

Special Issue Reprint

Recent Developments in the Synthesis and Functionalization of Nitrogen Heterocycles

Volume II

Edited by
Alexey M. Starosotnikov, Maxim A. Bastrakov and Igor L. Dalinger

[mdpi.com/journal/molecules](https://www.mdpi.com/journal/molecules)

**Recent Developments in the Synthesis
and Functionalization of Nitrogen
Heterocycles—Volume II**

Recent Developments in the Synthesis and Functionalization of Nitrogen Heterocycles—Volume II

Editors

Alexey M. Starosotnikov

Maxim A. Bastrakov

Igor L. Dalinger



Basel • Beijing • Wuhan • Barcelona • Belgrade • Novi Sad • Cluj • Manchester

Editors

Alexey M. Starosotnikov
N.D. Zelinsky Institute of
Organic Chemistry RAS
Moscow
Russia

Maxim A. Bastrakov
N.D. Zelinsky Institute of
Organic Chemistry RAS
Moscow
Russia

Igor L. Dalinger
N.D. Zelinsky Institute of
Organic Chemistry RAS
Moscow
Russia

Editorial Office

MDPI AG
Grosspeteranlage 5
4052 Basel, Switzerland

This is a reprint of articles from the Special Issue published online in the open access journal *Molecules* (ISSN 1420-3049) (available at: https://www.mdpi.com/journal/molecules/special_issues/Synthesis_Nitrogen_Heterocycles).

For citation purposes, cite each article independently as indicated on the article page online and as indicated below:

Lastname, A.A.; Lastname, B.B. Article Title. <i>Journal Name</i> Year , <i>Volume Number</i> , Page Range.
--

Volume II

ISBN 978-3-7258-2081-8 (Hbk)

ISBN 978-3-7258-2082-5 (PDF)

doi.org/10.3390/books978-3-7258-2082-5

Set

ISBN 978-3-7258-2077-1 (Hbk)

ISBN 978-3-7258-2078-8 (PDF)

© 2024 by the authors. Articles in this book are Open Access and distributed under the Creative Commons Attribution (CC BY) license. The book as a whole is distributed by MDPI under the terms and conditions of the Creative Commons Attribution-NonCommercial-NoDerivs (CC BY-NC-ND) license.

Contents

About the Editors	vii
Preface	ix
Vladislav V. Fedin, Sergey A. Usachev, Dmitrii L. Obydenov and Vyacheslav Y. Sosnovskikh Reactions of Trifluoroacetic Acid Lactone and Hexafluoroacetic Acid with Amines: Synthesis of Trifluoromethylated 4-Pyridones and Aminoenones Reprinted from: <i>Molecules</i> 2022 , <i>27</i> , 7098, doi:10.3390/molecules27207098	1
Ebenezer Ametsetor, Spencer Farthing and Richard A. Bunce Domino Aza-Michael-S _N Ar-Heteroaromatization Route to C5-Substituted 1-Alkyl-1 <i>H</i> -Indole-3-Carboxylic Esters Reprinted from: <i>Molecules</i> 2022 , <i>27</i> , 6998, doi:10.3390/molecules27206998	18
Lingamurthy Macha, Ranjith Jala, Sang-Yun Na and Hyun-Joon Ha Atom Economical Multi-Substituted Pyrrole Synthesis from Aziridine Reprinted from: <i>Molecules</i> 2022 , <i>27</i> , 6869, doi:10.3390/molecules27206869	34
Natalia A. Danilkina, Ekaterina A. Khmelevskaya, Anna G. Lyapunova, Alexander S. D'yachenko, Alexander S. Bunev, Rovshan E. Gasanov, et al. Functionalized 10-Membered Aza- and Oxaenediynes through the Nicholas Reaction Reprinted from: <i>Molecules</i> 2022 , <i>27</i> , 6071, doi:10.3390/molecules27186071	47
Dmitry M. Bystrov, Alla N. Pivkina and Leonid L. Fershtat An Alliance of Polynitrogen Heterocycles: Novel Energetic Tetrazinedioxide-Hydroxytetrazole-Based Materials Reprinted from: <i>Molecules</i> 2022 , <i>27</i> , 5891, doi:10.3390/molecules27185891	67
Sudheer S. Kurup, Natalie M. Woodland, Richard L. Lord and Stanislav Groysman Aziridination Reactivity of a Manganese(II) Complex with a Bulky Chelating Bis(Alkoxide) Ligand Reprinted from: <i>Molecules</i> 2022 , <i>27</i> , 5751, doi:10.3390/molecules27185751	81
Vladislav V. Nikol'skiy, Mikhail E. Minyaev, Maxim A. Bastrakov and Alexey M. Starosotnikov Nucleophilic Functionalization of 2-R-3-Nitropyridines as a Versatile Approach to Novel Fluorescent Molecules Reprinted from: <i>Molecules</i> 2022 , <i>27</i> , 5692, doi:10.3390/molecules27175692	95
Pavel A. Sakharov, Nikolai V. Rostovskii, Alexander F. Khlebnikov and Mikhail S. Novikov Copper(II)-Catalyzed (3+2) Cycloaddition of 2 <i>H</i> -Azirines to Six-Membered Cyclic Enols as a Route to Pyrrolo[3,2- <i>c</i>]quinolone, Chromeno[3,4- <i>b</i>]pyrrole, and Naphtho[1,8- <i>ef</i>]indole Scaffolds Reprinted from: <i>Molecules</i> 2022 , <i>27</i> , 5681, doi:10.3390/molecules27175681	110
Vanessa Judit Kolcsár and György Szöllösi Synthesis of a Pyrrolo[1,2- <i>a</i>]quinazoline-1,5-dione Derivative by Mechanochemical Double Cyclocondensation Cascade Reprinted from: <i>Molecules</i> 2022 , <i>27</i> , 5671, doi:10.3390/molecules27175671	127
Elvira R. Zaitseva, Dmitrii S. Ivanov, Alexander Yu. Smirnov, Andrey A. Mikhaylov, Nadezhda S. Baleeva and Mikhail S. Baranov [1,5]-Hydride Shift Triggered <i>N</i> -Dealkylative Cyclization into 2-Oxo-1,2,3,4-tetrahydroquinoline-3-carboxylates via Boronate Complexes Reprinted from: <i>Molecules</i> 2022 , <i>27</i> , 5270, doi:10.3390/molecules27165270	140

Daniil N. Lyapustin, Svetlana K. Kotovskaya, Ilya I. Butorin, Evgeny N. Ulomsky, Vladimir L. Rusinov, Denis A. Babkov, et al. CK2 Inhibition and Antitumor Activity of 4,7-Dihydro-6-nitroazolo[1,5-a]pyrimidines Reprinted from: <i>Molecules</i> 2022 , <i>27</i> , 5239, doi:10.3390/molecules27165239	149
Eurico Lima and Lucinda V. Reis Photodynamic Therapy: From the Basics to the Current Progress of <i>N</i> -Heterocyclic-Bearing Dyes as Effective Photosensitizers Reprinted from: <i>Molecules</i> 2023 , <i>28</i> , 5092, doi:10.3390/molecules28135092	163
Illia Lenko, Carole Alayrac, Igor Božek and Bernhard Witulski 1,3-Butadienamides the Ethynylogous Ynamides: Synthesis, Properties and Applications in Heterocyclic Chemistry Reprinted from: <i>Molecules</i> 2023 , <i>28</i> , 4564, doi:10.3390/molecules28114564	205
R. Bernadett Vlocskó, Guoshu Xie and Béla Török Green Synthesis of Aromatic Nitrogen-Containing Heterocycles by Catalytic and Non-Traditional Activation Methods Reprinted from: <i>Molecules</i> 2023 , <i>28</i> , 4153, doi:10.3390/molecules28104153	251
Zizhen Lei, Wenxu Chang, Hong Guo, Jiyao Feng and Zhenhua Zhang A Brief Review on the Synthesis of the <i>N</i> -CF ₃ Motif in Heterocycles Reprinted from: <i>Molecules</i> 2023 , <i>28</i> , 3012, doi:10.3390/molecules28073012	287
Yulia Volkova and Igor Zavarzin Synthesis of Phosphorus(V)-Substituted Six-Membered <i>N</i> -Heterocycles: Recent Progress and Challenges Reprinted from: <i>Molecules</i> 2023 , <i>28</i> , 2472, doi:10.3390/molecules28062472	313
Heber Victor Tolomeu and Carlos Alberto Manssour Fraga Imidazole: Synthesis, Functionalization and Physicochemical Properties of a Privileged Structure in Medicinal Chemistry Reprinted from: <i>Molecules</i> 2023 , <i>28</i> , 838, doi:10.3390/molecules28020838	344
Siva S. Panda, Marian N. Aziz, Jacek Stawinski and Adel S. Girgis Azomethine Ylides—Versatile Synthons for Pyrrolidinyl-Heterocyclic Compounds Reprinted from: <i>Molecules</i> 2023 , <i>28</i> , 668, doi:10.3390/molecules28020668	371
Igor S. Kovalev, Grigory V. Zyryanov, Sougata Santra, Adinath Majee, Mikhail V. Varaksin and Valery N. Charushin Folic Acid Antimetabolites (Antifolates): A Brief Review on Synthetic Strategies and Application Opportunities Reprinted from: <i>Molecules</i> 2022 , <i>27</i> , 6229, doi:10.3390/molecules27196229	452
Badrud Duza Mohammad, Mirza Shahed Baig, Neeraj Bhandari, Falak A. Siddiqui, Sharuk L. Khan, Zubair Ahmad, et al. Heterocyclic Compounds as Dipeptidyl Peptidase-IV Inhibitors with Special Emphasis on Oxadiazoles as Potent Anti-Diabetic Agents Reprinted from: <i>Molecules</i> 2022 , <i>27</i> , 6001, doi:10.3390/molecules27186001	475
Pezhman Shiri, Atefeh Roosta, Wim Dehaen and Ali Mohammad Amani Recent Strategies in Transition-Metal-Catalyzed Sequential C–H Activation/Annulation for One-Step Construction of Functionalized Indazole Derivatives Reprinted from: <i>Molecules</i> 2022 , <i>27</i> , 4942, doi:10.3390/molecules27154942	492

About the Editors

Alexey M. Starosotnikov

Alexey M. Starosotnikov was born in 1978 in Moscow, Russia. He graduated from the Higher Chemical College of the Russian Academy of Sciences in 2000. He obtained his Ph.D. (2003) and Doctor of Science (2016) degrees at the N.D. Zelinsky Institute of Organic Chemistry of the Russian Academy of Sciences. At present, he serves as a Research Group Leader within this institute. His research interests include the chemistry of nitrogen heterocycles and aromatic nitro-compounds, as well as the pericyclic reactivity of aromatic systems.

Maxim A. Bastrakov

Maxim A. Bastrakov was born in Yoshkar-Ola, Russia, in 1982. He graduated from Mary State University in 2005. In 2008, he defended his Ph.D. theses under the supervision of Professor Svyatoslav A. Shevelev. Currently, Dr. Bastrakov is a Senior Scientist of the Laboratory of Aromatic Nitrogen Compounds at the N.D. Zelinsky Institute of Organic Chemistry. In 2014, he was awarded a Gold Medal of the Russian Science Academy for his work as a young scientist. His research interests cover the chemistry of heterocyclic compounds and nitroarenes and the synthesis of multi-purpose compounds on this basis.

Igor L. Dalinger

Igor L. Dalinger was born in 1961 in Moscow, Russia. He graduated from the Lomonosov Moscow State University (Department of Chemistry) in 1983. He received his Ph.D. (1988) and Doctor of Chemical Science (2013) degrees from the N.D. Zelinsky Institute of Organic Chemistry. At present he serves as Head of the Laboratory of Aromatic Nitrogen Compounds at the same institute. His research interests include the molecular design, synthesis, and characterization of nitrogen-rich heterocycles and their use as energetic materials.

Preface

Nitrogen heterocycles constitute a broad class of organic compounds. Many of their representatives have found applications in pharmaceuticals, high-energy substances, dyes, and non-linear optical materials, among many others. The rapid development of the pharmaceutical industry and material science has stimulated the search for new synthetic approaches and new methods for the functionalization of N-heterocycles; these are some of the key objectives of modern organic chemistry. As a result of such research, in addition to achieving these objectives, new and sometimes unexpected applications of N-heterocycles may arise. This reprint brings together recent original research papers and high-quality reviews on the synthesis, reactivity, and applications of aromatic and saturated nitrogen heterocyclic compounds, contributed by an international team of leading experts in this field. This reprint offers useful information for a wide range of synthetic chemists.

Alexey M. Starosotnikov, Maxim A. Bastrakov, and Igor L. Dalinger

Editors

Article

Reactions of Trifluoroacetic Acid Lactone and Hexafluorodehydroacetic Acid with Amines: Synthesis of Trifluoromethylated 4-Pyridones and Aminoenones

Vladislav V. Fedin, Sergey A. Usachev, Dmitrii L. Obydenov and Vyacheslav Y. Sosnovskikh *

Institute of Natural Sciences and Mathematics, Ural Federal University, 51 Lenina Ave., 620000 Ekaterinburg, Russia

* Correspondence: vy.sosnovskikh@urfu.ru; Tel.: +7-343-389-9597

Abstract: Dehydroacetic acid and triacetic acid lactone are known to be versatile substrates for the synthesis of a variety of azaheterocycles. However, their fluorinated analogs were poorly described in the literature. In the present work, we have investigated reactions of trifluoroacetic acid lactone and hexafluorodehydroacetic acid with primary amines, phenylenediamine, and phenylhydrazine. While hexafluorodehydroacetic acid reacted the same way as non-fluorinated analog giving 2,6-bis(trifluoromethyl)-4-pyridones, trifluoroacetic acid lactone had different regioselectivity of nucleophilic attack compared to the parent structure, and corresponding 3-amino-6,6,6-trifluoro-5-oxohex-3-enamides were formed as the products. In the case of binucleophiles, further cyclization took place, forming corresponding benzodiazepine and pyrazoles. The obtained 2,6-bis(trifluoromethyl)-4-pyridones were able to react with active methylene compounds giving fluorinated merocyanine dyes.

Keywords: 4-hydroxy-2-pyrone; 4-pyridone; aminoenone; trifluoromethylated heterocycles; regioselective reactions

Citation: Fedin, V.V.; Usachev, S.A.; Obydenov, D.L.; Sosnovskikh, V.Y. Reactions of Trifluoroacetic Acid Lactone and Hexafluorodehydroacetic Acid with Amines: Synthesis of Trifluoromethylated 4-Pyridones and Aminoenones. *Molecules* **2022**, *27*, 7098. <https://doi.org/10.3390/molecules27207098>

Academic Editors: Alexey M. Starosotnikov, Maxim A. Bastrakov and Igor L. Dalinger

Received: 19 September 2022

Accepted: 17 October 2022

Published: 20 October 2022

Publisher's Note: MDPI stays neutral with regard to jurisdictional claims in published maps and institutional affiliations.



Copyright: © 2022 by the authors. Licensee MDPI, Basel, Switzerland. This article is an open access article distributed under the terms and conditions of the Creative Commons Attribution (CC BY) license (<https://creativecommons.org/licenses/by/4.0/>).

1. Introduction

Oxygen heterocycles are common precursors in organic synthesis and have a special place in the synthesis of important nitrogen heterocycles by various methodologies. Among others, pyrones attract significant interest both due to a variety of chemical properties and a wide distribution in nature [1–4]. Particular attention is paid to 4-hydroxy-2-pyrones, namely, triacetic acid lactone (TAL), dehydroacetic acid (DHA, Figure 1), and their derivatives, which belong to polyketides and occur widely in living organisms [5–8]. The availability of these compounds and the possibility of their biochemical synthesis contributed to their extensive research and to the development of a wide range of options for their modification, considering them as platform compounds [9–12].

On the other hand, the introduction of fluorine into the structure of molecules often leads to a modification of their chemical properties [13] and is a common strategy in drug design [14–18], pesticides synthesis [19,20], and other areas [21–24]. However, there are very limited data on fluorine-containing analogs of TAL and DHA in the literature, which practically do not cover their properties. The only synthesis of 4-hydroxy-3-trifluoroacetyl-6-trifluoromethyl-2H-pyran-2-one (hexafluorodehydroacetic acid, DHA-*f*₆, Figure 1) was performed by the heating of trifluoroacetoacetic ester in the presence of P₂O₅ and proceeds through formation and dimerization of trifluoroacetylketene [25]. Hydrolysis of DHA-*f*₆ in aqueous NaHCO₃ leads to 4-hydroxy-6-trifluoromethyl-2H-pyran-2-one (trifluoroacetic acid lactone, TAL-*f*₃, Figure 1) [25]. The second route for the synthesis of TAL-*f*₃ presented in the literature comprises cyclization of the corresponding trifluorodioxocaproic acid with acetic anhydride [26]. Among the properties of TAL-*f*₃, only modification of the 4-OH group is known, which was methylated with Me₂SO₄ [27] and triflated with Tf₂O [26]. The ring-opening of the O-methyl derivative on treatment with magnesium methylate gave

methyl 3-methoxy-5-oxo-6,6,6-trifluoro-5-hexenoate [27] and the 4-OTf derivative reacted with 4-(methylthio)phenylboronic acid to give a Suzuki coupling product [26].

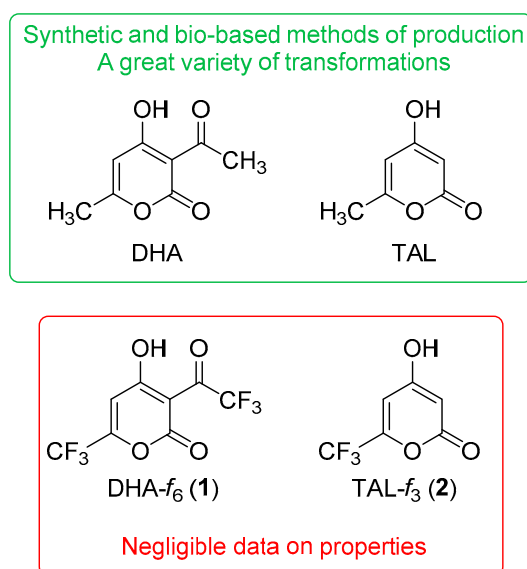
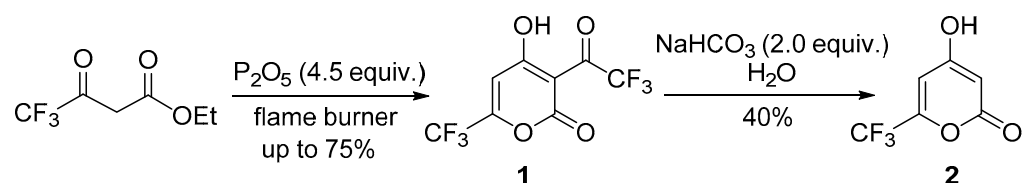


Figure 1. Structure of DHA, TAL, DHA-*f*₆, and TAL-*f*₃.

Thus, compounds that are attractive in terms of reactivity and properties of possible products turned out to be completely unexplored, and in this work, we have studied the interaction of DHA-*f*₆ and TAL-*f*₃ with primary amines as typical nucleophiles.

2. Results and Discussion

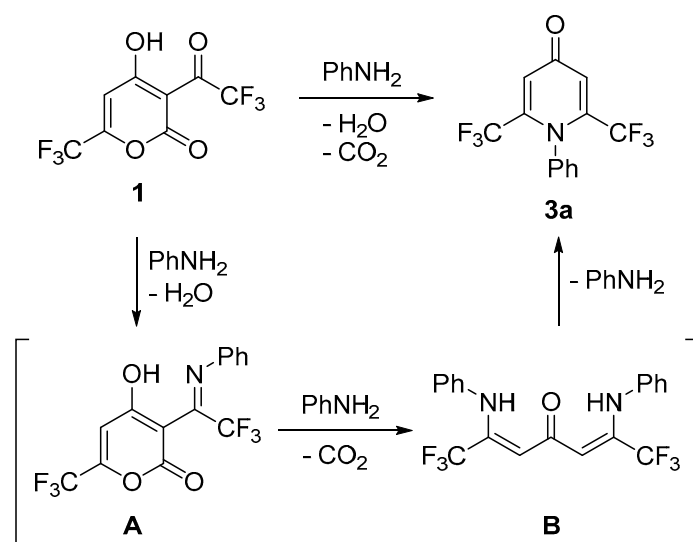
To begin with, we reproduced the synthesis described by German et al. (Scheme 1) [25], as it gives access both to DHA-*f*₆ and TAL-*f*₃. The results of the first step were quite inconsistent, and the yield ranged from 0% to 75%, presumably due to heating with a flame burner, which is hard to control. Nevertheless, the product was obtained in a satisfactory quantity for the further research. It should be noted that no variation in reaction conditions has improved the yield. Thus, the lowering of P₂O₅ loading or increasing reaction time resulted in the formation of complex mixtures, either of open-chain condensation products and trimerization ones characterized by the ester methylene quartets in ¹H NMR spectra or triads of equal intensity in ¹⁹F NMR spectra correspondingly. The hydrolysis of DHA-*f*₆ was more reproducible; however, we could never achieve the literature yield of 95% and had 40% on average (Scheme 1). Apart from NaHCO₃, we have used NaOH and Na₂CO₃ as a base, but the yields were slightly lower. Adjusting pH to 4–5 during hydrolysis as the original procedure claims was quite difficult because it dropped down in time due to trifluoroacetic acid formation, so 2.0 equiv. of NaHCO₃ was used instead. Moreover, crystallization of TAL-*f*₃ did not occur until acidification to pH 0–1. We tried, as well, to carry out the detrifluoroacetylation of DHA-*f*₆ by boiling it in water or by treatment with 93% H₂SO₄ or 70% HClO₄ at room temperature, but the conversion was negligible.



Scheme 1. Synthesis of DHA-*f*₆ (1) and TAL-*f*₃ (2).

At the first step, we studied the reaction of DHA-*f*₆ with aniline. There are three main consecutive products that can be expected based on the literature data (Scheme 2) [28,29].

While a formation of Schiff bases usually proceeds readily in acidic media, no conversion was observed when we attempted the synthesis of intermediate **A** in aqueous HCl with 1.5 equiv. of PhNH₂ (Table 1, entry 1). When EtOH was used as a solvent, spontaneous decarboxylation took place and *N*-phenylpyridone **3a** was isolated in 60% yield (Table 1, entry 2). Formation of intermediate **B** was also observed and will be discussed later. Increasing the amount of PhNH₂ and carrying out the reaction in a less polar solvent or without it as well as raising the temperature did not improve the yield (Table 1, entries 3–10).



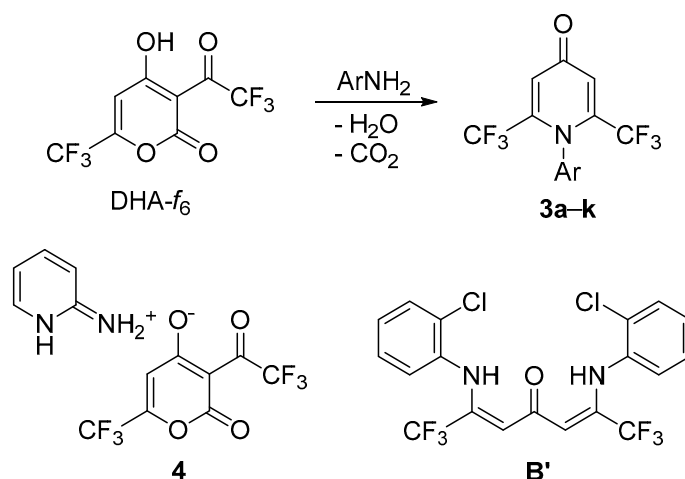
Scheme 2. Reaction of DHA-*f*₆ with aniline.

Table 1. Optimization of the reaction conditions of DHA-*f*₆ with aniline ^a.

Entry	PhNH ₂ , Equiv.	Solvent	Yield 3a , %
1	1.5	HCl (0.5 M) ^b	n.r. ^c
2	2.3	ethanol	60
3	3.5	ethanol	40
4	4.0	ethanol	45
5	2.3	ethanol	37 ^d
6	4.0	1,4-dioxane	36
7	3.5	1,4-dioxane	27 ^e
8	4.0	toluene	17
9	2.3	toluene	19
10	2.3	neat	25

^a A solution of PhNH₂ in 1 mL of a solvent was added to DHA-*f*₆ (**1**) (100 mg, 0.36 mmol) and the reaction mixture was stirred at room temperature for 24 h. ^b Aqueous solution. ^c No reaction. ^d The reaction was carried out at 65 °C for 12 h. ^e The reaction was carried out at reflux for 4 h.

Exploring the scope of the synthesis of 4-pyridones **3** from DHA-*f*₆, we found that the reaction rates and the yields correlate with nucleophilicity of amine. Thus, aniline derivatives bearing π -donor substituents (MeO, F) at the 4-position react considerably faster, whereas those bearing strong acceptor substituents (Ac, CF₃) at the 3-position or a weak acceptor substituent (Br) at the 4-position react at a comparable rate but give slightly lower yields (Scheme 3, Table 2). Noteworthy, even extremely weakly nucleophilic 4-nitroaniline was able to react although the conversion was low even after 6 days, and pyridone **3k** was formed in only 8% yield. The characteristic signals of pyridones **3** in the NMR spectra acquired in CDCl₃ are the singlet of vinylic CH with double intensity at 6.95–7.02 ppm (¹H NMR) and the quartets of symmetric carbons at 119.2–119.4 ppm (CF₃), 140.8–141.6 ppm (C-2 and C-6), and 119.0–119.6 ppm (C-3 and C-5).



Scheme 3. Reaction of DHA-*f*₆ with aromatic amines.

Table 2. The scope of 4-pyridone synthesis from DHA-*f*₆ ^a.

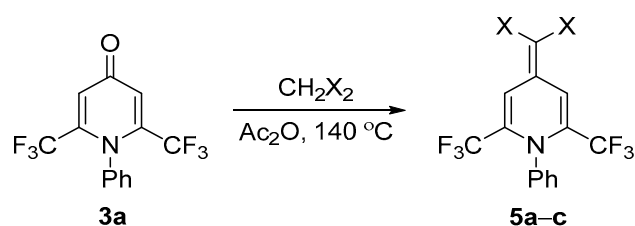
Pyridone	Ar	Time, h	Yield, %	Mp, °C
3a	Ph	24	60	135–136
3b	4-MeOC ₆ H ₄	8	56	125–126
3c	3,4-F ₂ C ₆ H ₃	6	57	142–143
3d	4-BrC ₆ H ₄	24	47	129–131
3e	3-AcC ₆ H ₄	24	47	118–119
3f	3-F ₃ CC ₆ H ₄	24	47	91–92
3g	2,5-F ₂ C ₆ H ₃	48	46	116–119
3h	2-ClC ₆ H ₄	40	49	132–136
3i	2-MeC ₆ H ₄	24	65	Liq.
3j	2,5-Me ₂ C ₆ H ₃	24	48	105–107
3k	4-O ₂ NC ₆ H ₄	144	8 ^b	– ^c

^a A solution of ArNH₂ (0.83 mmol) in EtOH was added to DHA-*f*₆ (1) (100 mg, 0.36 mmol) and the reaction mixture was stirred at room temperature for a given amount of time. ^b Based on ¹H NMR spectrum. ^c The product was obtained in the mixture with 4-nitroaniline.

The existence of an *ortho*-substituent did not affect the initial two steps of the reaction sequence and CO₂ evolution occurred during first 1–2 h; however, the cyclization of bisenamines **B** depends on electron properties of the substituent. In the case of more reactive *o*-toluidine and 2,5-xylidine, the overall duration was 24 h, whereas 2-chloro- and 2,5-difluoroaniline required twice as much time (Table 2). It allowed us to isolate and characterize the intermediate **B'** (Scheme 3), although in the mixture with starting 2-chloroaniline, which did not separate by the column chromatography. Its structure was confirmed by very distinguishable singlets of symmetric groups at 5.78 ppm (vinylic CH) and 11.49 ppm (enaminone NH) in ¹H NMR and at 97.8 ppm in ¹⁹F NMR spectra in CDCl₃. The formation of adducts with the structure of **B** was observed by TLC in all the cases, but for most of them the simultaneous cyclization to pyridones **3** occurred, so their isolation was impractical.

Surprisingly, aliphatic amines such as butylamine, *N,N*-dimethylethylenediamine and benzylamine did not react with DHA-*f*₆ under the conditions found, even after several weeks. It can be attributed to their much higher basicity and fixation of the substrate in an anionic form that prevents further nucleophilic attack. This assumption was supported by the formation of the salt **4** (Scheme 3) in the reaction with 2-aminopyridine, which precipitated in nearly quantitative yield and remained unchanged after 8 days at 60 °C in EtOH. The signals in the ¹⁹F NMR spectrum of compound **4** in DMSO-*d*₆ almost exactly match the signals of DHA-*f*₆ (91.0 and 89.8 ppm compared to 91.1 and 89.6 ppm, respectively) and the singlet of pyrone CH in the ¹H NMR spectrum is shifted upfield by 0.09 ppm (6.15 compared to 6.24 ppm) in agreement with its anionic character.

Reactivity of 4-pyridones **3** is greatly affected by strongly acceptor CF₃-groups. Thus, electrophilic bromination of **3a** with NBS proceeded poorly compared to the non-fluorinated analog [30] and no distinct product was obtained. On the contrary, Knoevenagel condensation did well with malononitrile, barbituric acid, and indane-1,3-dione in acetic anhydride, leading to fluorinated merocyanine dyes **5** (Scheme 4, Table 3). This reveals that the electron deficiency of a heterocycle plays an important role for this reaction, as 1-aryl-2,6-dimethyl-4-pyridones are less active [31,32] compared both to the CF₃-substituted pyridone **3a** and to the oxygen analog, 2,6-dimethyl-4-pyrone [33]. The time required for the reaction completion is in accordance with the acidity of an active methylene compound, so one can assume that deprotonation is a rate-limiting step, and a high activity of a substrate is necessary to prevent self-condensation of CH₂X₂.



Scheme 4. Reaction of 4-pyridone **3a** with active methylene compounds.

Table 3. Synthesis and structure of adducts **5a–c**^a.

Compound	Structure	Time, h	Yield, %	Mp, °C
5a		10	65	172–173
5b		4	58	270–271
5c		6	43	208–209

^a A solution of 4-pyridone **3a** (100 mg, 0.33 mmol) and the corresponding CH₂X₂ (0.4 mmol) in Ac₂O was stirred at 140 °C for a given amount of time.

The prepared compounds, **5a–c**, are found to be yellow solids and exhibit an absorbance major maximum at 382–437 nm in the visible region of the spectra. For barbituric derivative **5b**, the high molar extinction coefficient (91406 M⁻¹·cm⁻¹ at 412 nm) is observed and probably indicates the intramolecular charge-transfer described by the aromatic resonance form **5'** (Figure 2). For dihydropyridine **5c** bearing the indanedione moiety, additional intensive absorption maxima are observed at 246 and 224 nm. An interesting feature in NMR spectra of compounds **5** is a large difference compared to each other in chemical shifts of CH-groups in the dihydropyridine fragment attributed to the magnetic anisotropy of carbonyl and cyano groups, which have a closer proximity in derivative **5b** ($\delta_{\text{H}3}$ = 9.77 ppm, $\delta_{\text{C}3}$ = 116.8 ppm) than in **5c** ($\delta_{\text{H}3}$ = 9.10 ppm, $\delta_{\text{C}3}$ = 113.4 ppm) and in **5a** ($\delta_{\text{H}3}$ = 7.26 ppm, $\delta_{\text{C}3}$ = 112.7 ppm). Another possible explanation for the difference is a greater contribution of the betaine resonance form **5'** (Figure 2) for the adduct with barbituric acid, but this seems to have a smaller effect as the chemical shifts of the rest of carbon atoms diverge much less (Table S2 in Supplementary Materials).

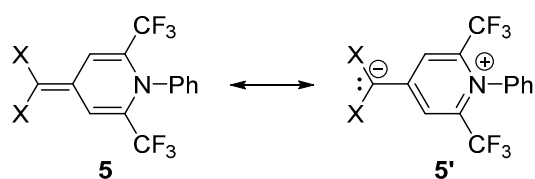
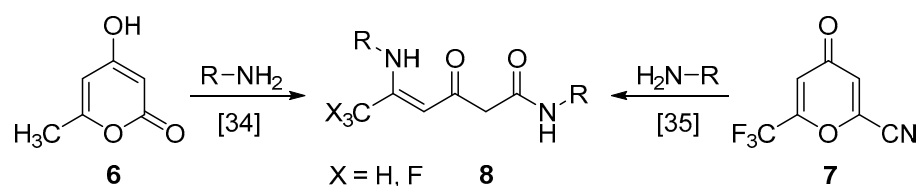


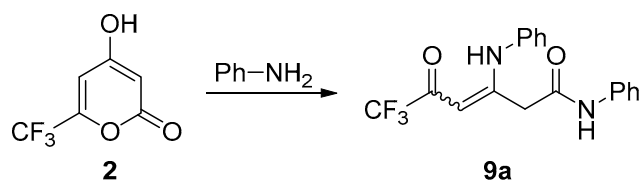
Figure 2. Resonance forms of compound 5.

Moving on to the investigation of trifluorotriacetic acid lactone (**2**) properties, we focused on our previous work on the study of triacetic acid lactone (**6**) [34] and 2-cyano-6-(trifluoromethyl)-4*H*-pyran-4-one (**7**) [35], which gave carbamoylated enaminones **8** (Scheme 5), which proved to be a versatile building blocks for nitrogen heterocycles. In both cases, the substrates were attacked with two equivalents of amine at positions 2 and 6.



Scheme 5. Reaction of TAL and 2-cyano-6-(trifluoromethyl)-4-pyrone with primary amines.

We started the optimization of the reaction conditions of TAL-*f*₃ (**2**) with aniline in EtOH using various amount of amine (Scheme 6, Table 4, entries 1–3). The product **9a** with unexpected regiochemistry was formed with the best yield of 64% when only little excess of PhNH₂ was applied. The reaction performs better in aprotic polar 1,4-dioxane (Table 4, entry 4) and worse in non-polar toluene or without a solvent (Table 4; entries 5, 6). It should be noted that an increase in the reaction temperature did not improve the yield of enaminone **9a**.



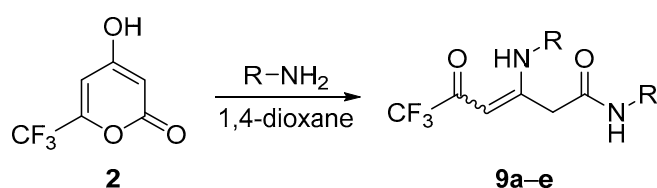
Scheme 6. Reaction of TAL-*f*₃ with aniline.

Table 4. Optimization of the reaction conditions of TAL-*f*₃ with aniline ^a.

Entry	PhNH ₂ , Equiv.	Solvent	Yield 9a , %
1	5	ethanol	43
2	3.5	ethanol	63
3	2.1	ethanol	64
4	2.1	1,4-dioxane	72
5	2.1	toluene	30
6	2.1	neat	12

^a A solution of PhNH₂ was added to TAL-*f*₃ (**2**) (100 mg, 0.56 mmol). The reaction mixture was stirred at room temperature for 24 h.

The reaction with electron-rich *p*-anisidine proceeded equally well, whereas electron-poor *p*-bromoaniline gave lower yield (Scheme 7, Table 5). The reaction with aliphatic amines again has difficulties, probably due to the formation of salts; however, the lower acidity of TAL-*f*₃ compared to DHA-*f*₆ allowed enaminones **9d,e** to form in low yields. In the case of butylamine, the heating to 60 °C was also needed. All amines reacted with the same regioselectivity, and no alternative isomers **8** were isolated.



Scheme 7. Reaction of TAL-*f*₃ with primary amines.

Table 5. The scope of reaction of TAL-*f*₃ with primary amines ^a.

Enaminone	R	Time, h	Yield, %	Z/E ratio ^b
9a	Ph	24	72	59:41 (44:56 °)
9b	4-MeOC ₆ H ₄	17	69	65:35
9c	4-BrC ₆ H ₄	15	41	59:41
9d	Bn	17	24	58:42 (67:33 °)
9e	Bu	72	7 ^d	65:35

^a A solution of RNH₂ (1.17 mmol) in 1,4-dioxane was added to TAL-*f*₃ (**2**) (100 mg, 0.56 mmol). The reaction mixture was stirred at room temperature for a given amount of time. ^b Assessed by ¹H and ¹⁹F NMR in CDCl₃. ^c Assessed by ¹H and ¹⁹F NMR in DMSO-*d*₆. ^d The reaction was carried out at 60 °C.

Although Z-form of enaminones is predominant because of an effective intramolecular hydrogen bonding, the contribution of an *E*-isomer may be affected by the electronic nature of a substituent at a nitrogen atom [36] or by an alternative hydrogen bond formation [37], which is the case for product **9** (Figure 3). The ratio of isomers is solvent-dependent, and Z-form mostly prevails, except for compound **4a** in DMSO-*d*₆ (Table 5). The assignment of isomers was conducted on the basis of ¹H and ¹³C NMR spectra (Table S3 in Supplementary Materials). The key signals are low-field NH-protons of Z-**9** isomers at 12.39–12.58 ppm (for N-arylenaminones **9a–c** in CDCl₃) and at 11.08–11.32 ppm (for N-alkylenaminones **9d,e** in CDCl₃). The corresponding signals for the *E*-isomers of **9** are under a much higher field in accordance with the literature [37,38]. Among the other features of the NMR spectra of compounds **9** is the existence of methylene protons and amide NH-protons at a lower field and methyne carbons at a higher field for the *E*-isomer (Figure 3).

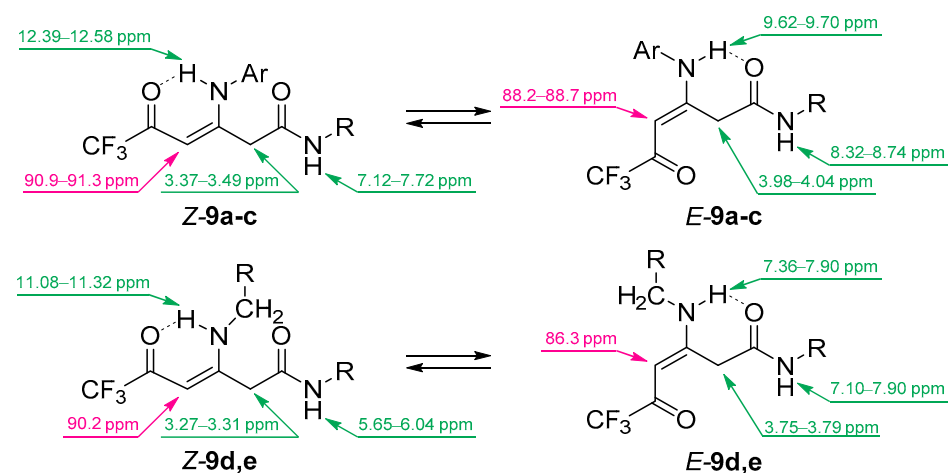
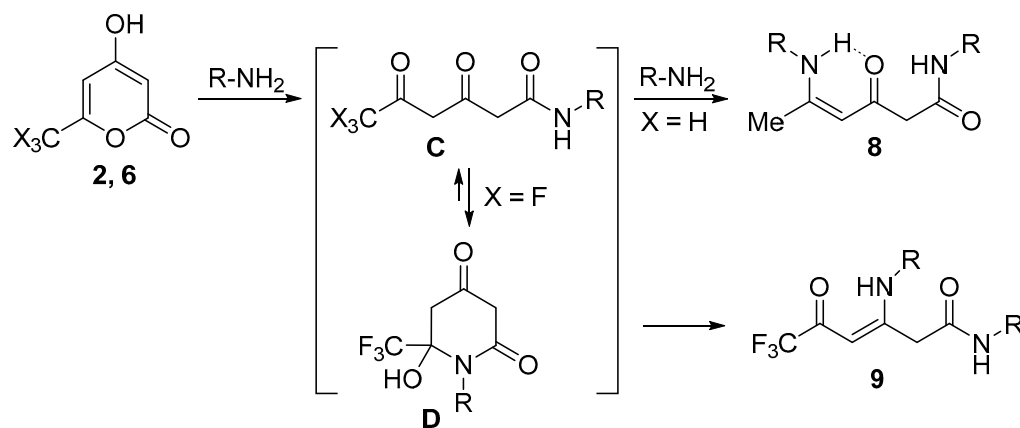


Figure 3. Equilibrium between Z- and *E*-isomers of enaminones **9** and their characteristic chemical shifts in ¹H (in green) and ¹³C (in magenta) NMR in CDCl₃.

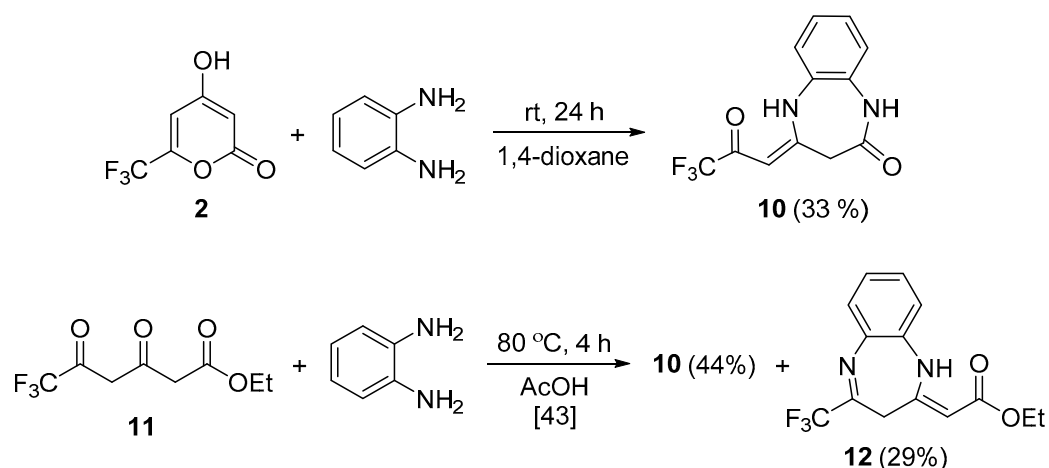
For an explanation of the difference in the regioselectivity of the interaction of TAL and TAL-*f*₃ with amines, we propose the following mechanism. The addition of the first equivalent of RNH₂ leads to the formation of dioxoamide **C** (Scheme 8), which was isolated earlier (X = H) [39]. The intermediate **C** is then attacked by the second amine molecule at the less hindered atom, C-5, in the case of X = H forming product **8**. A preference of the attack at C-3 for the fluorinated derivative may be attributed to a high content of cyclic

form **D** (Scheme 8), analogs of which were described in the literature as the only tautomer in CDCl_3 and $\text{DMSO-}d_6$ solutions [40,41]. The semiaminal carbon atom is less susceptible to nucleophiles than the free keto group that leads to the selective formation of product **9**. It also should be noted that a mixture of regioisomers is usually produced when linear aliphatic CF_3 -diketones react with aniline [42].



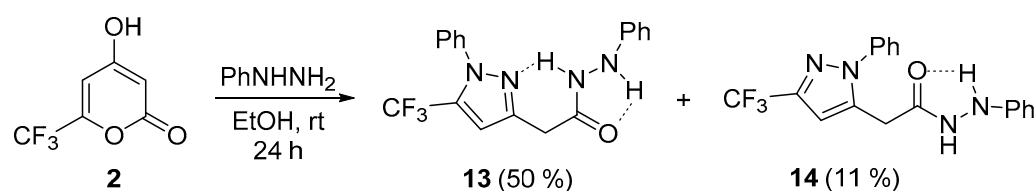
Scheme 8. Proposed mechanism of the reaction of TAL and TAL- f_3 with primary amines.

No change in selectivity was observed when bifunctional aromatic amine, *o*-phenylenediamine, was used in the optimized conditions. Benzodiazepinone **10** was formed as the only isolated product, although the yield was moderate (Scheme 9). Compound **10** was previously obtained from the corresponding dioxoester **11** in the mixture with diazepine **12** [43] (Scheme 9), so our method represents a good alternative with no specific separation needed.



Scheme 9. Reaction of TAL- f_3 and ethyl 6,6,6-trifluoro-3,5-dioxohexanoate with *o*-phenylenediamine.

Phenylhydrazine also reacted with TAL- f_3 (**2**) regioselectively in 1,4-dioxane, giving pyrazolohydrazide **13**, but the yield was poor. Changing the solvent to EtOH substantially increased the outcome, though isomer **14** was also formed and did not separate by the column chromatography (Scheme 10). Compound **14** was previously synthesized from cyanopyrone **7** [35] and its spectral characteristics are in a good correlation with our data. Both isomers appear as two sets of signals corresponding to a major *syn*- (presented at Scheme 10) and a minor *anti*-rotamer about the N–N bond. The key differences in the NMR spectra of the regioisomer **13** are the more downfield signal of the CF_3 group in ^{19}F NMR (106.2 ppm compared to 101.9 ppm for **14**) due to deshielding from the adjacent phenyl substituent, and more downfield signals of NH groups in ^1H NMR (9.91 and 7.82 ppm compared to 9.84 and 7.73 ppm for **14**) due to additional hydrogen bonding.



Scheme 10. Reaction of TAL-*f*₃ with phenylhydrazine.

Thus, hexafluorodehydroacetic acid and trifluorotriacetic acid lactone were shown to be active electrophiles and represent interesting fluorinated building blocks, which were transformed to a number of nitrogen heterocycles. Reaction of hexafluorodehydroacetic acid with primary aromatic amines leads to the formation of 2,6-bis(trifluoromethyl)-4-pyridones that are able to undergo Knoevenagel condensation to give merocyanine dyes. Trifluorotriacetic acid lactone undergoes ring-opening transformations with mono- and binucleophilic primary amines at the positions 2 and 4 and differs in regioselectivity compared to the non-fluorinated analog.

3. Materials and Methods

NMR spectra were recorded on Bruker DRX-400 (Bruker BioSpin GmbH, Ettlingen, Germany, work frequencies: ¹H–400 MHz, ¹³C–100 MHz, ¹⁹F–376.5 MHz) and Bruker Avance III-500 (Bruker BioSpin GmbH, Rheinstetten, Germany, work frequencies: ¹H–500 MHz, ¹³C–126 MHz, ¹⁹F–471 MHz) spectrometers in DMSO-*d*₆ and CDCl₃. The chemical shifts (δ) are reported in ppm relative to the internal standard TMS (¹H NMR), C₆F₆ (¹⁹F NMR), and residual signals of the solvents (¹³C NMR). IR spectra were recorded on a Shimadzu IRSpirit-T spectrometer (Shimadzu Corp., Kyoto, Japan) using an attenuated total reflectance (ATR) unit (FTIR mode, ZnSe crystal), and the absorbance maxima (ν) are reported in cm⁻¹. UV-visible spectra were recorded on a Shimadzu UV-1900 spectrophotometer (Shimadzu Corp., Kyoto, Japan) using EtOH as a solvent, the absorbance maxima (λ) are reported in nm, and the molar attenuation coefficients are reported in L·mol⁻¹·cm⁻¹. Elemental analyses were performed on an automatic analyzer PerkinElmer PE 2400 Series II (Perkin Elmer Instruments, Waltham, MA, USA). Melting points were determined using a Stuart SMP40 melting point apparatus (Bibby Scientific Ltd., Stone, Staffordshire, UK). Column chromatography was performed on silica gel (Merck 60, 70–230 mesh). All solvents and reagents were obtained commercially and used without purification.

3.1. Synthesis of Pyrones **1** and **2**

4-Hydroxy-3-(2,2,2-trifluoroacetyl)-6-(trifluoromethyl)-2H-pyran-2-one (1). A mixture of ethyl 4,4,4-trifluoroacetoacetate (9.1 g, 0.032 mol) and P₂O₅ (40 g, 0.141 mol) was heated with a gas burner flame for 10 min. Then, the mixture was distilled in a vacuum (~20 torr), collecting the fraction 90–110 °C. The target fraction was redistilled in the same interval. Yield 4.1 g (75%), yellowish needles, mp 40–42 °C. ¹H NMR (500 MHz, DMSO-*d*₆) δ 6.24 (1H, s, H-5), 11.12 (1H, s, OH). ¹⁹F NMR (471 MHz, DMSO-*d*₆) δ 89.6 (s, COCF₃), 91.1 (s, 6-CF₃) [25].

4-Hydroxy-6-(trifluoromethyl)-2H-pyran-2-one (2). A saturated aqueous solution of NaHCO₃ (0.5 mL, 0.55 mmol) was added with stirring to an aqueous solution of hexafluorodehydroacetic acid (**1**) (2.5 mL, 1 M). The mixture was stirred for 10 min and acidified with aqueous HCl (1 mL, 3 M). The precipitate was filtered off and dried. Yield 180 mg (40%), white solid, mp 135–138 °C (lit. mp 135–137 °C [25]). ¹H NMR (500 MHz, DMSO-*d*₆) δ 5.59 (1H, d, *J* = 1.8 Hz, H-3), 6.83 (1H, d, *J* = 1.7 Hz, H-5), 12.60 (1H, s, OH). ¹⁹F NMR (471 MHz, DMSO-*d*₆) δ 92.0 (s, CF₃).

3.2. Synthesis of Compounds **3a–k**

General Procedure

An aromatic amine (0.83 mmol) was added to a solution of hexafluorodehydroacetic acid (**1**) (100 mg, 0.36 mmol) in EtOH (1 mL). The reaction mixture was stirred at room

temperature for a given amount of time and acidified with aqueous HCl (3 mL, 1 M). The precipitate was filtered off and washed with water. The crude product was recrystallized from hexane.

1-Phenyl-2,6-bis(trifluoromethyl)pyridin-4(1H)-one (3a). The reaction was carried out for 24 h. Yield 66 mg (60%), yellow powder, mp 135–136 °C. ¹H NMR (400 MHz, CDCl₃) δ 6.97 (2H, s, H-3, H-5), 7.39 (2H, d, *J* = 7.6 Hz, H Ph), 7.50 (2H, t, *J* = 7.9 Hz, H Ph), 7.59 (1H, t, *J* = 7.5 Hz, H Ph). ¹H NMR (500 MHz, DMSO-*d*₆) δ 6.97 (2H, s, H-3, H-5), 7.55 (2H, t, *J* = 7.7 Hz, H Ph), 7.59 (1H, t, *J* = 7.5 Hz, H Ph), 7.70 (2H, d, *J* = 7.8 Hz, H Ph). ¹⁹F NMR (471 MHz, CDCl₃) δ 100.6 (s, CF₃). ¹⁹F NMR (471 MHz, DMSO-*d*₆) δ 102.5 (s, CF₃). ¹³C NMR (126 MHz, CDCl₃) δ 119.1 (2C, q, *J* = 4.7 Hz, C-3, C-5), 119.4 (2C, q, *J* = 275.7 Hz, CF₃), 128.7 (2C Ph), 130.1 (2C Ph), 131.3 (C Ph), 135.0 (C Ph), 141.2 (2C, q, *J* = 33.3 Hz, C-2, C-6), 177.4 (CO). IR (ATR) ν 3297, 1700 (C=O), 1658, 1398 (N–C), 1128–1116 (CF₃). Anal. Calculated for C₁₃H₇F₆NO: C 50.83; H 2.30; N 4.56. Found: C 50.77; H 2.38; N 4.46.

1-(4-Methoxyphenyl)-2,6-bis(trifluoromethyl)pyridin-4(1H)-one (3b). The reaction was carried out for 8 h. Yield 68 mg (56%), gray powder, mp 125–126 °C. ¹H NMR (400 MHz, CDCl₃) δ 3.88 (3H, s, CH₃), 6.95 (2H, s, H-3, H-5), 6.95 (2H, d, *J* = 8.9 Hz, H Ar), 7.28 (2H, d, *J* = 8.9 Hz, H Ar). ¹⁹F NMR (471 MHz, CDCl₃) δ 100.5 (s, CF₃). ¹³C NMR (126 MHz, CDCl₃) δ 55.6 (OCH₃), 113.7 (2C Ar), 119.1 (2C, q, *J* = 4.7 Hz, C-3, C-5), 119.4 (2C, q, *J* = 275.6 Hz, CF₃), 127.2 (C Ar), 131.2 (2C Ar), 141.6 (2C, q, *J* = 32.7 Hz, C-2, C-6), 161.3 (C Ar), 177.5 (CO). IR (ATR) ν 3061, 1653 (C=O), 1602, 1510, 1397 (N–C), 1250, 1397, 1158 (CF₃). HRMS (ESI) *m/z* [M + H]⁺. Calculated for C₁₄H₁₀F₆NO₂: 338.0616. Found: 338.0613.

1-(3,4-Difluorophenyl)-2,6-bis(trifluoromethyl)pyridin-4(1H)-one (3c). The reaction was carried out for 6 h. Yield 71 mg (57%), gray powder, mp 142–143 °C. ¹H NMR (500 MHz, CDCl₃) δ 6.96 (2H, s, H-3, H-5), 7.21 (1H, d, *J* = 8.6 Hz, H Ar), 7.31 (2H, m, H Ar). ¹⁹F NMR (471 MHz, CDCl₃) δ 28.3 (1F, dt, *J* = 21.3, 8.8 Hz, F Ar), 31.0 (1F, dddd, *J* = 21.3, 9.5, 6.7, 3.8 Hz, F Ar), 100.7 (6F, s, CF₃). ¹³C NMR (101 MHz, CDCl₃) δ 117.4 (d, *J* = 18.9 Hz, C Ar), 119.3 (2C, q, *J* = 275.7 Hz, CF₃), 119.4 (2C, q, *J* = 4.7 Hz, C-3, C-5), 120.2 (d, *J* = 19.1 Hz, C Ar), 127.3 (C Ar), 130.6 (C Ar), 140.9 (2C, q, *J* = 33.3 Hz, C-2, C-6), 149.5 (dd, *J* = 254.1, 13.8 Hz, C Ar), 152.1 (dd, *J* = 256.4, 12.2 Hz, C Ar), 177.1 (CO). IR (ATR) ν 3091, 3056, 1655 (C=O), 1615, 1519, 1397 (N–C), 1144 (CF₃). Anal. Calculated for C₁₃H₅F₈NO: C 45.50; H 1.47; N 4.08. Found: C 45.33; H 1.46; N 4.09.

1-(4-Bromophenyl)-2,6-bis(trifluoromethyl)pyridin-4(1H)-one (3d). The reaction was carried out for 24 h. Yield 65 mg (47%), yellow powder, mp 129–131 °C (decomp.). ¹H NMR (400 MHz, CDCl₃) δ 6.97 (2H, s, H-3, H-5), 7.27 (2H, d, *J* = 8.1 Hz, H Ar), 7.64 (1H, d, *J* = 8.5 Hz, H Ar). ¹⁹F NMR (471 MHz, CDCl₃) δ 100.7 (s, CF₃). ¹³C NMR (101 MHz, CDCl₃) δ 119.26 (2C, q, *J* = 4.5 Hz, C-3, C-5), 119.33 (2C, q, *J* = 275.8 Hz, CF₃), 126.0 (C Ar), 131.7 (2C, C Ar), 132.1 (2C, C Ar), 133.9 (C Ar), 141.0 (2C, q, *J* = 32.8 Hz, C-2, C-6), 177.3 (CO). IR (ATR) ν 3071, 1652 (C=O), 1589, 1480, 1397 (N–C), 1249, 1175 (CF₃). HRMS (ESI) *m/z* [M + H]⁺. Calculated for C₁₃H₇BrF₆NO: 385.9615. Found: 385.9606.

1-(3-Acetylphenyl)-2,6-bis(trifluoromethyl)pyridin-4(1H)-one (3e). The reaction was carried out for 24 h. Yield 60 mg (47%), pale pink powder, mp 118–119 °C. ¹H NMR (400 MHz, CDCl₃) δ 2.65 (3H, s, CH₃), 6.99 (2H, s, H-3, H-5), 7.57–7.69 (2H, m, H Ar), 8.00 (1H, s, H Ar), 8.17 (1H, dt, *J* = 7.4, 1.5 Hz, H Ar). ¹⁹F NMR (376 MHz, CDCl₃) δ 100.8 (s, CF₃). ¹³C NMR (126 MHz, CDCl₃) δ 26.6 (CH₃), 119.0 (2C, unres. q, C-3, C-5), 119.2 (2C, q, *J* = 276.1 Hz, CF₃), 129.2 (C Ar), 129.8 (C Ar), 131.2 (C Ar), 134.1 (C Ar), 135.4 (C Ar), 137.7 (C Ar), 141.6 (2C, unres. q, C-2, C-6), 177.2 (4-CO), 195.6 (COCH₃). IR (ATR) ν 3068, 1700 (C=O), 1665 (C=O), 1610, 1480, 1402 (N–C), 1138 (CF₃). Anal. Calculated for C₁₅H₉F₆NO₂: C 51.59; H 2.60; N 4.01. Found: C 51.50; H 2.63; N 3.99.

1-(3-(Trifluoromethyl)phenyl)-2,6-bis(trifluoromethyl)pyridin-4(1H)-one (3f). The reaction was carried out for 24 h. Yield 63 mg (47%), light-yellow powder, mp 91–92 °C. ¹H NMR (600 MHz, CDCl₃) δ 7.00 (2H, s, H-3, H-5), 7.64 (1H, d, *J* = 8.2 Hz, H Ar), 7.69 (1H, t, *J* = 8.0 Hz, H Ar), 7.72 (1H, s, H Ar), 7.89 (1H, d, *J* = 7.8 Hz, H Ar). ¹⁹F NMR (376 MHz, CDCl₃) δ 98.7 (3F, s, CF₃ Ar), 100.7 (6F, s, 2-CF₃, 6-CF₃). ¹³C NMR (126 MHz, CDCl₃) δ 119.3 (2C, q, *J* = 275.5 Hz, 2-CF₃, 6-CF₃), 119.4 (2C, q, *J* = 4.7 Hz, C-3, C-5), 122.9 (q, *J* = 272.5 Hz,

CF₃ Ar), 127.6 (C Ar), 128.3 (C Ar), 129.6 (C Ar), 131.8 (q, *J* = 33.8 Hz, C-3 Ar), 133.6 (C Ar), 135.4 (C Ar), 140.9 (2C, q, *J* = 33.4 Hz, C-2, C-6), 177.2 (CO). IR (ATR) ν 3091, 1655 (C=O), 1395 (N–C), 1327, 1252, 1126 (CF₃). HRMS (ESI) *m/z* [M + H]⁺. Calculated for C₁₄H₇F₉NO: 376.0384. Found: 376.0397.

1-(2,5-Difluorophenyl)-2,6-bis(trifluoromethyl)pyridin-4(1H)-one (3g). The reaction was carried out for 48 h. Yield 58 mg (46%), yellow powder, mp 116–119 °C. ¹H NMR (500 MHz, CDCl₃) δ 6.99 (2H, s, H-3, H-5), 7.20–7.26 (2H, m, H-3, H-6 Ar), 7.35 (1H, dddd, *J* = 9.3, 7.4, 3.8, 3.0 Hz, H-4 Ar). ¹⁹F NMR (376 MHz, CDCl₃) δ 38.6–38.8 (m, F-2 Ar), 46.0 (1F, dtd, *J* = 15.4, 7.4, 4.7 Hz, F-5 Ar), 98.5 (dd, *J* = 3.2, 0.9 Hz, CF₃). ¹³C NMR (126 MHz, CDCl₃) δ 117.1 (dd, *J* = 22.4, 8.8 Hz, C Ar), 119.1 (d, *J* = 25.9 Hz, C Ar), 119.3 (2C, q, *J* = 275.5 Hz, CF₃), 119.5 (2C, q, *J* = 4.6 Hz, C-3, C-5), 120.8 (dd, *J* = 23.6, 8.1 Hz, C Ar), 123.4 (dd, *J* = 16.3, 10.5 Hz, C Ar), 140.8 (2C, q, *J* = 34.1 Hz, C-2, C-6), 155.9 (dd, *J* = 252.0, 3.3 Hz, C Ar), 157.4 (dd, *J* = 247.8, 2.8 Hz, C Ar), 177.2 (CO). IR (ATR) ν 3072, 1666 (C=O), 1615, 1508, 1397 (N–C), 1251, 1136 (CF₃). HRMS (ESI) *m/z* [M + H]⁺. Calculated for C₁₃H₆F₈NO: 344.0322. Found: 344.0316.

1-(2-Chlorophenyl)-2,6-bis(trifluoromethyl)pyridin-4(1H)-one (3h). The reaction was carried out for 40 h. Yield is 61 mg (49%), yellow powder, mp 132–136 °C. ¹H NMR (500 MHz, CDCl₃) δ 6.99 (2H, s, H-3, H-5), 7.41–7.48 (1H, m, H Ar), 7.51–7.58 (3H, m, H Ar). ¹⁹F NMR (471 MHz, CDCl₃) δ 98.6 (s, CF₃). ¹³C NMR (126 MHz, CDCl₃) δ 119.3 (2C, q, *J* = 275.8 Hz, CF₃), 119.6 (2C, q, *J* = 4.5 Hz, C-3, C-5), 127.2 (C Ar), 130.1 (C Ar), 131.9 (C Ar), 132.7 (C Ar), 132.9 (C Ar), 135.9 (C Ar), 140.9 (2C, q, *J* = 33.9 Hz, C-2, C-6), 177.6 (CO). IR (ATR) ν 3056, 1743, 1651 (C=O), 1476, 1389 (N–C), 1247, 1136 (CF₃). HRMS (ESI) *m/z* [M + H]⁺. Calculated for C₁₃H₇ClF₆NO: 342.0120. Found: 342.0131.

1-(*o*-Tolyl)-2,6-bis(trifluoromethyl)pyridin-4(1H)-one (3i). The reaction was carried out for 24 h. Yield 74 mg (65%), brown viscous liquid. ¹H NMR (400 MHz, CDCl₃) δ 2.08 (3H, s, CH₃), 7.01 (2H, s, H-3, H-5), 7.35–7.30 (3H, m, H Ar), 7.47 (1H, td, *J* = 7.5, 1.6 Hz, H Ar). ¹⁹F NMR (471 MHz, CDCl₃) δ 99.0 (d, *J* = 1.0 Hz, CF₃). ¹³C NMR (151 MHz, CDCl₃) δ 17.0 (CH₃), 119.3 (2C, q, *J* = 275.8 Hz, CF₃), 119.6 (2C, q, *J* = 4.2 Hz, C-3, C-5), 126.2 (C Ar), 130.3 (C Ar), 130.7 (C Ar), 131.5 (C Ar), 134.1 (C Ar), 138.5 (C Ar), 141.3 (2C, q, *J* = 33.2 Hz, C-2, C-6), 177.9 (CO). IR (ATR) ν 3054, 1696 (C=O), 1620, 1508, 1391 (N–C), 1252, 1135 (CF₃). HRMS (ESI) *m/z* [M + H]⁺. Calculated for C₁₄H₁₀F₆NO: 322.0667. Found: 322.0679.

1-(2,5-Dimethylphenyl)-2,6-bis(trifluoromethyl)pyridin-4(1H)-one (3j). The reaction was carried out for 24 h. Yield 58 mg (48%), brown viscous liquid, crystallizes on standing, mp 105–107 °C. ¹H NMR (500 MHz, CDCl₃) δ 2.02 (3H, s, CH₃), 2.38 (3H, s, CH₃), 7.01 (2H, s, H-3, H-5), 7.16 (1H, s, H-2 Ar), 7.18 (1H, d, *J* = 7.7 Hz, H-5 Ar), 7.27 (1H, d, *J* = 7.7 Hz, H-4 Ar). ¹⁹F NMR (471 MHz, CDCl₃) δ 99.0 (s, CF₃). ¹³C NMR (126 MHz, CDCl₃) δ 16.6 (CH₃), 20.6 (CH₃), 119.3 (2C, q, *J* = 275.8 Hz, CF₃), 119.5 (2C, q, *J* = 4.8 Hz, C-3, C-5), 130.3 (C Ar), 130.6 (C Ar), 132.2 (C Ar), 133.9 (C Ar), 135.2 (C Ar), 136.2 (C Ar), 141.1 (2C, q, *J* = 33.4 Hz, C-2, C-6), 177.5 (CO). IR (ATR) ν 3091, 1655 (C=O), 1608, 1395 (N–C), 1328, 1251, 1125 (CF₃). HRMS (ESI) *m/z* [M + H]⁺. Calculated for C₁₅H₁₂F₆NO: 336.0823. Found: 336.0802.

1-(4-Nitrophenyl)-2,6-bis(trifluoromethyl)pyridin-4(1H)-one (3k). The reaction was carried out for 6 d. Pale yellow powder, a mixture of **3k** (10 mg, 8%) and 4-nitroaniline (32 mg). ¹H NMR (500 MHz, CDCl₃) δ 7.00 (2H, s, H-3, H-5), 7.64 (2H, d, *J* = 8.4 Hz, H Ar), 8.39 (2H, d, *J* = 8.9 Hz, H Ar). ¹⁹F NMR (471 MHz, CDCl₃) δ 100.9 (s, CF₃). HRMS (ESI) *m/z* [M + H]⁺. Calculated for C₁₃H₇F₆N₂O₃: 353.0361. Found: 353.0357.

3.3. Synthesis of Compound B'

o-Chloroaniline (106 mg, 0.83 mmol) was added to a solution of hexafluoroacetic acid (**1**) (100 mg, 0.36 mmol) in EtOH (1 mL). The reaction mixture was stirred at room temperature for a 15 h and acidified with aqueous HCl (3 mL, 1 M). The precipitate was filtered off and washed with water. The crude product was purified by column chromatography (CHCl₃).

(2*Z*,5*Z*)-2,6-Bis((2-chlorophenyl)amino)-1,1,1,7,7,7-hexafluorohepta-2,5-dien-4-one (**B'**). Dark-yellow solid, a mixture of **B'** (108 mg, 64%) and 2-chloroaniline (11 mg), mp 84–85 °C. ¹H

NMR (400 MHz, CDCl₃) δ 5.78 (2H, s, 3-CH, 5-CH), 7.18–7.29 (4H, m, H Ar), 7.33 (2H, d, J = 7.3 Hz, H Ar), 7.44 (2H, dd, J = 7.8, 1.5 Hz, H Ar), 11.49 (2H, s, NH). ¹⁹F NMR (376 MHz, CDCl₃) δ 97.8 (s, CF₃).

3.4. Synthesis of Compound 4

2-Aminopyridine (78 mg, 0.83 mmol) was added to a solution of hexafluoroacetic acid (1) (100 mg, 0.36 mmol) in EtOH (1 mL). The precipitate was filtered and washed with a small amount of EtOH.

2-Aminopyridin-1-ium 2-oxo-3-(2,2,2-trifluoroacetyl)-6-(trifluoromethyl)-2H-pyran-4-olate (4). Yield 127 mg (95%), white solid, mp 205–206 °C. ¹H NMR (400 MHz, DMSO-*d*₆) δ 6.15 (1H, s, H-5 pyrone), 6.86 (1H, td, J = 6.8, 1.0 Hz, H-5 pyridine), 6.97 (1H, dd, J = 9.6, 1.0 Hz, H-3 pyridine), 7.92 (4H, m, NH₂, H-4, H-6 pyridine), 13.27 (1H, s, NH). ¹⁹F NMR (376 MHz, DMSO-*d*₆) δ 89.8 (s, COCF₃), 91.1 (s, CF₃). ¹³C NMR (126 MHz, DMSO-*d*₆) δ 98.4 (C-3), 109.7 (q, J = 2.9 Hz, C-5), 112.1 (C Py), 113.4 (C Py), 116.6 (q, J = 292.1 Hz, CF₃), 118.9 (q, J = 272.8 Hz, CF₃), 136.0 (C Py), 144.1 (C Py), 146.8 (q, J = 37.1 Hz, C-6), 153.9 (C Py), 160.0 (C-2), 176.8 (C-4), 177.7 (q, J = 33.5 Hz, COCF₃). IR (ATR) ν 3366, 3310, 3191, 1712 (C=O), 1699 (C=O), 1535, 1372 (N–C), 1134 (CF₃). Anal. Calculated for C₁₃H₈F₆N₂O₄: C 42.18; H 2.18; N 7.57. Found: C 42.28; H 2.07; N 7.57.

3.5. Synthesis of Compounds 5

General Procedure

A mixture of 1-phenyl-2,6-bis(trifluoromethyl)pyridin-4(1H)-one (100 mg, 0.33 mmol) and a corresponding active methylene compound (0.4 mmol) in Ac₂O (1.5 mL) was heated at 140 °C for a given amount of time. The reaction mixture was then cooled and left overnight for crystallization of a product. The precipitate was filtered and washed with EtOH (1 mL). The product was dried at 120 °C for 4 h.

2-(1-Phenyl-2,6-bis(trifluoromethyl)pyridin-4(1H)-ylidene)malononitrile (5a). Synthesized from malononitrile (10 h). Yield 77 mg (65%). Dark-yellow crystals, mp 172–173 °C. ¹H NMR (500 MHz, DMSO-*d*₆) δ 7.26 (2H, s, H-3', H-5'), 7.59 (2H, t, J = 7.8 Hz, H Ph), 7.66 (1H, t, J = 7.6 Hz, H Ph), 7.74 (2H, d, J = 7.8 Hz, H Ph). ¹⁹F NMR (471 MHz, DMSO-*d*₆) δ 102.5 (s, CF₃). ¹³C NMR (126 MHz, DMSO-*d*₆) δ 57.1 (C(CN)₂), 112.7 (2C, q, J = 5.3 Hz, C-3', C-5'), 114.8 (2C, CN), 118.7 (2C, q, J = 275.9 Hz, CF₃), 128.7 (2C Ph), 130.1 (2C Ph), 131.7 (C Ph), 134.6 (C Ph), 138.2 (2C, q, J = 33.0 Hz, C-2', C-6'), 154.2 (C-4'). IR (ATR) ν 3058, 2922, 2852, 2215, 1643, 1518, 1302 (N–C), 1275, 1142 (CF₃). UV/vis (EtOH): λ_{\max} (ϵ_{\max}) = 382 (18222). HRMS (ESI) m/z [M + H]⁺. Calculated for C₁₆H₈F₆N₃: 356.0622. Found: 356.0624.

5-(1-Phenyl-2,6-bis(trifluoromethyl)pyridin-4(1H)-ylidene)pyrimidine-2,4,6(1H,3H,5H)-trione (5b). Synthesized from barbituric acid (4 h). Yield 81 mg (58%). Dark-yellow powder, mp 270–271 °C (decomp.). ¹H NMR (500 MHz, DMSO-*d*₆) δ 7.59 (2H, t, J = 7.7 Hz, H Ph), 7.66 (1H, t, J = 7.5 Hz, H Ph), 7.80 (2H, d, J = 7.9 Hz, H Ph), 9.77 (2H, s, H-3', H-5'), 10.78 (2H, s, NH). ¹⁹F NMR (471 MHz, DMSO-*d*₆) δ 103.2 (s, CF₃). ¹³C NMR (151 MHz, DMSO-*d*₆) δ 95.0 (C-5), 116.8 (2C, q, J = 5.7 Hz, C-3', C-5'), 119.8 (2C, q, J = 275.5 Hz, CF₃), 129.0 (2C Ph), 130.4 (2C Ph), 132.1 (C Ph), 135.6 (C Ph), 138.3 (2C, q, J = 32.3 Hz, C-2', C-5'), 150.1 (2-CO), 153.0 (C-4'), 165.6 (2C, 4-CO, 6-CO). IR (ATR) ν 3021, 1712, 1673, 1483, 1354 (N–C), 1145 (CF₃). UV/vis (EtOH): λ_{\max} (ϵ_{\max}) = 412 (91406), 234 (37760). HRMS (ESI) m/z [M + H]⁺. Calculated for C₁₇H₁₀F₆N₃O₃: 418.0626. Found: 418.0591.

2-(1-Phenyl-2,6-bis(trifluoromethyl)pyridin-4(1H)-ylidene)1,3-indandione (5c). Synthesized from 1,3-indandione (6 h). Yield 62 mg (43%). Dark-yellow crystals, mp 208–209 °C. ¹H NMR (500 MHz, DMSO-*d*₆) δ 7.60 (2H, t, J = 7.7 Hz, H Ph), 7.67 (1H, t, J = 7.4 Hz, H Ph), 7.70–7.78 (4H, m, H Ar), 7.80 (2H, d, J = 7.9 Hz, H Ph), 9.10 (2H, s, H-3', H-5'). ¹⁹F NMR (471 MHz, DMSO-*d*₆) δ 102.8 (s, CF₃). ¹³C NMR (126 MHz, DMSO-*d*₆) δ 107.2 (C-2), 113.4 (2C, q, J = 5.9 Hz, C-3', C-5'), 119.2 (2C, q, J = 275.2 Hz, CF₃), 121.3 (2C Ar), 128.5 (2C Ph), 130.0 (2C Ph), 131.6 (C Ph), 134.0 (2C Ar), 135.1 (C Ph), 138.9 (2C, q, J = 32.7 Hz, C-2', C-6'), 139.8 (2C Ar), 146.0 (C-4'), 191.0 (2C, CO). IR (ATR) ν 3101, 3065, 1693, 1648, 1518, 1319 (N–C), 1141 (CF₃). UV/vis (EtOH): λ_{\max} (ϵ_{\max}) = 437 (21948), 415 (15988), 246

(74128), 224 (151744). HRMS (ESI) m/z $[M + H]^+$. Calculated for $C_{22}H_{12}F_6NO_2$: 436.0772. Found: 436.0779.

3.6. Synthesis of Compounds 9

General Procedure

To a solution of trifluoroacetic acid (**2**) (100 mg, 0.56 mmol) in 1,4-dioxane (1 mL), a corresponding amine (1.17 mmol) was added with stirring. The reaction was monitored by TLC ($CHCl_3$:EtOH, 20:1). After completion, the reaction mixture was acidified with aqueous HCl (1 mL, 3 M). The precipitate was filtered and washed with water. The crude product was recrystallized from hexane.

6,6-Trifluoro-5-oxo-N-phenyl-3-(phenylamino)hex-3-enamide (9a). The reaction was carried out for 24 h. Yield 139 mg (72%), small yellow crystals, mp 135–137 °C. 1H NMR (500 MHz, $DMSO-d_6$) δ **Z-9a** (44%): 3.65 (2H, s, 2- CH_2), 5.79 (1H, s, 4-CH), 7.05 (2H, t, J = 7.3 Hz, H Ph), 7.30–7.34 (2H, m, H Ph), 7.40 (2H, d, J = 7.5 Hz, H Ph), 7.45 (4H, t, J = 7.0 Hz, H Ph), 10.08 (1H, s, NH amide), 12.56 (1H, s, NH enamine); **E-9a** (56%): 4.06 (2H, s, 2- CH_2), 5.59 (1H, s, 4-CH), 7.25–7.38 (6H, m, H Ph), 7.52 (2H, t, J = 6.8 Hz, H Ph), 7.61 (2H, d, J = 7.4 Hz, H Ph), 10.23 (1H, s, NH), 10.31 (1H, s, NH). ^{19}F NMR (376 MHz, $DMSO-d_6$) δ **Z-9a** (44%): 87.1 (s, CF_3); **E-9a** (56%): 86.6 (s, CF_3). ^{19}F NMR (376 MHz, $CDCl_3$) δ **Z-9a** (59%): 85.1 (s, CF_3); **E-9a** (41%): 84.8 (s, CF_3). ^{13}C NMR (101 MHz, $CDCl_3$) δ **Z-9a** (59%): 41.5 (CH_2), 91.3 (4-CH), 117.2 (q, J = 288.3 Hz, CF_3), 120.2 (2C Ph), 125.2 (C Ph), 125.9 (2C Ph), 128.3 (C Ph), 129.1 (2C Ph), 129.82 (2C Ph), 136.4 (C Ph), 136.9 (C Ph) 163.4 (1-CO), 164.0 (C-3), 177.8 (q, J = 33.7 Hz, 5-CO); **E-9a** (41%): 42.3 (CH_2), 88.7 (CH), 117.6 (q, J = 290.2 Hz, CF_3), 120.4 (2C Ph), 124.7 (2C Ph), 124.9 (C Ph), 127.8 (C Ph), 129.0 (2C Ph), 129.78 (2C Ph), 136.6 (C Ph), 137.5 (C Ph), 162.5 (1-CO), 166.3 (C-3), 178.5 (q, J = 32.1 Hz, 5-CO). IR (ATR) ν 3299, 3061, 3032, 1658 (C=O), 1578, 1242, 1172, 1116 (CF_3). Anal. Calculated for $C_{18}H_{15}F_3N_2O_2$: C 62.07; H 4.34; N 8.04. Found: C 61.81; H 4.12; N 7.94.

6,6-Trifluoro-N-(4-methoxyphenyl)-3-((4-methoxyphenyl)amino)-5-oxohex-3-enamide (9b). The reaction was carried out for 17 h. Yield 160 mg (69%), fine gray crystals, mp 163–165 °C. 1H NMR (400 MHz, $CDCl_3$) δ **Z-9b** (65%): 3.38 (2H, s, 2- CH_2), 3.79 (3H, s, OCH_3) 3.80 (3H, s, OCH_3), 5.68 (1H, s, 4-CH), 6.85 (2H, d, J = 8.7 Hz, H Ar), 6.91 (2H, d, J = 8.6 Hz, H Ar), 7.16 (1H, d, J = 8.6 Hz, H Ar), 7.29 (1H, d, J = 8.7 Hz, H Ar), 7.12 (1H, s, NH amide), 12.39 (1H, s, NH enamine); **E-9b** (35%): 3.79 (3H, s, OCH_3) 3.83 (3H, s, OCH_3), 4.00 (2H, s, 2- CH_2), 5.68 (1H, s, 4-CH), 6.84 (2H, d, J = 8.7 Hz, H Ar), 6.90 (2H, d, J = 8.6 Hz, H Ar), 7.11 (1H, d, J = 8.6 Hz, H Ar), 7.42 (1H, d, J = 8.7 Hz, H Ar), 8.74 (1H, s, NH amide), 9.63 (1H, s, NH enamine). ^{19}F NMR (376 MHz, $CDCl_3$) δ **Z-9b** (65%): 85.1 (s, CF_3); **E-9b** (35%): 84.9 (s, CF_3). ^{13}C NMR (126 MHz, $CDCl_3$) δ **Z-9b** (65%): 41.4 (CH_2), 55.47 (OCH_3), 55.52 (OCH_3), 90.9 (4-CH), 114.3 (2C Ar), 114.88 (2C Ar), 117.3 (q, J = 288.6 Hz, CF_3), 122.1 (2C Ar), 127.4 (2C Ar), 129.0 (C Ar), 129.9 (C Ar), 157.1 (C Ar), 159.4 (C Ar), 164.0, 164.2, 177.5 (q, J = 33.6 Hz, 5-CO); **E-9b** (35%): 42.0 (CH_2), 55.47 (OCH_3), 55.49 (OCH_3), 88.2 (4-CH), 114.1 (2C Ar), 114.91 (2C Ar), 117.7 (q, J = 290.2 Hz, CF_3), 122.0 (2C Ar), 126.4 (2C Ar), 129.3 (C Ar), 130.8 (C Ar), 156.7 (C Ar), 159.0 (C Ar), 163.2 (1-CO), 165.9 (C-3), 177.9 (q, J = 31.3 Hz, 5-CO). IR (ATR) ν 3282, 2999, 2842, 1651 (C=O), 1530, 1237, 1169, 1116 (CF_3). Anal. Calculated for $C_{20}H_{19}F_3N_2O_4 \cdot 0.25H_2O$: C 58.18; H 4.76; N 6.79. Found: C 58.25; H 4.48; N 6.54.

N-(4-Bromophenyl)-3-((4-bromophenyl)amino)-6,6,6-trifluoro-5-oxohex-3-enamide (9c). The reaction was carried out for 15 h. Yield 118 mg (41%), fine yellow crystals, mp 209–210 °C (decomp.). 1H NMR (500 MHz, $CDCl_3$) δ **Z-9c** (58%): 3.41 (2H, s, 2- CH_2), 5.70 (1H, s, 4-CH), 7.14 (2H, d, J = 8.4 Hz, H Ar), 7.31 (2H, d, J = 8.6 Hz, H Ar), 7.43 (1H, s, NH amide), 7.46 (2H, d, J = 8.6 Hz, H Ar), 7.54 (2H, d, J = 8.4 Hz, H Ar), 12.42 (1H, s, NH enamine); **E-9c** (42%): 3.98 (1H, s, 2- CH_2), 5.78 (1H, s, 4-CH), 7.09 (2H, d, J = 8.5 Hz, H Ar), 7.41–7.46 (4H, m, H Ar), 7.55 (2H, d, J = 8.5 Hz, H Ar), 8.32 (1H, s, NH amide), 9.62 (1H, s, NH enamine). ^{19}F NMR (471 MHz, $CDCl_3$) δ **Z-9c** (58%): 85.0 (s, CF_3); **E-9c** (42%): 84.8 (s, CF_3). IR (ATR) ν 3262, 3018, 3046, 1664 (C=O), 1589, 1533, 1246, 1111 (CF_3). Anal. Calculated for $C_{18}H_{13}Br_2F_3N_2O_2 \cdot 0.33H_2O$: C 42.22; H 2.69; N 5.47. Found: C 42.44; H 2.58; N 5.19.

N-Benzyl-3-(benzylamino)-6,6,6-trifluoro-5-oxohex-3-enamide (**9d**). The reaction was carried out for 17 h. Yield 51 mg (24%), colorless powder, mp 124–125 °C. ¹H NMR (500 MHz, DMSO-*d*₆) δ *Z*-**9d** (68%): 3.55 (2H, s, 2-CH₂), 4.30 (2H, d, *J* = 5.8 Hz, NCH₂), 4.72 (2H, d, *J* = 6.1 Hz, NCH₂), 5.50 (1H, s, 4-CH), 7.09–7.49 (10H, m, H Ph), 8.76 (1H, t, *J* = 5.8 Hz, NH amide), 11.29 (1H, t, *J* = 6.1 Hz, NH enamine); *E*-**9d** (32%): 3.84 (2H, s, 2-CH₂), 4.31 (2H, d, *J* = 6.0 Hz, NCH₂), 4.46 (2H, d, *J* = 5.6 Hz, NCH₂), 5.27 (1H, s, 4-CH), 7.09–7.49 (10H, m, H Ph), 8.45 (1H, t, *J* = 5.9 Hz, NH amide), 9.08 (1H, t, *J* = 5.8 Hz, NH enamine). ¹H NMR (500 MHz, CDCl₃) δ *Z*-**9d** (58%): 3.31 (2H, s, 2-CH₂), 4.39 (2H, d, *J* = 5.7 Hz, NCH₂), 4.61 (2H, d, *J* = 6.1 Hz, NCH₂), 5.44 (1H, s, 4-CH), 6.04 (1H, unres. t, NH) 7.20–7.40 (10H, m, H Ph), 11.32 (1H, unres. t, NH); *E*-**9d** (42%): 3.79 (2H, s, 2-CH₂), 4.32 (2H, d, *J* = 5.9 Hz, NCH₂), 4.33 (2H, d, *J* = 4.9 Hz, NCH₂), 5.41 (1H, s, 4-CH), 7.15 (2H, d, *J* = 7.0 Hz), 7.20–7.40 (8H, m), 7.90 (2H, unres. t, NH). ¹⁹F NMR (471 MHz, CDCl₃) δ *Z*-**9d** (58%): 85.1 (s, CF₃); *E*-**9d** (42%): 84.9 (s, CF₃). ¹³C NMR (126 MHz, CDCl₃) δ *Z*-**9d** (58%): 41.1 (2-CH₂), 44.0 (NCH₂), 48.0 (NCH₂), 90.1 (4-CH), 117.3 (q, *J* = 288.4 Hz), 127.1 (2C Ph), 127.8 (2C Ph), 127.9 (C Ph), 128.2 (C Ph), 128.9 (2C Ph), 129.2 (2C Ph), 135.7 (C Ph), 137.3 (C Ph), 164.9 (1-CO), 165.3 (C-3), 177.0 (q, *J* = 33.4 Hz, 5-CO). *E*-**9d** (42%): 40.5 (2-CH₂), 43.5 (NCH₂), 48.3 (NCH₂), 86.3 (4-CH), 117.7 (q, *J* = 290.5 Hz, CF₃), 127.2 (2C Ph), 127.4 (C Ph), 127.7 (2C Ph), 128.3 (C Ph), 128.6 (2C Ph), 129.1 (2C Ph), 134.8 (C Ph), 137.6 (C Ph), 163.5 (1-CO), 168.0 (C-3), 176.9 (q, *J* = 32.1 Hz, 5-CO). IR (ATR) ν 3308, 3062, 3033, 1641 (C=O), 1549, 1264, 1165, 1124 (CF₃). Anal. Calculated for C₂₀H₁₉F₃N₂O₂·0.33H₂O: C 62.82; H 5.18; N 7.33. Found: C 63.01; H 5.10; N 7.09.

N-Butyl-3-(butylamino)-6,6,6-trifluoro-5-oxohex-3-enamide (**9e**). The reaction was carried out for 72 h at 60 °C. Yield 12 mg (7%), large gray crystals, mp 79–80 °C. ¹H NMR (500 MHz, CDCl₃) δ *Z*-**9e** (65%): 0.93 (3H, t, *J* = 7.2 Hz, CH₃), 0.95 (3H, t, *J* = 7.2 Hz, CH₃), 1.32 (quint, 2H, *J* = 7.2 Hz, NCH₂CH₂), 1.43 (2H, sex, *J* = 7.2 Hz, CH₂CH₃), 1.49 (2H, sex, *J* = 7.2 Hz, CH₂CH₃), 1.63 (2H, quint, *J* = 7.2 Hz, NCH₂CH₂), 3.27 (2H, s, 2-CH₂), 3.28 (2H, q, *J* = 6.3 Hz, NCH₂), 3.42 (2H, q, *J* = 6.6 Hz, NCH₂), 5.36 (1H, s, 4-CH), 5.65 (1H, s, NH amide), 11.08 (1H, s, NH enamine); *E*-**9e** (35%): 0.90 (3H, t, *J* = 7.2 Hz, CH₃), 0.96 (3H, t, *J* = 7.2 Hz, CH₃), 1.34 (quint, 2H, *J* = 7.2 Hz, NCH₂CH₂), 1.39–1.53 (4H, masked, CH₂CH₃), 1.65 (2H, quint, *J* = 7.2 Hz, NCH₂CH₂), 3.15–3.24 (4H, m, NCH₂), 3.75 (2H, s, 2-CH₂), 5.32 (1H, s, 4-CH), 7.10 (1H, s, NH amide), 7.36 (1H, s, NH enamine). ¹⁹F NMR (471 MHz, CDCl₃) δ *Z*-**9e** (65%): 85.04 (s, CF₃); *E*-**9e** (35%): 84.90 (s, CF₃). IR (ATR) ν 3289, 2958, 2872, 1591 (C=O), 1548, 1306, 1184, 1114 (CF₃). HRMS (ESI) *m/z* [M + H]⁺. Calculated for C₁₄H₂₅F₃N₂O₂: 309.1790. Found: 309.1799.

3.7. Synthesis of Compound 10

1,3,4,5-Tetrahydro-4-(3,3,3-trifluoro-2-oxopropylidene)-2H-1,5-benzodiazepin-2-one (**10**). Benzene-1,2-diamine (63 mg, 0.58 mmol) was added to a solution of trifluoroacetic acid (**2**) (100 mg, 0.56 mmol) in 1,4-dioxane (1 mL) with stirring. The reaction was carried out for 24 h at room temperature. Then, the reaction mixture was acidified with aqueous HCl (1 mL, 3M). The precipitate was filtered and washed with water. The crude product was recrystallized from hexane. Yield 51 mg (33%), fine white powder, mp 244–245 °C (decomp.; lit. mp 243–245 °C [43]). ¹H NMR (500 MHz, CDCl₃) δ 3.31 (2H, s, CH₂), 5.68 (1H, s, CH), 7.12 (1H, dd, *J* = 7.6, 1.6 Hz, H Ar), 7.24–7.34 (3H, m, H Ar), 8.17 (1H, s, 1-NH), 12.57 (1H, s, 5-NH). ¹⁹F NMR (471 MHz, CDCl₃) δ 84.8 (s, CF₃). HRMS (ESI) *m/z* [M + H]⁺. Calculated for C₁₄H₂₅F₃N₂O₂: 271.0694. Found: 271.0673. The analytical data are in consistence with the literature [43].

3.8. Synthesis of Compounds 13 and 14

N'-Phenyl-2-(1-phenyl-5-(trifluoromethyl)-1H-pyrazol-3-yl)acetohydrazide (**13**) and *N'*-phenyl-2-(1-phenyl-3-(trifluoromethyl)-1H-pyrazol-5-yl)acetohydrazide (**14**). Phenylhydrazine (126 mg, 1.17 mmol) was added to a solution of trifluoroacetic acid (**2**) (100 mg, 0.56 mmol) in EtOH (1 mL) with stirring. The reaction was carried out for 24 h at room temperature. Then, the reaction mixture was acidified with aqueous HCl (1 mL, 3M). The precipitate

was filtered and washed with water. The crude product was recrystallized from hexane. Yield 122 mg (61%), yellow powder, mp 136–138 °C. The mixture of isomers **13** and **14** (82:18) did not separate by column chromatography. IR (ATR) ν 3281, 1657 (C=O), 1603, 1504, 1356, 1083 (CF₃). HRMS (ESI) m/z [M + H]⁺. Calculated for C₁₈H₁₆F₃N₄O: 361.1276. Found: 361.1276.

13: ¹H NMR (500 MHz, DMSO-*d*₆) δ *syn*-isomer (88%): 3.65 (2H, s, CH₂), 6.67–6.71 (1H, m, H Ph), 6.73 (2H, d, *J* = 7.8 Hz, H Ph), 7.03 (1H, s, H pyraz.), 7.11 (2H, t, *J* = 7.8 Hz, H Ph), 7.49–7.52 (2H, m, H Ph), 7.56–7.62 (3H, m, H Ph), 7.60–8.03 (br. s, 1H, PhNH), 9.91 (1H, s, CONH); *anti*-isomer (12%): 3.71 (2H, s, CH₂), 6.67–6.71 (2H, m, H Ph), 6.76 (1H, t, *J* = 7.3 Hz, H Ph), 6.95 (1H, s, H pyraz.), 7.18 (2H, t, *J* = 7.8 Hz, H Ph), 7.40–7.43 (2H, m, H Ph), 7.52–7.56 (3H, m, H Ph), 8.06 (1H, s, PhNH), 9.22 (1H, s, CONH). ¹⁹F NMR (471 MHz, DMSO-*d*₆) δ *anti*-isomer (12%): 106.18 (s, CF₃); *syn*-isomer (88%): 106.13 (s, CF₃). ¹³C NMR (126 MHz, CDCl₃) δ *syn*-isomer: 34.3 (CH₂), 109.0 (C-4 pyraz.), 113.5 (2C Ph), 119.4 (q, *J* = 269.4 Hz, CF₃), 121.3 (C Ph), 125.6 (2C Ph), 129.16 (2C Ph), 129.20 (2C Ph), 129.6 (C Ph), 133.9 (q, *J* = 39.7 Hz, C-5 pyraz.), 138.7 (C Ph), 146.2 (C Ph), 147.6 (C-3 pyraz.), 168.9 (CO); *anti*-isomer: most of the signals are masked due to low concentration.

14: ¹H NMR (500 MHz, DMSO-*d*₆) δ *syn*-isomer (71%): 3.78 (2H, s, CH₂), 6.55 (2H, d, *J* = 7.6 Hz, H Ph), 6.69 (1H, t, *J* = 7.4 Hz, H Ph), 6.87 (1H, s, H pyraz.), 7.10 (2H, t, *J* = 7.5 Hz, H Ph), 7.56–7.62 (5H, m, H Ph), 7.73 (1H, s, PhNH), 9.83 (1H, s, CONH); *anti*-isomer (29%): 3.79 (2H, s, CH₂), 6.56 (2H, d, *J* = 7.3 Hz, H Ph), 6.76 (1H, t, *J* = 7.3 Hz, H Ph), 6.83 (1H, s, H pyraz.), 7.14 (2H, t, *J* = 7.5 Hz, H Ph), 7.43–7.47 (2H, m, H Ph), 7.51–7.55 (3H, m, H Ph), 7.95 (1H, s, PhNH), 9.25 (1H, s, CONH). ¹⁹F NMR (471 MHz, DMSO-*d*₆) δ *anti*-isomer (29%): 101.91 (s, CF₃), *syn*-isomer (71%): 101.83 (s, CF₃). The analytical data are in consistence with the literature [35].

Supplementary Materials: The following supporting information can be downloaded at: <https://www.mdpi.com/article/10.3390/molecules27207098/s1>. Figure S1: UV/Vis spectra of compounds **5**; Table S1: Characteristic chemical shifts in ¹H, ¹³C, and ¹⁹F NMR spectra of compounds **3**; Table S2: Characteristic chemical shifts in ¹H, ¹³C, and ¹⁹F NMR spectra of compounds **5**; Table S3: Characteristic chemical shifts in ¹H, ¹³C, and ¹⁹F NMR spectra of *E*- and *Z*-isomers of enaminones **9**; full ¹H, ¹⁹F, and ¹³C NMR spectra of all synthesized compounds.

Author Contributions: Conceptualization and methodology were provided by V.Y.S., S.A.U. and D.L.O. conceived and designed the experiments. The experimental work was conducted by V.V.F. and S.A.U., S.A.U. and V.V.F. analyzed the results. S.A.U. studied and systemized the NMR data. S.A.U. and V.Y.S. wrote the paper. Project administration and funding acquisition were carried out by V.Y.S. and D.L.O. All authors have read and agreed to the published version of the manuscript.

Funding: This research was funded by the Russian Science Foundation, grant number 18-13-00186 (<https://rscf.ru/project/18-13-00186/> accessed on 18 October 2022).

Institutional Review Board Statement: Not applicable.

Informed Consent Statement: Not applicable.

Data Availability Statement: Data are contained within the article and Supplementary Materials.

Acknowledgments: Analytical studies were carried out using equipment at the Center for Joint Use ‘Spectroscopy and Analysis of Organic Compounds’ at the Postovsky Institute of Organic Synthesis of the Russian Academy of Sciences (Ural Branch) and the Laboratory of Complex Investigations and Expert Evaluation of Organic Materials of the Center for Joint Use at the Ural Federal University.

Conflicts of Interest: The authors declare no conflict of interest.

Sample Availability: Samples of the compounds are not available from the authors.

References

1. McClacken, G.P.; Fairlamb, I.J.S. 2-Pyrone natural products and mimetics: Isolation, characterisation and biological activity. *Nat. Prod. Rep.* **2005**, *22*, 369–385. [CrossRef] [PubMed]
2. Goel, A.; Ram, V.J. Natural and synthetic 2H-pyran-2-ones and their versatility in organic synthesis. *Tetrahedron* **2009**, *65*, 7865–7913. [CrossRef]
3. Pratap, R.; Ram, V.J. 2H-Pyran-2-ones and their annelated analogs as multifaceted building blocks for the fabrication of diverse heterocycles. *Tetrahedron* **2017**, *73*, 2529–2590. [CrossRef]
4. Dobler, D.; Leitner, M.; Moor, N.; Reiser, O. 2-Pyrone—A privileged heterocycle and widespread motif in nature. *Eur. J. Org. Chem.* **2021**, *2021*, 6180–6205. [CrossRef]
5. Hickey, A.; Pardo, L.M.; Reen, F.J.; McClacken, G.P. Pyrones identified as LuxR signal molecules in photorhabdus and their synthetic analogues can alter multicellular phenotypic behavior of *Bacillus atropheaus*. *ACS Omega* **2021**, *6*, 33141–33148. [CrossRef]
6. Yadav, J.S.; Ganganna, B.; Dutta, P.; Singarapu, K.K. Synthesis and determination of absolute configuration of α -pyrones isolated from *Penicillium corylophilum*. *J. Org. Chem.* **2014**, *79*, 10762–10771. [CrossRef] [PubMed]
7. Lee, I.K.; Yun, B.S. Styrylpyrone-class compounds from medicinal fungi *Phellinus* and *Inonotus* spp., and their medicinal importance. *J. Antibiot.* **2011**, *64*, 349–359. [CrossRef] [PubMed]
8. Bhat, Z.S.; Rather, M.A.; Maqbool, M.; Lah, H.U.; Yousuf, S.K.; Ahmad, Z. α -pyrones: Small molecules with versatile structural diversity reflected in multiple pharmacological activities—an update. *Biomed. Pharmacother.* **2017**, *91*, 265–277. [CrossRef]
9. Aggarwal, R.; Walia, S.; Rani, C. Dehydroacetic acid and its derivatives as starting synthons for synthesis of heterocyclic compounds. *Heterocycles* **2017**, *94*, 1197–1244. [CrossRef]
10. Obydenov, D.L.; El-Tantawy, A.I.; Sosnovskikh, V.Y. Triacetic acid lactone as a bioprivileged molecule in organic synthesis. *Mendeleev Commun.* **2019**, *29*, 1–10. [CrossRef]
11. Prakash, O.; Kumar, A.; Singh, S.P. Synthesis of heterocyclic compounds from the reactions of dehydroacetic acid (DHA) and its derivatives. *Heterocycles* **2004**, *63*, 1193–1220. [CrossRef]
12. Moreno-Mañas, M.; Pleixats, R. Dehydroacetic acid, triacetic acid lactone, and related pyrones. *Adv. Heterocycl. Chem.* **1992**, *53*, 1–84. [CrossRef]
13. Politanskaya, L.V.; Selivanova, G.A.; Panteleeva, E.V.; Tretyakov, E.V.; Platonov, V.E.; Nikul'shin, P.V.; Vinogradov, A.S.; Zonov, Y.V.; Karpov, V.M.; Mezhenkova, T.V.; et al. Organofluorine chemistry: Promising growth areas and challenges. *Russ. Chem. Rev.* **2019**, *88*, 425–569. [CrossRef]
14. Han, J.; Remete, A.M.; Dobson, L.S.; Kiss, L.; Izawa, K.; Moriwaki, H.; Soloshonok, V.A.; O'Hagan, D. Next generation organofluorine containing blockbuster drugs. *J. Fluor. Chem.* **2020**, *239*, 109639. [CrossRef]
15. Isanbor, C.; O'Hagan, D. Fluorine in medicinal chemistry: A review of anti-cancer agents. *J. Fluor. Chem.* **2006**, *127*, 303–319. [CrossRef]
16. O'Hagan, D. Fluorine in health care: Organofluorine containing blockbuster drugs. *J. Fluor. Chem.* **2010**, *131*, 1071–1081. [CrossRef]
17. Purser, S.; Moore, P.R.; Swallow, S.; Gouverneur, V. Fluorine in medicinal chemistry. *Chem. Soc. Rev.* **2008**, *37*, 320–330. [CrossRef] [PubMed]
18. Wang, J.; Sánchez-Roselló, M.; Aceña, J.L.; del Pozo, C.; Sorochinsky, A.E.; Fustero, S.; Soloshonok, V.A.; Liu, H. Fluorine in pharmaceutical industry: Fluorine-containing drugs introduced to the market in the last decade (2001–2011). *Chem. Rev.* **2014**, *114*, 2432–2506. [CrossRef] [PubMed]
19. Fujiwara, T.; O'Hagan, D. Successful fluorine-containing herbicide agrochemicals. *J. Fluor. Chem.* **2014**, *167*, 16–29. [CrossRef]
20. Jeschke, P. The unique role of fluorine in the design of active ingredients for modern crop protection. *ChemBioChem* **2004**, *5*, 570–589. [CrossRef] [PubMed]
21. Berger, R.; Resnati, G.; Metrangolo, P.; Weber, E.; Hulliger, J. Organic fluorine compounds: A great opportunity for enhanced materials properties. *Chem. Soc. Rev.* **2011**, *40*, 3496–3508. [CrossRef] [PubMed]
22. Granqvist, L.; Virta, P. Characterization of G-quadruplex/hairpin transitions of RNAs by ^{19}F NMR spectroscopy. *Chem. Eur. J.* **2016**, *22*, 15360–15372. [CrossRef] [PubMed]
23. Marsh, E.N.G.; Suzuki, Y. Using ^{19}F NMR to probe biological interactions of proteins and peptides. *ACS Chem. Biol.* **2014**, *9*, 1242–1250. [CrossRef] [PubMed]
24. Resnick, P.R. Practical uses of fluorinated heterocycles. In *Fluorinated Heterocyclic Compounds*; John Wiley & Sons, Inc.: Hoboken, NJ, USA, 2009; pp. 493–506.
25. German, L.S.; Sterlin, S.R.; Cherstkov, V.F. Hexafluorodehydroacetic acid. *Bull. Acad. Sci. USSR Div. Chem. Sci.* **1982**, *31*, 1476–1477. [CrossRef]
26. Li, C.-S.; Lau, C.K.; Therien, M.; Prasit, P. Pyrones as Inhibitors of Cyclooxygenase-2. U.S. Patent 0058690, 16 May 2002.
27. Hanselmann, P.; Wenger, W. Method for the Production of 6,6,6-Trihalo-3,5-dioxohexanoic Acid Esters. WO Patent 040087, 6 May 2005.
28. Garratt, S. The Mechanism of the reaction between dehydroacetic acid and alkylamines. *J. Org. Chem.* **1963**, *28*, 1886–1888. [CrossRef]
29. Cook, D. The preparation, properties, and structure of 2,6-bis-(alkylamino)-2,5-heptadien-4-ones. *Can. J. Chem.* **1963**, *41*, 1435–1440. [CrossRef]

30. Pierce, J.B.; Ariyan, Z.S.; Ovenden, G.S. Preparation and antiinflammatory activity of 2- and 4-pyridones. *J. Med. Chem.* **1982**, *25*, 131–136. [CrossRef]
31. Schmidt, R.; Stolte, M.; Grüne, M.; Würthner, F. Hydrogen-bond-directed formation of supramolecular polymers incorporating head-to-tail oriented dipolar merocyanine dyes. *Macromolecules* **2011**, *44*, 3766–3776. [CrossRef]
32. Würthner, F.; Schmidt, J.; Stolte, M.; Wortmann, R. Hydrogen-bond-directed head-to-tail orientation of dipolar merocyanine dyes: A strategy for the design of electrooptical materials. *Angew. Chem. Int. Ed.* **2006**, *45*, 3842–3846. [CrossRef] [PubMed]
33. Eiden, F. Untersuchungen an γ -Pyronen. 4. Mitteilung: Die Kondensation von γ -Pyronen mit cyclischen Malonsäureamiden. *Arch. Pharm.* **1960**, *293*, 404–414. [CrossRef] [PubMed]
34. Obydenov, D.L.; El-Tantawy, A.I.; Sosnovskikh, V.Y. Bio-based triacetic acid lactone in the synthesis of azaheterocycles via a ring-opening transformation. *New J. Chem.* **2018**, *42*, 8943–8952. [CrossRef]
35. Usachev, B.I.; Obydenov, D.L.; Rösenthaller, G.-V.; Sosnovskikh, V.Y. 2-Cyano-6-(trifluoromethyl)-4H-pyran-4-one: A novel versatile CF₃-containing building block. *J. Fluor. Chem.* **2012**, *137*, 22–26. [CrossRef]
36. Zheglova, D.K.; Genov, D.G.; Gribanov, A.V.; Kol'tsov, A.I.; Smirnov, S.N. NMR spectroscopic study of the (Z)/(E)-isomerism of 1-aryl-3-arylamino-2-propen-1-ones in solution and in the crystalline state. *Monatsh. Chem.* **1994**, *125*, 1443–1446. [CrossRef]
37. Gerus, I.I.; Balabon, O.A.; Pazenok, S.V.; Lui, N.; Kondratov, I.S.; Tarasenko, K.V.; Shaitanova, E.N.; Ivasyshyn, V.E.; Kukhar, V.P. Synthesis and properties of polyfunctional cyclic β -alkoxy- α,β -unsaturated ketones based on 4-methylene-1,3-dioxolanes. *Eur. J. Org. Chem.* **2018**, *2018*, 3853–3861. [CrossRef]
38. Wójcik, J.; Domalewski, W.; Kamieńska-Trela, K.; Stefaniak, L.; Vdovienko, S.I.; Gerus, I.I.; Gorbunova, M.G. Conformational behaviour of some trifluoroenaminones by multinuclear magnetic resonance. *Magn. Reson. Chem.* **1993**, *31*, 808–814. [CrossRef]
39. Kiang, A.K.; Tan, S.F.; Wong, W.S. Reactions of acetonedicarboxylic anhydride (tetrahydropyrantrione) and its mono- and di-acetyl derivatives with amines. *J. Chem. Soc. C* **1971**, 2721–2726. [CrossRef]
40. Usachev, S.A.; Usachev, B.I.; Sosnovskikh, V.Y. Synthesis of 6-hydroxy-5,6-dihydro-2-pyrones and -pyridones by reaction of 4-aryl-6-trifluoromethyl-2-pyrones with water, hydrazine, and hydroxylamine. *Chem. Heterocycl. Compd.* **2017**, *53*, 1294–1301. [CrossRef]
41. Gerus, I.I.; Tolmachova, N.A.; Vdovenko, S.I.; Fröhlich, R.; Haufe, G. A convenient synthesis and chemical properties of 3-acylamino-6-poly-fluoroalkyl-2H-pyran-2-ones. *Synthesis* **2005**, *2005*, 1269–1278. [CrossRef]
42. Ye, W.-P.; Mu, H.-L.; Shi, X.-C.; Cheng, Y.-X.; Li, Y.-S. Synthesis and characterization of the titanium complexes bearing two regioisomeric trifluoromethyl-containing enaminketonato ligands and their behavior in ethylene polymerization. *Dalt. Trans.* **2009**, *2009*, 9452–9465. [CrossRef] [PubMed]
43. Desens, W.; Winterberg, M.; Michalik, D.; Langer, P. Synthesis and solution structure of 1H-benzo-1,5-diazepine derivatives with a perfluoroalkyl side chain. *Helv. Chim. Acta* **2016**, *99*, 361–372. [CrossRef]

Article

Domino Aza-Michael- S_NAr -Heteroaromatization Route to C5-Substituted 1-Alkyl-1*H*-Indole-3-Carboxylic Esters

Ebenezer Ametsetor, Spencer Farthing and Richard A. Bunce *

Department of Chemistry, Oklahoma State University, Stillwater, OK 74078-3071, USA

* Correspondence: rab@okstate.edu; Tel.: +1-405-744-5952

Abstract: A new synthesis of C5-substituted 1-alkyl-1*H*-indole-3-carboxylic esters is reported. A series of methyl 2-arylacrylate aza-Michael acceptors were prepared with aromatic substitution to activate them towards S_NAr reaction. Subsequent reaction with a series of primary amines generated the title compounds. Initially, the sequence was expected to produce indoline products, but oxidative heteroaromatization intervened to generate the indoles. The reaction proceeded under anhydrous conditions in DMF at 23–90 °C using equimolar quantities of the acrylate and the amine with 2 equiv. of K_2CO_3 to give 61–92% of the indole products. The reaction involves an aza-Michael addition, followed by S_NAr ring closure and heteroaromatization. Since the reactions were run under nitrogen, the final oxidation to the indole likely results from reaction with dissolved oxygen in the DMF. Substrates incorporating a 2-arylacrylonitrile proved too reactive to prepare using our protocol. The synthesis of the reaction substrates, their relative reactivities, and mechanistic details of the conversion are discussed.

Keywords: domino reaction; 1*H*-indole synthesis; aza-Michael reaction; S_NAr reaction; heteroaromatization

Citation: Ametsetor, E.; Farthing, S.; Bunce, R.A. Domino Aza-Michael- S_NAr -Heteroaromatization Route to C5-Substituted 1-Alkyl-1*H*-Indole-3-Carboxylic Esters. *Molecules* **2022**, *27*, 6998. <https://doi.org/10.3390/molecules27206998>

Academic Editors: Alexey M. Starosotnikov, Maxim A. Bastrakov and Igor L. Dalinger

Received: 24 September 2022

Accepted: 14 October 2022

Published: 18 October 2022

Publisher's Note: MDPI stays neutral with regard to jurisdictional claims in published maps and institutional affiliations.



Copyright: © 2022 by the authors. Licensee MDPI, Basel, Switzerland. This article is an open access article distributed under the terms and conditions of the Creative Commons Attribution (CC BY) license (<https://creativecommons.org/licenses/by/4.0/>).

1. Introduction

Indoles are among the most widely distributed heterocycles in nature and many have critical functions in living organisms. Due to their potent biological profiles, numerous natural and synthetic indoles have been prepared and studied by chemists to mitigate the effects of various diseases [1,2]. To date, numerous synthetic approaches have been developed and this family of compounds remains a highly active area of research in organic and medicinal chemistry.

The major “named” synthetic routes to indoles have been nicely summarized in the review cited above [1]. Other less general methods include: (1) intramolecular cyclization of a side chain amine on a neighboring benzyne triple bond [3], (2) cyclization of a benzylic anion to an ortho-substituted isocyanide [4], (3) intramolecular addition of a nitrene to a styryl double bond [5], and (4) palladium catalyzed ring closure of 2-iodo-1-allylaminobenzenes [6] among other variations [7]. Beyond direct syntheses, indoles can also be accessed from indolines through dehydrogenation [8,9] or elimination of functionality on the five-membered ring [10]. Finally, once prepared, methods for the introduction of alkyl substitution to the indole nitrogen have been reported by a number of routes [11–15].

The current study sought to develop a new synthetic approach to these systems through a domino aza-Michael- S_NAr -heteroaromatization sequence from acrylate esters substituted at C2 by an aromatic system substituted to promote nucleophilic aromatic substitution by an addition-elimination (S_NAr) mechanism. Previously, indole derivatives have been prepared by a domino-reduction-reductive amination reaction from 2-nitrophenylacetone [16] and a domino reduction-aza-Michael-elimination process from ethyl 2-(2-nitrophenyl)-b-ketoesters [17]. These procedures differ from the current route in aromatizing via elimination of water from the initial adduct. The present study involves (1) aza-Michael addition to a polarized 2-arylacrylate double bond, (2) ring formation by

S_NAr of the added nitrogen to the electron-deficient aromatic ring, and (3) aromatization by reaction with molecular oxygen which is either dissolved in the reaction solvent or admitted to the flask during removal of TLC samples. The conversion is clean and provides the indoles in high yield.

Indoles are prevalent in many drug compounds showing a wide range of activities. Filtering for compounds that possess similar structural features to the compounds prepared here—an alkylated nitrogen at position 1 and an acyl group at C3—revealed a number of structures that are pictured in Figure 1. Pravadoline (1) has potent analgesic properties via binding to the cannabinoid CB_1/CB_2 receptors [18] and is closely related to neuroprotective compounds that inhibit inflammation caused by β -amyloid proteins involved in Alzheimer's disease [19]. The iodinated naphthoylindole 2 is a strong analgesic as it also binds to the CB_1/CB_2 receptors [20]. Arbidol (Umifenovir, 3) is a potent antiviral [21], used primarily in Russia and China, against influenza A [22]. Finally, 3-indolyl-5-amino-2-phenyl-1,2,3-triazine 4 has shown highly promising antimicrobial activity towards both Gram positive and Gram negative bacteria [23].

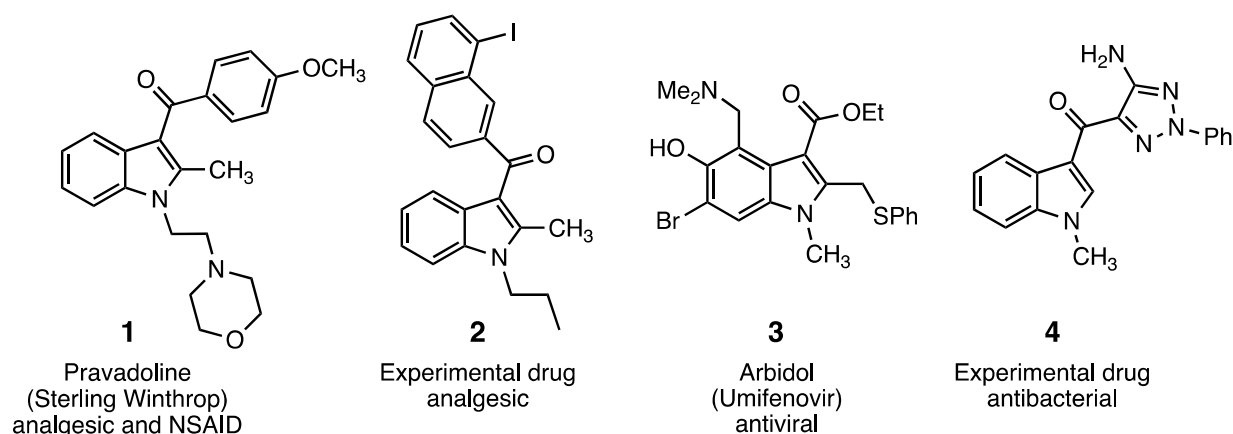
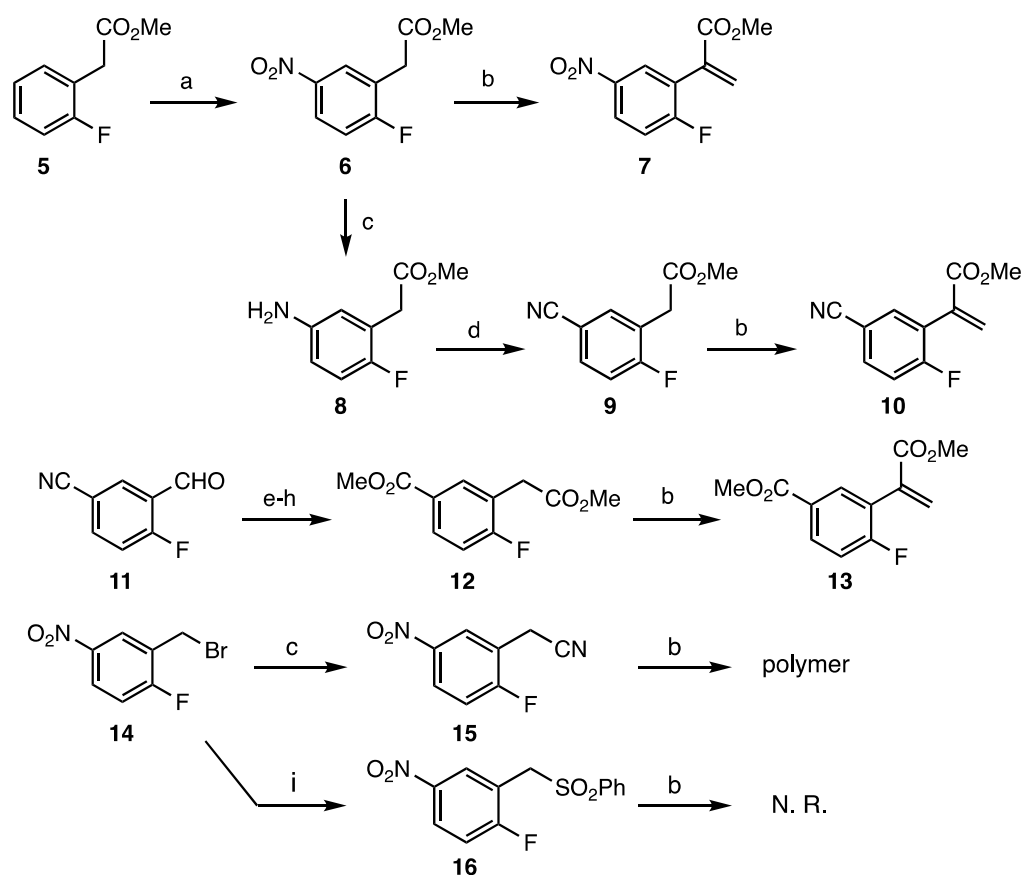


Figure 1. Indole-containing drug compounds incorporating the *N*-alkyl and 3-acyl groups.

2. Results and Discussion

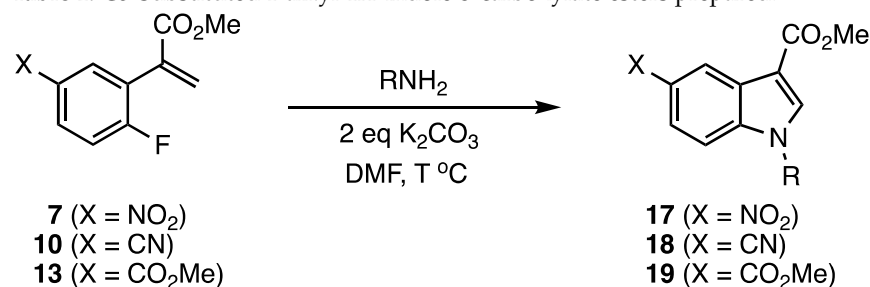
The 2-arylacrylate indole precursors 7, 10 and 13 were prepared using standard techniques (Scheme 1). Methyl 2-fluorophenylacetate (5) was converted to methyl 2-(2-fluoro-5-nitrophenyl)acrylate (6) by nitration using $NaNO_3$ in H_2SO_4 at 0–23 °C for 2 h [24]. Installation of the acrylate double bond to give 7 was accomplished by aldol condensation with formaldehyde (37% aq. formaldehyde (formalin), K_2CO_3 , DMF, 23 °C) [25]. The 2-(5-cyano-2-fluorophenyl)acrylate substrate (10) was prepared from the aforementioned intermediate nitration product 6. Reduction of the nitro group to give aniline 8 (Fe/NH_4Cl , aq. EtOH, 70 °C) [26] was followed by diazotization (HONO) and Sandmeyer replacement of nitrogen by cyanide ($CuCN$) [27,28] to afford 9. Final conversion to acrylate 10 was accomplished as above. Finally, the diester substituted substrate 13 was prepared from 5-cyano-2-fluorobenzaldehyde (11). Reduction of the aldehyde to the benzyl alcohol ($NaBH_4$, EtOH, 23 °C), conversion to the bromide (PBr_3 , Et_2O , 0–23 °C) [29], S_N2 displacement of bromide by cyanide (KCN , aq. EtOH) and methanolysis of the dicyano compound (25% H_2SO_4 in MeOH, 90 °C) generated diester 12. Aldol condensation with formaldehyde then led to 13. Yields were reasonable for all steps and each synthesis was performed on a multigram scale. It should be noted that attempts to install the aza-Michael accepting double bond in 2-(2-fluoro-5-nitrophenyl)acetonitrile (15), generated from 2-fluoro-5-nitrobenzyl bromide (14) [30], yielded polymeric material under the aldol conditions used and 1-fluoro-4-nitro-2-((phenylsulfonyl)methyl)benzene (16), prepared from this same bromide [31], failed to aldolize under the conditions used.



Scheme 1. Synthesis of the reaction substrates to prepare methyl 1-alkyl-1H-indole-3-carboxylates. Key: (a) NaNO₂, H₂SO₄, 0–23 °C, 91%; (b) 37% aq. HCHO, K₂CO₃, DMF, 23 °C, 58–62%; (c) Fe, NH₄Cl, aq. EtOH, 85 °C, 93%; (d) HONO, CuCN, 65%; (e) NaBH₄, EtOH, 23 °C, 91%; (f) PBr₃, Et₂O, 0–23 °C 90%; (g) KCN, aq. EtOH, 23 °C, 76–88%; (h) 25% H₂SO₄, MeOH, 90 °C, 60%; (i) PhSO₂Na, EtOH, 78 °C, 70%.

Our cyclization results are summarized in Table 1. The reaction was carried out in anhydrous DMF using 1 mmol of the acrylate, 1 mmol of the RNH₂ and 2 mmol of K₂CO₃. Primary amines incorporating a primary, secondary or tertiary alkyl group were all successful in the reaction but anilines failed to initiate the sequence due to their diminished reactivity. We also found that hydrazine reacted with nitro activated substrate 7 but not the cyano and ester activated substrates 10 and 13, respectively [32]. Despite the α -effect which increases the nucleophilicity of hydrazine [33], the less S_NAr active substrates 10 and 13 primarily afforded products resulting from reaction at the pendant ester and cyano groups. As expected, the five-membered ring was entropically favored over the six-membered ring in the reaction of hydrazine with 7. Additionally, the five-membered ring also benefited from stabilization gained via heteroaromatization.

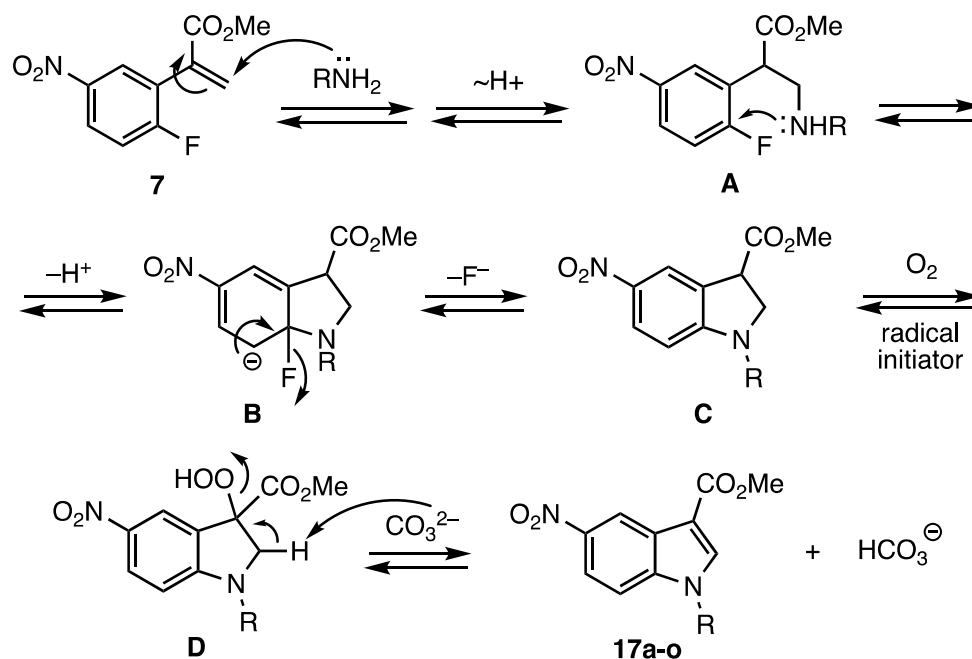
Substrates incorporating nitro and cyano activation on the S_NAr acceptor ring proceeded at room temperature while the ester-bearing substrate required heating up to 90 °C. This observation likely reflects the relative activating ability of the different groups in the S_NAr process. In all cases, the work-up required adding the crude reaction mixture to aq. NH₄Cl, extracting with ether, and washing the combined organic layers with aq. NaCl. The ether layers were dried and concentrated to give a crude product that was purified by column chromatography. All products exhibited spectral and analytical data in accord with the assigned structures (see Supplementary Materials).

Table 1. C5-Substituted 1-alkyl-1*H*-indole-3-carboxylate esters prepared.

Substrate	R	T (°C)	Product	Yield
7	<i>n</i> -C ₆ H ₁₃	23	17a	80
7	-CH ₂ CH(CH ₃) ₂	23	17b	88
7	-CH ₂ CH = CH ₂	23	17c	90
7	<i>c</i> -C ₃ H ₅	23	17d	75
7	<i>c</i> -C ₆ H ₁₁	23	17e	78
7	-C(CH ₃) ₃	23	17f	77
7	-CH ₂ CH ₂ C ₆ H ₅	23	17g	85
7	-CH ₂ C ₆ H ₅	23	17h	85
7	-CH ₂ C ₆ H ₄ -4-Me	23	17i	86
7	-CH ₂ C ₆ H ₄ -4-Me	23	17j	83
7	-CH ₂ C ₆ H ₄ -4-Me	23	17k	87
7	-CH ₂ C ₆ H ₄ -4-Cl	23	17l	81
7	-CH ₂ C ₆ H ₄ -4-CF ₃	23	17m	89
7	-CH ₂ C ₆ H ₄ -3-NO ₂	23	17n	91
7	-NH ₂	23	17o	83
10	<i>n</i> -C ₆ H ₁₃	23	18a	74
10	-CH ₂ CH(CH ₃) ₂	23	18b	67
10	<i>c</i> -C ₃ H ₅	23	18d	78
10	<i>c</i> -C ₆ H ₁₁	23	18e	79
10	-CH ₂ CH ₂ C ₆ H ₅	23	18g	91
10	-CH ₂ C ₆ H ₅	23	18h	88
10	-CH ₂ C ₆ H ₄ -4-Me	23	18i	81
10	-CH ₂ C ₆ H ₄ -3-OMe	23	18j	83
10	-CHC ₆ H ₄ -4-OMe	23	18k	89
10	-CH ₂ C ₆ H ₄ -4-Cl	23	18l	87
10	-CH ₂ C ₆ H ₄ -3-NO ₂	23	18n	92
13	<i>n</i> -C ₆ H ₁₃	90	19a	67
13	-CH ₂ CH(CH ₃) ₂	90	19b	69
13	-CH ₂ CH = CH ₂	50	19c	80
13	<i>c</i> -C ₃ H ₅	90	19d	61
13	<i>c</i> -C ₆ H ₁₁	90	19e	65
13	-CH ₂ CH ₂ C ₆ H ₅	90	19g	89
13	-CH ₂ C ₆ H ₅	50	19h	86
13	-CH ₂ C ₆ H ₄ -4-Me	50	19i	82
13	-CH ₂ C ₆ H ₄ -3-OMe	50	19j	86
13	-CH ₂ C ₆ H ₄ -4-OMe	50	19k	86
13	-CH ₂ C ₆ H ₄ -4-Cl	50	19l	80
13	-CH ₂ C ₆ H ₄ -3-NO ₂	50	19n	91

The exact chronology of events in the reaction sequence is unknown, but a plausible sequence is outlined for substrate **7** in Scheme 2. Due to the low temperatures employed, the initiating step was assumed to involve aza-Michael addition of the amine to the unhindered 2-arylacrylate double bond followed by loss of a proton to give amine adduct **A**. The nitrogen in this intermediate is positioned to add to the activated aromatic ring by a S_NAr reaction via Meisenheimer intermediate **B** to give indoline **C**. The heteroaromatization process likely occurs due to exposure of the compound to dissolved oxygen in the DMF [34] or oxygen introduced during removal of TLC samples. Since indoline **C** has a highly activated benzylic C-H substituted by an ester group, insertion of oxygen at this site to

form a peroxide intermediate **D** should be facile. This process often requires a radical initiator [32], but it is unclear what could perform this function in the current reaction. Once oxygen inserts into the activated C–H bond, elimination under the basic conditions would install the double bond to afford the indole **17** (Scheme 2). In no case was indoline **C** detected during the reaction or in the final product. A similar process was hypothesized for the formation of quinolones in an earlier study [35].



Scheme 2. Plausible mechanism for the domino aza-Michael- $\text{S}_{\text{N}}\text{Ar}$ -heteroaromatization of **7**.

3. Materials and Methods

3.1. General Methods

Unless otherwise indicated, all reactions were performed under dry N_2 in oven-dried glassware. All reagents and solvents were used as received. All wash solutions in work-up procedures were aqueous. Reactions were monitored by thin layer chromatography on Analtech No 21521 silica gel GF plates (Newark, DE, USA). Preparative separations were performed by flash chromatography on silica gel (Davisil[®], grade 62, 60–200 mesh) containing 0.5% of UV-05 UV-active phosphor (both from Sorbent Technologies, Norcross, GA, USA) slurry packed into quartz columns. Band elution for all chromatographic separations was monitored using a hand-held UV lamp (Fisher Scientific, Pittsburgh, PA, USA). Melting points were obtained using a MEL-TEMP apparatus (Cambridge, MA, USA) and are uncorrected. FT-IR spectra (0.09 cm^{-1} resolution between $4000\text{--}500\text{ cm}^{-1}$) were run as thin films on NaCl disks using a Nicolet iS50 spectrophotometer (Madison, WI, USA). ^1H - and ^{13}C -NMR spectra were measured using a Bruker Avance 400 system (Billerica, MA, USA) at 400 MHz and 101 MHz, respectively, in the indicated solvents containing 0.05% $(\text{CH}_3)_4\text{Si}$ as the internal standard; coupling constants (J) are given in Hz. Low-resolution mass spectra were obtained using a Hewlett-Packard Model 1800A GCD GC-MS system (Palo Alto, CA, USA). Elemental analyses ($\pm 0.4\%$) were determined by Atlantic Microlabs (Norcross, GA, USA).

3.2. Methyl 2-(2-Fluoro-5-nitrophenyl)acetate (**6**)

The procedure was modified from that of Gale and Wilshire [24]. Methyl 2-(2-fluorophenyl)acetate (**5**, 10.0 g, 59.5 mmol), was added drop-wise over 1 h to an ice-cooled solution of sodium nitrate (5.60 g, 65.8 mmol) in concentrated sulfuric acid (102 g, 55.3 mL). After a further 30 min at $5\text{--}10\text{ }^\circ\text{C}$, the solution was poured onto ice and the resulting mixture was extracted with ether ($3 \times 50\text{ mL}$). The combined ether layers

were washed with water (2 × 50 mL), saturated NaHCO₃ (1 × 50 mL), and saturated NaCl (1 × 50 mL) and then dried (Na₂SO₄). Filtration and concentration under vacuum gave the crude nitrated product as a yellow solid that was purified by trituration with 2% ether in pentane to give **6** (11.5 g, 91%) as a light yellow solid, m.p. 51–53 °C. IR: 1741, 1527, 1350 cm⁻¹; ¹H NMR (400 MHz, CDCl₃): δ 8.25–8.18 (complex, 2H), 7.23 (t, *J* = 8.8 Hz, 1H), 3.78 (d, *J* = 1.4 Hz, 2H), 3.75 (s, 3H); ¹³C NMR (101 MHz, CDCl₃): δ 169.8, 164.6 (d, *J* = 258.1 Hz), 144.2, 127.6 (d, *J* = 5.9 Hz), 125.2 (d, *J* = 10.1 Hz), 123.2 (d, *J* = 18.3 Hz), 116.4 (d, *J* = 24.6 Hz), 52.6, 34.1 (d, *J* = 2.6 Hz); MS (*m/z*) 213 (M⁺); Anal. Calcd for C₉H₈FNO₄: C, 50.71; H, 3.78; N, 6.57. Found: C, 50.77; H, 3.83; N, 6.55.

3.3. Methyl 2-(5-Amino-2-fluorophenyl)acetate (**8**)

The procedure of Zhou and co-workers was used [26]. Nitroester **7** (5.00 g, 23.5 mmol) was dissolved in a mixture of EtOH (165 mL) and H₂O (45 mL). The solution was heated at 70 °C under N₂, NH₄Cl (1.26 g, 23.5 mmol) and iron powder (3.92 g, 70.1 mmol) were cautiously added, and heating was continued for 2–3 h. The reaction mixture was filtered through celite, treated with saturated NaHCO₃ (100 mL), and extracted with ethyl acetate (3 × 50 mL). The combined organic extracts were washed with saturated NaCl, dried (Na₂SO₄), filtered, and concentrated under vacuum to give amino ester **8** (4.00 g, 93%) as a light tan solid, m.p. 35–37 °C. This material was spectroscopically pure and was used without further purification. IR: 3445, 3369, 3232, 1732 cm⁻¹; ¹H NMR (400 MHz, CDCl₃): δ 6.84 (t, *J* = 8.9 Hz, 1H), 6.57–6.49 (complex, 2H), 3.70 (s, 3H), 3.58 (d, *J* = 1.4 Hz, 2H), 3.37 (br s, 2H); ¹³C NMR (101 MHz, CDCl₃): δ 171.3, 154.5 (d, *J* = 236.6 Hz), 142.5 (d, *J* = 2.4 Hz), 121.7 (d, *J* = 17.2 Hz), 117.4 (d, *J* = 3.4 Hz), 115.8 (d, *J* = 23.1 Hz), 115.2 (d, *J* = 7.6 Hz), 52.2, 34.3 (d, *J* = 2.9 Hz); MS (*m/z*): 183 (M⁺).

3.4. Methyl 2-(5-Cyano-2-fluorophenyl)acetate (**9**)

The general procedure of Clarke and Read was used [27]. All water and aqueous solutions in this procedure used deionized H₂O. CuCl was prepared from CuSO₄·5H₂O (3.42 g, 13.7 mmol), NaCl (0.90 g, 15.5 mmol) and Na₂SO₃ (from 0.72 g of NaHSO₃/Na₂S₂O₅ and 0.48 g (18 mmol) of NaOH) in H₂O (14 mL) as described by Marvel and McElvain [28]. The CuCl was purified by decantation and suspended in H₂O (10 mL). To the magnetically stirred suspension, a solution of NaCN (1.82 g, 37.1 mmol) in H₂O (5 mL) was added drop-wise over 10 min and the CuCl dissolved with the generation of heat.

Aminoester **8** (2.00 g, 10.9 mmol) was mixed with crushed ice (ca 5 g) and 28% HCl (3 mL) was added. The flask was surrounded by an ice bath to maintain the temperature at 0–5 °C and a solution of NaNO₂ (0.84 g, 12.1 mmol) in H₂O (3 mL) was added with stirring over 15 min. This mixture was neutralized to pH 7 by slow addition of solid anhydrous Na₂CO₃ to give a solution of the diazonium salt.

The above CuCN solution was cooled to 0–5 °C, toluene (4 mL) was added and vigorous stirring was initiated. To this was added drop-wise the cold solution of the diazonium salt during 15–20 min keeping the temperature at 0–5 °C. N₂ was evolved during the addition. The mixture was warmed to 23 °C over 2 h and then heated to 50 °C for 5 min. The heat was removed and the reaction was allowed to return to 23 °C over 1 h. The crude reaction mixture was transferred to a separatory funnel and the mixture was extracted with EtOAc (3 × 25 mL). The combined organic extracts were washed with saturated NaCl (3 × 50 mL), dried (Na₂SO₄), and concentrated under vacuum. The product from two runs at the above scale was purified by silica gel column chromatography (50 cm × 2.5 cm) eluted with 10–20% EtOAc in hexanes to give nitrile ester **9** (2.73 g, 65%) as a yellow solid, m.p. 51–53 °C. IR: 2232, 1741 cm⁻¹; ¹H NMR (400 MHz, CDCl₃): δ 7.66–7.58 (complex, 2H), 7.19 (t, *J* = 8.8 Hz, 1H), 3.74 (s, 3H), 3.71 (d, *J* = 1.5 Hz, 2H); ¹³C NMR (101 MHz, CDCl₃): δ 169.9, 163.4 (d, *J* = 256.8 Hz), 135.9 (d, *J* = 5.5 Hz), 133.6 (d, *J* = 9.6 Hz), 123.5 (d, *J* = 17.4 Hz), 117.9, 116.9 (d, *J* = 23.7 Hz), 108.7 (d, *J* = 4.0 Hz), 52.5, 33.8 (d, *J* = 2.9 Hz); MS (*m/z*): 193 (M⁺); Anal. Calcd for C₁₀H₈FNO₂: C, 62.18; H, 4.17; N, 7.25. Found: C, 62.25; H, 4.19; N, 7.14.

3.5. Methyl (4-Carbomethoxy-2-fluorophenyl)acetate (12)

To a solution of the 5-cyano-2-fluorobenzaldehyde (**11**, 10.0 g, 67.1 mmol) in absolute ethanol (80 mL) at 0 °C (ice-water bath), NaBH₄ (1.27 g, 33.5 mmol) was added portion-wise with stirring during 10–15 min. The cooling bath was removed and the reaction was allowed to warm to room temperature for 1 h. The reaction was quenched by addition to saturated NaCl (250 mL) and extracted with ether (3 × 50 mL). The combined ether layers were washed with saturated NaCl (3 × 50 mL) and dried (Na₂SO₄). Filtration and concentration under vacuum gave the alcohols as off-white solids that were purified by trituration with 2% ether in pentane to give (5-cyano-2-fluorophenyl)methanol (9.22 g, 91%) as an off-white solid, m.p. 48–50 °C; IR: 3429, 2234 cm⁻¹; ¹H NMR (400 MHz, CDCl₃): δ 7.84 (dd, *J* = 6.7, 2.1 Hz, 1H), 7.61 (ddd, *J* = 8.3, 4.8, 2.1 Hz, 1H), 7.16 (t, *J* = 9.0 Hz, 1H), 4.80 (s, 2H), 2.16 (br s, 1H); ¹³C NMR (101 MHz, CDCl₃): δ 162.5 (d, *J* = 256.6 Hz), 133.5 (d, *J* = 9.5 Hz), 133.1 (d, *J* = 6.2 Hz), 130.1 (d, *J* = 16.1 Hz), 118.4, 116.5 (d, *J* = 22.9 Hz), 108.6 (d, *J* = 3.9 Hz), 58.2 (d, *J* = 4.4 Hz); MS (*m/z*) 151 (M⁺); Anal. Calcd for C₈H₆FNO: C, 63.58; H, 4.00; N, 9.27. Found: C, 63.65; H, 3.97; N, 9.22.

A solution of (5-cyano-2-fluorophenyl)methanol (9.22 g, 61.1 mmol) in anhydrous ether (100 mL) was cooled to 0 °C. To the stirred solution was added drop-wise PBr₃ (8.32 g, 2.89 mL, 30.7 mmol) during 1 h. The reaction was allowed to warm to 23 °C overnight at which time it was quenched by addition to saturated NaCl (150 mL). The ether layer was separated and the aqueous layer was washed with ether (2 × 50 mL). The combined ether layers were washed with saturated NaCl (3 × 50 mL) and dried (Na₂SO₄). Filtration and concentration under vacuum gave the bromide as an off-white solid which was purified by trituration with 2% ether in pentane to give 2-(bromomethyl)-4-cyano-1-fluorobenzene (11.8 g, 90%) as an off-white solid, m.p. 55–56 °C; IR: 2238 cm⁻¹; ¹H NMR (400 MHz, CDCl₃): δ 7.76 (dd, *J* = 6.9, 2.2 Hz, 1H), 7.64 (ddd, *J* = 8.6, 4.8, 2.2 Hz, 1H), 7.20 (t, *J* = 8.9 Hz, 1H), 4.48 (s, 2H); ¹³C NMR (101 MHz, CDCl₃): δ 162.9 (d, *J* = 260.0 Hz), 135.5 (d, *J* = 4.5 Hz), 134.6 (d, *J* = 9.7 Hz), 127.3 (d, *J* = 16.0 Hz), 117.5, 117.3 (d, *J* = 22.9 Hz), 109.1 (d, *J* = 4.0 Hz), 23.5 (d, *J* = 4.3 Hz); MS (*m/z*) 213, 215 (*ca* 1:1, M⁺); Anal. Calcd for C₈H₅FBrN: C, 44.89; H, 2.35; N, 6.54. Found: C, 44.97; H, 2.39; N, 6.44.

To a solution of KCN (5.16 g, 79.2 mmol) in water (6 mL) at 23 °C was added drop-wise a solution of the 2-(bromomethyl)-4-cyano-1-fluorobenzene (11.3 g, 52.8 mmol) in ethanol (75–90 mL) during 1 h. The solution was stirred for 16 h and quenched by addition to saturated NaCl (250 mL) and extracted with ether (3 × 50 mL). The combined ether layers were washed with saturated NaCl (3 × 50 mL) and dried (Na₂SO₄). Filtration and concentration under vacuum gave 3-(cyanomethyl)-4-fluorobenzonitrile as a light tan solid which was subjected to methanolysis without further purification.

A solution of concentrated sulfuric acid in methanol (100 mL, 25% *v/v*) was prepared at 0 °C. The benzylic nitrile was added slowly and the mixture was heated to boiling for 16 h (bath temperature 90 °C). After cooling, the reaction was quenched by addition to saturated NaCl (250 mL) and extracted with ether (3 × 50 mL). The combined ether layers were washed with saturated NaCl (3 × 50 mL) and dried (Na₂SO₄). Filtration and concentration under vacuum gave the ester as a yellow oil. Purification was accomplished by silica gel column chromatography (40 cm × 2.5 cm) eluted with 10–15% ether in hexanes to give 7.05 g (60%, 2 steps) of diester **12** as a light yellow oil. IR: 1735, 1720 cm⁻¹; ¹H NMR (400 MHz, CDCl₃): δ 7.98 (m, 2H), 7.12 (t, *J* = 9.1 Hz, 1H), 3.91 (d, *J* = 2.6 Hz, 2H), 3.73 (s, 3H), 3.72 (s, 3H); ¹³C NMR (101 MHz, CDCl₃): δ 170.6, 166.0, 164.0 (d, *J* = 254.4 Hz), 133.5 (d, *J* = 5.4 Hz), 131.1 (d, *J* = 9.5 Hz), 126.5 (d, *J* = 3.4 Hz), 121.8 (d, *J* = 16.9 Hz), 115.6 (d, *J* = 22.9 Hz), 53.3, 52.2, 34.2 (d, *J* = 2.7 Hz); MS (*m/z*) 226 (M⁺); Anal. Calcd for C₁₁H₁₁FO₄: C, 58.41; H, 4.90. Found: C, 58.39; H, 4.94.

3.6. General Procedure for Conversion of the 2-Arylacetate Esters to Acrylates

The basic procedure of Selvakumar and co-workers was used [25]. To a mixture of the methyl 2-arylacetate (8.0 mmol) in formalin (37%, 18 mL) was added a suspension of anhydrous K₂CO₃ (1.66 g, 12.0 mmol) in DMF (5 mL). The resulting mixture was heated

to 60 °C for 2 h and then cooled to 23 °C. The crude reaction mixture was quenched with water (75 mL) and extracted with ether (3 × 50 mL). The combined ether extracts were washed with saturated NaCl (3 × 50 mL) and dried (Na₂SO₄). Filtration and concentration under vacuum gave the crude product as a light yellow oil. Purification by silica gel column chromatography (25 cm × 2.5 cm) eluted with increasing concentrations of ether in hexanes afforded the pure acrylate esters, which solidified on standing.

3.6.1. Methyl 2-(2-Fluoro-5-nitrophenyl)acrylate (7)

Yield: 1.97 g (60%) as an off-white solid, m.p. 52–54 °C; IR: 1730, 1634, 1527, 1350 cm⁻¹; ¹H NMR (400 MHz, CDCl₃): δ 8.24 (m, 2H), 7.24 (t, *J* = 8.8 Hz, 1H), 6.68 (s, 1H), 6.03 (s, 1H), 3.83 (s, 3H); ¹³C NMR (101 MHz, CDCl₃): δ 165.3, 163.4 (d, *J* = 259.7 Hz), 144.1, 134.5, 131.6 (d, *J* = 1.7 Hz), 126.9 (d, *J* = 5.3 Hz), 126.4 (d, *J* = 17.4 Hz), 125.8 (d, *J* = 10.3 Hz), 116.6 (d, *J* = 24.9 Hz), 52.7; MS (*m/z*) 225 (M⁺); Anal. Calcd for C₁₀H₈FNO₄: C, 53.34; H, 3.58; N, 6.22. Found: C, 53.37; H, 3.61; N, 6.13.

3.6.2. Methyl 2-(5-Cyano-2-fluorophenyl)acrylate (10)

Yield: 1.66 g (58%) as a yellow solid, m.p. 69–70 °C; IR: 2231, 1723 cm⁻¹; ¹H NMR (400 MHz, CDCl₃): δ 7.66 (ddd, *J* = 8.5, 4.7, 2.2 Hz, 1H), 7.63 (dd, *J* = 6.7, 2.2 Hz, 1H), 7.20 (dd, *J* = 9.2, 8.5 Hz, 1H), 6.64 (d, *J* = 0.8 Hz, 1H), 5.97 (d, *J* = 0.7 Hz, 1H), 3.82 (s, 3H); ¹³C NMR (101 MHz, CDCl₃): δ 165.4, 162.3 (d, *J* = 258.4 Hz), 135.2 (d, *J* = 4.5 Hz), 134.5, 134.3 (d, *J* = 9.8 Hz), 131.3 (d, *J* = 1.6 Hz), 126.9 (d, *J* = 16.7 Hz), 117.8, 117.1 (d, *J* = 23.9 Hz), 108.6 (d, *J* = 4.0 Hz), 52.6; MS (*m/z*): 205 (M⁺); Anal. Calcd for C₁₁H₈FNO₂: C, 64.39; H, 3.93; N, 6.83. Found: C, 64.33; H, 3.96; N, 6.78.

3.6.3. Methyl 2-(5-Carbomethoxy-2-fluorophenyl)acrylate (13)

Yield: 2.03 g (62%) as an off-white solid, m.p. 52–54 °C; IR: 1724, 1627 cm⁻¹; ¹H NMR (400 MHz, CDCl₃): δ 8.04 (ddd, *J* = 8.6, 5.0, 2.3 Hz, 1H), 8.00 (dd, *J* = 7.1, 2.3 Hz, 1H), 7.13 (t, *J* = 9.0 Hz, 1H), 6.58 (d, *J* = 1.1 Hz, 1H), 5.95 (d, *J* = 1.1 Hz, 1H), 3.92 (s, 3H), 3.81 (s, 3H); ¹³C NMR (101 MHz, CDCl₃): δ 166.0, 165.9, 162.8 (d, *J* = 256.0 Hz), 135.7, 132.8 (d, *J* = 4.7 Hz), 132.0 (d, *J* = 9.7 Hz), 130.3, 126.4 (d, *J* = 3.3 Hz), 125.4 (d, *J* = 16.0 Hz), 115.7 (d, *J* = 23.1 Hz), 52.5, 52.3; MS (*m/z*) 238 (M⁺); Anal. Calcd for C₁₂H₁₁FO₄: C, 60.51; H, 4.65. Found: C, 60.48; H, 4.64.

3.7. General Procedure for Preparing C5-Substituted Methyl 1-Alkyl-1H-indole-3-carboxylates

A solution of the C5-substituted 2-arylacrylate (1 mmol) and the primary amine (1 mmol) in DMF (4 mL) was treated with anhydrous K₂CO₃ (276 mg, 2 mmol) and stirred for 12 h at 23 °C. At this time, TLC indicated that the reaction was complete. The crude reaction mixture was added to saturated NH₄Cl (50 mL) and extracted with ether (3 × 25 mL). The combined organic extracts were washed with saturated NaCl (50 mL), dried (Na₂SO₄), filtered, and concentrated under vacuum. The crude product was purified by passing through a short silica gel column (25 × 2.5 cm) eluted with increasing concentrations of ether in hexanes. The compounds prepared are summarized below. *Notes:* (1) When 3-nitrobenzylamine hydrochloride was used as the amine, 3 equiv of K₂CO₃ were used. (2) When the substrate incorporated an ester activating group on the S_NAr acceptor ring, the reaction was stirred for 12 h at 50–90 °C as indicated in Table 1.

3.8. Reactions with Methyl 2-(2-Fluoro-5-nitrophenyl)acrylate (7)

3.8.1. Methyl 1-Hexyl-5-nitro-1H-indole-3-carboxylate (17a)

Yield: 243 mg (80%) as a light yellow solid, m.p. 52–54 °C; IR: 1707, 1612, 1537, 1341 cm⁻¹; ¹H NMR (400 MHz, CDCl₃): δ 9.08 (d, *J* = 2.3 Hz, 1H), 8.18 (dd, *J* = 9.1, 2.3 Hz, 1H), 7.97 (s, 1H), 7.41 (d, *J* = 9.1 Hz, 1H), 4.19 (t, *J* = 7.1 Hz, 2H), 3.97 (s, 3H), 1.88 (quintet, *J* = 7.1 Hz, 2H), 1.31 (m, 6H), 0.88 (t, *J* = 6.9 Hz, 3H); ¹³C NMR (101 MHz, CDCl₃): δ 164.5, 143.4, 139.2, 136.9, 125.9, 119.0, 118.3, 110.2, 109.5, 51.5, 47.5, 31.2, 29.9, 26.4, 22.4, 13.9;

MS (m/z): 304 (M^+); Anal. Calcd for $C_{16}H_{20}N_2O_4$: C, 63.14; H, 6.62; N, 9.20. Found: C, 63.11; H, 6.59; N, 9.14.

3.8.2. Methyl 1-Isobutyl-5-nitro-1*H*-indole-3-carboxylate (17b)

Yield: 243 mg (88%) as a light yellow solid, m.p. 131–133 °C; IR: 1706, 1614, 1539, 1347 cm^{-1} ; 1H NMR (400 MHz, $CDCl_3$): δ 9.06 (d, $J = 2.3$ Hz, 1H), 8.16 (dd, $J = 9.1, 2.3$ Hz, 1H), 7.96 (s, 1H), 7.40 (d, $J = 9.1$ Hz, 1H), 4.00 (d, $J = 7.4$ Hz, 2H), 3.96 (s, 3H), 2.21 (nonet, $J = 6.9$ Hz, 1H), 0.97 (d, $J = 6.7$ Hz, 6H); ^{13}C NMR (101 MHz, $CDCl_3$): δ 164.4, 143.3, 139.5, 137.5, 125.8, 119.8, 118.2, 110.4, 109.3, 55.0, 51.5, 29.5, 20.1; MS (m/z): 276 (M^+); Anal. Calcd for $C_{14}H_{16}N_2O_4$: C, 60.86; H, 5.84; N, 10.14. Found: C, 60.83; H, 5.82; N, 10.17.

3.8.3. Methyl 1-Allyl-5-nitro-1*H*-indole-3-carboxylate (17c)

Yield: 234 mg (90%) as a light yellow solid, m.p. 119–121 °C; IR: 1704, 1620, 1534, 1342 cm^{-1} ; 1H NMR (400 MHz, $CDCl_3$): δ 9.06 (d, $J = 2.3$ Hz, 1H), 8.16 (dd, $J = 9.1, 2.3$ Hz, 1H), 7.96 (s, 1H), 7.40 (d, $J = 9.1$ Hz, 1H), 6.01 (ddt, $J = 17.0, 10.6, 5.4$ Hz, 1H), 5.35 (d, $J = 10.6$ Hz, 1H), 5.18 (d, $J = 17.0$ Hz, 1H), 4.82 (d, $J = 5.4$ Hz, 2H), 3.96 (s, 3H); ^{13}C NMR (101 MHz, $CDCl_3$): δ 164.3, 143.5, 139.3, 137.0, 131.2, 126.0, 119.4, 118.8, 118.4, 110.4, 109.7, 51.5, 49.8; MS (m/z): 260 (M^+); Anal. Calcd for $C_{13}H_{12}N_2O_4$: C, 60.00; H, 4.65; N, 10.76. Found: C, 59.97; H, 4.67; N, 10.58.

3.8.4. Methyl 1-Cyclopropyl-5-nitro-1*H*-indole-3-carboxylate (17d)

Yield: 195 mg (75%) as a light yellow solid, m.p. 133–134 °C; IR: 1698, 1607, 1533, 1334 cm^{-1} ; 1H NMR (400 MHz, $CDCl_3$): δ 9.03 (d, $J = 2.3$ Hz, 1H), 8.19 (dd, $J = 9.1, 2.3$ Hz, 1H), 7.98 (s, 1H), 7.64 (d, $J = 9.1$ Hz, 1H), 3.95 (s, 3H), 3.48 (septet, $J = 3.8$ Hz, 1H), 1.24 (m, 2H), 1.08 (m, 2H); ^{13}C NMR (101 MHz, $CDCl_3$): δ 164.3, 143.7, 140.7, 137.3, 125.9, 118.8, 118.4, 111.0, 109.4, 51.5, 28.0, 6.5; MS (m/z): 260 (M^+); Anal. Calcd for $C_{13}H_{12}N_2O_4$: C, 60.00; H, 4.65; N, 10.76. Found: C, 60.04; H, 4.65; N, 10.61.

3.8.5. Methyl 1-Cyclohexyl-5-nitro-1*H*-indole-3-carboxylate (17e)

Yield: 236 mg (78%) as a light yellow solid, m.p. 133–134 °C; IR: 1708, 1614, 1532, 1339 cm^{-1} ; 1H NMR (400 MHz, $CDCl_3$): δ 9.07 (d, $J = 2.3$ Hz, 1H), 8.16 (dm, $J = 9.1$ Hz, 1H), 8.09 (s, 1H), 7.46 (d, $J = 9.1$ Hz, 1H), 4.28 (tt, $J = 12.0, 3.7$ Hz, 1H), 3.96 (s, 3H), 2.20 (d, $J = 12.0$ Hz, 2H), 2.00 (d, $J = 13.5, 3.6$ Hz, 2H), 1.85 (d, $J = 13.1$ Hz, 1H), 1.74 (q, $J = 13.1, 3.6$ Hz, 2H), 1.55 (qt, $J = 13.1, 3.6$ Hz, 2H), 1.31 (qt, $J = 13.1, 3.6$ Hz, 1H); ^{13}C NMR (101 MHz, $CDCl_3$): δ 164.6, 143.3, 138.9, 133.8, 125.8, 118.9, 118.0, 110.1, 109.5, 56.4, 51.4, 33.4, 25.7, 25.3; MS (m/z): 302 (M^+); Anal. Calcd for $C_{16}H_{18}N_2O_4$: C, 63.56; H, 6.00; N, 9.27. Found: C, 63.63; H, 6.05; N, 9.23.

3.8.6. Methyl 1-(*tert*-Butyl)-5-nitro-1*H*-indole-3-carboxylate (17f)

Yield: 213 mg (77%) as a light yellow solid, m.p. 161–163 °C; IR: 1708, 1615, 1536, 1342 cm^{-1} ; 1H NMR (400 MHz, $CDCl_3$): δ 9.11 (d, $J = 2.4$ Hz, 1H), 8.15 (s, 1H), 8.14 (dd, $J = 9.3, 2.4$ Hz, 1H), 7.72 (d, $J = 9.3$ Hz, 1H), 3.96 (s, 3H), 1.79 (s, 9H); ^{13}C NMR (101 MHz, $CDCl_3$): δ 164.6, 142.8, 138.3, 135.1, 127.6, 118.8, 117.4, 113.8, 108.4, 58.0, 51.4, 29.7; MS (m/z): 276 (M^+); Anal. Calcd for $C_{14}H_{16}N_2O_4$: C, 60.86; H, 5.84; N, 10.14. Found: C, 60.84; H, 5.81; N, 10.06.

3.8.7. Methyl 5-Nitro-1-phenethyl-1*H*-indole-3-carboxylate (17g)

Yield: 275 mg (85%) as a light yellow solid, m.p. 165–167 °C; IR: 1705, 1619, 1536, 1341 cm^{-1} ; 1H NMR (400 MHz, $CDCl_3$): δ 9.05 (d, $J = 2.3$ Hz, 1H), 8.11 (dd, $J = 9.1, 2.3$ Hz, 1H), 7.77 (s, 1H), 7.28–7.22 (complex, 4H), 7.00 (complex, 2H), 4.43 (t, $J = 7.0$ Hz, 2H), 3.94 (s, 3H), 3.15 (t, $J = 7.0$ Hz, 2H); ^{13}C NMR (101 MHz, $CDCl_3$): δ 164.4, 143.4, 139.1, 137.0, 136.9, 129.0, 128.6, 127.3, 125.8, 118.9, 118.3, 110.0, 109.6, 51.5, 49.2, 36.6; MS (m/z): 324 (M^+); Anal. Calcd for $C_{18}H_{16}N_2O_4$: C, 66.66; H, 4.97; N, 8.64. Found: C, 66.71; H, 4.96; N, 8.57.

3.8.8. Methyl 1-Benzyl-5-nitro-1H-indole-3-carboxylate (17h)

Yield: 263 mg (85%) as a light yellow solid, m.p. 112–113 °C; IR: 1705, 1618, 1537, 1341 cm^{-1} ; ^1H NMR (400 MHz, CDCl_3): δ 9.09 (d, $J = 2.2$ Hz, 1H), 8.14 (dd, $J = 9.1, 2.2$ Hz, 1H), 7.98 (s, 1H), 7.39–7.32 (complex, 4H), 7.17–7.14 (complex, 2H), 5.39 (s, 2H), 3.96 (s, 3H); ^{13}C NMR (101 MHz, CDCl_3): δ 164.3, 143.5, 139.4, 137.3, 134.8, 129.3, 128.7, 127.1, 126.1, 118.9, 118.6, 110.6, 110.0, 51.5, 51.3; MS (m/z): 310 (M^+); Anal. Calcd for $\text{C}_{17}\text{H}_{14}\text{N}_2\text{O}_4$: C, 65.80; H, 4.55; N, 9.03. Found: C, 65.74; H, 4.51; N, 8.98.

3.8.9. Methyl 1-(4-Methylbenzyl)-5-nitro-1H-indole-3-carboxylate (17i)

Yield: 279 g (86%) as a light yellow solid, m.p. 163–164 °C; IR: 1706, 1616, 1538, 1349 cm^{-1} ; ^1H NMR (400 MHz, CDCl_3): δ 9.07 (d, $J = 2.2$ Hz, 1H), 8.13 (dd, $J = 9.1, 2.2$ Hz, 1H), 7.96 (s, 1H), 7.37 (d, $J = 9.1$ Hz, 1H), 7.16 (d, $J = 7.9$ Hz, 2H), 7.06 (d, $J = 7.9$ Hz, 2H), 5.33 (s, 2H), 3.95 (s, 3H), 2.33 (s, 3H); ^{13}C NMR (101 MHz, CDCl_3): δ 164.4, 143.5, 139.4, 138.6, 137.2, 131.7, 129.9, 127.2, 126.1, 118.9, 118.5, 110.6, 109.8, 51.5, 51.1, 21.1; MS (m/z): 324 (M^+); Anal. Calcd for $\text{C}_{18}\text{H}_{16}\text{N}_2\text{O}_4$: C, 66.66; H, 4.97; N, 8.64. Found: C, 66.61; H, 4.95; N, 8.62.

3.8.10. Methyl 1-(3-Methoxybenzyl)-5-nitro-1H-indole-3-carboxylate (17j)

Yield: 282 mg (83%) as a light yellow solid, m.p. 112–113 °C; IR: 2840, 1704, 1611, 1547, 1338 cm^{-1} ; ^1H NMR (400 MHz, CDCl_3): δ 9.09 (d, $J = 2.2$ Hz, 1H), 8.14 (dd, $J = 9.1, 2.2$ Hz, 1H), 7.98 (s, 1H), 7.37 (d, $J = 9.1$ Hz, 1H), 7.27 (t, $J = 7.8$ Hz, 1H), 6.87 (dd, $J = 8.6, 2.2$ Hz, 1H), 6.73 (d, $J = 7.8$ Hz, 1H), 6.67 (t, $J = 2.2$ Hz, 1H), 5.35 (s, 2H), 3.96 (s, 3H), 3.76 (s, 3H); ^{13}C NMR (101 MHz, CDCl_3): δ 164.3, 160.2, 143.5, 139.4, 137.3, 136.3, 130.4, 126.1, 119.3, 118.9, 118.6, 113.5, 113.2, 110.6, 110.0, 55.3, 51.5, 51.2; MS (m/z): 340 (M^+); Anal. Calcd for $\text{C}_{18}\text{H}_{16}\text{N}_2\text{O}_5$: C, 63.53; H, 4.74; N, 8.23. Found: C, 63.44; H, 4.77; N, 8.17.

3.8.11. Methyl 1-(4-Methoxybenzyl)-5-nitro-1H-indole-3-carboxylate (17k)

Yield: 296 mg (87%) as a light yellow solid, m.p. 153–154 °C; IR: 2838, 1705, 1614, 1537, 1342 cm^{-1} ; ^1H NMR (400 MHz, CDCl_3): δ 9.08 (d, $J = 2.3$ Hz, 1H), 8.14 (dd, $J = 9.1, 2.3$ Hz, 1H), 7.95 (s, 1H), 7.39 (d, $J = 9.1$ Hz, 1H), 7.12 (d, $J = 8.7$ Hz, 2H), 6.88 (d, $J = 8.7$ Hz, 2H), 5.31 (s, 2H), 3.95 (s, 3H), 3.80 (s, 3H); ^{13}C NMR (101 MHz, CDCl_3): δ 164.4, 159.9, 143.5, 139.3, 137.1, 128.8, 126.6, 126.1, 118.9, 118.5, 114.6, 110.6, 109.8, 55.4, 51.5, 50.8; MS (m/z): 340 (M^+); Anal. Calcd for $\text{C}_{18}\text{H}_{16}\text{N}_2\text{O}_5$: C, 63.53; H, 4.74; N, 8.23. Found: C, 63.49; H, 4.74; N, 8.21.

3.8.12. Methyl 1-(4-Chlorobenzyl)-5-nitro-1H-indole-3-carboxylate (17l)

Yield: 279 mg (81%) as a light yellow solid, m.p. 167–169 °C; IR: 1706, 1611, 1537, 1342 cm^{-1} ; ^1H NMR (400 MHz, CDCl_3): δ 9.07 (d, $J = 2.2$ Hz, 1H), 8.13 (dd, $J = 9.1, 2.2$ Hz, 1H), 7.96 (s, 1H), 7.33 (d, $J = 8.5$ Hz, 2H), 7.32 (d, $J = 9.1$ Hz, 1H), 7.09 (d, $J = 8.5$ Hz, 2H), 5.37 (s, 2H), 3.96 (s, 3H); ^{13}C NMR (101 MHz, CDCl_3): δ 164.2, 149.6, 139.2, 137.1, 134.7, 133.3, 129.5, 128.4, 126.1, 119.0, 118.7, 110.5, 110.2, 51.6, 50.6; MS (m/z): 344 (M^+); Anal. Calcd for $\text{C}_{17}\text{H}_{13}\text{ClN}_2\text{O}_4$: C, 59.23; H, 3.80; N, 8.13. Found: C, 59.16; H, 3.77; N, 8.07.

3.8.13. Methyl 5-Nitro-1-((4-trifluoromethyl)benzyl)-1H-indole-3-carboxylate (17m)

Yield: 336 mg (89%) as a light yellow solid, m.p. 162–164 °C; IR: 1707, 1616, 1538, 1343, 1325 cm^{-1} ; ^1H NMR (400 MHz, CDCl_3): δ 9.11 (d, $J = 2.3$ Hz, 1H), 8.15 (dd, $J = 9.1, 2.3$ Hz, 1H), 7.99 (s, 1H), 7.62 (d, $J = 8.1$ Hz, 2H), 7.43 (s, 1H), 7.32 (d, $J = 9.1$ Hz, 1H), 7.24 (dt, $J = 8.1$ Hz, 1H), 5.47 (s, 2H), 3.97 (s, 3H); ^{13}C NMR (101 MHz, CDCl_3): δ 164.1, 143.7, 139.2, 138.9, 137.1, 131.0 (q, $J = 32.8$ Hz), 127.2, 126.3 (q, $J = 3.7$ Hz), 126.1, 123.7 (q, $J = 272.4$ Hz), 119.1, 118.8, 110.5, 110.4, 51.6, 50.7; MS (m/z): 378 (M^+); Anal. Calcd for $\text{C}_{18}\text{H}_{13}\text{F}_3\text{N}_2\text{O}_4$: C, 57.15; H, 3.46; N, 7.41. Found: C, 57.24; H, 3.49; N, 7.30.

3.8.14. Methyl 5-Nitro-1-(3-nitrobenzyl)-1H-indole-3-carboxylate (17n)

Yield: 323 mg (91%) as a yellow solid, m.p. 147–149 °C; IR: 1706, 1618, 534, 1344 cm^{-1} ; ^1H NMR (400 MHz, CDCl_3): δ 9.11 (d, $J = 2.3$ Hz, 1H), 8.24 (d, $J = 8.1$ Hz, 1H), 8.16 (dd, $J = 9.1, 2.3$ Hz, 1H), 8.08 (br s, 1H), 8.02 (s, 1H), 7.56 (t, $J = 8.0$ Hz, 1H), 7.41 (d, $J = 8.0$ Hz,

1H), 7.33 (t, $J = 9.1$ Hz, 1H), 5.52 (s, 2H), 3.98 (s, 3H); ^{13}C NMR (101 MHz, CDCl_3): δ 164.1, 148.8, 143.8, 139.1, 137.1, 136.9, 132.6, 130.5, 126.2, 123.7, 121.9, 119.2, 119.0, 110.8, 110.2, 51.7, 50.4; MS (m/z): 355 (M^+); Anal. Calcd for $\text{C}_{17}\text{H}_{13}\text{N}_3\text{O}_6$: C, 57.47; H, 3.69; N, 11.83. Found: C, 57.39; H, 3.65; N, 11.72.

3.8.15. Methyl 1-Amino-5-nitro-1H-indole-3-carboxylate (17o)

Yield: 195 mg (83%) as a tan solid, m.p. 199–200 °C; IR: 3333, 3125, 1698 cm^{-1} ; ^1H NMR (400 MHz, $\text{DMSO}-d_6$): δ 8.86 (d, $J = 2.3$ Hz, 1H), 8.19 (s, 1H), 8.18 (dd, $J = 9.1, 2.3$ Hz, 1H), 7.75 (d, $J = 9.1$ Hz, 1H), 6.49 (s, 2H), 3.86 (s, 3H); ^{13}C NMR (101 MHz, $\text{DMSO}-d_6$): δ 163.0, 142.0, 139.2, 138.5, 122.5, 117.1, 116.4, 111.1, 104.3, 50.6; MS (m/z): 235 (M^+); Anal. Calcd for $\text{C}_{10}\text{H}_9\text{N}_3\text{O}_4$: C, 51.07; H, 3.86; N, 17.87. Found: C, 51.08; H, 3.83; N, 17.77.

3.9. Reactions with Methyl 2-(5-Cyano-2-fluorophenyl)acrylate (10)

3.9.1. Methyl 5-cyano-1-hexyl-1H-indole-3-carboxylate (18a)

Yield: 210 mg (74%) as a white solid, m.p. 71–73 °C; IR: 2223, 1705, 1612 cm^{-1} ; ^1H NMR (400 MHz, CDCl_3): δ 8.53 (br s, 1H), 7.92 (s, 1H), 7.51 (dd, $J = 8.6, 1.6$ Hz, 1H), 7.42 (dd, $J = 8.6, 0.8$ Hz, 1H), 4.15 (t, $J = 7.1$ Hz, 2H), 3.94 (s, 3H), 1.88 (quintet, $J = 7.1$ Hz, 2H), 1.31 (m, 6H), 0.87 (t, $J = 6.8$ Hz, 3H); ^{13}C NMR (101 MHz, CDCl_3): δ 164.6, 138.0, 136.1, 127.4, 126.3, 125.6, 120.2, 111.0, 108.0, 105.1, 51.4, 47.3, 31.2, 29.7, 26.4, 22.4, 14.1; MS (m/z): 284 (M^+); Anal. Calcd for $\text{C}_{17}\text{H}_{20}\text{N}_2\text{O}_2$: C, 71.81; H, 7.09; N, 9.85. Found: C, 71.87; H, 7.13; N, 9.73.

3.9.2. Methyl 5-Cyano-1-isobutyl-1H-indole-3-carboxylate (18b)

Yield: 172 mg (67%) as a white solid, m.p. 70–72 °C; IR: 2223, 1705, 1612 cm^{-1} ; ^1H NMR (400 MHz, CDCl_3): δ 8.53 (br s, 1H), 7.90 (s, 1H), 7.50 (dd, $J = 8.6, 1.6$ Hz, 1H), 7.42 (dd, $J = 8.6, 0.7$ Hz, 1H), 3.98 (d, $J = 7.4$ Hz, 2H), 3.94 (s, 3H), 2.21 (nonet, $J = 6.9$ Hz, 1H), 0.95 (d, $J = 6.7$ Hz, 6H); ^{13}C NMR (101 MHz, CDCl_3): δ 164.6, 138.3, 136.6, 127.4, 126.3, 125.6, 120.2, 111.2, 108.0, 105.1, 54.8, 51.4, 29.4, 20.1; MS (m/z): 256 (M^+); Anal. Calcd for $\text{C}_{15}\text{H}_{16}\text{N}_2\text{O}_2$: C, 70.29; H, 6.29; N, 10.93. Found: C, 70.26; H, 6.27; N, 10.87.

3.9.3. Methyl 5-Cyano-1-cyclopropyl-1H-indole-3-carboxylate (18d)

Yield: 187 mg (78%) as a white solid, m.p. 132–134 °C; IR: 2222, 1706, 1614 cm^{-1} ; ^1H NMR (400 MHz, CDCl_3): δ 8.48 (br s, 1H), 7.94 (s, 1H), 7.65 (dd, $J = 8.5, 0.8$ Hz, 1H), 7.51 (dd, $J = 8.5, 1.6$ Hz, 1H), 3.92 (s, 3H), 3.45 (apparent septet, $J = 3.6$ Hz, 1H), 1.21 (m, 2H), 1.06 (m, 2H); ^{13}C NMR (101 MHz, CDCl_3): δ 164.4, 139.5, 136.4, 127.3, 126.4, 125.8, 120.2, 111.8, 108.0, 105.5, 51.4, 27.8, 6.4; MS (m/z): 240 (M^+); Anal. Calcd for $\text{C}_{14}\text{H}_{12}\text{N}_2\text{O}_2$: C, 69.99; H, 5.03; N, 11.66. Found: C, 69.94; H, 4.97; N, 11.59.

3.9.4. Methyl 5-Cyano-1-cyclohexyl-1H-indole-3-carboxylate (18e)

Yield: 223 mg (79%) as a white solid, m.p. 132–134 °C; IR: 2223, 1705, 1614 cm^{-1} ; ^1H NMR (400 MHz, CDCl_3): δ 8.53 (br s, 1H), 8.05 (s, 1H), 7.50 (dd, $J = 8.6, 1.6$ Hz, 1H), 7.47 (dd, $J = 8.6, 0.8$ Hz, 1H), 4.25 (tt, $J = 11.9, 3.7$ Hz, 1H), 3.94 (s, 3H), 2.17 (d, $J = 12.8$ Hz, 2H), 2.00 (dt, $J = 13.5, 3.5$ Hz, 2H), 1.84 (dd, $J = 13.2$ Hz, 1H), 1.76 (qd, $J = 13.2, 3.5$ Hz, 2H), 1.53 (qt, $J = 13.2, 3.5$ Hz, 2H), 1.33 (qt, $J = 13.0, 3.5$ Hz, 1H); ^{13}C NMR (101 MHz, CDCl_3): δ 164.7, 137.7, 132.9, 127.4, 126.3, 125.4, 120.3, 111.0, 108.1, 105.1, 56.1, 51.3, 33.4, 25.7, 25.3; MS (m/z): 282 (M^+); Anal. Calcd for $\text{C}_{17}\text{H}_{18}\text{N}_2\text{O}_2$: C, 72.32; H, 6.43; N, 9.92. Found: C, 72.34; H, 6.44; N, 9.85.

3.9.5. Methyl 5-Cyano-1-phenethyl-1H-indole-3-carboxylate (18g)

Yield: 277 mg (91 %) as a white solid, m.p. 112–114 °C; IR: 2222, 1702, 1615 cm^{-1} ; ^1H NMR (400 MHz, CDCl_3): δ 8.51 (s, 1H), 7.73 (s, 1H), 7.45 (d, $J = 8.5$ Hz, 1H), 7.30 (d, $J = 8.5$ Hz, 1H), 7.27–7.20 (complex, 3H), 7.04–6.96 (complex, 2H), 4.42 (t, $J = 7.0$ Hz, 2H), 3.91 (s, 3H), 3.13 (t, $J = 7.0$ Hz, 2H); ^{13}C NMR (101 MHz, CDCl_3): δ 164.5, 137.9, 137.1, 136.1, 128.9, 128.6, 127.4, 127.3, 126.2, 125.7, 120.2, 110.9, 108.1, 105.1, 51.4, 48.9, 36.5; MS (m/z):

304 (M^+); Anal. Calcd for $C_{19}H_{16}N_2O_2$: C, 74.98; H, 5.30; N, 9.20. Found: C, 74.95; H, 5.28; N, 9.14.

3.9.6. Methyl 1-Benzyl-5-cyano-1*H*-indole-3-carboxylate (**18h**)

Yield: 255 mg (88%) as a white solid, m.p. 131–133 °C; IR: 2223, 1705, 1614 cm^{-1} ; 1H NMR (400 MHz, $CDCl_3$): δ 8.55 (d, $J = 1.5$ Hz, 1H), 7.94 (s, 1H), 7.47 (dd, $J = 8.5, 1.5$ Hz, 1H), 7.40–7.32 (complex, 4H), 7.15–7.13 (complex, 2H), 5.36 (s, 2H), 3.93 (s, 3H); ^{13}C NMR (101 MHz, $CDCl_3$): δ 164.5, 138.2, 136.4, 134.9, 129.2, 128.6, 127.5, 127.1, 126.5, 125.9, 120.1, 111.3, 108.6, 105.4, 51.4, 51.1; MS (m/z): 290 (M^+); Anal. Calcd for $C_{18}H_{14}N_2O_2$: C, 74.47; H, 4.86; N, 9.65. Found: C, 74.44; H, 4.86; N, 9.63.

3.9.7. Methyl 5-Cyano-1-(4-methylbenzyl)-1*H*-indole-3-carboxylate (**18i**)

Yield: 246 mg (81%) as a white solid, m.p. 139–141 °C; IR: 2222, 1704, 1615 cm^{-1} ; 1H NMR (400 MHz, $CDCl_3$): δ 8.54 (br s, 1H), 7.92 (s, 1H), 7.46 (dd, $J = 8.5, 1.6$ Hz, 1H), 7.38 (dd, $J = 8.5, 0.8$ Hz, 1H), 7.15 (d, $J = 7.8$ Hz, 2H), 7.05 (d, $J = 7.8$ Hz, 2H), 5.31 (s, 2H), 3.93 (s, 3H), 2.33 (s, 3H); ^{13}C NMR (101 MHz, $CDCl_3$): δ 164.5, 138.5, 138.2, 136.4, 131.8, 129.9, 127.4, 127.2, 126.5, 125.9, 120.1, 111.4, 108.4, 105.4, 51.4, 50.9, 21.1; MS (m/z): 304 (M^+); Anal. Calcd for $C_{19}H_{16}N_2O_2$: C, 74.98; H, 5.30; N, 9.20. Found: C, 74.94; H, 5.29; N, 9.16.

3.9.8. Methyl 5-Cyano-1-(3-methoxybenzyl)-1*H*-indole-3-carboxylate (**18j**)

Yield: 265 mg (83%) as a white solid, m.p. 118–120 °C; IR: 2837, 2222, 1702, 1612 cm^{-1} ; 1H NMR (400 MHz, $CDCl_3$): δ 8.55 (br s, 1H), 7.94 (s, 1H), 7.47 (dd, $J = 8.6, 1.6$ Hz, 1H), 7.37 (dd, $J = 8.6, 0.7$ Hz, 1H), 7.27 (t, $J = 8.1$ Hz, 1H), 6.86 (dd, $J = 8.1, 2.5$ Hz, 1H), 6.71 (d, $J = 7.6$ Hz, 1H), 6.65 (br t, $J = 2.1$ Hz, 1H), 5.32 (s, 2H), 3.94 (s, 3H), 3.75 (s, 3H); ^{13}C NMR (101 MHz, $CDCl_3$): δ 164.5, 160.2, 138.2, 136.4, 130.4, 127.5, 126.5, 126.0, 120.1, 119.2, 113.5, 113.2, 111.3, 108.6, 105.5, 55.3, 51.4, 51.0 (one aromatic carbon unresolved); MS (m/z): 320 (M^+); Anal. Calcd for $C_{19}H_{16}N_2O_3$: C, 71.24; H, 5.03; N, 8.74. Found: C, 71.17; H, 4.99; N, 8.68.

3.9.9. Methyl 5-Cyano-1-(4-methoxybenzyl)-1*H*-indole-3-carboxylate (**18k**)

Yield: 285 mg (89%) as a white solid, m.p. 130–132 °C; IR: 2840, 2222, 1703, 1613 cm^{-1} ; 1H NMR (400 MHz, $CDCl_3$): δ 8.54 (br s, 1H), 7.90 (s, 1H), 7.47 (dd, $J = 8.6, 1.6$ Hz, 1H), 7.40 (dd, $J = 8.6, 0.7$ Hz, 1H), 7.11 (d, $J = 8.7$ Hz, 2H), 6.88 (d, $J = 8.7$ Hz, 2H), 5.28 (s, 2H), 3.93 (s, 3H), 3.79 (s, 3H); ^{13}C NMR (101 MHz, $CDCl_3$): δ 164.5, 159.8, 138.1, 136.2, 128.7, 127.4, 126.7, 126.5, 125.8, 120.1, 114.6, 111.3, 108.4, 105.4, 55.3, 51.4, 50.6; MS (m/z): 320 (M^+); Anal. Calcd for $C_{19}H_{16}N_2O_3$: C, 71.24; H, 5.03; N, 8.74. Found: C, 71.23; H, 5.01; N, 8.66.

3.9.10. Methyl 1-(4-Chlorobenzyl)-5-cyano-1*H*-indole-3-carboxylate (**18l**)

Yield: 282 mg (87%) as a white solid, m.p. 193–195 °C; IR: 2223, 1704, 1614 cm^{-1} ; 1H NMR (400 MHz, $CDCl_3$): δ 8.54 (br s, 1H), 7.93 (s, 1H), 7.46 (dd, $J = 8.6, 1.6$ Hz, 1H), 7.34 (dd, $J = 8.6, 0.7$ Hz, 1H), 7.31 (d, $J = 8.5$ Hz, 2H), 7.08 (d, $J = 8.5$ Hz, 2H), 5.34 (s, 2H), 3.93 (s, 3H); ^{13}C NMR (101 MHz, $CDCl_3$): δ 164.3, 138.0, 136.2, 134.6, 133.4, 129.5, 128.4, 127.5, 126.5, 126.0, 120.0, 111.2, 108.8, 105.6, 51.5, 50.4; MS (m/z): 324 (M^+); Anal. Calcd for $C_{18}H_{13}ClN_2O_2$: C, 66.57; H, 4.03; N, 8.63. Found: C, 66.57; H, 4.02; N, 8.59.

3.9.11. Methyl 5-Cyano-1-(3-nitrobenzyl)-1*H*-indole-3-carboxylate (**18n**)

Yield: 308 mg (92%) as a light yellow solid, m.p. 165–167 °C; IR: 2223, 1702, 1614, 1533, 1350 cm^{-1} ; 1H NMR (400 MHz, $CDCl_3$): δ 8.57 (br s, 1H), 8.21 (dd, $J = 8.2, 1.3$ Hz, 1H), 8.07 (br t, $J = 2.1$ Hz, 1H), 7.98 (s, 1H), 7.55 (t, $J = 8.0$ Hz, 1H), 7.49 (dd, $J = 8.6, 1.6$ Hz, 1H), 7.39 (d, $J = 7.7$ Hz, 1H), 7.33 (d, $J = 8.6$ Hz, 1H), 5.49 (s, 2H), 3.95 (s, 3H); ^{13}C NMR (101 MHz, $CDCl_3$): δ 164.2, 148.8, 137.9, 137.2, 136.1, 132.6, 130.5, 127.8, 126.6, 126.4, 123.7, 121.9, 119.8, 111.0, 109.5, 106.0, 51.6, 50.2; MS (m/z): 335 (M^+); Anal. Calcd for $C_{18}H_{13}N_3O_4$: C, 64.48; H, 3.91; N, 12.53. Found: C, 64.42; H, 3.88; N, 12.47.

3.10. Methyl 2-(5-Carbomethoxy-2-fluorophenyl)acrylate (13)

3.10.1. Dimethyl 1-Hexyl-1*H*-indole-3,5-dicarboxylate (19a)

Yield: 212 mg (67%) as a white solid, m.p. 64–66 °C; IR: 1719, 1634 cm⁻¹; ¹H NMR (400 MHz, CDCl₃): δ 8.88 (d, *J* = 1.7 Hz, 1H), 7.98 (dd, *J* = 8.7, 1.7 Hz, 1H), 7.87 (s, 1H), 7.37 (d, *J* = 8.7 Hz, 1H), 4.14 (t, *J* = 7.2 Hz, 2H), 3.95 (s, 3H), 3.94 (s, 3H), 1.86 (quintet, *J* = 7.2 Hz, 2H), 1.31 (m, 6H), 0.86 (t, *J* = 6.8 Hz, 3H); ¹³C NMR (101 MHz, CDCl₃): δ 167.9, 165.1, 139.0, 135.6, 126.1, 124.5, 124.1, 123.8, 109.8, 108.3, 52.0, 51.2, 47.2, 31.3, 29.9, 26.5, 22.5, 14.0; MS (*m/z*): 317 (M⁺); Anal. Calcd for C₁₈H₂₃NO₄: C, 68.12; H, 7.30; N, 4.41. Found: C, 68.19; H, 7.31; N, 4.33.

3.10.2. Dimethyl 1-Isobutyl-1*H*-indole-3,5-dicarboxylate (19b)

Yield: 199 mg (69%) as a white solid, m.p. 125–126 °C; IR: 1717, 1631 cm⁻¹; ¹H NMR (400 MHz, CDCl₃): δ 8.88 (dd, *J* = 1.7, 0.7 Hz, 1H), 7.98 (dd, *J* = 8.7, 1.7 Hz, 1H), 7.86 (s, 1H), 7.37 (dd, *J* = 8.7, 0.7 Hz, 1H), 3.96 (d, *J* = 7.2 Hz, 2H), 3.952 (s, 3H), 3.948 (s, 3H), 2.22 (septet, *J* = 6.8 Hz, 1H), 0.95 (d, *J* = 6.7 Hz, 6H); ¹³C NMR (101 MHz, CDCl₃): δ 167.9, 165.1, 139.2, 136.1, 126.0, 124.5, 124.1, 123.9, 110.0, 108.3, 54.8, 52.0, 51.2, 29.3, 20.2; MS (*m/z*): 289 (M⁺); Anal. Calcd for C₁₆H₁₉NO₄: C, 66.42; H, 6.62; N, 4.84. Found: C, 66.47; H, 6.65; N, 4.78.

3.10.3. Dimethyl 1-Allyl-1*H*-indole-3,5-dicarboxylate (19c)

Yield: 218 mg (80 %) as a white solid, m.p. 102–103 °C; IR: 1710, 1645, 1617 cm⁻¹; ¹H NMR (400 MHz, CDCl₃): δ 8.88 (d, *J* = 1.7 Hz, 1H), 7.98 (dd, *J* = 8.7, 1.7 Hz, 1H), 7.88 (s, 1H), 7.36 (d, *J* = 8.7 Hz, 1H), 6.00 (ddt, *J* = 15.8, 10.3, 5.4 Hz, 1H), 5.60 (d, *J* = 10.3 Hz, 1H), 5.35 (d, *J* = 15.8 Hz, 1H), 4.78 (d, *J* = 5.4 Hz, 2H), 3.95 (s, 3H), 3.94 (s, 3H); ¹³C NMR (101 MHz, CDCl₃): δ 167.9, 165.0, 139.0, 135.6, 131.7, 126.1, 124.5, 124.2, 124.0, 118.9, 110.0, 108.7, 52.0, 51.3, 49.5; MS (*m/z*): 273 (M⁺); Anal. Calcd for C₁₅H₁₅NO₄: C, 65.92; H, 5.53; N, 5.13. Found: C, 65.87; H, 5.48; N, 5.09.

3.10.4. Dimethyl 1-Cyclopropyl-1*H*-indole-3,5-dicarboxylate (19d)

Yield: 166 mg (61%) as a white solid, m.p. 136–137 °C; IR: 1709, 1621 cm⁻¹; ¹H NMR (400 MHz, CDCl₃): δ 8.84 (d, *J* = 1.7 Hz, 1H), 8.00 (dd, *J* = 8.7, 1.7 Hz, 1H), 7.90 (s, 1H), 7.60 (d, *J* = 8.7 Hz, 1H), 3.95 (s, 3H), 3.93 (s, 3H), 3.44 (m, 1H), 1.17 (m, 2H), 1.05 (m, 2H); ¹³C NMR (101 MHz, CDCl₃): δ 167.9, 165.0, 140.4, 135.9, 126.1, 124.4, 124.3, 124.2, 110.6, 108.4, 52.0, 51.2, 27.8, 6.3; MS (*m/z*): 273 (M⁺); Anal. Calcd for C₁₅H₁₅NO₄: C, 65.92; H, 5.53; N, 5.13. Found: C, 65.81; H, 5.55; N, 5.06.

3.10.5. Dimethyl 1-Cyclohexyl-1*H*-indole-3,5-dicarboxylate (19e)

Yield: 205 mg (65%) as a white solid, m.p. 138–140 °C; IR: 1703, 1618 cm⁻¹; ¹H NMR (400 MHz, CDCl₃): δ 8.88 (d, *J* = 1.7 Hz, 1H), 8.01 (s, 1H), 7.98 (dd, *J* = 8.7, 1.7 Hz, 1H), 7.42 (d, *J* = 8.7 Hz, 1H), 4.26 (tt, *J* = 11.9, 3.7 Hz, 1H), 3.95 (s, 3H), 3.94 (s, 3H), 2.18 (d, *J* = 12.8 Hz, 2H), 1.98 (dd, *J* = 13.5, 3.5 Hz, 2H), 1.83 (d, *J* = 13.2 Hz, 1H), 1.74 (qd, *J* = 13.2, 3.5 Hz, 2H), 1.53 (qt, *J* = 13.2, 3.5 Hz, 2H), 1.33 (tt, *J* = 13.0, 3.5 Hz, 1H); ¹³C NMR (101 MHz, CDCl₃): δ 167.9, 165.2, 138.6, 132.4, 126.0, 124.5, 123.88, 123.86, 109.8, 108.4, 54.9, 52.0, 51.2, 33.4, 25.7, 25.4; MS (*m/z*): 315 (M⁺); Anal. Calcd for C₁₈H₂₁NO₄: C, 68.55; H, 6.71; N, 4.44. Found: C, 68.61; H, 6.73; N, 4.42.

3.10.6. Dimethyl 1-Phenethyl-1*H*-indole-3,5-dicarboxylate (19g)

Yield: 300 mg (89 %) as a white solid, m.p. 152–154 °C; IR: 1706 cm⁻¹; ¹H NMR (400 MHz, CDCl₃): δ 8.87 (d, *J* = 1.7 Hz, 1H), 7.96 (dd, *J* = 8.7, 1.7 Hz, 1H), 7.70 (s, 1H), 7.30 (d, *J* = 8.7 Hz, 1H), 7.28–7.21 (complex, 3H), 7.04–7.01 (complex, 2H), 4.39 (t, *J* = 7.2 Hz, 2H), 3.95 (s, 3H), 3.92 (s, 3H), 3.14 (t, *J* = 7.2 Hz, 2H); ¹³C NMR (101 MHz, CDCl₃): δ 167.9, 165.0, 138.8, 137.3, 135.6, 128.8, 128.6, 127.1, 126.1, 124.5, 124.2, 123.9, 109.7, 108.4, 52.0, 51.2, 48.8, 36.5; MS (*m/z*): 337 (M⁺); Anal. Calcd for C₂₀H₁₉NO₄: C, 71.20; H, 5.68; N, 4.15. Found: C, 71.18; H, 5.68; N, 4.10.

3.10.7. Dimethyl 1-Benzyl-1*H*-indole-3,5-dicarboxylate (19h)

Yield: 278 mg (86%) as a white solid, m.p. 140–142 °C; IR: 1709, 1611 cm⁻¹; ¹H NMR (400 MHz, CDCl₃): δ 8.90 (d, *J* = 1.7 Hz, 1H), 7.94 (dd, *J* = 8.7, 1.7 Hz, 1H), 7.89 (s, 1H), 7.37–7.30 (complex, 4H), 7.17–7.13 (complex, 2H), 5.35 (s, 2H), 3.942 (s, 3H), 3.937 (s, 3H); ¹³C NMR (101 MHz, CDCl₃): δ 167.8, 165.0, 139.2, 135.9, 135.4, 129.1, 128.4, 127.1, 126.2, 124.5, 124.4, 124.1, 110.1, 109.0, 52.0, 51.3, 50.9; MS (*m/z*): 323 (M⁺); Anal. Calcd for C₁₉H₁₇NO₄: C, 70.58; H, 5.30; N, 4.33. Found: C, 70.56; H, 5.27; N, 4.25.

3.10.8. Dimethyl 1-(4-Methylbenzyl)-1*H*-indole-3,5-dicarboxylate (19i)

Yield: 276 mg (82%) as a white solid, m.p. 146–147 °C; IR: 1710, 1609 cm⁻¹; ¹H NMR (400 MHz, CDCl₃): δ 8.89 (d, *J* = 1.7 Hz, 1H), 7.95 (dd, *J* = 8.7, 1.7 Hz, 1H), 7.87 (s, 1H), 7.34 (d, *J* = 8.7 Hz, 1H), 7.14 (d, *J* = 7.9 Hz, 2H), 7.05 (d, *J* = 7.9 Hz, 2H), 5.29 (s, 2H), 3.94 (s, 3H), 3.93 (s, 3H), 2.32 (s, 3H); ¹³C NMR (101 MHz, CDCl₃): δ 167.8, 165.0, 139.1, 138.3, 135.8, 132.3, 129.8, 127.2, 126.2, 124.5, 124.3, 124.1, 110.1, 108.8, 52.0, 51.2, 50.7, 21.1; MS (*m/z*): 337 (M⁺); Anal. Calcd for C₂₀H₁₉NO₄: C, 71.20; H, 5.68; N, 4.15. Found: C, 71.14; H, 5.64; N, 4.11.

3.10.9. Dimethyl 1-(3-Methoxybenzyl)-1*H*-indole-3,5-dicarboxylate (19j)

Yield: 303 mg (86%) as a white solid, m.p. 131–132 °C; IR: 2831, 1705, 1622 cm⁻¹; ¹H NMR (400 MHz, CDCl₃): δ 8.89 (br s, 1H), 7.96 (dd, *J* = 8.7, 1.7 Hz, 1H), 7.89 (s, 1H), 7.34 (d, *J* = 8.7 Hz, 1H), 7.25 (t, *J* = 8.1 Hz, 1H), 6.84 (t, *J* = 2.5 Hz, 1H), 6.74 (d, *J* = 7.5 Hz, 1H), 6.66 (t, *J* = 2.5 Hz, 1H), 5.32 (s, 2H), 3.945 (s, 3H), 3.941 (s, 3H), 3.74 (s, 3H); ¹³C NMR (101 MHz, CDCl₃): δ 167.8, 165.0, 160.1, 139.2, 136.9, 135.9, 130.2, 126.2, 124.5, 124.4, 124.2, 119.3, 113.4, 113.0, 110.1, 109.0, 55.3, 52.0, 51.3, 50.9; MS (*m/z*): 353 (M⁺); Anal. Calcd for C₂₀H₁₉NO₅: C, 67.98; H, 5.42; N, 3.96. Found: C, 67.91; H, 5.40; N, 3.88.

3.10.10. Dimethyl 1-(4-Methoxybenzyl)-1*H*-indole-3,5-dicarboxylate (19k)

Yield: 304 mg (86%) as a white solid, m.p. 135–136 °C; IR: 2833, 1705, 1620 cm⁻¹; ¹H NMR (400 MHz, CDCl₃): δ 8.89 (d, *J* = 1.7 Hz, 1H), 7.96 (dd, *J* = 8.7, 1.7 Hz, 1H), 7.86 (s, 1H), 7.36 (d, *J* = 8.7 Hz, 1H), 7.12 (d, *J* = 8.6 Hz, 2H), 6.87 (d, *J* = 8.6 Hz, 2H), 5.28 (s, 2H), 3.94 (s, 3H), 3.93 (s, 3H), 3.79 (s, 3H); ¹³C NMR (101 MHz, CDCl₃): δ 167.8, 165.0, 159.7, 139.1, 135.7, 128.7, 127.2, 126.3, 124.5, 124.3, 124.1, 114.5, 110.1, 108.8, 55.3, 52.0, 51.3, 50.5; MS (*m/z*): 353 (M⁺); Anal. Calcd for C₂₀H₁₉NO₅: C, 67.98; H, 5.42; N, 3.96. Found: C, 68.02; H, 5.41; N, 3.93.

3.10.11. Dimethyl 1-(4-Chlorobenzyl)-1*H*-indole-3,5-dicarboxylate (19l)

Yield: 286 mg (80%) as a white solid, m.p. 140–142 °C; IR: 1709, 1617 cm⁻¹; ¹H NMR (400 MHz, CDCl₃): δ 8.90 (d, *J* = 1.7 Hz, 1H), 7.96 (dd, *J* = 8.7, 1.7 Hz, 1H), 7.88 (s, 1H), 7.31 (d, *J* = 8.5 Hz, 2H), 7.29 (d, *J* = 8.7 Hz, 1H), 7.08 (d, *J* = 8.5 Hz, 2H), 5.32 (s, 2H), 3.946 (s, 3H), 3.943 (s, 3H); ¹³C NMR (101 MHz, CDCl₃): δ 167.7, 164.9, 139.0, 135.6, 134.4, 133.9, 129.3, 128.4, 126.2, 124.6, 124.5, 124.3, 110.0, 109.2, 52.0, 51.3, 50.3; MS (*m/z*): 357 (M⁺); Anal. Calcd for C₁₉H₁₆ClNO₄: C, 63.78; H, 4.51; N, 3.91. Found: C, 63.72; H, 4.47; N, 3.83.

3.10.12. Dimethyl 1-(3-Nitrobenzyl)-1*H*-indole-3,5-dicarboxylate (19n)

Yield: 334 mg (91%) as a white solid, m.p. 234–236 °C; IR: 1695, 1615, 1514, 1330 cm⁻¹; ¹H NMR (400 MHz, CDCl₃): δ 8.92 (d, *J* = 1.7 Hz, 1H), 8.19 (d, *J* = 8.1 Hz, 1H), 8.08 (s, 1H), 7.97 (dd, *J* = 8.7, 17 Hz, 1H), 7.93 (s, 1H), 7.52 (t, *J* = 8.0 Hz, 1H), 7.38 (d, *J* = 8.1 Hz, 1H), 7.28 (d, *J* = 8.7 Hz, 1H), 5.48 (s, 2H), 3.96 (s, 3H), 3.95 (s, 3H); ¹³C NMR (101 MHz, CDCl₃): δ 167.6, 164.7, 148.7, 138.9, 137.7, 135.5, 132.6, 130.4, 126.3, 124.84, 124.80, 124.6, 123.5, 121.9, 109.9, 109.8, 52.1, 51.4, 50.1; MS (*m/z*): 368 (M⁺); Anal. Calcd for C₁₉H₁₆N₂O₆: C, 61.96; H, 4.38; N, 7.61. Found: C, 61.93; H, 4.39; N, 7.57.

4. Conclusions

A method has been developed for the efficient synthesis of 1-alkyl-1*H*-indole-3-carboxylic esters that uses a domino aza-Michael-S_NAr-heteroaromatization sequence. Following synthesis of the substrates, the reaction was performed using an equimolar mixture of the acrylate and the amine in the presence of 2 equiv of K₂CO₃ in anhydrous DMF. The reaction proceeded at room temperature for substrates with nitro and cyano activated S_NAr acceptor rings and at 50–90 °C for rings activated by an ester. The amines were all primary alkylamines with no restriction on the structure of the alkyl group. Anilines did not undergo the ring formation due to their reduced nucleophilicity. The entire process occurred in a single reaction flask to give the aromatized product. The anticipated indoline products were not produced, but instead, oxidation to the aromatic indoles was observed. The heteroaromatization is believed to be promoted by oxygen dissolved in the DMF solvent or introduced during removal of samples for TLC analysis. In no case was an indoline observed or isolated from the reaction. Hydrazine reacted with the nitro activated substrate, but failed for substrates with less active S_NAr acceptor rings, giving products resulting from reaction with the cyano and ester substituents. The corresponding 2-arylacrylonitrile substrate polymerized under the aldol conditions with formalin while the phenylsulfonyl precursor to the vinyl sulfone failed to undergo aldol condensation with formaldehyde using K₂CO₃ as the base.

Supplementary Materials: The following supporting information can be downloaded at <https://www.mdpi.com/article/10.3390/molecules27206998/s1>, copies of the ¹H-NMR and ¹³C-NMR spectra for all new compounds.

Author Contributions: Project conception, project administration, formal analysis and writing the manuscript text, R.A.B.; investigation, methodology, analysis and writing the experimental, E.A. and S.F.; reviewing and editing, R.A.B., E.A. and S.F. All authors have read and agreed to the published version of the manuscript.

Funding: Financial support for this work was obtained from the Oklahoma State University Foundation and the College of Arts and Sciences at Oklahoma State University. The authors are indebted to the OSU College of Arts and Sciences for funds to purchase several departmental instruments including an FT-IR and a 400 MHz NMR unit for the State-wide NMR facility. The NMR facility was initially established with support from the NSF (BIR-9512269), the Oklahoma State Regents for Higher Education, the W. M. Keck Foundation and Conoco, Inc.

Institutional Review Board Statement: Not applicable.

Informed Consent Statement: Not applicable.

Data Availability Statement: Not applicable.

Acknowledgments: E.A. wishes to thank the OSU Foundation for a K. D. Berlin Fellowship in Summer 2020. S.F., an undergraduate researcher, acknowledges support from R.A.B. in Summer 2022.

Conflicts of Interest: The authors declare no conflict of interest.

References

1. Navriti, N.; Silakari, O. Indoles as therapeutics of interest in medicinal chemistry: Bird's eye view. *Eur. J. Med. Chem.* **2017**, *134*, 159–184. [CrossRef]
2. Sravanthi, T.V.; Manju, S.I. Indoles—A promising scaffold for drug development. *Eur. J. Pharm. Sci.* **2016**, *91*, 1–10. [CrossRef] [PubMed]
3. Fleming, I.; Woolias, M. A benzyne route to indoles from *o*- or *m*-bromoaryl ketones. *J. Chem. Soc. Perkin Trans. 1* **1979**, 827–828. [CrossRef]
4. Ito, Y.; Kobayashi, K.; Saegusa, T. An efficient synthesis of indole. *J. Am. Chem. Soc.* **1977**, *99*, 3532–3534. [CrossRef]
5. Scriven, E.F.V.; Turnbull, K. Azides: Their preparation and synthetic uses. *Chem. Rev.* **1988**, *88*, 297–368. [CrossRef]
6. Hegedus, L.S.; Allen, G.F.; Bozell, J.J.; Waterman, E.L. Palladium-assisted intramolecular amination of olefins. Synthesis of nitrogen heterocycles. *J. Am. Chem. Soc.* **1978**, *100*, 5800–5807. [CrossRef]
7. Organic Chemistry Portal: Synthesis of Indoles. Available online: <https://www.organic-chemistry.org/synthesis/heterocycles/benzofused/indoles.htm> (accessed on 11 August 2022).

8. Tilstam, U.; Harre, M.; Heckrodt, T.; Weinmann, H. A mild efficient dehydrogenation of indolines. *Tetrahedron Lett.* **2001**, *42*, 5385–5387. [CrossRef]
9. Karki, M.; Araujo, H.C.; Magolan, J. Dehydroaromatization with V₂O₅. *Synth. Lett.* **2013**, *24*, 1675–1678. [CrossRef]
10. Gribble, G.W. Indolines to indoles by functionalized elimination in indole ring synthesis. In *Indole Ring Synthesis: From Natural Products to Drug Discovery*; Wiley: New York, NY, USA, 2016; pp. 553–557. [CrossRef]
11. Caddick, S.; Aboutayab, K.; Jenkins, K.; West, R.I. Intramolecular radical substitution reactions: A novel approach to fused [1,2-*a*]-indoles. *J. Chem. Soc., Perkin Trans. 1* **1996**, 675–682. [CrossRef]
12. Giles, P.R.; Rogers-Evans, M.; Soukup, M.; Knight, J. An improved process for the *N*-alkylation of indoles using chiral *N*-protected 2-methylaziridines. *Org. Proc. Res. Dev.* **2003**, *7*, 22–24. [CrossRef]
13. Bayindir, S.; Erdogan, E.; Kilic, H.; Aydin, O.; Saracoglu, N. Synthesis of *N*-alkylated indolines and indoles from indoline and aliphatic ketones. *J. Heterocycl. Chem.* **2015**, *52*, 1589–1594. [CrossRef]
14. Ling, L.; Cao, J.; Hu, J.; Zhang, H. Copper-catalyzed *N*-alkylation of indoles by *N*-tosylhydrazones. *RSC Adv.* **2017**, *7*, 27974–27980. [CrossRef]
15. Sun, L.; Zhang, X.; Wang, C.; Teng, H.; Ma, J.; Li, M.; Chen, H.; Jiang, H. Direct electrosynthesis of *N*-alkyl-C3-haloindoles using alkyl halide as both alkylating and halogenating building blocks. *Green Chem.* **2019**, *21*, 2732–2738. [CrossRef]
16. Augustine, R.L.; Gustavsen, A.J.; Wanat, S.F.; Pattison, I.C.; Houghton, K.S.; Koletar, G. Synthesis of α -monosubstituted indoles. *J. Org. Chem.* **1973**, *38*, 3004–3011. [CrossRef]
17. Bunce, R.A.; Randall, M.H.; Applegate, K.G. 2-Alkylindole-3-carboxylate esters by a tandem reduction-addition-elimination reaction. *Org. Prep. Proced. Int.* **2002**, *34*, 493–499. [CrossRef]
18. D’Ambra, T.E.; Estep, K.G.; Bell, M.R.; Eissenstat, M.A.; Josef, K.A.; Ward, S.J.; Haycock, D.A.; Baizman, E.R.; Casiano, F.M.; Beglin, N.C.; et al. Conformationally restrained analogs of pravastatin: Nanomolar potent, enantioselective, (aminoalkyl) indole agonists of the cannabinoid receptor. *J. Med. Chem.* **1992**, *35*, 124–135. [CrossRef]
19. Sun, Y.; Alexander, S.P.H.; Garle, M.J.; Gibson, C.L.; Hewitt, K.; Murphy, S.P.; Kendall, D.A.; Bennett, A.J. Cannabinoid activation of PPAR α ; a novel neuroprotective mechanism. *Br. J. Pharmacol.* **2007**, *152*, 734–743. [CrossRef]
20. Smith, V. Synthesis and pharmacology of *N*-alkyl-3-halonaphthoylindoles. *All Diss* **2008**, 253. Available online: https://tigerprints.clemson.edu/all_dissertations/253 (accessed on 7 September 2022).
21. Boriskin, Y.S.; Leneva, I.A.; Pécheur, E.-I.; Polyak, S.J. Arbidol: A broad-spectrum antiviral compound that blocks viral fusion. *Curr. Med. Chem.* **2008**, *15*, 997–1005. [CrossRef]
22. Liu, M. COVID-19 pandemic: Case studies and perspectives. In *Side Effects Annual*; Elsevier: Amsterdam, The Netherlands, 2020; Volume 42, pp. 291–297.
23. Behbehani, H.; Ibrahim, H.M.; Makhseed, S.; Mahmoud, H. Applications of 2-arylhydrazonitriles in synthesis: Preparation of new indole containing 1,2,3-triazole, pyrazole and pyrazolo[1,5-*a*]pyrimidine derivatives and evaluation of their antimicrobial activities. *Eur. J. Med. Chem.* **2011**, *46*, 1813–1820. [CrossRef]
24. Gale, D.J.; Wilshire, J.F.K. The preparation of sole polymethine astrazon dyes. *Aust. J. Chem.* **1970**, *23*, 1063–1068. [CrossRef]
25. Selvakumar, N.; Azhagan, A.M.; Srinivas, D.; Krishna, G.G. A direct synthesis of 2-arylpropenoic acid esters having nitro in the aromatic ring: A short synthesis of (\pm)-coerulescine and (\pm)-horsfiline. *Tetrahedron Lett.* **2002**, *43*, 9175–9178. [CrossRef]
26. Zhao, G.; Souers, A.J.; Voorbach, M.; Falls, H.D.; Droz, B.; Brodjian, S.; Lau, Y.Y.; Iyengar, R.R.; Gao, J.; Judd, A.S.; et al. Validation of diacyl glycerolacyltransferase I as a novel target for the treatment of obesity and dyslipidemia using a potent and selective small molecule inhibitor. *J. Med. Chem.* **2008**, *51*, 380–383. [CrossRef]
27. Clarke, H.T.; Read, R.R. *o*-Tolunitrile and *p*-tolunitrile. In *Organic Syntheses, Collective Volume 1*; Gilman, H., Blatt, A.H., Eds.; Wiley: New York, NY, USA, 1941; pp. 514–516. [CrossRef]
28. Marvel, C.S.; McElvain, S.M. *o*-Chlorotoluene and *p*-chlorotoluene. In *Organic Syntheses, Collective Volume 1*; Gilman, H., Blatt, A.H., Eds.; Wiley: New York, NY, USA, 1941; pp. 170–172. [CrossRef]
29. Bunce, R.A.; Rogers, D.; Nago, T.; Bryant, S.A. 4*H*-Benzopyrans by a tandem S_N2-S_NAr reaction. *J. Heterocycl. Chem.* **2008**, *45*, 547–550. [CrossRef]
30. Bunce, R.A.; Nago, T.; Sonobe, N.; Slaughter, L.M. Benzo-fused heterocycles and carbocycles by intramolecular S_NAr and tandem S_N2-S_NAr reactions. *J. Heterocycl. Chem.* **2008**, *45*, 551–557. [CrossRef]
31. Grossert, J.S.; Dubey, P.K.; Gill, G.H.; Cameron, S.; Gardner, P.A. The preparation, spectral properties, structures and base-induced cleavage reactions of some α -halo- β -ketosulfones. *Can. J. Chem.* **1984**, *62*, 967–968. [CrossRef]
32. Smith, M.B.; March, J. *March’s Advanced Organic Chemistry Reactions Mechanisms and Structure*, 6th ed.; Wiley-Interscience: Hoboken, NJ, USA, 2007; pp. 864–968.
33. Carey, F.A.; Sundberg, R.J. *Advanced Organic Chemistry Part A: Structure and Mechanisms*, 4th ed.; Kluwer Academic/Plenum: New York, NY, USA, 2000; pp. 293–294.
34. Achord, J.M.; Hussey, C.L. Determination of dissolved oxygen in nonaqueous electrochemical solvents. *Anal. Chem.* **1980**, *52*, 601–602. [CrossRef]
35. Annor-Gyamfi, J.K.; Ametsetor, E.; Meraz, K.; Bunce, R.A. Dihydroquinolines, dihydronaphthyridines and quinolones by domino reactions of Morita-Baylis-Hillman acetates. *Molecules* **2021**, *26*, 890. [CrossRef]

Article

Atom Economical Multi-Substituted Pyrrole Synthesis from Aziridine

Lingamurthy Macha, Ranjith Jala, Sang-Yun Na and Hyun-Joon Ha *

Department of Chemistry, Hankuk University of Foreign Studies, Yongin 17035, Korea

* Correspondence: hjha@hufs.ac.kr; Tel.: +82-31-330-4369

Abstract: Multi-substituted pyrroles are synthesized from regiospecific aziridine ring-opening and subsequent intramolecular cyclization with a carbonyl group at the γ -position in the presence of Lewis acid or protic acid. This method is highly atom economical where all the atoms of the reactants are incorporated into the final product with the removal of water. This new protocol is applied to the synthesis of various pyrroles, including natural products.

Keywords: aziridine; non-activated; nucleophilic; ring-opening; regioselectivity; pyrrole

1. Introduction

Pyrroles are molecules of great interest as key structural elements of various compounds, including pharmaceuticals and natural products [1,2]. For example, inonotus obliquus [3–5]. The white rot fungus that belongs to the family *Hymenochaetaceae* (*Basidiomycetes*) and is mainly distributed in Europe, Asia, and North America has been used for the treatment of gastrointestinal cancer, cardiovascular disease, and diabetes since the sixteenth century in Russia, Poland, and the Baltic countries. Moreover, the fungus has been reported to have anti-inflammatory [6], antioxidant [7–10], immunomodulatory [11], and hepatoprotective effects [12]. Some representative examples of 5-hydroxymethyl pyrrole-2-carbaldehydes found in the inonotus obliquus, sometimes referred to as 2-formylpyrroles or pyrrolines, are displayed in Figure 1.

Citation: Macha, L.; Jala, R.; Na, S.-Y.; Ha, H.-J. Atom Economical Multi-Substituted Pyrrole Synthesis from Aziridine. *Molecules* **2022**, *27*, 6869. <https://doi.org/10.3390/molecules27206869>

Academic Editor: Alexey M. Starostnikov

Received: 28 September 2022

Accepted: 11 October 2022

Published: 13 October 2022

Publisher's Note: MDPI stays neutral with regard to jurisdictional claims in published maps and institutional affiliations.



Copyright: © 2022 by the authors. Licensee MDPI, Basel, Switzerland. This article is an open access article distributed under the terms and conditions of the Creative Commons Attribution (CC BY) license (<https://creativecommons.org/licenses/by/4.0/>).

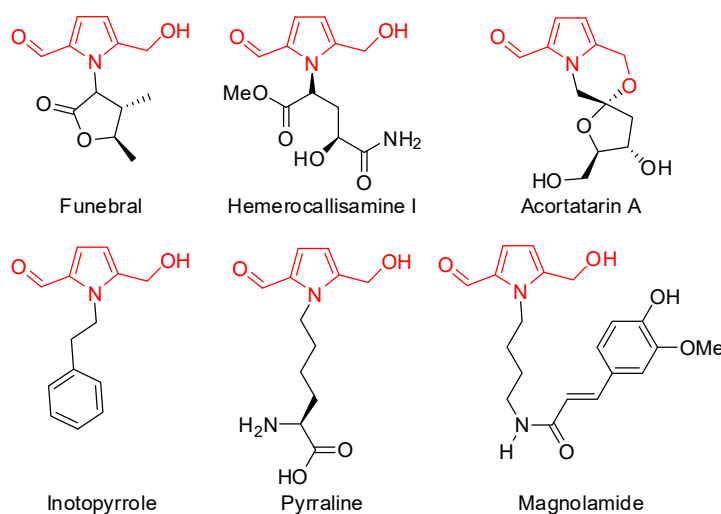
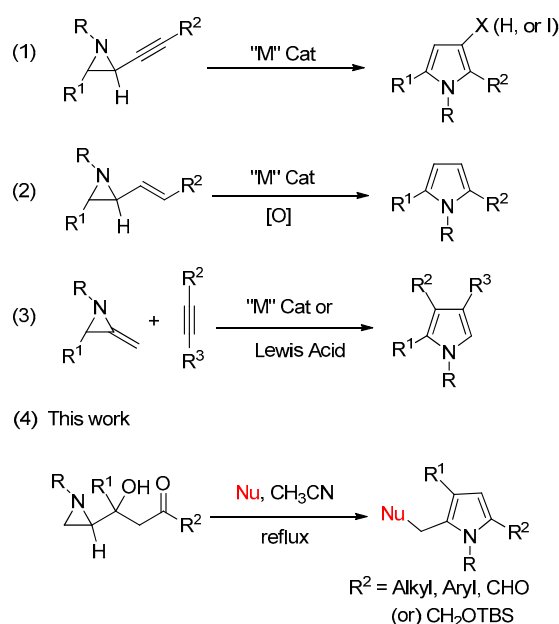


Figure 1. Structures of 2-formyl pyrrole-containing bioactive natural products.

The synthesis of highly functionalized pyrroles has drawn considerable attention from organic and medicinal chemists. In general, the classical synthesis routes for multi-substituted pyrroles, including the Knorr condensation [13], the Paal–Knorr reaction [14],

the Hantzsch reaction [15], transition metal-catalyzed reactions [16,17], and multicomponent coupling reactions [18–20], have been in existence for many years. However, most of them are limited by the inefficient synthesis of highly functionalized pyrroles; it is challenging to introduce various substituents to the pyrrole ring due to its harsh reaction conditions and the instability of widely used keto functionality. The construction of the pyrrole ring allows regioselective functionalization and subsequent diversification of the pyrrole ring with various substituents.

Many synthetic methods have commenced from aziridine and its derivatives by expanding the ring whose nitrogen ends at the pyrrole ring. Specifically, pyrroles are synthesized from propargyl aziridines through intramolecular cyclization and breaking of the aziridine ring with the assistance of various metal catalysts (“M”) including “Au(I)” followed by rearrangement for aromatization (Scheme 1, (1)) [16,17]. Our group developed a similar pyrrole synthesis method with 3-(aziridine-2-yl)-3-hydroxypropyne taking an advantage of nucleophilic aziridine ring-opening prior to cyclization [18–20]. Vinyl aziridines also served as starting materials for pyrrole after 1,3-sigmatropic shift and oxidation or 2+3 cycloaddition reaction with olefin via the cleavage of the C-N bond (Scheme 1, (2)). Similar [3+2]-cycloadditions were used to generate five-membered rings from 2-methyleneaziridine as a 1,3-dipole with an olefin (Scheme 1, (3)). However, most of these reported methods have two critical drawbacks. First, most of the methods require a metal (“M”) catalyst. Second, only a single substituted pyrrole is generated from one set of aziridine substituents properly decorated as a starting material with the necessary counterparts, including olefins and alkynes [21,22].



Scheme 1. Previous works for construction of pyrroles from activated-aziridines.

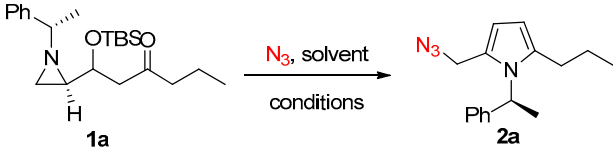
In this report, we describe an atom economical synthesis of multi-substituted pyrroles from regiospecific aziridine ring-opening by various nucleophiles [23–26] and the following cyclization in Knorr-type reactions.

2. Results and Discussion

Treatment of hydroxy keto aziridine **1a** [25,26] with TMSN_3 in THF or dioxane under reflux did not yield the desired pyrrole product **2a** (entries 1 and 2, Table 1). In dichloromethane, under reflux conditions, we obtained the expected pyrrole with a 70% yield (entry 3), whereas in CH_3CN the yield increased to 85% (entry 4). In the presence of various Lewis acids such as $\text{BF}_3\cdot\text{OEt}_2$ and FeCl_3 with NaN_3 nucleophile, we did not obtain

the desired pyrrole product **2a** (entries 5 and 6, Table 1) with all the starting materials remaining.

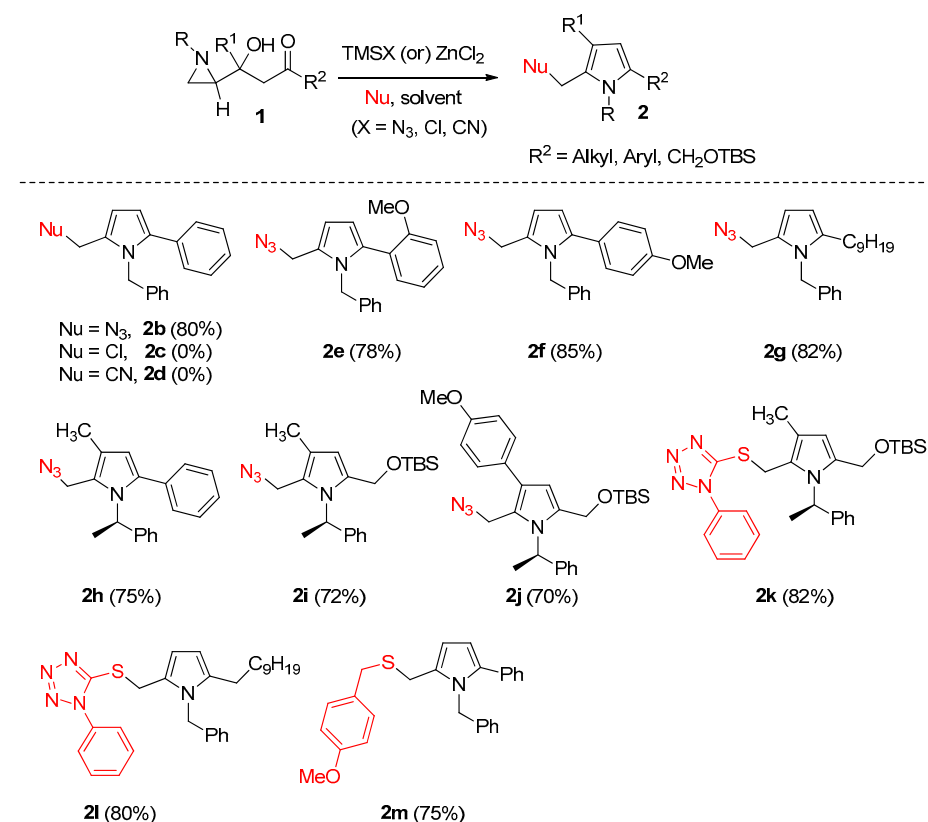
Table 1. Optimization of the reaction conditions.



Entry ^a	Nucleophile	Solvent	Temp	Time (h)	Yield ^b (%)
1	TMSN ₃	THF	85	4	0
2	TMSN ₃	Dioxane	85	4	0
3	TMSN ₃	CH ₂ Cl ₂	50	4	70
4	TMSN ₃	CH ₃ CN	85	4	85
5	BF ₃ ·OEt ₂ /NaN ₃	CH ₂ Cl ₂	rt	4	0
6	FeCl ₃ /NaN ₃	CH ₂ Cl ₂	rt	4	0

^a Reaction conditions: **1a** (1.0 mmol); ^b Yield of the isolated compound.

Next, the generality of the method was evaluated under optimized conditions that had been cyclization. This protocol provided a versatile entry for a variety of pyrroles (**2**) is well determined in Table 1. Then, we examined the scope and limitations of several β -(aziridin-2-yl)- β -hydroxy ketones (**1**) through the one-step regioselective ring-opening of aziridine followed by intramolecular to moderate yields (Scheme 2).

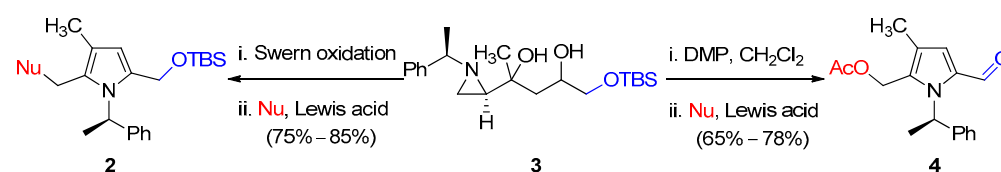


Scheme 2. Representative scheme and various examples of multi-substituted pyrroles (**2**) from substituted aziridines (**1**).

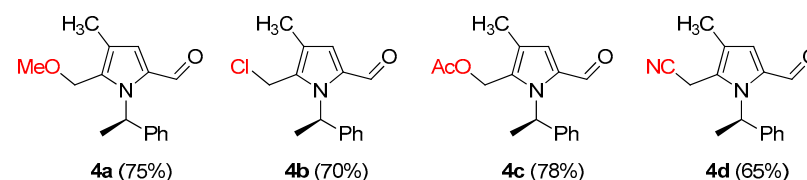
In the successive reactions of regioselective ring opening in CH₃CN under reflux and Knorr cyclization, the pyrrole compound **2b** was obtained in an 80% yield from

the aziridine starting compounds bearing a substituent at R^2 such as phenyl (**1b**) using TMSN_3 , whereas no pyrrole product **2c** or **2d** was obtained using TMSCl or TMSCN (see Scheme 2). After TMSN_3 screening (as mentioned in Table 1), we next screened a substrate variant using aziridines bearing a substituent at R^2 , such as *o*-methoxyphenyl (**1e**), *p*-methoxyphenyl (**1f**), and *n*-nonanyl (**1g**), as starting materials, which gave a pyrrole variant (**2e–2g**) in moderate to good yield under TMSN_3 conditions. The starting substrates with an additional substituent (R^2 as phenyl and *t*-butyldimethylsilyloxymethyl) and R^1 as methyl and *p*-methoxyphenyl) gave pyrroles (**2h**, **2i**, and **2j**) in 75%, 72%, and 70% yields, respectively. We also applied various thiol nucleophiles under the ZnCl_2 catalyst in MeOH to compounds (**1k–1m**) with substituents at C2 and C4, resulting in high yields of pyrroles (**2k–2m**) (Scheme 2).

Next, oxidation of the secondary alcohol of compound **3** at the γ -position of aziridine with Dess–Martin periodinane in CH_2Cl_2 yielded a complex mixture of compounds, which were directly reacted for the ring-opening with various nucleophiles such as OMe, OAc, Cl, and CN to afford 2,3-disubstituted pyrrole 5-aldehydes (**4a–4d**) in the one-pot procedure as shown in Scheme 3 with examples in the Scheme 4. Whereas Swern oxidation of secondary alcohol of compound **3**, followed by regio and stereoselective aziridine ring-opening with incoming nucleophile, yielded OTBS-protected pyrrole **2** as shown in Scheme 3 (see compounds **2k–2l** in Scheme 2).

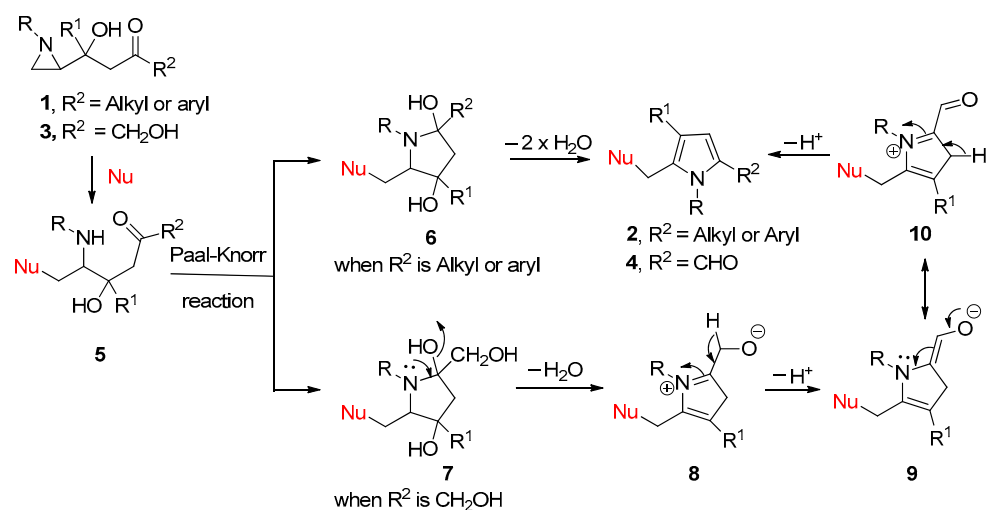


Scheme 3. Oxidation-state controlled synthesis of pyrrole product.



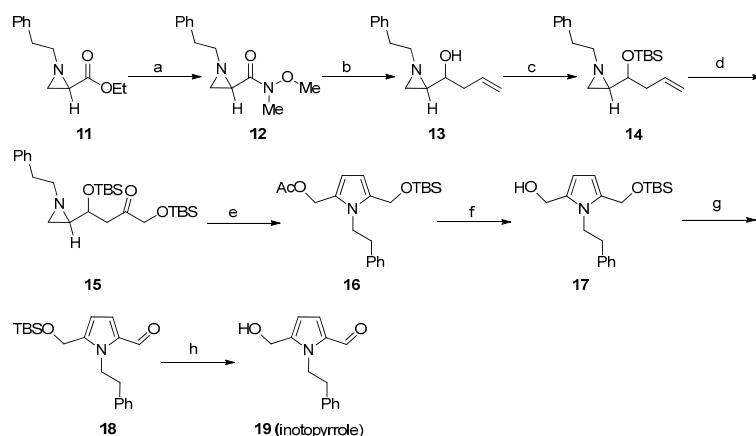
Scheme 4. Examples of synthesis of 2-formyl pyrroles.

The difference in cyclization is raised by the substituent of R^2 , whether the substituent R^2 is a simple alkyl or aryl, or hydroxymethyl in Scheme 2. The initial Paal–Knorr cyclization step gives either **6** or **7**, regardless of the characteristics of R^2 , with the removal of water molecules. After the generation of the hydroxy pyrrolidine intermediate **6**, generated from most substrates with alkyl or aryl substituent on R^2 , the reaction proceeds to aromatization to yield **2** as shown in Scheme 2. From the substrate-bearing hydroxymethyl group, the ammonium ion intermediate **8** was generated, from which the deprotonation occurs to give **9** and its resonance form as **10**. One more deprotonation from **10** gives rise to the final 2-formyl pyrroles **4**, as shown in Scheme 4 (Scheme 5).



Scheme 5. Proposed reaction mechanism for the formation of **2** and **4** from **1** and **3** in two different pathways.

This method was extended to the synthesis of the natural product inotopyrrole **19** (Scheme 5). Treatment of compound **11** with Weinreb salt and *i*-PrMgCl to give compound **12**, followed by allyl magnesium bromide and a subsequent reduction of aziridine ketone by NaBH₄ yielded the alcohol compound **13** in 68% yield for two steps. Protection of the secondary alcohol with TBSOTf and 2,6-lutidine to furnish olefin **14** at a 73% yield. Olefin **14** was subjected to simple dihydroxylation using OsO₄ and NMO to give a diol compound, followed by selective protection of the primary alcohol with TBSCl to afford secondary alcohol, and subsequently, Swern oxidation of alcohol afforded key intermediate keto compound **15** in a 62% yield. Then, we applied our optimized method on compound **15** for the synthesis of pyrrole derivative **16** from a one-step regioselective ring-opening followed by cyclization of keto compound by using AcOH and CH₂Cl₂ at 0 °C in 82% yield. Then, deacetylation of **16** with K₂CO₃ to give alcohol **17**, followed by Dess-martin oxidation of primary alcohol, afforded aldehyde **18** with a 74% yield. Removal of the TBS group with TBAF gave rise to the desired natural product, inotopyrrole (**19**), in an 84% yield. Spectral data (¹H, ¹³C NMR) and HRMS data of our synthetic inotopyrrole (**19**) were in full agreement with those reported for the natural product (Scheme 6) [3–5].



Scheme 6. Synthesis of inotopyrrole (**19**) from aziridine (**11**). (a) NHMe(OMe), *i*-PrMgCl, THF, 0 °C, 2 h, 78%. (b) (i) Allylmagnesium bromide, THF, 0 °C, 1 h; (ii) NaBH₄, MeOH, 0 °C, 1 h; 87% (over two steps). (c) TBSOTf, 2,6-Lutidine, CH₂Cl₂, 0 °C to rt, 2 h, 73%. (d) (i) OsO₄, NMO, 0 °C to rt, 4 h; (ii) TBSCl, Imidazole, CH₂Cl₂, 0 °C to rt, 2 h; (iii) DMSO, (COCl)₂, CH₂Cl₂, −78 °C, 2 h; 62% (over three steps). (e) AcOH, CH₂Cl₂, 0 °C, 12 h, 82%. (f) K₂CO₃, MeOH, 0 °C, 12 h, 80%. (g) DMP, CH₂Cl₂, 0 °C, 2 h, 74%. (h) TBAF, THF, 0 °C, 1 h, 84%.

3. Materials and Methods

3.1. General Information

Chiral aziridines are available from Sigma-Aldrich as reagents. They are also available from Imogene Co., Ltd. (<http://www.imogene.co.kr/>) in bulk quantities. All commercially available compounds were used as received unless stated otherwise. All reactions were carried out under an atmosphere of nitrogen in oven-dried glassware with magnetic stirrer. Dichloromethane was distilled from calcium hydride. Reactions were monitored by thin layer chromatography (TLC) with 0.25 mm E. Merck pre-coated silica gel plates (60 F254). Visualization was accomplished with either UV light, or by immersion in solutions of ninhydrin, *p*-anisaldehyde, or phosphomolybdic acid (PMA) followed by heating on a hot plate for about 10 sec. Purification of reaction products was carried out by flash chromatography using Kieselgel 60 Art 9385 (230–400 mesh). The ¹H-NMR and ¹³C-NMR spectra were obtained using Varian unity INOVA 400WB (400 MHz) or Bruker AVANCE III HD (400 MHz) spectrometer. Chemical shifts are reported relative to chloroform ($\delta = 7.26$) for ¹H NMR, chloroform ($\delta = 77.2$) for ¹³C NMR, acetonitrile ($\delta = 1.94$) for ¹H NMR, and acetonitrile ($\delta = 1.32$) for ¹³C NMR (see Supplementary Materials). Data are reported as br = broad, s = singlet, d = doublet, t = triplet, q = quartet, p = quintet, m = multiplet. Coupling constants are given in Hz. Ambiguous assignments were resolved using standard one-dimensional proton decoupling experiments. Optical rotations were obtained using a Rudolph Autopol III digital polarimeter and JASCO P-2000. Optical rotation data are reported as follows: $[\alpha]^{20}$ (concentration $c = \text{g}/100 \text{ mL}$, solvent). High-resolution mass spectra were recorded on a 4.7 Tesla IonSpec ESI-TOFMS, JEOL (JMS-700), and an AB Sciex 4800 Plus MALDI TOFTM, (2,5-dihydroxybenzoic acid (DHB) matrix was used to prepare samples for MS. Data were obtained in the reflector positive mode with internal standards for calibration).

3.2. General Procedure for the Synthesis of Pyrroles

To a stirred solution of **1a** (100 mg, 0.38 mmol) in CH₃CN (3 mL) was added trimethylsilyl azide (0.1 mL, 0.76 mmol) at 90 °C. After being stirred for 4 h, the mixture was concentrated under reduced pressure. The crude product was purified by column chromatography (EtOAc/hexane = 1:9) to afford pyrrole compound **2a**.

(*R*)-2-(Azidomethyl)-1-(1-phenylethyl)-5-propyl-1*H*-pyrrole (**2a**)

Yellow liquid, (80 mg) 85% yield. The ¹H NMR (400 MHz, CDCl₃) δ 7.32 (ddd, $J = 7.6, 5.0, 2.0 \text{ Hz}$, 3H), 7.07–7.02 (m, 2H), 6.17 (d, $J = 3.5 \text{ Hz}$, 1H), 5.92 (d, $J = 3.5 \text{ Hz}$, 1H), 5.53 (q, $J = 7.2 \text{ Hz}$, 1H), 4.17 (d, $J = 14.5 \text{ Hz}$, 1H), 3.93 (d, $J = 14.4 \text{ Hz}$, 1H), 2.49–2.41 (m, 1H), 2.35–2.25 (m, 1H), 1.90 (d, $J = 7.2 \text{ Hz}$, 3H), 1.61–1.50 (m, 2H), 0.88 (t, $J = 7.3 \text{ Hz}$, 3H). The ¹³C NMR (101 MHz, CDCl₃) δ 141.9, 136.1, 128.5, 127.1, 125.9, 124.7, 110.9, 105.6, 52.6, 47.6, 29.6, 22.1, 19.6, 14.0. HRMS-ESI (m/z): $[\text{M} + \text{H}]^+$ calcd. for C₁₆H₂₁N₄, 269.6121, found 269.6128. Copies of ¹H and ¹³C NMR could be found in Supplementary Materials.

2-(Azidomethyl)-1-benzyl-5-phenyl-1*H*-pyrrole (**2b**)

Yellow liquid, (90 mg) 80% yield. The ¹H NMR (400 MHz, CDCl₃) δ 7.28 (ddd, $J = 10.9, 6.7, 3.5 \text{ Hz}$, 8H), 6.89 (d, $J = 7.2 \text{ Hz}$, 2H), 6.33 (d, $J = 3.6 \text{ Hz}$, 1H), 6.25 (d, $J = 3.6 \text{ Hz}$, 1H), 5.21 (s, 2H), 4.15 (s, 2H). The ¹³C NMR (101 MHz, CDCl₃) δ 138.6, 137.3, 133.0, 128.9, 128.8, 128.5, 127.4, 127.3, 127.0, 125.5, 111.3, 108.4, 47.7, 47.2. HRMS-ESI (m/z): $[\text{M} + \text{H}]^+$ calcd. for C₁₈H₁₇N₄, 289.1358, found 289.1362. Copies of ¹H and ¹³C NMR could be found in Supplementary Materials.

2-(Azidomethyl)-1-benzyl-5-(2-methoxyphenyl)-1*H*-pyrrole (**2e**)

Yellow liquid, (93 mg) 78% yield. The ¹H NMR (400 MHz, CDCl₃) δ 7.39–7.03 (m, 5H), 7.00–6.78 (m, 4H), 6.34 (d, $J = 3.5 \text{ Hz}$, 1H), 6.16 (d, $J = 3.5 \text{ Hz}$, 1H), 5.03 (s, 2H), 4.14 (s, 2H), 3.65 (s, 3H). The ¹³C NMR (101 MHz, CDCl₃) δ 157.4, 138.6, 133.6, 132.7, 129.6, 128.4, 127.0, 126.4, 126.0, 122.1, 120.6, 111.0, 110.8, 108.6, 55.3, 48.2. HRMS-ESI (m/z): $[\text{M} + \text{H}]^+$ calcd.

for C₁₉H₁₉N₄O, 319.0446, found 319.0449. Copies of ¹H and ¹³C NMR could be found in Supplementary Materials.

2-(Azidomethyl)-1-benzyl-5-(4-methoxyphenyl)-1H-pyrrole (**2f**)

Yellow liquid, (89 mg) 85% yield. The ¹H NMR (400 MHz, CDCl₃) δ 7.01 (ddd, *J* = 6.6, 5.2, 2.7 Hz, 5H), 6.67–6.65 (m, 2H), 6.62–6.59 (m, 2H), 6.09 (d, *J* = 3.5 Hz, 1H), 5.96 (d, *J* = 3.5 Hz, 1H), 4.95 (s, 2H), 3.89 (s, 2H), 3.54 (s, 3H). The ¹³C NMR (101 MHz, CDCl₃) δ 159.1, 138.7, 137.0, 130.3, 128.8, 127.2, 126.4, 125.5, 125.5, 113.9, 111.1, 107.8, 55.3, 47.6, 47.3. HRMS-ESI (*m/z*): [M + H]⁺ calcd. for C₁₉H₁₉N₄O, 319.1228, found 319.1230. Copies of ¹H and ¹³C NMR could be found in Supplementary Materials.

2-(Azidomethyl)-1-benzyl-5-nonyl-1H-pyrrole (**2g**)

Yellow liquid, (85 mg) 82% yield. The ¹H NMR (400 MHz, CDCl₃) δ 7.37–7.28 (m, 3H), 6.92 (d, *J* = 7.0 Hz, 2H), 6.27 (d, *J* = 3.5 Hz, 1H), 6.01 (d, *J* = 3.5 Hz, 1H), 5.18 (s, 2H), 4.20 (s, 2H), 2.51 (dd, *J* = 13.6, 6.0 Hz, 2H), 1.67–1.59 (m, 2H), 1.38–1.29 (m, 12H), 0.94 (t, *J* = 6.9 Hz, 3H). The ¹³C NMR (101 MHz, CDCl₃) δ 138.3, 136.2, 128.7, 127.2, 125.5, 125.4, 125.0, 110.2, 105.3, 47.2, 46.9, 31.8, 29.3, 28.6, 26.5, 22.5, 13.8. HRMS-ESI (*m/z*): [M + H]⁺ calcd. for C₂₁H₃₁N₄, 339.4618, found 339.4620. Copies of ¹H and ¹³C NMR could be found in Supplementary Materials.

(R)-2-(Azidomethyl)-3-methyl-5-phenyl-1-(1-phenylethyl)-1H-pyrrole (**2h**)

Yellow liquid, (83 mg) 75% yield. The ¹H NMR (400 MHz, CDCl₃) δ 7.35–7.24 (m, 8H), 7.04–7.02 (m, 2H), 6.08 (s, 1H), 5.59 (q, *J* = 7.3 Hz, 1H), 4.23 (d, *J* = 14.7 Hz, 1H), 3.75 (d, *J* = 14.8 Hz, 1H), 2.16 (s, 3H), 1.88 (d, *J* = 7.2 Hz, 3H). The ¹³C NMR (101 MHz, CDCl₃) δ 142.4, 133.8, 129.4, 128.6, 128.4, 127.4, 127.1, 125.8, 122.6, 121.7, 110.3, 53.2, 45.1, 19.9, 11.3. HRMS-ESI (*m/z*): [M + H]⁺ calcd. for C₂₀H₂₁N₄, 317.5973, found 317.5975. Copies of ¹H and ¹³C NMR could be found in Supplementary Materials.

(R)-2-(Azidomethyl)-5-(((*tert*-butyldimethylsilyl)oxy)methyl)-3-methyl-1-(1-phenylethyl)-1H-pyrrole (**2i**)

Yellow liquid, (91 mg) 72% yield. The ¹H NMR (400 MHz, CDCl₃) δ 7.34–7.26 (m, 3H), 7.18–7.14 (m, 2H), 5.97 (s, 1H), 5.72 (q, *J* = 7.2 Hz, 1H), 4.53 (s, 2H), 4.22 (d, *J* = 14.7 Hz, 1H), 3.81 (d, *J* = 14.7 Hz, 1H), 2.12 (s, 3H), 1.94 (d, *J* = 7.2 Hz, 3H), 0.88 (s, 9H), 0.05 (d, *J* = 7.1 Hz, 6H). The ¹³C NMR (101 MHz, CDCl₃) δ 142.0, 133.0, 128.4, 127.1, 126.2, 122.6, 119.9, 109.7, 57.8, 53.1, 44.6, 25.8, 19.6, 18.2, 11.2, −5.2. HRMS-ESI (*m/z*): [M + Na]⁺ calcd. for C₂₁H₃₂N₄NaOSi, 407.8471, found 407.8474. Copies of ¹H and ¹³C NMR could be found in Supplementary Materials.

(R)-2-(Azidomethyl)-5-(((*tert*-butyldimethylsilyl)oxy)methyl)-3-(4-methoxyphenyl)-1-(1-phenylethyl)-1H-pyrrole (**2j**)

Yellow liquid, (87 mg) 70% yield. The ¹H NMR (400 MHz, CDCl₃) δ 7.40–7.34 (m, 4H), 7.32–7.29 (m, 1H), 7.22 (dd, *J* = 5.1, 4.2 Hz, 2H), 6.97 (d, *J* = 8.8 Hz, 2H), 6.25 (s, 1H), 5.82 (q, *J* = 7.1 Hz, 1H), 4.55 (s, 2H), 4.34 (d, *J* = 14.6 Hz, 1H), 4.05 (d, *J* = 14.6 Hz, 1H), 3.87 (s, 3H), 2.04 (d, *J* = 7.2 Hz, 3H), 0.91 (s, 9H), 0.08 (d, *J* = 3.9 Hz, 6H). The ¹³C NMR (101 MHz, CDCl₃) δ 158.2, 141.6, 133.7, 129.6, 128.6, 128.5, 127.3, 126.4, 126.3, 122.5, 113.9, 109.1, 57.9, 55.3, 53.6, 45.4, 25.9, 19.6, 18.2, −5.2. HRMS-ESI (*m/z*): [M + H]⁺ calcd. for C₂₇H₃₇N₄O₂Si, 477.0417, found 477.0419. Copies of ¹H and ¹³C NMR could be found in Supplementary Materials.

(R)-5-(((5-(((tert-Butyldimethylsilyloxy)methyl)-3-methyl-1-(1-phenylethyl)-1H-pyrrol-2-yl)methyl)thio)-1-phenyl-1H-tetrazole (2k)

Yellow liquid, (107 mg) 82% yield. The ^1H NMR (400 MHz, CDCl_3) δ 7.83–7.80 (m, 2H), 7.56–7.48 (m, 3H), 7.21 (t, $J = 7.6$ Hz, 2H), 7.11–7.03 (m, 3H), 6.08 (s, 1H), 5.85 (q, $J = 7.1$ Hz, 1H), 5.28 (s, 2H), 4.53 (s, 2H), 2.19 (s, 3H), 1.93 (d, $J = 7.2$ Hz, 3H), 0.88 (s, 9H), 0.06 (d, $J = 2.8$ Hz, 6H). The ^{13}C NMR (101 MHz, CDCl_3) δ 162.1, 141.3, 134.7, 133.6, 129.4, 129.1, 128.2, 126.8, 126.1, 123.6, 121.4, 120.3, 110.5, 58.0, 53.5, 42.6, 25.9, 19.9, 18.3, 11.5, –5.2. HRMS-ESI (m/z): $[\text{M} + \text{H}]^+$ calcd. for $\text{C}_{28}\text{H}_{38}\text{N}_5\text{OSSi}$, 520.4336, found 520.4340. Copies of ^1H and ^{13}C NMR could be found in Supplementary Materials.

5-(((1-Benzyl-5-nonyl-1H-pyrrol-2-yl)methyl)thio)-1-phenyl-1H-tetrazole (2l)

Yellow liquid, (115 mg) 81% yield. The ^1H NMR (400 MHz, CDCl_3) δ 7.66 (dd, $J = 8.2, 1.5$ Hz, 2H), 7.51–7.43 (m, 3H), 7.17 (t, $J = 7.4$ Hz, 2H), 7.11 (d, $J = 7.3$ Hz, 1H), 6.67 (d, $J = 7.5$ Hz, 2H), 6.52 (d, $J = 3.5$ Hz, 1H), 6.03 (d, $J = 3.5$ Hz, 1H), 5.44 (s, 2H), 5.32 (s, 2H), 2.44–2.39 (m, 2H), 1.57 (dd, $J = 15.0, 7.4$ Hz, 2H), 1.30–1.22 (m, 12H), 0.87 (t, $J = 6.8$ Hz, 3H). The ^{13}C NMR (101 MHz, CDCl_3) δ 162.4, 137.9, 136.5, 134.5, 129.4, 128.9, 128.4, 127.0, 124.9, 123.8, 123.4, 111.9, 105.7, 46.9, 43.6, 31.8, 29.5, 29.4, 29.3, 28.5, 26.4, 22.6, 14.1. HRMS-ESI (m/z): $[\text{M} + \text{H}]^+$ calcd. for $\text{C}_{28}\text{H}_{36}\text{N}_5\text{S}$, 474.3226, found 474.3228. Copies of ^1H and ^{13}C NMR could be found in Supplementary Materials.

1-Benzyl-2-(((4-methoxybenzyl)thio)methyl)-5-phenyl-1H-pyrrole (2m)

Yellow liquid, (105 mg) 75% yield. The ^1H NMR (400 MHz, CDCl_3) δ 7.32–7.29 (m, 4H), 7.25–7.15 (m, 6H), 6.86–6.79 (m, 4H), 6.22 (d, $J = 3.5$ Hz, 1H), 6.17 (d, $J = 3.5$ Hz, 1H), 5.25 (s, 2H), 3.79 (s, 3H), 3.62 (s, 2H), 3.44 (s, 2H). The ^{13}C NMR (101 MHz, CDCl_3) δ 158.5, 138.9, 136.2, 133.4, 130.3, 130.0, 128.8, 128.6, 128.3, 126.9, 125.6, 113.8, 110.0, 108.0, 55.3, 47.4, 34.9, 27.5. HRMS-ESI (m/z): $[\text{M} + \text{Na}]^+$ calcd. for $\text{C}_{26}\text{H}_{25}\text{NNaOS}$, 422.5371, found 422.5375. Copies of ^1H and ^{13}C NMR could be found in Supplementary Materials.

(R)-5-(methoxymethyl)-4-methyl-1-(1-phenylethyl)-1H-pyrrole-2-carbaldehyde (4a)

To a stirred solution of secondary alcohol **3** (200 mg, 0.527 mmol) was dissolved in CH_2Cl_2 (6 mL) under N_2 at 0 °C and Dess–Martin periodinane (335 mg, 0.791 mmol) was added to the reaction mixture and allowed to stir for 2 h. Ether was added to the reaction mixture and the solid was filtered. The filtrate was washed with saturated NaHCO_3 solution, dried over anhydrous Na_2SO_4 , and solvents were removed under vacuum to obtain a crude product, which was used for the next reaction without further purification.

To a stirred solution of above crude ketone compound was dissolved in MeOH (3 mL) under N_2 at 0 °C and ZnCl_2 (86 mg, 0.632 mmol) was added to the reaction mixture and allowed to stir for 2 h. After 2 h, the reaction mixture was diluted with CH_2Cl_2 (10 mL), quenched with water, and extracted with CH_2Cl_2 (2×10 mL). The organic layer was dried over Na_2SO_4 and concentrated in vacuo to obtain a crude product, which was purified by silica gel column chromatography (EtOAc/hexane, 1:9) to obtain pyrrole compound **4a** (102 mg, 75% yield) as a yellow liquid. The ^1H NMR (400 MHz, CDCl_3) δ 9.41 (s, 1H), 7.32–7.26 (m, 3H), 7.13 (d, $J = 8.1$ Hz, 2H), 6.80 (s, 1H), 6.56 (s, 1H), 4.20 (d, $J = 12.4$ Hz, 1H), 4.07 (d, $J = 12.4$ Hz, 1H), 3.21 (s, 3H), 2.12 (s, 3H), 1.91 (d, $J = 7.1$ Hz, 3H). The ^{13}C NMR (101 MHz, CDCl_3) δ 179.1, 141.5, 136.3, 131.4, 128.3, 127.0, 126.1, 125.1, 121.7, 63.5, 57.7, 53.9, 19.4, 11.1. HRMS-ESI (m/z): $[\text{M} + \text{H}]^+$ calcd. for $\text{C}_{16}\text{H}_{20}\text{NO}_2$, 258.2714, found 258.2718. Copies of ^1H and ^{13}C NMR could be found in Supplementary Materials.

(R)-5-(Chloromethyl)-4-methyl-1-(1-phenylethyl)-1H-pyrrole-2-carbaldehyde (4b)

Yellow liquid, (92 mg) 70% yield. The ^1H NMR (400 MHz, CDCl_3) δ 9.50 (s, 1H), 7.37–7.29 (m, 3H), 7.16–7.13 (m, 2H), 6.82 (s, 1H), 6.77 (s, 1H), 4.43 (d, $J = 12.8$ Hz, 1H), 4.27 (d, $J = 12.9$ Hz, 1H), 2.15 (s, 3H), 2.00 (d, $J = 7.2$ Hz, 3H). The ^{13}C NMR (101 MHz, CDCl_3) δ 179.6, 141.1, 135.3, 131.6, 128.6, 128.4, 127.3, 125.9, 125.3, 53.8, 35.4, 19.4, 10.8. HRMS-ESI

(m/z): $[M + H]^+$ calcd. for $C_{15}H_{17}ClNO$, 262.1479, found 262.1483. Copies of 1H and ^{13}C NMR could be found in Supplementary Materials.

(R)-(5-Formyl-3-methyl-1-(1-phenylethyl)-1H-pyrrol-2-yl)methyl acetate (**4c**)

Yellow liquid, (98 mg) 78% yield. The 1H NMR (400 MHz, $CDCl_3$) δ 9.47 (s, 1H), 7.32–7.26 (m, 3H), 7.11 (d, $J = 8.0$ Hz, 2H), 6.81 (s, 1H), 6.65 (s, 1H), 4.96 (d, $J = 13.4$ Hz, 1H), 4.69 (d, $J = 13.4$ Hz, 1H), 2.11 (s, 3H), 1.91 (t, $J = 3.5$ Hz, 6H). The ^{13}C NMR (101 MHz, $CDCl_3$) δ 179.5, 170.3, 141.0, 134.0, 131.8, 128.4, 127.2, 126.0, 125.4, 55.6, 53.9, 20.6, 19.4, 10.9. HRMS-ESI (m/z): $[M + H]^+$ calcd. for $C_{17}H_{20}NO_3$, 286.6442, found 286.6446. Copies of 1H and ^{13}C NMR could be found in Supplementary Materials.

(R)-2-(5-Formyl-3-methyl-1-(1-phenylethyl)-1H-pyrrol-2-yl)acetonitrile (**4d**)

Yellow liquid, (93 mg) 65% yield. The 1H NMR (400 MHz, $CDCl_3$) δ 9.47 (s, 1H), 7.32–7.27 (m, 3H), 7.12–7.09 (m, 2H), 6.81 (s, 1H), 6.65 (s, 1H), 4.96 (d, $J = 13.4$ Hz, 1H), 4.69 (d, $J = 13.3$ Hz, 1H), 2.11 (s, 3H), 1.90 (d, $J = 2.2$ Hz, 3H). The ^{13}C NMR (101 MHz, $CDCl_3$) δ 179.4, 141.0, 133.9, 131.8, 128.5, 128.4, 127.2, 126.0, 125.9, 125.3, 55.6, 53.9, 20.6, 19.4, 10.9. HRMS-ESI (m/z): $[M + H]^+$ calcd. for $C_{16}H_{17}N_2O$, 253.4441, found 253.4446. Copies of 1H and ^{13}C NMR could be found in Supplementary Materials.

Ethyl 1-phenethylaziridine-2-carboxylate (**11**)

To a stirred solution of ethyl 2,3-dibromopropanoate (5.0 g, 19.30 mmol, 1.0 equiv) dissolved in acetonitrile (60 mL), were added potassium carbonate (8.0 g, 57.9 mmol, 3.0 equiv) followed by 2-phenylethanamine (2.9 mL, 23.16 mmol, 1.2 equiv) in dropwise manner at room temperature and reaction mixture were allowed to stir for 12 h. After completion, quenched with water (25 mL) and filtered out over filter paper (pore size 8–10 μ m). The organic mixture was extracted with Et_2O (2×30 mL), dried over anhydrous magnesium sulfate, and concentrated under reduced pressure to obtain a crude mixture of Ethyl 1-phenethylaziridine-2-carboxylate **11** as a yellow liquid (3.8 g, 89%). The 1H NMR (400 MHz, $CDCl_3$) δ 7.27 (ddd, $J = 7.4, 3.1, 1.3$ Hz, 2H), 7.22–7.16 (m, 3H), 4.24–4.11 (m, 2H), 2.93 (dd, $J = 15.1, 6.9$ Hz, 2H), 2.65–2.49 (m, 2H), 2.14 (dd, $J = 3.1, 1.2$ Hz, 1H), 1.94 (dd, $J = 6.5, 3.1$ Hz, 1H), 1.52 (dd, $J = 6.5, 1.1$ Hz, 1H), 1.27 (t, $J = 7.1$ Hz, 3H). The ^{13}C NMR (101 MHz, $CDCl_3$) δ 170.7, 139.3, 128.7, 128.3, 126.1, 62.3, 61.0, 37.5, 36.0, 34.3, 14.1. HRMS-ESI (m/z): $[M + H]^+$ calcd. for $C_{13}H_{18}NO_2$, 220.6121, found 220.6128. Copies of 1H and ^{13}C NMR could be found in Supplementary Materials.

N-Methoxy-*N*-methyl-1-phenethylaziridine-2-carboxamide (**12**)

To a stirred solution of ester **11** (3.8 g, 17.35 mmol) and *N,O*-dimethylhydroxylamine hydrochloride (2.53 g, 26.0 mmol) in dry THF (50 mL) at 0 $^\circ$ C was slowly added *i*-PrMgCl (26.0 mL, 2.0 M in THF, 52.05 mmol), and the reaction mixture was stirred for 1 h. The reaction mixture was quenched with saturated NH_4Cl solution and extracted with EtOAc (3×20 mL). The combined organic layers were dried over anhydrous Na_2SO_4 and concentrated in vacuo to obtain the crude product, which was purified by silica gel column chromatography (EtOAc/hexanes, 1:1) to afford Weinreb amide **12** as a yellow color oil (3.2 g, 78.8%) yield. The 1H NMR (400 MHz, $CDCl_3$) δ 7.29–7.25 (m, 2H), 7.20 (d, $J = 7.2$ Hz, 3H), 3.68 (s, 3H), 3.21 (s, 3H), 2.99–2.88 (m, 2H), 2.71 (ddd, $J = 11.4, 8.7, 6.6$ Hz, 1H), 2.56–2.42 (m, 2H), 2.17 (dd, $J = 3.2, 1.3$ Hz, 1H), 1.51 (dd, $J = 6.5, 1.2$ Hz, 1H). The ^{13}C NMR (101 MHz, $CDCl_3$) δ 170.3, 139.6, 128.7, 128.3, 126.1, 62.7, 61.6, 36.1, 35.3, 34.0, 32.5. HRMS-ESI (m/z): $[M + H]^+$ calcd. for $C_{13}H_{19}N_2O_2$, 235.0336, found 234.0340. Copies of 1H and ^{13}C NMR could be found in Supplementary Materials.

1-(1-Phenethylaziridin-2-yl)but-3-en-1-ol (**13**)

To a stirred solution of Weinreb amide **12** (3.2 g, 13.67 mmol) was slowly added allylMgBr (8.2 mL, 2.0 M in THF, 16.4 mmol) in dry THF (40 mL) at 0 $^\circ$ C, and the reaction mixture was stirred for 1 h. The reaction mixture was quenched with saturated NH_4Cl

solution and extracted with EtOAc (2 × 20 mL). The combined organic layers were dried over anhydrous Na₂SO₄ and concentrated in vacuo to obtain the crude allyl product, which was used for the next reaction without further purification.

To a stirred solution of above keto compound (3.2 g, 14.86 mmol) was slowly added NaBH₄ (0.45 g, 11.88 mmol) in MeOH (40 mL) at 0 °C, and the reaction mixture was stirred for 1 h. Then, MeOH was removed under vacuum and extracted with CH₂Cl₂ (2 × 10 mL). The organic layer was dried over Na₂SO₄ and concentrated in vacuo to obtain the crude allyl alcohol product, which was purified by column chromatography (EtOAc/hexanes, 2:8) to give pure 1-(1-phenethylaziridin-2-yl)but-3-en-1-ol (**13**) as a yellow liquid (2.6 g, 87%) yield. The ¹H NMR (400 MHz, CDCl₃) δ 7.33–7.16 (m, 5H), 5.84 (ddt, *J* = 17.2, 10.2, 7.1 Hz, 1H), 5.16–5.06 (m, 2H), 3.66 (td, *J* = 6.3, 3.8 Hz, 1H), 2.85 (t, *J* = 7.4 Hz, 2H), 2.67 (dt, *J* = 11.6, 7.3 Hz, 1H), 2.52–2.43 (m, 1H), 2.24 (t, *J* = 6.7 Hz, 2H), 1.80 (d, *J* = 3.6 Hz, 1H), 1.49 (dt, *J* = 7.0, 3.7 Hz, 1H), 1.23 (d, *J* = 6.4 Hz, 1H). The ¹³C NMR (101 MHz, CDCl₃) δ 139.7, 134.3, 128.7, 128.3, 126.1, 117.4, 67.9, 61.7, 42.2, 39.3, 36.3, 29.3. HRMS-ESI (*m/z*): [M + H]⁺ calcd. for C₁₄H₂₀NO, 218.0231, found 218.0234. Copies of ¹H and ¹³C NMR could be found in Supplementary Materials.

2-(1-((*tert*-Butyldimethylsilyl)oxy)but-3-en-1-yl)-1-phenethylaziridine (**14**)

To a stirred solution of allyl alcohol **13** (2.5 g, 11.50 mmol) in dry CH₂Cl₂ (30 mL) was added imidazole (1.5 g, 23.0 mmol) and TBSCl (1.9 g, 12.65 mmol), sequentially, at 0 °C under an N₂ atmosphere. After 4 h of being stirred at rt, the reaction mixture was quenched with saturated aqueous NH₄Cl (10 mL). The organic layer was separated, and the aqueous layer was extracted with CH₂Cl₂ (2 × 20 mL). The organic layer was dried over Na₂SO₄ and concentrated in vacuo to obtain the crude product, which was purified by column chromatography (EtOAc/hexanes, 2:8) to give pure 2-(1-((*tert*-butyldimethylsilyl)oxy)but-3-en-1-yl)-1-phenethylaziridine **14** as a yellow liquid (2.8 g, 73%) yield. The ¹H NMR (400 MHz, CDCl₃) δ 7.30–7.24 (m, 2H), 7.19 (dd, *J* = 7.1, 5.2 Hz, 3H), 5.91 (ddt, *J* = 17.1, 10.2, 7.1 Hz, 1H), 5.13–5.04 (m, 2H), 3.20 (td, *J* = 7.0, 4.4 Hz, 1H), 2.86 (t, *J* = 8.0 Hz, 2H), 2.55 (dt, *J* = 11.5, 7.7 Hz, 1H), 2.48–2.33 (m, 3H), 1.69 (d, *J* = 3.4 Hz, 1H), 1.45 (ddd, *J* = 7.6, 6.4, 3.4 Hz, 1H), 1.29 (d, *J* = 6.3 Hz, 1H), 0.88 (s, 9H), 0.02 (d, *J* = 2.1 Hz, 6H). The ¹³C NMR (101 MHz, CDCl₃) δ 139.8, 135.0, 128.6, 128.3, 126.0, 116.9, 74.6, 62.7, 43.6, 40.9, 36.3, 33.9, 25.8, 18.1, −4.1, −4.6. HRMS-ESI (*m/z*): [M + H]⁺ calcd. for C₂₀H₃₄NOSi, 332.1222, found 332.1224. Copies of ¹H and ¹³C NMR could be found in Supplementary Materials.

Octamethyl-8-(1-phenethylaziridin-2-yl)-4,9-dioxa-3,10-disiladodecan-6-one (**15**)

To a stirred solution of 2-(1-((*tert*-butyldimethylsilyl)oxy)but-3-en-1-yl)-1-phenethylaziridine **14** (2.5 g, 7.5 mmol) and *N*-Methylmorpholine *N*-oxide (2.64 g, 22.61 mmol) in acetone: H₂O (4:1) (20 mL) at room temperature was slowly added OsO₄ (3.2 mL, 0.75 mmol), and the reaction mixture was stirred for 6 h. The reaction mixture was quenched with saturated NH₂SO₃ solution and extracted with EtOAc (3 × 20 mL). The combined organic layers were dried over anhydrous Na₂SO₄ and concentrated in vacuo to obtain the crude dihydroxy product, which was used for the next reaction without further purification.

To a stirred solution of dihydroxy alcohol (2.5 g, 6.8 mmol) in dry CH₂Cl₂ (30 mL) was added imidazole (0.93 g, 13.67 mmol) and TBSCl (1.13 g, 7.5 mmol), sequentially, at 0 °C under an N₂ atmosphere. After 2 h of being stirred at rt, the reaction mixture was quenched with saturated aqueous NH₄Cl (10 mL). The organic layer was separated, and the aqueous layer was extracted with CH₂Cl₂ (2 × 20 mL). The organic layer was dried over Na₂SO₄ and concentrated in vacuo to obtain the crude product, which was used for the next reaction without further purification.

To a solution of oxalyl chloride (0.67 mL, 7.81 mmol) in CH₂Cl₂ (20 mL) at −78 °C was added dimethyl sulfoxide (1.1 mL, 15.63 mmol) over 15 min. The resulting mixture was stirred for another 45 min and then a solution of alcohol (2.5 g, 5.21 mmol) in CH₂Cl₂ (20 mL) was added dropwise. The resulting white suspension was stirred for 2h before adding triethylamine (2.18 mL, 15.63 mmol). The reaction mixture was stirred for 30

min at $-78\text{ }^{\circ}\text{C}$ and then warmed to $0\text{ }^{\circ}\text{C}$ and allowed to stir for 15 min. The reaction mixture was quenched with water (20 mL) and the aqueous phase was extracted with CH_2Cl_2 (2×20 mL). The combined organic layers were washed with brine, dried over anhydrous Na_2SO_4 , and concentrated under reduced pressure to obtain a crude, which was purified by column chromatography (EtOAc/hexanes, 2:8) to give pure Octamethyl-8-(1-phenethylaziridin-2-yl)-4,9-dioxa-3,10-disiladodecan-6-one **15** as a yellow liquid (2.1 g, 62%) yield. The ^1H NMR (400 MHz, CDCl_3) δ 7.27–7.25 (m, 2H), 7.18 (t, $J = 7.6$ Hz, 3H), 4.17 (s, 2H), 4.00–3.90 (m, 1H), 2.82 (t, $J = 6.9$ Hz, 2H), 2.65–2.59 (m, 2H), 2.59–2.52 (m, 1H), 2.35–2.28 (m, 1H), 1.66 (d, $J = 2.5$ Hz, 1H), 1.54 (dd, $J = 9.0, 6.4$ Hz, 1H), 1.18 (d, $J = 6.0$ Hz, 1H), 0.92 (s, 9H), 0.87 (s, 9H), 0.10 (s, 6H), 0.08 (s, 6H). The ^{13}C NMR (101 MHz, CDCl_3) δ 208.1, 139.9, 128.6, 128.3, 126.0, 70.1, 70.0, 62.9, 43.9, 43.8, 36.3, 31.1, 25.8, 25.8, 18.3, 18.0, -3.5 , -4.3 , -4.9 , -5.4 . HRMS-ESI (m/z): $[\text{M} + \text{H}]^+$ calcd. for $\text{C}_{26}\text{H}_{47}\text{NO}_3\text{Si}_2$, 448.4378, found 448.4382. Copies of ^1H and ^{13}C NMR could be found in Supplementary Materials.

(5-(((*tert*-Butyldimethylsilyl)oxy)methyl)-1-phenethyl-1*H*-pyrrol-2-yl)methyl acetate (**16**)

To a stirred solution of Octamethyl-8-(1-phenethylaziridin-2-yl)-4,9-dioxa-3,10-disiladodecan-6-one **15** (1.5 g, 3.13 mmol) in dry CH_2Cl_2 (30 mL) was added acetic acid (0.56 mL, 6.27 mmol) at $0\text{ }^{\circ}\text{C}$ under an N_2 atmosphere. After 6 h stirred at $0\text{ }^{\circ}\text{C}$, the reaction mixture was quenched with saturated aqueous NH_2CO_3 (10 mL). The organic layer was separated, and the aqueous layer was extracted with CH_2Cl_2 (2×20 mL). The organic layer was dried over Na_2SO_4 and concentrated in vacuo to obtain the crude product, which was purified by column chromatography (EtOAc/hexanes, 2:8) to give pure (5-(((*tert*-butyldimethylsilyl)oxy)methyl)-1-phenethyl-1*H*-pyrrol-2-yl)methyl acetate **16** as a yellow liquid (1.0 g, 82%) yield. The ^1H NMR (400 MHz, CDCl_3) δ 7.30 (dd, $J = 7.9, 6.4$ Hz, 2H), 7.23 (d, $J = 7.4$ Hz, 1H), 7.14–7.11 (m, 2H), 6.15 (d, $J = 3.5$ Hz, 1H), 6.00 (d, $J = 3.5$ Hz, 1H), 4.96 (s, 2H), 4.53 (s, 2H), 4.17 (t, $J = 6.5$ Hz, 2H), 3.06 (t, $J = 6.2$ Hz, 2H), 2.06 (s, 3H), 0.89 (s, 9H), 0.05 (s, 6H). The ^{13}C NMR (101 MHz, CDCl_3) δ 170.7, 138.6, 133.5, 128.8, 128.6, 127.3, 126.6, 110.4, 108.0, 57.9, 57.6, 45.8, 38.0, 25.9, 21.1, 18.3, -5.2 . HRMS-ESI (m/z): $[\text{M} + \text{Na}]^+$ calcd. for $\text{C}_{22}\text{H}_{33}\text{NNaO}_3\text{Si}$, 410.6150, found 410.6158. Copies of ^1H and ^{13}C NMR could be found in Supplementary Materials.

(5-(((*tert*-Butyldimethylsilyl)oxy)methyl)-1-phenethyl-1*H*-pyrrol-2-yl)methanol (**17**)

To a stirred solution of (5-(((*tert*-butyldimethylsilyl)oxy)methyl)-1-phenethyl-1*H*-pyrrol-2-yl)methyl acetate **16** (0.7 g, 1.80 mmol) in MeOH (10 mL) was added potassium carbonate (0.249 g, 1.80 mmol) at $0\text{ }^{\circ}\text{C}$, and the mixture was stirred for 1 h at rt. Then, MeOH was removed under vacuum and extracted with CH_2Cl_2 (2×10 mL). The organic layer was dried over Na_2SO_4 and concentrated in vacuo to obtain the crude product, which was purified by column chromatography (EtOAc/hexanes, 4:6) to give pure (5-(((*tert*-butyldimethylsilyl)oxy)methyl)-1-phenethyl-1*H*-pyrrol-2-yl)methanol (**17**) as a yellow liquid (0.5 g, 80% yield). The ^1H NMR (400 MHz, CDCl_3) δ 7.32–7.20 (m, 3H), 7.15–7.10 (m, 2H), 6.01 (d, $J = 3.5$ Hz, 1H), 5.97 (d, $J = 3.5$ Hz, 1H), 4.55 (s, 2H), 4.42 (s, 2H), 4.24 (t, $J = 6.5$ Hz, 2H), 3.10 (t, $J = 6.2$ Hz, 2H), 0.90 (s, 9H), 0.06 (s, 6H). The ^{13}C NMR (101 MHz, CDCl_3) δ 138.9, 133.1, 132.7, 128.9, 128.5, 126.5, 107.8, 107.7, 57.6, 56.9, 45.7, 38.0, 25.9, 18.3, -5.2 . HRMS-ESI (m/z): $[\text{M} + \text{H}]^+$ calcd. for $\text{C}_{20}\text{H}_{32}\text{NO}_2\text{Si}$, 346.5226, found 346.5231.

5-(((*tert*-Butyldimethylsilyl)oxy)methyl)-1-phenethyl-1*H*-pyrrole-2-carbaldehyde (**18**)

To a stirred solution of alcohol **17** (0.5 g, 1.29 mmol) in dry CH_2Cl_2 (4 mL) was added Dess–Martin periodinane (0.820 g, 1.93 mmol) at $0\text{ }^{\circ}\text{C}$, and the mixture was stirred for 1 h at rt. Then, the reaction mixture was quenched with a 1:1 mixture of saturated solution of NaHCO_3 (10 mL) and extracted with CH_2Cl_2 (2×10 mL). The organic layer was dried over Na_2SO_4 and concentrated in vacuo to obtain the crude product, which was purified by column chromatography (EtOAc/hexanes, 2:8) to give pure aldehyde **18** as a yellow liquid (330 mg, 74% yield). The ^1H NMR (400 MHz, CDCl_3) δ 9.55 (s, 1H), 7.27 (dd, $J = 5.2, 2.1$ Hz, 3H), 7.16–7.13 (m, 2H), 6.90 (d, $J = 4.0$ Hz, 1H), 6.11 (d, $J = 4.0$ Hz, 1H), 4.53

(t, $J = 6.5$ Hz, 2H), 4.31 (s, 2H), 3.04 (t, $J = 6.2$ Hz, 2H), 0.89 (s, 9H), 0.04 (s, 6H). The ^{13}C NMR (101 MHz, CDCl_3) δ 179.2, 142.2, 138.6, 132.0, 129.0, 128.4, 126.5, 124.5, 109.6, 57.0, 47.6, 37.6, 25.8, 18.2, -5.3 . HRMS-ESI (m/z): $[\text{M} + \text{H}]^+$ calcd. for $\text{C}_{20}\text{H}_{30}\text{NO}_2\text{Si}$, 344.2264, found 344.2269. Copies of ^1H and ^{13}C NMR could be found in Supplementary Materials.

5-(Hydroxymethyl)-1-phenethyl-1H-pyrrole-2-carbaldehyde (19)

To a stirred solution of 5-(((*tert*-butyldimethylsilyl)oxy)methyl)-1-phenethyl-1H-pyrrole-2-carbaldehyde (18) (0.3 g, 0.87 mmol) in dry THF (10 mL) was added TBAF (0.94 mL, 1.0 M in THF, 0.96 mmol) at 0 °C and stirred for 1 h. After completion of the reaction was quenched with saturated aqueous NH_2CO_3 (10 mL). The organic layer was separated, and the aqueous layer was extracted with ethyl acetate (2×20 mL). The organic layer was dried over Na_2SO_4 and concentrated in vacuo to obtain the crude product, which was purified by column chromatography (EtOAc/hexanes, 3:7) to give pure 5-(hydroxymethyl)-1-phenethyl-1H-pyrrole-2-carbaldehyde 19 as a yellow oil (168 mg, 84% yield). The ^1H NMR (400 MHz, CDCl_3) δ 9.58 (s, 1H), 7.27–7.21 (m, 3H), 7.10 (d, $J = 6.5$ Hz, 2H), 6.93 (d, $J = 4.0$ Hz, 1H), 6.17 (d, $J = 4.0$ Hz, 1H), 4.55 (t, $J = 7.2$ Hz, 2H), 4.29 (s, 2H), 3.05 (t, $J = 7.2$ Hz, 2H). The ^{13}C NMR (101 MHz, CDCl_3) δ 179.4, 141.7, 138.5, 132.2, 129.0, 128.6, 126.7, 124.6, 110.0, 56.3, 47.6, 37.7. HRMS-ESI (m/z): $[\text{M} + \text{H}]^+$ calcd. for $\text{C}_{14}\text{H}_{16}\text{NO}_2$, 230.1178, found 230.1185. Copies of ^1H and ^{13}C NMR could be found in Supplementary Materials.

4. Conclusions

In summary, multi-substituted pyrroles were synthesized from regiospecific aziridine ring opening and subsequently intramolecular cyclization with a carbonyl group at the γ -position in the presence of Lewis acid (TMSN_3 or ZnCl_2) or protic acid (AcOH). This method is high atom economical in that all reactants are incorporated into the final product with the removal of water. This new protocol can be applied to the synthesis of various pyrroles, including natural products.

Supplementary Materials: The following supporting information can be downloaded at: <https://www.mdpi.com/article/10.3390/molecules27206869/s1>; All analytical data of compounds other than the representative example are reported along the copies of ^1H and ^{13}C NMR spectra.

Author Contributions: Conceptualization, H.-J.H. and L.M.; methodology, R.J. and S.-Y.N.; investigation, H.-J.H., L.M. and R.J.; experiments and data curation, L.M. and R.J.; writing—original draft preparation, H.-J.H.; writing—review and editing, H.-J.H. and L.M.; supervision, H.-J.H.; project administration, H.-J.H.; funding acquisition, H.-J.H. All authors have read and agreed to the published version of the manuscript.

Funding: This research was supported by the National Research Foundation of Korea (NRF-2012M3A7B4049645 and 2021R1A5A6002803 with the Centre for New Directions in Organic Synthesis). Additional financial support from 2020R1A2C1007102 and HUFs Grant 2022 (for the preparation of this manuscript) are also appreciated.

Institutional Review Board Statement: Not applicable.

Informed Consent Statement: Not applicable.

Data Availability Statement: Not applicable.

Acknowledgments: This work was supported by the National Research Foundation of Korea (NRF-2012M3A7B4049645 and 2014R1A5A1011165 with the Centre for New Directions in Organic Synthesis). Additional financial support from HUFs Grant 2018 is also appreciated.

Conflicts of Interest: The authors declare no conflict of interest.

Sample Availability: Samples of the compounds are available from the authors.

References

1. Gholap, S.S. Pyrrole: An emerging scaffold for construction of valuable therapeutic agents. *Eur. J. Med. Chem.* **2016**, *110*, 13–31. [CrossRef]
2. Estévez, V.; Villacampa, M.; Menéndez, J.C. Multicomponent reactions for the synthesis of pyrroles. *Chem. Soc. Rev.* **2010**, *39*, 4402–4421. [CrossRef]
3. Zhang, L.-Y.; Bai, H.-B.; Shan, W.-G.; Zhan, Z.-J. A new Alkaloid from the Mycelium of *Inonotus Obliquus*. *J. Chem. Res.* **2014**, *38*, 245–246. [CrossRef]
4. Wood, J.M.; Furkert, D.P.; Brimble, M.A. 2-Formylpyrrole natural products: Origin, structural diversity, bioactivity and synthesis. *Nat. Prod. Rep.* **2019**, *36*, 289–306. [CrossRef]
5. Mal, D.; Shome, B.; Dinda, B.K. Pyrrole and Its Derivatives. In *Heterocycles in Natural Product Synthesis*; Majumdar, K.C., Chattopadhyay, S.K., Eds.; Wiley: Hoboken, NJ, USA, 2011; Chapter 6; p. 187.
6. Park, Y.M.; Won, J.H.; Kim, Y.H.; Choi, J.W.; Park, H.J.; Lee, K.L. In vivo and in vitro anti-inflammatory and anti-nociceptive effects of the methanol extract of *Inonotus obliquus*. *J. Ethnopharmacol.* **2005**, *101*, 120–128. [CrossRef]
7. Lee, I.K.; Kim, Y.S.; Jang, Y.W.; Jung, J.Y.; Yun, B.S. New antioxidant polyphenols from the medicinal mushroom *Inonotus obliquus*. *Bioorg Med Chem Lett.* **2007**, *17*, 6678–6681. [CrossRef]
8. Szychowski, K.A.; Skora, B.; Pomianek, T.; Gminski, J. *Inonotus obliquus* - from folk medicine to clinical use. *J. Tradit. Complement. Med.* **2021**, *11*, 293–302. [CrossRef]
9. Zheng, W.; Zhang, M.; Zhao, Y.; Wang, Y.; Miao, K.; Wei, Z. Accumulation of antioxidant phenolic constituents in submerged cultures of *Inonotus obliquus*. *Bioresour. Technol.* **2009**, *100*, 1327–1335. [CrossRef]
10. Cui, Y.; Kim, D.-S.; Park, K.-C. Antioxidant effect of *Inonotus obliquus*. *J. Ethnopharmacol.* **2005**, *96*, 79–85. [CrossRef]
11. Kim, Y.O.; Han, S.B.; Lee, H.W.; Ahn, H.J.; Yoon, Y.D.; Jung, J.K.; Shin, C.S. Immuno-stimulating effect of the endo-polysaccharide produced by submerged culture of *Inonotus obliquus*. *Life Sci.* **2005**, *77*, 2438–2456. [CrossRef]
12. Cha, J.-Y.; Jun, B.-S.; Yoo, K.-S.; Hahm, J.-R.; Cho, Y.-S. Fermented Chaga Mushroom (*Inonotus obliquus*) Effects on Hypolipidemia and Hepatoprotection in Otsuka Long-Evans Tokushima Fatty (OLETF) Rats. *Food Sci. Biotechnol.* **2006**, *15*, 122–127.
13. Paal, C. Synthese von Thiophen-und Pyrrolderivaten. *Ber. Dtsch. Chem. Ges.* **1885**, *18*, 367. [CrossRef]
14. Knorr, L. Synthesis of pyrroline-derivatives II. *Chem. Ber.* **1884**, *17*, 1635. [CrossRef]
15. Hantzsch, A. Neue Bildungsweise von Pyrrolderivaten. *Ber. Dtsch. Chem. Ges.* **1890**, *23*, 1474–1476. [CrossRef]
16. Gulevich, A.V.; Dudnik, A.S.; Chernyak, N.; Gevorgyan, V. Transition Metal-Mediated Synthesis of Monocyclic Aromatic Heterocycles. *Chem. Rev.* **2013**, *113*, 3084–3213. [CrossRef] [PubMed]
17. Doyle, M.P.; Dong, K.; Humeidi, A.; Griffith, W.; Arman, H.; Xu, X. Ag^I-Catalyzed Reaction of Enol Diazoacetates and Imino Ethers: Synthesis of Highly Functionalized Pyrroles. *Angew. Chem., Int. Ed.* **2021**, *60*, 13394–13400.
18. Stankovic, S.; D'hooghe, M.; Catak, S.; Eum, H.; Waroquier, M.; Van Speybroeck, V.; De Kimpe, N.; Ha, H.-J. Regioselectivity in the ring-opening of non-activated aziridines. *Chem. Soc. Rev.* **2012**, *41*, 643–665. [CrossRef]
19. Choi, J.; Yu, T.; Ha, H.-J. Alkylative Aziridine Ring-Opening Reactions. *Molecules* **2021**, *26*, 1703. [CrossRef]
20. Ranjith, J.; Ha, H.-J. Synthetic Applications of Aziridinium Ions. *Molecules* **2021**, *26*, 1774. [CrossRef]
21. Chen, J.R.; Hu, X.Q.; Lu, L.Q.; Xiao, W.J. Exploration of Visible-Light Photocatalysis in Heterocycle Synthesis and Functionalization: Reaction Design and Beyond. *Acc. Chem. Res.* **2016**, *49*, 1911–1923. [CrossRef]
22. Estevez, V.; Villacampa, M.; Menendez, J.C. Recent advances in the synthesis of pyrroles by multicomponent reactions. *Chem. Soc. Rev.* **2014**, *43*, 4633–4657. [CrossRef] [PubMed]
23. Yadav, N.N.; Jeong, H.; Ha, H.-J. Atom-Economical and Metal-Free Synthesis of Multisubstituted Furans from Intramolecular Aziridine Ring Opening. *ACS Omega* **2017**, *2*, 7525–7531. [CrossRef] [PubMed]
24. Macha, L.; D'hooghe, M.; Ha, H.J. Deployment of Aziridines for the Synthesis of Alkaloids and Their Derivatives. *Synthesis* **2019**, *51*, 1491–1515.
25. Kim, J.H.; Lee, S.B.; Lee, W.K.; Yoo, D.-H.; Ha, H.-J. Synthesis of 1,2,5- and 1,2,3,5-substituted pyrroles from substituted aziridines via Ag(I)-catalyzed intramolecular cyclization. *Tetrahedron* **2011**, *67*, 3553–3558. [CrossRef]
26. Lee, H.; Kim, J.H.; Lee, W.K.; Jung, J.-H.; Ha, H.-J. Synthesis of 2,5-Disubstituted 6-Azaindoles from Substituted Aziridines via Intramolecular Cyclization. *Org. Lett.* **2012**, *14*, 3120–3122. [CrossRef]

Article

Functionalized 10-Membered Aza- and Oxaenediynes through the Nicholas Reaction

Natalia A. Danilkina ¹, Ekaterina A. Khmelevskaya ¹, Anna G. Lyapunova ¹, Alexander S. D'yachenko ¹, Alexander S. Bunev ², Rovshan E. Gasanov ², Maxim A. Gureev ^{3,4} and Irina A. Balova ^{1,*}

¹ Institute of Chemistry, Saint Petersburg State University (SPbU), Universitetskaya nab. 7/9, 199034 Saint Petersburg, Russia

² Medicinal Chemistry Center, Tolyatti State University, 445020 Tolyatti, Russia

³ Center of Chemo- and Bioinformatics, I. M. Sechenov First Moscow State Medical University, 119991 Moscow, Russia

⁴ Department of Computational Biology, Sirius University of Science and Technology, 354349 Sochi, Russia

* Correspondence: i.balova@spbu.ru

Abstract: The scope and limitations of the Nicholas-type cyclization for the synthesis of 10-membered benzothiophene-fused heterocyclic enediynes with different functionalities were investigated. Although the Nicholas cyclization through oxygen could be carried out in the presence of an ester group, the final oxaenediyne was unstable under storage. Among the N-type Nicholas reactions, cyclization via an arenesulfonamide functional group followed by mild Co-deprotection was found to be the most promising, yielding 10-membered azaenediynes in high overall yields. By contrast, the Nicholas cyclization through the acylated nitrogen atom did not give the desired 10-membered cycle. It resulted in the formation of a pyrroline ring, whereas cyclization via an alkylated amino group resulted in a poor yield of the target 10-membered enediyne. The acylated 4-aminobenzenesulfonamide nucleophilic group was found to be the most convenient for the synthesis of functionalized 10-membered enediynes bearing a clickable function, such as a terminal triple bond. All the synthesized cyclic enediynes exhibited moderate activity against lung carcinoma NCI-H460 cells and had a minimal effect on lung epithelial-like WI-26 VA4 cells and are therefore promising compounds in the search for novel antitumor agents that can be converted into conjugates with tumor-targeting ligands.

Keywords: alkynes; enediynes; heterocycles; benzo[*b*]thiophene; Bergman cyclization; Nicholas reaction; Sonogashira coupling; benzenesulfonamides

Citation: Danilkina, N.A.; Khmelevskaya, E.A.; Lyapunova, A.G.; D'yachenko, A.S.; Bunev, A.S.; Gasanov, R.E.; Gureev, M.A.; Balova, I.A. Functionalized 10-Membered Aza- and Oxaenediynes through the Nicholas Reaction. *Molecules* **2022**, *27*, 6071. <https://doi.org/10.3390/molecules27186071>

Academic Editors: Alexey M. Starosotnikov, Maxim A. Bastrakov and Igor L. Dalinger

Received: 4 September 2022

Accepted: 14 September 2022

Published: 17 September 2022

Publisher's Note: MDPI stays neutral with regard to jurisdictional claims in published maps and institutional affiliations.



Copyright: © 2022 by the authors. Licensee MDPI, Basel, Switzerland. This article is an open access article distributed under the terms and conditions of the Creative Commons Attribution (CC BY) license (<https://creativecommons.org/licenses/by/4.0/>).

1. Introduction

Enediyne antibiotics are an important class of natural products [1–7]. Although the first derivatives of 10-membered enediynes, Esperamicin [8] and Calicheamicin γ_1^I [9,10], were isolated from bacteria almost forty years ago, interest in these unusual natural products and their use has continued [11,12] due to the unprecedented toxicity of these products to various cell lines [13]. The described biological activity of cyclic enediynes is associated with their ability to undergo the Bergman cyclization [14,15] with the formation of highly reactive diradicals that damage DNA and kill cancer cells [16] (Figure 1a). Currently, enediynes are the focus of the search for novel anticancer drugs based on the conjugation of natural enediyne warheads with monoclonal antibodies (MABs) to obtain antibody-drug conjugates (ADCs) [17–19]. Thus, two ADSs of Calicheamicin γ_1^I , Gemtuzumab ozogamicin (Mylotarg[®]) [20] and Inotuzumab ozogamicin (Besponsa[®]) [21], have been approved for the targeted treatment of various types of cancer (Figure 1b,c).

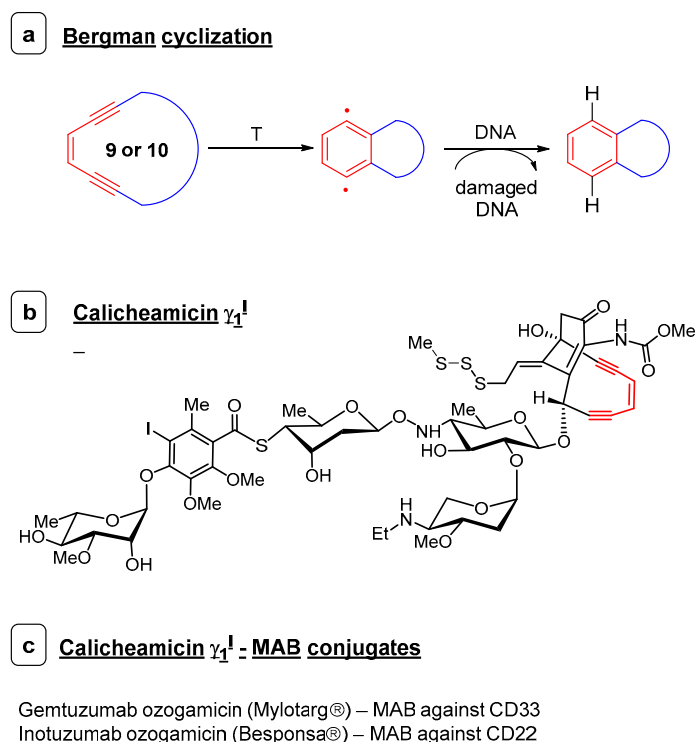


Figure 1. The Bergman Cyclization as a Mode of Action of Eneidyne Antibiotics (a); the Structure of Calicheamicin γ_1^I (b) and the Trademarks of Anticancer Drugs Based on Calicheamicin γ_1^I (c).

However, studies devoted to analogs of natural enediynes are also extremely important [22–31]. Recently, Nicolaou's group reported a synthetic approach to tiancimycin B and uncialamycin analogs with promising antitumor activity (Figure 2a) [32]. Ding and Hu's groups have successfully elaborated maleimide-assisted rearrangement and cycloaromatization (MARACA) of acyclic analogs of enediyne antibiotics that have been found to be active against different types of cancer cells [33–36] (Figure 2b).

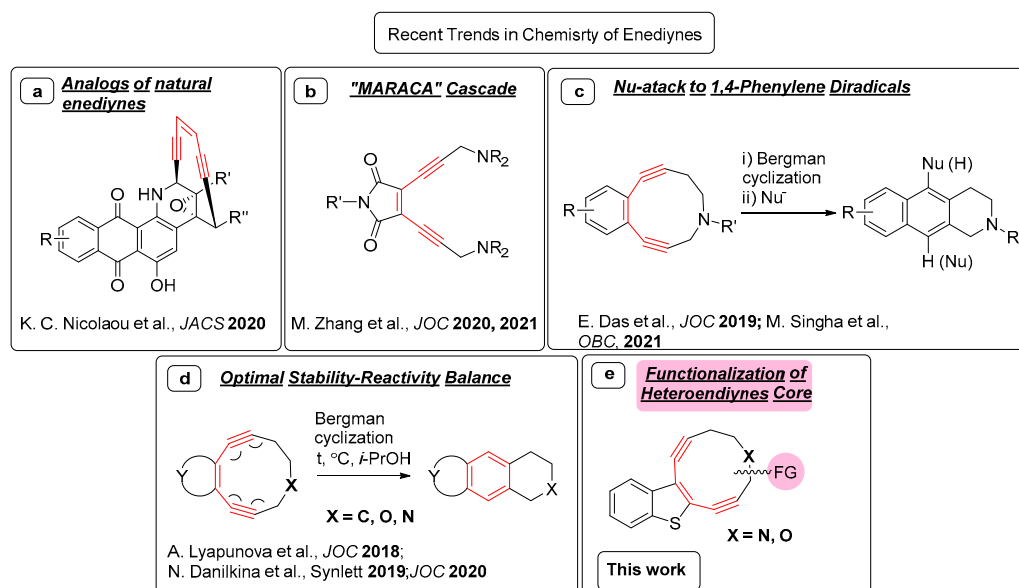


Figure 2. Recent Trends in the Chemistry of Eneidyne Systems (a–d) in Comparison with the Current Study (e).

Another recent focus in this field is the Bergman cyclization followed by the nucleophilic attack to 1,4-phenylene diradicals and the formation of halogen-substituted polyaromatic products [34,37] and the use of these products in organic synthesis (Figure 2c) [38]. Enolate ions as nucleophiles have recently been shown to be active in trapping 1,4-phenylene diradicals formed from 10-membered enediyne [39]. Moreover, intramolecular “nucleophilic trapping” of the diradicals formed by MARACA-type cyclization is possible [40].

Our efforts in this area have been concentrated on the intensive study of the molecular design of 10-membered heteroenediyne systems fused to heterocycles. Note that naturally occurring enediynes are protected from spontaneous Bergman cyclization due to specific structural features, and the enediyne core becomes reactive only after activation by special triggering [16]. Therefore, in the search for simple active cyclic analogs of natural enediynes lacking masking groups, the optimal balance between the stability of enediyne molecules during synthesis, isolation, and storage and the reactivity of these analogs in the Bergman cyclization is of decisive importance. We recently reported that this balance could be regulated by the nature of the fused heterocyclic core, as well as by the nature of the endocyclic σ -acceptor bound to the propargylic carbon atom of the enediyne system [41–43] (Figure 2d). Moreover, we proposed that the deviation of alkyne bond angles from 180° (alkyne bending) as well as the difference in bending of the ground state and the Bergman cyclization transition state can be used as parameters for the evaluation of the reactivity of annulated enediynes in the Bergman cyclization [41] instead of the «cd-distance» [44]. It is noteworthy that the same approach has recently been extended by Basak’s group to other families of enediyne [45].

Thus, the optimal balance between stability, the Bergman cyclization reactivity, and DNA cleavage ability was found for benzothiophene-fused azaenediynes [41,43], whereas O-enediynes were somewhat less stable but had slightly higher DNA damaging activity [42]. While searching for convenient synthetic methods for constructing strained 10-membered enediyne systems fused to a five-membered heterocycle, we found the Nicholas reaction to be the most promising and effective synthetic tool [42,43,46] because other reactions, such as ring-closing metathesis [47] and the Nozki–Hiama–Kishi reaction, do not work in this case [48].

The Nicholas reaction, namely, the alkylation of various nucleophilic functional groups with a stabilized $\text{Co}_2(\text{CO})_6$ -propargyl carbocation [49–54], has several characteristics necessary for the successful closing of a strained enediyne cycle. Thus, in acyclic precursors, the proximity of reaction centers contributes to the formation of a 10-membered ring; Co-protected enediynes are less strained and therefore more stable than their cobalt-free derivatives and can be stored for a long time as $\text{Co}_2(\text{CO})_6$ -enediyne complexes and simply can be deprotected from cobalt under mild conditions, if necessary.

However, all the heteroenediynes previously synthesized through the Nicholas-type cyclization lacked any functionality for further modification of the 10-membered core to control the solubility of target molecules, increase the affinity of these target molecules for cancer cells, and produce ADCs [41–43,46]. Here, we explored the possibilities of using Nicholas cyclization in the construction of functionalized aza- as well as oxanediynes suitable for further synthetic modifications. We show that the Nicholas reaction through O- and N-atoms, can be used to synthesize benzothiophene-fused enediynes with different functional groups (Figure 2e): ester, *o*-nosyl functional groups, or a terminal triple bond. Arenesulfonamide nucleophilic group was found to be the optimal moiety for the synthesis of functionalized enediynes.

2. Results

Searching for the optimal nucleophilic functional group for the synthesis of functionalized 10-membered oxa- and azaenediynes, we chose the target structures I–V (Figure 3), which can be obtained using cyclization through OH (I), NHSO_2Ar (II, III), NHBn (IV) and NHBz (V).

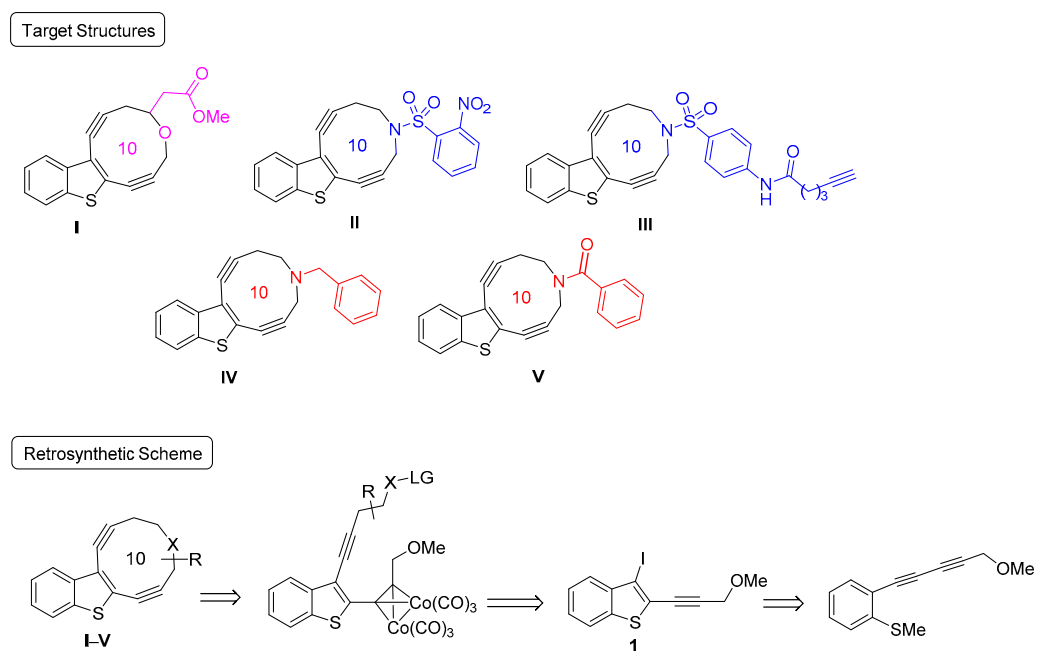


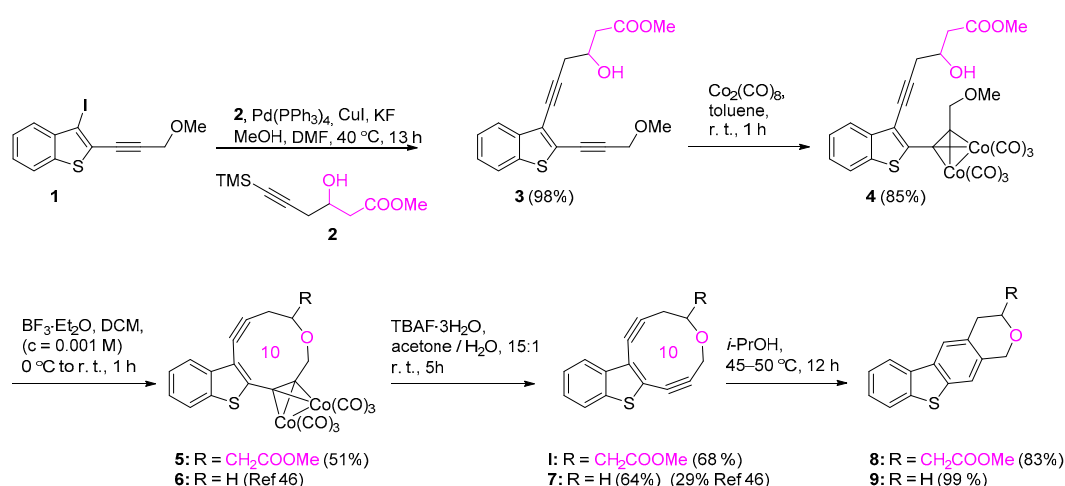
Figure 3. General Approach for Synthesizing the Target 10-Membered Heteroenediyne (LG–Leaving Group).

Synthesis of all the target structures is based on a combination of electrophile-promoted cyclization of the starting diacetylene and the subsequent Sonogashira coupling to construct unsymmetrically substituted acyclic enediyne with the required functionalities at both triple bonds followed by the regioselective formation of $\text{Co}_2(\text{CO})_6$ -complexes for the further Nicholas cyclization [42,46,55] (Figure 3). The key intermediate compound for all the structures was 3-iodo-2-(3-methoxyprop-1-yn-1-yl)benzo[*b*]thiophene (**1**), which is available synthetically at the multigram scale as has been previously reported [46].

2.1. Synthesis of Oxaenediyne I

A four-step synthesis of the ester-functionalized O-enediyne **I** was started from 3-iodobenzothiophene **1**. Desilylation of the functionalized alkyne **2** and the Sonogashira coupling were carried out in one pot using $\text{KF}/\text{MeOH}/\text{DMF}$ as the desilylation source (Scheme 1) [56]. Further complexation of the enediyne **3** with $\text{Co}_2(\text{CO})_8$ proceeded regioselectively with the formation of the cobalt complex **4** at the C2-triple bond. The higher selectivity for the C2-triple bond compared with the nonfunctionalized enediyne can be explained by the higher steric hindrance of the triple bond at the C3 position [46].

The Nicholas reaction of the ester-functionalized complex **4** proceeded under optimized conditions (1.5 equiv. of $\text{FB}_3 \cdot \text{Et}_2\text{O}$) to afford the cyclic product **5** in good yield. We recently showed that using tetrabutylammonium fluoride (TBAF) hydrate in an aqueous acetone solution increases the yield of cobalt-free 10-membered enediyne in the decomplexation step [43]. Therefore, we applied these conditions to the ester-functionalized Co-complex **5**, as well as to the previously reported Co-complex of the nonfunctionalized O-enediyne **6**, which allowed us to obtain the enediyne **I** and noticeably increase the yield of the enediyne **7** at the decomplexation step compared with previous results [46]. However, the target ester-containing enediyne **I** was significantly less stable than its unsubstituted analog **7** and gave traces of the Bergman cyclization product in experiments with NMR detection. Then, the Bergmann cyclization of the enediyne **I** and **7** was carried out in *i*-PrOH at 45–50 °C, and both cyclization products **8** and **9** were isolated in high yields.

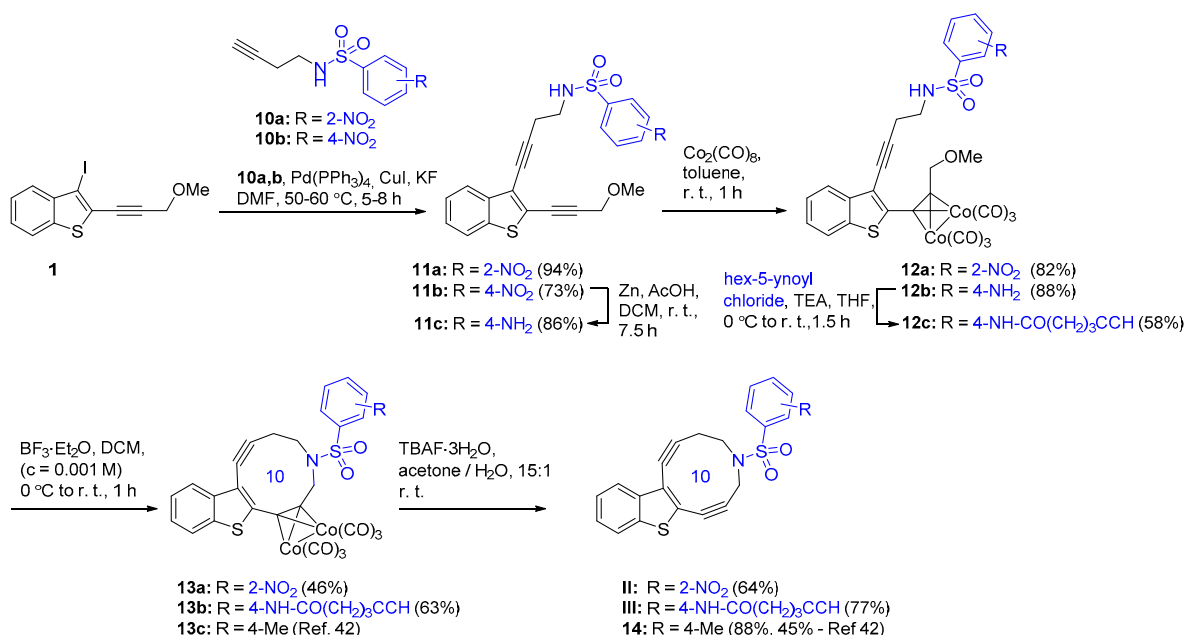


Scheme 1. Synthesis of O-enediynes I.

2.2. Synthesis of Azaenediynes II–V

We recently showed that the amino functional group protected by the tosyl group (NH-Ts) is very efficient for the synthesis of azaenediynes through the Nicholas cyclization, and there was an optimal balance between the stability and DNA-damaging activity of the resulting N-Ts-enediyne [42]. Therefore, we decided to use an arenesulfonamide fragment to introduce functional groups into the N-enediyne molecule. Two types of functionalized arenesulfonamide moieties were used: 2-nosyl as an easily removable protecting group and a sulfanilamide moiety with an NH_2 group acylated with hex-5-ynoic acid.

The N-Ns (2-nosyl, 2-nitrobenzenesulfonyl) enediyne **III** was synthesized similarly to the N-Ts enediyne [42] (Scheme 2).



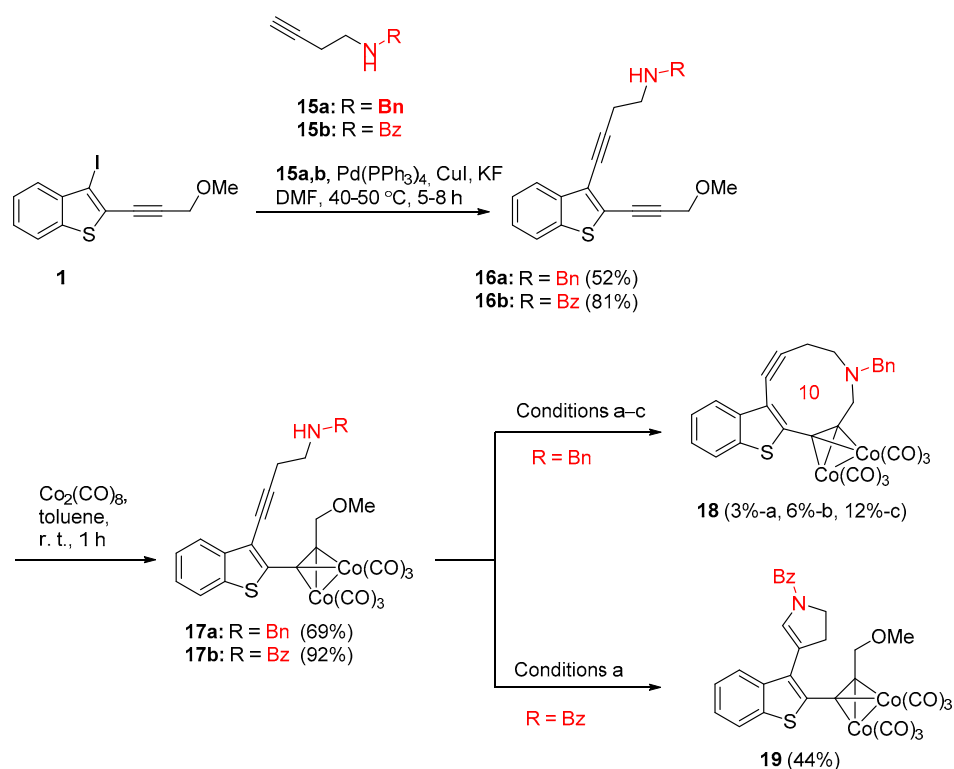
Scheme 2. Synthesis of N-enediynes via the Benzenesulfonamide Functional Group.

Thus, the starting Co-complex **12a** for the Nicholas reaction was obtained without any difficulties and in high yield. However, the Nicholas reaction of the NH-Ns group formed the product **13a** in a considerably lower yield (46%) compared with the NH-Ts function

(76%) and required a higher quantity of a Lewis acid (8 equiv. instead of 1.5 equiv.) [42], which can be explained both by the steric hindrance and lower nucleophilicity of NH-Ns.

To synthesize the *N*-hex-5-ynoyl enediyne **III**, the obtained *p*-NO₂Ph-substituted enediyne **11b** was reduced by Zn in the AcOH/DCM system to the NH₂-derivative **11c**, which was then converted to the Co-complex **12b**. Then, the Co-complex **12b** was acylated with hex-5-ynoyl chloride to produce the nontrivial triacetylenic compound **12c**, in which only one triple bond out of three was converted to the Co complex. The Nicholas cyclization of the *N*-protected/functionalized Co-complex **12c** proceeded smoothly to give the desired cyclic Co-complex **13b** in good yield (64%). It should be emphasized that the Nicholas cyclization of the Co-complex with the free NH₂ group **12b** did not proceed at all. Therefore, protection, along with functionalization at the stage of an acyclic Co-complex, is a necessary synthetic step for producing a 10-membered enediyne with a terminal triple bond. Finally, we investigated the last decomplexation step, which proceeded in good to high yields to give the *N*-enediynes **II** and **III**, which were stable under isolation and storage. We also tested decomplexation in aqueous acetone for the Co-complex of the *N*-Ts-enediyne **13c**, which has been previously reported [42]. In this case, we succeeded in increasing the yield of **14** at the decomplexation step from 45% (in anhydrous acetone) [42] to 88% (in aqueous acetone).

It is known that the Nicholas-type cyclization can proceed using amide functional groups [57] and even through secondary amino groups in the presence of DIPEA [58]. Therefore, we decided to test these functional groups, which could also be useful for the functionalization of enediynes. Therefore, cyclization using NHBn and NHBz groups was also studied (Scheme 3).



Reagents and conditions:

a) BF₃·OEt₂ (4.5 equiv.), 0 °C-r.t.; b) HBF₄·OEt₂ (3.6 equiv.), 0 °C-r.t.; c) HBF₄·OEt₂ (8 equiv.), DIPEA (9 equiv.), -20 °C-r.t.

Scheme 3. Attempts to Synthesize *N*-enediynes **IV** and **V** through NH-Benzyl and NH-Benzoyl Functionalities.

The corresponding starting materials, the Co-complexes **17a** and **17b**, were synthesized without any difficulties starting from iodobenzothiophene **1** and the corresponding

functionalized terminal alkynes **15a** and **15b** in two steps (Scheme 3); however, cyclization failed in both cases. Thus, the conditions tested for the Nicholas cyclization of the NHBn Co-complex **17a** ($\text{BF}_3 \cdot \text{Et}_2\text{O}$; $\text{HBF}_4 \cdot \text{Et}_2\text{O}$ and $\text{HBF}_4 \cdot \text{Et}_2\text{O}/\text{DIPEA}$) gave the desired cyclic compound **18** in low yields due to the complexation of the NHBn group with the acid. Even generation of the carbocation with $\text{HBF}_4 \cdot \text{OEt}_2$ followed by deprotonation of the $[\text{NH}_2\text{Bn}]^+$ group with DIPEA only gave a 12% yield of the cyclic enediyne **18**. Therefore, the basicity of the secondary amino function should be considered a strong limitation of the Nicholas reaction in the case of enediyne systems.

Cyclization of the complex **17b** using an NH-benzoyl moiety as a nucleophilic group did not give the desired 10-membered enediyne at all (Scheme 3). The main product of the reaction was the pyrroline derivative **19** due to the electrophile-promoted cyclization of the NHBz functional group at the free triple bond. This result can be explained by the higher steric hindrance of the planar NHBz group compared with that of the tetrahedral arenesulfonamide functional group. Thus, we have proven that the sulfonamide moiety remains the functional group of choice when using the aza-Nicholas reaction to synthesize 10-membered N-enediynes.

2.3. Biological Activity of Cyclic Enediynes

All the synthesized 10-membered enediynes (**I–III**, **7**, and **14**) were tested for their effect on the growth of NCI-H460 lung carcinoma and WI-26 VA4 lung epithelial-like cell lines using the MTT colorimetric test [59,60] with the cytotoxic drug etoposide as a positive control. All the enediynes at a concentration of 75 μM displayed moderate cytotoxicity toward cancer cells and had less effect on normal fibroblasts (Figure 4).

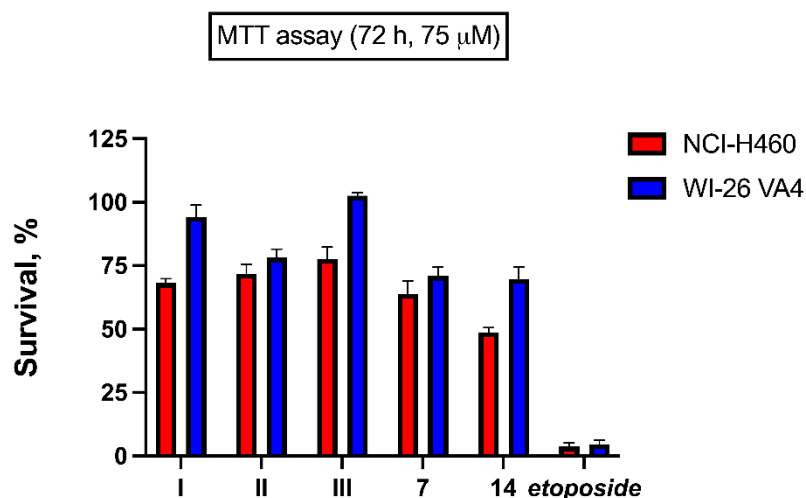


Figure 4. Screening for the Cytotoxicity of the Enediynes **I–III**, **7** and **14**.

These data correspond with the previously estimated ability of benzothiophene-fused enediynes to cleave plasmid DNA [41,42,46]. Therefore, the observed cytotoxic activity of enediynes is assumed to be associated with their DNA damaging effect. However, it is clear that for DNA to be affected and destroyed in cells, a molecule must have a sufficient hydrophilic-lipophilic balance and the ability to penetrate into cells and avoid various drug resistance mechanisms. Therefore, to improve the cytotoxic effect of enediynes, the functional design of benzothiophene-fused enediyne molecules should be elaborated. From this point of view, considering the absence of significant differences in cytotoxicity, N-enediynes are the most promising compounds for further development of antitumor agents. Thus, functionalized derivatives of N-enediynes are stable and synthetically accessible and can be used for further conjugation with ligands with an affinity for cancer cells.

3. Discussion

The scope and limitation of the Nicholas-type cyclization for the synthesis of various 10-membered azaenediynes, as well as oxa-analog were studied. We used two types of heteroatoms—oxygen and nitrogen, to choose which type of heteroenediynes and which type of nucleophilic functional groups are most suitable for the synthesis of heteroenediynes that have additional functionality for further modification with tumor-targeting ligands.

We showed that functionalized O-enediyne with an ester group attached to the enediyne core is synthetically accessible through the O-Nicholas reaction. However, further functionalization is limited because of the low stability of O-enediynes.

N-Nicholas cyclization through three types of N-containing nucleophilic groups—amino, amido, and arenesulfonamido, was studied. We proved that an arenesulfonamide fragment is the optimal functional group to realize a high-yielded synthesis of 10-membered azaenediynes. Moreover, this group can serve as a site for the introduction of additional functional groups for further modification of cyclic enediynes using click chemistry. For this purpose, the 4-aminobenzenesulfonamide moiety should be acylated with acid derivatives containing a functional group tolerant to the Nicholas cyclization conditions. We demonstrated that this strategy could be applied to the synthesis of azaenediyne with a free terminal triple bond in the arenesulfonamide linker part.

While amino and amido nucleophilic groups also offer great potential as linkers for attaching clickable groups to an enediyne core, neither the secondary amino group nor the amido functional group is suitable for the closure of the 10-membered azaenediyne, which is a limitation of the aza-Nicholas cyclization.

All the synthesized cyclic enediynes were tested as potential anticancer compounds and showed moderate activity against NCI-H460 lung carcinoma and had a minimal effect on WI-26 VA4 lung epithelial-like cells. Thus, the modification of azaenediynes through the 4-aminobenzenesulfonamide moiety can be used in the future to synthesize enediyne conjugates with higher antitumor efficacy.

4. Materials and Methods

4.1. General Information and Methods

Solvents, reagents, and chemicals used for reactions were purchased from commercial suppliers. The chemicals were used without further purification. Catalyst Pd(PPh₃)₄ and Co₂(CO)₈ were purchased from Sigma-Aldrich. 3-Iodo-2-(3-methoxyprop-1-yn-1-yl)benzo[*b*]thiophene (**1**) [46], methyl-3-hydroxy-6-(trimethylsilyl)hex-5-ynoate (**2**) [61], *N*-(but-3-yn-1-yl)-2-nitrobenzenesulfonamide (**10a**) [62], *N*-benzylbut-3-yn-1-amine (**15a**) [63], *N*-(but-3-yn-1-yl)benzamide (**15b**) [64], Co-complexes **6** [46] and **13c** [42] were synthesized according to known procedures without any modifications.

Solvents were dried under standard conditions. Purification and drying of DCM were carried out in accordance with the literature procedure using CaH₂ [65]. The Sonogashira coupling, the synthesis of Co-complexes, the Nicholas cyclization, and the Bergman cyclization were carried out under argon in oven-dried glassware. Other reactions were carried out under air unless stated otherwise. Evaporation of solvents and concentration of reaction mixtures were performed under vacuum at 20 °C (for the enediynes **I–III**, **7**, **14**) and 35 °C (for other compounds) on a rotary evaporator. TLC was carried out on silica gel plates (Silica gel 60, UV 254) with detection by UV or staining with a basic aqueous solution of KMnO₄. A normal-phase silica gel (Silica gel 60, 230–400 mesh) was used for preparative column chromatography. ¹H and ¹³C{¹H} and DEPT NMR spectra were recorded at 400 (or 500) and 101 (or 125) MHz, respectively, at 25 °C in CDCl₃, acetone-*d*₆, or CD₃CN without an internal standard. The ¹H NMR data are reported as chemical shifts (δ), multiplicity (s, singlet; d, doublet; t, triplet; q, quartet; m, multiplet; br, broad), coupling constants (*J*, given in Hz), and number of protons. The ¹³C{¹H} NMR data are reported as chemical shifts (δ). Chemical shifts for ¹H and ¹³C are reported as δ values (ppm) and referenced to residual solvents (δ = 7.26 ppm for ¹H; δ = 77.16 ppm for ¹³C for spectra recorded in CDCl₃ and δ = 2.05 ppm for ¹H; δ = 29.84 ppm for ¹³C for spectra recorded in acetone-*d*₆ and δ = 1.94

ppm for ^1H ; $\delta = 1.32$ ppm for ^{13}C for spectra in CD_3CN). For copies of NMR spectra of all new compounds see the Supporting Information. High-resolution mass spectra were determined for solutions of all compounds in MeOH using ESI in the mode of positive ion registration with a TOF mass analyzer. For copies of ESI HRMS spectra of key products I–III, 18, 19 see the Supporting Information.

4.2. Experimental Details: General Procedures

4.2.1. General Procedure (A) for the Synthesis of Acyclic Enediynes 11a,b; 16a,b

To a stirred, degassed solution of 3-iodo-2-(3-methoxyprop-1-yn-1-yl)benzo[*b*]thiophene (1) (1.00 equiv.) in anhydrous dimethylformamide (DMF) in a vial or a Schlenk flask were added alkyne (1.05–2.00 equiv.), KF (5.00–8.00 equiv.), $\text{Pd}(\text{PPh}_3)_4$ (5 mol%), and CuI (15 mol%) under atmosphere of an Ar. The reaction vessel was sealed, degassed, and flushed with Ar. The reaction mixture was stirred at 40–60 °C for the corresponding time (TLC monitoring). After completion of the reaction, the reaction mixture was cooled, poured into a saturated aqueous solution of NH_4Cl , and extracted with ethyl acetate. The combined organic layers were washed two times with brine and dried over anhydrous Na_2SO_4 . The solvent was evaporated under reduced pressure, and the residue was purified by column chromatography.

4.2.2. General Procedure (B) for the Synthesis of Acyclic Enediyne $\text{Co}_2(\text{CO})_6$ Complexes 4; 12a,b; 17a,b

To a 0.005 M solution of acyclic enediyne (1.00 equiv.) in anhydrous toluene was added octacarbonyl dicobalt (1.05–1.15 equiv.), and the mixture was stirred under argon at room temperature for the corresponding time. The solvent was evaporated under reduced pressure, and the residue was purified by column chromatography.

4.2.3. General Procedure (C) for the Synthesis of Cyclic $\text{Co}_2(\text{CO})_6$ -Complexes 5; 13a,b; 18 by the Nicholas Reaction and the Synthesis of Pyrroline Derivative 19

To an argon-flushed, cooled (0 °C) stirred solution of $\text{Co}_2(\text{CO})_6$ -complex of an acyclic enediyne (1.00 equiv.) in anhydrous DCM ($c = 0.001$ M) was added boron trifluoride diethyl etherate (1.50–8.00 equiv.). The resulting mixture was allowed to warm to room temperature and was stirred at room temperature until the reaction was complete (TLC). Then the reaction mixture was quenched with a saturated aqueous solution of NaHCO_3 . The organic layer was separated, washed with brine, dried over anhydrous Na_2SO_4 , and concentrated under reduced pressure to yield a crude product, which was purified by column chromatography.

4.2.4. General Procedure (D) for the Synthesis of 10-Mebered Enediynes I–III, 7, 14 by the Deprotection of Acyclic $\text{Co}_2(\text{CO})_6$ -complexes from Cobalt

To a stirred solution of cyclic $\text{Co}_2(\text{CO})_6$ complex (1.00 equiv., $c = 0.006$ M) in a mixture of acetone/water (15:1, *v/v*), tetrabutylammonium fluoride (TBAF) hydrate (calculated for $\text{TBAF} \times \text{H}_2\text{O}$) or trihydrate (calculated for $\text{TBAF} \times 3\text{H}_2\text{O}$), was added in several portions until the starting Co-complex was consumed, as indicated by TLC. The total amount of TBAF hydrate or TBAF·trihydrate varied from 23.5 to 65.8 equiv. After completion of the reaction, the reaction mixture was filtered through a pad of Celite using fritted filter funnel, the sorbent was washed with acetone, and the resulting solution was concentrated under reduced pressure at 20 °C to ~ 1/5 of the original volume; the resulting mixture was mixed with ethyl acetate and brine. The organic layer was separated, and the aqueous layer was extracted with ethyl acetate. The combined organic layers were washed three times with brine, dried over anhydrous Na_2SO_4 , and the solvent was evaporated under reduced pressure at 20 °C. The crude product was purified by column chromatography.

4.3. Experimental Details: Specific Procedures

Methyl 3-hydroxy-6-(2-(3-methoxyprop-1-yn-1-yl)benzo[*b*]thiophen-3-yl)hex-5-ynoate (3). To a stirred solution of 3-iodobenzothiophene 1 (391 mg, 1.19 mmol, 1.00 equiv.) in

DMF (8.00 mL) in a vial were added methyl-3-hydroxy-6-(trimethylsilyl)hex-5-ynoate (**2**) (383 mg, 1.79 mmol, 1.50 equiv.), KF (346 mg, 5.96 mmol, 5.00 equiv.), Pd(PPh₃)₄ (68.8 mg, 0.0600 mmol, 5 mol%). The reaction vial was evacuated and flushed with Ar several times. After that, CuI (34 mg, 0.179 mmol, 15 mol%) was added, and the reaction vial was sealed, evacuated, and flushed with Ar. Then, MeOH (382 mg, 11.9 mmol, 0.482 mL, 10.0 equiv.) was added with a syringe, and the reaction mixture was stirred at 40 °C for 13 h (TLC control). The reaction mixture was cooled, poured into a saturated aqueous solution of NH₄Cl (150 mL), and extracted with ethyl acetate (3 × 100 mL). The combined organic layers were washed with a saturated solution of NH₄Cl (200 mL) and two times with brine (2 × 200 mL), dried over anhydrous Na₂SO₄, and concentrated under reduced pressure to give the crude product, which was purified by column chromatography on silica using hexane/ethyl acetate (2:1) as the eluent to give enediyne **3** (400 mg, 98%) as a yellow solid. ¹H NMR (400 MHz, CDCl₃, δ): 7.86–7.80 (m, 1H), 7.75–7.69 (m, 1H), 7.44–7.38 (m, 2H), 4.43 (s, 2H), 4.38–4.32 (m, 1H), 3.74 (s, 3H), 3.48 (s, 3H), 2.90–2.69 (m, 5H). ¹³C{¹H}NMR (101 MHz, CDCl₃, δ): 172.9, 138.7, 138.6, 126.4, 125.5, 125.3, 123.5, 123.4, 122.3, 95.0, 92.6, 79.6, 76.6, 66.9, 60.7, 58.0, 52.0, 40.2, 27.9. HRMS (ESI) *m/z*: [M+Na]⁺ Calcd for C₁₉H₁₈O₄SNa⁺, 365.0804; Found, 365.0818.

Hexacarbonyl (methyl (3-hydroxy-6-(2-(3-methoxyprop-1-(1,2-η²)-yn-1-yl)benzo[*b*]thiophen-3-yl)hex-5-ynoate)dicobalt (4). Co-complex **4** was synthesized from enediyne **3** (209 mg, 0.610 mmol, 1.00 equiv.) and octa-carbonyl dicobalt (230 mg, 0.670 mmol, 1.10 equiv.) in absolute toluene (122 mL, *c* = 0.005M) in accordance with the General Procedure (B). The reaction time was 1 h. Purification of the crude product by column chromatography using hexane/ethyl acetate (2:1) as the eluent gave Co-complex **4** (326 mg, 85%) as a dark red solid. ¹H NMR (400 MHz, Acetone-*d*₆, δ): 7.91–7.88 (m, 2H), 7.49–7.44 (m, 2H), 4.99 (s, 2H), 4.46–4.38 (m, 2H: 1H–OH; 1H–CH), 3.65 (s, 3H), 3.61 (s, 3H), 2.87 (d, *J* = 5.8 Hz, 2H), 2.64 (dd, *J* = 15.5, 7.9 Hz, 1H), signal from one H atom overlaps with water signal at 2.81 ppm. ¹³C{¹H}NMR (101 MHz, Acetone-*d*₆, δ): 200.1, 172.4, 146.1, 141.8, 139.5, 126.8, 126.3, 123.9, 123.2, 118.8, 98.4, 97.8, 78.1, 77.2, 74.0, 67.4, 59.2, 51.7, 41.9, 29.2. HRMS (ESI) *m/z*: [M+Na]⁺ Calcd for C₂₅H₁₈Co₂O₁₀SNa⁺, 650.9177; Found, 650.9183.

Hexacarbonyl (methyl ((2-((1,2-η²)-1,2,7,8-tetradehydro-5,6-dihydro-3*H*-benzo[4,5]thieno[2,3-*e*]oxecin-5-yl)acetate)dicobalt (5). Compound **5** was synthesized from complex **4** (139 mg, 0.221 mmol, 1.00 equiv.) and boron trifluoride–diethyl ether (47.1 mg, 41.0 mmol, 0.331 mmol, 1.50 equiv.) in absolute DCM (222 mL, *c* = 0.001M) in accordance with the General Procedure (C); the reaction time was 1 h. Purification of the crude product by column chromatography using hexane/ethyl acetate (5:1) as the eluent gave unconverted complex **4** (26.7 mg, 19%) and cyclic Co-complex **5** (66.8 mg, 51%) as a dark red oil. ¹H NMR (400 MHz, Acetone-*d*₆, δ): 7.95–7.91 (m, 1H), 7.80–7.76 (m, 1H), 7.50–7.43 (m, 2H), 5.29 (d, *J* = 12.1 Hz, 1H), 5.20 (d, *J* = 12.1 Hz, 1H), 4.59–4.52 (m, 1H), 3.71 (s, 3H), 2.73–2.68 (m, 2H), signals from two H atom overlap with water signal at 2.79 ppm. ¹³C NMR (125 MHz, Acetone-*d*₆, δ): 200.0, 171.9, 150.4, 140.0, 139.4, 126.7, 126.5, 123.7, 123.6, 117.6, 99.8, 97.1, 80.7, 79.62, 79.58, 75.0, 51.9, 41.5, 27.5. HRMS (ESI) *m/z*: [M+H]⁺ Calcd for C₂₄H₁₅Co₂O₉S⁺, 596.9095; Found, 596.9106.

Methyl 2-(1,2,7,8-tetradehydro-5,6-dihydro-3*H*-benzo[4,5]thieno[2,3-*e*]oxecin-5-yl)acetate (I). The decomplexation from cobalt for complex **5** (66.0 mg, 0.111 mmol, 1.00 equiv.) was carried out in accordance with the General Procedure for the Co-complexes deprotection (D) using TBAF trihydrate (820.7 mg, 2.6 mmol, 23.5 equiv.) in an acetone/water mixture (15:1, *v/v*, 18.3 mL, *c* = 0.006 M). TBAF trihydrate was added in eight portions with an interval of 0.5 h. The reaction time was 3.5 h. The crude product was purified by column chromatography using hexane/acetone (30:1) as the eluent to give enediyne **I** (23.2 mg, 68%) as a light yellow solid. ¹H NMR (400 MHz, Acetone-*d*₆, δ): 7.97–7.95 (m, 1H), 7.79–7.76 (m, 1H), 7.51–7.45 (m, 2H), 4.67 (d, *J* = 17.7 Hz, 1H), 4.56 (d, *J* = 17.7 Hz, 1H), 4.48–4.42 (m, 1H), 3.69 (s, 3H), 2.76–2.69 (m, 4H). ¹³C{¹H} NMR cannot be measured due to the instability of the enediyne **I** under the measurements. HRMS (ESI) *m/z*: [M+Na]⁺ Calcd for C₁₈H₁₄O₃SNa⁺ 333.0556; Found, 333.0562.

1,2,7,8-Tetrahydro-5,6-dihydro-3H-benzo[4,5]thieno[2,3-*e*]oxecine (7). Enediynes 7 was synthesized in accordance with the General Procedure (D) for the Co-complexes deprotection from Co-complex 6 (78.6 mg, 0.150 mmol, 1.00 equiv.) and TBAF hydrate (1.88 g, 6.73 mmol, 45.0 equiv.) in an acetone/water mixture (15:1, *v/v*, 25.0 mL, *c* = 0.006 M). TBAF hydrate was added in six portions with an interval of 0.5 h. The reaction time was 2.5 h. The crude product was purified by column chromatography using hexane/ethyl acetate (15:1) as the eluent to give O-enediynes 7 (22.7 mg, 64%) as a light yellow solid. $^1\text{H NMR}$ (400 MHz, CDCl_3) δ 7.79–7.75 (m, 2H), 7.44–7.35 (m, 2H), 4.48 (s, 2H), 4.17 (d, *J* = 4.8 Hz, 2H), 2.74 (d, *J* = 4.8 Hz, 2H). $^1\text{H NMR}$ spectrum corresponds with the data reported earlier [46].

Methyl 2-(3,4-dihydro-1H-benzo[4,5]thieno[3,2-*g*]isochromen-3-yl)acetate (8). The solution of enediynes I (10.0 mg, 0.0322 mmol, 1.00 equiv.) and isopropanol (32.2 mL, *c* = 0.001 M) in a sealed vial were degassed accurately and flashed with Ar. Then the reaction mixture was stirred at 45 °C for 14 h. The solvent was evaporated under reduced pressure, and the crude product was purified by column chromatography using hexane/acetone (5:1) as the eluent to give the Bergman cyclization product 8 (8.4 mg, 83%) as a yellowish solid. $^1\text{H NMR}$ (400 MHz, CDCl_3) δ 8.11–8.07 (m, 1H), 7.88 (s, 1H), 7.84–7.80 (m, 1H), 7.49 (s, 1H), 7.46–7.41 (m, 2H), 4.99 (s, 2H), 4.28–4.21 (m, 1H), 3.76 (s, 3H), 3.05–2.94 (m, 2H), 2.78 (dd, *J* = 15.4, 7.8 Hz, 1H), 2.66 (dd, *J* = 15.4, 5.1 Hz, 1H). $^{13}\text{C}\{^1\text{H}\}$ NMR (100 MHz, CDCl_3) δ 171.7, 139.7, 137.6, 135.3, 134.6, 133.7, 129.5, 126.8, 124.5, 123.0, 121.6, 121.5, 118.3, 71.9, 68.7, 52.04, 41.0, 34.0. HRMS (ESI) *m/z*: $[\text{M}+\text{H}]^+$ Calcd for $\text{C}_{18}\text{H}_{17}\text{O}_3\text{S}$, 313.0893; Found, 313.0883.

3,4-dihydro-1H-benzo[4,5-*b*]thieno[3,2-*g*]isochromene (9). The solution of enediynes 7 (5.30 mg, 0.0222 mmol) in isopropanol (22.2 mL, *c* = 0.001 M) in a sealed vial was degassed accurately and flashed with Ar. Then the reaction mixture was stirred at 50 °C for 12 h. The solvent was evaporated under reduced pressure, and the crude product was purified by column chromatography using hexane/ethyl acetate (5:1) as the eluent to give the product of the Bergman cyclization 9 (5.3 mg, 100%) as a white solid. $^1\text{H NMR}$ (400 MHz, CDCl_3) δ 8.12–8.09 (m, 1H), 7.91 (s, 1H), 7.84–7.80 (m, 1H), 7.47 (s, 1H), 7.45–7.41 (m, 2H), 4.93 (s, 2H), 4.06 (t, *J* = 5.7 Hz, 2H), 3.07 (t, *J* = 5.7 Hz, 2H). $^{13}\text{C}\{^1\text{H}\}$ NMR (101 MHz, CDCl_3) δ 139.7, 137.4, 135.4, 134.5, 134.4, 130.1, 126.7, 124.5, 123.0, 121.8, 121.5, 118.4, 68.6, 65.8, 28.8. HRMS (ESI) *m/z*: $[\text{M}+\text{Na}]^+$ Calcd for $\text{C}_{15}\text{H}_{12}\text{OSNa}$, 263.0508; Found, 263.0501.

***N*-(But-3-yn-1-yl)-4-nitrobenzenesulfonamide (10b).** Compound 10b was synthesized in accordance with the procedure for the corresponding NHTs analogue [66] from *tert*-butyl but-3-yn-1-yl((4-nitrophenyl)sulfonyl)carbamate (2.53 g, 7.14 mmol, 1.0 equiv.) and trifluoroacetic acid (12.2 g, 7.97 mL, 0.107 mol, 15.0 equiv.). Yield 65% (1.19 g). $^1\text{H NMR}$ (400 MHz, Acetone-*d*₆) δ 8.51–8.36 (m, 2H), 8.26–7.91 (m, 2H), 7.06 (t, *J* = 5.5 Hz, 1H), 3.20–3.15 (m, 2H), 2.43–2.37 (m, 2H–CH₂, 1H–C≡CH). $^1\text{H NMR}$ spectrum corresponds with the data reported earlier [67].

***N*-(4-(2-(3-methoxyprop-1-yn-1-yl)benzo[*b*]thiophen-3-yl)but-3-yn-1-yl)-2-nitrobenzenesulfonamide (11a).** Enediynes 11a was synthesized in accordance with the General Procedure (A) for the Sonogashira coupling from 3-iodobenzothiophene 1 (100 mg, 0.303 mmol, 1.00 equiv.), *N*-(but-3-yn-1-yl)-2-nitrobenzenesulfonamide (10a) (100 mg, 0.394 mmol, 1.3 equiv.), KF (88.0 mg, 1.52 mmol, 5.00 equiv.), Pd(PPh₃)₄ (17.5 mg, 0.015 mmol, 5 mol%) and CuI (8.66 mg, 0.046 mmol, 15 mol%) in anhydrous DMF (5.00 mL) at 50 °C. The reaction time was 5 h. The crude product was purified by column chromatography using hexane/ethyl acetate (2:1) as the eluent to give enediynes 11a (130 mg, 94%) as a yellow oil. $^1\text{H NMR}$ (400 MHz, CDCl_3 , δ): 8.15 (dd, *J* = 7.7, 1.4 Hz, 1H), 7.73–7.69 (m, 3H), 7.65–7.55 (m, 2H), 7.42–7.38 (m, 2H), 5.83 (t, *J* = 6.0 Hz, 1H), 4.43 (s, 2H), 3.53–3.41 two signals overlap (m, 2H, s, 3H), 2.81 (t, *J* = 6.5 Hz, 2H). $^{13}\text{C}\{^1\text{H}\}$ NMR (100 MHz, CDCl_3 , δ): 148.0, 138.6, 138.4, 134.2, 133.5, 132.9, 130.8, 126.5, 125.8, 125.5, 125.3, 123.4, 122.7, 122.2, 95.4, 92.6, 79.2, 76.1, 60.7, 58.0, 42.9, 21.5. HRMS (ESI) *m/z*: $[\text{M}+\text{Na}]^+$ Calcd for $\text{C}_{22}\text{H}_{18}\text{N}_2\text{O}_5\text{S}_2\text{Na}^+$, 477.0549; Found, 477.0551.

***N*-(4-(2-(3-methoxyprop-1-yn-1-yl)benzo[*b*]thiophen-3-yl)but-3-yn-1-yl)-4-nitrobenzenesulfonamide (11b).** Eneidyne **11b** was synthesized in accordance with the General Procedure (A) for the Sonogashira coupling from 3-iodobenzothiophene **1** (1.07 g, 3.26 mmol, 1.00 equiv.), *N*-(but-3-yn-1-yl)-4-nitrobenzenesulfonamide (**10b**) (870 mg, 3.42 mmol, 1.05 equiv.), KF (1.52 g, 26.1 mmol, 8.00 equiv.), Pd(PPh₃)₄ (188 mg, 0.163 mmol, 5 mol%) and CuI (93.0 mg, 489 μmol, 15 mol%) in DMF (25.0 mL) at 60 °C. The reaction time was 8 h. The crude product was purified by column chromatography using hexane/ethyl acetate (3:1) as the eluent to give enedyne **11b** (1.08 g, 73%) as a light brown solid. ¹H NMR (400 MHz, CDCl₃, δ): 8.25–8.21 (m, 2H), 8.10–8.07 (m, 2H), 7.76–7.71 (m, 1H), 7.70–7.67 (m, 1H), 7.44–7.38 (m, 2H), 5.51 (t, *J* = 6.1 Hz, 1H), 4.46 (s, 2H), 3.50 (s, 3H), 3.40–3.35 (m, 2H), 2.73 (t, *J* = 6.1 Hz, 2H). ¹³C{¹H} NMR (100 MHz, CDCl₃, δ): 150.0, 146.5, 138.6, 138.2, 128.3, 126.7, 125.8, 125.4, 124.4, 123.3, 123.0, 122.4, 95.3, 92.6, 79.6, 76.7, 60.8, 58.3, 42.2, 21.4. HRMS (ESI) *m/z*: [M+Na]⁺ Calcd for C₂₂H₁₈N₂O₅S₂Na⁺, 477.0549; Found, 477.0557.

4-Amino-*N*-(4-(2-(3-methoxyprop-1-yn-1-yl)benzo[*b*]thiophen-3-yl)but-3-yn-1-yl)benzenesulfonamide (11c). To a stirred solution of enedyne **11b** (109 mg, 0.240 mmol, 1.00 equiv.) in DCM (3.20 mL) were added zinc dust (941 mg, 14.4 mmol, 60.0 equiv.). The reaction vial was cooled to 0 °C, and then glacial acetic acid (115 mg, 1.92 mmol, 0.110 mL, 8.00 equiv.) was added. The reaction mixture was allowed to warm to room temperature and was vigorously stirred at this temperature for 7.5 h (TLC control). After completion of the reaction, the reaction mixture was filtered through a pad of Celite; the sorbent was washed with ethyl acetate (75.0 mL). The resulting solution was washed two times with a saturated solution of NaHCO₃ (2 × 75.0 mL) and two times with brine (2 × 75.0 mL), dried over anhydrous Na₂SO₄, and concentrated under reduced pressure to give the crude product, which was purified by column chromatography using benzene/acetonitrile (8:1) as the eluent to give NH₂-enediyne **11c** (88.0 mg, 86%) as a light brown solid. ¹H NMR (400 MHz, CD₃CN, δ): 7.86–7.81 (m, 2H), 7.58–7.54 (m, 2H), 7.50–7.44 (m, 2H), 6.71–6.67 (m, 2H), 5.59 (t, *J* = 6.2 Hz, 1H), 4.79 (br s, 2H), 4.40 (s, 2H), 3.41 (s, 3H), 3.13–3.08 (m, 2H), 2.68 (t, *J* = 6.8 Hz, 2H). ¹³C{¹H} NMR (100 MHz, CD₃CN, δ): 153.2, 139.5, 139.2, 129.9, 127.9, 127.7, 126.5, 125.6, 124.3, 124.2, 123.4, 114.4, 96.6, 95.7, 79.5, 75.5, 60.9, 58.1, 42.9, 21.6. HRMS (ESI) *m/z*: [M+Na]⁺ Calcd for C₂₂H₂₀N₂O₃S₂Na⁺, 447.0808; Found, 447.0815.

Hexacarbonyl (*N*-(4-(2-(3-methoxyprop-1-(1,2-η²)-yn-1-yl)benzo[*b*]thiophen-3-yl)but-3-yn-1-yl)-2-nitrobenzenesulfonamide)dicobalt (12a). Cobalt complex **12a** was synthesized from enedyne **11a** (104 mg, 0.228 mmol, 1.00 equiv.) and octa-carbonyl dicobalt (82.0 mg, 0.239 mmol, 1.05 equiv) in absolute toluene (46.0 mL, *c* = 0.005 M) in accordance with the General Procedure (B). The reaction time was 1 h. Purification of the crude product by column chromatography using hexane/ethyl acetate (2:1) as the eluent gave complex **12a** (140 mg, 82%) as a dark red oil. ¹H NMR (500 MHz, Acetone-*d*₆, δ): 8.18 (br s, 1H), 7.90 (br s, 2H), 7.85 (br s, 3H), 7.45 (br s, 2H), 7.03 br (s, 1H), 4.94 (s, 2H), 3.59 (s, 3H), 3.55–3.51 (m, 2H), 2.93 (t, *J* = 6.6 Hz, 2H). ¹³C{¹H} NMR (100 MHz, Acetone-*d*₆, δ): 200.1, 149.1, 146.3, 141.7, 139.4, 134.9, 134.5, 133.6, 131.3, 126.9, 126.3, 125.8, 123.9, 123.2, 118.6, 98.0, 97.5, 77.8, 76.9, 73.9, 59.3, 43.2, 22.4. HRMS (ESI) *m/z*: [M+Na]⁺ Calcd for C₂₈H₁₈Co₂N₂O₁₁S₂Na⁺, 762.8908; Found, 762.8910.

Hexacarbonyl (4-amino-*N*-(4-(2-(3-methoxyprop-1-(1,2-η²)-yn-1-yl)benzo[*b*]thiophen-3-yl)but-3-yn-1-yl)benzenesulfonamide)dicobalt (12b). Cobalt complex **12b** was synthesized from enedyne **11c** (30.0 mg, 0.707 mmol, 1.00 equiv.) and octa-carbonyl dicobalt (27.8 mg, 0.0813 mmol, 1.15 equiv.) in absolute toluene (14.0 mL, *c* = 0.005 M) in accordance with the General Procedure (B). The reaction time was 1 h. Purification of the crude product by column chromatography using hexane/ethyl acetate (3:2) as the eluent gave cobalt complex **12b** (44.4 mg, 88%) as dark violet solid. ¹H NMR (400 MHz, CD₃CN, δ): 7.82 (br s, 2H), 7.55 (d, *J* = 7.5 Hz, 2H), 7.45 (br s, 2H), 6.69 (d, *J* = 7.5 Hz, 2H), 5.57 (br s, 1H), 4.86 (s, 2H), 4.78 (br s, 2H), 3.53 (s, 3H), 3.17–3.05 (m, 2H), 2.68 (br s, 2H). ¹³C{¹H} NMR (100 MHz, CD₃CN, δ): 200.3, 153.6, 146.5, 141.7, 139.4, 129.9, 127.9, 127.0, 126.5, 123.9, 123.3, 114.4 (one of the «aromatic» signals overlaps with the CD₃CN signal), 98.7, 97.2, 77.9, 76.7, 74.1, 59.4,

42.7, 22.1. HRMS (ESI) m/z : $[M+Na]^+$ Calcd for $C_{28}H_{20}Co_2N_2O_9S_2Na^+$, 732.9166; Found, 732.9169.

Hexacarbonyl (*N*-(4-(*N*-(4-(2-(3-methoxyprop-1-(1,2- η^2)-yn-1-yl)benzo[*b*]thiophen-3-yl)but-3-yn-1-yl)sulfamoyl)phenyl)hept-6-ynamide)dicobalt (12c). To a stirred solution of Co-complex **12b** (25.3 mg, 0.0356 mmol, 1.00 equiv.) in absolute THF (10.0 mL) under Ar, Et₃N (5.41 mg, 0.0534 mmol, 7.42 μ L, 1.50 equiv.) was added. The reaction mixture was cooled to 0 °C, and hex-5-ynoyl chloride (6.97 mg, 0.0534 mmol, 1.50 equiv.) was added. The reaction mixture was allowed to warm to room temperature and was stirred at room temperature for 1.5 h (TLC control). After completion of the reaction, the reaction mixture was poured into a saturated aqueous solution of NH₄Cl (50.0 mL) and extracted with ethyl acetate (3 \times 50.0 mL). The combined organic layers were washed two times with a 2% solution of NaOH (2 \times 50.0 mL) and three times with brine (2 \times 50.0 mL), dried over anhydrous Na₂SO₄, and concentrated under reduced pressure to give a crude product. The crude product was purified by column chromatography using hexane/acetone (2:1) as the eluent to give acylated Co-complex **12c** (16.7 mg, 58%) as a dark red oil. ¹H NMR (400 MHz, Acetone-*d*₆, δ): 9.48 (s, 1H), 7.91–7.81 (m, 6H), 7.48–7.44 (m, 2H), 6.75 (t, J = 6.1 Hz, 1H), 4.93 (s, 2H), 3.58 (s, 3H), 3.32–3.27 (m, 2H), 2.83 (t, J = 7.1 Hz, 2H), 2.55 (t, J = 7.4 Hz, 2H), 2.37 (t, J = 2.6 Hz, 1H), 2.29 (td, J = 7.0, 2.6 Hz, 2H), 1.92–1.85 (m, 2H). ¹³C{¹H} NMR (100 MHz, Acetone-*d*₆, δ): 200.1, 171.9, 146.2, 144.1, 141.7, 139.4, 135.8, 128.9, 126.8, 126.3, 124.0, 123.2, 119.7, 118.7, 98.4, 97.6, 84.3, 78.0, 76.7, 74.0, 70.5, 59.3, 42.8, 36.3, 24.9, 22.3, 18.3. Four signals (144.1, 135.8, 119.7, 42.8) double as a result of rotation around the amide bond. For the details, see the SI file. HRMS (ESI) m/z : $[M+Na]^+$ Calcd for $C_{34}H_{26}Co_2N_2O_{10}S_2Na^+$, 826.9585; Found, 826.9590.

Hexacarbonyl ((1,2- η^2)-1,2,7,8-tetrahydro-4-((2-nitrophenyl)sulfonyl)-3,4,5,6-tetrahydrobenzo[4,5]thieno[2,3-*e*]azecine)dicobalt (13a). Cyclic complex **13a** was synthesized in accordance with the general procedure (C) for the Nicholas reaction from Co-complex **12a** (44.0 mg, 0.0590 mmol, 1.00 equiv.) and boron trifluoride diethyl etherate (67.0 mg, 89.3 μ L, 0.475 mmol, 8.00 equiv.) in absolute DCM (60.0 mL, c = 0.001 M). The reaction time was 1 h. Purification of the crude product by column chromatography using hexane/ethyl acetate (2:1) as the eluent gave cyclic complex **13a** (19.3 mg, 46%) as a dark brown oil. ¹H NMR (400 MHz, Acetone-*d*₆, δ): 8.20 (d, J = 7.7 Hz, 1H), 8.00–7.91 (m, 4H), 7.76 (d, J = 7.0 Hz, 1H), 7.50–7.44 (m, 2H), 5.34 (s, 2H), 3.89 (d, J = 4.8 Hz, 2H), 2.88 (d, J = 4.8 Hz, 2H). ¹³C{¹H} NMR (100 MHz, Acetone-*d*₆, δ): 199.9, 151.7, 150.1, 139.8, 139.4, 135.6, 133.1, 131.9, 131.1, 126.6 (two overlapping signals), 125.5, 123.6, 123.5, 116.8, 101.5, 98.6, 80.7, 79.8, 57.7, 55.5, 22.9. HRMS (ESI) m/z : $[M+Na]^+$ Calcd for $C_{27}H_{14}Co_2N_2O_{10}S_2Na^+$, 730.8646; Found, 730.8657.

Hexacarbonyl (*N*-(4-(((1,2- η^2)-1,2,7,8-tetrahydro-5,6-dihydrobenzo[4,5]thieno[2,3-*e*]azecin-4(3*H*)-yl)sulfonyl)phenyl)hex-5-ynamide)dicobalt (13b). Cyclic complex **13b** was synthesized in accordance with the general procedure (C) for the Nicholas reaction from Co-complex from complex **12c** (42.0 mg, 0.052.0 mmol, 1.00 equiv.) and boron trifluoride diethyl etherate (14.8 mg, 12.9 μ L, 0.104 mmol, 2.00 equiv.) in absolute DCM (52.0 mL, c = 0.001 M). The reaction time was 1 h. Purification of the crude product by column chromatography using hexane/acetone (3:1) as the eluent gave cyclic complex **13b** (25.4 mg, 63%) as a dark red oil. ¹H NMR (400 MHz, Acetone-*d*₆, δ): 9.59 (br s, 1H), 7.96–7.90 (m, 5H), 7.76–7.74 (m, 1H), 7.49–7.39 (m, 2H), 4.97 (s, 2H), 3.74 (d, J = 5.3 Hz, 2H), 2.84 (d, J = 5.3 Hz, 2H), 2.57 (t, J = 7.3 Hz, 2H), 2.38 (t, J = 2.6 Hz, 1H), 2.30 (td, J = 7.0, 2.6 Hz, 2H), 1.93–1.86 (m, 2H). ¹³C{¹H} NMR (100 MHz, Acetone-*d*₆, δ): 200.1, 172.1, 151.5, 144.8, 139.8, 139.4, 132.8, 129, 126.5, 123.6, 123.5, 119.9, 116.8, 101.4, 99.1, 84.3, 80.6, 79.4, 70.5, 57.8, 56.4, 36.3, 24.8, 23.6, 18.3 (two «aromatic» CH signals overlap). Three signals (144.8, 119.9, 36.3) double as a result of rotation around the amide bond. For the details, see the SI file. HRMS (ESI) m/z : $[M+Na]^+$ Calcd for $C_{33}H_{22}Co_2N_2O_9S_2Na^+$, 794.9323; Found, 794.9311.

1,2,7,8-tetrahydro-4-((2-nitrophenyl)sulfonyl)-3,4,5,6-tetrahydrobenzo[4,5]thienoazecine (II). Eneidyne **II** was synthesized in accordance with the General Procedure (D) for the Co-complexes deprotection from complex **13a** (33.0 mg, 0.0466 mmol, 1.00 equiv.)

and TBAF trihydrate (557 mg, 1.77 mmol, 65.8 equiv.) in a mixture of acetone/water (15:1, *v/v*, 4.50 mL, *c* = 0.006 M). TBAF was added in ten portions with an interval of 30 min. The reaction time was 4.5 h. The crude product was purified by column chromatography using hexane/acetone (3:1) as the eluent to give enediyne II (7.30 mg, 64%) as an orange solid. ¹H NMR (400 MHz, Acetone-*d*₆, δ): 8.23 (d, *J* = 8.0 Hz, 2H), 7.99–7.79 (m, 5H), 7.53–7.47 (m, 2H), 4.63 (s, 2H), 3.91 (d, *J* = 5.1 Hz, 2H), 3.01 (d, *J* = 5.1 Hz, 2H). ¹³C{¹H} NMR (100 MHz, Acetone-*d*₆, δ): 139.0, 136.5, 135.6, 133.1, 132.1, 131.3, 130.5, 130.4, 129.0, 127.3, 126.5, 125.4, 124.0, 123.5, 104.5, 102.1, 82.9, 79.5, 52.4, 43.7, 22.9. HRMS (ESI) *m/z*: [M+H]⁺ Calcd for C₂₁H₁₅N₂O₄S₂⁺, 423.0468; Found, 423.0469.

***N*-(4-((1,2,7,8-tetrahydro-5,6-dihydrobenzo[4,5]thieno[2,3-*e*]azecin-4(3*H*)-yl)sulfonyl)phenyl)hex-5-ynamide (III)**. Enediyne III was synthesized in accordance with the General Procedure (D) for the Co-complexes deprotection from complex **13b** (22.0 mg, 0.0285 mmol, 1.00 equiv.) TBAF trihydrate (370 mg, 1.17 mmol, 41.0 equiv.) in a mixture of acetone/water (15:1, *v/v*, 4.80 mL, *c* = 0.006 M). TBAF trihydrate was added in eight portions with an interval of 40 min. The reaction time was 5.5 h. The crude product was purified by column chromatography using hexane/acetone (2:1) as the eluent to give enediyne III (10.5 mg, 77%) as a light red solid. ¹H NMR (400 MHz, Acetone-*d*₆, δ): 9.52 (br s, 1H), 7.98–7.94 (m, 1H), 7.90–7.85 (m, 4H), 7.80–7.76 (m, 1H), 7.52–7.45 (m, 2H), 4.38 (s, 2H), 3.64 (d, *J* = 5.0 Hz, 2H), 2.96 (d, *J* = 5.0 Hz, 2H), 2.54 (t, *J* = 7.4 Hz, 2H), 2.37 (t, *J* = 2.6 Hz, 1H), 2.28 (td, *J* = 7.0, 2.6 Hz, 2H), 1.91–1.83 (m, 2H). ¹³C{¹H} NMR (100 MHz, Acetone-*d*₆, δ): 172.0, 144.7, 138.9, 136.6, 133.0, 130.3, 129.4, 129.0, 127.2, 126.4, 124.0, 123.4, 119.8, 105.0, 102.3, 84.3, 82.5, 79.3, 70.5, 52.3, 43.3, 36.3, 24.8, 23.4, 18.3. Three signals (144.7, 119.8, 36.3) double as a result of rotation around the amide bond. For the details, see the SI file. HRMS (ESI) *m/z*: [M+H]⁺ Calcd for C₂₇H₂₃N₂O₃S₂⁺, 487.1145; Found, 487.1142.

1,2,7,8-tetrahydro-4-(phenylsulfonyl)-3,4,5,6-tetrahydrobenzo[4,5]thieno[2,3-*e*]azecine (14). Enediyne **14** was synthesized in accordance with the General Procedure (D) for the Co-complexes deprotection from Co-complex **13c** (120 mg, 0.177 mmol, 1.00 equiv.) and TBAF trihydrate (1.95 g, 6.195 mmol, 35.0 equiv.) in an acetone/water mixture (15:1, *v/v*, 25.0 mL, *c* = 0.006 M). TBAF trihydrate was added in eight portions with an interval of 0.5 h. The reaction time was 3.5 h. The crude product was purified by column chromatography using hexane/acetone (3:1) as the eluent to give NTs-enediyne **14** (52.1 mg, 75%) as a beige solid. ¹H NMR (400 MHz, Acetone-*d*₆, δ) 7.98–7.96 (m, 1H), 7.83 (d, *J* = 8.3 Hz, 2H), 7.79–7.77 (m, 1H), 7.53–7.46 (m, 2H), 7.44 (d, *J* = 8.3 Hz, 2H), 4.39 (s, 2H), 3.64 (d, *J* = 5.0 Hz, 2H), 2.97 (d, *J* = 5.0 Hz, 2H), 2.41 (s, 3H). ¹H NMR spectrum corresponds with the data reported earlier [42].

***N*-benzyl-4-(2-(3-methoxyprop-1-yn-1-yl)benzo[*b*]thiophen-3-yl)but-3-yn-1-amine (16a)**. Enediyne **16a** was synthesized in accordance with the General Procedure (A) for the Sonogashira coupling from 3-iodobenzothiophene **1** (328 mg, 1.00 mmol, 1.00 equiv.), *N*-benzylbut-3-yn-1-amine (**15a**) (249 mg, 1.50 mmol, 1.50 equiv.), KF (464 mg, 8.00 mmol, 8.00 equiv.), Pd(PPh₃)₄ (58.0 mg, 0.0500 mmol, 5 mol%) and CuI (28.0 mg, 0.150 mmol, 15 mol%) in DMF (10.0 mL) at 40 °C. The reaction time was 6 h. Purification of the crude product by column chromatography using hexane/ethyl acetate (2:1→1:1) as the eluent gave enediyne **16a** (185 mg, 52%) as an orange oil. ¹H NMR (400 MHz, Acetone-*d*₆, δ): 7.94–7.90 (m, 1H), 7.89–7.84 (m, 1H), 7.51–7.47 (m, 2H), 7.41 (d, *J* = 7.1 Hz, 2H), 7.33–7.29 (m, 2H), 7.23 (t, *J* = 7.3 Hz, 1H), 4.37 (s, 2H), 3.88 (s, 2H), 3.40 (s, 3H), 2.94 (t, *J* = 6.7 Hz, 2H), 2.78 (t, *J* = 6.7 Hz, 2H; br s, 1H–NH, the signal overlaps with the water signal). ¹³C{¹H} NMR (100 MHz, Acetone-*d*₆, δ): 141.8, 139.5, 139.0, 129.0, 128.9, 127.52, 127.51, 126.3, 125.1, 124.5, 124.1, 123.3, 97.3, 96.3, 79.5, 74.9, 60.6, 57.7, 53.8, 48.6, 21.4. HRMS (ESI) *m/z*: [M+H]⁺ Calcd for C₂₃H₂₁NOS⁺ 360.1417; Found, 360.1406.

***N*-(4-(2-(3-methoxyprop-1-yn-1-yl)benzo[*b*]thiophen-3-yl)but-3-yn-1-yl)benzamide (16b)**. Enediyne **16b** was synthesized in accordance with the General Procedure (A) for the Sonogashira coupling from 3-iodobenzothiophene **1** (100 mg, 0.303 mmol, 1.00 equiv.), *N*-(but-3-yn-1-yl)benzamide (**15b**) (68.0 mg, 0.394 mmol, 1.30 equiv.), KF (88.3 mg, 1.52 mmol, 5.00 equiv.), Pd(PPh₃)₄ (17.5 mg, 0.0152 mmol, 5 mol%) and CuI (8.6 mg, 0.0456 mmol,

15 mol%) in DMF (5.00 mL) at 50 °C. The reaction time was 5 h. Purification of the crude product by column chromatography using hexane/ethyl acetate (2:1) as the eluent gave enediyne **16a** (92.0 mg, 81%) as a yellow oil. ^1H NMR (400 MHz, CDCl_3 , δ): 7.84–7.80 (m, 2H), 7.72 (d, $J = 7.1$ Hz, 1H), 7.51–7.35 (m, 5H), 6.81 (br. s, 1H), 4.29 (s, 2H), 7.79–7.75 (m, 2H), 3.39 (s, 3H), 2.91 (t, $J = 6.2$ Hz, 2H). $^{13}\text{C}\{^1\text{H}\}$ NMR (101 MHz, CDCl_3 , δ): 167.8, 138.0, 138.5, 134.6, 131.7, 128.7, 127.1, 126.5, 125.3, 125.21, 123.49, 123.4, 122.3, 94.9, 94.5, 79.6, 75.6, 60.6, 58.0, 39.0, 21.0. HRMS (ESI) m/z : $[\text{M}+\text{Na}]^+$ Calcd for $\text{C}_{23}\text{H}_{19}\text{NO}_2\text{Sna}^+$, 396.1029; Found, 396.1030.

Hexacarbonyl (*N*-benzyl-4-(2-(3-methoxyprop-1-(1,2- η^2)-yn-1-yl)benzo[*b*]thiophen-3-yl)but-3-yn-1-amine)dicobalt (17a). Cobalt complex **17a** was synthesized from enediyne **16a** (89.9 mg, 0.250 mmol, 1.00 equiv.) and octa-carbonyl dicobalt (94.0 mg, 0.275 mmol, 1.1 equiv.) in absolute toluene (50.0 mL, $c = 0.005$ M) in accordance with the General Procedure (B). The reaction time was 1 h. Purification of the crude product by column chromatography using hexane/ethyl acetate (3:1) as the eluent gave cobalt complex **17a** (111 mg, 69%) as a dark red-brown solid. ^1H NMR (400 MHz, Acetone- d_6 , δ): 7.90–7.84 (m, 2H), 7.46–7.39 (m, 4H), 7.33–7.29 (m, 2H), 7.26–7.21 (m, 1H), 4.96 (s, 2H), 3.88 (s, 2H), 3.57 (s, 3H), 2.98 (br s, 2H), 2.86–2.78 (m, 2H, NH, overlaps with the water signal). $^{13}\text{C}\{^1\text{H}\}$ NMR (101 MHz, Acetone- d_6 , δ): 200.1, 145.8, 141.9, 141.8, 139.5, 129.0, 128.9, 127.5, 126.8, 126.3, 123.8, 123.2, 119.0, 100.4, 97.6, 78.2, 76.2, 74.0, 59.2, 54.0, 48.6, 22.0. HRMS (ESI) m/z : $[\text{M}+\text{H}]^+$ Calcd for $\text{C}_{29}\text{H}_{22}\text{Co}_2\text{NO}_7\text{S}^+$, 645.9775; Found, 645.9806.

Hexacarbonyl (*N*-(4-(2-(3-methoxyprop-1-(1,2- η^2)-yn-1-yl)benzo[*b*]thiophen-3-yl)but-3-yn-1-yl)benzamide)dicobalt (17b). Cobalt complex **17b** was synthesized from enediyne **16b** (70.0 mg, 0.186 mmol, 1.00 equiv.) and octa-carbonyl dicobalt (70.0 mg, 0.205 mmol, 1.10 equiv.) in absolute toluene (37.2 mL, $c = 0.005$ M) in accordance with the General Procedure (B). The reaction time was 1 h. Purification of the crude product by column chromatography using hexane/ethyl acetate (2:1) as the eluent gave cobalt complex **17b** (113 mg, 92%) as a burgundy oil. ^1H NMR (400 MHz, CDCl_3 , δ): 7.83–7.72 (m, 4H), 7.53–7.33 (m, 5H), 6.58 (br s, 1H), 4.87 (s, 2H), 3.81–3.77 (m, 2H), 3.59 (s, 3H), 2.91 (t, $J = 6.5$ Hz, 2H). Only signals from CO ligands and carbon atoms bonded to hydrogen atoms can be detected by $^{13}\text{C}\{^1\text{H}\}$ NMR. $^{13}\text{C}\{^1\text{H}\}$ NMR (125 MHz, CDCl_3 , δ): 199.2, 132.0, 129.0, 127.3, 126.1, 125.5, 123.1, 122.4, 73.7, 59.6, 39.1, 21.5. HRMS (ESI) m/z : $[\text{M}+\text{Na}]^+$ Calcd for $\text{C}_{29}\text{H}_{19}\text{Co}_2\text{NO}_8\text{SNa}^+$, 681.9388; Found, 681.9389.

Hexacarbonyl (4-benzyl-(1,2- η^2)-1,2,7,8-tetrahydro-3,4,5,6-tetrahydrobenzo[4,5]thieno[2,3-*e*]azecine)dicobalt (18). **(A)** Cyclic Co-complex **18** was synthesized in accordance with the general procedure (C) for the Nicholas reaction from Co-complex **17a** (30.0 mg, 0.0465 mmol, 1.00 equiv.) and boron trifluoride diethyl etherate (29.7 mg, 25.8 μL , 0.209 mmol, 4.50 equiv.) in absolute DCM (46.5 mL, $c = 0.001$ M). The reaction time was 20 h. Purification of the crude product by column chromatography using hexane/ethyl acetate (30:1) as the eluent gave cyclic complex **18** (1.50 mg, 4%) as a dark red-brown solid.

(B) Cyclic Co-complex **18** was synthesized in accordance with the general procedure (C) for the Nicholas reaction from Co-complex **17a** (73.4 mg, 0.114 mmol, 1.00 equiv.) and another acid-tetrafluoroboric acid diethyl ether complex (66.7 mg, 55.8 μL , 0.410 mmol, 3.60 equiv.) in absolute DCM (114 mL, $c = 0.001$ M). The reaction time was 20 h. Purification of the crude product by column chromatography using hexane/ethyl acetate (30:1) as the eluent gave cyclic complex **18** (3.90 mg, 6%) as a dark red-brown solid.

(C) To an argon-flushed, cooled (-20 °C) stirred solution of $\text{Co}_2(\text{CO})_6$ -complex of an acyclic enediyne **17a** (44.0 mg, 0.0682 mmol, 1.00 equiv.) in anhydrous DCM (44.0 mL, $c = 0.001$ M) was added tetrafluoroboric acid diethyl ether complex (33.1 mg, 28.1 μL , 0.205 mmol, 3.00 equiv.). The resulting mixture was stirred at -20 °C for 10 min; then *N,N*-diisopropylethylamine (DIPEA) (26.4 mg, 35.6 μL , 0.205 mmol, 3.00 equiv.) was added. The reaction mixture was allowed to warm to room temperature and was stirred at this temperature for 1 h. TLC analysis showed the presence of traces of the product **18**. Therefore, the reaction mixture was cooled to -20 °C and treated with an additional amount of $\text{HBF}_4 \times \text{Et}_2\text{O}$ (33.1 mg, 28.1 μL , 0.205 mmol, 3.00 equiv.) followed by the additional

amount of DIPEA (26.4 mg, 35.6 μ L, 0.205 mmol, 3.00 equiv.). The reaction mixture was allowed to warm to room temperature and was stirred at this temperature for 3 h. Then it was cooled to -20 °C once again and treated with $\text{HBF}_4 \times \text{Et}_2\text{O}$ (22.1 mg, 18.7 μ L, 0.136 mmol, 2.00 equiv.) and after 10 min additionally with DIPEA (26.4 mg, 35.6 μ L, 0.205 mmol, 3.00 equiv.). The reaction mixture was allowed to warm to room temperature and was stirred at this temperature for 3 h. Then the reaction mixture was quenched with a saturated aqueous solution of NaHCO_3 . The organic layer was separated, washed with brine, dried over anhydrous Na_2SO_4 , and concentrated under reduced pressure to yield a crude product, which was purified by column chromatography using hexane/ethyl acetate (30:1) as the eluent gave cyclic complex **18** (4.90 mg, 12%) as a dark red-brown solid. ^1H NMR (400 MHz, Acetone- d_6 , δ): 7.96–7.92 (m, 1H), 7.81–7.78 (m, 1H), 7.50–7.44 (m, 4H), 7.39–7.33 (m, 2H), 7.29–7.26 (m, 1H), 4.57 (s, 2H), 4.17 (s, 2H), 3.15 (t, $J = 5.8$ Hz, 2H), 2.55 (t, $J = 5.8$ Hz, 2H). $^{13}\text{C}\{^1\text{H}\}$ NMR (100 MHz, Acetone- d_6 , δ): 200.5, 150.2, 140.2, 139.8, 139.5, 129.5, 129.3, 128.0, 126.3, 126.5, 123.8, 123.6, 118.0, 102.1, 101.6, 81.2, 79.5, 61.6, 61.1, 55.5, 22.4. HRMS (ESI) m/z : $[\text{M}+\text{H}]^+$ Calcd for $\text{C}_{28}\text{H}_{18}\text{Co}_2\text{NO}_6\text{S}^+$ 613.9513; Found, 613.9531.

(5-(2-(3-Methoxyprop-(1,2- η^2)-1-yn-1-yl)benzo[*b*]thiophen-3-yl)-2,3-dihydro-1*H*-pyrrol-1-yl)(phenyl)methanone (19). Co-complex of pyrroline derivative **19** was synthesized in accordance with the general procedure (C) for the Nicholas reaction from Co-complex **17b** (52.0 mg, 0.079 mmol, 1.00 equiv.) and boron trifluoride diethyl etherate (14.5 mg, 13.0 μ L, 0.102 mmol, 1.30 equiv.) in absolute DCM (79.0 mL, $c = 0.001$ M). The reaction time was 2 h. Purification of the crude product by column chromatography using hexane/ethyl acetate (10:1) as the eluent gave Co-complex of pyrroline derivative **19** (22.0 mg, 44%) as a burgundy solid. ^1H NMR (400 MHz, CDCl_3 , δ): 7.51 (br s, 1H), 7.44 (br s, 1H), 7.29–7.12 (m, 4H), 7.12–6.87 (m, 3H), 5.46 (br s, 1H), 4.74 (d, $J = 12.9$ Hz, 1H), 4.70 (d, $J = 12.9$ Hz, 1H), 4.38–4.31 (m, 1H), 4.19 (br s, 1H), 3.61 (s, 3H), 2.92–2.75 (m, 2H). NMR DEPT (101 MHz, CDCl_3 , δ): 129.7 (CH), 126.9 (CH—two signals overlap), 124.9 (CH), 124.6 (CH), 122.4 (CH), 121.6 (CH), 117.1 (CH), 73.6 (OCH_2), 59.2 (OCH_3), 50.1 (CH_2), 28.0 (OCH_2). The ^{13}C NMR was too broad and had a low signal-to-noise ratio. For the details, see the Supporting Information. HRMS (ESI) m/z : $[\text{M}+\text{Na}]^+$ Calcd for $\text{C}_{29}\text{H}_{19}\text{Co}_2\text{NO}_8\text{SNa}^+$, 681.9388; Found, 681.9412.

4.4. Cell Culture

NCI-H460 lung carcinoma cells and WI-26 VA4 lung epithelial-like cells were purchased from the ATCC. NCI-H460 cells were maintained in Advanced RPMI-1640 (Gibco, UK) supplemented with 5% fetal bovine serum (FBS, Gibco, Leicestershire, UK), penicillin (100 UI mL^{-1}), streptomycin (100 $\mu\text{g mL}^{-1}$) and GlutaMax (2 mM, Gibco, UK). WI-26 VA4 cells were maintained in Advanced MEM (Gibco, UK) supplemented with 5% fetal bovine serum (FBS, Gibco, UK), penicillin (100 UI mL^{-1}), streptomycin (100 $\mu\text{g mL}^{-1}$), and GlutaMax (1.87 mM, Gibco, UK). All cells line cultivation under a humidified atmosphere of 95% air/5% CO_2 at 37 °C. Subconfluent monolayers, in the log growth phase, were harvested by a brief treatment with TrypLE Express solution (Gibco, UK) in phosphate-buffered saline (PBS, Capricorn Scientific, Ebsdorfergrund, Germany) and washed three times in serum-free PBS. The number of viable cells was determined by trypan blue exclusion.

4.5. Antiproliferative Assay

The effects of the synthesized compounds on cell viability were determined using the MTT colorimetric test. All examined cells were diluted with the growth medium to 3.5×10^4 cells per mL, and the aliquots (7×10^3 cells per 200 μL) were placed in individual wells in 96-multiplates (Eppendorf, Germany) and incubated for 24 h. The next day the cells were then treated with synthesized compounds separately at the final concentration of 75 μM and incubated for 72 h at 37 °C in a 5% CO_2 atmosphere. After incubation, the cells were then treated with 40 μL MTT solution (3-(4,5-dimethylthiazol-2-yl)-2,5-diphenyltetrazolium bromide, 5 mg mL^{-1} in PBS) and incubated for 4 h. After an additional 4 h incubation, the medium with MTT was removed, and DMSO (150 μL)

was added to dissolve the crystals formazan. The plates were shaken for 10 min. The optical density of each well was determined at 560 nm using a microplate reader GloMax Multi+ (Promega, Madison, WI, USA). Each of the tested compounds was evaluated for cytotoxicity in three separate experiments.

5. Conclusions

The scope and limitation of the Nicholas-type cyclization for the synthesis of various 10-membered heteroenediyne fused to a benzothiophene ring were studied. We proved that an arenesulfonamide fragment is the optimal functional group to realize a high-yield synthesis of 10-membered enediynes. Moreover, this group can serve as a site for the introduction of additional functional groups for further modification of cyclic enediynes via click chemistry. For this purpose, the 4-(*N*-acylamino)benzenesulfonamide functional group can be used as a nucleophile for cyclization and functionalization. The crucial point is that neither the secondary amino group nor the amido functional group is suitable for the closure of the 10-membered azaenediyne, which is a limitation of the aza-Nicholas cyclization. Functionalized O-enediynes are also synthetically accessible through the O-Nicholas reaction. Still, the use of such functionalization is limited because of the low stability of O-enediynes compared with that of N-enediynes. All the synthesized cyclic enediynes were tested as potential anticancer compounds and showed moderate activity against NCI-H460 lung carcinoma and had a minimal effect on WI-26 VA4 lung epithelial-like cells, demonstrating that the synthesized enediynes can be further used to synthesize active molecules with antitumor activity based on enediyne conjugates. Azaenediynes modified through acylated 4-aminobenzenesulfonamide nucleophilic group should be considered the most suitable structures for ongoing studies.

Supplementary Materials: The following supporting information can be downloaded at: <https://www.mdpi.com/article/10.3390/molecules27186071/s1>, copies of ^1H , $^{13}\text{C}\{^1\text{H}\}$, DEPT, 2D NMR spectra of the synthesized compounds (PDF); copies of ESI HRMS spectra of cyclic enediynes **I–III**, and of Co-complexes **18**, **19**.

Author Contributions: Conceptualization, N.A.D. and I.A.B.; methodology, N.A.D.; software, M.A.G.; validation, E.A.K.; formal analysis, R.E.G.; investigation, N.A.D., E.A.K., A.G.L. and A.S.D.; resources, I.A.B.; data curation, N.A.D., A.S.B.; writing—original draft preparation, N.A.D., E.A.K.; writing—review and editing, N.A.D., I.A.B.; visualization, N.A.D.; supervision, N.A.D.; project administration, N.A.D., I.A.B.; funding acquisition, I.A.B. All authors have read and agreed to the published version of the manuscript.

Funding: This research was funded by RSF, grant number 21-13-00218.

Institutional Review Board Statement: Not applicable.

Informed Consent Statement: Not applicable.

Data Availability Statement: Data supporting reported results (copies of ^1H , $^{13}\text{C}\{^1\text{H}\}$, DEPT, 2D NMR spectra in PDF) can be found in a Supporting Information File or can be sent as original files upon request.

Acknowledgments: The study was carried out using equipment from the SPbU Research Park: the Centre for Magnetic Resonance and the Centre for Chemical Analysis and Materials Research. The authors would like to thank Alexander Ivanov (SPbU) and Sergey Smirnov (SPbU) for measuring the NMR spectra of the Co-complexes.

Conflicts of Interest: The authors declare no conflict of interest.

Sample Availability: Samples of the all compounds are available from the authors.

References

1. Nicolaou, K.C.; Dai, W.-M. Chemistry and Biology of the Eneidyne Anticancer Antibiotics. *Angew. Chem. Int. Ed.* **1991**, *30*, 1387–1416. [CrossRef]
2. Kraka, E.; Cremer, D. Eneidyne, enyne-allenes, their reactions, and beyond. *Wiley Interdiscip. Rev. Comput. Mol. Sci.* **2014**, *4*, 285–324. [CrossRef]
3. Basak, A.; Roy, S.; Roy, B.; Basak, A. Synthesis of Highly Strained Eneidyne and Dienedynes. *Curr. Top. Med. Chem.* **2008**, *8*, 487–504. [CrossRef] [PubMed]
4. Jean, M.; Tomasi, S.; van de Weghe, P. When the nine-membered eneidyne play hide and seek. *Org. Biomol. Chem.* **2012**, *10*, 7453–7456. [CrossRef]
5. Hamann, P.R.; Upeslaciis, J.; Borders, D.B. *Anticancer Agents from Natural Products*; Cragg, G.M., Kingston, D.G.I., Newman, D.J., Eds.; CRC Press: Boca Raton, FL, USA, 2011; ISBN 9780429130854.
6. Shen, B.; Liu, W.; Nonaka, K. Eneidyne Natural Products: Biosynthesis and Prospect Towards Engineering Novel Antitumor Agents. *Curr. Med. Chem.* **2003**, *10*, 2317–2325. [CrossRef]
7. Yan, X. Anthraquinone-fused eneidyne: Discovery, biosynthesis and development. *Nat. Prod. Rep.* **2022**, *39*, 703–728. [CrossRef]
8. Konishi, M.; Ohkuma, H.; Saitoh, K.-I.; Kawaguchi, H.; Golik, J.; Dubay, G.; Groenewold, G.; Krishnan, B.; Doyle, T.W. Esperamicins, a novel class of potent antitumor antibiotics. I. Physico-chemical data and partial structure. *J. Antibiot.* **1985**, *38*, 1605–1609. [CrossRef]
9. Lee, M.D.; Dunne, T.S.; Siegel, M.M.; Chang, C.C.; Morton, G.O.; Borders, D.B. Calicheamicins, a novel family of antitumor antibiotics. 1. Chemistry and partial structure of calicheamicin γ_1^I . *J. Am. Chem. Soc.* **1987**, *109*, 3464–3466. [CrossRef]
10. Lee, M.D.; Dunne, T.S.; Chang, C.C.; Ellestad, G.A.; Siegel, M.M.; Morton, G.O.; McGahren, W.J.; Borders, D.B. Calicheamicins, a novel family of antitumor antibiotics. 2. Chemistry and structure of calicheamicin γ_1^I . *J. Am. Chem. Soc.* **1987**, *109*, 3466–3468. [CrossRef]
11. Igarashi, M.; Sawa, R.; Umekita, M.; Hatano, M.; Arisaka, R.; Hayashi, C.; Ishizaki, Y.; Suzuki, M.; Kato, C. Sealutomicins, new eneidyne antibiotics from the deep-sea actinomycete *Nonomuraea* sp. MM565M-173N2. *J. Antibiot.* **2021**, *74*, 291–299. [CrossRef]
12. Low, Z.J.; Ma, G.-L.; Tran, H.T.; Zou, Y.; Xiong, J.; Pang, L.; Nuryyeva, S.; Ye, H.; Hu, J.-F.; Houk, K.N.; et al. Sungeidines from a Non-canonical Eneidyne Biosynthetic Pathway. *J. Am. Chem. Soc.* **2020**, *142*, 1673–1679. [CrossRef] [PubMed]
13. Shao, R.-G. Pharmacology and Therapeutic Applications of Eneidyne Antitumor Antibiotics. *Curr. Mol. Pharmacol.* **2008**, *1*, 50–60. [CrossRef]
14. Jones, R.R.; Bergman, R.G. p-Benzyne. Generation as an Intermediate in a Thermal Isomerization Reaction and Trapping Evidence for the 1,4-Benzenediyl Structure. *J. Am. Chem. Soc.* **1972**, *94*, 660–661. [CrossRef]
15. Li, J.J. Bergman Cyclization. In *Name Reactions*; Springer International Publishing: Cham, Switzerland, 2021; pp. 35–37, ISBN 9783030508647.
16. Cosgrove, J.P.; Dedon, P.C. Binding and Reaction of Calicheamicin and Other Eneidyne Antibiotics with DNA. In *Small Molecule DNA and RNA Binders*; Wiley-VCH Verlag GmbH & Co. KGaA: Weinheim, Germany, 2003; Volume 2, pp. 609–642, ISBN 3527305955.
17. Nicolaou, K.C.; Rigol, S.; Pitsinos, E.N.; Das, D.; Lu, Y.; Rout, S.; Schammel, A.W.; Holte, D.; Lin, B.; Gu, C.; et al. Uncialamycin-based antibody–drug conjugates: Unique eneidyne ADCs exhibiting bystander killing effect. *Proc. Natl. Acad. Sci. USA* **2021**, *118*, e2107042118. [CrossRef]
18. Adhikari, A.; Shen, B.; Rader, C. Challenges and opportunities to develop eneidyne natural products as payloads for antibody–drug conjugates. *Antib. Ther.* **2021**, *4*, 1–15. [CrossRef] [PubMed]
19. Adhikari, A.; Teijaro, C.N.; Yan, X.; Chang, C.-Y.; Gui, C.; Liu, Y.-C.; Crnovcic, I.; Yang, D.; Annaval, T.; Rader, C.; et al. Characterization of TnmH as an O-Methyltransferase Revealing Insights into Tiancimycin Biosynthesis and Enabling a Biocatalytic Strategy to Prepare Antibody–Tiancimycin Conjugates. *J. Med. Chem.* **2020**, *63*, 8432–8441. [CrossRef] [PubMed]
20. Godwin, C.D.; Gale, R.P.; Walter, R.B. Gemtuzumab ozogamicin in acute myeloid leukemia. *Leukemia* **2017**, *31*, 1855–1868. [CrossRef]
21. Lamb, Y.N. Inotuzumab Ozogamicin: First Global Approval. *Drugs* **2017**, *77*, 1603–1610. [CrossRef]
22. Basak, A.; Mandal, S.; Bag, S.S. Chelation-Controlled Bergman Cyclization: Synthesis and Reactivity of Eneidyne Ligands. *Chem. Rev.* **2003**, *103*, 4077–4094. [CrossRef]
23. Joshi, M.C.; Rawat, D.S. Recent developments in eneidyne chemistry. *Chem. Biodivers.* **2012**, *9*, 459–498. [CrossRef]
24. Kar, M.; Basak, A. Design, Synthesis, and Biological Activity of Unnatural Eneidyne and Related Analogues Equipped with pH-Dependent or Phototriggering Devices. *Chem. Rev.* **2007**, *107*, 2861–2890. [CrossRef] [PubMed]
25. Romeo, R.; Giofre, S.V.; Chiacchio, M.A. Synthesis and Biological Activity of Unnatural Eneidyne. *Curr. Med. Chem.* **2017**, *24*, 3433–3484. [CrossRef] [PubMed]
26. Yan, X.; Ge, H.; Huang, T.; Hindra; Yang, D.; Teng, Q.; Crnovčić, I.; Li, X.; Rudolf, J.D.; Lohman, J.R.; et al. Strain Prioritization and Genome Mining for Eneidyne Natural Products. *MBio* **2016**, *7*, e02104-16. [CrossRef] [PubMed]
27. Bhattacharya, P.; Basak, A.; Campbell, A.; Alabugin, I.V. Photochemical Activation of Eneidyne Warheads: A Potential Tool for Targeted Antitumor Therapy. *Mol. Pharm.* **2018**, *15*, 768–797. [CrossRef]
28. Lessi, M.; Panattoni, A.; Guglielmero, L.; Minei, P.; Bellina, F. Imidazole-Fused Eneidyne by Selective C5–C4 Alkynylations of 4,5-Dibromoimidazoles. *Synthesis*. **2019**, *51*, 933–943.

29. Li, B.; Zhang, M.; Lu, H.; Ma, H.; Wang, Y.; Chen, H.; Ding, Y.; Hu, A. Coordination-Accelerated Radical Formation from Acyclic Eneidyne for Tumor Cell Suppression. *Chem. Asian J.* **2019**, *14*, 4352–4357. [CrossRef]
30. Li, B.; Wu, Y.; Wang, Y.; Zhang, M.; Chen, H.; Li, J.; Liu, R.; Ding, Y.; Hu, A. Light-Cross-linked Eneidyne Small-Molecule Micelle-Based Drug-Delivery System. *ACS Appl. Mater. Interfaces* **2019**, *11*, 8896–8903. [CrossRef]
31. Lu, H.; Ma, H.; Li, B.; Zhang, M.; Chen, H.; Wang, Y.; Li, X.; Ding, Y.; Hu, A. Facilitating Myers–Saito cyclization through acid-triggered tautomerization for the development of maleimide-based antitumor agents. *J. Mater. Chem. B* **2020**, *8*, 1971–1979. [CrossRef]
32. Nicolaou, K.C.; Das, D.; Lu, Y.; Rout, S.; Pitsinos, E.N.; Lyssikatos, J.; Schammel, A.; Sandoval, J.; Hammond, M.; Aujay, M.; et al. Total Synthesis and Biological Evaluation of Tancimycins A and B, Yangpumicin A, and Related Anthraquinone-Fused Eneidyne Antitumor Antibiotics. *J. Am. Chem. Soc.* **2020**, *142*, 2549–2561. [CrossRef]
33. Zhang, M.; Li, B.; Chen, H.; Lu, H.; Ma, H.; Cheng, X.; Wang, W.; Wang, Y.; Ding, Y.; Hu, A. Triggering the Antitumor Activity of Acyclic Eneidyne through Maleimide-Assisted Rearrangement and Cycloaromatization. *J. Org. Chem.* **2020**, *85*, 9808–9819. [CrossRef]
34. Singha, M.; Bhattacharya, P.; Ray, D.; Basak, A. Sterically hindering the trajectory of nucleophilic attack towards p-benzynes by a properly oriented hydrogen atom: An approach to achieve regioselectivity. *Org. Biomol. Chem.* **2021**, *19*, 5148–5154. [CrossRef] [PubMed]
35. Zhang, M.; Li, B.; Chen, H.; Lu, H.; Ma, H.; Cheng, X.; Wang, W.; Wang, Y.; Ding, Y.; Hu, A. Maleimides Allow for Cycloaromatization of Acyclic Eneidyne. *Synfacts* **2020**, *16*, 1232.
36. Wang, W.; Lu, H.; Zhang, M.; Ma, H.; Cheng, X.; Ding, Y.; Hu, A. Synthesis of maleimide-based eneidyne with cyclopropane moieties for enhanced cytotoxicity under normoxic and hypoxic conditions. *J. Mater. Chem. B* **2021**, *9*, 4502–4509. [CrossRef]
37. Das, E.; Basak, S.; Anoop, A.; Chand, S.; Basak, A. How To Achieve High Regioselectivity in Barrier-less Nucleophilic Addition to p -Benzynes Generated via Bergman Cyclization of Unsymmetrical Cyclic Azaenediynes? *J. Org. Chem.* **2019**, *84*, 2911–2921. [CrossRef]
38. Das, E.; Basak, A. Regioselective Synthesis of Benzo-Fused Tetrahydroisoquinoline-Based Biaryls through a Tandem One-Pot Halogenation of p -Benzynes from Eneidyne and Suzuki-Miyaura Coupling. *J. Org. Chem.* **2020**, *85*, 2697–2703. [CrossRef] [PubMed]
39. Shrinidhi, A.; Perrin, C.L. Cyclohexeno[3,4]cyclodec-1,5-diyne-3-ene: A Convenient Eneidyne. *Org. Lett.* **2021**, *23*, 6911–6915. [CrossRef]
40. Zhang, M.; Ma, H.; Li, B.; Sun, K.; Lu, H.; Wang, W.; Cheng, X.; Li, X.; Ding, Y.; Hu, A. Nucleophilic Addition to Diradicals Derived From Cycloaromatization of Maleimide-Based Eneidyne. *Asian J. Org. Chem.* **2021**, *10*, 1454–1462. [CrossRef]
41. Lyapunova, A.G.; Danilkina, N.A.; Rummyantsev, A.M.; Khlebnikov, A.F.; Chislov, M.V.; Starova, G.L.; Sambuk, E.V.; Govdi, A.I.; Bräse, S.; Balova, I.A. Relative Reactivity of Benzothiophene-Fused Eneidyne in the Bergman Cyclization. *J. Org. Chem.* **2018**, *83*, 2788–2801. [CrossRef]
42. Danilkina, N.; Rummyantsev, A.; Lyapunova, A.; D'yachenko, A.; Khlebnikov, A.; Balova, I. 10-Membered Azaenediynes Fused to a Benzothiophene through the Nicholas Macrocyclization: Synthesis and DNA Cleavage Ability. *Synlett* **2019**, *30*, 161–166.
43. Danilkina, N.A.; D'yachenko, A.S.; Govdi, A.I.; Khlebnikov, A.F.; Korniyakov, I.V.; Bräse, S.; Balova, I.A. Intramolecular Nicholas Reactions in the Synthesis of Heteroenediynes Fused to Indole, Triazole, and Isocoumarin. *J. Org. Chem.* **2020**, *85*, 9001–9014. [CrossRef]
44. Nicolaou, K.C.; Ogawa, Y.; Zuccarello, G.; Schweiger, E.J.; Kumazawa, T. Cyclic conjugated eneidyne related to calicheamicins and esperamicins: Calculations, synthesis, and properties. *J. Am. Chem. Soc.* **1988**, *110*, 4866–4868. [CrossRef]
45. Bhattacharya, P.; Chakraborty, S.; Balaji, A.; Basak, A. Angle distortion model for predicting eneidyne activation towards Bergman cyclization: An alternate to the distance theory. *RSC Adv.* **2022**, *12*, 23552–23565. [CrossRef] [PubMed]
46. Lyapunova, A.G.; Danilkina, N.A.; Khlebnikov, A.F.; Köberle, B.; Bräse, S.; Balova, I.A. Oxaenediynes through the Nicholas-Type Macrocyclization Approach. *Eur. J. Org. Chem.* **2016**, *2016*, 4842–4851. [CrossRef]
47. Danilkina, N.A.; Lyapunova, A.G.; Khlebnikov, A.F.; Starova, G.L.; Bräse, S.; Balova, I.A. Ring-Closing Metathesis of $\text{Co}_2(\text{CO})_6$ -Alkyne Complexes for the Synthesis of 11-Membered Dieneidyne: Overcoming Thermodynamic Barriers. *J. Org. Chem.* **2015**, *80*, 5546–5555. [CrossRef] [PubMed]
48. Kulyashova, A.E.; Ponomarev, A.V.; Selivanov, S.I.; Khlebnikov, A.F.; Popik, V.V.; Balova, I.A. Cr(II)-promoted internal cyclization of acyclic eneidyne fused to benzo[b]thiophene core: Macrocycles versus 2-methylenecycloalkane-1-ols formation. *Arab. J. Chem.* **2019**, *12*, 151–167. [CrossRef]
49. Nicholas, K.M.; Pettit, R. On the stability of α -(alkynyl)dicobalt hexacarbonyl carbonium ions. *J. Organomet. Chem.* **1972**, *44*, C21–C24. [CrossRef]
50. Magnus, P. A general strategy using $\eta^2\text{Co}_2(\text{CO})_6$ acetylene complexes for the synthesis of the eneidyne antitumor agents esperamicin, calicheamicin, dynemicin and neocarzinostatin. *Tetrahedron* **1994**, *50*, 1397–1418. [CrossRef]
51. Teobald, B.J. The Nicholas reaction: The use of dicobalt hexacarbonyl-stabilised propargylic cations in synthesis. *Tetrahedron* **2002**, *58*, 4133–4170. [CrossRef]
52. Kann, N. Applications of the Nicholas Reaction in the Synthesis of Natural Products. *Curr. Org. Chem.* **2012**, *16*, 322–334. [CrossRef]
53. Röse, P.; Hilt, G. Cobalt-Catalysed Bond Formation Reactions; Part 2. *Synthesis*. **2015**, *48*, 463–492.

54. Green, J.R.; Nicholas, K.M. Propargylic Coupling Reactions via Bimetallic Alkyne Complexes: The Nicholas Reaction. In *Organic Reactions*; Johnson, J.B., Ed.; Wiley: Hoboken, NJ, USA, 2020; pp. 931–1326.
55. Danilkina, N.A.; Kulyashova, A.E.; Khlebnikov, A.F.; Bräse, S.; Balova, I.A. Electrophilic Cyclization of Aryldiacetylenes in the Synthesis of Functionalized Eneidyne Fused to a Heterocyclic Core. *J. Org. Chem.* **2014**, *79*, 9018–9045. [CrossRef] [PubMed]
56. Lyapunova, A.G.; D'yachenko, A.S.; Danilkina, N.A. Potassium fluoride for one-pot desilylation and the Sonogashira coupling of ethynylsilanes and buta-1,3-diyne silanes. *Russ. J. Org. Chem.* **2017**, *53*, 800–804. [CrossRef]
57. Ni, R.; Mitsuda, N.; Kashiwagi, T.; Igawa, K.; Tomooka, K. Heteroatom-embedded Medium-Sized Cycloalkynes: Concise Synthesis, Structural Analysis, and Reactions. *Angew. Chem. Int. Ed.* **2015**, *54*, 1190–1194. [CrossRef] [PubMed]
58. Roth, K.D.; Mueller, U. Nicholas reactions of amines. *Tetrahedron Lett.* **1993**, *34*, 2919–2922. [CrossRef]
59. Mosmann, T. Rapid colorimetric assay for cellular growth and survival: Application to proliferation and cytotoxicity assays. *J. Immunol. Methods* **1983**, *65*, 55–63. [CrossRef]
60. Kazantsev, A.; Bakulina, O.; Dar'in, D.; Kantin, G.; Bunev, A.; Krasavin, M. Unexpected Ring Contraction of Homophthalic Anhydrides under Diazo Transfer Conditions. *Org. Lett.* **2022**, *24*, 4762–4765. [CrossRef]
61. Mulay, S.V.; Fernandes, R.A. Synthetic Studies on Actinorhodin and γ -Actinorhodin: Synthesis of Deoxyactinorhodin and Deoxy- γ -actinorhodin/Crisamicin A Isomer. *Chem. A Eur. J.* **2015**, *21*, 4842–4852. [CrossRef]
62. Van Rooden, E.J.; Kreekel, R.; Hansen, T.; Janssen, A.P.A.; Van Esbroeck, A.C.M.; Den Dulk, H.; Van Den Berg, R.J.B.H.N.; Codée, J.D.C.; Van Der Stelt, M. Two-step activity-based protein profiling of diacylglycerol lipase. *Org. Biomol. Chem.* **2018**, *16*, 5250–5253. [CrossRef]
63. Hess, W.; Burton, J.W. Palladium-Catalysed Cyclisation of N-Alkynyl Aminomalonates. *Chem. Eur. J.* **2010**, *16*, 12303–12306. [CrossRef]
64. Shen, S.; Hadley, M.; Ustinova, K.; Pavlicek, J.; Knox, T.; Noonpalle, S.; Tavares, M.T.; Zimprich, C.A.; Zhang, G.; Robers, M.B.; et al. Discovery of a New Isoxazole-3-hydroxamate-Based Histone Deacetylase 6 Inhibitor SS-208 with Antitumor Activity in Syngeneic Melanoma Mouse Models. *J. Med. Chem.* **2019**, *62*, 8557–8577. [CrossRef]
65. Armarego, W.L.F. Purification of Organic Chemicals. In *Purification of Laboratory Chemicals*; Elsevier: Amsterdam, The Netherlands, 2017; p. 135. ISBN 9780128054574.
66. Kim, S.; Chung, Y.K. Rhodium-Catalyzed Carbonylative [3 + 2 + 1] Cycloaddition of Alkyne-Tethered Alkylidenecyclopropanes to Phenols in the Presence of Carbon Monoxide. *Org. Lett.* **2014**, *16*, 4352–4355. [CrossRef] [PubMed]
67. Kalbarczyk, K.P.; Diver, S.T. Enyne Metathesis/Brønsted Acid-Promoted Heterocyclization. *J. Org. Chem.* **2009**, *74*, 2193–2196. [CrossRef] [PubMed]

Article

An Alliance of Polynitrogen Heterocycles: Novel Energetic Tetrazinedioxide-Hydroxytetrazole-Based Materials

Dmitry M. Bystrov ¹, Alla N. Pivkina ² and Leonid L. Fershtat ^{1,*}

¹ N. D. Zelinsky Institute of Organic Chemistry, Russian Academy of Sciences 47 Leninsky Prosp., 119991 Moscow, Russia

² N. N. Semenov Federal Research Center for Chemical Physics, Russian Academy of Sciences, 3 Kosygin Str., 119991 Moscow, Russia

* Correspondence: fershtat@bk.ru

Abstract: Energetic materials constitute one of the most important subtypes of functional materials used for various applications. A promising approach for the construction of novel thermally stable high-energy materials is based on an assembly of polynitrogen biheterocyclic scaffolds. Herein, we report on the design and synthesis of a new series of high-nitrogen energetic salts comprising the C-C linked 6-aminotetrazinedioxide and hydroxytetrazole frameworks. Synthesized materials were thoroughly characterized by IR and multinuclear NMR spectroscopy, elemental analysis, single-crystal X-ray diffraction and differential scanning calorimetry. As a result of a vast amount of the formed intra- and intermolecular hydrogen bonds, prepared ammonium and amino-1,2,4-triazolium salts are thermally stable and have good densities of 1.75–1.78 g·cm⁻³. All synthesized compounds show high detonation performance, reaching that of benchmark RDX. At the same time, as compared to RDX, investigated salts are less friction sensitive due to the formed net of hydrogen bonds. Overall, reported functional materials represent a novel perspective subclass of secondary explosives and unveil further opportunities for an assembly of biheterocyclic next-generation energetic materials.

Citation: Bystrov, D.M.; Pivkina, A.N.; Fershtat, L.L. An Alliance of Polynitrogen Heterocycles: Novel Energetic Tetrazinedioxide-Hydroxytetrazole-Based Materials. *Molecules* **2022**, *27*, 5891. <https://doi.org/10.3390/molecules27185891>

Academic Editor: Panayiotis A. Koutentis

Received: 17 August 2022

Accepted: 8 September 2022

Published: 11 September 2022

Publisher's Note: MDPI stays neutral with regard to jurisdictional claims in published maps and institutional affiliations.



Copyright: © 2022 by the authors. Licensee MDPI, Basel, Switzerland. This article is an open access article distributed under the terms and conditions of the Creative Commons Attribution (CC BY) license (<https://creativecommons.org/licenses/by/4.0/>).

Keywords: nitrogen heterocycles; energetic materials; tetrazine; hydroxytetrazole

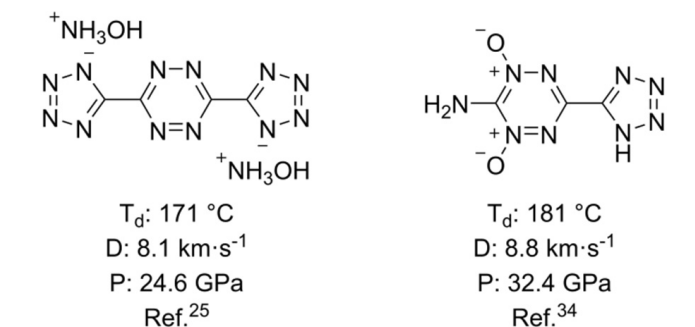
1. Introduction

A creation of novel functional organic materials remains one of the urgent goals in modern chemistry and materials science [1–4]. Such materials constitute a large variety of usually conjugated organic compounds with different chemical and physical properties. Recent achievements of numerous research groups worldwide confirmed that an incorporation of a nitrogen heteroaromatic motif usually enhances the quality of materials compared to their carbocyclic analogues [5–7]. In this regard, linear combinations of conjugated nitrogen heterocyclic moieties, especially of those mainly consisting of nitrogen atoms, demonstrate great application potential [8–10].

Among high-nitrogen heteroaromatic species, 1,2,4,5-tetrazine (six-membered ring with four nitrogen atoms) and tetrazole (five-membered ring with four nitrogen atoms) scaffolds retain leading positions in the chemistry community since materials derived thereof demonstrate improved functional properties. 1,2,4,5-Tetrazines may serve as components of photo- and electroactive materials [11,12], substrates for bioorthogonal processes [13,14] or precursors for diverse nitrogen heterocycles [15–18]. Tetrazoles are considered as carboxylic acid bioisosteres and are found in a wide range of pharmacological activity including some clinically approved pharmaceuticals [19–21]. Meanwhile, both tetrazine and tetrazole rings are used as paramount scaffolds in the construction of next-generation high-energy materials for mining, welding and other civil energetic applications [10,22]. As a rule, tetrazine- and tetrazole-based energy-rich compounds have a number of advantages including high nitrogen content, good thermal stability, acceptable sensitivity to mechanical stimuli and environmental compatibility [23,24]. A combination of C-C linked conjugated tetrazole

and tetrazine rings afforded several thermally stable energetic materials (Figure 1), which, however, have low amounts of oxygen [25]. Meanwhile, oxygen balance defined as the degree to which an explosive can be oxidized is an important parameter for high-energy materials. Several strategies for an incorporation of oxygen-rich explosophoric moieties, such as trinitromethyl group [26,27] or furoxan ring [28,29], are commonly used to enhance the oxygen content. Unfortunately, these approaches inevitably entail a decrease in thermal stability and an increase in mechanical sensitivity. Therefore, a compromise between these criteria still remains an urgent task and defines future trends in materials science.

Previous works:



This work:

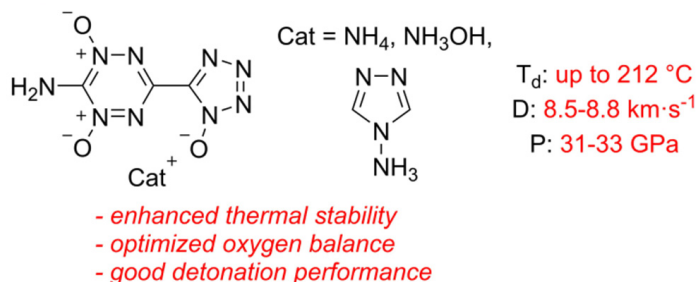


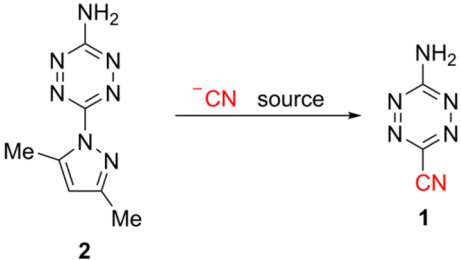
Figure 1. Previously known and newly synthesized energetic materials incorporating tetrazine–tetrazole framework.

Recent investigations demonstrated the utility of the N-oxide functionalization strategy to balance physicochemical properties, mechanical sensitivity and oxygen balance of energetic materials [30–33]. Importantly, N-oxide functionality not only increases oxygen balance, but also allows for better crystal packing, and efficiently enhances detonation performance. In the case of 1,2,4,5-tetrazine, a preparation of its mono- and dioxide derivatives with promising energetic properties was reported [34]. For the tetrazole ring, an installation of the N-oxide moiety is complicated due to the azole nature of the heterocycle and involvement of nitrogen lone pairs into ring conjugation. A solution to this issue may comprise the formation of the hydroxytetrazole motif, which is also capable of the formation of energy-rich salts due to high acidity of the OH-group [35,36]. In this regard, an alliance of the tetrazinedioxide and hydroxytetrazole scaffolds may contribute advantageously from both heterocycles in terms of thermal stability and mechanical sensitivity and provide an evolutionary step toward functional organic materials of the future. Herein, we report on the design and synthesis of a new series of high-nitrogen energetic salts comprising the C-C linked 6-aminotetrazinedioxide and hydroxytetrazole frameworks (Figure 1). The presence of the amino group is desirable in terms of intra- and intermolecular hydrogen bonds formed between amino group hydrogens and N-oxide oxygens, which contribute to the density and stability of target materials. Complex multidisciplinary investigation of the thus-prepared compounds reveals a balanced set of their physicochemical and detonation parameters enabling their ability to replace existing explosives (e.g., RDX).

2. Results and Discussion

For the synthesis of target energetic materials, we decided to use 6-amino-3-cyanotetrazine **1** as a starting compound, since the nitrile group can be easily converted to the hydroxytetrazole motif [35,36]. Thus, our research was started from the optimization of the reaction conditions of nucleophilic substitution of the dimethylpyrazolyl fragment in a readily available 3-amino-6-(3,5-dimethylpyrazol-1-yl)-1,2,4,5-tetrazine [37] **2**. Several different solvents as well as cyanide sources were screened, and the results are summarized in Table 1. It was found that the source and the concentration of cyanide anions were crucial for the reaction to proceed. TMSCN was ineffective (entry 1), while acetone cyanohydrin provided target tetrazine **1** in 31–71% yields depending on the reagent excess and additives used (entries 2–4). A combination of KCN in hexafluoroisopropanol (HFIP) did not result in the formation of compound **1** (entry 5), but a replacement of HFIP with MeCN or DMF provided cyanotetrazine **1** in moderate yields (entries 6–8). It was also found that low water content proved to be essential for high yields of 3-amino-6-cyanotetrazine **1** as can be seen from entries 8–10; thus, the best results were achieved using dry DMF with an addition of molecular sieves under inert atmosphere (entry 9). We consider that any water present in the reaction mixture reacts with KCN to form HO[−], which not only easily displaces dimethylpyrazolyl fragments to form a corresponding hydroxytetrazine derivative, but also induces the hydrolysis of the cyano group in the already formed product. It is also important that an excess of KCN can cause product hydrolysis upon aqueous work-up. To restrain this issue, the reaction mixture was poured into a slightly acidic aqueous ammonium chloride solution.

Table 1. Optimization of the reaction conditions for the synthesis of **1**^a.



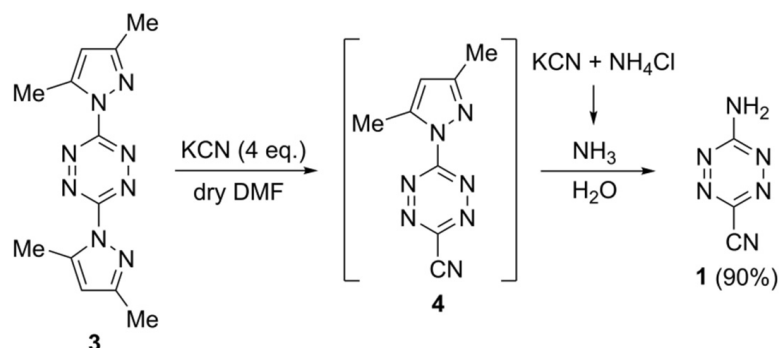
Entry	Cyanide Source	Base or Additive	Solvent	T, °C	Yield, ^b %
1	TMSCN (1 eq.)	NH ₄ F (1 eq.)	MeCN	82	0
2	Acetone cyanohydrin (1.5 eq.)	Net ₃ (1.5 eq.), 3Å MS	MeCN	82	31
3	Acetone cyanohydrin (2 eq.)	KHCO ₃ (2 eq.)	MeCN	82	48 ^c
4	Acetone cyanohydrin (4 eq.)	Net ₃ (4 eq.), 3Å MS	dry dioxane	101	71
5	KCN (2 eq.)	18-crown-6 (0.1 eq.)	HFIP	58	0
6	KCN (2 eq.)	-	MeCN	82	35 ^c
7	KCN (2 eq.)	-	DMF	85	61
8	KCN (1.2 eq.)	-	DMF	85	54
9	KCN (2 eq.)	3Å MS, Ar atm.	dry DMF	20	84
10	KCN (2 eq.)	3Å MS, Ar atm.	dry DMF	50	79

^a Reaction conditions: **2** (0.38 g, 2 mmol), cyanide source, base or additive, stirring at the indicated temperature.

^b Isolated yields. ^c Incomplete conversion of **2**.

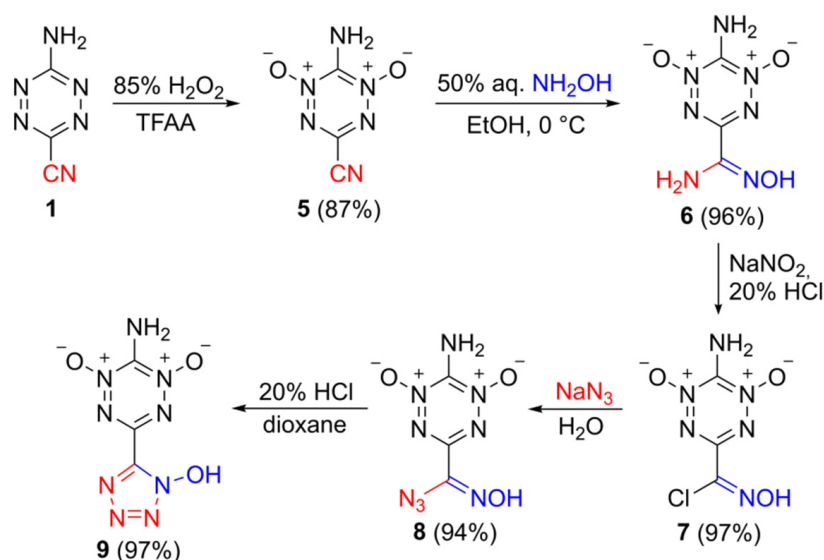
Curiously, an introduction of bis(dimethylpyrazolyl)tetrazine **3** in the same reaction under optimized conditions resulted again in a formation of 3-amino-6-cyano-1,2,4,5-tetrazine **1**. The great outcome was that not only was the yield of the target compound higher, but also the reaction time was reduced from 5 to 1.5 h. We supposed that 3-cyano-6-(3,5-dimethylpyrazol-1-yl)-1,2,4,5-tetrazine **4** formed initially. When the reaction mixture was poured into the ammonium chloride solution, the excess KCN neutralized the ammonium cation to form free ammonia, which then quickly displaced a second dimethylpyrazolyl fragment with the formation of 3-amino-6-cyano derivative **1** (Scheme 1). From the technological point of view, the utilization of substrate **3** is more convenient and

cost-effective since aminotetrazine **2** is synthesized from compound **3** [37]. Therefore, direct preparation of 3-amino-6-cyanotetrazine **1** from bis(dimethylpyrazolyl)tetrazine **3** allows to omit one reaction step.



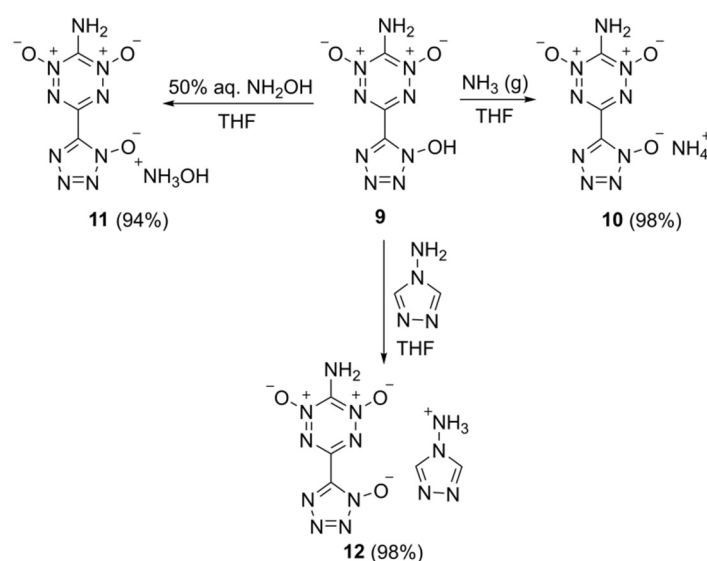
Scheme 1. Formation of 3-amino-6-cyanotetrazine **1** from bis(dimethylpyrazolyl)tetrazine **3**.

With a developed procedure for the synthesis of 3-amino-6-cyanotetrazine **1** in hand, we performed stepwise functionalization to install the hydroxytetrazole scaffold to the tetrazine backbone. At first, compound **1** was oxidized to the corresponding di-N-oxide **5** using peroxytrifluoroacetic acid generated in situ from 85% H_2O_2 and trifluoroacetic anhydride (TFAA). Addition of hydroxylamine to the thus-obtained di-N-oxide **5** occurred easily, providing amidoxime **6** with almost quantitative yield. The latter was subjected to diazotization in HCl to form the corresponding chloroxime **7**. The chlorine atom in **7** can be easily substituted with an azide anion to form azidooxime **8** with an excellent yield. Acid-induced cyclization of azidooxime functionality in **8** furnished the formation of the hydroxytetrazole **9** (Scheme 2). The overall yield of the target hydroxytetrazole **9** is remarkably high: 74% over five reaction steps starting from 3-amino-6-cyanotetrazine **1**.



Scheme 2. Synthesis of hydroxytetrazole **9**.

Upon treatment with nitrogen-rich bases, hydroxytetrazole **9** was converted to the corresponding salts **10–12** in quantitative yields (Scheme 3). Ammonia, hydroxylamine and 4-amino-1,2,4-triazole were used as commercially available and convenient base counterparts.



Scheme 3. Synthesis of nitrogen-rich hydroxytetrazole salts 10–12.

The structures of all synthesized compounds were confirmed by IR, ^1H and ^{13}C NMR spectroscopy as well as by elemental analysis. The structure of aminotriazolium salt **12** was additionally confirmed by ^{15}N NMR spectroscopy (Figure 2). The signals were assigned on the basis of the literature values of resonance peaks in similar compounds. The tetrazinedi-N-oxide motif is symmetric due to aromaticity; therefore, there are only two nitrogen signals attributable to the tetrazine ring [34]. The N4 and N5 signals are more upfield (-90.4 ppm) relative to N1 and N3 (-80.3 ppm). On the contrary, the hydroxytetrazole motif is asymmetric, which is clearly shown by the presence of four signals similar to the previously reported data [38]. 1,2,4-Triazole fragment is symmetric and is shown by two nitrogen signals (-89.9 ppm for N12 and -194.5 ppm for N10, N11) [39]. Both amino groups are located close to -300 ppm.

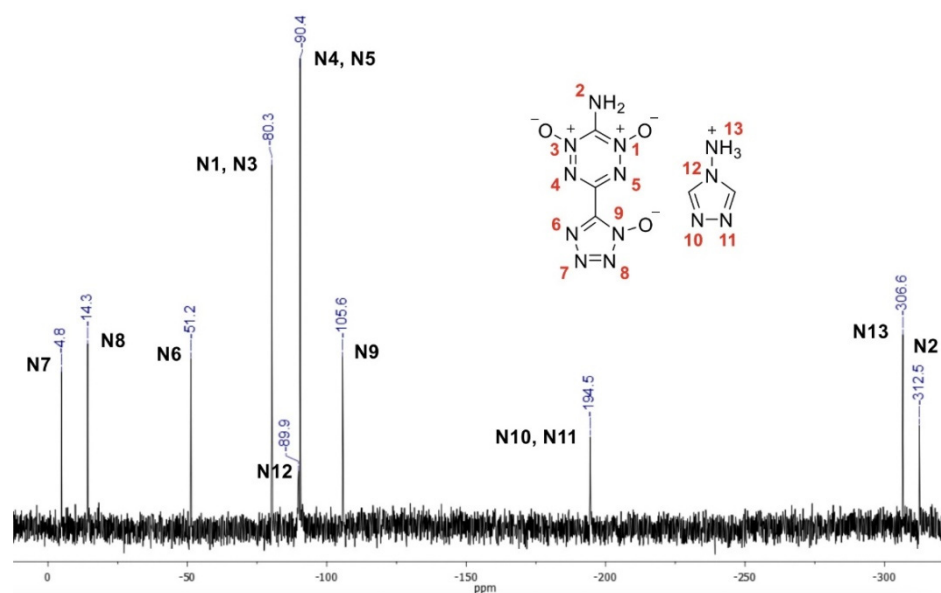


Figure 2. ^{15}N NMR spectra of aminotriazolium salt **12**.

The structure of salt **11** was further confirmed by X-ray diffraction study of a crystallohydrate grown from a methanol–water (1:1) mixture (Figure 3). Compound **11** crystallizes as a monohydrate in the monoclinic space group $P2_1/n$ with four formula units (4 anions, 4 cations, 4 water molecules) per cell and a density of $1.852 \text{ g}\cdot\text{cm}^{-3}$ at 100 K (Figure 3).

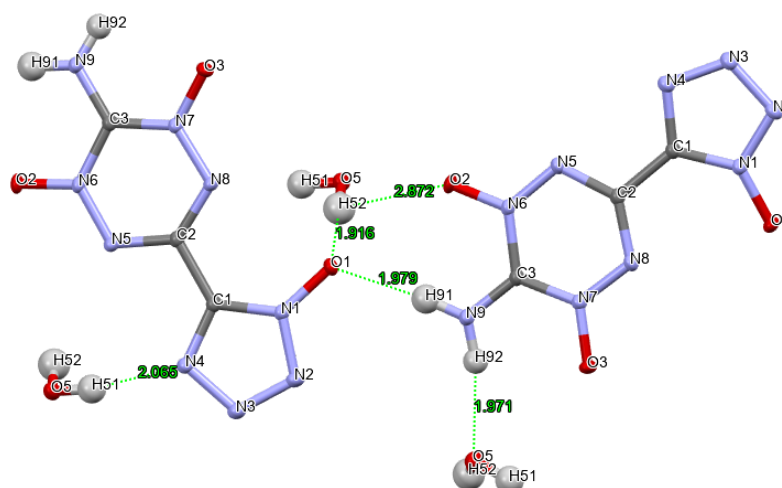


Figure 5. H-bonds formed by the hydroxytetrazole motif in the crystal of **11**. The values of the bond lengths are given in angstroms.

Contacts between parallel anion stacks are provided by two hydroxylammonium cations, which are interconnected head-to-tail between each other with two equal H-bonds (1.983 Å). These dimeric spacers are then linked to anionic units through hydroxylammonium OH⁻ and NH₃⁺ groups with two rather strong H-bonds (1.809 and 1.804 Å, respectively; Figure 6).

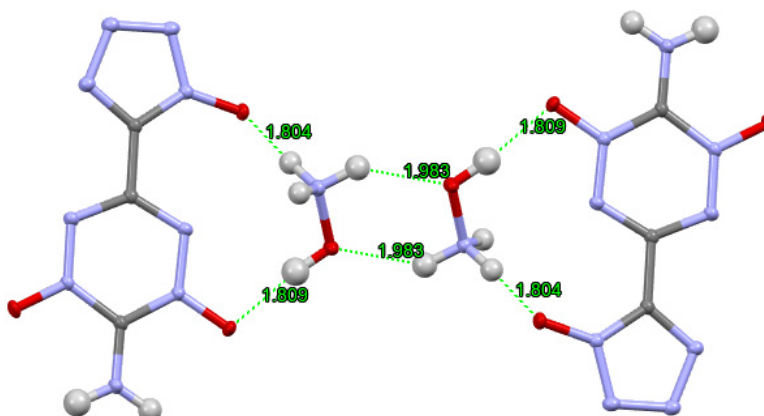


Figure 6. Hydroxylammonium-linked H-bonded dimers of **11**. The values of the bond lengths are given in angstroms.

The surrounding of the N-oxides is different: O(3) forms two moderate bonds with a water molecule and a hydroxylammonium cation, and O(2) only forms a weak H-bond with water (2.872 Å). This fact results in a slight difference between lengths of these two bonds in crystals: the N(7)-O(3) bond is longer than the N(6)-O(2) bond (1.283 and 1.256 Å, respectively). As a result of vast amount of the formed H-bonds, the density of the monohydrate is relatively high (1.852 g·cm⁻³) and even higher than that for the water-free salt (1.78 g·cm⁻³).

The physical and detonation properties, such as thermal stability, density, enthalpy of formation, detonation performance, as well as sensitivity of all target compounds, were investigated. The results are summarized in Table 2. With an exception of hydroxylammonium salt **11**, analyzed compounds have acceptable thermal stability: for **10** and **12**, the extrapolated onset of the decomposition peak by DSC is above 200 °C. Measured densities fall in the range of 1.75–1.78 g·cm⁻³, which is quite good for organic energetic salts. Compounds **10–12** store large amounts of nitrogen (>56%), much more than that of benchmark nitramine energetic material RDX (37.8%). High nitrogen content should

result in more eco-friendly reaction products. Combined nitrogen–oxygen contents of salts **10–12** are similar to that of RDX, while their oxygen balance to CO is slightly negative. Due to the presence of two additional carbon atoms in the amino-1,2,4-triazolium cation, the oxygen balance of salt **12** is the most negative in the presented series of energetic salts. At the same time, energetic materials **10–12** have high calculated enthalpies of formation within 413–780 kJ·mol^{−1}. The enthalpy of formation of salt **12** is the highest since the contribution of the heteroaromatic amino-1,2,4-triazolium cation to the resulting value is the most significant in comparison with ammonium and hydroxylammonium cations. Having the enthalpies of formation and experimental densities in hand, we calculated the detonation velocities (D) and pressures (P) using the empirical equations included in the PILEM application [42]. All synthesized compounds show the high detonation performance, reaching that of benchmark RDX. As compared to the RDX, investigated salts are less friction sensitive.

Table 2. Physical properties and detonation parameters of salts **10–12**.

Salt	T _d , ^a °C	ρ, ^b g·cm ^{−3}	N, ^c %	[N + O], ^d %	Ω _{CO} , ^e %	ΔH _f ^{o,f} kJ·mol ^{−1}	D, ^g km·s ^{−1}	P, ^h GPa	IS, ⁱ J	FS, ^j N
10	212	1.75	60.9	81.7	−20.9	417	8.5	31	9	265
11	155	1.78	56.9	82.9	−13.0	413	8.8	33	10	190
12	206	1.77	61.3	77.4	−29.6	779	8.5	32	15	260
RDX	204	1.81	37.8	81.1	0	68	8.8	34	10	130

^a Decomposition temperature (DSC, 5 K min^{−1}). ^b Density measured by gas pycnometer (298 K). ^c Nitrogen content. ^d Combined nitrogen and oxygen content. ^e Oxygen balance (based on CO) for C_aH_bO_cN_d, 1600(c − a − b/2)/MW. ^f Enthalpy of formation. ^g Detonation velocity. ^h Detonation pressure. ⁱ Impact sensitivity. ^j Friction sensitivity.

3. Materials and Methods

CAUTION! Although we encountered no difficulties during the preparation and handling of compounds described in this paper, they are potentially explosive energetic materials that are sensitive to impact and friction. Mechanical actions of these energetic materials, involving scratching or scraping, must be avoided. Any manipulations must be carried out by using appropriate standard safety precautions.

3.1. General Methods

All reactions were carried out in well-cleaned oven-dried glassware with magnetic stirring. ¹H and ¹³C NMR spectra were recorded on a Bruker AM-300 (300.13 and 75.47 MHz, respectively) spectrometer and referenced to residual solvent peak. ¹⁵N NMR spectrum was recorded on a Bruker AV-600 instrument (the frequency for ¹⁵N was 50.7 MHz) at room temperature. The chemical shifts are reported in ppm (δ). The IR spectra were recorded on a Bruker “Alpha” spectrometer in the range 400–4000 cm^{−1} (resolution 2 cm^{−1}). Elemental analyses were performed by the CHN Analyzer Perkin-Elmer 2400. All solvents were purified and dried using standard methods prior to use. All standard reagents were purchased from Aldrich or Acros Organics and used without further purification.

3.2. X-ray Crystallography

X-ray diffraction data were collected at 100 K on a four-circle Rigaku Synergy S diffractometer equipped with a HyPix600HE area-detector (kappa geometry, shutterless ω-scan technique), using graphite monochromatized Cu K_α-radiation. The intensity data were integrated and corrected for absorption and decay by the CrysAlisPro program [43]. The structure was solved by direct methods using SHELXT [44] and refined on F² using SHELXL-2018 [45] in the OLEX2 program [46]. All non-hydrogen atoms were refined with individual anisotropic displacement parameters. The locations of hydrogen atoms H4, H51, H52, H91, H92, H101, H102 and H103 were found from the electron density-difference map;

these hydrogen atoms were refined with individual isotropic displacement parameters. All other hydrogen atoms were placed in ideal calculated positions and refined as riding atoms with relative isotropic displacement parameters (for details, see Supplementary Materials, Tables S1–S7). CCDC 2169314 contains the supplementary crystallographic data for **11**. These data can be obtained free of charge via <http://www.ccdc.cam.ac.uk/conts/retrieving.html> (accessed on 17 July 2022) (or from the CCDC, 12 Union Road, Cambridge, CB21EZ, UK; or deposit@ccdc.cam.ac.uk).

3.3. Computational Methods

All calculations were performed with Gaussian09 software package [47]. The enthalpies of formation in the gas phase for all cases were calculated using the CBS-4M method [48]. The enthalpies of formation of salts in the solid phase were estimated on the basis of the crystal packing modeling method. Values for $\Delta_f H^\circ$ (atoms) were taken from the NIST database.

$$\Delta_f H^\circ_{(g, 298)} = H_{(Molecule, 298)} - \sum H^\circ_{(Atoms, 298)} + \sum \Delta_f H^\circ_{(Atoms, 298)}$$

Geometric optimization of all structures for crystal packing calculation was carried out using the DFT/B3LYP functional and the aug-cc-PVDZ basis set with a Grimme's D2 dispersion correction [49]. The optimized structures were conformed to be true local energy minima on the potential-energy surface by frequency analyses at the same level.

In the calculation of lattice energy, the molecules were treated as rigid bodies with fixed point groups. We applied pairwise atom–atom potentials to describe the van der Waals and electrostatic point charges for Coulomb components of intermolecular energy. At the initial stage, “6–12” Lennard-Jones (LJ)-type potential parameters were used [50]. The electrostatic energy was calculated with a set of displaced point charge sites by program FitMEP [51]. The lattice energy simulations were performed with the program PMC [52].

It is well known that the majority of organic crystal structures studied experimentally belong to a rather limited number of space groups [53]. For brief assessment of crystal packing, we obtained the following ordered list of the most likely structural classes: $P2_1/c$, $P2_12_12_1$, $P-1$, $Pca2_1$ and $P1$ with two independent molecules in cell, which cover more than 80% of the whole number of crystal structures in total [53]. Taking into account low deviation in the crystal lattice energies of polymorphs, such a calculation is considered reasonable.

Enthalpy of sublimation for **9** was calculated by the formula:

$$\Delta H_{\text{subl}} = -E_{\text{lat}} - 2RT$$

where R is the universal gas constant, E_{lat} is the lattice energy, T is temperature (298 K).

The new approach for salts proposes a technique based on modeling the crystal packing for a salt and a similar neutral compound (quasi-salt, cocrystal). The enthalpy of formation in this case is calculated as the average value between these two structures [54].

Detonation performance parameters (detonation velocity at maximal density and Chapman–Jouguet pressure) were calculated by a recently suggested set of empirical methods from PILEM application [42]. Note that the accuracy of the utilized PILEM empirical methods is comparable to benchmark thermodynamic code EXPLO5.

3.4. Thermal Analysis and Sensitivity Measurements

Thermal analysis was performed using the STA 449 F3 (Netzsch) apparatus. Samples of 0.5–1 mg mass were poured into alumina pans covered with pierced lids and heated to 600 °C with a constant rate of 5 K min^{−1}. Impact sensitivity tests were performed using BAM-type machine according to STANAG 4489 [55]. Friction sensitivity was evaluated in agreement with STANAG 4487 [56]. The reported values correspond to 50% probability of explosions; other details can be found elsewhere [57].

3.5. Synthetic Procedures

3-Amino-6-cyano-1,2,4,5-tetrazine (1). *Method A from 3-amino-6-(3,5-dimethyl-1H-pyrazol-1-yl)-1,2,4,5-tetrazine 2:* In a Schlenk flask under an argon atmosphere, 3-amino-6-(3,5-dimethyl-1H-pyrazol-1-yl)-1,2,4,5-tetrazine **2** (382 mg, 2 mmol), KCN (260 mg, 4 mmol) and oven-dried 3Å molecular sieves (300 mg) were mixed, and dry DMF (9 mL) was added. The reaction mixture was stirred at ambient temperature for 5.5 h, poured into a solution of NH₄Cl (16 g) in 200 mL of cold water and extracted with EtOAc (7 × 60 mL). The combined extracts were dried over MgSO₄ and evaporated at reduced pressure. The resulting crude solid was purified by flash chromatography on SiO₂ (eluent CH₂Cl₂-EtOAc, 4:1) yielding 206 mg (84%) of pure product. *Method B from 3,6-bis(3,5-dimethyl-1H-pyrazol-1-yl)-1,2,4,5-tetrazine 3:* In a Schlenk flask under an argon atmosphere, 3,6-bis(3,5-dimethyl-1H-pyrazol-1-yl)-1,2,4,5-tetrazine **3** (540 mg, 2 mmol), KCN (520 mg, 8 mmol) and oven-dried 3Å molecular sieves (400 mg) were mixed, and dry DMF (15 mL) was added. The reaction mixture was stirred at ambient temperature for 1.5 h, poured into a solution of NH₄Cl (12 g) in 150 mL of cold water and extracted with EtOAc (5 × 60 mL). The combined extracts were dried over MgSO₄ and evaporated at reduced pressure. The resulting crude solid was purified by flash chromatography on SiO₂ (eluent CH₂Cl₂-EtOAc, 4:1) yielding 220 mg (90%) of pure product. Red crystalline solid. mp = 176–177 °C (dec). IR (KBr), ν: 3432, 3331, 2253, 1670, 1637, 1531, 1501, 1038, 970 cm⁻¹. ¹H NMR (300 MHz, DMSO-*d*₆) δ_H, ppm: 9.12 (s, 2H). ¹³C{¹H} NMR (75.5 MHz, DMSO-*d*₆) δ_C, ppm: 160.9, 144.6, 115.6. Calcd. for C₃H₂N₆ (%): C, 29.51; H, 1.65; N, 68.84. Found (%): C, 29.59; H, 1.59; N, 68.67.

6-Amino-3-cyano-1,2,4,5-tetrazine 1,5-dioxide (5). First, 85% H₂O₂ (4.5 mL) was slowly added to trifluoroacetic anhydride (12 mL), cooled on an ice bath, and the temperature was kept below 10 °C. Then, a solution of 3-amino-6-cyanotetrazine (2.44 g, 20 mmol) in MeCN (30 mL) was added in one portion. The reaction mixture was stirred at 25 °C for 2 h, poured into water (250 mL) and extracted with EtOAc (10 × 50 mL). The combined extracts were dried over MgSO₄ and evaporated at reduced pressure yielding 2.68 g (87%) of pure product. Yellow solid. mp = 191–192 °C (dec). ¹H NMR (300 MHz, DMSO-*d*₆) δ_H, ppm: 9.69 (s, 2H). ¹³C{¹H} NMR (75.5 MHz, DMSO-*d*₆) δ_C, ppm: 150.1, 129.9, 112.5. Calcd. for C₃H₂N₆O₂ (%): C, 23.38; H, 1.31; N, 54.54. Found (%): C, 23.51; H, 1.19; N, 54.31.

6-Amino-3-(amino(hydroximino)methyl)-1,2,4,5-tetrazine 1,5-dioxide (6). First, 50% aqueous NH₂OH (1.22 mL, 19 mmol) was added dropwise to a suspension of 6-amino-3-cyano-1,2,4,5-tetrazine 1,5-dioxide **5** (2.54 g, 16.5 mmol) in ethanol (66 mL) at 0 °C under vigorous stirring. The reaction mixture was stirred at 0 °C for 10 min and then at ambient temperature for an additional 1 h. The resulting solid was filtered off, washed with EtOAc (30 mL) and dried in air. Yield 2.96 g (96%). Orange solid. T_d = 207–208 °C. IR (KBr), ν: 3459, 3403, 3353, 3111, 1685, 1633, 1502, 1402, 1319, 1092, 947 cm⁻¹. ¹H NMR (300 MHz, DMSO-*d*₆) δ_H, ppm: 10.32 (s, 1H), 8.71 (br. s, 2H), 5.79 (s, 2H). ¹³C{¹H} NMR (75.5 MHz, DMSO-*d*₆) δ_C, ppm: 147.1, 145.5, 145.2. Calcd. for C₃H₅N₇O₃ (%): C, 19.26; H, 2.69; N, 52.40. Found (%): C, 19.35; H, 2.61; N, 52.28.

6-Amino-3-(chloro(hydroxyimino)methyl)-1,2,4,5-tetrazine 1,5-dioxide (7). Conc. HCl (59 mL) was added to a suspension of amidoxime **6** (2.805 g, 15 mmol) in distilled water (48 mL) at 0 °C under vigorous stirring. Then, a solution of NaNO₂ (1.24 g, 18 mmol) in distilled water (18 mL) was added dropwise at 0 °C. The reaction mixture was stirred for 3.5 h at 0 °C, poured into 500 mL of water and extracted with EtOAc (8 × 60 mL). The combined extracts were dried over MgSO₄ and evaporated at reduced pressure yielding 3.01 g (97%) of pure chlorooxime. Yield 3.01 g (97%). Yellow solid. T_d = 207–208 °C. IR (KBr), ν: 3391, 3291, 3262, 1644, 1494, 1303, 1088, 1007, 900 cm⁻¹. ¹H NMR (300 MHz, DMSO-*d*₆) δ_H, ppm: 13.20 (s, 1H), 8.96 (s, 2H). ¹³C{¹H} NMR (75.5 MHz, DMSO-*d*₆) δ_C, ppm: 147.3, 145.1, 129.8. Calcd. for C₃H₃N₆O₃Cl (%): C, 17.45; H, 1.46; N, 40.69. Found (%): C, 17.40; H, 1.49; N, 40.61.

6-Amino-3-(azido(hydroxyimino)methyl)-1,2,4,5-tetrazine 1,5-dioxide (8). Chloroxime **7** (1.55 g, 7.5 mmol) was added in one portion to a solution of NaN₃ (975 mg, 15 mmol) in 40 mL of distilled water at 0 °C. The reaction mixture was stirred at 0 °C for 10 min and

then at ambient temperature for an additional 3.5 h. Then, conc. HCl (660 μ L) was added, the reaction mixture was stirred for 10 min, and the yellow product was filtered off, washed with water (10 mL) and dried in air. Additional amounts of product were obtained from the mother liquor, which was evaporated under reduced pressure. Then, THF (20 mL) was added to the residue, and insoluble NaCl was filtered off. The resulting solution containing target azidooxime was evaporated under reduced pressure. The obtained products were combined to yield 1.50 g (94%) of target compound **8**. Yellow solid. $T_d = 185$ – 186 °C. IR (KBr), ν : 3374, 3246, 2172, 2135, 1645, 1499, 1311, 1085, 1029, 926 cm^{-1} . ^1H NMR (300 MHz, DMSO- d_6) δ_{H} , ppm: 12.46 (s, 1H), 8.90 (s, 2H). $^{13}\text{C}\{^1\text{H}\}$ NMR (75.5 MHz, DMSO- d_6) δ_{C} , ppm: 147.4, 144.0, 136.6. Calcd. for $\text{C}_3\text{H}_3\text{N}_9\text{O}_3$ (%): C, 16.91; H, 1.42; N, 59.15. Found (%): C, 16.70; H, 1.49; N, 58.99.

6-Amino-3-(1-hydroxy-1H-tetrazol-5-yl)-1,2,4,5-tetrazine 1,5-dioxide (9). Azidooxime **8** (1.70 g, 8 mmol) was dissolved in a 20% HCl solution in dioxane (25 mL). The reaction mixture was stirred for 5 h at ambient temperature, poured into 100 mL of distilled water and evaporated at reduced pressure at 45 °C, adding water several times to completely remove any residual HCl. Yield 1.65 g (97%). Yellow solid. $T_d = 213$ – 214 °C. IR (KBr), ν : 3547, 3499, 1639, 1503, 1326, 1109, 956 cm^{-1} . ^1H NMR (300 MHz, DMSO- d_6) δ_{H} , ppm: 9.20 (s, 2H). $^{13}\text{C}\{^1\text{H}\}$ NMR (75.5 MHz, DMSO- d_6) δ_{C} , ppm: 148.0, 141.5, 139.6. HRMS (ESI) Calcd. for: $\text{C}_3\text{H}_4\text{N}_9\text{O}_3^+$: 214.0431; Found: 214.0441 [M+H] $^+$. Calcd. for: $\text{C}_3\text{H}_3\text{N}_9\text{O}_3\text{Na}^+$: 236.0251; Found: 236.0251 [M+Na] $^+$.

Ammonium salt of 6-amino-3-(1-hydroxy-1H-tetrazol-5-yl)-1,2,4,5-tetrazine 1,5-dioxide (10). Dry gaseous ammonia was bubbled through a solution of hydroxytetrazole **9** (1.065 g, 5 mmol) in 40 mL of dry THF, cooled to 0 °C, for 5 min. The reaction mixture was stirred for an additional 30 min at 0 °C. The formed red solid was filtered off, washed with THF (50 mL) and dried in air. Yield 1.13 g (98%). Red solid. $T_d = 212$ °C. IR (KBr), ν : 3302, 3208, 1613, 1418, 1309, 1114, 956 cm^{-1} . ^1H NMR (300 MHz, DMSO- d_6) δ_{H} , ppm: 6.40 (br. s, 6H). $^{13}\text{C}\{^1\text{H}\}$ NMR (75.5 MHz, DMSO- d_6) δ_{C} , ppm: 147.3, 140.9, 137.4. ^{14}N NMR (21.7 MHz, DMSO- d_6) δ_{N} : -362.1 . Calcd. for $\text{C}_3\text{H}_6\text{N}_{10}\text{O}_3$ (%): C, 15.66; H, 2.63; N, 60.86. Found (%): C, 15.81; H, 2.49; N, 60.59.

Hydroxylammonium salt of 6-amino-3-(1-hydroxy-1H-tetrazol-5-yl)-1,2,4,5-tetrazine 1,5-dioxide (11). First, 50% aqueous NH_2OH (313 μ L, 5.1 mmol) was added dropwise to a solution of hydroxytetrazole **9** (1.065 g, 5 mmol) in 20 mL of dry THF at 0 °C under vigorous stirring. The reaction mixture was additionally stirred at 0 °C for 30 min. The formed yellow solid was filtered off, washed with THF (30 mL) and dried in air. Yield 1.48 g (94%). Yellow solid. $T_d = 155$ °C. IR (KBr), ν : 3229, 2950, 1651, 1502, 1309, 1112, 956 cm^{-1} . ^1H NMR (300 MHz, DMSO- d_6) δ_{H} : 9.90 (br. s, 6H). $^{13}\text{C}\{^1\text{H}\}$ NMR (75.5 MHz, DMSO- d_6) δ_{C} , ppm: 146.7, 142.9, 137.5. Calcd. for $\text{C}_3\text{H}_6\text{N}_{10}\text{O}_4$ (%): C, 14.64; H, 2.46; N, 56.91. Found (%): C, 14.42; H, 2.57; N, 56.70.

4-Amino-1,2,4-triazolium salt of 6-amino-3-(1-hydroxy-1H-tetrazol-5-yl)-1,2,4,5-tetrazine 1,5-dioxide (12). A solution of 4-amino-1,2,4-triazole (378 mg, 4.5 mmol) in 2 mL of MeOH was added dropwise to a solution of hydroxytetrazole **9** (959 mg, 4.5 mmol) in 16 mL of dry THF at ambient temperature under vigorous stirring. The reaction mixture was additionally stirred at ambient temperature for 30 min. The formed yellow solid was filtered off, washed with THF (30 mL) and dried in air. Yield 1.31 mg (98%). Yellow solid. $T_d = 206$ °C. IR (KBr), ν : 3331, 3134, 1638, 1500, 1320, 1100, 960 cm^{-1} . ^1H NMR (300 MHz, DMSO- d_6) δ_{H} , ppm: 9.18 (s, 2H), 8.55 (s, 2H), 6.02 (br. s, 3H). $^{13}\text{C}\{^1\text{H}\}$ NMR (75.5 MHz, DMSO- d_6) δ_{C} , ppm: 147.8, 144.6, 140.9, 140.2. ^{15}N NMR (50.7 MHz, DMSO- d_6) δ_{N} , ppm: -4.8 , -14.3 , -51.2 , -80.3 , -89.9 , -90.4 , -105.6 , -194.5 , -306.6 , -312.5 . Calcd. for $\text{C}_5\text{H}_7\text{N}_{13}\text{O}_3$ (%): C, 20.21; H, 2.37; N, 61.27. Found (%): C, 20.36; H, 2.29; N, 60.97.

4. Conclusions

In conclusion, a series of novel energetic organic salts comprising C-C bridged tetrazinedi-N-oxide and hydroxytetrazole rings and nitrogen-rich cations was synthesized starting from the parent compound 3-amino-6-cyano-1,2,4,5-tetrazine. These energetic

materials were well characterized by IR and ^1H , ^{13}C , ^{15}N NMR spectroscopy, elemental analysis and differential scanning calorimetry. The molecular structure of the hydroxylammonium salt **11** was additionally confirmed by single-crystal X-ray diffraction. The anionic units in energetic salt **11** are stacked into infinite columns, which are supported by hydrogen bonds formed between exocyclic oxygen and ring nitrogen atoms of the anion and the hydroxylammonium counter-ions. Synthesized energetic salts have high enthalpies of formation and excellent detonation performance, which together with high nitrogen content, make these compounds promising green alternatives for commonly used secondary explosive RDX. Moreover, reported high-energy salts have lower friction sensitivity compared to RDX, which additionally confirms their suitability for energetic applications as secondary explosives.

Supplementary Materials: The following supporting information can be downloaded at: <https://www.mdpi.com/article/10.3390/molecules27185891/s1>, crystallographic data (Tables S1–S7), copies of NMR spectra.

Author Contributions: Conceptualization, D.M.B. and L.L.F.; methodology, D.M.B.; investigation, D.M.B. and A.N.P.; writing—original draft preparation, D.M.B. and L.L.F.; writing—review and editing, L.L.F.; supervision, L.L.F.; project administration, L.L.F.; funding acquisition, L.L.F. All authors have read and agreed to the published version of the manuscript.

Funding: This work was supported by the Russian Science Foundation (project 21-73-10109).

Institutional Review Board Statement: Not applicable.

Informed Consent Statement: Not applicable.

Data Availability Statement: Data obtained in this project are contained within this article and are available upon request from the authors.

Acknowledgments: Crystal structure determination was performed in the Department of Structural Studies of the Zelinsky Institute of Organic Chemistry, Moscow. We thank Artem N. Fakhrutdinov for registration of the ^{15}N NMR spectrum and Dmitry V. Khakimov for calculation of the enthalpies of formation.

Conflicts of Interest: The authors declare no conflict of interest.

Sample Availability: Samples of the compounds are not available from the authors.

References

1. Li, D.; Yu, G. Innovation of Materials, Devices, and Functionalized Interfaces in Organic Spintronics. *Adv. Funct. Mater.* **2021**, *31*, 2100550. [CrossRef]
2. Liu, C.-Y.; Lin, P.-H.; Lee, K.-M. Development of Step-Saving Alternative Synthetic Pathways for Functional π -Conjugated Materials. *Chem. Rec.* **2021**, *21*, 3498–3508. [CrossRef] [PubMed]
3. Sathiyar, G.; Wang, H.; Chen, C.; Miao, Y.; Zhai, M.; Cheng, M. Impact of fluorine substitution in organic functional materials for perovskite solar cell. *Dye. Pigment.* **2022**, *198*, 110029. [CrossRef]
4. Yang, X.-D.; Tan, L.; Sun, J.-K. Encapsulation of Metal Clusters within Porous Organic Materials: From Synthesis to Catalysis Applications. *Chem. Asian J.* **2022**, *17*, e202101289. [CrossRef]
5. Roy, S.; Das, S.K.; Khatua, H.; Das, S.; Chattopadhyay, B. Road Map for the Construction of High-Valued N-Heterocycles via Denitrogenative Annulation. *Acc. Chem. Res.* **2021**, *54*, 4395–4409. [CrossRef]
6. Odom, A.L.; McDaniel, T.J. Titanium-Catalyzed Multicomponent Couplings: Efficient One-Pot Syntheses of Nitrogen Heterocycles. *Acc. Chem. Res.* **2015**, *48*, 2822–2833. [CrossRef]
7. Makhova, N.N.; Belen'kii, L.I.; Gazieva, G.A.; Dalinger, I.L.; Konstantinova, L.S.; Kuznetsov, V.V.; Kravchenko, A.N.; Krayushkin, M.M.; Rakin, O.A.; Starosotnikov, A.M.; et al. Progress in the chemistry of nitrogen-, oxygen- and sulfur-containing heterocyclic systems. *Russ. Chem. Rev.* **2020**, *89*, 55–124. [CrossRef]
8. Verbitskiy, E.V.; Rusinov, G.L.; Chupakhin, O.N.; Charushin, V.N. Design of fluorescent sensors based on azaheterocyclic push-pull systems towards nitroaromatic explosives and related compounds: A review. *Dye. Pigment.* **2020**, *180*, 108414. [CrossRef]
9. Kerru, N.; Gummidi, L.; Maddila, S.; Gangu, K.K.; Jonnalagadda, S.B. A Review on Recent Advances in Nitrogen-Containing Molecules and Their Biological Applications. *Molecules* **2020**, *25*, 1909. [CrossRef]
10. O'Sullivan, O.T.; Zdilla, M.J. Properties and Promise of Catenated Nitrogen Systems As High-Energy-Density Materials. *Chem. Rev.* **2020**, *120*, 5682–5744. [CrossRef]

11. Miomandre, F.; Audebert, P. 1,2,4,5-Tetrazines: An intriguing heterocycles family with outstanding characteristics in the field of luminescence and electrochemistry. *J. Photochem. Photobiol. C Photochem. Rev.* **2020**, *44*, 100372. [CrossRef]
12. Lipunova, G.N.; Nosova, E.V.; Zyryanov, G.V.; Charushin, V.N.; Chupakhin, O.N. 1,2,4,5-Tetrazine derivatives as components and precursors of photo- and electroactive materials. *Organ. Chem. Front.* **2021**, *8*, 5182–5205. [CrossRef]
13. Wilkovitsch, M.; Haider, M.; Sohr, B.; Herrmann, B.; Klubnick, J.; Weissleder, R.; Carlson, J.C.T.; Mikula, H. A Cleavable C₂-Symmetric *trans*-Cyclooctene Enables Fast and Complete Bioorthogonal Disassembly of Molecular Probes. *J. Am. Chem. Soc.* **2020**, *142*, 19132–19141. [CrossRef]
14. Wu, H.; Devaraj, N.K. Advances in Tetrazine Bioorthogonal Chemistry Driven by the Synthesis of Novel Tetrazines and Dienophiles. *Acc. Chem. Res.* **2018**, *51*, 1249–1259. [CrossRef] [PubMed]
15. Schnell, S.D.; Schilling, M.; Sklyaruk, J.; Linden, A.; Lubner, S.; Gademann, K. Nucleophilic Attack on Nitrogen in Tetrazines by Silyl-Enol Ethers. *Organ. Lett.* **2021**, *23*, 2426–2430. [CrossRef] [PubMed]
16. Xie, Y.; Fang, Y.; Huang, Z.; Tallon, A.M.; am Ende, C.W.; Fox, J.M. Divergent Synthesis of Monosubstituted and Unsymmetrical 3,6-Disubstituted Tetrazines from Carboxylic Ester Precursors. *Angew. Chem. Int. Ed.* **2020**, *59*, 16967–16973. [CrossRef] [PubMed]
17. Sun, H.; Xue, Q.; Zhang, C.; Wu, H.; Feng, P. Derivatization based on tetrazine scaffolds: Synthesis of tetrazine derivatives and their biomedical applications. *Org. Chem. Front.* **2022**, *9*, 481–498. [CrossRef]
18. Zhu, Z.; Glinkerman, C.M.; Boger, D.L. Selective N1/N4 1,4-Cycloaddition of 1,2,4,5-Tetrazines Enabled by Solvent Hydrogen Bonding. *J. Am. Chem. Soc.* **2020**, *142*, 20778–20787. [CrossRef]
19. Mittal, R.; Awasthi, S.K. Recent Advances in the Synthesis of 5-Substituted 1H-Tetrazoles: A Complete Survey (2013–2018). *Synthesis* **2019**, *51*, 3765–3783. [CrossRef]
20. Popova, E.A.; Trifonov, R.E.; Ostrovskii, V.A. Tetrazoles for biomedicine. *Russ. Chem. Rev.* **2019**, *88*, 644–676. [CrossRef]
21. Ostrovskii, V.A.; Popova, E.A.; Trifonov, R.E. Chapter One—Developments in Tetrazole Chemistry (2009–2016). *Adv. Heterocycl. Chem.* **2017**, *123*, 1–62. [CrossRef]
22. Wang, T.; Gao, H.; Shreeve, J.M. Functionalized Tetrazole Energetics: A Route to Enhanced Performance. *Z. Anorg. Allg. Chem.* **2021**, *647*, 157–191. [CrossRef]
23. Chavez, D.E.; Hanson, S.K.; Veauthier, J.M.; Parrish, D.A. Electroactive Explosives: Nitrate Ester-Functionalized 1,2,4,5-Tetrazines. *Angew. Chem. Int. Ed.* **2013**, *52*, 6876–6879. [CrossRef] [PubMed]
24. Rudakov, G.F.; Kalinichenko, A.I.; Nguyen, T.Q.; Zinchenko, S.S.; Cherkaev, G.V.; Fedyanin, I.V.; Sinditskii, V.P. Monosubstituted Polynitroalkoxy-1,2,4,5-Tetrazines: A New Family of Melt-Castable Energetic Materials. *Propellants Explos. Pyrotech.* **2022**, *47*, e202100262. [CrossRef]
25. Klapötke, T.M.; Piercey, D.G.; Rohrbacher, F.; Stierstorfer, J. Synthesis and Characterization of Energetic Salts of the (C₄N₁₂²⁻) Dianion. *Z. Anorg. Allg. Chem.* **2012**, *638*, 2235–2242. [CrossRef]
26. Dalinger, I.L.; Kormanov, A.V.; Suponitsky, K.Y.; Muravyev, N.V.; Sheremetev, A.B. Pyrazole–Tetrazole Hybrid with Trinitromethyl, Fluorodinitromethyl, or (Difluoroamino) dinitromethyl Groups: High-Performance Energetic Materials. *Chem. Asian J.* **2018**, *13*, 1165–1172. [CrossRef]
27. Chaplygin, D.A.; Larin, A.A.; Muravyev, N.V.; Meerov, D.B.; Kosareva, E.K.; Kiselev, V.G.; Pivkina, A.N.; Ananyev, I.V.; Fershtat, L.L. Nitrogen-Rich Metal-Free Salts: A New Look at 5-(Trinitromethyl) tetrazolate Anion as an Energetic Moiety. *Dalton Trans.* **2021**, *50*, 13778–13785. [CrossRef]
28. Larin, A.A.; Muravyev, N.V.; Pivkina, A.N.; Suponitsky, K.Y.; Ananyev, I.V.; Khakimov, D.V.; Fershtat, L.L.; Makhova, N.N. Assembly of Tetrazolylfuroxan Organic Salts: Multipurpose Green Energetic Materials with High Enthalpies of Formation and Excellent Detonation Performance. *Chem. Eur. J.* **2019**, *25*, 4225–4233. [CrossRef]
29. Larin, A.A.; Shaferov, A.V.; Kulikov, A.S.; Pivkina, A.N.; Monogarov, K.A.; Dmitrienko, A.O.; Ananyev, I.V.; Khakimov, D.V.; Fershtat, L.L.; Makhova, N.N. Design and Synthesis of Nitrogen-Rich Azo-Bridged Furoxanylazoles as High-Performance Energetic Materials. *Chem. Eur. J.* **2021**, *27*, 14628–14637. [CrossRef]
30. Zhai, L.; Bi, F.; Luo, Y.; Wang, N.; Zhang, J.; Wang, B. New Strategy for Enhancing Energetic Properties by Regulating Trifuroxan Configuration: 3,4-Bis (3-nitrofuroxan-4-yl) furoxan. *Sci. Rep.* **2019**, *9*, 4321. [CrossRef]
31. Larin, A.A.; Shaferov, A.V.; Epishina, M.A.; Melnikov, I.N.; Muravyev, N.V.; Ananyev, I.V.; Fershtat, L.L.; Makhova, N.N. Pushing the Energy-Sensitivity Balance with High-Performance Bifuroxans. *ACS Appl. Energy Mater.* **2020**, *3*, 7764–7771. [CrossRef]
32. Song, S.; Wang, Y.; He, W.; Wang, K.; Yan, M.; Yan, Q.-L.; Zhang, Q. Melamine N-oxide based self-assembled energetic materials with balanced energy & sensitivity and enhanced combustion behavior. *Chem. Eng. J.* **2020**, *395*, 125114. [CrossRef]
33. Zlotin, S.G.; Churakov, A.M.; Egorov, M.P.; Fershtat, L.L.; Klenov, M.S.; Kuchurov, I.V.; Makhova, N.N.; Smirnov, G.A.; Tomilov, Y.V.; Tartakovskiy, V.A. Advanced energetic materials: Novel strategies and versatile applications. *Mendeleev Commun.* **2021**, *31*, 731–749. [CrossRef]
34. Wei, H.; Gao, H.; Shreeve, J.M. N-Oxide 1,2,4,5-Tetrazine-Based High-Performance Energetic Materials. *Chem. Eur. J.* **2014**, *20*, 16943–16952. [CrossRef] [PubMed]
35. He, P.; Zhang, J.-G.; Yin, X.; Wu, J.-T.; Wu, L.; Zhou, Z.-N.; Zhang, T.-L. Energetic Salts Based on Tetrazole N-Oxide. *Chem. Asian J.* **2016**, *22*, 7670–7685. [CrossRef]
36. Larin, A.A.; Fershtat, L.L. High-energy hydroxytetrazoles: Design, synthesis and performance. *Energ. Mater. Front.* **2021**, *2*, 3–13. [CrossRef]

37. Coburn, M.D.; Buntain, G.A.; Harris, B.W.; Hiskey, M.A.; Lee, K.-Y.; Ott, D.G. An improved synthesis of 3,6-diamino-1,2,4,5-tetrazine. II. From triaminoguanidine and 2,4-pentanedione. *J. Heterocycl. Chem.* **1991**, *28*, 2049–2050. [CrossRef]
38. Wei, H.; Zhang, J.; He, C.; Shreeve, J.M. Energetic Salts Based on Furazan-Functionalized Tetrazoles: Routes to Boost Energy. *Chem. Eur. J.* **2015**, *21*, 8607–8612. [CrossRef]
39. Ugrak, B.I.; Vinogradov, V.M.; Dalinger, I.L.; Shevelev, S.A. Nitropyrazoles 9.* Parameters of the ^1H , ^{13}C , and ^{15}N (^{14}N) spectra and the structures of N-aminonitropyrazoles. *Russ. Chem. Bull.* **1995**, *44*, 2087–2092. [CrossRef]
40. Liu, Y.; Zhao, G.; Yu, Q.; Tang, Y.; Imler, G.H.; Parrish, D.A.; Shreeve, J.M. Intermolecular Weak Hydrogen Bonding (Het-H-N/O): An Effective Strategy for the Synthesis of Monosubstituted 1,2,4,5-Tetrazine-Based Energetic Materials with Excellent Sensitivity. *J. Organ. Chem.* **2019**, *84*, 16019–16026. [CrossRef]
41. Snyder, C.J.; Wells, L.A.; Chavez, D.E.; Imler, G.H.; Parrish, D.A. Polycyclic N-oxides: High performing, low sensitivity energetic materials. *Chem. Commun.* **2019**, *55*, 2461–2464. [CrossRef] [PubMed]
42. Muravyev, N.V.; Wozniak, D.R.; Piercey, D.G. Progress and performance of energetic materials: Open dataset, tool, and implications for synthesis. *J. Mater. Chem. A* **2022**, *10*, 11054–11073. [CrossRef]
43. *CrysAlisPro*, Version 1.171.41.106a; Rigaku Oxford Diffraction: Oxford, UK, 2021.
44. Sheldrick, G.M. SHELXT—Integrated space-group and crystal-structure determination. *Acta Crystallogr. Sect. A* **2015**, *71*, 3–8. [CrossRef]
45. Sheldrick, G.M. Crystal structure refinement with SHELXL. *Acta Crystallogr. Sect. C* **2015**, *71*, 3–8. [CrossRef]
46. Dolomanov, O.V.; Bourhis, L.J.; Gildea, R.J.; Howard, J.A.K.; Puschmann, H. OLEX2: A complete structure solution, refinement and analysis program. *J. Appl. Cryst.* **2009**, *42*, 229–341. [CrossRef]
47. Frisch, M.J.; Trucks, G.W.; Schlegel, H.B.; Scuseria, G.E.; Robb, M.A.; Cheeseman, J.R.; Scalmani, G.; Barone, V.; Petersson, G.A.; Nakatsuji, H.; et al. *Gaussian 09*; Revision, D.01; Gaussian, Inc.: Wallingford, CT, USA, 2016.
48. Montgomery, J.J.A.; Frisch, M.J.; Ochterski, J.W.; Petersson, G.A. A complete basis set model chemistry. VII. Use of the minimum population localization method. *J. Chem. Phys.* **2000**, *112*, 6532–6542. [CrossRef]
49. Grimme, S.; Ehrlich, S.; Goerigk, L. Effect of the damping function in dispersion corrected density functional theory. *J. Comput. Chem.* **2011**, *32*, 1456–1465. [CrossRef] [PubMed]
50. Momany, F.A.; Carruthers, L.M.; McGuire, R.F.; Scheraga, H.A. Intermolecular potentials from crystal data. III. Determination of empirical potentials and application to the packing configurations and lattice energies in crystals of hydrocarbons, carboxylic acids, amines, and amides. *J. Phys. Chem.* **1974**, *78*, 1595–1620. [CrossRef]
51. Dzyabchenko, A.V. A multipole approximation of the electrostatic potential of molecules. *Russ. J. Phys. Chem. A* **2008**, *82*, 758–766. [CrossRef]
52. Dzyabchenko, A.V. From molecule to solid: The prediction of organic crystal structures. *Russ. J. Phys. Chem. A* **2008**, *82*, 1663–1671. [CrossRef]
53. Belsky, V.K.; Zorkaya, O.N.; Zorky, P.M. Structural Classes and Space Groups of Organic Homomolecular Crystals: New Statistical Data. *Acta Crystallogr. Sect. A* **1995**, *51*, 473–481. [CrossRef]
54. Khakimov, D.V.; Pivina, T.S. New Method for Predicting the Enthalpy of Salt Formation. *J. Phys. Chem. A* **2022**, *126*, 5207–5214. [CrossRef] [PubMed]
55. *STANAG 4489*; Explosives, Impact Sensitivity Tests. NATO: Brussels, Belgium, 1999.
56. *STANAG 4487*; Explosives, Friction Sensitivity Tests. NATO: Brussels, Belgium, 2002.
57. Muravyev, N.V.; Meerov, D.B.; Monogarov, K.A.; Melnikov, I.N.; Kosareva, E.K.; Fershtat, L.L.; Sheremetev, A.B.; Dalinger, I.L.; Fomenkov, I.V.; Pivkina, A.N. Sensitivity of energetic materials: Evidence of thermodynamic factor on a large array of Chnofol compounds. *Chem. Eng. J.* **2021**, *421*, 129804. [CrossRef]

Article

Aziridination Reactivity of a Manganese(II) Complex with a Bulky Chelating Bis(Alkoxide) Ligand

Sudheer S. Kurup¹, Natalie M. Woodland², Richard L. Lord^{2,*} and Stanislav Groysman^{1,*}¹ Department of Chemistry, Wayne State University, 5101 Cass Ave., Detroit, MI 48202, USA² Department of Chemistry, Grand Valley State University, 1 Campus Drive, Allendale, MI 49401, USA

* Correspondence: lordri@gvsu.edu (R.L.L.); groysman@wayne.edu (S.G.)

Abstract: Treatment of $\text{Mn}(\text{N}(\text{SiMe}_3)_2)(\text{THF})_2$ with bulky chelating bis(alkoxide) ligand [1,1':4',1''-terphenyl]-2,2''-diylbis(diphenylmethanol) ($\text{H}_2[\text{O-terphenyl-O}]^{\text{Ph}}$) formed a seesaw manganese(II) complex $\text{Mn}[\text{O-terphenyl-O}]^{\text{Ph}}(\text{THF})_2$, characterized by structural, spectroscopic, magnetic, and analytical methods. The reactivity of $\text{Mn}[\text{O-terphenyl-O}]^{\text{Ph}}(\text{THF})_2$ with various nitrene precursors was investigated. No reaction was observed between $\text{Mn}[\text{O-terphenyl-O}]^{\text{Ph}}(\text{THF})_2$ and aryl azides. In contrast, the treatment of $\text{Mn}[\text{O-terphenyl-O}]^{\text{Ph}}(\text{THF})_2$ with iminoiodinane PhINTs (Ts = *p*-toluenesulfonyl) was consistent with the formation of a metal-nitrene complex. In the presence of styrene, the reaction led to the formation of aziridine. Combining varying ratios of styrene and PhINTs in different solvents with 10 mol% of $\text{Mn}[\text{O-terphenyl-O}]^{\text{Ph}}(\text{THF})_2$ at room temperature produced 2-phenylaziridine in up to a 79% yield. Exploration of the reactivity of $\text{Mn}[\text{O-terphenyl-O}]^{\text{Ph}}(\text{THF})_2$ with various olefins revealed (1) moderate aziridination yields for *p*-substituted styrenes, irrespective of the electronic nature of the substituent; (2) moderate yield for 1,1'-disubstituted α -methylstyrene; (3) no aziridination for aliphatic α -olefins; (4) complex product mixtures for the β -substituted styrenes. DFT calculations suggest that iminoiodinane is oxidatively added upon binding to Mn, and the resulting formal imido intermediate has a high-spin Mn(III) center antiferromagnetically coupled to an imidyl radical. This imidyl radical reacts with styrene to form a sextet intermediate that readily reductively eliminates the formation of a sextet Mn(II) aziridine complex.

Keywords: alkoxides; aziridination; manganese; iminoiodinane

Citation: Kurup, S.S.; Woodland, N.M.; Lord, R.L.; Groysman, S. Aziridination Reactivity of a Manganese(II) Complex with a Bulky Chelating Bis(Alkoxide) Ligand. *Molecules* **2022**, *27*, 5751. <https://doi.org/10.3390/molecules27185751>

Academic Editors: Alexey M. Starosotnikov, Maxim A. Bastrakov and Igor L. Dalinger

Received: 15 August 2022
Accepted: 30 August 2022
Published: 6 September 2022

Publisher's Note: MDPI stays neutral with regard to jurisdictional claims in published maps and institutional affiliations.



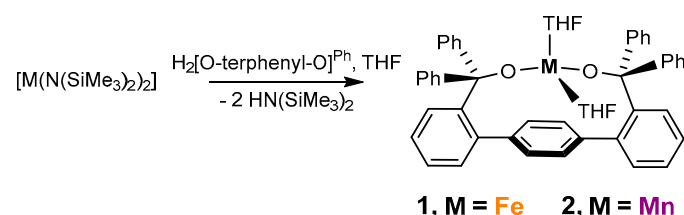
Copyright: © 2022 by the authors. Licensee MDPI, Basel, Switzerland. This article is an open access article distributed under the terms and conditions of the Creative Commons Attribution (CC BY) license (<https://creativecommons.org/licenses/by/4.0/>).

1. Introduction

The nitrogen equivalent of an epoxide, aziridine, is a three-membered heterocycle containing one nitrogen and two carbon atoms [1]. The combination of Baeyer strain and an electronegative element in a three-membered ring makes it susceptible to ring-opening reactions [2]. Because of the high reactivity of aziridines, they serve as intermediates in the total synthesis of natural products [3] and pharmaceuticals [4,5], exhibit diverse biological/biomedical functions [6,7], and have been used extensively in the synthesis of various heterocycles [8,9]. Different routes toward this useful functional group have been reported in the literature [1,2,10,11]. In the absence of transition metals, aziridine synthesis requires extreme conditions (high temperature and/or pressure) or the availability of highly reactive ylide-based precursors [12–14]. Generally, transition metal-catalyzed nitrene group transfer to olefins enables a more efficient route to aziridines, which also takes place under milder reaction conditions. Various nitrene transfer reagents, such as iminoiodinanes [15–18], organic azides [19], chloramine-T, and bromamine-T [20–22], can act as nitrene precursors to carry out this transformation. Catalysts based on noble metals, such as Ag [23–28], Rh [29–37], Ru [38–44], and Pd [45–47], were found to be reactive, with a wide variety of alkenes. Although these catalysts are often very efficient, the high cost and low availability of precious metals prompted interest in developing more sustainable catalysts based on earth-abundant and generally less toxic 3d metals [48,49]. Aziridination via nitrene transfer

using Mn and Fe porphyrins was reported early on by Breslow et al. [50]. The reactivity of porphyrinoid (porphyrin, corrole, and phthalocyanine), salen, and oxazoline ligands in aziridination has led to a growing interest among the scientific community in developing nitrogen-donor ligand-based aziridination catalysts with varying properties [48]. A significant number of Fe- and Co-based aziridination catalysts have been reported in the last decade, most of which are supported by nitrogen-donor ligands [51–66]. In recent years, a number of Fe-based aziridination catalysts supported by oxygen-donor [67,68] and carbon-donor [69–75] ligands have been reported as well. The stability and reactivity of formally high-oxidation state Fe and Co have been demonstrated to depend on ancillary ligand environments. While for weak-field nitrogen and oxygen ligand environments the reactions are generally postulated to proceed via highly reactive (and often not isolable) metal(III)-imidyl radical species, strong-field (carbene) ligation forms more stable Fe(IV) imides [76,77]. In contrast, the field of Mn-based aziridination catalysis has been less explored. Most reported Mn catalysts feature nitrogen-donor ligands [78–88], with the notable exception of the mixed nitrogen/oxygen donor set of salen ligands. The present work describes the aziridination reactivity of a Mn complex bearing an oxygen-ligand environment exclusively.

Group-transfer catalysts containing 3d transition metals coordinated with bulky bis(alkoxide) ligands are currently under investigation in our group [89,90]. Bis(alkoxide) ligand platforms provide weak-field ligand environments, leading to reactive nitrene- and carbene-transfer catalysts [91–96]. Using these systems, we demonstrated iron- and chromium-mediated nitrene transfer to form azoarenes and carbodiimides, respectively [91–94]. However, no aziridine formation was observed in the reactions of the chromium or iron systems with the combination of organoazides and styrene. To improve catalyst stability and performance, we recently synthesized a new chelating bis(alkoxide) ligand $\text{H}_2[\text{O-terphenyl-O}]^{\text{Ph}}$ ([1,1':4',1''-terphenyl]-2,2''-diylbis(diphenylmethanol)) [97,98]. The resulting iron complex $\text{Fe}[\text{O-terphenyl-O}]^{\text{Ph}}(\text{THF})_2$ (**1**, Scheme 1) demonstrated significantly more efficient catalytic performance in azoarene production [97]. The improved performance of the chelating bis(alkoxide) ligand $[\text{O-terphenyl-O}]^{\text{Ph}}$ in catalysis prompted us to investigate the application of its complexes in olefin aziridination. Herein, we report the first example of an Mn-based aziridination catalyst featuring a low-coordinate, oxygen-only, bulky bis(alkoxide) ligand environment.



Scheme 1. Synthesis of $\text{Mn}[\text{O-terphenyl-O}]^{\text{Ph}}(\text{THF})_2$ (**2**), along with the previously reported synthesis of iron analogue **1**.

2. Results and Discussion

2.1. Reactivity of $\text{Fe}[\text{O-terphenyl-O}]^{\text{Ph}}(\text{THF})_2$ (**1**) and Synthesis and Characterization of $\text{Mn}[\text{O-terphenyl-O}]^{\text{Ph}}(\text{THF})_2$ (**2**)

Complex **1** ($\text{Fe}[\text{O-terphenyl-O}]^{\text{Ph}}(\text{THF})_2$) was prepared as previously described (Scheme 1) [97]. The attempted aziridination using the combination of an organoazide precursor (*p*-tolyl azide), styrene, and **1** (10 mol%) (room temperature) did not produce the desired 2-phenyl-1-(*p*-tolyl)aziridine product (Figure S14). However, replacing organoazide with the more reactive nitrene precursor iminoiodinane (PhINTs, Ts = *p*-toluenesulfonyl) produced 2-phenyl-1-tosylaziridine in 32% yield (Figure S15). In selected cases, Mn-based catalysts exhibited reactivity superior to their Fe-based counterparts [88]. We decided to prepare the Mn(II) analogue of **1** and explore its aziridination reactivity.

Mn[O-terphenyl-O]^{Ph}(THF)₂ (**2**) was synthesized by treating Mn(N(SiMe₃)₂)(THF)₂ with H₂[O-terphenyl-O]^{Ph} in THF at room temperature (Scheme 1). The purple solution of the Mn(N(SiMe₃)₂)(THF)₂ precursor turned light yellow upon the addition of the ligand over a course of 8 hours. Recrystallization of the crude reaction product from CH₂Cl₂/THF mixture at −35 °C produced very pale yellow (nearly colorless) crystals of **2** in 74% yield. The product was characterized by solution magnetic measurements, X-ray crystallography, IR, and UV-vis spectroscopy, and elemental analysis. The solution state magnetic moment of **2** (measured in C₆D₆) was found to be 5.8 ± 0.2 μ_B (an average of two measurements), consistent with high-spin Mn(II) (Figures S3 and S4). ¹H NMR spectrum of the paramagnetic Mn(II) complex **2** demonstrated only two broad signals around 1.6 ppm and 3.8 ppm attributable to THF protons (Figures S1 and S2). The UV-vis spectrum in the 350–900 nm range was nearly featureless, as expected for high-spin Mn(II) (Figure S5).

The X-ray structure of **2** is presented in Figure 1 (crystal and refinement data are given in Table S4). As anticipated, [O-terphenyl-O]^{Ph} binds to the metal in a chelating fashion. The geometry at the metal is a distorted seesaw, with a narrow angle between the THF ligands (91.3(2)°) and a wide angle between the alkoxide donors (150.3(2)°) (see Figure 1 for selected bond distances and angles). The seesaw geometry in **2** is similar to the previously reported iron counterpart **1** [97]. The inter-alkoxide angle (RO-Mn-OR, ~150°) in **2** is significantly wider than the corresponding angle in the related Mn(II) complex with two monodentate alkoxides (Mn(OC^tBu₂Ph)₂(THF)₂, ~130°) [99]. A similar difference in this angle was observed for the corresponding iron isologues Fe[O-terphenyl-O]^{Ph}(THF)₂ (**1**) and Fe(OC^tBu₂Ph)₂(THF)₂, [97,99,100] and likely resulted from the rigidity of the chelating para-terphenyl bis(alkoxide) framework. The distance between the central phenyl and Mn is 3.09 Å, suggesting no interaction between the phenyl ring and the metal center, as previously observed for the iron analogue [97]. In contrast, a considerably shorter distance between the metal and the central phenyl (2.49 Å) in the chromium analogue Cr[O-terphenyl-O]^{Ph}(THF)₂, was consistent with a weak covalent interaction between chromium and the central phenyl [98].

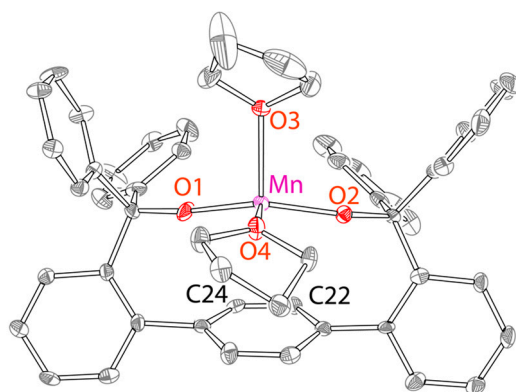


Figure 1. X-ray structure (50% probability) of Mn[O-terphenyl-O]^{Ph}(THF)₂ (**2**). Alternative conformations of one of the top THF ligands and one of the lateral phenyls, H atoms, and disordered solvent were omitted for clarity. Selected bond distances (Å) and angles (°): Mn-O1 1.888(5), Mn-O2 1.922(4), Mn-O3 2.205(4), Mn-O4 2.178(4), O1-Mn-O2 150.3(2), and O3-Mn-O4 91.23(2).

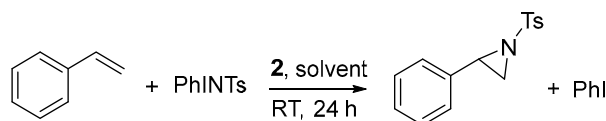
2.2. Reactivity of **2** in Aziridination

Following the synthesis and characterization of **2**, its reactivity in nitrene transfer was investigated. The reaction of **2** with representative organic aryl azides, including mesityl azide, *p*-tolyl azide, and tosyl azide in benzene, did not display any significant color change, even at elevated temperatures. No change in the ¹H NMR spectra of the reaction mixtures was observed, further suggesting a lack of reactivity. The reaction of **2** with organic azides in the presence of styrene or isocyanides similarly exhibited no change in the NMR spectrum of the reaction mixture. However, replacing the nitrene precursor with iminoiodinane (PhINTs, Ts = *p*-toluenesulfonyl) produced a rapid color change (colorless to brown). The

combination of PhINTs, styrene, and **2** (10 mol%, C₆D₆) for 24 h at room temperature led to the formation of the desired aziridine product, with 78% yield. The ¹H NMR spectrum of the reaction mixture (Figure S15) was relatively clean, exhibiting peaks attributable to the aziridine, styrene, and iodobenzene by-product. The control reaction of styrene (and other alkenes, see below) with PhINTs in the absence of a catalyst under similar reaction conditions formed trace amounts of TsNH₂; no formation of aziridines was observed.

To optimize catalyst performance, we carried out the aziridination of styrene at varying ratios of catalyst, PhINTs, and styrene (Table 1). In addition, we investigated the effects of different solvents on the reaction outcomes. All reactions were conducted at room temperature for 24 hours. Only small variations in product yields (74–78%) were observed for different ratios of styrene:PhINTs:catalyst in C₆D₆ (Table 1). These results are noteworthy, as a large excess of styrene is generally necessary in Mn-catalyzed aziridination reactions. The use of CD₂Cl₂ or CD₃CN as the reaction solvent produced similar yields at a 4:1 ratio of styrene:PhINTs (entries 1–3). However, in sharp contrast to C₆D₆, a significant decrease in the product yields was observed in these solvents when the styrene:PhINTs ratio was decreased to 1:1 (entries 6–8). It is feasible that a decrease in the product yields at a lower styrene:PhINTs ratio in polar solvents results from the increased solubility and therefore faster decomposition of reactive PhINTs in these solvents. As the reaction yield remained nearly optimal in benzene under less wasteful reaction conditions (reagent ratio of 1:1), it was used as a solvent in subsequent reactivity studies. Reducing catalyst loading to 5% (entry 5) led to a decline in the aziridine yield to 53%; a significant amount of undissolved PhINTs remained.

Table 1. Optimization of aziridination conditions.



Entry	2 (mol%)	Solvent	PhINTs (equiv)	Styrene (equiv)	Yield (%)
1	10	C ₆ D ₆	1	4	78
2	10	CD ₂ Cl ₂	1	4	79
3	10	CD ₃ CN	1	4	70
4	10	C ₆ D ₆	1	2	74
5	5	C ₆ D ₆	1	2	53
6	10	C ₆ D ₆	1	1	75
7	10	CD ₂ Cl ₂	1	1	17
8	10	CD ₃ CN	1	1	43
9	10	C ₆ D ₆	2	1	74
10	10	C ₆ D ₆	1.5	1	75

Following the optimization of reaction conditions for styrene aziridination, the aziridination of additional olefins was investigated. All reactions were conducted at room temperature for 24 h using 10 mol% catalyst and a ratio of 1:1 PhINTs:styrene. The formation of the products was confirmed by ¹H NMR spectroscopy and GC-MS (see Supplementary Material). Several different variables in the olefin structure were investigated (Figure 2), including the electronic effect (*para* substitution) in styrene, the aromatic vs. aliphatic nature of mono-substituted olefins, and α - and β -disubstituted styrenes. The catalyst showed moderate reactivity with *p*-^tBu, *p*-CN, and *p*-CF₃-substituted styrenes (52–54%); a slightly higher yield (62%) was obtained for electron-rich 4-methoxy styrene. In addition to the aziridine products, NMR spectra demonstrate the presence of an unreacted starting material (styrene) and the expected by-product iodobenzene. No additional products (e.g., TsNH₂ or C-H aminated products) were observed in significant quantities by ¹H NMR. However, the formation of these products in small quantities, or the formation of paramagnetic metal-based by-products, cannot be ruled out. The comparable reactivity of

electron-rich and electron-poor styrenes in Mn-catalyzed aziridination is consistent with previous reports [88]. No aziridination reactivity with non-aromatic olefins (methyl acrylate and 1-decene, Figures S21 and S22) was observed.

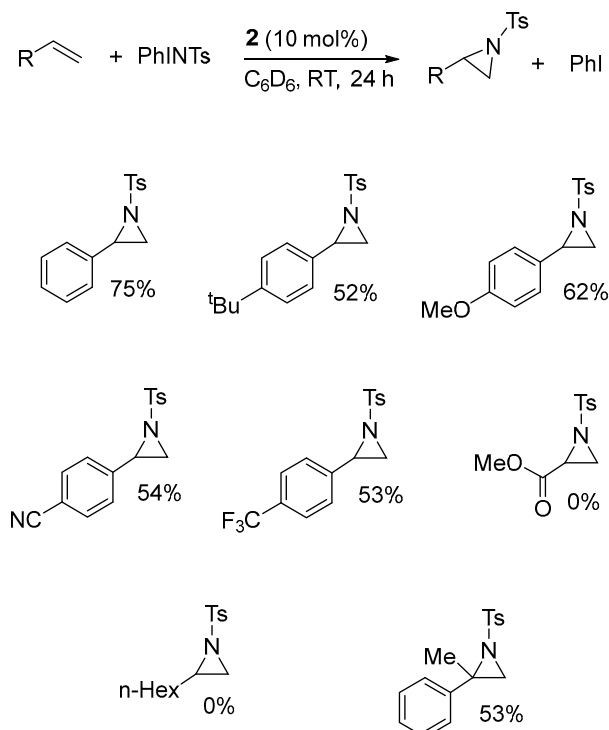


Figure 2. Aziridination of various olefins using **2**. The yields of the aziridine products were determined by ^1H NMR using internal standard (1,3,5-trimethylbenzene).

We also investigated the reactivity of α - and β -disubstituted styrenes. The reaction of α -methyl-styrene produced 1,1'-methylphenylaziridine relatively cleanly, with a moderate yield (53%). However, nitrene transfer onto β -disubstituted styrenes (*cis/trans* β -methylstyrene and *cis/trans* stilbene) formed significantly more complex mixtures of products exhibiting broad resonances. Our attempts to isolate the organic products of these reactions were unsuccessful.

2.3. Spectroscopic and Computational Probing of the Reaction Mechanism

How does the formation of aziridine occur with **2** as a catalyst? Different mechanistic hypotheses for manganese-mediated aziridination with PhINTs were proposed, including via a $\text{Mn-N}(\text{Ts})\text{IPh}$ adduct or $\text{Mn}=\text{NTs}$ imido [85,88]. We probed the nature of reactive intermediates by NMR spectroscopy and DFT calculations. PhINTs is insoluble in the reaction medium. Upon the combination of **2** with PhINTs in C_6D_6 , its dissolution occurs. The ^1H NMR spectrum collected immediately after the dissolution of PhINTs (approximately 10–15 min) showed the formation of free PhI (iodobenzene, Figures S7–S9). Thus, the formation of PhI occurs concurrently with the formation of brown intermediates and dissolution of PhINTs, suggesting that $\text{Mn}[\text{O-terphenyl-O}]^{\text{Ph}}\text{-N}(\text{Ts})\text{IPh}$ is not a long-lived reaction intermediate. The addition of styrene after the formation of the brown intermediate shows aziridine formation, suggesting that the nitrene transfer to styrene does not take place via a $\text{Mn}[\text{O-terphenyl-O}]^{\text{Ph}}\text{-N}(\text{Ts})\text{IPh}$ intermediate. No TsNH_2 was observed by ^1H NMR after 15 min; formation of TsNH_2 was observed after approximately 20 h (Figures S10–S12). The UV-vis spectra of the mixtures of **2** with PhINTs, taken at different time intervals, were not informative (Figure S13). Because our multiple attempts to isolate reaction intermediates were not successful, we used DFT calculations to probe the nature of the reaction intermediates and the reaction mechanism.

Additional support for the short-lived iminoiodinane adduct comes from computations. DFT calculations of putative iminoiodinane adducts showed significant activation, as evidenced by the long N-I distances of 2.94 and 3.10 Å for the two isomers vs. 2.06 Å in free iminoiodinane (Figure S28). Mayer bond orders of only 0.08 and 0.05 confirm that the N-I bond is broken in both isomers. Moreover, the electronic structure of this species is nearly identical to that of the formal imido species (*vide infra*) formed after the loss of PhI. The reaction of **2** with two equivalents of PhINTs is unlikely due to steric constraints [86,98]. We hypothesize that the aziridination of styrene takes place via a Mn-imido intermediate.

Multiple geometries and possible oxidation/spin states were evaluated for the manganese imido species. The lowest energy quartet optimized structure is shown in Figure 3. This species has a short Mn-NTs bond length of 1.72 Å that is slightly longer than the known Mn-imido species of ~1.6 Å [101–103] and shorter Mn-O bond lengths of 1.75 and 1.78 Å than the crystal structure of the Mn(II) species (Figure 1). The spin isosurface shows that spin is mostly localized at Mn and N, with opposite spins on each atom in Figure 3; Mulliken spin densities are 3.5 for Mn, 0.0 for [O-terphenyl-O]^{Ph}, and −0.5 for NTs. This suggests that this quartet has an electronic structure between a formal high-spin Mn(IV)-imido and high-spin Mn(III)-imidyl, with antiferromagnetic coupling between the metal and ligand radical. This geometric and electronic structure is similar to the one reported for Mn with a triphenylamido amine ligand; thus, we consider it Mn(III)-imidyl going forward and computationally probe the radical mechanism previously proposed [88]. Analysis of the electronic structure of the iminoiodinane adduct showed Mulliken spins of 3.4 for Mn, 0.0 for [O-terphenyl-O]^{Ph}, and −0.4 for TsNIPh, and visualization of the spin density (see Supplementary Material) shows that it is localized on the N. Thus, that adduct is probably better interpreted as manganese imidyl with a van der Waals-bound PhI.

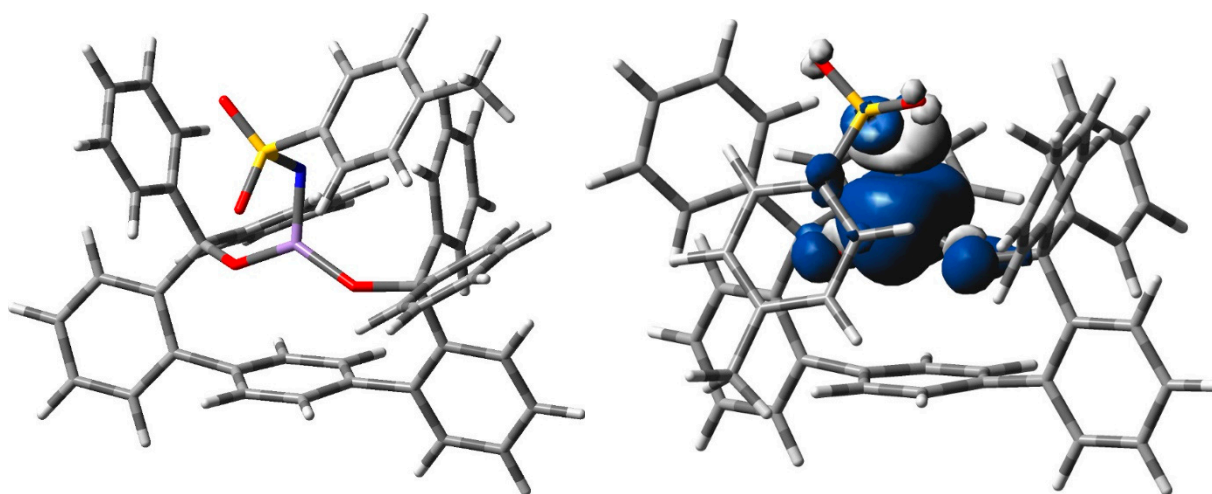


Figure 3. Optimized structure of the lowest energy quartet (**left**) and its spin density isosurface plotted using a cutoff value of 0.002 au (**right**). Blue and white surfaces correspond to excess alpha and beta spins, respectively.

Figure 4 summarizes the lowest energy structures along the reaction mechanism. Alternative regio and stereoisomers, and spin states are discussed in the Supporting Information. Starting with the bis-THF complex, the loss of both THF molecules is uphill by 13.2 kcal/mol. Binding of iminoiodinane to Mn[O-terphenyl-O]^{Ph} is exergonic by 28.3 kcal/mol and affords putative iminoiodinane adduct **A**, which we use as the reference point for this mechanism. As discussed above, **A** has a nearly identical electronic structure to Mn(III)-imidyl intermediate **B**, which is exergonic by 2.3 kcal/mol. **B** reacts with styrene on the quartet surface through a transition state that is 6.8 kcal/mol uphill in Gibbs free energy, and spin crossover occurs before the radical intermediate **C**, which is downhill in Gibbs energy by 12.4 kcal/mol relative to **B**. **C** has Mulliken spins of 4.0

for Mn, 0.0 for [O-terphenyl-O]^{Ph}, and 0.9 for NTsCH₂CHPh, the latter of which is mostly localized on CHPh (see Supplementary Material). The barrier between **C** and **D** is uphill by 4.9 kcal/mol, and **D** is exergonic by 7.0 kcal/mol. **D** has Mulliken spins of 4.8 for Mn, 0.1 for [O-terphenyl-O]^{Ph}, and 0.1 for aziridine. Thus, the high-spin Mn(III) intermediate **C** is well poised to reductively eliminate aziridine and re-form sextet Mn(II), **D**, in a spin-allowed step. This mechanism agrees well with the previously proposed mechanism [88].

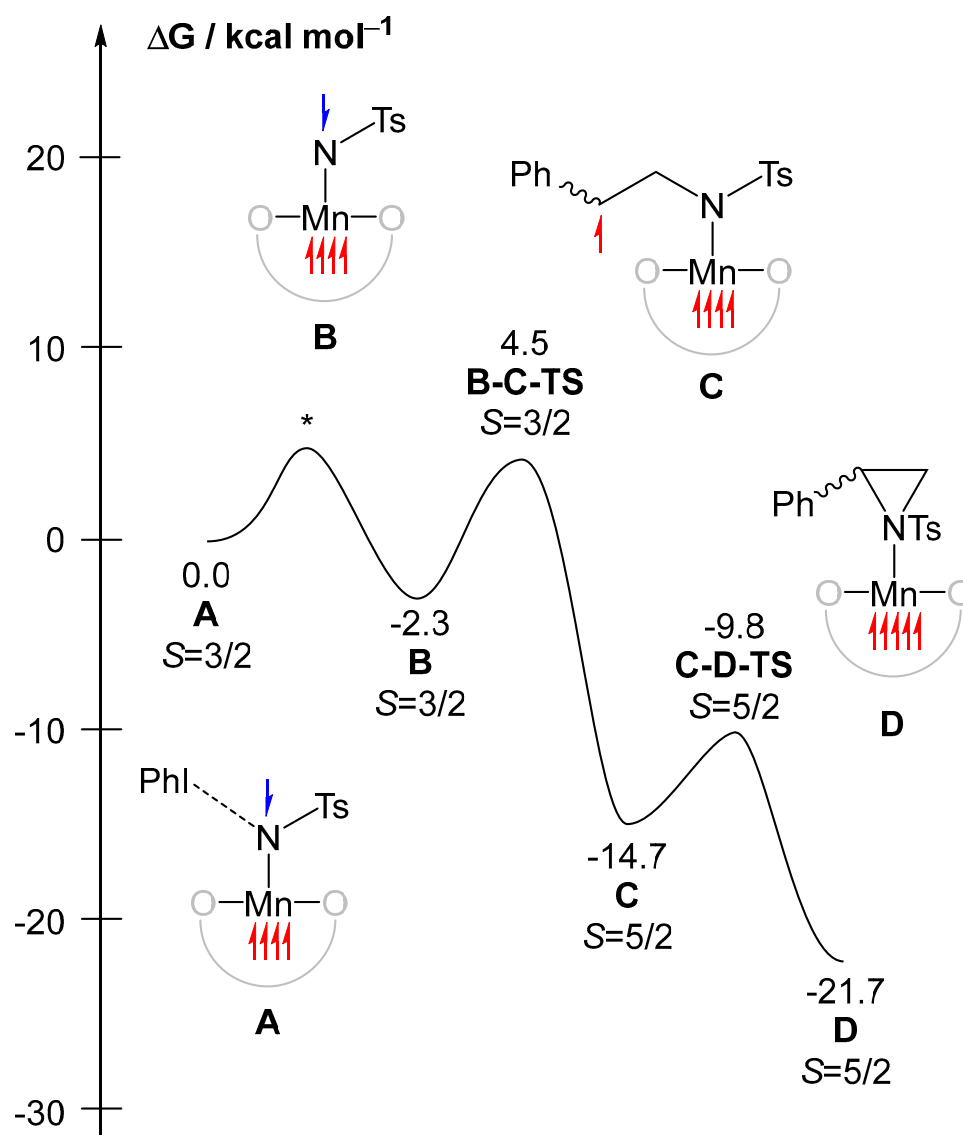
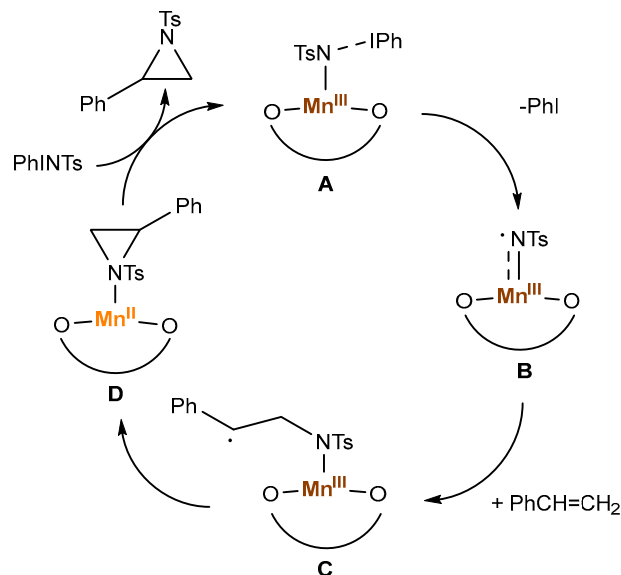


Figure 4. Reaction energy profile calculated at the B3LYP-D3(BJ)/def2-TZVP//BP86-D3(BJ)/def2-SVP level of theory. * indicates a missing transition state. Up and down spins are indicated by red and blue electrons, respectively.

The possible catalytic cycle (combining the spectroscopic and computational findings described above) is given in Scheme 2 below. The formation of PhINT adduct **A** is followed by the dissociation of PhI and facile formation of Mn(III)-imidyl radical **B** (free PhI is observed by NMR). While our computational studies focused on the reaction path in which PhINTs replace both THF ligands, it is possible that one THF remains coordinated to the metal throughout the reaction mechanism. Next, reactive (high-energy) species **B** reacts with styrene to form lower-energy radical intermediate **C**. As **C** is significantly more stable and the reaction barrier is low, little discrimination is observed between different para-substituted styrenes (featuring different electronic effects in the sterically remote para position). However, the reaction is anticipated to be sensitive to a more pronounced steric

effect, including styrene di-substitution. Likely due to the reactive radical nature of the reaction, complex mixtures of the reaction products were observed for the β -disubstituted styrenes. Subsequent C—N coupling forms azidine adduct **D**, which restores **A**, liberating the aziridine product.



Scheme 2. Possible mechanism for styrene aziridination catalyzed by **2**.

3. Summary and Conclusions

We have reported the synthesis and aziridination reactivity of a new manganese complex $\text{Mn}[\text{O-terphenyl-O}]^{\text{Ph}}(\text{THF})_2$, ligated by a bulky chelating bis(alkoxide) ligand. While the complex did not exhibit a reaction with an organoazide, its treatment with a mixture of PhINTs and styrene led to the formation of 2-phenyl-1-tosylaziridine in a good yield (up to 79%) with 10 mol% of the catalyst at room temperature. Various *p*-substituted styrenes, as well as the α -methyl-styrene produce the corresponding aziridines in comparable moderate yields; no reactivity with aliphatic olefins was observed. DFT calculations suggest a radical reaction intermediate, which is formed upon reaction of the high-spin imidyl radical $\text{Mn}^{\text{III}}[\text{O-terphenyl-O}]^{\text{Ph}}(=\text{NTs}\bullet)$ with styrene. Whereas the reactivity of the Mn bis(alkoxide) aziridination catalyst is not superior to the other known Mn aziridination catalysts (described in the Introduction), it (1) allows styrene aziridination relatively efficiently under sustainable (PhINTs:styrene 1:1 ratio) conditions, and (2) represents the first example of nitrene transfer into olefin by a 3d complex in a bulky bis(alkoxide) ligand environment. Our future studies will focus on the additional group-transfer reactions of middle and late 3d complexes in weak-field alkoxide ligand environments, and on the attempts to isolated and structurally and spectroscopically characterize various reaction intermediates.

4. Materials and Methods

4.1. General Methods and Characterization

Air-sensitive reactions were carried out in a nitrogen-filled glovebox. MnCl_2 and $\text{KN}(\text{SiMe}_3)_2$ were purchased from Strem chemicals and Sigma-Aldrich, respectively, and used as received. 2-bromophenylboronic acid, 1,4-diodobenzene, and K_2CO_3 were purchased from Sigma-Aldrich and used as received. $\text{H}_2[\text{O-terphenyl-O}]^{\text{Ph}}$ and PhINTs were synthesized based on the literature procedures [97,104]. Benzene- d_6 was purchased from Cambridge Isotope Laboratories and stored over 3 Å molecular sieves. HPLC-grade non-deuterated solvents were purchased from Sigma-Aldrich and purified using an MBraun solvent purification system. Compounds were generally characterized by ^1H and ^{13}C NMR, high-resolution mass spectrometry, and/or elemental analysis. Selected compounds were characterized by X-ray crystallography. NMR spectra were recorded at the Lumigen

Instrument Center on an Agilent 400 MHz Spectrometer and an Agilent DD2-600 MHz Spectrometer in C_6D_6 or $CDCl_3$ at room temperature. Chemical shifts and coupling constants (J) were reported in parts per million and Hertz, respectively. The solution state effective magnetic moment of **2** was determined using the Evans method. Elemental analysis was carried out by Midwest Microlab LLC under air-free conditions. A Thermo Fisher Scientific LTQ Orbitrap XL mass spectrometer at the Lumigen Instrument Centre was used for high-resolution mass spectra. IR spectra of powdered samples were recorded on a Shimadzu IR Affinity-1 FT-IR Spectrometer outfitted with an MIRacle10 attenuated total reflectance accessory with a monolithic diamond crystal stage and pressure clamp. UV-visible spectra were obtained using a Shimadzu UV-1800 spectrometer. GC-MS analysis was carried out using an Agilent 6890N spectrometer, Thermo TG5MS 30 m \times 0.32 mm \times 0.25 μ m column, 7683 series injector, and Agilent 5973 detector.

4.2. Synthesis of $Mn[O\text{-terphenyl-O}]^{Ph}(THF)_2$ (**2**)

A 57 mg solution of ligand (0.096 mmol, 1 eq.) in THF was added dropwise to a 5 mL THF solution of $Mn[N(SiMe_3)_2]_2(THF)_2$ [105] (0.050 g, 0.096 mmol, 1 eq.). The color of the reaction changed from purple to light brown over the course of 12 h. The volatiles were removed under vacuum, and the crude product was recrystallized using a DCM-THF solvent mixture at -35 $^\circ$ C to give the complex 88% yield (0.061 mg, 0.077 mmol). IR (cm^{-1} , selected peaks) 2942 (m), 2899 (m), 2366 (m), 1490 (s), 1439 (s), 1115 (s), 1173 (s), 1073 (s), 1026 (s), 909 (s), 888 (s), 832 (s), 790 (s), 755 (s), 700 (s), and 638 (s). The UV–vis spectrum was nearly featureless in the 350–800 nm region (Figure S5). The magnetic moment for the compound was determined using the Evans method; two measurements (Figures S1 and S2) yielded μ_{eff} values of 5.68 and 5.97 μ_B . Anal. Calc for $C_{52}H_{46}MnO_4$: C, 79.07; H, 5.87. Found: C, 79.84; H, 6.21.

4.3. General Procedure for Catalytic Formation of Aziridines

A vial containing solid PhINTs (1 eq.) was transferred to a stirred C_6D_6 solution containing mesitylene (internal standard), alkene (1 eq.) and $Mn[O\text{-terphenyl-O}]^{Ph}(THF)_2$ (0.1 eq.). The color of the solution changed from colorless to brown. The NMR of the solution was collected after 24 h, and the yield was calculated with reference to the internal standard. Major products were identified by NMR and GC-MS. C_6D_6 was removed under vacuum, and the crude mixture was dissolved in $CDCl_3$. A comparison of the NMR with literature reports confirmed the formation of aziridines [106–108].

4.4. Computational Methods

Calculations were performed using density functional theory, as implemented in Gaussian 09 [109]. Geometry optimizations and frequency calculations [110], and wavefunction stability analyses [111] were executed at the BP86-D3(BJ)/def2-SVP level of theory employing density fitting and ultrafine grids [112–116]. Subsequent single-point energy refinements were performed at the B3LYP-D3(BJ)/def2-TZVP level of theory with ultrafine grids [114,117–120]. Structural analysis and orbital/spin density visualization were done in GaussView 06 [121]. Mayer bond orders were calculated using Multiwfn 3.5 [122].

Supplementary Materials: The following supporting information can be downloaded at <https://www.mdpi.com/article/10.3390/molecules27185751/s1>, 1H NMR and GC-MS spectra of the aziridine products (Figures S14–S27), characterization data for complex **2** (Figures S1–S13), computational details, including energies, frequencies, and optimized geometries, for all species (Figures S28–S30, Tables S1–S3), crystal and refinement data for **2** (Table S4). CCDC 2183156.

Author Contributions: S.G. and S.S.K. designed and carried out the synthetic part of this work; N.M.W. and R.L.L. designed and carried out the computational part of this work; all authors participated in manuscript preparation. All authors have read and agreed to the published version of the manuscript.

Funding: This research was funded by the National Science Foundation, Division of Chemistry, grant number CHE 1855681. R.L.L. additionally acknowledges NSF for computational resources through MRI CHE-1919571.

Institutional Review Board Statement: Not applicable.

Informed Consent Statement: Not applicable.

Data Availability Statement: Information about Supplementary material is provided above in “Supplementary Materials” statement.

Acknowledgments: Experimental characterization was carried out at the Lumigen Instrument Center of Wayne State University.

Conflicts of Interest: The authors declare no conflict of interest.

References

1. Sweeney, J.B. Aziridines: Epoxides' Ugly Cousins? *Chem. Soc. Rev.* **2002**, *31*, 247–258. [PubMed]
2. Paik, V.V.; Kauthale, S.S.; Kumar, R.C.; Katariya, M.V.; More, R.R.; Ameta, K.L.; Mane, S.B. Aziridines: Synthesis and bioactivity. In *Bioactive Heterocycles*; Ameta, K.L., Pawar, R.P., Domb, A.J., Eds.; Nova Scientific Publishers: Hauppauge, NY, USA, 2013; pp. 41–68.
3. Kametani, T.; Honda, T. Application of Aziridines to the Synthesis of Natural Products. *Adv. Heterocycl. Chem.* **1986**, *39*, 181–236.
4. Werner, L.; Machara, A.; Sullivan, B.; Carrera, I.; Moser, M.; Adams, D.R.; Hudlicky, T. Several Generations of Chemoenzymatic Synthesis of Oseltamivir (Tamiflu): Evolution of Strategy, Quest for a Process-Quality Synthesis, and Evaluation of Efficiency Metrics. *J. Org. Chem.* **2011**, *76*, 10050–10067.
5. Hanessian, S.; Guesne, S.; Chenard, E. Total Synthesis of “Aliskiren”: The First Renin Inhibitor in Clinical Practice for Hypertension. *Org. Lett.* **2010**, *12*, 1816–1819. [PubMed]
6. Nikitjuka, A.; Jirgensons, A. Synthesis, Chemical And Biological Properties Of Aziridine-1-Carbaldehyde Oximes. *Chem. Heterocycl. Compd.* **2014**, *49*, 1669–1684.
7. Kinoshita, S.; Uzu, K.; Nakano, K.; Shimizu, M.; Takahashi, T.; Matsui, M. Mitomycin Derivatives. Preparation of Mitosane and Mitosene Compounds and Their Biological Activities. *J. Med. Chem.* **1971**, *14*, 103–109. [CrossRef] [PubMed]
8. Xie, Y.; Lu, C.; Zhao, B.; Wang, Q.; Yao, Y. Cycloaddition of Aziridine with CO₂/CS₂ Catalyzed by Amidato Divalent Lanthanide Complexes. *J. Org. Chem.* **2019**, *84*, 1951–1958.
9. Zhu, C.; Feng, J.; Zhang, J. Rhodium-catalyzed intermolecular [3+3] cycloaddition of vinyl aziridines with C,N-cyclic azomethine imines: Stereospecific Synthesis Of Chiral fused tricyclic 1,2,4-hexahydrotriazines. *Chem. Commun.* **2017**, *53*, 4688–4691.
10. Degennaro, L.; Trinchera, P.; Luisi, R. Recent Advances in the Stereoselective Synthesis of Aziridines. *Chem. Rev.* **2014**, *114*, 7881–7929.
11. Zhu, Y.; Wang, Q.; Cornwall, R.G.; Shi, Y. Organocatalytic Asymmetric Epoxidation and Aziridination of Olefins and Their Synthetic Applications. *Chem. Rev.* **2014**, *114*, 8199–8256.
12. Wenker, H. The Preparation of Ethylene Imine from Monoethanolamine. *J. Am. Chem. Soc.* **1935**, *57*, 2328. [CrossRef]
13. Marsini, M.A.; Reeves, J.T.; Desrosiers, J.N.; Herbage, M.A.; Savoie, J.; Li, Z.; Fandrick, K.R.; Sader, C.A.; McKibben, B.; Gao, D.A.; et al. Diastereoselective Synthesis of α -Quaternary Aziridine-2-Carboxylates via Aza-Corey-Chaykovsky Aziridination of N-Tert-Butanesulfinyl Ketimino Esters. *Org. Lett.* **2015**, *17*, 5614–5617. [CrossRef] [PubMed]
14. Dokli, I.; Matanovic, I.; Hamersak, Z. Sulfur ylide promoted synthesis of N-protected aziridines: A combined experimental and computational approach. *Chem. Eur. J.* **2010**, *16*, 11744–11752. [CrossRef] [PubMed]
15. Chang, J.W.W.; Ton, T.M.U.; Chan, P.W.H. Transition-Metal-Catalyzed Aminations and Aziridinations of C-H and C=C Bonds with Iminoiodinanes. *Chem. Rec.* **2011**, *11*, 331–357. [PubMed]
16. Darses, B.; Rodrigues, R.; Neuville, L.; Mazurais, M.; Dauban, P. Transition metal-catalyzed iodine(III)-mediated nitrene transfer reactions: Efficient tools for challenging syntheses. *Chem. Commun.* **2017**, *53*, 493–508.
17. Zhdankin, V.V.; Protasiewicz, J.D. Development of New Hypervalent Iodine Reagents with Improved Properties and Reactivity by Redirecting Secondary Bonds at Iodine Center. *Coord. Chem. Rev.* **2014**, *275*, 54–62. [CrossRef]
18. Karila, D.; Dodd, R.H. Recent Progress in Iminoiodane-Mediated Aziridination of Olefins. *Curr. Org. Chem.* **2011**, *15*, 1507–1538.
19. Uchida, T.; Katsuki, T. Asymmetric Nitrene Transfer Reactions: Sulfimidation, Aziridination and C-H Amination Using Azide Compounds as Nitrene Precursors. *Chem. Rec.* **2014**, *14*, 117–129.
20. Aujla, P.S.; Baird, C.P.; Taylor, P.C.; Mauger, H.; Vallée, Y. Can chloramine-T be a nitrene transfer agent? *Tetrahedron Lett.* **1997**, *38*, 7453–7456.
21. Cano, I.; Nicasio, M.C.; Pérez, P.J. Nitrene transfer reactions catalysed by copper(I) complexes in ionic liquid using chloramine-T. *Dalton Trans.* **2009**, *4*, 730–734. [CrossRef]
22. Antunes, A.M.M.; Marto, S.J.L.; Branco, P.S.; Prabhakar, S.; Lobo, A.M. Palladium(II)-promoted Aziridination of Olefins with Bromamine T as the Nitrogen Transfer Reagent. *Chem. Commun.* **2001**, *5*, 405–406.

23. Elkoush, T.; Mak, C.L.; Paley, D.W.; Campbell, M.G. Silver(II) and Silver(III) Intermediates in Alkene Aziridination with a Dinuclear Silver(I) Nitrene Transfer Cataly. *ACS Catal.* **2020**, *10*, 4820–4826.
24. Mat Lani, A.S.; Schomaker, J.M. Site-Selective, Catalyst-Controlled Alkene Aziridination. *Synthesis* **2018**, *50*, 4462–4470.
25. Ju, M.; Weatherly, C.D.; Guzei, I.A.; Schomaker, J.M. Chemo- and Enantioselective Intramolecular Silver-Catalyzed Aziridinations. *Angew. Chem. Int. Ed.* **2017**, *56*, 9944–9948. [CrossRef] [PubMed]
26. Weatherly, C.; Alderson, J.M.; Berry, J.F.; Hein, J.E.; Schomaker, J.M. Catalyst-controlled nitrene transfer by tuning metal:ligand ratios: Insight into the mechanisms of chemoselectivity. *Organometallics* **2017**, *36*, 1649–1661. [CrossRef]
27. Safin, D.A.; Pialat, A.; Korobkov, I.; Murugesu, M. Unprecedented Trinuclear AgI Complex with 2,4,6-Tris (2-pyrimidyl)-1,3,5-triazine as an Efficient Catalyst for the Aziridination of Olefins. *Chem. Eur. J.* **2015**, *21*, 6144–6149. [CrossRef]
28. Maestre, L.; Sameera, W.M.C.; Diaz-Requejo, M.M.; Maseras, F.; Perez, P.J. A General Mechanism for the Copper- and Silver-Catalyzed Olefin Aziridination Reactions: Concomitant Involvement of the Singlet and Triplet Pathways. *J. Am. Chem. Soc.* **2013**, *135*, 1338–1348.
29. Lee, S.; Jang, Y.J.; Phipps, E.J.T.; Lei, H.; Rovis, T. Rhodium(III)-Catalyzed Three-Component 1,2-Diamination of Unactivated Terminal Alkenes. *Synthesis* **2020**, *52*, 1247–1252. [CrossRef]
30. Azek, E.; Spitz, C.; Ernzerhof, M.; Lebel, H. A Mechanistic Study of the Stereochemical Outcomes of Rhodium-Catalysed Styrene Aziridinations. *Adv. Syn. Catal.* **2020**, *362*, 384–397.
31. Lee, S.; Lei, H.; Rovis, T. A Rh(III)-Catalyzed Formal [4+1] Approach to Pyrrolidines from Unactivated Terminal Alkenes and Nitrene Sources. *J. Am. Chem. Soc.* **2019**, *141*, 12536–12540. [CrossRef]
32. Sabir, S.; Pandey, C.B.; Yadav, A.K.; Tiwari, B.; Jat, J.L. Direct N-H/N-Me Aziridination of Unactivated Olefins Using O-(Sulfonyl)hydroxylamines as Aminating Agents. *J. Org. Chem.* **2018**, *83*, 12255–12260. [PubMed]
33. Su, J.Y.; Olson, D.E.; Ting, S.I.; Du Bois, J. Synthetic Studies Toward Pactamycin Highlighting Oxidative C-H and Alkene Amination Technologies. *J. Org. Chem.* **2018**, *83*, 7121–7134.
34. Ciesielski, J.; Dequierez, G.; Retailliau, P.; Gandon, V.; Dauban, P. Rhodium-Catalyzed Alkene Difunctionalization with Nitrenes. *Chem. Eur. J.* **2016**, *22*, 9338–9347. [PubMed]
35. Olson, D.E.; Su, J.Y.; Roberts, D.A.; Du Bois, J. Vicinal Diamination of Alkenes under Rh-Catalysis. *J. Am. Chem. Soc.* **2014**, *136*, 13506–13509.
36. Smith, D.T.; Njardarson, J.T. A scalable rhodium-catalyzed intermolecular aziridination reaction. *Angew. Chem. Int. Ed.* **2014**, *53*, 4278–4280.
37. Jat, J.L.; Paudyal, M.P.; Gao, H.; Xu, Q.-L.; Yousufuddin, M.; Devarajan, D.; Ess, D.H.; Kurti, L.; Falck, J.R. Direct Stereospecific Synthesis of Unprotected N-H and N-Me Aziridines from Olefins. *Science* **2014**, *343*, 61–65. [PubMed]
38. Wu, K.; Zhou, C.-Y.; Che, C.-M. Perfluoroalkyl Aziridines with Ruthenium Porphyrin Carbene Intermediates. *Org. Lett.* **2019**, *21*, 85–89.
39. Sengupta, G.; Pandey, P.; De, S.; Ramapanicker, R.; Bera, J.K. A bromo-capped diruthenium(II) N-heterocyclic carbene compound for in situ bromine generation with NBS: Catalytic olefin aziridination reactions. *Dalton Trans.* **2018**, *47*, 11917–11924.
40. Kim, C.; Uchida, T.; Katsuki, T. Asymmetric olefin aziridination using a newly designed Ru(CO)(salen) complex as the catalyst. *Chem. Commun.* **2012**, *48*, 7188–7190.
41. Tso, K.C.-H.; Chan, S.L.-F.; Huang, J.-S.; Che, C.-M. Wheel-to-rhomboid isomerization as well as nitrene transfer catalysis of ruthenium-thiolate wheels. *Chem. Commun.* **2017**, *53*, 2419–2422.
42. Rossi, S.; Puglisi, A.; Benaglia, M.; Carminati, D.M.; Intrieri, D.; Gallo, E. Synthesis in mesoreactors: Ru(porphyrin)CO-catalyzed aziridination of olefins under continuous flow conditions. *Catal. Sci. Technol.* **2016**, *6*, 4700–4704. [CrossRef]
43. Zardi, P.; Pozzoli, A.; Ferretti, F.; Manca, G.; Mealli, C.; Gallo, E. A mechanistic investigation of the ruthenium porphyrin catalyzed aziridination of olefins by aryl azides. *Dalton Trans.* **2015**, *44*, 10479–10489. [CrossRef] [PubMed]
44. Law, S.-M.; Chen, D.; Chan, S.L.-F.; Guan, X.; Tsui, W.-M.; Huang, J.-S.; Zhu, N.; Che, C.-M. Ruthenium Porphyrins with Axial π -Conjugated Arylamide and Arylimide Ligands. *Chem. Eur. J.* **2014**, *20*, 11035–11047. [CrossRef] [PubMed]
45. Zhang, J. Origins of the enantioselectivity of a palladium catalyst with BINOL-phosphoric acid ligands. *Org. Biomol. Chem.* **2018**, *16*, 8064–8071. [CrossRef]
46. Smalley, A.P.; Gaunt, M.J. Mechanistic Insights into the Palladium-Catalyzed Aziridination of Aliphatic Amines by C-H Activation. *J. Am. Chem. Soc.* **2015**, *137*, 10632–10641. [CrossRef]
47. Han, J.; Li, Y.; Zhi, S.; Pan, Y.; Timmons, C.; Li, G. Palladium-catalyzed aziridination of alkenes using N,N-dichloro-p-toluenesulfonamide as nitrogen source. *Tetrahedron Lett.* **2006**, *47*, 7225–7228. [CrossRef]
48. Fingerhut, A.; Serdyuk, O.V.; Tsogoeva, S.B. Non-heme iron catalysts for epoxidation and aziridination reactions of challenging terminal alkenes: Towards sustainability. *Green Chem.* **2015**, *17*, 2042–2058. [CrossRef]
49. Jenkins, D.M. Atom-economical C2 + N1 aziridination: Progress towards catalytic intermolecular reactions using alkenes and aryl azides. *Synlett* **2012**, *23*, 1267–1270. [CrossRef]
50. Breslow, R.; Gellman, S.H. Tosylamidation of Cyclohexane by a Cytochrome P-450 Model. *J. Chem. Soc. Chem. Commun.* **1982**, *24*, 1400–1401. [CrossRef]
51. Coin, G.; Patra, R.; Rana, S.; Biswas, J.P.; Dubourdeaux, P.; Clemancey, M.; de Visser, S.P.; Maiti, D.; Maldivi, P.; Latour, J.-M. Fe-Catalyzed Aziridination Is Governed by the Electron Affinity of the Active Imido-Iron Species. *ACS Catal.* **2020**, *10*, 10010–10020. [CrossRef]

52. Du, Y.-D.; Zhou, C.-Y.; To, W.-P.; Wang, H.-X.; Che, C.-M. Iron porphyrin catalysed light driven C-H bond amination and alkene aziridination with organic azides. *Chem. Sci.* **2020**, *11*, 4680–4686. [CrossRef] [PubMed]
53. Damiano, C.; Gadolini, S.; Intriери, D.; Lay, L.; Colombo, C.; Gallo, E. Iron and Ruthenium Glycopolyporphyrins: Active Catalysts for the Synthesis of Cyclopropanes and Aziridines. *Eur. J. Inorg. Chem.* **2019**, *41*, 4412–4420. [CrossRef]
54. Shehata, M.F.; Ayer, S.K.; Roizen, J.L. Iron(MCP) Complexes Catalyze Aziridination with Olefins As Limiting Reagents. *J. Org. Chem.* **2018**, *83*, 5072–5081. [CrossRef] [PubMed]
55. Damiano, C.; Intriери, D.; Gallo, E. Aziridination of Alkenes Promoted by Iron or Ruthenium Complexes. *Inorg. Chim. Acta* **2018**, *470*, 51–67. [CrossRef]
56. Hennessy, E.T.; Liu, R.Y.; Iovan, D.A.; Duncan, R.A.; Betley, T.A. Iron-mediated intermolecular N-group transfer chemistry with olefinic substrates. *Chem. Sci.* **2014**, *5*, 1526–1532. [CrossRef]
57. Liang, L.; Lv, H.; Yu, Y.; Wang, P.; Zhang, J.-L. Iron(III) Tetrakis(pentafluorophenyl)Porpholactone Catalyzes Nitrogen Atom Transfer to C:C and C-H Bonds with Organic Azides. *Dalton Trans.* **2012**, *41*, 1457–1460. [CrossRef]
58. Iovan, D.A.; Betley, T.A. Characterization of Iron-Imido Species Relevant for N-Group Transfer Chemistry. *J. Am. Chem. Soc.* **2016**, *138*, 1983–1993. [CrossRef]
59. Liu, Y.; Che, C.-M. [FeIII(F20-tpp)Cl] Is an Effective Catalyst for Nitrene Transfer Reactions and Amination of Saturated Hydrocarbons with Sulfonyl and Aryl Azides as Nitrogen Source under Thermal and Microwave-Assisted Conditions. *Chem. Eur. J.* **2010**, *16*, 10494–10501. [CrossRef]
60. Klotz, K.L.; Slominski, L.M.; Riemer, M.E.; Phillips, J.A.; Halfen, J.A. Mechanism of the Iron-Mediated Alkene Aziridination Reaction: Experimental and Computational Investigations. *Inorg. Chem.* **2009**, *48*, 801–803. [CrossRef]
61. Heins, S.P.; Morris, W.D.; Wolczanski, P.T.; Lobkovsky, E.B.; Cundari, T.R. Nitrene Insertion into C-C and C-H Bonds of Diamide Diimine Ligands Ligated to Chromium and Iron. *Angew. Chem. Int. Ed.* **2015**, *54*, 14407–14411. [CrossRef]
62. van Leest, N.P.; Tepaske, M.A.; Venderbosch, B.; Oudsen, J.-P.H.; Tromp, M.; van der Vlugt, J.I.; de Bruin, B. Electronically Asynchronous Transition States for C–N Bond Formation by Electrophilic [CoIII(TAML)]-Nitrene Radical Complexes Involving Substrate-to-Ligand Single-Electron Transfer and a Cobalt-Centered Spin Shuttle. *ACS Catal.* **2020**, *10*, 7449–7463. [CrossRef] [PubMed]
63. Hu, Y.; Lang, K.; Tao, J.; Marshall, M.K.; Cheng, Q.; Cui, X.; Wojtas, L.; Zhang, X.P. Next-Generation D2-Symmetric Chiral Porphyrins for Cobalt(II)-Based Metalloradical Catalysis: Catalyst Engineering by Distal Bridging. *Angew. Chem. Int. Ed.* **2019**, *58*, 2670–2674. [CrossRef] [PubMed]
64. Jiang, H.; Lang, K.; Lu, H.; Wojtas, L.; Zhang, X.P.J. Asymmetric Radical Bicyclization of Allyl Azidoformates via Cobalt(II)-Based Metalloradical Catalysis. *J. Am. Chem. Soc.* **2017**, *139*, 9164–9167. [CrossRef] [PubMed]
65. Lu, H.; Jiang, H.; Hu, Y.; Wojtas, L.; Zhang, X.P. Chemoselective intramolecular allylic C-H amination versus C:C aziridination through Co(II)-based metalloradical catalysis. *Chem. Sci.* **2011**, *2*, 2361–2366. [CrossRef]
66. Kalra, A.; Bagchi, V.; Paraskevopoulou, P.; Das, P.; Ai, L.; Sanakis, Y.; Raptopoulos, G.; Mohapatra, S. Choudhury, A.; Sun, Z.; et al. Is the Electrophilicity of the Metal Nitrene the Sole Predictor of Metal-Mediated Nitrene Transfer to Olefins? Secondary Contributing Factors as Revealed by a Library of High-Spin Co(II) Reagents. *Organometallics* **2021**, *40*, 1974–1996. [CrossRef]
67. Coin, G.; Patra, R.; Clemancey, M.; Dubourdeaux, P.; Pecaut, J.; Lebrun, C.; Castro, L.; Maldivi, P.; Chardon-Noblat, S.; Latour, J.-M. Fe-based Complexes as Styrene Aziridination Catalysts: Ligand Substitution Tunes Catalyst Activity. *ChemCatChem* **2019**, *11*, 5296–5299. [CrossRef]
68. Patra, R.; Coin, G.; Castro, L.; Dubourdeaux, P.; Clemancey, M.; Pecaut, J.; Lebrun, C.; Maldivi, P.; Latour, J.-M. Rational design of Fe catalysts for olefin aziridination through DFT-based mechanistic analysis. *Catal. Sci. Technol.* **2017**, *7*, 4388–4400. [CrossRef]
69. Blatchford, K.M.; Mize, C.J.; Roy, S.; Jenkins, D.M. Toward Asymmetric Aziridination with an Iron Complex Supported by a D2-symmetric Tetra-NHC. *Dalton Trans.* **2022**, *51*, 6153–6156. [CrossRef]
70. Isbill, S.B.; Chandrachud, P.P.; Kern, J.L.; Jenkins, D.M.; Roy, S. Elucidation of the Reaction Mechanism of C2 + N1 Aziridination from Tetracarbene Iron Catalysts. *ACS Catal.* **2019**, *9*, 6223–6233. [CrossRef]
71. Crandell, D.W.; Munoz, S.B.; Smith, J.M.; Baik, M.-H. Mechanistic study of styrene aziridination by iron(IV) nitrides. *Chem. Sci.* **2018**, *9*, 8542–8552. [CrossRef]
72. Chandrachud, P.P.; Bass, H.M.; Jenkins, D.M. Synthesis of Fully Aliphatic Aziridines with a Macrocyclic Tetracarbene Iron Catalyst. *Organometallics* **2016**, *35*, 1652–1657. [CrossRef]
73. Munoz, S.B., III; Lee, W.-T.; Dickie, D.A.; Scepaniak, J.J.; Subedi, D.; Pink, M.; Johnson, M.D.; Smith, J.M. Styrene Aziridination by Iron(IV) Nitrides. *Angew. Chem. Int. Ed.* **2015**, *54*, 10600–10603. [CrossRef] [PubMed]
74. Cramer, S.A.; Hernandez Sanchez, R.; Brakhage, D.F.; Jenkins, D.M. Probing the Role of an Fe(IV) Tetraene in Catalytic Aziridination. *Chem. Commun.* **2014**, *50*, 13967–13970. [CrossRef] [PubMed]
75. Cramer, S.A.; Jenkins, D.M. Synthesis of Aziridines from Alkenes and Aryl Azides with a Reusable Macrocyclic Tetracarbene Iron Catalyst. *J. Am. Chem. Soc.* **2011**, *133*, 19342–19345. [CrossRef] [PubMed]
76. Wang, L.; Hu, L.; Zhang, H.; Chen, H.; Deng, L. Three-Coordinate Iron(IV) Bisimido Complexes with Aminocarbene Ligation: Synthesis, Structure, and Reactivity. *J. Am. Chem. Soc.* **2015**, *137*, 14196–14207. [CrossRef]
77. Liu, Q.; Long, L.; Ma, P.; Ma, Y.; Leng, X.; Xiao, J.; Chen, H.; Deng, L. Synthesis, Structure, and C–H Bond Activation Reaction of An Iron(IV) Terminal Imido Complex Bearing Trifluoromethyl Groups. *Cell. Rep. Phys. Sci.* **2021**, *2*, 100454. [CrossRef]

78. Abu-Omar, M.M. High-valent iron and manganese complexes of corrole and porphyrin in atom transfer and dioxygen evolving catalysis. *Dalton Trans.* **2011**, *40*, 3435–3444. [CrossRef]
79. Fantauzzi, S.; Caselli, A.; Gallo, E. Nitrene transfer reactions mediated by metallo-porphyrin complexes. *Dalton Trans.* **2009**, *28*, 5434–5443. [CrossRef]
80. Chinkov, N. Catalytic enantioselective reactions using organomanganese compounds. In *The Chemistry of Organomanganese Compounds*; Rappoport, Z., Marek, I., Eds.; John Wiley & Sons Ltd.: Chichester, UK, 2011.
81. Mansuy, D.; Mahy, J.P.; Dureault, A.; Bedi, G.; Battioni, P. Iron- and Manganese-Porphyrin Catalysed Aziridination of Alkenes by Tosyl- and Acyl-Iminoiodobenzene. *J. Chem. Soc. Chem. Commun.* **1984**, *17*, 1161–1163. [CrossRef]
82. Liang, J.-L.; Huang, J.-S.; Yu, X.-Q.; Zhu, N.; Che, C.-M. Metalloporphyrin-mediated asymmetric nitrogen-atom transfer to hydrocarbons: Aziridination of alkenes and amidation of saturated C-H bonds catalyzed by chiral ruthenium and manganese porphyrins. *Chem. Eur. J.* **2002**, *8*, 1563–1572. [CrossRef]
83. Noda, K.; Hosoya, N.; Irie, R.; Ito, Y.; Katsuki, T. Asymmetric Aziridination by Using Optically Active (Salen) Manganese(III) Complexes. *Synlett* **1993**, *7*, 469–471. [CrossRef]
84. O'Connor, K.J.; Wey, S.J.; Burrows, C. Alkene aziridination and epoxidation catalyzed by chiral metal salen complexes. *Tetrahedron Lett.* **1992**, *33*, 1001–1004. [CrossRef]
85. Zdiilla, M.J.; Abu-Omar, M.M. Mechanism of Catalytic Aziridination with Manganese Corrole: The Often Postulated High-Valent Mn(V) Imido Is Not the Group Transfer Reagent. *J. Am. Chem. Soc.* **2006**, *128*, 16971–16979. [CrossRef] [PubMed]
86. Yan, S.Y.; Wang, Y.; Shu, Y.J.; Liu, H.H.; Zhou, X.G. Nitrene Transfer Reaction Catalyzed by Substituted Metallophthalocyanines. *J. Mol. Catal. A Chem.* **2006**, *248*, 148–151. [CrossRef]
87. Liang, S.; Jensen, M.P. Half-Sandwich Scorpionates as Nitrene Transfer Catalysts. *Organometallics* **2012**, *31*, 8055–8058. [CrossRef]
88. Bagchi, V.; Kalra, A.; Das, P.; Paraskevopoulou, P.; Gorla, S.; Ai, L.; Wang, Q.; Mohapatra, S.; Choudhury, A.; Sun, Z.; et al. Comparative Nitrene-Transfer Chemistry to Olefinic Substrates Mediated by a Library of Anionic Mn(II) Triphenylamido-Amine Reagents and M(II) Congeners (M = Fe, Co, Ni) Favoring Aromatic over Aliphatic Alkenes. *ACS Catal.* **2018**, *8*, 9183–9206. [CrossRef]
89. Grass, A.; Wannipurage, D.; Lord, R.L.; Groysman, S. Group-transfer chemistry at transition metal centers in bulky alkoxide ligand environments. *Coord. Chem. Rev.* **2019**, *400*, 1–16. [CrossRef]
90. Kurup, S.S.; Groysman, S. Catalytic Synthesis of Azoarenes via Metal-mediated Nitrene Coupling. *Dalton Trans.* **2022**, *51*, 4577–4589. [CrossRef]
91. Yousif, M.; Tjapkes, D.J.; Lord, R.L.; Groysman, S. Catalytic Formation of Asymmetric Carbodiimides at Mononuclear Chromium (II/IV) Bis(alkoxide) Complexes. *Organometallics* **2015**, *34*, 5119–5128. [CrossRef]
92. Yousif, M.; Wannipurage, D.; HuiZenga, C.D.; Washnock-Schmid, E.; Peraino, N.J.; Ozarowski, A.; Stoian, S.A.; Lord, R.L.; Groysman, S. Catalytic Nitrene Homocoupling by an Iron(II) Bis(alkoxide) Complex: Bulking Up the Alkoxide Enables a Wider Range of Substrates and Provides Insight into the Reaction Mechanism. *Inorg. Chem.* **2018**, *57*, 9425–9438. [CrossRef]
93. Bellow, J.A.; Yousif, M.; Cabelof, A.C.; Lord, R.L.; Groysman, S. Reactivity Modes of an Iron Bis(alkoxide) Complex with Aryl Azides: Catalytic Nitrene Coupling vs Formation of Iron(III) Imido Dimers. *Organometallics* **2015**, *34*, 2917–2923. [CrossRef]
94. Wannipurage, D.; Kurup, S.S.; Groysman, S. Heterocoupling of Different Aryl Nitrenes to Produce Asymmetric Azoarenes Using Iron-Alkoxide Catalysis and Investigation of the Cis-Trans Isomerism of Selected Bulky Asymmetric Azoarenes. *Organometallics* **2021**, *40*, 3637–3644. [CrossRef]
95. Grass, A.; Dewey, N.S.; Lord, R.L.; Groysman, S. Ketenimine Formation Catalyzed by a High Valent Cobalt Carbene in Bulky Alkoxide Ligand Environment. *Organometallics* **2019**, *38*, 962–972. [CrossRef]
96. Grass, A.; Bellow, J.A.; Morrison, G.; zur Loye, H.-C.; Lord, R.L.; Groysman, S. One electron reduction transforms high-valent low-spin cobalt alkylidene into high-spin cobalt(II) carbene radical. *Chem. Commun.* **2020**, *56*, 8416–8419. [CrossRef] [PubMed]
97. Kurup, S.S.; Wannipurage, D.; Lord, R.L.; Groysman, S. An iron complex with a new chelating bis(alkoxide) ligand leads to an active nitrene dimerization catalyst for a variety of para- and meta-substituted azide precursors. *Chem. Commun.* **2019**, *55*, 10780–10783. [CrossRef]
98. Kurup, S.S.; Staples, R.J.; Lord, R.L.; Groysman, S. Synthesis of Chromium(II) Complexes with Chelating Bis(alkoxide) Ligand and Their Reactions with Organoazides and Diazoalkanes. *Molecules* **2020**, *25*, 373. [CrossRef]
99. Bellow, J.A.; Yousif, M.; Fang, D.; Kratz, E.G.; Cisneros, G.A.; Groysman, S. Synthesis and reactivity of 3d metal complexes with the bulky alkoxide ligand [OC^tBu₂Ph]. *Inorg. Chem.* **2015**, *54*, 5624–5633. [CrossRef]
100. Bellow, J.A.; Martin, P.D.; Lord, R.L.; Groysman, S. Reductive Coupling of Azides Mediated by an Iron(II) Bis(alkoxide) Complex. *Inorg. Chem.* **2013**, *52*, 12335–12337. [CrossRef]
101. Eikey, R.A.; Khan, S.I.; Abu-Omar, M.M. The Elusive Terminal Imido of Manganese(V). *Angew. Chem. Int. Ed.* **2002**, *41*, 3591–3595. [CrossRef]
102. Lansky, D.E.; Kosack, J.R.; Narducci Sarjeant, A.A.; Goldberg, D.P. An Isolable, Nonreducible High-Valent Manganese(V) Imido Corrolazine Complex. *Inorg. Chem.* **2006**, *45*, 8477–8479. [CrossRef]
103. Shi, H.; Xie, J.; Lam, W.W.Y.; Man, W.-L.; Mak, C.-K.; Yiu, S.-M.; Lee, H.K.; Lau, T.-C. Generation and Reactivity of a One-Electron-Oxidized Manganese(V) Imido Complex with a Tetraamido Macrocyclic Ligand. *Chem. Eur. J.* **2019**, *25*, 12895–12899. [CrossRef]

104. Yamada, Y.; Yamamoto, T.; Okawara, M. Synthesis and Reaction of New Type I–N Ylide, N-Tosyliminoiodinane. *Chem. Lett.* **1975**, *4*, 361–362. [CrossRef]
105. Bradley, D.C.; Hursthouse, M.B.; Ibrahim, A.A.; Malik, K.M.A.; Motevalli, M.; Mösele, R.; Powell, H.; Runnacles, J.D.; Sullivan, A.C. Synthesis and chemistry of the bis(trimethylsilyl)amido bis-tetrahydrofuranates of the group 2 metals magnesium, calcium, strontium and barium. X-ray crystal structures of $\text{Mg}[\text{N}(\text{SiMe}_3)_2]_2 \cdot 2\text{THF}$ and related $\text{Mn}[\text{N}(\text{SiMe}_3)_2]_2 \cdot 2\text{THF}$. *Polyhedron* **1990**, *9*, 2959–2964. [CrossRef]
106. Johnson, S.L.; Hilinski, M.K. Organocatalytic Olefin Aziridination via Iminium-Catalyzed Nitrene Transfer: Scope, Limitations, and Mechanistic Insight. *J. Org. Chem.* **2019**, *84*, 8589–8595. [CrossRef]
107. Minakata, S.; Morino, Y.; Oderaotoshia, Y.; Komatsu, M. Novel aziridination of olefins: Direct synthesis from sulfonamides using t-BuOI. *Chem. Commun.* **2006**, *31*, 3337–3339. [CrossRef]
108. Evans, D.A.; Faul, M.M.; Bilodeau, M.T. Development of the Copper-Catalyzed Olefin Aziridination Reaction. *J. Am. Chem. Soc.* **1994**, *116*, 2742–2753. [CrossRef]
109. Frisch, M.J.; Trucks, G.W.; Schlegel, H.B.; Scuseria, G.E.; Robb, M.A.; Cheeseman, J.R.; Scalmani, G.; Barone, V.; Mennucci, B.; Petersson, G.A.; et al. *Gaussian 09*; Revision D.01; Gaussian, Inc.: Wallingford, CT, USA, 2013.
110. Schlegel, H.B. Geometry optimization. *WIREs Comput. Mol. Sci.* **2011**, *1*, 790–809. [CrossRef]
111. Bauernschmitt, R.; Ahlrichs, R. Stability analysis for solutions of the closed shell Kohn-Sham equation. *J. Chem. Phys.* **1996**, *104*, 9047–9052. [CrossRef]
112. Becke, A.D. Density-functional exchange-energy approximation with correct asymptotic-behavior. *Phys. Rev. A* **1988**, *38*, 3098–3100. [CrossRef]
113. Perdew, J.P. Density-functional approximation for the correlation energy of the inhomogeneous electron gas. *Phys. Rev. B* **1986**, *33*, 8822–8824. [CrossRef]
114. Weigend, F.; Ahlrichs, R. Balanced basis sets of split valence, triple zeta valence, and quadruple zeta valence quality for H to Rn: Design and assessment of accuracy. *Phys. Chem. Chem. Phys.* **2005**, *7*, 3297–3305. [CrossRef] [PubMed]
115. Weigend, F. Accurate Coloumb-fitting basis sets for H to Rn. *Phys. Chem. Chem. Phys.* **2006**, *8*, 1057–1065. [CrossRef] [PubMed]
116. Bootsma, A.N.; Wheeler, S.E. Popular Integration Grids Can Result in Large Errors in DFT-Computed Free Energies. *ChemRxiv* **2019**. [CrossRef]
117. Vosko, S.H.; Wilk, L.; Nusair, M. Accurate spin-dependent electron liquid correlation energies for local spin density calculations: A critical analysis. *Can. J. Phys.* **1980**, *58*, 1200–1211. [CrossRef]
118. Lee, C.; Yang, W.; Parr, R.G. Development of the Colle-Salvetti correlation-energy formula into a functional of the electron density. *Phys. Rev. B* **1988**, *37*, 785–789. [CrossRef] [PubMed]
119. Becke, A.D. Density-functional thermochemistry. III. The role of exact exchange. *J. Chem. Phys.* **1993**, *98*, 5648–5652. [CrossRef]
120. Stephens, P.J.; Devlin, F.J.; Chabalowski, C.F.; Frisch, M.J. *Ab Initio* Calculation of Vibrational Absorption and Circular Dichroism Spectra Using Density Functional Force Fields. *J. Phys. Chem.* **1994**, *98*, 11623–11627. [CrossRef]
121. Dennington, R.; Keith, T.A.; Millam, J.M. *GaussView*, 6th ed.; Semichem Inc.: Shawnee Mission, KS, USA, 2016.
122. Lu, T.; Chen, F. Multiwfn: A Multifunctional Wavefunction Analyzer. *J. Comp. Chem.* **2012**, *33*, 580–592. [CrossRef]

Article

Nucleophilic Functionalization of 2-R-3-Nitropyridines as a Versatile Approach to Novel Fluorescent Molecules

Vladislav V. Nikol'skiy, Mikhail E. Minyaev, Maxim A. Bastrakov and Alexey M. Starosotnikov *

N.D. Zelinsky Institute of Organic Chemistry RAS, Leninsky Prosp. 47, 11991 Moscow, Russia

* Correspondence: alexey41@list.ru

Abstract: A number of new 2-methyl- and 2-arylviny-3-nitropyridines were synthesized and their reactions with thiols were studied. It was found that 3-NO₂ tends to be selectively substituted under the action of sulfur nucleophiles in the presence of another nucleofuge in position 5. Correlations between the substitution pattern and regioselectivity as well as photophysical properties were established. Some synthesized compounds possessed a large Stokes shift.

Keywords: nitro group; nitropyridines; bis-(het)aryl ethenes; nucleophilic substitution; thiols; UV–Vis spectroscopy

1. Introduction

Pyridine is an important heterocyclic motif and a part of various natural products. The pyridine ring system is incorporated into alkaloids, medicines (for example, omeprazole, lorlatinib, ivosidenib and many others), fungicides, herbicides and insecticides. Application of the pyridine derivatives as biologically active precursors and coordination complexes was reviewed recently [1]. Nitropyridines are of particular interest due to their biological significance [2–5]. In addition, some nitropyridines are considered to be promising energetic compounds [6–10] and efficient organic optical materials [11]. The introduction of the nitro group into the pyridine ring facilitates its functionalization in different ways. Recently, we investigated reactions of 3-R-5-nitropyridines with various types of nucleophiles [12]. It was found that in the case of anionic S-, N- and O-nucleophiles, the substitution of the non-activated nitro group occurred while carbon nucleophiles underwent dearomatization of the pyridine ring with the formation of 1,2- or 1,4-addition products. As a result, a number of novel or hardly accessible pyridines and their dihydro derivatives were synthesized [12].

In this work we report on the synthesis, reactivity and photophysical properties of 2-methyl- and 2-(2-arylviny)-3-nitropyridines, as shown in Figure 1. 2-Alkenylpyridines are widely employed as precursors to pharmaceuticals (vorapaxar, axitinib, nifurpirinol) and other biologically active compounds [13]. In addition, 2-(2-arylviny)pyridines were proven to be the fluorescent molecules, with the fluorescence quantum yield showing a large dependence on the acidity of media [14].

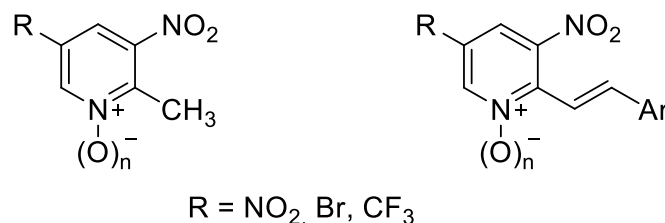


Figure 1. 2-Methyl- and 2-(2-arylviny)-3-nitropyridines synthesized and studied in this work.

Citation: Nikol'skiy, V.V.; Minyaev, M.E.; Bastrakov, M.A.; Starosotnikov, A.M. Nucleophilic Functionalization of 2-R-3-Nitropyridines as a Versatile Approach to Novel Fluorescent Molecules. *Molecules* **2022**, *27*, 5692. <https://doi.org/10.3390/molecules27175692>

Academic Editor: Antonio Massa

Received: 4 August 2022

Accepted: 31 August 2022

Published: 3 September 2022

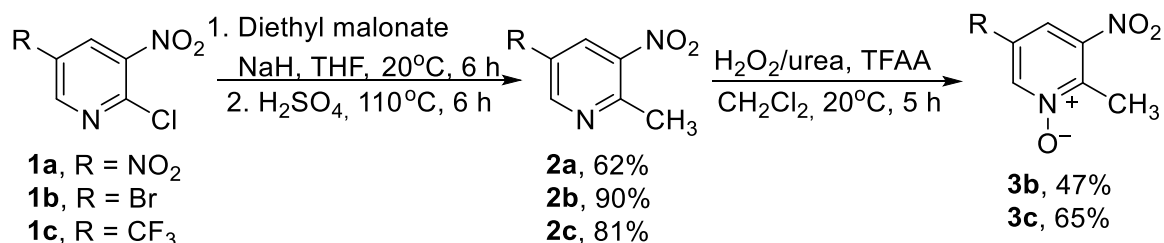
Publisher's Note: MDPI stays neutral with regard to jurisdictional claims in published maps and institutional affiliations.



Copyright: © 2022 by the authors. Licensee MDPI, Basel, Switzerland. This article is an open access article distributed under the terms and conditions of the Creative Commons Attribution (CC BY) license (<https://creativecommons.org/licenses/by/4.0/>).

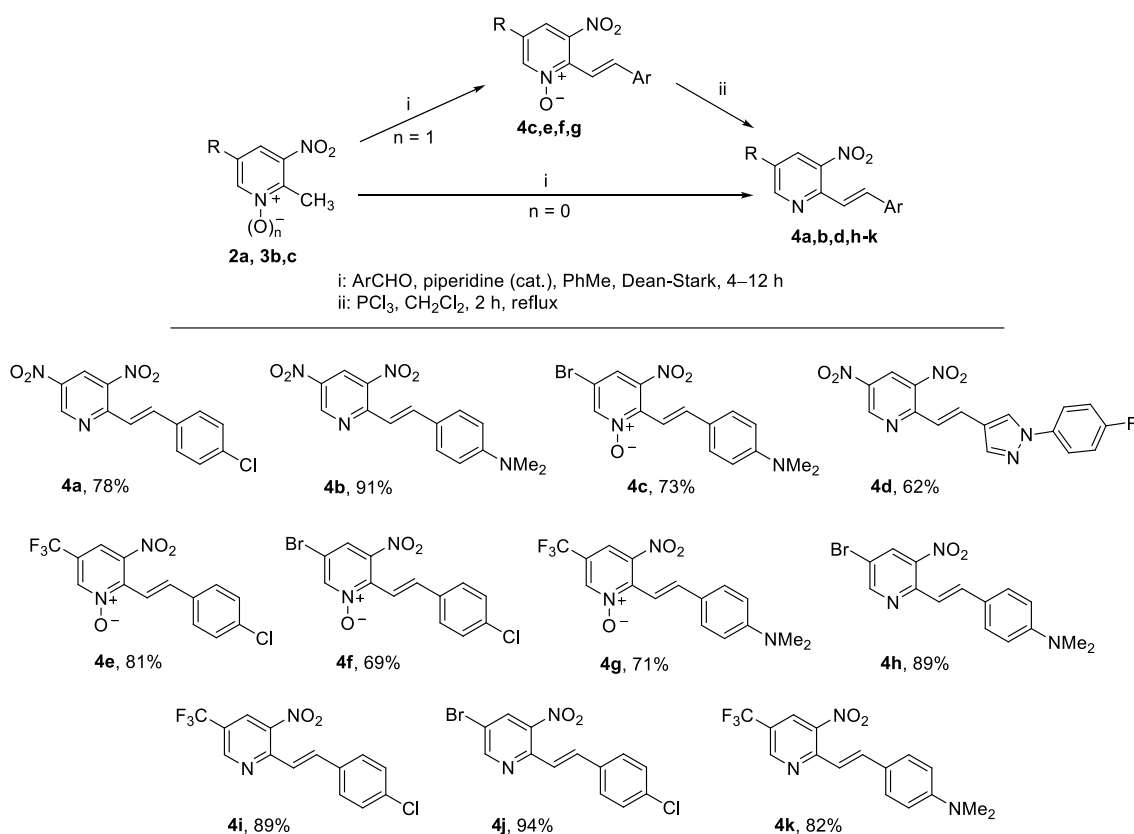
2. Results and Discussion

2-Methyl-3-nitropyridines **2a–c** were synthesized from the corresponding commercially available 2-chloro-3-nitropyridines **1a–c** by the reaction with diethyl malonate, followed by acidic hydrolysis/decarboxylation, as shown in Scheme 1. The oxidation of compounds **2b,c** with the hydrogen peroxide–urea complex gave *N*-oxides **3b,c** in moderate yields.



Scheme 1. Synthesis of 2-methyl-3-nitropyridines.

We examined 2-methylpyridines **2** and **3** in reactions with aldehydes under piperidine catalysis. Our attempts to isolate condensation products of compounds **2b,c** failed, whereas 2-methyl-3,5-dinitropyridine **2a** and *N*-oxides **3b,c** gave diarylethenes **4a–g** in high yields, as shown in Scheme 2. It should be noted that compound **2a** reacts several times faster than pyridine *N*-oxides **3b,c**, indicating that *para*-NO₂ is a more potent activating group for this reaction than the *N*-oxide moiety neighboring the 2-methyl group. The functional group tolerance, along with the relatively mild conditions and availability of aromatic aldehydes, makes this method a valid alternative for Pd-catalyzed coupling reactions [15–18]. Deoxygenation of pyridine *N*-oxides **4c,e–g** with PCl₃ allowed us to obtain four additional 2-ethenylpyridines **4h–k**, which were inaccessible via direct condensation of 2-methylpyridines **2b,c** with aldehydes, as shown in Scheme 2.



Scheme 2. Synthesis of 2-(2-arylvinyl)-3-nitropyridines.

In all cases, only *trans*-diarylethenes are formed, which was confirmed by NMR spectroscopy: coupling constants of 15–16 Hz were observed for proton signals of the double bonds. In addition, X-ray analysis for compounds **4a,i** was performed, undoubtedly proving our assumption, as shown in Figure 2.

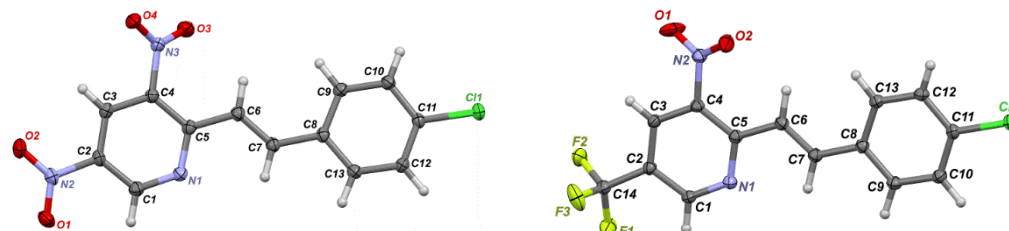
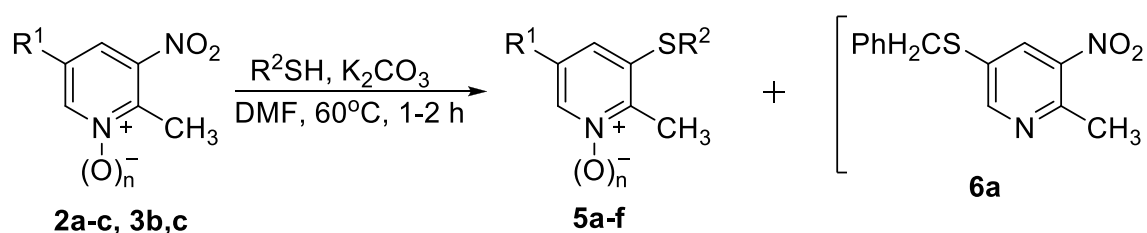


Figure 2. X-ray crystal structures of compounds **4a** (left) and **4i** (right) with thermal ellipsoids at 50% probability level.

The possibility of the substitution of the non-activated nitro group in pyridines was studied recently by our group [12]. In 3-nitro-5-Cl(Br)-pyridines, 3-NO₂ was found to be more nucleofugal than halogen in position 5. The reactions of 2-methyl-3-nitropyridines **2** and **3** with thiols are summarized in Scheme 3 and Table 1. Upon heating the reactants in DMF in the presence of K₂CO₃, the selective formation of 3-R²S-products **5** was observed in all cases; however, the reaction of **2a** with BnSH gave **5a** with a trace amount of the isomer **6a**.

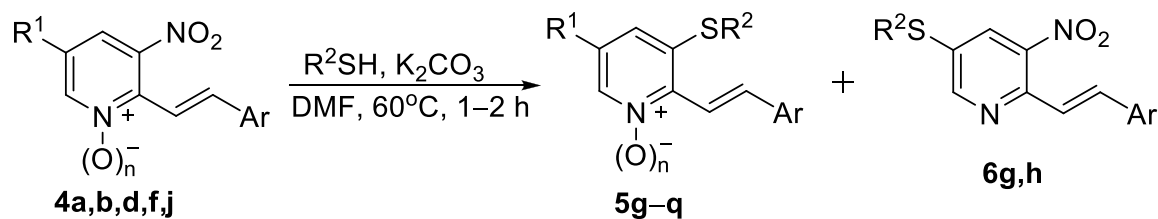


Scheme 3. Reactions of 2-methyl-3-nitropyridines with thiols.

Table 1. Reactions of 2-methyl-3-nitropyridines with thiols.

Substrate	R ¹	n	R ²	Product, Isolated Yield (%)
2a	NO ₂	0	PhCH ₂	5a , 70
3b	Br	1	PhCH ₂	5b , 96
3b	Br	1	4-Cl-C ₆ H ₄	5c , 95
2b	Br	0	PhCH ₂	5d , 65
2c	CF ₃	0	PhCH ₂	5e , 60
3c	CF ₃	1	PhCH ₂	5f , 52

Interestingly, diarylethenes **4** react with thiols under the same mild conditions, but with lower selectivity. ¹H NMR spectra of the crude products generally contain an additional set of signals corresponding to the 5-R²S-isomer, whereas the ratio of 5/6 varied from 2:1 to 20:1 depending on the substrate and thiol. Moreover, compounds **6g,h** were isolated and fully characterized, but in all other cases we were unable to isolate isomers **6**, as shown in Scheme 4 and Table 2.



Scheme 4. Reactions of 2-(arylvinylyl)-3-nitropyridines with thiols.

Table 2. Reactions of 2-(arylvinylyl)-3-nitropyridines with thiols.

Substrate	R ¹	Ar	n	R ²	Ratio 5/6 ^a	Product, Isolated Yield (%)
4a	NO ₂	4-Cl-C ₆ H ₄	0	PhCH ₂	3:1	5g, 56 6g, 18
4a	NO ₂	4-Cl-C ₆ H ₄	0	i-C ₄ H ₉	2:1	5h, 62 6h, 31
4a	NO ₂	4-Cl-C ₆ H ₄	0	2-furylmethyl	>20:1	5i, 56
4a	NO ₂	4-Cl-C ₆ H ₄	0	4-Cl-C ₆ H ₄	>20:1	5j, 67
4b	NO ₂	4-Me ₂ N-C ₆ H ₄	0	4-Cl-C ₆ H ₄	>20:1	5k, 83
4b	NO ₂	4-Me ₂ N-C ₆ H ₄	0	i-C ₄ H ₉	8:1	5l, 84
4b	NO ₂	4-Me ₂ N-C ₆ H ₄	0	PhCH ₂	10:1	5m, 88
4d	NO ₂	1-(4-fluorophenyl)pyrazol-4-yl	0	PhCH ₂	10:1	5n, 89
4d	NO ₂	1-(4-fluorophenyl)pyrazol-4-yl	0	4-Cl-C ₆ H ₄	>20:1	5o, 93
4j	Br	4-Cl-C ₆ H ₄	0	PhCH ₂	>20:1	5p, 60
4f	Br	4-Me ₂ N-C ₆ H ₄	1	PhCH ₂	>20:1	5q, 67

^a Determined from ¹H NMR spectrum of crude product.

Structures of compounds **5** and **6** were confirmed by NMR, HRMS, X-ray and elemental analysis. ¹H-¹H NOESY spectra of compounds **5m** and **5q** revealed interactions of the spatially close protons of the double bond and benzyl substituent, as shown in Figure 3. The structures of **5h, l** were determined by the X-ray diffraction single-crystal method, as shown in Figure 4.

The above-mentioned results allow us to conclude that electron-releasing substituents in the aryl group and the bulky thiolate anion favor substitution at position 3: the best selectivity was observed for reactions of **4b** with α -toluene thiol, whereas **4a** with isobutyl mercaptan gave the lowest selectivity (2:1). Reactions with 4-chlorothiophenol afforded exclusively a 3-substituted product.

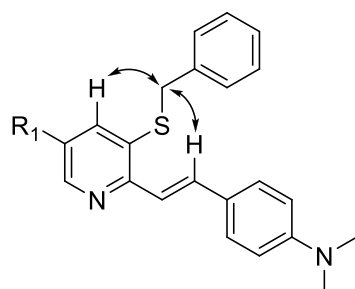


Figure 3. Cross-peaks observed in ¹H-¹H NOESY spectrum of compounds **5m** (R¹ = NO₂) and **5q** (R¹ = Br).

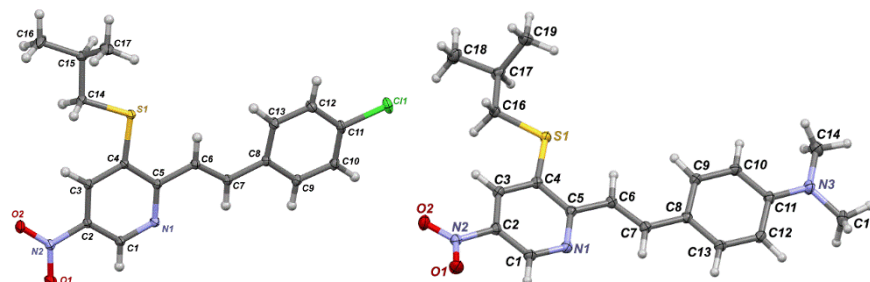


Figure 4. X-ray crystal structures of compounds **5h** (left) and **5l** (right) with thermal ellipsoids at 50% probability level.

Compounds with multiple conjugated double bonds, such as diarylethenes **4–6**, can be expected to have strong absorbance in the UV and visible region; therefore, the photophysical properties of some representative compounds with various substitution patterns were studied. Indeed, it was found that all recorded UV–Vis spectra in the MeCN solution have a strong and distinctive absorption band in the 326–509 nm region accompanied by one or more weaker and non-informative bands around 260–300 nm (Figure 5, Table 3). Notable exceptions are compounds **4a,i** with only one dominant absorption maximum and compound **4e** with a stronger shortwave band, which can be attributed to the *N*-oxide moiety.

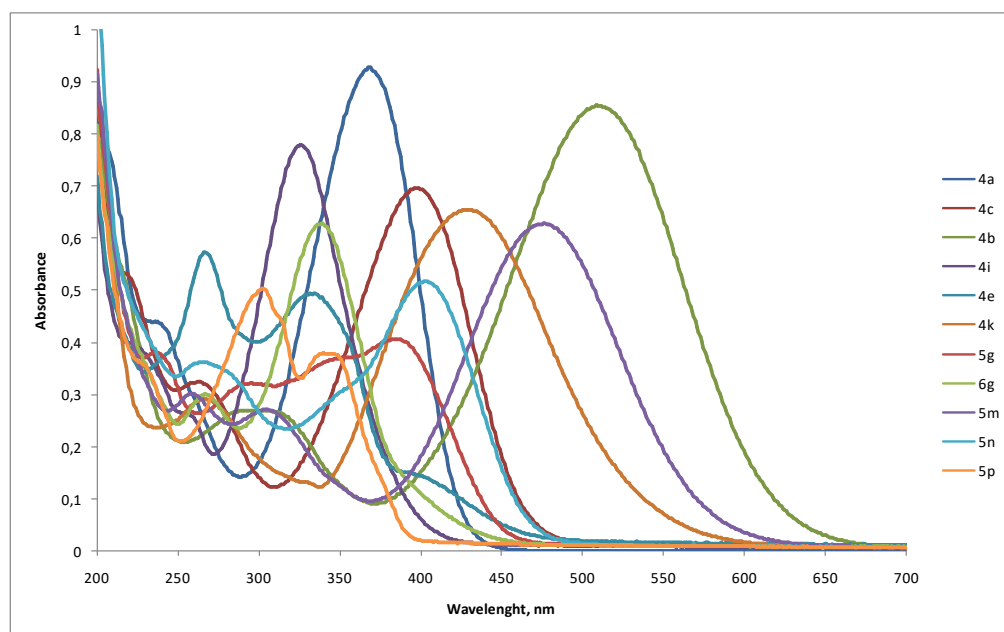


Figure 5. UV–Vis spectra of selected synthesized compounds in MeCN (2×10^{-5} M).

Table 3. Photophysical properties of some synthesized compounds.

Compound	λ_{\max} nm	ϵ_1 dm ³ mol ^{−1} cm ^{−1}	λ_{\max} nm	ϵ_2 dm ³ mol ^{−1} cm ^{−1}
4a	-	-	368	46,400
4b	302	13,500	509	42,800
4c	263	16,200	397	34,900
4e	267	28,700	332	24,700
4i	-	-	326	39,000
4k	266	14,600	429	32,800
5g	296	16,000	384	20,300

Table 3. Cont.

Compound	λ_{\max} nm	ϵ_1 dm ³ mol ⁻¹ cm ⁻¹	λ_{\max} nm	ϵ_2 dm ³ mol ⁻¹ cm ⁻¹
5m	305	13,600	476	31,400
5n	266	18,100	403	25,900
5p	302	25,200	344	19,000
6g	267	15,000	337	31,400

In the case of dinitro compounds **4a–c**, the electron-releasing Me₂N group in the phenyl ring leads to a considerable red shift of the absorption maximum (by 141 nm) with respect to the electron-withdrawing chlorine atom (compounds **4a** and **4b**, Figure 6). Compound **4b**, with a strong electron-releasing 4-dimethylaminophenyl group, absorbs light in the visible region, whereas compounds **4a** and **4c** have their absorption maxima at the border between the visible and UV regions. This can be explained by the difference in the degree of charge transfer along the conjugation chain between the strongly withdrawing nitropyridine ring and the second electron-donating ring through the double bond.

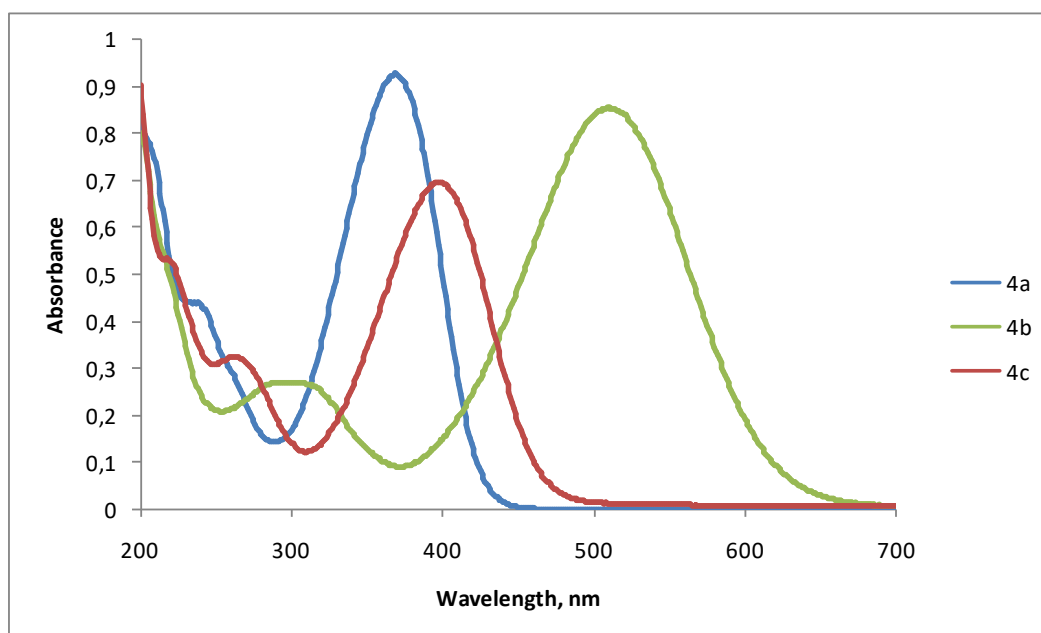


Figure 6. UV-Vis spectra of compounds **4a–c** in MeCN (2×10^{-5} M).

On the other hand, the replacement of 5-NO₂ with the CF₃ group in a pyridine cycle caused a 42 nm blue shift for compounds **4a/4i** and an 80 nm shift for 4-dimethylaminophenyl derivatives **4b/4k**, as well as a small decrease in molar absorptivity (Figure 7). It can be concluded that substituents at the double bond as well as in position 5 can be independently altered to predictably fine-tune absorption spectra of these compounds.

The study of isomeric substitution products of 3- and 5-NO₂ in compound **4a** revealed an important dependence, as shown in Figure 8. Substitution of the nitro group at position 5 gave compound **6g**, whose absorption spectrum generally resembles that of the parent compound and follows the same pattern described above for the 5-NO₂/5-CF₃ pair. On the other hand, substitution of the nitro group at position 3 gave compound **5g**, which is qualitatively different from both compounds. In this case, the absorption maximum shifts slightly towards the visible region, and the absorption spectrum itself acquires a more complex structure. From this we can conclude that the combination of 2-alkenyl and 3-alkylthio substituents leads to the appearance of a characteristic electronic structure. A similar pattern was observed for the substitution of 3-NO₂ in compound **4c**, but not for

compound **4b**, which can be explained by the predominance of a strong charge transfer over the finer electronic structure. It should be noted that the alkylthio substituent does not significantly affect the photophysical properties of the obtained compounds.

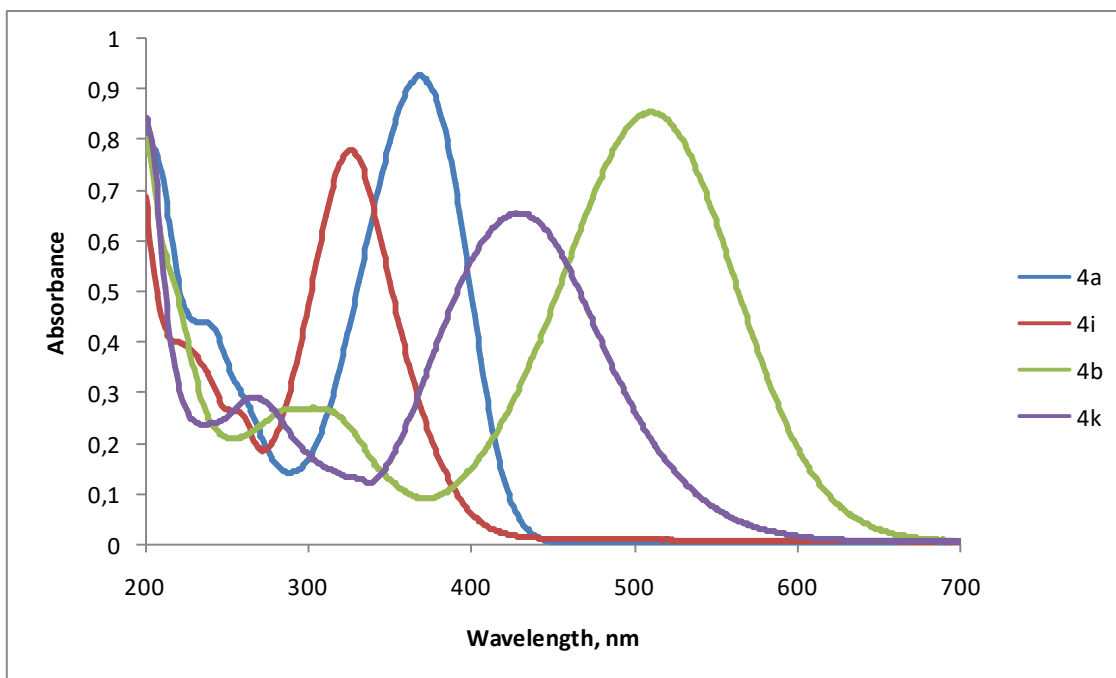


Figure 7. UV-Vis spectra of compounds **4a,b,i,k** in MeCN (2×10^{-5} M).

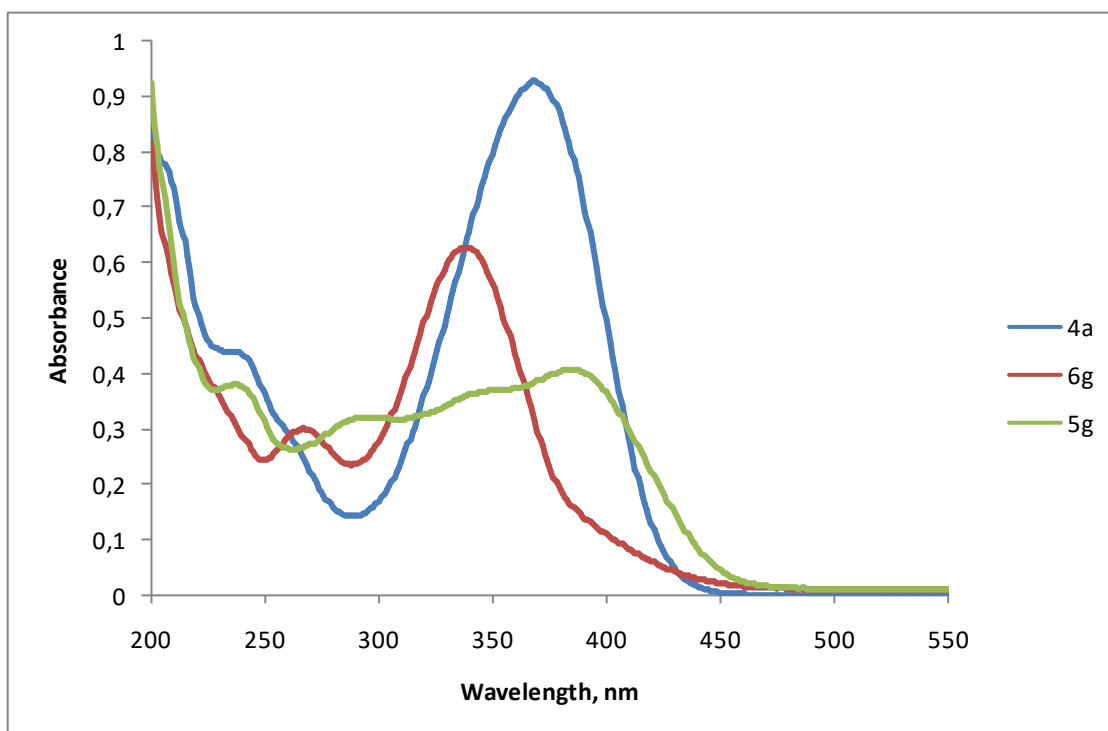


Figure 8. UV-Vis spectra of compounds **4a, 5g, 6g** in MeCN (2×10^{-5} M).

Compounds **5g,n** showed fluorescence upon excitation by light with the wavelength equal to the λ_{max} in the visible region, as shown in Figures 9 and 10. Compound **5g** has an emission maximum at 538 nm and a Stokes shift of 154 nm, whereas for compound **5n**, these values are 571 nm and 168 nm, respectively. The large values of Stokes shifts (150–170 nm) almost completely eliminate the overlap between the absorption and emission regions. In addition, the properties of these fluorescent molecules can be tuned by changing the substituent at the double bond.

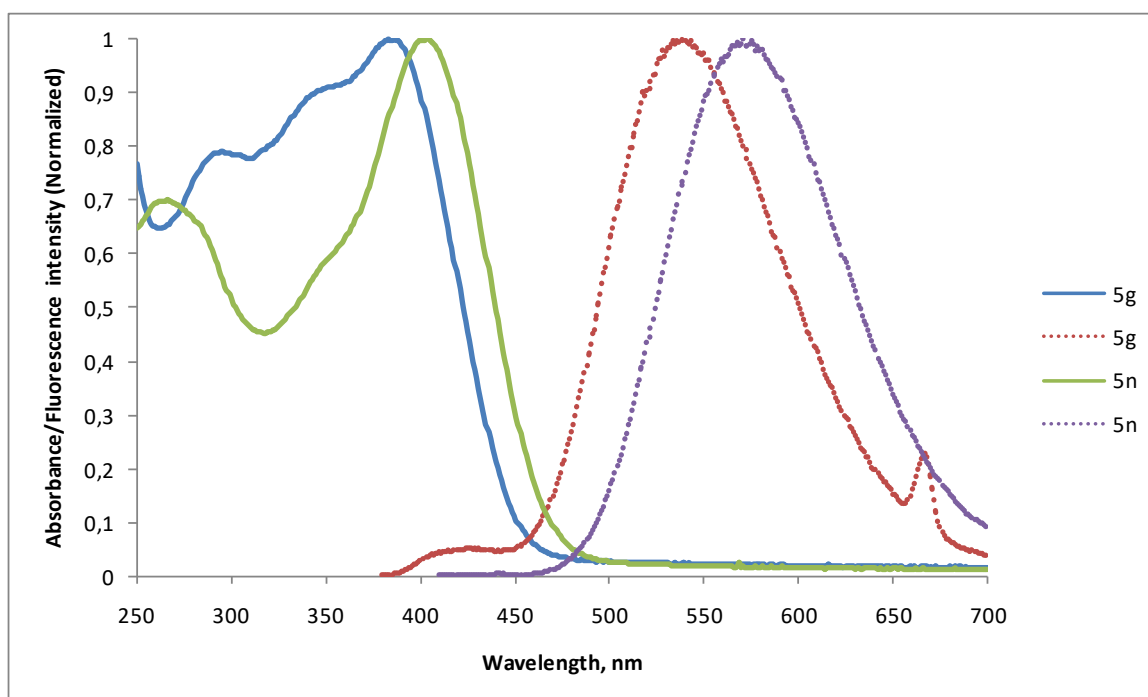


Figure 9. Normalized absorption and emission spectra of compounds **5g** and **5n** in MeCN.

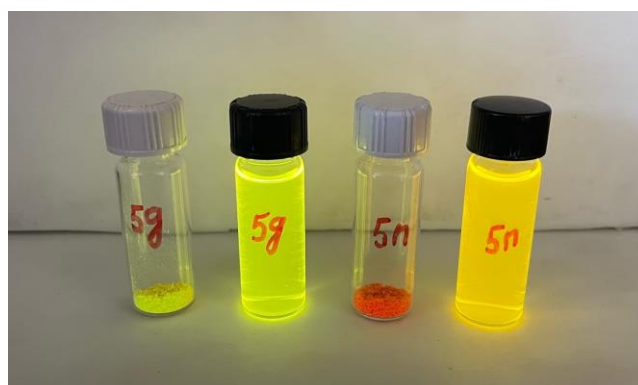


Figure 10. Fluorescence of compounds **5g** and **5n** in solid state and in MeCN solution under 365 nm UV lamp.

3. Conclusions

In conclusion, a number of the previously unknown 2-methyl- and 2-arylvinyl-3-nitropyridines were synthesized. Their reactions with *S*-nucleophiles proceeded under mild conditions and were found to be regioselective with a predominance of 3-NO₂ substitution; the influence of the substituents in positions 2 and 5 on the observed selectivity was revealed. The synthesized compounds showed promising tunable photophysical properties, such as large Stokes shifts. The reported synthetic approach can be considered as a convenient tool for rapid access to pyridine-based building blocks of various potential applications.

4. Materials and Methods

4.1. General Information

All chemicals were of commercial grade and used directly without purification. Melting points were measured on a Stuart SMP20 apparatus (Stuart (Bibby Scientific), UK). ^1H and ^{13}C NMR spectra were recorded on a Bruker AM-300 (at 300.13 and 75.13 MHz, respectively, Bruker Biospin, Germany) or Bruker Avance DRX 500 (at 500 and 125 MHz, respectively, Bruker Biospin, Germany) in DMSO-d_6 or CDCl_3 . J values are given in Hz. HRMS spectra were recorded on a Bruker micrOTOF II mass spectrometer using ESI. UV-Vis absorption spectra were recorded in MeCN (2×10^{-5} M) in standard $10 \times 10 \times 45$ mm quartz cuvettes on a Cary 60 UV-Vis spectrophotometer (Agilent Technologies, Santa Clara, CA, USA). Fluorescence spectra were recorded in MeCN (2×10^{-6} M) in standard $10 \times 10 \times 45$ mm quartz cuvettes on a Cary Eclipse fluorescence spectrophotometer (Agilent Technologies). All reactions were monitored by TLC analysis using ALUGRAM SIL G/UV254 plates, which were visualized with UV light. Compounds **1a–c** were purchased from commercial suppliers. In some cases we were unable to record the ^{13}C NMR spectra of products due to insufficient solubility in common organic solvents (compounds **4d**, **5i,j,o** and **6j**).

4.2. General Procedure for the Synthesis of 2-Methyl-3-nitropyridines **2a–c**

To a stirred suspension of NaH (60% in mineral oil, 0.80 g, 20 mmol) in anhydrous THF (30 mL), diethyl malonate (1.52 mL, 10 mmol) was added dropwise. The suspension was stirred for 15 min until hydrogen evolution ceased and a solution of the corresponding 2-chloropyridine **1** (10 mmol) in THF (20 mL) was added. The reaction mixture was stirred at r.t. (room temperature) for 6 h, poured in water (200 mL) and acidified with conc. HCl to pH 3. This was then extracted with CHCl_3 , evaporated and 50% H_2SO_4 (30 mL) was added to the residue. The mixture was stirred for 6 h at 120 °C, cooled, neutralized with Na_2CO_3 to pH 8 and extracted with CHCl_3 . The organic phase was dried over Na_2SO_4 , evaporated and the residue was purified via column chromatography ($\text{SiO}_2/\text{CHCl}_3$).

2-Methyl-3,5-dinitropyridin (2a) [19], brown oil; yield 62%; ^1H NMR (300 MHz, CDCl_3): δ 9.55 (d, 1H, $J = 2.1$ Hz), 9.06 (d, 1H, $J = 2.1$ Hz), 3.03 (s, 3H).

5-Bromo-2-methyl-3-nitropyridin (2b) [20], yellowish oil; yield 90%; ^1H NMR (300 MHz, CDCl_3): δ 8.80 (d, 1H, $J = 2.1$ Hz), 8.44 (d, 1H, $J = 2.1$ Hz), 2.84 (s, 3H).

2-Methyl-3-nitro-5-trifluoromethylpyridine (2c), yellowish oil; yield 81%; ^1H NMR (300 MHz, CDCl_3): δ 9.00 (s, 1H), 8.54 (s, 1H), 2.97 (s, 3H).

4.3. General Procedure for the Oxidation of 2-Methyl-3-nitropyridines **2b,c**

To a solution of the corresponding 2-methyl-3-nitropyridine **2** (10 mmol) in CH_2Cl_2 (30 mL), a freshly prepared complex urea/ H_2O_2 (1.88 g, 20 mmol) was added. The resulting suspension was cooled to 0 °C and trifluoroacetic anhydride (5 mL, 36 mol) was added dropwise. The reaction mixture was stirred for 30 min at 0 °C and 4 h at r.t. A saturated aqueous solution of $\text{Na}_2\text{S}_2\text{O}_3$ (50 mL) was added and the organic phase was separated. An aqueous layer was additionally extracted with CH_2Cl_2 and combined organic solutions were washed with the saturated solution of NaHCO_3 , dried over Na_2SO_4 and evaporated. The residue was recrystallized from aqueous EtOH.

5-Bromo-2-methyl-3-nitropyridine N-oxide (3b), pale-yellow solid; yield 47%; mp 104–105 °C; ^1H NMR (300 MHz, CDCl_3): δ 8.60 (s, 1H), 7.86 (s, 1H), 2.67 (s, 3H, CH_3). ^{13}C NMR (125 MHz, CDCl_3): δ 148.5, 145.5, 143.5, 122.9, 116.4, 13.8. HRMS (ESI, m/z): calcd for $\text{C}_6\text{H}_5\text{BrN}_2\text{O}_3$ [$\text{M} + \text{H}$] $^+$: 232.9556; found: 232.9563.

2-Methyl-3-nitro-5-trifluoromethylpyridine N-oxide (3c), pale-yellow solid; yield 65%; mp 82–83 °C; ^1H NMR (300 MHz, CDCl_3): δ 8.69 (s, 1H), 7.89 (s, 1H), 2.75 (s, 3H). ^{13}C NMR (75 MHz, CDCl_3): δ 149.9, 148.8, 139.5, 127.1 (q, $^2J_{\text{CF}} = 36$ Hz), 121.1 (q, $^1J_{\text{CF}} = 274$ Hz), 116.1, 14.3. HRMS (ESI, m/z): calcd for $\text{C}_7\text{H}_5\text{F}_3\text{N}_2\text{O}_3$ [$\text{M} + \text{H}$] $^+$: 223.0325; found: 223.0331.

4.4. General Procedure for the Synthesis of Compounds 4a–g

To a solution of the corresponding 2-methylpyridine **2** or **3** (5 mmol) in toluene (30 mL), aromatic aldehyde (5 mmol) and 50 μ L of piperidine was added. The reaction mixture was stirred under reflux with a Dean–Stark adapter until water separation was completed. The solvent was evaporated and the residue was triturated with 20 mL of cold EtOH. The precipitate was filtered off and air-dried.

(*E*)-2-[(4-Chlorophenyl)vinyl]-3,5-dinitropyridine (**4a**), yellow solid; yield 78%; mp 204–205 °C; ^1H NMR (300 MHz, CDCl_3): δ 9.58 (s, 1H), 9.05 (s, 1H), 8.30 (d, 1H, $J = 15.3$ Hz), 7.83 (d, 1H, $J = 15.3$ Hz), 7.64 (d, 2H, $J = 8.4$ Hz), 7.45 (d, 2H, $J = 8.4$ Hz). ^{13}C NMR (150 MHz, $\text{DMSO}-d_6$): δ 152.0, 147.5, 143.2, 141.9, 140.3, 135.0, 134.0, 130.2, 129.2, 129.1, 121.6. HRMS (ESI, m/z): calcd for $\text{C}_{13}\text{H}_8\text{ClN}_3\text{O}_4$ [$\text{M} + \text{H}$] $^+$: 306.0276; found: 306.0283.

(*E*)-4-(2-(3,5-Dinitropyridin-2-yl)vinyl)-*N,N*-dimethylaniline (**4b**), dark-violet solid; yield 91%; mp 260 °C (dec.); ^1H NMR (300 MHz, CDCl_3): δ 9.41 (d, 1H, $J = 2.1$ Hz), 8.93 (d, 1H, $J = 2.1$ Hz), 8.28 (d, 1H, $J = 15.0$ Hz), 7.64 (d, 1H, $J = 15.0$ Hz), 7.57 (d, 2H, $J = 8.8$ Hz), 6.77 (d, 2H, $J = 8.8$ Hz), 3.06 (s, 6H). ^{13}C NMR (125 MHz, CDCl_3): δ 154.8, 152.4, 147.3, 146.4, 139.5, 131.1, 128.9, 123.2, 114.4, 111.9, 40.1. HRMS (ESI, m/z): calcd for $\text{C}_{15}\text{H}_{14}\text{N}_4\text{O}_4$ [$\text{M} + \text{H}$] $^+$: 315.1088; found: 315.1085.

(*E*)-5-Bromo-2-(4-dimethylaminophenyl)vinyl-3-nitropyridine *N*-oxide (**4c**), red-brown solid; yield 73%; mp 217 °C (dec.); ^1H NMR (300 MHz, CDCl_3): δ 8.55 (d, 1H, $J = 15.9$ Hz), 8.49 (s, 1H), 7.64 (s, 1H), 7.49 (d, 2H, $J = 8.7$ Hz), 7.00 (d, 1H, $J = 15.6$ Hz), 6.69 (d, 2H, $J = 8.7$ Hz), 3.05 (s, 6H). ^{13}C NMR (75 MHz, CDCl_3): δ 151.8, 147.2, 143.9, 142.8, 141.2, 129.9, 123.8, 123.0, 113.0, 111.9, 107.1, 40.1. HRMS (ESI, m/z): calcd for $\text{C}_{15}\text{H}_{14}\text{BrNO}_3$ [$\text{M} + \text{H}$] $^+$: 364.0291; found: 364.0292.

(*E*)-2-(2-(1-(4-Fluorophenyl)-1H-pyrazol-4-yl)vinyl)-3,5-dinitropyridine (**4d**), brown solid; yield 62%; mp 255 °C; ^1H NMR (300 MHz, CDCl_3): δ 9.53 (d, 1H, $J = 2.1$ Hz), 9.03 (d, 1H, $J = 2.1$ Hz), 8.30 (d, 1H, $J = 15.3$ Hz), 8.19 (s, 1H), 8.06 (s, 1H), 7.70 (m, 3H), 7.20 (m, 2H). HRMS (ESI, m/z): calcd for $\text{C}_{16}\text{H}_{10}\text{FN}_5\text{O}_4$ [$\text{M} + \text{H}$] $^+$: 356.0790; found: 356.0789.

(*E*)-2-(4-Chlorophenyl)vinyl-3-nitro-5-trifluoromethylpyridine *N*-oxide (**4e**), yellow solid; yield 81%; mp 161–162 °C; ^1H NMR (300 MHz, CDCl_3): δ 8.65 (d, 1H, $J = 15.9$ Hz), 8.64 (s, 1H), 7.73 (s, 1H), 7.52 (d, 2H, $J = 8.4$ Hz), 7.39 (d, 2H, $J = 8.4$ Hz), 7.17 (d, 1H, $J = 15.9$ Hz). ^{13}C NMR (75 MHz, CDCl_3): δ 147.9, 143.6, 142.3, 140.4, 136.7, 134.1, 129.4, 129.3, 125.5 (q, $^2J_{\text{CF}} = 36$ Hz), 121.1 (q, $^1J_{\text{CF}} = 273$ Hz), 116.0 (d, $^3J_{\text{CF}} = 3.2$ Hz), 112.8. HRMS (ESI, m/z): calcd for $\text{C}_{14}\text{H}_8\text{ClF}_3\text{N}_2\text{O}_3$ [$\text{M} + \text{H}$] $^+$: 345.0248; found: 345.0239.

(*E*)-5-Bromo-2-(4-chlorophenyl)vinyl-3-nitropyridine *N*-oxide (**4f**), yellow solid; yield 69%; mp 173–174 °C; ^1H NMR (300 MHz, CDCl_3): δ 8.45 (s, 1H), 8.30 (d, 1H, $J = 16.1$ Hz), 7.60 (s, 1H), 7.41 (d, 2H, $J = 8.4$ Hz), 7.29 (d, 2H, $J = 8.4$ Hz), 7.02 (d, 1H, $J = 16.1$ Hz). ^{13}C NMR (125 MHz, CDCl_3): δ 147.8, 144.1, 140.3, 140.2, 136.1, 134.4, 129.2, 129.1, 122.7, 115.7, 113.1. HRMS (ESI, m/z): calcd for $\text{C}_{13}\text{H}_8\text{BrClN}_2\text{O}_3$ [$\text{M} + \text{H}$] $^+$: 354.9480; found: 354.9472.

(*E*)-2-(4-Dimethylaminophenyl)vinyl-3-nitro-5-trifluoromethylpyridine *N*-oxide (**4g**), red-brown solid; yield 71%; mp 198–199 °C; ^1H NMR (300 MHz, CDCl_3): δ 8.85 (d, 1H, $J = 15.6$ Hz), 8.58 (s, 1H), 7.68 (s, 1H), 7.52 (d, 2H, $J = 8.4$ Hz), 7.10 (d, 1H, $J = 15.6$ Hz), 6.69 (d, 2H, $J = 8.4$ Hz), 3.06 (s, 6H). ^{13}C NMR (125 MHz, CDCl_3): δ 152.2, 146.8, 145.1, 144.4, 140.1, 130.5, 123.4, 122.7 (q, $^2J_{\text{CF}} = 36$ Hz), 121.4 (q, $^1J_{\text{CF}} = 273$ Hz), 116.3 (q, $^3J_{\text{CF}} = 3.6$ Hz), 111.9, 106.6, 40.0. HRMS (ESI, m/z): calcd for $\text{C}_{16}\text{H}_{14}\text{F}_3\text{N}_3\text{O}_3$ [$\text{M} + \text{H}$] $^+$: 354.1060; found: 354.1060.

4.5. General Procedure for the Synthesis of Compounds 4h–k

To a solution of the corresponding pyridine *N*-oxide (0.5 mmol), CH_2Cl_2 (10 mL) was added PCl_3 (0.13 mL) and the mixture was stirred under reflux for 2 h. After cooling, the reaction was washed with a saturated NaHCO_3 solution, dried over Na_2SO_4 and evaporated.

(*E*)-4-(2-(5-Bromo-3-nitropyridin-2-yl)vinyl)-*N,N*-dimethylaniline (**4h**), dark-brown solid; yield 89%; mp 202–203 °C; ^1H NMR (300 MHz, CDCl_3): δ 8.75 (s, 1H), 8.34 (s, 1H), 8.05 (d, 1H,

$J = 15.3$ Hz), 7.55 (d, 1H, $J = 15.6$), 7.53 (d, 2H, $J = 8.4$), 6.71 (d, 2H, $J = 8.4$ Hz), 3.04 (s, 6H). ^{13}C NMR (75 MHz, CDCl_3): δ 153.8, 151.3, 148.8, 145.5, 142.8, 140.5, 135.0, 129.8, 115.5, 115.5, 112.3, 40.4, 29.7. HRMS (ESI, m/z): calcd for $\text{C}_{15}\text{H}_{14}\text{BrN}_3\text{O}_2$ $[\text{M} + \text{H}]^+$: 348.0342; found: 348.0342.

(*E*)-2-(4-Chlorophenyl)vinyl-3-nitro-5-trifluoromethylpyridine (**4i**), yellow solid; yield 89%; mp 138 °C; ^1H NMR (300 MHz, CDCl_3): δ 9.02 (s, 1H), 8.50 (s, 1H), 8.16 (d, 1H, $J = 15.6$ Hz), 8.77 (d, 1H, $J = 15.6$ Hz), 7.59 (d, 2H, $J = 8.4$ Hz), 7.41 (d, 2H, $J = 8.4$ Hz). ^{13}C NMR (75 MHz, CDCl_3): δ 152.0, 149.2 (q, $^3J_{\text{CF}} = 3.6$ Hz), 143.0, 140.8, 136.1, 133.9, 130.7 (q, $^3J_{\text{CF}} = 3.6$ Hz), 129.4, 129.3, 124.9 (q, $^2J_{\text{CF}} = 35$ Hz), 120.6. HRMS (ESI, m/z): calcd for $\text{C}_{14}\text{H}_8\text{ClF}_3\text{N}_2\text{O}_2$ $[\text{M} + \text{H}]^+$: 329.0299; found: 329.0311.

(*E*)-5-Bromo-2-(4-chlorostyryl)-3-nitropyridine (**4j**), yellow solid; yield 94%; mp 184–185 °C; ^1H NMR (300 MHz, CDCl_3): δ 8.83 (d, 1H, $J = 1.8$ Hz), 8.40 (d, 1H, $J = 1.8$ Hz), 8.02 (d, 1H, $J = 15.6$ Hz), 7.68 (d, 1H, $J = 15.6$ Hz), 7.56 (d, 2H, $J = 8.4$ Hz), 7.38 (d, 2H, $J = 8.4$ Hz). ^{13}C NMR (75 MHz, CDCl_3): δ 154.0, 147.4, 143.7, 138.4, 135.5, 135.1, 134.2, 129.2, 129.1, 124.9, 117.6. HRMS (ESI, m/z): calcd for $\text{C}_{13}\text{H}_8\text{BrClN}_2\text{O}_2$ $[\text{M} + \text{H}]^+$: 338.9530; found: 338.9533.

(*E*)-*N,N*-Dimethyl-4-(2-(3-nitro-5-trifluoromethylpyridin-2-yl)vinyl)aniline (**4k**), brown solid; yield 82%; mp 150–151 °C; ^1H NMR (300 MHz, CDCl_3): δ 8.40 (s, 1H), 8.36 (s, 1H), 8.12 (d, 1H, $J = 15.3$ Hz), 7.56 (d, 1H, $J = 15.3$ Hz), 7.49 (d, 2H, $J = 8.7$ Hz), 6.66 (d, 2H, $J = 8.7$ Hz), 2.99 (s, 6H). ^{13}C NMR (75 MHz, CDCl_3): δ 153.4, 151.9, 149.1 (q, $^3J_{\text{CF}} = 4$ Hz), 143.3, 141.8, 130.8 (q, $^3J_{\text{CF}} = 4$ Hz), 130.3, 122.8 (q, $^1J_{\text{CF}} = 271$ Hz), 123.6, 122.9 (q, $^2J_{\text{CF}} = 34$ Hz), 115.0, 112.1, 40.2. HRMS (ESI, m/z): calcd for $\text{C}_{16}\text{H}_{14}\text{F}_3\text{N}_3\text{O}_2$ $[\text{M} + \text{H}]^+$: 338.1111; found: 338.1120.

4.6. General Procedure for the Synthesis of Compounds 5 and 6

To a solution of compound **2**, **3** or **4** (1 mmol) in anhydrous DMF (5 mL), thiol (1 mmol) and K_2CO_3 (0.138 g, 1 mmol) were added. The reaction mixture was stirred for 1–2 h at 60 °C, poured into H_2O (50 mL), acidified with conc. HCl to pH 3 and extracted with CHCl_3 (3 \times 20 mL). The organic phase was dried over Na_2SO_4 , evaporated and the residue was purified via column chromatography ($\text{SiO}_2/\text{CHCl}_3$) or recrystallized from EtOH.

3-(Benzylsulfanyl)-2-methyl-5-nitropyridine (**5a**), beige solid; yield 70%; mp 79–80 °C; ^1H NMR (300 MHz, CDCl_3): δ 9.06 (d, 1H, $J = 2.1$ Hz), 7.35 (m, 5H), 4.24 (s, 2H, CH_2), 2.65 (s, 3H, CH_3). ^{13}C NMR (125 MHz, CDCl_3): δ 162.7, 142.8, 140.1, 134.9, 134.8, 128.9, 128.8, 128.0, 127.8, 37.1, 23.4. HRMS (ESI, m/z): calcd for $\text{C}_{13}\text{H}_{12}\text{N}_2\text{O}_2\text{S}$ $[\text{M} + \text{H}]^+$: 261.0692; found: 261.0699.

3-(Benzylsulfanyl)-5-bromo-2-methylpyridine *N*-oxide (**5b**), grey needles; yield 96%; mp 106–107 °C; ^1H NMR (300 MHz, CDCl_3): δ 8.25 (s, 1H), 7.26–7.32 (m, 5H), 7.24 (s, 1H), 4.14 (s, 2H, SCH_2), 2.49 (s, 3H, CH_3). ^{13}C NMR (75 MHz, CDCl_3): δ 147.3, 137.8, 136.8, 134.9, 128.9, 128.1, 127.7, 116.3, 38.5, 14.5. HRMS (ESI, m/z): calcd for $\text{C}_{13}\text{H}_{12}\text{BrNOS}$ $[\text{M} + \text{H}]^+$: 309.9896; found: 309.9896.

5-Bromo-3-(4-chlorophenylsulfanyl)-2-methylpyridine *N*-oxide (**5c**), brown solid; yield 95%; mp 131–132 °C; ^1H NMR (300 MHz, CDCl_3): δ 8.27 (s, 1H), 7.44 (d, 2H, $J = 8.4$ Hz), 7.38 (d, 2H, $J = 8.4$ Hz), 6.89 (s, 1H), 2.56 (s, 3H). ^{13}C NMR (75 MHz, CDCl_3): δ 146.7, 138.1, 137.3, 136.0, 134.8, 130.4, 129.0, 127.7, 116.6, 14.6. HRMS (ESI, m/z): calcd for $\text{C}_{12}\text{H}_9\text{BrClNOS}$ $[\text{M} + \text{H}]^+$: 329.9350; found: 329.9349.

3-(Benzylsulfanyl)-5-bromo-2-methylpyridine (**5d**), pale-yellow crystals; yield 65%; mp 55 °C; ^1H NMR (300 MHz, CDCl_3): δ 8.33 (s, 1H), 7.58 (s, 1H), 7.31 (m, 5H), 4.09 (s, 2H, SCH_2), 2.48 (s, 3H, CH_3). ^{13}C NMR (75 MHz, CDCl_3): δ 155.5, 146.5, 137.3, 135.6, 134.4, 128.9, 128.8, 127.8, 117.9, 37.8, 22.5. HRMS (ESI, m/z): calcd for $\text{C}_{13}\text{H}_{12}\text{BrNS}$ $[\text{M} + \text{H}]^+$: 293.9947; found: 293.9956.

3-(Benzylsulfanyl)-2-methyl-5-(trifluoromethyl)pyridine (**5e**), yellow oil; yield 60%; ^1H NMR (300 MHz, CDCl_3): δ 8.53 (s, 1H), 7.64 (s, 1H), 7.31 (s, 5H), 4.14 (s, 2H, SCH_2), 2.61 (s, 3H, CH_3). ^{13}C NMR (75 MHz, CDCl_3): δ 161.0, 142.3 (q, $^3J_{\text{CF}} = 4$ Hz), 135.5, 133.4, 131.7 (q,

$^3J_{CF} = 3.5$ Hz), 128.9, 128.8, 127.8, 124.7 (q, $^2J_{CF} = 34$ Hz), 123.5 (q, $^1J_{CF} = 273$ Hz), 37.5, 23.2. HRMS (ESI, m/z): calcd for $C_{14}H_{12}F_3NS$ $[M + H]^+$: 284.0715; found: 284.0719.

3-(Benzylsulfanyl)-2-methyl-5-(trifluoromethyl)pyridine *N*-oxide (**5f**), pale-yellow crystals; yield 52%; mp 85–86 °C; 1H NMR (300 MHz, $CDCl_3$): δ 8.33 (s, 1H), 7.29 (m, 5H), 7.22 (s, 1H), 4.15 (s, 2H, SCH_2), 2.57 (s, 3H, CH_3). ^{13}C NMR (75 MHz, $CDCl_3$): δ 151.8, 137.3, 134.7, 134.1, 128.9, 128.9, 128.1, 126.6 (q, $^2J_{CF} = 35$ Hz), 121.9 (q, $^1J_{CF} = 273$ Hz), 120.1, 38.4, 15.0. HRMS (ESI, m/z): calcd for $C_{14}H_{12}F_3NOS$ $[M + H]^+$: 300.0664; found: 300.0662.

(*E*)-3-(Benzylsulfanyl)-2-((4-chlorophenyl)vinyl)-5-nitropyridine (**5g**), yellow crystals; yield 56%; mp 146–147 °C; 1H NMR (300 MHz, $CDCl_3$): δ 9.17 (d, 1H, $J = 2.1$ Hz), 8.28 (d, 1H, $J = 2.1$ Hz), 7.92 (d, 1H, $J = 15.6$ Hz), 7.57 (d, 1H, $J = 15.6$ Hz), 7.53 (d, 2H, $J = 8.7$ Hz), 7.39 (d, 2H, $J = 8.7$ Hz), 7.30 (m, 5H), 4.18 (s, 2H, SCH_2). ^{13}C NMR (75 MHz, $CDCl_3$): δ 159.0, 142.2, 142.1, 138.1, 135.5, 135.2, 134.5, 132.4, 132.3, 129.2, 129.2, 129.0, 128.9, 128.1, 122.8, 38.7. HRMS (ESI, m/z): calcd for $C_{20}H_{15}ClN_2O_2S$ $[M + H]^+$: 383.0616; found: 383.0603.

(*E*)-5-(Benzylsulfanyl)-2-((4-chlorophenyl)vinyl)-3-nitropyridine (**6g**), yellow crystals; yield 18%; mp 183–184 °C; 1H NMR (300 MHz, $CDCl_3$): δ 8.63 (d, 1H, $J = 1.8$ Hz), 8.06 (d, 1H, $J = 2.1$ Hz), 7.97 (d, 1H, $J = 15.6$ Hz), 7.67 (d, 1H, $J = 15.6$ Hz), 7.56 (d, 2H, $J = 8.7$ Hz), 7.39 (d, 2H, $J = 8.7$ Hz), 7.33 (m, 5H), 4.22 (s, 2H, SCH_2). HRMS (ESI, m/z): calcd for $C_{20}H_{15}ClN_2O_2S$ $[M + H]^+$: 383.0616; found: 383.0621.

2-[(*E*)-(4-Chlorophenyl)vinyl]-3-(isobutylsulfanyl)-5-nitropyridine (**5h**), yellow crystals; yield 62%; mp 139–140 °C; 1H NMR (300 MHz, $CDCl_3$): δ 9.16 (d, 1H, $J = 2.4$ Hz), 8.31 (d, 1H, $J = 2.1$ Hz), 7.96 (d, 1H, $J = 15.3$ Hz), 7.63 (d, 1H, $J = 15.3$ Hz), 7.60 (d, 2H, $J = 8.4$ Hz), 7.41 (d, 2H, $J = 8.4$ Hz), 2.92 (d, 2H, $J = 6.9$ Hz), 1.99 (m, 1H), 1.14 (d, 6H, $J = 6.6$ Hz). ^{13}C NMR (75 MHz, $CDCl_3$): δ 158.0, 147.0, 142.4, 141.0, 137.9, 135.4, 134.5, 134.3, 129.9, 122.8, 42.3, 28.1, 22.2. HRMS (ESI, m/z): calcd for $C_{17}H_{17}ClN_2O_2S$ $[M + H]^+$: 349.0772; found: 349.0783.

2-[(*E*)-(4-Chlorophenyl)vinyl]-5-(isobutylsulfanyl)-3-nitropyridine (**6h**), yellow crystals; yield 31%; mp 106 °C; 1H NMR (300 MHz, $CDCl_3$): δ 8.68 (d, 1H, $J = 1.8$ Hz), 8.09 (d, 1H, $J = 1.8$ Hz), 7.97 (d, 1H, $J = 15.6$ Hz), 7.68 (d, 1H, $J = 15.6$ Hz), 7.56 (d, 2H, $J = 8.4$ Hz), 7.38 (d, 2H, $J = 8.4$ Hz), 2.92 (d, 2H, $J = 6.9$ Hz), 1.96 (m, 1H), 1.10 (d, 6H, $J = 6.6$ Hz). ^{13}C NMR (75 MHz, $CDCl_3$): δ 152.0, 145.4, 143.9, 136.8, 135.1, 134.9, 134.6, 130.9, 129.1, 129.0, 121.5, 42.1, 28.3, 22.0. HRMS (ESI, m/z): calcd for $C_{17}H_{17}ClN_2O_2S$ $[M + H]^+$: 349.0772; found: 349.0764.

2-[(*E*)-2-(4-Chlorophenyl)vinyl]-3-[(2-furylmethyl)sulfanyl]-5-nitropyridine (**5i**), yellow crystals; yield 56%; mp 156 °C; 1H NMR (300 MHz, $CDCl_3$): δ 9.24 (d, 1H, $J = 1.8$ Hz), 8.42 (d, 1H, $J = 2.1$ Hz), 7.95 (d, 1H, $J = 15.6$ Hz), 7.65 (d, 1H, $J = 15.6$ Hz), 7.58 (d, 2H, $J = 8.4$ Hz), 7.40 (d, 2H, $J = 8.4$ Hz), 7.33 (s, 1H), 6.26 (s, 1H), 6.14 (d, 1H, $J = 3.0$ Hz), 4.18 (s, 2H). HRMS (ESI, m/z): calcd for $C_{18}H_{13}ClN_2O_2S$ $[M + H]^+$: 373.0408; found: 373.0419.

3-[(4-Chlorophenyl)sulfanyl]-2-[(*E*)-2-(4-chlorophenyl)vinyl]-5-nitropyridine (**5j**), yellow solid; yield 67%; mp 172 °C; 1H NMR (300 MHz, $DMSO-d_6$): δ 9.26 (s, 1H), 8.22 (s, 1H), 7.98 (d, 1H, $J = 15.6$ Hz), 7.74 (d, 2H, $J = 8.4$ Hz), 7.66 (d, 1H, $J = 15.6$ Hz), 7.52 (br.s, 4H), 7.49 (d, 2H, $J = 8.4$ Hz). HRMS (ESI, m/z): calcd for $C_{19}H_{12}Cl_2N_2O_2S$ $[M + H]^+$: 403.0069; found: 403.0057.

(*E*)-4-(2-(3-((4-Chlorophenyl)sulfanyl)-5-nitropyridin-2-yl)vinyl)-*N,N*-dimethylaniline (**5k**), dark-red solid; yield 83%; mp 175 °C; 1H NMR (300 MHz, $DMSO-d_6$): δ 9.21 (s, 1H), 8.20 (s, 1H), 7.96 (d, 1H, $J = 15.6$ Hz), 7.50 (m, 6H), 7.36 (d, 1H, $J = 15.6$ Hz), 6.74 (d, 2H, $J = 8.4$ Hz), 2.99 (s, 6H). ^{13}C NMR (125 MHz, $CDCl_3$): δ 160.1, 151.6, 143.1, 141.3, 141.2, 134.9, 133.4, 133.2, 130.9, 130.1, 129.9, 123.7, 117.0, 111.9, 40.1. HRMS (ESI, m/z): calcd for $C_{21}H_{18}ClN_3O_2S$ $[M + H]^+$: 412.0881; found: 412.0870.

(*E*)-4-(2-(3-(Isobutylsulfanyl)-5-nitropyridin-2-yl)vinyl)-*N,N*-dimethylaniline (**5l**), dark-red solid; yield 84%; mp 165–166 °C; 1H NMR (300 MHz, $CDCl_3$): δ 9.14 (d, 1H, $J = 2.4$ Hz), 8.27 (d, 1H, $J = 2.1$ Hz), 8.01 (d, 1H, $J = 15.3$ Hz), 7.58 (d, 2H, $J = 8.7$ Hz), 7.46 (d, 1H, $J = 15.3$ Hz), 6.74 (d, 2H, $J = 8.7$ Hz), 3.06 (s, 6H), 2.89 (d, 2H, $J = 6.6$ Hz), 1.96 (m, 1H), 1.13 (d, 6H, $J = 6.6$ Hz). ^{13}C NMR (75 MHz, $CDCl_3$): δ 159.5, 151.5, 141.4, 141.3, 140.2, 132.5, 130.0, 129.8,

124.1, 117.4, 112.0, 43.0, 40.2, 28.1, 22.2. HRMS (ESI, m/z): calcd for $C_{19}H_{23}N_3O_2S$ $[M + H]^+$: 358.1584; found: 358.1583.

(*E*)-4-(2-(3-(Benzylsulfanyl)-5-nitropyridin-2-yl)vinyl)-*N,N*-dimethylaniline (**5m**), dark-red solid; yield 88%; mp 188 °C; 1H NMR (300 MHz, $CDCl_3$): δ 9.13 (d, 1H, $J = 2.1$ Hz), 8.20 (d, 1H, $J = 1.8$ Hz), 7.98 (d, 1H, $J = 15.3$ Hz), 7.54 (d, 2H, $J = 8.7$ Hz), 7.43 (d, 1H, $J = 15.3$ Hz), 7.30 (m, 5H), 6.70 (d, 2H, $J = 8.7$ Hz), 4.16 (s, 2H), 3.05 (s, 6H). ^{13}C NMR (75 MHz, $CDCl_3$): δ 160.4, 151.5, 142.3, 141.0, 140.5, 135.5, 132.2, 130.6, 129.9, 129.0, 128.8, 127.9, 124.0, 117.4, 112.0, 40.2, 38.5. HRMS (ESI, m/z): calcd for $C_{22}H_{21}N_3O_2S$ $[M + H]^+$: 392.1427; found: 392.1417.

(*E*)-3-(Benzylsulfanyl)-2-(2-(1-(4-fluorophenyl)-1H-pyrazol-4-yl)vinyl)-5-nitropyridine (**5n**), orange solid; yield 89%; mp 145–146 °C; 1H NMR (300 MHz, $CDCl_3$): δ 9.15 (d, 1H, $J = 2.1$ Hz), 8.26 (d, 1H, $J = 2.1$ Hz), 8.05 (s, 1H), 7.98 (s, 1H), 7.92 (d, 1H, $J = 15.3$ Hz), 7.67 (m, 2H), 7.40 (d, 1H, $J = 15.3$ Hz), 7.30 (m, 5H), 7.18 (m, 2H), 4.18 (s, 2H). ^{13}C NMR (75 MHz, $CDCl_3$): δ 161.4 (d, $^1J_{CF} = 247$ Hz), 159.3, 142.1, 141.8, 140.3, 136.0 (d, $^4J_{CF} = 3$ Hz), 135.3, 132.2, 131.5, 129.3, 129.0, 128.9, 128.0, 126.4, 121.9, 121.4, 121.1 (d, $^3J_{CF} = 8.5$ Hz), 116.5 (d, $^2J_{CF} = 23$ Hz), 38.6. HRMS (ESI, m/z): calcd for $C_{23}H_{17}FN_4O_2S$ $[M + H]^+$: 433.1129; found: 433.1123.

(*E*)-3-((4-Chlorophenyl)sulfanyl)-2-(2-(1-(4-fluorophenyl)-1H-pyrazol-4-yl)vinyl)-5-nitropyridine (**5o**), orange solid; yield 93%; mp 219 °C; 1H NMR (300 MHz, $DMSO-d_6$): δ 9.24 (s, 1H), 8.99 (s, 1H), 8.22 (s, 1H), 8.18 (s, 1H), 7.80 (m, 4H), 7.55 (s, 4H), 7.40 (m, 3H). HRMS (ESI, m/z): calcd for $C_{22}H_{14}ClFN_4O_2S$ $[M + H]^+$: 453.0583; found: 453.0573.

(*E*)-3-(Benzylsulfanyl)-5-bromo-2-[(4-chlorophenyl)vinyl]pyridine (**5p**), beige solid, yield 60%; mp 142–143 °C; 1H NMR (300 MHz, $CDCl_3$): δ 8.48 (s, 1H), 7.69–7.73 (m, 2H), 7.48–7.56 (m, 3H), 7.25–7.36 (m, 7H), 4.08 (s, 2H). ^{13}C NMR (125 MHz, $CDCl_3$): δ 153.2, 148.4, 141.1, 135.9, 135.1, 134.3, 133.6, 132.5, 128.9, 128.8, 128.7, 128.6, 127.7, 123.7, 118.3, 39.4. HRMS (ESI, m/z): calcd for $C_{20}H_{15}BrClNS$ $[M + H]^+$: 415.9869; found: 415.9870.

(*E*)-3-(Benzylsulfanyl)-5-bromo-2-[(4-(dimethylamino)phenyl)vinyl]pyridine *N*-oxide (**5q**), dark-red solid; yield 67%; mp 177 °C; 1H NMR (300 MHz, $CDCl_3$): δ 8.49 (d, 1H, $J = 15.9$ Hz), 8.23 (s, 1H), 7.51 (d, 2H, $J = 8.7$ Hz), 7.28 (m, 7H), 6.71 (d, 2H, $J = 8.7$ Hz), 4.14 (s, 2H), 3.03 (s, 6H, NCH_3). ^{13}C NMR (75 MHz, $CDCl_3$): δ 151.2, 144.9, 140.5, 139.0, 135.9, 135.0, 129.2, 129.1, 128.8, 128.4, 127.9, 127.8, 124.8, 114.1, 112.1, 40.3, 39.0. HRMS (ESI, m/z): calcd for $C_{22}H_{21}BrN_2OS$ $[M + H]^+$: 441.0631; found: 441.0635.

4.7. X-ray Crystallographic Data and Refinement Details

X-ray diffraction data for **5h** were collected at 100 K on a Bruker Quest D8 diffractometer (Karlsruhe, Germany) equipped with a Photon III area detector, using graphite-monochromatized Mo K_{α} -radiation and a shutterless φ - and ω -scan technique. The intensity data were integrated by the SAINT program (version 8.04A) [21] and were semi-empirically corrected for absorption and decay using SADABS (2016/2) [22]. X-ray diffraction data for **4a**, **4i** and **5l** were collected at 100 K on a four-circle Rigaku Synergy-S diffractometer (Wroclaw, Poland) equipped with a HyPix6000HE area detector, using monochromatized Cu K_{α} -radiation and a shutterless ω -scan technique. The intensity data were integrated and corrected for absorption and decay by the CrysAlisPro program [23]. All structures were solved by direct methods using SHELXT [24] and refined by the full-matrix least-squares method on F^2 using SHELXL-2018 [25]. Positions of all atoms were found from the electron density difference map. Atoms were refined with individual anisotropic (non-hydrogen atoms) or isotropic (hydrogen atoms) displacement parameters. The Mercury program [26] was used for molecular graphics. Crystal data, data collection and structure refinement details are summarized in Supplementary Materials Table S1. The structures were deposited at the Cambridge Crystallographic Data Center with the reference CCDC numbers 2191010–2191013; they also contain the supplementary crystallographic data. These data can be obtained free of charge from the CCDC via http://www.ccdc.cam.ac.uk/data_request/cif, accessed on 30 August 2022.

Supplementary Materials: The following are available online at <https://www.mdpi.com/article/10.3390/molecules27175692/s1>, X-ray data, ^1H and ^{13}C NMR spectra. References [19–26] are cited in the supplementary materials.

Author Contributions: Conceptualization, V.V.N. and A.M.S.; methodology, V.V.N. and M.A.B.; investigation, V.V.N. and M.E.M.; resources, M.E.M.; writing—original draft preparation, V.V.N. and M.A.B.; writing—review and editing, A.M.S.; supervision, A.M.S. All authors have read and agreed to the published version of the manuscript.

Funding: This research received no external funding.

Data Availability Statement: Not applicable.

Acknowledgments: In this section, you can acknowledge any support given which is not covered by the author contribution or funding sections. This may include administrative and technical support, or donations in kind (e.g., materials used for experiments).

Conflicts of Interest: The authors declare no conflict of interest.

Sample Availability: Samples of the compounds are not available from the authors.

References

- Khan, E. Pyridine Derivatives as Biologically Active Precursors; Organics and Selected Coordination Complexes. *ChemistrySelect* **2021**, *6*, 3041–3064. [CrossRef]
- Yang, S.; Yan, J.; Wang, L.; Guo, X.; Li, S.; Wu, G.; Zuo, R.; Huang, X.; Wang, H.; Wang, L.; et al. Nitropyridinyl ethyleneimine compound, the pharmaceutical composition containing it, the preparation method and use thereof. U.S. Patent 20140073796A1, 27 January 2015.
- Jhons, B.A.; Spaltenstein, A. HIV Integrase Inhibitors. U.S. Patent WO 2007/09101 A2, 18 January 2007.
- Romero, D.L.; Morge, R.A.; Biles, C.; Berrios-Pena, N.; May, P.D.; Palmer, J.R.; Johnson, P.D.; Smith, H.W.; Busso, M. Discovery, Synthesis, and Bioactivity of Bis(heteroaryl)piperazines. 1. A Novel Class of Non-Nucleoside HIV-1 Reverse Transcriptase Inhibitors. *J. Med. Chem.* **1994**, *37*, 999–1014. [CrossRef] [PubMed]
- Kuduk-Jaworska, J.; Puzsko, A.; Kubiak, M.; Pelczynska, M. Synthesis, structural, physico-chemical and biological properties of new palladium(II) complexes with 2,6-dimethyl-4-nitropyridine. *J. Inorg. Biochem.* **2004**, *98*, 1447–1456. [CrossRef] [PubMed]
- Klapötke, T.M.; Stierstorfer, J.; Weyrauther, M.; Witkowski, T.G. Synthesis and Investigation of 2,6-Bis(picrylamino)-3,5-dinitropyridine (PYX) and Its Salts. *Chem.—A Eur. J.* **2016**, *22*, 8619–8626. [CrossRef] [PubMed]
- Agrawal, J.P.; Prasad, U.S.; Surve, R.N. Synthesis of 1,3-bis(1,2,4-triazol-3-amino)-2,4,6-trinitrobenzene and its thermal and explosive behaviour. *New J. Chem.* **2000**, *24*, 583–585. [CrossRef]
- Balachari, D.; Trudell, M.L. Synthesis of new dipyridotetraazapentalenes. *Tetrahedron Lett.* **1997**, *38*, 8607–8610. [CrossRef]
- Balachari, D.; Stevens, E.D.; Trudell, M.L.; Beardall, D.; Wight, C.A. Synthesis, Thermal Stability and Impact Stability of Novel Tetranitro-Dipyridotetraazapentalene Derivatives. *Propell. Explos. Pyrotech.* **2000**, *25*, 75–80. [CrossRef]
- Kauer, J.C.; Carboni, R.A. Aromatic azapentalenes. III. 1,3a,6,6a-Tetraazapentalenes. *J. Am. Chem. Soc.* **1967**, *89*, 2633–2637. [CrossRef]
- Gryl, M.; Seidler, T.; Wojnarska, J.; Stadnicka, K.M.; Matulková, I.; Němec, I.; Němec, P. Co-Crystals of 2-Amino-5-Nitropyridine Barbitol with Extreme Birefringence and Large Second Harmonic Generation Effect. *Chem.—A Eur. J.* **2018**, *24*, 8727–8731. [CrossRef] [PubMed]
- Bastrakov, M.A.; Nikol'Skiy, V.V.; Starosotnikov, A.M.; Fedyanin, I.V.; Shevelev, S.A.; Knyazev, D.A. Reactions of 3-R-5-nitropyridines with nucleophiles: Nucleophilic substitution vs conjugate addition. *Tetrahedron* **2019**, *75*, 130659. [CrossRef]
- Frank, R.; Christoph, T.; Lesch, B.; Lee, J. Substituted heterocyclic aza derivatives. WO Patent 2013013817, 31 January 2013.
- Van der Eycken, E.; Jidong, Z.; Kilonda, A.; Compennolle, F.; Toppet, S.; Hoornaert, G.; Van der Auweraer, M.; Jackers, C.; Verbouwe, W.; De Schryver, F.C. Synthesis of (E)-5-(2-arylvinyl)-2-(hetero)arylpiperazines, (E)-2-(2-arylvinyl)-5-methoxycarbonylpiperazines and (E,E)-2,5-bis(2-arylvinyl)piperazines as polarity and pH probes. Electronic supplementary information (ESI). *J. Chem. Soc. Perkin Trans.* **2002**, *2*, 928–937. [CrossRef]
- Iyer, S.; Ramesh, C. Aryl-Pd covalently bonded palladacycles, novel amino and oxime catalysts {di- μ -chlorobis(benzaldehydeoxime-6-C,N)dipalladium(II), di- μ -chlorobis(dimethylbenzylamine-6-C,N)dipalladium(II)} for the Heck reaction. *Tetrahedron Lett.* **2000**, *41*, 8981–8984. [CrossRef]
- Amatore, C.; Jutand, A. Anionic Pd(0) and Pd(II) Intermediates in Palladium-Catalyzed Heck and Cross-Coupling Reactions. *Accounts Chem. Res.* **2000**, *33*, 314–321. [CrossRef] [PubMed]
- Lubisch, W.; Beckenbach, E.; Bopp, S.; Hofmann, H.-P.; Kartal, A.; Kästel, C.; Lindner, T.; Metz-Garrecht, M.; Reeb, J.; Regner, F.; et al. Benzoylalanine-Derived Ketoamides Carrying Vinylbenzyl Amino Residues: Discovery of Potent Water-Soluble Calpain Inhibitors with Oral Bioavailability. *J. Med. Chem.* **2003**, *46*, 2404–2412. [CrossRef] [PubMed]

18. Lee, D.-H.; Taher, A.; Hossain, S.; Jin, M.-J. An Efficient and General Method for the Heck and Buchwald–Hartwig Coupling Reactions of Aryl Chlorides. *Org. Lett.* **2011**, *13*, 5540–5543. [CrossRef] [PubMed]
19. Liu, M.-C.; Lin, T.-S.; Sartorelli, A.C. A One-Pot Synthesis of 3-Nitro- and 3,5-Dinitro-2-Picolines. *Synth. Commun.* **1990**, *20*, 2965–2970. [CrossRef]
20. Jones, C.D.; William, R.; Luke, A.; McCoull, W. Aminopyrimidine Derivatives with TIE2 Inhibiting Activity. U.S. Patent 20080194552 A1, 14 August 2008.
21. Bruker. *APEX-III*; Bruker AXS Inc.: Madison, WI, USA, 2019.
22. Krause, L.; Herbst-Irmer, R.; Sheldrick, G.M.; Stalke, D. Comparison of silver and molybdenum microfocus X-ray sources for single-crystal structure determination. *J. Appl. Crystallogr.* **2015**, *48*, 3–10. [CrossRef]
23. CrysAlisPro. Version 1.171.41.106a. In *Rigaku Oxford Diffraction*; Rigaku Corporation: Oxford, UK, 2021.
24. Sheldrick, G.M. *SHELXT*—Integrated space-group and crystal-structure determination. *Acta Crystallogr. Sect. A Found. Adv.* **2015**, *71*, 3–8. [CrossRef] [PubMed]
25. Sheldrick, G.M. Crystal structure refinement with *SHELXL*. *Acta Crystallogr. Sect. C Struct. Chem.* **2015**, *C71*, 3–8. [CrossRef] [PubMed]
26. Macrae, C.F.; Sovago, I.; Cottrell, S.J.; Galek, P.T.A.; McCabe, P.; Pidcock, E.; Platings, M.; Shields, G.P.; Stevens, J.S.; Towler, M.; et al. *Mercury 4.0*: From visualization to analysis, design and prediction. *J. Appl. Crystallogr.* **2020**, *53*, 226–235. [CrossRef] [PubMed]

Article

Copper(II)-Catalyzed (3+2) Cycloaddition of 2*H*-Azirines to Six-Membered Cyclic Enols as a Route to Pyrrolo[3,2-*c*]quinolone, Chromeno[3,4-*b*]pyrrole, and Naphtho[1,8-*ef*]indole Scaffolds

Pavel A. Sakharov, Nikolai V. Rostovskii *, Alexander F. Khlebnikov and Mikhail S. Novikov *

Institute of Chemistry, St. Petersburg State University, 7/9 Universitetskaya Nab., 199034 St. Petersburg, Russia

* Correspondence: n.rostovskiy@spbu.ru (N.V.R.); m.novikov@spbu.ru (M.S.N.)

Abstract: A method for the [2+3] pyrroline annulation to the six-membered non-aromatic enols using 3-aryl-2*H*-azirines as annulation agents is developed in the current study. The reaction proceeds as a formal (3+2) cycloaddition via the N1-C2 azirine bond cleavage and is catalyzed by both Cu(II) and Cu(I) compounds. The new annulation method can be applied to prepare pyrrolo[3,2-*c*]quinoline, chromeno[3,4-*b*]pyrrole, and naphtho[1,8-*ef*]indole derivatives in good to excellent yields from enols of the quinolin-2-one, 2*H*-chromen-2-one, and 1*H*-phenalen-1-one series.

Keywords: azirines; pyrrolines; cycloaddition; annulation; copper catalysis

Citation: Sakharov, P.A.; Rostovskii, N.V.; Khlebnikov, A.F.; Novikov, M.S. Copper(II)-Catalyzed (3+2) Cycloaddition of 2*H*-Azirines to Six-Membered Cyclic Enols as a Route to Pyrrolo[3,2-*c*]quinolone, Chromeno[3,4-*b*]pyrrole, and Naphtho[1,8-*ef*]indole Scaffolds. *Molecules* **2022**, *27*, 5681. <https://doi.org/10.3390/molecules27175681>

Academic Editor: Alexey M. Starosotnikov

Received: 16 August 2022

Accepted: 31 August 2022

Published: 2 September 2022

Publisher's Note: MDPI stays neutral with regard to jurisdictional claims in published maps and institutional affiliations.

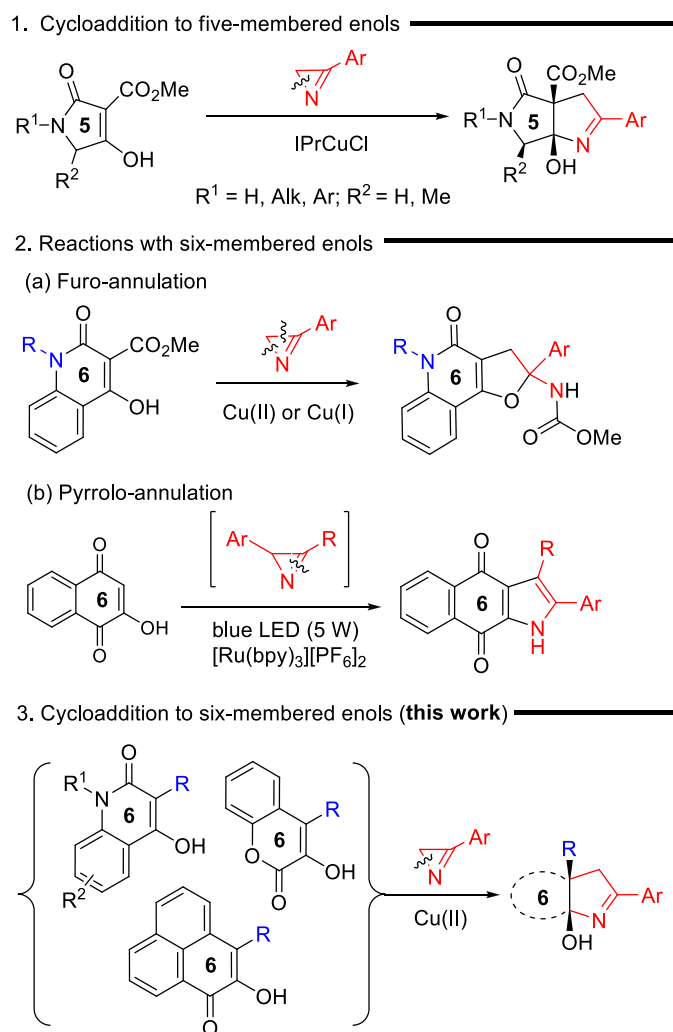


Copyright: © 2022 by the authors. Licensee MDPI, Basel, Switzerland. This article is an open access article distributed under the terms and conditions of the Creative Commons Attribution (CC BY) license (<https://creativecommons.org/licenses/by/4.0/>).

1. Introduction

2*H*-Azirines are widely used for the preparation of various 4–7-membered N-, N,N-, and N,O-heterocycles of varying degrees of unsaturation and different heteroatom arrangements [1,2]. The ability of azirines to open at any of the three bonds of the ring under the action of electrophilic and nucleophilic reagents, as well as transition metal compounds, underlies a powerful strategy for the synthesis of azete [3], pyrrole [4–6], oxazole [7–9], imidazole [10–12], 1,2,3-triazole [13], pyridine [14] derivatives, and other heterocycles, which are hardly accessible with conventional methods. Some of the azirine-ring opening reactions can be applied for the synthesis of *ortho*-fused, spiro-fused, and bridged heterocycles. These heteropolycycles can be the result of both intramolecular and intermolecular reactions of azirines [1]. Among them, intermolecular cycloaddition reactions are of particular interest, since they satisfy the requirements of green chemistry being atom-economical processes. In contrast to the (2+3)- and (2+4)-cycloaddition reactions of azirines with 1,3-dipoles and 1,3-dienes (or their aza-analogs) [15–19], in which azirines, without the ring opening, provide the incorporation of a diatomic N–C fragment in the resulting heterocycle, the reaction sequence “azirine-ring opening/cycloaddition” provides the incorporation of all atoms of the azirine ring into a new heterocyclic system. This annulation strategy includes transition-metal-catalyzed reactions of azirines with cyclic diazo compounds [20–22], Y(OTf)₃-catalyzed [3+6] cycloaddition of azirines to fulvenes [23] leading to 3,4-dihydro-2*H*-cyclopenta[*c*]pyridine derivatives, photoinduced (3+2) cycloaddition of nitrile ylides, generated via the azirine-ring opening (C2–C3 azirine bond cleavage), to quinones [24] or *N*-benzylmaleimide [25], synthesis of cycloalkane-fused pyrroles by the Fe(III)-catalyzed decarboxylative (3+2) cycloaddition of the 2*H*-azirines to cyclic β-ketoacids (N1–C3 azirine bond cleavage) [26], and synthesis of pyrrolo[3,4-*b*]pyrrole derivatives via Cu(I)-catalyzed (3+2) cycloaddition of azirines to the enol carbon–carbon double bond of 3-methoxycarbonyl-substituted tetramic acids (Scheme 1, reaction 1) [27]. The last of these methods can be effectively applied to the pyrroline annulation of tetronic and thiotetronic acids as well [28]. However, attempts to extend this method to six-membered enols of the quinoline-3-carboxylate series unexpectedly encountered a serious problem associated with the involvement of the ester substituent in the transformation (Scheme 1,

reaction 2a). This reaction also proceeds through azirine N1-C2 bond cleavage under both Cu(I) and Cu(II) catalysis, but exclusively produces the furo-annulation product [29]. A visible-light-promoted (3+2) cycloaddition of azirines, derived in situ from vinyl azides, to α -hydroxybenzoquinones is the only successful example of azirine cycloaddition to a multiple bond of a six-membered cyclic enol to date (Scheme 1, reaction 2b) [30]. However, this reaction cannot serve as an alternative to the method of copper-catalyzed annulation of enols with azirines, since it proceeds via the cleavage of not a single N-C2 azirine bond, but a multiple N-C3 bond, and provides a pyrrole ring with another substitution pattern. Thus, the search for the effective conditions for (3+2) cycloadditions of azirines to unsaturated cyclic systems, including cyclic enols, the elucidation of mechanisms of these reactions, assessing their scope and limitations still remains an outstanding challenge.



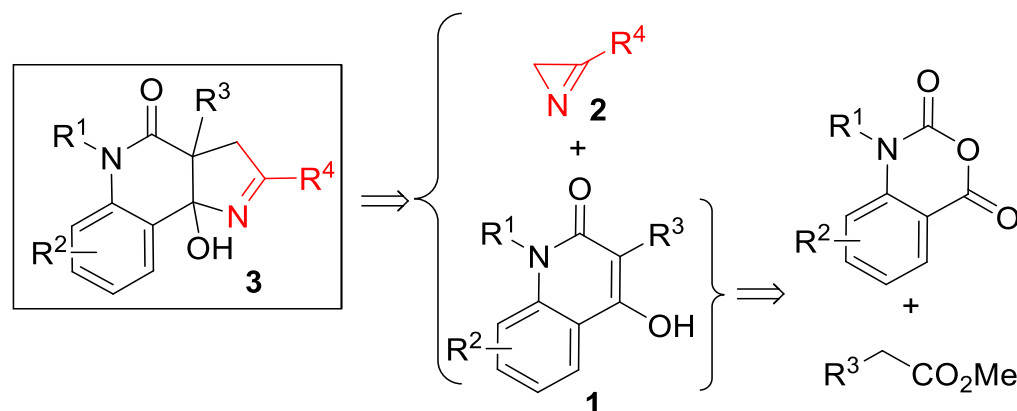
Scheme 1. Reactions of cyclic enols with 2*H*-azirines.

In this study, we describe a method for the pyrroline annulation of six-membered non-aromatic enols of the quinolin-2-one, 2*H*-chromen-2-one, and 1*H*-phenalen-1-one series. Additionally, a reaction mechanism is presented that allows us to define the scope of this method.

2. Results and Discussion

Our initial interest in (3+2)-cycloaddition reactions of azirines **2** was related to their possible use for the rapid assembly of 1*H*-pyrrolo[3,2-*c*]quinoline framework **3** from 4-hydroxyquinolone derivatives **1** (Scheme 2). The structural motif of 1*H*-pyrrolo[3,2-*c*]quinoline has always attracted the attention of synthetic chemists [31,32], as it is included

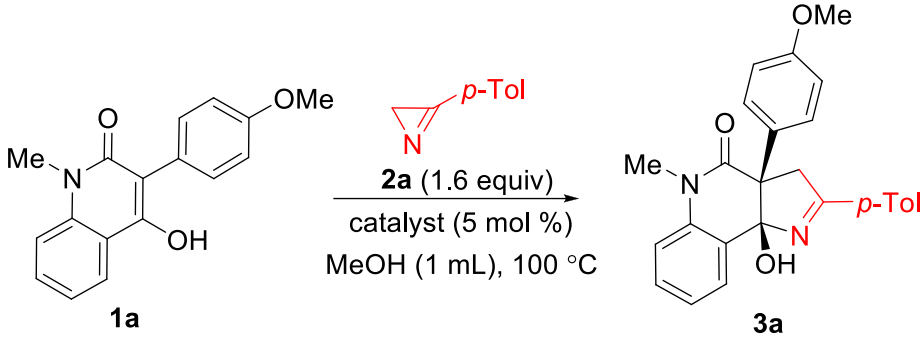
in many bioactive, natural products [33–36] and synthetic compounds that possess enzyme modulator [37], antitumor [38], and 5-hydroxytryptamine(6) receptor antagonist activities [39]. The attractiveness of the mentioned approach to these compounds lies in the easy availability of quinolones **1**, which can be prepared from isatoic anhydrides. It should also be noted that the synthesis of pyrroline-fused systems bearing a bridgehead hydroxy group is a challenge, since conventional annulation methods either produce unsatisfactory results [40] or require the use of an aggressive medium, such as liquid ammonia [41].



Scheme 2. Retrosynthetic scheme for 1*H*-pyrrolo[3,2-*c*]quinolones **3**.

In our initial experiments, we synthesized 3-(4-methoxyphenyl)-substituted quinolin-2-one **1a** from *N*-methylisatoic anhydride and methyl 4-methoxyphenylacetate according to the procedure described in the literature [42]. Enol **1a** turned out to be inactive toward azirine **2a** when heated at 100 °C in methanol, toluene, or 1,2-dichloroethane (DCE). At higher temperatures, the formation of azirine decomposition products without enol involvement was observed. The reaction between **1a** and **2a** commenced at 100 °C in methanol when catalytic amounts of the Cu(I)-NHC complex IPrCuCl (5 mol%) were added, and resulted in the formation of the desired annulation product, pyrroloquinolone **3a**, in 98% yield in 20 min (Table 1, entry 2). It was notable that a close to quantitative yield of **3a** was also achieved with all tested copper(II) catalysts (entries 3–5). The optimal ratio **1a**/**2a** was observed to be 1:1.6, whereas the reaction between equimolar amounts of the reagents provided only 65% yield (entry 6). Replacing anhydrous methanol with 96% aqueous ethanol led to a decrease in the yield (entry 7). A high yield of **3a** in the CuCl₂-catalyzed reaction was obtained by increasing the amount of the azirine to 2 equiv. To our surprise, cobalt(II) acetate as well as nickel(II) and iron(III) acetylacetonates also catalyzed the reaction, albeit with less efficiency (entries 9–11). As a result, we used the 1:1.6 mixture of enol **1** and azirine **2** in the presence of copper(II) acetate monohydrate (5 mol%) as a catalyst at 100 °C in methanol as optimal conditions for the further experiments.

The scope of hydroxyquinolones **1** was then evaluated under the optimized conditions using 3-(*p*-tolyl)-2*H*-azirine (**2a**) as the reaction partner (Scheme 3). The reaction displayed a low sensitivity to the electronic effects of the aryl substituent at C3 of the enol (compounds **3a–f**). In addition, the annulation product **3g** was synthesized from a quinolone with a 2-thienyl substituent at the C3 in 92% yield. The reaction was observed to be tolerant to the presence of a substituent at any position of the benzene ring of the quinolone moiety and provided high product yields (compounds **3h–k**). Additional *ortho*- and *peri*-fusion (as in quinolone **1m**) also did not influence the product yield (compound **3m**).

Table 1. Optimization of synthesis of 3a.


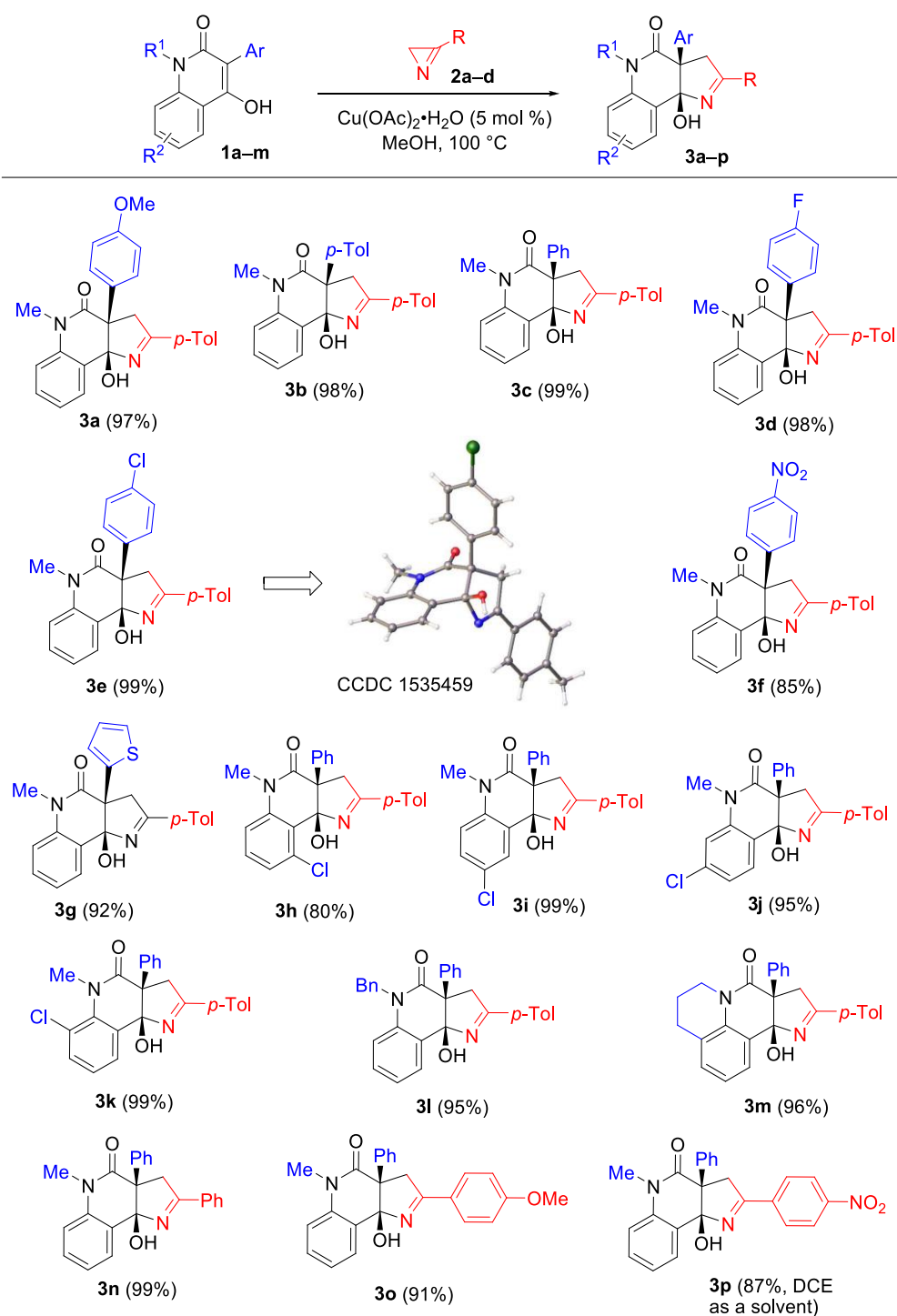
Entry	Catalyst	Deviation from Standard Conditions	Yield of 3a, % ^a
1	-		0
2	IPrCuCl ^b		98
3	CuCl ₂ ·2H ₂ O	2a (2 equiv)	95
4	Cu(acac) ₂		98
5	Cu(OAc) ₂ ·H ₂ O		98
6	Cu(OAc) ₂ ·H ₂ O	2a (1 equiv)	65
7	Cu(OAc) ₂ ·H ₂ O	solvent EtOH	77
8	Cu(OAc) ₂ ·H ₂ O	temperature 20 °C	53 ^c
9	Co(OAc) ₂ ·4H ₂ O		17
10	Ni(acac) ₂		64
11	Fe(acac) ₃		70

^a Yield is determined by ¹H NMR spectroscopy using CH₂Br₂ as an internal standard. ^b IPrCuCl = Chloro[1,3-bis(2,6-diisopropylphenyl)imidazol-2-ylidene]copper(I). ^c Reaction time: 48 h.

The structures of compounds **3a–p** were established using NMR spectroscopy and HRMS methods. The structure of compound **3e** was additionally verified by X-ray diffraction analysis.

The comparison of the obtained results with the data of our previous work [29] (Scheme 1, reaction 2a) revealed a dramatic dependence of the reaction outcome on the nature of the C3 substituent in quinolones **1**: 3-alkoxycarbonyl-substituted derivatives produced the products of furo-annulation, while 3-aryl-substituted derivatives exclusively produced pyrroline-fused products **3**. In order to find out how general this pattern was for six-membered enols, we examined compounds **4** and **7**, having carbonyl substituents both at the α - and β -carbon atoms of the enol moiety (Scheme 4). The Cu(OAc)₂- and IPrCuCl-catalyzed reactions of chromenone **4** with azirine **2a**, conducted in methanol at 100 °C, resulted in a complex, inseparable mixture of products. IPrCuCl did not catalyze the reaction in DCE at all, but, to our delight, the target chromenopyrrole **6a** was obtained in 67% yield in DCE using Cu(OAc)₂·H₂O (5 mol%) as a catalyst. According to the ¹H NMR spectrum of the reaction mixture, no traces of the furo-annulated product, compound **5**, were detected. The reaction of chromenone **4** with azirines **2b–d** occurred with almost the same efficiency, producing chromenopyrroles **6b–d** in 60–70% yields. The structure of compound **6c** was confirmed by X-ray diffraction analysis.

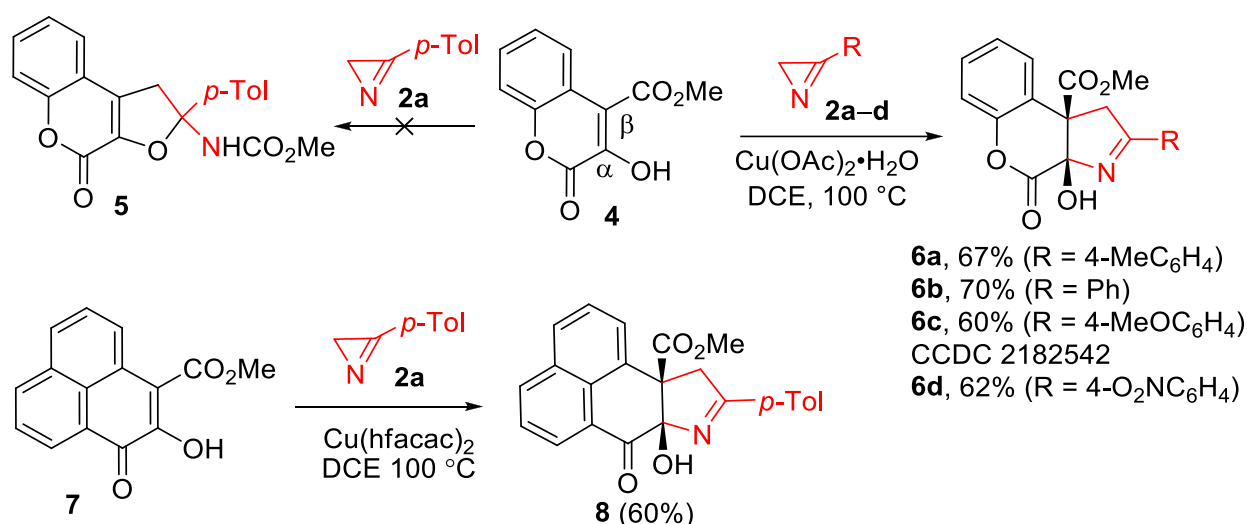
Phenalenone **7** with a similarly substituted enol moiety included in the *ortho*- and *peri*-fused system also reacted well with azirine **2a**, producing the tetracyclic annulation adduct **8** in a 60% yield. In this reaction, copper(II) hexafluoroacetylacetonate (10 mol%) was used as a catalyst since it provided a slightly higher product yield than copper(II) acetate.



Scheme 3. Synthesis of pyrroloquinolinones 3.

Thus, the substitution pattern of the enol moiety of six-membered cyclic enols controlled the outcome of their catalytic annulation with azirines directing the reaction toward either pyrroline- or furane-fused products. In the presence of an aryl substituent at the β -position of the enol moiety of quinolones 1, its (2+3) cycloaddition to azirines 2 smoothly proceeded to afford pyrroline-annulated products 3. In contrast, the CO_2Me group in the same position directs the process toward the formation of furo-annulated products as follows from the results of the previous studies [29]. However, this switching does not occur if the α -carbon of the enol moiety is adjacent to the endocyclic carbonyl carbon atom. We proposed the reaction mechanism (Scheme 5) to address the observed reactivity of

non-aromatic six-membered cyclic enols toward azirines under copper catalysis. The key step of the reaction was the azirine-ring opening across the N1-C2 bond to form radical **9** under the action of copper(I) enolate **1-Cu(I)/4-Cu(I)**. The latter resulted from the oxidative homocoupling of the enol with the copper(II) catalyst. Such an oxidation with copper(II) acetylacetonate was previously reported for tetramic acids [27]. Indeed, enol **1a** reacts with $\text{Cu}(\text{OAc})_2$ in boiling MeOH, but, unfortunately, our attempts to isolate the oxidative coupling product failed because of the low selectivity of the reaction, which yielded an inseparable mixture of products. Intramolecular radical attack in intermediate **9** afforded copper(I) iminide **10,11**. 3-Aryl-substituted iminide **10** underwent the cyclization at the keto group followed by a copper–hydrogen exchange to produce cycloadduct **3**. The expected intramolecular nucleophilic attack of the iminide nitrogen on the ester carbonyl in intermediate **11** to form furo-annulation product **5** did not occur because of two reasons: (1) the additional activation of the electrophilic keto group by the lactone carbonyl group, and (2) stabilization of alcoholate **13** by the chelation of the copper by the lactone carbonyl group. As a result, the cyclization in the keto group proceeded rapidly and irreversibly. The copper–hydrogen exchange between alcoholate **13** and enol **4** afforded the final cycloadduct **6** and regenerated enolate **4-Cu(I)**.

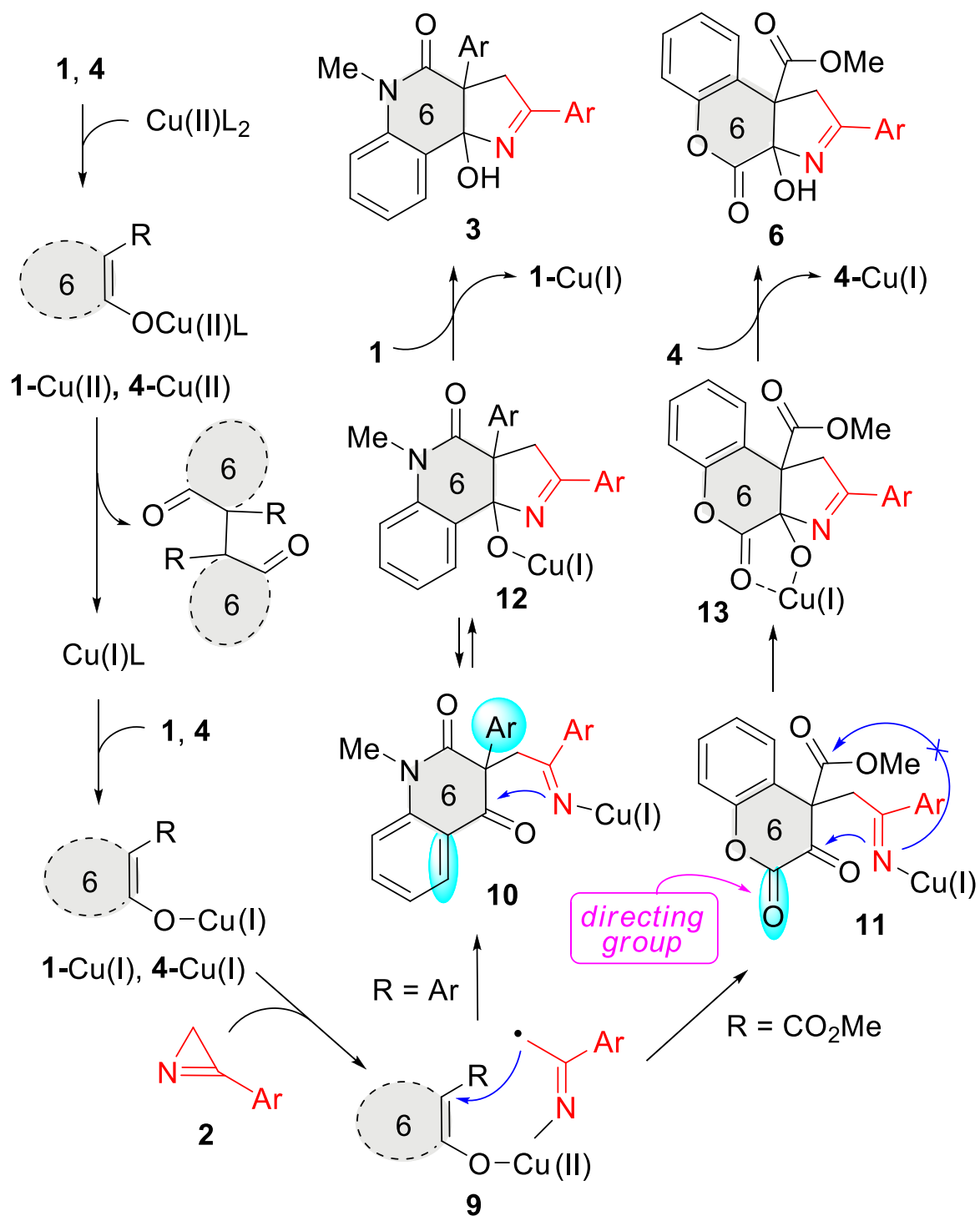


Scheme 4. Synthesis of chromenopyrrolones **6** and adduct **8**.

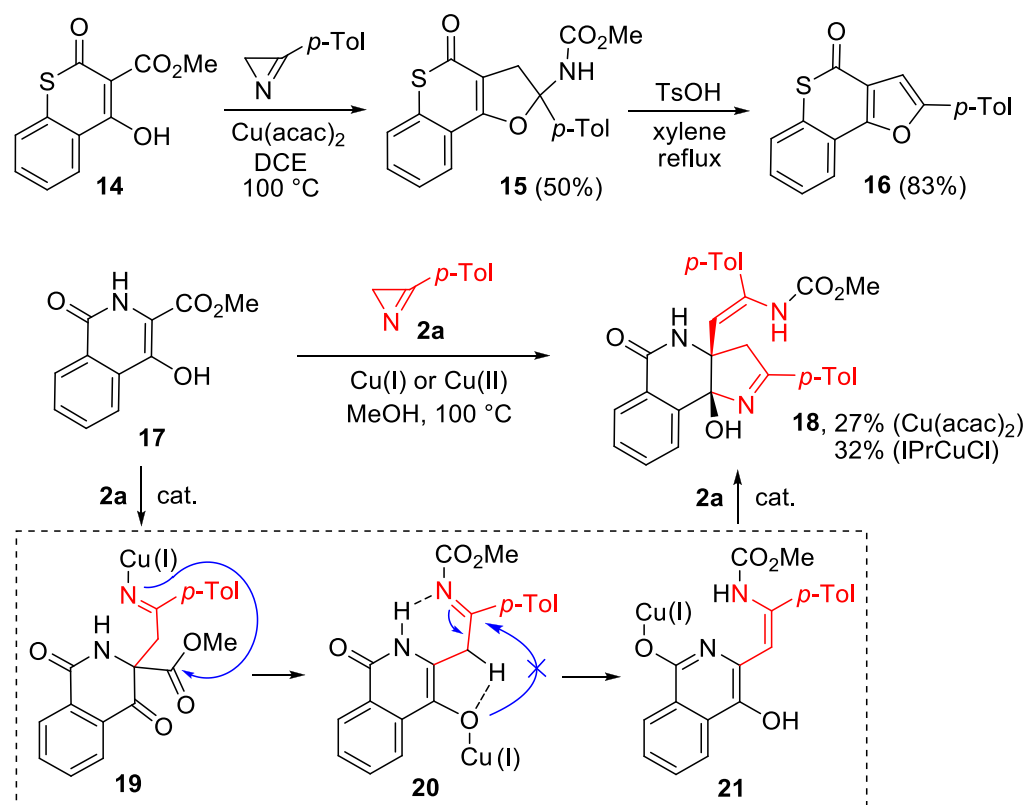
Thus, the lactone carbonyl in intermediate **11** acted as a directing group, enabling the annulation of the pyrroline ring even though the enol system bears an ester substituent at the β -C enol atom. The reaction of methoxycarbonyl-substituted 6-membered cyclic enols, having no directing carbonyl group, should proceed through a furo-annulation involving the CO_2Me group. This important conclusion was supported by the reaction between thiochromene-based enol **14** and azirine **2a** (Scheme 6). This reaction afforded carbamate **15** as a sole product in the presence of copper(II) acetylacetonate under the standard conditions. Compound **15** can be transformed under acidic conditions into thiochromenofuran **16** in good yields.

An unexpected result was obtained in the reaction of 4-hydroxyisoquinolinone **17** with azirine **2a** catalyzed with $\text{Cu}(\text{acac})_2$ (5 mol%) (Scheme 6). The formation of a furo-fused product (similar to **15**) did not occur from compound **17**, despite the presence of the methoxycarbonyl group at the β -C atom and the absence of the directing carbonyl group at the α -C atom of the enol moiety. Instead, pyrrolino-annulated 1:2 adduct **18** was isolated in 27% yield. Optimization experiments showed that the use of other copper(II) catalysts ($\text{Cu}(\text{OAc})_2$, $\text{Cu}(\text{hfacac})_2$) did not enhance the efficiency of the reaction, whereas NHC complex IPrCuCl (5 mol%) allowed a slight increase in the yield of **18** (32%). This product resulted from the addition of two molecules of azirine **2a** to isoquinolinone **17**, one of which modified the methoxycarbonyl group of **17** and another one formed the pyrroline ring. The

abnormal reaction course can be rationalized in terms of rapid copper–hydrogen exchange in intermediate **20**, which is more rapid than the furan ring closure. The (2+3) cycloaddition of aminovinyl-substituted enol **21** to azirine **2a** afforded compound **18**. The *Z* configuration of the C=C bond in compound **18** was established based on 2D ^1H - ^1H -NOESY spectrum data (see the Supplementary Materials).



Scheme 5. Plausible mechanism.



Scheme 6. Synthesis of compounds 15, 16, and 18.

3. Materials and Methods

3.1. General Instrumentation

Melting points were determined on a melting-point apparatus and were uncorrected. ^1H (400 MHz) and ^{13}C (100 MHz) NMR spectra were recorded on a Bruker Avance 400 spectrometer in solvent indicated below. ^1H NMR spectra were calibrated according to the residual peaks of CDCl_3 ($\delta = 7.26$ ppm), DMSO-d_6 ($\delta = 2.50$ ppm). $^{13}\text{C}\{^1\text{H}\}$ NMR spectra were calibrated according to the carbon atom peaks of CDCl_3 ($\delta = 77.0$ ppm), DMSO-d_6 ($\delta = 40.0$ ppm). High-resolution mass spectra were recorded with a Bruker maXis HRMS-QTOF, electrospray ionization. X-ray diffraction analysis was performed with an Agilent Technologies Xcalibur Eos (for **3e**) and Agilent Technologies Supernova (for **6c**) diffractometers. Crystallographic data for the structures **3e** (CCDC 1535459) and **6c** (CCDC 2182542) were deposited at the Cambridge Crystallographic Data Centre. Thin-layer chromatography (TLC) was conducted on aluminum sheets precoated with SiO_2 ALUGRAM SIL G/UV₂₅₄. Column chromatography was performed on silica gel 60 M (0.04–0.063 mm). Methanol was refluxed for 2 h with magnesium turnings and then distilled. 1,2-Dichloroethane was washed with concentrated H_2SO_4 , water, then distilled from P_2O_5 and stored over anhydrous K_2CO_3 .

Quinolones **1a–l** were prepared from isatoic anhydrides and corresponding methyl acetates according to the procedure described in the literature [42]. Quinolones **1a**, **1m** [43], and **1c** [42] are known compounds. Compounds **2a–c** [44], **2d** [45], **4** [46], **7** [47], **14** [48], and **17** [49] are known compounds, which were prepared by using the reported procedures.

3.2. Synthesis and Characterization of Quinolones

4-Hydroxy-1-methyl-3-(4-methylphenyl)quinolin-2(1H)-one (**1b**) [42]. Compound **1b** (1.09 g, 82%) was prepared from *N*-methylisatoic anhydride (0.89 g, 5 mmol), methyl 4-methylphenylacetate (0.82 g, 5 mmol), and KHDMS (1.99 g, 10 mmol) as a colorless solid. Mp: 204–205 °C (MeOH). ^1H NMR (400 MHz, DMSO-d_6), δ , ppm: 2.35 (s, 3H), 3.60 (s, 3H), 7.20–7.29 (m, 5H), 7.50 (d, $J = 8.4$ Hz, 1H), 7.61–7.65 (m, 1H), 8.02–8.04 (m, 1H), 9.92 (s, 1H).

^{13}C NMR (100 MHz, DMSO- d_6), δ , ppm: 21.4, 29.7, 112.6, 114.8, 116.8, 121.7, 124.0, 128.9, 131.1, 131.3, 131.5, 136.5, 139.3, 156.5, 162.5. HRMS-ESI: $[\text{M}+\text{H}]^+$ calcd for $\text{C}_{17}\text{H}_{16}\text{NO}_2^+$ 266.1176, found 216.1187.

3-(4-Fluorophenyl)-4-hydroxy-1-methylquinolin-2(1H)-one (1d) [42]. Compound **1d** (0.89 g, 66%) was prepared from *N*-methylisatoic anhydride (0.89 g, 5 mmol), methyl 4-fluorophenylacetate (0.84 g, 5 mmol), and KHDMS (1.99 g, 10 mmol) as a colorless solid. Mp: 288–290 °C (MeOH). ^1H NMR (400 MHz, DMSO- d_6), δ , ppm: 3.61 (s, ^3H), 7.20–7.24 (m, ^2H), 7.28 (t, $J = 7.5$ Hz, ^1H), 7.36–7.39 (m, ^2H), 7.52 (d, $J = 8.4$ Hz, ^1H), 7.65 (d, $J = 7.5$ Hz, ^1H), 8.05 (d, $J = 7.7$ Hz, ^1H), 10.11 (s, ^1H). ^{13}C NMR (100 MHz, DMSO- d_6), δ , ppm: 29.7, 111.7, 114.9, 115.1 (d, $J = 21.2$ Hz), 116.7, 121.8, 124.0, 130.4 (d, $J = 3.2$ Hz), 131.5, 133.6 (d, $J = 8.1$ Hz), 139.4, 156.8, 161.8 (d, $J = 243.0$ Hz), 162.4. HRMS-ESI: $[\text{M}+\text{H}]^+$ calcd for $\text{C}_{16}\text{H}_{13}\text{FNO}_2^+$ 270.0925, found 270.0931.

3-(4-Chlorophenyl)-4-hydroxy-1-methylquinolin-2(1H)-one (1e) [42]. Compound **1e** (1.24 g, 87%) was prepared from *N*-methylisatoic anhydride (0.89 g, 5 mmol), methyl 4-chlorophenylacetate (0.92 g, 5 mmol), and KHDMS (1.99 g, 10 mmol) as a colorless solid. Mp: 279–281 °C (MeOH). ^1H NMR (400 MHz, DMSO- d_6), δ , ppm: 3.60 (s, 3H), 7.28 (t, $J = 7.5$ Hz, 1H), 7.37 (d, $J = 8.4$ Hz, 2H), 7.45 (d, $J = 8.4$ Hz, 2H), 7.51 (d, $J = 8.4$ Hz, ^1H), 7.65 (t, $J = 7.3$ Hz, 1H), 8.05 (d, $J = 7.5$ Hz, 1H), 10.21 (br. s, 1H). ^{13}C NMR (100 MHz, DMSO- d_6), δ , ppm: 29.7, 111.5, 114.9, 116.7, 121.9, 124.1, 128.2, 131.6, 132.1, 133.1, 133.5, 139.5, 156.9, 162.2. HRMS-ESI: $[\text{M}+\text{H}]^+$ calcd for $\text{C}_{16}\text{H}_{13}^{35}\text{ClNO}_2^+$ 286.0629, found 286.0639.

4-Hydroxy-1-methyl-3-(4-nitrophenyl)quinolin-2(1H)-one (1f) [42]. Compound **1f** (0.77 g, 52%) was prepared from *N*-methylisatoic anhydride (0.89 g, 5 mmol), methyl 4-nitrophenylacetate (0.98 g, 5 mmol), and KHDMS (1.99 g, 10 mmol) as a colorless solid. Mp: 339–340 °C (MeOH). ^1H NMR (400 MHz, DMSO- d_6), δ , ppm: 3.62 (s, 3H), 7.32 (t, $J = 7.5$ Hz, 1H), 7.56 (d, $J = 8.5$ Hz, 1H), 7.67–7.71 (m, 3H), 8.10 (d, $J = 7.9$ Hz, 1H), 8.26 (d, $J = 8.5$ Hz, 2H), 10.61 (br. s, 1H). ^{13}C NMR (100 MHz, DMSO- d_6), δ , ppm: 29.3, 110.9, 114.5, 116.4, 121.5, 122.6, 123.9, 131.6, 132.6, 139.5, 141.8, 146.5, 157.3, 161.5. HRMS-ESI: $[\text{M}+\text{H}]^+$ calcd for $\text{C}_{16}\text{H}_{13}\text{N}_2\text{O}_4^+$ 297.0870, found 297.0885.

4-Hydroxy-1-methyl-3-(thiophen-2-yl)quinolin-2(1H)-one (1g) [42]. Compound **1g** (0.71 g, 55%) was prepared from *N*-methylisatoic anhydride (0.89 g, 5 mmol), methyl (thiophen-2-yl)acetate (0.78 g, 5 mmol), and KHDMS (1.99 g, 10 mmol) as a colorless solid. Mp: 175–176 °C (MeOH). ^1H NMR (400 MHz, DMSO- d_6), δ , ppm: 3.68 (s, 3H), 7.13 (dd, $J = 5.1$ and 3.8 Hz, 1H), 7.33 (t, $J = 7.2$ Hz, 1H), 7.52 (dd, $J = 5.2$ and 1.0 Hz, 1H), 7.56 (d, $J = 8.3$ Hz, 1H), 7.64–7.68 (m, 1H), 8.01 (dd, $J = 3.7$ and 1.0 Hz, 1H), 8.17 (dd, $J = 8.1$ and 1.0 Hz, 1H), 11.08 (br. s, 1H). ^{13}C NMR (100 MHz, DMSO- d_6), δ , ppm: 30.1, 107.0, 115.1, 116.4, 122.1, 123.9, 126.2, 126.6, 128.7, 131.5, 135.1, 138.4, 156.4, 161.6. HRMS-ESI: $[\text{M}+\text{H}]^+$ calcd for $\text{C}_{14}\text{H}_{12}\text{NO}_2\text{S}^+$ 258.0583, found 258.0595.

5-Chloro-4-hydroxy-1-methyl-3-phenylquinolin-2(1H)-one (1h) [42]. Compound **1h** (1.05 g, 74%) was prepared from *N*-methyl-5-chloroisatoic anhydride (1.06 g, 5 mmol), methyl phenylacetate (0.75 g, 5 mmol), and KHDMS (1.99 g, 10 mmol) as a colorless solid. Mp: 208–209 °C (MeOH). ^1H NMR (400 MHz, DMSO- d_6), δ , ppm: 3.61 (s, 3H), 7.31–7.57 (m, 8H), 9.78 (s, 1H). ^{13}C NMR (100 MHz, DMSO- d_6), δ , ppm: 30.7, 114.3, 114.6, 114.8, 125.7, 127.8, 128.5, 131.1 (2C), 131.7, 133.6, 141.8, 157.0, 161.6. HRMS-ESI: $[\text{M}+\text{H}]^+$ calcd for $\text{C}_{16}\text{H}_{13}^{35}\text{ClNO}_2^+$ 286.0629, found 286.0636.

6-Chloro-4-hydroxy-1-methyl-3-phenylquinolin-2(1H)-one (1i) [42]. Compound **1i** (0.97 g, 68%) was prepared from *N*-methyl-6-chloroisatoic anhydride (1.06 g, 5 mmol), methyl phenylacetate (0.75 g, 5 mmol), and KHDMS (1.99 g, 10 mmol) as a colorless solid. Mp: 265–267 °C (MeOH). ^1H NMR (400 MHz, DMSO- d_6), δ , ppm: 3.59 (s, 3H), 7.31–7.35 (m, 3H), 7.39–7.43 (m, 2H), 7.53 (d, $J = 9.1$ Hz, 1H), 7.65 (dd, $J = 9.0$ and 2.4 Hz, 1H), 8.02 (d, $J = 2.4$ Hz, 1H), 10.28 (br. s, 1H). ^{13}C NMR (100 MHz, DMSO- d_6), δ , ppm: 29.9, 113.8, 117.0, 118.2, 123.1, 126.2, 127.6, 128.2, 131.0, 131.5, 133.8, 138.2, 155.6, 162.2. HRMS-ESI: $[\text{M}+\text{H}]^+$ calcd for $\text{C}_{16}\text{H}_{13}^{35}\text{ClNO}_2^+$ 286.0629, found 286.0640.

7-Chloro-4-hydroxy-1-methyl-3-phenylquinolin-2(1H)-one (1j) [42]. Compound **1j** (1.0 g, 70%) was prepared from *N*-methyl-7-chloroisatoic anhydride (1.06 g, 5 mmol), methyl

phenylacetate (0.75 g, 5 mmol), and KHDMS (1.99 g, 10 mmol) as a colorless solid. Mp: 230–231 °C (MeOH). ¹H NMR (400 MHz, DMSO-d₆), δ, ppm: 3.58 (s, 3H), 7.29–7.35 (m, 4H), 7.39–7.43 (m, 2H), 7.57 (d, *J* = 1.7 Hz, 1H), 8.02 (d, *J* = 8.6 Hz, 1H), 10.22 (s, 1H). ¹³C NMR (100 MHz, DMSO-d₆), δ, ppm: 29.9, 113.0, 114.5, 115.7, 121.8, 125.9, 127.6, 128.3, 131.6, 133.8, 136.1, 140.4, 156.2, 162.4. HRMS-ESI: [M+H]⁺ calcd for C₁₆H₁₃³⁵ClNO₂⁺ 286.0629, found 286.0638.

8-Chloro-4-hydroxy-1-methyl-3-phenylquinolin-2(1H)-one (1k) [42]. Compound **1k** (0.87 g, 61%) was prepared from *N*-methyl-8-chloroisatoic anhydride (1.06 g, 5 mmol), methyl phenylacetate (0.75 g, 5 mmol), and KHDMS (1.99 g, 10 mmol) as a colorless solid. Mp: 238–239 °C (MeOH). ¹H NMR (400 MHz, DMSO-d₆), δ, ppm: 3.77 (s, 3H), 7.25 (t, *J* = 7.9 Hz, 1H), 7.31–7.43 (m, 5H), 7.69 (d, *J* = 7.7 Hz, 1H), 8.02 (d, *J* = 7.8 Hz, 1H), 10.32 (br. s, 1H). ¹³C NMR (100 MHz, DMSO-d₆), δ, ppm: 37.3, 113.0, 119.8, 121.0, 123.1, 123.6, 127.6, 128.3, 131.5, 133.7, 134.4, 137.8, 156.5, 164.2. HRMS-ESI: [M+Na]⁺ calcd for C₁₆H₁₂³⁵ClNNaO₂⁺ 308.0449, found 308.0461.

3.3. Synthesis of Pyrrolo[3,2-*c*]quinolin-4-ones **3**

General procedure. Quinolone **1a–m** (0.2 mmol), Cu(Oac)₂·H₂O (2 mg, 0.01 mmol), azirine **2** (0.32 mmol), and MeOH (3 mL) (or DCE for compound **3p**) were placed consequently into a screw-cap glass tube and heated at 100 °C for 15–20 min under stirring until full consumption of the quinolinone **1** was detected (control by TLC). The solvent was removed in vacuo and the residue was purified by column chromatography on silica gel (eluent hexane/EtOAc from 2:1 to 1:2) followed by recrystallization from hexane/CHCl₃ to produce adduct **3** as pure crystals (compounds **3c** and **3l**) or as solvates with chloroform (compounds **3a,b,d–k,m–p**).

*rac-(3aR,9bR)-9b-Hydroxy-3a-(4-methoxyphenyl)-5-methyl-2-(4-methylphenyl)-3,3a,5,9b-tetrahydro-4H-pyrrolo[3,2-*c*]quinolin-4-one (3a)*. Colorless solid (**3a** × 0.48CHCl₃, 91 mg, 97%). Mp: 144–145 °C (CHCl₃/hexane). ¹H NMR (400 MHz, DMSO-d₆), δ, ppm: 2.36 (s, 3H), 3.25 (s, 3H), 3.67 (s, 3H), 3.78 (d, *J* = 16.1 Hz, 1H), 4.27 (d, *J* = Hz, 1H), 6.17 (s, 1H), 6.78 (d, *J* = 8.8 Hz, 2H), 7.12 (d, *J* = 8.8 Hz, 2H), 7.20 (d, *J* = 8.1 Hz, 1H), 7.25–7.30 (m, 3H), 7.43–7.48 (m, 1H), 7.83 (d, *J* = 8.1 Hz, 2H), 7.96 (dd, *J* = 7.6 and 1.3 Hz, 1H). ¹³C NMR (100 MHz, DMSO-d₆), δ, ppm: 21.5, 30.5, 44.2, 55.4, 60.9, 97.5, 113.8, 115.0, 123.7, 127.2, 128.4 (2C), 129.4, 129.7, 129.9, 130.0, 131.3, 138.3, 142.0, 158.7, 171.5, 175.6. HRMS-ESI: [M+H]⁺ calcd for C₂₆H₂₅N₂O₃⁺ 413.1860, found 413.1858.

*rac-(3aR,9bR)-9b-Hydroxy-5-methyl-2,3a-di(4-methylphenyl)-3,3a,5,9b-tetrahydro-4H-pyrrolo[3,2-*c*]quinolin-4-one (3b)*. Colorless solid (**3b** × 1.47CHCl₃, 112 mg, 98%). Mp: 178–179 °C (CHCl₃/hexane). ¹H NMR (400 MHz, DMSO-d₆), δ, ppm: 2.21 (s, 3H), 2.36 (s, 3H), 3.25 (s, 3H), 3.82 (d, *J* = 16.1 Hz, 1H), 4.29 (d, *J* = 16.1 Hz, 1H), 6.19 (s, 1H), 7.02 (d, *J* = 7.6 Hz, 2H), 7.10 (d, *J* = 7.6 Hz, 2H), 7.19 (d, *J* = 8.0 Hz, 1H), 7.28–7.30 (m, 3H), 7.45 (t, *J* = 7.2 Hz, 1H), 7.85 (d, *J* = 7.6 Hz, 2H), 7.98 (d, *J* = 7.2 Hz, 1H). ¹³C NMR (100 MHz, DMSO-d₆), δ, ppm: 21.0, 21.5, 30.5, 44.1, 61.3, 97.5, 115.0, 123.6, 127.2, 128.2, 128.4 (2C), 128.9, 129.7, 129.9, 131.3, 135.0, 136.6, 138.3, 142.0, 171.4, 175.6. HRMS-ESI: [M+H]⁺ calcd for C₂₆H₂₅N₂O₂⁺ 397.1911, found 397.1914.

*rac-(3aR,9bR)-9b-Hydroxy-5-methyl-2-(4-methylphenyl)-3a-phenyl-3,3a,5,9b-tetrahydro-4H-pyrrolo[3,2-*c*]quinolin-4-one (3c)*. Pale-yellow solid (76 mg, 99%). Mp: 165–167 °C (CHCl₃/Et₂O). ¹H NMR (400 MHz, CDCl₃), δ, ppm: 2.44 (s, 3H), 3.33 (br. s, 3H), 3.53–3.57 (m, 1H), 4.11 (br. s, 1H), 4.27–4.29 (m, 1H), 7.10–7.49 (m, 10H), 7.44–7.53 (m, 1H), 7.67–7.80 (m, 1H), 8.06–8.09 (m, 1H). ¹³C NMR (100 MHz, CDCl₃), δ, ppm: 21.5, 30.4, 44.1, 61.4, 97.7, 114.4, 123.8, 127.0, 127.6 (2C), 128.4 (3C), 129.1, 129.9, 130.1, 136.6, 138.0, 142.5, 170.9, 177.6. HRMS-ESI: [M+H]⁺ calcd for C₂₅H₂₃N₂O₂⁺ 383.1754, found 383.1748.

*rac-(3aR,9bR)-3a-(4-Fluorophenyl)-9b-hydroxy-5-methyl-2-(4-methylphenyl)-3,3a,5,9b-tetrahydro-4H-pyrrolo[3,2-*c*]quinolin-4-one (3d)*. Colorless solid (**3d** × 0.56CHCl₃, 91 mg, 98%). Mp: 148–149 °C (CHCl₃/hexane). ¹H NMR (400 MHz, DMSO-d₆), δ, ppm: 2.36 (s, 3H), 3.26 (s, 3H), 3.82 (d, *J* = 16.2 Hz, 1H), 4.30 (d, *J* = 16.2 Hz, 1H), 6.29 (s, 1H), 7.06 (t, *J* = 8.9 Hz, 2H), 7.21–7.30 (m, 6H), 7.44–7.49 (m, 1H), 7.84 (d, *J* = 8.1 Hz, 2H), 7.97 (dd, *J* = 7.6 and

1.4 Hz, 1H). ^{13}C NMR (100 MHz, DMSO- d_6), δ , ppm: 21.5, 30.6, 44.5, 61.0, 97.5, 115.1 (d, $J = 21.1$ Hz), 115.2, 123.8, 127.2, 128.2, 128.4, 129.7, 130.0, 130.3 (d, $J = 8.0$ Hz), 131.1, 134.3 (d, $J = 3.1$ Hz), 138.1, 142.1, 161.7 (d, $J = 243.7$ Hz), 171.1, 175.5. HRMS-ESI: $[\text{M}+\text{H}]^+$ calcd for $\text{C}_{25}\text{H}_{22}\text{FN}_2\text{O}_2^+$ 401.1660, found 401.1655.

rac-(3*aR*,9*bR*)-3*a*-(4-Chlorophenyl)-9*b*-hydroxy-5-methyl-2-(4-methylphenyl)-3,3*a*,5,9*b*-tetrahydro-4*H*-pyrrolo[3,2-*c*]quinolin-4-one (**3e**). Colorless solid (**3e** \times 0.45 CHCl_3 , 93 mg, 99%). Mp: 202–203 °C (CHCl_3 /hexane). ^1H NMR (400 MHz, DMSO- d_6), δ , ppm: 2.35 (s, 3H), 3.27 (s, 3H), 3.84 (d, $J = 16.2$ Hz, 1H), 4.29 (d, $J = 16.2$ Hz, 1H), 6.33 (s, 1H), 7.21–7.31 (m, 8H), 7.44–7.48 (m, 1H), 7.84 (d, $J = 8.1$ Hz, 2H), 7.97 (dd, $J = 7.6$ and 1.4 Hz, 1H). ^{13}C NMR (100 MHz, DMSO- d_6), δ , ppm: 21.5, 30.7, 44.4, 61.2, 97.5, 115.2, 123.9, 127.2, 128.1, 128.4 (2C), 129.7, 130.0, 130.2, 131.1, 132.3, 137.0, 138.1, 142.2, 170.9, 175.4. HRMS-ESI: $[\text{M}+\text{H}]^+$ calcd for $\text{C}_{25}\text{H}_{22}^{35}\text{ClN}_2\text{O}_2^+$ 417.1364, found 417.1369.

rac-(3*aR*,9*bR*)-9*b*-Hydroxy-5-methyl-2-(4-methylphenyl)-3*a*-(4-nitrophenyl)-3,3*a*,5,9*b*-tetrahydro-4*H*-pyrrolo[3,2-*c*]quinolin-4-one (**3f**). Colorless solid (**3f** \times 0.39 CHCl_3 , 80 mg, 85%). Mp: 186–187 °C (CHCl_3 /hexane). ^1H NMR (400 MHz, DMSO- d_6), δ , ppm: 2.36 (s, 3H), 3.29 (s, 3H), 3.93 (d, $J = 16.3$ Hz, 1H), 4.33 (d, $J = 16.3$ Hz, 1H), 6.48 (s, 1H), 7.25–7.32 (m, 4H), 7.46–7.51 (m, 3H), 7.84 (d, $J = 8.1$ Hz, 2H), 7.96 (dd, $J = 7.7$ and 1.4 Hz, 1H), 8.11 (d, $J = 8.9$ Hz, 2H). ^{13}C NMR (100 MHz, DMSO- d_6), δ , ppm: 21.5, 30.8, 44.6, 61.9, 97.7, 115.4, 123.5, 124.1, 127.3, 127.8, 128.5, 129.7, 129.8, 130.2, 130.9, 137.9, 142.3, 145.5, 147.0, 170.2, 175.2. HRMS-ESI: $[\text{M}+\text{H}]^+$ calcd for $\text{C}_{25}\text{H}_{22}\text{N}_3\text{O}_4^+$ 428.1605, found 428.1608.

rac-(3*aR*,9*bR*)-9*b*-Hydroxy-5-methyl-2-(4-methylphenyl)-3*a*-(thiophen-2-yl)-3,3*a*,5,9*b*-tetrahydro-4*H*-pyrrolo[3,2-*c*]quinolin-4-one (**3g**). Colorless solid (**3g** \times 0.49 CHCl_3 , 82 mg, 92%). Mp: 112–114 °C (CHCl_3 /hexane). ^1H NMR (400 MHz, DMSO- d_6), δ , ppm: 2.36 (s, 3H), 3.28 (s, 3H), 3.77 (d, $J = 15.9$ Hz, 1H), 4.28 (d, $J = 15.9$ Hz, 1H), 6.35 (s, 1H), 6.82 (d, $J = 3.1$ Hz, 1H), 6.87–6.89 (m, 1H), 7.21–7.32 (m, 5H), 7.46 (t, $J = 7.2$ Hz, 1H), 7.81 (d, $J = 8.0$ Hz, 2H), 7.93 (d, $J = 7.5$ Hz, 1H). ^{13}C NMR (100 MHz, DMSO- d_6), δ , ppm: 21.5, 30.7, 45.0, 59.2, 97.6, 115.1, 123.8, 125.7, 126.3, 126.6, 127.3, 127.8, 128.4, 129.7, 130.1, 131.0, 138.2, 139.7, 142.2, 170.0, 176.1. HRMS-ESI: $[\text{M}+\text{H}]^+$ calcd for $\text{C}_{23}\text{H}_{21}\text{N}_2\text{O}_2\text{S}^+$ 389.1318, found 389.1333.

rac-(3*aR*,9*bS*)-9-Chloro-9*b*-hydroxy-5-methyl-2-(4-methylphenyl)-3*a*-phenyl-3,3*a*,5,9*b*-tetrahydro-4*H*-pyrrolo[3,2-*c*]quinolin-4-one (**3h**). Colorless solid (**3h** \times 0.60 CHCl_3 , 78 mg, 80%). Mp: 146–148 °C (CHCl_3 /hexane). ^1H NMR (400 MHz, DMSO- d_6), δ , ppm: 2.37 (s, 3H), 3.25 (s, 3H), 3.73 (d, $J = 16.4$ Hz, 1H), 4.29 (d, $J = 16.4$ Hz, 1H), 5.86 (s, 1H), 7.21–7.33 (m, 9H), 7.44 (t, $J = 8.2$ Hz, 1H), 7.87 (d, $J = 8.1$ Hz, 2H). ^{13}C NMR (100 MHz, DMSO- d_6), δ , ppm: 21.6, 31.6, 43.2, 62.5, 98.4, 114.8, 125.5, 126.9, 127.4, 128.4, 128.5 (2C), 129.7, 130.5, 131.0, 134.3, 138.7, 141.0, 142.3, 170.8, 176.2. HRMS-ESI: $[\text{M}+\text{H}]^+$ calcd for $\text{C}_{25}\text{H}_{22}^{35}\text{ClN}_2\text{O}_2^+$ 417.1364, found 417.1372.

rac-(3*aR*,9*bR*)-8-Chloro-9*b*-hydroxy-5-methyl-2-(4-methylphenyl)-3*a*-phenyl-3,3*a*,5,9*b*-tetrahydro-4*H*-pyrrolo[3,2-*c*]quinolin-4-one (**3i**). Colorless solid (**3i** \times 0.67 CHCl_3 , 98 mg, 99%). Mp: 124–126 °C (CHCl_3 /hexane). Compound **3i** can be obtained as a solvate with DMSO- d_6 by evaporation solution in DMSO- d_6 with identical NMR spectra. ^1H NMR (400 MHz, DMSO- d_6), δ , ppm: 2.36 (s, 3H), 3.25 (s, 3H), 3.86 (d, $J = 16.3$ Hz, 1H), 4.27 (d, $J = 16.3$ Hz, 1H), 6.41 (s, 1H), 7.17–7.31 (m, 8H), 7.52 (dd, $J = 8.7$ and 2.6 Hz, 1H), 7.84 (d, $J = 8.1$ Hz, 2H), 7.91 (d, $J = 2.6$ Hz, 1H). ^{13}C NMR (100 MHz, DMSO- d_6), δ , ppm: 21.5, 30.7, 44.2, 61.5, 97.1, 117.2, 126.8, 127.6, 128.0, 128.3, 128.5 (2C), 129.6, 129.7, 130.5, 131.0, 137.2, 137.6, 142.3, 171.1, 176.1. HRMS-ESI: $[\text{M}+\text{H}]^+$ calcd for $\text{C}_{25}\text{H}_{22}^{35}\text{ClN}_2\text{O}_2^+$ 417.1364, found 417.1376.

rac-(3*aR*,9*bR*)-7-Chloro-9*b*-hydroxy-5-methyl-2-(4-methylphenyl)-3*a*-phenyl-3,3*a*,5,9*b*-tetrahydro-4*H*-pyrrolo[3,2-*c*]quinolin-4-one (**3j**). Colorless solid (**3j** \times 0.47 CHCl_3 , 90 mg, 95%). Mp: 120–121 °C (CHCl_3 /hexane). ^1H NMR (400 MHz, DMSO- d_6), δ , ppm: 2.36 (s, 3H), 3.27 (s, 3H), 3.88 (d, $J = 16.2$ Hz, 1H), 4.29 (d, $J = 16.2$ Hz, 1H), 6.36 (s, 1H), 7.22–7.36 (m, 9H), 7.85 (d, $J = 7.7$ Hz, 2H), 7.96 (d, $J = 8.2$ Hz, 1H). ^{13}C NMR (100 MHz, DMSO- d_6), δ , ppm: 21.5, 30.7, 44.2, 61.6, 97.2, 115.1, 123.5, 127.3, 127.6, 128.3, 128.4, 128.5, 128.9, 129.7, 131.0, 134.4, 137.7, 139.6, 142.2, 171.5, 175.8. HRMS-ESI: $[\text{M}+\text{H}]^+$ calcd for $\text{C}_{25}\text{H}_{22}^{35}\text{ClN}_2\text{O}_2^+$ 417.1364, found 417.1374.

rac-(3*aR*,9*bR*)-6-Chloro-9*b*-hydroxy-5-methyl-2-(4-methylphenyl)-3*a*-phenyl-3,3*a*,5,9*b*-tetrahydro-4*H*-pyrrolo[3,2-*c*]quinolin-4-one (**3k**). Colorless solid (**3k** × 0.68CHCl₃, 98 mg, 99%). Mp: 170–171 °C (CHCl₃/hexane). ¹H NMR (400 MHz, DMSO-*d*₆), δ, ppm: 2.37 (s, 3H), 3.29 (s, 3H), 3.79 (d, *J* = 15.9 Hz, 1H), 4.31 (d, *J* = 15.9 Hz, 1H), 6.50 (s, 1H), 7.13–7.34 (m, 8H), 7.55 (d, *J* = 7.4 Hz, 1H), 7.85–7.90 (m, 3H). ¹³C NMR (100 MHz, DMSO-*d*₆), δ, ppm: 21.6, 38.1, 44.7, 62.3, 97.2, 122.1, 126.1, 126.2, 127.6, 128.2, 128.4, 128.5, 129.7, 131.2, 132.3, 134.1, 136.2, 137.2, 142.3, 173.3, 177.4. HRMS-ESI: [M+H]⁺ calcd for C₂₅H₂₂³⁵CIN₂O₂⁺ 417.1364, found 417.1372.

rac-(3*aR*,9*bR*)-5-Benzyl-9*b*-hydroxy-2-(4-methylphenyl)-3*a*-phenyl-3,3*a*,5,9*b*-tetrahydro-4*H*-pyrrolo[3,2-*c*]quinolin-4-one (**3l**). Colorless solid (87 mg, 95%). Mp: 173–175 °C (CHCl₃/hexane). ¹H NMR (400 MHz, DMSO-*d*₆), δ, ppm: 2.38 (s, 3H), 3.92 (d, *J* = 16.0 Hz, 1H), 4.34 (d, *J* = 16.0 Hz, 1H), 5.17 (s, 2H), 6.33 (s, 1H), 6.91–6.93 (m, 2H), 7.07–7.12 (m, 4H), 7.21–7.34 (m, 9H), 7.88 (d, *J* = 8.1 Hz, 2H), 7.98 (dd, *J* = 7.6 and 1.5 Hz, 1H). ¹³C NMR (100 MHz, DMSO-*d*₆), δ, ppm: 21.6, 44.2, 45.3, 61.9, 97.4, 115.7, 123.9, 126.5, 127.2 (2C), 127.6, 128.4 (2C), 128.5, 128.8, 129.0, 129.7, 129.8, 131.4, 137.1, 137.2, 137.8, 142.1, 171.8, 176.1. HRMS-ESI: [M+Na]⁺ calcd for C₃₁H₂₆N₂NaO₂⁺ 481.1886, found 481.1896.

rac-(8*aR*,11*aR*)-11*a*-Hydroxy-10-(4-methylphenyl)-8*a*-phenyl-5,6,9,11*a*-tetrahydro-4*H*-pyrrolo[3,2-*c*]quinolin-8(8*aH*)-one (**3m**). Colorless solid (**3m** × 1.20CHCl₃, 106 mg, 96%). Mp: 187–188 °C (CHCl₃/MeOH). ¹H NMR (400 MHz, DMSO-*d*₆), δ, ppm: 1.79 (s, 2H), 2.36 (s, 3H), 2.81 (br. s, 2H), 3.43–3.45 (m, 1H), 3.85 (d, *J* = 16.1 Hz, 1H), 3.99–4.02 (m, 1H), 4.29 (d, *J* = 16.1 Hz, 1H), 6.15 (s, 1H), 7.15–7.30 (m, 9H), 7.78–7.86 (m, 3H). ¹³C NMR (100 MHz, DMSO-*d*₆), δ, ppm: 21.1, 21.6, 27.5, 42.3, 44.0, 61.3, 97.6, 123.2, 125.0, 125.3, 127.4, 128.1, 128.3, 128.4 (2C), 129.7, 130.2, 131.3, 134.0, 138.2, 142.0, 170.6, 175.4. HRMS-ESI: [M+H]⁺ calcd for C₂₇H₂₅N₂O₂⁺ 409.1911, found 409.1916.

rac-(3*aR*,9*bR*)-9*b*-Hydroxy-5-methyl-2,3*a*-diphenyl-3,3*a*,5,9*b*-tetrahydro-4*H*-pyrrolo[3,2-*c*]quinolin-4-one (**3n**). Colorless solid (**3n** × 0.26CHCl₃, 79 mg, 99%). Mp: 174–175 °C (CHCl₃/hexane). ¹H NMR (400 MHz, DMSO-*d*₆), δ, ppm: 3.27 (s, 3H), 3.89 (d, *J* = 16.2 Hz, 1H), 4.32 (d, *J* = 16.2 Hz, 1H), 6.26 (s, 1H), 7.22–7.31 (m, 7H), 7.45–7.55 (m, 4H), 7.95–7.98 (m, 3H). ¹³C NMR (100 MHz, DMSO-*d*₆), δ, ppm: 30.6, 44.2, 61.6, 97.6, 115.1, 123.8, 127.1, 127.5, 128.3, 128.4 (3C), 129.1, 130.0, 132.1, 133.8, 138.0, 138.2, 171.2, 175.7. HRMS-ESI: [M+H]⁺ calcd for C₂₄H₂₁N₂O₂⁺ 369.1598, found 369.1592.

rac-(3*aR*,9*bR*)-9*b*-Hydroxy-2-(4-methoxyphenyl)-5-methyl-3*a*-phenyl-3,3*a*,5,9*b*-tetrahydro-4*H*-pyrrolo[3,2-*c*]quinolin-4-one (**3o**). Colorless solid (**3o** × 0.51CHCl₃, 83 mg, 91%). Mp: 99–100 °C (CHCl₃/hexane). ¹H NMR (400 MHz, DMSO-*d*₆), δ, ppm: 3.26 (s, 3H), 3.78–3.82 (m, 4H), 4.26 (d, *J* = 16.1 Hz, 1H), 6.16 (s, 1H), 7.02 (d, *J* = 8.8 Hz, 2H), 7.19–7.29 (m, 7H), 7.44–7.48 (m, 1H), 7.88–7.94 (m, 3H). ¹³C NMR (100 MHz, DMSO-*d*₆), δ, ppm: 30.6, 44.0, 55.9, 61.7, 97.4, 114.5, 115.1, 123.7, 126.5, 127.1, 127.4, 128.4 (2C), 128.5, 129.9, 130.2, 138.1, 138.2, 162.4, 171.3, 175.0. HRMS-ESI: [M+H]⁺ calcd for C₂₅H₂₃N₂O₃⁺ 399.1703, found 399.1693.

rac-(3*aR*,9*bR*)-9*b*-Hydroxy-5-methyl-2-(4-nitrophenyl)-3*a*-phenyl-3,3*a*,5,9*b*-tetrahydro-4*H*-pyrrolo[3,2-*c*]quinolin-4-one (**3p**). Compound **3p** was prepared according to the general procedure using DCE as a solvent. Colorless solid (**3p** × 0.45CHCl₃, 81 mg, 87%). Mp: 101–102 °C (CHCl₃/hexane). ¹H NMR (400 MHz, DMSO-*d*₆), δ, ppm: 3.27 (s, 3H), 3.96 (d, *J* = 16.5 Hz, 1H), 4.34 (d, *J* = 16.5 Hz, 1H), 6.40 (s, 1H), 7.21–7.31 (m, 7H), 7.47–7.51 (m, 1H), 7.95–7.98 (m, 1H), 8.20 (d, *J* = 8.8 Hz, 2H), 8.31–8.33 (m, 2H). ¹³C NMR (100 MHz, DMSO-*d*₆), δ, ppm: 30.7, 44.5, 61.7, 97.9, 115.2, 123.9, 124.3, 127.2, 127.6, 127.7, 128.3, 128.5, 129.7, 130.2, 137.6, 138.3, 139.3, 149.6, 171.0, 174.6. HRMS-ESI: [M+H]⁺ calcd for C₂₄H₂₀N₃O₄⁺ 414.1448, found 414.1440.

3.4. Synthesis of Chromenopyrroles **6**

General procedure. Hydroxycoumarin **4** (0.2 mmol), Cu(Oac)₂ × H₂O (2 mg, 0.01 mmol), azirine **2** (0.32 mmol), and DCE (3.0 mL) were consequently placed into a screw-cap glass tube and heated at 100 °C for 20–30 min until the full consumption of 3-hydroxycoumarin **4** was detected (control by TLC). The solvent was removed in vacuo and the residue was

purified by column chromatography on silica gel (eluent hexane/EtOAc from 2:1 to 1:2), followed by recrystallization from a hexane–Et₂O mixture to produce compound **6**.

Methyl rac-(3aR,9bR)-3a-hydroxy-2-(4-methylphenyl)-4-oxo-3a,4-dihydrochromeno[3,4-b]pyrrole-9b(1H)-carboxylate (6a). Colorless solid (47 mg, 67%). Mp: 203–204 °C (Et₂O/hexane). ¹H NMR (400 MHz, DMSO-d₆), δ, ppm: 2.32 (s, 3H), 3.59 (s, 3H), 4.02 and 3.88 (AB-q, J = 17.2 Hz, 2H), 7.11 (d, J = 8.1 Hz, 1H), 7.18 (t, J = 7.4 Hz, 1H), 7.26 (d, J = 7.9 Hz, 2H), 7.34 (t, J = 7.4 Hz, 1H), 7.46 (d, J = 7.5 Hz, 1H), 7.59 (s, 1H), 7.78 (d, J = 8.0 Hz, 2H). ¹³C NMR (100 MHz, DMSO-d₆), δ, ppm: 21.6, 44.6, 53.2, 60.8, 95.5, 117.4, 122.7, 125.8, 128.3, 128.7, 129.8, 130.0, 130.7, 143.3, 150.3, 166.2, 169.7, 179.8. HRMS-ESI: [M-H]⁻ calcd for C₂₀H₁₆NO₅⁻ 350.1034, found 350.1039.

Methyl rac-(3aR,9bR)-3a-hydroxy-4-oxo-2-phenyl-3a,4-dihydrochromeno[3,4-b]pyrrole-9b(1H)-carboxylate (6b). Colorless solid (47 mg, 70%). Mp: 171–172 °C (Et₂O/hexane). ¹H NMR (400 MHz, DMSO-d₆), δ, ppm: 3.59 (s, 3H), 3.92 and 4.07 (AB-q, J = 17.3 Hz, 2H), 7.12 (dd, J = 8.2 and 1.0 Hz, 1H), 7.19 (td, J = 7.6 and 1.1 Hz, 1H), 7.32–7.36 (m, 1H), 7.43–7.48 (m, 3H), 7.54 (t, J = 7.4 Hz, 1H), 7.66 (s, 1H), 7.88–7.90 (m, 2H). ¹³C NMR (100 MHz, DMSO-d₆), δ, ppm: 44.7, 53.3, 60.9, 95.5, 117.4, 122.6, 125.8, 128.3, 128.7, 129.3, 130.7, 132.6, 133.0, 150.3, 166.1, 169.7, 180.1. HRMS-ESI: [M+H]⁺ calcd for C₁₉H₁₆NO₅⁺ 338.1023, found 338.1039.

Methyl rac-(3aR,9bR)-3a-hydroxy-2-(4-methoxyphenyl)-4-oxo-3a,4-dihydrochromeno[3,4-b]pyrrole-9b(1H)-carboxylate (6c). Colorless solid (44 mg, 60%). Mp: 199–200 °C (Et₂O/hexane). ¹H NMR (400 MHz, DMSO-d₆), δ, ppm: 3.58 (s, 3H), 3.79 (s, 3H), 3.87 and 4.00 (AB-q, J = 17.1 Hz, 2H), 6.98 (d, J = 8.6 Hz, 2H), 7.11 (d, J = 8.1 Hz, 1H), 7.18 (t, J = 7.4 Hz, 1H), 7.34 (t, J = 7.5 Hz, 1H), 7.45 (d, J = 7.6 Hz, 1H), 7.52 (s, 1H), 7.84 (d, J = 8.6 Hz, 2H). ¹³C NMR (100 MHz, DMSO-d₆), δ, ppm: 44.5, 53.2, 55.9, 60.9, 95.4, 114.6, 117.4, 122.8, 125.3, 125.7, 128.3, 130.6, 130.7, 150.3, 163.1, 166.3, 169.8, 179.2. HRMS-ESI: [M+H]⁺ calcd for C₂₀H₁₈NO₆⁺ 368.1129, found 368.1138.

Methyl rac-(3aR,9bR)-3a-hydroxy-2-(4-nitrophenyl)-4-oxo-3a,4-dihydrochromeno[3,4-b]pyrrole-9b(1H)-carboxylate (6d). Colorless solid (47 mg, 62%). Mp: 190–191 °C (Et₂O/hexane). ¹H NMR (400 MHz, DMSO-d₆), δ, ppm: 3.61 (s, 3H), 3.99 and 4.16 (AB-q, J = 17.5 Hz, 2H), 7.13 (dd, J = 8.2 and 1.0 Hz, 1H), 7.20 (td, J = 7.7 and 1.1 Hz, 1H), 7.34–7.38 (m, 1H), 7.47 (dd, J = 7.8 and 1.3 Hz, 1H), 7.86 (s, 1H), 8.13 (d, J = 8.9 Hz, 2H), 8.27 (d, J = 8.9 Hz, 2H). ¹³C NMR (100 MHz, DMSO-d₆), δ, ppm: 45.1, 53.4, 61.0, 95.6, 117.5, 122.2, 124.3, 125.9, 128.4, 130.1, 130.9, 138.0, 150.1, 150.2, 165.8, 169.5, 178.9. HRMS-ESI: [M-H]⁻ calcd for C₁₉H₁₃N₂O₇⁻ 381.0728, found 381.0720.

3.5. Synthesis of Methyl Rac-(7aR,10aR)-7a-hydroxy-9-(4-methylphenyl)-7oxo-7a,10-dihydronaphtho[1,8-ef]indole-10a(7H)-carboxylate (**8**)

Enol **7** (51 mg, 0.2 mmol), Cu(hfacac)₂ (10 mg, 0.02 mmol), azirine **2a** (42 mg, 0.32 mmol), and DCE (3.0 mL) were consequently placed into a screw-cap glass tube and heated at 100 °C for 2.5 h until the full consumption of enol **7** was detected (control by TLC). The solvent was removed in vacuo and the residue was purified by column chromatography on silica gel (eluent hexane/EtOAc from 2:1 to 1:2). Yellow solid (46 mg, 60%). Mp: 208–209 °C (Et₂O/hexane). ¹H NMR (400 MHz, CDCl₃–DMSO-d₆ mixture), δ, ppm: 2.26 (s, 3H), 3.49 (s, 3H), 3.83 (d, J = 16.9 Hz, 1H), 4.32 (d, J = 16.9 Hz, 1H), 5.82 (s, 1H), 7.07 (d, J = 7.9 Hz, 2H), 7.48–7.52 (m, 1H), 7.60–7.64 (m, 4H), 7.80–7.82 (m, 1H), 8.08–8.10 (m, 1H), 8.32–8.34 (m, 1H). ¹³C NMR (100 MHz, CDCl₃–DMSO-d₆ mixture), δ, ppm: 20.7, 46.0, 51.9, 63.0, 97.0, 125.4, 125.8, 125.9, 126.3, 127.1, 127.3, 127.6, 128.4, 129.5, 130.1, 132.3, 132.6, 134.4, 141.8, 169.9, 177.8, 193.3. HRMS-ESI: [M+H]⁺ calcd for C₂₄H₂₀NO₄⁺ 386.1387, found 386.1393.

3.6. Synthesis of Methyl (2-(4-Methylphenyl)-4-oxo-2,3-dihydro-4H-thiochromeno[4,3-b]furan-2-yl)carbamate (**15**)

Enol **14** (60 mg, 0.25 mmol), Cu(acac)₂ (3 mg, 0.01 mmol), azirine **2a** (54 mg, 0.41 mmol), and DCE (3.0 mL) were consequently placed into a screw-cap glass tube and heated at 100 °C for 20 min until the full consumption of enol **14** was detected (control by TLC). The solvent was removed in vacuo and the residue was purified by column chromatography

on silica gel (eluent hexane/EtOAc 4:1). Colorless solid (46 mg, 50%). Mp: 183–184 °C (Et₂O/hexane). ¹H NMR (400 MHz, CDCl₃), δ, ppm: 2.38 (s, 3H), 3.46 (d, *J* = 16.1 Hz, 1H), 3.68 (s, 3H), 4.05 (d, *J* = 16.1 Hz, 1H), 6.04 (s, 1H), 7.23 (d, *J* = 7.8 Hz, 2H), 7.42–7.48 (m, 3H), 7.50–7.56 (m, 2H), 8.13 (d, *J* = 7.8 Hz, 1H). ¹³C NMR (100 MHz, CDCl₃), δ, ppm: 21.0, 41.2, 52.3, 98.9, 111.7, 119.9, 124.3, 125.5, 125.9, 126.1, 129.6, 130.4, 138.9, 139.1, 139.5, 154.5, 164.8, 180.1. HRMS-ESI: [M+Na]⁺ calcd for C₂₀H₁₇NNaO₄S⁺ 390.0770, found 390.0770.

3.7. Synthesis of 2-(4-Methylphenyl)-4H-thiochromeno[4,3-b]furan-4-one (16)

A solution of carbamate **15** (38 mg, 0.1 mmol) and anhydrous *p*-toluenesulfonic acid (2 mg, 0.01 mmol) in anhydrous *o*-xylene (2.0 mL) was refluxed for 15 min. The reaction mixture was diluted with EtOAc (10 mL), washed with 0.1M NaOH, and dried over Na₂SO₄. Following filtration and concentration under vacuum, the residue was purified by flash column chromatography on silica gel (eluent hexane/EtOAc 5:1) to produce compound **16**. Colorless solid (25 mg, 83%). Mp: 172–173 °C (Et₂O/hexane). ¹H NMR (400 MHz, CDCl₃), δ, ppm: 2.43 (s, 3H), 7.13 (s, 1H), 7.27–7.29 (m, 2H), 7.45–7.56 (m, 3H), 7.71 (d, *J* = 8.0 Hz, 2H), 8.22–8.25 (m, 1H). ¹³C NMR (100 MHz, CDCl₃), δ, ppm: 21.4, 100.6, 120.6, 121.3, 123.3, 124.5, 125.6, 126.3, 126.6, 128.7, 129.7, 135.2, 139.3, 155.7, 157.5, 180.4. HRMS-ESI: [M+Na]⁺ calcd for C₁₈H₁₃NaO₂S⁺ 293.0631, found 293.0633.

3.8. Synthesis of Methyl (2-(rac-(3aR,9bR)-9b-Hydroxy-2-(4-methylphenyl)-5-oxo-3,4,5,9b-tetrahydro-3aH-pyrrolo[3,2-c]isoquinolin-3a-yl)-1-(4-methylphenyl)vinyloxy)carbamate (18)

Enol **17** (44 mg, 0.2 mmol), IPrCuCl (5 mg, 0.01 mmol), azirine **2a** (42 mg, 0.32 mmol), and MeOH (3.0 mL) were consequently placed into a screw-cap glass tube and heated at 100 °C for 30 min until the full consumption of enol **17** was detected (control by TLC). The solvent was removed in vacuo and the residue was purified by column chromatography on silica gel (eluent hexane/EtOAc from 2:1 to 1:2). Light-yellow oil (31 mg, 32%). ¹H NMR (400 MHz, DMSO-d₆), δ, ppm: 2.27 (s, 3H), 2.37 (s, 3H), 3.35 (d, *J* = 17.0 Hz, 1H), 3.42 (d, *J* = 17.0 Hz, 1H), 3.54 (s, 3H), 5.48 (s, 1H), 6.29 (s, 1H), 7.10 (d, *J* = 8.0 Hz, 2H), 7.27 (d, *J* = 8.1 Hz, 2H), 7.32 (d, *J* = 8.0 Hz, 2H), 7.44–7.48 (m, 1H), 7.64–7.67 (s, 1H), 7.78–7.80 (m, 3H), 7.92–7.95 (m, 1H), 8.74 (s, 1H), 9.16 (br. s, 1H). ¹³C NMR (100 MHz, DMSO-d₆), δ, ppm: 21.2, 21.6, 51.4, 52.1, 79.0, 90.2, 115.9, 126.0, 126.6, 126.8, 127.5, 128.2, 128.3, 128.9, 129.7, 131.1, 132.8, 136.1, 137.6, 138.5, 141.9, 142.2, 154.8, 161.8, 175.6. HRMS-ESI: [M+Na]⁺ calcd for C₂₉H₂₇N₃NaO₄⁺ 504.1894, found 504.1897.

4. Conclusions

In conclusion, we described an effective one-step procedure for the [2+3] pyrroline annulation to six-membered non-aromatic enols with 3-aryl-2*H* azirines as annulation agents. The reaction could be catalyzed by both Cu(II) and Cu(I) compounds. It proceeded as a formal (2+3) cycloaddition via the N1–C2 azirine bond cleavage with high-atom economy and efficiency. The method can be applied to cyclic enols of the quinolin-2-one, 2*H*-chromen-2-one, and 1*H*-phenalen-1-one series. The reaction outcome can be rationalized from the reactivity of the amidine intermediate, which was obtained following the copper(I) enolate-induced azirine-ring opening.

Supplementary Materials: The following supporting information can be downloaded at: <https://www.mdpi.com/article/10.3390/molecules27175681/s1>: X-ray diffraction experiments; NMR spectra of compounds **1**, **3**, **6**, **8**, **18** [50–53].

Author Contributions: Conceptualization, P.A.S. and M.S.N.; methodology, P.A.S., N.V.R. and A.F.K.; investigation, P.A.S.; writing—original draft preparation, P.A.S. and M.S.N.; writing—review and editing, N.V.R. and A.F.K. All authors have read and agreed to the published version of the manuscript.

Funding: This research was supported by the Russian Science Foundation, grant number 20-13-00044.

Institutional Review Board Statement: Not applicable.

Informed Consent Statement: Not applicable.

Data Availability Statement: Data are contained within the article.

Acknowledgments: This research was conducted using resources from the Centre for Magnetic Resonance, the Research Centre for X-ray Diffraction Studies, and the Centre for Chemical Analysis and Materials of the Science Park of Saint Petersburg State University.

Conflicts of Interest: The authors declare no conflict of interest.

Sample Availability: Samples of compounds **3**, **6**, **8**, **15–18** are available from the authors.

References

1. Khlebnikov, A.F.; Novikov, M.S.; Rostovskii, N.V. Advances in 2*H*-azirine chemistry: A seven-year update. *Tetrahedron* **2019**, *75*, 2555–2624. [CrossRef]
2. Huang, C.-Y.; Doyle, A.G. The Chemistry of Transition Metals with Three-Membered Ring Heterocycles. *Chem. Rev.* **2014**, *114*, 8153–8198. [CrossRef] [PubMed]
3. Smetanin, I.A.; Novikov, M.S.; Agafonova, A.V.; Rostovskii, N.V.; Khlebnikov, A.F.; Kudryavtsev, I.V.; Terpilowski, M.A.; Serebriakova, M.K.; Trulioff, A.S.; Goncharov, N.V. A novel strategy for the synthesis of thermally stable and apoptosis-inducing 2,3-dihydroazetes. *Org. Biomol. Chem.* **2016**, *14*, 4479–4487. [CrossRef] [PubMed]
4. Pokhriyal, A.; Karki, B.S.; Kant, R.; Rastogi, N. Redox-Neutral 1,3-Dipolar Cycloaddition of 2*H*-Azirines with 2,4,6-Triarylpyrylium Salts under Visible Light Irradiation. *J. Org. Chem.* **2021**, *86*, 4661–4670. [CrossRef]
5. Zhao, M.-N.; Ren, Z.-H.; Yang, D.-S.; Guan, Z.-H. Iron-Catalyzed Radical Cycloaddition of 2*H*-Azirines and Enamides for the Synthesis of Pyrroles. *Org. Lett.* **2018**, *20*, 1287–1290. [CrossRef]
6. Zhao, M.-N.; Ning, G.-W.; Yang, D.-S.; Gao, P.; Fan, M.-J.; Zhao, L.-F. Nickel-catalyzed formal [3+2]-cycloaddition of 2*H*-azirines with 1,3-dicarbonyl compounds for the synthesis of pyrroles. *Tetrahedron Lett.* **2020**, *61*, 152319. [CrossRef]
7. Zeng, T.-T.; Xuan, J.; Ding, W.; Wang, K.; Lu, L.-Q.; Xiao, W.-J. [3+2] Cycloaddition/Oxidative Aromatization Sequence via Photoredox Catalysis: One-Pot Synthesis of Oxazoles from 2*H*-Azirines and Aldehydes. *Org. Lett.* **2015**, *17*, 4070–4073. [CrossRef]
8. Duan, X.; Yang, K.; Lu, J.; Kong, X.; Liu, N.; Ma, J. Base-Mediated Cascade Substitution–Cyclization of 2*H*-Azirines: Access to Highly Substituted Oxazoles. *Org. Lett.* **2017**, *19*, 3370–3373. [CrossRef] [PubMed]
9. Ning, Y.; Otani, Y.; Ohwada, T. Base-Induced Transformation of 2-Acyl-3-alkyl-2*H*-azirines to Oxazoles: Involvement of Deprotonation-Initiated Pathways. *J. Org. Chem.* **2017**, *82*, 6313–6326. [CrossRef] [PubMed]
10. Sun, S.; Huang, J.; Yuan, C.; Wang, G.; Guo, D.; Wang, J. Switchable assembly of substituted pyrimidines and 2*H*-imidazoles via Cu(I)-catalysed ring expansion of 2-methoxyl-2*H*-azirines. *Org. Chem. Front.* **2022**, *9*, 3006–3011. [CrossRef]
11. Angyal, A.; Demjén, A.; Wölfling, J.; Puskás, L.G.; Kanizsai, I. Acid-Catalyzed 1,3-Dipolar Cycloaddition of 2*H*-Azirines with Nitrones: An Unexpected Access to 1,2,4,5-Tetrasubstituted Imidazoles. *J. Org. Chem.* **2020**, *85*, 3587–3595. [CrossRef] [PubMed]
12. Rossa, T.A.; Fantinel, M.; Bortoluzzi, A.J.; Sá, M.M. Multicomponent Synthesis of Structurally Diverse Imidazoles Featuring Azirines, Amines and Aldehydes. *Eur. J. Org. Chem.* **2018**, *2018*, 4171–4177. [CrossRef]
13. Feng, F.-F.; Li, J.-K.; Liu, X.-Y.; Zhang, F.-G.; Cheung, C.W.; Ma, J.-A. General Synthesis of Tri-Carbo-Substituted N2-Aryl-1,2,3-triazoles via Cu-Catalyzed Annulation of Azirines with Aryldiazonium Salts. *J. Org. Chem.* **2020**, *85*, 10872–10883. [CrossRef]
14. Sujatha, C.; Bhatt, C.S.; Ravva, M.K.; Suresh, A.K.; Namitharan, K. Copper-Catalyzed Ring-Expansion Cascade of Azirines with Alkynes: Synthesis of Multisubstituted Pyridines at Room Temperature. *Org. Lett.* **2018**, *20*, 3241–3244. [CrossRef]
15. Khlebnikov, A.F.; Novikov, M.S.; Petrovskii, P.P.; Stoeckli-Evans, H. An Aza Cyclopropylcarbinyl-Homoallyl Radical Rearrangement–Radical Cyclization Cascade. Synthesis of Dibenzoimidazoazepine and Oxazepine Derivatives. *J. Org. Chem.* **2011**, *76*, 5384–5391. [CrossRef]
16. Borra, S.; Chandrasekhar, D.; Adhikary, S.; Rasala, S.; Gokulnath, S.; Maurya, R.A. Visible-Light Driven Photocascade Catalysis: Union of *N,N*-Dimethylanilines and α -Azidochalcones in Flow Microreactors. *J. Org. Chem.* **2017**, *82*, 2249–2256. [CrossRef]
17. Angyal, A.; Demjén, A.; Harmat, V.; Wölfling, J.; Puskás, L.G.; Kanizsai, I. 1,3-Dipolar Cycloaddition of Isatin-Derived Azomethine Ylides with 2*H*-Azirines: Stereoselective Synthesis of 1,3-Diazaspiro[bicyclo[3.1.0]hexane]oxindoles. *J. Org. Chem.* **2019**, *84*, 4273–4281. [CrossRef]
18. Colin, A.R.; Risberg, E.; Somfai, P. Diastereoselective Lewis acid-catalysed [4+2] cycloadditions of 3-alkyl-, 3-aryl- and 3-carboxyl-2*H*-azirines: A route to aziridine containing azabicyclo[4.1.0]heptanes and azatricyclo[2.2.1.0]nonanes. *Tetrahedron* **2002**, *58*, 5983–5987. [CrossRef]
19. Alves, M.J.; Lemos, A.; Rodriguez-Borges, J.E.; García-Mera, X.; Fortes, A.G. Ethyl 2-(diisopropoxyphosphoryl)-2*H*-azirine-3-carboxylate: Reactions with nucleophilic 1,3-dienes. *Synthesis* **2009**, *2009*, 3263–3266. [CrossRef]
20. Ding, H.; Wang, Z.; Bai, S.; Lu, P.; Wang, Y. Rh-Catalyzed Conversion of 3-Diazoindolin-2-imines to 5*H*-Pyrazino[2,3-*b*]indoles with Photoluminescent Properties. *Org. Lett.* **2017**, *19*, 6514–6517. [CrossRef]
21. Baek, Y.; Maeng, C.; Kim, H.; Lee, P.H. Regioselective Synthesis of Indolopyrazines through a Sequential Rhodium-Catalyzed Formal [3+3] Cycloaddition and Aromatization Reaction of Diazoindolinimines with Azirines. *J. Org. Chem.* **2018**, *83*, 2349–2360. [CrossRef] [PubMed]

22. Ruvinskaya, J.O.; Rostovskii, N.V.; Filippov, I.P.; Khlebnikov, A.F.; Novikov, M.S. A novel approach to 5H-pyrazino[2,3-b]indoles via annulation of 3-diazoindolin-2-imines with 2H-azirines or 5-alkoxyisoxazoles under Rh(II) catalysis. *Org. Biomol. Chem.* **2018**, *16*, 38–42. [CrossRef] [PubMed]
23. Gupta, A.K.; Wu, M.-F.; Liao, J.-H.; Hong, B.-C. Formal [6+3] cycloaddition of fulvenes with 2H-azirine: A facile approach to the [2]pyrindines system. *Tetrahedron Lett.* **2004**, *45*, 1663–1666. [CrossRef]
24. Wang, L.; Liu, C.; Li, L.; Wang, X.; Sun, R.; Zhou, M.-D.; Wang, H. Visible-Light-Promoted [3 + 2] Cycloaddition of 2H-Azirines with Quinones: Access to Substituted Benzo[f]isoindole-4,9-diones. *Chin. J. Chem.* **2022**, *40*, 719–724. [CrossRef]
25. Cludius-Brandt, S.; Kupracz, L.; Kirschning, A. [3+2]-Cycloadditions of nitrile ylides after photoactivation of vinyl azides under flow conditions. *Beilstein J. Org. Chem.* **2013**, *9*, 1745–1750. [CrossRef] [PubMed]
26. Hu, H.; Wang, C.; Lai, H.; Wang, S.; Ni, H.; Yu, W.; Cao, P. The Fe(III)-catalyzed decarboxylative cycloaddition of β -ketoacids and 2H-azirines for the synthesis of pyrrole derivatives. *Org. Chem. Front.* **2020**, *7*, 3686–3691. [CrossRef]
27. Rostovskii, N.V.; Sakharov, P.A.; Novikov, M.S.; Khlebnikov, A.F.; Starova, G.L. Cu(I)-NHC-Catalyzed (2+3)-Annulation of Tetramic Acids with 2H-Azirines: Stereoselective Synthesis of Functionalized Hexahydropyrrolo[3,4-b]pyrroles. *Org. Lett.* **2015**, *17*, 4148–4151. [CrossRef]
28. Sakharov, P.A.; Rostovskii, N.V.; Khlebnikov, A.F.; Novikov, M.S. Annulation of five-membered cyclic enols with 3-aryl-2H-azirines: Catalytic versus non-catalytic cycloaddition. *Tetrahedron* **2017**, *73*, 4663–4670. [CrossRef]
29. Sakharov, P.A.; Rostovskii, N.V.; Khlebnikov, A.F.; Panikorovskii, T.L.; Novikov, M.S. 2H-Azirines as C–C Annulation Reagents in Cu-Catalyzed Synthesis of Furo[3,2-c]quinolone Derivatives. *Org. Lett.* **2019**, *21*, 3615–3619. [CrossRef]
30. Borra, S.; Chandrasekhar, D.; Newar, U.D.; Maurya, R.A. Access to 2,3-Fused Pyrroles via Visible Light Driven Coupling of α -Azidochalcones with 1/2-Naphthols, or 2-Hydroxy-1,4-Naphthoquinone. *J. Org. Chem.* **2019**, *84*, 1042–1052. [CrossRef]
31. Mahto, P.; Shukla, K.; Das, A.; Singh, V.K. Organocatalytic asymmetric synthesis of pyrrolo[3,2-c]quinolines via a formal [3+2] cycloaddition-lactamization cascade reaction using a bifunctional squaramide catalyst. *Tetrahedron* **2021**, *87*, 132115. [CrossRef]
32. Nieman, J.A.; Ennis, M.D. Enantioselective Synthesis of the Pyrroloquinoline Core of the Martinellines. *Org. Lett.* **2000**, *2*, 1395–1397. [CrossRef] [PubMed]
33. Yugandar, S.; Misra, N.C.; Parameshwarappa, G.; Panda, K.; Ila, H. Reaction of Cyclic α -Oxoketene Dithioacetals with Methylene Isocyanides: A Novel Pyrrole Annulation–Ring-Expansion Domino Process. *Org. Lett.* **2013**, *15*, 5250–5253. [CrossRef] [PubMed]
34. Zhou, F.; Liu, J.; Ding, K.; Liu, J.; Cai, Q. Copper-Catalyzed Tandem Reaction of Isocyanides with N-(2-Haloaryl)propionamides for the Synthesis of Pyrrolo[3,2-c]quinolin-4-ones. *J. Org. Chem.* **2011**, *76*, 5346–5353. [CrossRef]
35. Ma, D.; Xia, C.; Jiang, J.; Zhang, J. First Total Synthesis of Martinellic Acid, a Naturally Occurring Bradykinin Receptor Antagonist. *Org. Lett.* **2001**, *3*, 2189–2191. [CrossRef]
36. Witherup, K.M.; Ransom, R.W.; Graham, A.C.; Bernard, A.M.; Salvatore, M.J.; Lumma, W.C.; Anderson, P.S.; Pitzenberger, S.M.; Varga, S.L. Martinelline and Martinellic Acid, Novel G-Protein Linked Receptor Antagonists from the Tropical Plant *Martinella iquitosensis* (Bignoniaceae). *J. Am. Chem. Soc.* **1995**, *117*, 6682–6685. [CrossRef]
37. Heidempergher, F.; Pevarello, P.; Pillan, A.; Pinciroli, V.; Della Torre, A.; Speciale, C.; Marconi, M.; Cini, M.; Toma, S.; Greco, F.; et al. Pyrrolo[3,2-c]quinoline derivatives: A new class of kynurenine-3-hydroxylase inhibitors. *Farmaco* **1999**, *54*, 152–160. [CrossRef]
38. Ohashi, T.; Oguro, Y.; Tanaka, T.; Shiokawa, Z.; Shibata, S.; Sato, Y.; Yamakawa, H.; Hattori, H.; Yamamoto, Y.; Kondo, S.; et al. Discovery of pyrrolo[3,2-c]quinoline-4-one derivatives as novel hedgehog signaling inhibitors. *Bioorg. Med. Chem.* **2012**, *20*, 5496–5506. [CrossRef]
39. Grychowska, K.; Satała, G.; Kos, T.; Partyka, A.; Colacino, E.; Chaumont-Dubel, S.; Bantreil, X.; Wesółowska, A.; Pawłowski, M.; Martinez, J.; et al. Novel 1H-Pyrrolo[3,2-c]quinoline Based 5-HT₆ Receptor Antagonists with Potential Application for the Treatment of Cognitive Disorders Associated with Alzheimer’s Disease. *ACS Chem. Neurosci.* **2016**, *7*, 972–983. [CrossRef]
40. Ohki, S.; Yoshino, M. Synthesis of nitrogen-containing heterocyclic compounds through nitrilium salt. I. Reaction of nitriles with 2-(α -hydroxy-methyl, -ethyl, and isopropyl)cyclohexanol in the presence of acid. *Chem. Pharm. Bull.* **1969**, *17*, 2142–2150. [CrossRef]
41. Maini, P.N.; Sammes, M.P. The synthesis and chemistry of azolenines. Part 8. The Paal-Knorr reaction with cyclic 2-(acylmethyl)-2-alkyl-1,3-diketones: Isolation of 1-acyl-1H-pyrroles. *J. Chem. Soc. Perkin Trans. 1* **1988**, 161–168. [CrossRef]
42. Coppola, G.M. An Efficient Synthesis of Arboricine. *Synth. Commun.* **1985**, *15*, 135–139. [CrossRef]
43. Choppakatla, S.; Dacheppally, A.K.; Bollikolla, H.B. Palladium-Catalyzed Double C–H Functionalization of 2-Aryl-1,3-Dicarbonyl Compounds: A Facile Access to Alkenylated Benzopyrans. *Tetrahedron Lett.* **2016**, *57*, 2488–2491. [CrossRef]
44. Hortmann, A.G.; Robertson, D.A.; Gillard, B.K. A Convenient Procedure for the Preparation of 2-Arylazirines. *J. Org. Chem.* **1972**, *37*, 322–324. [CrossRef]
45. Wang, Y.; Lei, X.; Tang, Y. Rh(II)-catalyzed cycloadditions of 1-tosyl 1,2,3-triazoles with 2H-azirines: Switchable reactivity of Rh-azavinylcarbene as [2C]- or aza-[3C]-synthon. *Chem. Commun.* **2015**, *51*, 4507–4510. [CrossRef]
46. Eistert, B.; Selzer, H. Umsetzungen Einiger Diazoalkane Mit Isatin, N-Methyl-Isatin, Cumarandion Und Thionaphthenchinon. *Chem. Ber.* **1963**, *96*, 1234–1255. [CrossRef]
47. Eistert, B.; Selzer, H. Ringerweiterung von Acenaphthenchinon Mit Diazoalkanen Unter Abfangen Der Produkte Als Enolate Bzw. Zinkchelat. *Chem. Ber.* **1963**, *96*, 314–319. [CrossRef]
48. Kikionis, S.; McKee, V.; Markopoulos, J.; Igglessi-Markopoulou, O. A prominent C-acylation–cyclisation synthetic sequence and X-ray structure elucidation of benzothiopyranone derivatives. *Tetrahedron* **2008**, *64*, 5454–5458. [CrossRef]

49. Gabriel, S.; Colman, J. Ueber Die Einwirkung von Natriumalkylaten Auf Phtalylglycinester Und Dessen Homologe. *Ber. Dtsch. Chem. Ges.* **1900**, *33*, 980–995. [CrossRef]
50. Dolomanov, O.V.; Bourhis, L.J.; Gildea, R.J.; Howard, J.A.K.; Puschmann, H. OLEX2: A complete structure solution, refinement and analysis program. *J. Appl. Cryst.* **2009**, *42*, 339–341. [CrossRef]
51. Sheldrick, G.M. A short history of SHELX. *Acta Cryst.* **2008**, *A64*, 112–122. [CrossRef] [PubMed]
52. Sheldrick, G.M. Crystal Structure Refinement with SHELXL. *Acta Cryst.* **2015**, *C71*, 3–8.
53. Sheldrick, G.M. SHELXT—Integrated Space-Group and Crystal-Structure Determination. *Acta Cryst.* **2015**, *A71*, 3–8. [CrossRef] [PubMed]

Article

Synthesis of a Pyrrolo[1,2-*a*]quinazoline-1,5-dione Derivative by Mechanochemical Double Cyclocondensation Cascade

Vanessza Judit Kolcsár¹ and György Szöllösi^{2,*}

¹ Department of Organic Chemistry, Faculty of Science and Informatics, Institute of Chemistry, University of Szeged, Dóm tér 8, 6720 Szeged, Hungary

² ELKH-SZTE, Stereochemistry Research Group, University of Szeged, Eötvös utca 6, 6720 Szeged, Hungary

* Correspondence: szollosi@chem.u-szeged.hu; Tel.: +36-62-544514

Abstract: *N*-heterocyclic compounds, such as quinazolinone derivatives, have significant biological activities. Nowadays, as the demand for environmentally benign, sustainable processes increases, the application of compounds from renewable sources, easily separable heterogeneous catalysts and efficient, alternative activation methods is of great importance. In this study, we have developed a convenient, green procedure for the preparation of 3a-methyl-2,3,3a,4-tetrahydropyrrolo[1,2-*a*]quinazoline-1,5-dione through a double cyclocondensation cascade using anthranilamide and ethyl levulinate. Screening of various heterogeneous Brønsted acid catalysts showed that Amberlyst[®] 15 is a convenient choice. By applying mechanochemical activation in the preparation of this *N*-heterocyclic compound for the first time, it was possible to shorten the necessary time to three hours compared to the 24 h needed under conventional conditions to obtain a high yield of the target product.

Keywords: anthranilamide; ethyl levulinate; Amberlyst[®] 15; Brønsted acid; cascade reaction; mechanochemistry; quinazolinone; ball mill

Citation: Kolcsár, V.J.; Szöllösi, G. Synthesis of a Pyrrolo[1,2-*a*]quinazoline-1,5-dione Derivative by Mechanochemical Double Cyclocondensation Cascade. *Molecules* **2022**, *27*, 5671. <https://doi.org/10.3390/molecules27175671>

Academic Editors: Alexey M. Starosotnikov, Maxim A. Bastrakov and Igor L. Dalinger

Received: 6 August 2022

Accepted: 30 August 2022

Published: 2 September 2022

Publisher's Note: MDPI stays neutral with regard to jurisdictional claims in published maps and institutional affiliations.



Copyright: © 2022 by the authors. Licensee MDPI, Basel, Switzerland. This article is an open access article distributed under the terms and conditions of the Creative Commons Attribution (CC BY) license (<https://creativecommons.org/licenses/by/4.0/>).

1. Introduction

The pharmaceutical importance of *N*-heterocyclic compounds is indisputable [1]. Due to the biological activities of quinazolinone derivatives, such as anticancer, diuretic and antibacterial properties, these molecules caught the attention of organic chemists [2–8]. Among these, 2,3-dihydroquinazolin-4(1*H*)-ones are privileged building blocks in drug design, which are readily prepared by the cyclocondensation of anthranilamides and aldehydes or ketones [2–4,9]. Various catalysts were used in these cyclocondensations, such as strong bases [10,11], strong mineral or weak organic Brønsted acids [10,12–16], sulfonic acids [4,10,17–21], Lewis acids [22–30] and ammonium salts [31,32].

Recent trends in the fine chemical industry require the development of sustainable, environmentally benign processes; thus, in the preparation of 2,3-dihydroquinazolin-4(1*H*)-ones, the application of catalyst- or solvent-free methods [33–36] and/or employing easily separable heterogeneous catalysts also became widely investigated [37–47]. Among the latter materials, surface-bonded sulfonic, sulfamic or sulfuric acids are privileged heterogeneous catalysts [48–56]. Methods replacing anthranilamide with compounds in situ transformed to 2-aminobenzamides, such as isatoic anhydride, 2-aminobenzonitrile, 2-nitro or 2-azidobenzamides, were also applied in cascade processes leading to 2,3-dihydroquinazolin-4(1*H*)-ones [13,57–63]. Besides their pharmaceutical use, 2,3-dihydroquinazolin-4(1*H*)-ones are easily transformed to quinazolinones by subsequent one-pot oxidation [11,19,20,64,65]. Moreover, the use of additionally functionalized carbonyl compounds allows the preparation of tricyclic hydroquinazoline derivatives through another consecutive one-pot cyclocondensation step [66–68]. Among the carbonyl compounds used in such cascade reactions, γ -keto carboxylic acids and esters were applied to obtain pyrrolo[1,2-*a*]quinazoline-1,5-dione derivatives [68–70]. As levulinic acid is a platform molecule obtained from biomass

and its esterification can be activated by microwave in a solventless organocatalytic system [71–73], these allow the sustainable preparation of such *N*-heterocyclic products using renewable resources.

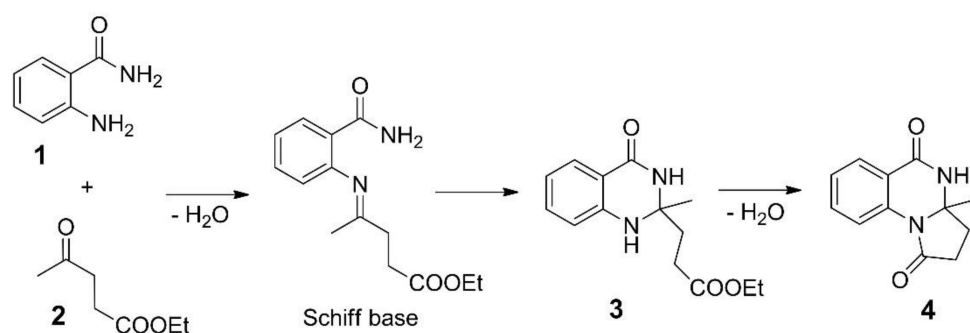
On the other hand, advancements in the development of environmentally friendly methods were achieved by the application of alternative energy transmissions [74,75]. Among these, mechanochemical activation became widespread due to its operational simplicity and broad applicability [76–80]. Mechanochemical reactions performed in easily available mixer mills may be carried out in a solventless manner or using a minor amount of liquid for ensuring the proper energy transmission and mixing, termed liquid-assisted grinding (LAG). A wide range of milling conditions can be optimized to achieve high efficiency in various organic reactions, such as the agitation speed, the milling time and the size, number and material of the grinding media [81,82]. Finding appropriate conditions to efficiently carry out certain organic transformations by mechanochemical activation is still a challenging task and requires detailed studies. A variety of organic reactions were carried out by mechanochemical activation at a laboratory scale [76–85]. These studies indicated that, in most of these reactions, the time can be decreased significantly compared to conventional batch systems. Studies on mechanochemical reactions were also extended to cascade processes, resulting in the formation of valuable heterocyclic compounds [86–89]. Initial attempts to use mechanochemical activation in catalytic cyclocondensations leading to 2,3-dihydroquinazolin-4(1*H*)-ones were carried out in mortars by grinding the reaction components often followed by heating the mixtures [90–94]. Later, with the widespread application of ball mills in organic synthetic procedures, reactions of anthranilamide and aldehydes or ketones were also efficiently carried out in mixer mills, either solventless or in aqueous media and catalyst-free or catalyzed by potassium iodide or iodine [95,96]. However, the applicability of the mechanochemical activation in cascade double cyclocondensations of anthranilamide and bifunctional carbonyl compounds, to our knowledge, has not yet been explored.

Having in sight the increased importance of one-pot reactions [97], our present study aimed at developing an economic, green and sustainable process for the preparation of a tricyclic pyrrolo[1,2-*a*]quinazoline-1,5-dione derivative by two consecutive cyclocondensations occurring upon reacting anthranilamide and ethyl levulinate. For this, we attempted to use solid acids as heterogeneous catalysts and mechanochemical activation.

2. Results and Discussions

2.1. Catalytic Cascade Reaction of Anthranilamide and Ethyl Levulinate in the Batch System

The condensations of anthranilamide (**1**) and aldehydes or ketones occur through the formation of the corresponding Schiff base followed by a ring-closing step with the participation of the amide moiety (Scheme 1). Products with three condensed rings may be achieved under appropriate conditions with bifunctional carbonyl compounds, such as ethyl levulinate (**2**), as shown in Scheme 1. Thus, in the reaction of **1** and **2** the quinazolinone derivative **3** is formed which, via a second ring-closing step, provides the three-fused ring-containing product **4**. Our initial goal was to choose an appropriate commercial heterogeneous catalyst which may ensure the formation of product **4** under convenient conditions. The study was carried out in a solventless manner in a batch system through magnetic stirring. To ensure proper mixing of the components, 1.5 equivalent (eq) **2** was applied. Measurements carried out without a catalyst showed that, at low temperature (60 °C), small conversion (**Conv**) of **1** could be achieved and that the second ring-closing step took place in a small ratio (see the selectivity of **4** (**S4**), Table 1, entry 1). However, the presence of the Schiff base was not detected at a significant amount, thus its formation rate may be the limiting step of **3** production. Increasing the reaction temperature (90 °C) had a positive effect on the conversion; however, production of **4** still resulted in a low yield (entry 2).



Scheme 1. The reaction of anthranilamide (**1**) and ethyl levulinate (**2**) resulting in the formation of 2,3-dihydroquinazolin-4(1H)-one (**3**) and pyrrolo[1,2-*a*]quinazoline-1,5-dione (**4**) derivatives.

Table 1. Effect of the catalyst in the reaction of **1** and **2**^a.

Entry	Catalyst	Catalyst Amount	T (°C) ^b	t (h) ^c	Conv (%) ^d	S3 (%) ^e	S4 (%) ^e
1	-	-	60	24	40	83	15
2	-	-	90	24	95	73 (60) ^f	24
3	Silica gel 60	125 mg	90	48	99	48	51
4	Mont K10	125 mg	90	24	>99	60	39
5	Mont K10	125 mg	90	48	>99	35	63
6	Mont KSF	125 mg	90	48	>99	40	58
7	<i>p</i> -TsOH	5 mol%	60	24	>99	48	51
8	<i>p</i> -TsOH	5 mol%	90	24	>99	-	99 (90) ^f
9	Deloxan [®] ASP	100 mg	60	24	>99	80 (70) ^f	19
10	Deloxan [®] ASP	125 mg	90	24	>99	-	98
11	Nafion [™] NR50	86 mg (2 pcs)	60	24	96	77 (61) ^f	21
12	Nafion [™] NR50	84 mg (2 pcs)	90	24	>99	-	99 (88) ^f
13	Amberlyst [®] XN-1010	100 mg	60	24	>99	-	99 (90) ^f
14	Amberlyst [®] 15	100 mg	60	24	>99	-	99 (91) ^f

^a Reactions were carried out using 1 mmol **1** and 1.5 mmol **2** with magnetic stirring (600 rpm). ^b Reaction temperature. ^c Reaction time. ^d Conversion of **1** determined by gas chromatography (GC-FID). ^e Selectivities of products **3** and **4** were determined by GC-FID, the selectivities of other products were 1–3%. ^f In parentheses, the yield of the corresponding product following purification by flash chromatography (**3**) or by crystallization in ethyl acetate (**4**).

Next, we employed various commercial Brønsted acidic catalysts, which all provided high conversions after 24 or 48 h, some even at 60 °C. The selectivities highly depended on the properties of the applied catalyst. Silica gel and acid-treated montmorillonite clays (Mont K10, Mont KSF) (entries 3–6) were not able to provide high **4** selectivities. On the other hand, catalysts bearing sulfonic acid groups were active in catalyzing the formation of the aimed pyrrolo[1,2-*a*]quinazolidione derivative (entries 7–14). The application of *p*-toluenesulfonic acid (*p*-TsOH) provided high **S4** only under harsher reaction conditions (90 °C). The propylsulfonic polysiloxane resin (Deloxan[®] ASP) and the perfluorinated resin bearing sulfonic acid groups (Nafion[™] NR50) were also efficient but, similarly to the *p*-TsOH, a higher temperature was necessary to obtain **4** (entries 9–12). The best results were provided by the polystyrene-based sulfonic acid-functionalized Amberlyst[®]-type catalysts (entries 13, 14), both of which afforded full conversions and close to exclusive formation of **4** at 60 °C. Based on these results, we choose to use Amberlyst[®] 15 in our further investigations.

Examination of the temperature effect was carried out both without a catalyst and with Amberlyst[®] 15 (see Supplementary Materials, Figure S1). In the absence of a catalyst, a temperature of 90 °C was necessary to achieve close to full conversion; however, **S4** was low over the investigated temperature range, i.e., thermally the second ring-closing step occurred with a low rate. In contrast, by applying Amberlyst[®] 15, **1** was completely transformed

and **S4** increased by raising the temperature, approaching 100% at 60 °C. Thus, under the conditions used in this study, the second cyclization step required the use of an acid catalyst. The same conclusion may be drawn from results regarding the influence of the catalyst amount (Supplementary Materials, Figure S2). At 60 °C, at least 100 mg Amberlyst® 15 was necessary to obtain the desired product **4** in high proportion. Amberlyst® 15 is available from a commercial source in bead-like form. We have powdered it by pre-grinding the material in a ball mill for 10 min to increase its exposed surface sites (denoted as Amberlyst® 15P). By this method, the activity of the catalyst in the second cyclization could be increased significantly, reaching almost 30% higher selectivity of **4** compared to the reaction with the same amount (50 mg) of the commercial form (Figure S2).

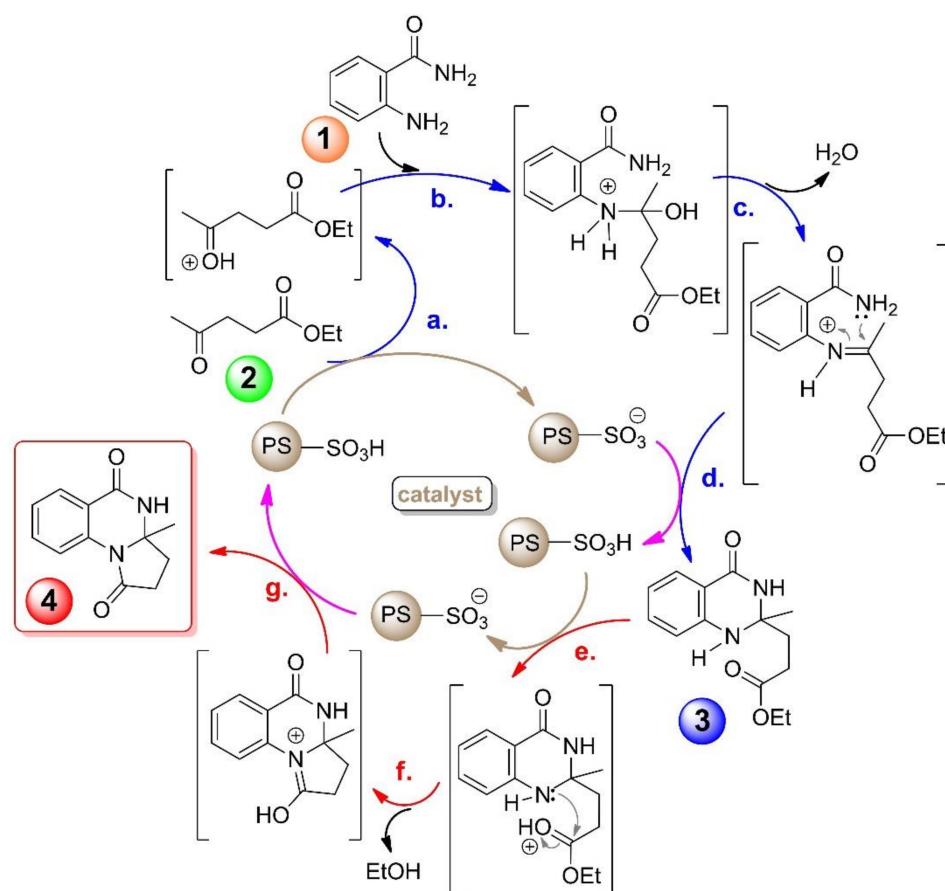
Based on the results achieved with Amberlyst® 15P, we further optimized the reaction conditions using this material (Table 2). Decreasing the excess of the reactant to 1.1 eq resulted in lower **4** selectivity, suspected to be due to less efficient mixing of the slurry (Table 2, entries 1, 2). To improve the mixing of the components, the missing volume of **2** was replaced with methanol (MeOH). Close to full conversion and high **S4** were obtained (entry 3). To further study the role of the catalyst, purified **3** (resulting from previous experiments) was used as the starting compound under identical conditions, both without (entry 4) and with Amberlyst® 15P (entry 5). In this case, the second ring-closing step did not occur unless the solid acid was present.

Table 2. Effect of **2** and methanol amount on the results obtained in the reaction of **1** and **2**^a.

Entry	EL Amount (eq)	MeOH Amount (μL)	Conv (%) ^b	S3 (%) ^c	S4 (%) ^c
1	1.5	-	>99	35	64
2	1.1	-	>99	55	42
3	1.1	57	>99	1	97 (89) ^f
4 ^{d,e}	1.1	57	-	96	2
5 ^e	1.1	57	-	-	99 (91) ^f

^a Reactions were carried out using 50 mg pre-milled Amberlyst® 15P and 1 mmol **1** at 60 °C for 24 h. ^b Conversion by GC-FID. ^c Selectivities of **3** and **4** by GC-FID. ^d Reaction without catalyst. ^e Using 1 mmol **3** as the starting material (isolated by flash chromatographic purification of previously obtained reaction mixtures). ^f In parentheses, the yield of crystallized **4**.

According to the above, the two cyclocondensation steps of this cascade reaction can be carried out neat, using as little as 1.1 eq **2** by applying a small amount of MeOH and pre-milled Amberlyst® 15 catalyst. The use of MeOH does not diminish the environmentally benign aspect of the method as it is among the organic solvents recommended for use even by some pharmaceutical companies [98]. Based on the obtained results so far and the known mechanism of the cyclocondensations [9,13,23,37,68,70], we could draw conclusions about the activation of the steps, as presented in Scheme 2. We observed that the first cyclization of the cascade reaction leading to **3** can be thermally promoted. Without using a catalyst at 60 °C, 40% conversion was obtained, which increased to 95% at a higher (90 °C) temperature. The product mixture mostly contained the intermediate product **3**, but the formation of a small amount of **4** was also observed, which shows that heating may also promote the second step (Table 1, entries 1, 2). The effect of heating seemed negligible starting from **3** (Table 2, entry 4); however, by introducing Amberlyst® 15 into the system, intramolecular amide formation was accelerated (Table 2, entry 5). According to these findings, the first part of the reaction marked with blue arrows on Scheme 2 (steps **a**–**d**.) can be promoted by heat as well as acid catalysts. Intramolecular amide formation, on the other hand, is mainly promoted by the acid catalyst (red arrows, steps **e**–**g**.); thus, in our further studies, the use of a catalyst was necessary to obtain the target compound **4**.



Scheme 2. The reaction mechanism of the cascade reaction: blue arrows are the catalytic steps which occurred thermally (a.–d.) and the red arrows are steps requiring an acid catalyst (e.–g.).

2.2. Mechanochemical Catalytic Cascade Reaction of Anthranilamide and Ethyl Levulinate

To make further steps towards the development of a sustainable method, we aimed to carry out the neat reaction of **1** and **2** in a ball mill. Based on the mechanochemical organic reactions recently reported in the literature [99,100], we started our experiments by applying grinding balls of different sizes (Table 3). The number of grinding beads was determined to have similar total volumes in each measurement.

Table 3. Effect of the size and number of grinding balls in the reaction of **1** and **2** ^a.

Entry	Diameters of Balls (mm)	Number of Balls (pcs)	Conv (%) ^b	S3 (%) ^c	S4 (%) ^c
1	15	1	98	36	62
2	12	1	98	54	42
3	5	25	97	13	85
4	3	125	>99	90 (80) ^d	8
5	5	35	98	4	94
6	5	40	>99	-	99 (92) ^d
7 ^e	5	35	77	78	20

^a Reactions were carried out using 100 mg Amberlyst® 15, 1 mmol **1** and 1.5 mmol **2** with an agitation speed of 30 Hz for 180 min. ^b Conversion by GC-FID. ^c Selectivities of **3** and **4** by GC-FID. ^d In parentheses, the yield of the purified **3** or **4**. ^e 90 min reaction.

Balls with a bigger diameter (Ø 15 and 12 mm) may provide high collision energy; however, only one piece fits into the jar without hindering another's movement. Thus, only a low collision number can be achieved. Better **4** selectivity was observed using the Ø 15 mm ball (Table 3, entry 1) than applying the Ø 12 mm ball (entry 2), which shows the importance of collision energy in the second cyclization step. Using 25 pieces (pcs) of

Ø 5 mm grinding balls provided an even better result (entry 3). In this case, the higher collision number compensated for the decreased collision energy. However, the use of 125 pcs of Ø 3 mm beads was not efficient, probably due to their very low energy (entry 4). Based on these results, the use of Ø 5 mm balls was the best choice. By increasing the number of Ø 5 mm balls, 4 selectivity can be further improved (entries 5, 6). Although 40 pcs afforded close to exclusive formation of 4, 35 pcs were used in further measurements to make the effect of the other reaction parameters visible. Thus, when the reaction mixture was milled for half of the previously used time, both the conversion and S4 decreased (entry 7).

Our results obtained in batch reactions showed that a small amount of MeOH may improve the selectivity of 4 in this cascade reaction. Moreover, many of the mechanochemical reactions that have been reported up to now are not completely neat; a small amount of additional liquid with an energy mediating role is often used, which also ensures the proper mixing of the system [79,80]. By decreasing the excess of 2 and replacing the missing volume with MeOH, conversion and S4 of the mechanochemical reaction were improved (Figure 1). With as little as 1.1 eq 2 and 0.057 mL MeOH, the reaction solely afforded product 4 in the mixer mill following 180 min of grinding.

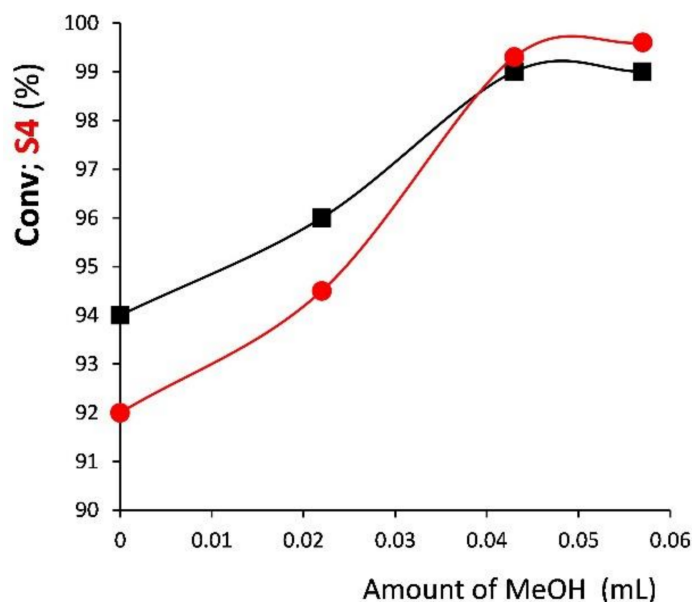


Figure 1. Effect of MeOH amount (■: Conv, conversion; ●: S4, selectivity of 4—both determined by GC-FID). Reaction condition: 100 mg Amberlyst[®] 15, 1 mmol 1, 1.5–1.1 mmol 2, total liquid volume of 0.213 mL, 35 pcs Ø 5 mm ZrO₂ balls, 30 Hz, 180 min.

Decreasing either the milling time or frequency had an unfavourable effect in reactions using 100 mg Amberlyst[®] 15, 0.057 mL MeOH and 35 pcs of Ø 5 mm grinding balls. Thus, at least 180 min of milling at 30 Hz was necessary to achieve high conversion and up to 99% S4 (Table 4). Importantly, the reaction time can be decreased significantly compared to the magnetically stirred system (3 vs. 24 h). Although the reaction is shorter, more catalyst is demanded to achieve a good result; 50 mg Amberlyst[®] 15 was not enough to promote the second ring-closing step properly (Table 4, entry 7). The use of pre-milled Amberlyst[®] 15P (entry 3, 5) gave similar results to the commercial form in mechanochemical reactions, probably due to grinding of the bead-like Amberlyst[®] 15 during the initial stages of the milling process, with pre-milling thus losing its importance.

Table 4. Effect of milling time and agitation frequency in the reaction of **1** and **2** ^a.

Entry	Reaction Time (min)	Agitation Frequency (Hz)	Conv (%) ^b	S3 (%) ^c	S4 (%) ^c
1	60	30	90	58	40
2	120	30	93	28	70
3 ^e	120	30	97	25	73
4	180	30	98	-	99 (88) ^d
5 ^e	180	30	>99	-	99 (92) ^d
6	180	20	99	80	18
7 ^f	180	30	99	38	60

^a Reactions were carried out using 100 mg Amberlyst[®] 15, 1 mmol **1**, 1.1 mmol **2** and 57 μ L MeOH with 35 pcs of \varnothing 5 mm ZrO₂ grinding balls. ^b Conversion by GC-FID. ^c Selectivities of **3** and **4** by GC-FID. ^d In parentheses, the yield of the crystallized **4**. ^e Reaction using 100 mg pre-milled Amberlyst[®] 15P. ^f Using 50 mg Amberlyst[®] 15.

Finally, a few other acidic Brønsted catalysts used in the batch system were also re-examined under mechanochemical conditions (Table 5). The reaction carried out without a catalyst gave low conversion and **S4** (entry 1). Although the system warms up during the milling process, i.e., the mixture is heated up to *cca* 55 °C after 3 h of milling (based on our previous studies) [100], the temperature in the jar is not high enough to promote either step. The best results so far were provided by the Amberlyst[®] 15 used in this study (entry 2). In the magnetically stirred system, Amberlyst[®] XN-1010 also gave similar results; however, the mechanochemical reaction was less efficient than with the former, probably due to its lower ion-exchange capacity (Amberlyst[®] 15: 4.7 meq/g, Amberlyst[®] XN-1010: 3.3 meq/g [101,102]; entry 3). Thus, a higher amount of this material should be used. Although Nafion[™] NR50 gave a similar result to the Amberlyst[®] resins in batch reactions at 90 °C, in the ball-milled reaction the former was much less efficient. Additionally, with the lower temperature reached in the mechanochemical system, the non-porous (and having low surface area) Nafion[™] NR50 polymer was not brittle and consequently was not ground into powder. Instead, this material formed a thick, sticky paste which was not mixed properly with the reactants. The acid-treated montmorillonite (Mont K-10) mostly catalyzed the first ring-closing step in the mixer mill, which may also be attributed to the low temperature of the mixture in the milling jars.

Table 5. Influence of the catalyst in the mechanochemical reaction of **1** and **2** ^a.

Entry	Catalyst	Catalyst Amount	Conv (%) ^b	S3 (%) ^c	S4 (%) ^c
1	-	-	5	80	18
2	Amberlyst [®] 15	100 mg	98	-	99
3	Amberlyst [®] XN-1010	100 mg	99	14	85
4	Nafion [™] NR50	85 mg (2 pcs)	48	63	35
5	Mont K10	125 mg	52	82	16

^a Reactions carried out using 1 mmol **1**, 1.1 mmol **2** and 57 μ L MeOH with 35 pcs \varnothing 5 mm ZrO₂ grinding balls at 30 Hz for 180 min. ^b Conversion by GC-FID. ^c Selectivities of **3** and **4** by GC-FID.

3. Materials and Methods

The anthranilamide (**1**), ethyl levulinate (**2**), *p*-toluenesulfonic acid monohydrate (*p*-TsOH) and the applied methanol were obtained from commercial sources (Sigma-Aldrich, St. Louis, MO, USA) and used as received. The heterogeneous acid catalysts were commercial materials: Amberlyst[®] 15 (Sigma-Aldrich, St. Louis, MO, USA; brown-grey beads, ion-exchange capacity: 4.7 meq/g, average pore diameters 265 Å, surface area: 45–55 m²/g, [101–103]); Amberlyst XN-1010 (Sigma-Aldrich Chem, Steighem, Germany, presently not available; dark grey beads, ion-exchange capacity: 3.3 meq/g, average pore diameters 51 Å, surface area: 540 m²/g [101,102]); Nafion[™] NR50 (Sigma-Aldrich, St. Louis, MO, USA, has been discontinued; opaque white pellet, ion-exchange capacity:

≥ 0.8 meq/g, non-porous, surface area: < 0.02 m²/g [101]); Deloxan[®] ASP (Degussa AG, Hanau, Germany; white powder, 0.80 mmol S/g [104]); montmorillonite K10 (Mont K10, Sigma-Aldrich, St. Louis, MO, USA) (light beige powder, surface area: 220–270 m²/g, total concentration of the acid centers 0.45 mmol/g [105]); montmorillonite KSF (Mont KSF, Sigma-Aldrich, St. Louis, MO, USA, currently is not available; off-white powder, surface area: 20–40 m²/g [106]); and Silica gel 60 (Merck Millipore, Darmstadt, Germany, white powder, particle size: 250–500 μ m, pore size: 150 Å, pore volume: 1.15 mL/g). In some reactions, Amberlyst[®] 15 was used after pre-milling for 10 min with 30 Hz agitation frequency in a 10-mL ZrO₂ grinding jar applying 35 pcs of \varnothing 5 mm ZrO₂ grinding balls (Retsch GmbH, Haan, Germany).

¹H and ¹³C NMR spectra of the purified products were recorded on a Bruker Ascend 500 instrument using CDCl₃ solvent. Products were isolated by crystallization in ethyl acetate (**4**) or purified by flash chromatography (**3**). Gas-chromatographic analysis of the reaction products was carried out using an Agilent Techn. 6890 N GC-5973 MSD (GC-MSD, Agilent Co., Santa Clara, CA, US) equipped with a 30 m long HP-1MS capillary column for mass spectrometric identification of the products. For quantitative analysis, an Agilent 7890A GC-FID (GC-FID, Agilent Co., Santa Clara, CA, US) chromatograph equipped with a capillary column (HP-5 30 m, J & W from Agilent Co., Santa Clara, CA, US) was used.

3.1. Reaction of Anthranilamide and Ethyl Levulinate in the Batch System: General Procedure

The reactions were carried out in 4-mL closed glass vials immersed in a heated oil bath and the slurries were stirred magnetically (600 rpm). In a typical reaction, 1 mmol **1**, 1.1–1.5 mmol **2** (0.022–0.057 mL MeOH) and the chosen catalyst were introduced into the vial and stirred at 60 or 90 °C for 24 or 48 h. Following the reactions, the products were dissolved in 3 mL MeOH, and the catalysts were separated by filtration or centrifugation. The liquid phases were analyzed by gas-chromatography using *n*-decane as the internal standard (GC-MSD and GC-FID). Conversions (**Conv**) and selectivities (**S3** and **S4**) were calculated based on the relative concentrations determined from chromatograms using the formulae given in the Supplementary Materials. The products that resulted in a few reactions were purified either by crystallization in ethyl acetate (**4**) or by flash chromatography using hexane/ethyl acetate 1/1 as eluent (**3**) for the determination of the yields. The identity of the isolated products was confirmed by ¹H and ¹³C NMR spectroscopic measurements using CDCl₃ as a solvent. The experiments were repeated at least 3 times and the reproducibility of product composition was found to be within $\pm 1\%$.

3.2. Reaction of Anthranilamide and Ethyl Levulinate by Ball Milling: General Procedure

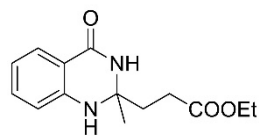
The reactions were carried out in 10-mL closed grinding jars with a ZrO₂ inner coat and ZrO₂ grinding balls (\varnothing 3, 5, 12, 15 mm). In a typical reaction, 1 mmol **1**, 1.1–1.5 mmol **2** (0.022–0.057 mL MeOH) and the chosen catalyst were introduced into the jars, and the chosen number of balls was then added to the system. The closed jars were placed into a Retsch MM400 mixer mill (Retsch GmbH, Haan, Germany) and agitated at a 30 Hz frequency for a maximum of 180 min. Following reactions, the products were dissolved in 1 mL MeOH, the jars and balls were washed twice with 1 mL MeOH and the unified liquid phase was filtrated and analyzed in the same manner as the products of the magnetically stirred reactions. The experiments were repeated at least 3 times and the reproducibility of product composition was found to be within $\pm 1\%$.

Analytical data of the products:

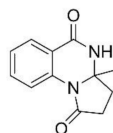
Ethyl 3-(2-methyl-4-oxo-1,2,3,4-tetrahydroquinazolin-2-yl)propanoate (**3**)

Flash chromatographic separation, eluent: hexane/ethyl acetate 1/1, off-white crystals, mp 88–91 °C.

GC-FID analysis (HP-5 column): R_t = 47.6 min.



GC-MSD m/z (rel. int.): 262(M^+ , 1), 201(24), 173(8), 161(100), 119(24), 92(16), 65(5), 42(4).
 ^1H NMR (500 MHz, CDCl_3) δ (ppm): 7.85 (d, 1H, J 7.7 Hz, Ar-H), 7.27 (m, 1H, Ar-H), 6.90 (s, 1H, N-H), 6.78 (t, 1H, J 7.7 Hz, Ar-H), 6.58 (d, 1H, J 8.0 Hz, Ar-H), 4.34 (s, 1H, N-H), 4.10 (q, 2H, J 7.1 Hz, CH_2), 2.65 (m, 2H, CH_2), 2.10 (m, 2H, CH_2), 1.54 (s, 3H, CH_3), 1.20 (t, 3H, J 7.1, CH_3).
 ^{13}C NMR (125 MHz, CDCl_3) δ (ppm): 173.7, 164.4, 145.9, 134.0, 128.3, 118.6, 114.5, 114.1, 69.9, 60.8, 36.6, 29.1, 29.0, 14.1.
 3a-Methyl-2,3,3a,4-tetrahydropyrrolo[1,2-*a*]quinazoline-1,5-dione (**4**)
 Separation by crystallization in ethyl acetate, white crystals, mp 162–165 °C.
 GC-FID analysis (HP-5 column): R_t = 52.4 min.



GC-MSD m/z (rel. int.): 216(M^+ , 6), 201(100), 1173(35), 161(6), 132(6), 90(6), 42(2).
 ^1H NMR (500 MHz, CDCl_3) δ (ppm): 8.16 (d, 1H, J 8.1 Hz, Ar-H), 8.07 (d, 1H, J 7.8 Hz, Ar-H), 7.89 (s, 1H, N-H), 7.59 (m, 1H, Ar-H), 7.29 (m, 1H, Ar-H), 2.70 (m, 2H, CH_2), 2.39 (m, 2H, CH_2), 1.57 (s, 3H, CH_3).
 ^{13}C NMR (125 MHz, CDCl_3) δ (ppm): 171.6, 163.3, 135.8, 133.8, 128.3, 125.0, 120.7, 119.5, 76.7, 74.5, 32.9, 30.0, 26.9.

4. Conclusions

In the present study, we have developed a method to increase the sustainability of the preparation of a pyrrolo[1,2-*a*]quinazoline-1,5-dione derivative through a one-pot cascade reaction occurring by reacting anthranilamide and ethyl levulinate. The application of a heterogeneous acid catalyst and mechanochemical activation in the two-step reaction was successful, resulting in a decrease in the necessary reaction time from 24 h in a magnetically stirred batch system to as little as three hours. The reaction was carried out in a ball mill via liquid-assisted grinding with only a minor excess of ethyl levulinate and using a slight amount of methanol. A polystyrene-based sulfonic acid-functionalized catalyst, i.e., Amberlyst[®] 15, provided the best results both in the batch and in the mechanochemical reactions. In the latter system, the use of an acid catalyst with appropriate properties was essential, as the heat generated by the collision and friction of the grinding media was not sufficient to promote the second ring-closing step thermally.

Supplementary Materials: The following supporting information can be downloaded at: <https://www.mdpi.com/article/10.3390/molecules27175671/s1>, General formulae; Figure S1: Effect of temperature on the reaction of anthranilamide (**1**) with ethyl levulinate (**2**) in the batch system; Figure S2: Effect of the catalyst amount on the reaction of anthranilamide (**1**) with ethyl levulinate (**2**) in the batch system; ^1H and ^{13}C NMR spectra of the isolated products; Chromatograms and mass spectra of the products.

Author Contributions: V.J.K. and G.S. contributed equally to the presented research. All authors have read and agreed to the published version of the manuscript.

Funding: The Hungarian Science Foundation funded this research, grant number K138871.

Institutional Review Board Statement: Not applicable.

Informed Consent Statement: Not applicable.

Data Availability Statement: The data presented in this study are available on request from the corresponding author.

Conflicts of Interest: The authors declare no conflict of interest.

Sample Availability: Not available.

References

1. Frank, É.; Szöllösi, G. Nitrogen-Containing Heterocycles as Significant Molecular Scaffolds for Medicinal and Other Applications. *Molecules* **2021**, *26*, 4617. [CrossRef]
2. Alaimo, R.J. Antibacterial 2,3-Dihydro-2-(5-nitro-2-thienyl)quinazolin-4-(1H)-ones. *J. Med. Chem.* **1972**, *15*, 335–336. [CrossRef]
3. Parish, H.A., Jr.; Gilliom, R.D. Syntheses and Diuretic Activity of 1,2-Dihydro-2-(3-pyridyl)-3H-pyrido[2,3-d]pyrimidin-4-one and Related Compounds. *J. Med. Chem.* **1982**, *25*, 98–102. [CrossRef] [PubMed]
4. Hour, M.-J.; Huang, L.-J.; Kuo, S.-C.; Xia, Y.; Bastow, K.; Nakanishi, Y.; Hamel, E.; Lee, K.-H. 6-Alkylamino- and 2,3-Dihydro-3'-methoxy-2-phenyl-4-quinazolinones and Related Compounds: Their Synthesis, Cytotoxicity, and Inhibition of Tubulin Polymerization. *J. Med. Chem.* **2000**, *43*, 4479–4487. [CrossRef] [PubMed]
5. Sharma, P.C.; Kaur, G.; Pahwa, R.; Sharma, A.; Rajak, H. Quinazolinone Analogs as Potential Therapeutic Agents. *Curr. Med. Chem.* **2011**, *18*, 4786–4812. [CrossRef]
6. He, D.; Wang, M.; Zhao, S.; Shu, Y.; Zeng, H.; Xiao, C.; Lu, C.; Liu, Y. Pharmaceutical prospects of naturally occurring quinazolinone and its derivatives. *Fitoterapia* **2017**, *119*, 136–149. [CrossRef] [PubMed]
7. Hameed, A.; Al-Rashida, M.; Uroos, M.; Ali, S.A.; Arshia; Ishtiaq, M.; Khan, K.M. Quinazoline and quinazolinone as important medicinal scaffolds: A comparative patent review (2011–2016). *Expert Opin. Ther. Patents* **2018**, *28*, 281–297. [CrossRef]
8. Wahan, S.K.; Sharma, B.; Chawla, P.A. Medicinal perspective of quinazolinone derivatives: Recent developments and structure-activity relationship studies. *J. Heterocycl. Chem.* **2022**, *59*, 239–257. [CrossRef]
9. Badolato, M.; Aiello, F.; Neamatti, N. 2,3-Dihydroquinazolin-4(1H)-one as a privileged scaffold in drug design. *RSC Adv.* **2018**, *8*, 20894–20921. [CrossRef] [PubMed]
10. Yale, H.L.; Kalkstein, M. Substituted 2,3-Dihydro-4(1H)-quinazolinones. A New Class of Inhibitors of Cell Multiplication. *J. Med. Chem.* **1967**, *10*, 334–336. [CrossRef] [PubMed]
11. Chavan, S.P.; Sivappa, R. A short and efficient general synthesis of luotonin A, B and E. *Tetrahedron* **2004**, *60*, 9931–9935. [CrossRef]
12. Klemm, L.H.; Weakly, T.J.R.; Gilbertson, R.D.; Song, Y.-H. Definitive Structural Assignment of Condensation Products from Antranilamide and 3-Amino-2-carbamoylthiophene with Ketones. Formation of Tetrahydroquinazolinones and Their Thiophene Isosteres. *J. Heterocycl. Chem.* **1998**, *35*, 1269–1273. [CrossRef]
13. Bunce, R.A.; Nammalwar, B. New Conditions for Synthesis of (\pm)-2-Monosubstituted and (\pm)-2,2-Disubstituted 2,3-Dihydro-4(1H)-quinazolinones from 2-Nitro and 2-Aminobenzamide. *J. Heterocycl. Chem.* **2011**, *48*, 991–997. [CrossRef]
14. Esfandiari, S.; Maghsoodlou, M.T.; Habibi-Khorassani, S.M.; Kiaee, S.; Aboonajmi, J. Malonic acid as a catalyst for efficient and simple synthesis of 2,3-dihydroquinazolin-4(1H)-one in green solvent. *Iranian J. Org. Chem.* **2012**, *4*, 827–830.
15. Zhaleh, S.; Hazeri, N.; Maghsoodlou, M.T. Green protocol for synthesis of 2,3-dihydroquinazolin-4(1H)-ones: Lactic acid as catalyst under solvent-free condition. *Res. Chem. Intermed.* **2016**, *42*, 6381–6390. [CrossRef]
16. Sarfraz, M.; Sultana, N.; Rashid, U.; Akram, M.S.; Sadiq, A.; Tariq, M.I. Synthesis, biological evaluation and docking studies of 2,3-dihydroquinazolin-4(1H)-one derivatives as inhibitors of cholinesterases. *Bioorg. Chem.* **2017**, *70*, 237–244. [CrossRef]
17. Sharma, S.D.; Kaur, V. Synthesis of 3-Oxa- and 3-Aza-1-dethiacepham Analogs. *Synthesis* **1989**, 677–680. [CrossRef]
18. Bhavani, A.K.D.; Reddy, P.S.N. Synthesis of Some Tetrahydro-3,3'-bisquinazolin-4,4'-diones. *Org. Prep. Proc. Int.* **1992**, *24*, 1–5. [CrossRef]
19. Naleway, J.J.; Fox, C.M.J.; Robinhold, D.; Terpetschnig, E.; Olson, N.A.; Haugland, R.P. Synthesis and Use of New Fluorogenic Precipitating Substrates. *Tetrahedron Lett.* **1994**, *35*, 8569–8572. [CrossRef]
20. Zappalà, M.; Grasso, S.; Micale, N.; Zuccalà, G.; Menniti, F.S.; Ferreri, G.; Di Sarro, G.; De Micheli, C. 1-Aryl-6,7-methylenedioxy-3H-quinazolin-4-ones as Anticonvulsant Agents. *Bioorg. Med. Chem. Lett.* **2003**, *13*, 4427–4430. [CrossRef]
21. Labade, V.B.; Shinde, P.V.; Shingare, M.S. A facile and rapid access towards the synthesis of 2,3-dihydroquinazolin-4(1H)-ones. *Tetrahedron Lett.* **2013**, *54*, 5778–5780. [CrossRef]
22. Chen, J.X.; Wu, H.Y.; Su, W.K. A facile synthesis of 2,3-dihydro-2-aryl-4(1H)-quinazolinones catalyzed by scandium(III) triflate. *Chin. Chem. Lett.* **2007**, *18*, 536–538. [CrossRef]
23. Wang, X.-S.; Yang, K.; Zhou, J.; Tu, S.-J. Facile Method for the Combinatorial Synthesis of 2,2-Disubstituted Quinazolin-4(1H)-one Derivatives Catalyzed by Iodine in Ionic Liquids. *J. Comb. Chem.* **2010**, *12*, 417–421. [CrossRef] [PubMed]
24. Abdollahi-Alibeik, M.; Shabani, E. Synthesis of 2,3-dihydroquinazolin-4(1H)-ones catalyzed by zirconium(IV) chloride as a mild and efficient catalyst. *Chin. Chem. Lett.* **2011**, *22*, 1163–1166. [CrossRef]
25. Englund, E.E.; Neumann, S.; Eliseeva, E.; McCoy, J.G.; Titus, S.; Zheng, W.; Southall, N.; Shinn, P.; Leister, W.; Thomas, C.J.; et al. The synthesis and evaluation of dihydroquinazolin-4-ones and quinazolin-4-ones as thyroid stimulating hormone receptor agonists. *Med. Chem. Commun.* **2011**, *2*, 1016–1020. [CrossRef] [PubMed]
26. Shang, Y.-H.; Fan, L.-Y.; Li, X.-X.; Liu, M.-X. Y(OTf)₃-catalyzed heterocyclic formation *via* aerobic oxygenation: An approach to dihydro quinazolinones and quinazolinones. *Chin. Chem. Lett.* **2015**, *26*, 1355–1358. [CrossRef]

27. Rajaka, L.; Penumati, N.R.; Nagaiah, K.; Poornachandra, Y.; Kumar, C.G. Convenient and Scalable Synthesis of 2,3-Dihydroquinazolin-4(1H)-one Derivatives and Their Anticancer Activities. *Synth. Commun.* **2015**, *45*, 1893–1901. [CrossRef]
28. Ramesh, N.; Rao, M.G.; Varala, R.; Rao, V.U.; Babu, B.H. Mercuric chloride catalyzed synthesis of some anticancer 2-aryl-2,3-dihydroquinazolin-4(1H)-ones. *Med. Chem. Res.* **2016**, *25*, 1945–1951. [CrossRef]
29. Sivaguru, P.; Parameswaran, K.; Lalitha, A. Synthesis of novel eight-membered dibenzo[*b,f*][1,5]oxazocin-6-ones. *Tetrahedron Lett.* **2016**, *57*, 2549–2553. [CrossRef]
30. Luo, Y.; Wu, Y.; Wang, Y.; Sun, H.; Xie, Z.; Zhang, W.; Gao, Z. Ethanol promoted titanocene Lewis acid catalyzed synthesis of quinazoline derivatives. *RSC Adv.* **2016**, *6*, 66074–66077. [CrossRef]
31. Shaabani, A.; Maleki, A.; Mofakham, H. Click Reaction: Highly Efficient Synthesis of 2,3-Dihydroquinazolin-4(1H)-ones. *Synth. Commun.* **2008**, *38*, 3751–3759. [CrossRef]
32. Li, S.-C.; Jhang, W.-F.; Liou, T.-J.; Yang, D.-Y. Photochemical synthesis of indazolo[3,2-*b*]quinazolines and their redox-switching properties. *Dyes Pigm.* **2015**, *114*, 259–266. [CrossRef]
33. Qiao, R.Z.; Xu, B.L.; Wang, Y.H. A facile synthesis of 2-substituted-2,3-dihydro-4(1H)-quinazolinones in 2,2,2-trifluoroethanol. *Chin. Chem. Lett.* **2007**, *18*, 656–658. [CrossRef]
34. Rostamizadeh, S.; Amani, A.M.; Aryan, R.; Ghaieni, H.R.; Shadjou, N. Synthesis of New 2-Aryl Substituted 2,3-Dihydroquinazolin-4(1H)-ones Under Solvent-Free Conditions, Using Molecular Iodine as a Mild and Efficient Catalyst. *Synth. Commun.* **2008**, *38*, 3567–3576. [CrossRef]
35. Karimi-Jaberi, Z.; Zarei, L. Rapid Synthesis of 2-Substituted-2,3-dihydro-4(1H)-quinazolinones using Boric Acid or Sodium Dihydrogen Phosphate under Solvent-Free Conditions. *S. Afr. J. Chem.* **2012**, *65*, 36–38.
36. Xie, Z.-B.; Zhang, S.-G.; Jiang, G.-F.; Sun, D.-Z.; Le, Z.-G. The green synthesis of 2,3-dihydroquinazolin-4(1H)-ones via direct cyclocondensation reaction under catalyst-free conditions. *Green Chem. Lett. Rev.* **2015**, *8*, 95–98. [CrossRef]
37. Roy, A.D.; Jayalakshmi, K.; Dasgupta, S.; Roy, R.; Mukhopadhyay, B. Real time HR-MAS NMR: Application in reaction optimization, mechanism elucidation and kinetic analysis for heterogeneous reagent catalyzed small molecule chemistry. *Magn. Reson. Chem.* **2008**, *46*, 1119–1126. [CrossRef]
38. Shaterian, H.R.; Oveisi, A.R. PPA-SiO₂ as a Heterogeneous Catalyst for Efficient Synthesis of 2-Substituted-1,2,3,4-tetrahydro-4-quinazolinones under Solvent-free Conditions. *Chin. J. Chem.* **2009**, *27*, 2418–2422. [CrossRef]
39. Dar, B.A.; Sahu, A.K.; Patidar, P.; Sharma, P.R.; Mupparapu, N.; Vyas, D.; Maity, S.; Sharma, M.; Singh, B. Heteropolyacid-clay nano-composite as a novel heterogeneous catalyst for the synthesis of 2,3-dihydroquinazolinones. *J. Ing. Eng. Chem.* **2013**, *19*, 407–412. [CrossRef]
40. Dindulkar, S.D.; Oh, J.; Arole, V.M.; Jeong, Y.T. Supported ceric ammonium nitrate: A highly efficient catalytic system for the synthesis of diversified 2,3-substituted 2,3-dihydroquinazolin-4(1H)-ones. *Comptes Rendus Chim.* **2014**, *17*, 971–979. [CrossRef]
41. Safari, J.; Gandomi-Ravandi, S. Efficient synthesis of 2-aryl-2,3-dihydroquinazolin-4(1H)-ones in the presence of nanocomposites under microwave irradiation. *J. Mol. Catal. A: Chem.* **2014**, *390*, 1–6. [CrossRef]
42. Havasi, F.; Ghorbani-Choghamarani, A.; Nikpour, F. Synthesis and characterization of nickel complex anchored onto MCM-41 as a novel and reusable nanocatalyst for the efficient synthesis of 2,3-dihydroquinazolin-4(1H)-ones. *Microporous Mesoporous Mat.* **2016**, *24*, 26–35. [CrossRef]
43. Kausar, N.; Roy, I.; Chattopadhyay, D.; Das, A.R. Synthesis of 2,3-dihydroquinazolinones and quinazolin-4(3H)-ones catalyzed by graphene oxide nanosheets in an aqueous medium: “on-water” synthesis accompanied by carbocatalysis and selective C-C bond cleavage. *RSC Adv.* **2016**, *6*, 22320–22330. [CrossRef]
44. Shiri, L.; Ghorbani-Choghamarani, A.; Kazemi, M. Cu(II) immobilized on Fe₃O₄-diethylenetriamine: A new magnetically recoverable catalyst for the synthesis of 2,3-dihydroquinazolin-4(1H)-ones and oxidative coupling of thiols. *Appl. Organometal. Chem.* **2017**, *31*, e3596. [CrossRef]
45. Mirjalili, B.B.F.; Bamoniri, A.; Azad, S. Synthesis of 2,3-dihydroquinazolin-4(1H)-ones catalyzed by nano-Fe₃O₄/TiCl₂/cellulose as a bio-based magnetic catalyst. *J. Iran. Chem. Soc.* **2017**, *14*, 47–55. [CrossRef]
46. Radfar, I.; Miraki, M.K.; Ghandi, L.; Esfandiary, N.; Abbasi, A.; Karimi, M.; Heydar, A. BF₃-grafted Fe₃O₄@Sucrose nanoparticles as a highly-efficient acid catalyst for syntheses of Dihydroquinazolinones (DHQZs) and Bis 3-Indolyl Methanes (BIMs). *Appl. Organometal. Chem.* **2018**, *32*, e4431. [CrossRef]
47. Efran, M.A.; Akhlaghinia, B.; Ghodsinia, S.S.E. An Efficient Green Protocol for Synthesis of 2,3-Dihydroquinazolin-4(1H)-ones Using SBA-16/GPTMS-TSC-Cu^I under Solvent-Free Conditions. *ChemistrySelect* **2020**, *5*, 2306–2316. [CrossRef]
48. Subba Reddy, B.V.; Venkateswarlu, A.; Madan, C.; Vinu, A. Cellulose-SO₃H: An efficient and biodegradable solid acid for the synthesis of quinazolin-4(1H)-ones. *Tetrahedron Lett.* **2011**, *52*, 1891–1894. [CrossRef]
49. Ghashang, M.; Mansoor, S.S.; Aswin, K. Synthesis of 2,3-dihydroquinazolin-4(1H)-ones catalyzed by succinimide-*N*-sulfonic acid as a mild and efficient catalyst. *Res. Chem. Intermed.* **2015**, *41*, 3447–3460. [CrossRef]
50. Ghorbani-Choghamarani, A.; Azadi, G. Synthesis, characterization, and application of Fe₃O₄-SA-PPCA as a novel nanomagnetic reusable catalyst for the efficient synthesis of 2,3-dihydroquinazolin-4(1H)-ones and polyhydroquinolines. *RSC Adv.* **2015**, *5*, 9752–9758. [CrossRef]
51. Rao, A.V.D.; Vykunteswararao, B.P.; Bhaskarkumar, T.; Jogdand, N.R.; Kalita, D.; Lilakar, J.K.D.; Siddaiah, V.; Sanasi, P.D.; Raghunadh, A. Sulfonic acid functionalized Wang resin (Wang-OSO₃H) as polymeric acidic catalyst for the eco-friendly synthesis of 2,3-dihydroquinazolin-4(1H)-ones. *Tetrahedron Lett.* **2015**, *56*, 4714–4717. [CrossRef]

52. Ghorbani-Choghamarani, A.; Tahmasbi, B. The first report on the preparation of boehmite silica sulfuric acid and its application in some multicomponent organic reactions. *New J. Chem.* **2016**, *40*, 1205–1212. [CrossRef]
53. Hajjami, M.; Ghorbani-Choghamarani, A.; Ghafouri-Nejad, R.; Tahmasbi, B. Efficient preparation of boehmite silica dopamine sulfamic acid as a novel nanostructured compound and its application as a catalyst in some organic reactions. *New J. Chem.* **2016**, *40*, 3066–3074. [CrossRef]
54. Bharate, S.B.; Mupparapu, N.; Manda, S.; Bharate, J.B.; Mudududdla, R.; Yadav, R.R.; Vishwakarma, R.A. Efficient synthesis of 2,3-dihydroquinazolin-4(1H)-ones using heterogeneous solid acid catalysts: Unexpected formation of 2,3-dihydro-2-(4-(tetrahydro-2H-pyran-2-yloxy)butyl)quinazolin-4(1H)-one. *Arkivoc* **2012**, *viii*, 308–318. [CrossRef]
55. Murthy, P.V.N.S.; Rambabu, D.; Krishna, G.R.; Reddy, C.M.; Prasad, K.R.S.; Rao, M.V.B.; Pal, M. Amberlyst-15 mediated synthesis of 2-substituted 2,3-dihydroquinazolin-4(1H)-ones and their crystal structure analysis. *Tetrahedron Lett.* **2012**, *53*, 863–867. [CrossRef]
56. Rambabu, D.; Kumar, S.K.; Sreenivas, B.Y.; Sandra, S.; Kandaale, A.; Misra, P.; Rao, M.V.B.; Pal, M. Ultrasound-based approach to spiro-2,3-dihydroquinazolin-4(1H)-ones: Their in vitro evaluation against chorismate mutase. *Tetrahedron Lett.* **2013**, *54*, 495–501. [CrossRef]
57. Cai, G.; Xu, X.; Li, Z.; Weber, W.P.; Lu, P. A One-Pot Synthesis of 2-Aryl-2,3-dihydro-4(1H)-quinazolinones by use of Samarium Iodide. *J. Heterocycl. Chem.* **2002**, *39*, 1271–1272. [CrossRef]
58. Su, W.; Yang, B. Reductive Cyclization of Nitro and Azide Compounds with Aldehydes and Ketones Promoted by Metallic Samarium and Catalytic Amount of Iodine. *Aust. J. Chem.* **2002**, *55*, 695–697. [CrossRef]
59. Shi, D.; Rong, L.; Wang, J.; Zhuang, Q.; Wang, X.; Hu, H. Synthesis of quinazolin-4(3H)-ones and 1,2-dihydroquinazolin-4(3H)-ones with the aid of a low-valent titanium reagent. *Tetrahedron Lett.* **2003**, *44*, 3199–3201. [CrossRef]
60. Surpur, M.P.; Singh, P.R.; Patil, S.B.; Samant, S.D. Expedient One-Pot and Solvent-Free Synthesis of Dihydroquinazolin-4(1H)-ones in the Presence of Microwaves. *Synth. Commun.* **2007**, *37*, 1965–1970. [CrossRef]
61. Rostamizadeh, S.; Amani, A.M.; Mahdavinia, G.H.; Sepehrian, H.; Ebrahimi, S. Synthesis of Some Novel 2-Aryl-Substituted 2,3-Dihydroquinazolin-4(1H)-ones under Solvent-Free Conditions Using MCM-41-SO₃H as a Highly Efficient Sulfonic Acid. *Synthesis* **2010**, 1356–1360. [CrossRef]
62. Tamaddon, F.; Pouramini, F. Amberlyst A26 OH as a Recyclable Catalyst for Hydration of Nitriles and Water-Based Synthesis of 4(1H)-Quinazolinones from 2-Aminobenzonitrile and Carbonyl Compounds. *Synlett* **2014**, *25*, 1127–1131. [CrossRef]
63. Shaterian, H.R.; Rigi, F. An efficient synthesis of quinazoline and xanthene derivatives using starch sulfate as a biodegradable solid acid catalyst. *Res. Chem. Intermed.* **2015**, *41*, 721–738. [CrossRef]
64. Wang, X.-S.; Yang, K.; Zhang, M.-M.; Yao, C.-S. Synthesis of 2-Arylquinazolin-4(3H)-one Derivatives Catalyzed by Iodine in [bmim⁺][BF₄⁻]. *Synth. Commun.* **2010**, *40*, 2633–2646. [CrossRef]
65. Nagasawa, Y.; Matsusaki, Y.; Nobuta, T.; Tada, N.; Miura, T.; Itoh, A. Aerobic photooxidative synthesis of 2-aryl-4-quinazolinones from aromatic aldehydes and aminobenzamide using catalytic amounts of molecular iodine. *RSC Adv.* **2015**, *5*, 63952–63954. [CrossRef]
66. Feng, E.; Zhou, Y.; Zhang, D.; Zhang, L.; Sun, H.; Jiang, H.; Liu, H. Gold(I)-Catalyzed Tandem Transformation: A Simple Approach for the Synthesis of Pyrrolo/Pyrido[2,1-a][1,3]benzoxazinones and Pyrrolo/Pyrido[2,1-a]quinazolinones. *J. Org. Chem.* **2010**, *75*, 3274–3282. [CrossRef]
67. Wang, M.; Dou, G.; Shi, D. Efficient and Convenient Synthesis of Pyrrolo[1,2-a]quinazoline Derivatives with the Aid of Tin(II) Chloride. *J. Comb. Chem.* **2010**, *12*, 582–586. [CrossRef]
68. Zhao, X.; Shi, D.-Q. An Efficient Synthesis of Pyrrolo[1,2-a]quinazolin-5(1H)-one Derivatives with the Aid of Low-Valent Titanium Reagent. *J. Heterocycl. Chem.* **2011**, *48*, 634–638. [CrossRef]
69. Safai, H.R.; Shekouhy, M.; Khademi, S.; Rahmanian, V.; Safaei, M. Diversity-oriented synthesis of quinazoline derivatives using zirconium tetrakis(dodecylsulfate) [Zr(DS)₄] as a reusable Lewis acid-surfactant-combined catalyst in tap water. *J. Ind. Eng. Chem.* **2014**, *20*, 3019–3024. [CrossRef]
70. Lu, L.; Yang, K.; Zhang, M.-M.; Wang, X.-S. An Efficient Synthesis of Pyrrolo[1,2-a]quinazoline Derivatives in Ionic Liquid Catalyzed by Iodine. *J. Heterocycl. Chem.* **2014**, *51*, 841–845. [CrossRef]
71. Zou, X.; Zhu, C.; Wang, Q.; Yang, G. Catalytic dehydration of hexose sugars to 5-hydroxymethylfural. *Biofuels Bioprod. Biorefining* **2019**, *13*, 153–173. [CrossRef]
72. Nzediegwu, E.; Dumont, M.-J. Chemo-Catalytic Transformation of Cellulose and Cellulosic-Derived Waste Materials into Platform Chemicals. *Waste Biomass Valorization* **2021**, *12*, 2825–2851. [CrossRef]
73. Castro, G.A.D.; Fernandes, S.A. Microwave-assisted green synthesis of levulinate esters as biofuel precursors using calix[4]arene as an organocatalyst under solvent-free conditions. *Sustain. Energ. Fuels* **2021**, *5*, 108–111. [CrossRef]
74. Zhang, W.; Cue, B.W. (Eds.) *Green Techniques for Organic Synthesis and Medicinal Chemistry*, 2nd ed.; John Wiley & Sons, Inc.: Hoboken, NJ, USA, 2018.
75. Protti, S.; Palmieri, A. (Eds.) *Sustainable Organic Synthesis: Tools and Strategies*; Royal Society of Chemistry: London, UK, 2022.
76. James, S.L.; Adams, C.J.; Bolm, C.; Braga, D.; Collier, P.; Friščić, T.; Grepioni, F.; Harris, K.D.M.; Hyett, G.; Jones, W.; et al. Mechanochemistry: Opportunities for new and cleaner synthesis. *Chem. Soc. Rev.* **2012**, *41*, 413–447. [CrossRef]
77. Wang, G.-W. Mechanochemical organic synthesis. *Chem. Soc. Rev.* **2013**, *42*, 7668–7700. [CrossRef]

78. Ranu, B.; Stolle, A. (Eds.) *Ball Milling Towards Green Synthesis: Applications, Projects, Challenges*; RSC Green Chemistry, No. 31; Royal Society of Chemistry: Cambridge, UK, 2015.
79. Margetić, D.; Štrukil, V. *Mechanochemical Organic Synthesis*; Elsevier Inc.: Amsterdam, The Netherland, 2016.
80. Avila-Ortiz, C.G.; Juaristi, E. Novel Methodologies for Chemical Activation in Organic Synthesis under Solvent-Free Reaction Conditions. *Molecules* **2020**, *25*, 3579. [CrossRef]
81. Prasad, D.V.N.; Theuerkauf, J. Effect of Grinding Media Size And Chamber Length on Grinding in a Spex Mixer Mill. *Chem. Eng. Technol.* **2009**, *32*, 1102–1106. [CrossRef]
82. Prasad, D.V.N.; Theuerkauf, J. Improvement in the Collision Intensity of Grinding Media in High Energy Impact Mills. *Chem. Eng. Technol.* **2010**, *33*, 1433–1437. [CrossRef]
83. Fulmer, D.A.; Shearouse, W.C.; Medonza, S.T.; Mack, J. Solvent-Free Sonogashira coupling reaction *via* high speed ball milling. *Green Chem.* **2009**, *11*, 1821–1825. [CrossRef]
84. Sawama, Y.; Yasukawa, N.; Ban, K.; Goto, R.; Niikawa, M.; Monguchi, Y.; Itoh, M.; Sajiki, H. Stainless Steel-Mediated Hydrogen Generation from Alkanes and Diethyl Ether and Its Application for Arene Reduction. *Org. Lett.* **2018**, *20*, 2892–2896. [CrossRef]
85. Bolm, C.; Hernández, J.G. Mechanochemistry of Gaseous Reactants. *Angew. Chem. Int. Ed.* **2019**, *58*, 3285–3299. [CrossRef]
86. Gérard, E.M.C.; Sahin, H.; Encinas, A.; Bräse, S. Systematic Study of a Solvent-Free Mechanochemically Induced Domino Oxa-Michael-Aldol Reaction in a Ball Mill. *Synlett* **2008**, 2702–2704. [CrossRef]
87. Dekamin, M.G.; Eslami, M. Highly efficient organocatalytic synthesis of diverse and densely functionalized 2-amino-3-cyano-4H-pyrans under mechanochemical ball milling. *Green Chem.* **2014**, *16*, 4914–4921. [CrossRef]
88. Gaudino, E.C.; Tagliapierta, S.; Mantegna, S.; Cravotto, G. Mechanochemical and sonochemical heterocyclizations. *Chem. Heterocycl. Compds.* **2016**, *52*, 856–865. [CrossRef]
89. El-Sayed, T.H.; Aboelnaga, A.; El-Atawy, M.A.; Hagar, M. Ball Milling Promoted N-Heterocycles Synthesis. *Molecules* **2018**, *23*, 1348. [CrossRef] [PubMed]
90. Wang, M.; Gao, J.J.; Song, Z.G.; Wang, L. Cerium(IV) ammonium nitrate catalyzed green synthesis of 2,3-dihydroquinazolin-4(1H)-ones using a grinding technique. *Chem. Heterocycl. Compds.* **2011**, *47*, 851–855. [CrossRef]
91. Ding, Q.-S.; Zhang, J.-L.; Chen, J.-X.; Liu, M.-C.; Ding, J.-C.; Wu, H.-Y. Tandem Synthesis of 2,3-Dihydroquinazolin-4(1H)-ones on Grinding under Solvent-Free Conditions. *J. Heterocycl. Chem.* **2012**, *49*, 375–380. [CrossRef]
92. Wang, M.; Gao, J.; Song, Z.; Wang, L. Cerous Methanesulfonate Catalyzed Facile Synthesis of 2-Substituted-2,3-dihydro-4(1h)-quinazolinones by Grinding Technique. *J. Heterocycl. Chem.* **2012**, *49*, 1250–1253. [CrossRef]
93. Sharma, R.; Pandey, A.K.; Chauhan, P.M.S. A Greener Protocol for Accessing 2,3-Dihydro/spiroquinazolin-4(1H)-ones: Natural Acid-SDS Catalyzed Three-Component Reaction. *Synlett* **2012**, *23*, 2209–2214. [CrossRef]
94. Wang, M.; Gao, J.-J.; Song, Z.-G.; Wang, L. Synthesis of 2-Substituted-2,3-dihydro-4(1H)-quinazolinones using Sodium Bisulfate as a Catalyst by the Grinding Technique. *Org. Prep. Proceed. Int.* **2012**, *44*, 159–163. [CrossRef]
95. Miklós, F.; Hum, V.; Fülöp, F. Eco-friendly syntheses of 2,2-disubstituted- and 2-Spiroquinazolinones. *Arkivoc* **2014**, *vi*, 25–37. [CrossRef]
96. Magyar, T.; Miklós, F.; Lázár, L.; Fülöp, F. Synthesis of 2-(hetero)arylquinazolinones in aqueous media. *Arkivoc* **2016**, *vi*, 247–258. [CrossRef]
97. Szöllösi, G. Asymmetric one-pot reactions using heterogeneous chemical catalysis: Recent steps towards sustainable processes. *Catal. Sci. Technol.* **2018**, *8*, 389–422. [CrossRef]
98. Byrne, F.P.; Jin, S.; Paggiola, G.; Petchey, T.H.M.; Clark, J.H.; Farmer, T.J.; Hunt, A.J.; McElroy, C.R.; Sherwood, J. Tools and techniques for solvent selection: The green solvent selection guides. *Sustain. Chem. Process.* **2016**, *4*, 7. [CrossRef]
99. Kolcsár, V.J.; Szöllösi, G. Mechanochemical, Water-Assisted Asymmetric Transfer Hydrogenation of Ketones Using Ruthenium Catalyst. *ChemCatChem* **2022**, *14*, e202101501. [CrossRef]
100. Kolcsár, V.J.; Szöllösi, G. Ru-catalyzed mechanochemical asymmetric transfer hydrogenations in aqueous media using chitosan as chirality source. *Mol. Catal.* **2022**, *520*, 112162. [CrossRef]
101. Lee, S.Y.; Kim, J.C.; Lee, J.S.; Kim, Y.G. Carbonylation of Formaldehyde over Ion Exchange Resin Catalysts. 1. Batch Reactor Studies. *Ind. Eng. Chem. Res.* **1993**, *32*, 253–259. [CrossRef]
102. Park, H.-S.; Ihm, S.-K. Alkylation of benzene with 1-dodecene by macroreticular resin catalysts. *Korean J. Chem. Eng.* **1985**, *2*, 69–74. [CrossRef]
103. Pal, R.; Sarkar, T.; Khasnobis, S. Amberlyst-15 in organic synthesis. *Arkivoc* **2012**, *i*, 570–609. [CrossRef]
104. Fraile, J.M.; Saavedra, C.J. Application of Heterogeneous Catalysts in the First Steps of the Oseltamivir Synthesis. *Catalysts* **2017**, *7*, 393. [CrossRef]
105. Kornas, A.; Śliwa, M.; Ruggiero-Mikołajczyk, M.; Samson, K.; Podobiński, J.; Karcz, R.; Duraczyńska, D.; Rutkowska-Zbik, D.; Grabowski, R. Direct hydrogenation of CO₂ to dimethyl ether (DME) over hybrid catalysts containing CuO/ZrO₂ as a metallic function and heteropolyacids as an acidic function. *Reac. Kin. Mech. Catal.* **2020**, *130*, 179–194. [CrossRef]
106. Habibi, D.; Marvi, O. Montmorillonite KSF clay as an efficient catalyst for the synthesis of 1,4-dioxo-3,4-dihydrophthalazine-2(1H)-carboxamides and -carbothioamides under solvent-free conditions using microwave irradiation. *Catal. Commun.* **2007**, *8*, 127–130. [CrossRef]

Article

[1,5]-Hydride Shift Triggered *N*-Dealkylative Cyclization into 2-Oxo-1,2,3,4-tetrahydroquinoline-3-carboxylates via Boronate Complexes

Elvira R. Zaitseva ¹, Dmitrii S. Ivanov ¹, Alexander Yu. Smirnov ^{1,2}, Andrey A. Mikhaylov ¹,
Nadezhda S. Baleeva ^{1,2} and Mikhail S. Baranov ^{1,2,*}

¹ Institute of Bioorganic Chemistry, Russian Academy of Sciences, Miklukho-Maklaya 16/10, 117997 Moscow, Russia

² Institute of Translational Medicine, Pirogov Russian National Research Medical University, Ostrovitianov 1, 117997 Moscow, Russia

* Correspondence: baranovmikes@gmail.com

Abstract: A new simple one-pot two-step protocol for the synthesis of 2-oxo-1,2,3,4-tetrahydroquinoline-3-carboxylate from 2-(2-(benzylamino)benzylidene)malonate under the action of BF₃·Et₂O was developed. It was shown that the reaction proceeds through the formation of a stable iminium intermediate containing a difluoroboryl bridge in the dicarbonyl fragment of the molecule.

Keywords: amides; BF₃·Et₂O; debenzilation; nitrogen heterocycles; 2-oxo-1,2,3,4-tetrahydroquinoline-3-carboxylate

Citation: Zaitseva, E.R.; Ivanov, D.S.; Smirnov, A.Y.; Mikhaylov, A.A.; Baleeva, N.S.; Baranov, M.S. [1,5]-Hydride Shift Triggered *N*-Dealkylative Cyclization into 2-Oxo-1,2,3,4-tetrahydroquinoline-3-carboxylates via Boronate Complexes. *Molecules* **2022**, *27*, 5270. <https://doi.org/10.3390/molecules27165270>

Academic Editor: Xinfang Xu

Received: 18 July 2022

Accepted: 16 August 2022

Published: 18 August 2022

Publisher's Note: MDPI stays neutral with regard to jurisdictional claims in published maps and institutional affiliations.



Copyright: © 2022 by the authors. Licensee MDPI, Basel, Switzerland. This article is an open access article distributed under the terms and conditions of the Creative Commons Attribution (CC BY) license (<https://creativecommons.org/licenses/by/4.0/>).

1. Introduction

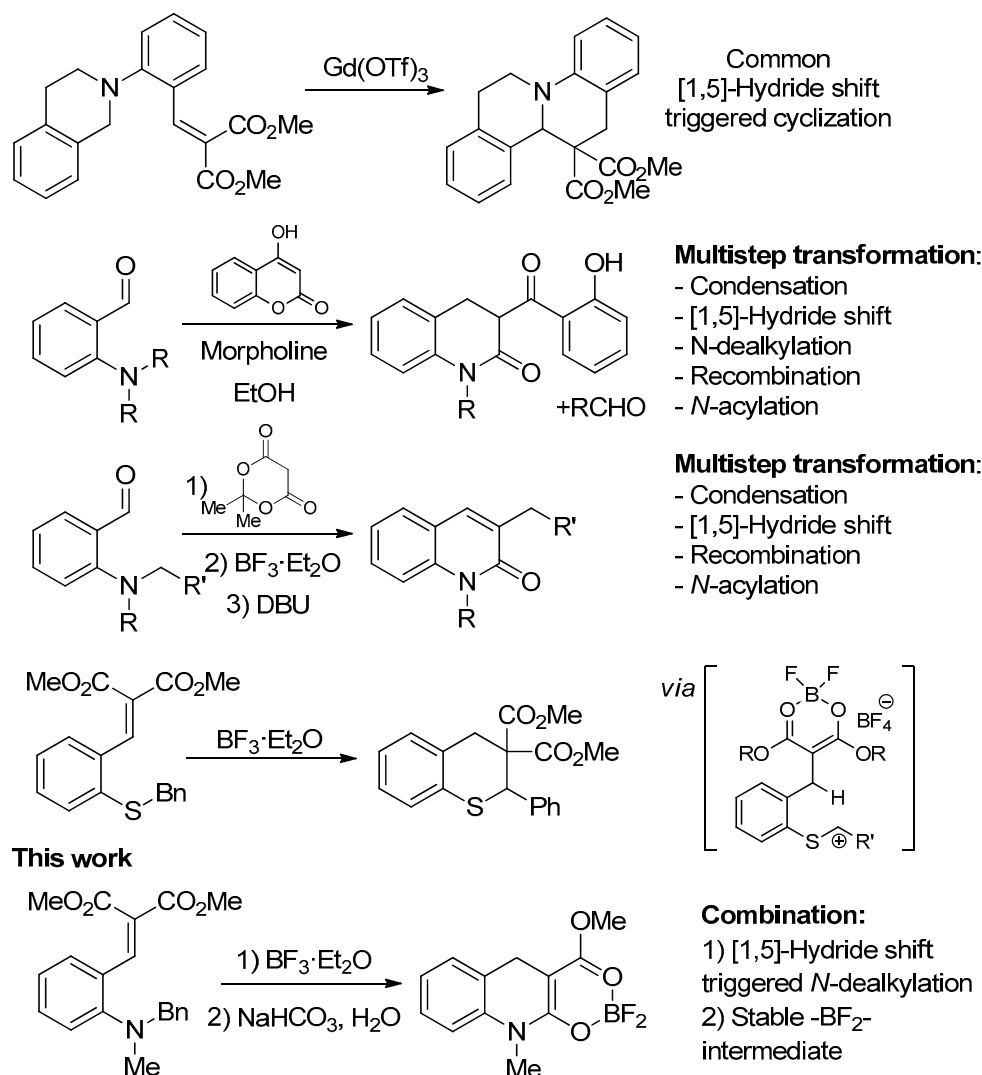
The redox economy concept plays an important role in modern organic synthesis and facilitates the efficiency of synthetic pathways [1,2]. The essential tools for such economy are various redox neutral reactions [2]. Incorporation of the reactions into tandem processes is one of the latest trends [3–5], which allows increasing molecular complexity in a straightforward and economical manner.

Cyclizations triggered by [1,5]-hydride shift are the most frequently employed variants of the internal redox process [6–10]. This cascade reaction involves the activation of thus an inert C–H bond and results in the formation of various heterocycles (Scheme 1, 1st line). For *ortho*-amino benzylidene malonates and other similar derivatives, the transformation proceeds in the presence of various Lewis acids and leads to valuable tetrahydroquinolines (Scheme 1) [11–13]. Tandem processes exploiting such a reaction are mostly limited to double 1,5-hydride shift triggered cyclization [14–17]. However, a few reactions involving more complex multistep transformations were recently reported (Scheme 1, 2nd and 3rd lines) [18,19]. In the first report, the hydride shift process can be also accompanied by the cleavage of a C–N bond and recyclization into the internal amide via an attack on the carbonyl group (Scheme 1) [18]. In the second report, the same recyclization takes place, but the amino substituent still remains in the molecule [19]. These transformations were reported to proceed only with strong acceptor functions, such as Meldrum's acid or 1,3-dicarbonyl derivatives.

In our previous work [20], we showed that BF₃·Et₂O can induce a hydride shift and subsequent cyclization of benzylidene-malonates containing a thioether group, which was shown to be a very poor hydride donor (Scheme 1, 4th line). The key factor driving this process is the formation of chelate species with the O–BF₂–O bridge, which compensates problems in the formation of an intermediate thionium cation (Scheme 1, 4th line). The reaction of this Lewis acid with similar amino derivatives with *N*-benzyl fragment leads to a more rapid consumption of the initial malonate [20]. In the present work, we studied

this process in more detail and showed that the reaction with $\text{BF}_3 \cdot \text{Et}_2\text{O}$ results in the formation of a stable iminium cation containing a difluoroboryl bridge. Treatment of this product with water leads to hydrolysis with formal *N*-dealkylation and formation of 2-oxotetrahydroquinoline-3-carboxylate or its boronate complex. It should be noted that no similar transformation of the dialkyl malonate derivatives was feasible in earlier reports [6,8,9], which demonstrates the efficiency of the activation approach via the boronate complex. The developed protocol allows the redox- and step-economical synthesis of 2-oxo-1,2,3,4-tetrahydroquinoline-3-carboxylates.

Previous works

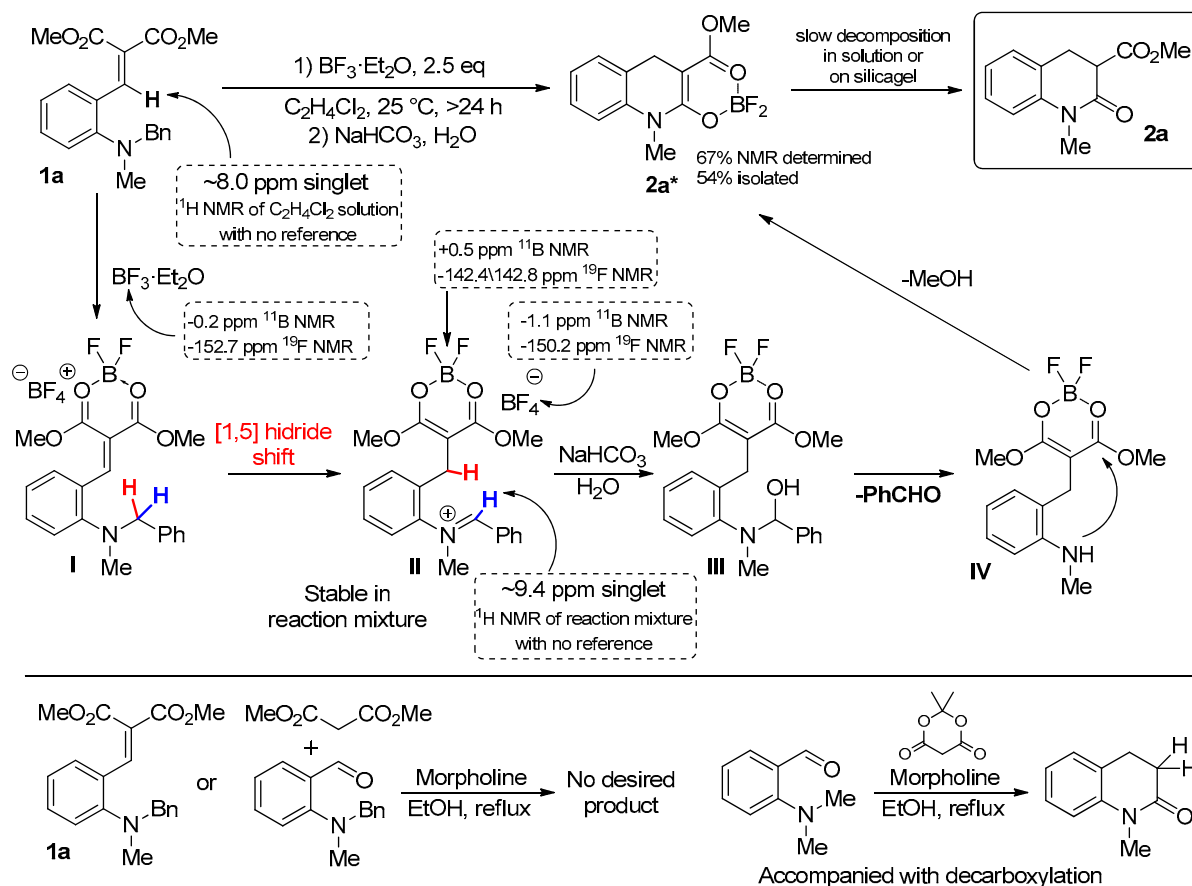


Scheme 1. [1,5]-Hydride shift triggered cyclization and dealkylation. Typical example of 1,5-hydride shift triggered cyclization (1st line) [11], previously proposed multistep transformations (2nd and 3rd lines) [18,19], $\text{BF}_3 \cdot \text{Et}_2\text{O}$ mediated 1,5-hydride shift triggered cyclization of thioethers (4th line) [20] and results of this work.

2. Results and Discussion

In a previous work [20], using quantum mechanical calculations, we showed that the [1,5]-hydride shift reaction of benzylidene malonates with boron trifluoride requires two BF_3 molecules and proceeds via the formation of a stable cation and a difluoroboryl bridge (Scheme 1). Such species were especially stable in case of an iminium cation and are probably capable to undergo various other reactions. This prompted us to carry out more detailed studies.

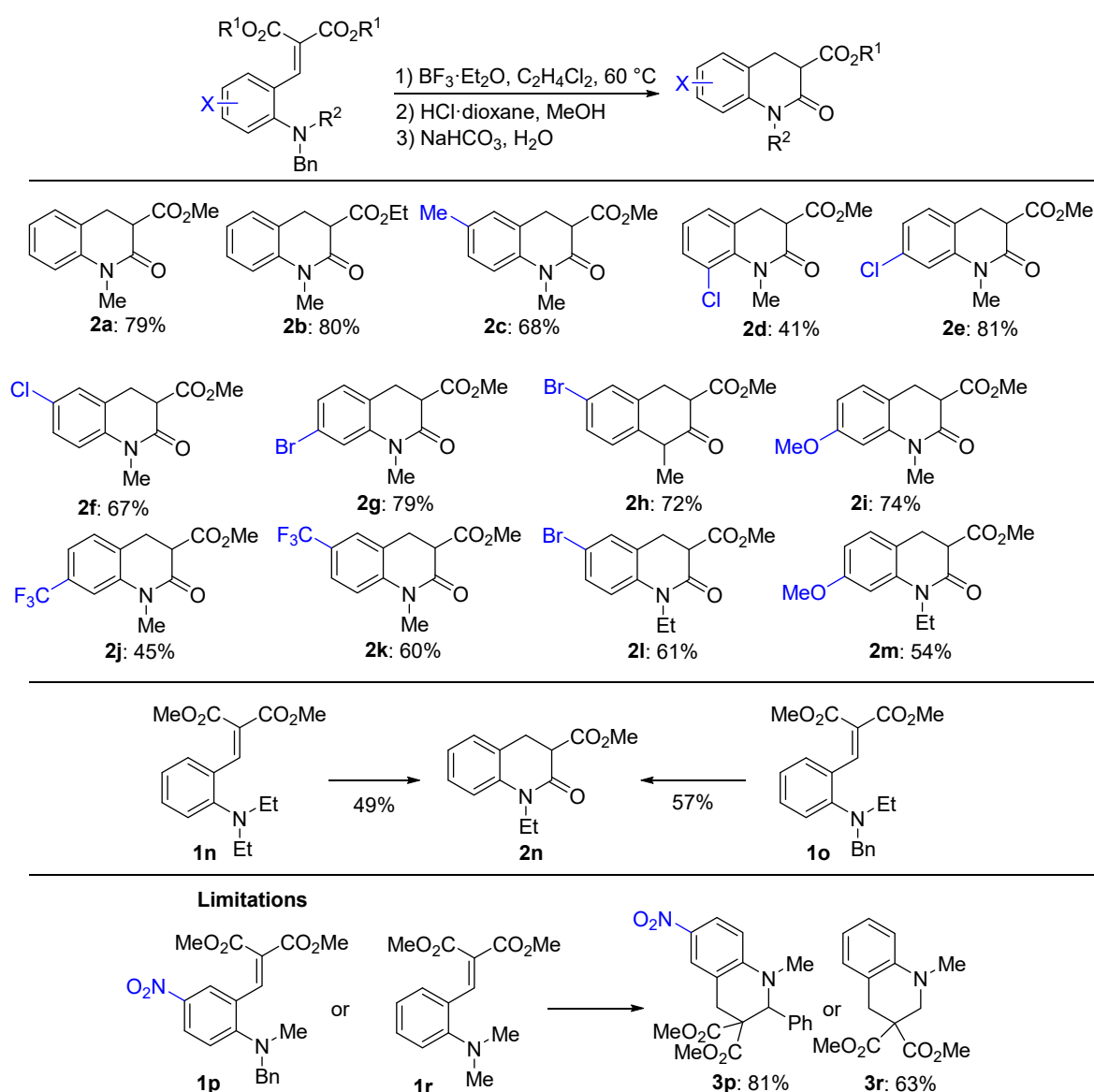
We showed that the prolonged action of the excess of boron trifluoride on malonate derivative **1a**, followed by aqueous treatment, leads to the formation of product **2a*** (Scheme 2). In addition, a noticeable amount of benzaldehyde and product **2a** was observed in the mixture. The amount of **2a** increased with prolonged treatment with water or upon purification on silica gel (Scheme 2).



Scheme 2. Reaction of **1a** with $\text{BF}_3 \cdot \text{Et}_2\text{O}$, proposed reaction mechanism, and comparison with the previously proposed [18] hydride shift triggered *N*-dealkylative cyclization of Meldrum's acid derivatives.

The results of the ^1H NMR spectroscopic analysis of the reaction mixture (SI, part 4, Figures S1 and S2) revealed the formation of the iminium cationic species **II** with $\text{N}^+=\text{CHPh}$ fragment. The presence of such a fragment was confirmed by the appearance of a singlet signal at 9.4 ppm, which significantly differs from the signal of the initial **1a** (8.0 ppm for $\text{CH}=\text{C}(\text{CO}_2\text{Me})_2$ in dichloroethane without additional reference). Formation of a difluoroboryl bridge and BF_4^- anion was confirmed by heteronuclear NMR (SI, part 4, Figures S3–S6). Similarly to the previously reported data [20,21], the transformation of $\text{BF}_3 \cdot \text{Et}_2\text{O}$ into the $\text{O}-\text{BF}_2-\text{O}$ bridge and BF_4^- anion results in the appearance of novel signals: -150.3 , -148.4 , and -142.4 ppm in ^{19}F as well as $+0.5$ and -1.1 ppm in ^{11}B spectra, contrary to -152.7 and -0.2 ppm signals of the initial $\text{BF}_3 \cdot \text{Et}_2\text{O}$.

The subsequent aqueous treatment leads to hydrolysis yielding benzaldehyde and secondary amino derivative **IV**, which readily converts into tetrahydroquinoline **2a*** (Scheme 3).



Scheme 3. Reaction scope.

Under these conditions, substituted malonates **1** can be easily converted into product **2***. However, most of them were even less stable than **2a***. Therefore, we added a HCl treatment step, which provided pure deboronated product **2**. In addition, we briefly examined the conditions of the first step and found that the best results could be obtained for various malonates **1** when 2.5 molar excess of BF_3 was used and the reaction proceeded for 24 h upon heating at 60 °C. We found that the formation of such a product was not observed if various metal triflates or other Lewis acids (AlCl_3 , TiCl_4 or SnCl_4) were used. The action of triflates results in “classical” 1,5-hydride shift triggered cyclization, while stronger action of Lewis acids results in the formation of more complex mixtures. However, the presence of product **2** was also not observed. We also examined the conditions for [1,5]-hydride shift triggered N-dealkylative cyclization (reported for Meldrum’s acid derivatives) by heating with morpholine in ethanol [18]. Heating of neither derivative **1a** nor a mixture of the corresponding aldehyde with diethylmalonate with morpholine did not lead to the formation of tetrahydroquinoline derivatives—the starting materials remained intact even after 24 h (Scheme 2, bottom).

Next, using the revealed conditions, we obtained a series of compound **2** (Scheme 3).

In contrast to the previously studied reaction of the sulfur derivatives [20], we did not observe any difference between the derivatives of dimethyl- (**1a**) and diethylmanolanate (**1b**). Aromatic substituents can influence the stability of boronate complex **2***, but the HCl workup step provided the desired product **2** in good yield in most cases. The exceptions were 8-chloro- (**2d**) and 7-trifluoromethyl- (**2j**) derivatives, which were obtained in the decreased yields of 41% and 45%, respectively. N-benzyl-N-ethyl- substrates **1l** and **1m** provided the target products **2l** and **2m**, respectively, containing an ethyl substituent at the nitrogen atom. In comparison with Mori's report [16], the recombination process was reasonably efficient also for diethylamino derivative **1n** (giving the same product as ethylbenzylamine derivative **1o**). This means that the described method was not limited to "debenzylation".

All the revealed limitations of the reaction correlate well with the stability of the iminium cation. In particular, compounds **1p** and **1r** upon a treatment with $\text{BF}_3 \cdot \text{Et}_2\text{O}$ underwent [1,5]-hydride shift and subsequent cyclization to give compounds **3p** and **3r** in good yield. In both cases, the resulting iminium cations were rather unstable, which shifted the equilibrium toward the classical cyclization product.

3. Materials and Methods

3.1. Materials

Commercially available reagents were used without additional purification. E. Merck Kieselgel 60 (Merck, Darmstadt, Germany) was used for column chromatography. Thin-layer chromatography (TLC) was performed on silica gel 60 F₂₅₄ glass-backed plates (Merck, Darmstadt, Germany). Visualization was performed using UV light (254 or 312 nm) or by staining with KMnO_4 .

NMR spectra were recorded on a 700 MHz Bruker Avance III NMR (Bruker, Rheinstetten, Germany) at 303K, Bruker Avance III 800 (Bruker, Rheinstetten, Germany) (with a 5 mm CPTXI cryoprobe), and Bruker Fourier 300 (Bruker, Rheinstetten, Germany). Chemical shifts were reported relative to the residue peaks of $\text{DMSO-}d_6$ (2.51 ppm for ^1H and 39.5 ppm for ^{13}C). Melting points were measured on an SMP 30 (Buch & Holm A/S, Herlev, Denmark) apparatus without correction. High-resolution mass spectra (HRMS) were recorded on AB Sciex TripleTOF[®] 5600+ System (AB Sciex, Framingham, MA, USA) using electrospray ionization (ESI). The measurements were performed in a positive ion mode (interface capillary voltage 5500 V); the mass ranged from m/z 50 to m/z 3000; external or internal calibration was performed with an ESI Tuning Mix, (Agilent, Santa-Clara, CA, USA). A syringe injection was used for solutions in acetonitrile, methanol, or water (flow rate of 20 $\mu\text{L}/\text{min}$). Nitrogen was applied as a dry gas; the interface temperature was set at 180 °C. IUPAC compound names were generated using ChemDraw Software (PerkinElmer, Waltham, MA, USA).

3.2. Experimental Procedures

3.2.1. Synthesis of Methyl2-((difluoroboranyl)oxy)-1-methyl-1,4-dihydroquinoline-3-carboxylate (**2a***)

Compound **1a** (1 mmol) was dissolved in dry $\text{C}_2\text{H}_4\text{Cl}_2$ (5 mL) under argon atmosphere. Freshly distilled $\text{BF}_3 \cdot \text{Et}_2\text{O}$ (355 mg, 2.5 mmol) was added dropwise, and the resulting mixture was stirred at 25 °C for 24 h. An aqueous solution of NaHCO_3 (3%, 50 mL) was added, and the resulting mixture was extracted with EtOAc (3×50 mL). Combined organic layers were washed with brine (3×50 mL), dried over anhydrous Na_2SO_4 . All volatiles were removed in vacuo, and the residue was purified by flash chromatography (an eluent mixture of hexane and EtOAc , v/v 10:1). Yield 144 mg (54%), white solid, m.p. 188–190 °C.

^1H NMR (700 MHz, $\text{DMSO-}d_6$) δ ppm: 3.39 (s, 3 H), 3.70 (s, 2 H), 3.97 (s, 3 H), 7.15 (td, $J = 7.4, 0.9$ Hz, 1 H), 7.23 (d, $J = 8.0$ Hz, 1 H), 7.26 (dd, $J = 7.5, 1.0$ Hz, 1 H), and 7.28–7.31 (m, 1 H); ^{13}C NMR (176 MHz, $\text{DMSO-}d_6$) δ ppm: 22.7, 30.1, 55.2, 72.3, 115.8, 122.4, 124.9, 127.5, 128.9, 136.8, 163.7, and 168.7. HRMS (ESI-TOF) found, m/z : 268.0957 [$\text{M}+\text{H}$]⁺. $\text{C}_{12}\text{H}_{13}\text{BF}_2\text{NO}^{3+}$. Calculated, m/z : 268.0951.

3.2.2. General Procedure for Synthesis of the Compounds 2

The corresponding substance **1** (1 mmol) was dissolved in dry C₂H₄Cl₂ (5 mL) under argon atmosphere. Freshly distilled BF₃·Et₂O (355 mg, 2.5 mmol) was added dropwise, and the resulting mixture was stirred at 60 °C for 24 h and cooled to 25 °C. A mixture of 5.4 M solution of HCl in dioxane (0.46 mL, 2.5 mmol) and MeOH (5 mL) was added dropwise, and the resulting mixture was stirred for 6 h at 25 °C. An aqueous solution of NaHCO₃ (3%, 50 mL) was added, and the resulting mixture was extracted with EtOAc (3 × 50 mL). The combined organic layers were washed with brine (3 × 50 mL), dried over anhydrous Na₂SO₄. All volatiles were removed in vacuo, and the residue was purified by column chromatography (an eluent mixture of hexane and EtOAc, *v/v* 5:1).

Methyl 1-methyl-2-oxo-1,2,3,4-tetrahydroquinoline-3-carboxylate (2a). Yield 173 mg (79%), light green solid, m.p. 83–85 °C; ¹H NMR (700 MHz, DMSO-*d*₆) δ ppm: 3.09–3.18 (m, 2H), 3.28 (s, 3H), 3.62 (s, 3H), 3.72 (*dd*, *J* = 9.4, 6.4 Hz, 1H), 7.03 (*td*, *J* = 7.4, 0.8 Hz, 1H), 7.12 (*d*, *J* = 8.0 Hz, 1H), 7.24 (*d*, *J* = 7.3 Hz, 1H), and 7.27–7.30 (m, 1H); ¹³C NMR (75 MHz, DMSO-*d*₆) δ ppm: 27.9, 29.5, 47.3, 52.1, 115.1, 122.9, 124.0, 127.7, 127.9, 139.6, 165.8, and 169.8; HRMS (ESI-TOF) found, *m/z*: 220.0969 [M+H]⁺. C₁₂H₁₄NO₃⁺. Calculated, *m/z*: 220.0968. This corresponds to literature data [22].

Ethyl 1-methyl-2-oxo-1,2,3,4-tetrahydroquinoline-3-carboxylate (2b). Yield 186 mg (80%), pale viscous oil; ¹H NMR (700 MHz, DMSO-*d*₆) δ ppm: 1.12 (t, *J* = 7.1 Hz, 3H), 3.09–3.16 (m, 2H), 3.28 (s, 3H), 3.67 (*dd*, *J* = 8.2, 7.3 Hz, 1H), 4.02–4.12 (m, 2H), 7.03 (t, *J* = 7.3 Hz, 1H), 7.12 (*d*, *J* = 8.0 Hz, 1H), 7.24 (*d*, *J* = 7.3 Hz, 1H), and 7.28 (t, *J* = 7.8 Hz, 1H); ¹³C NMR (75 MHz, DMSO-*d*₆) δ ppm: 14.0, 28.0, 29.5, 47.4, 60.7, 115.0, 122.8, 124.0, 127.7, 127.9, 139.6, 165.9, and 169.3; HRMS (ESI-TOF) found, *m/z*: 234.1125 [M+H]⁺. C₁₃H₁₆NO₃⁺. Calculated, *m/z*: 234.1125.

Methyl 1,6-dimethyl-2-oxo-1,2,3,4-tetrahydroquinoline-3-carboxylate (2c). Yield 158 mg (68%), pink solid, m.p. 108–110 °C; ¹H NMR (700 MHz, DMSO-*d*₆) δ ppm: 2.25 (s, 3H), 3.03–3.13 (m, 2H), 3.25 (s, 3H), 3.62 (s, 3H), 3.68 (*dd*, *J* = 9.5, 6.3 Hz, 1H), 7.01 (*d*, *J* = 8.2 Hz, 1H), 7.05 (s, 1H), and 7.08 (*d*, *J* = 8.2 Hz, 1H); ¹³C NMR (75 MHz, DMSO-*d*₆) δ ppm: 20.2, 27.9, 29.5, 47.3, 52.2, 115.0, 123.8, 128.0, 128.4, 131.9, 137.2, 165.6, and 169.8; HRMS (ESI-TOF) found, *m/z*: 234.1126 [M+H]⁺. C₁₃H₁₆NO₃⁺. Calculated, *m/z*: 234.1125.

Methyl 8-chloro-1-methyl-2-oxo-1,2,3,4-tetrahydroquinoline-3-carboxylate (2d). Yield 103 mg (41%), white solid, m.p. 107–109 °C; ¹H NMR (700 MHz, DMSO-*d*₆) δ ppm: 3.08–3.18 (m, 2H), 3.34 (s, 3H), 3.61 (s, 3H), 3.74 (*dd*, *J* = 9.7, 5.3 Hz, 1H), 7.11 (t, *J* = 7.8 Hz, 1H), 7.27 (*d*, *J* = 7.4 Hz, 1H), and 7.37 (*d*, *J* = 8.0 Hz, 1H); ¹³C NMR (75 MHz, DMSO-*d*₆) δ ppm: 28.5, 35.9, 47.7, 52.2, 122.8, 125.5, 126.7, 130.0, 131.0, 138.3, 168.2, and 169.0; HRMS (ESI-TOF) found, *m/z*: 254.0579 [M+H]⁺. C₁₂H₁₃ClNO₃⁺. Calculated, *m/z*: 254.0578.

Methyl 7-chloro-1-methyl-2-oxo-1,2,3,4-tetrahydroquinoline-3-carboxylate (2e). Yield 204 mg (81%), light green solid, m.p. 93–95 °C; ¹H NMR (700 MHz, DMSO-*d*₆) δ ppm: 3.12 (s, 1H), 3.13 (s, 1H), 3.27 (s, 3H), 3.63 (s, 3H), 3.75 (t, *J* = 7.8 Hz, 1H), 7.09 (*dd*, *J* = 7.9, 2.0 Hz, 1H), 7.19 (*d*, *J* = 1.9 Hz, 1H), and 7.27 (*d*, *J* = 8.0 Hz, 1H); ¹³C NMR (75 MHz, DMSO-*d*₆) δ ppm: 27.3, 29.6, 47.0, 52.3, 115.1, 122.4, 123.0, 129.3, 132.1, 141.0, 165.7, and 169.5; HRMS (ESI-TOF) found, *m/z*: 254.0583 [M+H]⁺. C₁₂H₁₃ClNO₃⁺. Calculated, *m/z*: 254.0578.

Methyl 6-chloro-1-methyl-2-oxo-1,2,3,4-tetrahydroquinoline-3-carboxylate (2f). Yield 173 mg (68%), white solid, m.p. 139–141 °C. ¹H NMR (700 MHz, DMSO-*d*₆) δ ppm: 3.10–3.18 (m, 2H), 3.26 (s, 3H), 3.63 (s, 3H), 3.75 (*dd*, *J* = 9.1, 6.8 Hz, 1H), 7.14 (*d*, *J* = 8.8 Hz, 1H), 7.33 (*dd*, *J* = 8.6, 2.5 Hz, 1H), and 7.35 (*d*, *J* = 2.5 Hz, 1H); ¹³C NMR (75 MHz, DMSO-*d*₆) δ ppm: 27.5, 29.6, 46.8, 52.3, 116.8, 126.4, 126.8, 127.3, 127.5, 138.6, 165.6, and 169.5; HRMS (ESI-TOF) found, *m/z*: 254.0582 [M+H]⁺. C₁₂H₁₃ClNO₃⁺. Calculated, *m/z*: 254.0578.

Methyl 7-bromo-1-methyl-2-oxo-1,2,3,4-tetrahydroquinoline-3-carboxylate (2g). Yield 234 mg (79%), white solid, m.p. 127–129 °C; ¹H NMR (700 MHz, DMSO-*d*₆) δ ppm: 3.10 (s, 1H), 3.11 (s, 1H), 3.27 (s, 3H), 3.63 (s, 3H), 3.75 (t, *J* = 7.7 Hz, 1H), 7.19–7.24 (m, 2H), and 7.31 (s, 1H); ¹³C NMR (75 MHz, DMSO-*d*₆) δ ppm: 27.4, 29.6, 46.9, 52.2, 117.8, 120.3, 123.4, 125.4, 129.6, 141.2, 165.7, and 169.5; HRMS (ESI-TOF) found, *m/z*: 298.0071 [M+H]⁺. C₁₂H₁₃BrNO₃⁺. Calculated, *m/z*: 298.0073.

Methyl 6-bromo-1-methyl-2-oxo-1,2,3,4-tetrahydroquinoline-3-carboxylate (2h). Yield 213 mg (72%), white solid, m.p. 141–143 °C; ^1H NMR (700 MHz, DMSO- d_6) δ ppm: 3.11–3.18 (m, 2H), 3.26 (s, 3H), 3.64 (s, 3H), 3.75 (dd, $J=9.2, 6.7$ Hz, 1H), 7.08 (d, $J = 8.6$ Hz, 1H), 7.45 (dd, $J = 8.6, 2.3$ Hz, 1H), and 7.47 (d, $J = 1.9$ Hz, 1H); ^{13}C NMR (75 MHz, DMSO- d_6) δ ppm: 27.4, 29.6, 46.8, 52.3, 114.8, 117.2, 126.7, 130.2, 130.3, 139.0, 165.6, and 169.5; HRMS (ESI-TOF) found, m/z : 298.0075 $[\text{M}+\text{H}]^+$. $\text{C}_{12}\text{H}_{13}\text{BrNO}_3^+$. Calculated, m/z : 298.0073.

Methyl 7-methoxy-1-methyl-2-oxo-1,2,3,4-tetrahydroquinoline-3-carboxylate (2i). Yield 179 mg (72%), colorless viscous oil; ^1H NMR (700 MHz, DMSO- d_6) δ ppm: 3.01–3.09 (m, 2H), 3.27 (s, 3H), 3.62 (s, 3H), 3.67 (dd, $J = 9.2, 6.5$ Hz, 1H), 3.76 (s, 3H), 6.61 (dd, $J = 8.2, 2.3$ Hz, 1H), 6.67 (d, $J = 2.3$ Hz, 1H), and 7.14 (d, $J = 8.2$ Hz, 1H); ^{13}C NMR (75 MHz, DMSO- d_6) δ ppm: 27.2, 29.6, 47.6, 52.1, 55.3, 102.2, 107.4, 115.9, 128.5, 140.6, 159.0, 165.9, and 169.8; HRMS (ESI-TOF) found, m/z : 250.1076 $[\text{M}+\text{H}]^+$. $\text{C}_{13}\text{H}_{16}\text{NO}_4^+$. Calculated, m/z : 250.1074.

Methyl 1-methyl-2-oxo-7-(trifluoromethyl)-1,2,3,4-tetrahydroquinoline-3-carboxylate (2j). Yield 129 mg (45%), colorless viscous oil; ^1H NMR (700 MHz, DMSO- d_6) δ ppm: 3.23 (br.d., $J = 7.8$ Hz, 2H), 3.33 (s, 3H), 3.64 (s, 3H), 3.81 (t, $J = 7.9$ Hz, 1H), 7.38 (s, 1H), 7.40 (d, $J = 7.8$ Hz, 1H), and 7.48 (d, $J = 7.8$ Hz, 1H); ^{13}C NMR (201 MHz, DMSO- d_6) δ ppm: 27.7, 29.6, 46.6, 52.2, 111.4 (q, $J=3.7$ Hz), 119.4 (q, $J = 3.7$ Hz), 124.1 (q, $J = 272.2$ Hz), 128.3 (q, $J = 32.3$ Hz), 128.6, 128.7, 128.8, 140.4, 165.6, and 169.4; HRMS (ESI-TOF) found, m/z : 288.0844 $[\text{M}+\text{H}]^+$. $\text{C}_{13}\text{H}_{13}\text{F}_3\text{NO}_3^+$. Calculated, m/z : 288.0842.

Methyl 1-methyl-2-oxo-6-(trifluoromethyl)-1,2,3,4-tetrahydroquinoline-3-carboxylate (2k). Yield 172 mg (60%), colorless viscous oil; ^1H NMR (700 MHz, DMSO- d_6) δ ppm: 3.24 (d, $J = 7.8$ Hz, 2H), 3.32 (s, 3H), 3.64 (s, 3H), 3.83 (t, $J = 8.0$ Hz, 1H), 7.31 (d, $J = 8.4$ Hz, 1H), and 7.61–7.67 (m, 2H); ^{13}C NMR (201 MHz, DMSO- d_6) δ ppm: 27.4, 29.7, 46.7, 52.2, 115.4, 123.0 (q, $J = 30.8$ Hz), 124.3 (q, $J = 271.4$ Hz), 124.6 (q, $J = 4.4$ Hz), 124.8 (q, $J = 4.4$ Hz), 125.1, 142.9, 165.9, and 169.4; HRMS (ESI-TOF) found, m/z : 288.0846 $[\text{M}+\text{H}]^+$. $\text{C}_{13}\text{H}_{13}\text{F}_3\text{NO}_3^+$. Calculated, m/z : 288.0842.

Methyl 6-bromo-1-ethyl-2-oxo-1,2,3,4-tetrahydroquinoline-3-carboxylate (2l). Yield 190 mg (61%), white solid, m.p. 96–98 °C; ^1H NMR (700 MHz, DMSO- d_6) δ ppm: 1.11 (t, $J = 7.1$ Hz, 3H), 3.09–3.16 (m, 2H), 3.63 (s, 3H), 3.74 (dd, $J = 9.1, 6.6$ Hz, 1H), 3.90 (q, $J = 7.3$ Hz, 2H), 7.12 (d, $J = 8.8$ Hz, 1H), 7.44 (dd, $J = 8.8, 2.3$ Hz, 1H), and 7.48 (d, $J = 2.1$ Hz, 1H); ^{13}C NMR (75 MHz, DMSO- d_6) δ ppm: 12.3, 27.5, 37.1, 46.8, 52.2, 114.6, 117.0, 127.1, 130.3, 130.7, 137.8, 165.1, and 169.5; HRMS (ESI-TOF) found, m/z : 312.0235 $[\text{M}+\text{H}]^+$. $\text{C}_{13}\text{H}_{15}\text{BrNO}_3^+$. Calculated, m/z : 312.0230.

Methyl 1-ethyl-7-methoxy-2-oxo-1,2,3,4-tetrahydroquinoline-3-carboxylate (2m). Yield 142 mg (54%), colorless viscous oil; ^1H NMR (700 MHz, DMSO- d_6) δ ppm: 1.12 (t, $J = 7.1$ Hz, 3H), 2.99–3.07 (m, 2H), 3.61 (s, 3H), 3.66 (dd, $J = 9.0, 6.5$ Hz, 1H), 3.76 (s, 3H), 3.91 (q, $J = 7.1$ Hz, 2H), 6.61 (dd, $J = 8.2, 2.5$ Hz, 1H), 6.67 (d, $J = 2.3$ Hz, 1H), and 7.14 (d, $J = 8.2$ Hz, 1H); ^{13}C NMR (75 MHz, DMSO- d_6) δ ppm: 12.4, 27.3, 37.0, 47.6, 52.1, 55.3, 102.0, 107.2, 116.2, 128.9, 139.3, 159.1, 165.5, and 169.8; HRMS (ESI-TOF) found, m/z : 264.1238 $[\text{M}+\text{H}]^+$. $\text{C}_{14}\text{H}_{18}\text{NO}_4^+$. Calculated, m/z : 264.1230.

Methyl 1-ethyl-2-oxo-1,2,3,4-tetrahydroquinoline-3-carboxylate (2n). Yield 109 mg (47%) from **1n** and 132 mg (57%) from **1o**, pale viscous oil; ^1H NMR (700 MHz, DMSO- d_6) δ ppm: 1.13 (t, $J = 7.1$ Hz, 3H), 3.06–3.15 (m, 2H), 3.62 (s, 3H), 3.70 (dd, $J = 9.4, 6.4$ Hz, 1H), 3.87–3.96 (m, 2H), 7.00–7.04 (m, 1H), 7.16 (d, $J = 8.0$ Hz, 1H), 7.24 (d, $J = 7.4$ Hz, 1H), and 7.26–7.29 (m, 1H); ^{13}C NMR (75 MHz, DMSO- d_6) δ ppm: 12.5, 28.0, 37.0, 47.3, 52.1, 114.9, 122.8, 124.3, 127.8, 128.2, 138.4, 165.3, and 169.7; HRMS (ESI-TOF) found, m/z : 234.1130 $[\text{M}+\text{H}]^+$. $\text{C}_{13}\text{H}_{16}\text{NO}_3^+$. Calculated, m/z : 234.1125.

Dimethyl 1-methyl-6-nitro-2-phenyl-1,4-dihydroquinoline-3,3(2H)-dicarboxylate (3p). Yield 310 mg (81%), yellow solid, m.p. 187–189 °C. ^1H NMR (700 MHz, DMSO- d_6) δ ppm: 3.01 (s, 3H), 3.12 (d, $J = 16.4$ Hz, 1H), 3.28 (m, 1H), 3.59 (d, $J = 6.3$ Hz, 6H), 5.22 (d, $J = 1.5$ Hz, 1H), 6.79 (d, $J = 9.4$ Hz, 1H), 7.02 (dd, $J = 7.3, 1.9$ Hz, 2H), and 7.32–7.36 (m, 3H), 8.02–8.06 (m, 2H); ^{13}C NMR (75 MHz, DMSO- d_6) δ ppm: 27.8, 38.2, 53.0, 53.3, 55.6, 65.1, 109.2, 116.6,

125.1, 125.3, 127.3, 128.7, 128.7, 135.9, 137.6, 149.3, 167.5, and 168.8; HRMS (ESI-TOF) found, m/z : 385.1393 $[M+H]^+$. $C_{20}H_{21}N_2O_6^+$. Calculated, m/z : 385.1394.

Dimethyl 1-methyl-1,4-dihydroquinoline-3,3(2H)-dicarboxylate (3r). Yield 166 mg (63%), yellow solid, m.p. 97–100 °C; 1H NMR (700 MHz, $CDCl_3$) δ ppm: 2.91 (s, 3H), 3.30 (s, 2H), 3.62 (s, 2H), 3.74 (s, 6H), 6.60 (d, J = 8.2 Hz, 1H), 6.69 (t, J = 7.2 Hz, 1H), 7.04 (d, J = 7.4 Hz, 1H), and 7.10 (t, J = 7.7 Hz, 1H); ^{13}C NMR (75 MHz, $CDCl_3$) δ ppm: 33.4, 39.0, 52.8, 52.9, 54.5, 111.2, 117.3, 119.7, 127.3, 128.9, 145.1, and 170.2; HRMS (ESI-TOF) found, m/z : 264.1235 $[M+H]^+$. $C_{14}H_{18}NO_4^+$. Calculated, m/z : 264.1230.

4. Conclusions

We developed a new, redox-neutral method for the synthesis of 2-oxo-1,2,3,4-tetrahydroquinoline-3-carboxylates from 2-(*N*-benzyl-*N*-alkylamino)benzylidene malonates. The process was based on the activation of a substrate with two equivalents of boron trifluoride. This activation leads to [1,5]-hydride shift and the formation of a stable iminium intermediate containing a difluoroboryl bridge. The formation of such an O–BF₂–O bridge was confirmed by a heteronuclear NMR study, while the presence of a stable iminium cation was confirmed by the 1H NMR analysis of a reaction mixture. This product undergoes cyclization upon hydrolysis, resulting in the formation of an amide product. In sum, this process can be described as [1,5]-hydride shift triggered *N*-dealkylative cyclization. The revealed transformation differs from the previously presented examples of hydride shift triggered *N*-dealkylative cyclization, as it does not require the presence of strong electron-accepting functions [18,19], and it is not accompanied with decarboxylation [18] or substituent rearrangements [19].

Supplementary Materials: The following supporting information can be downloaded at: <https://www.mdpi.com/article/10.3390/molecules27165270/s1>, Experimental procedures for the synthesis of initial compounds, Figure S1. copies of 1H and ^{13}C NMR data. Figure S2. 1H NMR spectrum of the reaction mixture in $C_2H_4Cl_2$. Figure S3. ^{11}B NMR spectrum of BF_3 in $C_2H_4Cl_2$. Figure S4. ^{19}F NMR spectrum of BF_3 in $C_2H_4Cl_2$. Figure S5. ^{11}B NMR spectrum of the reaction mixture in $C_2H_4Cl_2$. Figure S6. ^{19}F NMR spectrum of the reaction mixture in $C_2H_4Cl_2$. References [23–28] are cited in the supplementary materials.

Author Contributions: Conceptualization, M.S.B. and A.A.M.; methodology, M.S.B. and A.A.M.; validation, M.S.B. and N.S.B.; investigation, E.R.Z., D.S.I. and A.Y.S.; resources, M.S.B.; data curation, M.S.B. and N.S.B.; writing—original draft preparation, A.Y.S. and N.S.B.; writing—review and editing, M.S.B. and A.A.M.; visualization, N.S.B.; supervision, M.S.B.; project administration, M.S.B.; funding acquisition, N.S.B. All authors have read and agreed to the published version of the manuscript.

Funding: This research was funded by the Russian Science Foundation, grant No. 20–73–10195.

Data Availability Statement: All data are contained within the article or supplementary material.

Acknowledgments: The authors would like to acknowledge D. S. Perekalin (INEOS RAS) for helpful discussion.

Conflicts of Interest: The authors declare no conflict of interest.

Sample Availability: Samples of the compounds 1 and 2 are available from the authors.

References

1. Newhouse, T.; Baran, P.S.; Hoffmann, R.W. The economies of synthesis. *Chem. Soc. Rev.* **2009**, *38*, 3010–3021. [CrossRef]
2. Burns, N.Z.; Baran, P.S.; Hoffmann, R.W. Redox Economy in Organic Synthesis. *Angew. Chem. Int. Ed.* **2009**, *48*, 2854–2867. [CrossRef]
3. Seidel, D. The Azomethine Ylide Route to Amine C–H Functionalization: Redox-Versions of Classic Reactions and a Pathway to New Transformations. *Acc. Chem. Res.* **2015**, *48*, 317–328. [CrossRef]
4. Fiorito, D.; Scaringi, S.; Mazet, C. Transition metal-catalyzed alkene isomerization as an enabling technology in tandem, sequential and domino processes. *Chem. Soc. Rev.* **2021**, *50*, 1391–1406. [CrossRef]
5. Corma, A.; Navas, J.; Sabater, M.J. Advances in One-Pot Synthesis through Borrowing Hydrogen Catalysis. *Chem. Rev.* **2018**, *118*, 1410–1459. [CrossRef]

6. Mori, K. C(sp³)-H Bond Functionalization Mediated by Hydride a Shift/Cyclization System. *Bull. Chem. Soc. Jpn.* **2022**, *95*, 296–305. [CrossRef]
7. An, X.-D.; Xiao, J. Recent advances in hydride transfer-involved C(sp³)-H activation reactions. *Org. Chem. Front.* **2021**, *8*, 1364–1383. [CrossRef]
8. Wang, L.; Xiao, J. Hydrogen-Atom Transfer Reactions. *Top. Curr. Chem.* **2016**, *374*, 17.
9. Haibach, M.C.; Seidel, D. C-H bond functionalization through intramolecular hydride transfer. *Angew. Chem. Int. Ed.* **2014**, *53*, 5010–5036. [CrossRef]
10. Peng, B.; Maulide, N. The Redox-Neutral Approach to C-H Functionalization. *Chem. Eur. J.* **2013**, *19*, 13274–13287. [CrossRef]
11. Murarka, S.; Zhang, C.; Konieczynska, M.D.; Seidel, D. Lewis Acid Catalyzed Formation of Tetrahydroquinolines via an Intramolecular Redox Process. *Org. Lett.* **2009**, *11*, 129–132. [CrossRef] [PubMed]
12. Chen, L.; Zhang, L.; Lv, J.; Cheng, J.-P.; Luo, S. Catalytic Enantioselective tert -Aminocyclization by Asymmetric Binary Acid Catalysis (ABC): Stereospecific 1,5-Hydrogen Transfer. *Chem. Eur. J.* **2012**, *18*, 8891–8895. [CrossRef] [PubMed]
13. Cao, W.; Liu, X.; Wang, W.; Lin, L.; Feng, X. Highly Enantioselective Synthesis of Tetrahydroquinolines via Cobalt(II)-Catalyzed Tandem 1,5-Hydride Transfer/Cyclization. *Org. Lett.* **2011**, *13*, 600–603. [CrossRef]
14. Mori, K.; Kurihara, K.; Yabe, S.; Yamanaka, M.; Akiyama, T. Double C(sp³)-H Bond Functionalization Mediated by Sequential Hydride Shift/Cyclization Process: Diastereoselective Construction of Polyheterocycles. *J. Am. Chem. Soc.* **2014**, *136*, 3744–3747. [CrossRef] [PubMed]
15. Kataoka, M.; Otawa, Y.; Ido, N.; Mori, K. Highly Diastereoselective Synthesis of Medium-Sized Carbocycle-Fused Piperidines via Sequential Hydride Shift Triggered Double C(sp³)-H Bond Functionalization. *Org. Lett.* **2019**, *21*, 9334–9338. [CrossRef]
16. Yokoo, K.; Sakai, D.; Mori, K. Highly Stereoselective Synthesis of Fused Tetrahydropyrans via Lewis-Acid-Promoted Double C(sp³)-H Bond Functionalization. *Org. Lett.* **2020**, *22*, 5801–5805. [CrossRef]
17. Mori, K.; Isogai, R.; Kamei, Y.; Yamanaka, M.; Akiyama, T. Chiral magnesium bisphosphate-catalyzed asymmetric double C(sp³)-H bond functionalization based on sequential hydride shift/cyclization process. *Am. Chem. Soc.* **2018**, *140*, 6203–6207.
18. Yang, X.; Wang, L.; Hu, F.; Xu, L.; Li, S.; Li, S.-S. Redox-Triggered Switchable Synthesis of 3,4-Dihydroquinolin-2(1H)-one Derivatives via Hydride Transfer/N-Dealkylation/N-Acylation. *Org. Lett.* **2021**, *23*, 358–364. [CrossRef]
19. Yokoo, K.; Mori, K. Expedient Synthesis of Multisubstituted Quinolinone Derivatives Based on Ring Recombination Strategy. *Org. Lett.* **2020**, *22*, 244–248. [CrossRef]
20. Zaitseva, E.; Smirnov, A.; Timashev, V.; Malyshev, W.; Zhigileva, E.; Mikhaylov, A.; Medvedev, M.; Baleeva, N.; Baranov, M.S. BF₃ Mediated [1,5]-Hydride Shift Triggered Cyclization: Thioethers Join the Game. *Eur. J. Org. Chem.* **2022**, *2022*, e202200547. [CrossRef]
21. Borisov, D.D.; Novikov, R.A.; Tomilov, Y.V.J. Reactions of Styrylmalonates with Aromatic Aldehydes: Detailed Synthetic and Mechanistic Studies. *Org. Chem.* **2021**, *86*, 4457–4471. [CrossRef] [PubMed]
22. Lu, S.-L.; Li, X.; Qin, W.-B.; Liu, J.-J.; Huang, Y.-Y.; Wong, H.N.C.; Liu, G.-K. Air- and Light-Stable S-(Difluoromethyl)sulfonium Salts: C-Selective Electrophilic Difluoromethylation of β-Ketoesters and Malonates. *Org. Lett.* **2018**, *20*, 6925–6929. [CrossRef] [PubMed]
23. Yang, P.; Xu, W.; Wang, R.; Zhang, M.; Xie, C.; Zeng, X.; Wang, M. Potassium tert-Butoxide-Mediated Condensation Cascade Reaction: Transition Metal-Free Synthesis of Multisubstituted Aryl Indoles and Benzofurans. *Org. Lett.* **2019**, *21*, 3658–3662. [CrossRef] [PubMed]
24. Murarka, S.; Deb, I.; Zhang, C.; Seidel, D. Catalytic enantioselective intramolecular redox reactions: Ring-fused tetrahydroquinolines. *J. Am. Chem. Soc.* **2009**, *131*, 13226–13227. [CrossRef]
25. Zaitseva, E.R.; Smirnov, A.Y.; Myasnyanko, I.N.; Mineev, K.S.; Sokolov, A.I.; Volkina, T.N.; Mikhaylov, A.A.; Baleeva, N.S.; Baranov, M.S. Imidazol-5-ones as a substrate for [1, 5]-hydride shift triggered cyclization. *New J. Chem.* **2021**, *45*, 1805–1808. [CrossRef]
26. Josa-Culleré, L.; Hirst, M.G.; Lockett, J.P.; Thompson, A.L.; Moloney, M.G. Spirocyclic tetramates by sequential knoevenagel and [1, 5]-prototropic shift. *J. Org. Chem.* **2019**, *84*, 9671–9683. [CrossRef]
27. Rosevear, J.; Wilshire, J.F.K. The preparation of some 2-nitroacridines and related compounds. *Aust. J. Chem.* **1981**, *34*, 839–853. [CrossRef]
28. Mori, K.; Ehara, K.; Kurihara, K.; Akiyama, T. Selective Activation of Enantiotopic C(sp³)-Hydrogen by Means of Chiral Phosphoric Acid: Asymmetric Synthesis of Tetrahydroquinoline Derivatives. *J. Am. Chem. Soc.* **2011**, *133*, 6166–6169. [CrossRef]

Article

CK2 Inhibition and Antitumor Activity of 4,7-Dihydro-6-nitroazolo[1,5-a]pyrimidines

Daniil N. Lyapustin¹, Svetlana K. Kotovskaya¹, Ilya I. Butorin¹, Evgeny N. Ulomsky¹, Vladimir L. Rusinov^{1,*}, Denis A. Babkov², Alexander A. Pokhlebin², Alexander A. Spasov², Vsevolod V. Melekhin^{1,3}, Maria D. Tokhtueva¹, Anna V. Shcheglova^{1,3} and Oleg G. Makeev³

¹ Department of Organic and Biomolecular Chemistry, Ural Federal University, Mira St. 19, 620002 Ekaterinburg, Russia

² Department of Pharmacology & Bioinformatics, Scientific Center for Innovative Drugs, Volgograd State Medical University, 400131 Volgograd, Russia

³ Department of Biology, Ural State Medical University, Repina 3, 620014 Yekaterinburg, Russia

* Correspondence: v.l.rusinov@urfu.ru

Abstract: Today, cancer is one of the most widespread and dangerous human diseases with a high mortality rate. Nevertheless, the search and application of new low-toxic and effective drugs, combined with the timely diagnosis of diseases, makes it possible to cure most types of tumors at an early stage. In this work, the range of new polysubstituted 4,7-dihydro-6-nitroazolo[1,5-a]pyrimidines was extended. The structure of all the obtained compounds was confirmed by the data of ¹H, ¹³C NMR spectroscopy, IR spectroscopy, and elemental analysis. These compounds were evaluated against human recombinant CK2 using the ADP-Glo™ assay. In addition, the IC₅₀ parameters were calculated based on the results of the MTT test against glioblastoma (A-172), embryonic rhabdomyosarcoma (Rd), osteosarcoma (Hos), and human embryonic kidney (Hek-293) cells. Compounds **5f**, **5h**, and **5k** showed a CK2 inhibitory activity close to the reference molecule (staurosporine). The most potential compound in the MTT test was **5m** with an IC₅₀ from 13 to 27 μM. Thus, our results demonstrate that 4,7-dihydro-6-nitroazolo[1,5-a]pyrimidines are promising for further investigation of their antitumor properties.

Keywords: nitro compounds; Azolo[1,5-a]pyrimidines; CK2 inhibition; antitumor activity; multicomponent reaction

Citation: Lyapustin, D.N.; Kotovskaya, S.K.; Butorin, I.I.; Ulomsky, E.N.; Rusinov, V.L.; Babkov, D.A.; Pokhlebin, A.A.; Spasov, A.A.; Melekhin, V.V.; Tokhtueva, M.D.; et al. CK2 Inhibition and Antitumor Activity of 4,7-Dihydro-6-nitroazolo[1,5-a]pyrimidines. *Molecules* **2022**, *27*, 5239. <https://doi.org/10.3390/molecules27165239>

Academic Editor: Alexander F. Khlebnikov

Received: 8 July 2022

Accepted: 12 August 2022

Published: 17 August 2022

Publisher's Note: MDPI stays neutral with regard to jurisdictional claims in published maps and institutional affiliations.



Copyright: © 2022 by the authors. Licensee MDPI, Basel, Switzerland. This article is an open access article distributed under the terms and conditions of the Creative Commons Attribution (CC BY) license (<https://creativecommons.org/licenses/by/4.0/>).

1. Introduction

Cancer is one of the world's leading causes of death, with an estimated number of 10 million deaths in 2020 [1]. However, many types of cancer are curable with early diagnosis and treatment. The establishment of alternative ways to treat tumor diseases allows for the use of new effective and low-toxic drugs in the early stages of the disease. One of the current trends is the inhibition of biological targets responsible for the growth, proliferation, and survival of tumor cells. From this point of view, type 2 casein kinase is a promising target for chemotherapy. The overexpression of casein kinase 2 (CK2) is closely associated with several cancers, including cancers of the head and neck, breast, kidney, lung, etc. [2–9], thus making CK2 a promising target for chemotherapy [10–14]. The ATP binding site of CK2 is smaller than that of most other kinases due to the presence of unique bulky residues, such as Val66 and Ile174, which create the prerequisites for the development of selective small molecule ATP-competitive inhibitors [15,16]. In the review article of CK2 and its inhibitors [17] by Iegre and colleagues, compounds of the azolo[1,5-a]pyrimidine series are noted as one of the most significant types of inhibitors over the past decade [18,19], along withazole derivatives (Figure 1) [20,21].

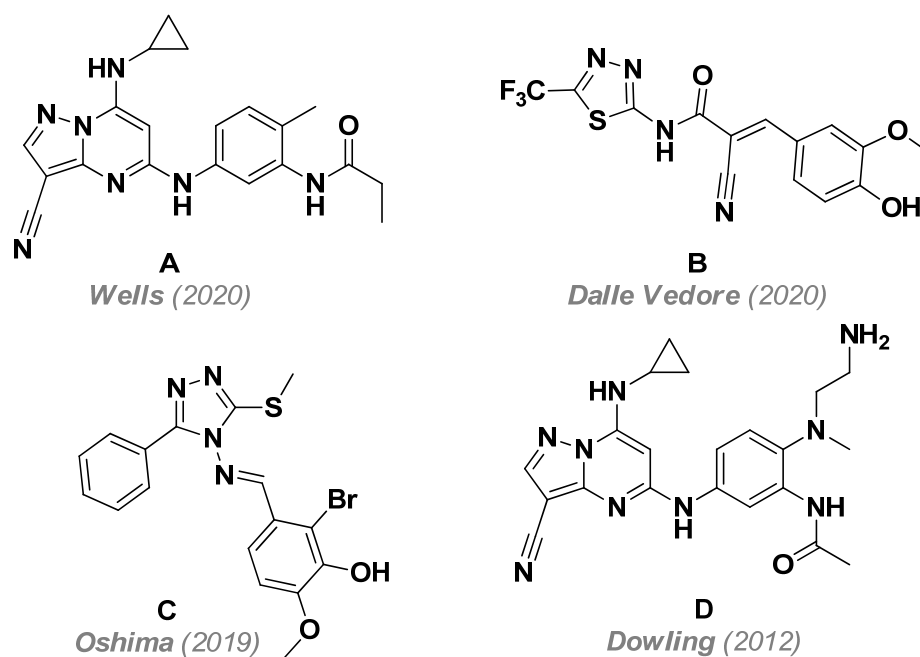


Figure 1. Most significant ATP-competitive CK2 inhibitors: **A** [19], **B** [20], **C** [21], **D** [18].

The antitumor activity of azolo[1,5-a]pyrimidines [22–27] has been related to the inhibition of cancer-associated kinases [28,29] (cyclin-dependent kinase 2 and phosphoinositide-3-kinase). However, recent Safari's work demonstrates a positive trend in the cytotoxic effect of nitro-containing azolo[1,5-a]pyrimidines against human malignant melanoma cells (A375) and prostate cancer (PC3 cells, LNCaP cells) [30]. Examples of azolo[1,5-a]pyrimidines exhibiting antitumor activities are shown in Figure 2.

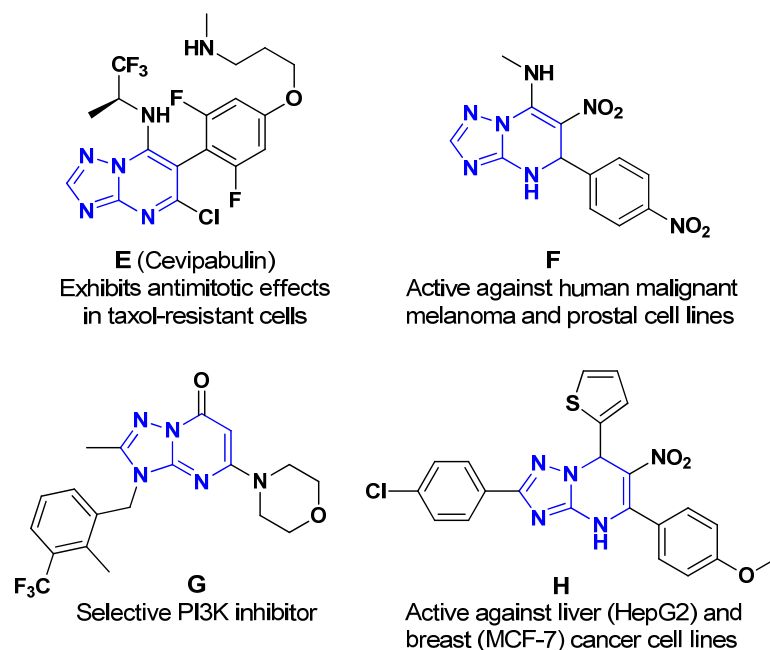


Figure 2. Azolo[1,5-a]pyrimidines exhibiting antitumor activity: **E** [22–25], **F** [30], **G** [26], **H** [27].

To continue our research on polysubstituted 6-nitroazolo[1,5-a]pyrimidines [31–33], we would like to present the synthesis of new compounds of this series, as well as their inhibitory activity against protein kinase CK2 and their cytotoxic effect against cultured tumor cells of human glioblastoma (A-172, ATCC CRL 1620), embryonic rhabdomyosarcoma

(Rd, ATCC CRL 136), human osteosarcoma (Hos, ATCC CRL 1543), and human embryonic kidney (HEK-293).

2. Results and Discussion

2.1. Synthesis

In the present work, we studied compounds of the 4,7-dihydro-6-nitroazolo[1,5-a]pyrimidine **5a-o** and **6a-e** series. These compounds were obtained by a multicomponent reaction between aminoazoles **1,2**, 1-morpholino-2-nitroalkenes **3**, and aldehydes **4** (Scheme 1). It was shown [31] that an initial reaction occurs between 1-morpholino-2-nitroalkenes **3** and aminoazoles **1,2**, followed by heterocyclization to products **5**, and the interaction of boron trifluoride etherate with the morpholinenoitroalkene **3** leads to the formation of a corresponding alkyne and morpholinium tetrafluoroborate. The structure of all the obtained products **5,6** was confirmed by the data of ^1H , ^{13}C NMR spectroscopy, IR spectroscopy, and elemental analysis. The signals H-7 and C-7 are the characteristic for products **5,6** in the corresponding NMR spectra. It is interesting to note that in compounds **5a-d** obtained from 3-aminopyrazole **3a**, in the ^1H spectra, the H-7 signal is in the region of 5.43–5.84 ppm, while in the ^{13}C spectra, the characteristic C-7 signal is in the region of 34–40 ppm. In all other structures **5e-o**, **6a-d**, these signals are shifted to a weaker region of the spectrum in the region of 6.44–6.94 and 55–60 ppm, respectively (see Supplementary Materials). Apparently, the substituent and heteroatom in the azole ring affect the position of these signals.

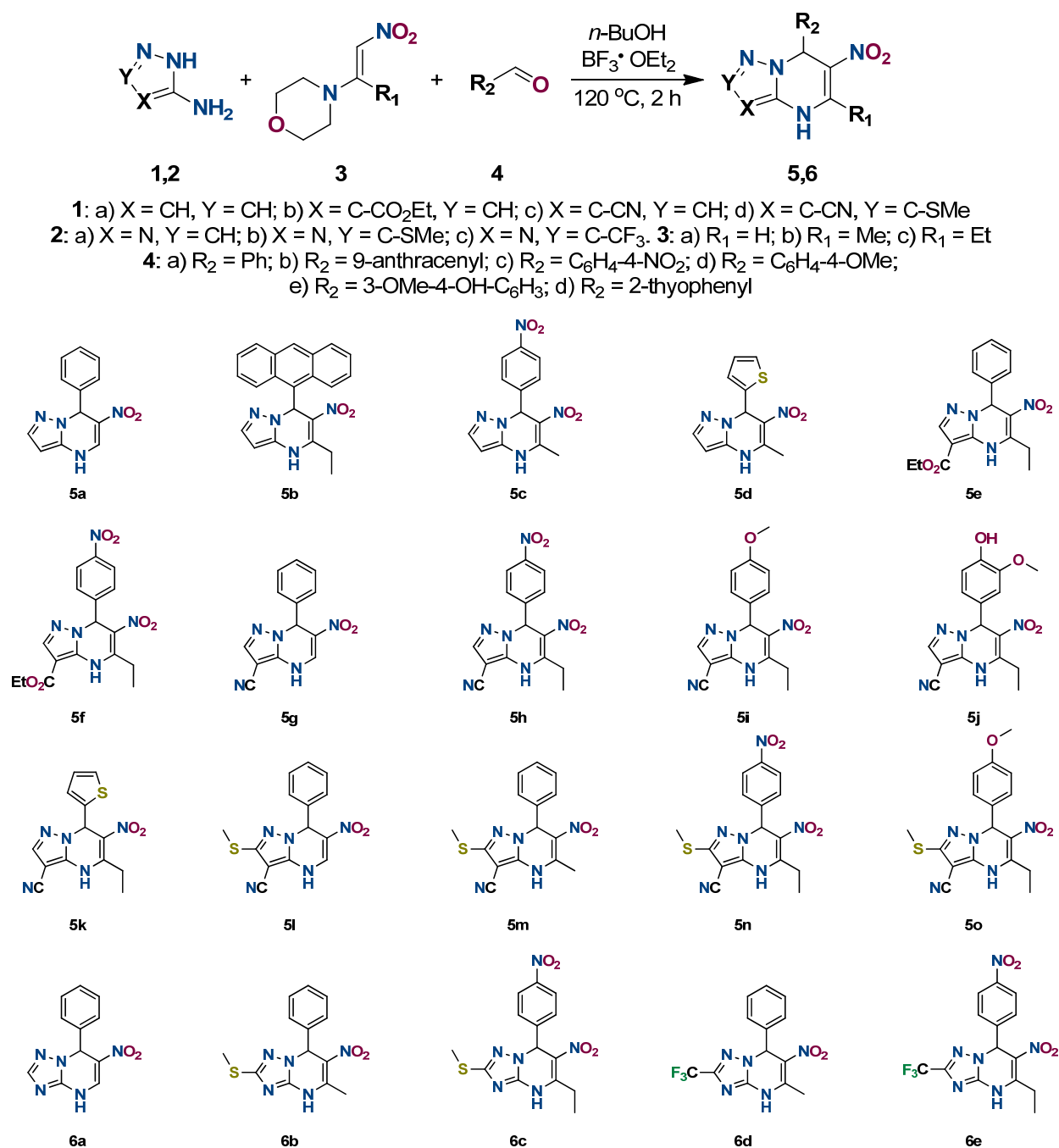
2.2. CK2 Inhibition

Once in hand, target compounds were evaluated against human recombinant CK2 using the ADP-GloTM assay (Table 1). Initial screening at 50 μM revealed that compounds **5a**, **5c**, **5g**, **5m**, **5o**, **6a**, **6c**, and **6d** paradoxically enhance CK2 activity. Moderate inhibition was demonstrated by compounds **5f**, **5h**, **5k**, **5l**, and **6e**. Derivatives **5f**, **5h**, and **5k** were the most active inhibitors. One can notice that compounds bearing alkyl or alkylthio substituents at position C-2 and at position C-6 simultaneously tend to be more active, though the high structural similarity in this series does not allow us to define more comprehensive SAR. A dose–response study confirmed that compounds **5f**, **5h**, **5k**, and **5l** are micromolar CK2 inhibitors, while **6e** has a low potency (Table 2). A hill coefficient around (–1) indicates that lead compounds as well as staurosporine behave like classical inhibitors that bind to a single kinase site.

Table 1. Screening of the target compounds against CK2 activity.

Compound	CK2 Inhibition at 50 μM , $m \pm \text{SD}$ (%)	Compound	CK2 Inhibition at 50 μM , $m \pm \text{SD}$ (%)
5a	n.a.	5k	66.81 \pm 7.97 **
5b	n.a.	5l	48.35 \pm 4.48 *
5c	n.a.	5m	n.a.
5d	n.a.	5n	19.80 \pm 24.53
5e	n.a.	5o	n.a.
5f	53.81 \pm 0.42	6a	n.a.
5g	n.a.	6b	n.a.
5h	54.80 \pm 0.87	6c	n.a.
5i	3.66 \pm 37.60	6d	n.a.
5j	n.a.	6e	39.82 \pm 19.52
	Staurosporine		72.34 \pm 6.39 **

n.a.-not active; * $p < 0.05$, ** $p < 0.01$ -significance vs. DMSO-control. Kruskal–Wallis test.



Scheme 1. Preparation of 4,7-dihydro-6-nitroazolo[1,5-a]pyrimidines 5,6.

Table 2. Inhibition of CK2 by the most active compounds.

Compound	CK2 IC ₅₀ , μM	95% C.I., μM	Hill Coefficient
5f	52.83	39.12–59.08	−1.369
5h	59.47	32.99–66.81	−1.566
5k	52.26	30.10–105.80	−1.183
5l	57.20	57.14–57.26	−2.947
6e	>100	-	-
Staurosporine	69.85	50.96–98.39	−0.974

2.3. Antitumor Activity

The IC₅₀ parameters were calculated based on the results of the MTT test (Table 3). The values are defined in the range from 13 μM to >650 μM. It should be noted that the study of the **5a**, **5b**, and **5c** cytotoxic effects was limited to exclude because of their low solubility.

Table 3. Cytotoxicity index (IC₅₀ ± SE) of 4,7-dihydro-6-nitroazolo[1,5-a]pyrimidines on glioblastoma (A-172), embryonic rhabdomyosarcoma (Rd), osteosarcoma (Hos), and human embryonic kidney (Hek-293) cells, μM.

Compound	IC ₅₀ , μM			
	A-172	Rd	Hos	Hek-293
5d	28.91 ± 4.58	105.54 ± 16.81	103.53 ± 18.27	543.74 ± 70.79
5e	256.72 ± 12.20	99.46 ± 4.43	126.60 ± 7.17	222.84 ± 6.33
5f	212.36 ± 42.85	121.97 ± 13.53	170.14 ± 11.16	35.86 ± 4.30
5g	171.74 ± 8.63	149.72 ± 11.01	181.14 ± 7.47	483.09 ± 37.61
5h	323.41 ± 22.70	378.59 ± 20.39	234.97 ± 25.80	153.47 ± 12.35
5i	145.19 ± 8.96	105.10 ± 10.70	88.44 ± 5.85	69.52 ± 8.69
5j	566.09 ± 17.12	673.44 ± 20.70	522.38 ± 16.16	581.39 ± 43.90
5k	110.23 ± 2.97	89.43 ± 10.46	77.32 ± 3.06	107.57 ± 11.10
5l	77.79 ± 4.02	124.66 ± 6.80	92.91 ± 3.91	162.30 ± 9.95
5m	13.36 ± 0.98	27.52 ± 2.77	18.54 ± 1.79	211.7 ± 10.77
5n	119.75 ± 8.49	151.44 ± 7.28	112.26 ± 8.19	78.70 ± 9.75
5o	22.49 ± 2.93	36.33 ± 3.40	28.09 ± 3.91	169.30 ± 10.88
6a	434.08 ± 18.02	448.21 ± 22.53	542.85 ± 21.45	1131.79 ± 77.86
6b	71.03 ± 2.07	110.11 ± 4.93	92.03 ± 3.08	237.40 ± 11.99
6c	41.27 ± 4.10	71.15 ± 6.84	40.88 ± 4.11	227.50 ± 25.20
6d	27.49 ± 1.67	37.28 ± 3.77	23.31 ± 1.84	50.07 ± 4.43
6e	82.44 ± 2.22	192.69 ± 10.27	93.72 ± 5.89	54.16 ± 5.32
cPt	3.64 ± 0.21	4.99 ± 0.31	2.36 ± 0.12	4.41 ± 0.24

Compounds **5j** and **6a** possessed the least pronounced cytotoxic effect on cells (in all cases IC₅₀ > 0.4 mM), while the greatest decrease in the viability of tumor cells was noted with the addition of compounds **5m**, **5o**, **6c**, and **6d**. It is important to note that these azolopyrimidine compounds are characterized by a more pronounced suppression of the viability of tumor cells A-172, Rd, and Hos in comparison with the effect on human embryonic kidney cells Hek-293 (Figures 3 and 4).

It was found that the IC₅₀ for compounds **5m**, **5o**, **6c**, and **6d** in tumor cell lines studies, mostly, did not exceed 50 μM, whereas the cytotoxicity index on embryonic cells was higher than 169 μM (**5m**, **5o**, and **6c**). It should be noted that compounds **6d** containing a triazole fragment with a CF₃-substituent in the structure had similar micromolar IC₅₀ values for kidney cells and tumor cells. The least cytotoxic effect on non-tumor cells was determined for compound **6c** (227.50 μM). At the same time, our results indicate that compound **5m** may have the most pronounced antitumor properties.

Meanwhile, the mechanisms for the suppression of cultured cells growth remain unclear and require further research. We can assume, that experimental data of cytotoxic action are not fully explained by the effect on CK2. On the one hand, it was noted that azolo[1,5-a]pyrimidines **5k**, **5l**, and **6e** inhibit both the enzymatic activity of CK2 and the viability of tumor cells. On the other hand, compounds **5m**, **5o**, **6c**, and **6d** significantly inhibit the growth of neoplastic cells without affecting CK2. We can assume that the cytotoxic effect of the synthesized compounds may be due to the effect on other intracellular targets.

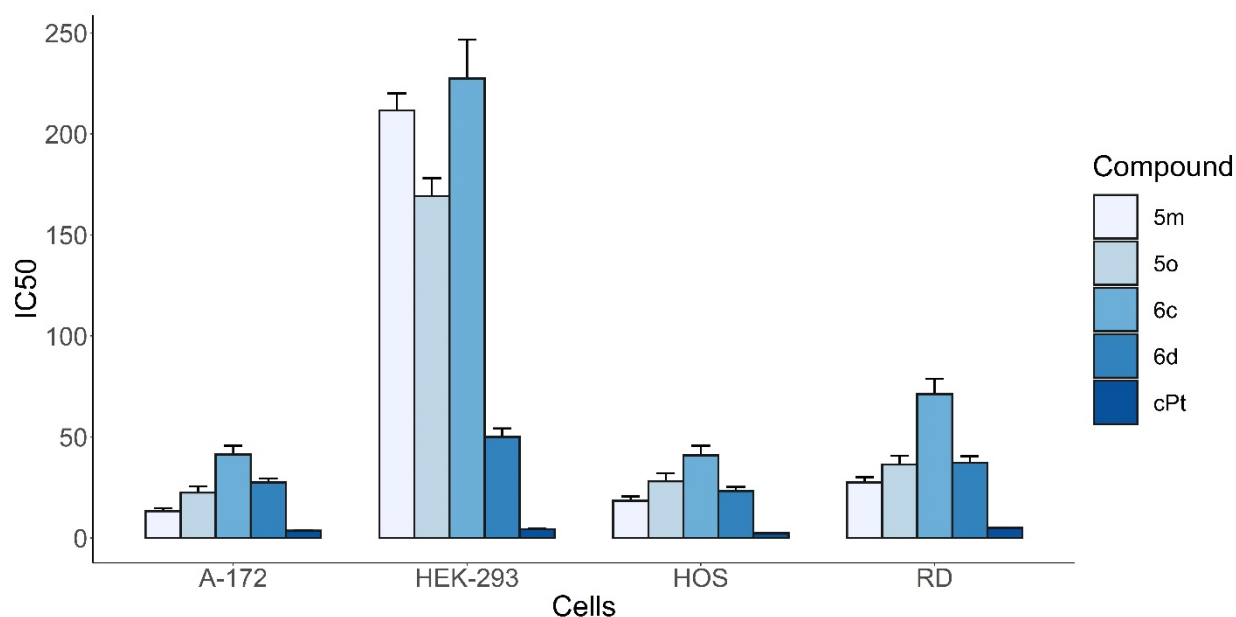


Figure 3. Cytotoxicity index IC₅₀ ± SE for compounds 5m, 5o, 6c, 6d, and cPt in comparison.

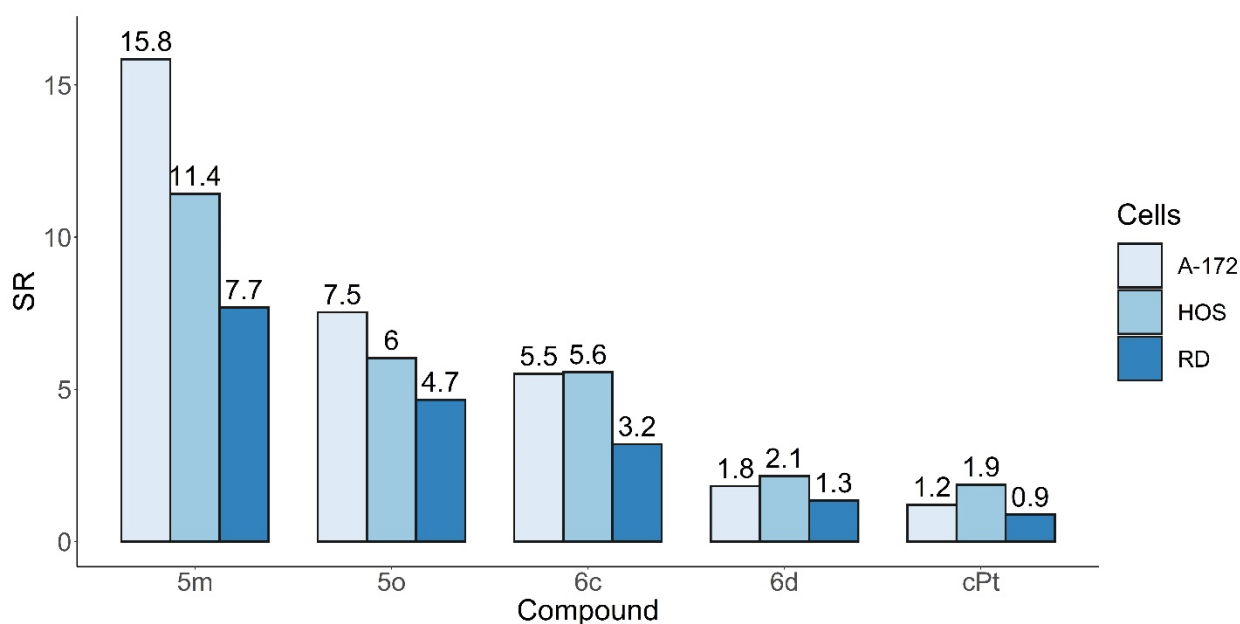


Figure 4. Comparison of the selectivity ratio (normal/cancer cell).

3. Materials and Methods

3.1. Chemical Experiment

Unless stated otherwise, all solvents and commercially available reactants/reagents were used as received. Non-commercial starting materials were prepared as described below or according to literature procedures. One-dimensional ¹H and ¹³C NMR spectra, as well as two-dimensional ¹H–¹³C HMBC experiments were acquired on a Bruker DRX-400 instrument (400 and 101 MHz, respectively) or a Bruker Avance NEO 600 instrument (600 and 151 MHz, respectively), equipped with a Prodigy broadband gradient cryoprobe, utilizing DMSO-*d*₆ as solvent and TMS as internal standard. IR spectra were recorded on a Bruker Alpha FTIR spectrometer equipped with a ZnSe ATR accessory. Elemental analysis was performed on a PerkinElmer 2400 CHN analyzer. The reaction progress was controlled by TLC on Silufol UV-254 plates, eluent—EtOAc. Melting points were determined on a Stuart SMP3 apparatus

at the heating rate of 7 °C/min. 1-Morpholino-2-nitroethylenes **3** were prepared according to a literature procedure [34].

4,7-Dihydro-6-nitroazolo[1,5-a]pyrimidines 5,6; General procedure 1.

A total of 3 Mmol (1.5 equiv., 0.37 mL) of $\text{BF}_3 \cdot \text{Et}_2\text{O}$ was added to a suspension 2 mmol (1.0 equiv.) of corresponding aminoazole **1,2**, 2 mmol (1.0 equiv.) of nitroalkene **3**, and 2 mmol (1.0 equiv.) of aldehyde **4** in 5 mL *n*-BuOH. The reaction mixture was heated on oil bath at 120 °C for 2 h. The resulting solution was cooled to room temperature and stirred 15 min. The obtained precipitate was filtered off, washed with 15 mL of *i*-PrOH. The precipitate was suspended in 50 mL of water, stirred for 5 min, filtered off again, and washed with 15 mL of water.

4,7-Dihydro-6-nitroazolo[1,5-a]pyrimidines 5,6; General procedure 2.

A total of 3 Mmol (1.5 equiv., 0.37 mL) of $\text{BF}_3 \cdot \text{Et}_2\text{O}$ was added to a suspension 2 mmol (1.0 equiv.) of corresponding aminoazole **1,2**, 2 mmol (1.0 equiv.) of nitroalkene **3**, and 2 mmol (1.0 equiv.) of aldehyde **4** in 5 mL *n*-BuOH. The reaction mixture was heated on oil bath at 120 °C for 2 h. After heating, the resulting solution was concentrated under reduced pressure. To the residue, 20 mL of 2M Na_2CO_3 and 50 mL of water was added and stirred for 20 min. Solution was extracted twice with 20 mL of EtOAc. To a water phase, 15 mL of hexane was added and mixture was neutralized by diluted HCl to pH 7. Resulting mixture was stirred for 30 min, filtered off, and washed with water.

6-Nitro-7-phenyl-4,7-dihydropyrazolo[1,5-a]pyrimidine (5a). The reaction was performed according to the general procedure 1 employing 0.166 g (2 mmol, 1 equiv.) of 3-aminopyrazole **1a**, 0.316 g (2 mmol, 1 equiv.) of 1-morpholino-2-nitroethylene **3a**, and 0.20 mL (2 mmol, 1 equiv.) of benzaldehyde **4a**. The product was recrystallized from DMF. The substance was dried over P_2O_5 at 170 °C. Yellow solid. Yield 0.387 g (80%). mp 295–297 °C. IR Spectrum, ν cm^{-1} : 1528, 1417 (NO_2). ^1H NMR (400 MHz, $\text{DMSO}-d_6$): δ = 5.43 (1H, s, H-7); 7.10–7.30 (5H, m, Ph); 7.41 (1H, s, H-2); 8.36 (1H, d, H-5, J = 6.1 Hz); 10.88 (1H, d, NH, J = 6.4 Hz); 12.45 (1H, s, H-3). ^{13}C $\{^1\text{H}\}$ NMR (101 MHz, $\text{DMSO}-d_6$): δ = 38.2; 106.8; 124.3; 126.2; 126.5; 128.4; 127.3; 139.0; 144.2; 146.0. Anal. Calcd. for $\text{C}_{12}\text{H}_{10}\text{N}_4\text{O}_2$: C, 59.50; H, 4.16; N, 23.13. Found: C, 59.61; H, 4.20; N, 23.01.

7-(Anthracen-9-yl)-5-ethyl-7-nitro-4,7-dihydropyrazolo[1,5-a]pyrimidine (5b). The reaction was performed according to the general procedure 1 employing 0.166 g (2 mmol, 1 equiv.) of 3-aminopyrazole **1a**, 0.372 g (2 mmol, 1 equiv.) of 1-morpholino-2-nitroethylene **3a** and 0.412 g (2 mmol, 1 equiv.) of 9-anthracenecarbaldehyde **4b**. The product was recrystallized from *n*-BuOH. The substance was dried over P_2O_5 at 170 °C. Yellow solid. Yield 0.385 g (53%). mp 215 °C with decomp. IR Spectrum, ν cm^{-1} : 1518, 1277 (NO_2). ^1H NMR (400 MHz, $\text{DMSO}-d_6$): δ = 1.38 (3H, t, $\text{CH}_2\text{-CH}_3$, J = 7.3 Hz); 2.73–2.84, 3.16–3.26 (2H, m, $\text{CH}_2\text{-CH}_3$); 8.40 (1H, s, H-2); 6.88 (1H, s, H-7); 7.08 (1H, s, H-9'); 7.26 (1H, m, H-7'); 7.35 (1H, m, H-2'); 7.52 (2H, m, H-6'); 7.60 (2H, m, H-3'); 7.98 (1H, d, H-5', J = 8.4 Hz); 8.06 (1H, d, H-4', J = 8.4 Hz); 8.11 (1H, d, H-8', J = 9.1 Hz); 8.40 (1H, s, H-2); 8.71 (1H, d, H-1', J = 9.1 Hz); ^{13}C $\{^1\text{H}\}$ NMR (101 MHz, $\text{DMSO}-d_6$): δ = 13.5; 28.0; 34.8; 106.7; 124.6 (2C); 124.9; 125.0; 125.2; 125.5; 126.8; 126.9; 127.1; 128.7; 129.4; 129.9; 130.4; 131.5; 132.2; 137.5; 145.1; 155.6. Anal. Calcd. for $\text{C}_{22}\text{H}_{18}\text{N}_4\text{O}_2$: C, 71.34; H, 4.90; N, 15.13. Found: C, 71.52; H, 4.72; N, 14.99.

6-Nitro-5-methyl-7-(4'-nitrophenyl)-4,7-dihydropyrazolo[1,5-a]pyrimidine (5c). A total of 3 Mmol (1.5 equiv., 0.37 mL) of $\text{BF}_3 \cdot \text{Et}_2\text{O}$ was added to a suspension of 0.166 g (2 mmol, 1 equiv.) of 3-aminopyrazole **1a** and 0.344 g (2 mmol, 1 equiv.) of 1-morpholino-2-nitropropylene **3b** in 5 mL *n*-BuOH. The reaction mixture was heated on oil bath at 80 °C for 15 min. After this, 0.302 g (2 mmol, 1 equiv.) of 4-nitrobenzaldehyde **4c** was added to the obtained solution. The reaction mixture was heated on oil bath at 120 °C for 2 h. The resulting solution was cooled to room temperature and stirred for 15 min. The obtained precipitate was filtered off, washed with 15 mL of *i*-PrOH. The precipitate was suspended in 50 mL of water, stirred for 5 min, filtered off again and washed with 15 mL of water. To the residue, 20 mL of 2 M Na_2CO_3 and 50 mL of water were added and stirred for 20 min. The solution was extracted twice with 20 mL of EtOAc. To the water phase, 15 mL of hexane was added, and the mixture was neutralized by diluted HCl to pH 7. The resulting mixture was stirred overnight, filtered off, and washed

with water. Yellow solid. Yield 0.355 g (59%). mp 198 °C with decomp. IR Spectrum, ν cm^{-1} : 1535, 1352 (NO_2); 1508, 1268 (NO_2). ^1H NMR (600 MHz, $\text{DMSO-}d_6$): δ = 2.66 (3H, s, C-5- CH_3); 5.64 (1H, s, H-5); 7.45 (1H, s, H-2); 7.50 (2H, d, H-2', J = 8.3 Hz); 8.12 (2H, d, H-3', J = 8.3 Hz); 10.95 (1H, s, NH); 12.49 (1H, s, H-3). ^{13}C $\{^1\text{H}\}$ NMR (151 MHz, $\text{DMSO-}d_6$): δ = 22.0; 39.8; 105.6; 121.8; 123.8; 127.0; 127.6; 144.2; 145.9; 152.5; 154.1. Anal. Calcd. for $\text{C}_{13}\text{H}_{11}\text{N}_5\text{O}_4$: C, 51.83; H, 3.68; N, 23.25 Found: C, 51.89; H, 3.73; N, 23.19.

6-Nitro-5-methyl-7-(thiophen-2'-yl)-4,7-dihydropyrazolo[1,5-a]pyrimidine (5d). The reaction was performed according to the general procedure 1 employing 0.166 g (2 mmol, 1 equiv.) of 3-aminopyrazole **1a**, 0.344 g (2 mmol, 1 equiv.) of 1-morpholino-2-nitropropylene **2b** and 0.184 mL (2 mmol, 1 equiv.) of thiophen-2-carbaldehyde **4f**. Pale green solid. Yield 0.278 (53%). mp 210 °C with decomp. IR Spectrum, ν , cm^{-1} : 1511, 1256 (NO_2). ^1H NMR (400 MHz, $\text{DMSO-}d_6$): δ = 2.58 (3H, s, C-5- CH_3); 5.84 (1H, s, H-7); 6.80–6.82 (1H, m, H-3'); 6.83–6.87 (1H, m, H-4'); 7.23 (1H, d, H-5', J = 5.0 Hz); 7.56 (1H, s, H-2); 10.85 (1H, s, NH); 12.49 (1H, s, H-3). ^{13}C $\{^1\text{H}\}$ NMR (101 MHz, $\text{DMSO-}d_6$): δ = 21.8; 34.3; 106.2; 122.9; 123.1; 123.6; 126.5; 126.7; 144.5; 150.6; 151.1. Anal. Calcd. for $\text{C}_{11}\text{H}_{10}\text{N}_4\text{O}_2\text{S}$: C, 50.37; H, 3.84; N, 21.36. Found: C, 50.20; H, 3.99; N, 21.49.

3-Etoxycarbonyl-5-ethyl-6-nitro-7-phenyl-4,7-dihydropyrazolo[1,5-a]pyrimidine (5e). The reaction was performed according to the general procedure 1 employing 0.31 g (2 mmol, 1 equiv.) of 3-amino-4-etoxy carbonylpyrazole **1b**, 0.372 g (2 mmol, 1 equiv.) of 1-morpholino-2-nitrobutylene **3c** and 0.2 mL (2 mmol, 1 equiv.) of benzaldehyde **4a**. Orange yellow solid. Yield 0.424 g (62%). mp 127–129 °C. IR Spectrum, ν , cm^{-1} : 1669 (C=O); 1584, 1289 (NO_2). ^1H NMR (600 MHz, $\text{DMSO-}d_6$): δ = 1.32 (6H, t, $\text{CH}_2\text{-CH}_3$, J = 7.1 Hz); 3.19 (2H, q, C-5- $\text{CH}_2\text{-CH}_3$, J = 7.2 Hz); 4.18–4.38 (2H, m, C(O)- $\text{CH}_2\text{-CH}_3$); 6.55 (1H, s, H-7); 7.22–7.36 (5H, m, Ph); 7.66 (1H, s, H-2); 10.29 (1H, s, NH). ^{13}C $\{^1\text{H}\}$ NMR (151 MHz, $\text{DMSO-}d_6$): δ = 12.5; 14.3; 25.2; 59.4; 59.8; 97.6; 122.0; 127.1; 139.6; 128.4; 128.6; 137.4; 140.8; 152.7; 161.7. Anal. Calcd. for $\text{C}_{17}\text{H}_{18}\text{N}_4\text{O}_4$: C, 59.64; H, 5.30; N, 16.37. Found: C, 59.69; H, 5.32; N, 16.49.

3-Etoxycarbonyl-5-ethyl-6-nitro-7-(4'-nitrophenyl)-4,7-dihydropyrazolo[1,5-a]pyrimidine (5f). The reaction was performed according to the general procedure 2 employing 0.31 g (2 mmol, 1 equiv.) of 3-amino-4-etoxy carbonylpyrazole **1b**, 0.372 g (2 mmol, 1 equiv.) of 1-morpholino-2-nitrobutylene **3c** and 0.302 g (2 mmol, 1 equiv.) of 4-nitrobenzaldehyde **4c**. Pale yellow solid. Yield 0.425 g (55%). mp 156–158 °C. IR Spectrum, ν , cm^{-1} : 1720 (C=O); 1579, 1519, 1350, 1307 (NO_2). ^1H NMR (600 MHz, $\text{DMSO-}d_6$): δ = 1.34 (6H, m, $\text{CH}_2\text{-CH}_3$); 3.23 (3H, q, C-5- $\text{CH}_2\text{-CH}_3$); 4.30 (2H, q, C(O)- $\text{CH}_2\text{-CH}_3$); 6.72 (1H, s, H-7); 7.59 (2H, d, H-2', J = 8.4 Hz); 7.69 (1H, s, H-2); 8.19 (2H, d, H-3', J = 8.4 Hz); 10.48 (1H, s, NH). ^{13}C $\{^1\text{H}\}$ NMR (151 MHz, $\text{DMSO-}d_6$): δ = 12.5; 14.3; 25.2; 58.8; 59.9; 97.9; 121.3; 123.9; 128.6; 141.2; 146.4; 147.4; 153.5; 161.6. Anal. Calcd. for $\text{C}_{17}\text{H}_{17}\text{N}_5\text{O}_6$: C, 52.95; H, 4.57; N, 18.10. Found: C, 52.71; H, 4.42; N, 18.08.

3-Cyano-6-nitro-7-phenyl-4,7-dihydropyrazolo[1,5-a]pyrimidine (5g). The reaction was performed according to the general procedure 1 employing 0.216 g (2 mmol, 1 equiv.) of 3-amino-3-cyanopyrazole **1c**, 0.316 g (2 mmol, 1 equiv.) of 1-morpholino-2-nitroethylene **3c** and 0.20 mL (2 mmol, 1 equiv.) of benzaldehyde **4a**. The product was recrystallized from MeOH. Yellow solid. Yield 0.219 g (41%). mp 262 °C with decomp. IR Spectrum, ν , cm^{-1} : 2232 (CN); 1593, 1333 (NO_2). ^1H NMR (400 MHz, $\text{DMSO-}d_6$): δ = 6.62 (1H, s, H-7); 7.20–7.47 (5H, m, Ph); 7.95 (1H, s, H-2); 8.47 (1H, s, H-5); 12.43 (1H, br.s.; NH). ^{13}C $\{^1\text{H}\}$ NMR (101 MHz, $\text{DMSO-}d_6$): δ = 59.6; 76.2; 112.6; 124.3; 127.5; 128.6; 128.7; 134.6; 138.8; 139.6; 143.1. Anal. Calcd. for $\text{C}_{13}\text{H}_9\text{N}_5\text{O}_2$: C, 58.43; H, 3.39; N, 26.21. Found: C, 58.49; H, 3.33; N, 26.29.

3-Cyano-5-ethyl-6-Nitro-7-(4'-nitrophenyl)-4,7-dihydropyrazolo[1,5-a]pyrimidine (5h). The reaction was performed according to the general procedure 1 employing 0.216 g (2 mmol, 1 equiv.) of 3-amino-4-cyanopyrazole **1c**, 0.372 g (2 mmol, 1 equiv.) of 1-morpholino-2-nitrobutylene **3c** and 0.302 g (2 mmol, 1 equiv.) of 4-nitrobenzaldehyde **4c**. The substance was dried over P_2O_5 at 170 °C. Yellow solid. Yield 0.394 g (58%). mp 230 °C with decomp. IR Spectrum, ν , cm^{-1} : 2231 (CN); 1584, 1350 (NO_2); 1520, 1315 (NO_2). ^1H NMR (400 MHz, $\text{DMSO-}d_6$): δ = 1.32 (3H, t, $\text{CH}_2\text{-CH}_3$; J = Hz); 2.90–3.15 (2H, m, $\text{CH}_2\text{-CH}_3$); 6.76 (1H, s, H-7); 7.63 (2H, d, H-2', J = 8.3 Hz); 7.95 (1H, s, H-2); 8.17 (2H, d, H-3', J = 8.3 Hz); 12.07 (1H,

s, NH). ^{13}C $\{^1\text{H}\}$ NMR (101 MHz, DMSO- d_6): δ = 12.4; 25.5; 59.1; 75.9; 112.7; 121.0; 123.8; 128.8; 139.3; 143.5; 146.1; 147.5; 153.0. Anal. Calcd. for $\text{C}_{15}\text{H}_{12}\text{N}_6\text{O}_4$: C, 52.94; H, 3.55; N, 24.70. Found: C, 52.89; H, 3.47; N, 24.69.

3-Cyano-5-ethyl-6-Nitro-7-(4'-methoxyphenyl)-4,7-dihydropyrazolo[1,5-a]pyrimidine (5i).

The reaction was performed according to the general procedure 1 employing 0.216 g (2 mmol, 1 equiv.) of 3-aminopyrazole **1c**, 0.372 g (2 mmol, 1 equiv.) of 1-morpholino-2-nitrobutylene **3c** and 0.24 mL (2 mmol, 1 equiv.) of 4-methoxybenzaldehyde **4c**. The product was recrystallized from MeOH. Light-yellow solid. Yield 0.338 g (52%). mp 249 °C with decomp. IR Spectrum, ν , cm^{-1} : 2229 (CN); 1577, 1307 (NO_2). ^1H NMR (400 MHz, DMSO- d_6): δ = 1.10–1.48 (3H, m, $\text{CH}_2\text{-CH}_3$); 2.87–3.13 (2H, m, $\text{CH}_2\text{-CH}_3$); 3.71 (3H, s, O- CH_3); 6.54 (1H, s, H-7); 6.79–6.94 (2H, m, H-3'); 7.13–7.30 (2H, m, H-2'); 7.92 (1H, s, H-2); 11.83 (1H, s, NH). ^{13}C $\{^1\text{H}\}$ NMR (101 MHz, DMSO- d_6): δ = 12.4; 25.4; 55.1; 59.2; 75.3; 112.9; 114.0; 122.0; 128.5; 131.5; 139.1; 143.1; 151.8; 159.3. Anal. Calcd. for $\text{C}_{16}\text{H}_{15}\text{N}_5\text{O}_3$: C, 59.07; H, 4.65; N, 21.53. Found: C, 59.17; H, 4.69; N, 21.44.

3-Cyano-5-Ethyl-6-nitro-7-(3'-methoxy-4'-hydroxyphenyl)-4,7-dihydropyrazolo[1,5-a]pyrimidine (5j). The reaction was performed according to the general procedure 1 employing 0.216 g (2 mmol, 1 equiv.) of 3-amino-4-cyanopyrazole **1c**, 0.372 g (2 mmol, 1 equiv.) of 1-morpholino-2-nitrobutylene **3c** and 0.304 g (2 mmol, 1 equiv.) of 3-methoxy-4-hydroxybenzaldehyde **4e**. Pale yellow solid. Yield 0.355 g (52%). mp 241 °C with decomp. IR Spectrum, ν , cm^{-1} : 3181 (OH); 2234 (CN); 1579, 1306 (NO_2). ^1H NMR (400 MHz, DMSO- d_6): δ = 1.32 (3H, t, $\text{CH}_2\text{-CH}_3$, J = 7.3 Hz); 2.90–3.13 (2H, m, $\text{CH}_2\text{-CH}_3$); 3.74 (1H, s, O- CH_3); 6.50 (1H, s, H-7); 6.62–6.69 (1H, m, H-5'); 6.72 (1H, d, H-6', J = 8.1 Hz); 7.93 (1H, s, H-2); 9.13 (1H, s, OH); 11.79 (1H, s, NH). ^{13}C $\{^1\text{H}\}$ NMR (101 MHz, DMSO- d_6): δ = 12.5; 25.5; 55.7; 59.5; 75.3; 111.8; 112.9; 115.5; 119.5; 121.9; 130.2; 143.0; 147.0; 147.4; 151.7. Anal. Calcd. for $\text{C}_{16}\text{H}_{15}\text{N}_5\text{O}_4$: C, 56.30; H, 4.43; N, 20.52. Found: C, 56.39; H, 4.36; N, 20.44.

3-Cyano-5-ethyl-6-nitro-7-(thiophen-2-yl)-4,7-dihydropyrazolo[1,5-a]pyrimidine (5k). The reaction was performed according to the general procedure 1 employing 0.216 g (2 mmol, 1 equiv.) of 3-amino-4-cyanopyrazole **1c**, 0.372 g (2 mmol, 1 equiv.) of 1-morpholino-2-nitrobutylene **3c** and 0.18 mL (2 mmol, 1 equiv.) of thiophene-2-carbaldehyde **4f**. Pale red solid. Yield 0.307 g (51%). mp 188–190 °C with decomp. IR Spectrum, ν , cm^{-1} : 2232 (CN); 1576, 1300 (NO_2). ^1H NMR (400 MHz, DMSO- d_6): δ = 1.30 (3H, t, $\text{CH}_2\text{-CH}_3$, J = 7.4 Hz); 2.84–3.14 (2H, m, $\text{CH}_2\text{-CH}_3$); 6.94 (1H, s, H-7); 6.89–6.98 (1H, s, H-3'); 7.01–7.08 (1H, m, H-4'); 7.41–7.49 (1H, d, H-5', J = 4.9 Hz); 8.00 (1H, s, H-2); 12.00 (1H, s, NH). ^{13}C $\{^1\text{H}\}$ NMR (101 MHz, DMSO- d_6): δ = 12.8; 25.9; 55.1; 76.1; 113.2; 122.1; 127.0; 127.1; 127.5; 139.6; 142.4; 143.8; 152.7. Anal. Calcd. for $\text{C}_{13}\text{H}_{11}\text{N}_5\text{O}_2\text{S}$: C, 51.82; H, 3.68; N, 23.24. Found: C, 51.69; H, 3.66; N, 23.36.

3-Cyano-2-methylthio-6-nitro-7-phenyl-4,7-dihydropyrazolo[1,5-a]pyrimidine (5l). The reaction was performed according to the general procedure 1 employing 0.308 g (2 mmol, 1 equiv.) of 3-amino-4-cyano-5-methylthiopyrazole **1d**, 0.316 g (2 mmol, 1 equiv.) of 1-morpholino-2-nitroethylene **3a** and 0.20 mL (2 mmol, 1 equiv.) of benzaldehyde **4a**. Yellow solid. Yield 0.319 g (51%). mp 219 °C with decomp. IR Spectrum, ν , cm^{-1} : 2229 (CN); 1596, 1325 (NO_2). ^1H NMR (400 MHz, DMSO- d_6): δ = 2.41 (3H, s, S- CH_3); 6.56 (1H, s, H-7); 7.11–7.56 (5H, m, Ph); 8.45 (1H, s, H-2); 12.44 (1H, br s, NH). ^{13}C $\{^1\text{H}\}$ NMR (101 MHz, DMSO- d_6): δ = 13.8; 59.6; 76.1; 111.9; 124.6; 127.6; 128.6; 128.8; 134.3; 138.5; 140.8; 150.8. Anal. Calcd. for $\text{C}_{14}\text{H}_{11}\text{N}_5\text{O}_2\text{S}$: C, 53.67; H, 3.54; N, 22.35. Found: C, 53.75; H, 3.61; N, 22.19.

3-Cyano-5-methyl-2-methylthio-6-nitro-7-phenyl-4,7-dihydropyrazolo[1,5-a]pyrimidine (5m). The reaction was performed according to the general procedure 1 employing 0.308 g (2 mmol, 1 equiv.) of 3-amino-4-cyano-5-methylthiopyrazole **1d**, 0.344 g (2 mmol, 1 equiv.) of 1-morpholino-2-nitropropylene **3b** and 0.20 mL (2 mmol, 1 equiv.) of benzaldehyde **4a**. Sand color solid. Yield 0.294 g (45%). mp 251–253 °C with decomp. IR Spectrum, ν , cm^{-1} : 2229 (CN); 1575, 1306 (NO_2). ^1H NMR (400 MHz, DMSO- d_6): δ = 2.42 (3H, s, S- CH_3); 2.67 (3H, s, C-5- CH_3); 6.53 (1H, s, H-7); 7.27–7.47 (5H, m, Ph); 11.90 (1H, s, NH). ^{13}C $\{^1\text{H}\}$ NMR (101 MHz, DMSO- d_6): δ = 13.8; 19.6; 59.8; 75.3; 112.1; 122.6; 127.4 (2C); 128.6; 139.0;

140.4; 147.4; 150.9. Anal. Calcd. for C₁₅H₁₃N₅O₂S: C, 55.04; H, 4.00; N, 21.39. Found: C, 55.00; H, 4.04; N, 21.50.

5-Ethyl-3-cyano-2-methylthio-6-nitro-7-(4'-nitrophenyl)-4,7-dihydropyrazolo[1,5-a]pyrimidine (5n). The reaction was performed according to the general procedure 1 employing 0.308 g (2 mmol, 1 equiv.) of 3-amino-4-cyano-5-methylthiopyrazole **1d**, 0.376 g (2 mmol, 1 equiv.) of 1-morpholino-2-nitrobutylene **3c** and 0.302 g (2 mmol, 1 equiv.) of 4-nitrobenzaldehyde **4c**. The substance was dried over P₂O₅ at 170 °C. Yellow solid. Yield 0.363 g (47%). mp 220 °C with decomp. IR Spectrum, ν , cm⁻¹: 2236 (CN); 1580, 1331 (NO₂); 1524, 1350 (NO₂). ¹H NMR (400 MHz, DMSO-*d*₆): δ = 1.30 (3H, t, CH₂-CH₃, *J* = 7.4 Hz); 2.40 (3H, s, S-CH₃); 2.90–3.10 (2H, m, CH₂-CH₃); 6.71 (1H, s, H-7); 7.65 (2H, d, H-2', *J* = 8.3 Hz); 8.19 (2H, d, H-3', *J* = 8.3 Hz); 12.06 (1H, br.s.; NH). ¹³C {¹H} NMR (101 MHz, DMSO-*d*₆): δ = 12.3; 13.7; 59.0; 75.7; 112.0; 121.4; 129.9; 128.9; 140.6; 145.8; 147.5; 151.4; 152.7. Anal. Calcd. for C₁₆H₁₄N₆O₄S: C, 49.74; H, 3.65; N, 21.75. Found: C, 49.69; H, 3.60; N, 21.81.

3-Cyano-2-methylthio-6-nitro-7-(4'-nitrophenyl)-4,7-dihydropyrazolo[1,5-a]pyrimidine (5o). The reaction was performed according to the general procedure 2 employing 0.308 g (2 mmol, 1 equiv.) of 3-amino-4-cyano-5-methylthiopyrazole **1d**, 0.372 g (2 mmol, 1 equiv.) of 1-morpholino-2-nitrobutylene **3c** and 0.243 mL (2 mmol, 1 equiv.) of 4-methoxybenzaldehyde **4d**. Yellow solid. Yield 0.378 g (51%). mp 183 °C with decomp. IR Spectrum, ν , cm⁻¹: 2224 (CN); 1577, 1302 (NO₂). ¹H NMR (400 MHz, DMSO-*d*₆): δ = 1.33 (3H, t, CH₂-CH₃, *J* = 7.3 Hz); 2.44 (1H, s, S-CH₃); 3.01 (2H, q, CH₂-CH₃; *J* = 7.3 Hz); 3.75 (1H, s, O-CH₃); 6.44 (1H, s, H-7); 6.84 (2H, d, H-3', *J* = 8.3 Hz); 7.19 (2H, d, H-2', *J* = 7.19 Hz); 11.68 (1H, s, NH). ¹³C {¹H} NMR (101 MHz, DMSO-*d*₆): δ = 12.8; 14.3; 25.9; 55.6; 59.7; 75.8; 112.6; 114.5; 122.8; 129.0; 131.7; 140.9; 151.3; 152.0; 159.9. Anal. Calcd. for C₁₇H₁₇N₅O₃S: C, 54.98; H, 4.61; N, 18.86. Found: C, 55.08; H, 4.59; N, 18.89.

6-Nitro-7-phenyl-4,7-dihydro-1,2,4-triazolo[1,5-a]pyrimidine (6a). The reaction was performed according to the general procedure 1 employing 0.168 g (2 mmol, 1 equiv.) of 3-amino-1,2,4-triazole **2a**, 0.316 g (2 mmol, 1 equiv.) of 1-morpholino-2-nitroethylene **3a** and 0.20 mL (2 mmol, 1 equiv.) of benzaldehyde **4a**. Yellow solid. Yield 0.253 g (52%). mp 269 °C with decomp. IR Spectrum, ν , cm⁻¹: 1593, 1314 (NO₂). ¹H NMR (400 MHz, DMSO-*d*₆): δ = 6.65 (1H, s, H-7); 7.15–7.60 (5H, m, Ph); 7.79 (1H, s, H-5); 8.54 (1H, s, H-2); 12.09 (1H, br. s., NH). ¹³C {¹H} NMR (101 MHz, DMSO-*d*₆): δ = 59.5; 123.8; 127.4; 128.6; 128.6; 136.5; 38.8; 145.7; 151.0. Anal. Calcd. for C₁₁H₉N₅O₂: C, 54.32; H, 3.73; N, 28.79. Found: C, 54.21; H, 3.79; N, 28.69.

5-Methyl-2-methylthio-6-nitro-7-phenyl-4,7-dihydro-1,2,4-triazolo[1,5-a]pyrimidine (6b). The reaction was performed according to the general procedure 1 employing 0.260 g (2 mmol, 1 equiv.) of 3-amino-5-methylthio-1,2,4-triazole **2b**, 0.344 g (2 mmol, 1 equiv.) of 1-morpholino-2-nitropropylene **3b** and 0.20 mL (2 mmol, 1 equiv.) of benzaldehyde **4a**. Pale yellow solid. Yield 0.327 g (54%). mp 274–276 °C. IR Spectrum, ν , cm⁻¹: 1557, 1320 (NO₂). ¹H NMR (400 MHz, DMSO-*d*₆): δ = 2.42 (3H, s, S-CH₃); 2.64 (3H, s, C-5-CH₃); 6.56 (1H, s, H-7); 7.27–7.38 (5H, m, Ph); 11.90 (1H, s, NH). ¹³C {¹H} NMR (101 MHz, DMSO-*d*₆): δ = 13.5; 20.2; 59.8; 122.2; 127.4; 128.5; 128.6; 139.1; 146.2; 148.8; 160.0. Anal. Calcd. for C₁₃H₁₃N₅O₂S: C, 51.49; H, 4.41; N, 23.02. Found: C, 51.47; H, 4.32; N, 23.09.

5-Methyl-2-methylthio-6-nitro-7-(4'-nitrophenyl)-4,7-dihydro-1,2,4-triazolo[1,5-a]pyrimidine (6c). The reaction was performed according to the general procedure 2 employing 0.260 g (2 mmol, 1 equiv.) of 3-amino-5-methylthio-1,2,4-triazole **2b**, 0.372 g (2 mmol, 1 equiv.) of 1-morpholino-2-nitrobutylene **2b** and 0.302 mL (2 mmol, 1 equiv.) of 4-nitrobenzaldehyde **4c**. Yellow solid. Yield 0.384 g (53%). mp 239–241 °C. IR Spectrum, ν , cm⁻¹: 1581, 1555, 1345, 1303 (NO₂). ¹H NMR (400 MHz, DMSO-*d*₆): δ = 1.34 (3H, t, CH₂-CH₃, *J* = 7.3 Hz); 2.44 (3H, s, S-CH₃); 2.91–3.11 (2H, m, CH₂-CH₃); 6.71 (1H, s, H-7); 7.64 (2H, d, H-2', *J* = 8.5 Hz); 8.22 (2H, d, H-3', *J* = 8.6 Hz); 12.00 (1H, s, NH). ¹³C {¹H} NMR (101 MHz, DMSO-*d*₆): δ = 12.3; 13.5; 26.0; 59.0; 120.9; 123.84; 128.8; 146.0; 146.3; 147.5; 154.2; 160.5. Anal. Calcd. for C₁₄H₁₄N₆O₄S: C, 46.40; H, 3.89; N, 23.19. Found: C, 46.55; H, 3.77; N, 23.10.

5-Methyl-6-nitro-7-phenyl-2-trifluoromethyl-4,7-dihydro-1,2,4-triazolo[1,5-a]pyrimidine (6d).

To a suspension of 0.304 g (2 mmol, 1 equiv.) of 3-amino-5-trifluoromethyl-1,2,4-triazole **2c**, 0.344 g (2 mmol, 1 equiv.) of 1-morpholino-2-nitropropylene **3b** and 0.20 mL (2 mmol, 1 equiv.) of benzaldehyde **4a** in 5 mL *n*-BuOH 3 mmol (1.5 equiv., 0.37 mL) of BF₃·Et₂O was added. The reaction mixture was heated on oil bath at 120 °C for 2 h. The resulting solution was cooled to room temperature and evaporated. To residue 5 mL of *n*-heptane was added. The obtained suspension was stirred for 10 min, filtered off and washed with 20 mL of water. The product was recrystallized from *i*-PrOH-H₂O 1/1. Yellow solid. Yield 0.273 g (42%); mp 233–235 °C. IR Spectrum, ν , cm⁻¹: 1573, 1321 (NO₂), 1133 (CF₃). ¹H NMR (400 MHz, DMSO-*d*₆): δ = 2.66 (3H, s, C-5-CH₃); 6.74 (1H, s, H-7); 7.31–7.45 (5H, m, Ph); 12.13 (1H, s, NH). ¹³C {¹H} NMR (101 MHz, DMSO-*d*₆): δ = 20.1; 60.4; 118.9 (q, *J* = 269.7 Hz); 122.5; 127.6; 128.7; 128.9; 138.4; 147.0; 148.8; 151.1 (q, *J* = 39.1 Hz). Anal. Calcd. for C₁₃H₁₀F₃N₅O₂: C, 48.01; H, 3.10; N, 21.53. Found: C, 48.15; H, 3.24; N, 21.40.

*5-Methyl-6-nitro-7-(4'-nitrophenyl)-2-trifluoromethyl-4,7-dihydro-1,2,4-triazolo[1,5-*a*]pyrimidine (6e)*. 3 Mmol (1.5 equiv., 0.37 mL) of BF₃·Et₂O was added to a suspension of 0.304 g (2 mmol, 1 equiv.) of 3-amino-5-trifluoromethyl-1,2,4-triazole **2c**, 0.372 g (2 mmol, 1 equiv.) of 1-morpholino-2-nitrobutylene **3c** in 5 mL *n*-BuOH. The reaction mixture was heated on oil bath at 80 °C for 15 min. After this, 0.302 g (2 mmol, 1 equiv.) of 4-nitrobenzaldehyde **4c** was added to the obtained solution. The reaction mixture was heated on oil bath at 120 °C for 2 h. The resulting solution was cooled to room temperature and evaporated. To residue, 5×3 mL of *n*-heptane was added, and the obtained mixture was decanted. The same procedure was carried out with water. The crude oil was dissolved in 5 mL of *i*-PrOH, and the obtained solution was left overnight. The obtained suspension was filtered off and recrystallized from *i*-PrOH/H₂O 1/1. Pale yellow solid. Yield 0.322 g (42%). mp 228 °C with decomp. IR Spectrum, ν , cm⁻¹: 1573, 1309 (NO₂); 1152 (CF₃). ¹H NMR (400 MHz, DMSO-*d*₆): δ = 1.32 (3H, t, CH₂-CH₃, *J* = 7.4 Hz); 2.85–3.11 (2H, m, CH₂-CH₃); 6.93 (1H, s, H-7); 7.75 (2H, d, H-2', *J* = 8.3 Hz); 8.21 (2H, d, H-3', *J* = 8.3 Hz); 12.29 (1H, s, NH). ¹³C {¹H} NMR (101 MHz, DMSO-*d*₆): δ = 12.2; 26.0; 59.6; 118.81 (q, *J* = 269.9 Hz); 121.3; 124.0; 129.2; 145.1; 147.2; 147.8; 151.5 (q, *J* = 39.2 Hz); 154.3. Anal. Calcd. for C₁₄H₁₁F₃N₆O₄: C, 43.76; H, 2.89; N, 21.87. Found: C, 43.69; H, 2.80; N, 21.98.

3.2. Biological Experiments

3.2.1. CK2 Assay

Kinase activity was determined using the enzyme system CK2 α 1 (Promega V4482, Madison, WI, USA) and the ADP-Glo™ kit (Promega V9101, Madison, WI, USA) in white 96-well plates (Nunc U96 Microwell 267350, Denmark). The reaction was carried out using 50 ng/well of N-GST labeled human recombinant CK2 α 1, 0.1 μ g/ μ L bovine casein as a substrate, 10 μ M ATP in 40 mM Tris buffer solution (pH 7.50) containing 20 mM MgCl₂, 0.1 mg/mL of BSA, and 50 μ M of DTT. Test compounds were added to 1.25% DMSO (final concentration 0.25%) and preincubated with kinase for 10 min. The reaction was carried out for 60 min at 25 °C in a thermostatically controlled PST-60HL shaker (Biosan. Beresfield, NSW, Latvia). ATP-dependent luminescence was measured at an integration time of 1000 ms using the Infinite M200 PRO microplate reader (Tecan. Austria). The ATP-competitive inhibitor Staurosporin (CAS 62996–74-1, Alfa Aesar J62837, 99+%) was used as a positive control. The experiments were performed in two parallels.

3.2.2. Cytotoxicity Study

Cell Culture

The studies were carried out on cultured cells of human glioblastoma (A-172, ATCC CRL 1620) [35], human osteosarcoma (Hos, ATCC CRL 1543) [36–38], human embryonic rhabdomyosarcoma (Rd, ATCC CRL 136) [39], and human embryonic kidney 293 cells (Hek-293, ATCC CRL 1573) [40] obtained from the Shared research facility “Vertebrate cell culture collection” (Institute of Cytology RAS, Saint-Petersburg, Russia). The cells were cultured using DMEM / F-12 medium containing 10% fetal bovine serum at 37 °C, 5% CO₂, and 98% humidity. Subculturing was performed using 0.25% trypsin solution when the culture reached \geq 90% confluency.

Viability Assessment

The compounds were dissolved in DMSO. The solutions were diluted with DMEM/F-12 culture medium with 10% fetal bovine serum to the studied concentrations: 8, 16, 32, 64, 128, 256, 512, and 1024 μM . In all cases, the concentration of DMSO in the final solution did not exceed 1%. Cisplatin (cPt) was used as a positive control.

Cells were seeded in 96-well plates at a concentration of 4×10^3 cells per well. After 24 h, test compounds were added to the wells in a given concentration range. Then the cells were incubated for 72 h, after which a solution of MTT (3-(4,5-dimethyl-2-thiazolyl)-2,5-diphenyl-2H-tetrazolium bromide) was added to the cultures at 20 μL (5 mg/mL) to the well. After 2.5 h, the medium was removed from the wells and 200 μL of a mixture of DMSO/*i*-PrOH 1/1 was added. Optical density was measured on a plate spectrophotometer at a wavelength of 570 nm.

Statistical Analysis

Statistical data processing was carried out in the RStudio program (Version 1.4.1106 © 2022–2021 RStudio, PBC, Boston, MA, USA) using the R package (version 4.1.2). The cytotoxicity index (IC_{50}) was calculated by plotting dose–response curves using the “drc” package [41].

4. Conclusions

Thus, in this work we extended the library of the 4,7-dihydro-6-nitroazolo[1,5-a]pyrimidine series, and also studied their antitumor properties. The inhibitory activity of these compounds against CK2 has been established, as well as their cytotoxic effect. Compounds of this series are comparable in inhibitory activity with the reference drug and exhibit a cytotoxic effect on tumor cells at micromolar concentrations. It is evident that the herein reported 4,7-dihydro-6-nitroazolo[1,5-a]pyrimidines have the potential to be studied as a new class of antitumor compounds.

Supplementary Materials: The following are available online at <https://www.mdpi.com/article/10.3390/molecules27165239/s1>, NMR Spectra of compounds 5,6, and biological experiments.

Author Contributions: Synthesis, D.N.L. and I.I.B.; methodology, D.N.L. and E.N.U.; writing, D.N.L., S.K.K. and V.L.R.; CK2 inhibition investigation, D.A.B., A.A.P. and A.A.S.; cytotoxicity study, V.V.M., M.D.T., A.V.S. and O.G.M. All authors have read and agreed to the published version of the manuscript.

Funding: This work was financially supported by the Ministry of Science and Higher Education of the Russian Federation, State Contract № FEUZ-2020–0058 (H687.42B.223/20).

Institutional Review Board Statement: Not applicable.

Informed Consent Statement: Not applicable.

Data Availability Statement: Data are contained within article.

Acknowledgments: The team of authors would like to thank the Laboratory for Comprehensive Research and Expert Evaluation of Organic Materials under the direction of O.S. Eltsov.

Conflicts of Interest: The authors declare no conflict of interest.

Sample Availability: Samples of the compounds 5,6 are available from the authors.

References

1. Ferlay, J.; Ervik, M.; Lam, F.; Colombet, M.; Mery, L.; Piñeros, M.; Znaor, A.; Soerjomataram, I.; Bray, F. *Global Cancer Observatory: Cancer Today*; International Agency for Research on Cancer: Lyon, France, 2020; Available online: <https://gco.iarc.fr/today> (accessed on 28 February 2021).
2. Charoenrat, P.; Rusch, V.; Talbot, S.G.; Sarkaria, I.; Viale, A.; Socci, N.; Ngai, I.; Rao, P.; Singh, B. Casein Kinase II Alpha Subunit and C1-Inhibitor Are Independent Predictors of Outcome in Patients with Squamous Cell Carcinoma of the Lung. *Clin. Cancer Res.* **2004**, *10*, 5792–5803. [CrossRef] [PubMed]
3. Ortega, C.E.; Seidner, Y.; Dominguez, I. Mining CK2 in Cancer. *PLoS ONE* **2014**, *9*, e115609. [CrossRef] [PubMed]

4. Faust, R.A.; Gapany, M.; Tristani, P.; Davis, A.; Adams, G.L.; Ahmed, K. Elevated Protein Kinase CK2 Activity in Chromatin of Head and Neck Tumors: Association with Malignant Transformation. *Cancer Lett.* **1996**, *101*, 31–35. [CrossRef]
5. Faust, R.A.; Niehans, G.; Gapany, M.; Hoistad, D.; Knapp, D.; Cherwitz, D.; Davis, A.; Adams, G.L.; Ahmed, K. Subcellular Immunolocalization of Protein Kinase CK2 in Normal and Carcinoma Cells. *Int. J. Biochem. Cell Biol.* **1999**, *31*, 941–949. [CrossRef]
6. Gapany, M.; Faust, R.A.; Tawfic, S.; Davis, A.; Adams, G.L.; Ahmed, K. Association of Elevated Protein Kinase CK2 Activity with Aggressive Behavior of Squamous Cell Carcinoma of the Head and Neck. *Mol. Med.* **1995**, *1*, 659. [CrossRef]
7. Kim, H.S.; Chang, Y.G.; Bae, H.J.; Eun, J.W.; Shen, Q.; Park, S.J.; Shin, W.C.; Lee, E.K.; Park, S.; Ahn, Y.M.; et al. Oncogenic Potential of CK2 α and Its Regulatory Role in EGF-Induced HDAC2 Expression in Human Liver Cancer. *FEBS J.* **2014**, *281*, 851–861. [CrossRef]
8. Rabjerg, M.; Bjerregaard, H.; Halekoh, U.; Jensen, B.L.; Walter, S.; Marcussen, N. Molecular Characterization of Clear Cell Renal Cell Carcinoma Identifies CSNK2A1, SPP1 and DEFB1 as Promising Novel Prognostic Markers. *APMIS* **2016**, *124*, 372–383. [CrossRef]
9. Nitta, R.T.; Gholamin, S.; Feroze, A.H.; Agarwal, M.; Cheshier, S.H.; Mitra, S.S.; Li, G. Casein Kinase 2 α Regulates Glioblastoma Brain Tumor-Initiating Cell Growth through the β -Catenin Pathway. *Oncogene* **2014**, *34*, 3688–3699. [CrossRef]
10. Pagano, M.A.; Cesaro, L.; Meggio, F.; Pinna, L.A. Protein Kinase CK2: A Newcomer in the ‘Druggable Kinome’. *Biochem. Soc. Trans.* **2006**, *34*, 1303–1306. [CrossRef]
11. Guerra, B.; Issinger, O.-G. Protein Kinase CK2 in Human Diseases. *Curr. Med. Chem.* **2008**, *15*, 1870–1886. [CrossRef]
12. Silva-Pavez, E.; Tapia, J. Protein Kinase CK2 in Cancer Energetics. *Front Oncol.* **2020**, *10*. [CrossRef] [PubMed]
13. Borgo, C.; D’Amore, C.; Sarno, S.; Salvi, M.; Ruzzene, M. Protein Kinase CK2: A Potential Therapeutic Target for Diverse Human Diseases. *Curr. Signal Transduct. Ther.* **2021**, *6*, 1–20. [CrossRef] [PubMed]
14. Chua, M.M.J.; Lee, M.; Dominguez, I. Cancer-Type Dependent Expression of CK2 Transcripts. *PLoS ONE* **2017**, *12*, e0188854. [CrossRef]
15. Pagano, M.A.; Bain, J.; Kazimierczuk, Z.; Sarno, S.; Ruzzene, M.; di Maira, G.; Elliott, M.; Orzeszko, A.; Cozza, G.; Meggio, F.; et al. The Selectivity of Inhibitors of Protein Kinase CK2: An Update. *Biochem. J.* **2008**, *415*, 353–365. [CrossRef] [PubMed]
16. Trembley, J.H.; Chen, Z.; Unger, G.; Slaton, J.; Kren, B.T.; van Waes, C.; Ahmed, K. Emergence of Protein Kinase CK2 as a Key Target in Cancer Therapy. *BioFactors.* **2010**, *36*, 187–195. [CrossRef]
17. Iegre, J.; Atkinson, E.L.; Brear, P.D.; Cooper, B.M.; Hyvönen, M.; Spring, D.R. Chemical Probes Targeting the Kinase CK2: A Journey Outside the Catalytic Box. *Org. Biomol. Chem.* **2021**, *19*, 4380–4396. [CrossRef]
18. Dowling, J.E.; Alimzhanov, M.; Bao, L.; Chuaqui, C.; Denz, C.R.; Jenkins, E.; Larsen, N.A.; Lyne, P.D.; Pontz, T.; Ye, Q.; et al. Potent and Selective CK2 Kinase Inhibitors with Effects on Wnt Pathway Signaling in Vivo. *ACS Med. Chem. Lett.* **2016**, *7*, 300–305. [CrossRef] [PubMed]
19. Wells, C.I.; Drewry, D.H.; Pickett, J.E.; Tjaden, A.; Krämer, A.; Müller, S.; Gyenis, L.; Menyhart, D.; Litchfield, D.W.; Knapp, S.; et al. Development of a Potent and Selective Chemical Probe for the Pleiotropic Kinase CK2. *Cell Chem. Biol.* **2021**, *28*, 546–558.e10. [CrossRef]
20. Dalle Vedove, A.; Zonta, F.; Zanforlin, E.; Demitri, N.; Ribaudò, G.; Cazzanelli, G.; Ongaro, A.; Sarno, S.; Zagotto, G.; Battistutta, R.; et al. A Novel Class of Selective CK2 Inhibitors Targeting Its Open Hinge Conformation. *Eur. J. Med. Chem.* **2020**, *195*, 112267. [CrossRef]
21. Oshima, T.; Niwa, Y.; Kuwata, K.; Srivastava, A.; Hyoda, T.; Tsuchiya, Y.; Kumagai, M.; Tsuyuguchi, M.; Tamaru, T.; Sugiyama, A.; et al. Cell-Based Screen Identifies a New Potent and Highly Selective CK2 Inhibitor for Modulation of Circadian Rhythms and Cancer Cell Growth. *Sci. Adv.* **2019**, *5*, 9060–9083. [CrossRef]
22. Zhang, N.; Ayrál-Kaloustian, S.; Nguyen, T.; Afragola, J.; Hernandez, R.; Lucas, J.; Gibbons, J.; Beyer, C. Synthesis and SAR of [1,2,4]Triazolo [1,5-a]Pyrimidines, a Class of Anticancer Agents with a Unique Mechanism of Tubulin Inhibition. *J. Med. Chem.* **2007**, *50*, 319–327. [CrossRef] [PubMed]
23. Beyer, C.F.; Zhang, N.; Hernandez, R.; Vitale, D.; Lucas, J.; Nguyen, T.; Discafani, C.; Ayrál-Kaloustian, S.; Gibbons, J.J. TTI-237: A Novel Microtubule-Active Compound with In Vivo Antitumor Activity. *Cancer Res.* **2008**, *68*, 2292–2300. [CrossRef] [PubMed]
24. Wang-Gillam, A.; Arnold, S.M.; Bukowski, R.M.; Rothenberg, M.L.; Cooper, W.; Wang, K.K.; Gauthier, E.; Lockhart, A.C. A Phase I Dose Escalation Study of TTI-237 in Patients with Advanced Malignant Solid Tumors. *Investig. New Drugs* **2012**, *30*, 266–272. [CrossRef] [PubMed]
25. Ayrál-Kaloustian, S.; Zhang, N.; Beyer, C. Cevipabulin (TTI-237): Preclinical and Clinical Results for a Novel Antimicrotubule Agent. *Methods Find. Exp. Clin. Pharmacol.* **2009**, *31*, 443–447. [CrossRef] [PubMed]
26. Sanchez, R.M.; Erhard, K.; Hardwicke, M.A.; Lin, H.; McSurdy-Freed, J.; Plant, R.; Raha, K.; Rominger, C.M.; Schaber, M.D.; Spengler, M.D.; et al. Synthesis and Structure–Activity Relationships of 1,2,4-Triazolo [1,5-a]Pyrimidin-7(3H)-Ones as Novel Series of Potent β Isoform Selective Phosphatidylinositol 3-Kinase Inhibitors. *Bioorg. Med. Chem. Lett.* **2012**, *22*, 3198–3202. [CrossRef]
27. Hassan, A.Y.; Sarg, M.T.; Bayoumi, A.H.; El-Deeb, M.A. Synthesis and Anticancer Evaluation of Some Novel 5-Amino [1,2,4]Triazole Derivatives. *J. Het. Chem.* **2018**, *55*, 1450–1478. [CrossRef]
28. Oukoloff, K.; Lucero, B.; Francisco, K.R.; Brunden, K.R.; Ballatore, C. 1,2,4-Triazolo [1,5-a]Pyrimidines in Drug Design. *Eur. J. Med. Chem.* **2019**, *165*, 332–346. [CrossRef]
29. Pinheiro, S.; Pinheiro, E.M.C.; Muri, E.M.F.; Pessôa, J.C.; Cadorini, M.A.; Greco, S.J. Biological Activities of [1,2,4]Triazolo [1,5-a]Pyrimidines and Analogs. *Med. Chem. Res.* **2020**, *29*, 1751–1776. [CrossRef]

30. Safari, F.; Bayat, M.; Nasri, S.; Karami, S. Synthesis and Evaluation of Anti-Tumor Activity of Novel Triazolo [1,5-a]Pyrimidine on Cancer Cells by Induction of Cellular Apoptosis and Inhibition of Epithelial-to-Mesenchymal Transition Process. *Bioorg. Med. Chem. Lett.* **2020**, *30*, 127111. [CrossRef]
31. Lyapustin, D.N.; Ulomsky, E.N.; Zanakhov, T.O.; Rusinov, V.L. Three-Component Coupling of Aromatic Aldehydes, 1-Morpholino-2-Nitroalkenes, and 3-Aminoazoles via Boron Trifluoride Etherate Catalysis: Reaction Pathway and Features of the Formation of Intermediates. *J. Org. Chem.* **2019**, *84*, 15267–15275. [CrossRef]
32. Lyapustin, D.N.; Ulomsky, E.N.; Rusinov, V.L. 6-Nitro-4,7-Dihydroazolo[1,5-a]Pyrimidines: An Alternative Mechanism of Formation and Studies of Alkylation. *Chem. Het. Comp.* **2020**, *56*, 1465–1472. [CrossRef]
33. Lyapustin, D.N.; Ulomsky, E.N.; Balyakin, I.A.; Shchepochkin, A.v.; Rusinov, V.L.; Chupakhin, O.N. Oxidative Aromatization of 4,7-Dihydro-6-Nitroazolo[1,5-a]Pyrimidines: Synthetic Possibilities and Limitations, Mechanism of Destruction, and the Theoretical and Experimental Substantiation. *Molecules* **2021**, *26*, 4719. [CrossRef] [PubMed]
34. Rusinov, V.L.; Drokin, R.A.; Tiufiakov, D.V.; Voinkov, E.K.; Ulomsky, E.N. Synthesis and Properties of the Salts of 1-Nitropropan-2-One and 1-Nitrobutan-2-One. *Mendeleev Commun.* **2020**, *30*, 177–179. [CrossRef]
35. Giard, D.J.; Aaronson, S.A.; Todaro, G.J.; Arnstein, P.; Kersey, J.H.; Dosik, H.; Parks, W.P. In Vitro Cultivation of Human Tumors: Establishment of Cell Lines Derived From a Series of Solid Tumors. *J. Natl. Cancer Inst.* **1973**, *51*, 1417–1423. [CrossRef]
36. Rhim, J.S.; Cho, H.Y.; Huebner, R.J. Non-Producer Human Cells Induced by Murine Sarcoma Virus. *Int. J. Cancer* **1975**, *15*, 23–29. [CrossRef]
37. McAllister, R.M.; Gardner, M.B.; Greene, A.E.; Bradt, C.; Nichols, W.W.; Landing, B.H. Cultivation in vitro of cells derived from a human osteosarcoma. *Cancer* **1971**, *27*, 397–402. [CrossRef]
38. Rhim, J.S.; Cho, H.Y.; Vernon, M.L.; Arnstein, P.; Huebner, R.J.; Gilden, R.v.; Nelson-Rees, W.A. Characterization of Non-Producer Human Cells Induced by Kirsten Sarcoma Virus. *Int. J. Cancer* **1975**, *16*, 840–849. [CrossRef]
39. McAllister, R.M.; Melenyk, J.; Finklestein, J.Z.; Adams, E.C.; Gardner, M.B. Cultivation in Vitro of Cells Derived from a Human Rhabdomyosarcoma. *Cancer* **1969**, *24*, 520–526. [CrossRef]
40. Graham, F.L.; Smiley, J.; Russell, W.C.; Nairn, R. Characteristics of a Human Cell Line Transformed by DNA from Human Adenovirus Type 5. *J. Gen. Virol.* **1977**, *36*, 59–72. [CrossRef]
41. Ritz, C.; Baty, F.; Streibig, J.C.; Gerhard, D. Dose-Response Analysis Using R. *PLoS ONE* **2015**, *10*, e0146021. [CrossRef]

Review

Photodynamic Therapy: From the Basics to the Current Progress of *N*-Heterocyclic-Bearing Dyes as Effective Photosensitizers

Eurico Lima ^{1,2} and Lucinda V. Reis ^{1,*}

¹ CQ-VR—Chemistry Centre of Vila Real, University of Trás-os-Montes and Alto Douro, Quinta de Prados, 5001-801 Vila Real, Portugal; eurico_lima@icloud.com

² CICS-UBI—Health Sciences Research Centre, University of Beira Interior, Av. Infante D. Henrique, 6201-506 Covilhã, Portugal

* Correspondence: lucinda.reis@utad.pt

Abstract: Photodynamic therapy, an alternative that has gained weight and popularity compared to current conventional therapies in the treatment of cancer, is a minimally invasive therapeutic strategy that generally results from the simultaneous action of three factors: a molecule with high sensitivity to light, the photosensitizer, molecular oxygen in the triplet state, and light energy. There is much to be said about each of these three elements; however, the efficacy of the photosensitizer is the most determining factor for the success of this therapeutic modality. Porphyrins, chlorins, phthalocyanines, boron-dipyrromethenes, and cyanines are some of the *N*-heterocycle-bearing dyes' classes with high biological promise. In this review, a concise approach is taken to these and other families of potential photosensitizers and the molecular modifications that have recently appeared in the literature within the scope of their photodynamic application, as well as how these compounds and their formulations may eventually overcome the deficiencies of the molecules currently clinically used and revolutionize the therapies to eradicate or delay the growth of tumor cells.

Keywords: *N*-heterocyclic-based dyes; photosensitizers; photodynamic therapy

Citation: Lima, E.; Reis, L.V.

Photodynamic Therapy: From the Basics to the Current Progress of *N*-Heterocyclic-Bearing Dyes as Effective Photosensitizers. *Molecules* **2023**, *28*, 5092. <https://doi.org/10.3390/molecules28135092>

Academic Editors: Alexey M. Starosotnikov, Maxim A. Bastrakov and Igor L. Dalinger

Received: 1 June 2023

Revised: 16 June 2023

Accepted: 27 June 2023

Published: 29 June 2023



Copyright: © 2023 by the authors. Licensee MDPI, Basel, Switzerland. This article is an open access article distributed under the terms and conditions of the Creative Commons Attribution (CC BY) license (<https://creativecommons.org/licenses/by/4.0/>).

1. Introduction

Photodynamic therapy (PDT) is a minimally invasive therapeutic strategy that intends to be applied to the most diverse problems of our society's daily lives: as an anticancer therapy [1–3], as a way of combating multi-resistant bacteria [4] or certain fungi [5] that may compromise human health, and, more recently, as a way of eradicating certain viral strains [6,7]. PDT already plays a role in treating several non-oncological and oncological diseases, mainly of dermatological origin [8]. Its slow clinical progression in cancer treatment is primarily due to the lack of approved photosensitizers (PSs). Nevertheless, researchers have tried to find new attractive molecules and their formulations that perform better than those currently used.

Focusing on cancer, this term refers to a wide range of diseases that trigger abnormal growth and division due to cell proliferation and regulation mechanism modifications. Given their uncontrolled behavior, they become highly invasive and can even reach the bloodstream and migrate to places where extravasation allows the formation of metastases [9]. In addition to environmental and hereditary factors, lifestyle, and exposure to carcinogens, aging is one of the factors that most contribute to the onset of this disease [10,11]. Although the scientific, pharmaceutical, and medical communities have made efforts to improve the available treatments, the long-term response of patients treated with radiotherapy and chemotherapy is still insufficient due to the severe side effects [12,13]. These gaps highlight the need to explore emerging therapies such as PDT. Clinical studies have shown that this therapeutic modality can be curative, especially in less advanced tumors [14,15]. In addition, it can prolong survival in cases of inoperable tumors and improve patients' quality of life [3,15].

Featuring heterocyclic units accompanied by nitrogen atoms in their molecular structure as well as conjugated double bonds that allow the design of chromophores, *N*-heterocyclic-bearing dyes constitute several families of compounds that, thanks to their relevant “photoproperties”, have been addressed concerning their potential application as PDT photosensitizing agents. Hundreds of new synthetic or hemisynthetic origin molecules have been reported in recent years to find the compound that combines desirable characteristics for its phototherapeutic application and better understand how and why certain structural modifications result in such diverse photobiological effects.

This review aims to present the reader with a concise approach to what PDT is and its fundamental principles, its importance as a therapeutic approach to complement or even replace conventional therapies in the treatment of diseases of oncological origin, several parameters to take into account to guarantee better efficiency and efficacy, as well as some of the families of *N*-heterocyclic-bearing dyes and the structural modifications or their formulation strategies that have been recently carried out to create new light-absorbing potential drugs with photodynamic interest (Figure 1).

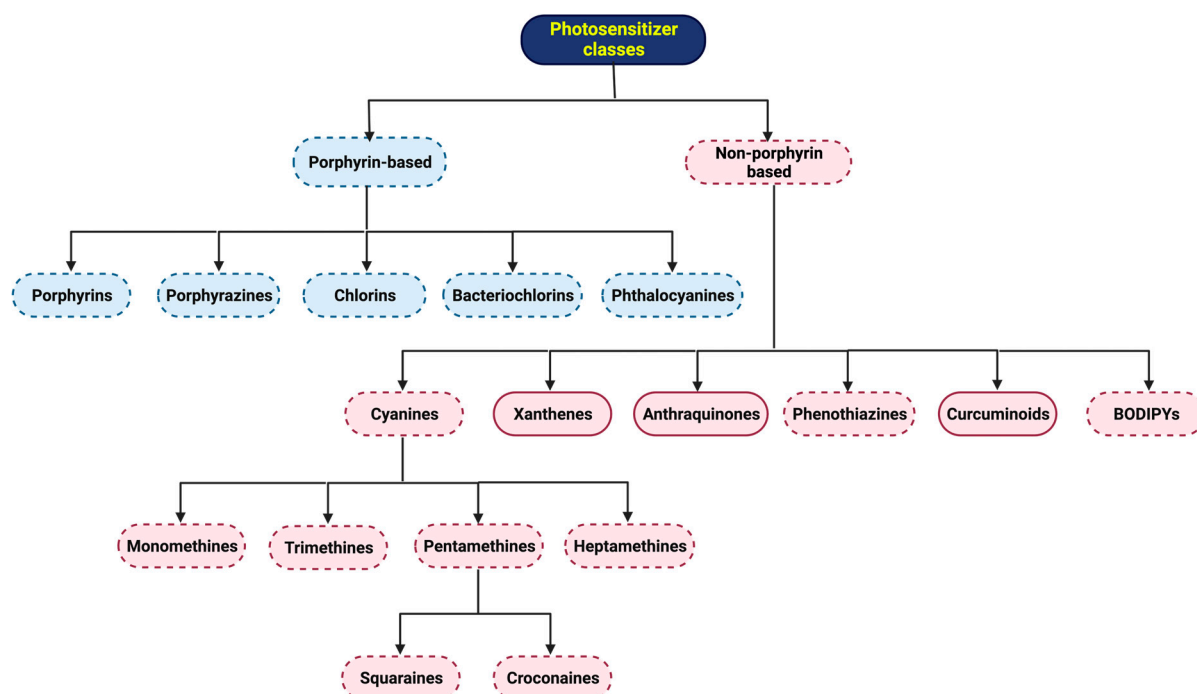


Figure 1. Flowchart hierarchy of the photosensitizer classes currently studied. The categories and respective sub-categories whose box limits are in dashed lines are related to dyes with *N*-heterocyclic units in their basic structure.

2. Photodynamic Therapy

2.1. A Piece of Photodynamic Therapy's Origin and History

Dating back to 1550 B.C., the Ebers papyrus is the oldest medical document that reports the use of sunlight as a treatment, using powder from various plants such as bishop's flower (*Ammi majus*), wild parsnip (*Pastinaca sativa*), parsley (*Petroselinum crispum*), and St. John's wort (*Hypericum perforatum*) for the application and treatment of depigmented skin lesions [16]. Also in Egyptian culture, pharaohs called for the construction of roofless temples dedicated to the Aton god of the sun for body light exposure and to benefit from its healing powers, and the use of *Ammi majus* plant extracts was common in the treatment of diseases of a dermatological nature [17]. Indian medical literature dated 1400 BC, the Atharva Veda, reports treating vitiliginous skin with babchi (*Psoralea corylifolia*) extracts, a plant from which it is now known that 8-methoxypsoralen is the furan-containing coumarin-based molecule that induced the photodynamic effect [16,18]. Even today, this

core of photosensitizing molecules is widely studied for its potential phototherapeutic use [19,20]. Also, in Greek, Chinese, and Roman civilizations, there is evidence of the use of energy from the sun as a remedy for the treatment of various diseases.

Arnold Rikli, a Swiss healer and physician, reintroduced the use of the powers of sunlight during the late 1800s and early 1900s. A believer that nature was the basis for treating many of the complications related to human health (mentioning his famous phrase, “Water is good; air is better and light is the best of all”), Rikli trusted in the power of light in therapy, introducing “sunbathing” as a therapy for chronic diseases and functional disorders in an attempt to apply the knowledge that had been known for hundreds of years but had been forgotten [16,21].

Until then, the effectiveness of using sunlight to treat various diseases had been proven, namely for vitiligo, lupus, acne, pulmonary tuberculosis, and rickets, using (or not) extracts and powders from plant species administered topically or orally. However, it was only in 1900 that the concept of a “photosensitizing molecule” emerged, with the potential use of dyes in this therapy having been recognized: Oscar Raab, a medical student, reported that the light factor was lethal for species of *Paramecium caudatum* in the presence of the acridine dye and that these two elements, individually, did not cause any consequences to this unicellular organism [22]. Taking advantage of these discoveries, von Tappeiner continued Raab’s research with the dermatologist Jesionek, who published works detailing clinical trials using dyes such as eosin, fluorescein, and sodium dichloroanthracene disulfonate in the treatment of topical disorders, including skin cancer [23,24]. At the same time, they also reported data on the possible use of eosin in facial basal cell carcinoma after sun exposure or using light from arc lamps. Von Tappeiner was the first to speculate about the need for triplet molecular oxygen, introducing the term “photodynamic therapy” [16].

Despite the significant findings of Raab and von Tappeiner, Niels Finsen, a Danish physician, is considered by many to be the pioneer of modern clinical PDT. Finsen owned a medical institute in Copenhagen, to which he attached a “sun garden” to allow his patients to benefit from the healing powers of sunlight. Later, he abandoned the sunlight to start using artificial lights and noticed that exposure to red or ultraviolet light could have therapeutic effects since red light prevented the formation of pustules in patients with smallpox and that ultraviolet light allowed the treatment of cutaneous tuberculosis [16,23,25]. Due to the impact of his discoveries, Finsen was awarded the Medicine Nobel Prize in 1903.

A noteworthy milestone demonstrating the acceptance of PDT as a therapeutic modality was the approval of Photofrin in 1993 for treating bladder tumors in Canada and later in the United States, Japan, and some European countries [26,27]. Today, the Photofrin oligomer is used worldwide in treating oesophageal, endobronchial, and lung cancer, in addition to being used in Japan for gastric cancer. Since its discovery, new molecules have been clinically approved, namely 5-aminolevulinic acid and methyl 5-aminolevulinic acid (Levulan and Metvix, respectively), precursors of porphyrins, in the treatment of basal cell carcinoma and squamous cell carcinoma; in Japan, Talaporfin chlorin (also known as Laserphyrin) in the treatment of glioblastoma and lung cancer; in Russia, the chlorin mixture Radachlorin in basal cell carcinoma and the sulfonated phthalocyanine Photosens for lung, liver, breast, skin and gastrointestinal cancer; and in the European Union, Foscan chlorin and Redaporfin bacteriochlorin have gained a role in the therapy of head and neck cancer, and Tookad bacteriochlorin in prostate cancer [28].

However, from then on, there was a growing need to synthesize new molecules with greater efficacy and fewer side effects, giving rise to new “second- and third-generation PSs” [29,30].

These and other milestones in the history and progress of PDT to date are highlighted in the timeline in Figure 2.

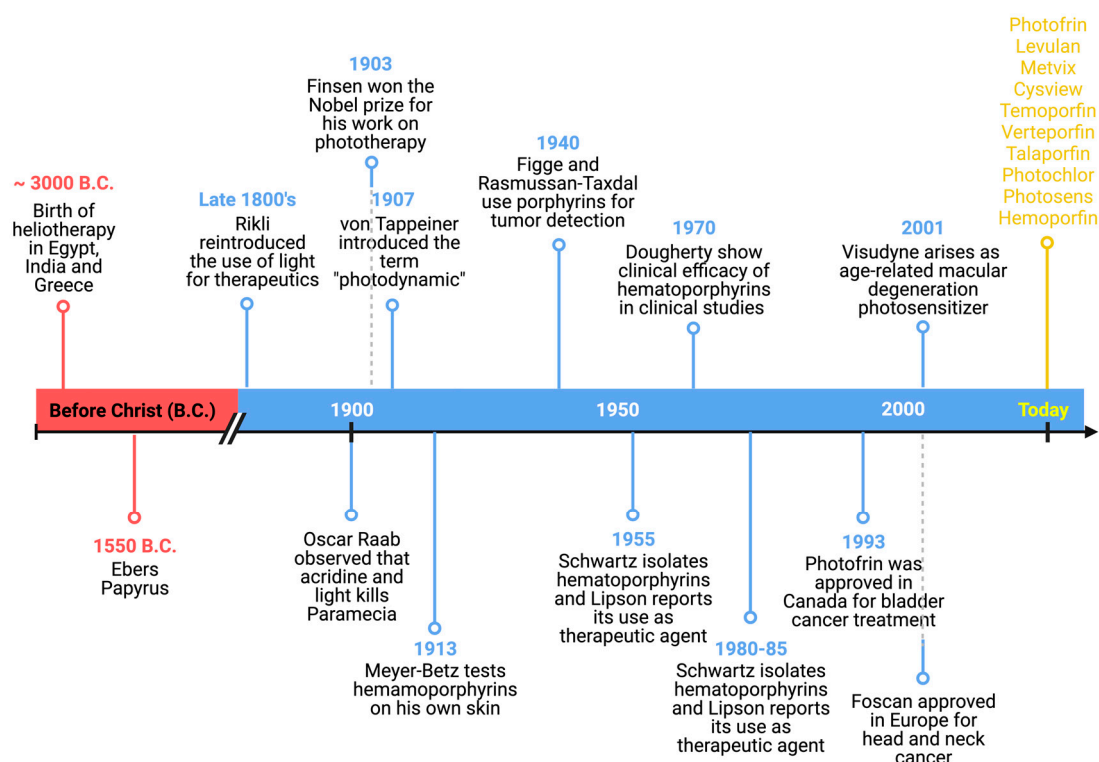


Figure 2. Timeline of photodynamic therapy, highlighting some of the events that most marked its evolution up to the present day.

2.2. Principles of Photodynamic Therapy

Clinically, the PS is administered through the most convenient route, depending on its pharmacokinetic and pharmacodynamic properties and the location of the target tissue. When administered intravenously, the photosensitizing agent is distributed throughout the body, ideally directing and accumulating selectively in the tissue to be treated. At the time of administration, the patient must be deprived of any light source to avoid premature activation. Retained by the target tissue and before being eliminated from the body, the same tissue is irradiated using a suitable light source, preferably emitting where radiation permeates tissues more efficiently, at wavelengths coincident with the molecule absorption, and with sufficient energy for its activation. Activation of the compound culminates in cell death and consequent ablation of the target tissue [3,31,32].

According to how the photosensitizing molecule acts, in general, it can produce reactive oxygen species (ROS) [33] that, despite being essential for the normal functioning of the cell [34,35], in high concentrations, become cytotoxic [34]. Thus, this therapeutic approach results from combining three individually innocuous components that are lethal when combined: the PS, light, and triplet state oxygen molecules.

The Perrin-Jablonski energy diagram explains photophysically and photochemically the activity of PS compounds (Figure 3). This diagram elucidates that these molecules, in their ground state, are in the lowest possible energy configuration with opposite spins. When appropriate radiation is applied, an electron is transferred to a higher energy state, transiting the PS to the excited singlet state, a highly unstable energy configuration that easily returns to its fundamental state, emitting a photon in the form of fluorescence. The ground state PS does not result in therapeutic activity; however, the ability of dyes to fluoresce can be harnessed to create diagnostic or even theranostic techniques. Only if the PS transitions from the excited singlet state to the excited triplet state by intersystem crossing (ISC), that is, the inversion of the excited electron spin, is the drug capable of carrying out photodynamic reactions (of type I or type II). The loss of energy resulting

from the transition of the PS from the triplet state to the ground state occurs through phosphorescence emission [1,31].

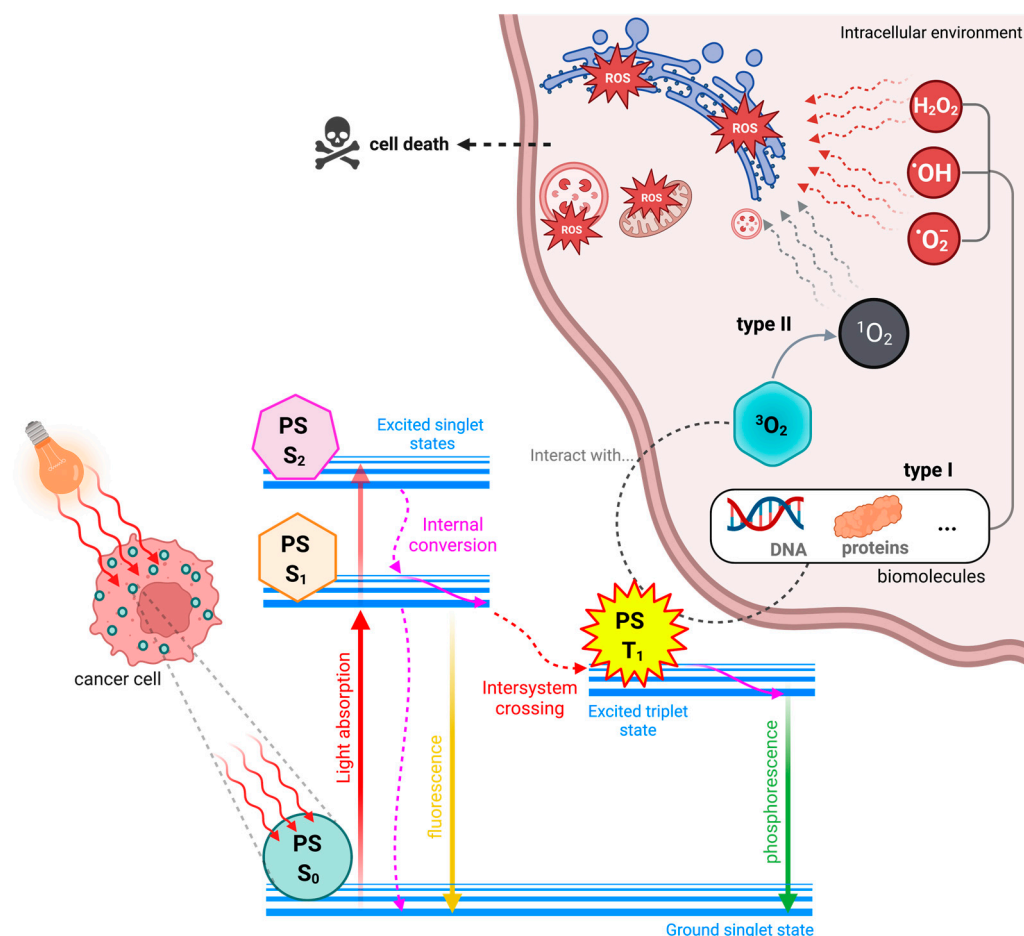


Figure 3. Photodynamic therapy-customized Perrin–Jablonski energy diagram. After cellular uptake of the photosensitizer (PS) and irradiation with light emitting a specific wavelength, this radiation is absorbed by the PS in the ground state (PS S_0), which transitions to the first or second excited singlet state (PS S_1 and PS S_2 , respectively). Variations between PS S_1 and PS S_2 or between the various energy levels of the same state occur by internal conversion. Radiative (fluorescence and consequent return to S_0) or nonradiative (intersystem crossing to the PS T_1) processes can occur in the PS S_1 . The PS T_1 can interact with biological substrates, forming reactive oxygen species (ROS), such as hydrogen peroxide (H_2O_2), hydroxyl radical ($\bullet OH$), or superoxide anion ($\bullet O_2^-$), by type I reactions, or singlet oxygen (1O_2) by type II reactions. In high concentrations, these ROS led to cell damage in essential structures for normal cell functioning, culminating in cell death.

Type I reactions are characterized by the interaction of the triplet excited state PS with cellular substrates and the consequent formation of free radicals through the transfer of electrons or protons to form anion or cation substrates, respectively [36,37]. An electron transfer from these radical substrates to molecular oxygen in the triplet state results in superoxide anions, which can produce hydrogen peroxide when reacting with water. If the production of hydrogen peroxide and superoxide anions is exacerbated, highly cytotoxic hydroxyl radicals may be formed through the Haber–Weiss reaction. Hydroxyl radicals can also be produced in the presence of, for example, iron or copper metal ions by the well-known Fenton reaction. The production of these radicals is desirable for photodynamic activity due to their distinct reactivity and ability to oxidize any molecule of biological interest [38,39].

Type II reactions are responsible for forming singlet oxygen through direct energy transfer between the triplet state PS and the triplet state molecular oxygen. Despite its high cytotoxicity, singlet oxygen has a minimal lifetime, so its action is mainly limited to the place of its generation [40]. Type I and type II reactions can coexist, and the prevalence of one type over the other is mainly related to the intrinsic properties of the PS [41]. Other conditioning factors are how the PS is distributed in the cellular environment, its proximity to biological substrates, and the triplet molecular oxygen concentration around it.

Photosensitizing molecules capable of tissue destruction through mechanisms independent of the presence of molecular oxygen in the triplet state (type III reactions) have also been reported. These type III PSs have the intrinsic property of specific targeting for biomolecules, such as proteins and nucleic acids, among other biomacromolecules. As a result, these target biological elements are efficiently destroyed when irradiated, compromising normal functioning and survival [42]. Recently, new type III *N*-heterocyclic dyes called “NBEX” were reported, which, after self-assembling and forming NBEX nanoparticles, bind specifically to ribonucleic acid (RNA) molecules, destroying them after irradiation and inhibiting the normal synthesis of proteins essential for vital cellular processes [43] (Figure 4).

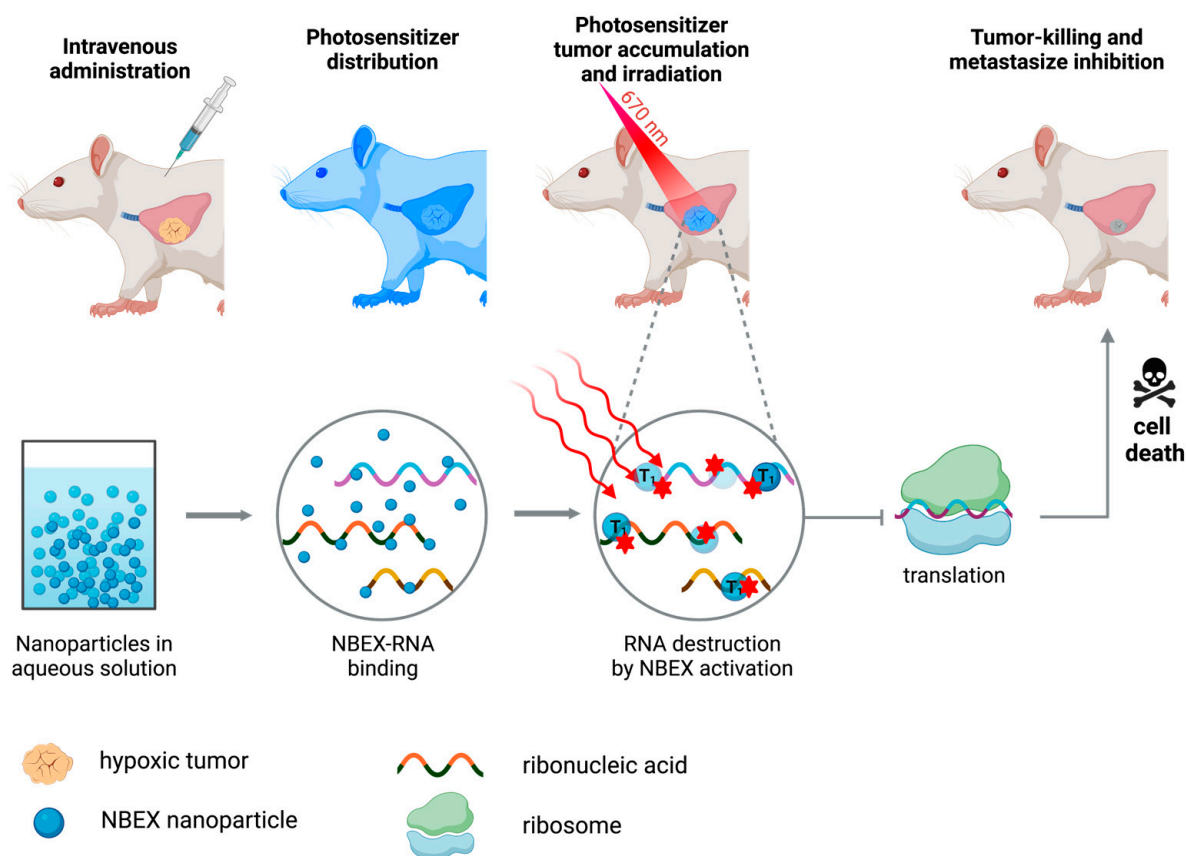


Figure 4. Photodynamic action mechanism of ribonucleic acid (RNA)-targeting self-assembling NBEX dyes type III-photosensitizer prepared by Yao *et al.* [43]. Nanoparticles were prepared in an aqueous medium by self-assembly of NBEX dyes. After administration, distribution, and accumulation in the target tissue, it was irradiated using a light source at 670 nm. At that moment, the NBEX, found linked to RNA molecules of interest for normal cell functioning and maintenance, were destroyed by the photosensitizer in the triplet state, regardless of the coexistence of molecular oxygen. As no RNA molecules are available for the regular production of proteins essential to cell integrity, the death process is triggered, resulting in the eradication of the tumor.

2.3. Photodynamic Therapy Clinical Applications

The clinical application of PDT began in dermatology. In this medical specialty, its purpose is much easier since drugs and their formulations can be administered topically, and access to the lesion is facilitated [44]. In addition, given the restricted penetration of light into biological tissues and the difficulty in delivering the energy required for PS activation to deeper tissues [45], the cutaneous surface is an organ of excellence concerning phototherapeutics. Photodynamic treatments in dermatology have shown promising results, with aesthetic improvements and similar therapeutic outcomes to surgery or radiotherapy in treating actinic keratosis, Bowen's disease, and basal cell carcinoma [46]. This reinforces the need to expand PDT into other areas of medicine.

As such, strategies were gradually created for treating diseases of various medical natures, such as in the field of ophthalmology, in the fight against age-related macular degeneration, pachychoroid disease, and oncological disorders such as choroidal hemangioma, and retinal hemangioblastoma [47,48]; urology, in the treatment of bladder, prostate, urethra, ureter, penis and kidney malignancies [49,50]; otorhinolaryngology, in the control of tumors in the head and neck [51,52], including carcinomas of the mouth, pharynx, larynx and ear; gynecology, in the treatment of carcinoma of the cervix, vulva and vagina [53–55]; and being applied to tissues of the gastrointestinal tract, such as in the therapy of high-grade Barrett's esophagus and esophageal cancer [56–58].

Despite being recognized worldwide for their comparative promise with conventional strategies, all potential drugs, before being clinically applied, must undergo clinical trials that prove their safety, effectiveness, and possible side effects in the short and long term. For PDT, clinical approval is difficult, as it is necessary to consider not only the therapeutic properties of the PS but also its combination with an energy radiation application system and its light dosimetry.

2.4. Photodynamic Therapy Advantages and Disadvantages Compared to Other Strategies

Chemotherapy, a therapeutic strategy based on the systemic administration of a cytotoxic product, despite allowing it to reach tumor cells in different parts of the body and efficiently eradicate them, has the most significant disadvantage of causing damage to healthy cells [59]. Furthermore, numerous side effects have been observed depending on the chemotherapeutic agent used, such as nephrotoxicity, hepatotoxicity, ototoxicity, neurotoxicity, cytopenia (leukopenia, neutropenia, anemia, and thrombocytopenia), nausea, vomiting, and alopecia [60]. Similarly, radiotherapy, in addition to the numerous adverse effects it causes in patients (fatigue, hair loss, damage to the epidermal layer, swelling, loss of memory and tenderness, fertility issues, and cardiovascular complications) [61], is unable to induce death in tumor cells that cannot be seen in imaging exams [62], is ineffective in the treatment of tumors with little blood supply [63], and needs to be administered for a continuous period of 1 to 2 months for best results [64].

To improve these negative features, research has been guided toward searching for more viable, safer, and more successful alternatives for treating cancer. Photodynamic therapy has precisely this objective, offering advantages such as:

- Minimal invasiveness: The PS administration is carried out intravenously, intratumorally, or topically, followed by irradiation to the surface or light delivery performed through endoscopy techniques, avoiding surgical strategies [3,65];
- Double selectivity: It is spatially selective, as the light beam is focused on the precise location of the target tissue, and, as the PS preferentially accumulates and retains at the site to be treated, systemic toxicity is minimized [66]. Furthermore, as the half-life of the ROS produced, such as singlet oxygen and hydroxyl radicals, is less than a microsecond, reactions of an oxidative nature hardly occur in adjacent healthy tissues;
- Combinable with other therapies: If PDT does not produce the desired effect, it can be used in combination with other therapeutic modalities, such as chemotherapy, radiotherapy, surgery, and immunotherapy, among other more invasive means, since drug interactions do not occur as therapeutic targets are different from those of PDT,

and irradiation treatment does not interfere with the activity of other antineoplastics [67,68]. Therapeutic targets differ, making their combination non-competitive and capable of producing improved effects compared to single treatments;

- Fewer adverse effects: Compared to conventional therapeutic strategies, which cause intensive wear and tear on the patient, PDT has some adverse effects at the cutaneous level, such as pain, burns, erythema, edema, itching, desquamation, and pustular formation [67,69];
- High effectiveness: At an early stage and for localized solid tumors, PDT can be a very effective treatment. In the case of patients in a palliative state, this therapeutic modality can be an alternative to the conventional ones since it can significantly improve the quality of life [70,71];
- Reduced recovery time [72];
- Repeatable in case of tumor recurrence: Photodynamic treatment can be repeated in the event of the appearance of a new primary tumor in a previously treated area without risk of damage to surrounding normal tissues or development of resistance to therapy, mechanisms recurrently observed and reported in the literature regarding conventional medicines, which limit their effectiveness [66,73,74];
- Lead to better aesthetic results: Especially in cases of skin cancer, good aesthetic results are observed compared to surgical methods [75]. Photodynamic treatment should not cause an increase in the temperature of the tissues, causing no destruction of the connective tissue and allowing the anatomical and functional integrity of the tissues to be maintained [76].

On the other hand, and like any therapeutic approach, PDT has several limitations that condition it clinically:

- Few commercially available PSs: Not many PS molecules are approved for clinical use. Furthermore, most PS currently applied are derived from porphyrins, a family of molecules whose molar absorptivity at higher wavelengths, in the regions of the electromagnetic spectrum where tissues are more transparent to light, is relatively low [77];
- Reduced penetration of light into tissues: The wavelengths used in therapy can induce cell death within a maximum radius of 10 mm from the illuminated area, which is often insufficient for eradicating a larger tumor mass [78,79];
- Dependence on the presence of triplet molecular oxygen: PSs whose mechanisms of action are type I and type II reactions depend on triplet molecular oxygen since this is necessary for forming reactive species that induce cell death [80]. Developing new type III PSs could circumvent this limitation [43];
- Absence of contact with light sources for significant periods: Depending on the pharmacokinetic and pharmacodynamic properties of the PS, the time it takes to reach and accumulate preferentially in the target tissue is variable. However, during this period, designated by many as the “drug-light interval”, the patient cannot be exposed to any light, as this would activate the compound prematurely [26,81];
- Persistent cutaneous photosensitivity: Even after photodynamic treatment, the patient should not be exposed directly to light sources since the PS takes some time to be eliminated from the body. From light incidence until the patient can be exposed to radiation, it depends mainly on the photosensitizing molecule. Early exposure results in skin photosensitivity, an effect that may last over time [82];
- Dosimetry is difficult to prescribe because several parameters must be optimized before applying therapy. The PS dose to be administered, the “drug-light interval”, as well as the light source to be used, the irradiation area, and the dose of light to be applied must be determined considering factors such as the size and location of the tumor and the level of oxygenation of the tissues to be eliminated [83].

3. The “Three Elements” of Photodynamic Therapy

3.1. Light Source

Illumination is a critical element of PDT, as its clinical effectiveness depends on the accuracy of light delivery at an appropriate dose [84]. Thanks to technological advances, delivering light accurately and in adequate amounts to a large part of the human body is possible. Therefore, this therapeutic approach can be applied to a wide range of diseases [78]. The choice of radiation source (Table 1) should depend on the location of the tumor and its depth. However, its dosimetry is still difficult to estimate, including the time of radiation exposure, the fluence of light, and the mode of light delivery (whether continuous or fractionated). Nevertheless, dosimetry is crucial for therapeutic success, knowing that delivering a high dose of light in a short period of time can lead to a rapid depletion of triplet molecular oxygen, compromising the destruction of the target tissue [31,85]. There is evidence that the most viable methodology is to carry out prolonged photodynamic treatments using lower irradiation energies [86,87].

Table 1. Comparison of various light sources used in photodynamic therapy and their main advantages and disadvantages.

Light Source	Description	References
Sun light	The use of sunlight as a treatment for dermatological conditions such as actinic keratosis is a cost-free and less painful option that can be easily performed at home. However, it is highly dependent on the weather conditions of the region, and there is no way to regulate the amount of energy emitted.	[88,89]
Lamp lights	Lamp lights are cheap, portable, easy to use, and emit at a wide range of wavelengths. In addition, filters eliminate radiation emitted without interest in the excitation of the photosensitizer, namely at short wavelengths. However, they have the disadvantage of losing energy in the form of heat, which is why they emit low-intensity light and are mainly limited to treating dermatological diseases.	[84]
Light-emitting diodes (LEDs)	LEDs are light sources with high power stability, capable of irradiating large areas, thermally non-destructive, inexpensive, small in size, and easily transportable. Combining lamps emitting at different wavelengths to excite several photosensitizers is possible with the same equipment. The light is incoherent and polychromatic, emitting in a narrow region of the electromagnetic spectrum.	[90,91]
Lasers	Lasers are currently the most commonly used clinically and produce high-intensity, coherent monochromatic light. The coherence contributes to the precise control of the fluence applied to the target tissue, which is more difficult to assess using incoherent sources. They can be coupled to optical fibers to deliver light to highly inaccessible tissues. It is the most expensive light source compared to those above. Comparative studies show comparable photodynamic efficacy using lasers or LEDs.	[78,84,92,93]

More recently, alternatives to conventional light sources have been studied to create a therapeutic strategy independent of external light that overcomes the fact that light cannot permeate tissues as efficiently as desired [94]. An example of these alternatives is chemiluminescence-mediated PDT (CL-PDT), based on the joint use of the PS and a chemiluminescent molecule [95] (Figure 5). These chemiluminescent molecules can emit energy in the form of radiation directly or indirectly: directly when the chemiluminescent molecule is activated by oxidation, forming a high-energy intermediate that dissipates energy by emitting photons until it returns to the ground state, and indirectly when these intermediates release energy that is subsequently absorbed by nearby fluorophores [96]. Luminol and its derivatives are direct chemiluminescent compounds that emit energy in the presence of oxidizing agents [97]. They were already studied for potential application in PDT [98]. To ensure that luminol irradiates the photosensitizing molecule, unique molecules resulting from the conjugation by covalent bonds of the chemiluminescent agent and PS were recently reported [99].

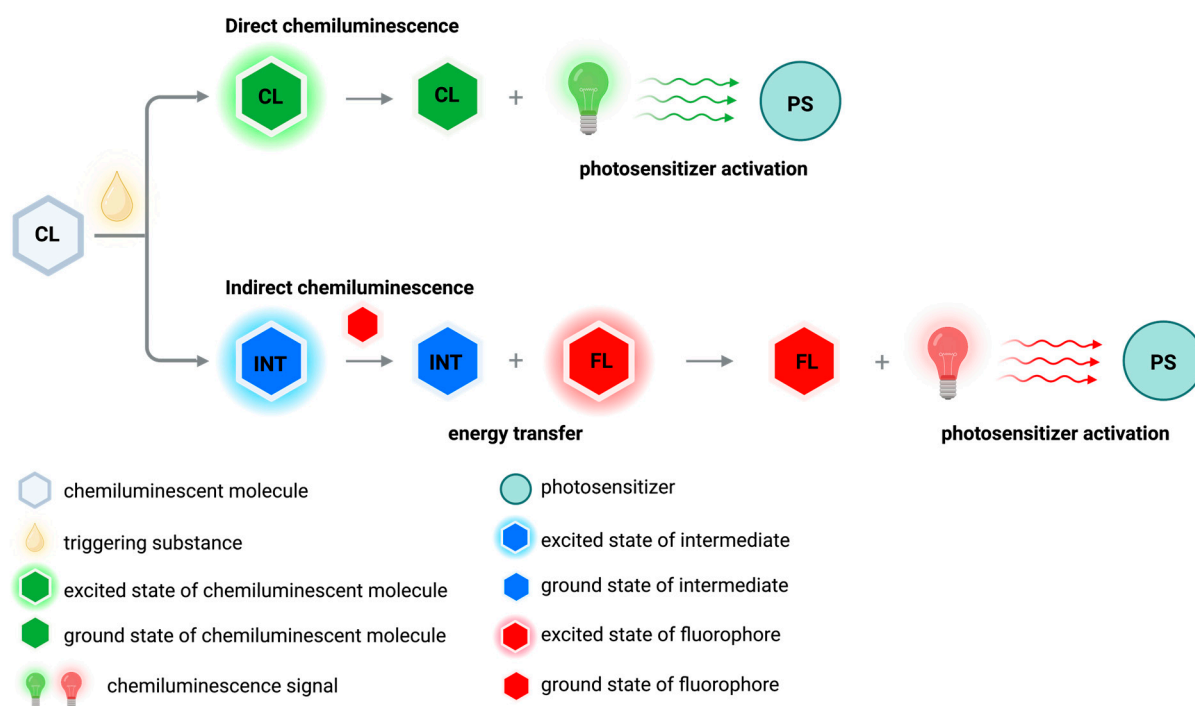


Figure 5. Basic principles of chemiluminescence-mediated photodynamic therapy as an alternative to treatment using external light sources. While in direct chemiluminescence, the excited material (CL) itself is capable of emitting light, during the process of indirect chemiluminescence, the energy is passed from the chemiexcited molecule (the intermediate (INT)) to another molecule (known as the acceptor or fluorophore (FL)) which becomes further excited. The emitted energy is absorbed by the photosensitizer (PS), activating it.

In addition to visible light, there are several alternatives for activating PSs [100], including microwaves, near-infrared (NIR) and infrared light, x-rays, and ultrasounds [101].

3.2. Triplet Molecular Oxygen

Triplet molecular oxygen plays a significant role in the PDT process, and its availability in the target tissue critically affects the treatment outcome when using PSs whose mechanism of action concerns mainly type I or type II reactions.

Since triplet molecular oxygen is essential for therapeutic success, hypoxia conditions can considerably jeopardize the effectiveness of the treatment [102]. One of the consequences inherent to PDT is tumor hypoxia itself since this strategy is based on the consumption of oxygen present in the tissues for its destruction and, in several cases, the vasculature that irrigates it [103]. Furthermore, tissue molecular oxygen concentration can vary significantly between tumors and regions of the same tumor, depending on the density of the vasculature that irrigates it and the rates of diffusion and consumption of oxygen [104]. Thus, irradiation with high-power light sources can be disadvantageous as it leads to total oxygen consumption [86,105].

Monitoring the concentration of oxygen in the tissues is a remarkable tool that allows the adjustment of the power of the incident light so that, ideally, the amount of oxygen consumed is equivalent to that diffused to the tumor tissue to guarantee the continued production of ROS during the period of irradiation without depletion of the component from which they are produced [106,107]. In addition, in tumors of a hypoxic nature, it is predictable that there will be evidence of resistance to therapy when type I or type II PSs are administered [108,109], so the use of PSs that produce type III reactions is desirable in this circumstance [43]. Alternatively, PDT experiments carried out with patients in hyperbaric chambers significantly improves the efficiency of the treatment of tissue ablation [110,111].

3.3. Photosensitizer

Thousands of compounds, dyes, and pigments with photosensitizing capacity have already been identified, either of natural [112], synthetic [113], or hemi-synthetic origin [114]. Porphyrins are the most widely studied of the various classes of PSs reported in the literature. However, due to several limitations that these dyes have, such as the low absorption in the red and NIR regions and higher absorption in blue and green, where tissues are less transparent to light, new alternatives have been sought to improve them [115].

Proof that efficient photoreactive molecules are present in nature is that insects that fed on the green fungus *Cortinarius austrovenetus*, after exposure to solar radiation, ended up dying, revealing the presence of compounds with photocytotoxic activity. It was discovered that this is a fungus-specific mechanism: damaged tissues of the green mushroom become violet due to the oxidation of the pigment austrovenetin in hypericin [116,117], one of the most studied PSs today [118]. Nowadays, it is known that, in addition to *Cortinarius austrovenetus*, a greater diversity of plants, such as *Matricaria chamomilla*, *Spinacia oleracea*, and *Aloe vera*, have similar defense strategies [116]. With advances in analytical technology, photosensitizing substances are becoming more easily discovered in natural extracts. As the identification of these “biophotoactive” molecules continues to increase, it is expected that many more will be found in the coming years [119,120]. Therefore, using PSs derived from plants can be considered an eco-friendly method of PDT [120].

Because families of natural compounds exhibit desirable properties for their phototherapeutic application, structural modifications have been carried out to enhance them, make them more biologically active, or give them more attractive photophysicochemical properties [121,122]. In addition to the porphyrins themselves, widely found in nature in a wide variety of organisms, synthetic analogs of pyranoanthocyanines, dyes that form during the maturation of red wine, have also been explored for their photobiological effects with promising results [122].

Regardless of their natural or synthetic nature, the photosensitizing candidate must exhibit specific properties for their phototherapeutic applicability. Table 2 presents the characteristics of an ideal PS for PDT, on which research has focused when looking for new candidates to be applied in this therapeutic strategy. However, it is crucial to remember that finding a PS with all these qualities is difficult. Furthermore, depending on the application, the most efficient PSs will likely compromise these properties.

Table 2. Ideal properties of a photosensitizer (PS) for photodynamic therapy (PDT).

Property	Description	References
Easy synthesis	Optimizing PS synthesis is crucial for high yields and purity, affecting production scale and cost.	
Absorption in the visible and near-infrared regions	Low-energy radiation reduces harm to healthy tissues and increases light permeability in biological tissues for deeper activation of PS.	[3,113]
Amphiphilicity	Amphiphilic compounds are water-soluble and can easily cross the lipid membranes of cells, ensuring their availability and distribution, allowing the PS to target and accumulate in abnormal tissues more efficiently.	[123]
Various routes of administration	The PS or its formulation must allow safe and painless administration, whether performed orally, topically, or intravenously. In addition, several administration routes will enable the use of the same molecule in a broader range of diseases.	[124]
Selective tumor accumulation	It should be able to reach the neoplasia in a short time as well as selectively accumulate in tumor cells.	[125]
Harmless in the absence of light	Molecules that intrinsically have cytotoxicity should not be studied as potential PSs. To be applied in PDT, photosensitizing candidates must exhibit zero to low toxicity in the dark and significant cytotoxicity only when irradiated.	[123,126]

Table 2. Cont.

Property	Description	References
Resistance to photobleaching	The term “photobleaching” refers to the loss of the ability of the PS to absorb light due to its degradation during irradiation. Resistance to this phenomenon allows the use of higher energy light sources, which may result in deeper tissue penetration and greater therapeutic efficacy.	[127,128]
Long-term triplet state lifetime	The triplet state PS reacts with triplet molecular oxygen to produce ROS for type I and II PSs. Long-term triplet state lifetime enables a prolonged generation of cytotoxic species, which is crucial for the death of target cells.	[129]
Rapid clearance from the body	A rapidly cleared PS from the organism significantly decreases the duration of its presence in the body, thereby minimizing the risk of toxicity to healthy tissue and reducing the risk of side effects such as skin photosensitivity.	[126]

4. N-Heterocyclic-Bearing Dyes as Photodynamic Therapy Photosensitizers

In an endless search for molecule structures that combine the most significant number of properties inherent to those of an ideal PS, several dyes have been described in the literature, namely *N*-heterocyclic-bearing dyes (Figure 6). These dyes have the characteristic of having at least one heterocyclic unit in their molecular structure, that is, at least one cyclic structure with at least two different elements, in this case, carbon and nitrogen. Thus, this nucleus of dyes comprises a wide variety of families of compounds of porphyrin- and non-porphyrin nature. Several structural modifications and formulations, including their encapsulation in nanoparticles, have been studied to understand and make known to the scientific community how advantageous they are for their potential phototherapeutic applicability and to create diagnostic or therapeutic approaches.

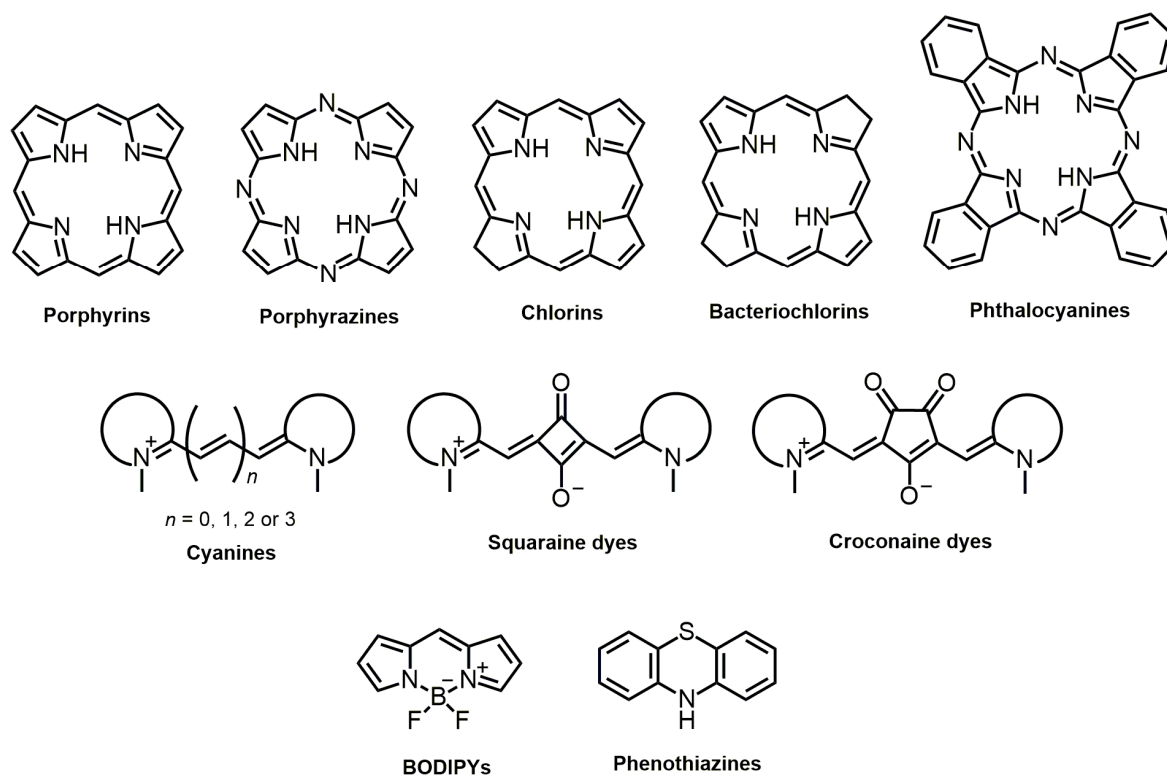


Figure 6. Skeleton structures of *N*-heterocyclic-bearing family dyes addressed in this review article.

4.1. Most Recent Studies Regarding Photosensitizing Candidates' Discovery

4.1.1. Porphyrin-Based Photosensitizers

Porphyrins

Porphyrins are a class of organic compounds whose chemical structure is composed of a ring formed by four *N*-heterocyclic pyrrole-type units connected by four methine bridges [130]. Its presence in nature and its role in various biological processes are well documented [131,132]. Generally, these dyes family can efficiently absorb visible light, preferentially in the blue and green regions, and produce singlet oxygen and free radicals proficiently [113,133]. However, due to their low solubility in water, short circulation time, and lack of specificity for tumors, traditional porphyrins have limited effectiveness as PDT PSs and diagnostic tools [134–136]. To address these shortcomings, scientists have developed various methods to improve the efficiency of porphyrins through chemical modification and nanofunctionalization techniques [137].

Concerning structural modifications carried out in porphyrins, the research focus has been directed to the functionalization of methine protons in the *meso* position by groups of diverse natures and the coordination of free base protons by metallic ions. Additionally, since it is the oldest known class of PSs and given that structure-activity effects are already relatively well known, the preparation of nanoparticles that incorporate these compounds and allow improving specific gaps in these candidates for PSs has been highly reported in recent literature.

The preparation of metalloporphyrins can significantly improve the phototherapeutic effects of analogous free-base porphyrins. For example, very recently, in the study by Hou *et al.* [138], the activity of water-soluble porphyrins coordinated with zinc and copper was compared with that of uncoordinated porphyrins, and it was verified that the one bearing zinc exhibited increased singlet oxygen and peroxide formation. Contrary to zinc, the copper coordinate did not reveal any therapeutic effect.

In addition, several investigators have studied biological effect variations for porphyrins coordinated with other metals such as palladium, manganese, and nickel [139–143]. According to these studies, coordination with palladium was not as advantageous as with platinum [139], and for porphyrin dyes complexed with copper, nickel, and zinc ions, the copper derivative showed the worst photodynamic effects [140]. In contrast to most research involving metalloporphyrins, Frant *et al.* [142] conclude in their work that manganese-metalized porphyrin is, by itself, cytotoxic, while its free-base analog induces effects only when irradiated on colorectal cancer cells. *N*-heterocyclic carbene, gold, *meso*-functionalized zinc, and palladium coordinated porphyrins prepared by Scoditti *et al.* [143] showed no cumulative impact on the ISC rate, revealing that the introduction of metals at different porphyrin positions does not induce a synergistic effect.

Regarding the modifications made to the *meso* porphyrin position, several functional groups have been reported, depending mainly on the therapeutic or functional aim:

- Inferring the functioning of specific cell receptors, Manathanath *et al.* [144] synthesized a series of tetrahydroxyphenyl-derived porphyrins (THPP) appended with the 4,6-diamino-1,3,5-triazine group. This moiety was introduced since triazines are known for their attractive bioactivity due to their kinase receptor inhibitory nature, particularly their ability to inhibit the epidermal growth factor receptor-tyrosine kinase, overexpressed in tumor cells, which is involved in tumor proliferation, metastasis, and angiogenesis processes [145,146];
- Responsiveness to elements overexpressed in the tumor environment: Huang *et al.* [147] designed a “dual response” porphyrin-based PS capable of responding to the typical increase in glutathione (GSH) and hydrogen sulfide concentration in tumor cells. For this purpose, they prepared a reversible derivative of the already known THPP esterified with 2,4-dinitrobenzoyl chloride, which presented low to moderate toxicity and zero formation of singlet oxygen. Furthermore, the investigators testified that only in the presence of GSH and hydrogen sulfide occurs the photosensitizing

- agent activation by the quenching group departure, stating that it has a high clinical potential in reducing the effect of cutaneous photosensitivity;
- Improvement of functional properties of this family of PSs: Certain functional groups can significantly contribute to refining physiological and chemical stability and biocompatibility [148]. The introduction of polyethylene glycol (PEG) moieties into porphyrin cores, for example, has been reported several times in the literature [149–151]. Lazewski *et al.* [151] demonstrated that, irrespective of the coordinated metal, short-PEGylated porphyrins reveal reduced dark cytotoxicity, increased ability to produce singlet oxygen, and that the structural location where the polymer is introduced can result in the variation of the biological effects;
 - As an interface between single-PSs and nano-PSs, Li *et al.* [152] demonstrate that the chain conjugation of PEG-bearing porphyrins with perylene diimide units resulted, by self-assembly, in a kind of nanoparticle with attractive properties: (i) high biocompatibility; (ii) intense absorption in the visible and NIR regions; (iii) therapeutic efficiency *in vitro* and *in vivo* with reduced side effects; (iv) potential use as a theranostic agent by obtaining second near-infrared (NIR-II) fluorescence images.

The incorporation of porphyrins in nanostructures is also recurrently reported in the literature to improve these first- and second-generation PSs, which, due to their several shortcomings that make their therapeutic efficacy unfeasible in their single form, when encapsulated, improve many properties related to their phototherapeutic effects.

As an example of a nanosystem that incorporates porphyrins, Shang *et al.* [153] reported a new theranostic nanomaterial targeting mitochondria called “PTPF-MitP”, by combining three functional groups: a lipocationic selective peptide as a mitochondrial targeting unit (MitP), *meso*-tetra(4-carboxyphenyl)porphyrin (TCPP) as a NIR fluorescent signaling unit, and platinum nanoparticles functionalized with polydopamine and TCPP as photothermal and PDT agents, respectively. In A549 human lung adenocarcinoma cells, the nanomaterial was in the mitochondria, proving the usefulness of the MitP unit in its targeting. In addition, the authors showed that this targeting was essential for the best therapeutic activity since nanomaterials not functionalized with MitP saw their photocytotoxicity reduced by half under 650 nm laser irradiation. Thus, its improved cytotoxicity, the fact that the death pathway adopted after photodynamic treatment is apoptotic given the release of cytochrome C, the increase in temperature observed after irradiation, and its visualization in real-time by imaging encourage the use of this “nanomissile” as a theranostic agent for lung adenocarcinoma.

The conception of porphyrin-containing nanoparticles may also contribute, for example, to better cell permeation and increased efficiency in a tumor environment poor in triplet molecular oxygen. This is proof of the study by Jiao *et al.* [154], in which they couple porphyrin metallacages capable of concentrating triplet molecular oxygen to proteolytic enzymes to break down hyaluronic acid (HA) moieties in an amphiphilic polymeric nanostructure 1,2-distearoyl-*sn*-glycero-3-phosphoethanolamine-*N*-(methoxy-polyethylene glycol)-2000 (DSPE-PEG₂₀₀₀; Figure 7). In this way, the incorporation of proteases allowed better permeation of the drug in cancer tissues since HA is overexpressed in tumor cells and is one of the main components of the extracellular matrix [155]; after irradiation at 660 nm, porphyrin was capable of producing singlet oxygen more proficiently than porphyrin in the free state, and the assembly of amphiphilic molecules made it possible to overcome the hydrophobicity of the PS candidate.

Dozens of other highly innovative strategies have been recently reported within the scope of porphyrin encapsulation, such as the design of triple action nanostructures (PDT, chemotherapy, and immunotherapy) [156], the combination of graphene quantum dots given their recognized photostability, biocompatibility, and minimal toxicity [157], as well as a vast array of techniques that make it possible to complement the therapeutic branch with prevention and diagnosis in the design of new and increasingly attractive porphyrin-based theranostic methods [158–160].

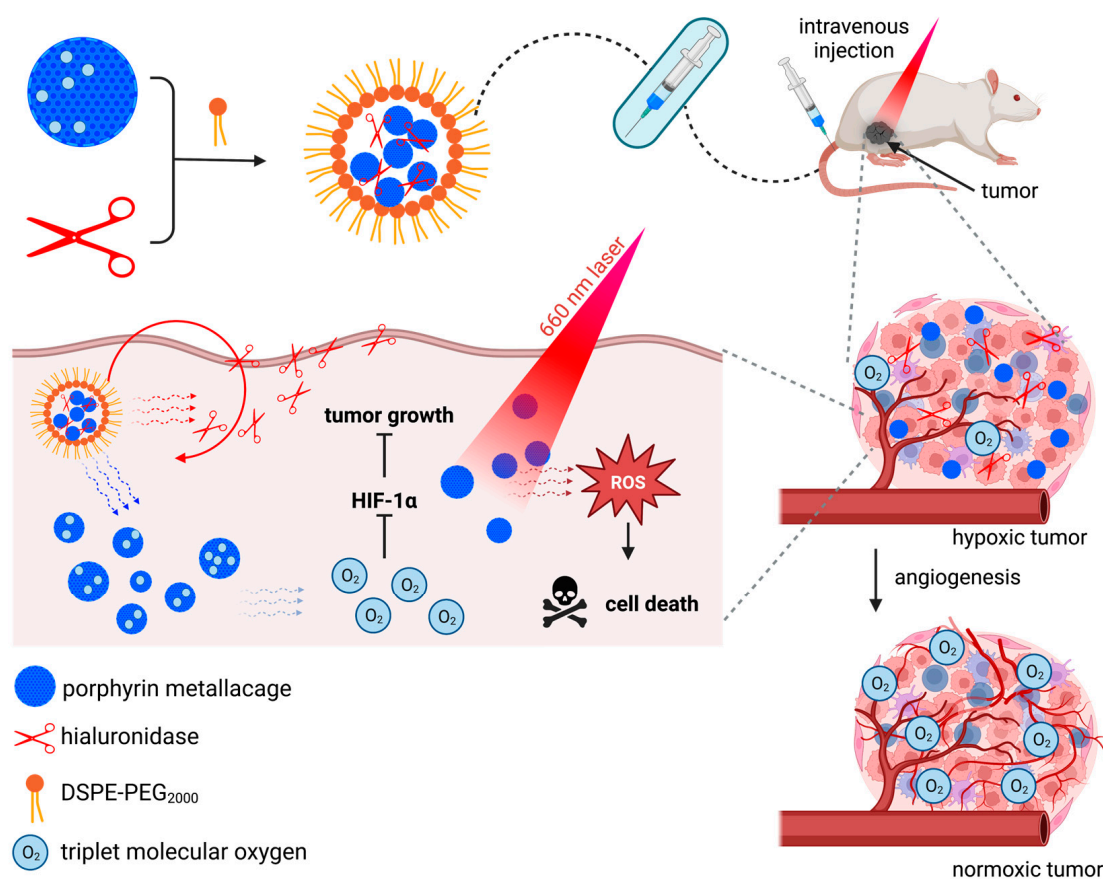


Figure 7. Formulation and mechanism of action of porphyrin metallacages nanoparticles containing hyaluronidase against hypoxic tumors reported by Jiao *et al.* [154]. The nanocarrier was prepared by combining a porphyrin metallacage, in which cavities are concentrated with triplet molecular oxygen, and the enzyme hyaluronidase, coated with 1,2-distearoyl-*sn*-glycero-3-phosphoethanolamine-*N*-(methoxy-polyethylene glycol)-2000 (DSPE-PEG₂₀₀₀). Hyaluronidase allowed the degradation of the extracellular matrix, resulting in greater formulation accumulation inside tumor cells. Molecular oxygen release from metallacages combined with hypoxia relieved by angiogenesis suppresses the expression of hypoxia-inducible factor-1 α (HIF-1 α) and consequent tumor growth inhibition. Irradiation with a laser emitting at 660 nm activates porphyrin, which, once activated, produces singlet oxygen, culminating in cell death.

Porphyrazines

Porphyrazines are synthetic derivatives of the porphyrin class, which, instead of the typical methine carbons, have nitrogen atoms in their structural places. Although less known than porphyrins in their phototherapeutic application, these derivatives already have well-defined synthesis pathways and a wide range of structures associated with this family of dyes [161,162]. Like porphyrins, porphyrazines also have the ability to absorb light at specific wavelengths and generate ROS after light activation, which can lead to the destruction of cancer cells [163].

The cellular location of new photosensitizing molecules is usually one of the focuses of investigation since they should accumulate in organelles of high significance for cellular integrity and maintenance, guaranteeing the occurrence of cell death after light activation. The most desired target is usually the mitochondria, since this is crucial for the cell's energy metabolism, and variations in the permeability of its membrane can trigger the release of cytochrome C and the consequent occurrence of the apoptotic death mechanism [164,165]. Despite this, studies prove that other organelles, including the Golgi apparatus, lysosomes, peroxisomes, and the cytosol, can be sites where photosensitization successfully occurs [166,167]. Additionally, demonstrating that mitochondrial uptake is not

necessary for photodynamic success, in 2021, Tasso *et al.* [168] synthesized a series of five magnesium porphyrazine complexes in which photobleaching inside cellular plasmatic membranes occurs through an electron abstraction of the lipid double bond, resulting in irreversible damage to the membrane. Interestingly, they observed that the higher the PS photobleaching rate, the faster the membrane leakage was induced. This research also challenges the commonly held belief that photostability is a crucial requirement when developing new PSs and suggests that a defined photobleaching rate can be beneficial for developing dosimetry in hypoxic target regions and drug elimination.

A particularly studied subclass of porphyrazines is the cyanoarylporphyrazines, whose researchers have been introducing different aryl groups and complexing them with various metals, as is the example of the study by Yuzhakova *et al.* [169]. They prepared two cyanoporphyrazines complexed with gadolinium, differing in the side chains: one functionalized with fluorobenzene and the other with (benzyloxy)benzene. *In vivo*, both dyes showed intense fluorescence in tumor regions compared to healthy tissues, indicating selective accumulation. The authors also showed that these porphyrazines have promise as contrast agents and can be used in magnetic resonance imaging. Despite being interesting from a diagnostic point of view, only the (benzyloxy)benzene derivative caused moderate tumor growth inhibition. Complexation with iron of other analogs of tetracyanoporphyrazines [170], this time functionalized with naphthyl groups, despite seeing their cellular uptake reduced, proves to have distinct photodynamic interest since much higher photodynamic indices were observed for the metal-complexed dye. In addition to their interest as potential PSs, the authors show that they may serve as possible fluorescent probes for determining the viscosity of solutions [171]. Other recent studies report other aryl groups that potentiate this subclass of porphyrazines [166,172].

The encapsulation of porphyrazines has also been the subject of study [173,174], one of the most attractive studies recently reported being that of Mlynarczyk *et al.* [175]. These authors report the synthesis of a *seco*-porphyrazine, a derivative possessing one of the pyrrole units opened by oxidative processes. These derivatives are little studied due to their complex synthesis and isolation, as well as their high chemical instability. However, once obtained with high purity, it was studied for its potential in PDT in CAL27 and HSC-3 oral squamous cell carcinoma cells and HeLa cervical epithelial adenocarcinoma cells. With distinct phototherapeutic activity in its free form, it was encapsulated in different liposomes made up of four types of lipids: phosphatidylcholine (POPC), dioleoylphosphatidylethanolamine (DOPE), phosphatidylglycerol (PG), and 1,2-dioleoyl-3-trimethylammonium-propane chloride (DOTAP). Mixtures of DOTAP:POPC or PG:DOPE lipids showed more attractive effects than PG:POPC or DOTAP:DOPE, with researchers demonstrating that the lipid constitution of these nanostructures can condition the photoactivity of the compounds internalized in them.

Assigning a particular favorable characteristic to the phototherapeutic application can be challenging, generally requiring a large set of molecules so that it can be confidently stated that the introduction of a specific functional group confers a particular property. Yagodin *et al.* [176], in their recent study and based on all their knowledge about porphyrin-based molecules, have prepared a tetraquinoxalineporphyrazine that has attractive photodynamic properties: maximum absorption at wavelengths around 760–770 nm, improved stability compared to other derivatives, and a high relative singlet oxygen quantum yield. The authors explain that the bathochromic shift is justified by the π -extension of the quinoxaline group directly linked to the porphyrazine ring, that light stability is conferred particularly by pyrazine, and that the eight anionic carboxylate substituents explain its increased water solubility. Based on the well-known Warburg effect, which describes the efficient uptake of glucose by tumor tissues to produce energy *via* glycolysis, several authors, including Klein and Ziegler [163], prepared candidates for glycoconjugate PSs to increase the uptake of these molecules by the tumor cells, “deceiving” them. Despite exhibiting appealing properties, their biological activity has not been evaluated.

Chlorins

Chlorins, also known as dihydroporphyrins, are porphyrinic dyes with attractive photophysical characteristics, namely improved absorption in the red region compared to traditional porphyrins [177]. The preparation of these molecules is usually initiated by derivatizing porphyrins; however, their purification is hampered by the fact that they are critically unstable, either because of the ease of retro-oxidation in porphyrins or because they are not very stable to light, as well as because, generally, multi-step synthesis is necessary, making their preparation even more challenging [178].

Clinically, chlorins already play a role, some of the most important being Temoporfin, Verteporfin, and Radachlorin. These commercial molecules are still a source of inspiration for creating new chlorins with improved properties and developing formulations that can improve them therapeutically or promote their theranostic application. Chlorophyll itself, a photosynthetic pigment present in the chloroplasts of plants and some algae, is used as a starting point for the synthesis of various chlorins [179,180], namely the well-known and recognized chlorin-e6 [181].

An example of this inspiration is, for example, the study by Qin *et al.* [182], where the researchers present a derivative of chlorin-e6, a PS whose hydrophobic nature and reduced activity in hypoxic environments strongly compromise its therapeutic action. Thus, based on these two shortcomings, Qin had two challenges that resulted in the preparation of a nanoplatform of undoubted significance: functionalizing structural chlorin with amphiphilic D- α -tocopherol polyethylene glycol 1000 succinate (TPGS) to modulate its hydrophobicity and, additionally, to induce the production of ROS by the interaction of TPGS with mitochondrial complex II, as well as its assembly into α -cyano-4-hydroxycinnamate units for the formulation of nanostructures capable of intervening in the regulation of lactate metabolism and therefore saving intracellular molecular oxygen (Figure 8). Another example that shows the relevance of working on already known PSs is the study by Kawasaki *et al.* [183], in which, through chlorin-e6 self-assembly in polymeric polysaccharides from maltotriose units, they prepared a PS system 780 times more potent than Photofrin. However, a disadvantage of chlorins, and most classes of PSs, is their poor targeting. As such, in a study of extreme significance, Yang *et al.* [184] developed chlorin-e6-loaded silica nanoparticles and, to specifically target gastric cancer cells, covered them with a cell membrane derived from cells of the same disease, obtaining excellent results both *in vitro* and *in vivo*. Other strategies have been adopted, such as integrating chlorins in maltotriose-functionalized nanoparticles [185] and HA-based carbon nanotubes [186].

The conjugation of dyes with molecules used as chemotherapeutic agents in a fusion approach of PDT with chemotherapy is a therapeutic strategy called chemophotodynamic therapy (chemoPDT). As an example, one of the most recent studies addressing this subject is that of Yang *et al.* [187], in which chondroitin sulfate-based nanoparticles co-charged with chlorin-e6 and paclitaxel are prepared. These nanosystems showed efficient photodynamic and chemotherapeutic synergy *in vivo*, releasing paclitaxel after the destruction of the nanostructure by laser irradiation for chlorin activation.

Structurally, several adaptations in the core of chlorins have been carried out, from the preparation of new pyrazolopyridine-bearing diphenyl chlorins designed from molecules with very relevant theranostic properties [178,188], their functionalization with fatty acids such as myristic acid to increase their cellular permeability [189], the introduction of groups with sulfur atoms such as thiophenes in order to improve their ability to form singlet oxygen [190], to their structural conjugation with sugar molecules and other compounds of biological interest [191,192].

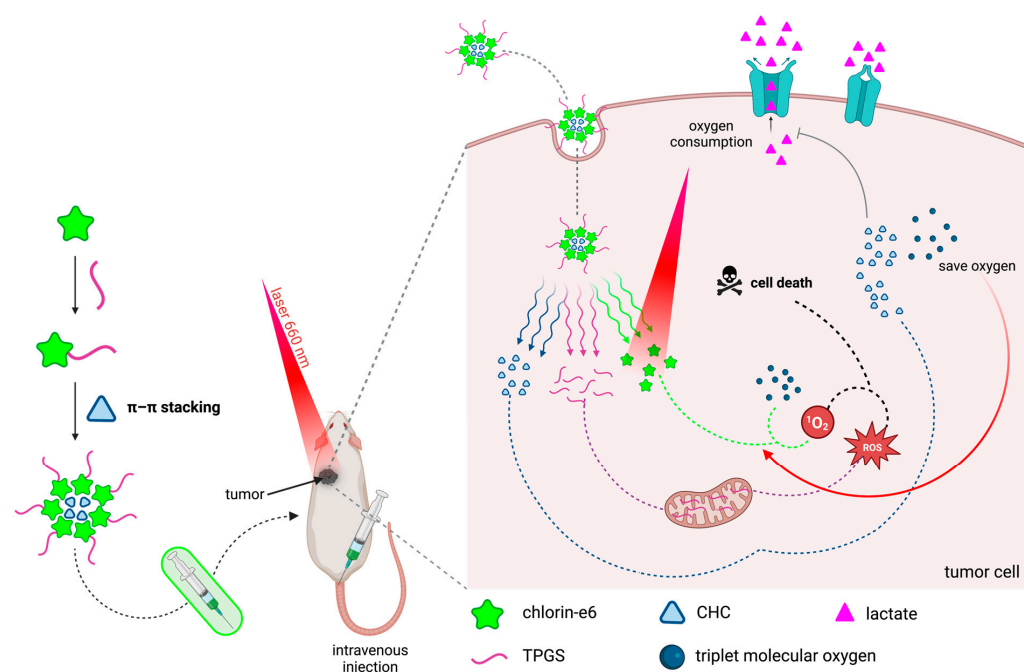


Figure 8. Preparation and mechanism of action of the lactate-aerobic respiration-inhibiting photodynamic therapy strategy suggested by Qin *et al.* [182]. The nanostructure was prepared by chemically conjugating chlorin-e6 with D- α -tocopherol polyethylene glycol 1000 succinate (TPGS) and, by hydrophobic π - π stacking interactions, α -cyano-4-hydroxycinnamate (CHC) units were co-assembled. Each of these elements was important for the therapeutic activity of the nanoparticle: CHC allowed the inhibition of lactate aerobic respiration, allowing the saving of triplet molecular oxygen required for the improved photodynamic activity of chlorin-e6, as well as TPGS, which, interacting with the mitochondrial complex II, induces reactive oxygen species (ROS) formation. These ROS, conjugated to singlet oxygen produced by chlorin-e6 activated after irradiation, culminate in cell death.

Bacteriochlorins

Plant photosynthesis mainly involves chlorophylls, which have been extensively studied due to their spectroscopic and photophysical properties [193–195]. However, bacteriochlorophylls, natural bacteriochlorins found in some photosynthetic bacteria species, are also relevant in understanding fundamental processes and potential applications [196,197]. Structurally, bacteriochlorins differ from chlorins as they present two reduced pyrroles on opposite sides of the porphyrin-derived macrocycle (Figure 6).

Bacteriochlorins can absorb electronic radiation in the visible to NIR region of 700 to 900 nm, penetrating deep into tissues [198]. While naturally occurring metal complexes derived from bacteriochlorophylls are unstable and have limited use, there are now synthetic compounds recently described that belong to the bacteriochlorin family and are highly photostable [199,200]. Therefore, two significant issues with bacteriochlorophylls must be addressed for their phototherapeutic application: firstly, they are prone to instability, which can lead to unintended dehydrogenation and subsequently the formation of a chlorin; and secondly, the rigidity of their macrocycle makes it challenging to perform synthetic transformations [198,201,202].

In the recent literature, one of the most reported strategies is the functionalization of bacteriochlorins with naphthalimides since these last molecules have an excellent ability to fluoresce, are endowed with good light stability, and have high Stokes shifts. Morozova *et al.* [203] showed that this conjugation resulted in the selective accumulation of malignant cells from murine tumor cells of S37 sarcoma, that excitation at the maximum wavelengths of the bacteriochlorin unit resulted in activity as high as that of individual bacteriochlorin, and that the additional excitation of the naphthalimide unit results in increased therapeutic efficiency due to the transfer of energy from the fluorophore to the

PS. In addition, the fluorescence properties of the fluorophore unit enhance the use of these molecules for theranostics. Other similar studies based on naphthalimide-bearing bacteriochlorins are also reported in recent original articles [202,204,205].

Current research is focused on developing new therapeutic strategies using Redaporfin and understanding its mechanism of action. Studies by Lobo *et al.* have shown that low doses of light-activated PS can destroy the primary tumor and reduce the formation of metastases while also triggering antitumor immune responses in mice with CT26 tumors [206]. In addition, Karwicka *et al.* found that depriving the tumor of blood supply using this PS molecule led to a highly effective antineoplastic response *in vivo*, with tumors not reappearing in 67% of mice after more than a year [207]. Lastly, Mendes and Arnaut explored the potential of combining Redaporfin with glycolysis inhibitors 3-bromopyruvate and 2-deoxyglucose [208] (Figure 9). The authors explain that glucose transporters serve cells to absorb glucose and 2-deoxyglucose, which is analogous to glucose but cannot be metabolized. 2-Deoxyglucose acts as an inhibitor of hexokinase and phosphoglucose isomerase. Meanwhile, 3-bromopyruvate is taken up by cells through monocarboxylate transporters, which are overexpressed in tumor cells, inhibiting hexokinase and glyceraldehyde-3-phosphate dehydrogenase, crucial enzymes in the glycolytic pathway. The combined action, particularly of 3-bromopyruvate, with the excellent photobiological properties of the PS, studied in mice with large subcutaneous CT26 tumors, showed cure rates that were 22% higher than using Redaporfin alone and 33% higher than using only the glycolysis inhibitor.

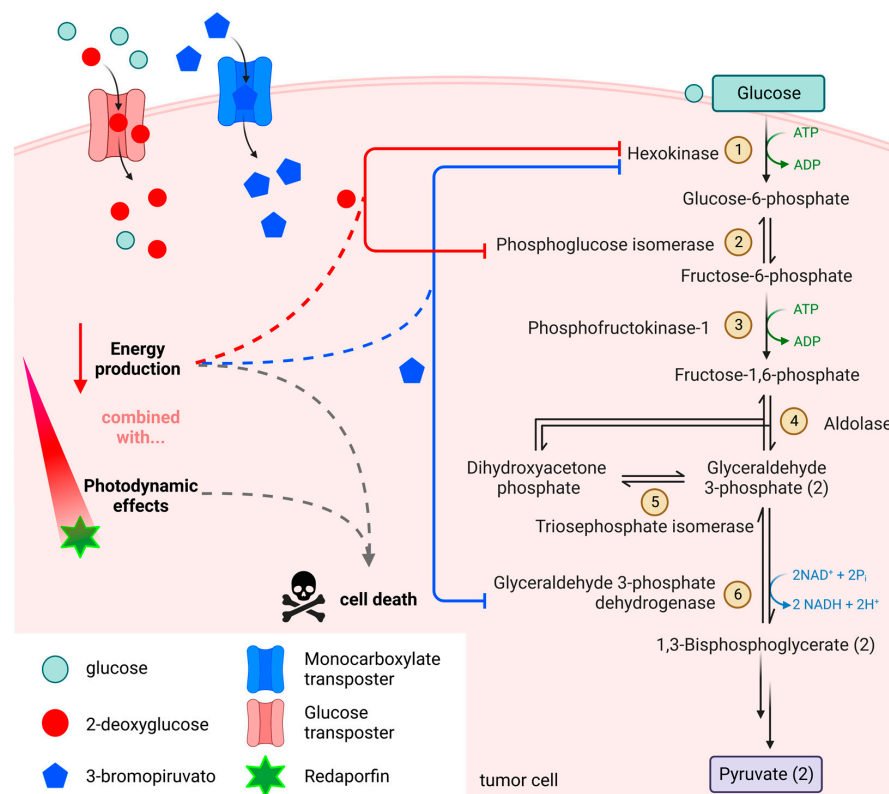


Figure 9. Role of glycolysis inhibitors combined with the photodynamic activity of Redaporfin in developing an efficient antitumor strategy proposed by Mendes and Arnaut [208]. 2-Deoxyglucose acts as an inhibitor of hexokinase and phosphoglucose isomerase, while 3-bromopyruvate is uptaken by cells through monocarboxylate transporters, which are overexpressed in tumor cells, targeting hexokinase and glyceraldehyde-3-phosphate dehydrogenase enzymes, both of which are decisive for the glycolytic pathway's regulation. The energy imbalance due to the glycolysis blockade, mainly triggered by 3-bromopyruvate conjugated with the photosensitizer's production of singlet oxygen, led to cell death.

Conjugation with chemotherapeutics such as erlotinib [209], the introduction of groups that allow improvements in their biocompatibility through hydrophilicity enhancement (e.g., Trizma and spermine groups [210,211]), and the functionalization of bacteriochlorins of natural origin or the design of new bioinspired bacteriochlorins [199,212], are other approaches described in recent works that deserve the scientific community's attention.

In the field of oncology, and among the previously mentioned works, the study by Cheruku *et al.* is one of the most attractive. The authors prepared a series of chlorophyll-a and bacteriochlorophyll-a derivatives structurally conjugated with the erlotinib chemotherapeutic agent in different positions of the macrocycles through linking groups of different nature, having concluded that these two latter factors interestingly conditioned in a significant way their *in vivo* tumor selectivity and therapeutic effects.

Phthalocyanines

Phthalocyanines (Pcs) are porphyrin-based dyes composed of four isoindole nuclei joined by four nitrogen atoms. Among the porphyrinic PSs, Pcs may have been most recently studied due to their superior photochemical and photophysical properties [213]. Compared to conventional porphyrins such as Photofrin and Foscan, for which treatments are typically associated with skin photosensitivity, the fact that Pcs exhibit strong and sharp absorption wavelengths in the range of 650 to 800 nm causes this to be minimized, allowing for better light penetration into tissues and consequently the treatment of deeper pathologies [214]. Highlighting this class as potential PSs, several Pcs and their formulations are in clinical trials, namely the aluminum-complexed Photosens [215] and the liposome-loaded ZnPc "CGP55847" formulation [216].

Photosens sees an improvement compared to most Pcs in its biocompatibility. Structurally, this property is explained by the sulfonic groups, which indicated neurotoxicity in *in vivo* studies for tetrasubstituted dyes. Interestingly, the sulfonic groups' number reduction contributed to filling this gap, with those disubstituted with sulfonic groups in opposite positions showing greater effectiveness. Phthalocyanines with sulfonyl groups are still studied nowadays [217].

Summarizing several examples of the structural changes made over the last few years, Table 3 gives a general overview of their influence on the therapeutic potential of Pcs.

Table 3. Summary of the main structural modifications made to phthalocyanines (Pcs) in recent years, main aspects and conclusions that can be drawn from their photobiological effects.

Structural Variation	Specification	Main Aspects and Conclusions	References
Metal coordination	Zn, In and GaPcs	Various metals were introduced into benzimidazole tetrasubstituted Pcs. The In-complexed one showed highly efficient singlet oxygen generation and <i>in vitro</i> phototoxicity.	[218]
	RuPcs	Ruthenium complexation can create effective Pcs for PDT, known for its medicinal properties. In addition, loading NO ⁺ and NO ₂ ⁻ units onto metal allows the release of nitric oxide, boosting light toxicity and causing selective effects seen <i>in vitro</i> .	[219,220]
Presence of chalcogen atoms	O, S, Se	Bathochromic shifts were observed for S and Se-bearing Pcs. The Se proved beneficial in increasing absorptivity and singlet oxygen production. PDT effects were observed for both derivatives, but the first derivative showed greater efficiency <i>in vitro</i> .	[221]
Charges number	0, 4 or 8 positive charges	Improved properties (singlet oxygen production, water solubility, and cellular uptake) were perceived for cationic compounds compared to neutral ones, and lower half-maximal inhibitory values were observed for eight times positively charged compounds for MCF-7 cells.	[222]

Table 3. Cont.

Structural Variation	Specification	Main Aspects and Conclusions	References
Functionalization with biomolecules	Sugar units	Ruthenium-complexed Pcs were functionalized with glucose, galactose, and mannose. Adding sugar did not enhance cellular uptake, but one-bearing mannose proved better for PDT use.	[223]
		Lactose Si-complexed Pcs proved to be biocompatible, stable in aqueous media, and efficient in ROS generation, showing <i>in vitro</i> high photocytotoxicity and selective tumor accumulation <i>in vivo</i> .	[224]
	Biotin	Biotin-PEG-bearing SiPc has been shown to selectively accumulate in tumor tissue and reduce biotin receptor-overexpressed tumor growth progression <i>in vivo</i> . In addition, PEG units made the potential PS more soluble in water and less prone to aggregation.	[225]
		It was perceived that self-assembled biotin-amine SiPc of different sizes (10, 20, 40, and 90 nm), depending on the percentage of surfactant, exhibited targeting and improved photoactivity <i>in vivo</i> , especially for the 20 nm particles after avidin-presence disassembly.	[226]
		Glycyrrhetic acid	The interest in conjugating glycyrrhetic acid to SiPc is due to its overexpressed receptors in liver cancer. The PS candidate was shown to effectively destroy the liver tumor tissue <i>via</i> necrosis and apoptosis. Side effects have not been observed <i>in vivo</i> .
Chalcones	Chalcone-bearing cationic Zn- and In-complexed Pcs saw, for MCF-7 breast adenocarcinoma cells, half-maximal inhibitory concentration values reduced to less than half after irradiation. Despite its promise, mechanisms of action still need to be studied.	[228]	

The mediation of the therapeutic activity of PSs by other molecules of biological interest is also reported in the literature as an approach that significantly increases their cytotoxicity. Two of the most recent examples in the literature involve biomolecules, such as catechins [229] and cannabidiol [230], and chemotherapeutic agents, for example, doxorubicin [231] and dacarbazine [232].

Within the scope of the use of biomolecules, Nkune *et al.* [230] report the synthesis of a tetra 2-mercaptoacetate, ZnPc, that accumulates into the lysosome and mitochondria of A375 human metastatic melanoma cells, which, combined with cannabidiol, proved to be lethal for the cells under investigation, reducing cell viability by about 20%. This value becomes interesting since the photosensitizing agent, by itself, when irradiated, like cannabidiol, decreases only 50% of cell viability under the same experimental conditions.

Concerning chemoPDT, Doustvandi *et al.* [231] demonstrated that by combining doxorubicin and ZnPc and applying low doses of radiation, synergistic effects occur: death by autophagy and apoptosis, cell cycle arrest in G2/M, and a significant reduction in cell migration capacity were some of the phenomena observed with a higher incidence compared to treatments with a PS or chemotherapeutic agent separately.

Researchers have also focused on the encapsulation of Pcs in drug delivery systems, such as micelles [233], liposomes [234], nanocapsules [235], nanoemulsions [236], and, interestingly, in “nanodiamonds” [237,238].

These so-called “nanodiamonds”, as they contain several functional groups on the surface, such as amine-, amide-, hydroxyl-, carbonyl-, and carboxyl-groups, some of which are not present in ordinary graphene quantum dots, facilitate the binding of potential PSs. In 2019, Matshitse *et al.* [237] published a study involving nanodiamonds covalently bonded to boron-dipyrromethenes (BODIPYs) by amide bonds and stacked on a ZnPc derivative. This nanodiamond structure saw a very significant increase in its singlet oxygen quantum yield compared to individual molecules. Evaluated against MCF-7 cells, the nanodiamond bearing both PSs showed harmlessness in the dark and high photocytotoxicity. However,

modest differences from nanodiamonds functionalized exclusively with BODIPYs or ZnPc were witnessed. Three years later, the same investigation group presented a new study evaluating benzothiazole-substituted ZnPcs with zero, three, or four positive charges linked or not covalently to the nanodiamonds [238]. The asymmetry and cationic character resulted in superior PDT activity.

Finally, another strategy of sublime significance that has been used to improve targeting is the loading of nanostructures with specific biomolecules, such as lipid carriers [239] and titanium dioxide nanoparticles [240], with folic acid, explained by the difference in expression of its receptors between normal cells and tumor cells, in which they are overexpressed, namely in prostate, breast, and ovarian tumors.

4.1.2. Cyanine-Based Photosensitizers

Cyanines are a class of photosensitizing dyes consisting of two heterocyclic rings containing carbon atoms and at least one nitrogen atom, which are connected by a polymethine chain comprising an odd number of carbon atoms necessary for the resonance of the lone pair of electrons between the two nitrogen atoms of heterocyclic rings [241,242].

Although they are structurally simpler than molecules derived from porphyrin-based dyes, a wide range of molecules can be built from their skeleton. In their design, there are several constraints to consider for them to perform a potential phototherapeutic activity, namely:

- Polymethine chain length: The number of carbons present in the polymethine chain is the property that defines which class cyanines belong to. Cyanine-based compounds with a single carbon in the methine chain are called monomethine cyanines (Cy1), with three trimethines (Cy3), five pentamethines (Cy5), and seven heptamethine cyanines (Cy7). Cy5 and Cy7 are the most noted in the literature in the study of their photobiology properties since they efficiently absorb at higher wavelengths: while Cy1 absorbs at around 400 nm, Cy7 sees its maximum absorption peaks around 800 nm [243];
- Heterocycle units: For PDT purposes, the preparation of cyanines bearing heterocycles derived from indolenine, benzoindole, benzothiazole, benzoselenazole, benzoxazole, and quinolines is the most common. Among those mentioned above, indolenine and benz[e]indole derivatives are the most highlighted in the recent literature. Furthermore, anthracene units serving as heterocyclic units have been reported [244,245]. The nature of the heterocycles may condition the biological activity of cyanines, varying, for example, the stability of dyes to light [246];
- Central ring: The introduction of cyclic structures in the center of cyanines is a strategy that allows for improving the rigidity and chemical stability of this class of molecules. It is especially common in the case of Cy5, where there are rings with four or five members (squaraine and croconaine dyes, respectively [247,248]) and, in the case of Cy7, cyclohexane rings or their derivatives (for example, a boron fluoride complex within the core structure [128]). The functionalization of Cy7's cyclohexane ring with halogenated atoms such as bromine and chloride is common [249], which serve as excellent leaving groups for functionalization with other groups of interest [250–252];
- *N*-alkyl chains: Since cyanines are intrinsically lipophilic compounds, this characteristic can be modulated by increasing or decreasing the length of *N*-aliphatic chains. This modulation of biocompatibility is also carried out, for example, by introducing sulfonic groups [249,252], carboxylic acids [253,254], pyridines [255], or even more attractively, by functionalizing them with PEG chains [253] or HA units [256]. The conjugation of cyanines with porphyrin-based dyes, adding them *via N*-alkyl chains, is another recently reported strategy to formulate new promising PSs [257]. A further attractive approach is the dimerization of these dyes, building molecules with two covalently linked cyanine nuclei, these chains serving as bridges between units [258]. The targeting of these compounds can also be enhanced, for example, by introducing specific antibodies to these chains [259];

- Halogenation and the so-called “heavy atom effect”: The introduction of halogens and other heavy atoms, such as selenium [260,261], contributes above all to more efficient anticancer activity and, by increasing the lifetime of these dyes in the triplet state, to the improvement of their singlet oxygen production. The presence of iodine atoms is highlighted as the form of halogenation that most actively increases therapeutic activity [249,254,262]. Interestingly, Semenova *et al.* provide evidence that, effectively, there is no linearity between the therapeutic effects and the number of iodine atoms introduced, reporting that the “ideal” number for the Cy7 they prepared is two iodine atoms [263]. Despite this, for indolenine-based Cy5, bromination proved to be more advantageous [264]. However, for benz[e]indole-based brominated Cy5, the same research group shows that there is no advantage in these halogenated ones compared to non-halogenated ones, indicating that the heterocycle may play a role [265]. Intending to improve its bioavailability, Shi *et al.* introduce the trifluoromethyl group into the Cy7 *N*-alkyl chains, stating that this structural modification can improve the cellular uptake of the dye [266].

Concerning cyanines, two very recent works should be highlighted: the first in which the authors take advantage of the fact that the prepared Cy3 forms J-aggregates in a strategy that serves to enhance therapeutic efficacy [267], and the second in which analogous iodinated and non-iodinated cyanines with an antibody covalently joined to them through an amide linker are synthesized to develop a methodology that also allows simultaneous treatment and monitoring of tumors (Figure 10) [259].

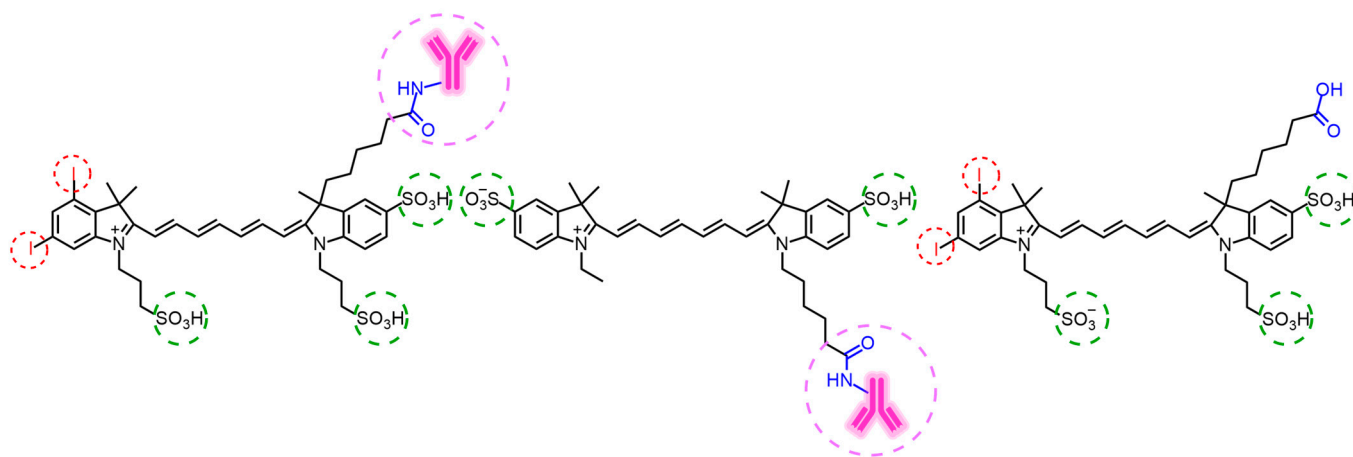


Figure 10. Trastuzumab antibody-functionalized iodinated and non-iodinated heptacyanines prepared by Kobzev *et al.* [259] for photoimmunotherapy. The structural combination with the antibody (pink) contributed to the immunotherapeutic activity of the dyes; the sulfonyl groups (green) made the cyanines more biocompatible; and the iodine atoms (red) allowed an increase in the production of singlet oxygen.

In the first work, Li *et al.* [267] prepared an iodo-indolenine- and quinoline-based Cy3, which, in its free form, has maximum absorption at 630 nm. However, as soon as it is administered intravenously, the dye aggregates under the control of anions with maximum absorption at 700 nm and is directed towards the tumor *via* the enhanced permeability and retention (EPR) effect, a mechanism in which macromolecular compounds can accumulate progressively in the vascularized cancer area. In an intracellular environment, RNA molecules constituted the negatively charged microenvironment for reconstructing these aggregates, accumulating preferentially and gradually in the nucleoli of tumor cells. The authors predict that this “smart J-aggregation” can be used in future studies since it integrates the ability of tumor targeting and improves the therapeutic efficacy of the potential PS molecule.

In the second study, Kobzev *et al.* [259] combine PDT with immunotherapy through the design of new photoimmunotherapeutic agents resulting from the conjugation of Cy7s,

iodinated and non-iodinated, with the antibody trastuzumab (Figure 10). The iodinated conjugate demonstrates a greater capacity to produce singlet oxygen, as expected according to the effect of the heavy atom. The non-iodinated conjugate did not show significant phototoxicity under 730 nm light-emitting diode (LED) irradiation, acting only as an immunotherapeutic agent. In contrast, the iodinated one, in addition to exhibiting intense fluorescence signals that allow monitoring of the conjugate's distribution in the body, suppresses tumor growth about five times. The immunotherapeutic effect is demonstrated when comparing tumor suppression with the dye without antibody conjugation, which only suppresses about 1.4 times. With such impressive results, the researchers believe that PS-antibody conjugation could be a tool further explored in other cyanine-based PSs.

Incorporating central rings in Cy5 is also common in preparing squaraine dyes, with a four-membered central ring derived from squaric acid, and croconaine dyes, with a five-membered ring derivative from croconic acid. Between these two sub-classes, squaraines are the most discussed in the recent literature, showing interesting photoproperties. Furthermore, compared to Cy5 with conventional methine chains, these structures, as they contain carbon rings, are known to be more chemically stable.

Regarding the photodynamic activity of squaraines, our last review focuses on the effect of the various structural modifications carried out on them on their biological activity [247]. Nonetheless, it should be noted that the main structural changes carried out more recently in these molecules are mostly the replacement of one of the oxygen atoms of the four-membered central ring by amines (for example, ethanolamines, picolylamines, and sulfonamides) [268–270] and the functionalization of that same ring with barbituric acid derivatives [271].

Since their debut in 1970, croconaine dyes have been mentioned in the scientific and patent literature [248]. However, the level of research conducted on croconaine dyes has not matched that of squaraines. Croconaines can absorb in the NIR region at higher wavelengths than squaraines and exhibit enhanced fluorescence properties, making them outstanding for biomedical applications [272]. As such, they are described in the recent literature as extraordinary molecules with potential use in diagnostic techniques (for example, brain tumors [273]), as well as in PDT approaches and photothermal [274,275] and, consequently, as theranostic agents [272].

An example of work that validates the theranostic potential of croconaines by addressing their photodynamic activity is that of Sun *et al.* [276] (Figure 11). Because there are few amphiphilic PSs with absorption capacity in the NIR range and pH-responsive NIR-II fluorescence, the researchers combined all these properties in a croconaine dye. The dye was coordinated with ferric ions, resulting in its absorption loss, fluorescence ability, and photocytotoxicity. It was subsequently encapsulated with a pH-responsive polymer connected to the glypican-3 (GPC-3) receptor-specific peptide GP2633. By EPR, croconaine-containing nanoparticles were routed to the target tissue and endocytosed by GPC-3 receptors. Given the acidic pH characteristic of the tumor microenvironment, the polymer was degraded and the coordination bonds were broken, causing its NIR-II fluorescence activation. After 808 nm laser irradiation, the croconaine showed singlet oxygen generation ability. The released ferric cations induce ferroptosis as, in addition to being used for nuclear magnetic resonance imaging, they are reduced to ferrous by the consumption of GSH, inhibiting tumor growth, and through Fenton's reaction, the production of cytotoxic hydroxyl radicals is promoted.

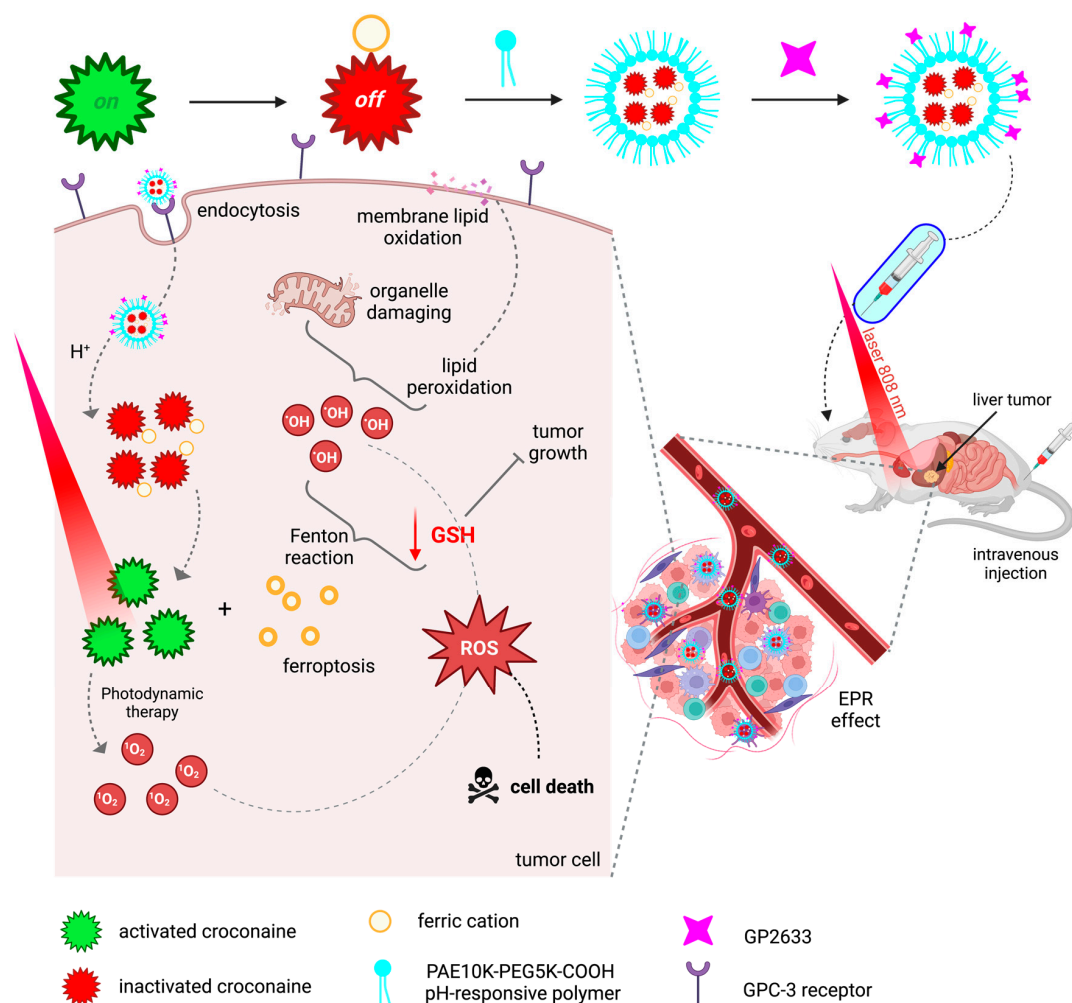


Figure 11. Synthesis and mechanism of action of the “on/off” croconaine-containing nanoparticle reported by Sun *et al.* [276]. They created a croconaine dye that exhibits absorption capacity in the near-infrared range and pH-responsive NIR-II fluorescence (“on”) that complexed with ferric ions and conducted its absorption loss, fluorescence ability, and photocytotoxicity (“off”). The dye-ferric complex (“off”) was then encapsulated with a pH-responsive polymer connected to the GP2633 glypican-3 (GPC-3) receptor-specific peptide. Through the “enhanced permeability and retention” effect (EPR), the nanoparticles were endocytosed by GPC-3 receptors. The proton-rich microenvironment led both the polymer degradation and the ferric-dye coordination bonds to break, activating its second near-infrared fluorescence (“on”). Singlet oxygen was generated after exposing the croconaine dye to 808 nm laser irradiation. The ferric cations released induced ferroptosis, were reduced to ferrous by consuming glutathione (GSH), and consequently inhibited tumor growth. Ferrous ions promote the production of cytotoxic hydroxyl radicals through Fenton’s reaction.

4.1.3. Phenothiazine-Based Photosensitizers

Phenothiazines are dyes with a central thiazine core and two benzene rings condensed to the thiazine ring. Given their biological, photochemical, and photophysical qualities [277,278], these dyes have recently been studied as PSs, more focused on the inactivation of bacterial, viral, and parasite strains [279–282]. Two of the best-known phenothiazines are methylene blue and toluidine blue O, with methylene blue recurrently reported in clinical cases in medical approaches to the treatment of bacterial infections, including for dental diseases, proving to be effective, safe, and with interesting aesthetic results [280,283]. In addition, derivatives of methylene blue, that is, 3,7-disubstituted dyes of the phenothiazine nucleus, have been synthesized, functionalizing these positions with several amines to be studied for photobiological and optoelectronic applications

(for example, as sensitizers of organic solar cells and for the construction of dye-based lasers) [278]. Inspired by these molecules' core, sonodynamic therapy agents have been investigated [284].

Although less common than its antibacterial activity, some molecules derived from phenothiazines are still created within the scope of their application in cancer PDT. One of the most attractive examples is that of Yang *et al.* [285], where they conjugate methylene blue with camptothecin through an activatable linker that contains a disulfide bond susceptible to breakage by GSH. Administered *in vivo*, the authors did not observe physiological toxicity, suggesting safety and biocompatibility, making them believe that they created a molecule capable of overcoming the limitations of methylene blue and camptothecin in their individuality.

4.1.4. Boron-Dipyrromethene-Based Photosensitizers

In recent years, research has significantly increased on the 4,4-difluoro-4-bora-3a,4a-diaza-s-indacene dyes, boron-dipyrromethenes, or BODIPYs. This has resulted in a notable rise in publications related to this chromophore core, showing its high versatility concerning its technological [286,287] and biomedical applications [99,288–290]. Within the scope of its phototherapeutic application, it is important to emphasize that BODIPYs offer a viable alternative to porphyrin-based compounds, owing to their flexibility in synthesis and photochemical properties [291], and consequently exhibit unique properties when modified and functionalized (Table 4).

Table 4. Strategies recently reported on how to structurally improve or enhance certain aspects of boron-dipyrromethene (BODIPY)-based photosensitizers (PSs).

Aim	How?	Main Aspects and Conclusions	References
Long-wavelength absorption	Conjugated double bonds and heavy atom introduction	The length of π -conjugate bonds influences the ability to absorb at redshifted lengths, which is why authors have invested in the synthesis of thiophene- and phenyl-fused BODIPYs, in the introduction of pyrrole rings, and, alternatively, in heavy atoms.	[292–294]
	Halogenation	The inefficient intersystem crossing (ISC) of BODIPYs limits their usefulness in PDT. As for most PS classes, halogenation is a way to improve this photophysical property. Introducing iodine atoms helps the ISC in a more pronounced way than bromination.	[295–297]
Improve singlet oxygen production ability	Organic metal complexes	Aksakal <i>et al.</i> examined new ruthenium and iridium BODIPY complexes. They discovered that singlet oxygen generation increased by twenty times with ruthenium. Meanwhile, Jana <i>et al.</i> achieved quantum yields of 67% for a cobalt-complexed dye. These and other findings suggest a connection between these complexes and the singlet oxygen production ability.	[298–300]
	Anthracene, pyrene, and fullerene conjugation	Callaghan <i>et al.</i> studied several BODIPY dyes with diverse anthracenes and the pyrene group, all showing greater ISC than the phenyl group bearing one. Fullerene derivatives are also effective PSs, producing ROS efficiently with good biocompatibility and easy body clearance.	[301,302]
	Sulfur core-fusion	Thiophene-fused BODIPYs have shown improved singlet oxygen quantum yields (from 4% to 85%). Oscillations in its ability to carry out type II reactions were due to different functional groups introduced in its <i>meso</i> position.	[292]
	BODIPY dimers and trimers	Combining several BODIPY units covalently linked in the same structure can influence properties, namely the increase in the production capacity of singlet oxygen. This effect is shown by Lu <i>et al.</i> for dimeric dyes and by Prieto-Castañeda <i>et al.</i> , whose molecular geometry of analogous trimers is also shown to influence this photophysical property.	[303,304]

Table 4. Cont.

Aim	How?	Main Aspects and Conclusions	References
Targeting specific organelles	Cationic character	Cationic BODIPYs can become more hydrophilic and gain the ability to target mitochondria. They are attracted to the negatively charged inner mitochondrial membrane, accumulating in the mitochondrial matrix through a concentration gradient.	[305–307]
	Morpholine group introduction	The introduction of the morpholine into the core of BODIPYs induces their directing to the lysosome organelle. This finding was observed by several research groups in BODIPY dyes, as this group was introduced to the dyes through a linker.	[308–310]
	Amphiphilicity and biomolecule mimetize	Wang <i>et al.</i> have designed a phospholipid-mimetizing BODIPY-based fluorescent surfactant with two hydrophobic chains for cell membrane imaging and PDT. Concerning the latter, its effect is induced by damaging the tumor cells' cytoplasmic membrane.	[311]
Enhance biocompatibility	Aminoacid functionalization	Amino acid conjugation is a practical approach to improving aqueous solubility and ameliorating their biocompatibility and photobiological efficacy. For example, the aspartic acid-modified BODIPY reported by Yu <i>et al.</i> exhibited enhanced aqueous solubility, singlet oxygen generation ability, and a good phototoxicity ratio.	[312]
	Polymer-junction self-assembly	To enhance the biocompatibility of BODIPYs, these molecules can be modified by attaching PEG derivatives or other hydrophilic polymers. This modification helps to reduce non-specific interactions with biomolecules and improves the stability of self-assembled BODIPY-based polymer-conjugated nanoparticles.	[306,313]
Enhance tumor targeting	Polyamine chain introduction	Tumor cells require amine growth factors and regularly exhibit polyamine transporter overexpression. This makes it possible for BODIPY-polyamine molecules to be transported to cancerous cells, which can improve the effectiveness of these tumor-targeting drugs. In addition, these transporters tolerate the uptake of diverse amines, making them a valuable tool for drug delivery.	[314]
	Sugar-conjugate structures	Recent research has revealed that galactose-containing macromolecules can successfully target various types of cancer. Combining lactose with BODIPYs efficiently targets and impacts tumor cells through enhanced recognition and interaction with overexpressed specific receptors.	[315,316]
		Glucose Transporter 1 is often overexpressed in cancer cells, increasing glucose intake and metabolism. As a result, glycosylated BODIPY triangular skeletons were designed by Durán-Sampedro <i>et al.</i> to promote cellular uptake through the Warburg effect.	[317]
	Polysaccharide-conjugate structures	For example, hyaluronic acid (HA) is commonly used as a polysaccharide-based drug carrier since it is water-soluble, has excellent biocompatibility, and is harmless. Chen <i>et al.</i> prepared an HA-BODIPY through an azide linker group that only triggered phototherapeutics inside tumor cells. This behavior is due to its self-assembled form in the extracellular environment; therefore, ROS production is inhibited.	[318]

One of the most attractive and vaguely reported approaches is the creation of structures made up of BODIPY PS units designed by self-assembly directed by the coordination of metallic ions, such as platinum and ruthenium, called supramolecular coordination complexes. These complexes can exhibit various shapes, including prisms, rectangles, hexagons, and triangles, among others, with the geometry they adopt highly influencing their photodynamic success [319,320]. Furthermore, the fact that they are coordinated prevents their aggregation and, consequently, their more efficient generation of ROS, and given the metal “heavy atom effect”, singlet oxygen production is also augmented [321].

Additionally, coordinating metals can also serve as chemotherapeutic agents, this being a chemoPDT modality [320].

There is nothing more thoughtful than taking the chemical and biological differences between tumor and healthy cells and, from these, building systems that allow their accumulation and activation only at the target site. Although not exclusive to BODIPYs, many “on/off” strategies, such as the one previously detailed on croconaines (Figure 11), have been extensively reported for this class of dyes [322,323]: the development of polymers, nanoparticles, or pH-responsive PSs that are only activated in acidic media characteristic of the tumor microenvironment [324,325]; the creation of GSH-cleavable quencher moieties containing PSs since the concentration of GSH in tumors is exacerbated higher than in normal cells [326,327]; and the design of systems that undergo activation by enzymatic degradation [328,329].

On the last topic, and by way of example, Juang *et al.* [329] took advantage of the fact that the level of tyrosinase, the enzyme that regulates melanin production through melanogenesis, is closely associated with melanoma severity by functionalizing a BODIPY dye with its inhibitor phenylthiourea to improve therapeutic efficacy against a tyrosinase-positive melanoma cell line. The authors verified an increase in its cellular uptake compared to a phenylthiourea-free compound, as well as the ability to produce ROS and significant effects on cell viability when irradiated. These results denote that this is a successful method and could be used to create even more efficient PSs for treating melanoma in the future.

5. Conclusions and Future Perspectives

Photodynamic therapy is a therapeutic strategy that, in recent years, has been growing exponentially in the most diverse areas that concern it to create new approaches that allow solving problems in today’s society, such as diseases of oncological origin. In this review, the authors intended to show how multidisciplinary PDT is, depending on knowledge about several scientific subjects, and whose combination is essential to its development and progression. Thus, based on this knowledge, we present the PDT basic principles from a clinical and photophysical-chemical point of view, showing how, theoretically, PS molecules act on the target tissue and what mechanisms they can adopt to produce cytotoxicity, the role of the three essential elements to improve phototherapeutic results, as well as the progression and alternatives that have been explored in recent years for the conception of improved therapeutic modalities to overcome the PDT weaknesses.

Regarding PSs, we emphasize that the slow progression of PDT is mainly due to the lack of clinically approved molecules, so the need to design new compounds that potentially exhibit properties inherent to those of an ideal PS is highly pertinent. As such, the concerns of current research in the preparation of new PSs are related to photophysical properties such as singlet oxygen production and absorption capacity at red and NIR wavelengths, modulation of lipophilicity inherent to most of the nuclei of these classes of compounds, as well as their direction to the precise location to be treated. To this end, approaches of high scientific interest have been created, with desirable results and elucidating how prominent the progress in oncology and medicine can be, especially when chemistry and nanotechnology subjects are merged.

Thus, given the colossal range of results that reinforce the proficiency of this therapeutic approach, there is a need to make “leads” the most relevant and best-founded based on encouraging results to be applied clinically soon. Furthermore, the development of new PS classes as well as the analysis of the therapeutic effects of the hitherto less explored ones, the creation of new delivery systems, and new targeting methods are equally desired since a more extensive and comprehensive spectrum of treatment methodologies will allow for a more successful fight against this very heterogeneous disease.

Author Contributions: Writing—original draft preparation, E.L.; writing—review and editing, L.V.R. All authors have read and agreed to the published version of the manuscript.

Funding: The authors are thankful to the Portuguese Foundation for Science and Technology and the European Regional Development Fund for financial support to the research centres the Chemistry Centre of Vila Real (UID/QUI/UI0616/2019) and the Health Sciences Research Centre (UIDB/00709/2020 and Project POCI-01-0145-FEDER-007491). E.L. is grateful to Portuguese Foundation for Science and Technology for his Ph.D. grant SFRH/BD/147645/2019. Figures 1–5 and 7–11 were created with Biorender.

Conflicts of Interest: The authors declare no conflict of interest.

References

- Correia, J.H.; Rodrigues, J.A.; Pimenta, S.; Dong, T.; Yang, Z. Photodynamic Therapy Review: Principles, Photosensitizers, Applications, and Future Directions. *Pharmaceutics* **2021**, *13*, 1332. [CrossRef] [PubMed]
- Allison, R.R. Photodynamic therapy: Oncologic horizons. *Futur. Oncol.* **2014**, *10*, 123–124. [CrossRef] [PubMed]
- Agostinis, P.; Berg, K.; Cengel, K.A.; Foster, T.H.; Girotti, A.W.; Gollnick, S.O.; Hahn, S.M.; Hamblin, M.R.; Juzeniene, A.; Kessel, D.; et al. Photodynamic therapy of cancer: An update. *CA Cancer J. Clin.* **2011**, *61*, 250–281. [CrossRef] [PubMed]
- Jia, Q.; Song, Q.; Li, P.; Huang, W. Rejuvenated Photodynamic Therapy for Bacterial Infections. *Adv. Healthc. Mater.* **2019**, *8*, e1900608. [CrossRef]
- Wu, X.; Hu, Y. Photodynamic Therapy for the Treatment of Fungal Infections. *Infect. Drug Resist.* **2022**, *15*, 3251–3266. [CrossRef]
- Mfouo-Tynga, I.S.; Mouinga-Ondeme, A.G. Photodynamic Therapy: A Prospective Therapeutic Approach for Viral Infections and Induced Neoplasia. *Pharmaceutics* **2022**, *15*, 1273. [CrossRef]
- Conrado, P.C.; Sakita, K.M.; Arita, G.S.; Galinari, C.B.; Gonçalves, R.S.; Lopes, L.D.; Lonardoni, M.V.; Teixeira, J.J.; Bonfim-Mendonça, P.S.; Kioshima, E.S. A systematic review of photodynamic therapy as an antiviral treatment: Potential guidance for dealing with SARS-CoV-2. *Photodiagnosis Photodyn. Ther.* **2021**, *34*, 102221. [CrossRef]
- Wan, M.T.; Lin, J. Current evidence and applications of photodynamic therapy in dermatology. *Clin. Cosmet. Investig. Dermatol.* **2014**, *7*, 145–163. [CrossRef]
- Gensbittel, V.; Kräter, M.; Harlepp, S.; Busnelli, I.; Guck, J.; Goetz, J.G. Mechanical Adaptability of Tumor Cells in Metastasis. *Dev. Cell* **2021**, *56*, 164–179. [CrossRef]
- Laconi, E.; Marongiu, F.; DeGregori, J. Cancer as a disease of old age: Changing mutational and microenvironmental landscapes. *Br. J. Cancer* **2020**, *122*, 943–952. [CrossRef]
- Anisimov, V.N. The relationship between aging and carcinogenesis: A critical appraisal. *Crit. Rev. Oncol.* **2003**, *45*, 277–304. [CrossRef] [PubMed]
- Gebauer, J.; Higham, C.; Langer, T.; Denzer, C.; Brabant, G. Long-Term Endocrine and Metabolic Consequences of Cancer Treatment: A Systematic Review. *Endocr. Rev.* **2019**, *40*, 711–767. [CrossRef]
- Hodgson, D.C. Long-term toxicity of chemotherapy and radiotherapy in lymphoma survivors: Optimizing treatment for individual patients. *Clin. Adv. Hematol. Oncol.* **2015**, *13*, 103–112. [PubMed]
- Gu, B.; Wang, B.; Li, X.; Feng, Z.; Ma, C.; Gao, L.; Yu, Y.; Zhang, J.; Zheng, P.; Wang, Y.; et al. Photodynamic therapy improves the clinical efficacy of advanced colorectal cancer and recruits immune cells into the tumor immune microenvironment. *Front. Immunol.* **2022**, *13*, 1050421. [CrossRef] [PubMed]
- Alsaab, H.O.; Alghamdi, M.S.; Alotaibi, A.S.; Alzhrani, R.; Alwuthaynani, F.; Althobaiti, Y.S.; Almalki, A.H.; Sau, S.; Iyer, A.K. Progress in Clinical Trials of Photodynamic Therapy for Solid Tumors and the Role of Nanomedicine. *Cancers* **2020**, *12*, 2793. [CrossRef]
- Abdel-Kader, M.H. (Ed.) History of Photodynamic Therapy. In *Photodynamic Therapy*; Springer: Berlin/Heidelberg, Germany, 2014; pp. 3–22. ISBN 978-3-642-39628-1.
- Abdel-kader, M.H. CHAPTER 1. The Journey of PDT Throughout History: PDT from Pharos to Present. In *Comprehensive Series in Photochemical & Photobiological Sciences*; Kostron, H., Hasan, T., Eds.; Royal Society of Chemistry: Cambridge, UK, 2016; pp. 1–21; ISBN 978-1-78262-451-6.
- Daniell, M.D.; Hill, J.S. A History of Photodynamic Therapy. *ANZ J. Surg.* **1991**, *61*, 340–348. [CrossRef]
- Hashimoto, A.; Takamura-Enya, T.; Oda, Y. Synthesis and In Vitro Biological Evaluation of Psoralen-Linked Fullerenes. *Photochem. Photobiol.* **2019**, *95*, 1403–1411. [CrossRef]
- Hübinger, L.; Runge, R.; Rosenberg, T.; Freudenberg, R.; Kotzerke, J.; Brogsitter, C. Psoralen as a Photosensitizers for Photodynamic Therapy by Means of In Vitro Cherenkov Light. *Int. J. Mol. Sci.* **2022**, *23*, 15233. [CrossRef]
- Grzybowski, A.; Sak, J.; Pawlikowski, J. A brief report on the history of phototherapy. *Clin. Dermatol.* **2016**, *34*, 532–537. [CrossRef]
- Spikes, J.D. The origin and meaning of the term “photodynamic” (as used in “photodynamic therapy”, for example). *J. Photochem. Photobiol. B Biol.* **1991**, *9*, 369–371. [CrossRef]

23. Moan, J.; Peng, Q. An Outline of the History of PDT. In *Photodynamic Therapy*; Patrice, T., Ed.; The Royal Society of Chemistry: London, UK, 2003; pp. 1–18. ISBN 978-0-85404-306-4.
24. Szeimies, R.-M.; Dräger, J.; Abels, C.; Landthaler, M. Chapter 1 History of Photodynamic Therapy in Dermatology. In *Comprehensive Series in Photosciences*; Elsevier: Amsterdam, The Netherlands, 2001; Volume 2, pp. 3–15; ISBN 978-0-444-50828-7.
25. Finsen, N.R. REMARKS on the RED-LIGHT TREATMENT of SMALL-POX: Is the Treatment of Small-pox Patients in Broad Daylight Warrantable? *BMJ* **1903**, *1*, 1297–1298. [CrossRef] [PubMed]
26. Hamblin, M.R. Photodynamic Therapy for Cancer: What's Past is Prologue. *Photochem. Photobiol.* **2020**, *96*, 506–516. [CrossRef] [PubMed]
27. Dougherty, T.J.; Gomer, C.J.; Henderson, B.W.; Jori, G.; Kessel, D.; Korbely, M.; Moan, J.; Peng, Q. Photodynamic Therapy. *Gynecol. Oncol.* **1998**, *90*, 889–905. [CrossRef] [PubMed]
28. Karges, J. Clinical Development of Metal Complexes as Photosensitizers for Photodynamic Therapy of Cancer. *Angew. Chem. Int. Ed.* **2022**, *61*, e202112236. [CrossRef] [PubMed]
29. Wöhrle, D.; Hirth, A.; Bogdahn-Rai, T.; Schnurpfeil, G.; Shopova, M. Photodynamic therapy of cancer: Second and third generations of photosensitizers. *Russ. Chem. Bull.* **1998**, *47*, 807–816. [CrossRef]
30. Mfouo-Tynga, I.S.; Dias, L.D.; Inada, N.M.; Kurachi, C. Features of third generation photosensitizers used in anticancer photodynamic therapy: Review. *Photodiagnosis Photodyn. Ther.* **2021**, *34*, 102091. [CrossRef]
31. Celli, J.P.; Spring, B.Q.; Rizvi, I.; Evans, C.L.; Samkoe, K.S.; Verma, S.; Pogue, B.W.; Hasan, T. Imaging and Photodynamic Therapy: Mechanisms, Monitoring, and Optimization. *Chem. Rev.* **2010**, *110*, 2795–2838. [CrossRef]
32. Li, X.; Lee, S.; Yoon, J. Supramolecular photosensitizers rejuvenate photodynamic therapy. *Chem. Soc. Rev.* **2018**, *47*, 1174–1188. [CrossRef]
33. Ming, L.; Cheng, K.; Chen, Y.; Yang, R.; Chen, D. Enhancement of tumor lethality of ROS in photodynamic therapy. *Cancer Med.* **2021**, *10*, 257–268. [CrossRef]
34. Patel, R.; Rinker, L.; Peng, J.; Chilian, W.M. Reactive Oxygen Species: The Good and the Bad. In *Reactive Oxygen Species (ROS) in Living Cells*; Filip, C., Albu, E., Eds.; InTech: London, UK, 2018; ISBN 978-1-78923-134-2.
35. Milkovic, L.; Cipak Gasparovic, A.; Cindric, M.; MOUTHUY, P.-A.; Zarkovic, N. Short Overview of ROS as Cell Function Regulators and Their Implications in Therapy Concepts. *Cells* **2019**, *8*, 793. [CrossRef]
36. Juarranz, Á.; Jaén, P.; Sanz-Rodríguez, F.; Cuevas, J.; González, S. Photodynamic therapy of cancer. Basic principles and applications. *Clin. Transl. Oncol.* **2008**, *10*, 148–154. [CrossRef] [PubMed]
37. Baptista, M.S.; Cadet, J.; Greer, A.; Thomas, A.H. Practical Aspects in the Study of Biological Photosensitization Including Reaction Mechanisms and Product Analyses: A Do's and Don'ts Guide. *Photochem. Photobiol.* **2023**, *99*, 313–334. [CrossRef] [PubMed]
38. Plaetzer, K.; Krammer, B.; Berlanda, J.; Berr, F.; Kiesslich, T. Photophysics and photochemistry of photodynamic therapy: Fundamental aspects. *Lasers Med. Sci.* **2009**, *24*, 259–268. [CrossRef] [PubMed]
39. Yoo, J.O.; Ha, K.S. New insights into the mechanisms for photodynamic therapy-induced cancer cell death. *Int. Rev. Cell. Mol. Biol.* **2012**, *295*, 139–174.
40. Maharjan, P.S.; Bhattarai, H.K. Singlet Oxygen, Photodynamic Therapy, and Mechanisms of Cancer Cell Death. *J. Oncol.* **2022**, *2022*, 7211485. [CrossRef] [PubMed]
41. Huang, L.; Xuan, Y.; Koide, Y.; Zhiyentayev, T.; Tanaka, M.; Hamblin, M.R. Type I and Type II mechanisms of antimicrobial photodynamic therapy: An in vitro study on gram-negative and gram-positive bacteria. *Lasers Surg. Med.* **2012**, *44*, 490–499. [CrossRef]
42. Dong, C.; Yi, Q.; Fang, W.; Zhang, J. A mini review of nanomaterials on photodynamic therapy. *J. Photochem. Photobiol. C Photochem. Rev.* **2023**, *54*, 100568. [CrossRef]
43. Yao, Q.; Fan, J.; Long, S.; Zhao, X.; Li, H.; Du, J.; Shao, K.; Peng, X. The concept and examples of type-III photosensitizers for cancer photodynamic therapy. *Chem* **2022**, *8*, 197–209. [CrossRef]
44. Nguyen, K.; Khachemoune, A. An update on topical photodynamic therapy for clinical dermatologists. *J. Dermatol. Treat.* **2019**, *30*, 732–744. [CrossRef]
45. Mallidi, S.; Anbil, S.; Bulin, A.-L.; Obaid, G.; Ichikawa, M.; Hasan, T. Beyond the Barriers of Light Penetration: Strategies, Perspectives and Possibilities for Photodynamic Therapy. *Theranostics* **2016**, *6*, 2458–2487. [CrossRef]
46. Lucena, S.R.; Salazar, N.; Gracia-Cazaña, T.; Zamarrón, A.; González, S.; Juarranz, Á.; Gilaberte, Y. Combined Treatments with Photodynamic Therapy for Non-Melanoma Skin Cancer. *Int. J. Mol. Sci.* **2015**, *16*, 25912–25933. [CrossRef] [PubMed]
47. Lin, Z.; Zhou, L.; Huang, C.; Li, Z.; Lu, T.; Cong, Q.; Liang, J.; Zhong, X.; Lu, L.; Jin, C. Twenty-year outcome in neovascular age-related macular degeneration treated with photodynamic therapy and intravitreal bevacizumab/ranibizumab injections: A case report. *Photodiagnosis Photodyn. Ther.* **2023**, *42*, 103349. [CrossRef] [PubMed]
48. Di Nicola, M.; Williams, B.K. Current Indications for Photodynamic Therapy in Retina and Ocular Oncology. *Curr. Ophthalmol. Rep.* **2021**, *9*, 107–116. [CrossRef]
49. Kubrak, T.; Karakula, M.; Czop, M.; Kawczyk-Krupka, A.; Aebisher, D. Advances in Management of Bladder Cancer—The Role of Photodynamic Therapy. *Molecules* **2022**, *27*, 731. [CrossRef] [PubMed]

50. Bozzini, G.; Colin, P.; Betrouni, N.; Nevoux, P.; Ouzzane, A.; Puech, P.; Villers, A.; Mordon, S. Photodynamic therapy in urology: What can we do now and where are we heading? *Photodiagnosis Photodyn. Ther.* **2012**, *9*, 261–273. [CrossRef]
51. Ibarra, A.M.C.; Cecatto, R.B.; Motta, L.J.; Franco, A.L.D.S.; Silva, D.D.F.T.D.; Nunes, F.D.; Hamblin, M.R.; Rodrigues, M.F.S.D. Photodynamic therapy for squamous cell carcinoma of the head and neck: Narrative review focusing on photosensitizers. *Lasers Med. Sci.* **2021**, *37*, 1441–1470. [CrossRef]
52. Zhan, Q.; Wu, C.; Ding, H.; Huang, Y.; Jiang, Z.; Liao, N.; Wang, K.; Li, Y. Emerging trends in photodynamic therapy for head and neck cancer: A 10-year bibliometric analysis based on CiteSpace. *Photodiagnosis Photodyn. Ther.* **2022**, *38*, 102860. [CrossRef]
53. Maździarz, A. Successful pregnancy and delivery following selective use of photodynamic therapy in treatment of cervix and vulvar diseases. *Photodiagnosis Photodyn. Ther.* **2019**, *28*, 65–68. [CrossRef]
54. Matoba, Y.; Banno, K.; Kisu, I.; Aoki, D. Clinical application of photodynamic diagnosis and photodynamic therapy for gynecologic malignant diseases: A review. *Photodiagnosis Photodyn. Ther.* **2018**, *24*, 52–57. [CrossRef]
55. Filonenko, E.V.; Trushina, O.I.; Novikova, E.G.; Zarochentseva, N.V.; Rovinskaya, O.V.; Ivanova-Radkevich, V.I.; Kaprin, A.D. Photodynamic therapy in the treatment of intraepithelial neoplasia of the cervix, vulva and vagina. *Biomed. Photonics* **2021**, *9*, 31–39. [CrossRef]
56. Yano, T.; Minamide, T.; Takashima, K.; Nakajo, K.; Kadota, T.; Yoda, Y. Clinical Practice of Photodynamic Therapy Using Talaporfin Sodium for Esophageal Cancer. *J. Clin. Med.* **2021**, *10*, 2785. [CrossRef] [PubMed]
57. Yano, T.; Wang, K.K. Photodynamic Therapy for Gastrointestinal Cancer. *Photochem. Photobiol.* **2020**, *96*, 517–523. [CrossRef] [PubMed]
58. Casas, A. Clinical uses of 5-aminolaevulinic acid in photodynamic treatment and photodetection of cancer: A review. *Cancer Lett.* **2020**, *490*, 165–173. [CrossRef]
59. Corrie, P.G. Cytotoxic chemotherapy: Clinical aspects. *Medicine* **2008**, *36*, 24–28. [CrossRef]
60. Oun, R.; Moussa, Y.E.; Wheate, N.J. The side effects of platinum-based chemotherapy drugs: A review for chemists. *Dalton Trans.* **2018**, *47*, 6645–6653. [CrossRef]
61. Bhatia, K.; Bhumika; Das, A. Combinatorial drug therapy in cancer—New insights. *Life Sci.* **2020**, *258*, 118134. [CrossRef] [PubMed]
62. de Crevoisier, R.; Lafond, C.; Mervoyer, A.; Hulot, C.; Jaksic, N.; Bessières, I.; Delpon, G. Image-guided radiotherapy. *Cancer/Radiothérapie* **2022**, *26*, 34–49. [CrossRef]
63. Busk, M.; Overgaard, J.; Horsman, M.R. Imaging of Tumor Hypoxia for Radiotherapy: Current Status and Future Directions. *Semin. Nucl. Med.* **2020**, *50*, 562–583. [CrossRef]
64. Garbutcheon-Singh, K.B.; Veness, M.J. The role of radiotherapy in the management of non-melanoma skin cancer. *Australas. J. Dermatol.* **2019**, *60*, 265–272. [CrossRef]
65. Hopper, C. Photodynamic therapy: A clinical reality in the treatment of cancer. *Lancet Oncol.* **2000**, *1*, 212–219. [CrossRef]
66. Wilson, B.C. Photodynamic Therapy for Cancer: Principles. *Can. J. Gastroenterol.* **2002**, *16*, 393–396. [CrossRef] [PubMed]
67. Gunaydin, G.; Gedik, M.E.; Ayan, S. Photodynamic Therapy for the Treatment and Diagnosis of Cancer—A Review of the Current Clinical Status. *Front. Chem.* **2021**, *9*, 686303. [CrossRef] [PubMed]
68. Kwon, N.; Kim, H.; Li, X.; Yoon, J. Supramolecular agents for combination of photodynamic therapy and other treatments. *Chem. Sci.* **2021**, *12*, 7248–7268. [CrossRef]
69. Borgia, F.; Giuffrida, R.; Caradonna, E.; Vaccaro, M.; Guarneri, F.; Cannavò, S.P. Early and Late Onset Side Effects of Photodynamic Therapy. *Biomedicines* **2018**, *6*, 12. [CrossRef] [PubMed]
70. Mohammad, T.; Kahaleh, M. Comparing palliative treatment options for cholangiocarcinoma: Photodynamic therapy vs. radiofrequency ablation. *Clin. Endosc.* **2022**, *55*, 347–354. [CrossRef] [PubMed]
71. Simone, C.B.; Friedberg, J.S.; Glatstein, E.; Stevenson, J.P.; Serman, D.H.; Hahn, S.M.; Cengel, K.A. Photodynamic therapy for the treatment of non-small cell lung cancer. *J. Thorac. Dis.* **2012**, *4*, 63–75. [CrossRef]
72. Overholt, B.F.; Panjehpour, M.; Haydek, J.M. Photodynamic therapy for Barrett’s esophagus: Follow-up in 100 patients. *Gastrointest. Endosc.* **1999**, *49*, 1–7. [CrossRef]
73. Singh, H.; Benn, B.S.; Jani, C.; Abdalla, M.; Kurman, J.S. Photodynamic therapy for treatment of recurrent adenocarcinoma of the lung with tracheal oligometastasis. *Respir. Med. Case Rep.* **2022**, *37*, 101620. [CrossRef]
74. Succo, G.; Rosso, S.; Fadda, G.; Fantini, M.; Crosetti, E. Salvage photodynamic therapy for recurrent nasopharyngeal carcinoma. *Photodiagnosis Photodyn. Ther.* **2014**, *11*, 63–70. [CrossRef]
75. Queirós, C.; Garrido, P.M.; Silva, J.M.; Filipe, P. Photodynamic therapy in dermatology: Beyond current indications. *Dermatol. Ther.* **2020**, *33*, e13997. [CrossRef]
76. Bown, S.G. Photodynamic therapy for photochemists. *Philos. Trans. R. Soc. A Math. Phys. Eng. Sci.* **2013**, *371*, 20120371. [CrossRef]
77. Kou, J.; Dou, D.; Yang, L. Porphyrin photosensitizers in photodynamic therapy and its applications. *Oncotarget* **2017**, *8*, 81591–81603. [CrossRef]
78. Algorri, J.F.; Ochoa, M.; Roldán-Varona, P.; Rodríguez-Cobo, L.; López-Higuera, J.M. Light Technology for Efficient and Effective Photodynamic Therapy: A Critical Review. *Cancers* **2021**, *13*, 3484. [CrossRef] [PubMed]

79. Stolik, S.; Delgado, J.; Pérez, A.; Anasagasti, L. Measurement of the penetration depths of red and near infrared light in human “ex vivo” tissues. *J. Photochem. Photobiol. B Biol.* **2000**, *57*, 90–93. [CrossRef] [PubMed]
80. Zhao, J.; Duan, L.; Wang, A.; Fei, J.; Li, J. Insight into the efficiency of oxygen introduced photodynamic therapy (PDT) and deep PDT against cancers with various assembled nanocarriers. *WIREs Nanomed. Nanobiotechnol.* **2020**, *12*, e1583. [CrossRef] [PubMed]
81. Ris, H.-B.; Altermatt, H.J.; Nachbur, B.; Stewart, J.C.M.; Wang, Q.; Lim, C.K.; Bonnett, R.; Althaus, U. Effect of drug-light interval on photodynamic therapy with meta-tetrahydroxyphenylchlorin in malignant mesothelioma. *Int. J. Cancer* **1993**, *53*, 141–146. [CrossRef]
82. Trehan, M.; Taylor, C.R. Chapter 21 Cutaneous Photosensitivity and Photoprotection for Photodynamic Therapy Patients. In *Comprehensive Series in Photosciences*; Elsevier: Amsterdam, The Netherlands, 2001; Volume 2, pp. 321–337; ISBN 978-0-444-50828-7.
83. Pogue, B.W.; Elliott, J.T.; Kanick, S.C.; Davis, S.C.; Samkoe, K.S.; Maytin, E.V.; Pereira, S.P.; Hasan, T. Revisiting photodynamic therapy dosimetry: Reductionist & surrogate approaches to facilitate clinical success. *Phys. Med. Biol.* **2016**, *61*, R57–R89. [CrossRef]
84. Kim, M.M.; Darafsheh, A. Light Sources and Dosimetry Techniques for Photodynamic Therapy. *Photochem. Photobiol.* **2020**, *96*, 280–294. [CrossRef]
85. Nichols, M.G.; Foster, T.H. Oxygen diffusion and reaction kinetics in the photodynamic therapy of multicell tumour spheroids. *Phys. Med. Biol.* **1994**, *39*, 2161–2181. [CrossRef]
86. Seshadri, M.; Bellnier, D.; Vaughan, L.A.; Sperryak, J.A.; Mazurchuk, R.; Foster, T.; Henderson, B.W. Light Delivery over Extended Time Periods Enhances the Effectiveness of Photodynamic Therapy. *Clin. Cancer Res.* **2008**, *14*, 2796–2805. [CrossRef]
87. Rodrigues, J.A.; Amorim, R.; Silva, M.; Baltazar, F.; Wolffenbuttel, R.; Correia, J.H. Photodynamic Therapy at Low-Light Fluence Rate: In vitro Assays on Colon Cancer Cells. *IEEE J. Sel. Top. Quantum Electron.* **2019**, *25*, 1–6. [CrossRef]
88. Cheng, Y.; Chang, Y.; Feng, Y.; Liu, N.; Sun, X.; Feng, Y.; Li, X.; Zhang, H. Simulated Sunlight-Mediated Photodynamic Therapy for Melanoma Skin Cancer by Titanium-Dioxide-Nanoparticle-Gold-Nanocluster-Graphene Heterogeneous Nanocomposites. *Small* **2017**, *13*, 1603935. [CrossRef] [PubMed]
89. Lee, C.-N.; Hsu, R.; Chen, S.; Wong, T.-W. Daylight Photodynamic Therapy: An Update. *Molecules* **2020**, *25*, 5195. [CrossRef] [PubMed]
90. Erkiert-Polguj, A.; Halbina, A.; Polak-Pacholczyk, I.; Rotsztein, H. Light-emitting diodes in photodynamic therapy in non-melanoma skin cancers—own observations and literature review. *J. Cosmet. Laser Ther.* **2016**, *18*, 105–110. [CrossRef]
91. Neupane, J.; Ghimire, S.; Shakya, S.; Chaudhary, L.; Shrivastava, V.P. Effect of light emitting diodes in the photodynamic therapy of rheumatoid arthritis. *Photodiagnosis Photodyn. Ther.* **2010**, *7*, 44–49. [CrossRef]
92. Mang, T.S. Lasers and light sources for PDT: Past, present and future. *Photodiagnosis Photodyn. Ther.* **2004**, *1*, 43–48. [CrossRef] [PubMed]
93. Yu, C.-H.; Lin, H.-P.; Chen, H.-M.; Yang, H.; Wang, Y.-P.; Chiang, C.-P. Comparison of clinical outcomes of oral erythroleukoplakia treated with photodynamic therapy using either light-emitting diode or laser light. *Lasers Surg. Med.* **2009**, *41*, 628–633. [CrossRef] [PubMed]
94. Gao, J.; Chen, Z.; Li, X.; Yang, M.; Lv, J.; Li, H.; Yuan, Z. Chemiluminescence in Combination with Organic Photosensitizers: Beyond the Light Penetration Depth Limit of Photodynamic Therapy. *Int. J. Mol. Sci.* **2022**, *23*, 12556. [CrossRef]
95. Bessière, A.; Durand, J.-O.; Noûs, C. Persistent luminescence materials for deep photodynamic therapy. *Nanophotonics* **2021**, *10*, 2999–3029. [CrossRef]
96. Tzani, M.A.; Giftofidou, D.K.; Kallitsakis, M.G.; Pliatsios, N.V.; Kalogiouri, N.P.; Angaridis, P.A.; Lykakis, I.N.; Terzidis, M.A. Direct and Indirect Chemiluminescence: Reactions, Mechanisms and Challenges. *Molecules* **2021**, *26*, 7664. [CrossRef]
97. Periyasami, G.; Martelo, L.; Baleizão, C.; Berberan-Santos, M.N. Strong green chemiluminescence from naphthalene analogues of luminol. *New J. Chem.* **2014**, *38*, 2258–2261. [CrossRef]
98. Chen, T.-C.; Huang, L.; Liu, C.-C.; Chao, P.-J.; Lin, F.-H. Luminol as the light source for in situ photodynamic therapy. *Process. Biochem.* **2012**, *47*, 1903–1908. [CrossRef]
99. Degirmenci, A.; Sonkaya, Ö.; Soylukan, C.; Karaduman, T.; Algi, F. BODIPY and 2,3-Dihydrophthalazine-1,4-Dione Conjugates as Heavy Atom-Free Chemiluminogenic Photosensitizers. *ACS Appl. Bio Mater.* **2021**, *4*, 5090–5098. [CrossRef] [PubMed]
100. Rodrigues, J.A.; Correia, J.H. Enhanced Photodynamic Therapy: A Review of Combined Energy Sources. *Cells* **2022**, *11*, 3995. [CrossRef]
101. Foglietta, F.; Macri, M.; Panzanelli, P.; Francovich, A.; Durando, G.; Garello, F.; Terreno, E.; Serpe, L.; Canaparo, R. Ultrasound boosts doxorubicin efficacy against sensitive and resistant ovarian cancer cells. *Eur. J. Pharm. Biopharm.* **2023**, *183*, 119–131. [CrossRef]
102. Nkune, N.W.; Abrahamse, H. Anti-Hypoxia Nanoplatforms for Enhanced Photosensitizer Uptake and Photodynamic Therapy Effects in Cancer Cells. *Int. J. Mol. Sci.* **2023**, *24*, 2656. [CrossRef]
103. Li, X.; Chen, L.; Huang, M.; Zeng, S.; Zheng, J.; Peng, S.; Wang, Y.; Cheng, H.; Li, S. Innovative strategies for photodynamic therapy against hypoxic tumor. *Asian J. Pharm. Sci.* **2023**, *18*, 100775. [CrossRef]
104. Siemann, D.W.; Horsman, M.R. Modulation of the tumor vasculature and oxygenation to improve therapy. *Pharmacol. Ther.* **2015**, *153*, 107–124. [CrossRef]

105. Anand, S.; Ortel, B.J.; Pereira, S.P.; Hasan, T.; Maytin, E.V. Biomodulatory approaches to photodynamic therapy for solid tumors. *Cancer Lett.* **2012**, *326*, 8–16. [CrossRef]
106. Woodhams, J.H.; MacRobert, A.J.; Bown, S.G. The role of oxygen monitoring during photodynamic therapy and its potential for treatment dosimetry. *Photochem. Photobiol. Sci.* **2007**, *6*, 1246–1256. [CrossRef]
107. Zang, L.; Zhao, H. A strategy for monitoring oxygen concentration, oxygen consumption, and generation of singlet oxygen using a phosphorescent photosensitizer. *J. Lumin.* **2020**, *224*, 117282. [CrossRef]
108. Hong, L.; Li, J.; Luo, Y.; Guo, T.; Zhang, C.; Ou, S.; Long, Y.; Hu, Z. Recent Advances in Strategies for Addressing Hypoxia in Tumor Photodynamic Therapy. *Biomolecules* **2022**, *12*, 81. [CrossRef] [PubMed]
109. Sun, Y.; Zhao, D.; Wang, G.; Wang, Y.; Cao, L.; Sun, J.; Jiang, Q.; He, Z. Recent progress of hypoxia-modulated multifunctional nanomedicines to enhance photodynamic therapy: Opportunities, challenges, and future development. *Acta Pharm. Sin. B* **2020**, *10*, 1382–1396. [CrossRef] [PubMed]
110. Wei, F.; Rees, T.W.; Liao, X.; Ji, L.; Chao, H. Oxygen self-sufficient photodynamic therapy. *Co-Ord. Chem. Rev.* **2021**, *432*, 213714. [CrossRef]
111. Maier, A.; Anegg, U.; Fell, B.; Rehak, P.; Ratzenhofer, B.; Tomaselli, F.; Sankin, O.; Pinter, H.; Smolle-Jüttner, F.M.; Friehs, G.B. Hyperbaric Oxygen and Photodynamic Therapy in the Treatment of Advanced Carcinoma of the Cardia and the Esophagus. *Lasers Surg. Med.* **2000**, *26*, 308–315. [CrossRef]
112. Aziz, B.; Aziz, I.; Khurshid, A.; Raoufi, E.; Esfahani, F.N.; Jalilian, Z.; Mozafari, M.R.; Taghavi, E.; Ikram, M. An Overview of Potential Natural Photosensitizers in Cancer Photodynamic Therapy. *Biomedicines* **2023**, *11*, 224. [CrossRef]
113. Abrahamse, H.; Hamblin, M.R. New photosensitizers for photodynamic therapy. *Biochem. J.* **2016**, *473*, 347–364. [CrossRef]
114. Khurana, B.; Ouk, T.-S.; Lucas, R.; Senge, M.O.; Sol, V. Photosensitizer-hyaluronic acid complexes for antimicrobial photodynamic therapy (aPDT). *J. Porphyr. Phthalocyanines* **2022**, *26*, 585–593. [CrossRef]
115. O'Connor, A.E.; Gallagher, W.M.; Byrne, A.T. Porphyrin and Nonporphyrin Photosensitizers in Oncology: Preclinical and Clinical Advances in Photodynamic Therapy. *Photochem. Photobiol.* **2009**, *85*, 1053–1074. [CrossRef]
116. Siewert, B. Does the chemistry of fungal pigments demand the existence of photoactivated defense strategies in basidiomycetes? *Photochem. Photobiol. Sci.* **2021**, *20*, 475–488. [CrossRef]
117. Gill, M.; Giménez, A. Austrovenetin, the principal pigment of the toadstool *Dermocybe austroveneta*. *Phytochemistry* **1991**, *30*, 951–955. [CrossRef]
118. Dong, X.; Zeng, Y.; Zhang, Z.; Fu, J.; You, L.; He, Y.; Hao, Y.; Gu, Z.; Yu, Z.; Qu, C.; et al. Hypericin-mediated photodynamic therapy for the treatment of cancer: A review. *J. Pharm. Pharmacol.* **2021**, *73*, 425–436. [CrossRef] [PubMed]
119. Kubrak, T.P.; Kołodziej, P.; Sawicki, J.; Mazur, A.; Kozirowska, K.; Aebischer, D. Some Natural Photosensitizers and Their Medicinal Properties for Use in Photodynamic Therapy. *Molecules* **2022**, *27*, 1192. [CrossRef]
120. Sulaiman, C.; George, B.P.; Balachandran, I.; Abrahamse, H. Photoactive Herbal Compounds: A Green Approach to Photodynamic Therapy. *Molecules* **2022**, *27*, 5084. [CrossRef]
121. Cieckiewicz, E.; Angenot, L.; Mathieu, V.; Pirotte, B.; de Tullio, P.; Frédérich, M. Hemisynthesis of glycosylated derivatives of pheophorbide a. *Planta Med.* **2014**, *80*, P2O2. [CrossRef]
122. Martins, L.M.O.S.; Wang, X.; Silva, G.T.M.; Junqueira, H.C.; Fornaciari, B.; Lopes, L.F.; Silva, C.P.; Zhou, P.; Cavalcante, V.F.; Baptista, M.S.; et al. Red Wine Inspired Chromophores as Photodynamic Therapy Sensitizers. *Photochem. Photobiol.* **2022**, *99*, 732–741. [CrossRef]
123. Ethirajan, M.; Chen, Y.; Joshi, P.; Pandey, R.K. The role of porphyrin chemistry in tumor imaging and photodynamic therapy. *Chem. Soc. Rev.* **2011**, *40*, 340–362. [CrossRef] [PubMed]
124. Ma, C.-H.; Yang, J.; Mueller, J.L.; Huang, H.-C. Intratumoral Photosensitizer Delivery and Photodynamic Therapy. *Nano LIFE* **2021**, *11*, 2130003. [CrossRef] [PubMed]
125. Ivanova-Radkevich, V.I. Biochemical Basis of Selective Accumulation and Targeted Delivery of Photosensitizers to Tumor Tissues. *Biochemistry* **2022**, *87*, 1226–1242. [CrossRef]
126. Castano, A.P.; Demidova, T.N.; Hamblin, M.R. Mechanisms in photodynamic therapy: Part one—Photosensitizers, photochemistry and cellular localization. *Photodiagn. Photodyn. Ther.* **2004**, *1*, 279–293. [CrossRef]
127. Bonnett, R.; Martínez, G. Photobleaching of sensitizers used in photodynamic therapy. *Tetrahedron* **2001**, *57*, 9513–9547. [CrossRef]
128. Zhao, X.; Yang, Y.; Yu, Y.; Guo, S.; Wang, W.; Zhu, S. A cyanine-derivative photosensitizer with enhanced photostability for mitochondria-targeted photodynamic therapy. *Chem. Commun.* **2019**, *55*, 13542–13545. [CrossRef] [PubMed]
129. Li, B.; Lin, L.; Lin, H.; Wilson, B.C. Photosensitized singlet oxygen generation and detection: Recent advances and future perspectives in cancer photodynamic therapy. *J. Biophotonics* **2016**, *9*, 1314–1325. [CrossRef]
130. Bryden, F.; Boyle, R.W. Metalloporphyrins for Medical Imaging Applications. In *Advances in Inorganic Chemistry*; Elsevier: Amsterdam, The Netherlands, 2016; Volume 68, pp. 141–221. ISBN 978-0-12-803526-9.
131. Tahoun, M.; Gee, C.T.; McCoy, V.E.; Sander, P.M.; Müller, C.E. Chemistry of porphyrins in fossil plants and animals. *RSC Adv.* **2021**, *11*, 7552–7563. [CrossRef]
132. Park, J.M.; Hong, K.-I.; Lee, H.; Jang, W.-D. Bioinspired Applications of Porphyrin Derivatives. *Acc. Chem. Res.* **2021**, *54*, 2249–2260. [CrossRef] [PubMed]

133. Buglak, A.A.; Filatov, M.A.; Hussain, M.A.; Sugimoto, M. Singlet oxygen generation by porphyrins and metalloporphyrins revisited: A quantitative structure-property relationship (QSPR) study. *J. Photochem. Photobiol. A Chem.* **2020**, *403*, 112833. [CrossRef]
134. Tsolekile, N.; Nelana, S.; Oluwafemi, O.S. Porphyrin as Diagnostic and Therapeutic Agent. *Molecules* **2019**, *24*, 2669. [CrossRef]
135. Tope, W.D.; Martin, A.; Grevelink, J.M.; Starr, J.C.; Fewkes, J.L.; Flotte, T.J.; Deutsch, T.F.; Anderson, R.R. Lack of selectivity of protoporphyrin IX fluorescence for basal cell carcinoma after topical application of 5-aminolevulinic acid: Implications for photodynamic treatment. *Arch. Dermatol. Res.* **1995**, *287*, 665–674. [CrossRef]
136. Li, Y.; Zheng, X.; Zhang, X.; Liu, S.; Pei, Q.; Zheng, M.; Xie, Z. Porphyrin-Based Carbon Dots for Photodynamic Therapy of Hepatoma. *Adv. Healthc. Mater.* **2017**, *6*, 1600924. [CrossRef]
137. Montaseri, H.; Kruger, C.A.; Abrahamse, H. Recent Advances in Porphyrin-Based Inorganic Nanoparticles for Cancer Treatment. *Int. J. Mol. Sci.* **2020**, *21*, 3358. [CrossRef]
138. Hou, B.; Zhang, W.; Li, C.; Sun, X.; Feng, X.; Liu, J. Synthesis and in vitro biological evaluation of novel water-soluble porphyrin complexes for cancer photodynamic therapy. *Appl. Organomet. Chem.* **2022**, *36*, e6598. [CrossRef]
139. Wu, F.; Yang, M.; Zhang, J.; Zhu, S.; Shi, M.; Wang, K. Metalloporphyrin–indomethacin conjugates as new photosensitizers for photodynamic therapy. *JBIC J. Biol. Inorg. Chem.* **2019**, *24*, 53–60. [CrossRef] [PubMed]
140. Couto, G.K.; Rodrigues, J.C.; Pacheco, B.S.; Simões, L.D.; Paschoal, J.D.; Seixas, F.K.; Acunha, T.V.; Iglesias, B.A.; Collares, T. Zinc(II), copper(II) and nickel(II) ions improve the selectivity of tetra-cationic platinum(II) porphyrins in photodynamic therapy and stimulate antioxidant defenses in the metastatic melanoma lineage (A375). *Photodiagnosis Photodyn. Ther.* **2020**, *31*, 101942. [CrossRef]
141. Yang, M.; Deng, J.; Guo, D.; Sun, Q.; Wang, Z.; Wang, K.; Wu, F. Mitochondria-targeting Pt/Mn porphyrins as efficient photosensitizers for magnetic resonance imaging and photodynamic therapy. *Dye. Pigment.* **2019**, *166*, 189–195. [CrossRef]
142. Frant, M.P.; Trytek, M.; Paduch, R. Assessing the In Vitro Activity of Selected Porphyrins in Human Colorectal Cancer Cells. *Molecules* **2022**, *27*, 2006. [CrossRef]
143. Scoditti, S.; Chiodo, F.; Mazzone, G.; Richeter, S.; Sicilia, E. Porphyrins and Metalloporphyrins Combined with N-Heterocyclic Carbene (NHC) Gold(I) Complexes for Photodynamic Therapy Application: What Is the Weight of the Heavy Atom Effect? *Molecules* **2022**, *27*, 4046. [CrossRef]
144. Manathanath, M.; Sasidharan, S.; Saudagar, P.; Panicker, U.G.; Sujatha, S. Photodynamic evaluation of triazine appended porphyrins as anti-leishmanial and anti-tumor agents. *Polyhedron* **2022**, *217*, 115711. [CrossRef]
145. Wieduwilt, M.J.; Moasser, M.M. The epidermal growth factor receptor family: Biology driving targeted therapeutics. *Cell. Mol. Life Sci.* **2008**, *65*, 1566–1584. [CrossRef]
146. Ranson, M. Epidermal growth factor receptor tyrosine kinase inhibitors. *Br. J. Cancer* **2004**, *90*, 2250–2255. [CrossRef]
147. Huang, K.; Xie, S.; Jiang, L.; Li, J.; Chen, J. A glutathione and hydrogen sulfide responsive photosensitizer for enhanced photodynamic therapy. *Dye. Pigment.* **2022**, *205*, 110529. [CrossRef]
148. Xie, J.; Wang, Y.; Choi, W.; Jangili, P.; Ge, Y.; Xu, Y.; Kang, J.; Liu, L.; Zhang, B.; Xie, Z.; et al. Overcoming barriers in photodynamic therapy harnessing nano-formulation strategies. *Chem. Soc. Rev.* **2021**, *50*, 9152–9201. [CrossRef]
149. Sibrian-Vazquez, M.; Jensen, T.J.; Vicente, M.G.H. Synthesis and cellular studies of PEG-functionalized meso-tetraphenylporphyrins. *J. Photochem. Photobiol. B Biol.* **2007**, *86*, 9–21. [CrossRef] [PubMed]
150. Zheng, N.; Li, X.; Huangfu, S.; Xia, K.; Yue, R.; Wu, H.; Song, W. Linear and high-molecular-weight poly-porphyrins for efficient photodynamic therapy. *Biomater. Sci.* **2021**, *9*, 4630–4638. [CrossRef] [PubMed]
151. Lazewski, D.; Kucinska, M.; Potapkiy, E.; Kuzminska, J.; Tezyk, A.; Popenda, L.; Jurga, S.; Teubert, A.; Gdaniec, Z.; Kujawski, J.; et al. Novel Short PEG Chain-Substituted Porphyrins: Synthesis, Photochemistry, and In Vitro Photodynamic Activity against Cancer Cells. *Int. J. Mol. Sci.* **2022**, *23*, 10029. [CrossRef] [PubMed]
152. Li, C.; Luo, Z.; Yang, L.; Chen, J.; Cheng, K.; Xue, Y.; Liu, G.; Luo, X.; Wu, F. Self-assembled porphyrin polymer nanoparticles with NIR-II emission and highly efficient photothermal performance in cancer therapy. *Mater. Today Bio* **2022**, *13*, 100198. [CrossRef] [PubMed]
153. Shang, D.; Yu, Q.; Liu, W.; Zhang, S.; Li, Y.; Chen, J.; Zhang, Z.; Lu, X. Enhanced porphyrin-based fluorescence imaging-guided photodynamic/photothermal synergistic cancer therapy by mitochondrial targeting. *Sci. China Mater.* **2022**, *65*, 527–535. [CrossRef]
154. Jiao, J.; He, J.; Li, M.; Yang, J.; Yang, H.; Wang, X.; Yang, S. A porphyrin-based metallacage for enhanced photodynamic therapy. *Nanoscale* **2022**, *14*, 6373–6383. [CrossRef]
155. Luo, Z.; Dai, Y.; Gao, H. Development and application of hyaluronic acid in tumor targeting drug delivery. *Acta Pharm. Sin. B* **2019**, *9*, 1099–1112. [CrossRef]
156. Song, H.; Cai, Z.; Li, J.; Xiao, H.; Qi, R.; Zheng, M. Light triggered release of a triple action porphyrin-cisplatin conjugate evokes stronger immunogenic cell death for chemotherapy, photodynamic therapy and cancer immunotherapy. *J. Nanobiotechnol.* **2022**, *20*, 329. [CrossRef]

157. Magaela, N.B.; Matshitse, R.; Babu, B.; Managa, M.; Prinsloo, E.; Nyokong, T. Sn(IV) porphyrin-biotin decorated nitrogen doped graphene quantum dots nanohybrids for photodynamic therapy. *Polyhedron* **2022**, *213*, 115624. [CrossRef]
158. Hou, M.; Chen, W.; Zhao, J.; Dai, D.; Yang, M.; Yi, C. Facile synthesis and in vivo bioimaging applications of porphyrin derivative-encapsulated polymer nanoparticles. *Chin. Chem. Lett.* **2022**, *33*, 4101–4106. [CrossRef]
159. Liang, X.; Li, X.; Jing, L.; Yue, X.; Dai, Z. Theranostic porphyrin dyad nanoparticles for magnetic resonance imaging guided photodynamic therapy. *Biomaterials* **2014**, *35*, 6379–6388. [CrossRef] [PubMed]
160. Schmitt, J.; Jenni, S.; Sour, A.; Heitz, V.; Bolze, F.; Pallier, A.; Bonnet, C.S.; Toth, E.; Ventura, B. A Porphyrin Dimer–GdDOTA Conjugate as a Theranostic Agent for One- and Two-Photon Photodynamic Therapy and MRI. *Bioconjugate Chem.* **2018**, *29*, 3726–3738. [CrossRef] [PubMed]
161. Kopranev, V.N.; Luk'yanets, E.A. Porphyrazines: Synthesis, properties, application. *Russ. Chem. Bull.* **1995**, *44*, 2216–2232. [CrossRef]
162. Rodríguez-Morgade, M.S.; Stuzhin, P.A. The chemistry of porphyrazines: An overview. *J. Porphyr. Phthalocyanines* **2004**, *8*, 1129–1165. [CrossRef]
163. Klein, T.; Ziegler, T. First example of an octa-glycoconjugated magnesium(II)porphyrazine. *Tetrahedron Lett.* **2016**, *57*, 495–497. [CrossRef]
164. Wen, S.; Zhu, D.; Huang, P. Targeting cancer cell mitochondria as a therapeutic approach. *Future Med. Chem.* **2013**, *5*, 53–67. [CrossRef]
165. Benov, L. Photodynamic Therapy: Current Status and Future Directions. *Med. Princ. Pract.* **2015**, *24*, 14–28. [CrossRef]
166. Turubanova, V.D.; Mishchenko, T.A.; Balalaeva, I.V.; Efimova, I.; Peskova, N.N.; Klapshina, L.G.; Lermontova, S.A.; Bachert, C.; Krysko, O.; Vedunova, M.V.; et al. Novel porphyrazine-based photodynamic anti-cancer therapy induces immunogenic cell death. *Sci. Rep.* **2021**, *11*, 7205. [CrossRef]
167. Peskova, N.N.; Brilkina, A.A.; Gorokhova, A.A.; Shilyagina, N.Y.; Kutova, O.M.; Nerush, A.S.; Orlova, A.G.; Klapshina, L.G.; Vodeneev, V.V.; Balalaeva, I.V. The localization of the photosensitizer determines the dynamics of the secondary production of hydrogen peroxide in cell cytoplasm and mitochondria. *J. Photochem. Photobiol. B Biol.* **2021**, *219*, 112208. [CrossRef]
168. Tasso, T.T.; Schlothauer, J.C.; Junqueira, H.C.; Matias, T.A.; Araki, K.; Liandra-Salvador, É.; Antonio, F.C.T.; Homem-De-Mello, P.; Baptista, M.S. Photobleaching Efficiency Parallels the Enhancement of Membrane Damage for Porphyrazine Photosensitizers. *J. Am. Chem. Soc.* **2019**, *141*, 15547–15556. [CrossRef] [PubMed]
169. Yuzhakova, D.V.; Lermontova, S.A.; Grigoryev, I.S.; Muravieva, M.S.; Gavrina, A.I.; Shirmanova, M.V.; Balalaeva, I.V.; Klapshina, L.G.; Zagaynova, E.V. In vivo multimodal tumor imaging and photodynamic therapy with novel theranostic agents based on the porphyrazine framework-chelated gadolinium (III) cation. *Biochim. Biophys. Acta (BBA) Gen. Subj.* **2017**, *1861*, 3120–3130. [CrossRef] [PubMed]
170. Shestakova, L.N.; Lyubova, T.S.; Lermontova, S.A.; Belotelov, A.O.; Peskova, N.N.; Klapshina, L.G.; Balalaeva, I.V.; Shilyagina, N.Y. Comparative Analysis of Tetra(2-naphthyl)tetracyano-porphyrazine and Its Iron Complex as Photosensitizers for Anticancer Photodynamic Therapy. *Pharmaceutics* **2022**, *14*, 2655. [CrossRef] [PubMed]
171. Balalaeva, I.V.; Mishchenko, T.A.; Turubanova, V.D.; Peskova, N.N.; Shilyagina, N.Y.; Plekhanov, V.I.; Lermontova, S.A.; Klapshina, L.G.; Vedunova, M.V.; Krysko, D.V. Cyanoarylporphyrazines with High Viscosity Sensitivity: A Step towards Dosimetry-Assisted Photodynamic Cancer Treatment. *Molecules* **2021**, *26*, 5816. [CrossRef]
172. Mishchenko, T.A.; Turubanova, V.D.; Mitroshina, E.V.; Alzeibak, R.; Peskova, N.N.; Lermontova, S.A.; Klapshina, L.G.; Balalaeva, I.V.; Vedunova, M.V.; Krysko, D.V. Effect of novel porphyrazine photosensitizers on normal and tumor brain cells. *J. Biophotonics* **2020**, *13*, e201960077. [CrossRef]
173. Shilyagina, N.Y.; Peskova, N.N.; Lermontova, S.A.; Brilkina, A.A.; Vodeneev, V.A.; Yakimansky, A.V.; Klapshina, L.G.; Balalaeva, I.V. Effective delivery of porphyrazine photosensitizers to cancer cells by polymer brush nanocontainers. *J. Biophotonics* **2017**, *10*, 1189–1197. [CrossRef]
174. Yudin, A.V.; Shilyagina, N.Y.; Dyakova, D.V.; Lermontova, S.A.; Klapshina, L.G.; Guryev, E.L.; Balalaeva, I.V.; Vodeneev, V.A. Liposomal Form of Tetra(Aryl)Tetracyanoporphyrazine: Physical Properties and Photodynamic Activity In Vitro. *J. Fluoresc.* **2018**, *28*, 513–522. [CrossRef]
175. Mlynarczyk, D.; Piskorz, J.; Popenda, L.; Stolarska, M.; Szczolko, W.; Konopka, K.; Jurga, S.; Sobotta, L.; Mielcarek, J.; Düzgüneş, N.; et al. S-seco-porphyrazine as a new member of the seco-porphyrazine family—Synthesis, characterization and photocytotoxicity against cancer cells. *Bioorganic Chem.* **2020**, *96*, 103634. [CrossRef]
176. Yagodin, A.V.; Mikheev, I.A.; Bunin, D.A.; Sinelshchikova, A.A.; Martynov, A.G.; Gorbunova, Y.G.; Tsivadze, A.Y. Tetraquinoxalinoporphyrazine— π -extended NIR-absorbing photosensitizer with improved photostability. *Dye. Pigment.* **2023**, *216*, 111326. [CrossRef]
177. Linares, I.A.; Martinelli, L.P.; Moritz, M.N.; Selistre-De-Araujo, H.S.; de Oliveira, K.T.; Perussi, J.R. Cytotoxicity of structurally-modified chlorins aimed for photodynamic therapy applications. *J. Photochem. Photobiol. A Chem.* **2022**, *425*, 113647. [CrossRef]
178. Pereira, N.A.; Laranjo, M.; Pina, J.; Oliveira, A.S.; Ferreira, J.D.; Sánchez-Sánchez, C.; Casalta-Lopes, J.; Gonçalves, A.C.; Sarmiento-Ribeiro, A.B.; Piñeiro, M.; et al. Advances on photodynamic therapy of melanoma through novel ring-fused 5,15-diphenylchlorins. *Eur. J. Med. Chem.* **2018**, *146*, 395–408. [CrossRef] [PubMed]

179. Dong, Y.; Li, G.; Wang, L.; Cao, L.; Li, Y.; Zhao, W. Anti-tumor evaluation of a novel methoxyphenyl substituted chlorin photosensitizer for photodynamic therapy. *J. Photochem. Photobiol. B Biol.* **2020**, *211*, 112015. [CrossRef] [PubMed]
180. Kang, E.S.; Lee, T.H.; Liu, Y.; Han, K.-H.; Lee, W.K.; Yoon, I. Graphene Oxide Nanoparticles Having Long Wavelength Absorbing Chlorins for Highly-Enhanced Photodynamic Therapy with Reduced Dark Toxicity. *Int. J. Mol. Sci.* **2019**, *20*, 4344. [CrossRef]
181. Hak, A.; Ali, M.S.; Sankaranarayanan, S.A.; Shinde, V.R.; Rengan, A.K. Chlorin e6: A Promising Photosensitizer in Photo-Based Cancer Nanomedicine. *ACS Appl. Bio Mater.* **2023**, *6*, 349–364. [CrossRef] [PubMed]
182. Qin, X.; Zhang, M.; Hu, X.; Du, Q.; Zhao, Z.; Jiang, Y.; Luan, Y. Nanoengineering of a newly designed chlorin e6 derivative for amplified photodynamic therapy via regulating lactate metabolism. *Nanoscale* **2021**, *13*, 11953–11962. [CrossRef] [PubMed]
183. Kawasaki, R.; Ohdake, R.; Yamana, K.; Eto, T.; Sugikawa, K.; Ikeda, A. Photodynamic therapy using self-assembled nanogels comprising chlorin e6-bearing pullulan. *J. Mater. Chem. B* **2021**, *9*, 6357–6363. [CrossRef]
184. Yang, J.; Teng, Y.; Fu, Y.; Zhang, C. Chlorins e6 loaded silica nanoparticles coated with gastric cancer cell membrane for tumor specific photodynamic therapy of gastric cancer. *Int. J. Nanomed.* **2019**, *14*, 5061–5071. [CrossRef]
185. Sakamaki, Y.; Ozdemir, J.; Heidrick, Z.; Azzun, A.; Watson, O.; Tsuji, M.; Salmon, C.; Sinha, A.; Batta-Mpouma, J.; McConnell, Z.; et al. A Bioconjugated Chlorin-Based Metal–Organic Framework for Targeted Photodynamic Therapy of Triple Negative Breast and Pancreatic Cancers. *ACS Appl. Bio Mater.* **2021**, *4*, 1432–1440. [CrossRef]
186. Sundaram, P.; Abrahamse, H. Effective Photodynamic Therapy for Colon Cancer Cells Using Chlorin e6 Coated Hyaluronic Acid-Based Carbon Nanotubes. *Int. J. Mol. Sci.* **2020**, *21*, 4745. [CrossRef]
187. Yang, X.; Shi, X.; Zhang, Y.; Xu, J.; Ji, J.; Ye, L.; Yi, F.; Zhai, G. Photo-triggered self-destructive ROS-responsive nanoparticles of high paclitaxel/chlorin e6 co-loading capacity for synergetic chemo-photodynamic therapy. *J. Control. Release* **2020**, *323*, 333–349. [CrossRef]
188. Laranjo, M.; Aguiar, M.C.; Pereira, N.A.; Brites, G.; Nascimento, B.F.; Brito, A.F.; Casalta-Lopes, J.; Gonçalves, A.C.; Sarmiento-Ribeiro, A.B.; Pineiro, M.; et al. Platinum(II) ring-fused chlorins as efficient theranostic agents: Dyes for tumor-imaging and photodynamic therapy of cancer. *Eur. J. Med. Chem.* **2020**, *200*, 112468. [CrossRef] [PubMed]
189. Kustov, A.V.; Kustova, T.V.; Belykh, D.V.; Khudyaeva, I.S.; Berezin, D.B. Synthesis and investigation of novel chlorin sensitizers containing the myristic acid residue for antimicrobial photodynamic therapy. *Dye. Pigment.* **2020**, *173*, 107948. [CrossRef]
190. Babu, B.; Sindelo, A.; Mack, J.; Nyokong, T. Thien-2-yl substituted chlorins as photosensitizers for photodynamic therapy and photodynamic antimicrobial chemotherapy. *Dye. Pigment.* **2020**, *185*, 108886. [CrossRef]
191. Kataoka, H.; Nishie, H.; Tanaka, M.; Sasaki, M.; Nomoto, A.; Osaki, T.; Okamoto, Y.; Yano, S. Potential of Photodynamic Therapy Based on Sugar-Conjugated Photosensitizers. *J. Clin. Med.* **2021**, *10*, 841. [CrossRef]
192. Almeida, J.; Zhang, G.; Wang, M.; Queirós, C.; Cerqueira, A.F.R.; Tomé, A.C.; Barone, G.; Vicente, M.G.H.; Hey-Hawkins, E.; Silva, A.M.G.; et al. Synthesis, characterization, and cellular investigations of porphyrin- and chlorin-indomethacin conjugates for photodynamic therapy of cancer. *Org. Biomol. Chem.* **2021**, *19*, 6501–6512. [CrossRef]
193. Hemelrijk, P.W.; Kwa, S.L.; van Grondelle, R.; Dekker, J.P. Spectroscopic properties of LHC-II, the main light-harvesting chlorophyll a/b protein complex from chloroplast membranes. *Biochim. Biophys. Acta (BBA) Bioenerg.* **1992**, *1098*, 159–166. [CrossRef]
194. Bucks, R.R.; Boxer, S.G. Synthesis and spectroscopic properties of a novel cofacial chlorophyll-based dimer. *J. Am. Chem. Soc.* **1982**, *104*, 340–343. [CrossRef]
195. Li, Y.; Cai, Z.-L.; Chen, M. Spectroscopic Properties of Chlorophyll *f*. *J. Phys. Chem. B* **2013**, *117*, 11309–11317. [CrossRef]
196. Niedzwiedzki, D.; Blankenship, R.E. Singlet and triplet excited state properties of natural chlorophylls and bacteriochlorophylls. *Photosynth. Res.* **2010**, *106*, 227–238. [CrossRef]
197. Scherz, A.; Parson, W.W. Oligomers of bacteriochlorophyll and bacteriopheophytin with spectroscopic properties resembling those found in photosynthetic bacteria. *Biochim. Et Biophys. Acta (BBA) Bioenerg.* **1984**, *766*, 653–665. [CrossRef]
198. Pucelik, B.; Sulek, A.; Dąbrowski, J.M. Bacteriochlorins and their metal complexes as NIR-absorbing photosensitizers: Properties, mechanisms, and applications. *Co-Ord. Chem. Rev.* **2020**, *416*, 213340. [CrossRef]
199. Wu, M.; Liu, Z.; Zhang, W. An ultra-stable bio-inspired bacteriochlorin analogue for hypoxia-tolerant photodynamic therapy. *Chem. Sci.* **2021**, *12*, 1295–1301. [CrossRef] [PubMed]
200. Le, N.A.; Babu, V.; Kalt, M.; Schneider, L.; Schumer, F.; Spingler, B. Photostable Platinated Bacteriochlorins as Potent Photodynamic Agents. *J. Med. Chem.* **2021**, *64*, 6792–6801. [CrossRef] [PubMed]
201. Otvagin, V.F.; Kuzmina, N.S.; Kudriashova, E.S.; Nyuchev, A.V.; Gavryushin, A.E.; Fedorov, A.Y. Conjugates of Porphyrinoid-Based Photosensitizers with Cytotoxic Drugs: Current Progress and Future Directions toward Selective Photodynamic Therapy. *J. Med. Chem.* **2022**, *65*, 1695–1734. [CrossRef]
202. Pavlova, M.A.; Panchenko, P.A.; Alekhina, E.A.; Ignatova, A.A.; Plyutinskaya, A.D.; Pankratov, A.A.; Pritmov, D.A.; Grin, M.A.; Feofanov, A.V.; Fedorova, O.A. A New Glutathione-Cleavable Theranostic for Photodynamic Therapy Based on Bacteriochlorin e and Styrylnaphthalimide Derivatives. *Biosensors* **2022**, *12*, 1149. [CrossRef]
203. Morozova, N.B.; Pavlova, M.A.; Plyutinskaya, A.D.; Pankratov, A.A.; Efendiev, K.T.; Semkina, A.S.; Pritmov, D.A.; Mironov, A.F.; Panchenko, P.A.; Fedorova, O.A. Photodiagnosis and photodynamic effects of bacteriochlorin-naphthalimide conjugates on tumor cells and mouse model. *J. Photochem. Photobiol. B Biol.* **2021**, *223*, 112294. [CrossRef]

204. Zakharko, M.A.; Panchenko, P.A.; Zarezin, D.P.; Nenajdenko, V.G.; Pritmov, D.A.; Grin, M.A.; Mironov, A.F.; Fedorova, O.A. Conjugates of 3,4-dimethoxy-4-styrylnaphthalimide and bacteriochlorin for theranostics in photodynamic therapy. *Russ. Chem. Bull.* **2020**, *69*, 1169–1178. [CrossRef]
205. Panchenko, P.A.; Zakharko, M.A.; Grin, M.A.; Mironov, A.F.; Pritmov, D.A.; Jonusauskas, G.; Fedorov, Y.V.; Fedorova, O.A. Effect of linker length on the spectroscopic properties of bacteriochlorin—1,8-naphthalimide conjugates for fluorescence-guided photodynamic therapy. *J. Photochem. Photobiol. A Chem.* **2020**, *390*, 112338. [CrossRef]
206. Lobo, A.C.S.; Gomes-Da-Silva, L.C.; Rodrigues-Santos, P.; Cabrita, A.; Santos-Rosa, M.; Arnaut, L.G. Immune Responses after Vascular Photodynamic Therapy with Redaporfin. *J. Clin. Med.* **2019**, *9*, 104. [CrossRef]
207. Karwicka, M.; Pucelik, B.; Gonet, M.; Elas, M.; Dąbrowski, J.M. Effects of Photodynamic Therapy with Redaporfin on Tumor Oxygenation and Blood Flow in a Lung Cancer Mouse Model. *Sci. Rep.* **2019**, *9*, 12655. [CrossRef]
208. Mendes, M.I.P.; Arnaut, L.G. Redaporfin Development for Photodynamic Therapy and its Combination with Glycolysis Inhibitors. *Photochem. Photobiol.* **2023**, *99*, 769–776. [CrossRef]
209. Cheruku, R.R.; Cacaccio, J.; Durrani, F.A.; Tabaczynski, W.A.; Watson, R.; Sifers, K.; Missert, J.R.; Tracy, E.C.; Dukh, M.; Guru, K.; et al. Synthesis, Tumor Specificity, and Photosensitizing Efficacy of Erlotinib-Conjugated Chlorins and Bacteriochlorins: Identification of a Highly Effective Candidate for Photodynamic Therapy of Cancer. *J. Med. Chem.* **2021**, *64*, 741–767. [CrossRef] [PubMed]
210. Pratavieira, S.; Uliana, M.P.; Lopes, N.S.D.S.; Donatoni, M.C.; Linares, D.R.; Anibal, F.D.F.; de Oliveira, K.T.; Kurachi, C.; de Souza, C.W.O. Photodynamic therapy with a new bacteriochlorin derivative: Characterization and in vitro studies. *Photodiagnosis Photodyn. Ther.* **2021**, *34*, 102251. [CrossRef]
211. Ballatore, M.B.; Milanesio, M.E.; Fujita, H.; Lindsey, J.S.; Durantini, E.N. Bacteriochlorin-bis(spermine) conjugate affords an effective photodynamic action to eradicate microorganisms. *J. Biophotonics* **2020**, *13*, e201960061. [CrossRef]
212. Tikhonov, S.; Ostroverkhov, P.; Suvorov, N.; Mironov, A.; Efimova, Y.; Plutinskaya, A.; Pankratov, A.; Ignatova, A.; Feofanov, A.; Diachkova, E.; et al. Tin Carboxylate Complexes of Natural Bacteriochlorin for Combined Photodynamic and Chemotherapy of Cancer. *Int. J. Mol. Sci.* **2021**, *22*, 13563. [CrossRef] [PubMed]
213. Santos, K.L.M.; Barros, R.M.; Lima, D.P.D.S.; Nunes, A.M.A.; Sato, M.R.; Faccio, R.; Damasceno, B.P.G.D.L.; Oshiro-Junior, J.A. Prospective application of phthalocyanines in the photodynamic therapy against microorganisms and tumor cells: A mini-review. *Photodiagnosis Photodyn. Ther.* **2020**, *32*, 102032. [CrossRef]
214. Lo, P.-C.; Rodriguez-Morgade, M.S.; Pandey, R.K.; Ng, D.K.P.; Torres, T.; Dumoulin, F. The unique features and promises of phthalocyanines as advanced photosensitisers for photodynamic therapy of cancer. *Chem. Soc. Rev.* **2020**, *49*, 1041–1056. [CrossRef]
215. Brilkina, A.A.; Dubasova, L.V.; Sergeeva, E.A.; Pospelov, A.; Shilyagina, N.Y.; Shakhova, N.M.; Balalaeva, I.V. Photobiological properties of phthalocyanine photosensitizers Photosens, Holosens and Phthalosens: A comparative in vitro analysis. *J. Photochem. Photobiol. B Biol.* **2019**, *191*, 128–134. [CrossRef]
216. Love, W.G.; Duk, S.; Biolo, R.; Jori, G.; Taylor, P.W. Liposome-Mediated Delivery of Photosensitizers: Localization of Zinc (II)-Phthalocyanine within Implanted Tumors after Intravenous Administration. *Photochem. Photobiol.* **1996**, *63*, 656–661. [CrossRef]
217. De Simone, B.C.; Alberto, M.E.; Russo, N.; Toscano, M. Photophysical properties of heavy atom containing tetrasulfonyl phthalocyanines as possible photosensitizers in photodynamic therapy. *J. Comput. Chem.* **2021**, *42*, 1803–1808. [CrossRef] [PubMed]
218. Sen, P.; Managa, M.; Nyokong, T. New type of metal-free and Zinc(II), In(III), Ga(III) phthalocyanines carrying biologically active substituents: Synthesis and photophysicochemical properties and photodynamic therapy activity. *Inorg. Chim. Acta* **2019**, *491*, 1–8. [CrossRef]
219. Lee, S.Y.; Kim, C.Y.; Nam, T.-G. Ruthenium Complexes as Anticancer Agents: A Brief History and Perspectives. *Drug Des. Dev. Ther.* **2020**, *14*, 5375–5392. [CrossRef] [PubMed]
220. Negri, L.B.; Martins, T.J.; da Silva, R.S.; Hamblin, M.R. Photobiomodulation combined with photodynamic therapy using ruthenium phthalocyanine complexes in A375 melanoma cells: Effects of nitric oxide generation and ATP production. *J. Photochem. Photobiol. B Biol.* **2019**, *198*, 111564. [CrossRef] [PubMed]
221. Riega, S.D.E.; Valli, F.; Rodríguez, H.B.; Marino, J.; Roguin, L.P.; Lantaño, B.; Vior, M.C.G. Chalcogen bearing tetrasubstituted zinc (II) phthalocyanines for CT26 colon carcinoma cells photodynamic therapy. *Dye. Pigment.* **2022**, *201*, 110110. [CrossRef]
222. Magadla, A.; Babu, B.; Mack, J.; Nyokong, T. Positively charged styryl pyridine substituted Zn(II) phthalocyanines for photodynamic therapy and photoantimicrobial chemotherapy: Effect of the number of charges. *Dalton Trans.* **2021**, *50*, 9129–9136. [CrossRef]
223. Ferreira, J.T.; Pina, J.; Ribeiro, C.A.F.; Fernandes, R.; Tomé, J.P.C.; Rodríguez-Morgade, M.S.; Torres, T. Highly Efficient Singlet Oxygen Generators Based on Ruthenium Phthalocyanines: Synthesis, Characterization and in vitro Evaluation for Photodynamic Therapy. *Chem. A Eur. J.* **2020**, *26*, 1789–1799. [CrossRef]
224. Li, D.; Hu, Q.-Y.; Wang, X.-Z.; Li, X.; Hu, J.-Q.; Zheng, B.-Y.; Ke, M.-R.; Huang, J.-D. A non-aggregated silicon(IV) phthalocyanine-lactose conjugate for photodynamic therapy. *Bioorganic Med. Chem. Lett.* **2020**, *30*, 127164. [CrossRef]

225. Li, K.; Dong, W.; Liu, Q.; Lv, G.; Xie, M.; Sun, X.; Qiu, L.; Lin, J. A biotin receptor-targeted silicon(IV) phthalocyanine for in vivo tumor imaging and photodynamic therapy. *J. Photochem. Photobiol. B Biol.* **2019**, *190*, 1–7. [CrossRef]
226. Li, D.; Wang, X.-Z.; Yang, L.-F.; Li, S.-C.; Hu, Q.-Y.; Li, X.; Zheng, B.-Y.; Ke, M.-R.; Huang, J.-D. Size-Tunable Targeting-Triggered Nanophotosensitizers Based on Self-Assembly of a Phthalocyanine–Biotin Conjugate for Photodynamic Therapy. *ACS Appl. Mater. Interf.* **2019**, *11*, 36435–36443. [CrossRef]
227. Kim, J.; Lee, S.; Na, K. Glycyrrhetic Acid-Modified Silicon Phthalocyanine for Liver Cancer-Targeted Photodynamic Therapy. *Biomacromolecules* **2021**, *22*, 811–822. [CrossRef]
228. Openda, Y.I.; Babu, B.; Nyokong, T. Novel cationic-chalcone phthalocyanines for photodynamic therapy eradication of *S. aureus* and *E. coli* bacterial biofilms and MCF-7 breast cancer. *Photodiagnosis Photodyn. Ther.* **2022**, *38*, 102863. [CrossRef] [PubMed]
229. Senapathy, G.J.; George, B.P.; Abrahamse, H. Enhancement of Phthalocyanine Mediated Photodynamic Therapy by Catechin on Lung Cancer Cells. *Molecules* **2020**, *25*, 4874. [CrossRef] [PubMed]
230. Nkune, N.W.; Matlou, G.G.; Abrahamse, H. Photodynamic Therapy Efficacy of Novel Zinc Phthalocyanine Tetra Sodium 2-Mercaptoacetate Combined with Cannabidiol on Metastatic Melanoma. *Pharmaceutics* **2022**, *14*, 2418. [CrossRef] [PubMed]
231. Doustvandi, M.A.; Mohammadnejad, F.; Mansoori, B.; Tajalli, H.; Mohammadi, A.; Mokhtarzadeh, A.; Baghbani, E.; Khaze, V.; Hajiasgharzadeh, K.; Moghaddam, M.M.; et al. Photodynamic therapy using zinc phthalocyanine with low dose of diode laser combined with doxorubicin is a synergistic combination therapy for human SK-MEL-3 melanoma cells. *Photodiagnosis Photodyn. Ther.* **2019**, *28*, 88–97. [CrossRef]
232. Reis, S.R.R.D.; Helal-Neto, E.; Barros, A.O.D.S.D.; Pinto, S.R.; Portilho, F.L.; Siqueira, L.B.d.O.; Alencar, L.M.R.; Dahoumane, S.A.; Alexis, F.; Ricci-Junior, E.; et al. Dual Encapsulated Dacarbazine and Zinc Phthalocyanine Polymeric Nanoparticle for Photodynamic Therapy of Melanoma. *Pharm. Res.* **2021**, *38*, 335–346. [CrossRef] [PubMed]
233. Yang, Z.; Li, P.; Chen, Y.; Dong, E.; Feng, Z.; He, Z.; Zhou, C.; Wang, C.; Liu, Y.; Feng, C. Preparation of zinc phthalocyanine-loaded amphiphilic phosphonium chitosan nanomicelles for enhancement of photodynamic therapy efficacy. *Colloids Surf. B Biointerfaces* **2021**, *202*, 111693. [CrossRef]
234. Rak, J.; Kabesova, M.; Benes, J.; Pouckova, P.; Vetvicka, D. Advances in Liposome-Encapsulated Phthalocyanines for Photodynamic Therapy. *Life* **2023**, *13*, 305. [CrossRef]
235. Pinto, B.C.; Ambrósio, J.A.; Marmo, V.L.M.; Pinto, J.G.; Raniero, L.J.; Ferreira-Strixino, J.; Simioni, A.R.; Beltrame, M. Synthesis, characterization, and evaluation of chloroaluminium phthalocyanine incorporated in poly(ϵ -caprolactone) nanoparticles for photodynamic therapy. *Photodiagnosis Photodyn. Ther.* **2022**, *38*, 102850. [CrossRef]
236. Rodrigues, M.C.; Vieira, L.G.; Horst, F.H.; de Araújo, E.C.; Ganassin, R.; Merker, C.; Meyer, T.; Böttner, J.; Venus, T.; Longo, J.P.F.; et al. Photodynamic therapy mediated by aluminium-phthalocyanine nanoemulsion eliminates primary tumors and pulmonary metastases in a murine 4T1 breast adenocarcinoma model. *J. Photochem. Photobiol. B Biol.* **2020**, *204*, 111808. [CrossRef]
237. Matshitse, R.; Ngoy, B.P.; Managa, M.; Mack, J.; Nyokong, T. Photophysical properties and photodynamic therapy activities of detonated nanodiamonds-BODIPY-phthalocyanines nanoassemblies. *Photodiagnosis Photodyn. Ther.* **2019**, *26*, 101–110. [CrossRef]
238. Matshitse, R.; Nwaji, N.; Managa, M.; Chen, Z.-L.; Nyokong, T. Photodynamic therapy characteristics of phthalocyanines in the presence of boron doped detonation nanodiamonds: Effect of symmetry and charge. *Photodiagnosis Photodyn. Ther.* **2022**, *37*, 102705. [CrossRef] [PubMed]
239. Oshiro-Junior, J.A.; Sato, M.; Boni, F.I.; Santos, K.L.M.; de Oliveira, K.T.; de Freitas, L.M.; Fontana, C.R.; Nicholas, D.; McHale, A.P.; Callan, J.F.; et al. Phthalocyanine-loaded nanostructured lipid carriers functionalized with folic acid for photodynamic therapy. *Mater. Sci. Eng. C* **2020**, *108*, 110462. [CrossRef]
240. Liang, X.; Xie, Y.; Wu, J.; Wang, J.; Petković, M.; Stepić, M.; Zhao, J.; Ma, J.; Mi, L. Functional titanium dioxide nanoparticle conjugated with phthalocyanine and folic acid as a promising photosensitizer for targeted photodynamic therapy in vitro and in vivo. *J. Photochem. Photobiol. B Biol.* **2021**, *215*, 112122. [CrossRef] [PubMed]
241. Lange, N.; Szlasa, W.; Saczko, J.; Chwiłkowska, A. Potential of Cyanine Derived Dyes in Photodynamic Therapy. *Pharmaceutics* **2021**, *13*, 818. [CrossRef]
242. Delaey, E.; van Laar, F.; De Vos, D.; Kamuhabwa, A.; Jacobs, P.; de Witte, P. A comparative study of the photosensitizing characteristics of some cyanine dyes. *J. Photochem. Photobiol. B Biol.* **2000**, *55*, 27–36. [CrossRef] [PubMed]
243. Serrano, J.L.; Maia, A.; Santos, A.O.; Lima, E.; Reis, L.V.; Nunes, M.J.; Boto, R.E.F.; Silvestre, S.; Almeida, P. An Insight into Symmetrical Cyanine Dyes as Promising Selective Antiproliferative Agents in Caco-2 Colorectal Cancer Cells. *Molecules* **2022**, *27*, 5779. [CrossRef]
244. Ebaston, T.; Nakonechny, F.; Talalai, E.; Gellerman, G.; Patsenker, L. Iodinated xanthene-cyanine NIR dyes as potential photosensitizers for antimicrobial photodynamic therapy. *Dye. Pigment.* **2021**, *184*, 108854. [CrossRef]
245. Thankarajan, E.; Walunj, D.; Bazylevich, A.; Prasad, C.; Hesin, A.; Patsenker, L.; Gellerman, G. A novel, dual action chimera comprising DNA methylating agent and near-IR xanthene-cyanine photosensitizer for combined anticancer therapy. *Photodiagnosis Photodyn. Ther.* **2022**, *37*, 102722. [CrossRef]
246. Martins, T.D.; Lima, E.; Boto, R.E.; Ferreira, D.; Fernandes, J.R.; Almeida, P.; Ferreira, L.F.V.; Silva, A.M.; Reis, L.V. Red and Near-Infrared Absorbing Dicyanomethylene Squaraine Cyanine Dyes: Photophysicochemical Properties and Anti-Tumor Photosensitizing Effects. *Materials* **2020**, *13*, 2083. [CrossRef]

247. Lima, E.; Reis, L.V. 'Lights, squaraines, action!'—The role of squaraine dyes in photodynamic therapy. *Futur. Med. Chem.* **2022**, *14*, 1375–1402. [CrossRef]
248. Lynch, D.E.; Hamilton, D.G. Croconaine Dyes—The Lesser Known Siblings of Squaraines. *Eur. J. Org. Chem.* **2017**, *2017*, 3897–3911. [CrossRef]
249. Usama, S.M.; Thavornpradit, S.; Burgess, K. Optimized Heptamethine Cyanines for Photodynamic Therapy. *ACS Appl. Bio Mater.* **2018**, *1*, 1195–1205. [CrossRef] [PubMed]
250. Zhang, Y.; Lv, T.; Zhang, H.; Xie, X.; Li, Z.; Chen, H.; Gao, Y. Folate and Heptamethine Cyanine Modified Chitosan-Based Nanotheranostics for Tumor Targeted Near-Infrared Fluorescence Imaging and Photodynamic Therapy. *Biomacromolecules* **2017**, *18*, 2146–2160. [CrossRef] [PubMed]
251. Yang, Q.; Jin, H.; Gao, Y.; Lin, J.; Yang, H.; Yang, S.-P. Photostable Iridium(III)–Cyanine Complex Nanoparticles for Photoacoustic Imaging Guided Near-Infrared Photodynamic Therapy in Vivo. *ACS Appl. Mater. Interfaces* **2019**, *11*, 15417–15425. [CrossRef] [PubMed]
252. Yang, X.; Bai, J.; Qian, Y. The investigation of unique water-soluble heptamethine cyanine dye for use as NIR photosensitizer in photodynamic therapy of cancer cells. *Spectrochim. Acta Part A Mol. Biomol. Spectrosc.* **2020**, *228*, 117702. [CrossRef] [PubMed]
253. Maltanava, H.; Belko, N.; Lugovski, A.; Brezhneva, N.; Bondarenko, E.; Chulkin, P.; Gusakov, G.; Vileishikova, N.; Samtsov, M.; Poznyak, S. Spectroelectrochemical and ESR investigation of free radicals derived from indotricarbocyanine dyes for photodynamic therapy. *Dye. Pigment.* **2022**, *205*, 110599. [CrossRef]
254. Liu, H.; Yin, J.; Xing, E.; Du, Y.; Su, Y.; Feng, Y.; Meng, S. Halogenated cyanine dyes for synergistic photodynamic and photothermal therapy. *Dye. Pigment.* **2021**, *190*, 109327. [CrossRef]
255. Thomas, A.P.; Palanikumar, L.; Jeena, M.T.; Kim, K.; Ryu, J.-H. Cancer-mitochondria-targeted photodynamic therapy with supramolecular assembly of HA and a water soluble NIR cyanine dye. *Chem. Sci.* **2017**, *8*, 8351–8356. [CrossRef]
256. Huang, B.; Zhang, C.; Tian, J.; Tian, Q.; Huang, G.; Zhang, W. A Cascade BIME-Triggered Near-IR Cyanine Nanoplatfrom for Enhanced Antibacterial Photodynamic Therapy. *ACS Appl. Mater. Interfaces* **2023**, *15*, 10520–10528. [CrossRef]
257. James, N.S.; Cheruku, R.R.; Missert, J.R.; Sunar, U.; Pandey, R.K. Measurement of Cyanine Dye Photobleaching in Photosensitizer Cyanine Dye Conjugates Could Help in Optimizing Light Dosimetry for Improved Photodynamic Therapy of Cancer. *Molecules* **2018**, *23*, 1842. [CrossRef]
258. Huang, H.; Ma, D.; Liu, Q.; Huang, D.; Zhao, X.; Yao, Q.; Xiong, T.; Long, S.; Du, J.; Fan, J.; et al. Enhancing Intersystem Crossing by Intermolecular Dimer-Stacking of Cyanine as Photosensitizer for Cancer Therapy. *CCS Chem.* **2022**, *4*, 3627–3636. [CrossRef]
259. Kobzev, D.; Semenova, O.; Tatarets, A.; Bazylevich, A.; Gellerman, G.; Patsenker, L. Antibody-guided iodinated cyanine for near-IR photoimmunotherapy. *Dye. Pigment.* **2023**, *212*, 111101. [CrossRef]
260. Debnath, S.; Agarwal, A.; Kumar, N.R.; Bedi, A. Selenium-Based Drug Development for Antioxidant and Anticancer Activity. *Futur. Pharmacol.* **2022**, *2*, 595–607. [CrossRef]
261. Sun, J.; Feng, E.; Shao, Y.; Lv, F.; Wu, Y.; Tian, J.; Sun, H.; Song, F. A Selenium-Substituted Heptamethine Cyanine Photosensitizer for Near-Infrared Photodynamic Therapy. *ChemBiochem* **2022**, *23*, e202200421. [CrossRef]
262. Siritwibool, S.; Kaekratoke, N.; Chansaenpak, K.; Siwawannapong, K.; Panajapo, P.; Sagarik, K.; Noisa, P.; Lai, R.-Y.; Kamkaew, A. Near-Infrared Fluorescent pH Responsive Probe for Targeted Photodynamic Cancer Therapy. *Sci. Rep.* **2020**, *10*, 1283. [CrossRef]
263. Semenova, O.; Kobzev, D.; Yazbak, F.; Nakonechny, F.; Kolosova, O.; Tatarets, A.; Gellerman, G.; Patsenker, L. Unexpected effect of iodine atoms in heptamethine cyanine dyes on the photodynamic eradication of Gram-positive and Gram-negative pathogens. *Dye. Pigment.* **2021**, *195*, 109745. [CrossRef]
264. Pontremoli, C.; Chinigò, G.; Galliano, S.; Plata, M.M.; Dereje, D.; Sansone, E.; Gilardino, A.; Barolo, C.; Pla, A.F.; Visentin, S.; et al. Photosensitizers for photodynamic therapy: Structure-activity analysis of cyanine dyes through design of experiments. *Dye. Pigment.* **2023**, *210*, 111047. [CrossRef]
265. Ciubini, B.; Visentin, S.; Serpe, L.; Canaparo, R.; Fin, A.; Barbero, N. Design and synthesis of symmetrical pentamethine cyanine dyes as NIR photosensitizers for PDT. *Dye. Pigment.* **2019**, *160*, 806–813. [CrossRef]
266. Shi, H.; Tan, X.; Wang, P.; Qin, J. A novel near-infrared trifluoromethyl heptamethine cyanine dye with mitochondria-targeting for integration of collaborative treatment of photothermal and sonodynamic therapy. *Mater. Today Adv.* **2022**, *14*, 100251. [CrossRef]
267. Li, M.; Sun, W.; Tian, R.; Cao, J.; Tian, Y.; Gurrarn, B.; Fan, J.; Peng, X. Smart J-aggregate of cyanine photosensitizer with the ability to target tumor and enhance photodynamic therapy efficacy. *Biomaterials* **2020**, *269*, 120532. [CrossRef]
268. Lima, E.; Barroso, A.G.; Sousa, M.A.; Ferreira, O.; Boto, R.E.; Fernandes, J.R.; Almeida, P.; Silvestre, S.M.; Santos, A.O.; Reis, L.V. Picolyamine-functionalized benz[e]indole squaraine dyes: Synthetic approach, characterization and in vitro efficacy as potential anticancer phototherapeutic agents. *Eur. J. Med. Chem.* **2022**, *229*, 114071. [CrossRef] [PubMed]
269. Lima, E.; Barroso, A.G.; Ferreira, O.; Boto, R.E.; Fernandes, J.R.; Almeida, P.; Silvestre, S.M.; Santos, A.O.; Reis, L.V. Benz[e]indole-bearing aminosquaraine dyes: Which of the amines introduced into the squaric ring will be able to induce the best in vitro photodynamic effect? *Dye. Pigment.* **2023**, *215*, 111239. [CrossRef]
270. Li, J.-H.; You, P.-D.; Lu, F.; Huang, J.-T.; Fu, J.-L.; Tang, H.-Y.; Zhou, C.-Q. Single aromatics sulfonamide substituted dibenzothiazole squaraines for tumor NIR imaging and efficient photodynamic therapy at low drug dose. *J. Photochem. Photobiol. B Biol.* **2023**, *240*, 112653. [CrossRef] [PubMed]

271. Lima, E.; Ferreira, O.; Gomes, V.S.; Santos, A.O.; Boto, R.E.; Fernandes, J.R.; Almeida, P.; Silvestre, S.M.; Reis, L.V. Synthesis and in vitro evaluation of the antitumoral phototherapeutic potential of squaraine cyanine dyes derived from indolenine. *Dye. Pigment.* **2019**, *167*, 98–108. [CrossRef]
272. Lei, S.; Zhang, Y.; Blum, N.T.; Huang, P.; Lin, J. Recent Advances in Croconaine Dyes for Bioimaging and Theranostics. *Bioconjugate Chem.* **2020**, *31*, 2072–2084. [CrossRef]
273. Liu, N.; Gujrati, V.; Malekzadeh-Najafabadi, J.; Werner, J.P.F.; Klemm, U.; Tang, L.; Chen, Z.; Prakash, J.; Huang, Y.; Stiel, A.; et al. Croconaine-based nanoparticles enable efficient optoacoustic imaging of murine brain tumors. *Photoacoustics* **2021**, *22*, 100263. [CrossRef]
274. Alejo, T.; Font, C.; Abad, M.; Andreu, V.; Sebastian, V.; Mendoza, G.; Arruebo, M. Spatiotemporal control of photothermal heating using pH sensitive near-infrared croconaine-based dyes. *J. Photochem. Photobiol. A Chem.* **2019**, *382*, 111936. [CrossRef]
275. Wen, Y.; McGarraugh, H.H.; Schreiber, C.L.; Smith, B.D. Cell organelle targeting of near-infrared croconaine dye controls photothermal outcome. *Chem. Commun.* **2020**, *56*, 6977–6980. [CrossRef]
276. Sun, R.; Ma, W.; Ling, M.; Tang, C.; Zhong, M.; Dai, J.; Zhu, M.; Cai, X.; Li, G.; Xu, Q.; et al. pH-activated nanoplatform for visualized photodynamic and ferroptosis synergistic therapy of tumors. *J. Control. Release* **2022**, *350*, 525–537. [CrossRef]
277. Vara, J.; Gualdesi, M.S.; Bertolotti, S.G.; Ortiz, C.S. Two phenothiazine dyes as photosensitizers for the production of singlet oxygen. Photophysics, photochemistry and effects of aggregation. *J. Mol. Struct.* **2019**, *1181*, 1–7. [CrossRef]
278. Padnya, P.; Khadieva, A.; Stoikov, I. Current achievements and perspectives in synthesis and applications of 3,7-disubstituted phenothiazines as Methylene Blue analogues. *Dye. Pigment.* **2023**, *208*, 110806. [CrossRef]
279. Vara, J.; Gualdesi, M.S.; Aiassa, V.; Ortiz, C.S. Evaluation of physicochemical properties and bacterial photoinactivation of phenothiazine photosensitizers. *Photochem. Photobiol. Sci.* **2019**, *18*, 1576–1586. [CrossRef] [PubMed]
280. Shen, X.; Dong, L.; He, X.; Zhao, C.; Zhang, W.; Li, X.; Lu, Y. Treatment of infected wounds with methylene blue photodynamic therapy: An effective and safe treatment method. *Photodiagnosis Photodyn. Ther.* **2020**, *32*, 102051. [CrossRef]
281. Barbosa, A.F.S.; Santos, I.P.; Santos, G.M.P.; Bastos, T.M.; Rocha, V.P.C.; Meira, C.S.; Soares, M.B.P.; Pitta, I.R.; Pinheiro, A.L.B. Anti-Trypanosoma cruzi effect of the photodynamic antiparasitic chemotherapy using phenothiazine derivatives as photosensitizers. *Lasers Med. Sci.* **2019**, *35*, 79–85. [CrossRef] [PubMed]
282. Almeida, A.; Faustino, M.A.F.; Neves, M.G.P.M.S. Antimicrobial Photodynamic Therapy in the Control of COVID-19. *Antibiotics* **2020**, *9*, 320. [CrossRef] [PubMed]
283. Theodoro, L.H.; da Rocha, T.E.; Wainwright, M.; Nuernberg, M.A.A.; Ervolino, E.; Souza, E.Q.M.; Brandini, D.A.; Garcia, V.G. Comparative effects of different phenothiazine photosensitizers on experimental periodontitis treatment. *Photodiagnosis Photodyn. Ther.* **2021**, *34*, 102198. [CrossRef]
284. Chang, C.-C.; Hsieh, C.-F.; Wu, H.-J.; Ameen, M.; Hung, T.-P. Investigation of Sonosensitizers Based on Phenothiazinium Photosensitizers. *Appl. Sci.* **2022**, *12*, 7819. [CrossRef]
285. Yang, Y.; Zhang, Y.; Wang, R.; Rong, X.; Liu, T.; Xia, X.; Fan, J.; Sun, W.; Peng, X. A glutathione activatable pro-drug-photosensitizer for combined chemotherapy and photodynamic therapy. *Chin. Chem. Lett.* **2022**, *33*, 4583–4586. [CrossRef]
286. Squeo, B.M.; Ganzer, L.; Virgili, T.; Pasini, M. BODIPY-Based Molecules, a Platform for Photonic and Solar Cells. *Molecules* **2020**, *26*, 153. [CrossRef]
287. Ray, C.; Schad, C.; Moreno, F.; Maroto, B.L.; Bañuelos, J.; Arbeloa, T.; García-Moreno, I.; Villafuerte, C.; Muller, G.; de la Moya, S. BCl₃-Activated Synthesis of COO-BODIPY Laser Dyes: General Scope and High Yields under Mild Conditions. *J. Org. Chem.* **2020**, *85*, 4594–4601. [CrossRef]
288. Mei, Y.; Li, H.; Song, C.-Z.; Chen, X.-G.; Song, Q.-H. An 8-arylselenium BODIPY fluorescent probe for rapid and sensitive discrimination of biothiols in living cells. *Chem. Commun.* **2021**, *57*, 10198–10201. [CrossRef] [PubMed]
289. Xu, H.; Shen, G.; Peng, C.; Han, X.; Duan, L.; Cheng, T. BODIPY-based fluorescent probe for selective detection of HSA in urine. *Dye. Pigment.* **2022**, *197*, 109915. [CrossRef]
290. Zhu, M.; Zhang, G.; Hu, Z.; Zhu, C.; Chen, Y.; James, T.D.; Ma, L.; Wang, Z. A BODIPY-based probe for amyloid- β imaging in vivo. *Org. Chem. Front.* **2023**, *10*, 1903–1909. [CrossRef]
291. Turksoy, A.; Yildiz, D.; Akkaya, E.U. Photosensitization and controlled photosensitization with BODIPY dyes. *Coordin. Chem. Rev.* **2019**, *379*, 47–64. [CrossRef]
292. Qi, S.; Kwon, N.; Yim, Y.; Nguyen, V.-N.; Yoon, J. Fine-tuning the electronic structure of heavy-atom-free BODIPY photosensitizers for fluorescence imaging and mitochondria-targeted photodynamic therapy. *Chem. Sci.* **2020**, *11*, 6479–6484. [CrossRef] [PubMed]
293. Yu, T.; Zhang, D.; Wang, J.; Sun, C.; Cui, T.; Xu, Z.; Jiang, X.-D.; Du, J. Near-infrared upper phenyl-fused BODIPY as a photosensitizer for photothermal–photodynamic therapy. *J. Mater. Chem. B* **2022**, *10*, 3048–3054. [CrossRef]
294. Gorbe, M.; Costero, A.M.; Sancenón, F.; Martínez-Mañez, R.; Ballesteros-Cillero, R.; Ochando, L.E.; Chulvi, K.; Gotor, R.; Gil, S. Halogen-containing BODIPY derivatives for photodynamic therapy. *Dye. Pigment.* **2018**, *160*, 198–207. [CrossRef]
295. Miao, X.; Hu, W.; He, T.; Tao, H.; Wang, Q.; Chen, R.; Jin, L.; Zhao, H.; Lu, X.; Fan, Q.; et al. Deciphering the intersystem crossing in near-infrared BODIPY photosensitizers for highly efficient photodynamic therapy. *Chem. Sci.* **2019**, *10*, 3096–3102. [CrossRef]
296. Yu, Z.; Zhou, J.; Ji, X.; Lin, G.; Xu, S.; Dong, X.; Zhao, W. Discovery of a Monoiodo Aza-BODIPY Near-Infrared Photosensitizer: In vitro and in vivo Evaluation for Photodynamic Therapy. *J. Med. Chem.* **2020**, *63*, 9950–9964. [CrossRef]

297. Zhang, Y.; Yang, Z.; Zheng, X.; Yang, L.; Song, N.; Zhang, L.; Chen, L.; Xie, Z. Heavy atom substituted near-infrared BODIPY nanoparticles for photodynamic therapy. *Dye. Pigment.* **2020**, *178*, 108348. [CrossRef]
298. Aksakal, N.E.; Ççik, E.T.; Kazan, H.H.; Çiftçi, G.Y.; Yuksel, F. Novel ruthenium(II) and iridium(III) BODIPY dyes: Insights into their application in photodynamic therapy in vitro. *Photochem. Photobiol. Sci.* **2019**, *18*, 2012–2022. [CrossRef] [PubMed]
299. Jana, A.; Kundu, P.; Paul, S.; Kondaiah, P.; Chakravarty, A.R. Cobalt(III) Complexes for Light-Activated Delivery of Acetylacetonate-BODIPY, Cellular Imaging, and Photodynamic Therapy. *Inorg. Chem.* **2022**, *61*, 6837–6851. [CrossRef] [PubMed]
300. Paul, S.; Kundu, P.; Kondaiah, P.; Chakravarty, A.R. BODIPY-Ruthenium(II) Bis-Terpyridine Complexes for Cellular Imaging and Type-I/-II Photodynamic Therapy. *Inorg. Chem.* **2021**, *60*, 16178–16193. [CrossRef]
301. Callaghan, S.; Filatov, M.A.; Savoie, H.; Boyle, R.W.; Senge, M.O. In vitro cytotoxicity of a library of BODIPY-anthracene and -pyrene dyads for application in photodynamic therapy. *Photochem. Photobiol. Sci.* **2019**, *18*, 495–504. [CrossRef]
302. Gündüz, E.Ö.; Gedik, M.E.; Günaydın, G.; Okutan, E. Amphiphilic Fullerene-BODIPY Photosensitizers for Targeted Photodynamic Therapy. *ChemMedChem* **2022**, *17*, e202100693. [CrossRef] [PubMed]
303. Lu, S.; Lei, X.; Ren, H.; Zheng, S.; Qiang, J.; Zhang, Z.; Chen, Y.; Wei, T.; Wang, F.; Chen, X. PEGylated Dimeric BODIPY Photosensitizers as Nanocarriers for Combined Chemotherapy and Cathepsin B-Activated Photodynamic Therapy in 3D Tumor Spheroids. *ACS Appl. Bio Mater.* **2020**, *3*, 3835–3845. [CrossRef]
304. Prieto-Castañeda, A.; García-Garrido, F.; Díaz-Norambuena, C.; Escriche-Navarro, B.; García-Fernández, A.; Bañuelos, J.; Rebolgar, E.; García-Moreno, I.; Martínez-Máñez, R.; de la Moya, S.; et al. Development of Geometry-Controlled All-Orthogonal BODIPY Trimers for Photodynamic Therapy and Phototheragnosis. *Org. Lett.* **2022**, *24*, 3636–3641. [CrossRef]
305. Badon, I.W.; Jee, J.-P.; Vales, T.P.; Kim, C.; Lee, S.; Yang, J.; Yang, S.K.; Kim, H.-J. Cationic BODIPY Photosensitizers for Mitochondrion-Targeted Fluorescence Cell-Imaging and Photodynamic Therapy. *Pharmaceutics* **2023**, *15*, 1512. [CrossRef]
306. Badon, I.W.; Kim, C.; Lim, J.M.; Mai, D.K.; Vales, T.P.; Kang, D.; Cho, S.; Lee, J.; Kim, H.-J.; Yang, J. Mitochondrion-targeting PEGylated BODIPY dyes for near-infrared cell imaging and photodynamic therapy. *J. Mater. Chem. B* **2022**, *10*, 1196–1209. [CrossRef]
307. Masood, M.A.; Wu, Y.; Chen, Y.; Yuan, H.; Sher, N.; Faiz, F.; Yao, S.; Qi, F.; Khan, M.I.; Ahmed, M.; et al. Optimizing the photodynamic therapeutic effect of BODIPY-based photosensitizers against cancer and bacterial cells. *Dye. Pigment.* **2022**, *202*, 110255. [CrossRef]
308. Bai, J.; Qian, Y. Construction of an NIR and lysosome-targeted quinoline-BODIPY photosensitizer and its application in photodynamic therapy for human gastric carcinoma cells. *Dye. Pigment.* **2020**, *181*, 108615. [CrossRef]
309. Liu, Y.; Gao, J.; Li, H.; Yang, M.; Lv, J.; Zhou, Y.; Yuan, Z.; Li, X. A near-infrared and lysosome-targeted BODIPY photosensitizer for photodynamic and photothermal synergistic therapy. *Org. Biomol. Chem.* **2023**, *21*, 4672–4682. [CrossRef] [PubMed]
310. Wang, C.; Qian, Y. A novel BODIPY-based photosensitizer with pH-active singlet oxygen generation for photodynamic therapy in lysosomes. *Org. Biomol. Chem.* **2019**, *17*, 8001–8007. [CrossRef] [PubMed]
311. Wang, H.; Zhao, W.; Liu, X.; Wang, S.; Wang, Y. BODIPY-Based Fluorescent Surfactant for Cell Membrane Imaging and Photodynamic Therapy. *ACS Appl. Bio Mater.* **2020**, *3*, 593–601. [CrossRef]
312. Yu, Z.; Wang, H.; Chen, Z.; Dong, X.; Zhao, W.; Shi, Y.; Zhu, Q. Discovery of an Amino Acid-Modified Near-Infrared Aza-BODIPY Photosensitizer as an Immune Initiator for Potent Photodynamic Therapy in Melanoma. *J. Med. Chem.* **2022**, *65*, 3616–3631. [CrossRef]
313. Li, C.; Lin, W.; Liu, S.; Zhang, W.; Xie, Z. Self-destructive PEG-BODIPY nanomaterials for photodynamic and photothermal therapy. *J. Mater. Chem. B* **2019**, *7*, 4655–4660. [CrossRef]
314. Song, W.; Liu, H.; Wang, S.; Zhi, X.; Shen, Z. Photodynamically inactive prodrug based-on leuco-BODIPY: In vivo tumor targeting and microenvironment activated photodynamic therapy. *J. Photochem. Photobiol. A Chem.* **2023**, *435*, 114319. [CrossRef]
315. Mai, D.K.; Kim, C.; Lee, J.; Vales, T.P.; Badon, I.W.; De, K.; Cho, S.; Yang, J.; Kim, H.-J. BODIPY nanoparticles functionalized with lactose for cancer-targeted and fluorescence imaging-guided photodynamic therapy. *Sci. Rep.* **2022**, *12*, 2541. [CrossRef]
316. Khuong Mai, D.; Kang, B.; Pagarro Vales, T.; Badon, I.W.; Cho, S.; Lee, J.; Kim, E.; Kim, H.-J. Synthesis and Photophysical Properties of Tumor-Targeted Water-Soluble BODIPY Photosensitizers for Photodynamic Therapy. *Molecules* **2020**, *25*, 3340. [CrossRef]
317. Durán-Sampedro, G.; Xue, E.Y.; Moreno-Simoni, M.; Paramio, C.; Torres, T.; Ng, D.K.P.; de la Torre, G. Glycosylated BODIPY-Incorporated Pt(II) Metallacycles for Targeted and Synergistic Chemo-Photodynamic Therapy. *J. Med. Chem.* **2023**, *66*, 3448–3459. [CrossRef]
318. Chen, B.; Cao, J.; Zhang, K.; Zhang, Y.-N.; Lu, J.; Iqbal, M.Z.; Zhang, Q.; Kong, X. Synergistic photodynamic and photothermal therapy of BODIPY-conjugated hyaluronic acid nanoparticles. *J. Biomater. Sci. Polym. Ed.* **2021**, *32*, 2028–2045. [CrossRef]
319. Sepehrpour, H.; Fu, W.; Sun, Y.; Stang, P.J. Biomedically Relevant Self-Assembled Metallacycles and Metallacages. *J. Am. Chem. Soc.* **2019**, *141*, 14005–14020. [CrossRef] [PubMed]
320. Lv, S.; Miao, Y.; Zheng, D.; Li, X.; Liu, D.; Song, F. Self-Assembled Platinum Supramolecular Metallacycles Based on a Novel TADF Photosensitizer for Efficient Cancer Photochemotherapy. *Mol. Pharm.* **2021**, *18*, 1229–1237. [CrossRef] [PubMed]
321. Lin, X.; Chen, F.; Yu, X.; Wang, H.; Qiu, H.; Li, Y.; Yin, S.; Stang, P.J. Phenylthiol-BODIPY-based supramolecular metallacycles for synergistic tumor chemo-photodynamic therapy. *Proc. Natl. Acad. Sci. USA* **2022**, *119*, e2203994119. [CrossRef]
322. Malacarne, M.C.; Gariboldi, M.B.; Caruso, E. BODIPYs in PDT: A Journey through the Most Interesting Molecules Produced in the Last 10 Years. *Int. J. Mol. Sci.* **2022**, *23*, 10198. [CrossRef] [PubMed]

323. Zhang, W.; Ahmed, A.; Cong, H.; Wang, S.; Shen, Y.; Yu, B. Application of multifunctional BODIPY in photodynamic therapy. *Dye. Pigment.* **2020**, *185*, 108937. [CrossRef]
324. Chang, Z.; Ye, J.-H.; Qi, F.; Fang, H.; Lin, F.; Wang, S.; Mu, C.; Zhang, W.; He, W. A PEGylated photosensitizer-core pH-responsive polymeric nanocarrier for imaging-guided combination chemotherapy and photodynamic therapy. *New J. Chem.* **2021**, *45*, 6180–6185. [CrossRef]
325. Lin, W.; Zhang, W.; Liu, S.; Li, Z.; Hu, X.; Xie, Z.; Duan, C.; Han, G. Engineering pH-Responsive BODIPY Nanoparticles for Tumor Selective Multimodal Imaging and Phototherapy. *ACS Appl. Mater. Interfaces* **2019**, *11*, 43928–43935. [CrossRef] [PubMed]
326. Cao, J.-J.; Zhang, M.-S.; Li, X.-Q.; Yang, D.-C.; Xu, G.; Liu, J.-Y. A glutathione-responsive photosensitizer with fluorescence resonance energy transfer characteristics for imaging-guided targeting photodynamic therapy. *Eur. J. Med. Chem.* **2020**, *193*, 112203. [CrossRef]
327. Zhu, Y.; Song, N.; Chen, L.; Xie, Z. Reduction responsive BODIPY decorated mesoporous silica nanoscale platforms for photodynamic therapy. *Microporous Mesoporous Mater.* **2021**, *311*, 110689–110698. [CrossRef]
328. Shi, H.; Sun, W.; Liu, C.; Gu, G.; Ma, B.; Si, W.; Fu, N.; Zhang, Q.; Huang, W.; Dong, X. Tumor-targeting, enzyme-activated nanoparticles for simultaneous cancer diagnosis and photodynamic therapy. *J. Mater. Chem. B* **2016**, *4*, 113–120. [CrossRef] [PubMed]
329. Jung, E.; Shim, I.; An, J.; Ji, M.S.; Jangili, P.; Chi, S.-G.; Kim, J.S. Phenylthiourea-Conjugated BODIPY as an Efficient Photosensitizer for Tyrosinase-Positive Melanoma-Targeted Photodynamic Therapy. *ACS Appl. Bio Mater.* **2021**, *4*, 2120–2127. [CrossRef] [PubMed]

Disclaimer/Publisher’s Note: The statements, opinions and data contained in all publications are solely those of the individual author(s) and contributor(s) and not of MDPI and/or the editor(s). MDPI and/or the editor(s) disclaim responsibility for any injury to people or property resulting from any ideas, methods, instructions or products referred to in the content.

Review

1,3-Butadiynamides the Ethynylogous Ynamides: Synthesis, Properties and Applications in Heterocyclic Chemistry

Illia Lenko, Carole Alayrac *, Igor Božek and Bernhard Witulski *

Laboratoire de Chimie Moléculaire et Thio-Organique (LCMT), CNRS UMR 6507, ENSICAEN & UNICAEN, Normandie University, 6 Bd Maréchal Juin, 14050 Caen, France

* Correspondence: carole.witulski-alayrac@ensicaen.fr (C.A.); bernhard.witulski@ensicaen.fr (B.W.)

Abstract: 1,3-butadiynamides—the ethynylogous variants of ynamides—receive considerable attention as precursors of complex molecular scaffolds for organic and heterocyclic chemistry. The synthetic potential of these C4-building blocks reveals itself in sophisticated transition-metal catalyzed annulation reactions and in metal-free or silver-mediated HDDA (Hexa-dehydro-Diels–Alder) cycloadditions. 1,3-Butadiynamides also gain significance as optoelectronic materials and in less explored views on their unique helical twisted frontier molecular orbitals (Hel-FMOs). The present account summarizes different methodologies for the synthesis of 1,3-butadiynamides followed by the description of their molecular structure and electronic properties. Finally, the surprisingly rich chemistry of 1,3-butadiynamides as versatile C4-building blocks in heterocyclic chemistry is reviewed by compiling their exciting reactivity, specificity and opportunities for organic synthesis. Besides chemical transformations and use in synthesis, a focus is set on the mechanistic understanding of the chemistry of 1,3-butadiynamides—suggesting that 1,3-butadiynamides are not just simple alkynes. These ethynylogous variants of ynamides have their own molecular character and chemical reactivity and reflect a new class of remarkably useful compounds.

Keywords: 1,3-dynamides; ynamides; alkynes; homogeneous catalysis; heterocycles; annulation reactions; cycloaddition cascade reactions; helical twisted frontier molecular orbitals (Hel-FMO); Hexa-dehydro-Diels–Alder (HDDA) reaction; quinolines; indoles; carbazoles

Citation: Lenko, I.; Alayrac, C.;

Božek, I.; Witulski, B.

1,3-Butadiynamides the

Ethynylogous Ynamides: Synthesis,

Properties and Applications in

Heterocyclic Chemistry. *Molecules*

2023, 28, 4564. [https://doi.org/](https://doi.org/10.3390/molecules28114564)

10.3390/molecules28114564

Academic Editors: Alexey M.

Starosotnikov, Maxim A. Bastrakov

and Igor L. Dalinger

Received: 16 May 2023

Revised: 30 May 2023

Accepted: 1 June 2023

Published: 5 June 2023



Copyright: © 2023 by the authors. Licensee MDPI, Basel, Switzerland. This article is an open access article distributed under the terms and conditions of the Creative Commons Attribution (CC BY) license (<https://creativecommons.org/licenses/by/4.0/>).

1. Introduction

Since the disclosure of a first reliable and widely applicable synthesis of ynamides (*N*-alkynylamides) in 1998 [1], these functionalized acetylenes combining the diverse reactivity of a carbon–carbon triple bond with one of the most important functional groups of organic chemistry—the amino function—found widespread interest within the chemical community. Ynamides distinguish from their long-time known electron-rich variants—the ynamines (*N*-alkynylamines)—by having at least one electron-withdrawing group (EWG) attached to the nitrogen heteroatom. This EWG is capable of serving as a protective group in further chemical manipulations—but most importantly—it guarantees a decent chemical stability of the otherwise electron-rich acetylenic unit by lowering its HOMO. As such, the nitrogen bound EWG decreases the electron density of the adjacent alkyne moiety by inducing a more or less—but significantly—polarized carbon–carbon triple bond (Figure 1). Consequently, this results in tuning reactivity and selectivity. Ynamides are habitually bench-stable functionalized acetylenes that withstand an aqueous work-up procedure as well as purification by column chromatography on silica gel—both important features that are required for being useful molecular building blocks in organic synthesis. Over the years, the chemistry of ynamides became well-recognized. Ynamides nowadays serve as multipurpose substrates in organic synthesis including transition metal, ionic, radical and photoredox-mediated processes leading to *N*-heterocyclic compounds, natural products and other molecular targets for life and material sciences. Their exceptional rich and diverse chemistry covers several review articles [2–16].

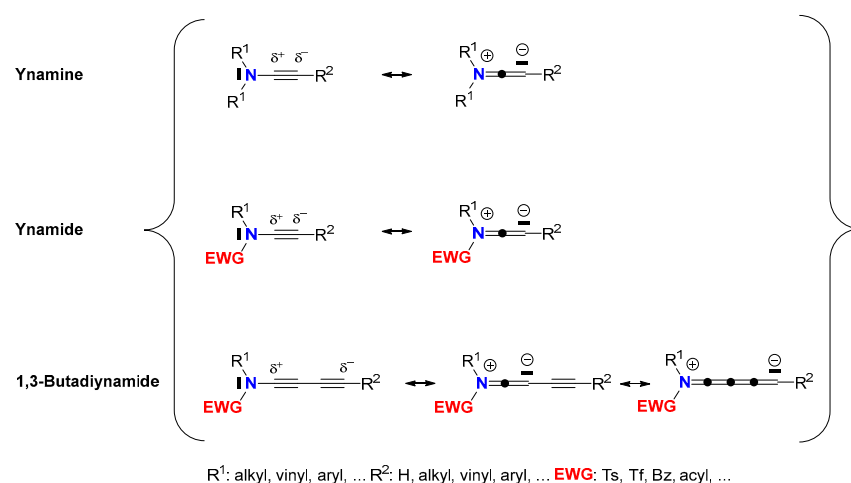
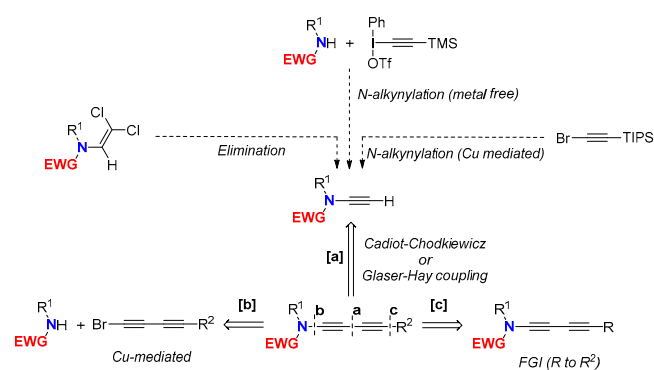


Figure 1. Mesomeric resonance structures of ynamines, ynamides and 1,3-butadiynamides.

More recently, the ethynylogous variants of ynamides—the 1,3-butadiynamides—likewise received considerable attention in organic and heterocyclic chemistry. They found interesting use in transition metal-catalyzed annulation reactions, like the Hexa-dehydro-Diels–Alder (HDDA) reaction [17–21], and as optoelectronic materials due to their underlying push–pull character. Notably, the intrinsic polarization of ynamides is not only preserved in 1,3-butadiynamides. It is furthermore extendable via the ethynylogous principle from a 1,2- to a formal 1,4-polarization. Therefore, 1,3-butadiynamides are appealing for nitrogen-functionalized C4-building blocks for the construction of complex structural motifs. As both triple bonds can be simultaneously or consecutively functionalized via an electrophilic and/or nucleophilic reaction step, the selective introduction of more than one substituent might be achievable selectively. Other important features of molecular 1,3-butadiynamide scaffolds are their facile synthesis and their often superb stability. This not only accounts for 1,4-dynamides, but also for the higher conjugated oligoynamides. Some chemistry associated with 1,3-butadiynamides has been briefly mentioned in reviews covering synthesis and use of ynamines and ynamides [3–5,12–16]. However, there is so far no comprehensive article focusing on the ethynylogous variant of ynamides—the 1,3-butadiynamides. Highlighting the chemistry of 1,3-butadiynamides and compiling their reactivity, specificity and miscellaneous synthetic potential is the purpose of our present review.

2. Synthesis of 1,3-Butadiynamides

The majority of described 1,3-butadiynamides are derived from arylsulfonamides (EWG = Toluenesulfonyl (Ts), Methanesulfonyl (Ms), etc.), and only a few examples rely on carbamates (EWG = CO₂Me) or oxazolidinones. Syntheses of 1,3-butadiynamides follow the basic three retrosynthesis disconnections [a–c] as shortlisted in Scheme 1.

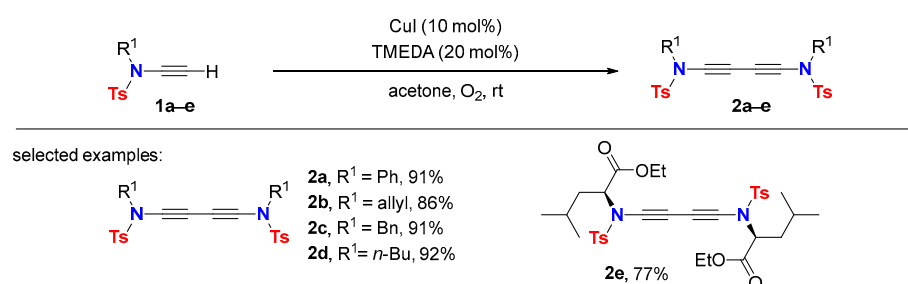


Scheme 1. Retrosynthesis of 1,3-butadiynamide.

2.1. Disconnection [a]: Cu-Catalyzed Cross-Coupling Reactions

Disconnection [a] to 1,3-butadiynamides follows common strategies for the assembly of 1,3-bisacetylenes starting from various terminal acetylenes (Glaser–Hay coupling) or cross-couplings of terminal acetylenes with 1-bromoalkynes (Cadiot–Chodkiewicz reaction). The use of terminal ynamides in copper-catalyzed cross-coupling reactions is the major strategy to access both symmetrical and unsymmetrical 1,3-butadiynamides. The required terminal ynamides are readily available by rendering the synthetic strategies outlined in Scheme 1 [13].

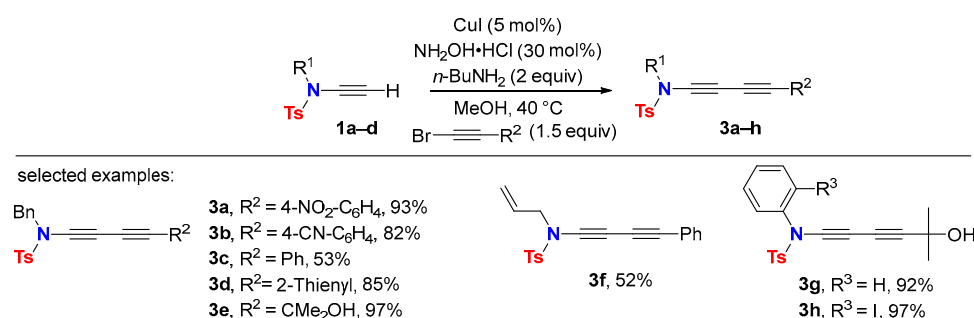
Application of the Glaser–Hay reaction to terminal ynamides proceeds readily affording various sets of symmetrical substituted 1,3-butadiynamides **2a–e** (Scheme 2) [22,23].



Scheme 2. Symmetrical substituted 1,3-diyamides via oxidative Glaser–Hay coupling.

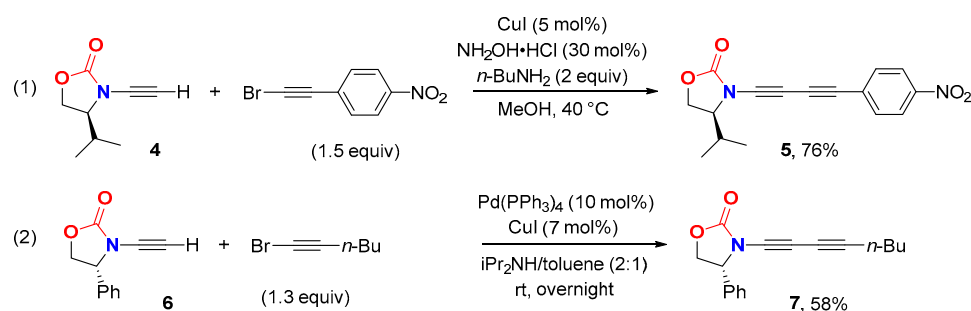
The oxidative homocoupling of terminal ynamides is usually carried out in acetone at room temperature with CuI–TMEDA (tetramethylethylenediamine) as the catalyst and by exposure to atmospheric oxygen. It is also applicable to chiral amino acid-derived terminal ynamides to deliver 1,3-diyamide **2e** [24].

Unsymmetrical 1,3-butadiynamides **3a–h** are available via the Cadiot–Chodkiewicz cross-coupling between terminal ynamides and 1-bromoalkynes (Scheme 3) [25,26]. Reactions are usually performed in methanol at 40 °C and require copper(I) iodide as the catalyst, *n*-butylamine as the base and sub-stoichiometric quantities of hydroxylamine hydrochloride. The use of the latter is crucial to avoid ynamide homocoupling by reducing any copper(II) salts present in the reaction medium. Notably, the complementary approach utilizing bromine- or iodine-terminated ynamides with terminal acetylenes was unsuccessful so far. This is reasoned by the fact that bromine- or iodine-terminated ynamides are difficult to obtain and are quite unstable [27].



Scheme 3. 1,3-Butadiynamides via Cadiot–Chodkiewicz cross-coupling reaction.

The Cadiot–Chodkiewicz reaction with *N*-ethynylated oxazolidinone **4** is also suitable for the synthesis of oxazolidinone-2-one-derived 1,3-butadiynamides, which, for example, delivers the chiral push–pull 1,3-butadiynamides **5** in high yields (Scheme 4, (1)) [25].

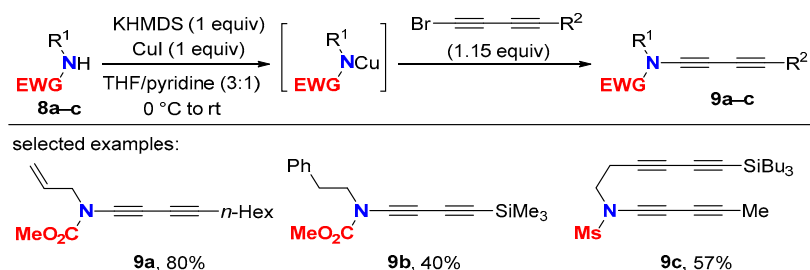


Scheme 4. Synthesis of oxazolidine-2-one-derived 1,3-butadiynamides.

Furthermore, but limited in scope, the palladium-mediated cross-coupling of ynamide **6** with 1-bromohexyne in (*i*-Pr)₂NH/toluene (2:1 (*v/v*)) gives the corresponding 1,3-butadiynamide **7** via a Sonogashira type reaction (Scheme 4, (2)) [28].

2.2. Disconnection [b]: Amide *N*-Alkynylations

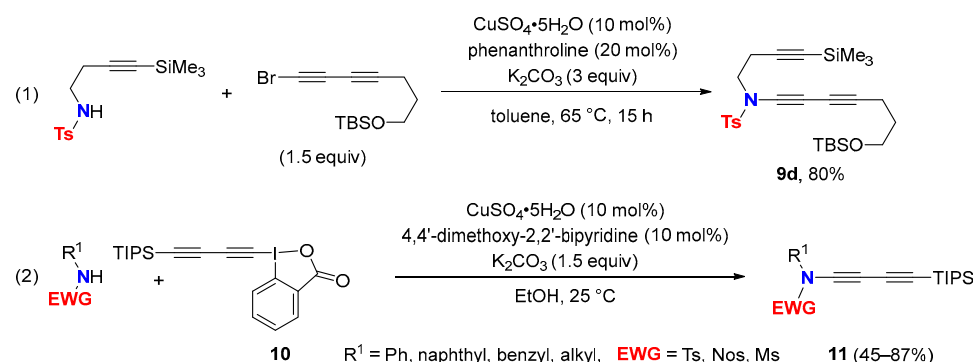
In analogy to related ynamide approaches, the synthesis of 1,3-butadiynamides via a copper-mediated C-N bond formation between suitable amides and 1-bromo-1,3-butadiynes was described, though only a few examples have been realized so far. Here, the stabilization of the acting copper amide complex prior to the coupling with the 1-bromo-1,3-diyne is mandatory. This is necessary to overpower the quite facile homocoupling of 1-bromodiyne (Scheme 5) [29,30]. C-N bond formation takes place at room temperature, but the drawbacks of requiring stoichiometric amounts of copper iodide and the need of high-quality pyridine should be taken into consideration. Indeed, the use of dry pyridine, freshly distilled over CaH₂ under inert atmosphere, is required. The reaction conditions are also suitable for and were applied in the synthesis of the *N*-methanesulfonyl 1,3-butadiynamide **9c** (EWG = Ms) [31].



Scheme 5. Synthesis of 1,3-butadiynamide via Cu-mediated C-N bond formation.

Ynamide syntheses relying on sub-stoichiometric amounts of copper sulfate/1,10-phenanthroline as the catalyst in toluene at 60–95 °C [32] were extended to gain access to 1,3-butadiynamides. Efficiency, however, is lower compared to the protocol leading to carbamate-derived 1,3-butadiyne **9a** via stoichiometric amounts of copper salt (36 vs. 80% yield) [29]. Notably, *N*-alkyl *N*-tosylamides are better substrates, and the synthesis of *N*-tosyl-1,3-butadiynamide **9d** proceeds with high yields under copper-catalyzed cross-coupling conditions (Scheme 6, (1)) [33].

It is worth noting that the synthesis of *N*-aryl *N*-toluenesulfonyl ynamides ($R^1 = Ar$) via copper-catalyzed C-N bond-forming protocols with 1-bromo alkynes does not proceed at all, or proceeds in very low yields after several days of heating [34]. Probably, this is due to the weaker nucleophilicity of *N*-aryl *N*-toluenesulfonylamides. Therefore, the Cadiot–Chodkiewicz reaction with terminal ynamides remains the state of the art to obtain 1,3-diyne derivatives having an *N*-aryl group. However, more recently, a copper-catalyzed electrophilic *N*-1,3-diyne synthesis with triisopropylsilyl 1,3-diyne benziodoxolone (**10**) was described to give straightforward TIPS protected 1,3-butadiynamides **11** including examples with *N*-aryl tosylamides (Scheme 6, (2)) [35].

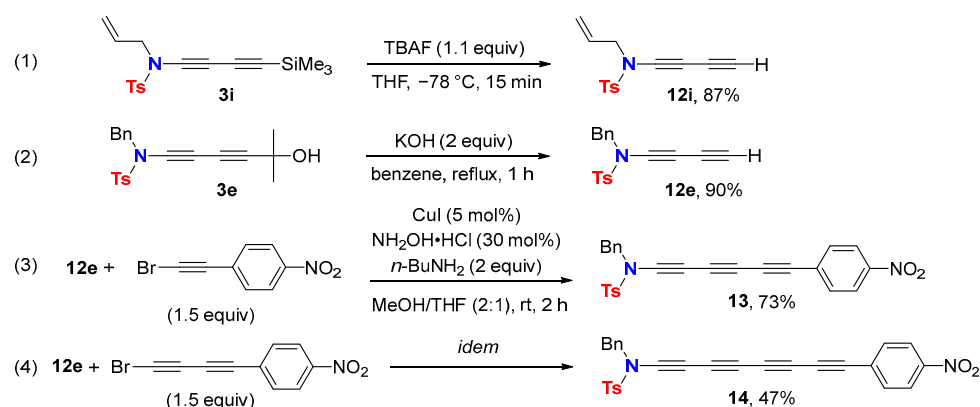


Scheme 6. Copper-catalyzed synthesis of 1,3-butadiynamides.

2.3. Disconnection [c]: Functional Group Interconversion (FGI) at the C-Terminus

Chemical modifications of ynamides without affecting the triple bond have been scarcely explored until recently [13]. In the case of 1,3-butadiynamides, examples of modifications of the C-terminus are even fewer.

The synthesis of a terminal 1,3-butadiynamide through desilylation of the corresponding trimethylsilyl protected precursor with tributylammonium fluoride (TBAF) at $-78\text{ }^{\circ}\text{C}$ in dry THF proceeds in high yield (Scheme 7, (1)) [36]. Alternatively, access to terminal 1,3-butadiynamides is provided under basic conditions starting from the parent 1,3-butadiynamide terminated by the acetone adduct (Scheme 7, (2)) [25].



Scheme 7. Modification of the 1,3-butadiynamide C-terminus.

1,3-Butadiynamide synthesis followed by transformation to a terminal 1,3-butadiynamide via protective group strategies allows for the development of iterative Cadiot–Chodkiewicz couplings to higher order ethynylogous ynamides. Such iterative cross-couplings offer a straightforward entry to conjugated tri- and tetraynamides **13** and **14** using as coupling partners diynamide **12e** and a 1-bromoalkyne or a 1-bromo-1,3-diyne, respectively (Scheme 7, (3) and (4)) [25].

3. Molecular Structure and Electronic Properties

1,3-Butadiynamides and their higher homologues not only gain interest as molecular building blocks in organic synthesis, but they also receive considerable attention for their unique conformation on basis of principal helical twisted molecular orbitals delocalized over the entire conjugated carbon rod, with their optoelectronic properties including NLO performance, and their possible function as molecular wire or as monomer in solid-state topo-chemical polymerizations.

Whilst axial chirality in certain odd numbered cumulenes like allenes is well-documented, the understanding of chirality based on helical twisted frontier molecular orbitals (Hel-FMO) and its impact on chemical, optical and physical properties is still in its early infancy.

Markedly, it is mainly limited to the theoretical and computational description of conjugated cumulenes [37,38], spiroconjugated systems [39] and suitable extended conjugated oligoynes (ECOs) [40–43]. The latter favor a twisted near orthogonal conformation caused by the combination of repulsive interactions between the terminating functional groups and the constructive orbital overlap upon twisting. Nitrogen atom-terminated oligoynes are predicted of being important members of the ECO family because of both being stable and having helical molecular orbitals delocalized over the entire conjugated polyynes carbon rod (Figure 2).

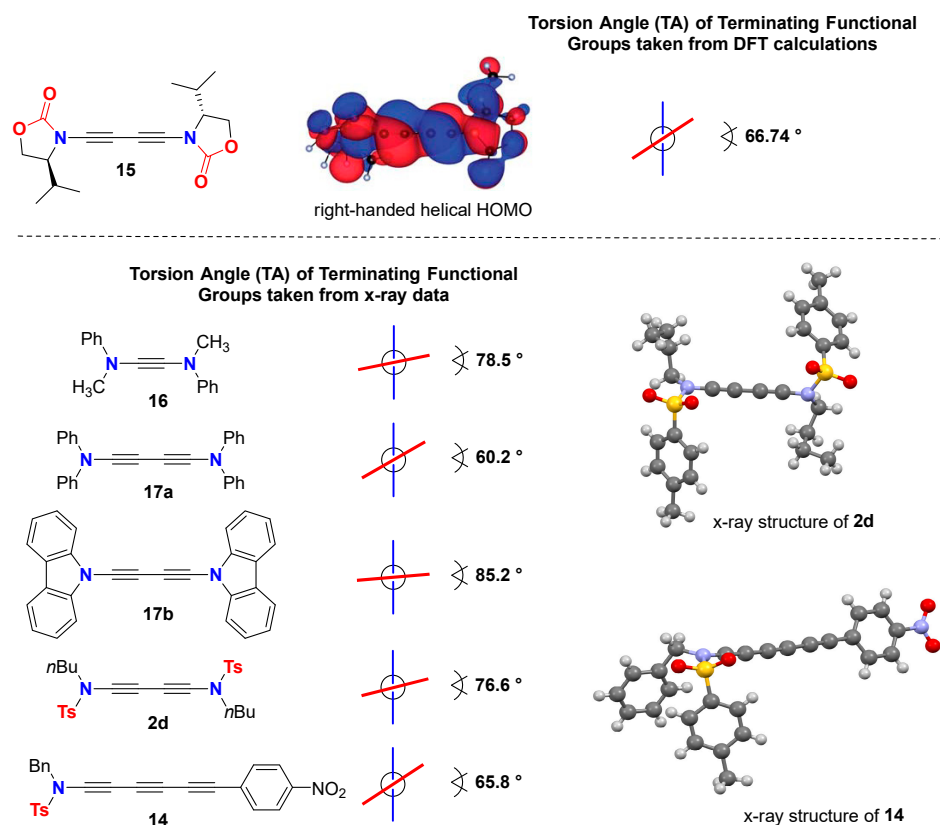


Figure 2. Helical twisted molecular orbitals in extended conjugated oligoynamides.

For example, the high-level density functional theory (DFT) calculation of the still unknown—but synthetically feasible—diynamide **15** predict helical twisted molecular frontier orbitals with axial chiral geometry [41]. For the 1,3-diynamide **15**, a torsion angle (TA) of TA = 66.74° was calculated together with a right-handed helical HOMO (Figure 2). Notably, similar values of TAs can be found in the single crystal structure data of the ynamine **16** (TA = 78.5°) [44], the 1,3-diynamines **17a** (TA = 60.2°) [45] and **17b** (TA = 85.2°) [46], the 1,3-diynamide **2d** (TA = 76.6°) [23] and the 1,3,5-triynamide **14** (TA = 65.8°) [25]. Although these data are taken from solid-state structures, and conformational changes due to crystal structure-packing effects cannot be neglected, all TAs are of similar magnitudes and underline the influence of helical twisted molecular orbitals on the conformational output of 1,3-diynamides and their higher homologues.

A set of donor- π -spacer-acceptor “push-pull” ynamides end-capped with nitrogen donor and 4-nitro or 4-cyanophenyl acceptor units was investigated by the electro-optical absorption method (EOAM). The aim of the study was to examine their intramolecular charge transfer (ICT) properties in relation to the extent of the spacing-conjugated oligoyne units [25]. Dipole moments in solution of the ground (μ_g), the Franck–Condon excited state ($\mu_{\epsilon}^{\text{FC}}$) and their respective change of dipole moment ($\Delta^a\mu$) were obtained. Values of dipole moments for measurements in 1,4-dioxane of selected *para*-nitro-phenyl substituted ynamide derivatives are compiled in Table 1. The observed very high values for the

change of dipole moments after transition from the ground to the Franck–Condon excited state show effective ICTs and consequently potential non-linear optical properties for these electronically tunable, extended, conjugated oligoynamides. Notably, the increase of change of dipole moments reaches a maximum for push–pull 1,3-diyynamides with two spacing-conjugated alkyne units. Elongation of the conjugated alkyne units from one to two triple bonds results in an increase of the $\Delta^a\mu$ values, while the ground-state dipole moments μ_g are almost unaffected. Increasing to three conjugated alkyne units, however, leads to a decrease of $\Delta^a\mu$ (Figure 3).

Table 1. Electrooptical absorption measurement (EOAM) of selected “push–pull” ynamides end-capped with a nitrogen donor and a 4-nitro-phenyl acceptor unit [25].

Ynamide	μ_g	$\Delta^a\mu$	μ_a^{FC}
		[10 ^{−30} Cm] in 1,4-dioxane	
	9.7	74.6	84.3
	9.5	92.3	101.8
	10.9	30.8	41.7
	11.8	69.7	81.5

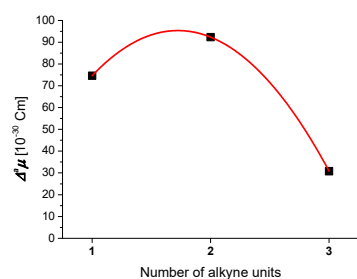


Figure 3. Correlation of the number of alkyne units in ynamides with the magnitude of change of dipole moment from ground to Franck–Condon excited state $\Delta^a\mu$.

Topochemical solid-state polymerization of 1,3-diacetylenes in single crystals gives conjugated polymers that have attracted attention on their physical properties such as conductivity, optical nonlinearity and mechanical strength. Consequently, 1,3-butadiynamides that are often crystalline materials were also investigated in topochemical polymerizations [23,47,48].

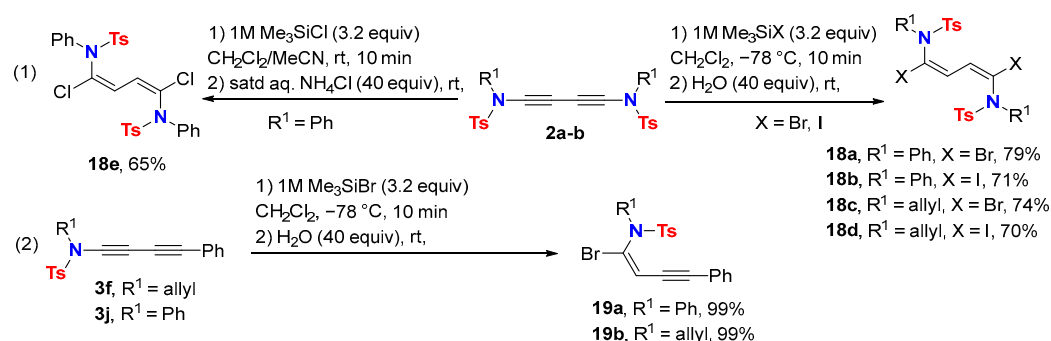
4. Addition, Cycloaddition and Oxidation Reactions

Non-symmetrical 1,3-butadiynamides—unlike their symmetrical counterparts—often act as internal ynamides. In many examples of addition and cycloaddition reactions, the 1,2-activation of the 1,3-diyne is superior to the 1,4-activation, and the second triple bond remains unaffected in the underlying transformation. However, in view of the richness of acetylene chemistry, the obtained products can often undergo further chemical transformations, broadening the array of available molecular and heterocyclic structures.

4.1. Addition Reactions

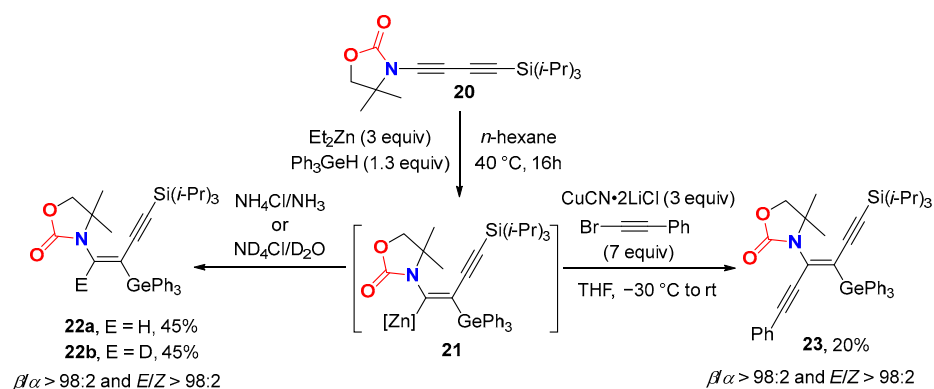
Stereodefined 1,3-dienes bearing *N*-substituents are important building blocks in organic synthesis. Simple access to versatile 1,4-dihalogenated *E,E*-1,4-dienamides was

achieved from readily available symmetrical 1,3-butadiynamides **2a–b** in regio- and stereoselective hydrohalogenations (Scheme 8, (1)) [49].



Scheme 8. Regio- and stereoselective hydrohalogenation of 1,3-butadiynamide.

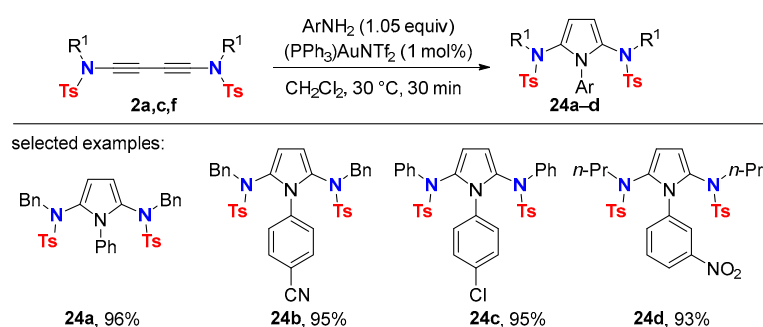
Hydrogen halides are generated in situ from halotrimethylsilane (Br, I) and water–or chlorotrimethylsilane and saturated ammonium chloride. Under these conditions, the perfect *syn*-addition of H-X (X = Cl, Br) across the ynamide triple bond occurs. The hydrobromination of non-symmetrical 1,3-butadiynamides **3f,j** ensues only on the triple bond linked to the nitrogen atom, i.e., the more electron-rich carbon-carbon triple bond, affording the 1-en-3-ynamides **19a–b** (Scheme 8, (2)). Notably, the hydrobromination of 1,4-diphenyl-butadiyne does not occur under similar reaction conditions. Gernylzincation of 1,3-butadiynamide **20** was achieved with excellent regio- and stereoselectivity using a combination of hydrogermanes and ZnEt₂ (Scheme 9) [50].



Scheme 9. Radical gernylzincation towards stereodefined ynenamides.

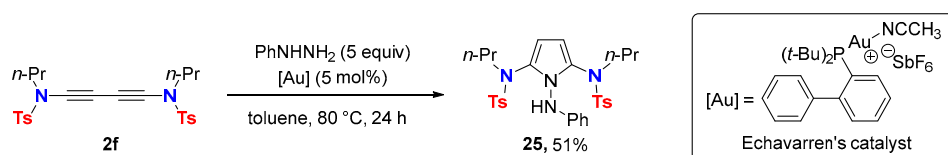
Addition of germanium did not occur in the absence of Et₂Zn. The proposed mechanism involves the addition of a germanium-centered radical across the triple bond on β -position to the *N*-atom in agreement with the underlying polarization of the 1,3-butadiynamide. The resulting α -heteroatom-substituted vinyl radical undergoes ethylzinc group transfer to give the β -zincated vinylgermane **21** along with an ethyl radical keeping the radical chain propagation. The (*E*)-form of the vinylgermane radical is favored. Retention of the double bond geometry of the vinylzinc intermediate **21** is observed upon hydrolysis or Cu(I)-mediated C-C bond formation with 1-bromophenylacetylene. The resulting stereodefined tri- and tetrasubstituted ynenamides **22a–b** and **23** can be further functionalized through displacement of germanium. Vinylgermanes gain increasing attention as alternatives to vinylsilanes and vinylstannanes for the preparation of stereodefined alkenes because of their low toxicity, increased stability towards protonolysis and facile transformation into vinyl halides.

Gold-catalyzed double hydroaminations of symmetrical substituted 1,3-butadiynamides **2a,c,f** with anilines readily proceed at room temperature and deliver the corresponding 2,5-diamido-*N*-arylpyrroles **24a–d** (Scheme 10) [51].



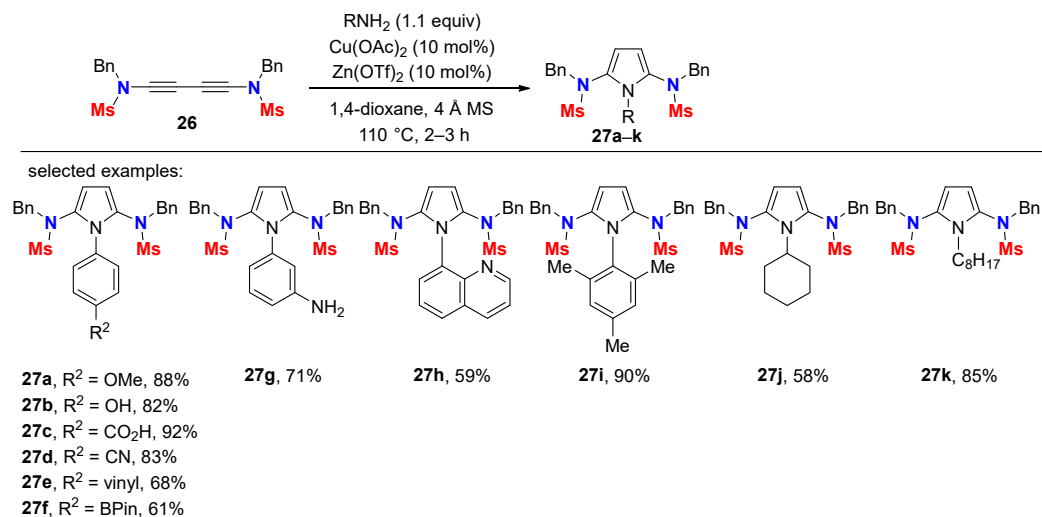
Scheme 10. Gold-catalyzed synthesis of 2,5-diamidopyrroles.

Moreover, the 1,2,5-trisubstituted pyrrole **25** is accessible by using phenylhydrazine as the hydroamination reagent. In this case, thermal activation is required, as well as the use of the more reactive Echavarren's gold catalyst derived from the bulky and electron-rich di-*t*-butylphosphinobiphenyl ligand (Scheme 11) [51].



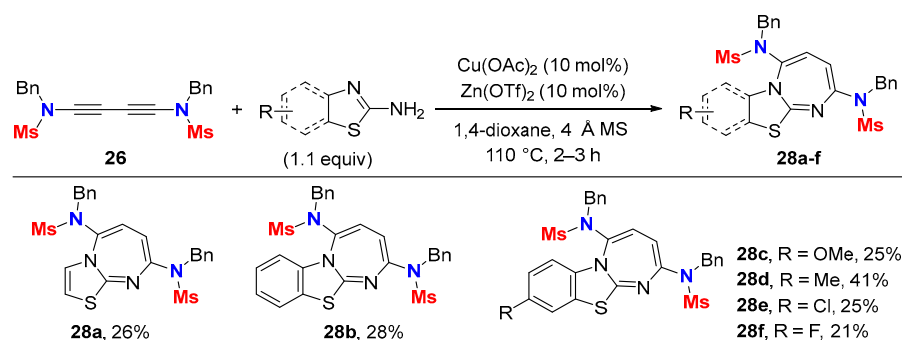
Scheme 11. Gold-catalyzed synthesis of a 1,2,5-trisubstituted pyrrole with phenylhydrazine.

Copper catalysis in the presence of a zinc additive is also effective in the pyrrole series and proceeds with excellent functional group tolerance [52]. In comparison to the gold-catalyzed protocol, the scope of 2,5-diamidopyrroles available from 1,3-butadienylidene di-N-mesitylamides is considerably broadened as primary aliphatic amines, and sterically hindered anilines are now suitable hydroamination reagents (Scheme 12).



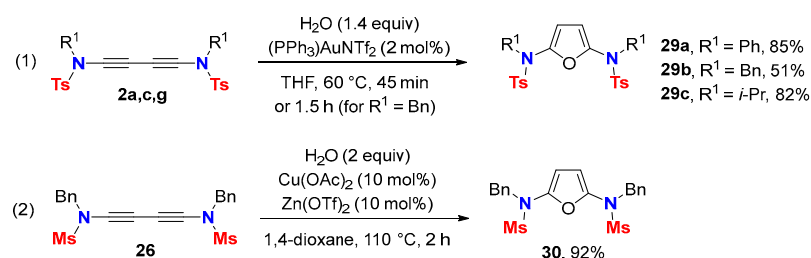
Scheme 12. Copper-catalyzed synthesis of 2,5-diamidopyrroles.

Interestingly, the copper-catalyzed reaction of 1,3-butadienylidene di-N-mesitylamide **26** with 2-amino (benzo)thiazoles as nucleophiles does not deliver pyrrole derivatives. Now, fused diazepines **28a–f** are formed via a formal [4+3] annulation sequence (Scheme 13) [52].



Scheme 13. Copper-catalyzed synthesis of diazepines derived from 1,3-diyne.

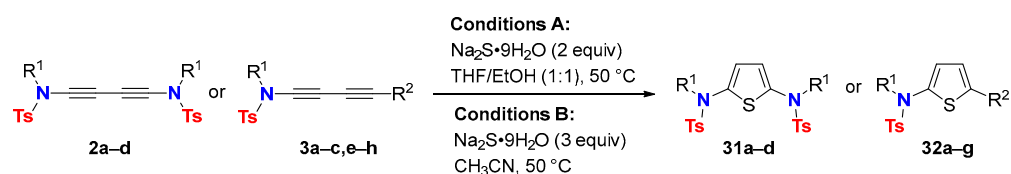
Symmetrical substituted 1,3-butadiynamides also serve as substrates in gold catalyzed hydration leading to the 2,5-diamidofurans **29a–c** (Scheme 14, (1)) [51]. Interestingly, the dimethanesulfonyl analogue of **29b**—the 2,5-diamidofuran **30**—was obtained in a better yield using a copper(II) catalyst in the presence of a zinc additive (Scheme 14, (2)) [52].



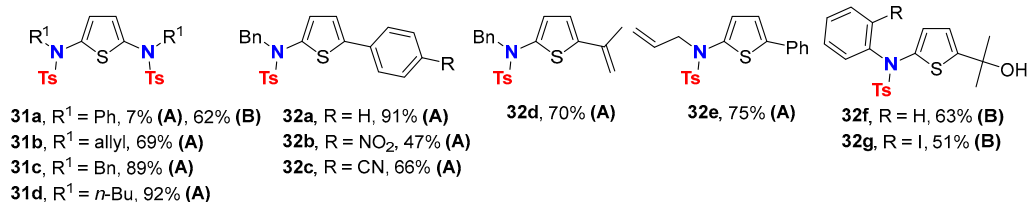
Scheme 14. Gold- or copper-catalyzed synthesis of 2,5-diamidofurans.

The metal-catalyst-free synthesis of 2,5-diamidothiophenes **31a–d** using 1,3-butadiynamides **2a–d** and $\text{Na}_2\text{S}\cdot 9\text{H}_2\text{O}$ as the sulfur-providing source proceeds under very mild conditions (Scheme 15, Conditions A) [26]. Both symmetrical as well as the non-symmetrical 1,3-diyne units undergo a formal 1,4-functionalization of the parent 1,3-diyne unit. In the case of diyne **2a** ($\text{R}^1 = \text{Ph}$), whose electrophilicity is enhanced by conjugation of the ynamide unit with the *N*-phenyl group, these reaction conditions were not suitable. This is probably because of side reactions resulting from the addition of ethanol across the triple bond. Switching to acetonitrile as the solvent was the key for success (Conditions B). Now, the corresponding thiophene **31a** is obtained in 62% yield. Importantly, the method is likewise effective with unsymmetrical 1,3-butadiynamides **3a–c,e–h** giving a straightforward entry to variously functionalized 2-amidothiophenes **32a–g** (Scheme 15).

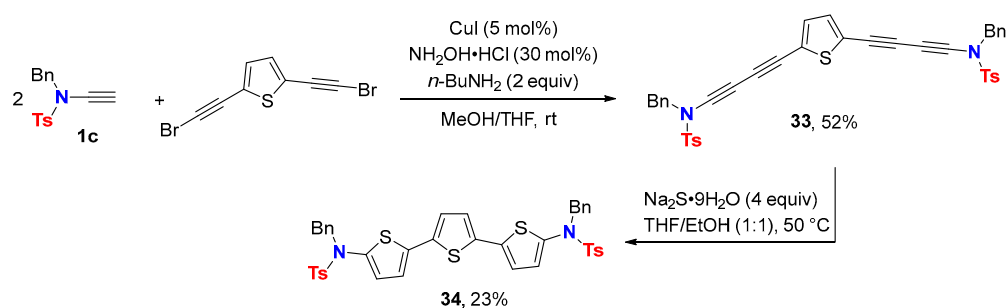
This new approach to 2-amido- or 2,5-diamidothiophenes is extendable to the synthesis of terthiophenes (Scheme 16). The required tetrayne **33** bearing two linked 1,3-diyne units is accessible via a double Cadiot–Chodkiewicz coupling between a terminal ynamide and bis(bromoalkynyl)thiophene. Application of the developed reaction conditions to substrate **33** delivers the diamido-capped terthiophene **34** having a string of *N,S* heteroatoms embedded in a highly π -conjugated molecular scaffold. Electron-rich terthiophenes are interesting as active materials in organic electronics such as organic transistors or organic photovoltaic cells.



selected examples:



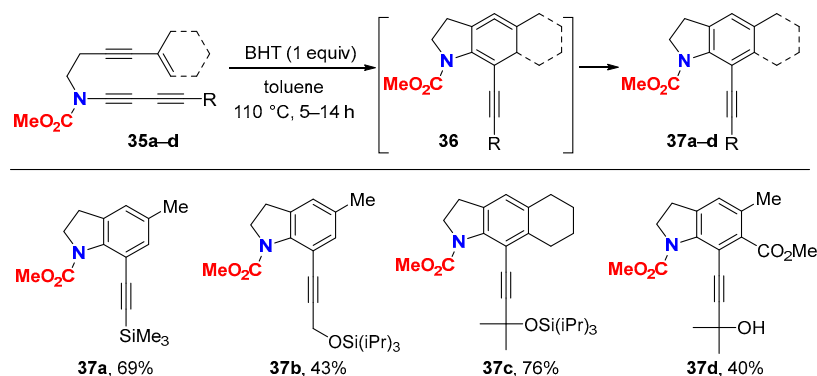
Scheme 15. Metal-catalyst-free synthesis of 2-amido- and 2,5-diamidothiophenes.



Scheme 16. Synthesis of a terthiophene.

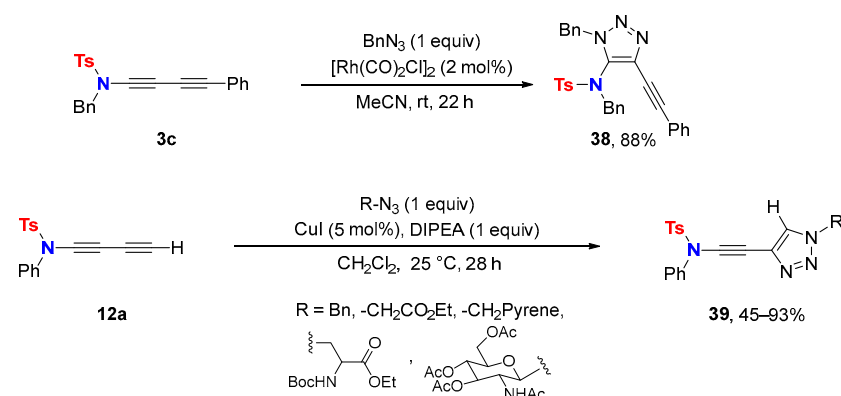
4.2. Cycloaddition Reactions

Intramolecular [4+2] cycloadditions of 1,3-butadiynamides **35a–d** tethered to an enyne moiety furnish functionalized 7-alkynyl indolines **37a–d** (Scheme 17) [53]. Yields improve in the presence of BHT, which not only suppresses the polymerization of enyne substrates, but also facilitates the isomerization of the cyclic allene intermediate **36** into indoline **37** via proton/hydrogen atom transfer. As alkyl-substituted ynamides with only one C–C triple bond give low yields in related [4+2] cycloadditions, the hydrogenation of the triple bond of indolines **37a–d** is an alternative and offers a valuable entry to the parent alkyl-substituted indolines. In these Didehydro–Diels–Alder (DHDA) reactions the 1,3-butadiynamide serves as the formal dienophile. Notably, this has to be distinguished from its use in Hexa-Dehydro-Diels–Alder (HDDA) reactions that will be discussed in Chapter 6, where the 1,3-butadiynamide unit functions as the formal 4π cycloaddition partner.



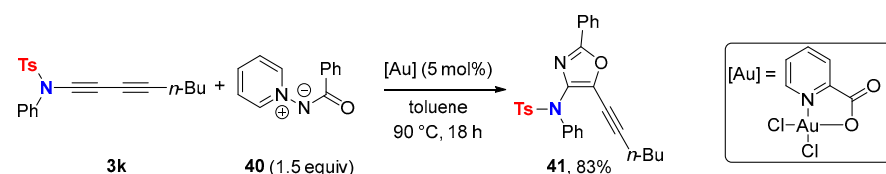
Scheme 17. Intramolecular [4+2] cycloaddition with 1,3-butadiynamides to give 7-alkynyl indolines via DHDA reaction.

Azide-alkyne [3+2] cycloadditions of 1,3-butadiynamide **3c** using rhodium catalysis afford 4-alkynyl 5-amino-triazole **38** [54], whereas the copper-catalyzed addition of azides to terminal 1,3-butadiynamides provide alternative ynamide-derived azide-alkyne click-products **39** (Scheme 18) [35]. Click reactions with 1,3-diyndamides are exclusively chemo- and regioselective with stoichiometric amounts of azides. The exclusion of air and moisture is unnecessary in the case of the rhodium catalysis, whereas high yields in copper-mediated azide-alkyne [3+2] cycloadditions are obtained only under strict anhydrous conditions.



Scheme 18. Intermolecular azide-alkyne [3+2] cycloaddition with 1,3-butadiynamides to give 4-alkynyl triazoles.

The gold-catalyzed cycloaddition of 1,3-butadiynamide **3k** with aminide **40** as *N*-acyl nitrene equivalent gives 5-alkynyl oxazole **41** as a single regioisomer in 83% yield (Scheme 19) [55]. This formal [3+2] cycloaddition is based on the use of the robust and air-stable dichloro(pyridine-2-carboxylato)gold(III) complex as a pre-catalyst.



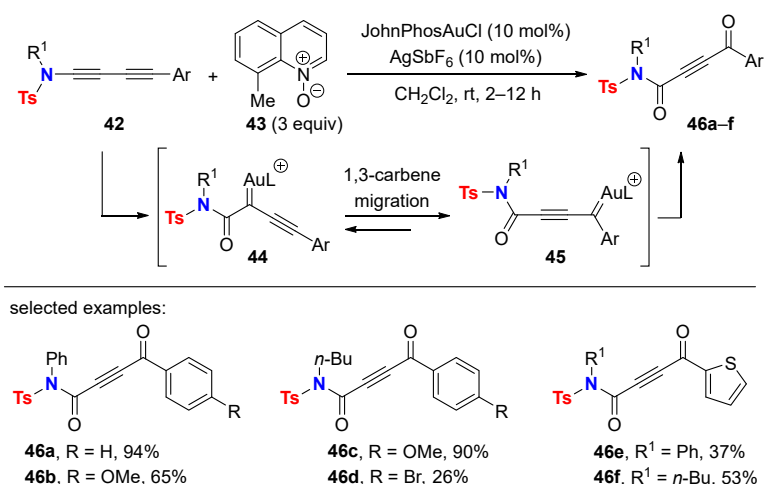
Scheme 19. Intermolecular [3+2] cycloaddition of aminide **40** to 1,3-butadiynamide **3k** to give 5-alkynyl oxazole **41**.

4.3. Oxidation Reactions

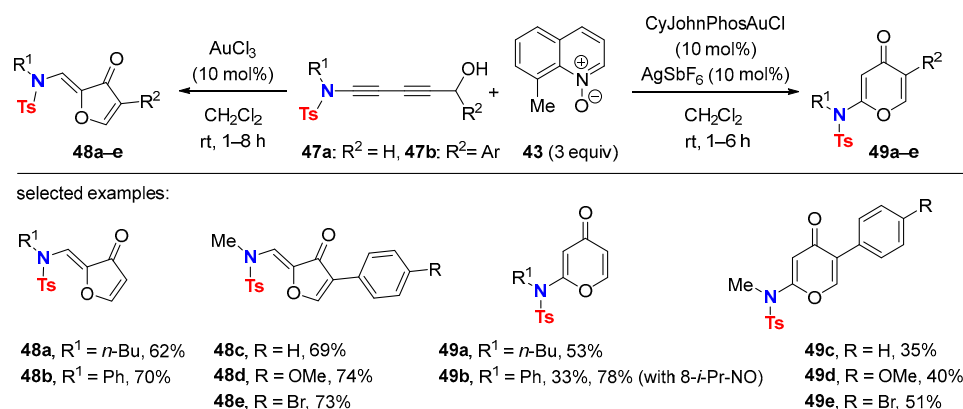
The catalytic oxidation of aryl 1,3-butadiynamides **42** with 8-methylquinoline oxide (**43**) using a cationic gold catalyst in the presence of a silver salt delivers the 1,4-oxidation products **46** (Scheme 20) [56].

In agreement with other gold-catalyzed oxidations of ynamides with pyridine *N*-oxides, a striking chemoselectivity for C(1) oxidations is observed leading to the α -carbonyl gold carbene intermediate **44**, which, in the case of the ethynylogous ynamide, undergoes a 1,3-carbene migration affording intermediate **45** [57]. The 1,3-migration tautomer **45** is then further oxidized to give the double oxidation products **46**. Finally, this oxidative process results in a 1,4-functionalization of the 1,3-diyndamide moiety.

Interestingly, a different chemical outcome is observed with 5-hydroxy-1,3-butadiynamides **47a–b**, which refrain from C(1) oxidation. Here, an atypical C(3) oxidation and a further gold-mediated oxidative cyclization lead to either furan-3-ones **48a–e** or to pyran-4-ones **49a–e** with AuCl₃ and CyJohnPhosAuCl/AgSbF₆, respectively (Scheme 21) [56]. The formation of pyran-4-ones **49** from the less basic *N*-phenyl *N*-toluenesulfonylamide-derived substrates **47** (R¹ = Ph) is more efficient with 8-*iso*-propylquinoline oxide, which is illustrated in the synthesis of product **49b** with 78 vs. 33% yield. Importantly no exchange between the two cyclic ketones occurs in the presence of the gold catalysts.

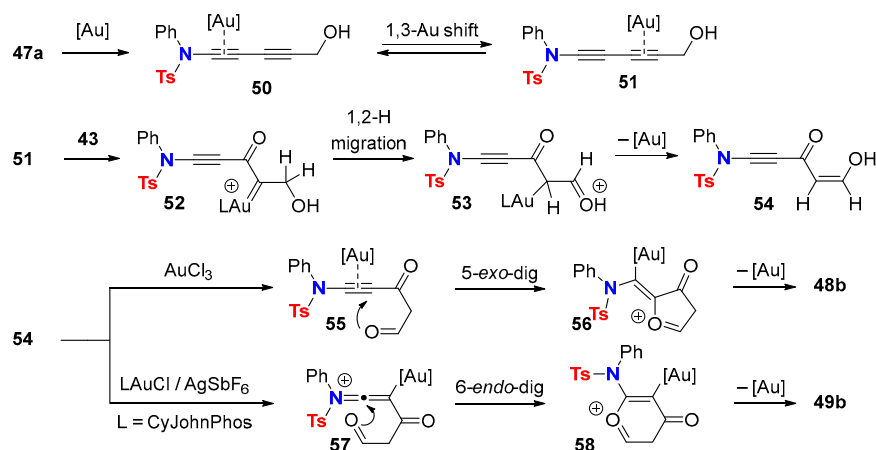


Scheme 20. Au(I)-catalyzed 1,4-oxidation of 1,3-butadienamides.



Scheme 21. Au(I)- and Au(III)-mediated oxidative cyclization of 5-hydroxy-1,3-butadienamides.

DFT calculations support a mechanism for the chemoselective conversion of **47a** (R¹ = Ph, R² = H) into cyclic ketones **48b** or **49b** (Scheme 22).



Scheme 22. Proposed mechanism for the Au-catalyzed oxidative formation of cyclic ketones.

The gold π -complexed alkynes **50** and **51** in Scheme 22 are interconvertible. The 1,4-functionalization through the oxidation at C(3) relies on an energetically favored complex **51** in comparison to **50** because the energy barrier of the oxidation of **51** with 8-methylquinoline oxide (**43**) is calculated as lower. The resulting α -oxo gold carbene **52** undergoes 1,2-hydride migration leading to intermediate **53**, which evolves to the 3-oxo-5-enol intermediate **54** by

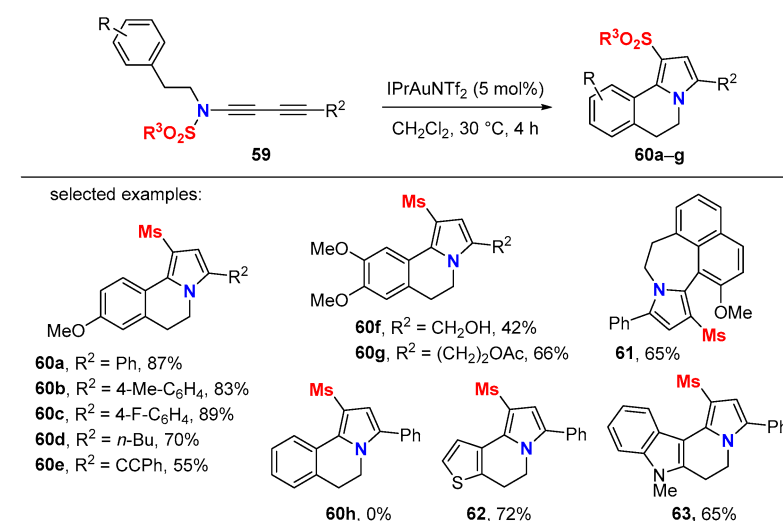
releasing a gold species. Complexation of the triple bond of **54** with less alkynophilic (more Lewis acidic) Au(III)Cl₃ induces an intramolecular carbonyl addition to the alkyne moiety via a 5-exo-dig cyclization. The latter affords intermediate **56**, whereas the formation of a keteniminium species **57** in the case of the cationic gold catalyst facilitates 6-endo-dig cyclization to give intermediate **58**. A mechanism for the transformation of the 1,3-diyynamide **47b** bearing an *aryl*-substituted hydroxy moiety was unfortunately not provided by the authors. The structure of the corresponding products **48c–e** and **49c–e**, however, suggests that a less often observed 1,2-aryl migration takes place [58]. This might also explain the net result with substrate **47** bearing an *alkyl*-substituted hydroxy moiety. The migratory aptitude of an alkyl group to an electron deficient center typically follows the order H > Ph > alkyl.

5. Metal-Catalyzed Cascade-Type Cyclization and Annulation Reactions

5.1. Intramolecular Processes

The activation of 1,3-butadiynamides with transition metal π -acids to form keteniminium ions provide superb opportunities of cascade-type cyclization and annulation reactions. For intramolecular processes, only gold catalysts have been used so far [59]. The involved gold catalysts often vary according to the 1,3-butadiynamides or to the reaction conditions applied.

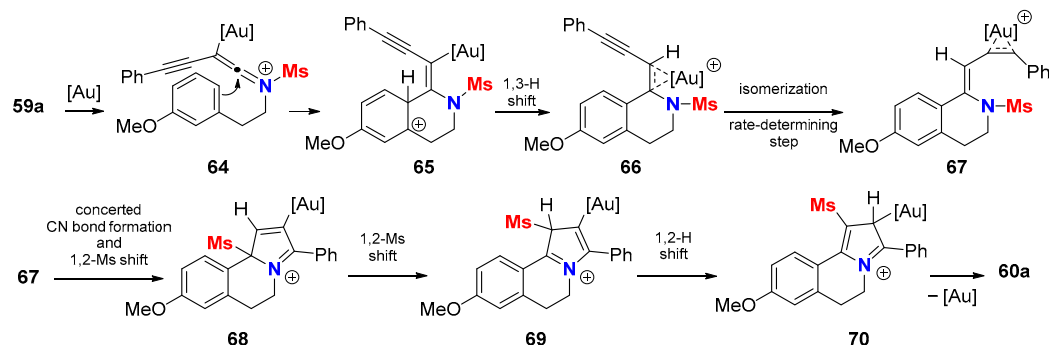
1,3-Butadiynamides **59** that are linked via the ynamide nitrogen by a two carbon tether to electron-rich benzenes or electron excess heteroaromatics readily undergo a gold-catalyzed cascade reaction with IPrAuNTf₂ (IPr = 1,3-bis(diisopropylphenyl)imidazole-2-ylidene), leading to sulfone-containing pyrrolo[2,1-*a*]tetrahydroisoquinolines **60a–g** (Scheme 23) [60]. The cationic nature of the gold catalyst is crucial. The counter anion NTf₂[−] acts as a proton transfer shuttle and facilitates the overall process, which notably involves a formal 1,4-sulfonyl migration. No reaction takes place in the absence of an electron-donating group on the phenyl ring (see **60h**). This stands for the electrophilic aromatic substitution step within the reaction cascade. Further functional groups susceptible to react with the gold catalyst, such as alkyne, hydroxy or acetate groups, are tolerated (see **60e–g**). Remarkably, other structural motifs are also accessible through this process, such as the pyrrolo-azepine **61** or the heterocyclic systems **62** and **63**.



Scheme 23. Gold-catalyzed synthesis of sulfone-containing pyrrolo[2,1-*a*]tetrahydroisoquinolines.

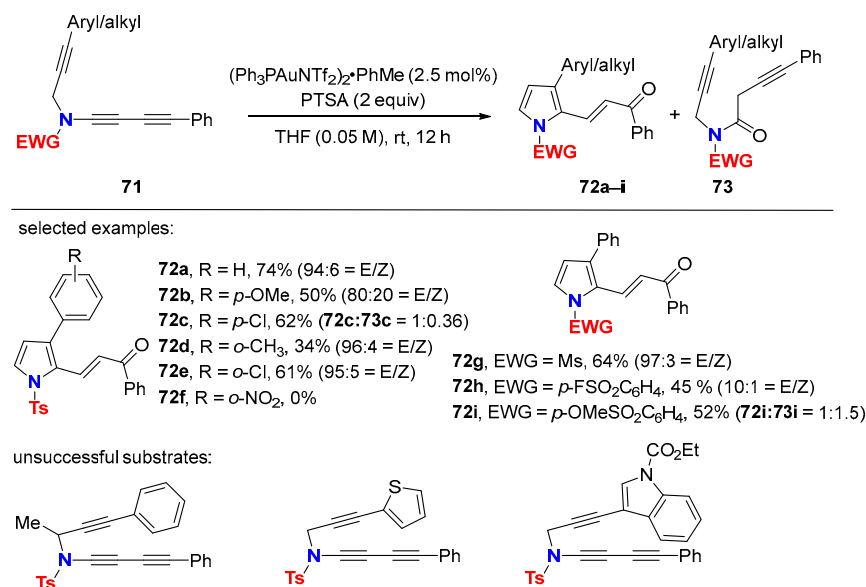
The main intermediates involved in this cascade reaction find support from DFT calculations (Scheme 24). The gold keteniminium species **64** resulting from a regioselective attack of the electrophilic gold catalyst to the 1,3-diyynamide moiety undergoes an intramolecular arylation (Vilsmeier–Haack-type reaction) followed by re-aromatization through a 1,3-H shift mediated by the counter anion NTf₂[−] to deliver intermediate **66**.

The isomerization of *cis*-**66** to *trans*-**67** required for the second annulation process is the proposed rate-determining step. This second cyclization takes place via a concerted C-N bond formation and includes a 1,2-methanesulfonyl-(Ms) migration to give intermediate **68**. A second 1,2-Ms shift followed by a 1,2-H shift, which is greatly facilitated by the counter anion NTf₂[−], delivers intermediate **70**, which finally furnishes product **60a** after demetallation.



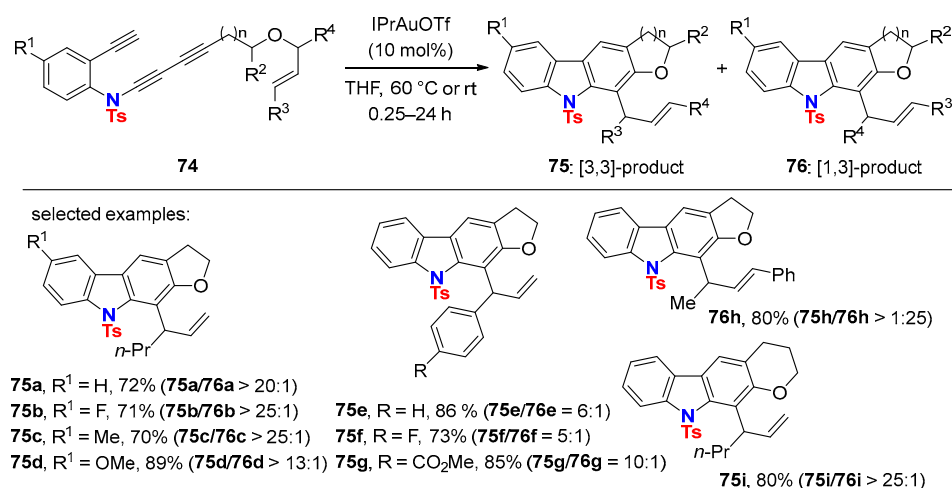
Scheme 24. Proposed mechanism for the gold-catalyzed transformation of 1,3-butadienyl amides into sulfone-containing pyrrolo[2,1-*a*]tetrahydroisoquinolines.

A related gold(I)-catalyzed *para*-toluenesulfonic acid (PTSA) promoted cycloisomerization of 1,3-dienamides **71** gives access to α,β -unsaturated ketones **72** together with minor amounts of the 1,3-dienamide hydration product **73** (Scheme 25) [61]. The studied transformation was limited to 1,3-dienamides terminated with a phenyl group, and the other substitution pattern was incompatible mismatched with the desired reactivity.



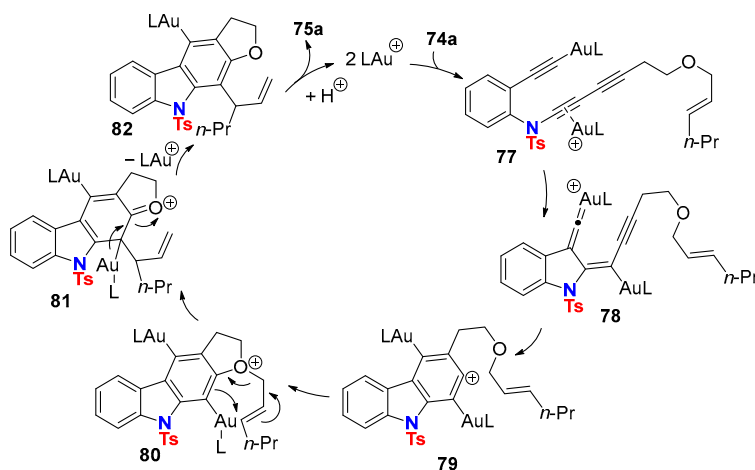
Scheme 25. Gold(I)-catalyzed *para*-toluenesulfonic acid (PTSA) promoted the cycloisomerization of 1,3-dienamides to α,β -unsaturated ketones.

C-terminal-functionalized 1,3-butadienyl amides **74** linked to a terminal alkyne and an allylic ether were used in a reaction cascade involving a dual gold-catalyzed process. The reaction cascade includes an intramolecular carboalkoxylation and a subsequent charge-accelerated [3,3] sigmatropic rearrangement to deliver carbazoles **75** as the major products (Scheme 26) [62]. Compound **76**, resulting from a [1,3] sigmatropic rearrangement, was formed as the minor side product in most cases. However, reversal of regioselectivity took place when the latter process was electronically favored (see **76h**).



Scheme 26. Gold-catalyzed formal HDDA/carboalkoxylation reaction cascade.

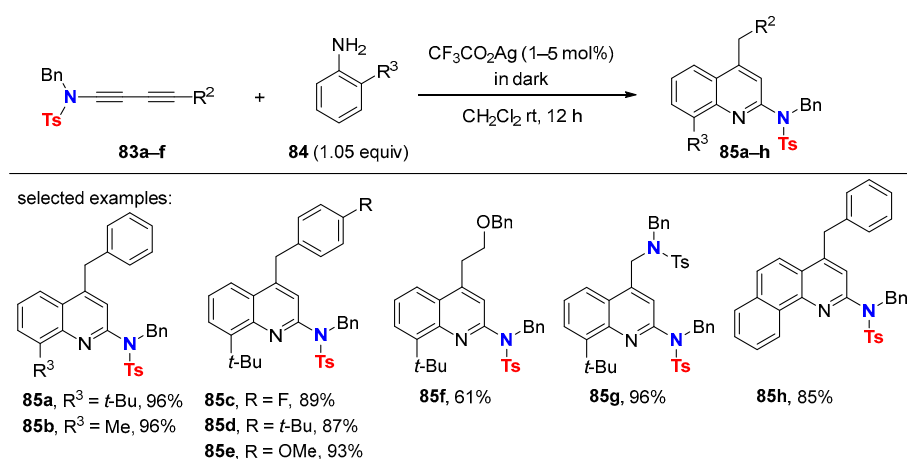
Triynes bearing an internal instead of a terminal alkyne moiety are unsuitable for this reaction cascade in agreement with the proposed mechanism that is being initiated by a σ,π dual activation of triyne **74a** to give intermediate **77** (Scheme 27). The latter undergoes a 5-*exo*-dig cyclization to give the gold vinylidene carbenoid **78**, which then cyclizes to furnish the *ortho*-Au phenyl cation **79**. The gold-complexed aryne **79** is trapped by the ether group leading to the oxonium species **80**. A charge-accelerated [3,3] sigmatropic rearrangement of **80** gives intermediate **81** followed by re-aromatization delivering **82** along the release of the gold ion. The final step of the proposed mechanism is the protodeauration of **82** to furnish product **75a** by releasing the active gold catalyst.



Scheme 27. Proposed mechanism for the Au-catalyzed carboalkoxylation reaction cascade.

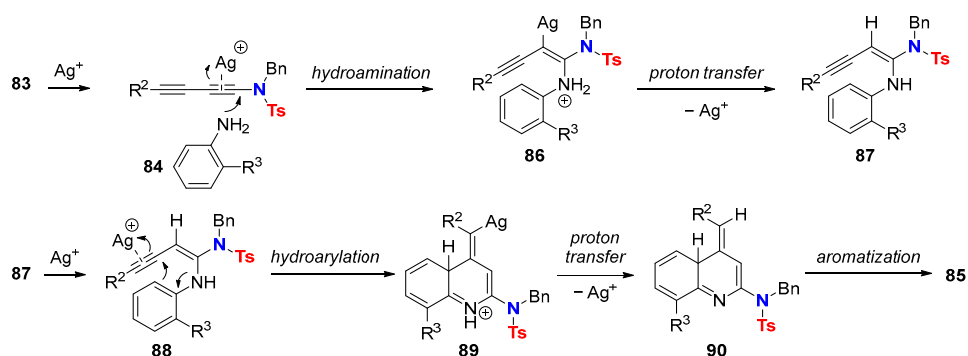
5.2. Intermolecular Processes

As highlighted in chapter 4, the metal-catalyzed double hydroaminations of symmetrical 1,3-butadiynamides with anilines gives 2,5-diamido-*N*-arylpyrroles. Surprisingly, in related transformations, *ortho*-substituted anilines as hydroamination reagent trigger a cationic driven reaction cascade after the first hydroamination step. For example, silver(I)-catalyzed transformations of 1,3-butadiynamides **83a–f** with *ortho*-substituted anilines **84** bearing electron-donating substituents give 2-amidoquinolines **85a–h** (Scheme 28) [63]. The combination of steric and electronic factors is crucial to gain preference for the formation of quinoline over pyrrole-derived products. One purpose of the electron-donating group in *ortho* position of the aniline is to facilitate the sequential electrophilic aromatic substitution step that rationalizes product formation. Symmetrical substituted 1,3-butadiynamides are also suitable substrates as shown in the example of bis-amido quinoline **85g** (96% yield).



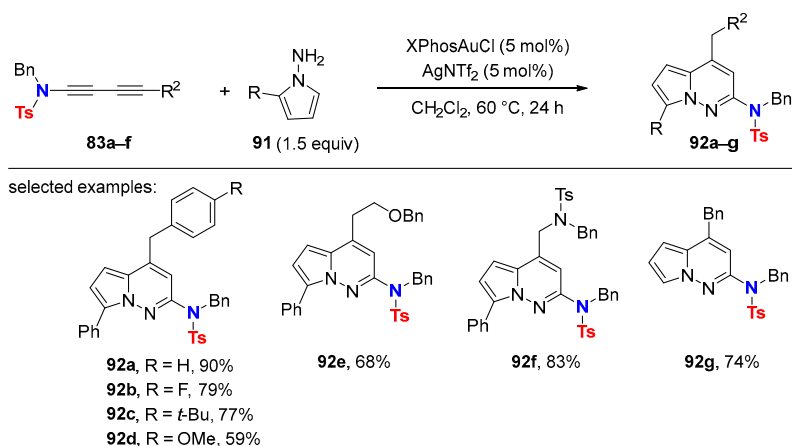
Scheme 28. Ag(I)-catalyzed synthesis of 2-amidoquinolines.

The proposed mechanism is depicted in Scheme 29. Silver-catalyzed intermolecular hydroamination of 1,3-butadiynamide **83** with aniline **84** delivers the enyne intermediate **86**, which, after proton transfer and protodeargentation, leads to **87**. Silver complexation of the remaining triple bond in **87** facilitates intramolecular hydroarylation via an electrophilic aromatic substitution process to give **89**. Subsequent proton transfer and re-aromatization results in the final quinoline **85**.



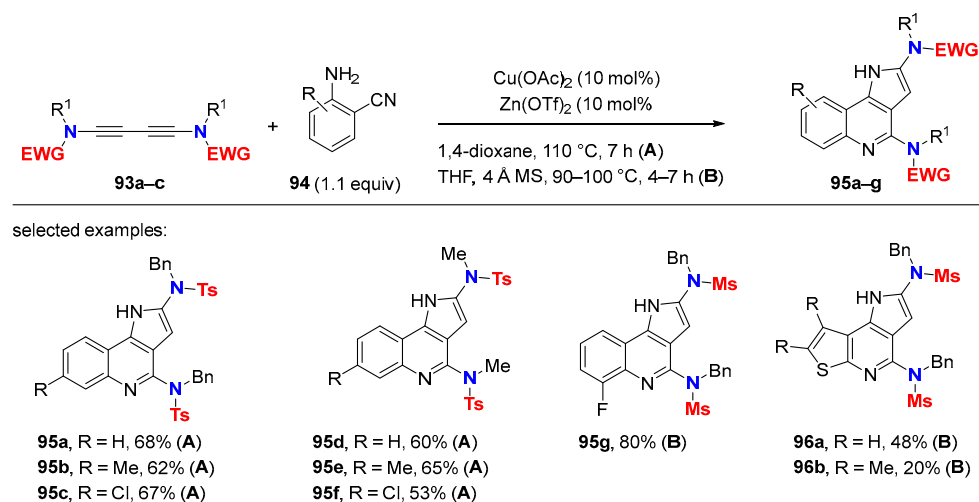
Scheme 29. Proposed mechanism for the Ag(I)-catalyzed synthesis of 2-amidoquinolines.

The synthesis of 2-aminopyrrolo[1,2-*b*]pyridazines **92a-g** from non-symmetrical 1,3-butadiynamides **83a-f** and 1-aminopyrroles **91** via a related strategy is also reported (Scheme 30) [64]. The overall reaction cascade proceeds through Au(I)/Ag(I)-mediated C-N/C-C bond formations to end up with readily substituted 2-aminopyrrolo[1,2-*b*]pyridazines **92**.



Scheme 30. Au(I)-catalyzed synthesis of 2-aminopyrrolo[1,2-*b*]pyridazines.

The reaction of symmetrical substituted 1,3-butadiynamides **93a–c** with *ortho*-cyano anilines **94** provides aryl-fused 1*H*-pyrrolo[3,2-*c*]quinolines **95a–g** within a single step via a dual catalyst process (Scheme 31) [65]. Heteroaryl-fused 1*H*-pyrrolo[3,2-*c*]quinolines **96a–b** are also accessible using 2-amino-3-cyano thiophenes as nucleophiles. Both catalysts—copper(II) acetate and zinc(II) triflate—are necessary for the cascade reaction to be effective. Finally, the overall sequence realizes the formation of one C–C and two new C–N bonds.



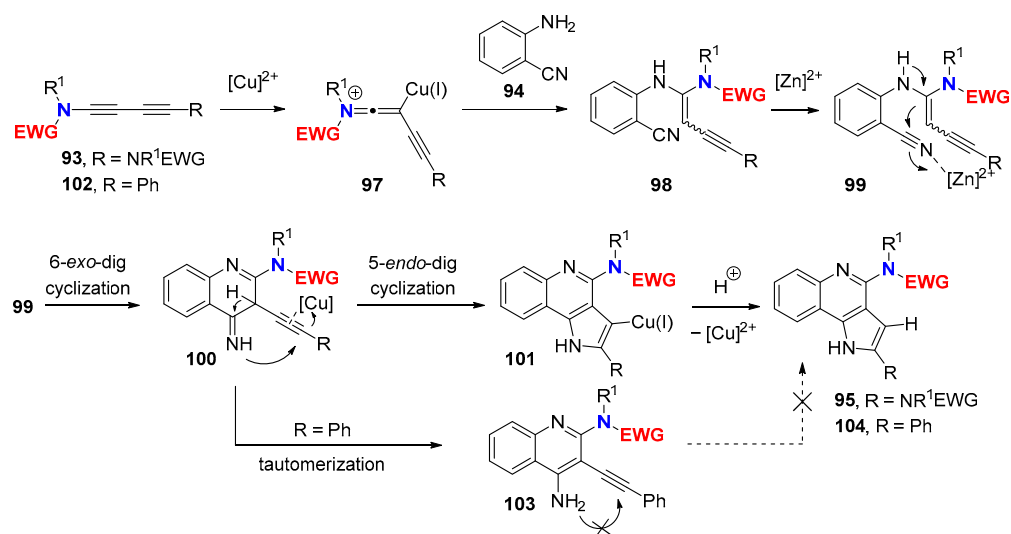
Scheme 31. Cu(II)/Zn(II)-catalyzed synthesis of 1*H*-pyrrolo[3,2-*c*]quinolines.

Activation of 1,3-butadiynamides via metal– π coordination of a π -acidic copper(II)-species to form the metal keteniminium **97** is the initiating step of the proposed mechanism (Scheme 32). This facilitates the intermolecular hydroamination to give enamine **98** followed by activation of the cyano group in **98** through coordination with the Zn catalyst. The resulting Zn-complexed **99** can undergo a 6-*exo*-dig cyclization via intramolecular nucleophilic attack of the enamine moiety producing **100**. Activation of the remaining carbon–carbon triple bond by Cu(II) facilitates a 5-*endo*-dig cyclization providing **101**, which upon protodemetalation leads to the 1*H*-pyrrolo[3,2-*c*]quinoline product **95**. In the case of non-symmetrical 1,3-butadiynamides **102** (R = Ph), tautomerization of intermediate **100** leads to the monocyclization product **103**, which is a major side product in the reaction. Quinoline **103** is unable to provide **104** through a second annulation sequence, as shown in a separate control experiment. Therefore, an equimolar mixture of products **103** and **104** resulting from both pathways is observed starting from 1,3-butadiynamide **102** even after prolongation of the reaction time. Notably, diphenyl-1,3-diacetylene did not undergo any reaction under these reaction conditions. This one more time underlines the differences in reactivity between 1,3-diyndamides and other 1,3-butadiynes.

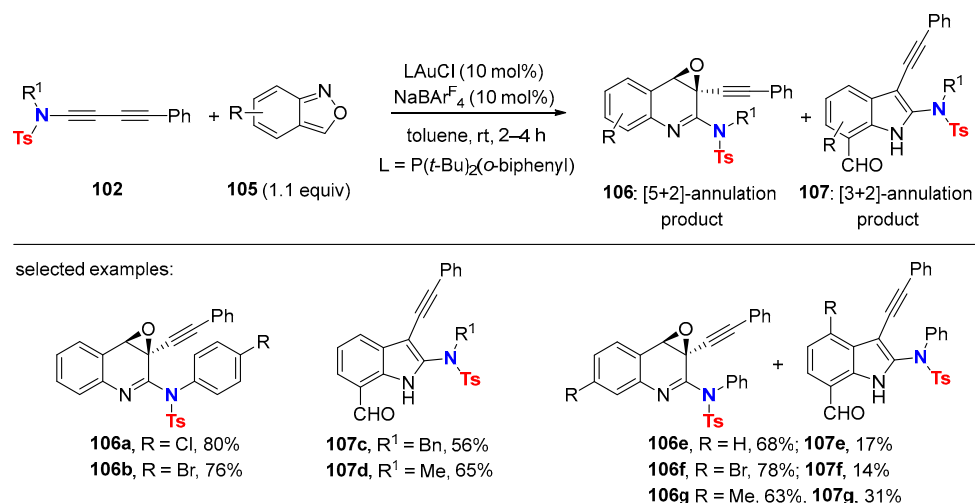
The outcome of gold-catalyzed reactions of 1,3-butadiynamides **102** with anthranils **105** is substrate-dependent, preferentially affording the formal [5+2] annulation products **106** in the case of 1,3-butadiynamides bearing an electron-deficient *N*-aryl group, while in contrast, [3+2] annulation products **107** are preferentially formed with more electron-rich *N*-alkyl 1,3-butadiynamides (Scheme 33) [66].

DFT calculations rationalize the observed chemoselectivity. Gold activation of the 1,3-butadiynamide followed by *N*-attack of anthranils leads to intermediate **109**, which evolves into the energetically more favorable α -imino gold carbene **110** (Scheme 34). The latter undergoes carbonyl addition to give **111** bearing a seven-membered cycle (**path a**). Although intermediate **111** is higher in energy than intermediate **112**, resulting from carbene arylation (**path b**), the free energy barrier for the formation of **111** is smaller than the one of **112**. Moreover, the conversion of **111** into quinoline oxide **106** is highly exothermic and expected to be almost barrierless. The preference for **path a** relies on the presence of the alkynyl substituent, which brings favorable steric and electronic effects to facilitate

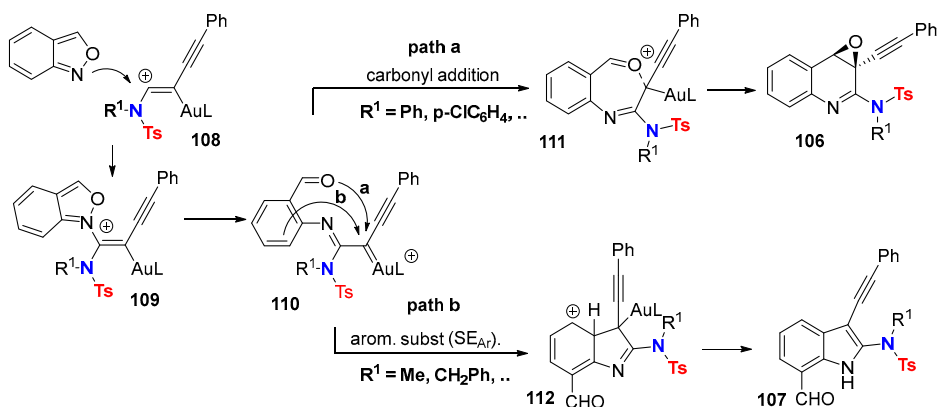
the formation of seven-membered ring intermediate **111**. These results are specific to 1,3-butadiynamides [67].



Scheme 32. Proposed mechanism of Cu(II)/Zn(II)-catalyzed synthesis of 1H-pyrrolo[3,2-c]quinolines.



Scheme 33. Gold-catalyzed reaction between 1,3-butadiynamides and anthranils.

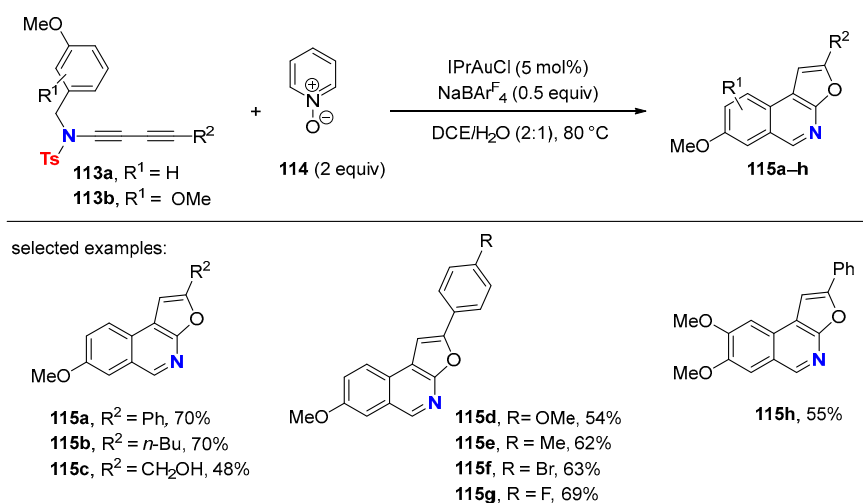


Scheme 34. Proposed mechanism for Au(I)-catalyzed reaction of 1,3-butadiynamides with anthranil.

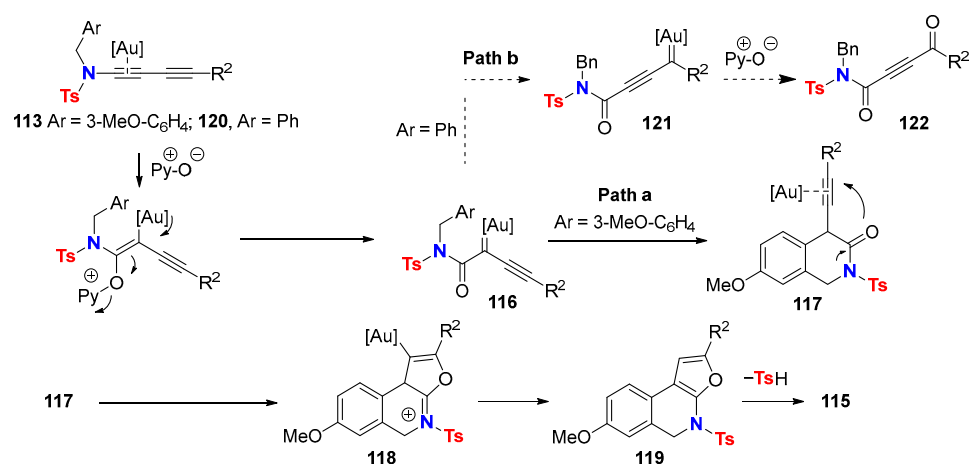
Gold-catalyzed oxidative cascade reactions of (het)aryl-tethered 1,3-butadiynamides, using pyridine *N*-oxide as the oxidant, encompass efficient protocols to access complex

polycyclic heteroaromatics within a single step. Here, the active gold species is an α -carbonyl gold carbene, whose obviously faster reaction with the proximal electron-rich aromatic group overrides the otherwise typical 1,4-dicarbonyl formation (Section 4.3, Scheme 20).

The reaction of 3-methoxyphenyl-tethered 1,3-butadiynamides **113a–b** with pyridine *N*-oxide (**114**), using catalytic amounts of IPrAuCl in the presence of NaBAr^F₄, leads to furo [2,3-*c*]isoquinolines **115a–h** (Scheme 35) [68]. The nature of the substituent at the terminal 1,3-diynamide end—alkyl or phenyl—for the outcome of the reaction cascade is negligible, but the presence of the 3-methoxy group on the tethered aryl ring is mandatory for the reaction cascade to occur. In the absence of the 3-methoxy group, in the case of substrates *N*-benzyl 1,3-butadiynamide **120** (Ar = Ph, Scheme 36), the double oxidation product **122** is the only product formed under the reaction conditions (**Path b**, Scheme 36).



Scheme 35. Au(I)-catalyzed synthesis of furo[2,3-*c*]isoquinolines.

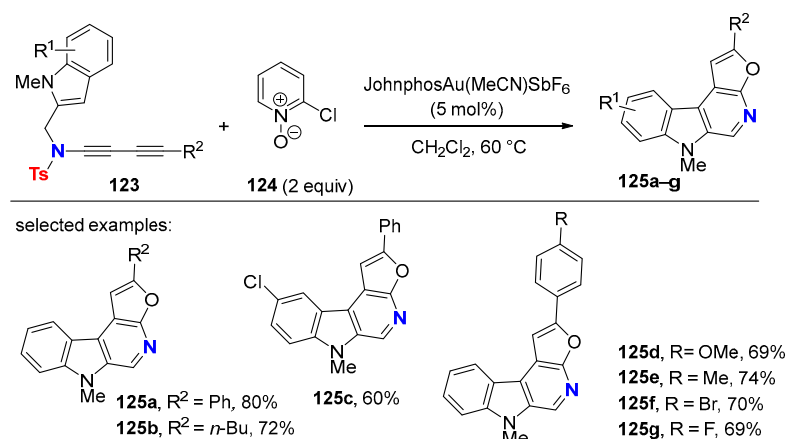


Scheme 36. Proposed mechanism for the synthesis of furo[2,3-*c*]isoquinolines.

According to the proposed mechanism, the gold-activated 1,3-butadiynamide **113** is oxidized by pyridine *N*-oxide (**114**) to give α -carbonyl gold carbenoid **116**, which is in situ trapped by the aryl group through CH insertion delivering intermediate **117** (**path a**, Scheme 36). Carbonyl addition on the activated second triple bond of **117** leads to the fused tricyclic intermediate **118**, which undergoes protodeauration to **119**. The transformation of intermediate **119** into the final polycyclic heteroaromatic product **115** via release of sulfonic acid is highly favorable and might be the driving force of the total transformation according to the authors. The involvement of **119a** (R² = Ph) was evidenced by conducting the

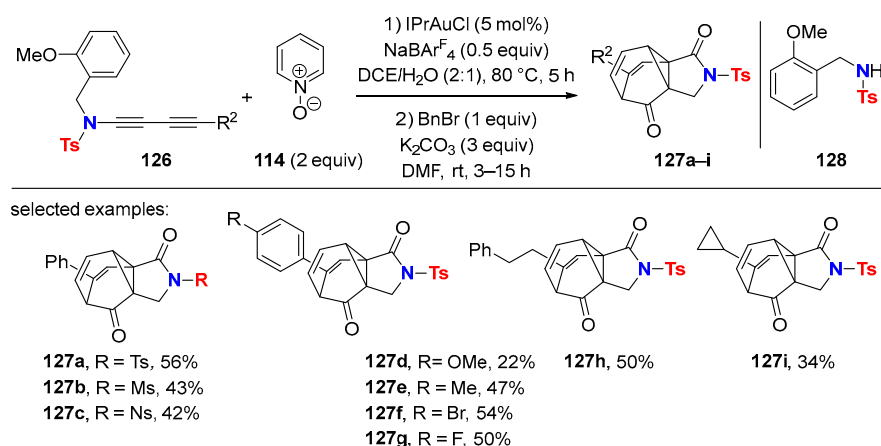
reaction at room temperature that provided **119a** (25% isolated yield) along with unreacted 1,3-butadiynamide **113a**. Full conversion of **119a** into product **115a** was achieved upon heating at 80 °C.

Accordingly, as extension, the assembly of fused tetracyclic heteroaromatics **125a–g** was achieved via the same strategy using *N*-methyl indolyl-tethered 1,3-butadiynamides **123** as the substrates and 2-chloropyridine *N*-oxide (**124**) as the oxidant (Scheme 37).



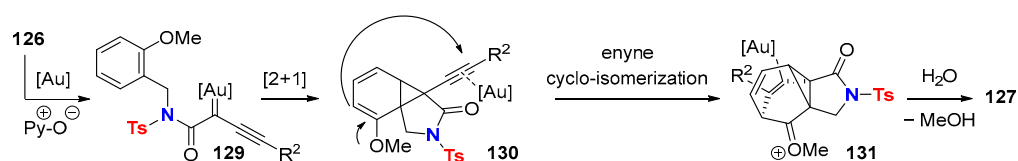
Scheme 37. Gold-catalyzed synthesis of 6*H*-furo[3',2':5,6]pyrido[3,4-*b*]indoles.

Strikingly, the outcome of the gold-catalyzed oxidative cascade cyclization of methoxyphenyl-tethered 1,3-butadiynamides is tunable by modifying the position of the methoxy group [69]. Indeed, the gold-catalyzed reaction of 2-methoxyphenyl-tethered 1,3-butadiynamides **126** with pyridine *N*-oxide (**114**) selectively delivers the polycyclic compounds **127a–i** with a barbalan-type carbon skeleton along with the byproduct **128**, resulting from hydrolysis and saponification of **126** (Scheme 38).



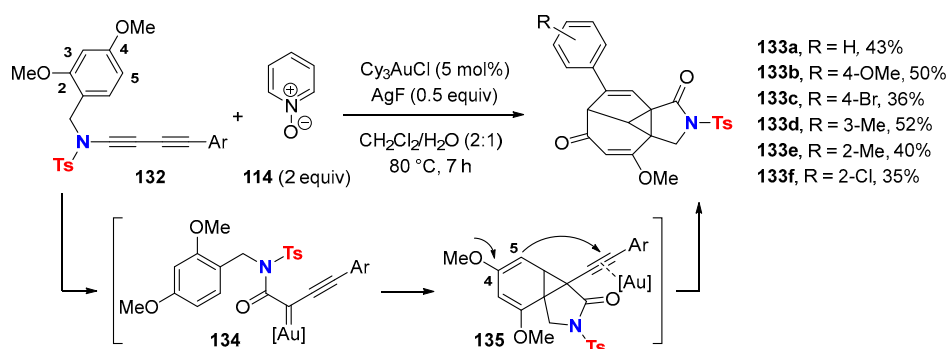
Scheme 38. Gold-catalyzed synthesis of polycyclic product **127**.

Arene CH insertion from in situ generated α -carbonyl gold carbenoids is not involved here in comparison to the case of the parent α -carbonyl gold carbenoid **116** depicted in Scheme 36. The preferential mechanistic path now is the intramolecular cyclopropanation of the arene unit by the carbenoid **129** to give norcaradiene **130** (Scheme 39). [3,3] Sigmatropic enyne cycloisomerization between the vinyl methoxy ether and the gold-activated alkynyl moiety leads to the formation of oxocarbenium ion **131**, which after hydrolysis delivers the polycycle **127**.



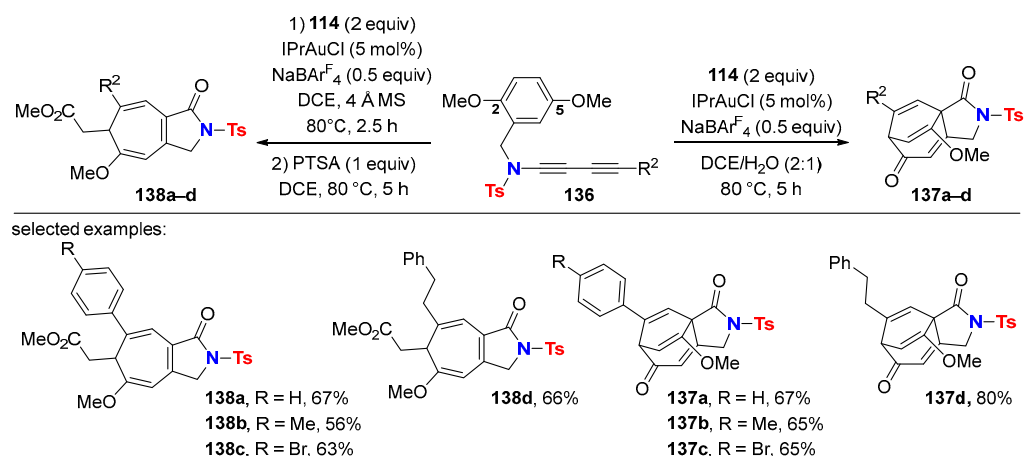
Scheme 39. Proposed mechanism for the synthesis of **127**.

A different set of polycycles now having an eight-membered ring moiety is available through a related gold-catalyzed dearomatization/cycloisomerization process by placing an additional methoxy group and varying the substitution pattern of dimethoxyphenyl-tethered 1,3-butadiynamides substrates. For example, 2,4-dimethoxyphenyl-tethered 1,3-butadiynamides **132** are selectively converted into the polycyclic products **133a–f** upon reaction with pyridine *N*-oxide (**114**) using $\text{Cy}_3\text{AuCl}/\text{AgF}$ as the catalyst (Scheme 40). In this case, the 2-methoxy group remains intact, whereas the additional 4-methoxy group is involved in the formal [3,3] sigmatropic enyne rearrangement.



Scheme 40. Au(I)-catalyzed reaction of 2,4-dimethoxyphenyl-tethered 1,3-butadiynamide **132** with pyridine *N*-oxide (**114**).

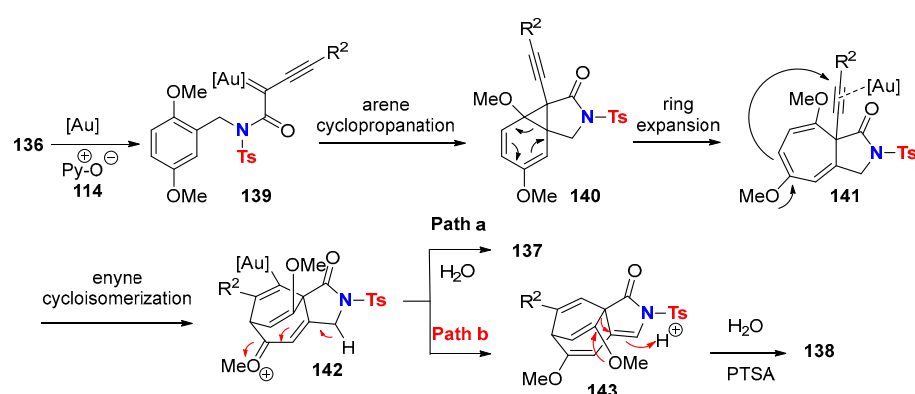
Using 2,5-dimethoxyphenyl-tethered 1,3-butadiynamides **136** as substrates makes the two fused *N*-heterocyclic structures **137a–d** and **138a–d** available, depending on whether the reaction is carried out in the presence of water or under anhydrous conditions, respectively (Scheme 41).



Scheme 41. Au(I)-catalyzed reaction of 2,5-dimethoxyphenyl-tethered 1,3-butadiynamides **136** with pyridine *N*-oxide (**114**).

The proposed mechanism involves the generation of a reactive α -carbonyl gold carbene species **139**, which undergoes a formal [2+1] cycloaddition with the adjacent arene moiety to give norcaradiene intermediate **140** (Scheme 42). The methoxy-substituted cyclo-

propane unit facilitates norcaradiene to cycloheptatriene ring expansion, leading to **141**. Subsequent intramolecular enyne cycloisomerization delivers intermediate **142**, whose hydrolysis furnishes the tricyclic products **137**. Under anhydrous conditions, intermediate **142** converts into product **143** via deprotonation and protodeauration. Acidic treatment of **143** induces the cleavage of one carbocycle, delivering the bicyclic compounds **138**. Importantly, such a pathway is supported by the isolation of compound **143a** ($R^2 = \text{Ph}$) and its conversion into the corresponding product **138a** by treatment with PTSA.



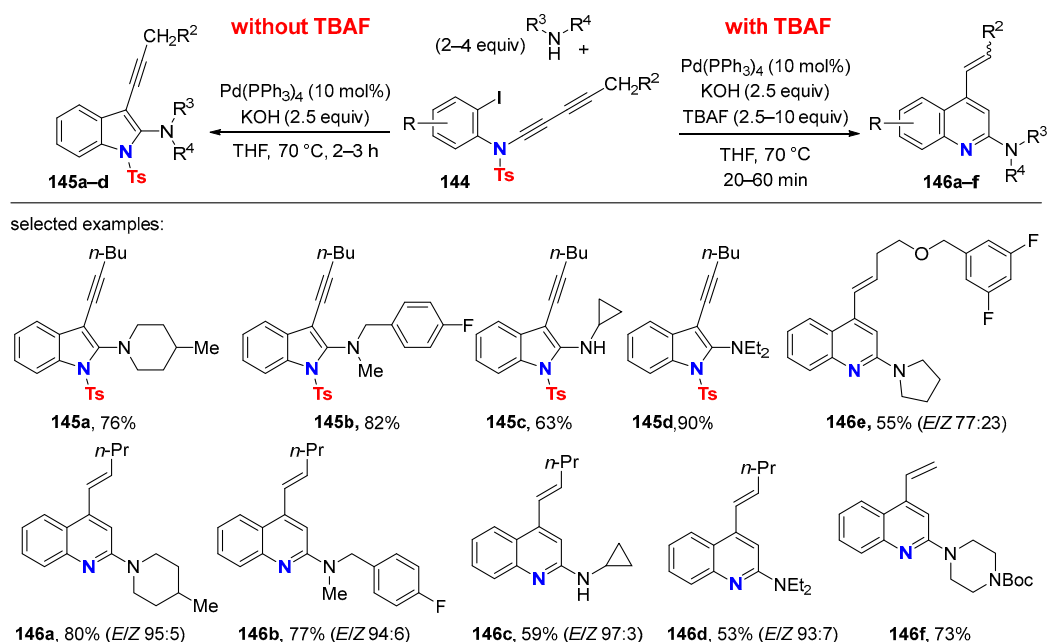
Scheme 42. Proposed mechanism for the Au(I)-catalyzed reaction of 2,5-dimethoxyphenyl-tethered 1,3-butadiynamides **136** with pyridine *N*-oxide (**114**).

Whereas the majority of the so far reviewed transformations of 1,3-butadiynamides rely on activation of one or two of its carbon–carbon triple bonds by either Brønsted or Lewis acids, or by transition metal catalysts acting both as π -acid and Lewis acid, or Au catalysts transforming 1,3-dynamides into metal carbenoid intermediates, other principles of ynamide activation might result from transforming 1,3-butadiynamides into [4]cumulenimines or related highly unsaturated π -conjugated molecular scaffolds.

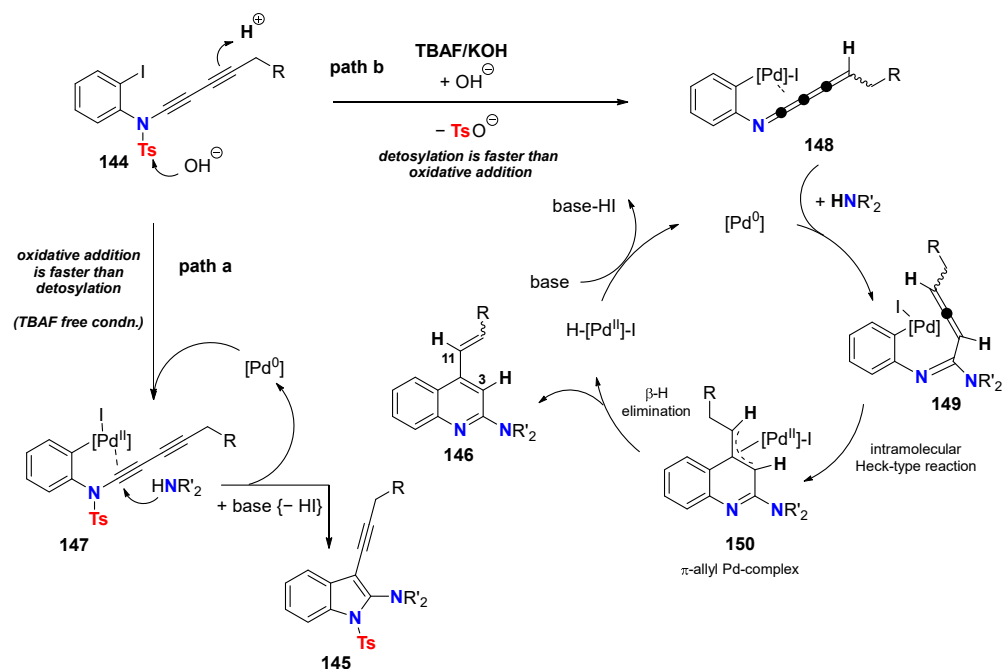
Recently, divergent palladium-catalyzed reaction cascades for the selective synthesis of either 2-amino-3-alkynyl-indoles **145a–d** or 2-amino-4-alkenylquinolines **146a–f** from 1,3-butadiynamides **144** and primary or secondary amines were established (Scheme 43) [70]. Starting from identical or similar substrates, the outcome of the reaction giving either indole or quinoline motifs is switchable, respectively, by the absence or presence of TBAF.

Under similar reaction conditions than those applied for the synthesis of 2-aminoindoles through Pd-catalyzed heteroannulation reaction from *N*-alkynyl-2-haloanilides [71], the 1,3-butadiynamides **144** behave like internal ynamides. The second triple bond remains unaffected through the transformation, whose key intermediate is the σ,π -chelated palladium species **147** (Scheme 44, **path a**). The latter results from the initial oxidative addition of the Pd(0) catalyst to the iodophenyl moiety of 1,3-butadiynamides **144**. Metal– π complexation of the ynamide triple bond in **147** facilitates intermolecular amine addition delivering the 3-alkynyl indoles **145** selectively. Strikingly, in the presence of TBAF, both triple bonds are engaged to convert 1,3-butadiynamides **144** in 2-aminoquinolines **146a–f** in one pot (Scheme 44, **path b**). The combination TBAF/KOH is believed to induce cleavage of the tosyl group either as the first step or after the oxidative addition of the palladium catalyst to the iodophenyl moiety. Now, the key intermediate is the palladium-chelated [4]cumulenimine **148**. The intermolecular amine addition to **148** selectively occurs at the α -carbon delivering the allene-derived intermediate **149**. Subsequent intramolecular Heck-type reaction furnishes the annulated π -allyl palladium species **150**, which undergoes β -hydrogen elimination to produce 4-alkenyl quinolines **146**.

The [4]cumulenimine structure in **148** is unprecedented. However, the deuterium labeling experiment shows the selective deuterium incorporation into the C3 and C11 positions of the quinoline products **146** in agreement with the formation of the transient species **148**.



Scheme 43. Divergent Pd-catalyzed reaction cascades towards indole and quinoline motifs.



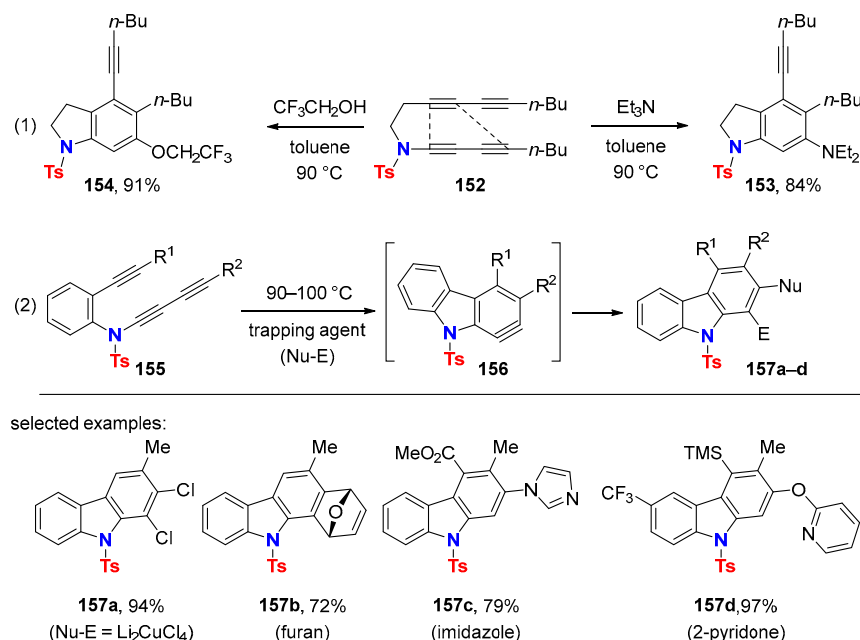
Scheme 44. Proposed mechanism for the Pd-catalyzed divergent synthesis of either 2-amino-3-alkynyl-indoles (**path a**) or 2-amino-4-alkenylquinolines via [4]cumulenimine intermediate (**path b**).

6. HDDA Cascade Reactions

The hexa-dehydro-Diels–Alder (HDDA) reaction of 1,3-dynamides tethered to 1,3-butadiynes delivers highly reactive arynes (dehydrobenzenes) after a formal intramolecular [4π + 2π] cycloaddition process [17]. They are subsequently trapped by in situ intra- or inter-molecular additions to the dehydrobenzene carbon–carbon triple bond, leading to a variety of new heterocyclic structures and useful products. The HDDA reaction itself was discovered in 1997 [72,73] and further developed. However, since 2012, it has received considerable attention, and the underlying process was coined with the term HDDA [18]. The field of HDDA reactions is rapidly expanding, including substrate variations and development of new aryne-trapping modes. The latter takes vast advantage

of the fact that typical reagents necessary for generating arynes are absent and therefore cannot interfere [19–21]. Studies have shown that reagent-free HDDA reactions proceed through a stepwise mechanism via diradical intermediates. Significant acceleration of the process is observed when the formal 2π cycloaddition partner in the underlying $[4\pi + 2\pi]$ cycloaddition process bears an alkynyl substituent (1,3-butadiynyl unit) [33,74]. This is why tetraynes rather than triynes are frequently used in HDDA cascade reactions.

1,3-Butadiynamides tethered to monoalkynes or 1,3-butadiyne moieties are privileged substrates for HDDA reactions because aryne formation proceeds chemo- and regioselectively due to the intrinsic polarization of the 1,3-diyamide unit. Notably, intramolecular HDDA reactions with 1,3-diyamides belong to transformations relying on a 1,4-functionalization of 1,3-diyamides, although the underlying process is step-wise. The follow-up reaction of those 1,3-diyamide-originated arynes continues being highly regioselective, i.e., for the addition of nucleophiles to the aryne. For example, the thermal reaction of tetrayne **152** with triethylamine or trifluoroethanol regioselectively furnishes indolines **153** and **154**, respectively (Scheme 45, (1)) [75]. A novel entry to functionalized carbazoles **157a–d** from triyne substrates **155** is accessible through perfectly regioselective nucleophilic addition to HDDA-generated carbazolynes **156** (Scheme 45, (2)) [76].

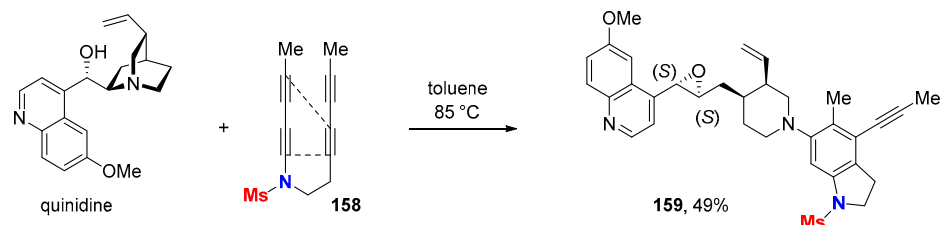


Scheme 45. Regioselective “trapping reactions” of 1,3-butadiynamide-derived arynes.

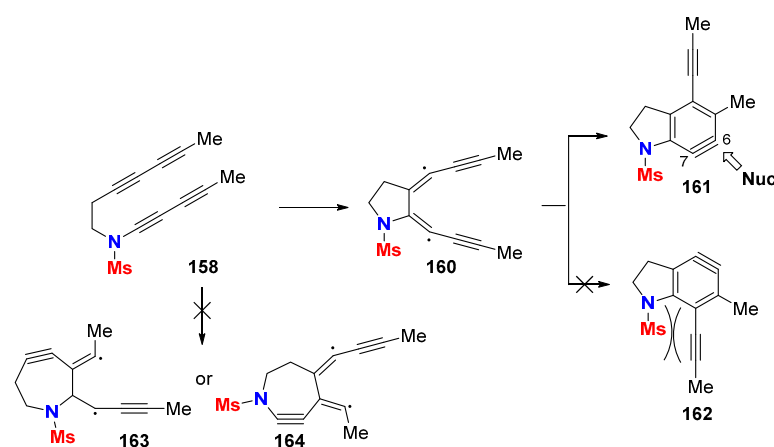
The discriminating reactivity of HDDA-generated arynes from 1,3-butadiynamides was further highlighted by chemo- and regioselective transformations using structurally complex multifunctionalized “aryne-trapping agents” taken from the nature pool. For example, the reaction of tetrayne **158** with the cinchona alkaloid quinidine, which displays several potential reacting sites and/or reacting modes, delivers the single indoline product **159** (Scheme 46) [77].

Experimental results of intramolecular HDDA reactions with 1,3-diyamide were rationalized by DFT calculations (Scheme 47) [78]. Amongst possible diradical intermediates formed in the principal first step of the HDDA reaction of tetrayne **158**, the aza-cycloheptynes **163** and **164** can be ruled out, because they are higher in energy by 35.9 and 41.7 kcal/mol, respectively, compared to the pyrrolidine species **160**. This largely originates from the twofold propynyl stabilization inherent in biradical **160** and the high triple bond strain energy in arynes **163** and **164**. The formation of intermediate **160** is the rate-determining step. Steric factors govern the selective formation of aryne **161** in the second step. The activation barrier to aryne **161** and **162** is 4.3 and 6.6 kcal/mol, respec-

tively, and relates to differences in product stability. Aryne **162** is less stable than **161** by 3.4 kcal/mol because of the steric hindrance between the methanesulfonyl group and the propynyl moiety.



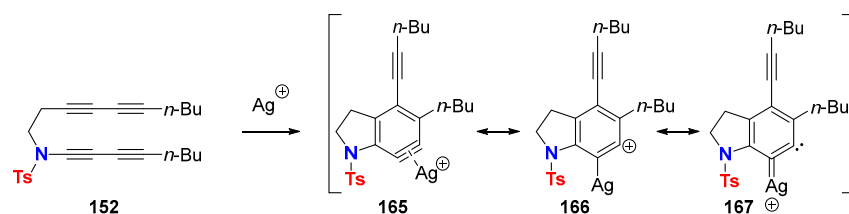
Scheme 46. Reaction of a HDDA-generated aryne with quinidine.



Scheme 47. Mechanistic pathway of the formation of a single HDDA-generated aryne from 1,3-butadienamide-derived substrates.

Computational studies, moreover, explain why nucleophilic additions to indoline aryne **161** take place selectively on the C-6 rather than the C-7 position (Scheme 47) [79]. Transition state distortion energies determine regioselectivity. In other words, the aryne **161** displays unsymmetrical bending distortion, and the nucleophilic addition occurs at its flatter and more electropositive end.

The silver-catalyzed HDDA reaction is an interesting alternative to the sole thermal version, eventually affording different reaction outcomes [80]. Ag(I) complexation of the aryne allows for its stabilization while retaining high reactivity. The reactive intermediate resulting from the interaction of aryne with silver salts is described as the silver-bound aryl cations **165**, **166** or by its mesomeric 1,2-carbene-silver carbenoid **167** (Scheme 48).

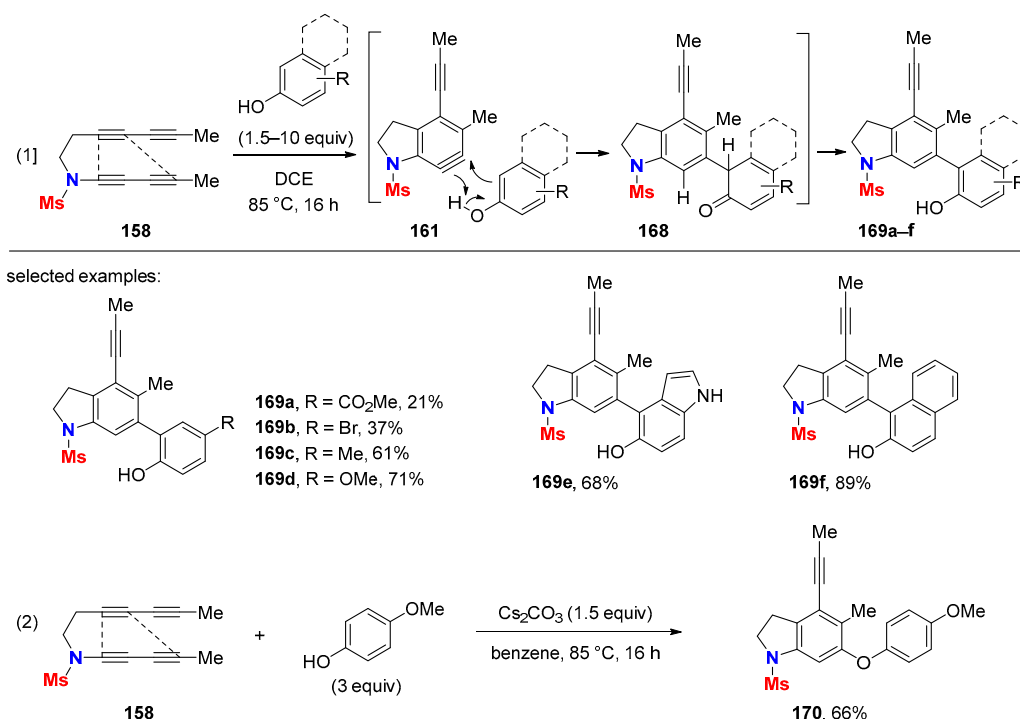


Scheme 48. Ag(I)-complexed aryne species in silver-catalyzed HDDA reactions.

6.1. Sole Thermally Induced HDDA Cascade Reactions

Aryne trapping via C-C bond formation: The HDDA-generated benzyne **161** reacts selectively with phenols and delivers 2-hydroxybiaryl compounds **169a–f**, and not the expected diaryl ethers, which are archetypal products of arynes generated by elimination reactions (Scheme 49, (1)) [81]. Indeed, sole thermal HDDA reactions proceed under neutral

conditions, without the presence of any base or metal reagent, in contrast to classical methods of benzyne generation. The biaryl junction occurs at the *ortho*-position to the hydroxyl group via a “concerted phenol-ene-type” reaction. On the other hand, in the presence of cesium carbonate, the thermal reaction of tetrayne **158** with 4-methoxyphenol gives diaryl ether **170** as a single product (Scheme 49, (2)) [81].



Scheme 49. Biaryl vs. diaryl ether synthesis through aryne reactions with phenols.

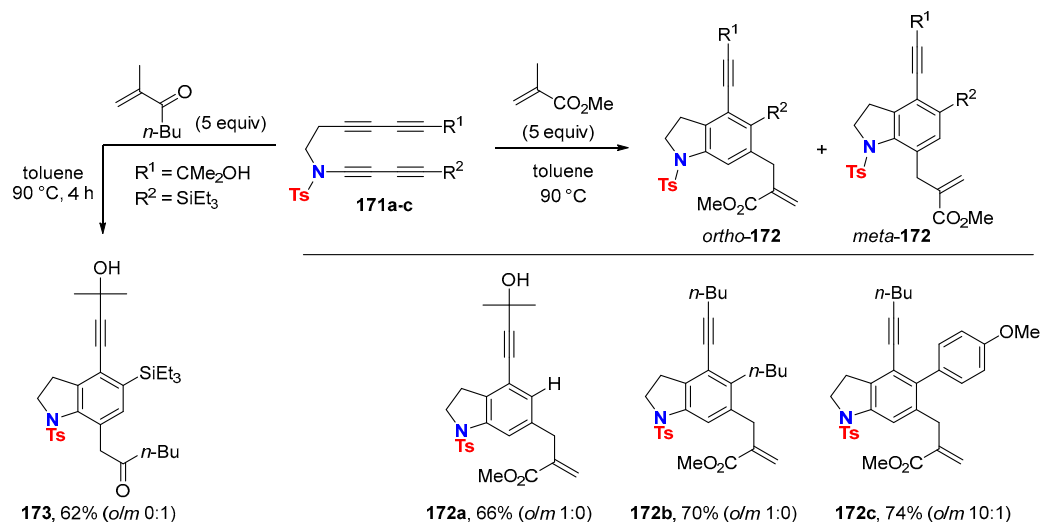
Inter- and intramolecular Alder-ene reactions with HDDA-generated arynes lead to a variety of differently substituted indolines. The reaction between 1,3-butadienamides **171a–c** with methyl methacrylate regioselectively delivers the *ortho*-isomers of indolines *ortho*-**172a–c** (Scheme 50) [82].

However, the steric bulk of the R² substituent has an influence on the Alder-ene reaction outcome. The conversion of 1,3-butadienamide **171c** substituted with a bulky silyl group (R² = SiEt₃) preferentially gives indoline *meta*-**173** with 2-methyl-hepten-3-one.

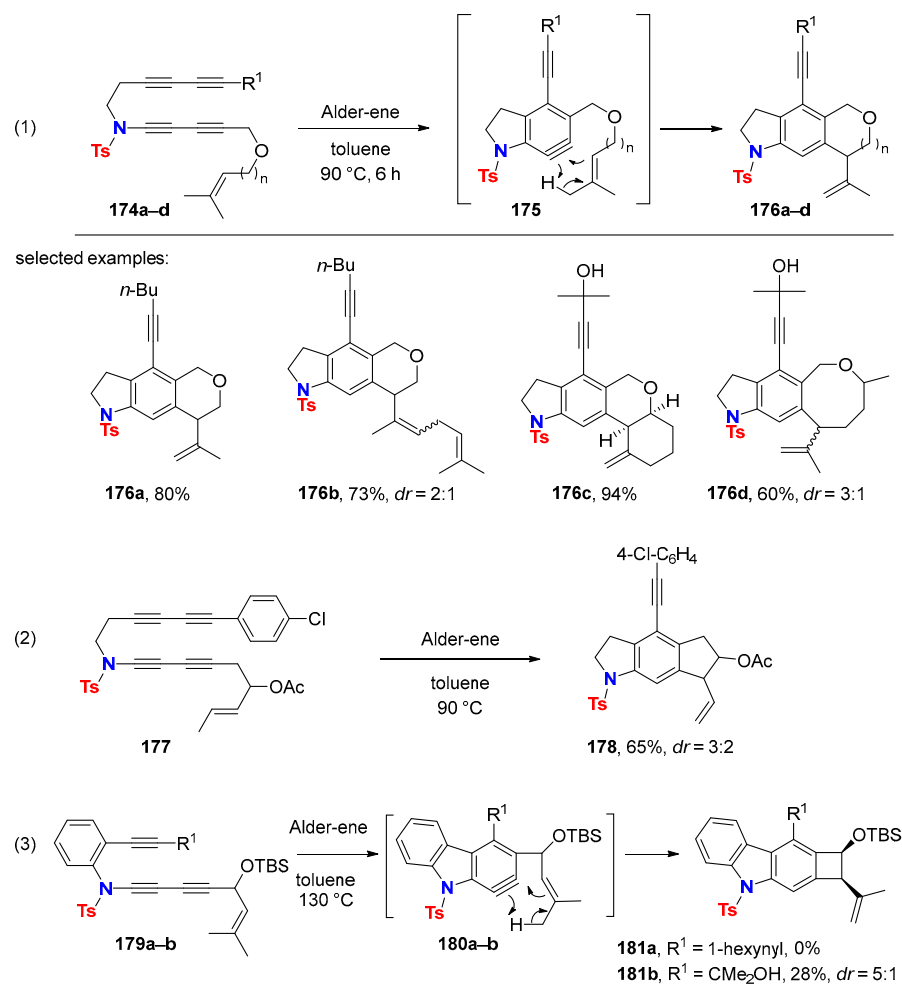
Intramolecular HDDA reactions followed by intramolecular Alder-ene sequences were realized with 1,3-dienamides **174a–d** to deliver the linear annulated indolines **176a–d** (Scheme 51, (1)) [83]. The chemoselective formation of aryne **175** makes the Alder-ene reaction the most favorable pathway amongst all other possible aryne reacting modes. Extending the tether from three to four atoms delivers eight-membered ring products like compound **176d**. Tetrayne **177** bearing a shorter two-atom tether with a methyl-substituted alkene also undergoes an Alder-ene reaction to deliver tricyclic compound **178** (Scheme 51, (2)) [84]. Isoprenyl-tethered tetrayne **179a** displaying an even shorter one-atom link fails to produce the corresponding Alder-ene product **181a** (R¹ = 1-hexynyl) even under more drastic conditions [85]. However, increase of steric pressure with the rather bulky isopropanol group in triyne **179b** (R¹ = C(Me)₂OH) facilitates the formation of the corresponding benzocyclobutene **181b** (Scheme 51, (3)).

Thermal HDDA reactions of allene-tethered 1,3-butadienamides **182** deliver the corresponding aryne intermediates **183**, whose reactivity and selectivity are divergent. The outcome of the intramolecular reaction of the allene with the aryne moiety depends on the substitution pattern of the allene and on the length of the tether (Scheme 52) [86]. The Alder-ene reaction involving an allylic C-H bond is favored with trisubstituted allenes (**path a**) leading to the eight-membered ring containing product **184**. In contrast, the allenic

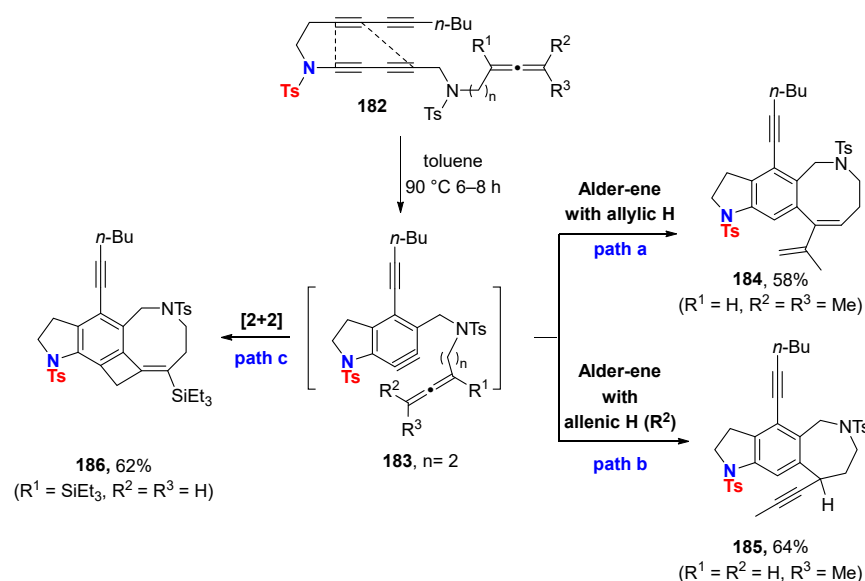
C-H bond is preferentially involved with mono- and 1,3-disubstituted allenes affording the seven-membered Alder-ene product **185** (path b). Finally, [2+2] cycloaddition is the preferred path of intramolecular arynes reactions with a 1,1-disubstituted terminal allene furnishing the tetracyclic compound **186** (path c).



Scheme 50. Intermolecular Alder-ene reactions with 1,3-butadiynamide-derived arynes.



Scheme 51. Alder-ene reactions of 1,3-butadiynamide-(**179a-b**)-derived arynes **180a-b**.



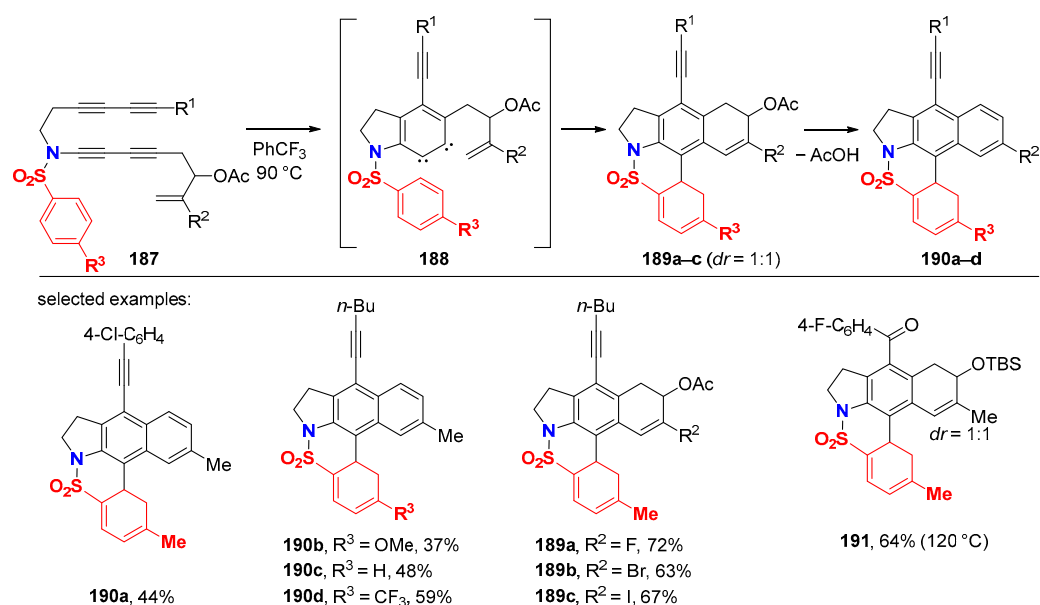
Scheme 52. Intramolecular Alder-ene reactions or [2+2] cycloadditions with ynamide-derived tetraynes tethered with an allene.

The sole thermal reaction of *N*-arenesulfonyl 1,3-butadiynamides **187**, spacing a terminal alkene moiety by a two-atom tether, leads to the pentacyclic structures **189** or **190** via an unprecedented aryne-mediated dearomatization of the phenyl connected to the sulfonyl moiety (Scheme 53) [84]. This transformation reveals the 1,2-dicarbene character of HDDA-generated arynes (intermediate **188**). The efficiency of the reaction increases with cation-stabilizing substituents on the alkene (R^2) and electron-withdrawing substituents on the arenesulfonyl group (R^3). Interestingly, compounds **189a–c**, bearing a haloalkene moiety ($R^2 = \text{halogen}$), do not undergo subsequent acetic acid elimination to give the corresponding aromatization products **190**. It is also worth noting that a ketone-containing triyne is a suitable substrate delivering the corresponding pentacyclic product **191** at a slightly higher reaction temperature of 120 °C.

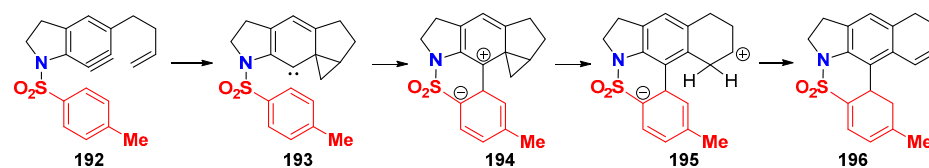
A plausible mechanism, underlined by DFT calculations carried out on the simplified aryne structure **192**, is given in Scheme 54. Alkene cyclopropanation is feasible due to the 1,2-dicarbene character of the HDDA-generated aryne and gives carbene **193**. The latter undergoes nucleophilic addition onto the electron-deficient phenylsulfonyl moiety delivering 1,3-zwitterion **194**. Subsequent ring expansion of the cyclopropane generates the 1,6-zwitterion **195**, which leads to the final product **196** via intramolecular proton transfer.

Acenes with indolynaphthalene or indolynanthracene units are accessible through iterative intramolecular HDDA reaction cascades starting from 1,3-butadiynamide **197** (Scheme 55) [87]. A first intramolecular HDDA cycloaddition gives aryne **198** consecutively undergoing a second intramolecular HDDA reaction to provide the new aryne **199** as the reactive intermediate. The latter is trapped either by [4+2] cycloaddition with α -pyrone to give indolynanthracene **200** or by dichlorination with dilithium tetrachlorocuprate, leading to indolynaphthalene **201**, respectively, as the sole products.

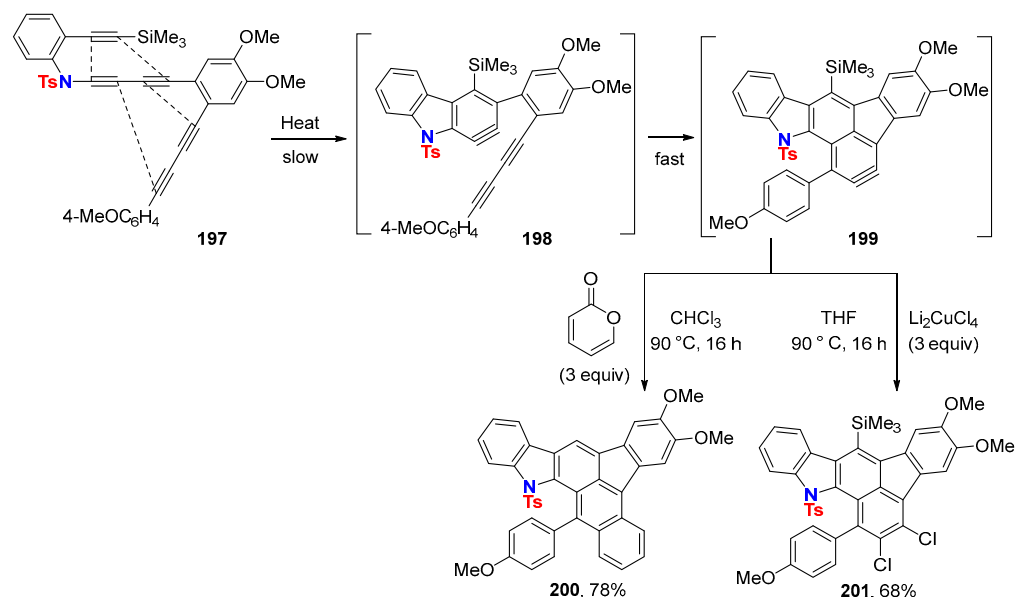
Aryne trapping via C–N bond formation: In situ trapping of HDDA-generated aryne **202** with simple tertiary amines such as triethylamine leads to the zwitterionic species **203**, which delivers the same product **204** as being provided from **152** with diethylamine. Disproportionation of the zwitterion **203** by release of ethylene delivers the final product **204** (Scheme 56, (1)) [75]. This olefin elimination sequence was confirmed in the case of tertiary amines bearing activated β -protons such as β -aminoester **205** (Scheme 56, (2)) [88].



Scheme 53. Synthesis of pentacyclic products via HDDA-aryne-mediated arene dearomatization reaction.



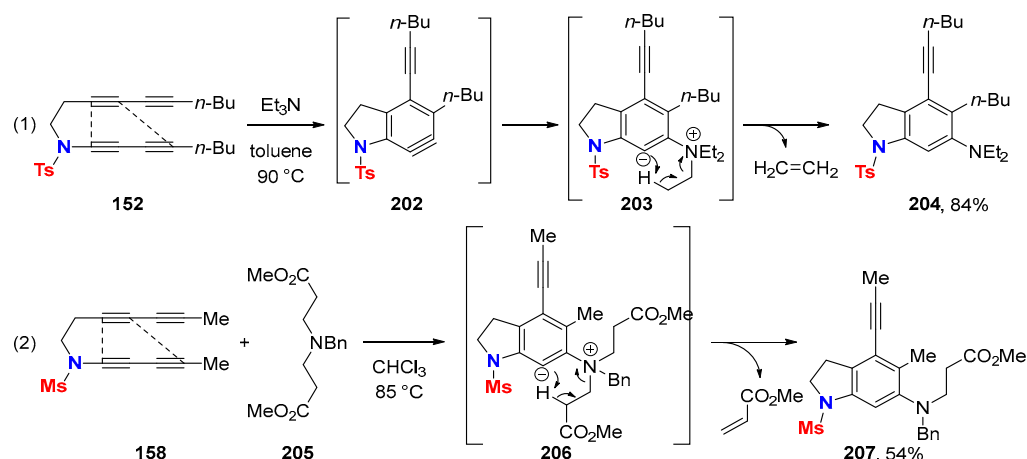
Scheme 54. Main intermediates of the proposed mechanistic pathway.



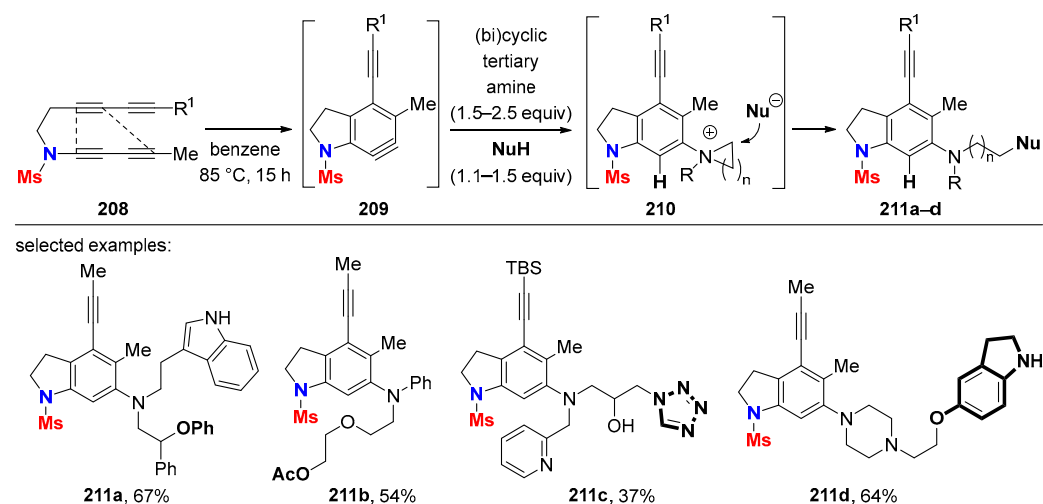
Scheme 55. Domino HDDA reactions towards polyacenes.

However, in protic solvents, the preferential pathway does not involve intra- but intermolecular protonation of the zwitterionic species (**209** → **210**). Now, a quaternary ammonium center is formed following ring opening by a nucleophile in the case of cyclic tertiary amines (**210** → **211**) [88]. This reaction sequence also delivers poly-heterocyclic structures **211a–d** based on three-component reactions (TCR) with HDDA-generated arynes

209 (Scheme 57) [31]. The addition of the amine onto benzyne **209** must be faster than that of the protic nucleophile. In some cases, such as acetic acid, the expected TCR product **211b** (54%) was formed along with the direct benzyne–acetate addition product (27%). Thus, a two-step sequence based on the addition of triflic acid to generate ammonium triflates and their subsequent nucleophilic ring opening by nucleophilic displacement of the triflate in the second step broadens the scope of suitable nucleophiles.



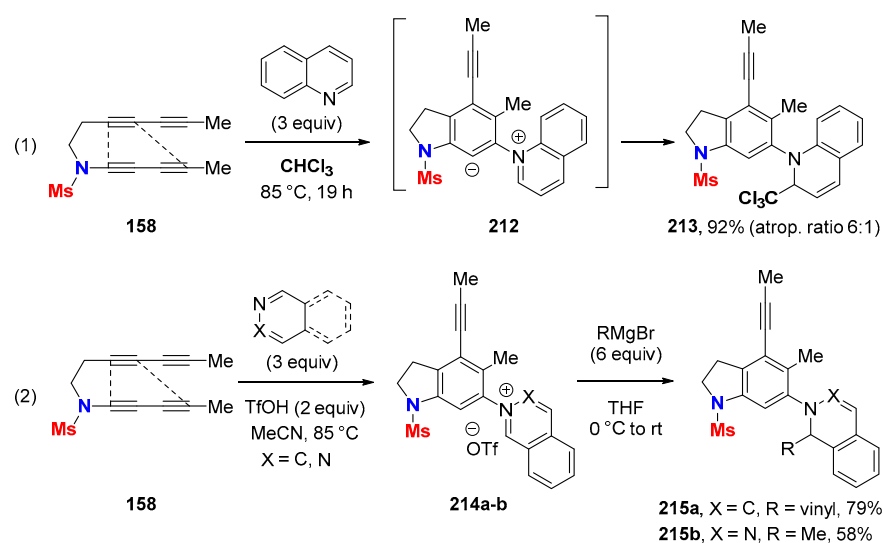
Scheme 56. Tertiary amine addition onto HDDA-generated aryne.



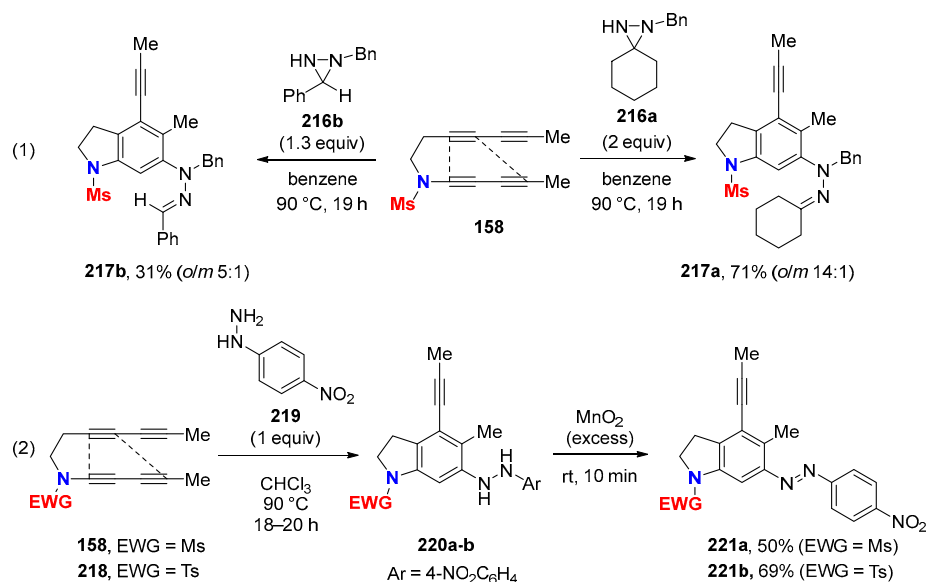
Scheme 57. Three-component reactions of HDDA-generated benzynes with (bi)cyclic tertiary amines and protic nucleophiles.

The TCR strategy is applicable to six-membered *N*-heteroaromatics as the nitrogen nucleophile. For instance, the reaction of 1,3-butadienylamine **158** with quinoline in chloroform provides the addition product **213** via betaine **212** (Scheme 58, (1)) [89]. Catching the aryne generated from **158** with triflic acid and *N*-heteroaromatics like quinoline or quinazolines delivers isolable *N*-arylium triflates **214a–b**, which undergo nucleophilic addition of Grignard reagents in a second reaction to give the heterocyclic products **215a–b** (Scheme 58, (2)).

The reaction of HDDA-generated benzyne starting from 1,3-butadienylamine **158** and diaziridines **216a–b** delivers *N*-arylhydrazones **217a–b** (Scheme 59, (1)) [90]. The more nucleophilic but also more hindered *N*-benzyl nitrogen atom in **216a–b** adds to the aryne moiety. This reasons the formation of *meta*-isomer of **217a–b** along with the expected major *ortho*-isomer.



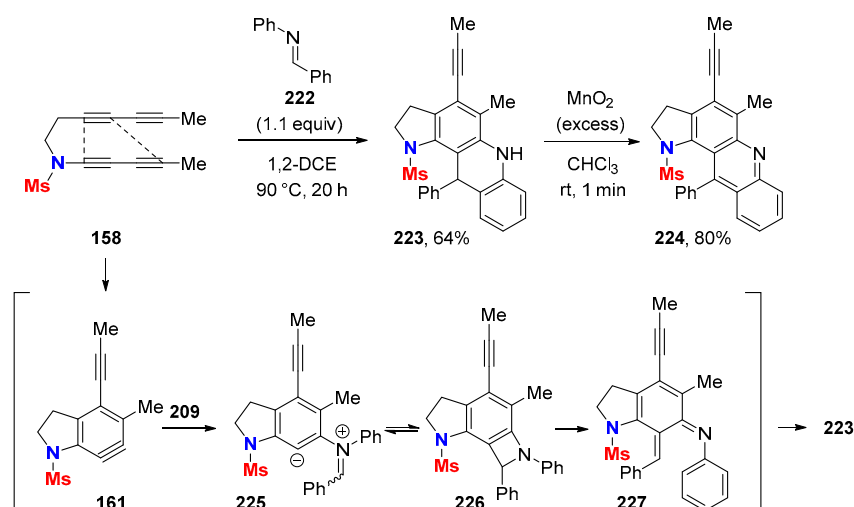
Scheme 58. Reaction of HDDA-generated arynes with six-membered *N*-heteroaromatics.



Scheme 59. Trapping of HDDA-generated benzynes with (1) diaziridines and (2) arylhydrazines.

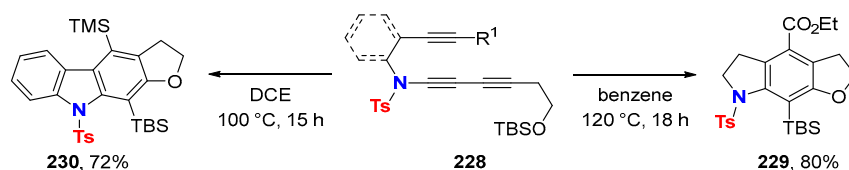
Arylhydrazines are ambident nucleophiles, but in the case of *para*-nitro-phenylhydrazine **219**, only the β -nitrogen atom (NH_2) engages in the trapping of arynes thermally generated from tetraynes **158** (EWG = Ms) or **18** (EWG = Ts) (Scheme 59, (2)) [91]. The reaction is highly regioselective and subsequent oxidation of the resulting 1,2-diarylhydrazines **220a–b** with MnO_2 delivers azoarene products **221a–b**.

The reaction of HDDA-generated arynes with *C,N*-diarylimine **222** proceeds efficiently, whereas this reaction is known to be poor yielding with *o*-benzynes generated by classical methods, i.e., by *ortho*-elimination of arene compounds (Scheme 60) [92]. Aromatization of the resulting dihydroacridine **223** by oxidation with MnO_2 gives acridine **224**. The conversion of **158** to **223** probably involves a formal [2+2] cycloaddition of an imine to a highly reactive aryne species. Initial imine addition on benzyne **161** provides betaine **225**, which cyclizes to benzazetidone intermediate **226** to provide azo-quinomethide **227** after electrocyclic ring opening. Finally, a 6π electrocyclic ring closure followed by a proton shift gives dihydroacridine **223**.



Scheme 60. Trapping of HDDA-generated benzynes with a *C,N*-diarylimine.

Aryne trapping via C-O bond formation: Intramolecular HDDA reactions generated with 1,3-butadienamide **228**, linked via two carbons to a silyl ether unit, result in fully substituted benzene derivatives via formal aryne insertion into the *O*-silicon bond. For example, furanyl-annulated indoline **229** and carbazole **230** are products from aryne reactions involving C-O bond formation (Scheme 61) [18,76].

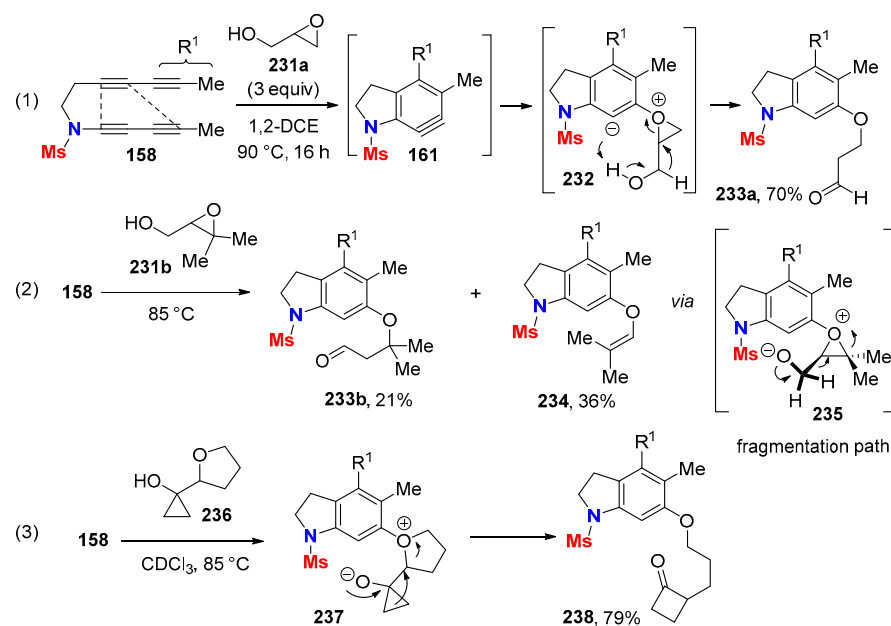


Scheme 61. Intramolecular reaction of HDDA-generated benzynes from 1,3-butadienamides tethered with a silyl ether.

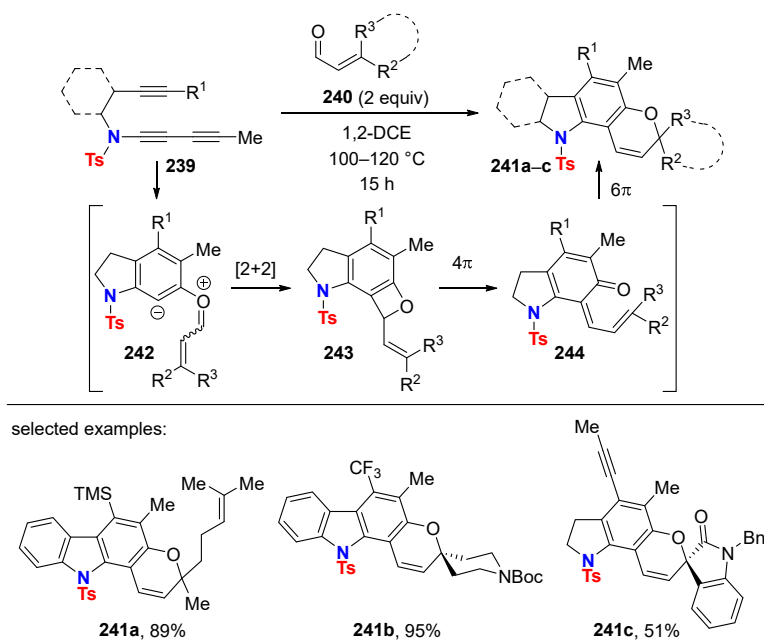
Intermolecular trapping of HDDA-generated benzynes from tetrayne **158** with hydroxy-containing cyclic ethers such as glycidol **231a** is also possible (Scheme 62, (1)) [93]. The reaction preferentially proceeds via the addition of the cyclic ether oxygen to the aryne. The resulting betaine **232** is protonated followed by ring opening of the cyclic oxonium ion delivering aryl ether **233a**. Addition of the alcohol hydroxy of **231a** to the aryne becomes a competitive pathway when a large excess of glycidol (100 equiv) is used. In the case of trisubstituted epoxide **231b**, another concurrent pathway based on C-C-bond cleavage and aldehyde liberation is observed leading to aryl enol derivative **234** (Scheme 62, (2)). The use of the cyclopropanol derivative **236** as the nucleophile readily delivered the cyclobutanone compound **238** via a cationic-driven cyclopropanol to the cyclobutanone ring-enlargement reaction (Scheme 62, (3)).

HDDA reaction-generated arynes trapped by 3,3-disubstituted enals **240** offer a new entry to benzopyran motifs, in particular to the pyranocarbazole skeleton, as found in the products **241a–b** (Scheme 63) [76]. Betaine **242** is the primary addition product and undergoes a formal [2+2] cycloaddition to the benzoxetene **243**. Subsequent 4π -electrocyclic ring opening gives (*Z*)-dienone **244**, which finally undergoes 6π -electrocyclic ring closure to restore the aromaticity and gives the pyran moiety. The use of exocyclic conjugated enals delivered a variety of fused spirocyclic benzopyran structures like **241c** [94].

With di(4-methoxy)phenyl sulfoxide (**246**) as an aryne-trapping agent, dimeric dibenzofuran *S*-shaped helicene **247** is obtained as major product along with carbazoles **248** and **249** starting from triyne **245** (Scheme 64) [95]. Remarkably, five new fused rings assemble within a single step under sole thermal activation.



Scheme 62. Diversity of HDDA–aryne reaction modes with glycidol derivatives via Pinacol-like rearrangements or oxirane fragmentation.

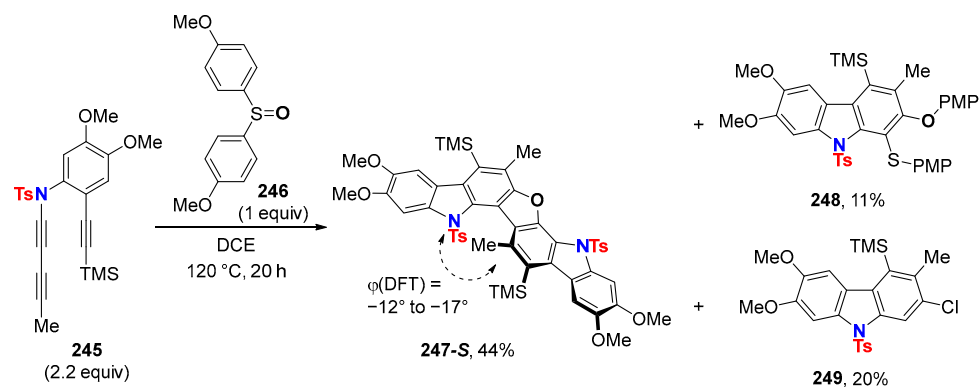


Scheme 63. Catching HDDA-generated arynes with conjugated enals towards benzopyran structures.

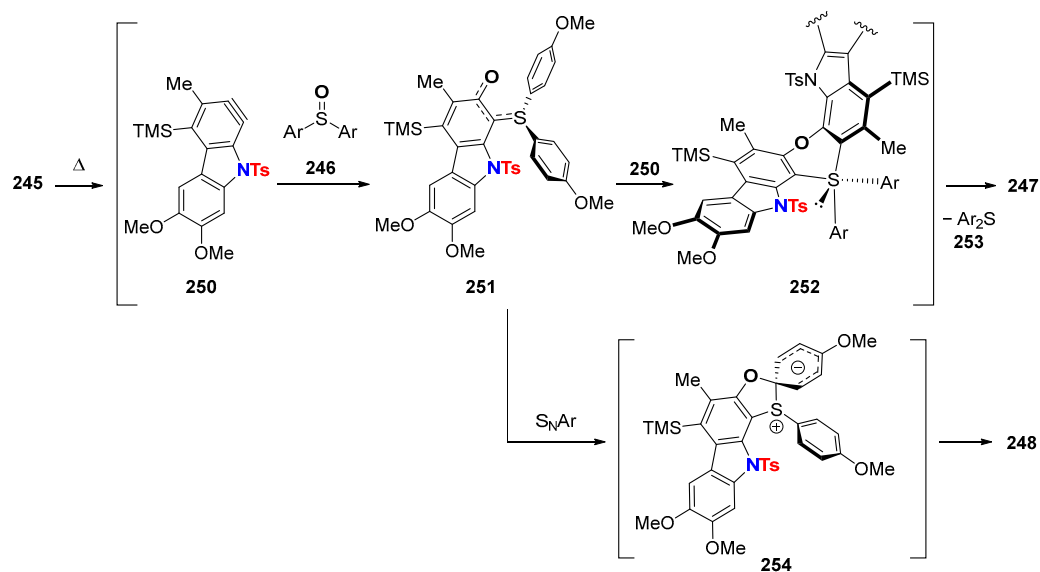
Mechanistically, the reaction of HDDA-generated benzyne **250** with sulfoxide **246** first leads to adduct **251** (Scheme 65). The latter interacts with a second benzyne molecule **250** to give tetracarbo-ligated σ -sulfurane **252**. The hypervalent S(IV) species **252** is the key intermediate of this novel process. Reductive elimination of diarylsulfide **253** delivers the helicene product **247**. The 1:1 adduct carbazole **248** is the $\text{S}_{\text{N}}\text{Ar}$ reaction product of **251** via the Meisenheimer intermediate **254** (Scheme 65).

Aryne trapping via C–S bond formation: HDDA reactions of tetrayne **218** with its 1,3-butadiynamide moiety in the presence of either thiirane (**255a**) or tetrahydrothiophene **255b** both furnish vinyl sulfide **258** (Scheme 66, (1)) [96]. The initial formation of a betaine **256** (*o*-sulfonium/arylcarbanion) is followed by intramolecular proton transfer leading to a more stable S-aryl sulfur ylide **257**, which undergoes ring cleavage. Moreover, in the

presence of a protic nucleophile, a three-component reaction takes place (Scheme 66, (2)). This becomes possible when the sulfide reacts faster with the aryne than the protic nucleophile. Intermolecular protonation of the resulting aryl carbanion leads to sulfonium **259**. Subsequent ring opening by nucleophile addition affords the final products **260a–c**. It is worthy of note that thiirane (**255a**) is not a suitable component for such a process because fragmentation to the vinyl sulfide is faster than nucleophile addition.



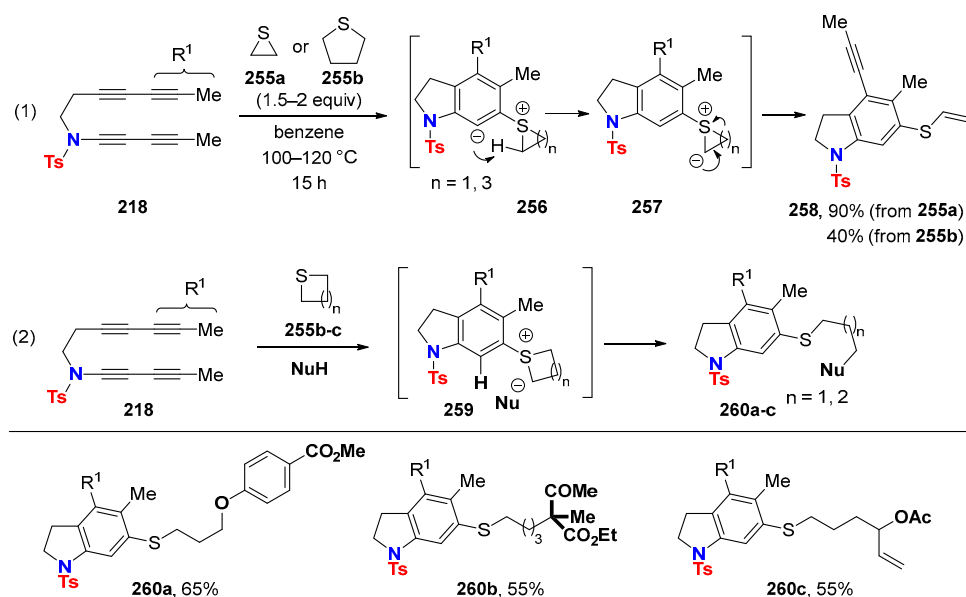
Scheme 64. Synthesis of dimeric dibenzofuran helicenes.



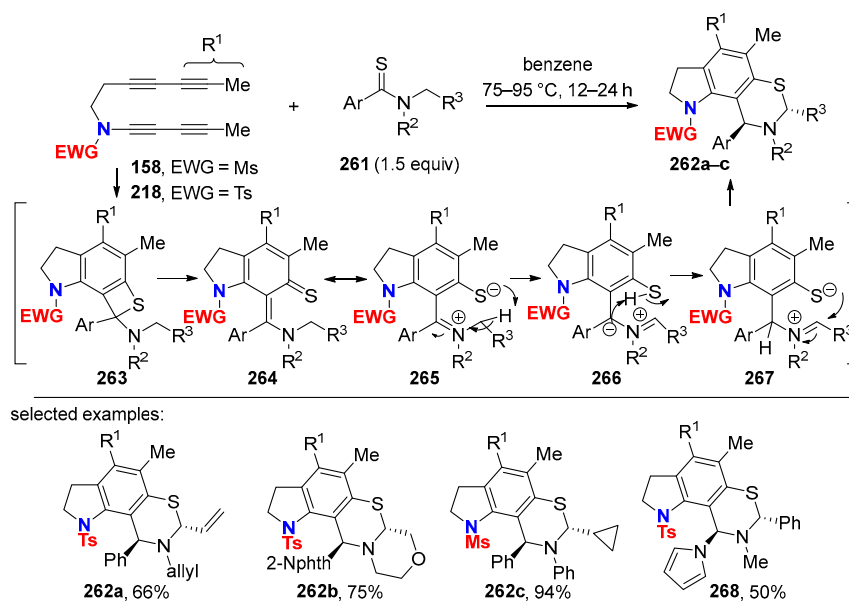
Scheme 65. Mechanistic rationale for the formation of dibenzohelicene **247**.

The HDA reaction of tetraynes **158** (EWG = Ms) or **218** (EWG = Ts) with aryl thioamides **261** affords the dihydrobenzothiazine-derived molecules **262a–c** in a regio- and diastereoselective fashion (Scheme 67) [97]. Notably, these are the first examples of the use of thioamides as aryne-trapping agents. The proposed mechanism involves the formation of benzothietene **263** and its ring opening to give intermediate **264** or its resonance form *o*-thiolatoaryliminium **265**. Intramolecular 1,3-hydrogen atom migration delivers the iminium zwitterion **267**, whose cyclization leads to products **262a–c**. The analogous product **268** was also obtained using a thiourea as reaction partner.

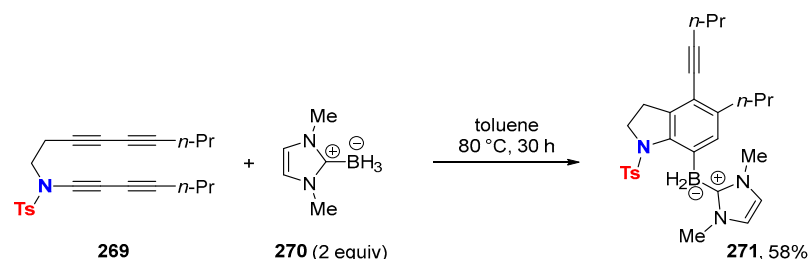
Aryne trapping via C–B bond formation: The hydroboration of the aryne that was generated by an HDA reaction with tetrayne **269**, with the *N*-heterocyclic carbene borane (NHC-borane) **270**, provides the highly functionalized arylborane compound **271** as a single isomer (Scheme 68) [98]. The feasibility of the reaction relies on the fact that NHC-boranes are deactivated and do not hydroborate the starting tetrayne unlike most other borane reagents.



Scheme 66. Reaction of HDDA-generated arynes with cyclic sulfides.



Scheme 67. Reaction of HDDA-generated arynes with aromatic thioamides.

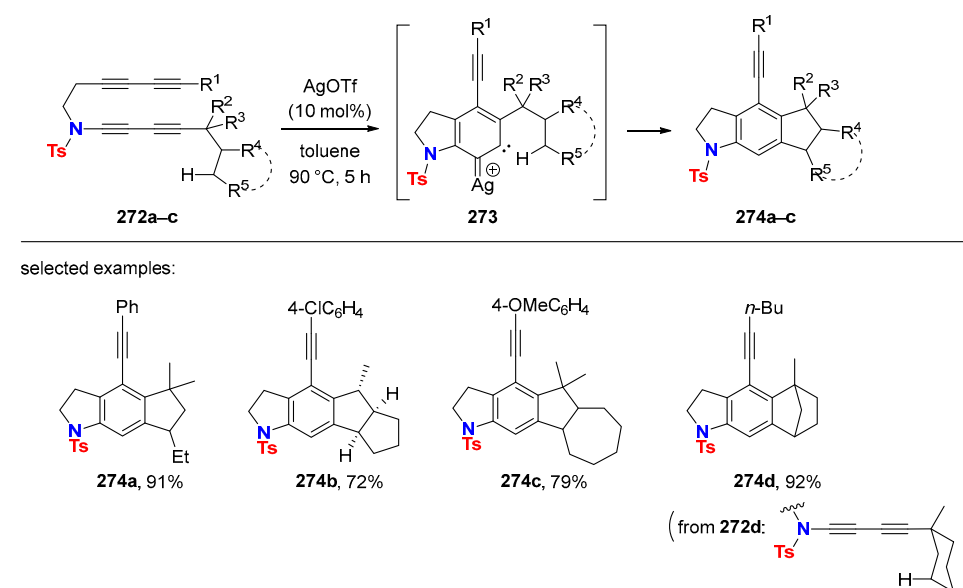


Scheme 68. Trapping of HDDA-generated arynes with NHC-boranes.

6.2. Silver-Catalyzed HDDA Reactions

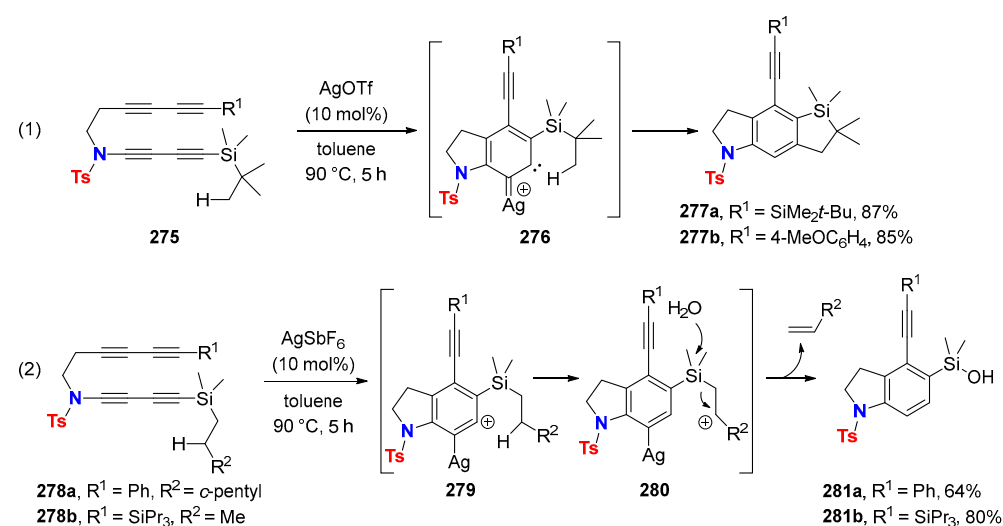
Ag(I)-bound aryne trapping via C–C bond formation: Alkane C–H bonds can be activated by 1,3-butadiyne–HDDA–reaction generated arynes in the presence of silver(I) salts (Scheme 69) [99]. Importantly, under Ag(I)-free reaction conditions, the alkane C–H insertion fails to appear. According to mechanistic studies, the C(sp³)-H bond-breaking

and C(sp²)-H bond-forming processes are concerted and induced via the silver-carbenoid intermediate **273**.



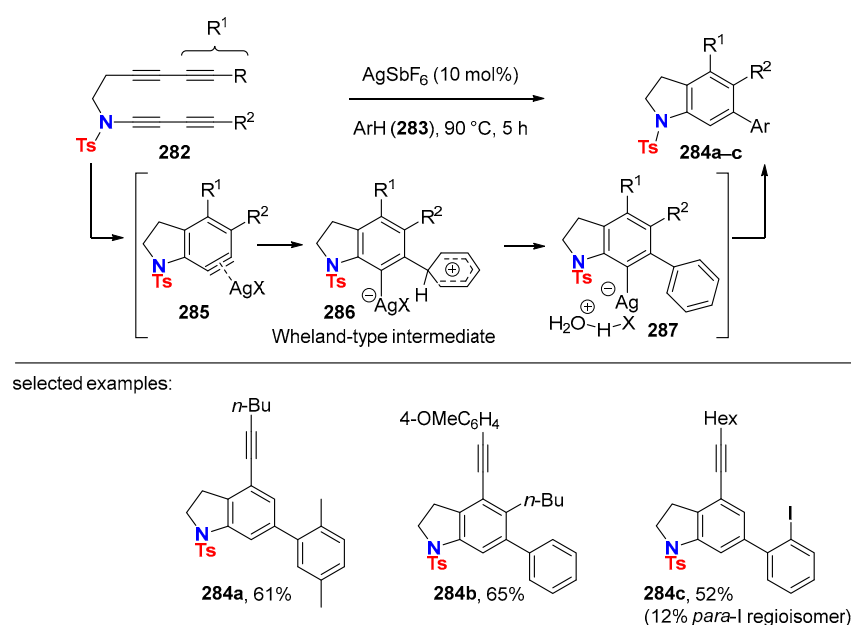
Scheme 69. Reaction of HDDA-generated aryne via silver-catalyzed alkane C-H insertion.

The fact that Ag(I) salts drive the character of the aryne reactivity from an alkyne towards a carbene character was nicely shown with the silyl-substituted substrates **275** bearing a primary C-H bond (Scheme 70, (1)) [100]. In the presence of a secondary or tertiary C-H bond on the β -carbon of the silyl group, hydride transfer occurs instead of C-H insertion (Scheme 70, (2)). This result is plausible considering a favorable hyperconjugation of the β -silicon stabilized carbocation **280**, whose reaction with water delivers the formal aryne hydrogenation products **281a–b**.



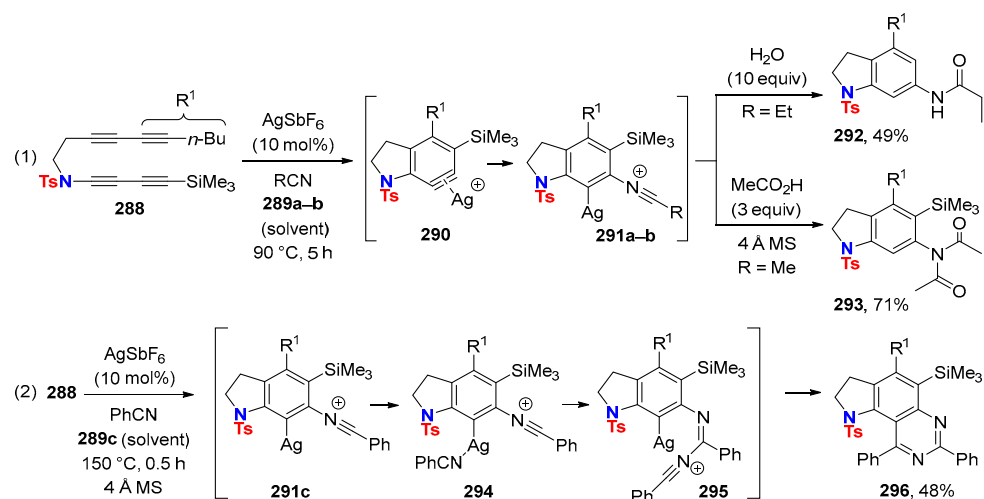
Scheme 70. Intramolecular trapping of HDDA-generated aryne from silyl-substituted substrates.

Silver-catalyzed reactions of non-activated benzenes **283** with 1,3-butadiynamide-**282**–HDDA reaction-generated arynes lead to the hydroarylation products **284a–c** (Scheme 71) [101]. Diels–Alder reaction products of arynes with arenes, as usually found with “free arynes”, stay out and are not formed. The chemical outcome of this transformation is rationalized by an electrophilic aromatic substitution through the formation of a Wheland-type intermediate **286** (arenium ion) and subsequent water-catalyzed proton transfer.



Scheme 71. Intermolecular hydroarylation of silver-complexed HDDA-generated arynes.

Ag(I)-bound aryne trapping via C-N bond formation: Nitriles are too weak nucleophiles to react with arynes. However, in the presence of a silver catalyst, the trapping of HDDA-generated aryne is taking place with nitriles readily via the formation of nitrilium ion intermediates **291a–b**. The latter can react with water or with acetic acid under anhydrous conditions to give indolylamide **292** or imide **293**, respectively, starting from tetrayne **288** (Scheme 72, (1)) [102].

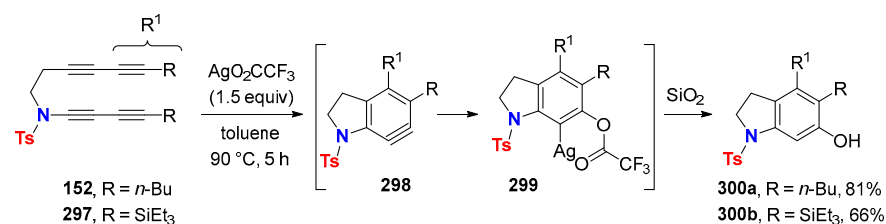


Scheme 72. Reaction of silver-complexed HDDA-generated arynes with nitriles.

Under anhydrous conditions and in the absence of carboxylic acids, tetrayne **288** converts into quinazoline **296** by incorporation of two benzonitrile molecules (**289c**) (Scheme 72, (2)) [103]. Now, the nitrilium ion **291c** interacts with a second nitrile molecule to give the resonance-stabilized complex **294**. Transformation of **294** into *bis*-nitrile adduct **295** and the subsequent ring closure finally delivers quinazoline **296**.

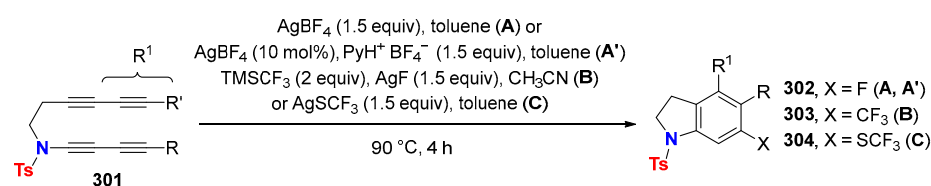
Ag(I)-bound aryne trapping via C-O bond formation: Water, unlike alcohols or carboxylic acids, is a less suitable aryne-trapping agent to deliver subsequent phenols. This is probably because of the immiscibility of water in organic solvents where transient arynes are generated. Silver trifluoroacetate (AgO_2CCF_3) turned out to be a suitable water surrogate to obtain phenol-related compounds [75,104]. Indeed, the reaction of 1,3-butadiynes **152**

or **297** with AgO_2CCF_3 leads via transient HDDA reaction-generated arynes **298** to trifluoroacetoxymethyl organosilver arenes **299**, whose hydrolysis on silica gel furnishes the phenolic compounds **300a–b** (Scheme 73).

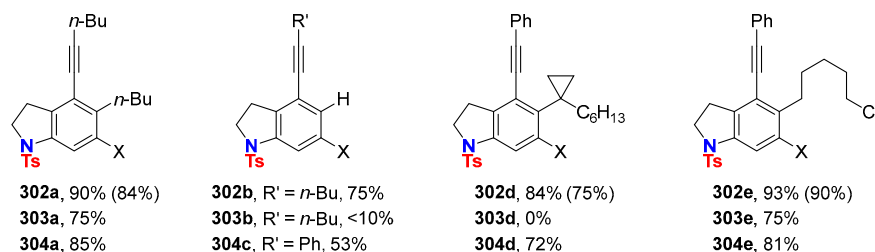


Scheme 73. Synthesis of phenolic compounds from HDDA-generated arynes.

Ag(I)-bound aryne trapping with fluorine-containing reagents: Fluorination, trifluoromethylation and trifluoromethylthiolation of HDDA-generated arynes from 1,3-butadiynes **301** were successfully achieved by using AgBF_4 , AgCF_3 (in situ generated from AgF and TMSCF_3) and AgSCF_3 in stoichiometric quantities, respectively (Scheme 74) [105]. The trifluoromethylation reaction is not proceeding with terminal (R = H) or tertiary alkyl-substituted 1,3-butadiynamides as starting materials (see **303b**, **303d**). A catalytic protocol for aryne fluorination appeared. It relies on the use of AgBF_4 (10 mol%) as the catalyst and the $\text{BF}_4 \bullet \text{pyridinium}$ salt (1.5 equiv) as the fluoride source. Importantly, fluorination fails in the absence of silver salts.



selected examples:



Scheme 74. Silver-mediated fluorination, trifluoromethylation and trifluoromethylthiolation of HDDA-generated arynes.

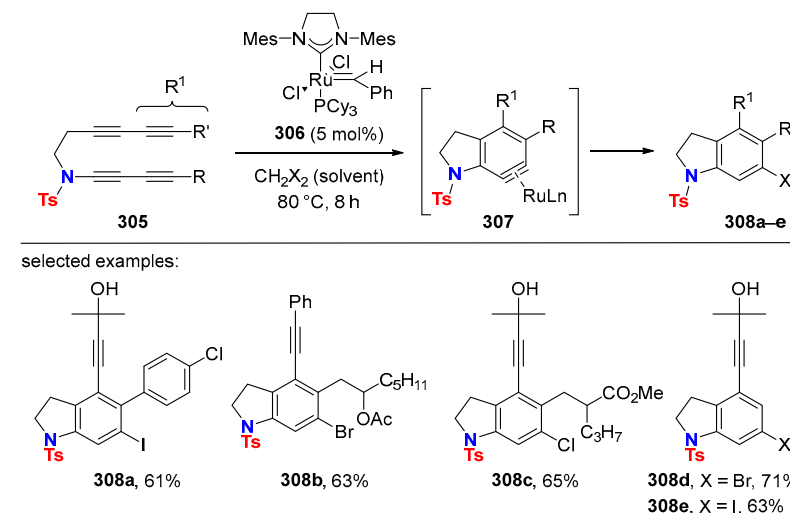
6.3. HDDA Reactions Catalyzed by Other Metals Than Silver

The hydrohalogenative aromatization of ynamide-derived tetraynes **305** readily proceeds in halogenated hydrocarbons CH_2X_2 (X = Cl, Br, I) as the solvent in the presence of Grubbs-type ruthenium alkylidene complex **306** and delivers novel halogenated indoline derivatives **308a–e** (Scheme 75) [106]. The proposed mechanism involves the activation of $\text{CH}_2 \times 2$ by the ruthenium catalyst for the HX transfer to ruthenium-complexed aryne intermediate **307**.

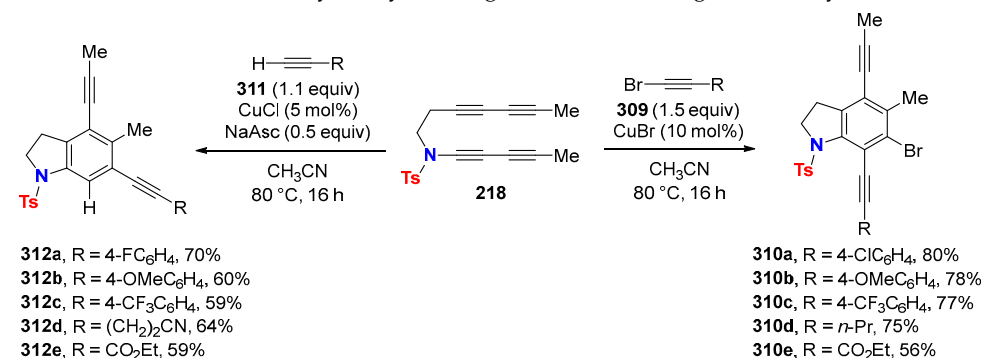
The addition of 1-bromoalkynes **309** or terminal alkynes **311** to 1,3-butadiyne-218-HDDA-reaction generated aryne proceeds efficiently under copper catalysis (Scheme 76) [107]. Interestingly, the insertion of the alkynyl moiety into the aryne carbon–carbon triple bond to give either indolines **310a–e** or **312a–e**, respectively, takes place at complementary positions.

Two different catalytic cycles **A** and **B** are proposed to rationalize the outcome of these reactions (Scheme 77). In the case of the bromoalkynylation, CuBr adds to in situ generated aryne **313** (from 1,3-dynamide **218**) to give aryl copper (I) species **314**. Oxidative addition of this Cu(I) species to 1-bromoalkyne **309** gives the aryl copper(III) intermediate

315. Subsequent reductive elimination produces the 4,7-diethynyldihydroindole **310** and regenerates the copper(I) catalyst. In the case of the catalytic hydroalkynylation reaction (catalytic cycle B), aryne **313** undergoes carbocupration with in situ generated copper acetylide **316** from terminal alkyne **311**, providing aryl copper species **317**. Proton exchange with terminal alkyne **311** delivers compound **312** and closes the catalytic cycle.

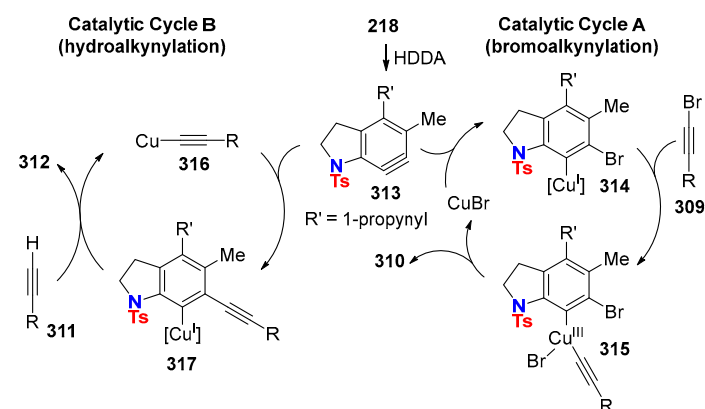


Scheme 75. Ruthenium-catalyzed hydrohalogenation of HDDA-generated arynes.

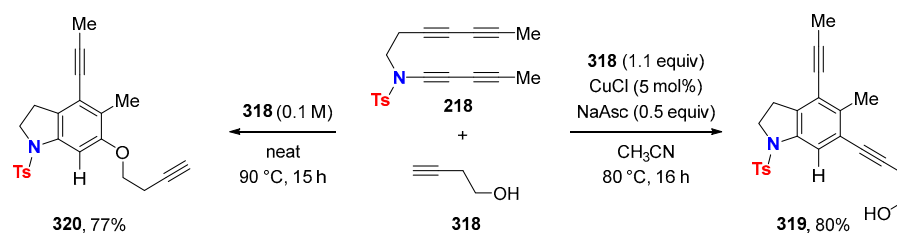


Scheme 76. Copper-catalyzed bromo- and hydroalkynylation of HDDA-generated arynes.

The catalytic reaction of tetrayne **218** with homopropargyl alcohol (**318**) selectively gives the hydroalkynylation product **319**, whereas compound **320** resulting from the addition of the alcohol moiety on the transient aryne **313** is the major compound in the absence of copper catalyst (Scheme 78).



Scheme 77. Proposed mechanism of copper-catalyzed bromoalkynylation and hydroalkynylation of HDDA-generated arynes.



Scheme 78. Different outcomes of the reaction of HDDA-generated aryne with homopropargyl alcohol with and without copper catalyst.

7. Conclusions and Perspectives

The present review covers the synthesis, molecular properties and use of 1,3-butadiynamides in heterocyclic chemistry. Based on this comprehensive summary and its compiled reactions, which not only focused on applications in organic synthesis, but also on mechanistic aspects, it becomes obvious that 1,3-butadiynamides—the ethynyl-ogous variant of ynamides—are more than just simple alkynes: they should be considered as a new class of compounds showing its own specific reactivity.

Their potential as building blocks for the construction of complex molecular scaffolds has emerged only recently, although the synthesis of symmetrical and unsymmetrical 1,3-butadiynamides was described more than 15 years ago. Terminal ynamides are useful precursors of 1,3-butadiynamides for their use in the Glaser–Hay coupling reaction or the Cadiot–Chodkiewicz cross-coupling reaction with 1-bromoalkynes. The latter emerged to a broadly used and indispensable synthetic method to access various highly functionalized non-symmetrical 1,3-butadiynamides. Alternative protocols based on the direct *N*-buta-1,3-diynylation of amides appeared just recently and will find further attention.

The extended conjugation and polarized character of 1,3-butadiynamides facilitate their use in addition and cycloaddition reactions with predictable regioselectivity. Many of them involve gold catalysis along with the successful use of other metal salts (Pd, Ag, Cu/Zn). Moreover, 1,3-butadiynamides are easily derivatized by introducing judicious functional groups tethered to the *N*-atom and/or to the *C*-terminal of the 1,3-diynyl moiety. Such diversely functionalized 1,3-butadiynamides serve as highly useful molecular scaffolds in the development of new reaction cascades.

Intensive studies have been dedicated to thermal or metal-catalyzed reactions with 1,3-butadiynamides tethered to a monoalkyne or 1,3-butadiyne moiety. These tetra- or triynes having a 1,3-butadiynamide unit are privileged substrates for the HDDA reaction because they lead to the in situ formation of a single aryne isomer, and its intermolecular trapping takes place regioselectively. Reagent-free, highly chemo- and regioselective aryne formation with regioselective follow-up reactions by inter- or intramolecular aryne trapping not only enhanced the chemistry of 1,3-butadiynamides, but also boosted the understanding of different reaction channels available for in situ generated aryne species. HDDA reactions with 1,3-butadiynamide units can be performed solely thermally or in the presence of sub-stoichiometric amounts of Ag(I)-salts. The latter often changes the mode of reactivity towards a more carbenoid character of the aryne intermediate and opens new alternative reaction channels.

Most described 1,3-butadiynamides are derived from sulfonamides. It is conceivable that the synthesis of carbamate- or oxazolidinone-related 1,3-butadiynamides will be further explored and that new reaction sequences will be discovered, as the strength of the nitrogen bound EWG group will alter the 1,3-butadiynamide reactivity.

The more classical activation of 1,3-butadiynamides relies on the in situ generation of a keteniminium species to accelerate follow-up transformations. Recently, a new reaction mode—the in situ liberation of [4]cumuleniminines from 1,3-butadiynamides—was revealed. This finding will probably initiate the development of novel reaction cascades and broaden the array of available structurally complex molecules.

Finally, the examples of optically active 1,3-butadiynamides are scarce, and the possibility of chirality transfer during reaction cascades has not been investigated yet. Asymmetric or enantioselective synthesis relying on the transformation of 1,3-butadiynamides will certainly be a future topic to gain access to the chiral world of heterocycles. Surely, the chemistry of 1,3-butadiynamides is still at its infancy and more new reactions and more sophisticated applications, especially in the field of heterocyclic chemistry, will appear in near future.

Author Contributions: All authors contributed equally to this article. All authors have read and agreed to the published version of the manuscript.

Funding: This work was funded by the Agence Nationale de la Recherche (ANR-22-CE07-0010).

Institutional Review Board Statement: Not applicable.

Informed Consent Statement: Not applicable.

Data Availability Statement: Not applicable.

Acknowledgments: The continuous support of our work by the CNRS, the Conseil Régional de Normandie, the European FEDER funding, and the Agence Nationale de la Recherche (ANR-22-CE07-0010) is gratefully acknowledged.

Conflicts of Interest: The authors declare no conflict of interest.

References

1. Witulski, B.; Stengel, T. *N*-Functionalized 1-Alkynylamides: New Building Blocks for Transition Metal Mediated Inter- and Intramolecular [2+2+1] Cycloadditions. *Angew. Chem. Int. Ed.* **1998**, *37*, 489–492. [CrossRef]
2. Iftikhar, R.; Mazhar, A.; Iqbal, M.S.; Khan, F.Z.; Askary, S.H.; Sibtain, H. Ring Forming Transformation of Ynamides via Cycloaddition. *RSC. Adv.* **2023**, *13*, 10715–10756. [CrossRef]
3. Hu, Y.-C.; Zhao, Y.; Wan, B.; Chen, Q.-A. Reactivity of Ynamides in Catalytic Intermolecular Annulations. *Chem. Soc. Rev.* **2021**, *50*, 2582–2625. [CrossRef]
4. Shandilya, S.; Gogoi, M.P.; Dutta, S.; Sahoo, A.K. Gold-Catalyzed Transformation of Ynamides. *Chem. Rec.* **2021**, *21*, 4123–4149. [CrossRef]
5. Campeau, D.; Rayo, D.F.L.; Mansour, A.; Muratov, K.; Gagosz, F. Gold-Catalyzed Reactions of Specially Activated Alkynes, Allenes and Alkenes. *Chem. Rev.* **2021**, *121*, 8756–8867. [CrossRef]
6. Chen, Y.-B.; Qian, P.-C.; Ye, L.-W. Brønsted Acid-Mediated Reactions of Ynamides. *Chem. Soc. Rev.* **2020**, *49*, 8897–8909. [CrossRef] [PubMed]
7. Lynch, C.C.; Sripada, A.; Wolf, C. Asymmetric Synthesis with Ynamides: Unique Reaction Control, Chemical Diversity and Applications. *Chem. Soc. Rev.* **2020**, *49*, 8543–8583. [CrossRef] [PubMed]
8. Tan, T.-D.; Wang, Z.-S.; Qian, P.-C.; Ye, L.-W. Radical Reactions of Ynamides. *Small Methods* **2021**, *5*, 2000673. [CrossRef] [PubMed]
9. Mahe, C.; Cariou, K. Ynamides in Free Radical Reactions. *Adv. Synth. Catal.* **2020**, *362*, 4820–4832. [CrossRef]
10. Hong, F.-L.; Ye, L.-W. Transition Metal-Catalyzed Tandem Reactions of Ynamides for Divergent *N*-Heterocycle Synthesis. *Acc. Chem. Res.* **2020**, *53*, 2003–2019. [CrossRef]
11. Zhou, B.; Tan, T.-D.; Zhu, X.-Q.; Shang, M.; Ye, L.-W. Reversal of Regioselectivity in Ynamide Chemistry. *ACS Catal.* **2019**, *9*, 6393–6406. [CrossRef]
12. Prabagar, B.; Ghosh, N.; Sahoo, A.K. Cyclization and Cycloisomerization of π -Tethered Ynamides: An Expedient Synthetic Method to Construct Carbo- and Heterocycles. *Synlett* **2017**, *28*, 2539–2555.
13. Cook, A.M.; Wolf, C. Terminal Ynamides: Synthesis, Coupling Reactions, and Additions to Common Electrophiles. *Tetrahedron Lett.* **2015**, *56*, 2377–2392. [CrossRef]
14. Wang, X.-N.; Yeom, H.-S.; Fang, L.-C.; He, S.; Ma, Z.-X.; Kedrowski, B.L.; Hsung, R.P. Ynamides in Ring Forming Transformations. *Acc. Chem. Res.* **2014**, *47*, 560–578. [CrossRef] [PubMed]
15. Evans, G.; Coste, A.; Jouvin, K. Ynamides: Versatile Tools in Organic Synthesis. *Angew. Chem. Int. Ed.* **2010**, *49*, 2840–2859. [CrossRef] [PubMed]
16. DeKorver, K.A.; Li, H.; Lohse, A.G.; Hayashi, R.; Lu, Z.; Zhang, Y.; Hsung, R.P. Ynamides: A Modern Functional Group for the New Millennium. *Chem. Rev.* **2010**, *110*, 5064–5106. [CrossRef]
17. Fluegel, L.L.; Hoye, T.R. Hexadehydro-Diels–Alder Reaction: Benzyne Generation via Cycloisomerization of Tethered Triynes. *Chem. Rev.* **2021**, *121*, 2413–2444. [CrossRef]
18. Hoye, T.R.; Baire, B.; Niu, D.; Willoughby, P.H.; Woods, B.P. The hexadehydro-Diels–Alder reaction. *Nature* **2012**, *490*, 208–212. [CrossRef]

19. Holden (née Hall), C.; Greaney, M.F. The Hexadehydro-Diels–Alder Reaction: A New Chapter in Aryne Chemistry. *Angew. Chem. Int. Ed.* **2014**, *53*, 5746–5749. [CrossRef]
20. Diamond, O.J.; Marder, T.B. Methodology and Applications of the Hexadehydro-Diels–Alder (HDDA) Reaction. *Org. Chem. Front.* **2017**, *4*, 891–910. [CrossRef]
21. Yu, H.; Xu, F. Advances in the Synthesis of Nitrogen-Containing Heterocyclic Compounds by in situ Benzyne Cycloaddition. *RSC Adv.* **2023**, *13*, 8238–8253. [CrossRef] [PubMed]
22. Rodriguez, D.; Castedo, L.; Saa, C. Homocoupling of 1-Alkynyl Tosylamides. *Synlett* **2004**, *2004*, 377–379. [CrossRef]
23. Doan, T.-H.; Talbi, I.; Lohier, J.-F.; Touil, S.; Alayrac, C.; Witulski, B. Synthesis, Crystal Structure, Optical, Electrochemical and Thermal Properties of the Ynamide: Bis-(*N*-4-methylbenzenesulfonyl, *N*-*n*-butyl)-1,3-butadiyne-1,4-diamide. *J. Mol. Struct.* **2016**, *1116*, 127–134. [CrossRef]
24. Takai, R.; Shimbo, D.; Tada, N.; Itoh, A. Ligand-Enabled Copper-Catalyzed *N*-Alkynylation of Sulfonamide with Alkynyl Benziodoxolone: Synthesis of Amino Acid-Derived Ynamide. *J. Org. Chem.* **2021**, *86*, 4699–4713. [CrossRef]
25. Witulski, B.; Schweikert, T.; Schollmeyer, D.; Nemkovich, N.A. Synthesis and Molecular Properties of Donor- π -Spacer-Acceptor Ynamides with up to Four Conjugated Alkyne Units. *Chem. Commun.* **2010**, *46*, 2953–2955. [CrossRef]
26. Talbi, I.; Alayrac, C.; Lohier, J.-F.; Touil, S.; Witulski, B. Application of Ynamides in the Synthesis of 2-(Tosylamido)- and 2,5-Bis(tosylamido)thiophenes. *Org. Lett.* **2016**, *18*, 2656–2659. [CrossRef]
27. Wang, Y.-P.; Danheiser, R.L. Synthesis of 2-Iodoynamides and Regioselective [2+2] Cycloadditions with Ketene. *Tetrahedron Lett.* **2011**, *52*, 2111–2114. [CrossRef]
28. Tracey, M.R.; Zhang, Y.; Frederick, M.O.; Mulder, J.A.; Hsung, R.P. Sonogashira Cross-Couplings of Ynamides. Syntheses of Urethane- and Sulfonamide-Terminated Conjugated Phenylacetylenic Systems. *Org. Lett.* **2004**, *6*, 2209–2212. [CrossRef]
29. Dunetz, J.R.; Danheiser, R.L. Copper-Mediated *N*-Alkynylation of Carbamates, Ureas, and Sulfonamides. A General Method for the Synthesis of Ynamides. *Org. Lett.* **2003**, *5*, 4011–4014. [CrossRef]
30. Kohnen, A.L.; Dunetz, J.R.; Danheiser, R.L. Synthesis of Ynamides by *N*-Alkynylation of Amine Derivatives. Preparation of *N*-Allyl-*N*-(Methoxycarbonyl)-1,3-Decadiynylamine. *Org. Synth.* **2007**, *84*, 88–101.
31. Ross, S.P.; Hoye, T.R. Multiheterocyclic Motifs via Three-Component Reactions of Benzyne, Cyclic Amines, and Protic Nucleophiles. *Org. Lett.* **2018**, *20*, 100–103. [CrossRef] [PubMed]
32. Zhang, Y.; Hsung, R.P.; Tracey, M.R.; Kurtz, K.C.M.; Vera, E.L. Copper Sulfate-Pentahydrate-1,10-Phenanthroline Catalyzed Amidations of Alkynyl Bromides. Synthesis of Heteroaromatic Amine Substituted Ynamides. *Org. Lett.* **2004**, *6*, 1151–1154. [CrossRef] [PubMed]
33. Wang, T.; Niu, D.; Hoye, T.R. The Hexadehydro-Diels–Alder Cycloisomerization Reaction Proceeds by a Stepwise Mechanism. *J. Am. Chem. Soc.* **2016**, *138*, 7832–7835. [CrossRef] [PubMed]
34. Mansfield, S.J.; Smith, R.C.; Yong, J.R.J.; Garry, O.L.; Anderson, E.A. A General Copper-Catalyzed Synthesis of Ynamides from 1,2-Dichloroenamides. *Org. Lett.* **2019**, *21*, 2918–2922. [CrossRef]
35. Kawakami, R.; Usui, S.; Tada, N.; Itoh, A. Late-Stage Diversification Strategy for Synthesizing Ynamides through Copper-Catalyzed Diynylation and Azide-Alkyne Cycloaddition. *Chem. Commun.* **2023**, *59*, 450–453.
36. Gohrai, S.; Lee, D. Selectivity for Alkynyl or Allenyl Imidamides and Imidates in Copper-Catalyzed Reactions of Terminal 1,3-Diynes and Azides. *Org. Lett.* **2021**, *23*, 697–701. [CrossRef]
37. Garner, M.H.; Hoffmann, R.; Rettrup, S.; Solomon, G.C. Coarctate and Möbius: The Helical Orbitals of Allene and Other Cumulenes. *ACS Cent. Sci.* **2018**, *4*, 688–700. [CrossRef]
38. Garner, M.H.; Jensen, A.; Hyllested, L.O.H.; Solomon, G.C. Helical Orbitals and Circular Currents in Linear Carbon Wires. *Chem. Sci.* **2019**, *10*, 4598–4608. [CrossRef]
39. Garner, M.H.; Corminboeuf, C. Helical Electronic Transitions of Spiroconjugated Molecules. *Chem. Commun.* **2021**, *57*, 6408–6411. [CrossRef]
40. Ohashi, S.; Inagaki, S. Orbital Phase Control of Conformations of Alkyne Derivatives. *Tetrahedron* **2001**, *57*, 5361–5367. [CrossRef]
41. Hendon, C.H.; Tiana, D.; Murray, A.T.; Carbery, D.R.; Walsh, A. Helical Frontier Orbitals of Conjugated Linear Molecules. *Chem. Sci.* **2013**, *4*, 4278–4284. [CrossRef]
42. Balakrishnan, A.R.; Suresh, R.; Vijayakumar, S. Amine Terminated Polyyne as Candidates for Molecular Wire Applications: A DFT Study. *Phys. E Low-Dimens. Syst. Nanostruct.* **2022**, *137*, 115045. [CrossRef]
43. Bro-Jørgensen, W.; Garner, M.H.; Solomon, G.C. Quantification of the Helicality of Helical Molecular Orbitals. *J. Phys. Chem. A* **2021**, *125*, 8107–8115. [CrossRef] [PubMed]
44. Petrov, A.R.; Daniliuc, C.G.; Jones, P.G.; Tamm, M. A Novel Synthetic Approach to Diaminoacetylenes: Structural Characterization and Reactivity of Aromatic and Aliphatic Ynediamines. *Chem. Eur. J.* **2010**, *16*, 11804–11808. [CrossRef]
45. Tokutome, Y.; Okuno, T. Preparations, Crystal Polymorphs and DFT Calculations of N^1, N^1, N^4, N^4 -Tetraphenylbuta-1,3-diyne-1,4-diamine. *J. Mol. Struct.* **2013**, *1047*, 136–142. [CrossRef]
46. Mayerle, J.J.; Flandera, M.A. Bis(1-carbazolyl)butadiyne. *Acta Cryst.* **1978**, *B34*, 1374–1376. [CrossRef]
47. Matsuda, H.; Nakanishi, H.; Hosomi, T.; Kato, M. Synthesis and Solid-State Polymerization of a New Diacetylene: 1-(*N*-Carbazolyl)penta-1,3-diyne-5-ol. *Macromolecules* **1988**, *21*, 1238–1240. [CrossRef]
48. Tabata, H.; Kuwamoto, K.; Okuno, T. Conformational Polymorphs and Solid-State Polymerization of 9-(1,3-Butadiynyl)carbazole Derivatives. *J. Mol. Struct.* **2016**, *1106*, 452–459. [CrossRef]

49. Ide, M.; Ohashi, K.; Mihara, S.; Iwasaha, T. Regio- and Stereoselective hydrohalogenation of Ynamide Components in 1,3-Butadiynes with in situ Generated HX. *Tetrahedron Lett.* **2014**, *55*, 2130–2133. [CrossRef]
50. De la Vega-Hernandez, K.; Romain, E.; Coffinet, A.; Bijouard, K.; Gontard, G.; Chemla, F.; Ferreira, F.; Jackowski, O.; Perez-Luna, A. Radical Germylzincation of α -Heteroatom-Substituted Alkynes. *J. Am. Chem. Soc.* **2018**, *140*, 17632–17642. [CrossRef]
51. Kramer, S.; Madsen, J.L.H.; Rottländer, M.; Skrydstrup, T. Access to 2,5-Diamidopyrroles and 2,5-Diamidofurans by Au(I)-Catalyzed Double Hydroamination or Hydration of 1,3-Diynes. *Org. Lett.* **2010**, *12*, 2758–2761. [CrossRef] [PubMed]
52. Choudhary, S.; Gayyur; Ghosh, N. Cu(II)-Catalyzed [4+1] and [4+3] Annulation Reactions: A Modular Approach to *N*-Aryl/Alkyl Substituted 2,5-Diamidopyrroles and Diazepines. *Org. Biomol. Chem.* **2022**, *20*, 7017–7021. [CrossRef] [PubMed]
53. Dunetz, J.R.; Danheiser, R.L. Synthesis of Highly Substituted Indolines and Indoles via Intramolecular [4+2] Cycloaddition of Ynamides and Conjugated Enynes. *J. Am. Chem. Soc.* **2005**, *127*, 5776–5777. [CrossRef] [PubMed]
54. Liao, Y.; Lu, Q.; Chen, G.; Yu, Y.; Li, C.; Huang, X. Rhodium-Catalyzed Azide-Alkyne Cycloaddition of Internal Ynamides: Regioselective Assembly of 5-Amino-Triazoles under Mild Conditions. *ACS Catal.* **2017**, *7*, 7529–7534. [CrossRef]
55. Davies, P.W.; Cremonesi, A.; Dumitrescu, L. Intermolecular and Selective Synthesis of 2,4,5-Trisubstituted Oxazoles by a Gold-Catalyzed Formal [3+2] Cycloaddition. *Angew. Chem. Int. Ed.* **2011**, *50*, 8931–8935. [CrossRef]
56. Skaria, M.; Hsu, Y.-C.; Jiang, Y.-T.; Lu, M.-Y.; Kuo, T.-C.; Cheng, M.-J.; Liu, R.-S. Gold-Catalyzed Oxidations of 1,3-Diynamides with C(1) versus C(3) Regioselectivity: Catalyst-Dependent Oxidative Cyclizations in the C(3) Oxidation. *Org. Lett.* **2020**, *22*, 4478–4482. [CrossRef]
57. Lee, D.; Kim, M. Advances in the Metallotropic [1,3]-Shift of Alkynyl Carbenoids. *Org. Biomol. Chem.* **2007**, *5*, 3418–3427. [CrossRef]
58. Yanai, H.; Kawazoe, T.; Ishii, N.; Witulski, B.; Matsumoto, T. Regioselective Synthesis of 4-Aryl-1,3-dihydroxy-2-naphthoates through 1,2-Aryl-Migrative Ring Rearrangement Reaction and their Photoluminescence Properties. *Chem. Eur. J.* **2021**, *27*, 11442–11449. [CrossRef]
59. Kumar, M.; Kaliya, K.; Maurya, S.K. Recent Progress in the Homogeneous Gold-Catalysed Cycloisomerisation Reactions. *Org. Biomol. Chem.* **2023**, *21*, 3276–3295. [CrossRef]
60. Liu, J.; Chakraborty, P.; Zhang, H.; Zhong, L.; Wang, Z.-X.; Huang, X. Gold-Catalyzed Atom-Economic Synthesis of Sulfone-Containing Pyrrolo [2,1-*a*]isoquinolines from Diynamides: Evidence for Consecutive Sulfonyl migration. *ACS Catal.* **2019**, *9*, 2610–2617. [CrossRef]
61. Choudhary, S.; Gayyur; Ghosh, N. Gold(I)-Catalyzed and PTSA-Promoted Cycloisomerization of Ynamides to Access Pyrrole Substituted α,β -Unsaturated Ketones. *Eur. J. Org. Chem.* **2023**, *26*, e202201223. [CrossRef]
62. Wang, H.F.; Guo, L.N.; Fan, Z.B.; Tang, T.H.; Zi, W. Gold-Catalyzed Formal Hexadehydro-Diels–Alder/Carboalkoxylation Reaction Cascades. *Org. Lett.* **2021**, *23*, 2676–2681. [CrossRef]
63. Liu, N.; Sun, H.; Wang, J.; Zhang, Z.; Wang, T. Ag(I)-Catalyzed Synthesis of 2-Aminoquinolines from 1-Aminobutadiynes and Anilines. *Adv. Synth. Catal.* **2021**, *363*, 5443–5447. [CrossRef]
64. Wang, J.; Du, J.; Wang, T. Synthesis of 2-Aminopyrrolo[1,2-*b*]pyridazines via Gold(I)-Catalyzed Chemoselective Hydroamination/Hydroarylation Cascade of 1,3-Diynamides with 1-Aminopyrroles. *Adv. Synth. Catal.* **2023**, *365*, 1088–1092. [CrossRef]
65. Gayyur; Choudhary, S.; Kant, R.; Ghosh, N. Synergetic Copper/Zinc Catalysis: Synthesis of Aryl/Heteroaryl-Fused 1*H*-Pyrrolo[3,2-*c*]pyridines. *Chem. Commun.* **2022**, *58*, 1974–1977. [CrossRef]
66. Pandit, Y.B.; Jiang, Y.-T.; Jian, J.-J.; Chen, T.-C.; Kuo, T.-C.; Cheng, M.-J.; Liu, R.-S. Gold-Catalyzed [5+2]-Annulations of 1,3-Diyn-1-amides with Anthranils Bearing no C(6)-Substituents. *Org. Chem. Front.* **2021**, *8*, 2563–2568. [CrossRef]
67. Tian, X.; Song, L.; Farshadfar, K.; Rudolph, M.; Rominger, F.; Oeser, T.; Ariafard, A.; Hashmi, A.S.K. Acyl Migration *versus* Epoxidation in Gold Catalysis: Facile, Switchable, and Atom-Economic Synthesis of Acylindoles and Quinoline Derivatives. *Angew. Chem. Int. Ed.* **2020**, *59*, 471–478. [CrossRef]
68. Liu, J.; Zhu, L.; Wan, W.; Huang, X. Gold-Catalyzed Cascade Cyclization of 1,3-Diynamides: Polycyclic *N*-Heterocycle Synthesis via Construction of a Furopyridinyl Core. *Org. Lett.* **2020**, *22*, 3279–3285. [CrossRef]
69. Xia, J.; Liu, J.; Yu, Y.; Zhang, J.; Huang, X. Divergent Access to Polycyclic *N*-Heterocyclic Compounds through Büchner-Type Dearomatisation Enabled Cycloisomerization of Diynamides under Gold Catalysis. *Org. Lett.* **2022**, *24*, 4298–4303. [CrossRef] [PubMed]
70. Lenko, I.; Mamontov, A.; Alayrac, C.; Legay, R.; Witulski, B. Media-Driven Pd-Catalyzed Reaction Cascades with 1,3-Diynamides Leading Selectively to Either Indoles or Quinolines. *Angew. Chem. Int. Ed.* **2021**, *60*, 22729–22734. [CrossRef] [PubMed]
71. Witulski, B.; Alayrac, C.; Tevzadze-Saefel, L. Palladium-Catalyzed Synthesis of 2-Aminoindoles by a Heteroannulation Reaction. *Angew. Chem. Int. Ed.* **2003**, *42*, 4257–4260. [CrossRef] [PubMed]
72. Bradley, A.Z.; Johnson, R.P. Thermolysis of 1,3,8-Nonatriyne: Evidence for Intramolecular [2+4] Cycloaromatization to a Benzyne Intermediate. *J. Am. Chem. Soc.* **1997**, *119*, 9917–9918. [CrossRef]
73. Miyawaki, K.; Suzuki, R.; Kawano, T.; Ueda, I. Cycloaromatization of a Non-Conjugated Polyenyne System: Synthesis of 5*H*-Benzo[*d*]fluoreno[3,2-*b*]pyrans via Diradicals Generated from 1-[2-{4-(2-Alkoxyethyl)phenyl}butan-1,3-diynyl]phenylpentan-2,4-diyn-1-ols and Trapping Evidence for the 1,2-Didehydrobenzene Diradical. *Tetrahedron Lett.* **1997**, *38*, 3943–3946.
74. Liang, Y.; Hong, X.; Yu, P.; Houk, K.N. Why Alkynyl Substituents Dramatically Accelerate Hexadehydro-Diels–Alder (HDDA) Reactions: Stepwise Mechanisms of HDDA Cycloadditions. *Org. Lett.* **2014**, *16*, 5702–5705. [CrossRef] [PubMed]

75. Karmakar, R.; Yun, S.Y.; Wang, K.-P.; Lee, D. Regioselectivity in the Nucleophile Trapping of Arynes: The Electronic and Steric Effects of Nucleophiles and Substituents. *Org. Lett.* **2014**, *16*, 6–9. [CrossRef]
76. Wang, T.; Hoyer, T.R. Hexadehydro-Diels–Alder (HDDA)-Enabled Carbazolyne Chemistry: Single Step, de Novo Construction of the Pyranocarbazole Core of Alkaloids of the *Murraya koenigii* (Curry Tree) Family. *J. Am. Chem. Soc.* **2016**, *138*, 13870–13873. [CrossRef]
77. Ross, S.P.; Hoyer, T.R. Reactions of Hexadehydro-Diels–Alder Benzyne with Structurally Complex Multifunctional Natural Products. *Nat. Chem.* **2017**, *9*, 523–530. [CrossRef]
78. Chen, M.; He, C.Q.; Houk, K.N. Mechanism and Regioselectivity of an Unsymmetrical Hexadehydro-Diels–Alder (HDDA) Reaction. *J. Org. Chem.* **2019**, *84*, 1959–1963. [CrossRef]
79. Cheong, P.H.-Y.; Paton, R.S.; Bronner, S.M.; Im, G.-Y.J.; Garg, N.K.; Houk, K.N. Indolyne and Aryne Distortions and Nucleophilic Regioselectivities. *J. Am. Chem. Soc.* **2010**, *132*, 1267–1269. [CrossRef]
80. Karmakar, R.; Lee, D. Reactions of Arynes Promoted by Silver Ions. *Chem. Soc. Rev.* **2016**, *45*, 4459–4470. [CrossRef]
81. Zhang, J.; Niu, D.; Brinker, V.A.; Hoyer, T.R. The Phenol–Ene Reaction: Biaryl Synthesis via Trapping Reactions between HDDA-Generated Benzyne and Phenolics. *Org. Lett.* **2016**, *18*, 5596–5599. [CrossRef] [PubMed]
82. Gupta, S.; Xie, P.; Xia, Y.; Lee, D. Reactivity and Selectivity in the Intermolecular Alder–Ene Reactions of Arynes with Functionalized Alkenes. *Org. Lett.* **2017**, *19*, 5162–5165. [CrossRef]
83. Karmakar, R.; Mamidipalli, P.; Yun, S.Y.; Lee, D. Alder–Ene Reactions of Arynes. *Org. Lett.* **2013**, *15*, 1938–1941. [CrossRef] [PubMed]
84. Karmakar, R.; Le, A.; Xie, P.; Xia, Y.; Lee, D. Reactivity of Arynes for Arene Dearomatization. *Org. Lett.* **2018**, *20*, 4168–4172. [CrossRef] [PubMed]
85. Gupta, S.; Lin, Y.; Xia, Y.; Wink, D.J.; Lee, D. Alder–Ene Reactions Driven by High Steric Strain and Bond Angle Distortion to Form Benzocyclobutenes. *Chem. Sci.* **2019**, *10*, 2212–2217. [CrossRef] [PubMed]
86. Le, A.; Lee, D. Selectivity between an Alder–ene Reaction and a [2+2] Cycloaddition in the Intramolecular Reactions of Allene-Tethered Arynes. *Org. Chem. Front.* **2021**, *8*, 3390–3397. [CrossRef]
87. Xiao, X.; Hoyer, T.R. The Domino Hexadehydro-Diels–Alder Reaction Transforms Polyyne to Benzyne to Naphthyne to Anthracene to Tetracyne (and Beyond?). *Nat. Chem.* **2018**, *10*, 838–844. [CrossRef]
88. Ross, S.P.; Baire, B.; Hoyer, T.R. Mechanistic Duality in Tertiary Amine Additions to Thermally Generated Hexadehydro-Diels–Alder Benzyne. *Org. Lett.* **2017**, *19*, 5705–5708. [CrossRef]
89. Arora, S.; Zhang, J.; Pogula, V.; Hoyer, T.R. Reactions of Thermally Generated Benzyne with Six-Membered *N*-Heteroaromatics: Pathway and Product Diversity. *Chem. Sci.* **2019**, *10*, 9069–9076. [CrossRef]
90. Arora, S.; Palani, V.; Hoyer, T.R. Reactions of Diaziridines with Benzyne Give *N*-Arylhydrazones. *Org. Lett.* **2018**, *20*, 8082–8085. [CrossRef]
91. Sneddon, D.S.; Hoyer, T.R. Arylhydrazine Trapping of Benzyne: Mechanistic Insights and a Route to Azoarenes. *Org. Lett.* **2021**, *23*, 3432–3436. [CrossRef] [PubMed]
92. Arora, S.; Sneddon, D.S.; Hoyer, T.R. Reactions of HDDA Benzyne with *C,N*-Diarylimines ($\text{ArCH} = \text{NAr}'$). *Eur. J. Org. Chem.* **2020**, *2020*, 2379–2383. [CrossRef]
93. Zhang, J.; Hoyer, T.R. Divergent Reactivity during the Trapping of Benzyne by Glycidol Analogs: Ring Cleavage via Pinacol-Like Rearrangements vs. Oxirane Fragmentations. *Org. Lett.* **2019**, *21*, 2615–2619. [CrossRef] [PubMed]
94. Wang, T.; Oswood, C.J.; Hoyer, T.R. Trapping of Hexadehydro-Diels–Alder Benzyne with Exocyclic, Conjugated Enals as a Route to Fused Spirocyclic Benzopyran Motifs. *Synlett* **2017**, *28*, 2933–2935. [CrossRef]
95. Ritts, C.B.; Hoyer, T.R. Sulfurane [S(IV)]-Mediated Fusion of Benzyne Leads to Helical Dibenzofurans. *J. Am. Chem. Soc.* **2021**, *143*, 13501–13506. [CrossRef]
96. Chen, J.; Palani, V.; Hoyer, T.R. Reactions of HDDA-Derived Benzyne with Sulfides: Mechanism, Modes, and Three-Component Reactions. *J. Am. Chem. Soc.* **2016**, *138*, 4318–4321. [CrossRef]
97. Palani, V.; Chen, J.; Hoyer, T.R. Reactions of Hexadehydro-Diels–Alder (HDDA)-Derived Benzyne with Thioamides: Synthesis of Dihydrobenzothiazino-Heterocyclics. *Org. Lett.* **2016**, *18*, 6312–6315. [CrossRef] [PubMed]
98. Watanabe, T.; Curran, D.P.; Taniguchi, T. Hydroboration of Aryne Formed by Hexadehydro Diels–Alder Cyclizations with *N*-Heterocyclic Carbene Boranes. *Org. Lett.* **2015**, *17*, 3450–3453. [CrossRef]
99. Yun, S.Y.; Wang, K.P.; Lee, N.-K.; Mamidipalli, P.; Lee, D. Alkane C–H Insertion by Aryne Intermediates with a Silver Catalyst. *J. Am. Chem. Soc.* **2013**, *135*, 4668–4671. [CrossRef]
100. Mamidipalli, P.; Yun, S.Y.; Wang, K.-P.; Zhou, T.; Xia, Y.; Lee, D. Formal Hydrogenation of Aryne with Silyl C_β -H Bonds as an Active Hydride Source. *Chem. Sci.* **2014**, *5*, 2362–2367. [CrossRef]
101. Lee, N.-K.; Yun, S.Y.; Mamidipalli, P.; Salzman, R.M.; Lee, D.; Zhou, T.; Xia, Y. Hydroarylation of Aryne Catalyzed by Silver for Biaryl Synthesis. *J. Am. Chem. Soc.* **2014**, *136*, 4363–4368. [CrossRef] [PubMed]
102. Ghorai, S.; Lee, D. Aryne Formation via the Hexadehydro Diels–Alder Reaction and their Ritter-Type Transformations Catalyzed by a Cationic Silver Complex. *Tetrahedron* **2017**, *73*, 4062–4069. [CrossRef]
103. Ghorai, S.; Lin, Y.; Xia, Y.; Wink, D.J.; Lee, D. Silver-Catalyzed Annulation of Aryne with Nitriles for Synthesis of Structurally Diverse Quinazolines. *Org. Lett.* **2020**, *22*, 626–630. [CrossRef]

104. Karmakar, R.; Ghorai, S.; Xia, Y.; Lee, D. Synthesis of Phenolic Compounds by Trapping Arynes with a Hydroxy Surrogate. *Molecules* **2015**, *20*, 15862–15880. [CrossRef] [PubMed]
105. Wang, K.-P.; Yun, S.Y.; Mamidipalli, P.; Lee, D. Silver-Mediated Fluorination, Trifluoromethylation, and Trifluoromethylthiolation of Arynes. *Chem. Sci.* **2013**, *4*, 3205–3211. [CrossRef]
106. Karmakar, R.; Wang, K.P.; Yun, S.Y.; Mamidipalli, P.; Lee, D. Hydrohalogenative Aromatization of Multiynes Promoted by Ruthenium Alkylidene Complexes. *Org. Biomol. Chem.* **2016**, *14*, 4782–4788. [CrossRef]
107. Xiao, X.; Wang, T.; Xu, F.; Hoye, T.R. Cu^I-Mediated Bromoalkynylation and Hydroalkynylation Reactions of Unsymmetrical Benzyne: Complementary Modes of Addition. *Angew. Chem. Int. Ed.* **2018**, *57*, 16564–16568. [CrossRef]

Disclaimer/Publisher's Note: The statements, opinions and data contained in all publications are solely those of the individual author(s) and contributor(s) and not of MDPI and/or the editor(s). MDPI and/or the editor(s) disclaim responsibility for any injury to people or property resulting from any ideas, methods, instructions or products referred to in the content.

Review

Green Synthesis of Aromatic Nitrogen-Containing Heterocycles by Catalytic and Non-Traditional Activation Methods

R. Bernadett Vločskó [†], Guoshu Xie [†] and Béla Török ^{*}

Department of Chemistry, University of Massachusetts Boston, 100 Morrissey Blvd., Boston, MA 02125, USA

^{*} Correspondence: bela.torok@umb.edu[†] These authors contributed equally to this work.

Abstract: Recent advances in the environmentally benign synthesis of aromatic N-heterocycles are reviewed, focusing primarily on the application of catalytic methods and non-traditional activation. This account features two main parts: the preparation of single ring N-heterocycles, and their condensed analogs. Both groups include compounds with one, two and more N-atoms. Due to the large number of protocols, this account focuses on providing representative examples to feature the available methods.

Keywords: sustainable synthesis; aromatic N-heterocycles; solid acids; nanoparticles; microwaves; ultrasounds; visible light activation; high hydrostatic pressure; electrochemistry; biomass

1. Introduction

Heterocycles are a broad variety of compounds including aromatic and non-aromatic compounds with various heteroatoms, most commonly N, O and S. Many of them are natural compounds and a large majority are biologically active. They are used in large quantities in the pharmaceutical, agrochemical, dyestuff or polymer industries. Accordingly, the preparation and functionalization of heterocycles have attracted overwhelming interest [1–3]. The high-volume industrial production of heterocycles, however, brings about a serious environmental issue; the traditional processes yield large amounts of toxic waste and often represent hazardous conditions. Both must be avoided if at all possible, leading recent synthesis development efforts into the realm of green chemistry. These methods are effective, and at the same time they also comply with contemporary guidelines for safety and environmental sustainability [4,5]. Due to the extremely high activity in this field, the advances toward the sustainable production of heterocycles have been reported in thousands of papers. In this work we will survey the green synthesis of nitrogen-containing heterocycles focusing on representative example protocols that apply either solid catalysts [6–8] and/or non-traditional activation methods [9] that significantly decrease the amount of waste as well as the energy need of these processes. We mostly focused on the last five years from 2017–2023. However, occasionally representative examples were cited from earlier periods. Given that a large majority of the derivatives of aromatic N-heterocycles are biologically active, the question of chirality arose naturally. Due to the aromaticity of these heterocycles, there were no examples where the ring itself had any chiral center. Hence we could not include such examples. There are many papers that report chiral derivatives of N-heterocycles. However, all of them were prepared by the functionalization of the core heterocycles, and functionalization was beyond the scope of this work.

2. Five-Membered Rings

2.1. One-Nitrogen-Containing Heterocycles: Pyrroles

The Paal–Knorr reaction [10,11], is one of the most well-known preparation methods to obtain pyrroles. Although effective in producing the desired pyrrole derivatives, the use

Citation: Vločskó, R.B.; Xie, G.; Török, B. Green Synthesis of Aromatic Nitrogen-Containing Heterocycles by Catalytic and Non-Traditional Activation Methods. *Molecules* **2023**, *28*, 4153. <https://doi.org/10.3390/molecules28104153>

Academic Editors: Alexey M. Starosotnikov, Maxim A. Bastrakov and Igor L. Dalinger

Received: 4 April 2023

Revised: 10 May 2023

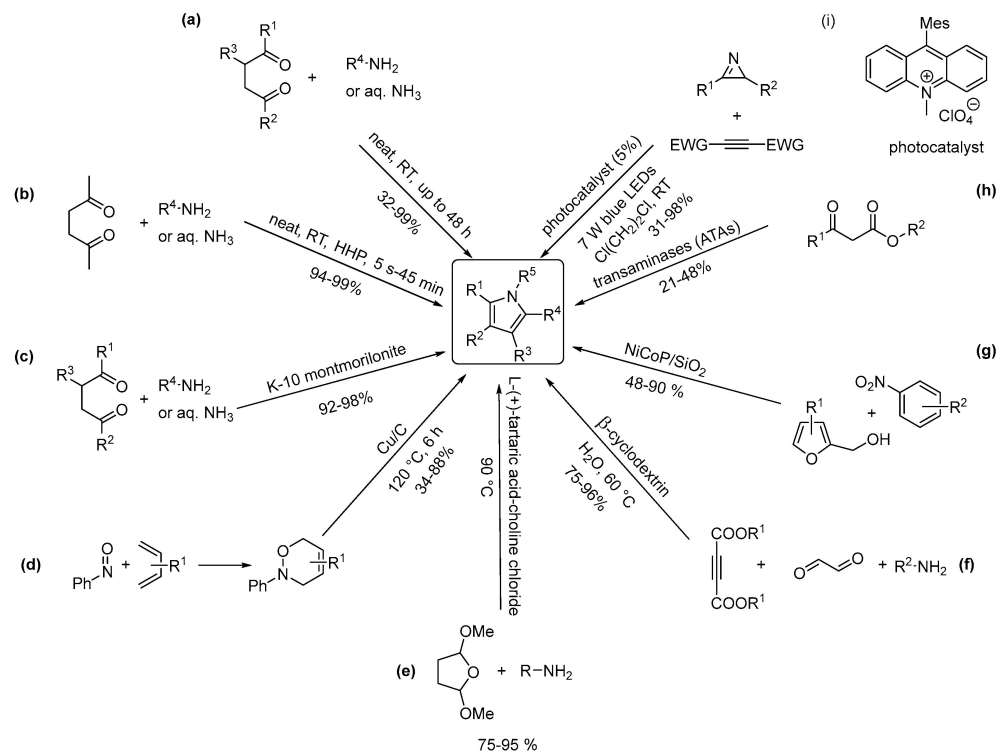
Accepted: 11 May 2023

Published: 17 May 2023



Copyright: © 2023 by the authors. Licensee MDPI, Basel, Switzerland. This article is an open access article distributed under the terms and conditions of the Creative Commons Attribution (CC BY) license (<https://creativecommons.org/licenses/by/4.0/>).

of mineral acid catalysis renders it obsolete. There have been several attempts to make this reaction more environmentally benign [12]. A summary of representative green protocols is depicted in Scheme 1.



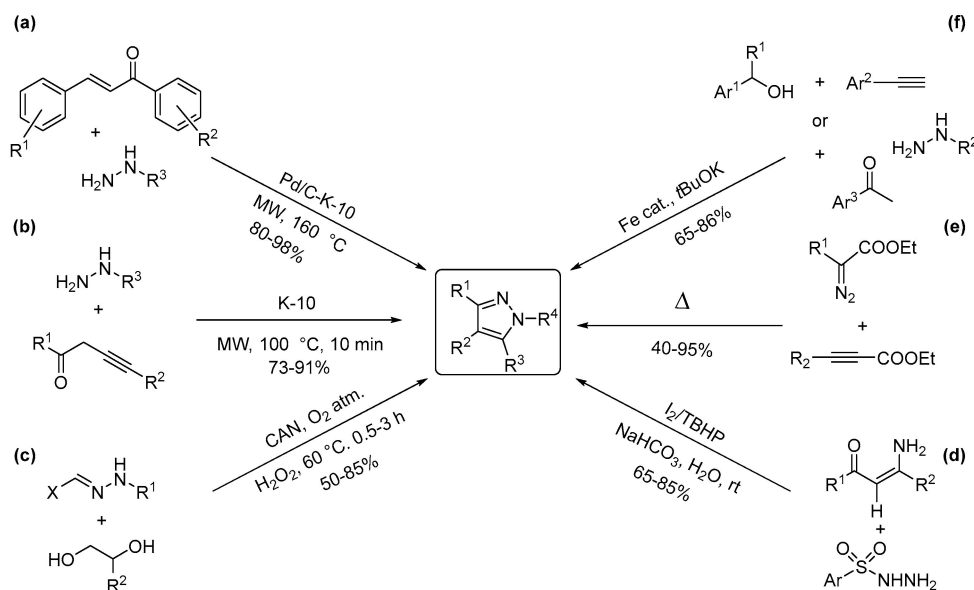
Scheme 1. Representative green protocols for the synthesis of pyrroles.

The greenest examples describe acid and solvent-free protocols that produce the pyrroles in high yields using 1,4-diketones and amines or aq. NH_4OH . One process even occurs at room temperature, although the required reaction times are quite long (up to 24 h) (Scheme 1a) [13]. A recent protocol, applying similar starting materials at ambient temperature and using high hydrostatic pressure as an activation method, significantly reduced the reaction time to 5 s–45 min, while maintaining quantitative yields (Scheme 1b) [14]. A similar acid-free method utilized water as a solvent, which is abundant and non-toxic, though its recycling has a high energy demand [15]. Another green solvent (MeOH) was applied in the catalyst-free coupling of nitroolefins with enaminoesters, producing multi-substituted pyrroles in good yields [16]. Other reports include solid-acid catalysis by K-10 montmorillonite (Scheme 1c) [17] and even extend the scope to monosubstituted N-alkylpyrroles and N-sulfonyl-pyrroles using 2,5-dimethoxy-tetrahydrofuran to replace the diketones [18,19]. Most of the solid-acid-catalyzed protocols use microwave irradiation as activation [20,21]. Other heterogeneous catalytic methods used carbon-supported copper (Cu/C) to promote a hetero Diels–Alder reaction of nitroso dienophiles and 1,3-dienes in good yields (Scheme 1d) [22]. 2,5-Dimethoxy-tetrahydrofuran can also undergo cyclization with amines in deep eutectic solvents (DES) (Scheme 1e) [23]. The DES also acted as an organocatalyst and provided stable yields in five consecutive reactions. Similarly to DES, ionic liquids [24] can also catalyze the reaction. Anilines, acetylenedicarboxylic acid esters and glyoxal underwent a multicomponent cyclization catalyzed by β -cyclodextrin to afford pyrroles (Scheme 1f) [25]. β -Cyclodextrin, which is well-known for forming inclusion complexes [26] provides an appropriate nonpolar space in its cavity while the highly polar external wall keeps the catalyst–substrate complex stable in the aqueous medium. Essentially, β -cyclodextrin acted as a phase transfer catalyst and remained reusable in four subsequent reactions. The biomass-product furan alcohols reacted efficiently with nitrobenzenes over the surface of a bifunctional catalyst, metal phosphides (Scheme 1g) [27]. The

catalyst possessed dual active sites namely solid acidic and metallic sites for ring opening, and the abstraction of H from the starting material and the in situ hydrogenation of the nitrobenzenes to anilines. The mixed NiCoP appeared to be the best catalyst providing the N-arylpyrroles in moderate to good yields. Another green example is a biocatalytic process using transaminases (ATAs) (Scheme 1h) [28]. In this protocol, α -diketones were aminated in a classical Knorr pyrrole synthesis. The pH of this biocatalytic system must be closely monitored to avoid the dimerization of the α -amino carbonyl intermediate. An emerging activation method, visible light LEDs, was applied in the synthesis of pyrroles. In general, visible-light-LED-assisted processes are widely applied in the synthesis of many heterocycles and are the target of frequent reviews [29–32]. In a photoredox reaction 2-azirines were combined with internal alkynes to afford pyrroles [33]. The energy from blue light LEDs utilized the intrinsic strain of 2-azirines to initiate a [3+2] cycloaddition with the alkyne in the presence of a 9-mesityl-10-methylacridinium perchlorate photocatalyst (Scheme 1i). The protocol provides a broad scope of pyrroles with moderate to excellent yields.

2.2. Two-Nitrogen-Containing Heterocycles: Pyrazoles and Imidazoles

Pyrazoles are two N-containing five-membered aromatic heterocycles, possessing widespread biological effects and are crucial building blocks. Thus, their preparation is at the forefront of synthesis research, focusing on contemporary green and sustainable approaches that include catalytic, multicomponent and solvent-free protocols [34–37] as described in several reviews [38–40]. The classic synthesis of pyrazoles relies on the domino reaction of hydrazines with 1,3-bifunctional substrates often suffering from low regioselectivity. Representative recent advances are illustrated in Scheme 2.

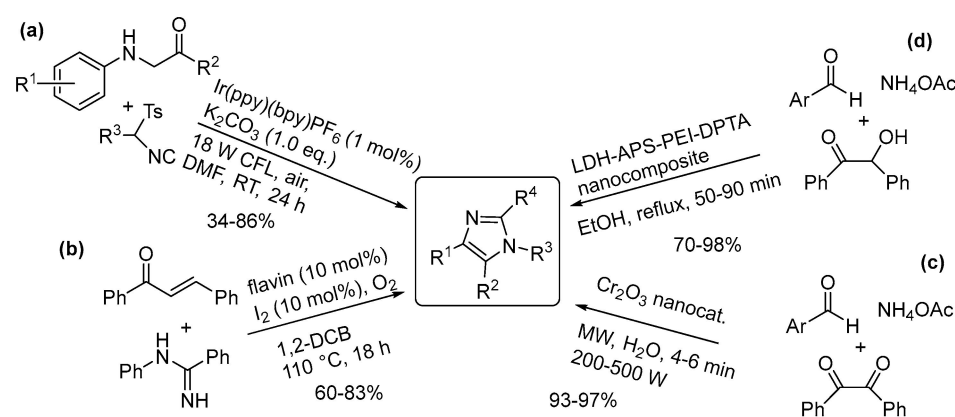


Scheme 2. Representative green protocols for the synthesis of pyrazoles.

The above-mentioned classic route was modified to a solid-acid-catalyzed process. The cyclization and aromatization of chalcones and arylhydrazones were catalyzed by Pd/C and K-10 montmorillonite and afforded the products in excellent yields [41]. The solid acid K-10 initiated the cyclization and then Pd oxidized the intermediate to pyrazoles (Scheme 2a). The same setup worked well with alk-3-yn-1-ones as well (Scheme 2b) [42]. In another catalytic method, cerium ammonium nitrate (CAN) was applied as a catalyst in the regioselective tandem oxidation and intermolecular ring cyclization of vicinal diols with hydrazones to pyrazoles (Scheme 2c) [43]. The products were isolated in moderate to excellent yields under mild conditions in an aqueous medium. Another hydrazine-based annulation protocol was also carried out in aqueous medium in a metal-free system (Scheme 2d) [44].

Molecular iodine was applied as a catalyst in the presence of *tert*-butylhydroperoxide and NaHCO₃. The reaction occurred through domino C–H sulfonylation and annulation steps with good functional group tolerance affording the pyrazoles in good to excellent yields. The thermal cycloaddition of diazo compounds with alkynes occurred in a catalyst- and reagent-free system with moderate to excellent yields (Scheme 2e). The α -diazocarbonyl compounds readily formed the pyrazole derivatives in high yields in a simple solvent-free thermal reaction eliminating work-up or purification steps [45]. An efficient iron-catalyzed multicomponent synthesis of trisubstituted pyrazoles was developed using biomass-derived alcohols in an Fe(II)-catalyzed process (Scheme 2f) [46]. This protocol possessed a broad scope that was achieved by dehydrogenative coupling of alcohols, aryl hydrazines and secondary alcohols or using alkynes as an alternative to the *sec*-alcohols. This protocol eliminated the need for pre-functionalization, toxic noble metal catalysts, harmful oxidants or other additives. A recent protocol applied a silver-catalyzed [3 + 2] cycloaddition of aryl diazonium salts and allenes, providing the target pyrazoles in moderate to excellent yields, however, in high selectivity [47]. A similar approach, using aryl diazonium salts with arylcyclopropanols produced the target pyrazoles by a photocatalytic cycloaddition [48].

The green synthesis of imidazoles also attracted extensive attention. A few representative examples are depicted in Scheme 3.



Scheme 3. Representative green protocols for the synthesis of imidazoles.

The visible-light-assisted photochemical processes have also been applied for the synthesis of imidazoles. The [3+2] cycloaddition-photooxidative aromatization sequence of glycine derivatives and isocyanides provided moderate to good yields for the synthesis of trisubstituted imidazoles (Scheme 3a) [49]. The reaction conditions were mild (rt etc.) and the protocol could be scaled up to a gram scale. A metal-free organocatalytic synthesis of imidazoles was carried out from amidines and chalcones. A natural product, flavin (with iodine), was used as a catalyst for the cross-dehydrogenative coupling (Scheme 3b) [50]. The reaction produced tetrasubstituted imidazoles in good yields (60–87%) in an atom economic design, consuming one equivalent of O₂ and producing water as the only byproduct in an otherwise waste-free protocol. A heterogeneous catalytic synthesis of imidazoles was designed by using the Cr₂O₃ nanoparticle-catalyzed reaction of aromatic aldehydes with ammonium acetate and benzil under microwave-assisted conditions in water as solvent (Scheme 3c) [51]. The protocol offers operational simplicity, short reaction times and excellent yields. Another heterogeneous catalytic method applied nanoarchitectonics of LDH/polymer (layered double hydroxide) composite, and LDH/polymer nanocomposites (LDH-APS-PEI-DTPA). The polymer portion of the catalysts was prepared from diethylenetriaminepentaacetic acid (DTPA), polyethylenimine and used LDH to form a nanocomposite with high thermal stability. The product nanocomposite is an active and recyclable (five times) heterogeneous catalyst for the synthesis of imidazoles (Scheme 3d) [52].

2.3. Three-Nitrogen-Containing Heterocycles: Triazoles

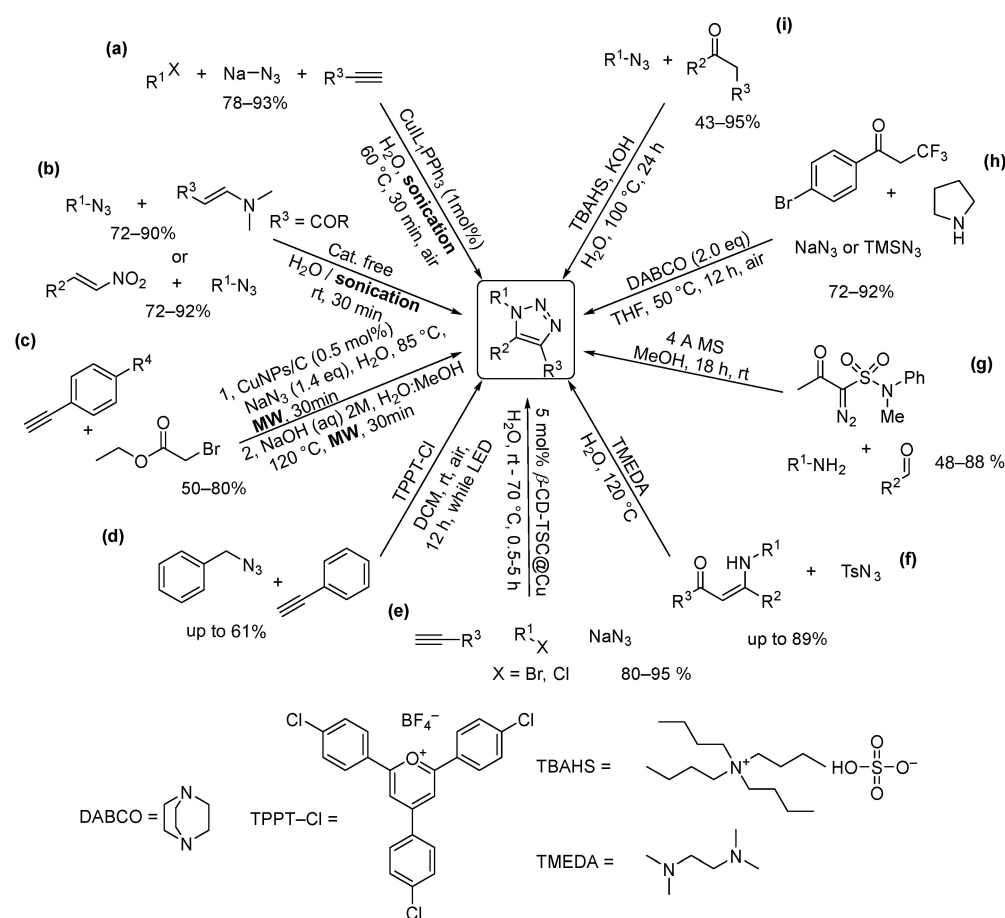
Triazoles are five-membered heterocycles with three nitrogen atoms and two double bonds. Depending on the position of the nitrogens and the double bonds, four triazole isomers can be distinguished (Figure 1). All triazole isomers are planar and aromatic.



Figure 1. Various isomeric forms of triazole.

Many of the 1,2,3- and 1,2,4-triazole derivatives show extensive pharmacological activities such as antifungal (fluconazole), herbicide (propiconazole), anticancer (carboxyamidotriazole) and antibacterial (cefatrizine), just to mention a few [53–57]. Not only are they good pharmacophores, but they have a wide range of applications in polymer and paint production [58–60]. The physiological and industrial significance of nitrogen-containing heterocycles, including triazoles, can be explained by their unique electronic and coordination properties, not to mention their H-bonding affinity due to which they can form many weak non-bonded or secondary interactions. One of the most widely applied synthesis methods to generate triazole and other heterocyclic derivatives is ‘click chemistry’. These are easy-to-perform, high-yielding stereospecific chemical transformations with wide substrate scope creating only innocuous by-products that can be removed without chromatography. These reactions in most cases are conducted in benign solvents, preferably in water and result in only one product. As we can see, the principles of click and green chemistry overlap in many ways [61]. Several known reactions meet these criteria such as addition reactions to C-C double or triple bonds, hydrazone formation and cycloaddition reactions. The predominant synthesis protocol for triazole synthesis has been, and still is, the use of organic azides and terminal alkynes as building blocks in a cycloaddition reaction, such as the classic 1,3-dipolar cycloaddition [62]. Unfortunately, this reaction requires elevated temperature and at the end of the reaction a mixture of the 1,4-substituted and the 1,5-substituted regioisomers is generated. The reaction was improved by adding a Cu(I) salt to the system, which accelerated it to 10^7 – 10^8 times the original rate and was selective in favor of the 1,4- isomer [63]. Later Fokin and Jia introduced the use of Ru-based catalysts in cycloaddition reactions which selectively leads to the 1,5-disubstituted 1,2,3-triazole isomer [64]. Recently Hong et al. also described a highly selective 1,5-disubstituted triazole synthesis using Cp_2Ni /Xantphos catalytic system [65]. Herein we present the latest trends and innovations of sustainable synthesis of relevant triazoles. Representative examples are shown in Scheme 4.

Most of the listed reactions (Scheme 4a,b,e,f,i) are carried out in water under transition metal-free conditions. For example, Joshi et al. used TBAHS phase transfer catalyst in a [3+2]-cycloaddition to generate 1,4-diaryl-5-alkyl-1,2,3-triazole derivatives in up to 95% yields and excellent regioselectivity (Scheme 4i) [66]. To reach these good results, elevated temperature and the presence of strong base (KOH) were necessary. The use of triazole-based linkage is also significant in bioconjugation for labeling of biomolecules inside the living cells. The pioneer of bioorthogonal chemistry, Bertozzi, was awarded the Nobel Prize in Chemistry (2023) along with Meldal and Sharpless (click chemistry) [67]. Following the bioorthogonal concept, Li et al. have recently described a metal-free, open-air multicomponent reaction of α -CF₃ carbonyls, NaN₃ and amines to generate 5-amino NH-1,2,3-triazole derivatives selectively (Scheme 4h) [68]. It was also shown how the resulting products are converted into their *N*-2 alkylated derivatives. Bubyrev et al. also introduced two three-component synthetic strategies without using any catalyst or chemical promoter [69]. First, they observed the formation of 1,5-di-substituted-1,2,3-triazoles by mixing *N*-methyl, *N*-phenyl α -acetyl- α -diazomethane sulfonamide, primary amines and aldehydes.



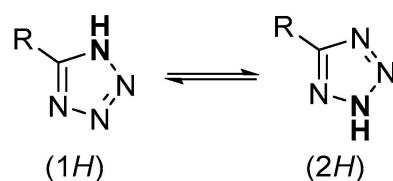
Scheme 4. Representative green strategies for synthesis of triazoles.

The reaction occurred in a two-step fashion, and elevated temperature was needed to eliminate sulfur(IV) oxide and *N*-methyl aniline and obtain the desired triazoles. To avoid thermal promotion, the authors developed a second one-step, single purification protocol as well, where the reaction was conducted at room temperature for 18 h, in the presence of 4 Å molecular sieves (Scheme 4g). A further example of metal and organic solvent free synthesis of triazoles was presented by Wan et al. (Scheme 4f) [70]. Readily available β-thioenaminones and tosyl azide building blocks were used in the presence of TMEDA (*N,N,N',N'*-tetramethyl- ethylenediamine) base promoter. No additional catalyst or reagent was needed to achieve the formation of several 5-thiolated 1,2,3-triazoles in good to excellent yields. There are also examples of building alternative, greener metal catalytic systems. Tajbakhsh and Naimi-Jamal described a classic azide-alkyne cycloaddition (AAC) reaction in aqueous media using a Cu@TSC-β-CD (immobilized Cu(I) in thiosemicarbazide-functionalized β-cyclodextrin) nanocatalyst (Scheme 4e) [71]. In the presence of the water soluble and stable catalyst, the desired 1,4-disubstituted-1,2,3-triazoles were obtained in up to 98% yield. The catalyst was reused seven times without significant leaching of Cu(I) and its recovery only required anti-solvent precipitation and filtration. However, the use of copper is often cited as a negative feature of click reactions, due to its cytotoxic effect. Pan and co-workers presented a photocatalytic and metal-free alternative and synthesized various 1,4-disubstituted 1,2,3-triazoles under mild conditions (Scheme 4d) [72]. In the presence of TPPT-Cl (2,4,6-tris(4-chloro-phenyl)pyrylium tetrafluoroborate) photocatalyst, with visible light activation, the corresponding 1,4-disubstituted 1,2,3-triazoles were obtained in moderate yield. The presented protocol shows promising results, but at the same time it still requires further development to match the efficiency of transition metal catalysts. In addition to photochemistry, other non-traditional activation methods have also been adopted to synthesize triazoles [73–76]. Rodríguez et al. have introduced a microwave-

assisted, one-pot multicomponent copper-catalyzed azide-alkyne cycloaddition (CuAAC) followed by a hydrolysis reaction to obtain the corresponding triazoles (Scheme 4c) [77]. As a catalyst, they used copper-based nanoparticles in biorenewable solvents (H₂O and methanol). Another example of implementing sonochemical activation in cycloaddition reactions has described a catalyst-free synthesis protocol to generate 4-acyl-1,2,3-triazoles and 1,5-disubstituted-1,2,3-triazoles using ultrasound irradiation in an aqueous medium (Scheme 4b) [78]. The protocol is characterized by excellent regioselectivity, scalability, short reaction time and broad substrate scope. Another group has developed a similar water-based ultrasonic method with the exception that a catalyst (1 mol%) was added to the reaction mixture (Scheme 4a) [79]. The multicomponent click reaction, mediated by a Cu(I) complex, afforded 1,4-disubstituted 1,2,3-triazoles in yields up to 93%. In similar approaches, a novel hybrid nano catalyst, silica-tethered cuprous acetophenone thiosemicarbazone (STCATSC) [80] or a silica gel-immobilized [Cu(cdsalMeen)] [81], were used respectively, to promote the synthesis of new 1,2,3-triazoles.

2.4. Four-Nitrogen-Containing Heterocycles: Tetrazoles

Tetrazoles are five-membered heterocycles with four nitrogen atoms in the aromatic ring. They are not natural products; they can only be produced synthetically. Based on how many substituents are attached to the ring, we can distinguish un-, mono-, di- and trisubstituted tetrazoles. The 5-substituted tetrazole is of particular interest because of its similar physical chemical properties to carboxylic acids (mobile H, comparable pK_a, similar size) which suggests similar receptor ligand interactions as well. At the same time, they typically have better ADME properties. There are two tautomeric forms of the mono 5-substituted tetrazoles (Scheme 5). Interestingly, while the 2*H*-tautomer is more stable in gas phase, the 1*H*-tautomer is prevalent in solution.

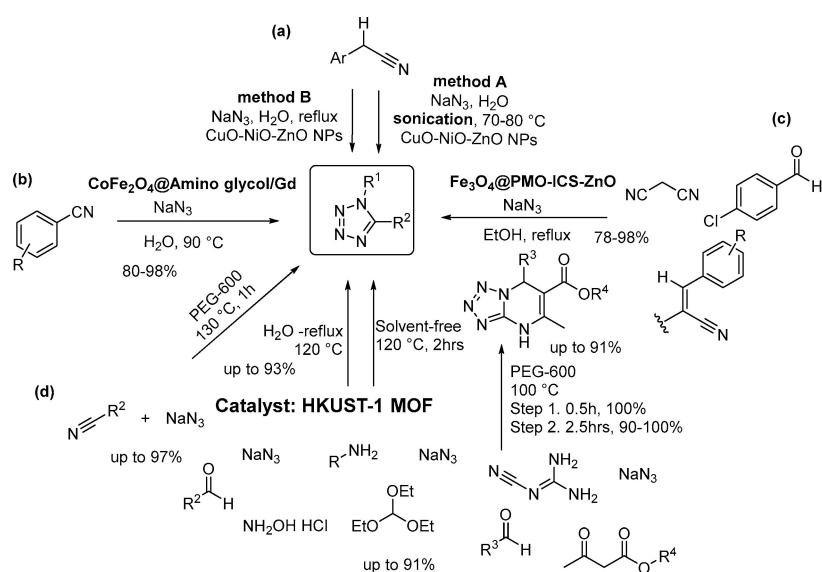


Scheme 5. The tautomers of tetrazole derivatives.

The occurrence of tetrazole moiety in industrially relevant compounds is extensive and has increased dramatically in the last decade. It can be found in photography, imaging chemicals and military applications [82,83], not to mention its significance in medicine and thus the pharmaceutical industry [84,85]. Amongst others, it is the building block of several antibiotics (Cefotiam, Cefmetazole), antihypertensive (Valsartan, Losartan) and antiallergic agents (Pemirolast). Accordingly, there is still a great demand for the development of efficient and sustainable synthesis procedures.

Heterogeneous synthesis methods have been prominent in the last few years among sustainable protocols for tetrazole synthesis. Scheme 6 illustrates a few highly efficient and selective nanoparticle-based catalyst systems.

Tebyanian and his coworkers have demonstrated a combination ultrasound/nanoparticle catalytic system in regioselective synthesis of 1-aryl-5-amino-1*H*-tetrazoles (Scheme 6a) [86]. The authors tested the CuO–NiO–ZnO mixed metal oxide catalyst in a traditional as well as in an ultrasound-assisted system. Better yield and selectivity were achieved with ultrasounds. The improvement was explained by a probable synergistic effect between the ultrasound irradiation and the nanocatalyst.



$\text{CoFe}_2\text{O}_4@\text{Amino glycol/Gd}$ = (gadolinium 2-amino-2-methyl-1,3-propanediol (Amino glycol) complex immobilized covalently on CoFe_2O_4 magnetite nanoparticles)

$\text{Fe}_3\text{O}_4@\text{PMO-ICS-ZnO}$ = ZnO nanoparticles embedded in a magnetic isocyanurate-based periodic mesoporous organosilica

HKUST-1 MOF = Cu-BTC(1,3,5 benzene tricarboxylate) metal organic framework

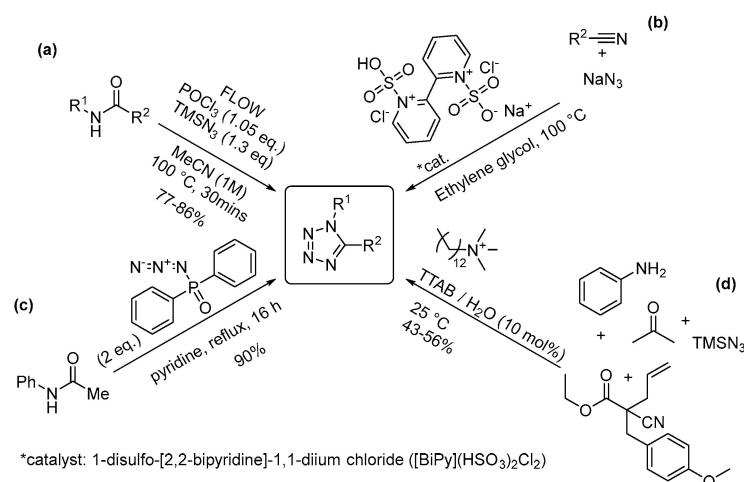
Scheme 6. Heterogeneous catalytic tetrazole synthesis protocols.

In another example, Ghadermazi et al. have developed a $\text{CoFe}_2\text{O}_4@\text{amino glycol/Gd}$ nanocomposite to catalyze the oxidation of sulfides and to generate 5-substituted 1*H*-tetrazoles under benign conditions (Scheme 6b) [87]. The corresponding products were obtained in good to excellent yields, and the optimized conditions were tested for broad substrate tolerance. Due to its magnetic nature, the catalyst could be easily removed with the help of an external magnet. Magnetic nanoparticles in general are known to have many favorable properties, such as low toxicity, high surface-to-volume ratio, good thermal stability and high activity, and can be easily modified and dispersed. Another group, Akbari and Naimi-Jamal, have developed an environmentally friendly procedure for cascade condensation and concerted 1,3-cycloaddition reactions catalyzed by magnetic $\text{Fe}_3\text{O}_4@\text{PMO-ICS-ZnO}$ nanomaterial (Scheme 6c) [88]. The catalyst retained its activity in five consecutive runs in a water/EtOH mixture under reflux. The 5-substituted-1*H*-tetrazole derivatives were obtained in high to quantitative yields. Lastly, Soroush et al. have demonstrated a new metal organic framework (MOF)-based heterogeneous catalytic system for the multicomponent synthesis of tetrazole derivatives (Scheme 6d) [89]. The hydrothermal technique proved to be the best for preparing the catalyst. In the presence of HKUST-1 MOF, two-, three- and four-component reactions were carried out under mild reaction conditions, using PEG-600, water or solvent-free media. All reactions yielded the desired products with good to excellent yield. Other heterogeneous catalytic protocols include a [3+2] cycloaddition of alkyl nitriles and sodium azide using a silica-anchored copper bis(diacetylcurcumin) 1,2-diamino benzene Schiff base complex with ascorbic acid in a water/*i*-PrOH (50:50, V/V) medium [90].

In addition to heterogeneous catalysis, homogeneous processes have also been applied in recent years as shown in Scheme 7.

An example of using amides as one of the starting materials was illustrated by Kappe's group in a continuous flow system (Scheme 7a) [91]. The amide was activated by POCl_3 to imidoyl chloride which in the following step reacts with the azide (TMSN_3). The reaction reaches full conversion in 10 min and the products were obtained in good yield (77–86%) after recrystallization. No further purification was necessary. Gholizadeh and coworkers have developed a novel protocol for a [2+3] cycloaddition reaction catalyzed by an ionic liquid system to synthesize 5-substituted 1*H*-tetrazole derivatives (Scheme 7b) [92]. Ionic

liquids are considered as easily available, non-volatile and non-flammable materials with good thermal and chemical stability.



Scheme 7. Environmentally benign synthesis methods for tetrazole derivatives.

They are also generally well miscible with both inorganic and organic solvents and reagents. In a short reaction time, the desired products were obtained in very good yields (92–99%) with a wide range of substrates. Ishihara et al. have developed a tetrazole synthesis, starting from amides and working with an alternative azide source [93]. To convert the amides, the authors used diphenyl phosphorazidate (DPPA, (C₆H₅O)₂P(O)N₃) or bis(*p*-nitrophenyl) phosphorazidate (*p*-NO₂DPPA, (*p*-NO₂C₆H₄O)₂P(O)N₃) in the presence of aromatic bases (Scheme 7c). Both DPPA and *p*-NO₂-DPPA act as an activator of amide-oxygen for elimination and thus an azide source. Mechanistically, what makes this reaction safer compared to the conventional click protocol is that the phosphorus atom stabilizes the azide. This practical and simple protocol is a great example of how toxic and explosive reagents in click reactions can be replaced by safer alternatives. Using water in organic reactions often causes difficulties in terms of solubility. To overcome this challenge, Abdessalam and his coworkers presented a micelle-based Ugi-azide four-component synthesis of 1,5-disubstituted tetrazoles (Scheme 7d) [94]. As starting material, the authors used aldehyde, various amines, isocyanides and trimethylazides in the presence of tetradecyltrimethylammonium bromide (TTAB) with a load of 10 mol% in an aqueous medium. Broad substrate scope was investigated and the corresponding tetrazole derivatives were obtained in moderate yield (43–56%).

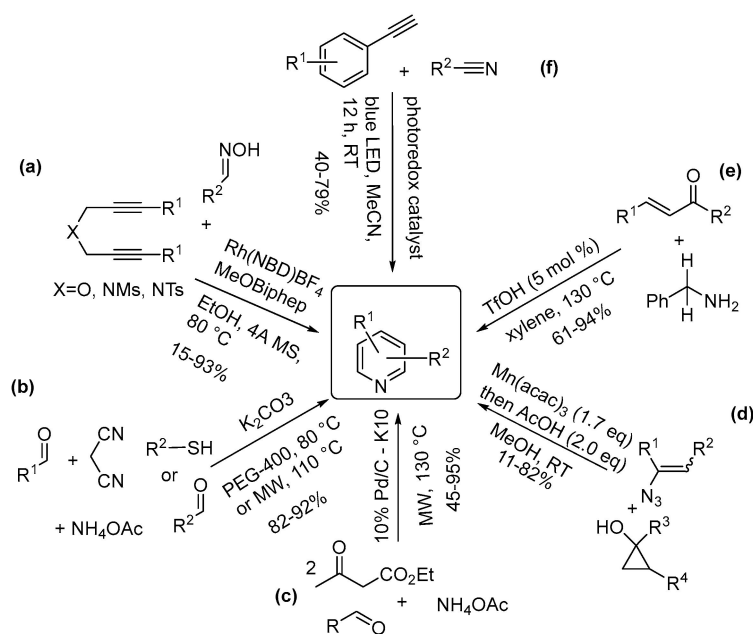
3. Six-Membered Rings

3.1. One-Nitrogen-Containing Heterocycles: Pyridines

Pyridines are six-membered heterocycles with one N atom in their ring. They are biologically active compounds, and the pyridine scaffold is often used as part of drugs. Thus, they are common building blocks. Their practical utility generated significant interest in their synthesis [95]. Some representative environmentally benign methods are depicted in Scheme 8.

The Rh-catalyzed [2+2+2] cycloaddition of diynes with oximes affords the formation of pyridine derivatives in low to excellent yields (Scheme 8a) [96]. The reaction can be carried out by the preformed oxime or as a multicomponent reaction. Ketoxime acetates also appeared to work in this reaction with aldehydes. FeCl₃ was used as a water tolerant Lewis acid [97]. These protocols have demonstrated good functional group tolerance and scalability. Similar three- and four component reactions of aryl aldehydes, malonitrile and thiophenols and ammonium acetate yielded a broad variety of substituted pyridines (Scheme 8b) [98]. The reactions were carried out in PEG-400 or methanol as solvent with K₂CO₃ on NH₄OAc as a base catalyst [99]. Solvent-free conditions combined

with microwave activation appeared to work sufficiently as well [100,101]. In an enhanced microwave-assisted effort, symmetrically substituted pyridines were prepared by a bifunctional metal–solid acid catalyst via a domino cyclization–aromatization approach [102]. The solid acid catalyzed the cyclization to dihydropyridine and the added Pd promoted the dehydrogenation to pyridines resulting in the aromatic products in moderate to high yields (Scheme 8c). Tetrasubstituted pyridines were prepared by Wang and Chiba using a synthetically diverse approach. The authors used a Mn(III)-assisted addition of vinyl azides and cyclopropanols in a green solvent, methanol at room temperature (Scheme 8d) [103], although the yields showed a great variety from 11–82%. A water tolerant Brønsted acid, triflic acid, was used as a catalyst in a one-pot protocol for the synthesis of pyridines, without the need of harmful oxidizing reagents (Scheme 8e) [104]. The reaction occurred via a tandem reverse aldol reaction/condensation/cyclization /aromatization sequence with enones and primary amines. The excellent functional group tolerance, air as a naturally abundant and green oxidant and the water tolerant acid catalyst are the major green advantages of the procedure. Finally, visible-light-promoted processes have also found use in the synthesis of pyridines. A blue LED irradiation-initiated [2+2+2] cyclization of alkynes and nitriles led to the successful synthesis of a broad variety of pyridines (Scheme 8e) [105]. The process was catalyzed by a photoredox catalyst and occurred with excellent functional group tolerance in moderate to good yields.



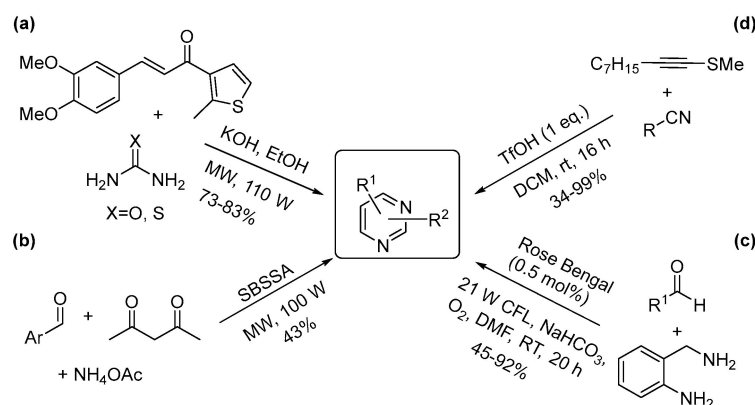
Scheme 8. Representative examples of environmentally benign synthesis methods for the preparation of pyridines.

3.2. Two-Nitrogen-Containing Heterocycles: Pyrimidines, Pyrazines

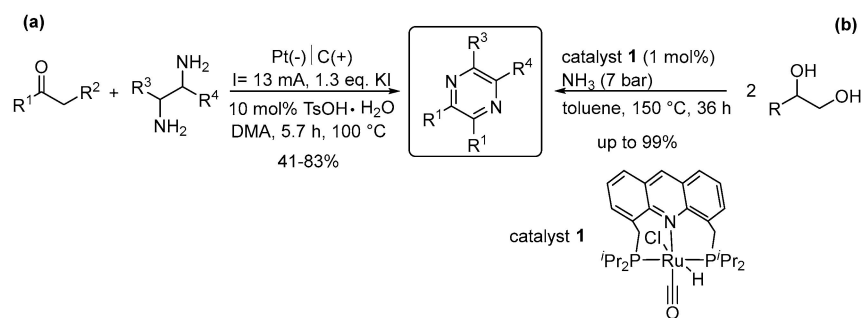
Pyrimidines are six membered ring heterocyclic compounds containing two nitrogen atoms. They make up an important group of compounds and have thus attracted significant attention, and their synthesis development is still at the forefront of organic synthesis [106–108].

Well-known and widely available starting materials such as chalcones with urea and thiourea were used for the preparation of pyrimidines (Scheme 9a) [109]. Microwave irradiation was used to activate the process that provided the substituted pyrimidines in good yields under green conditions e.g., using ethanol, a sustainable and green solvent. Other similar applications include the use of guanidine nitrate instead of urea derivatives [110], or a CuI and base-catalyzed protocol [111]. The synthesis of pyrimidines was also accomplished by a three-component reaction that was catalyzed by a silica-bound S-sulfonic acid (SBSSA) (Scheme 9b) [112]. The microwave-assisted protocol involved a solvent-free reaction, in <1 min reaction times. Urea could be used to replace ammonium

acetate; however, the major limitation of the reaction is the moderate yield (43%) and that the non-aromatic tetrahydropyrimidines were isolated. Condensed pyrimidines were prepared by a visible-light-LED-initiated cyclization of primary amines and aldehydes in moderate to excellent yields under mild conditions (Scheme 9c) [113]. The reaction was catalyzed by 0.5% of Rose Bengal as a photocatalyst and was carried out in air at ambient temperature. Using DMF as a solvent somewhat decreases the green synthetic value of the protocol. The water tolerant triflic acid has been applied as a catalyst for the synthesis of pyrimidines as well. The regioselective combination of alkynes and nitriles was catalyzed by Brønsted superacid, TfOH providing the pyrimidines with high yield and selectivity (Scheme 9d) [114]. An extensive list of diverse and readily available nitriles was applied in the cycloaddition under a simple protocol and mild conditions, although the use of dichloromethane is not desirable. Pyrazines contain their two nitrogen atoms in a 1,4-position. Their synthesis is highly attractive due to their broad-spectrum biological activity. Among the several examples we highlight an electrochemical process and a catalytic process. The electrochemical dehydrogenative [4+2] annulation of a broad variety of commercially available ketones and diamines resulted in the formation of pyrazines in moderate to high yields (Scheme 10a) [115]. The electrochemical oxidation combined with Brønsted acid catalysis led to the target products. In another example, a Ru-pincer complex was used as a catalyst in the synthesis of pyrazines from diols. The oxidative coupling of 1,2-diols and ammonia as the nitrogen source resulted in the formation of pyrazines in nearly quantitative yields (Scheme 10b) [116]. Although the protocol has some drawbacks (using toluene, and long reaction time at high temperature) the use of NH_3 , the catalyst, the high atom economy and low amount of nontoxic waste are clear green benefits.



Scheme 9. Representative examples of environmentally benign synthesis methods for the preparation of pyrimidines.

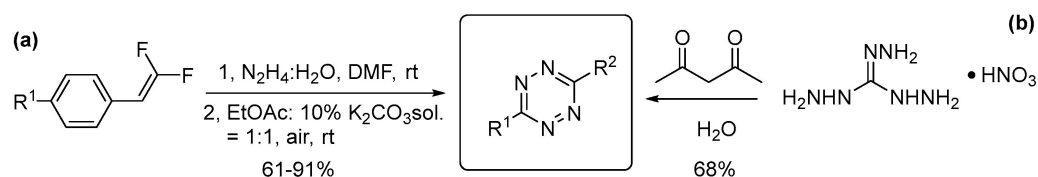


Scheme 10. Representative examples for the environmentally benign synthesis of pyrazines by an electrochemical and a catalytic method.

3.3. Three- and Four- Nitrogen-Containing Heterocycles: Triazines and Tetrazines

Both triazine and tetrazine molecular scaffolds are widely used in biorthogonal chemistry as cell labeling, diagnostic, coordination, drug release or live cell imaging agents. Due to their broad application, they attracted extensive attention in the last few years [117–120]. The Pinner reaction is considered the classic tetrazine synthesis when the reaction of activated nitriles with hydrazines occurs followed by an oxidation step. There are highly efficient transition metal-based tetrazine synthesis protocols, mostly for biorthogonal chemistry applications [121,122].

Recently, the replacement of old synthetic methods with sustainable processes has been gaining ground. Fang et al., have presented a [3+3] addition reaction starting from *gem*-difluoroalkenes to synthesize both symmetric and asymmetric 3,6-disubstituted 1,2,4,5-tetrazine derivatives under benign conditions (Scheme 11a) [123]. The reaction was carried out in an aqueous medium at room temperature under air, which also serves as an oxidant replacing the commonly used toxic nitric acid. The gram scale of the reaction was presented, and the corresponding products were obtained with a moderate to good yield (61–91%). Another green synthesis protocol was developed to generate secondary explosive materials, 3,6-bis[2-(4,6-diazido-1,3,5-triazin-2-yl)-hydrazinyl]-1,2,4,5-tetrazine and 3,6-bis-[2-(4,6-diazido-1,3,5-triazin-2-yl)-diazenyl]-1,2,4,5-tetrazine (Scheme 11b) [124]. The major goal was to replace $\text{Pb}(\text{N}_3)_2$ and generate a metal-free alternative. Due to their high nitrogen content, tetrazines often serve as building blocks for the preparation of high-energy, low-sensitivity explosives.

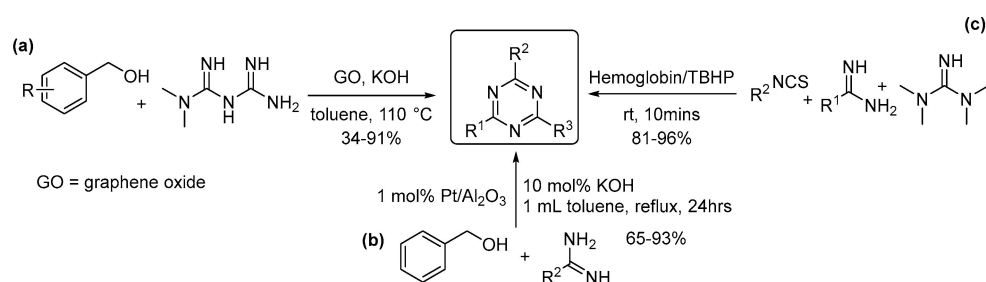


Scheme 11. Environmentally benign protocols to synthesize 1,2,4,5-tetrazoles.

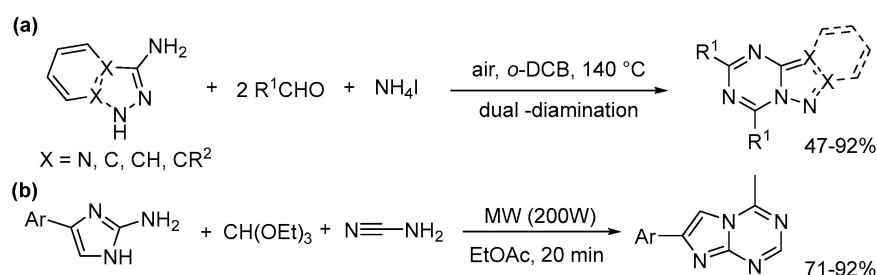
Triazines are six-membered aromatic heterocyclic compounds containing three nitrogen atoms. One of the most common isomers is 1,3,5-triazine, which exhibits several biological activities, such as antimalarial and anti-HIV activity. A novel graphene oxide-based catalyst was developed for the synthesis of triazines (Scheme 12a) [125]. The catalyst was used at moderate loading (10 mol%) and proved to be reusable in six runs without significant loss of activity. At the end of the reaction, the desired products were obtained in moderate to good yields up to 91%. In another example, Poly et al. demonstrated the use of primary alcohols and amidines as molecular building blocks for triazine synthesis by applying alumina-supported Pt ($\text{Pt}/\text{Al}_2\text{O}_3$) nanoparticle catalyst (Scheme 12b) [126]. The acceptorless dehydrogenative coupling reaction was carried out in one pot with high atom economy and good yields of up to 93%. Separation of the catalyst was easy after reuse and no extra oxidants were needed to complete the reaction. Biomolecules have also been reported to catalyze the synthesis of triazines. Wang et al. introduced an efficient asymmetric synthesis of 1,3,5-triazines in the presence of hemoglobin (heme concentration: 0.05 mol%) and *tert*-butyl hydroperoxide (TBHP), using isothiocyanate, amidines and 1,1,3,3-tetramethylguanidine [127]. The presented procedure resulted in high yields (81–96%) in a short reaction time at room temperature (Scheme 12c).

Like most heterocycles, the triazines are often present in fused ring systems. Purine is one of the most biologically relevant fused heterocycles as one of the fundamental building blocks of DNA and RNA. Therefore, the synthesis of its isosteres is of great interest due to their therapeutic potential. Scheme 13 shows two examples of the synthesis of pharmaceutically relevant derivatives. The first example illustrates an open-air dual-diamination annulation to generate 5-aza-9-deazapurine derivatives (Scheme 13a) [128]. Commercially available aromatic aldehydes and aminoazoles afforded *N*-azolo amidines in the first step

which then reacted with ammonium iodide to yield the corresponding fused triazines in good yield, up to 92%. No catalyst or further additives were required. As another example, a novel efficient synthesis of 5-aza-7-deaza-adenine scaffold was developed using a catalyst-free, microwave-assisted multicomponent reaction of triethyl orthoformate and cyanamide (Scheme 13b) [129]. The protocol afforded the desired 4-aminoimidazo[1,2-a][1,3,5]triazine derivatives in good yield and selectivity, in short reactions with good scalability and reproducibility.



Scheme 12. Sustainable, green protocols to synthesize 1,3,5 triazine derivatives.



Scheme 13. Green protocols for the synthesis of purine isosteres.

4. One-Nitrogen-Containing Condensed Heterocycles

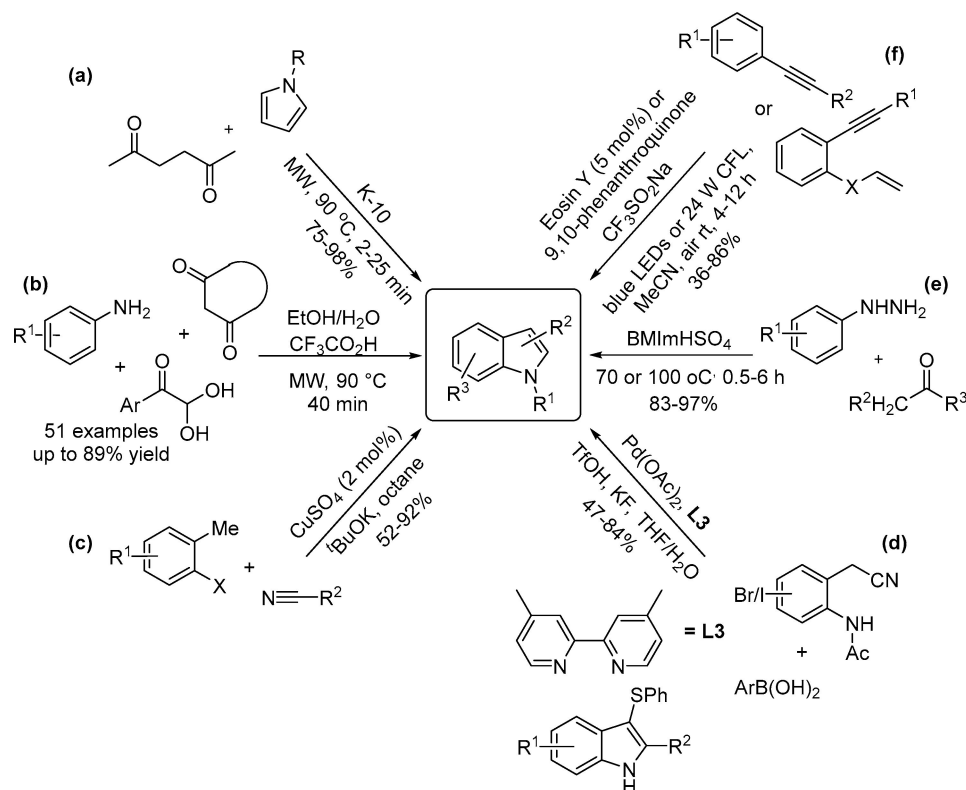
Condensed heterocycles contain multiple rings and commonly serve as the backbone of natural products such as alkaloids, amino acids or nucleic acids. Their structures inspired extensive synthetic efforts to build bioactive compounds that could be applied as drug candidates. Several strategies outlined above already involved the preparation of condensed heterocycles; however, here the emphasis will be on these specific structures.

4.1. Indoles

Indoles are one of the most frequently used and synthesized condensed heterocycles. Representative, environmentally benign, synthesis protocols are depicted in Scheme 14.

Pyrroles readily formed indoles in a reaction with 1,4-dicarbonyl compounds. The solvent-free microwave-assisted reaction was catalyzed by K-10 montmorillonite (Scheme 14a) [17]. K-10 is a solid acid that is also an effective microwave absorber, serving as the medium for the process. The protocol has many green advantages: recyclable solid catalyst, solvent-free conditions, microwave heating, high atom economy and excellent yields, short reactions and a small amount of nontoxic waste (water). Another report described a microwave-assisted catalytic method for the synthesis of indole derivatives from anilines, arylglyoxal monohydrates and cyclic 1,3-dicarbonyl compounds (Scheme 14b) [17]. The reactions occurred in short times in green solvents with high yields and regioselectivity. A simple CuSO₄-catalyzed carbanion-radical redox relay was reported by Shan et al. for the synthesis of N-H indoles (Scheme 14c) [130]. This process could be applied in large-scale preparations as it applies inexpensive reagents. The indole core can also be synthesized by a novel addition/cyclization of 2-(2-aminoaryl)acetonitriles with arylboronic acids catalyzed by a Pd complex (Scheme 14d) [131]. This protocol tolerates a broad range of functional groups and

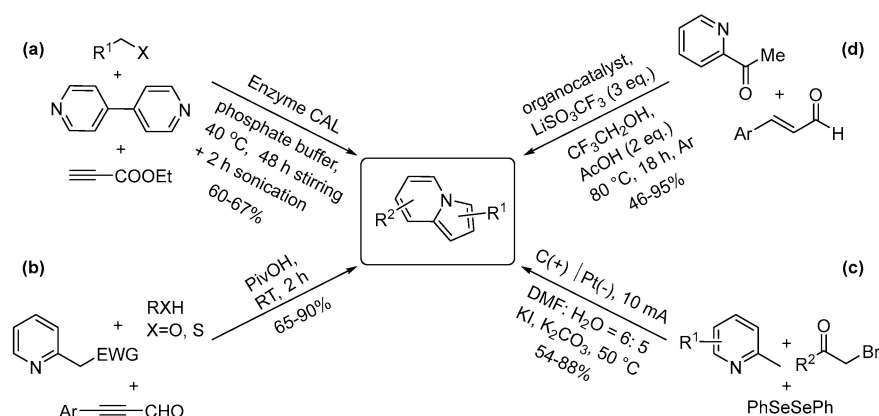
occurs with high selectivity. Ionic liquids (ILs), proposed green solvents, have been used for the preparation of indoles via a modified Fischer indole synthesis providing excellent yields (Scheme 14e) [132,133]. The IL-based methodology occurs without additional solvents and the ILs are generally reusable without any loss in their activity. The emerging, visible-light-promoted activation was also applied for the synthesis of indoles. Using different photoredox catalysts, Eosin Y or 9,10-phenanthroquinone, indoles were synthesized by the vicinal thioamination of alkynes or an intramolecular cyclization of alkynes with alkenes in moderate to good yields under mild conditions (Scheme 14f) [134,135].



Scheme 14. Representative green protocols for the synthesis of indoles.

4.2. Indolizines

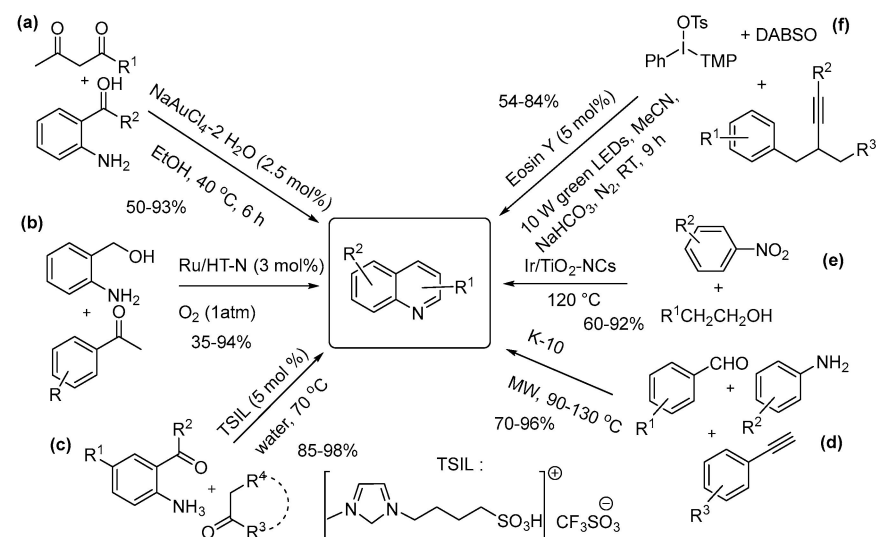
Indolizines, a group of indole analogs, have the N atom positioned to the annulation position between the two rings [136]. Their synthesis can be carried out by cycloadditions of 4,4'-bipyridine, halide derivatives and ethyl propiolate using a biocatalytic method [137]. The enzyme *Candida antarctica* lipase (CAL) showed the best performance in the reaction. (Scheme 15a). The protocol carries many green advantages: it is biocatalytic, the products form in good yields and high purity and it occurs in water under mild conditions. Another multicomponent reaction using similar starting materials, such as 2-(pyridin-2-yl) acetates, ynals and alcohols or thiols was catalyzed by pivalic acid under mild and solvent-free conditions (Scheme 15b) [138]. A similar organocatalytic process was also reported for the synthesis of a broad variety of indolizines (Scheme 15d) [139]. Electrochemical activation was also found to be effective for the preparation of indolizines from 2-methylpyridines, α -bromoketones and diselenides (Scheme 15c) [140], without the use of transition metal catalyst or external oxidant.



Scheme 15. Representative green protocols for the synthesis of indolizines.

4.3. Quinolines, Isoquinolines

The quinoline and isoquinoline skeletons are frequent core units in many bioactive natural products, most prominently alkaloids. Thus, the development of green synthetic protocols is at the forefront of organic synthesis research. A representative group of environmentally benign processes for the synthesis of quinolines are depicted in Scheme 16.

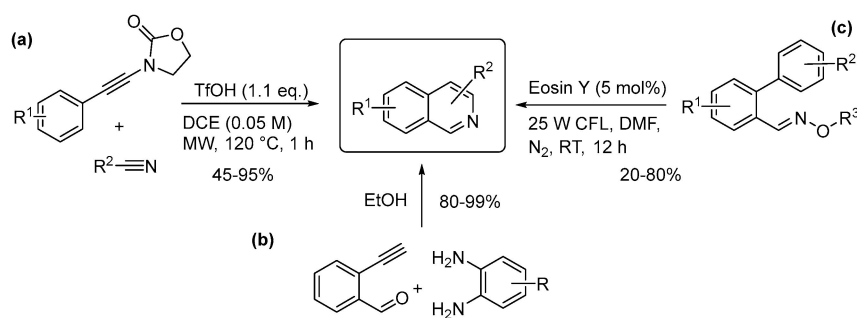


Scheme 16. Representative green protocols for the synthesis of quinolines.

Gold has gained significant attention as a catalytic material [141]. A gold catalyst has been applied in a modified Friedländer synthesis [142] of quinolines, to make the old protocol comply with current safety and environmental standards. The Au (III)-based catalyst promoted the condensation/annulation pathway under mild conditions using 2-aminoacetophenones and 1,3-dicarbonyl compounds (Scheme 16a) [143]. In a heterogeneous catalytic approach Ru-grafted hydrotalcite (HT) [144] catalyzed the reaction of 2-aminobenzyl alcohol with carbonyl compounds (Scheme 16b) [145]. Ru-HT was described as a bifunctional catalyst, the basic HT catalyzed the aldol reaction and Ru promoted the oxidative aromatization. Ionic liquids have also been applied for the synthesis of quinolones. The reusable SO_3H -functionalized alkyl-imidazole, a water tolerant acid, efficiently catalyzed the cyclization of 2-aminoaryl ketones and β -ketoesters/ketones in an aqueous medium in high yields (Scheme 16c) [146]. As a green feature, the products precipitated from the medium and were isolated by a simple filtration thus avoiding solvent demanding purification. In another solid-acid-catalyzed procedure, the recyclable K-10 montmorillonite, was applied in a microwave-assisted solid phase multicomponent reaction (MCR). The reaction

of anilines, benzaldehydes and terminal phenylacetylenes yielded 2,4-disubstituted quinolines (Scheme 16d) [147]. K-10 also catalyzed another MCR to provide quinolines [148]. A bifunctional metal–solid acid catalyst, Ir/TiO₂-NCs (nanoclusters), catalyzed the reaction of nitroarenes and aliphatic alcohols. The reduction–condensation–dehydrogenation pathway provided the quinolines in moderate to excellent yields (Scheme 16e) [149]. As described above the visible-light-promoted photoredox catalysis is attracting much attention in green synthesis. The Eosin Y-catalyzed, green LEDs irradiation-promoted reaction of N-propargyl aryl amines, diaryliodonium salts and sulfur dioxide was carried out at room temperature providing the quinolines in moderate to good yields (Scheme 16f) [150].

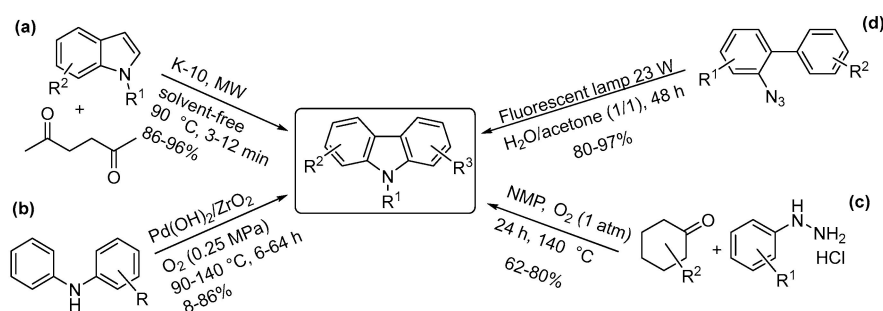
Similar protocols have been explored for the synthesis of isoquinolines as well. The water-tolerant Brønsted superacid, triflic acid (TfOH), efficiently catalyzed the regioselective intermolecular cycloaddition of ynamides-alkynes and nitriles (Scheme 17a) [103]. The protocol affords high yields to synthesize a broad variety of isoquinolines from readily available nitriles as the C–N sources. The high atom economy, microwave activation, short reaction times and the water tolerant acid catalyst are all green advantages, although dichloromethane is an undesirable solvent. Another report described the catalyst-free synthesis of benzimidazo[2,1-a]isoquinolines by the coupling of 2-ethynylbenzaldehyde with *ortho*-phenylenediamines. The reactions occurred in ethanol, a not only green but renewable solvent at room temperature (Scheme 17b) [151] generating high yields and minimal environmental impact. Similarly to 4.3.1.f, eosin Y was found to be an efficient photoredox catalyst for the cyclization of O-2,4-dinitrophenyloximes to produce isoquinolines as well (Scheme 17c) [152].



Scheme 17. Synthesis of isoquinolines by environmentally benign processes.

4.4. Carbazoles

Carbazoles are indole derivatives having an additional aromatic ring on both sides of the central pyrrole. Similarly to the above applications, K-10 montmorillonite was found to be effective for the synthesis of substituted carbazoles as well [153]. The microwave-assisted heterogeneous catalytic method resulted in high yields and excellent selectivities under very short reaction times (Scheme 18a). The protocol has high atom economy combined with excellent yields. It is a solvent-free reaction with a solid catalyst and minimal energy consumption, and it is nearly waste-free, producing water as a byproduct. The Pd-catalyzed oxidative intramolecular coupling of diarylamines also led to the formation of carbazoles. The process was catalyzed by a ZrO₂-supported Pd(OH)₂ (Pd(OH)₂/ZrO₂) with air as the oxidant (Scheme 18b) [154,155]. The synthesis of carbazoles was achieved in a catalyst-free reaction from cyclohexanones and arylhydrazine hydrochlorides in moderate to good yield (Scheme 18c) [156]. The catalyst-free nature and the use of molecular oxygen as an oxidant are the main green advantages of the protocol. A visible-light-activated process successfully cyclized 2-azidobiphenyls to carbazoles in high to excellent yields (Scheme 18d) [157]. This high atom economy/high yielding process occurs in water and produces nitrogen as the only byproduct.



Scheme 18. Synthesis of carbazoles by green processes (NMP-N-methyl-pyrrolidone).

4.5. N and Other Heteroatom

When designing the synthesis of fused heteroarenes, one of the first things to decide is which ring should be formed first. Baran et al. gave the following guidelines in an extensive literature review [158]. In essence, it always leaves the easier synthesis for later. For example, if there is a five and a six membered ring fused together, one should start with the six membered ring as a building block and then annulate the five membered one, mainly because in most cases the substitution of the six-membered ring system is easier, as is the synthesis of the five-membered rings. Therefore, it is recommended to first place the necessary functional groups on the six-membered ring for the sequential synthesis of the five-membered ring. Furthermore, if one of the rings in the fused ring system contains multiple heteroatoms, that ring should be synthesized later. It is rooted in the general observation that the synthesis of heteroarenes containing more heteroatoms is easier than the synthesis of heteroarenes with fewer. If each ring contains several heteroatoms, the position of the heteroatoms is decisive. Retrosynthetically, one should first cleave the ring with successive heteroatoms.

Here, our goal is to give a representative account of recent developments in green and environmentally benign procedures for synthesis of condensed heterocycles containing one nitrogen atom and another heteroatom (e.g., O, S or Se). The examples were grouped based on the extra heteroatom atom and their position relative to the nitrogen atom. The first group illustrates the oxygen-containing condensed heterocycles (Figure 2).

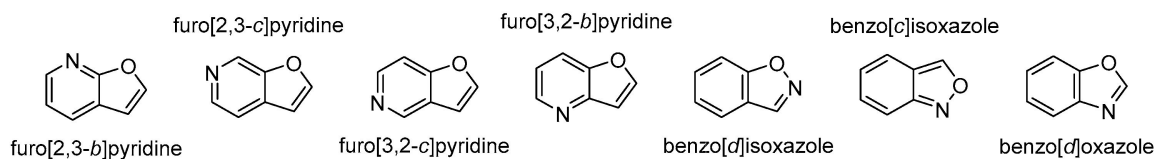
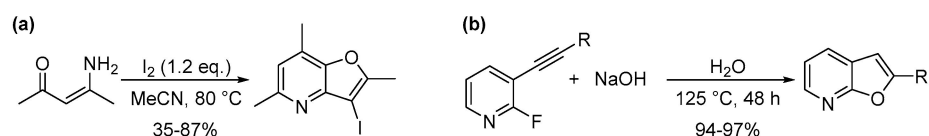


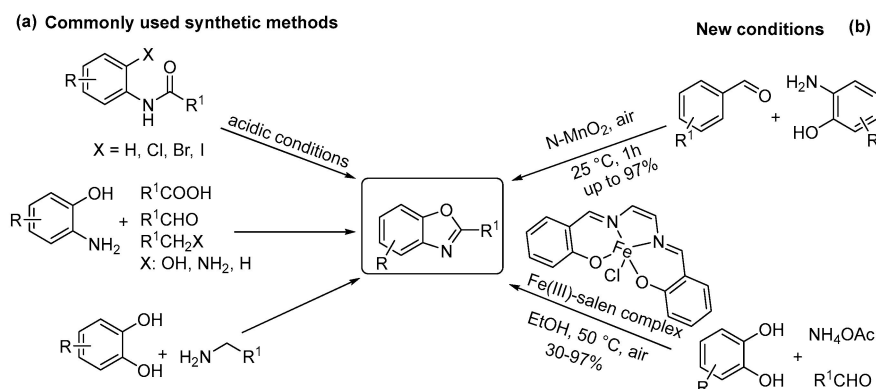
Figure 2. Oxygen-containing *N*-heterocycle isomers.

Huang et al. presented a one-pot synthesis of substituted furopyridines. (Scheme 19a) [159]. Simple enaminone amides underwent an iodine-mediated and metal-free oxidative tandem cyclization reaction to generate the corresponding furopyridine derivatives in moderate to good yield (35–87%). Furopyridines show biological activity against HIV protease inhibitor, therefore their green and benign synthesis is of great interest. Another synthesis protocol was presented by Katz et al. for generating furo[2,3-*b*]pyridine derivatives (Scheme 19b) [160]. Reacting the electrophilic 2-fluorophenylacetylene with sodium hydroxide in an aqueous medium gave the desired furopyridine derivative with an excellent yield (94–97%), but it should be noted that excessive substrate tolerance was not investigated. Further acetylene-activated S_NAr /intramolecular cyclizations in the synthesis of indole and benzofuran derivatives were also discussed.



Scheme 19. A tandem metal-free cyclization of enaminones in the presence of iodine. Reaction of electrophilic 2-fluorophenylacetylene and sodium hydroxide in an aqueous medium.

Benzoxazole is one of the most widely used isomers of *N*-containing condensed heterocycles. Over the years several procedures have been demonstrated for its synthesis (Scheme 20a) [161]. Recently, Han and Ke have presented a highly efficient, nitrogen-doped manganese dioxide (*N*-MnO₂)-catalyzed controllable reaction of 2-amino-phenols and carboxylic acid derivatives for generating benzoxazoles (Scheme 20b) [162–165]. The procedure was carried out at room temperature, and the benzoxazole was obtained with >99% yield and up to >87% for additional benzoxazole derivatives. No significant decay in catalytic activity was observed during 10 catalytic cycles. The introduction of nitrogen into the defect and the coordinatively unsaturated Mn sites proved to be crucial for the catalytic activity. Sharghi et al. presented a one-pot multicomponent reaction for the synthesis of benzoxazole in the presence of Fe(III)-salen complex (Scheme 20b) [166]. The use of catechols, ammonium acetate and aldehydes as starting materials under mild reaction conditions resulted in the desired benzoxazole derivatives in a short time and with moderate to excellent yield (30–97%). Although the catalysts of both reactions contained metal, the processes yielded the desired product with excellent results, and the catalysts were easily separated at the end of the process.



Scheme 20. Traditional and novel, environmentally friendly synthetic protocols for generating benzo[*d*]oxazole derivatives.

After the oxygen-containing condensed 1*N* containing heterocycles, we continue with the discussion of the synthesis of sulfur containing heterocycles (Figure 3).

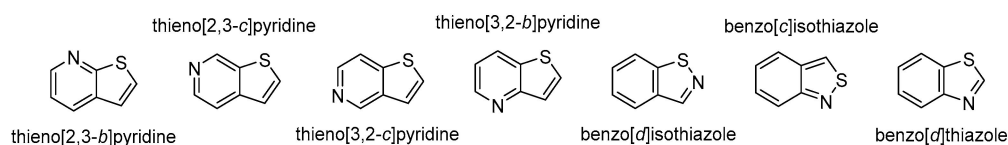
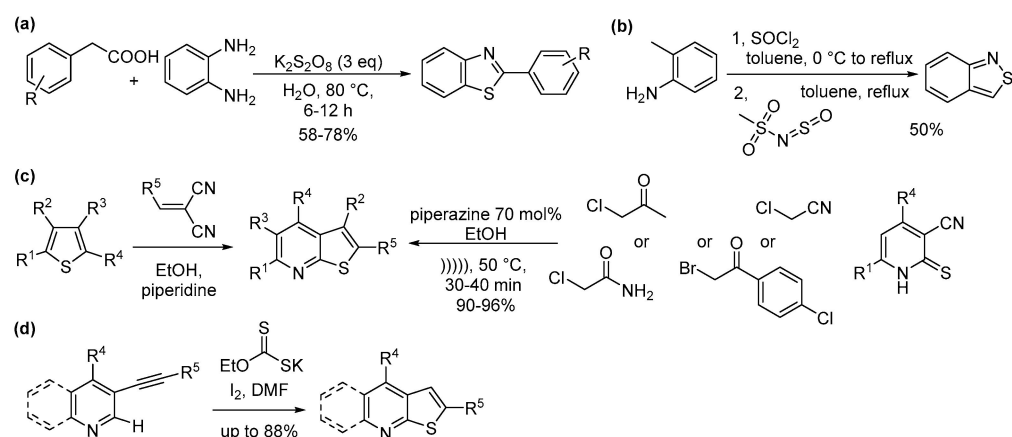


Figure 3. Sulfur-containing *N*-heterocycles.

As part of the development of a green gram-scale sildenafil protocol, Laha's group introduced a new synthetic strategy for constructing the 2-arylbenzo[*d*]thiazole fused ring system. (Scheme 21a) [167]. The innovation of the procedure is the use of arylacetic acid as an acyl source in the formation of the key pyrrazolo[4,3-*d*]pyrimidin-7-one ring. In addition, the organic solvent was replaced by an aqueous medium. In the presence of the oxidant K₂S₂O₈, a number of additional 2-arylbenzo[*d*]thiazoles were synthesized using

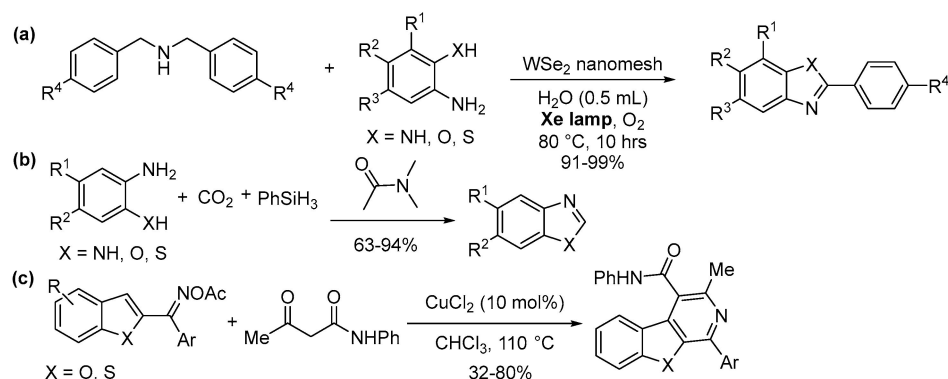
the same protocol in moderate to good yield (58–78%). An Agios Pharmaceuticals patent illustrated a new family of compounds with synthesis procedures that activate pyruvate kinase, making it a potential therapeutic agent for a disease related to PKR function and/or PKM2 function, such as certain cancers, diabetes or obesity (Scheme 21b) [168]. Although the described two-step process did not require the use of metal, toluene as a solvent does not fully comply with the principles of green chemistry. Nossier and Anwar have presented a practical synthesis protocol on how to build a thieno[2,3-b]pyridine scaffold (Scheme 21c) [169]. Thiophene and thiazole often exert a strong antiproliferative effect against various human cell lines, so the development of an efficient and benign synthesis of these compounds and their derivatives is very important. Another environmentally benign synthesis protocol for thieno[2,3-b]pyridine derivatives was reported by Mekky and coworkers (Scheme 21c) [170]. Pyridine-2(1H)-thiones were used as key intermediates to convert into thieno[2,3-b]pyridine derivatives. Excellent yields (90–96%) were achieved in a reaction of pyridine-2(1H)-thiones and α -halo compounds containing acidic C-H bond using eco-friendly piperazine as catalyst with ultrasonic activation. In addition to thienopyridines, this protocol was applied to produce nicotinonitrile derivatives, also with excellent results. Both groups of compounds showed a strong antibacterial effect. The last example of thienopyridine synthesis was presented by He et al. (Scheme 21d) [171]. In this metal-free highly selective cascade thiolation and cyclization reaction, EtOCS₂K was used as a sulfur source in the presence of molecular iodine. Direct C-H functionalization of alkynylpyridine (and alkynylquinoline) derivatives resulted in the formation of thienopyridines (and thienoquinolines) in good yields of up to 88% and showed broad substrate tolerance.



Scheme 21. Environmentally friendly synthetic protocols for generating benzothiazole, benzoisothiazole and thieno[2,3-b]pyridine derivatives.

Finally, some protocols are presented that can be either used for the synthesis of fused 1*N*-heterocycles containing another nitrogen, oxygen or sulfur. For example, Chai et al. designed and synthesized a WSe₂ nanomesh material that showed excellent photocatalytic activity in the oxidative coupling reaction of dibenzylamine and 2-amino/hydroxy/mercaptoaniline to produce benzimidazoles, benzoxazoles and benzothiazoles (Scheme 22a) [172]. The products were obtained in excellent yields (91–99%) under benign conditions, using only water as solvent and oxygen as an oxidizing agent, in the presence of visible light. The catalyst showed excellent stability over several catalytic cycles. A highly efficient catalyst-free green procedure was also developed to generate various N-containing benzoheterocycles in the presence of CO₂ (Scheme 22b) [173]. The reaction conditions are decisive in terms of selectivity, such as the solvent, CO₂ pressure, time, temperature and the hydrosilane quantity. Finally, Rong et al. presented a synthetic protocol for the annulation reaction of ketoxime acetates and acetoacetanilide in the presence of a copper catalyst (Scheme 22c) [174]. The simple, inexpensive synthetic strategy resulted in the desired benzofuro- and benzothieno[2,3-c]pyridines in good yields and with good substrate tolerance. Overall, all three processes are great examples of

environmentally friendly methods to produce the therapeutically significant benzimidazole, benzoxazole and benzothiazole moiety.



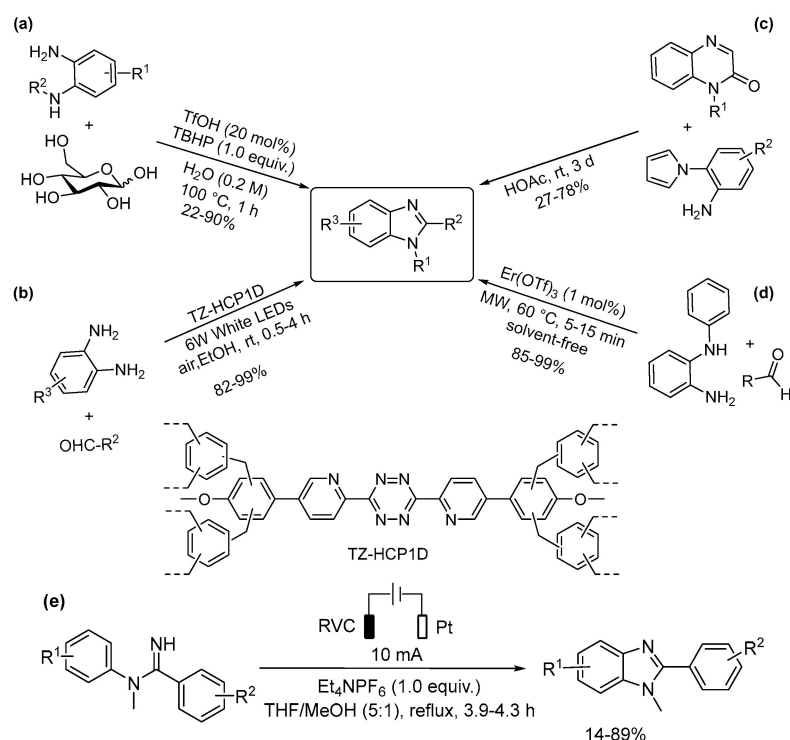
Scheme 22. Environmentally benign synthesis protocols to generate benzimidazoles, benzoxazoles and benzothiazoles.

5. Two-Nitrogen-Containing-Condensed Heterocycles with Multiple N Atoms

5.1. Benzimidazoles and Indazoles

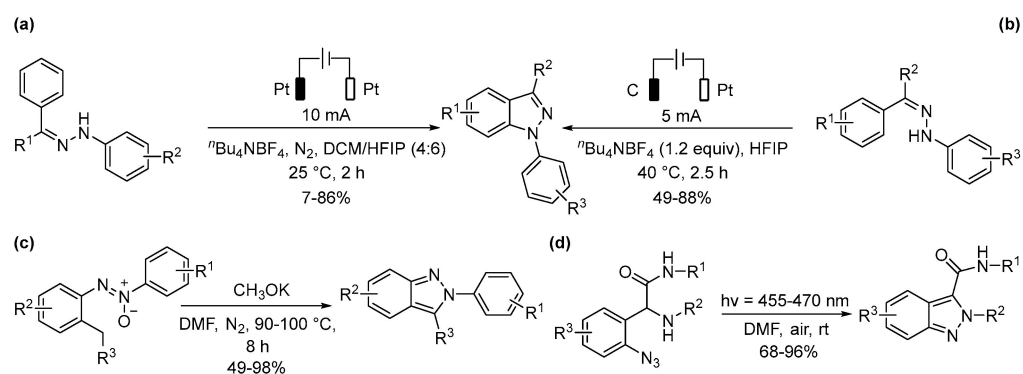
Benzimidazole and its derivatives are explicitly acknowledged as important skeletons which possess various biological activities such as anticancer activity [175], antihypertensive [176], anti-inflammatory [177], antimicrobial [178], antioxidant activity [179] and anticoagulant activity [180]. Due to its significant role in drug applications, extensive efforts were devoted to the green synthesis of benzimidazoles.

Raja et al. [181] developed an oxidative cyclization strategy by using the efficient C1 synthon *D*-glucose for the synthesis of benzimidazoles with yields 22–90% from *o*-phenylenediamines (Scheme 23a). This protocol possesses many advantages including short reaction time, broad functional group tolerance, metal-free, using environmentally benign solvent, water and bio-renewable methine sources. Hypercrosslinked polymers (HCPs) are of great interest due to their lightweight properties and high surface areas which makes them promising materials for catalysis [182]. An et al. successfully constructed a versatile photocatalyst TZ-HCP1D through Friedel–Crafts alkylation reaction (82–99% yield) (Scheme 23b) [183]. TZ-HCP1D was proved to be efficient in photocatalytic benzimidazole synthesis in EtOH. The heterogeneous system is considered green because of avoiding the use of metals, strong oxidants, acid and high temperature. In 2000, an unexpected rearrangement was discovered by Kalinin et al., when they mixed *o*-phenylenediamine with 3-benzoylquinoxalin-2(1*H*)one in boiling acetic acid [184] and obtained a benzimidazole derivative. Based on this finding, many valuable studies have been carried out. Among them, Li et al. explored a simple and environmentally friendly protocol to synthesize benzimidazoles [185]. A series of substituted products were obtained in moderate to good yields 27–78% with the only requirement of the solvent AcOH at room temperature (Scheme 23c). Since the clinically available benzimidazole-based drug is crucial, a rapid, cheap, clean and environmentally sustainable method for its synthesis has been reported. 1,2-disubstituted benzimidazoles (85–99% yield) were synthesized under microwave-assisted conditions without solvents, but 1% Er(OTf)₃ was required as an efficient and environmentally mild catalyst (Scheme 23d) [186]. In recent years, dehydrogenative cross-coupling reactions under electrochemical oxidative conditions have gained significant attention [187,188]. An efficient and sustainable method that utilized electricity as a green reagent was developed for the synthesis of benzimidazoles (14–89% yield) through dehydrogenative cyclization of *N*-aryl amidines (Scheme 23e) [189]. The tandem cyclization was conducted without catalysts, oxidants or additives, generating H₂ as the only byproduct. Another catalyst-free room temperature synthesis of isoquinoline-fused benzimidazoles was recently reported using 2-alkynylbenzaldehydes and *o*-phenylenediamines in good to excellent yields in a green solvent, EtOH [190].



Scheme 23. Green synthesis of benzimidazoles via non-traditional activation methods.

Substantial efforts have been made toward designing facile and efficient synthetic methods to access indazoles due to their biological and pharmaceutical applications [191]. *1H*-indazole and its tautomer *2H*-indazole have been known as crucial units in many pharmaceuticals [192,193]. A catalyst-free and chemical oxidant-free electrochemical synthesis of *1H*-indazoles (7–86% yield) was demonstrated by Wan and co-workers (Scheme 24a) [194]. This indazole formation involves electrochemical oxidative radical Csp²-H/N-H cyclization of arylhydrazones. Cyclic voltammetry indicates that DCM/HFIP is essential in which the substrate has the lowest oxidation potential. Pt anode and *n*Bu₄NBF₄ electrolyte were the most effective for the activation of arylhydrazones.



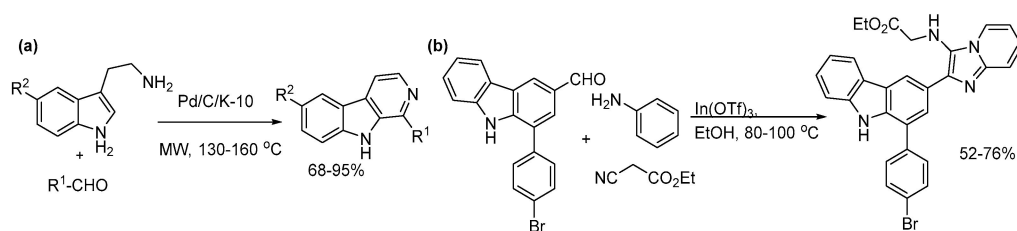
Scheme 24. Facile and efficient synthetic methods to access *1H*-indazole and *2H*-indazole.

Zhang et al. [195] reported another metal- and oxidant-free electrochemical protocol for the synthesis of *1H*-indazoles from easily available hydrazones. This series of reactions was carried out in an undivided cell which was equipped with a carbon anode, a Pt cathode and *n*Bu₄NBF₄ electrolytes (49–88% yield) (Scheme 24b). It is worth noting that a wide range of functional groups are tolerated, and gram-scale reactions were accomplished under mild conditions. *2H*-indazoles are important scaffolds in medicinal chemistry, exhibiting a broad range

of pharmacological and biological activities such as antimicrobial and anti-inflammatory [196]. In particular, 2-aryl-2*H*-indazoles are crucial scaffolds found in various biologically active molecules. Additionally, its derivatives display attractive fluorophoric properties for cellular imaging [197]. Jin et al. synthesized several fluorescent and bioactive 2*H*-indazoles molecules via base-catalyzed benzylic C–H deprotonation and cyclization without using transition-metal catalysts (Scheme 24c) [198]. This synthetic strategy employs inexpensive CH₃OK as the base and has good tolerance for halogen, electron-neutral methyl, electron-donating or electron-withdrawing groups, and provides the products in good to excellent yields, 49–98%. Liu et al. [199] reported a green and sustainable method to access 2*H*-indazole-3-carboxamides in moderate to excellent yields (68–96%) (Scheme 24d). Inspired by the Davis–Beirut reaction for the conversion of aromatic nitro compounds to *N*-aryl 2*H*-indazoles [200], a visible-light-driven N–N coupling of aryl azides to 2*H*-indazole-3-carboxamides has been developed without the presence of a photocatalyst and external additive addition. These reactions were carried out at room temperature under air, possessing additional advantages such as the broad substrate scope, excellent functional group compatibility and environment friendliness.

5.2. Carbolines

Carbolines are three-ring heterocycles with two N-atoms one in the middle ring and another in either side rings, β -carbolines being the most common [201]. These compounds exhibit multiple types of biological activities, such as being multifunctional anti AD compounds [202], anticancer agents [203] or angiogenesis inhibitors [204]. A combined heterogeneous catalytic microwave-assisted synthesis was developed by using a Pd/C and K-10 montmorillonite-containing bifunctional catalyst. Tryptamines and carbonyl compounds were reacted to form β -carbolines in a green Pictet–Spengler cyclization in a three-step domino sequence affording the products in good to excellent yields (Scheme 25a) [205]. Another method used In(OTf)₃ catalysis in a multicomponent reaction, using the Groebke–Blackburn–Bienayme (GBB) reaction [206]. The method provided good yields for the products and possessed several green advantages, such as operational simplicity, high atom economy, structural diversity, easy purification and the use of EtOH, a green solvent (Scheme 25b).



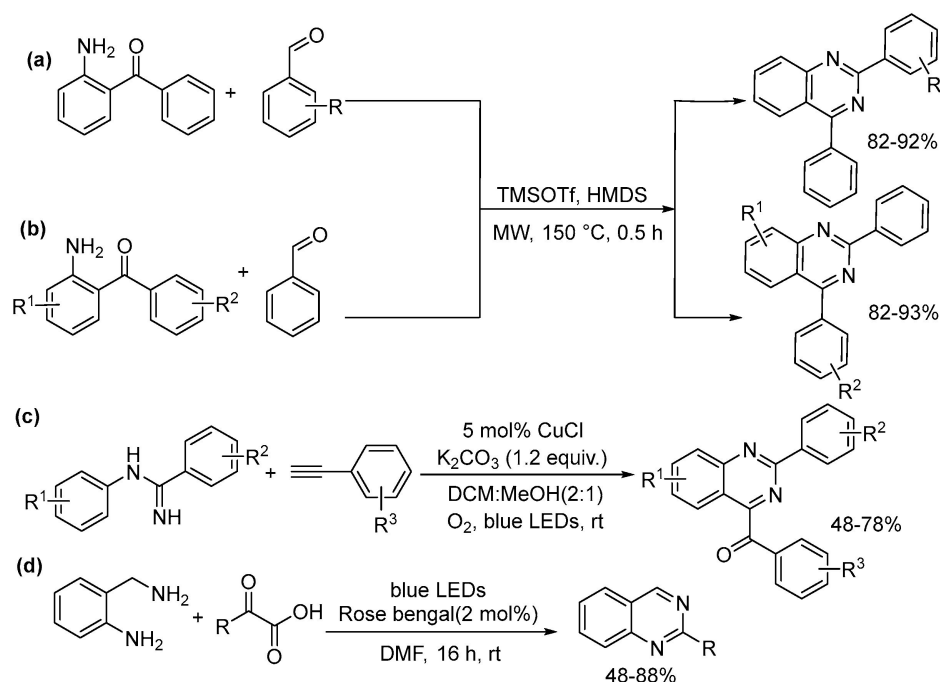
Scheme 25. Catalytic syntheses of β -carbolines and derivatives.

5.3. Quinazoline, Quinoxaline, Cinnoline

Quinazolines are important nitrogen-containing heterocycles many of them are bioactive natural and synthetic products of pharmaceutical interest with diverse properties such as antimicrobial [207], antiviral [208], antimalarial [209], antituberculosis [210], etc.

Chan et al. [211] constructed substituted quinazolines from functionalized 2-amino-benzophenones and aromatic aldehydes (Scheme 26a,b). This efficient and mild protocol employed TMSOTf/hexamethyldisilazane (HMDS) catalytic system under neat, metal-free and microwave-assisted conditions. Notably, HMDS served as N sources and the reaction was catalyzed by TMSOTf, generating gaseous ammonia in situ. Most protocols for C–H functionalization/C–H annulation use transition metal catalysts under conventional thermal conditions. Owing to its common drawbacks, Charpe et al. [212] reported the visible light-initiated copper-catalyzed oxidative Csp²–H annulation of amidines with terminal alkynes to form 2,4-disubstituted quinazolines using molecular O₂ as an oxidant at room temperature (48–78%; Scheme 26c). These reactions were carried out under mild

conditions, which did not require any expensive, toxic external photocatalysts or organic oxidants. Water is the only byproduct of the reactions. In terms of green chemistry metrics, the E-factor is ~1.9 times better than that of the reported thermal method. Another transition metal catalyst- and additive-free quinazoline synthesis has been described by Yang et al. [213]. In this study, visible-light catalysis was applied as a green and clean way to access the coupling, decarboxylation and cyclization of 2-aminobenzylamine and α -ketoacids under room temperature in air (48–88% yield; Scheme 26d).



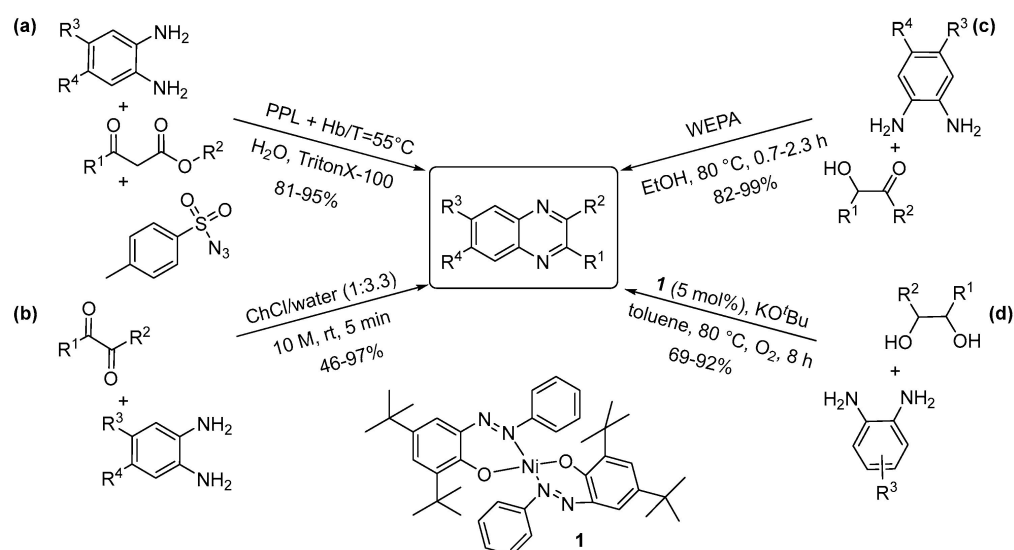
Scheme 26. Green synthesis of functionalized quinazolines under microwave- (a,b) and visible light (c,d) activation.

Quinoxalines and their derivatives have gained a great deal of attention in medicinal chemistry due to their diverse biological activities [214]. Additionally, quinoxaline derivatives have been reported for applications in fields such as organic semiconductors [215], dyes [216], organic photovoltaics [217] etc.

Li et al. [218] designed an efficient dual-protein (lipase and hemoglobin) system which successfully catalyzed the regioselective synthesis of quinoxalines in water. This system represents an environmentally benign, efficient and regioselective synthesis of quinoxalines. In this green and efficient protocol, lipase was used to access the in situ generations of diazodicarbonyls by a diazo transfer reaction to 1,3-dicarbonyl compounds with sulfonyl azides (Scheme 27a). The obtained α -diazo carbonyl compounds and 1,2-diamines were catalyzed by hemoglobin to afford the condensed quinoxaline products in excellent yield (81–95%). It is worth noting that this method can be easily scaled up, maintaining moderate regioselectivity.

Natural deep eutectic solvents (NADESs) are considered functional liquid media which can dissolve natural or synthetic chemicals of low water solubility. Owing to the special properties such as high biodegradability and biocompatibility, NADESs can serve as alternative candidates for organic solvents and ionic liquids [219]. Lupidi et al. [220] reported a sustainable and rapid method for the synthesis of functionalized quinoxalines, via the condensation of 1,2-dicarbonyls with 1,2-diamino compounds in a ChCl/water NADES in 5 min at room temperature (46–97%) (Scheme 27b). The involvement of NADESs enabled the fast activation of reactants, providing pure enough products to avoid further purification. Based on universal sustainable development goals, reusable biomass-based resources for organic synthesis are encouraged to develop cleaner, sustainable and safer chemistry [221]. The water extract of

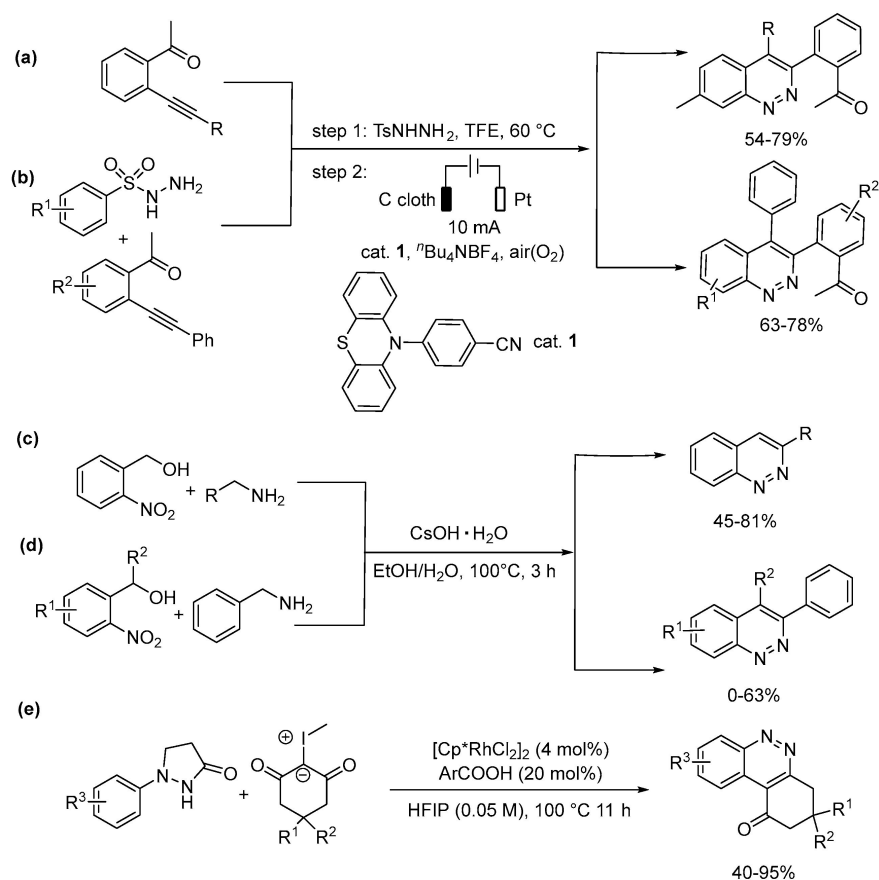
pomegranate peel ash (WEPA) was applied to catalyze a condensation–cyclization–oxidation process between α -hydroxy ketones and 1,2-diamines, affording quinoxalines with excellent yield (82–99%) at 80 °C in air (Scheme 27c). This sustainable protocol has many advantages, such as deploying oxygen from air, using recrystallization for purification in an aqueous medium and the ability to be scaled up. Bains et al. [222] investigated a bis(azophenolate) nickel complex in quinoxaline synthesis. The inexpensive, air-stable nickel catalyst successfully yielded quinoxalines (69–92%) under aerobic atmosphere at a mild reaction temperature of 80 °C via double dehydrogenative coupling of diamine and diol (Scheme 27d). A similar, but even more environmentally benign process provided quinoxalines in nearly quantitative yields in a catalyst and solvent-free process [223].



Scheme 27. Environmentally benign and sustainable method for the synthesis of functionalized quinoxalines.

Cinnolines are vital building blocks that are present in many compounds with considerable pharmaceutical properties such as antibacterial, antifungal, antimalarial, anti-inflammatory, analgesic, anxiolytic and antitumor activities [224], creating considerable interest in their preparation. Cai et al. [225] introduced a straightforward synthesis of cinnoline derivatives through aerobic electrochemical oxidation–cyclization and migration under metal-free conditions. This methodology utilized electrochemistry to promote a one-pot two-step cascade cyclization of *ortho*-alkynyl acetophenones and sulfonyl hydrazides (Scheme 28a,b). Moreover, this strategy has many benefits such as good to excellent yield 54–79%, broad functional group tolerance, good step economy and green reaction conditions.

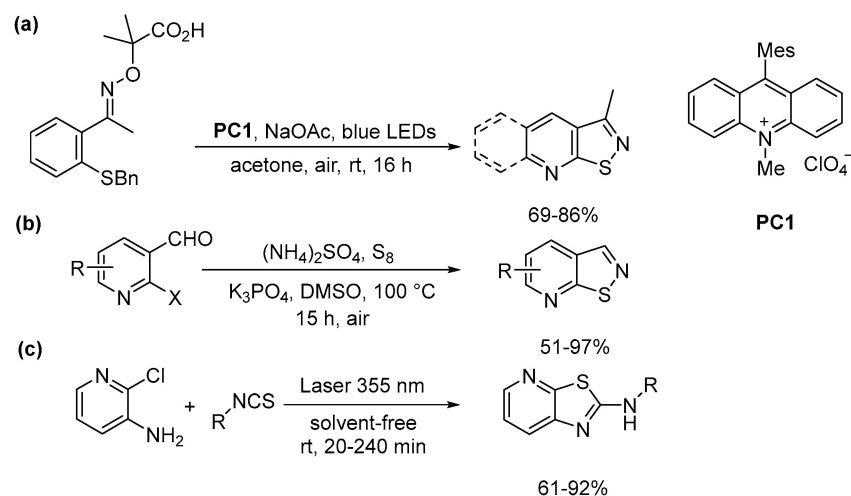
A transition-metal-free intramolecular redox cyclization reaction [226] was developed for the straightforward synthesis of cinnolines from 2-nitrobenzyl alcohol and benzylamine by a simple treatment with $C_5OH \cdot H_2O$ in EtOH/ H_2O (45–81% yield; Scheme 28c). This method involves the formation of intermediate 2-nitrosobenzaldehyde and (*E*)-2-(2-benzylidenediaziridinyl) benzaldehyde which play an important role in the intramolecular redox cyclization. A rhodium-catalyzed [4+2] cyclization of readily available pyrazolidinones and iodonium ylides [227] was applied to synthesize cinnolines (Scheme 28d). The reactions were carried out in HFIP with 2,4,6-trimethylbenzoic acid additive. Moderate to excellent yields (40–95%) and broad scope were achieved under mild reaction conditions.



Scheme 28. Straightforward access to cinnolines under mild reaction conditions.

5.4. N and Other Heteroatoms

Heterocyclic compounds having isothiazole moiety exhibit analgesic, anorectic and antidepressant activities. Traditional methods for the synthesis of isothiazolo[5,4-b]pyridines, however, require high temperatures (250 °C) [228]. To address such issues, Cabrera-Afonso et al. [229] disclosed a sustainable synthesis of isothiazoles from α -imino-oxy acids. This efficient method applied an organo-photoredox generation of iminyl radicals by oxidative single-electron transfer (SET) to the formation of N–S bonds (up to 86%). The reactions were carried out under air and 450 nm single LED at room temperature without transition metals or stoichiometric oxidants (Scheme 29a). Wang et al. [230] used elemental sulfur and ammonium sulfate as heteroatom components to synthesize isothiazolo[5,4-b]pyridines via a three-component reaction under transition metal-free conditions (Scheme 29b). Elemental sulfur has the advantages of being inexpensive, industrially available, stable, non-volatile, easily stored, non-hygroscopic and non-toxic in nature compared to other sulfur sources such as KSCN, thiadiazole, etc. These reactions are moisture and oxygen tolerant and can easily be scaled up, providing products in good to excellent yields 51–97%. Jemili et al. [231] described a new laser-assisted synthesis of phenylthiazolo[5,4-b]pyridine derivatives (Scheme 29c). This rapid and straightforward approach benefits from the absence of solvent, yielding 61–92% product. It was also noted that increasing laser energy input increased the yields. Moreover, the conditions are solvent-, metal- and base-free.

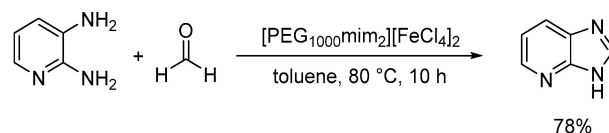


Scheme 29. Sustainable synthesis of isothiazolo[5,4-b]pyridines (a,b) and phenylthiazolo[5,4-b]pyridines (c).

6. Three- and Four-N-containing Condensed Heterocycles

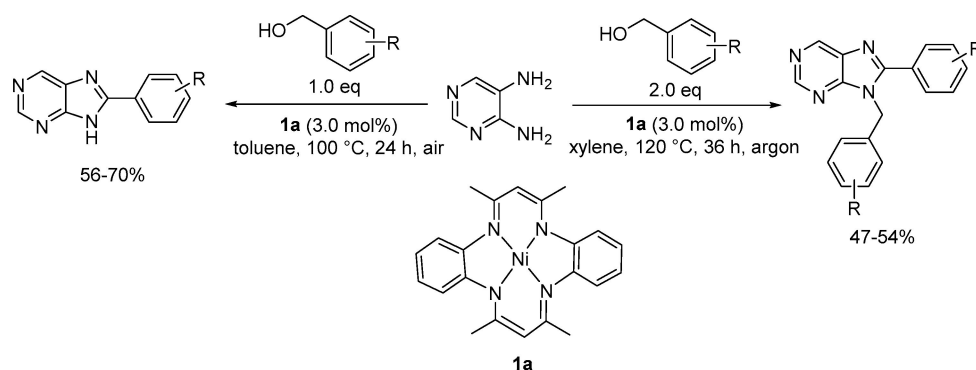
Purine, 3H-imidazo[4,5-b]pyridine, Imidazo[1,2-c]pyrimidine

Polyethylene glycol-based dicationic ionic liquid [232] has been applied in a green protocol to synthesize 3H-imidazo[4,5-b]pyridine. Fe(III)-based PEG₁₀₀₀ dicationic imidazolium ionic liquid ([PEG₁₀₀₀mim₂][FeCl₄]₂)/toluene biphasic system served as a medium and catalyst as well to promote the reaction effectively providing 78% yield (Scheme 30) [233]. As a further green advantage the solvent could be recycled and maintained good catalytic activity after seven runs.



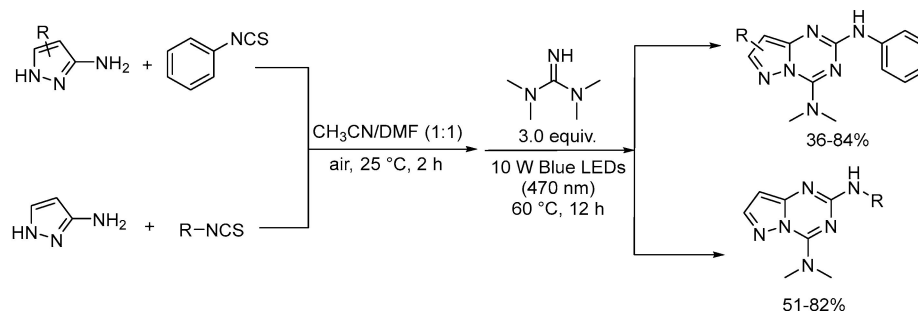
Scheme 30. Synthesis of 3H-imidazo[4,5-b]pyridine from aryldiamines with formaldehyde.

Chakraborty et al. reported a sustainable nickel-catalyzed methodology for the synthesis of various purines via dehydrogenative functionalization with benzyl alcohols [234]. The bench stable catalyst was easily prepared and could catalyze the selective formation of 8-substituted (56–70% yield) and 8,9-disubstituted (47–54% yield) purine derivatives under different reaction conditions. Moreover, 8-substituted purine derivatives were obtained via using toluene as a solvent at 100 °C under air, while 8,9-disubstituted purine derivatives were obtained with xylene as a solvent at 120 °C under argon atmosphere (Scheme 31).



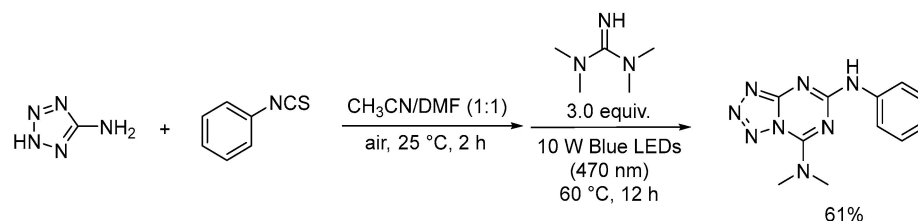
Scheme 31. Synthesis of various purines via acceptorless dehydrogenative coupling.

Guo et al. [235] reported an efficient synthesis of pyrazolo[1,5-*a*][1,3,5]triazine-2,4-diamines via a visible-light-enhanced annulation of 1*H*-pyrazol-3-amines and isothiocyanates [236]. This strategy generated in situ pyrazolthiourea intermediates in the first step, which then underwent a formal [4+2] annulation with 1,1,3,3-tetramethylguanidines (TMG) to give the corresponding products in 36–84% yield (Scheme 32). This method featured green advantages such as the use of a photocatalyst-, metal-, oxidant-, ligand-, base-free and broad substrate scope.



Scheme 32. Visible-light-enhanced annulation approach to pyrazolo[1,5-*a*][1,3,5]triazine-2,4-diamines.

Additionally, this protocol can be applied to synthesize a potential biologically active product (61% yield) when using 2*H*-tetrazol-5-amine as the substrate (Scheme 33).



Scheme 33. Synthesis of a potential biologically active compound under visible light activation.

7. Summary and Conclusions

As described above, the preparation of N-heterocycles is still at the forefront of organic synthesis research, although the focus has shifted toward the application of contemporary synthetic methods that comply with the major principles of green chemistry and engineering. In this work the highlight was placed on the use of catalytic methods and energy efficient activations by nontraditional methods, such as microwaves, ultrasounds, photo- and electrochemistry and high hydrostatic pressure. The protocols listed in this account are representative examples of the new developments illustrating the synthesis of the target compounds through a green and sustainable perspective.

Author Contributions: Conceptualization, B.T., R.B.V. and G.X.; data curation, B.T., R.B.V. and G.X.; writing—original draft preparation, B.T., R.B.V. and G.X.; writing—review and editing, B.T., R.B.V. and G.X.; visualization, B.T., R.B.V. and G.X.; supervision, B.T.; project administration, B.T. All authors have read and agreed to the published version of the manuscript.

Funding: This research received no external funding.

Institutional Review Board Statement: Not applicable.

Informed Consent Statement: Not applicable.

Data Availability Statement: No new data were created.

Acknowledgments: The support of this work by the University of Massachusetts Boston is gratefully acknowledged.

Conflicts of Interest: The authors declare no conflict of interest.

References

- Schäfer, C.; Cho, H.; Vlocskó, R.B.; Xie, G.; Török, B. Recent Advances in the Green Synthesis of Heterocycles: From Building Blocks to Biologically Active Compounds. *Curr. Org. Synth.* **2022**, *19*, 426–462. [CrossRef]
- Brahmachari, G. *Catalyst-Free Organic Synthesis*; RSC: London, UK, 2018.
- Gilchrist, T.L. *Heterocyclic Chemistry*, 3rd ed; Addison-Wesley-Longman, Ltd.: London, UK, 1997.
- Török, B.; Dransfield, T. (Eds.) *Green Chemistry: An Inclusive Approach*; Elsevier: Amsterdam, The Netherlands; Oxford, UK; Cambridge, MA, USA, 2018.
- Török, M. (Ed.) *Contemporary Chemical Approaches for Green and Sustainable Drugs*; Elsevier: Amsterdam, The Netherlands; Oxford, UK; Cambridge, MA, USA, 2022.
- Siddiki, S.M.A.H.; Toyao, T.; Shimizu, K. Acceptorless dehydrogenative coupling reactions with alcohols over heterogeneous catalysts. *Green Chem.* **2018**, *20*, 2933–2952. [CrossRef]
- Török, B.; Schäfer, C.; Kokel, A. Multicomponent reactions. In *Heterogeneous Catalysis in Sustainable Synthesis*; Elsevier: Cambridge, MA, USA; Oxford, UK, 2021; Chapter 3.7; pp. 443–490.
- Török, B.; Schäfer, C.; Kokel, A. Ring transformations by heterogeneous catalysis. In *Heterogeneous Catalysis in Sustainable Synthesis*; Elsevier: Cambridge, MA, USA; Oxford, UK, 2021; Chapter 3.8; pp. 491–542.
- Török, B.; Schäfer, C. (Eds.) *Non-Traditional Activation Methods in Green and Sustainable Applications: Microwaves, Ultrasounds, Photo, Electro and Mechanochemistry and High Hydrostatic Pressure*; Elsevier: Cambridge, MA, USA; Oxford, UK, 2021.
- Knorr, L. Synthese von Furfuranderivaten aus dem Diacetbernsteinsäureester. *Ber. Dtsch. Chem. Ges.* **1884**, *17*, 2863–2870. [CrossRef]
- Paal, C. Ueber die Derivate des Acetophenonacetessigesters und des Acetylacetessigesters. *Ber. Dtsch. Chem. Ges.* **1884**, *17*, 2756–2767. [CrossRef]
- Balakrishna, A.; Aguiar, A.; Sobral, P.J.M.; Wani, M.Y.; Almeida, J.; Sobral, S.A.J.N.F. Paal–Knorr synthesis of pyrroles: From conventional to green synthesis. *Catal. Rev. Sci. Eng.* **2019**, *61*, 84–110. [CrossRef]
- Cho, H.; Madden, R.; Nisanci, B.; Török, B. The Paal–Knorr reaction revisited. A catalyst and solvent-free synthesis of underivatized and N-substituted pyrroles. *Green Chem.* **2015**, *17*, 1088–1099. [CrossRef]
- Xie, G.; Lazarev, A.; Török, B. High Pressure Initiated Solvent and Catalyst-Free Instant Paal–Knorr Reactions. *Green Chem.* **2023**, *25*, 1582–1587. [CrossRef]
- Akbaslar, D.; Demirkol, O.; Giray, S. Paal–Knorr pyrrole synthesis in water. *Synth. Commun.* **2014**, *44*, 1323–1332. [CrossRef]
- Guan, Z.-H.; Li, L.; Ren, Z.-H.; Li, J.; Zhao, M.N. A facile and efficient synthesis of multisubstituted pyrroles from enaminoesters and nitroolefins. *Green Chem.* **2011**, *13*, 1664–1668. [CrossRef]
- Abid, M.; Spaeth, A.; Török, B. Solvent-Free Solid Acid Catalyzed Electrophilic Annulations: A New Green Approach for the Synthesis of Substituted Five-Membered N-Heterocycles. *Adv. Synth. Catal.* **2006**, *348*, 2191–2196. [CrossRef]
- Abid, M.; Landge, S.M.; Török, B. An Efficient and Rapid Synthesis of N-substituted Pyrroles by Microwave Assisted Solid Acid Catalysis. *Org. Prep. Proced. Int.* **2006**, *35*, 495–500. [CrossRef]
- Abid, M.; Teixeira, L.; Török, B. Triflic acid controlled successive annelation of aromatic sulfonamides: An efficient one-pot synthesis of N-sulfonyl pyrroles, indoles and carbazoles. *Tetrahedron Lett.* **2007**, *48*, 4047–4050. [CrossRef]
- Daştan, A.; Kulkarni, A.; Török, B. Environmentally Benign Synthesis of Heterocyclic Compounds by Combined Microwave-Assisted Heterogeneous Catalytic Approaches. *Green Chem.* **2012**, *14*, 17–37. [CrossRef]
- Kokel, A.; Schäfer, C.; Török, B. Application of microwave-assisted heterogeneous catalysis in sustainable synthesis design. *Green Chem.* **2017**, *19*, 3729–3751. [CrossRef]
- Yasukawa, N.; Kuwata, M.; Imai, T.; Monguchi, Y.; Sajiki, H.; Sawama, Y. Copper-catalyzed pyrrole synthesis from 3,6-dihydro-1,2-oxazines. *Green Chem.* **2018**, *20*, 4409–4413. [CrossRef]
- Wang, P.; Ma, F.-P.; Zhang, Z.-H. L-(+)-Tartaric acid and choline chloride based deep eutectic solvent: An efficient and reusable medium for synthesis of N-substituted pyrroles via Clauson-Kaas reaction. *J. Mol. Liq.* **2014**, *198*, 259–262. [CrossRef]
- Naeimi, H.; Dadaei, M. Efficient and Green Synthesis of N-aryl Pyrroles Catalyzed by Ionic Liquid [H-NMP][HSO₄] in Water at Room Temperature. *J. Chin. Chem. Soc.* **2014**, *61*, 1127–1132. [CrossRef]
- Singh, S.B.; Verma, P.K.; Tiwari, K.; Srivastava, M.; Ankit, P.; Singh, M.; Singh, J.; Tiwari, K.P. Supramolecular catalysis in the synthesis of polyfunctionalised pyrroles. *Supramol. Chem.* **2014**, *26*, 882–889. [CrossRef]
- Mhadgut, S.C.; Palaniappan, K.; Thimmaiah, M.; Hackney, S.A.; Török, B.; Liu, J. A Metal Nanoparticle-Based Supramolecular Approach for Aqueous Biphasic Reactions. *Chem. Commun.* **2005**, 3207–3209. [CrossRef]
- Li, X.; Zhang, L.; Wu, Z.; Chen, S.; Wang, J.; Zeng, Z.; Zou, J.-J.; Deng, S.; Deng, Q. Breaking binary competitive adsorption in the domino synthesis of pyrroles from furan alcohols and nitroarenes over metal phosphide. *Appl. Catal. B Environ.* **2022**, *316*, 21665. [CrossRef]
- Xu, J.; Green, A.P.; Turner, N.J. Chemo-Enzymatic Synthesis of Pyrazines and Pyrroles. *Angew. Chem. Int. Ed.* **2018**, *57*, 16760–16763. [CrossRef]
- Chen, J.-R.; Hu, X.-Q.; Lu, L.-Q.; Xiao, W.-J. Exploration of Visible-Light Photocatalysis in Heterocycle Synthesis and Functionalization: Reaction Design and Beyond. *Acc. Chem. Res.* **2016**, *49*, 1911–1923. [CrossRef] [PubMed]
- Cao, H.; Tang, X.; Tang, H.; Yuan, Y.; Wu, J. Photoinduced intermolecular hydrogen atom transfer reactions in organic synthesis. *Chem. Catal.* **2021**, *1*, 523–598. [CrossRef]

31. Lenardon, G.V.A.; Nicchio, L.; Fagnoni, M. Photogenerated electrophilic radicals for the umpolung of enolate chemistry. *J. Photochem. Photobiol. C Photochem. Rev.* **2021**, *46*, 100387. [CrossRef]
32. Pawlowski, R.; Stanek, F.; Stodulski, M. Recent Advances on Metal-Free, Visible-Light-Induced Catalysis for Assembling Nitrogen- and Oxygen-Based Heterocyclic Scaffolds. *Molecules* **2019**, *24*, 1533. [CrossRef]
33. Xuan, J.; Xia, X.-D.; Zeng, T.-T.; Feng, Z.-J.; Chen, J.-R.; Lu, L.-Q.; Xiao, W.-J. Visible-Light-Induced Formal [3 + 2] Cycloaddition for Pyrrole Synthesis under Metal-Free Conditions. *Angew. Chem. Int. Ed.* **2014**, *53*, 5653–5656. [CrossRef]
34. Li, X.T.; Liu, Y.H.; Liu, X.; Zhang, Z.H. Meglumine Catalyzed One-Pot, Three-Component Combinatorial Synthesis of Pyrazoles Bearing a Coumarin Unit. *RSC Adv.* **2015**, *5*, 25625–25633. [CrossRef]
35. Schmitt, D.C.; Taylor, A.P.; Flick, A.C.; Kyne, R.E. Synthesis of Pyrazoles from 1,3-Diols via Hydrogen Transfer Catalysis. *Org. Lett.* **2015**, *17*, 1405–1408. [CrossRef]
36. Matcha, K.; Antonchick, A.P. Cascade Multicomponent Synthesis of Indoles, Pyrazoles and Pyridazinones by Functionalization of Alkenes. *Agnew. Chem. Int. Ed.* **2014**, *53*, 11960–11964. [CrossRef] [PubMed]
37. Rostami, H.; Shiri, L.; Khani, Z. Recent advances in the synthesis of pyrazole scaffolds via nanoparticles: A review. *Tetrahedron* **2022**, *110*, 132688. [CrossRef]
38. Dias, D.; Pacheco, B.S.; Cunico, W.; Pizzuti, L.; Pereira, C.M.P. Recent Advances on the Green Synthesis and Antioxidant Activities of Pyrazoles. *Mini-Rev. Med. Chem.* **2014**, *14*, 1078–1092. [CrossRef]
39. Fustero, S.; Sanchez-Rosello, M.; Barrio, P.; Simon-Fuentes, A. From 2000 to Mid-2010: A Fruitful Decade for the Synthesis of Pyrazoles. *Chem. Rev.* **2011**, *111*, 6984–7034. [CrossRef] [PubMed]
40. Ilamanova, M.; Mastyugin, M.; Schäfer, C.; Kokel, A.; Török, B. Heterogeneous Metal Catalysis for the Environmentally Benign Synthesis of Medicinally Important Scaffolds, Intermediates and Building Blocks. *Curr. Org. Chem.* **2021**, *25*, 2304–2330. [CrossRef]
41. Landge, S.M.; Schmidt, A.; Outerbridge, V.; Török, B. Synthesis of Pyrazoles by a One-Pot Tandem Cyclization-Dehydrogenation Approach on Pd/C/K-10 Catalyst. *Synlett* **2007**, 1600–1604. [CrossRef]
42. Borkin, D.A.; Puscau, M.; Carlson, A.; Solan, A.; Wheeler, K.A.; Török, B.; Dembinski, R. Synthesis of diversely 1,3,5-trisubstituted pyrazoles via 5-exo-dig cyclization. *Org. Biomol. Chem.* **2012**, *10*, 4505–4508. [CrossRef] [PubMed]
43. Kumar Pal, C.; Kumar Jena, A. Ce-catalyzed regioselective synthesis of pyrazoles from 1,2-diols via tandem oxidation and C–C/C–N bond formation. *Org. Biomol. Chem.* **2023**, *21*, 59–64.
44. Guo, Y.; Wang, G.; Wei, L.; Wan, J.-P. Domino C–H Sulfonylation and Pyrazole Annulation for Fully Substituted Pyrazole Synthesis in Water Using Hydrophilic Enaminones. *J. Org. Chem.* **2019**, *84*, 2984–2990. [CrossRef]
45. Vuluga, D.; Legros, J.; Crousse, B.; Bonnet-Delpon, D. Synthesis of Pyrazoles through Catalyst-Free Cycloaddition of Diazo Compounds to Alkynes. *Green Chem.* **2009**, *11*, 156–159. [CrossRef]
46. Mondal, R.; Kumar Guin, A.; Pal, S.; Mondal, S.; Paul, N.D. Sustainable synthesis of pyrazoles using alcohols as the primary feedstock by an iron catalyzed tandem C–C and C–N coupling approach. *Org. Chem. Front.* **2022**, *9*, 5246–5258. [CrossRef]
47. Peng, X.; Zheng, M.-M.; Qin, P.; Xue, X.-S.; Zhang, F.-G.; Ma, J.-A. Silver-catalysed [3+2] annulation reaction of aryl diazonium salts with allenes enabled by boronate direction. *Org. Chem. Front.* **2023**, *10*, 74–82. [CrossRef]
48. Cardinale, L.; Neumeier, M.; Majek, M.; von Wangelin, A.J. Aryl Pyrazoles from Photocatalytic Cycloadditions of Arenediazonium. *Org. Lett.* **2020**, *22*, 7219–7224. [CrossRef]
49. Deng, Q.-H.; Zou, Y.-Q.; Lu, L.-Q.; Tang, Z.-L.; Chen, J.-R.; Xiao, W.-J. De Novo Synthesis of Imidazoles by Visible-Light-Induced Photocatalytic Aerobic Oxidation/[3+2] Cycloaddition/Aromatization Cascade. *Chem. Asian J.* **2014**, *9*, 2432–2435. [CrossRef]
50. Takeda, A.; Okai, H.; Watabe, K.; Iida, H. Metal-Free Atom-Economical Synthesis of Tetra-Substituted Imidazoles via Flavin-Iodine Catalyzed Aerobic Cross-Dehydrogenative Coupling of Amidines and Chalcones. *J. Org. Chem.* **2022**, *87*, 10372–10376. [CrossRef]
51. Kafi-Ahmadi, L.; Khademinia, S.; Poursattar, A.; Nozad, M.; Nozad, E. Microwave-assisted preparation of polysubstituted imidazoles using Zingiber extract synthesized green Cr₂O₃ nanoparticles. *Sci. Rep.* **2022**, *12*, 19942. [CrossRef]
52. Ghanbari, N.; Ghafari, H. Design and preparation of nanoarchitectonics of LDH/polymer composite with particular morphology as catalyst for greensynthesis of imidazole derivatives. *Sci. Rep.* **2022**, *12*, 11288. [CrossRef]
53. Kumar, S.; Khokra, S.L.; Yadav, A. Triazole analogues as potential pharmacological agents: A brief review. *Future J. Pharm. Sci.* **2021**, *7*, 106. [CrossRef] [PubMed]
54. Kazeminejad, Z.; Marzi, M.; Shiroudi, A.; Kouhpayeh, S.A.; Farjam, M.; Zarenezhad, E. Novel 1, 2, 4-Triazoles as Antifungal Agents. *BioMed Res. Int.* **2022**, *2022*, 4584846. [CrossRef] [PubMed]
55. Tratat, C. 1,2,4-Triazole: A Privileged Scaffold for the Development of Potent Antifungal Agents—A Brief Review. *Curr. Top. Med. Chem.* **2020**, *20*, 2235–2258. [CrossRef] [PubMed]
56. Xu, Z.; Zhao, S.-J.; Liu, Y. 1,2,3-Triazole-containing hybrids as potential anticancer agents: Current developments, action mechanisms and structure-activity relationships. *Eur. J. Med. Chem.* **2019**, *183*, 111700. [CrossRef]
57. Matin, M.M.; Matin, P.; Rahman, M.; Hadda, T.B.; Almalk, F.A.; Mahmud, S.; Ghoneim, M.M.; Alruwaily, M.; Alshehri, S. Triazoles and Their Derivatives: Chemistry, Synthesis, and Therapeutic Applications. *Front. Mol. Biosci.* **2020**, *9*, 864286. [CrossRef]
58. Brunel, D.; Dumur, F. Recent advances in organic dyes and fluorophores comprising a 1,2,3-triazole moiety. *New J. Chem.* **2020**, *44*, 3546–3561. [CrossRef]
59. Kaya, M.; Mentese, E. Synthesis and solvent-dependent photophysics of a novel fluorescent triazole-coumarin-based dye. *J. Heterocycl. Chem.* **2020**, *57*, 1714–1719. [CrossRef]

60. Song, S.; Ko, Y.-G.; Lee, H.; Wi, D.; Ree, B.J.; Li, Y.; Michinobu, T.; Ree, M. High-performance triazole-containing brush polymers via azide–alkyne click chemistry: A new functional polymer platform for electrical memory devices. *NPG Asia Mater.* **2015**, *7*, 228. [CrossRef]
61. Kolb, H.C.; Finn, M.G.; Sharpless, K.B. Click Chemistry: Diverse Chemical Function from a Few Good Reactions. *Angew. Chem. Int. Ed.* **2001**, *40*, 2004–2021. [CrossRef]
62. Marzi, M.; Farjam, M.; Kazeminejad, Z.; Shiroudi, A.; Kouhpayeh, A.; Zarenezhad, E. A Recent Overview of 1,2,3-Triazole-Containing Hybrids as Novel Antifungal Agents: Focusing on Synthesis, Mechanism of Action, and Structure-Activity Relationship (SAR). *J. Chem.* **2022**, *2022*, 7884316. [CrossRef]
63. Nino, A.D.; Maiuolo, L.; Costanzo, P.; Algieri, V.; Jiritano, A.; Olivito, F.; Tallarida, M.A. Recent Progress in Catalytic Synthesis of 1,2,3-Triazoles. *Catalysts* **2021**, *11*, 1120. [CrossRef]
64. Zhang, L.; Chen, X.; Xue, P.; Sun, H.H.Y.; Williams, I.D.; Sharpless, K.B.; Fokin, V.V.; Jia, G. Ruthenium-Catalyzed Cycloaddition of Alkynes and Organic Azides. *J. Am. Chem. Soc.* **2005**, *127*, 15998–15999. [CrossRef]
65. Kim, W.G.; Kang, M.E.; Lee, J.B.; Jeon, M.H.; Lee, S.; Lee, J.; Choi, B.; Cal, P.M.S.D.; Kang, S.; Kee, J.-M.; et al. Nickel-Catalyzed Azide-Alkyne Cycloaddition to Access 1,5-Disubstituted 1,2,3-Triazoles in Air and Water. *J. Am. Chem. Soc.* **2017**, *139*, 12121–12124. [CrossRef]
66. Tripathi, A.; Rode, C.V.; Llop, J.; Chavan, S.P.; Joshi, S.M. An enolate-mediated regioselective synthesis of 1,2,3-triazoles via azidealdehydes or ketones [3+2]-cycloaddition reactions in aqueous phase. *Tetrahedron Lett.* **2020**, *61*, 151662. [CrossRef]
67. Sletten, E.M.; Bertozzi, C.R. Bioorthogonal Chemistry: Fishing for Selectivity in a Sea of Functionality. *Angew. Chem. Int. Ed.* **2009**, *48*, 6974–6998. [CrossRef]
68. Lv, L.; Gao, G.; Luo, Y.; Mao, K.; Li, Z. Three-Component Reactions of α -CF₃ Carbonyls, NaN₃, and Amines for the Synthesis of NH-1,2,3-Triazoles. *J. Org. Chem.* **2021**, *86*, 17197–17212. [CrossRef] [PubMed]
69. Bubyrev, A.; Malkova, K.; Kantin, G.; Dar'in, D.; Krasavin, M. Metal-Free Synthesis of 1,5-Disubstituted 1,2,3-Triazoles. *J. Org. Chem.* **2021**, *86*, 17516–17522. [CrossRef]
70. Deng, L.; Cao, X.; Liu, Y.; Wan, J.-P. In-Water Synthesis of 5-Thiolated 1,2,3-Triazoles from β -Thioenaminones by Diazo Transfer Reaction. *J. Org. Chem.* **2019**, *84*, 14179–14186. [CrossRef] [PubMed]
71. Tajbakhsh, M.; Naimi-Jamal, M.R. Copper-doped functionalized β -cyclodextrin as an efficient green nanocatalyst for synthesis of 1,2,3-triazoles in water. *Sci. Rep.* **2022**, *12*, 4948. [CrossRef] [PubMed]
72. Wu, Z.-G.; Liao, X.-J.; Yuan, L.; Wang, Y.; Zheng, Y.-X.; Zuo, J.-L.; Pan, Y. Visible-Light-Mediated Click Chemistry for Highly Regioselective Azide–Alkyne Cycloaddition by a Photoredox Electron-Transfer Strategy. *Chem. Eur. J.* **2020**, *26*, 5694–5700. [CrossRef]
73. Henary, M.; Kananda, C.; Rotolo, L.; Savino, B.; Owensab, E.A.; Cravotto, G. Benefits and applications of microwave-assisted synthesis of nitrogen containing heterocycles in medicinal chemistry. *RSC Adv.* **2020**, *10*, 14170. [CrossRef] [PubMed]
74. Garg, A.; Sarma, D.; Ali, A.A. Microwave assisted metal-free approach to access 1,2,3-triazoles through multicomponent synthesis. *Curr. Res. Green Sustain. Chem.* **2020**, *3*, 100013. [CrossRef]
75. Ye, Z.; Ding, M.; Wu, Y.; Li, Y.; Huaa, W.; Zhang, F. Electrochemical synthesis of 1,2,4-triazole-fused heterocycles. *Green Chem.* **2018**, *20*, 1732. [CrossRef]
76. Zhao, Z.; He, Y.; Li, M.; Xu, J.; Li, X.; Zhang, L.; Gu, L. An electrochemical multicomponent [3+1+1] annulations to synthesize polysubstituted 1,2,4-triazoles. *Tetrahedron* **2021**, *87*, 132111. [CrossRef]
77. Rodríguez, D.F.; Durán-Osorio, F.; Duarte, Y.; Olivares, P.; Moglie, Y.; Dua, K.; Zacconi, F.Z. Green by Design: Convergent Synthesis, Computational Analyses, and Activity Evaluation of New FXa Inhibitors Bearing Peptide Triazole Linking Units. *Pharmaceutics* **2022**, *14*, 33. [CrossRef]
78. Kiranmye, T.; Vadivelu, M.; Sampath, S.; Muthu, K.; Karthikeyan, K. Ultrasound-assisted catalyst free synthesis of 1,4-/1,5-disubstituted-1,2,3-triazoles in aqueous medium. *Sustain. Chem. Pharm.* **2021**, *19*, 100358. [CrossRef]
79. Castillo, J.-C.; Bravo, N.-F.; Tamayo, L.-V.; Mestizo, P.-D.; Hurtado, J.; Macías, M.; Portilla, J. Water-Compatible Synthesis of 1,2,3-Triazoles under Ultrasonic Conditions by a Cu(I) Complex-Mediated Click Reaction. *ACS Omega* **2020**, *5*, 30148–30159. [CrossRef] [PubMed]
80. Rad, M.N.S.; Behrouz, S.; Mohammadtaghi-Nezhad, J.; Zarenezhad, E.; Agholi, M. Silica-tethered cuprous acetophenone thiosemicarbazone (STCATSC) as a novel hybrid nano-catalyst for highly efficient synthesis of new 1,2,3-triazolyl-based metronidazole hybrid analogues having potent anti-giardial activity. *Appl. Organomet. Chem.* **2019**, *33*, e4799.
81. Zarenezhad, E.; Rad, M.N.S.; Behrouz, S.; Esmailzadeh, S.; Farjam, M. Immobilized [Cu(cdsalMeen)] on silicagel: A highly efficient heterogeneous catalyst for 'Click' [3+2] Huisgen cycloaddition. *J. Iran. Chem. Soc.* **2017**, *14*, 509–519. [CrossRef]
82. Lv, F.; Liu, Y.; Zou, J.; Zhang, D.; Yao, Z. Synthesis of the Novel Photographic DIAR Couplers. *Dyes Pigm.* **2006**, *68*, 211–216. [CrossRef]
83. Manzoor, S.; Tariq, Q.; Yin, X.; Zhang, J.-G. Nitro-tetrazole based high performing explosives: Recent overview of synthesis and energetic properties. *Def. Technol.* **2021**, *17*, 1995–2010. [CrossRef]
84. Wei, C.-X.; Bian, M.; Gong, G.-H. Tetrazolium Compounds: Synthesis and Applications in Medicine. *Molecules* **2015**, *20*, 5528–5553. [CrossRef]
85. Myznikov, L.V.; Hrabalek, A.; Koldobskii, G.I. Drugs in the Tetrazole Series. *Chem. Heterocycl. Compd.* **2007**, *43*, 1–9. [CrossRef]

86. Ataroda, M.; Safaria, J.; Tebyanianb, H. Ultrasound irradiation and green synthesized CuO-NiO-ZnO mixed metal oxide: An efficient sono/nano-catalytic system toward a regioselective synthesis of 1-aryl-5-amino-1H-tetrazoles. *Synth. Commun.* **2020**, *50*, 1993–2006. [CrossRef]
87. Molaie, S.; Moeini, N.; Ghadermazi, M. Synthesis of CoFe₂O₄@Amino glycol/Gd nanocomposite as a high-efficiency and reusable nanocatalyst for green oxidation of sulfides and synthesis of 5-substituted 1H-tetrazoles. *J. Organomet. Chem.* **2022**, *977*, 122459. [CrossRef]
88. Safapoor, S.; Dekamin, M.G.; Akbari, A.; Naimi-Jamal, M.R. Synthesis of (E)-2-(1H-tetrazole-5-yl)-3-phenylacrylenitrile derivatives catalyzed by new ZnO nanoparticles embedded in a thermally stable magnetic periodic mesoporous organosilica under green conditions. *Sci. Rep.* **2022**, *12*, 10723. [CrossRef]
89. Kal-Koshvandi, A.T.; Maleki, A.; Tarlani, A.; Soroush, M.R. Synthesis and Characterization of Ultrapure HKUST-1 MOFs as Reusable Heterogeneous Catalysts for the Green Synthesis of Tetrazole Derivatives. *ChemistrySelect* **2020**, *5*, 3164–3172. [CrossRef]
90. Afsarian, M.H.; Farjam, M.; Zarenezhad, E.; Behrouz, S.; Rad, M.N.S. Synthesis, Antifungal Evaluation and Molecular Docking Studies of Some Tetrazole Derivatives. *Acta Chim. Slov.* **2019**, *66*, 874–887. [CrossRef] [PubMed]
91. Sagmeister, P.; Kaldre, D.; Sedelmeier, J.; Moessner, C.; Püntener, K.; Kummli, D.; Williams, J.D.; Kappe, C.O. Intensified Continuous Flow Synthesis and Workup of 1,5-Disubstituted Tetrazoles Enhanced by Real-Time Process Analytics. *Org. Process Res. Dev.* **2021**, *25*, 1206–1214. [CrossRef]
92. Aali, E.; Gholizadeh, M.; Noroozi-Shad, N. 1-Disulfo-[2,2-bipyridine]-1,1-dium chloride ionic liquid as an efficient catalyst for the green synthesis of 5-substituted 1 H -tetrazoles. *J. Mol. Struct.* **2022**, *1247*, 131289. [CrossRef]
93. Ishihara, K.; Ishihara, K.; Tanaka, Y.; Shioiri, T.; Matsugi, M. Practical synthesis of tetrazoles from amides and phosphorazidates in the presence of aromatic bases. *Tetrahedron* **2022**, *108*, 132642. [CrossRef]
94. Abdessalam, M.; Sidhoum, M.A.; Zradni, F.-Z.; Ilikti, H. Synthesis of 1,5-Disubstituted Tetrazoles in Aqueous Micelles at Room Temperature. *Molbank* **2021**, *2021*, M1194. [CrossRef]
95. Allais, C.; Grassot, J.-M.; Rodriguez, J.; Constantieux, T. Metal-Free Multicomponent Syntheses of Pyridines. *Chem. Rev.* **2014**, *114*, 10829–10868. [CrossRef]
96. Xu, F.; Wang, C.; Wang, H.; Li, X.; Wan, B. Eco-friendly synthesis of pyridines via rhodium-catalyzed cyclization of diynes with oximes. *Green Chem.* **2015**, *17*, 799–803. [CrossRef]
97. Yi, Y.K.; Zhao, M.N.; Ren, Z.H.; Wang, Y.Y.; Guan, Z.H. Synthesis of symmetrical pyridines by iron-catalyzed cyclization of ketoxime acetates and aldehydes. *Green Chem.* **2017**, *19*, 1023–1027. [CrossRef]
98. Kidwai, M.; Chauhan, R. K₂CO₃ catalyzed green and rapid access to 2-amino-3,5-dicarbonitrile-6-thio-pyridines. *J. Iran. Chem. Soc.* **2014**, *11*, 1005–1013. [CrossRef]
99. Shaikh, Y.I.; Shaikh, A.A.; Nazeruddin, G.M. Ammonia solution catalyzed one-pot synthesis of highly functionalized pyridine derivatives. *J. Chem. Pharm. Res.* **2012**, *4*, 4953–4956.
100. Yang, X.-H.; Zhou, Y.-H.; Zhang, P.-H.; Zhang, L.Y. An effective, one-pot synthesis of fully substituted pyridines under microwave irradiation in the absence of solvent. *J. Heterocycl. Chem.* **2013**, *50*, 1346–1350. [CrossRef]
101. Yin, G.; Liu, Q.; Ma, J. Solvent- and catalyst-free synthesis of new hydroxylated trisubstituted pyridines under microwave irradiation. *Green Chem.* **2012**, *14*, 1796–1798. [CrossRef]
102. De Paolis, O.; Baffoe, J.; Landge, S.M.; Török, B. Multicomponent Domino Cyclization-Oxidative Aromatization on a Bifunctional Pd/C/K-10 Catalyst: An Environmentally Benign Approach toward the Synthesis of Pyridines. *Synthesis* **2008**, *21*, 3423–3428. [CrossRef]
103. Wang, Y.F.; Chiba, S. Mn(III)-Mediated Reactions of Cyclopropanols with Vinyl Azides: Synthesis of Pyridine and 2-Azabicyclo[3.3.1]non-2-en-1-ol Derivatives. *J. Am. Chem. Soc.* **2009**, *131*, 12570–12572. [CrossRef]
104. Mao, Z.Y.; Liao, X.Y.; Wang, H.S.; Wang, C.G.; Huang, K.B.; Pan, Y.M. Acid-catalyzed tandem reaction for the synthesis of pyridine derivatives via C=C/C(sp³)-N bond cleavage of enones and primary amines. *RSC Adv.* **2017**, *7*, 13123–13129. [CrossRef]
105. Wang, K.; Meng, L.G.; Wang, L. Visible-Light-Promoted [2+2+2] Cyclization of Alkynes with Nitriles to Pyridines Using Pyrylium Salts as Photoredox Catalysts. *Org. Lett.* **2017**, *19*, 1958–1961. [CrossRef]
106. Lou, S.; Zhang, J. Pyrimidines. In *Heterocyclic Chemistry in Drug Discovery*; Jie, J.L., Ed.; John Wiley & Sons, Inc.: Hoboken, NJ, USA, 2013; pp. 569–613.
107. Zarenezhad, E.; Farjam, M.; Iraj, A. Synthesis and biological activity of pyrimidines-containing hybrids: Focusing on pharmacological application. *J. Mol. Struct.* **2021**, *1230*, 129833. [CrossRef]
108. Gore, R.P.; Rajput, A.P. A review on recent progress in multicomponent reactions of pyrimidine synthesis. *Drug Invent. Today* **2013**, *5*, 148–152. [CrossRef]
109. Khan, S.A.; Asiri, A.M.; Kumar, S.; Sharma, K. Green synthesis, antibacterial activity and computational study of pyrazoline and pyrimidine derivatives from 3-(3,4-dimethoxy-phenyl)-1-(2,5-dimethylthiophen-3-yl)-propenone. *Eur. J. Chem.* **2014**, *5*, 85–90. [CrossRef]
110. Ezhilarasi, M.R.; Prabha, B.; Prabakaran, S. Microwave assisted synthesis and spectral studies of thiophenyl pyrimidine derivatives. *J. Appl. Chem.* **2014**, *3*, 1929–1935.
111. Babu, K.R.; Paul, V.L.; Rao, V.M. Substituted pyridine catalyzed domino synthesis of pyrazolines and pyrimidines. *World J. Pharm. Res.* **2014**, *3*, 389–398.

112. Sivagamisundari, G.; Pushpalatha, A.M.; Rane, S.J. Silica bonded S-sulphonic acid as a green catalyst in the synthesis of functionalized pyrimidine under solvent-free microwave irradiation conditions. *Int. J. Sci. Eng. Technol.* **2014**, *3*, 852–855.
113. Yamaguchi, T.; Sugiura, Y.; Yamaguchi, E.; Tada, N.; Itoh, A. Synthetic Method for the Preparation of Quinazolines by the Oxidation of Amines Using Singlet Oxygen. *Asian J. Org. Chem.* **2017**, *6*, 432–435. [CrossRef]
114. Xie, L.G.; Niyomchon, S.; Mota, A.J.; Maulide, N. Metal-free intermolecular formal cycloadditions enable an orthogonal access to nitrogen heterocycles. *Nat. Commun.* **2016**, *7*, 10914. [CrossRef]
115. Liu, K.; Song, C.; Wu, J. Electrochemical Oxidation Synergizing with Brønsted-Acid Catalysis Leads to [4+2] Annulation for the Synthesis of Pyrazines. *Green Chem.* **2019**, *21*, 765–769. [CrossRef]
116. Daw, P.; Ben-David, Y.; Milstein, D. Acceptorless Dehydrogenative Coupling using Ammonia: Direct Synthesis of N-Heteroaromatics from Diols Catalyzed by Ruthenium. *J. Am. Chem. Soc.* **2018**, *140*, 11931–11934. [CrossRef] [PubMed]
117. Mondal, J.; Sivaramakrishna, A. Functionalized Triazines and Tetrazines: Synthesis and Applications. *Top. Curr. Chem.* **2022**, *380*, 34. [CrossRef] [PubMed]
118. Sun, H.; Xue, Q.; Zhang, C.; Wu, H.; Feng, P. Derivatization based on tetrazine scaffolds: Synthesis of tetrazine derivatives and their biomedical applications. *Org. Chem. Front.* **2022**, *9*, 481. [CrossRef]
119. Choi, S.-K.; Kim, J.; Kim, E. Overview of Syntheses and Molecular-Design Strategies for Tetrazine-Based Fluorogenic Probes. *Molecules* **2021**, *26*, 1868. [CrossRef] [PubMed]
120. Kedzia, A.; Kudelko, A.; Świątkowski, M.; Kruszyński, R. Microwave-promoted synthesis of highly luminescent s-tetrazine-1,3,4-oxadiazole and s-tetrazine-1,3,4-thiadiazole hybrids. *Dyes Pigment.* **2020**, *172*, 107865. [CrossRef]
121. Lambert, W.D.; Fang, Y.; Mahapatra, S.; Huang, Z.; Am Ende, C.W.; Fox, J.F. Installation of Minimal Tetrazines through Silver-Mediated Liebeskind–Srogl Coupling with Arylboronic Acids. *J. Am. Chem. Soc.* **2019**, *141*, 17068–17074. [CrossRef]
122. Xie, Y.; Fang, Y.; Huang, Z.; Tallon, A.M.; Am Ende, C.W.; Fox, J.M. Divergent Synthesis of Monosubstituted and Unsymmetrical 3,6-Disubstituted Tetrazines from Carboxylic Ester Precursors. *Angew. Chem. Int. Ed.* **2020**, *59*, 16967–16973. [CrossRef] [PubMed]
123. Fang, Z.; Hu, W.-L.; Liu, D.-Y.; Yua, C.-Y.; Hu, X.-G. Synthesis of tetrazines from gem-difluoroalkenes under aerobic conditions at room temperature. *Green Chem.* **2017**, *19*, 1299. [CrossRef]
124. Tang, J.; Chen, D.; Zhang, G.; Yang, H.; Cheng, G. A “Green” Primary Explosive: Design, Synthesis, and Testing. *Synlett* **2019**, *30*, 885–892.
125. Chaurasia, S.R.; Dange, R.; Bhanage, B.M. Graphene oxide as a carbo-catalyst for the synthesis of tri-substituted 1,3,5-triazines using biguanides and alcohols. *Catal. Commun.* **2020**, *137*, 105933. [CrossRef]
126. Poly, S.S.; Hashiguchi, Y.; Nakamura, I.; Fujitani, T.; Siddiki, S.M., A.H. Direct synthesis of triazines from alcohols and amidines using supported Pt nanoparticle catalysts via the acceptorless dehydrogenative methodology. *Catal. Sci. Technol.* **2022**, *12*, 4679. [CrossRef]
127. Li, F.; Wang, C.; Xu, Y.; Zhao, Z.; Su, J.; Luo, C.; Ning, Y.; Li, Z.; Li, C.; Wang, L. Efficient synthesis of unsymmetrical trisubstituted 1,3,5-triazines catalyzed by hemoglobin. *Mol. Catal.* **2021**, *505*, 111519. [CrossRef]
128. Gao, Q.; Wu, M.; Zhang, L.; Xu, P.; Wang, H.; Sun, Z.; Fang, L.; Duan, Y.; Bai, S.; Zhou, X.; Han, M.; et al. Open-Air Dual-Diamination of Aromatic Aldehydes: Direct Synthesis of Azolo-Fused 1,3,5-Triazines Facilitated by Ammonium Iodide. *J. Org. Chem.* **2021**, *86*, 17265–17273. [CrossRef]
129. Lim, F.P.L.; Low, S.T.; Ho, E.L.K.; Halcovitch, N.R.; Tiekink, E.R.T.; Dolzhenko, A.V. A multicomponent reaction of 2-aminoimidazoles: Microwave-assisted synthesis of novel 5-aza-7-deaza-adenines. *RSC Adv.* **2017**, *7*, 51062–51068. [CrossRef]
130. Lin, W.; Zheng, Y.X.; Xun, Z.; Huang, Z.B.; Shi, D.Q. Microwave-Assisted Regioselective Synthesis of 3-Functionalized Indole Derivatives via Three-Component Domino Reaction. *ACS Comb. Sci.* **2017**, *19*, 708–713. [CrossRef] [PubMed]
131. Shan, X.H.; Zheng, H.X.; Yang, B.; Tie, L.; Fu, J.L.; Qu, J.P.; Kang, Y.B. Copper-catalyzed oxidative benzylic C-H cyclization via iminyl radical from intermolecular anion-radical redox relay. *Nat. Commun.* **2019**, *10*, 908. [CrossRef] [PubMed]
132. Yu, S.; Qi, L.; Hu, K.; Gong, J.L.; Cheng, T.X.; Wang, Q.Z.; Chen, J.X.; Wu, H.Y. The Development of a Palladium-Catalyzed Tandem Addition/Cyclization for the Construction of Indole Skeletons. *J. Org. Chem.* **2017**, *82*, 3631–3638. [CrossRef]
133. Xu, D.; Yang, W.; Luo, S.; Wang, B.; Wu, J.; Xu, Z. Fischer indole synthesis in Brønsted acidic ionic liquids: A green, mild, and regioselective reaction system. *Eur. J. Org. Chem.* **2007**, 1007–1012. [CrossRef]
134. Xu, D.; Wu, J.; Luo, S.; Zhang, J.; Wu, J.; Du, X.; Xu, Z. Fischer indole synthesis catalyzed by novel SO₃H-functionalized ionic liquids in water. *Green Chem.* **2009**, *11*, 1239–1246. [CrossRef]
135. Tambe, S.D.; Rohokale, R.S.; Kshirsagar, U.A. Visible-Light-Mediated Eosin Y Photoredox-Catalyzed Vicinal Thioamination of Alkynes: Radical Cascade Annulation Strategy for 2-Substituted-3-sulphenylindoles. *Eur. J. Org. Chem.* **2018**, *18*, 2117–2121. [CrossRef]
136. Jana, S.; Verma, A.; Kadu, R.; Kumar, S. Visible-light-induced oxidant and metal-free dehydrogenative cascade trifluoromethylation and oxidation of 1,6-enynes with water. *Chem. Sci.* **2017**, *8*, 6633–6644. [CrossRef]
137. Sadowski, B.; Klajn, J.; Gryko, D.T. Recent advances in the synthesis of indolizines and their π -expanded analogues. *Org. Biomol. Chem.* **2016**, *14*, 7804–7828. [CrossRef]
138. Dinica, R.; Furdui, B.; Ghinea, I.; Bahrim, G.; Bonte, S.; Demeunynck, M. Novel one-pot green synthesis of indolizines biocatalysed by *Candida antarctica* lipases. *Mar. Drugs* **2013**, *11*, 431–439. [CrossRef] [PubMed]
139. Yang, D.; Yu, Y.; Wu, Y. One-Pot Regiospecific Synthesis of Indolizines: A Solvent-Free, Metal-Free, Three-Component Reaction of 2-(Pyridin-2-yl)acetates, Ynals, and Alcohols or Thiols. *Org. Lett.* **2018**, *20*, 2477–2480. [CrossRef]

140. Zeng, K.; Mei, R.; Dechert, S.; Ackermann, L.; Zhang, K. A recyclable stereoauxiliary aminocatalyzed strategy for one-pot synthesis of indolizine-2-carbaldehydes. *Nat. Commun. Chem.* **2023**, *6*, 40. [CrossRef]
141. Li, J.; Liu, X.; Deng, J.; Huang, Y.S.; Pan, Z.H.; Yu, Y.; Cao, H. Electrochemical Diselenylation of Indolizines via Intermolecular C-Se Formation of 2-Methylpyridines, α -Bromoketones with Diselenides. *Chem. Commun.* **2019**, *56*, 735–738. [CrossRef]
142. Török, B.; Schäfer, C.; Kokel, A. *Heterogeneous Catalysis in Sustainable Synthesis*; Elsevier: Cambridge, MA, USA; Oxford, UK, 2021.
143. Cheng, C.C.; Yan, S.J. *The Friedländer Synthesis of Quinolines*; Organic Reactions; Wiley: New York, NY, USA, 2005.
144. Arcadi, A.; Chiarini, M.; Giuseppe, S.D.; Marinelli, F. A new approach to the Friedländer synthesis of quinolines. *Synlett* **2003**, 203–206. [CrossRef]
145. Sels, B.F.; De Vos, D.E.; Jacobs, P.A. Hydrotalcite-like anionic clays in catalytic organic reactions. *Catal. Rev.* **2001**, *43*, 443–448. [CrossRef]
146. Motokura, K.; Mizugaki, T.; Ebitani, K.; Kaneda, K. Multifunctional catalysis of a ruthenium-grafted hydrotalcite: One-pot synthesis of quinolines from 2-aminobenzyl alcohol and various carbonyl compounds via aerobic oxidation and aldol reaction. *Tetrahedron Lett.* **2004**, *45*, 6029–6032. [CrossRef]
147. Akbari, J.; Heydari, A.; Kalhor, H.R.; Kohan, S.A. Sulfonic acid functionalized ionic liquid in combinatorial approach, a recyclable and water tolerant-acidic catalyst for one-pot Friedländer quinoline synthesis. *J. Comb. Chem.* **2010**, *12*, 137–140. [CrossRef]
148. Kulkarni, A.; Török, B. Microwave-assisted multicomponent domino cyclization–aromatization: An efficient approach for the synthesis of substituted quinolines. *Green Chem.* **2010**, *12*, 875–878. [CrossRef]
149. Reddy, T.R.; Reddy, L.S.; Reddy, G.R.; Yarbaji, K.; Lingappa, Y.; Rambabu, D.; Krishna, G.R.; Reddy, C.M.; Kumar, K.S.; Pal, M. Construction of quinoline ring via a 3-component reaction in water: Crystal structure analysis and H-bonding patterns of a 2-aryl quinoline. *Green Chem.* **2012**, *14*, 1870–1872. [CrossRef]
150. He, L.; Wang, J.Q.; Gong, Y.; Liu, Y.M.; Cao, Y.; He, H.Y.; Fan, K.N. Titania-Supported Iridium Subnanoclusters as an Efficient Heterogeneous Catalyst for Direct Synthesis of Quinolines from Nitroarenes and Aliphatic Alcohols. *Angew. Chem. Int. Ed.* **2011**, *50*, 10216–10220. [CrossRef]
151. Sun, D.; Yin, K.; Zhang, R. Visible-light-induced multicomponent cascade cycloaddition involving N-propargyl aromatic amines, diaryliodonium salts and sulfur dioxide: Rapid access to 3-arylsulfonylquinolines. *Chem. Commun.* **2018**, *54*, 1335–1338. [CrossRef]
152. Mishra, M.; Twardy, D.; Ellstrom, C.; Wheeler, K.A.; Dembinski, R.; Török, B. Catalyst-free ambient temperature synthesis of isoquinoline-fused benzimidazoles from 2-alkynylbenzaldehydes via alkyne hydroamination. *Green Chem.* **2019**, *21*, 99–108. [CrossRef]
153. Liu, X.; Qing, Z.; Cheng, P.; Zheng, X.; Zeng, J.; Xie, H. Metal-Free Photoredox Catalyzed Cyclization of O-(2,4-Dinitrophenyl)oximes to Phenanthridines. *Molecules* **2016**, *21*, 1690. [CrossRef]
154. Abid, M.; DePaolis, O.; Török, B. A Novel One-Pot Synthesis of N-Acylindoles from Primary Aromatic Amides. *Synlett* **2008**, 410–413. [CrossRef]
155. Kulkarni, A.; Zhou, W.-H.; Török, B. Heterogeneous catalytic hydrogenation of unprotected indoles in water: A green solution to a long-standing challenge. *Org. Lett.* **2011**, *13*, 5124–5127. [CrossRef]
156. Ishida, T.; Tsunoda, R.; Zhang, Z.; Hamasaki, A.; Honma, T.; Ohashi, H.; Yokoyama, T.; Tokunaga, M. Supported palladium hydroxide-catalyzed intramolecular double C-H bond functionalization for synthesis of carbazoles and dibenzofurans. *Appl. Catal. B Environ.* **2014**, *150–151*, 523–531. [CrossRef]
157. Xiao, F.; Liao, Y.; Wu, M.; Deng, G.J. One-pot synthesis of carbazoles from cyclohexanones and arylhydrazine hydrochlorides under metal-free conditions. *Green Chem.* **2012**, *14*, 3277–3280. [CrossRef]
158. Yang, L.; Zhang, Y.; Zou, X.; Lu, H.J.; Li, G.G. Visible-Light-Promoted Intramolecular C–H Amination in Aqueous Solution: Synthesis of Carbazoles. *Green Chem.* **2018**, *20*, 1362–1366. [CrossRef]
159. Ishihara, Y.; Montero, A.; Baran, P.S. *The Portable Chemist's Consultant*; Apple Publishing Group: New York, NY, USA, 2013.
160. Yan, R.; Li, X.; Yang, X.; Kang, X.; Xiang, L.; Huang, G. A novel one-pot method for the synthesis of substituted furopyridines: Iodine-mediated oxidation of enamines by tandem metal-free cyclization. *Chem. Commun.* **2015**, *51*, 2573. [CrossRef]
161. Hudson, R.; Bizier, N.P.; Esdalea, K.N.; Katz, J.L. Synthesis of indoles, benzofurans, and related heterocycles via an acetylene-activated S_NAr /intramolecular cyclization cascade sequence in water or DMSO. *Org. Biomol. Chem.* **2015**, *13*, 2273. [CrossRef] [PubMed]
162. Ueda, S.; Nagasawa, H. Synthesis of 2-Arylbenzoxazoles by Copper-Catalyzed Intramolecular Oxidative C–O Coupling of Benzanilides. *Angew. Chem. Int. Ed.* **2008**, *47*, 6411–6413. [CrossRef]
163. Evindar, G.; Batey, R.A. Parallel Synthesis of a Library of Benzoxazoles and Benzothiazoles Using Ligand-Accelerated Copper-Catalyzed Cyclizations of ortho-Halobenzanilides. *J. Org. Chem.* **2006**, *71*, 1802–1808. [CrossRef] [PubMed]
164. Chen, X.; Ji, F.; Zhao, Y.; Liu, Y.; Zhou, Y.; Chen, T.; Yin, S.F. Copper-Catalyzed Aerobic Oxidative C(aryl)-OH Bond Functionalization of Catechols with Amines Affording Benzoxazoles. *Adv. Synth. Catal.* **2015**, *357*, 2924–2930. [CrossRef]
165. Meng, X.; Wang, Y.; Wang, Y.; Chen, B.; Jing, Z.; Chen, G.; Zhao, P. OMS-2-Supported Cu Hydroxide-Catalyzed Benzoxazoles Synthesis from Catechols and Amines via Domino Oxidation Process at Room Temperature. *J. Org. Chem.* **2017**, *82*, 6922–6931. [CrossRef] [PubMed]
166. Tang, J.; Cao, Y.; Ruan, F.; Li, F.; Jin, Y.; Ha, M.N.; Han, X.; Ke, Q. New Approach for Controllable Synthesis of N-MnOx Microflowers and Their Superior Catalytic Performance for Benzoxazole Synthesis. *Ind. Eng. Chem. Res.* **2020**, *59*, 9408–9413. [CrossRef]

167. Sharghi, H.; Aboonajmi, J.; Aberi, M. One-Pot Multicomponent Reaction of Catechols, Ammonium Acetate, and Aldehydes for the Synthesis of Benzoxazole Derivatives Using the Fe(III)–Salen Complex. *J. Org. Chem.* **2020**, *85*, 6567–6577. [CrossRef]
168. Laha, J.K.; Gulati, U.; Saima; Gupta, A.; Indurthi, H.K. Improved, gram-scale synthesis of sildenafil in water using acylacetic acid as the acyl source in the pyrazolo[4,3-d]pyrimidin-7-one ring formation. *New J. Chem.* **2021**, *45*, 2643–2648. [CrossRef]
169. Agios Pharmaceuticals Inc. *Therapeutic Compounds and Compositions*; WO2014/139144; Agios Pharmaceuticals Inc.: Cambridge, MA, USA, 2014.
170. Alamshany, Z.M.; Tashkandi, N.Y.; Othman, I.M.M.; Anwar, M.M.; Nossier, E.S. New thiophene, thienopyridine and thiazoline-based derivatives: Design, synthesis and biological evaluation as antiproliferative agents and multitargeting kinase inhibitors. *Bioorg. Chem.* **2022**, *127*, 105964. [CrossRef]
171. Sanad, S.M.H.; Mekky, A.E.M. Novel Nicotinonitriles and Thieno[2,3-b]pyridines as Potent Biofilm and COX-2 Inhibitors: Synthesis, In Vitro and In Silico Studies. *ChemistrySelect* **2020**, *5*, 8494–8503. [CrossRef]
172. He, R.; Liu, Y.; Feng, Y.; Chen, L.; Huang, Y.; Xie, F.; Li, Y. Access to Thienopyridine and Thienoquinoline Derivatives via Site-Selective C–H Bond Functionalization and Annulation. *Org. Lett.* **2022**, *24*, 3167–3172. [CrossRef]
173. Chai, K.; Shi, Y.; Wang, Y.; Zou, P.; Yuan, Q.; Xu, W.; Zhang, P. Visible light-driven oxidative coupling of dibenzylamine and substituted anilines with a 2D WSe₂ nanomesh material. *Nanoscale* **2020**, *12*, 21869. [CrossRef] [PubMed]
174. Wu, H.; Dai, W.; Saravanamurugan, S.; Li, H.; Yang, S. Endogenous X–C=O species enable catalyst-free formylation prerequisite for CO₂ reductive upgrading. *Green Chem.* **2020**, *22*, 5822. [CrossRef]
175. Rong, B.; Xu, G.; Yan, H.; Zhang, S.; Wu, Q.; Zhu, N.; Fang, Z.; Duan, J.; Guo, K. Synthesis of benzofuro- and benzothieno[2,3-c]pyridines via copper-catalyzed [4+2] annulation of ketoxime acetates with acetoacetanilide. *Org. Chem. Front.* **2021**, *8*, 2939–2943. [CrossRef]
176. Morais, G.R.; Palma, E.; Marques, F.; Gano, L.; Oliveira, M.C.; Abrunhosa, A.; Miranda, H.V.; Outeiro, T.F.; Santos, I.; Paulo, A. Synthesis and biological evaluation of novel 2-aryl benzimidazoles as chemotherapeutic agents. *J. Heterocycl. Chem.* **2015**, *54*, 255–267. [CrossRef]
177. Kankate, R.S.; Pagare, A.H.; Kakad, R.D.; Gide, P.S.V.C.; Nathe, V.C. Nathe Synthesis and biological evaluation of benzimidazolyl biphenyl derivatives as antihypertensive agents. *Int. J. Chem. Concepts.* **2016**, *2*, 111–119.
178. Sethi, P.; Bansal, Y.; Bansal, G. Synthesis and pass-assisted evaluation of coumarin–benzimidazole derivatives as potential anti-inflammatory and anthelmintic agents. *Med. Chem. Res.* **2017**, *27*, 61–71. [CrossRef]
179. Ajani, O.; Aderohunmu, D.; Olorunshola, S.; Ikpo, C.; Olanrewaju, I. Facile synthesis, characterization and antimicrobial activity of 2-alkanamino benzimidazole derivatives. *Orient. J. Chem.* **2016**, *32*, 109–120. [CrossRef]
180. Bellam, M.; Gundluru, M.; Sarva, S.; Chadive, S.; Netala, V.R.; Tartte, V.; Cirandur, S.R. Synthesis and antioxidant activity of some new n-alkylated pyrazole-containing benzimidazoles. *Chem. Heterocycl. Comp.* **2017**, *53*, 173–178. [CrossRef]
181. Yang, H.; Ren, Y.; Gao, X.; Gao, Y. Synthesis and anticoagulant bioactivity evaluation of 1,2,5-trisubstituted benzimidazole fluorinated derivatives. *Chem. Res. Chin. Univ.* **2016**, *32*, 973–978. [CrossRef]
182. Raja, D.; Philips, A.; Palani, P.; Lin, W.-Y.; Devikala, S.; Senadi, G.C. Metal-free synthesis of benzimidazoles via oxidative cyclization of d-glucose with o-phenylenediamines in water. *J. Org. Chem.* **2020**, *85*, 11531–11540. [CrossRef]
183. Xu, S.; Luo, Y.; Tan, B. Recent development of hypercrosslinked microporous organic polymers. *Macromol. Rapid Commun.* **2013**, *34*, 471–484. [CrossRef]
184. An, W.-K.; Zheng, S.-J.; Zhang, H.-X.; Shang, T.-T.; Wang, H.-R.; Xu, X.-J.; Jin, Q.; Qin, Y.; Ren, Y.; Jiang, S.; et al. s-tetrazine-functionalized hyper-crosslinked polymers for efficient photocatalytic synthesis of benzimidazoles. *Green Chem.* **2021**, *23*, 1292–1299. [CrossRef]
185. Kalinin, A.A.; Mamedov, V.A.; Levin, Y.A. Unexpected quinoxalinobenzimidazole rearrangement. *Chem. Heterocycl. Comp.* **2000**, *36*, 882–883. [CrossRef]
186. Li, S.; Feng, L.; Ma, C. Simple and green synthesis of benzimidazoles and pyrrolo[1,2-a]quinoxalines via mamedov heterocycle rearrangement. *New J. Chem.* **2021**, *45*, 9320–9323. [CrossRef]
187. Nardi, M.; Bonacci, S.; Herrera Cano, N.; Oliverio, M.; Procopio, A. The highly efficient synthesis of 1,2-disubstituted benzimidazoles using microwave irradiation. *Molecules* **2022**, *27*, 1751. [CrossRef]
188. Yu, Y.; Yuan, Y.; Liu, H.; He, M.; Yang, M.; Liu, P.; Yu, B.; Dong, X.; Lei, A. Electrochemical oxidative C–H/N–H cross-coupling for C–N bond formation with hydrogen evolution. *Chem. Commun.* **2019**, *55*, 1809–1812. [CrossRef] [PubMed]
189. Lv, S.; Han, X.; Wang, J.Y.; Zhou, M.; Wu, Y.; Ma, L.; Niu, L.; Gao, W.; Zhou, J.; Hu, W.; et al. Tunable electrochemical C–N versus N–N bond formation of nitrogen-centered radicals enabled by dehydrogenative dearomatization: Biological applications. *Angew. Chem. Int. Ed.* **2020**, *132*, 11680–11687. [CrossRef]
190. Zhao, H.B.; Zhuang, J.L.; Xu, H.C. Electrochemical synthesis of benzimidazoles via dehydrogenative cyclization of amidines. *ChemSusChem* **2021**, *14*, 1692–1695. [CrossRef]
191. Twardy, D.J.; Wheeler, K.A.; Török, B.; Dembinski, R. Recent Advances in the Synthesis of Isoquinoline-fused Benzimidazoles. *Molecules* **2022**, *27*, 2062. [CrossRef]
192. Cerecetto, H.; Gerpe, A.; Gonzalez, M.; Aran, V.; de Ocariz, C. Pharmacological properties of indazole derivatives: Recent developments. *Mini-Rev. Med. Chem.* **2005**, *5*, 869–878. [CrossRef]
193. Shrivastava, A.; Chakraborty, A.K.; Upmanyu, N.; Singh, A. Recent progress in chemistry and biology of indazole and its derivatives: A brief review. *Austin J. Anal. Pharm. Chem.* **2016**, *3*, 1076.

194. Denya, I.; Malan, S.F.; Joubert, J. Indazole derivatives and their therapeutic applications: A Patent Review (2013–2017). *Expert Opin. Ther. Pat.* **2018**, *28*, 441–453. [CrossRef] [PubMed]
195. Wan, H.; Li, D.; Xia, H.; Yang, L.; Alhumade, H.; Yi, H.; Lei, A. Synthesis of 1h-indazoles by an electrochemical radical CSP2-h/N-H cyclization of arylhydrazones. *Chem. Commun.* **2022**, *58*, 665–668. [CrossRef]
196. Zhang, H.; Ye, Z.; Chen, N.; Chen, Z.; Zhang, F. Electrochemical dehydrogenative C–N coupling of hydrazones for the synthesis of 1h-indazoles. *Green Chem.* **2022**, *24*, 1463–1468. [CrossRef]
197. Pérez-Villanueva, J.; Yépez-Mulia, L.; González-Sánchez, I.; Palacios-Espinosa, J.; Soria-Arteche, O.; Sainz-Espuñes, T.; Cerbón, M.; Rodríguez-Villar, K.; Rodríguez-Vicente, A.; Cortés-Gines, M.; et al. Synthesis and biological evaluation of 2H-indazole derivatives: Towards antimicrobial and anti-inflammatory dual agents. *Molecules* **2017**, *22*, 1864. [CrossRef] [PubMed]
198. Lian, Y.; Bergman, R.G.; Lavis, L.D.; Ellman, J.A. Rhodium(III)-catalyzed indazole synthesis by C–H bond functionalization and Cyclative Capture. *J. Am. Chem. Soc.* **2013**, *135*, 7122–7125. [CrossRef]
199. Jin, G.-Q.; Gao, W.-X.; Zhou, Y.-B.; Liu, M.-C.; Wu, H.-Y. Efficient synthesis of 2-aryl-2h-indazoles by base-catalyzed benzyl C–H deprotonation and cyclization. *Chem. Commun.* **2020**, *56*, 14617–14620. [CrossRef] [PubMed]
200. Liu, J.; Liu, N.; Yang, Q.; Wang, L. Visible-light-driven photocyclization reaction: Photocatalyst-free mediated intramolecular N–N coupling for the synthesis of 2h-indazole-3-carboxamides from aryl azides. *Org. Chem. Front.* **2021**, *8*, 5296–5302. [CrossRef]
201. Kraemer, N.; Li, C.J.; Zhu, J.S.; Larach, J.M.; Tsui, K.Y.; Tantillo, D.J.; Haddadin, M.J.; Kurth, M.J. Davis–Beirut reaction: A photochemical Brønsted acid catalyzed route to n-aryl 2h-indazoles. *Org. Lett.* **2019**, *21*, 6058–6062. [CrossRef]
202. Szabó, T.; Volk, B.; Milen, M. Recent Advances in the Synthesis of β -Carboline Alkaloids. *Molecules* **2021**, *26*, 663. [CrossRef]
203. Horton, W.; Sood, A.; Peerannawar, S.; Kugyela, N.; Tulsan, R.; Tran, C.D.; Soule, J.; LeVine III, H.; Török, B.; Török, M. Synthesis and Application of β -Carbolines as Novel Multi-functional Anti-Alzheimer’s Disease Agents. *Bioorg. Med. Chem. Lett.* **2017**, *27*, 232–236. [CrossRef] [PubMed]
204. Du, H.; Gu, H.; Li, N.; Wang, J. Synthesis and biological evaluation of bivalent β -carbolines as potential anticancer agents. *Med. Chem. Commun.* **2016**, *7*, 636–645. [CrossRef]
205. Chen, W.; Zhang, G.; Guo, L.; Fan, V.; Ma, Q.; Zhang, X.; Du, R.; Cao, R. Synthesis and biological evaluation of novel alkyl diamine linked bivalent β -carbolines as angiogenesis inhibitors. *Eur. J. Med. Chem.* **2016**, *124*, 249–261. [CrossRef] [PubMed]
206. Kulkarni, A.; Abid, M.; Török, B.; Huang, X. A direct synthesis of β -carbolines via a three-step one-pot domino approach with a bifunctional Pd/C/K-10 catalyst. *Tetrahedron Lett.* **2009**, *50*, 1791–1794. [CrossRef]
207. Devi, N.; Singh, D.; Kaur, G.; Mor, S.; Kishore Putta VP, R.; Polina, S.; Malakard, C.C.; Singh, V. In(OTf)₃ assisted synthesis of β -carboline C-3 tethered imidazo[1,2-a]azine derivatives. *New J. Chem.* **2017**, *41*, 1082–1093. [CrossRef]
208. Vijayakumar, K.; Ahamed, A.J.; Thiruneelakandan, G. Synthesis, antimicrobial, and Anti-HIV1 activity of Quinazoline-4(3H)-one derivatives. *J. Appl. Chem.* **2013**, *5*, 387191. [CrossRef]
209. Krishnan, S.K.; Ganguly, S.; Veeramy, R.; Jan, B. Synthesis, antiviral and cytotoxic investigation of 2-phenyl-3-substituted quinazolin-4(3H)-ones. *Eur. Rev. Med. Pharmacol. Sci.* **2011**, *15*, 673–681.
210. Jiang, S.; Zeng, Q.; Gettayacamin, M.; Tungtaeng, A.; Wannaying, S.; Lim, A.; Hansukjariya, P.; Okunji, C.O.; Zhu, S.; Fang, D. Antimalarial activities and therapeutic properties of Febrifugine analogs. *Antimicrob. Agents Chemother.* **2005**, *49*, 1169–1176. [CrossRef] [PubMed]
211. Khosropour, A.R.; Mohammadpoor-Baltork, I.; Ghorbankhani, H. Bi(TFA)₃–[NBP]FeCl₄: A new, efficient and reusable promoter system for the synthesis of 4(3H)-quinazolinone derivatives. *Tetrahedron Lett.* **2006**, *47*, 3561–3564. [CrossRef]
212. Chan, C.-K.; Lai, C.-Y.; Wang, C.-C. TMSOTf-catalyzed synthesis of substituted quinazolines using hexamethyldisilazane as a nitrogen source under neat and microwave irradiation conditions. *Org. Biomol. Chem.* **2020**, *18*, 7201–7212. [CrossRef]
213. Charpe, V.P.; Ragupathi, A.; Sagadevan, A.; Hwang, K.C. Photoredox synthesis of functionalized quinazolines via copper-catalyzed aerobic oxidative Csp²-h annulation of amidines with terminal alkynes. *Green Chem.* **2021**, *23*, 5024–5030. [CrossRef]
214. Yang, J.; Xie, Z.; Jin, L.; Chen, X.; Le, Z. Synthesis of quinazoline by decarboxylation of 2-aminobenzylamine and α -keto acid under visible light catalysis. *Org. Biomol. Chem.* **2022**, *20*, 3558–3563. [CrossRef] [PubMed]
215. Pereira, J.A.; Pessoa, A.M.; Cordeiro, M.N.; Fernandes, R.; Prudêncio, C.; Noronha, J.P.; Vieira, M. Quinoxaline, its derivatives and applications: A state of the art review. *Eur. J. Med. Chem.* **2015**, *97*, 664–672. [CrossRef]
216. Dailey, S.; Feast, W.J.; Peace, R.J.; Sage, I.C.; Till, S.; Wood, E.L. Synthesis and device characterisation of side-chain polymer electron transport materials for organic semiconductor applications. *J. Mater. Chem.* **2001**, *11*, 2238–2243. [CrossRef]
217. Podsiadły, R. Photoreaction and photopolymerization studies on Fluoroflavin Dye–Pyridinium Salt Systems. *J. Photochem. Photobiol. A Chem.* **2008**, *198*, 60–68. [CrossRef]
218. Gedefaw, D.; Prosa, M.; Bolognesi, M.; Seri, M.; Andersson, M.R. Recent development of quinoxaline based polymers/small molecules for organic photovoltaics. *Adv. Energy Mater.* **2017**, *7*, 1700575. [CrossRef]
219. Li, F.; Tang, X.; Xu, Y.; Wang, C.; Wang, Z.; Li, Z.; Wang, L. A dual-protein cascade reaction for the regioselective synthesis of quinoxalines. *Org. Lett.* **2020**, *22*, 3900–3904. [CrossRef]
220. Liu, Y.; Friesen, J.B.; McAlpine, J.B.; Lankin, D.C.; Chen, S.N.; Pauli, G.F. Natural deep eutectic solvents: Properties, applications, and perspectives. *J. Nat. Prod.* **2018**, *81*, 679–690. [CrossRef]
221. Lupidi, G.; Palmieri, A.; Petrini, M. Sustainable and fast synthesis of functionalized quinoxalines promoted by natural deep eutectic solvents (NADESs). *Green Chem.* **2022**, *24*, 3629–3633. [CrossRef]
222. Queneau, Y.; Han, B. Biomass: Renewable carbon resource for chemical and Energy Industry. *Innovation* **2022**, *3*, 100184. [CrossRef]

223. Bains, A.K.; Singh, V.; Adhikari, D. Homogeneous nickel-catalyzed sustainable synthesis of quinoline and quinoxaline under aerobic conditions. *J. Org. Chem.* **2020**, *85*, 14971–14979. [CrossRef]
224. Zarenezhad, E.; Mosslemin, M.H.; Alborzi, A.; Anaraki-Ardakani, H.; Shams, N.; Khoshnood, M.M.; Zarenezhad, A. Efficient synthesis of 3,4-dihydro-1H-quinoxalin-2-ones and 1H-quinolin-2-ones and evaluation of their anti-bacterial activity. *J. Chem. Res.* **2014**, *38*, 337–340. [CrossRef]
225. Szumilak, M.; Stanczak, A. Cinnoline scaffold—A molecular heart of medicinal chemistry? *Molecules* **2019**, *24*, 2271. [CrossRef] [PubMed]
226. Cai, C.; Lu, Y.; Yuan, C.; Fang, Z.; Yang, X.; Liu, C.; Guo, K. Organocatalytic electro-synthesis of cinnolines through Cascade Radical Cyclization and migration. *ACS Sustain. Chem. Eng.* **2021**, *9*, 16989–16996. [CrossRef]
227. Sa, Y.; Cai, M.-X.; Lv, X.; Wu, A.-B.; Shu, W.-M.; Yu, W.-C. Intramolecular redox cyclization reaction access to cinnolines from 2-Nitrobenzyl Alcohol and benzylamine via intermediate 2-nitrosobenzaldehyde. *RSC Adv.* **2022**, *12*, 33260–33263. [CrossRef]
228. Li, R.; Hou, Y.-X.; Xu, J.-H.; Gao, Y.; Hu, X.-Q. Divergent synthesis of fused N-heterocycles via rhodium-catalysed [4+2] cyclization of pyrazolidinones with iodonium ylides. *Org. Chem. Front.* **2022**, *9*, 2181–2186. [CrossRef]
229. Mukherjee, A.; Sarkar, M.; Mahalanabis, K.K. The synthesis of novel ethyl 4-(substituted amino)isothiazolo[5,4-B]-pyridine-5-carboxylates. *J. Chem. Res.* **2006**, 437–439. [CrossRef]
230. Cabrera-Afonso, M.J.; Cembellín, S.; Halima-Salem, A.; Berton, M.; Marzo, L.; Miloudi, A.; Maestro, M.C.; Alemán, J. Metal-free visible light-promoted synthesis of isothiazoles: A catalytic approach for N-S bond formation from IMINYL radicals under batch and flow conditions. *Green Chem.* **2020**, *22*, 6792–6797. [CrossRef]
231. Wang, M.; Meng, X.; Cai, C.; Wang, L.; Gong, H. Synthesis of benzisothiazoles by a three-component reaction using elemental sulfur and ammonium as heteroatom components under transition metal-free conditions. *Green Synth. Catal.* **2022**, *3*, 168–174. [CrossRef]
232. Jemili, R.; Campos, J.F.; Dumuis, N.; Rabat, H.; Semmar, N.; Berteina-Raboin, S. Laser synthesis: A solvent-free approach for the preparation of phenylthiazolo[5,4-b]pyridine derivatives. *RSC Adv.* **2021**, *11*, 5003–5007. [CrossRef]
233. Cecchini, M.M.; Charnay, C.; De Angelis, F.; Lamaty, F.; Martinez, J.; Colacino, E. Poly(ethylene glycol)-based ionic liquids: Properties and uses as alternative solvents in organic synthesis and catalysis. *ChemSusChem* **2013**, *7*, 45–65. [CrossRef]
234. Wang, Z.-G.; Xia, Y.-G.; Jin, Y.; Lu, M. Efficient aerobic oxidative synthesis of benzimidazoles with Fe(III) based PEG₁₀₀₀ dicationic imidazolium ionic liquid/toluene temperature-dependent biphasic system. *J. Chin. Chem. Soc.* **2014**, *62*, 103–106. [CrossRef]
235. Guo, W.; Xie, Z.; Cai, L.; Liu, G.; Deng, L.; Mei, W.; Zou, X.; Zhong, Y.; Zhuo, X.; Zheng, L.; et al. Synthesis of purine analogues: Photocatalyst-free visible-light-enhanced annulation approach to pyrazolo[1,5-a][1,3,5]triazine-2,4-diamines. *J. Org. Chem.* **2021**, *86*, 8365–8380. [CrossRef] [PubMed]
236. Chakraborty, G.; Mondal, R.; Guin, A.K.; Paul, N.D. Nickel catalyzed sustainable synthesis of benzazoles and purines via acceptorless dehydrogenative coupling and borrowing hydrogen approach. *Org. Biomol. Chem.* **2021**, *19*, 7217–7233. [CrossRef] [PubMed]

Disclaimer/Publisher's Note: The statements, opinions and data contained in all publications are solely those of the individual author(s) and contributor(s) and not of MDPI and/or the editor(s). MDPI and/or the editor(s) disclaim responsibility for any injury to people or property resulting from any ideas, methods, instructions or products referred to in the content.

Review

A Brief Review on the Synthesis of the $N\text{-CF}_3$ Motif in Heterocycles

Zizhen Lei ^{1,2}, Wenxu Chang ^{1,2}, Hong Guo ^{1,2}, Jiyao Feng ^{1,2,*} and Zhenhua Zhang ^{1,2,*}¹ College of Science, China Agricultural University, Beijing 100193, China² College of Plant Protection, China Agricultural University, Beijing 100193, China

* Correspondence: b20183190860@cau.edu.cn (J.F.); zhangzh@cau.edu.cn (Z.Z.);

Tel.: +86-1861-263-9845 (J.F.); +86-1381-199-9084 (Z.Z.)

Abstract: The trifluoromethyl group is widely recognized for its significant role in the fields of medicinal chemistry and material science due to its unique electronic and steric properties that can alter various physicochemical properties of the parent molecule, such as lipophilicity, acidity, and hydrogen bonding capabilities. Compared to the well-established C-trifluoromethylation, *N*-trifluoromethylation has received lesser attention. Considering the extensive contribution of nitrogen to drug molecules, it is predicted that constructing *N*-trifluoromethyl ($N\text{-CF}_3$) motifs will be of great significance in pharmaceutical and agrochemical industries. This review is mainly concerned with the synthesis of heterocycles containing this motif. In three-membered heterocycles containing the $N\text{-CF}_3$ motif, the existing literature mostly demonstrated the synthetic strategy, as it does for four- and larger-membered heterocycles. Certain structures, such as oxaziridines, could serve as an oxidant or building blocks in organic synthesis. In five-membered heterocycles, it has been reported that $N\text{-CF}_3$ azoles showed a higher lipophilicity and a latent increased metabolic stability and Caco-2-permeability compared with their $N\text{-CH}_3$ counterparts, illustrating the potential of the $N\text{-CF}_3$ motif. Various $N\text{-CF}_3$ analogues of drugs or bioactive molecules, such as sildenafil analogue, have been obtained. In general, the $N\text{-CF}_3$ motif is developing and has great potential in bioactive molecules or materials. Give the recent development in this motif, it is foreseeable that its synthesis methods and applications will become more and more extensive. In this paper, we present an overview of the synthesis of $N\text{-CF}_3$ heterocycles, categorized on the basis of the number of rings (three-, four-, five-, six- and larger-membered heterocycles), and focus on the five-membered heterocycles containing the $N\text{-CF}_3$ group.

Keywords: *N*-trifluoromethyl group; heterocycles

Citation: Lei, Z.; Chang, W.; Guo, H.; Feng, J.; Zhang, Z. A Brief Review on the Synthesis of the $N\text{-CF}_3$ Motif in Heterocycles. *Molecules* **2023**, *28*, 3012. <https://doi.org/10.3390/molecules28073012>

Academic Editors: Alexey M. Starosotnikov, Maxim A. Bastrakov and Igor L. Dalinger

Received: 28 February 2023

Revised: 21 March 2023

Accepted: 24 March 2023

Published: 28 March 2023



Copyright: © 2023 by the authors. Licensee MDPI, Basel, Switzerland. This article is an open access article distributed under the terms and conditions of the Creative Commons Attribution (CC BY) license (<https://creativecommons.org/licenses/by/4.0/>).

1. Introduction

Organic fluorine chemistry, as a prominent research area, has garnered significant attention for several decades and has also become essential to the evolution of many different but interconnected research fields [1]. The introduction of the fluorine group, especially the trifluoromethyl group, into organic compounds has become known as one of the most efficient methods for modulating molecular properties, for example, lipophilicity and metabolic stability [2]. Due to its potential utility, many methods have been studied extensively [3,4]. However, in contrast to the well-developed C-trifluoromethylations, the *N*-trifluoromethyl ($N\text{-CF}_3$) motif has rarely been investigated to date. Considering the widespread dissemination of nitrogen (especially nitrogen-containing heterocycles) in drug molecules [5–7], constructing the $N\text{-CF}_3$ motif in molecules is of great significance in pharmaceutical and agrochemical industries. Drug analogues and potential agents containing the $N\text{-CF}_3$ motif are partially shown in Figure 1 [8–13].

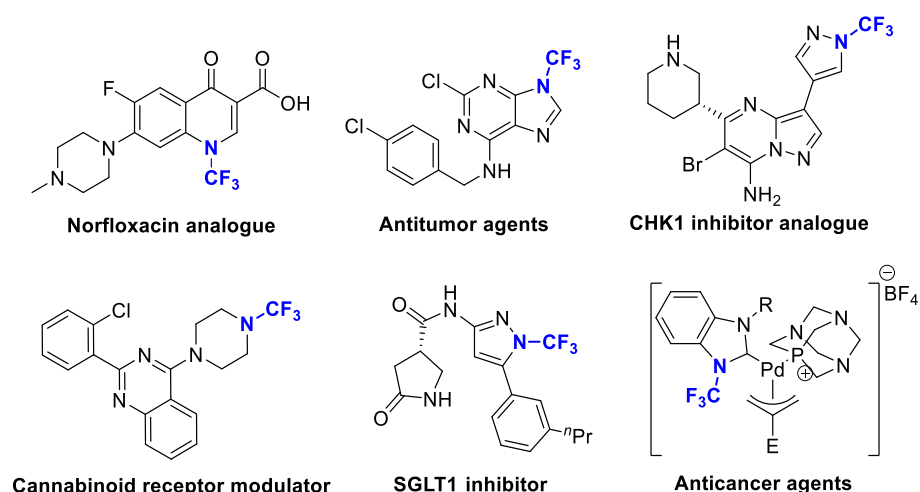


Figure 1. Drug analogues containing *N*-trifluoromethyl motif.

Despite the great potential of the *N*-CF₃ motif, the synthesis of this moiety and its relative chemistry have been rarely explored. The limited use of *N*-CF₃ compounds is primarily due to the absence of scalable methods for their preparation [14–16]. Recently, thanks to the new reagents and methods, this motif has increasingly been featured in the literature.

In terms of constructing the *N*-CF₃ motif in heterocycles, there are two main approaches. The first involves utilizing starting materials containing the *N*-CF₃ motif to generate heterocycles directly, while the second strategy entails introducing the CF₃ group via trifluoromethylation or fluorination of nitrogen-containing species. In this paper we review the construction of *N*-CF₃ heterocycles on the basis of the size of the cycles, involving three-, four-, five-, six- and larger-membered heterocycles. This article covers as much literature as possible, from the 1960s to early 2023. The structures mentioned in this paper are shown in Figure 2.

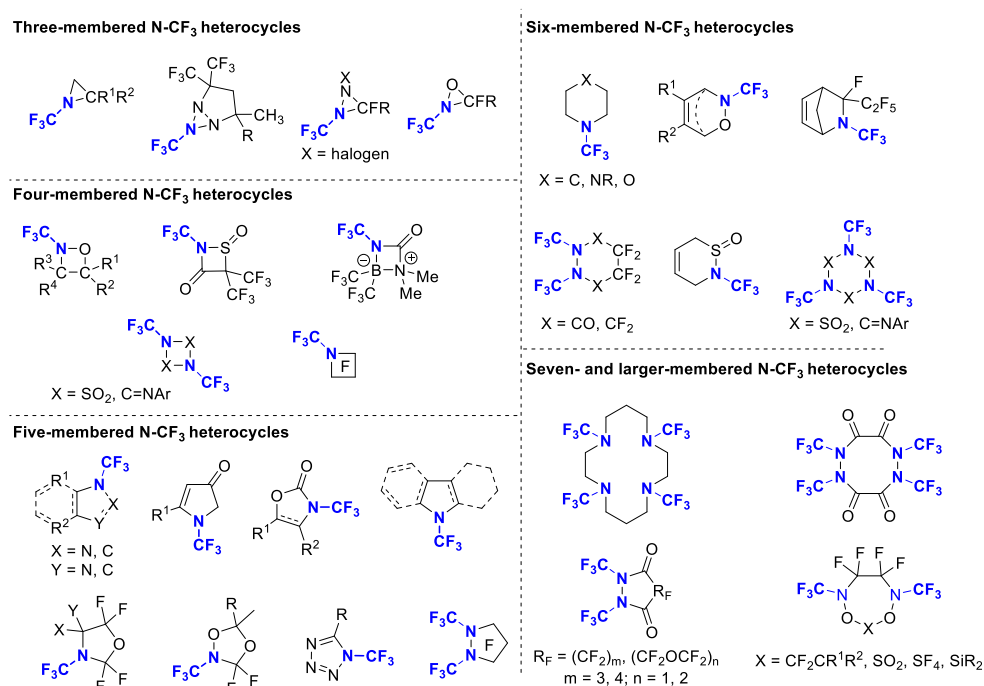
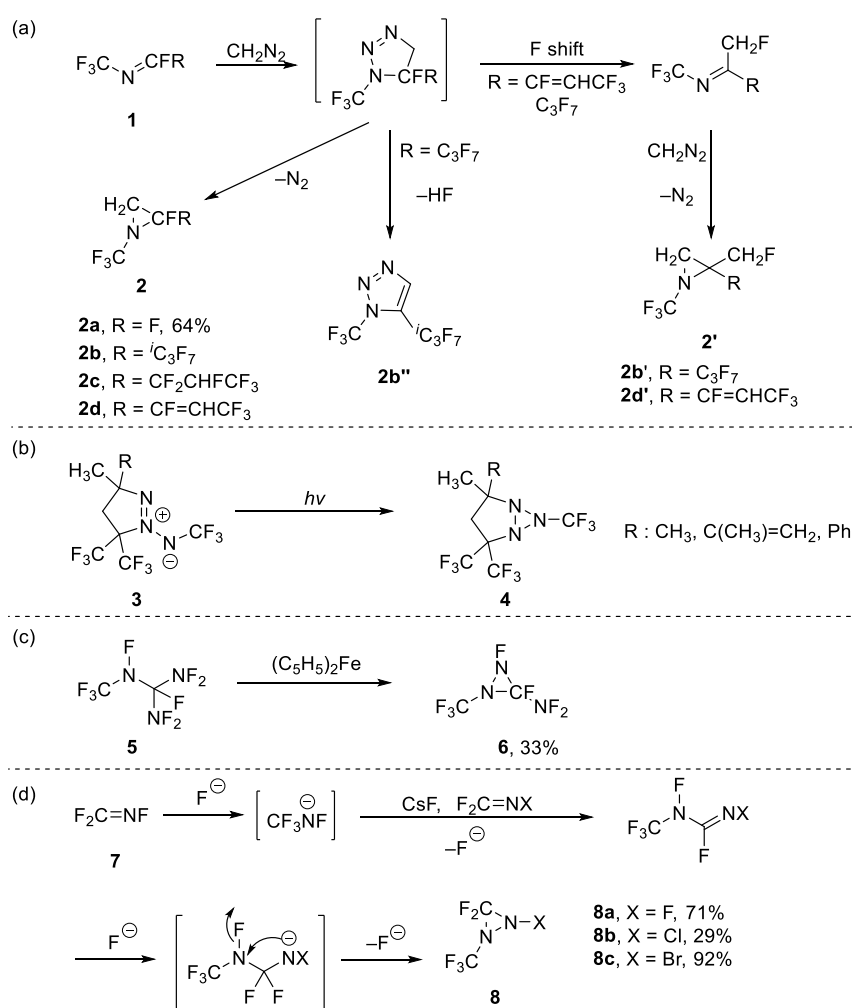


Figure 2. Variably sized *N*-heterocycles containing the *N*-trifluoromethyl motif.

2. Three-Membered Heterocycles

In previous reports, the synthesis of three-membered $N\text{-CF}_3$ heterocycles mainly relied on starting materials containing the $N\text{-CF}_3$ motif. In 1964, Logothetis reported the aziridination of $N\text{-CF}_3$ imines **1a** in the presence of diazomethane, which obtained aziridine **2a** in the yield of 64% (Scheme 1a) [17]. Subsequently, Coe et al. investigated the substructure scope of imines [18]. Unfortunately, poor selectivity was exhibited when R was replaced with $i\text{C}_3\text{F}_7$ (perfluoroisopropyl) or $\text{CF}=\text{CHCF}_3$. When $\text{R} = i\text{C}_3\text{F}_7$, a mixture of three components in the ratio of **2b**:**2b''**:**2b'** = 6:9:1 was obtained and when $\text{R} = \text{CF}=\text{CHCF}_3$, a mixture of two products was obtained in the ratio of **2d**:**2d'** = 71:29 by F shift and further CH insertion into a C-F bond. Kaupp et al. synthesized some stable triaziridines **4** which could be purified by fractional distillation by the irradiation of aziridines **3** at room temperature (Scheme 1b) [19]. However, not much attention has been paid to $N\text{-CF}_3$ triaziridine.

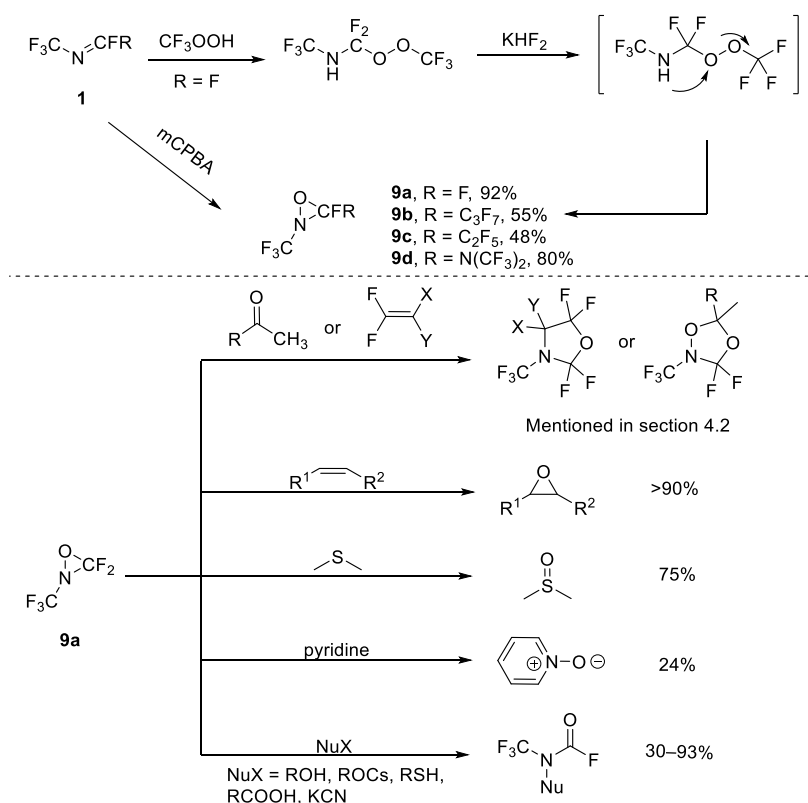


Scheme 1. Synthesis of (a) aziridines, (b) triaziridines and (c,d) diaziridines.

Compared to the structures mentioned above, diaziridine attracted more attention, and its synthesis could be divided into two strategies: Mitsch et al., while studying the reductive defluorination-cyclization of organic fluoronitrogens, found that diaziridine **6** could be generated from 1,1-bis(difluoroamino)perfluoro-2-azapropen **5** in the presence of ferrocene (Scheme 1c) [20]. Later DesMarteau et al. obtained another diaziridine **6** by nucleophilic cyclization when studying perfluoroalkylamine ions (Scheme 1d) [21]. In the presence of CsF , $\text{CF}_2=\text{NX}$ (when $\text{X} = \text{F}$) yielded perfluoroalkylamine ion (CF_3NF^-), which underwent further reaction with another $\text{CF}_2=\text{NX}$ to form perfluoro-1-methylformamidine **8**. On the basis of previous work, DesMarteau group achieved synthesis of other diaziridines (when X

= Br, Cl) through perfluoroalkanamine ions [22,23]. Meanwhile, other electrophilic species, such as *N*-CF₃ imine **1a**, could also be attacked by CF₃NF⁻, leading to 3,3-difluoro-1,2-bis(trifluoromethyl)diaziridine [24].

Furthermore, perfluorinated oxaziridine **9** has drawn wide attention and its structure, synthesis and applications have been studied. Petrov and Resnati have already summarized the synthesis and reactivity of perfluorinated oxaziridines, in which *N*-CF₃ oxaziridines are included [25]. In previous reports, the most common methods of synthesis were oxidative cyclization. In 1976, DesMarteau et al. reported that oxaziridine was obtained by the oxidation of a *N*-CF₃ imines **1a** by CF₃OOH [26]. This reaction was performed in two steps: addition, and further cyclization mediated by NaF. Later, different metal fluorides were investigated by the authors of [27] and KHF₂ was found to be the most suitable reagent for the yield of oxaziridine **7** (the yield was up to 92%). This method was difficult and the starting materials were potentially explosive. In order to make the reaction safer and more convenient, different oxidants, such as hydrogen peroxide [28] and chlorine gas in the presence of metal carbonate [29], etc., have been developed, but these methods were still difficult. Finally, using meta-chloroperbenzoic acid (mCPBA) as the oxidant was determined to be a safer and more attractive choice (Scheme 2) [30,31].



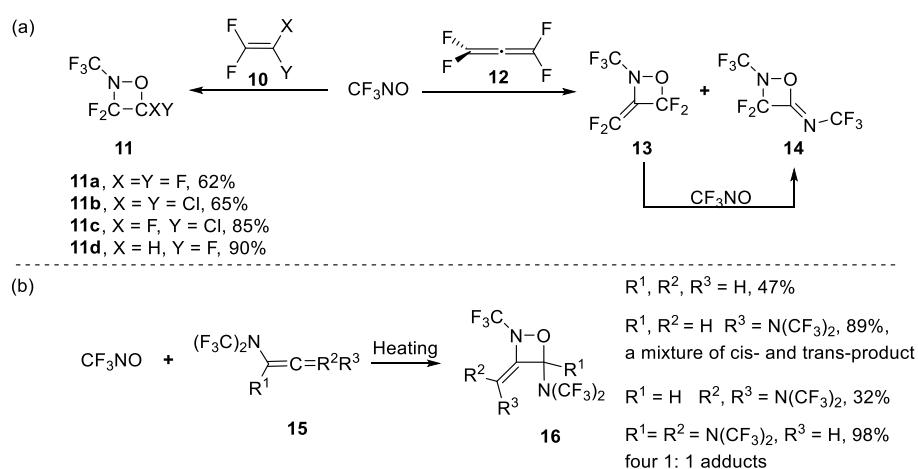
Scheme 2. Synthesis and applications of oxaziridines.

To date, *N*-CF₃ aziridine, triaziridine and diaziridine have still gained less attention and their properties and applications are less-developed. On the other hand, there have been studies into the structure, properties, and applications of oxaziridine [25] (shown in Scheme 2), such as its reaction with nucleophiles [32,33] and its use as an oxidant [34] or as building blocks. These studies are included in Section 4.2 of this paper.

3. Four-Membered Heterocycles

Similarly, the synthesis of four-membered *N*-CF₃ heterocycles was based on starting materials containing the *N*-CF₃ motif.

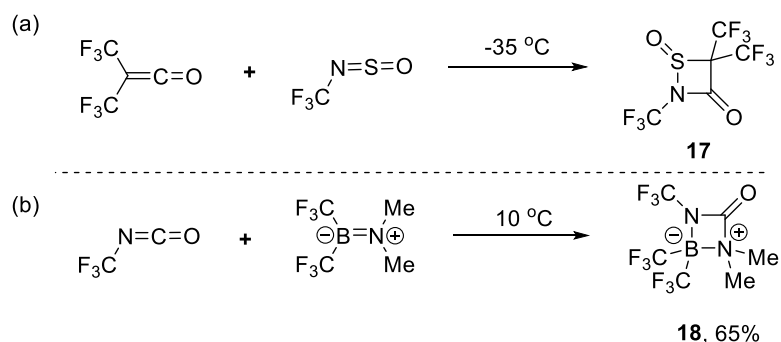
The predominant approach to oxazetidine was [2+2] cycloaddition reaction. Trifluoronitrosomethane (CF_3NO) was the most common starting material. In the 1950s, Barr and Haszeldine reported that CF_3NO reacted with tetrafluoroethylene **10a** to give two products: an oxazetidine **11a** and a copolymer (consisting of two monomers in a 1:1 ratio) [35,36]. The oxazetidine predominated in this reaction at a high temperature (ca. 100 °C) and the copolymer at room temperature (Scheme 3a). Since then, several halogenated tetrafluoroethylenes ($\text{CF}_2=\text{CXY}$) have been investigated (Scheme 3b) [37,38]. It was found that the formation of an oxazetidine and the copolymer from CF_3NO occurred most readily with the olefins $\text{CF}_2=\text{CF}_2$, $\text{CF}_2=\text{CHF}$ (adducts were a 99:1 mixture of 3,3,4-trifluoro-2-trifluoromethyl-1,2-oxazetidine and 3,4,4-trifluoro-2-trifluoromethyl-1,2-oxazetidine), $\text{CF}_2=\text{CFCl}$, and $\text{CF}_2=\text{CCl}_2$, and less readily with perfluoro-olefins containing more than two carbon atoms, or with ethylenes containing two or more vinylic hydrogens [38].



Scheme 3. Synthesis of oxazetidines through trifluoronitrosomethane.

Meanwhile, it was reported that an attack on the substituted allene by CF_3NO led to another form of oxazetidine. Banks et al. found that tetrafluoroallene **12** reacted with CF_3NO to yield a complex mixture of oxazetidine **13** and **14** [39]. By adjusting the reaction conditions, the highest yields of oxazetidine **13** and **14** can reach 43% and 42%, respectively. They also found that compound **14** could be obtained (82% yield) when heating oxazetidine **13** with CF_3NO . Later, Haszeldine et al. synthesized a series of oxazetidines **16** with limited regioselectivity and stereoselectivity through the reaction of N, N-bis(trifluoromethyl)amino-substituted allenes **15** with CF_3NO (Scheme 3b) [40,41].

In addition to CF_3NO , there were other reagents used in [2+2] cycloaddition. For example, in 1986, Sundermeyer and co-workers found that $\text{CF}_3\text{N}=\text{S}=\text{O}$ could react with ketene to generate thiazetidins **17** (Scheme 4a) [42]. Burger et al. reported that the reaction of $\text{CF}_3\text{N}=\text{C}=\text{O}$ and boranamine led to diazaboretidins **18** (Scheme 4b) [43].



Scheme 4. Synthesis of (a) thiazetidins and (b) diazaboretidins through [2+2] cycloaddition reaction.

4. Five-Membered Heterocycles

The literature on three- and four-membered $N\text{-CF}_3$ heterocycles was more focused on their synthesis, with limited exploration of their properties and potential applications. However, in contrast, five- and six-membered heterocycles featuring the $N\text{-CF}_3$ motif have recently been receiving more and more attention [8,44–46]. Their synthesis methods, as well as biological activities and derivatization, are gradually being studied.

To evaluate the suitability of the $N\text{-CF}_3$ motif on amines and azoles in drug design, Schiesser et al. synthesized a series of $N\text{-CF}_3$ amines and azoles (shown in Figure 3), and determined their stability in aqueous media and other properties [45]. For example, the stability of $N\text{-CF}_3$ analogues of known bioactive compounds (sulfamethoxazole derivative **19a**, tetracaine derivative **20a**, inhibitors of hedgehog pathway **21a** [47,48], inhibitors of methionine aminopeptidase **22a** [49], inhibitors of interleukin-1 receptor associated kinase 4 (IRAK4) **23a** [50], and sildenafil analogue **24a**) were studied and are shown in Table 1.

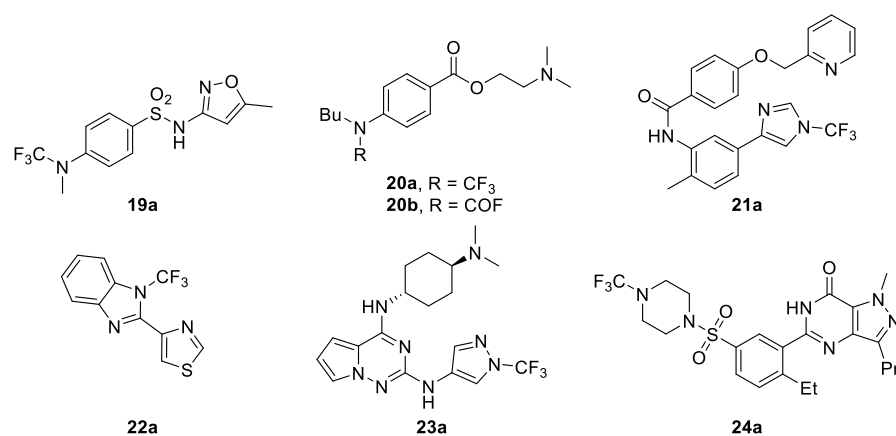


Figure 3. Synthesis of N -trifluoromethyl compounds to determine their aqueous stability and additional key in vitro properties.

Table 1. Half-life of $N\text{-CF}_3$ compounds **19a–24a** [a].

Structure	pH 1.0 [d]	pH 7.4 [d]	pH 10.0 [d]
19a	0.2	0.4	0.3
20a	<0.6	<0.6	<0.6
21a	>72	>72	>72
22a	>72	>72	>72
23a	>72	>72	71
24a	<1.3	<0.8	<0.5

[a] The experiment was carried out at 25 °C in 0.1 M HCl solution (pH 1.0), 20 mM sodium phosphate buffer (pH 7.4), and 20 mM carbonate buffer (pH 10.0).

Two anilines **19a** and **20a**, as well as piperazine **24a**, showed fast hydrolysis at all three pH values investigated, with half-lives of less than 1.5 days at 25 °C (Table 1). It should be noted that for **20a**, the corresponding carbamoyl fluoride **20b** was the main product at pH 1.0, with a small amount of product where both the carbamoyl fluoride had been further hydrolyzed to the secondary amine and the ester bond had been cleaved. The latter compound was also the main product at pH 7.4 and pH 10.0. In contrast to the $N\text{-CF}_3$ anilines and piperazine, for all the $N\text{-CF}_3$ azoles they investigated no corresponding carbamoyl fluoride of free azole was detected in aqueous media at any of the three pH values studied.

Moreover, they then compared the key in vitro properties in medicinal chemistry (log D , experimentally determined polar surface area (ePSA) [51,52], permeability in human

epithelial colorectal adenocarcinoma cells (Caco-2), and metabolic stability for the *N*-CF₃ compounds **19a–24a** and their *N*-CH₃ counterparts (Table 2).

Table 2. Overview of the change in key in vitro properties when exchanging *N*-CH₃ and *N*-CF₃ [f].

Structure	Number	Log <i>D</i> _{7.4} [a]	Chrom-log <i>D</i> _{7.4} [a]	ePSA [b] [Å ²]	Caco-2 <i>P</i> _{app} [c] [10 ^{−6} cm/s]	HLM [d] [L/min/mg]
	19a R = CF ₃	1.6 (0.1)	1.5 (0.1)	82 (1)	nd [e]	nd [e]
	19b R = CH ₃	0.6 (0.1)	1.3 (0.1)	81 (1)	nd [e]	nd [e]
	20a R = CF ₃	>4.0	4.9 (0.2)	38 (2)	nd [e]	nd [e]
	20c R = CH ₃	2.8 (0.1)	3.3 (0.1)	50 (1)	nd [e]	nd [e]
	21a R = CF ₃	3.7 (0.1)	3.3 (0.0)	73 (1)	61 (27)	47 (11)
	21b R = CH ₃	2.7 (0.1)	2.2 (0.1)	92 (1)	72 (1)	4.8 (1.9)
	22a R = CF ₃	3.0 (0.1)	3.3 (0.0)	39 (2)	58 (18)	39 (18)
	22b R = CH ₃	2.3 (0.0)	1.5 (0.1)	56 (1)	72 (20)	172 (41)
	23a R = CF ₃	2.2 (0.1)	2.2 (0.0)	92 (1)	12 (8)	<3.0
	23b R = CH ₃	0.6 (0.1)	<0.0	98 (0)	2.4 (0.9)	<3.0
	24a R = CF ₃	>4.0	>5.3	67 (1)	nd [e]	nd [e]
	24b R = CH ₃	2.7 (0.1)	3.3 (0.1)	73 (0)	nd [e]	nd [e]

[a] Due to limitations in the determination of log *D*_{7.4} using the shake-flask method, exact values for measured log *D*_{7.4} > 4 are given as >4.0. [b] Experimentally determined polar surface area. [c] Apical to basolateral passive permeability across the Caco-2 cell monolayer in the presence of inhibitors against the three major efflux transporters: P-glycoprotein (P-gp), breast cancer resistance protein (BCRP), and multidrug-associated protein 2 (MRP2). [d] Metabolic stability of the compound measured as the disappearance of the parent compound over time when incubated with human liver microsomes. [e] Due to the low stability of compounds **19a**, **20a**, and **24a** in an aqueous environment, which would interfere with the proper determination of their metabolic stability or Caco-2 permeability, no metabolic stability or Caco-2 permeability was determined for these compounds or for their *N*-methyl analogues. [f] Each experimental value is the mean of at least three independent replicates. The standard deviation is given in brackets.

In the compounds investigated, the exchange of a methyl for trifluoromethyl led to the expected higher lipophilicity as proven by an increased log *D*_{7.4} and chromlog *D*_{7.4} and a decreased ePSA. Log *D*_{7.4} increases by on average 1.1 log units and chromlog *D*_{7.4} by 1.6 log units. However, the extent of this change can vary significantly and was dependent on both the individual compound and type of log *D*_{7.4} analysis used. Changes in permeability and metabolic stability were less consistent. Stability to human liver microsomes (HLMs)

can be significantly increased for the trifluoromethyl analogue as seen for **22a** ($p = 0.004$) or decreased as for **21a**. The decreased metabolic stability of the latter two compounds could be due to an increased lipophilicity, rendering the potential metabolic soft spots (benzylic methyl group in **21a**) more susceptible to metabolism.

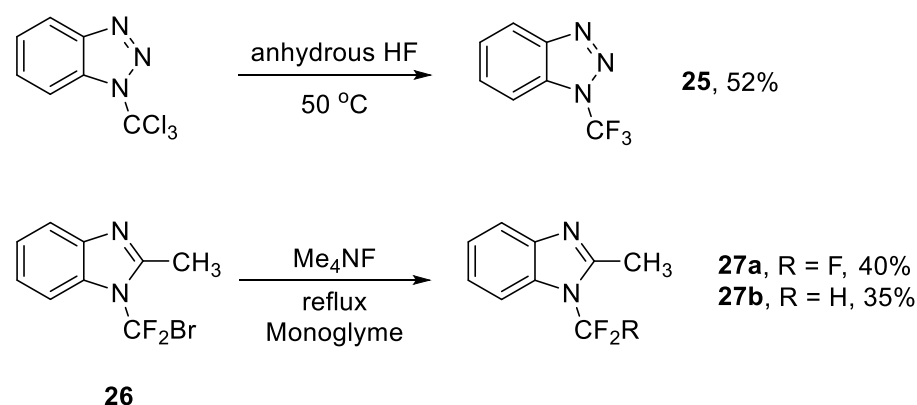
According to Schiesser's research [45], $N\text{-CF}_3$ amines were prone to hydrolysis, whereas $N\text{-CF}_3$ azoles have excellent aqueous stability. Compared to $N\text{-CH}_3$ analogues, $N\text{-CF}_3$ azoles showed a higher lipophilicity and a latent increase in metabolic stability and Caco-2-permeability, which illustrated the value and potentiality of $N\text{-CF}_3$ diazole in medicinal chemistry.

In terms of synthesizing these five-membered $N\text{-CF}_3$ structures, both types of constructing $N\text{-CF}_3$ were included. In this section, the synthesis of five-membered heterocycles would be divided into the three parts: nucleophilic fluorination, cyclization based on $N\text{-CF}_3$ starting materials, and electrophilic trifluoromethylation.

4.1. Nucleophilic Fluorination

4.1.1. Fluorine/Halogen Exchange

Fluorine/halogen exchange was one of the first reactions to obtain the trifluoromethyl group on the nitrogen atom (Scheme 5) [16]. Yagupolskii et al. achieved fluorine/halogen exchange with N -trichloromethyl derivatives in the presence of HF or Me_4NF [53]. This strategy was also capable of generating $N\text{-CF}_3$ pyrazoles [54,55] and $N\text{-CF}_3$ 1,2,4-triazoles [55]. However, highly toxic or environmentally unfriendly reagents (such as CF_2Br_2 , a known ozone-depleting reagent [56]) would be used in this method for fluorine/halogen exchange or in the preparation of the precursors (such as **26**) for fluorine/halogen exchange, which limited its use.

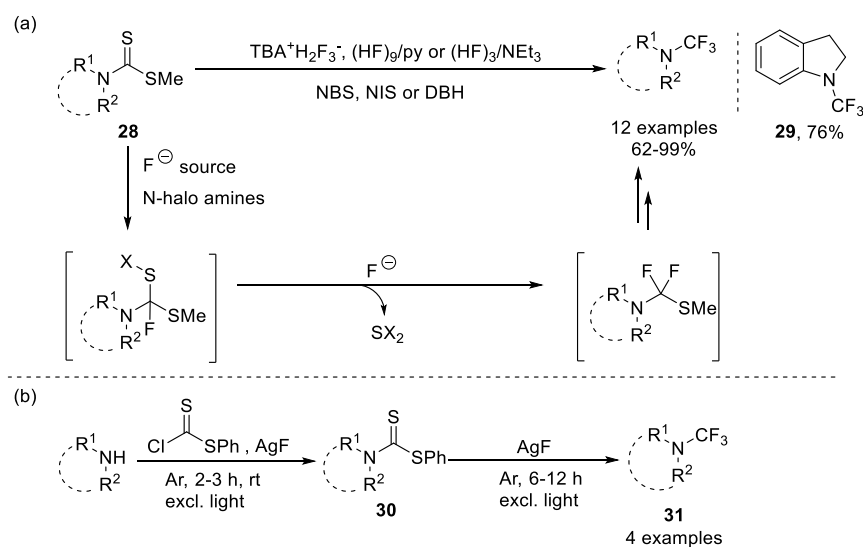


Scheme 5. Synthesis of N -trifluoromethyl benzotriazole or benzimidazole through fluorine/halogen exchange.

4.1.2. Oxidative Desulfurization and Fluorination

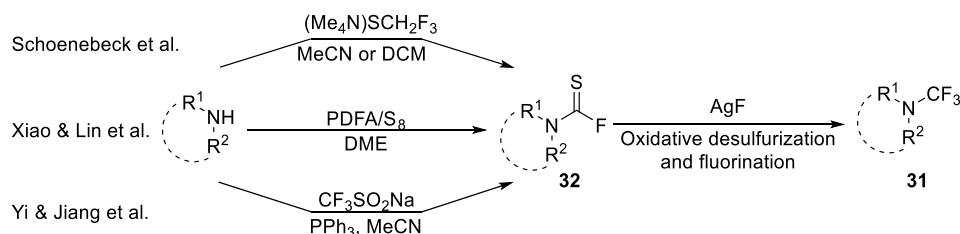
Compared to fluorine/halogen exchange, this method has been much more thoroughly studied. This method allowed people to replace C-S bonds with C-F bonds under extremely mild conditions compared to the fluorination of formamides [57] or fluorination induced by SF_4 [58].

Hiyama et al. reported conversion from methyl dithiocarbamates to trifluoromethylamines in the presence of readily available fluoride ions (Scheme 6a) [59]. The reaction conditions were applicable to a wide range of disubstituted nitrogen, with substituents including phenyl, heteroaromatic or alkyl. Recently, Schindler et al. applied chlorodithiophenylformiate as an electrophile and successfully obtained phenyl aminodithioate **30** [60]. Then trifluoromethylamines **31** were generated after the desulfurization and fluorination. Additionally, Hagooly et al. used BrF_3 for desulfurization and fluorination and obtained 2-(trifluoromethyl)isoindoline-1,3-dione and 1-(trifluoromethyl)azepan-2-one [61].



Scheme 6. Synthesis of *N*-trifluoromethyl amines from (a) methyl dithiocarbamate or (b) phenyl dithiocarbamate.

Furthermore, Schoenebeck et al. reported that amines and SCF_3^- source $(\text{Me}_4\text{N})\text{SCF}_3$ could generate the highly electrophilic thiocarbomoyl fluoride **32** followed by a reaction with AgF to yield trifluoromethyl amines **31** [62]. Furthermore, there were other approaches to the intermediate **32**. Lin and Xiao et al. [63] generated this intermediate from difluorocarbene and sulfur (S_8), while Jiang and Yi et al. [64] reported a method using $\text{CF}_3\text{SO}_2\text{Na}$ (Scheme 7). These strategies have been used to synthesize interesting analogues of biologically active compounds (examples are shown in Section 5.1).

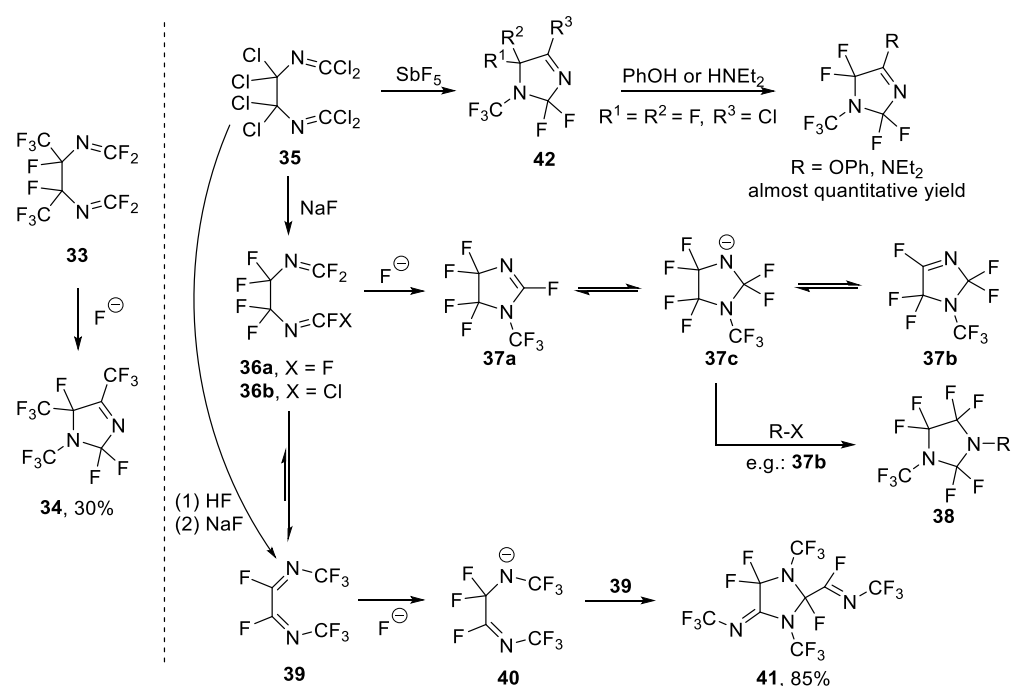


Scheme 7. Synthesis of thiocarbomoyl fluoride intermediate and further oxidative desulfurization and fluorination to access *N*-trifluoromethyl amines.

4.1.3. Cyclization Induced by Fluoride Ion

Fluoro-olefins containing terminal double bonds have been shown to isomerize in the presence of fluoride ion (Scheme 8) [65]. There is a considerable amount of literature on the transformation of perfluoro-2,5-diazahexa-2,4-diene ($\text{CF}_2=\text{NCF}_2\text{CF}_2\text{N}=\text{CF}_2$, **36a**) and its precursor $\text{CCl}_2=\text{NCCl}_2\text{CCl}_2\text{N}=\text{CCl}_2$, **35**. In 1967, Ogden and Mitsch reported that isomerization of perfluoro-, -diazomethines with CsF could form a cyclic five-membered *N*- CF_3 heterocycle as a minor product (**34**, 30% yield) [66].

Scholl et al. synthesized **36a** from **35** via two steps, and found that **36a** could cyclize to form two isomers (**37a** and **37b**) in the presence of fluoride ion [67]. Both isomers could form nitrogen anion **37c** in the presence of fluoride ion. **37c** could also react with **37b** to generate substituted *N*- CF_3 imidazolidine **38**. Subsequently, the same group found another transformation of **35** and obtained **39** in two steps [68]. In the presence of fluoride ion, another nitrogen anion **40** could be generated, which subsequently reacted with another **39** to obtain imidazolidine **41**.



Scheme 8. Synthesis of *N*-trifluoromethyl compounds through cyclization of fluoro-olefins induced by fluoride ion.

Later in 1984, Banks et al. [69] investigated in some detail the effect of temperature and metal fluoride on the systems used by Scholl. The product composition depends on the reactivity of the fluoride source and the reaction conditions, i.e., the product may be under kinetic or equilibrium control. In addition to the substances reported earlier by Scholl, they detected others. Later, Chambers et al. [70,71] reacted the nitrogen anion **37c** with different trapping agents including haloalkane, perfluoro azaarene, perfluoro cyclobutene, etc., and obtained diverse heterocycles **38**.

Meanwhile, Pawelke et al. [72] investigated the transformation of **35** or its derivative in the presence of fluoride source. Cyclization of compound **35** led to the perfluorinated 1H-imidazole **42**, whose chlorine atom could be further substituted by OPh or NEt₂.

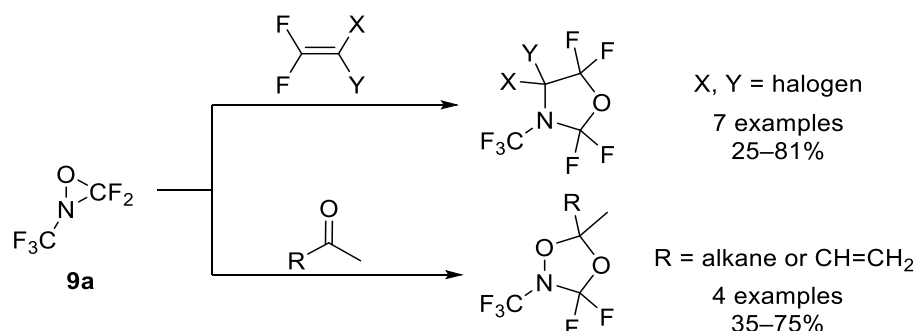
4.2. Cyclization Based on *N*-CF₃ Starting Materials

4.2.1. [3+2] Cycloaddition

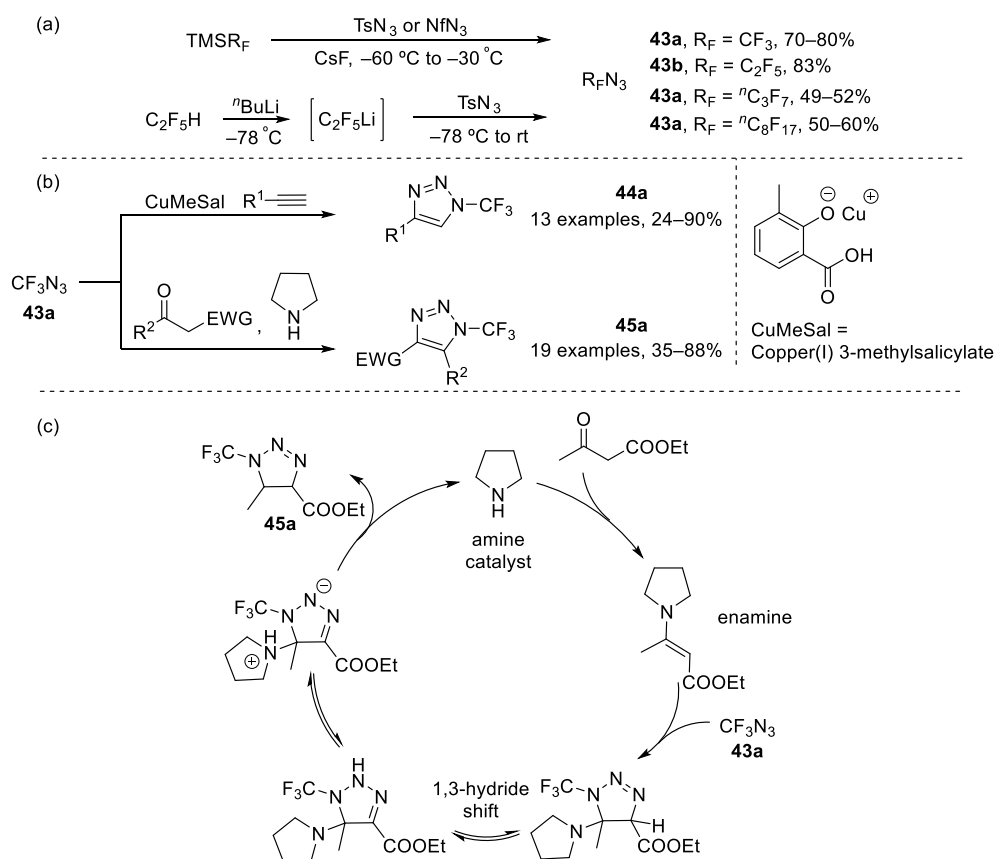
Utilization of starting materials containing the *N*-CF₃ motif is a commonly employed strategy for achieving the target heterocyclic compounds. As mentioned in Section 2, perfluorinated oxaziridine **9a** could serve as building blocks in organic chemistry. DesMarteau et al. reported that some cycloaddition of oxaziridine **9a** with electron-rich alkenes and ketones resulted in oxazolidines or dioxazolidines (Scheme 9) [73,74]. However, perfluorinated oxaziridine **9a** also had certain limitations as a building block: attempts to achieve the cycloaddition of **9a** with CH₂=CH₂, CFCl=CFCl, perfluorocyclopentene, acrylonitrile, and acetylene have failed. Additionally, the reaction could not occur with fluorinated ketones such as hexafluoroacetone.

In recent decades [3+2] cycloaddition between azide and alkyne has attracted significant attention, and copper-catalyzed azide-alkyne cycloaddition is one of the most widely used forms of this technique [75]. In 2017, Beier et al. reported the synthesis of azidoperfluoroalkanes **43** which could be synthesized from perfluoroalkyl trimethylsilane (TMSR_F) with *p*-toluenesulfonyl azide (TsN₃) in the presence of CsF, or synthesized from (perfluoroethyl)lithium (R_F = C₂F₅) with TsN₃ [76]. These azidoperfluoroalkanes could undergo [3+2] cycloaddition with alkynes catalyzed by copper to access diverse *N*-perfluoroalkyl 1,2,3-triazoles **44** (Scheme 10). Later in 2018, Beier et al. reported a mild

and efficient and synthesis of highly functionalized 1-perfluoroalkyl-1H-1,2,3-triazoles **45** via in situ generated enamines in azide-ketone [3+2] cycloaddition (Scheme 10) [77].

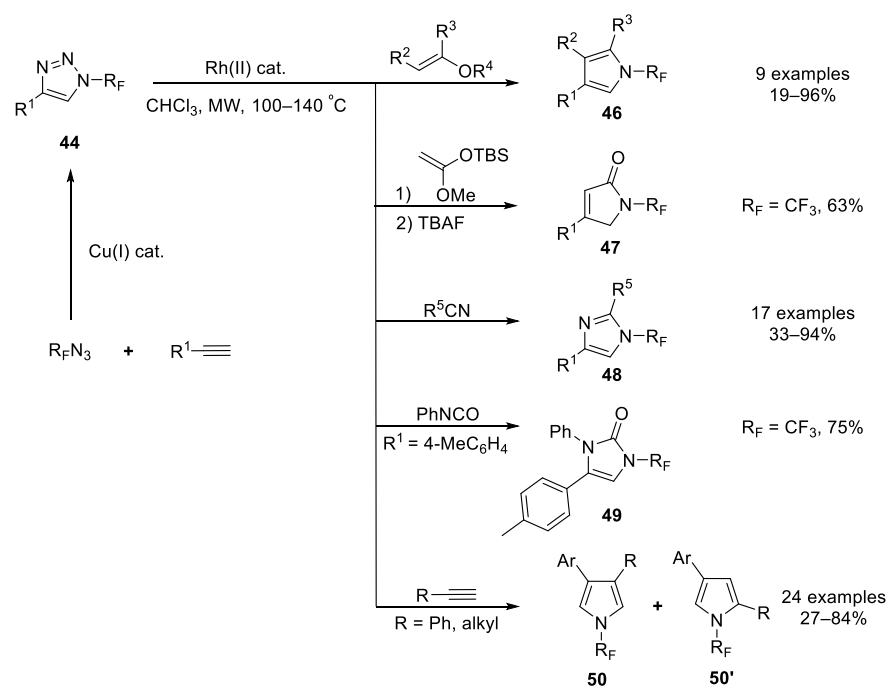


Scheme 9. Synthesis of oxazolidines or dioxazolidines through [3+2] cycloaddition of perfluorinated oxaziridine.

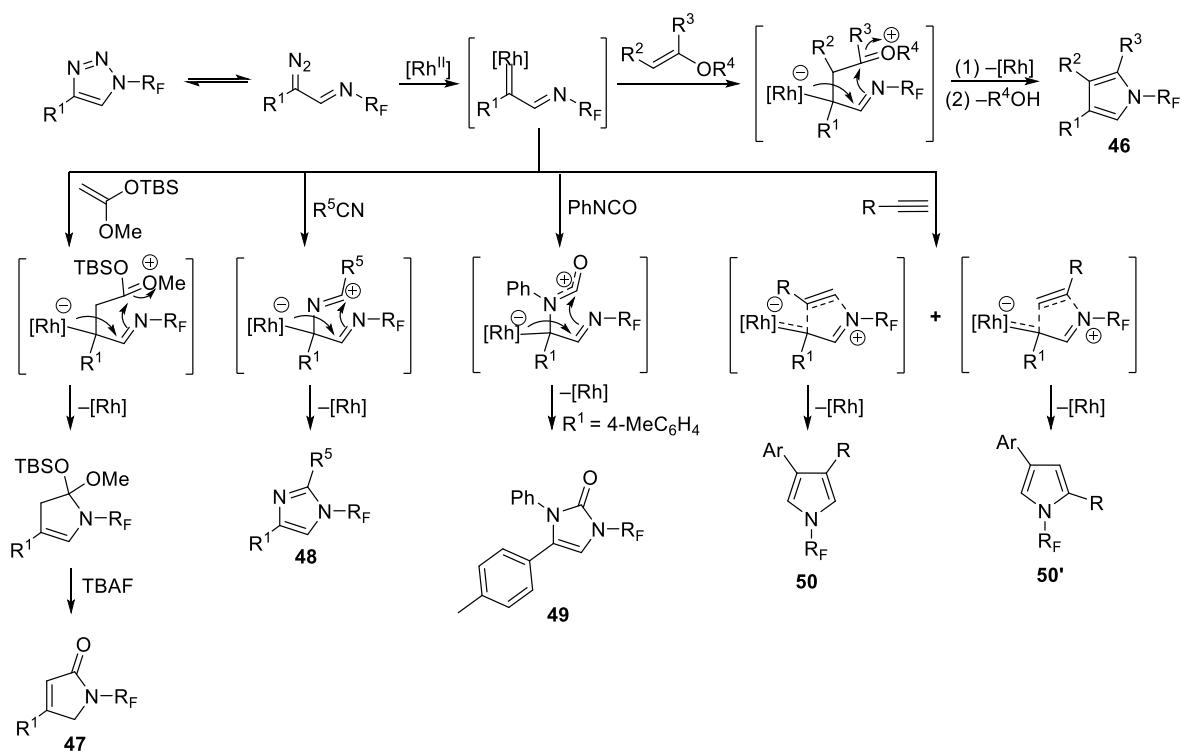


Scheme 10. (a) Synthesis of perfluoroalkyl azides; (b) cycloaddition of trifluoromethyl azides with alkynes or ketones; (c) mechanism of the cycloaddition of trifluoromethyl azides with ketones.

In the same year, the Beier group developed a highly efficient method for the synthesis of a broad range of previously unreported N-fluoroalkyl-substituted five-membered heterocycles with microwave heating-assisted rhodium-catalyzed transannulation of N-fluoroalkyl-substituted 1,2,3-triazoles **44** [78]. Subsequently, the same group expanded this approach to acetylene substrates and successfully generated N-fluoroalkyl pyrrole (Scheme 11) [79]. The mechanism proposed by authors is shown in Scheme 12.



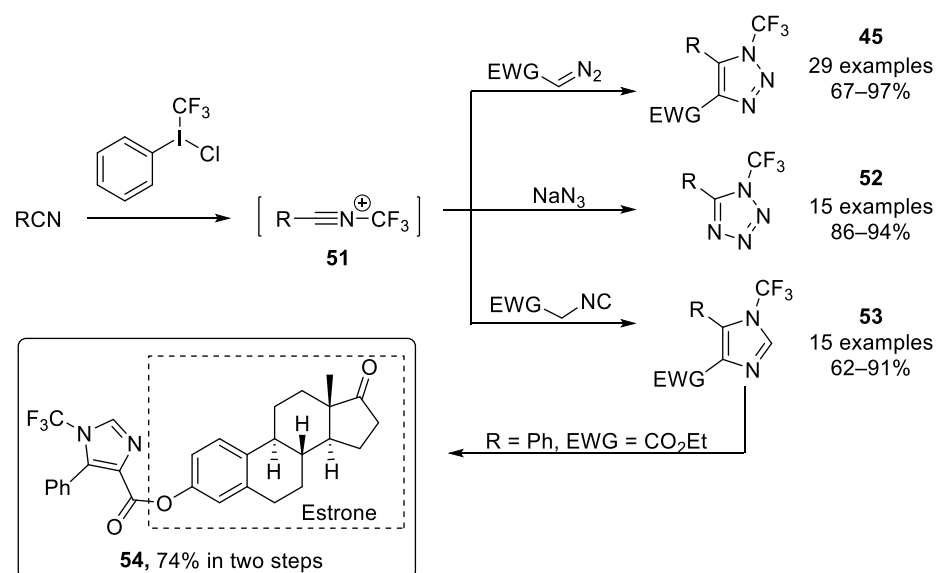
Scheme 11. Synthesis of diverse *N*-trifluoromethyl heterocycles through transannulation catalyzed by rhodium.



Scheme 12. Mechanism of transannulation catalyzed by rhodium.

Xu, Guan, and Wang et al. [80] reported an alternative and scalable cyclization strategy based on *N*- CF_3 -containing synthons for constructing diverse *N*- CF_3 azoles, including *N*- CF_3 tetrazoles, *N*- CF_3 imidazoles, and *N*- CF_3 1,2,3-triazoles (Scheme 13). This method involved using a hypervalent iodine reagent for trifluoromethylation in combination with a base to efficiently carry out the reaction. Furthermore, estrone analogue **54** could be generated in two steps in a total of 74% yield. Subsequently, the authors' group developed the reaction of the *N*- CF_3 nitrilium ions **51** with *N*-, *O*-, and *S*-nucleophiles, resulting in various

N-CF₃ amidines, imidates, and Thioimidates [81]. Very recently, they utilized hypervalent iodine reagent for the trifluoromethylation of 4-alkylamino-pyridine to generate *N*-CF₃ pyridinium salt which could be further translated to 2-functionized nicotinaldehydes [82].



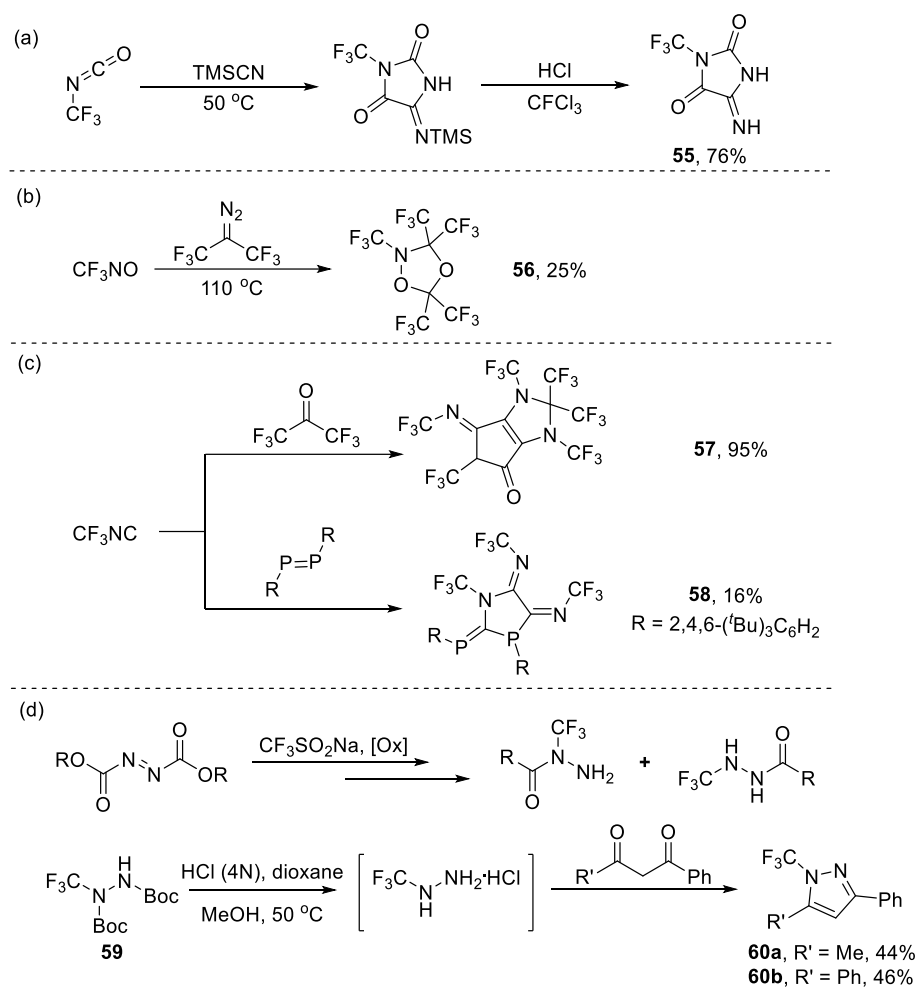
Scheme 13. Synthesis of *N*-trifluoromethyl heterocycles through 1,3-dipoles generated by hypervalent iodine reagent with nitriles.

4.2.2. Other Cyclization

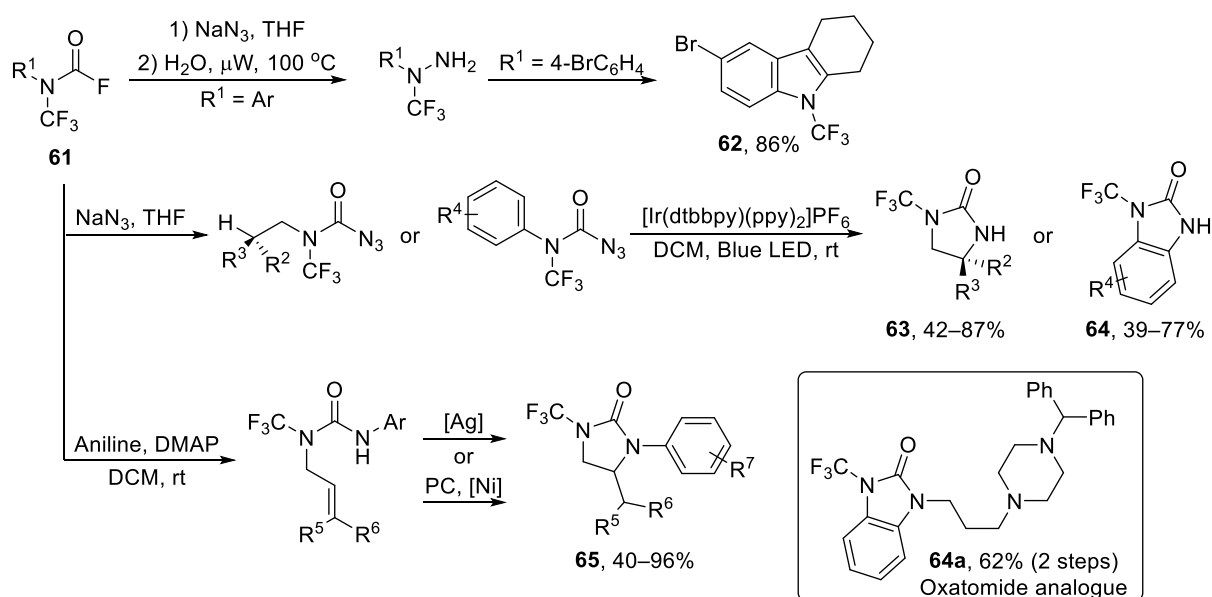
In addition to [3+2] cycloaddition, other cyclization pathways have been explored for the synthesis of *N*-CF₃-containing five-membered heterocycles. For instance, Sundermeyer and co-workers reported access to the preparation of imidazolidinedione **55** through the reaction of trifluoromethyl isocyanate with trimethylsilyl cyanide, followed by hydrolysis [83]. In 1977, Rudiger Mews synthesized dioxazolidine **56** from CF₃NO and bis(trifluoromethyl)diazomethane [84]. Lentz reported that trifluoromethyl isocyanide reacted with hexafluoroacetone to yield compound **57** [85]. Later, the same group reacted trifluoromethyl isocyanide with diphosphene, leading to the formation of azaphospholidine **58** [86]. In addition, Crousse et al. developed a direct approach to obtaining *N*-CF₃ hydrazines from CF₃SO₂Na. Among the family of *N*-CF₃ hydrazines, hydrazides **59** showed hydrolysis in the presence of HCl and reacted further with diketone, leading to *N*-CF₃-1*H*-pyrazoles **60** in 44% yield totally (Scheme 14d) [87].

In 2019, Schoenebeck et al. reported straight access to *N*-CF₃ amides, carbamates, thiocarbamates or ureas via *N*-CF₃ carbomoyl building blocks **61** [88]. After that, the same group developed the transformation of the building blocks and generated non-cyclic or heterocyclic *N*-CF₃ compounds as shown in Scheme 15 [89–92]. Additionally, antihistamine derivative oxatamide analogue **64a** could be generated in 62% in two steps by *N*-H functionalization of **64**.

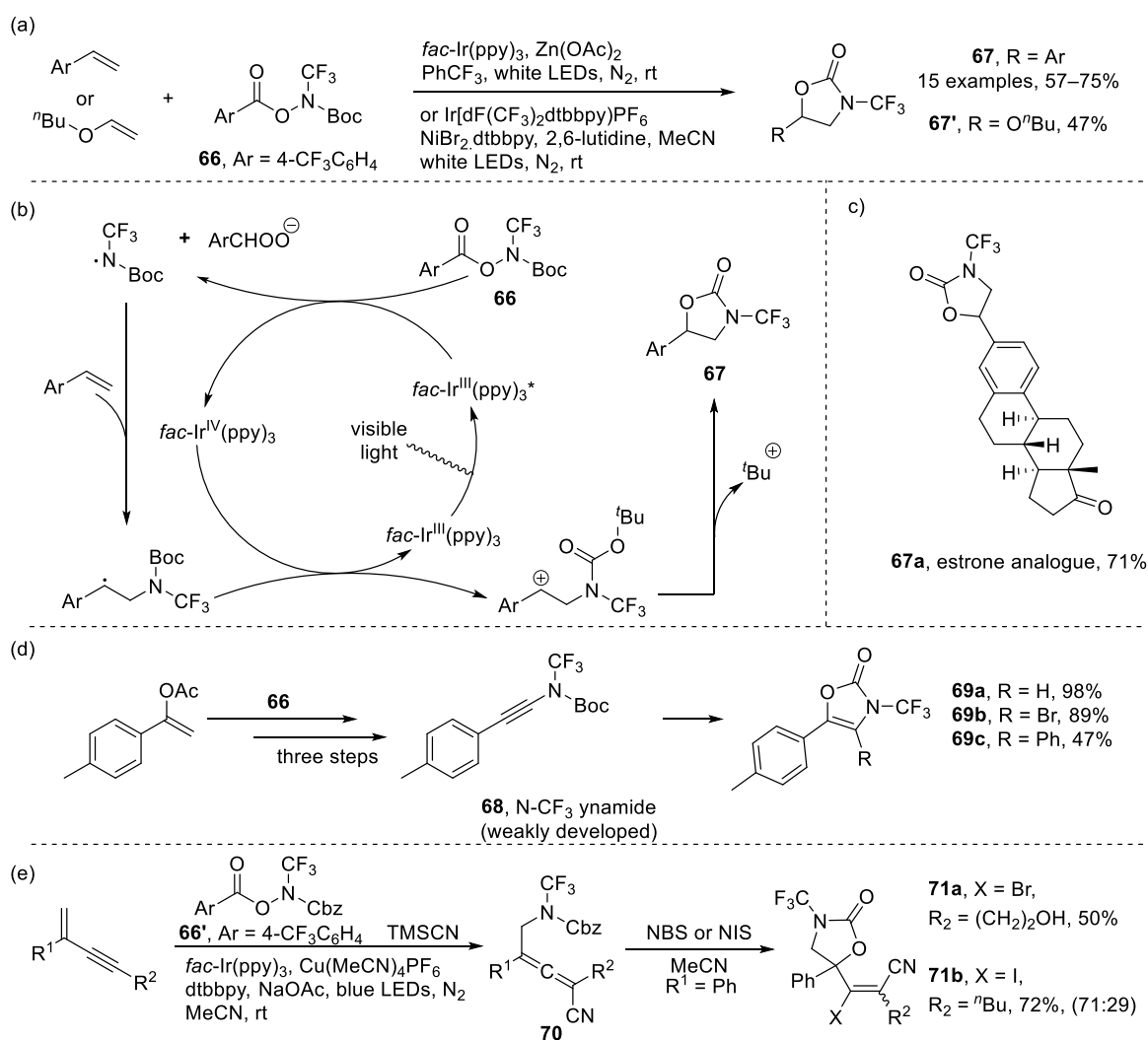
Meanwhile, Huang and Xu et al. reported the design and synthesis of novel *N*-CF₃ hydroxylamine reagents **66** as well as their applications in preparation of *N*-CF₃ compounds [93]. Some oxazolidinones **67** and **67'** could be generated from trifluoromethylamination/cyclization of styrenes or vinyl ether (Scheme 16a). For example, estrone analogue **67a**, could be generated in 71% yield. Furthermore, ynamide **68** could be generated from reagent **66**, which could further form heterocycles **69** via Pd-catalyzed cyclization (Scheme 16d). Subsequently, the same group employed reagent **66'** and trimethylsilyl cyanide to convert 1,3-enynes to trifluoromethylaminated allenes under a photoredox/copper-catalyzed 1,4-difunctionalization, in which allenes **70** could further yield oxazolidinones **71** in the presence of *N*-bromosuccinimide (NBS) or *N*-iodosuccinimide (NIS) (Scheme 16e) [94].



Scheme 14. Synthesis of other *N*-trifluoromethyl heterocycles through cyclization of (a) trifluoromethyl isocyanate, (b) trifluoronitrosomethane, (c) trifluoromethyl isocyanide, and (d) *N*-trifluoromethyl hydrazides.



Scheme 15. Synthesis of diverse *N*-trifluoromethyl heterocycles through *N*-trifluoromethyl carbonyl building blocks.

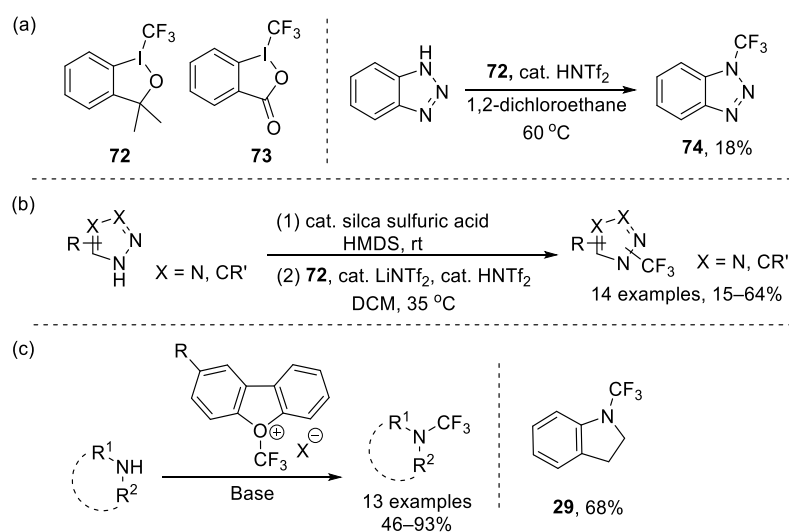


Scheme 16. (a) Synthesis of *N*-trifluoromethyl oxazolidinones through trifluoromethylamination/cyclization of styrenes or vinyl; (b) Proposed reaction mechanism; (c) estrone analogue **67a**; (d) Synthesis of *N*-trifluoromethyl oxazolidinones through trifluoromethylamination of vinyl acetate **66** and further cyclization; (e) Synthesis of oxazolidinones through cyclization of allenes.

4.3. Electrophilic Trifluoromethylation

In 2006, Togni et al. developed two new trifluoromethylation reagents (**72** and **73**) based on hypervalent iodine [95,96]. Subsequently, in 2011, the same group reported a Ritter-type direct electrophilic trifluoromethylation at nitrogen atoms using hypervalent iodine reagent **72** and obtained *N*-CF₃ benzotriazole **74** as a side product (Scheme 17a) [97]. Subsequently, they further refined the method and successfully conducted the trifluoromethylation of a variety of heterocycles (Scheme 17b) [98].

Meanwhile, Umemoto developed diverse derivatives of (trifluoromethyl)dibenzofuranylium that could generate CF₃⁺ anion at a low temperature, which facilitated the electrophilic trifluoromethylation of primary, secondary, or aromatic amines (Scheme 17c) [99]. For example, 1-(trifluoromethyl)indoline could be generated in 68% yield.



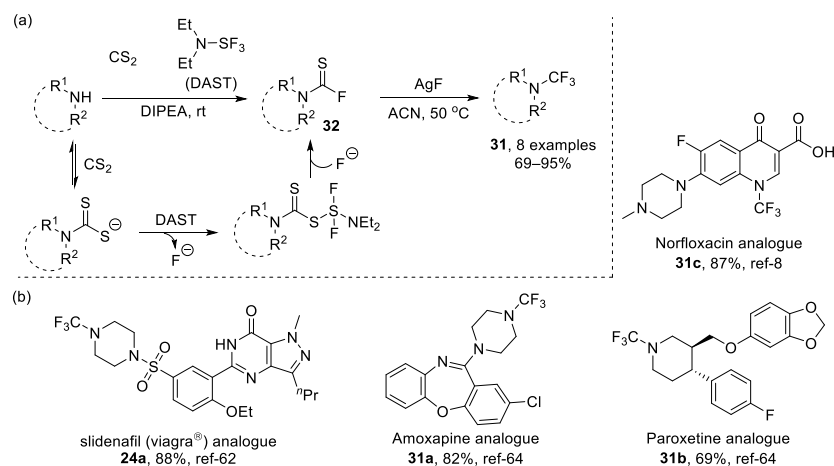
Scheme 17. (a) Togni's reagents and trifluoromethylation of benzotriazole; (b) Synthesis of various five-membered *N*-trifluoromethyl heterocycles through Togni's reagent; (c) Synthesis of trifluoromethyl amines through Umemoto's reagents.

5. Six-Membered Heterocycles

From the existing literature, the synthetic methodologies of six-membered heterocycles were similar to the five-membered heterocycles containing the *N*-CF₃ motif. Therefore, in this section, some examples are shown briefly.

5.1. Nucleophilic Trifluoromethylation

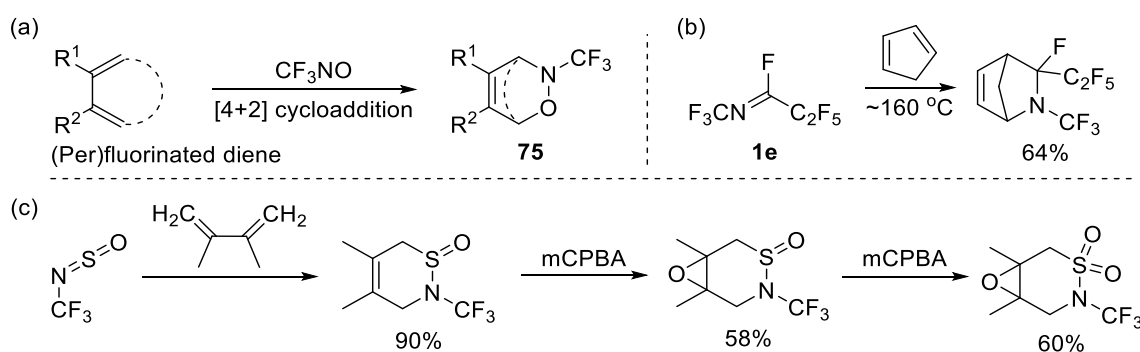
Similarly, oxidative desulfurization and subsequent fluorination was also an efficient way to achieve six-membered heterocycles containing the *N*-CF₃ motif, such as piperazines and piperidines. For example, Tili et al. [100] used carbon disulfide and (diethylamino)sulfur trifluoride (DAST) to generate thiocarbomoyl fluoride intermediate **32**, and then synthesized a series of *N*-CF₃ piperazines. Borbas et al. employed DAST and NBS to generate *N*-CF₃ morpholine while studying *N*-fluoroalkylated nucleoside analogues [101]. In addition to AgF, pyridinium poly(hydrogen fluoride [8] could also be employed for oxidative desulfurization and fluorination to give the product **31c** which exhibited antibacterial activity. These methods allowed the introduction of the CF₃ group into the nitrogen of pharmaceuticals or their analogues, demonstrating the potential of bioactive molecule modification (Scheme 18) [8,62,64].



Scheme 18. (a) Synthesis of thiocarbomoyl fluoride intermediate through DAST and CS₂ and subsequently Oxidative desulfurization and fluorination; (b) examples of drug analogues obtained by Oxidative desulfurization and fluorination.

5.2. [4+2] Cycloaddition

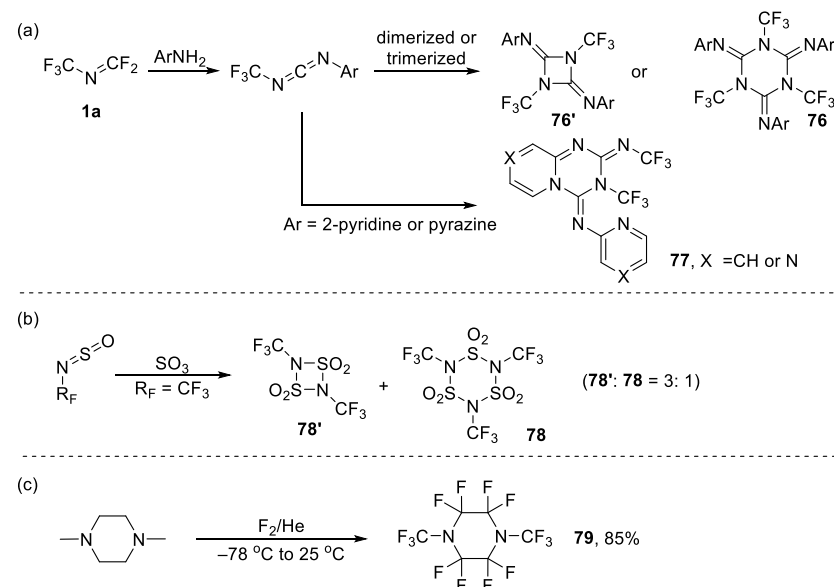
As described in Section 3, CF_3NO could serve as building blocks in cycloaddition. The application of CF_3NO in [4+2] cycloaddition has been investigated [39,102–107], yielding various adducts **75** (Scheme 19a). Carson et al. have studied the nucleophilic displacements of fluorine atoms in perfluoro-1,2-oxazines, in particular amino-defluorination reactions [107]. It was established that perfluoro-(3,6-dihydro-2-methyl-2H-1,2-oxazine) reacted with ammonia at room temperature to give a mixture of 4- and 5-amino derivatives, while when reacted with disubstituted amines in diethyl ester at $-78\text{ }^\circ\text{C}$ it only gave 5-amino compounds. Furthermore, other starting materials featuring $N\text{-CF}_3$ were utilized in [4+2] cycloaddition, as shown in Scheme 19b,c [108,109].



Scheme 19. Synthesis of six-membered N -trifluoromethyl heterocycles through [2+2] cycloaddition: (a) trifluoronitrosomethane with substituted diene; (b) N -trifluoromethyl imines with cyclopentadiene; (c) Trifluoromethyl-substituted N -sulfinylamine with diene and further oxidation.

5.3. Other Approaches

In 1976, Haszeldine et al. reported the formation of triazine via unsymmetrical carbodiimide intermediate, which was subsequently dimerized, trimerized or intramolecular cyclized (Scheme 20a) [110]. Similarly, Mews et al. reported that $\text{R}_F\text{N}=\text{S}=\text{O}$ reacted with SO_3 , leading to the formation of sulfonimide [111]. The degree of oligomer depended on the size of the substituent, and at what time $\text{R}_F = \text{CF}_3$, dimer and trimer were formed in the ratio of 3:1 (Scheme 20b).



Scheme 20. Synthesis of diverse six-membered heterocycles: (a) Dimerization or trimerization of N -trifluoromethyl carbodiimide; (b) Dimerization or trimerization of trifluoromethyl-substituted N -sulfinylamine; (c) direct fluorination of N,N -dimethyl piperidine.

Direct fluorination of hydrocarbons by fluorine gas was indeed also a method used to synthesize the corresponding fluorinated compounds. Lagow et al. reported the synthesis of perfluoro highly-branched heterocyclic fluorine compounds by direct fluorination, and also reported that 1,4-bis(trifluoromethyl)piperazine **79** was highly generated in 85% yield (Scheme 20c) [112].

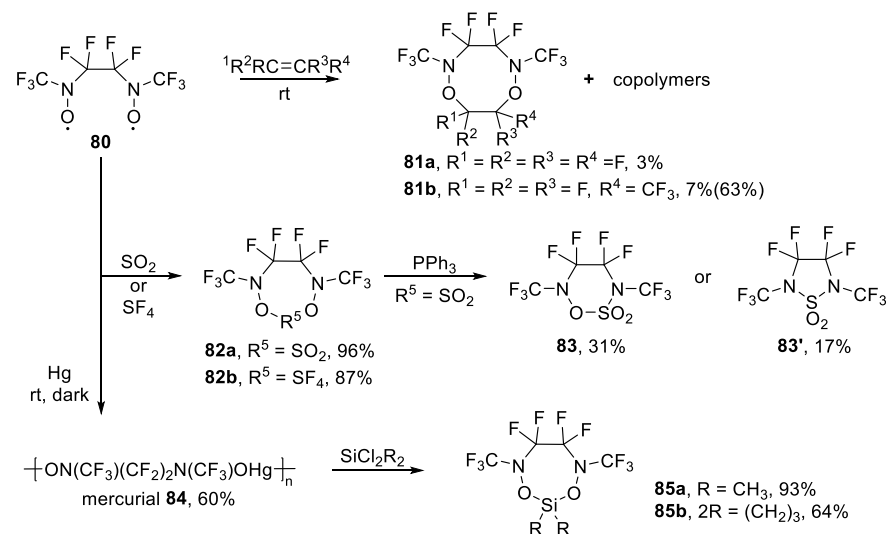
6. Seven- and Larger-Membered Heterocycles

Perfluoro-2,5-diazahexane-2,5-dioxy **80** could readily attack nitric oxide and hydrogen-atom donors, giving adducts, such as its monofunctional analogue, bis-trifluoromethyl nitroxide ((CF₃)₂NO) [113,114], which could readily react with fluoro-olefins. In some cases, the reaction of bis-trifluoromethyl nitroxide with a variable valence element compound led to an increase in the oxidation state of that element.

Banks et al. reported that an attack by dioxy **80** on tetrafluoroethylene or hexafluoropropene led mainly to the formation of copolymers in, and also to a smaller number of adducts (**81a**, **81b**) [115]. It should be noted that the yield of **81b** could rise to 63% if the reactants were mixed at room temperature and at ca. 25 mmHg pressure. In addition, Banks et al. pointed out that the formation of adducts would require a gas-phase reaction [113]. Subsequently, Tipping et al. investigated the scope of the cycloadduct formation by using fluoroalkenes and a wide variety of hydrogen-containing alkenes [116]. Their report clearly illustrated the limitations of gas-phase reaction. Such reactions must be restricted to simple ethenes or halogenated propenes due to the possibility of hydrogen abstraction occurring.

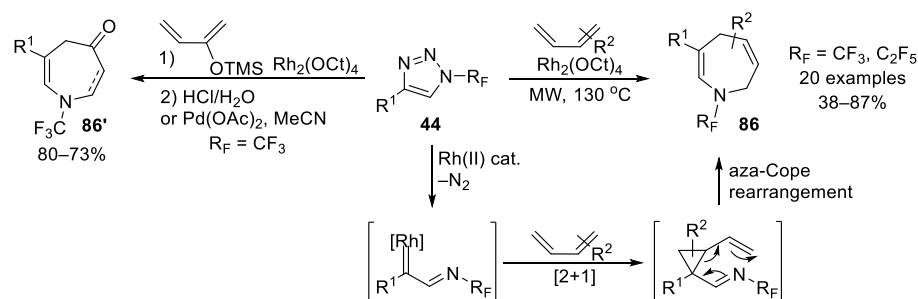
Later, Tipping et al. synthesized mercurial **84** from dioxy **80** and investigated the reaction of mercurial **84** with halogenated alkanes, acid chlorides, and dichlorosilanes [117]. The reaction of mercurial **84** with dichlorodimethylsilane resulted in the formation of silicon-containing heterocycle in 93% yield, while with 1,1-dichlorosilacyclobutane, the spiro compound was isolated in 64% yield. On the other hand, Booth et al. reported that the dioxy **80** could react readily by oxidative addition to [Pt(PPh₃)₄] or [IrCl(CO)L₂] (L = PPh₃, AsPh₃, PMePh₂) to afford the corresponding metal–nitroso complex containing a seven-membered chelate ring [118]. The resulting complexes were stable in air for several days or in N₂ atmosphere for several months.

Meanwhile, Smith et al. reported the reaction of SO₂ and SF₄ with dioxy **80** and obtained two heterocycles **82a** and **82b** (Scheme 21) [119]. In neither case was a copolymer formed, something which differed from the results from the reaction of dioxy **80** with tetrafluoroethylene and hexafluoropropene in a previous report [113]. Compound **82a** slowly reacted with PPh₃ at room temperature giving deoxidation products **83** and **83'**.



Scheme 21. Synthesis of larger-membered *N*-trifluoromethyl heterocycles through addition reaction of dioxy **80** or its mercurial **84**.

Moreover, in 2018, Beier et al. reported another strategy based on *N*-perfluoroalkyl 1,2,3-triazoles (Scheme 22) [120]. A series of then-unknown *N*-perfluoroalkyl azepine derivatives were obtained via the aza-[4+3]-annulation of triazoles **44** with both (*E*)-1-substituted and 2-substituted dienes. When silyloxy-substituted butadiene was employed, *N*-CF₃ azepinone **86'** could be prepared.

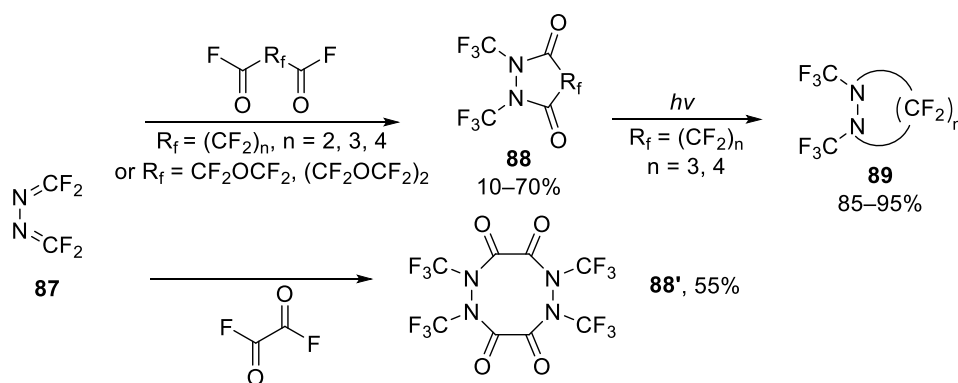


Scheme 22. Synthesis of *N*-trifluoromethyl azepine and azepinone via rhodium-catalyzed annulation of 1,2,3-triazoles.

7. Other Methods

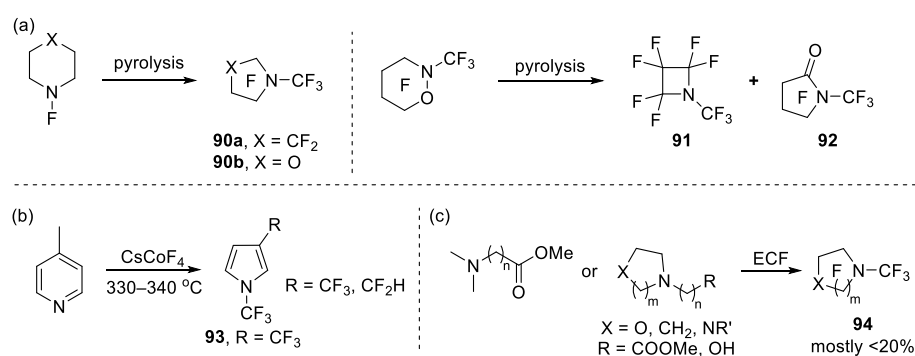
In addition to the methods mentioned above, various other synthetic routes have been explored for the generation of heterocycles containing the *N*-CF₃ motif. However, considering the involvement of multiple cyclic structures in these methods, their classification is challenging. Therefore, these approaches are described in this section.

In 1971, Ogden [121] reported a route to some perfluoroheterocyclic compounds via fluoride ion. In his work, tetrafluoroformaldazine **87** reacted with oxalyl fluoride and other carbonyl fluorides and obtained the heterocycles **88**, which could be further photolysis to smaller heterocycles **89** (Scheme 23).



Scheme 23. Synthesis of perfluoro heterocycles through reaction of tetrafluoroformaldazine with oxalyl fluoride or carbonyl fluoride.

In early organic chemistry, pyrolysis was an effective tool used to study the composition and properties of substances. For example, Banks et al. found that pyrolysis of perfluoropiperidine or perfluoromorpholine led to the generation of *N*-CF₃ pyrrolidine **90a** or *N*-CF₃ oxazolidine **90b**, respectively [102,122–124]. The pyrolysis of perfluorooxazirane in platinum at 480 °C led to the formation of perfluoro-(1-methylazetidene) **91** in 73% yield and trace perfluoro-(1-methyl-2-pyrrolidone) **92**, while at 580 °C/19 mm, the yield of **91** and **92** changed to 48% and 24%, respectively (Scheme 24a).



Scheme 24. Synthesis of diverse *N*-trifluoromethyl heterocycles: (a) pyrolysis of perfluoropiperidine, perfluoromorpholine or perfluorooxazinane; (b) fluorination of 4-methylpyridine in the presence of caesium tetrafluorocobaltate; (c) electrochemical fluorination of various nitrogen-containing materials.

Tatlow et al. investigated the fluorination of 4-methylpyridine in the presence of caesium tetrafluorocobaltate (CsCoF_4) and obtained perfluoro-(1,3-dimethylpyrrolidine) **93** and its analogue, together with a range of (per)fluoro-pyridine bearing CF_3 , CHF_2 , and CH_2F groups (Scheme 24b) [125]. Similar to CsCoF_4 , CoF_3 was a useful reagent for the preparation of a wide array of highly fluorinated organic molecules including open chain/cyclic aliphatics and aromatics. However, the high reactivity of CoF_3 meant that most of these reactions were relatively unselective with poor functional compatibility [126].

In addition, electrochemical fluorination (ECF) was one of the most commonly used methods for the fluorination of nitrogen-containing materials [127]. In the past few decades, many different nitrogen-containing materials [128–133] have been used in the ECF (Scheme 24c), but the yield was generally unsatisfactory (mostly $<20\%$) and side products were inevitable, which limited the scope.

8. Conclusions

Over the last decades, the chemistry of the *N*- CF_3 motif has been weakly developed because of the limited approaches and an incompatibility with functionalized molecules. Very recently, some new simpler, safer, and powerful methods of obtaining this motif have been explored. In general, the existing literature mainly focuses on synthesis, with limited properties or applications. In three-membered heterocycles containing the *N*- CF_3 motif, cycloaddition, reductive defluorination-cyclization, nucleophilic cyclization, and oxidative cyclization can reach the motif. Among them, properties and applications of oxaziridine were reported (oxidant or building blocks [25,34,73,74]), while other three-membered heterocycles were not reported. In four-membered heterocycles, cycloaddition was the predominant approach, while trifluoronitrosomethane was the most common starting material. Similarly, there were limited reports on the applications of four-membered heterocycles containing the *N*- CF_3 motif. In five-membered heterocycles, Scheiesser et al. [45] studied, for example, the stability in aqueous media, lipophilicity and metabolic stability of various *N*- CF_3 amines or azoles, illustrating the potential of the *N*- CF_3 motif in medicinal chemistry. Generally, five-membered heterocycles containing this motif can be synthesized from nucleophilic fluorination, cyclization, and electrophilic trifluoromethylation. Furthermore, *N*-fluoroalkyl 1,2,3-triazoles could serve as the building blocks to access some other *N*-fluoroalkyl heterocycles [78,79,120]. In six-membered heterocycles, the synthetic approaches were similar. In larger-membered heterocycles, the perfluoro-2,5-diazahexane-2,5-dioxyl showed its potential in coordination chemistry. The dioxyl could react readily with $[\text{Pt}(\text{PPh}_3)_4]$ or $[\text{IrCl}(\text{CO})\text{L}_2]$ to form the corresponding metal–nitroso complex containing a seven-membered chelate ring which was stable in air for several days or in N_2 atmosphere for several months [118].

Overall, the literature has concentrated on the synthesis of this motif in recent years, and research investigating its properties or applications is becoming more frequent. We believe that the chemistry of the motif will become more and more clear, thereby extending

its fields of application. We expect that this review will help to inspire the development of new synthetic strategies or the application of certain structures.

Author Contributions: Conceptualization, Z.Z.; writing—original draft preparation, Z.L. and H.G.; writing—review and editing, W.C. and J.F.; visualization, Z.L. and J.F.; supervision, Z.Z. and J.F.; project administration, Z.Z. All authors have read and agreed to the published version of the manuscript.

Funding: This research was funded by [National Key Research and Development Program of China] grant number [2022YFD1700302] and [2115 Talent Development Program of China Agricultural University] grant number [201324].

Institutional Review Board Statement: Not applicable.

Informed Consent Statement: Not applicable.

Data Availability Statement: Not applicable.

Conflicts of Interest: The authors declare no conflict of interest.

References

- Zhou, Y.; Wang, J.; Gu, Z.; Wang, S.; Zhu, W.; Acena, J.L.; Soloshonok, V.A.; Izawa, K.; Liu, H. Next Generation of Fluorine-Containing Pharmaceuticals, Compounds Currently in Phase II-III Clinical Trials of Major Pharmaceutical Companies: New Structural Trends and Therapeutic Areas. *Chem. Rev.* **2016**, *116*, 422–518. [CrossRef] [PubMed]
- Purser, S.; Moore, P.R.; Swallow, S.; Gouverneur, V. Fluorine in medicinal chemistry. *Chem. Soc. Rev.* **2008**, *37*, 320–330. [CrossRef] [PubMed]
- Tomashenko, O.A.; Grushin, V.V. Aromatic trifluoromethylation with metal complexes. *Chem. Rev.* **2011**, *111*, 4475–4521. [CrossRef]
- Besset, T.; Schneider, C.; Cahard, D. Tamed Arene and Heteroarene Trifluoromethylation. *Angew. Chem. Int. Ed.* **2012**, *51*, 5048–5050. [CrossRef]
- Vitaku, E.; Smith, D.T.; Njardarson, J.T. Analysis of the Structural Diversity, Substitution Patterns, and Frequency of Nitrogen Heterocycles among U.S. FDA Approved Pharmaceuticals. *J. Med. Chem.* **2014**, *57*, 10257–10274. [CrossRef]
- Matiadis, D.; Sagnou, M. Pyrazoline hybrids as promising anticancer agents: An up-to-date overview. *Int. J. Mol. Sci.* **2020**, *21*, 5507. [CrossRef]
- Prasher, P.; Sharma, M.; Zacconi, F.; Gupta, G.; Aljabali, A.A.A.; Mishra, V.; Tambuwala, M.M.; Kapoor, D.N.; Negi, P.; de Jesus Andreoli Pinto, T.; et al. Synthesis and Anticancer Properties of ‘Azole’ Based Chemotherapeutics as Emerging Chemical Moieties: A Comprehensive Review. *Curr. Org. Chem.* **2021**, *25*, 654–668.
- Asahina, Y.; Araya, I.; Iwase, K.; Inuma, F.; Hosaka, M.; Ishizaki, T. Synthesis and antibacterial activity of the 4-quinolone-3-carboxylic acid derivatives having a trifluoromethyl group as a novel N-1 substituent. *J. Med. Chem.* **2005**, *48*, 3443–3446. [CrossRef]
- Schow, S.R.; Mackman, R.L.; Blum, C.L.; Brooks, E.; Horsma, A.G.; Joly, A.; Kerwar, S.S.; Lee, G.; Shiffman, D.; Nelson, M.G.; et al. Synthesis and activity of 2,6,9-trisubstituted purines. *Bioorg. Med. Chem. Lett.* **1997**, *7*, 2697–2702. [CrossRef]
- Samadder, P.; Suchankova, T.; Hylse, O.; Khirsariya, P.; Nikulenkov, F.; Drapela, S.; Strakova, N.; Vanhara, P.; Vasickova, K.; Kolarova, H.; et al. Synthesis and Profiling of a Novel Potent Selective Inhibitor of CHK1 Kinase Possessing Unusual N-trifluoromethylpyrazole Pharmacophore Resistant to Metabolic N-dealkylation. *Mol. Cancer Ther.* **2017**, *16*, 1831–1842. [CrossRef]
- Gahman, T.C.; Thomas, D.J.; Lang, H.; Massari, M.E. Aminoquinazoline Cannabinoid Receptor Modulators for Treatment of Disease and Their Preparation. U.S. Patent WO2008157500 A1, 24 December 2008.
- Miura, T.; Tamatani, Y. Preparation of a Methylactam Ring Compound and Its Medicinal Uses. U.S. Patent WO2019168096 A1, 6 September 2019.
- Scattolin, T.; Bortolamiol, E.; Visentin, F.; Palazzolo, S.; Caligiuri, I.; Perin, T.; Canzonieri, V.; Demitri, N.; Rizzolio, F.; Togni, A. Palladium(II)- η^3 -Allyl Complexes Bearing N-Trifluoromethyl N-Heterocyclic Carbenes: A New Generation of Anticancer Agents that Restrain the Growth of High-Grade Serous Ovarian Cancer Tumors. *Chem.-Eur. J.* **2020**, *26*, 11868–11876. [CrossRef] [PubMed]
- Leroux, F.; Jeschke, P.; Schlosser, M. α -Fluorinated Ethers, Thioethers, and Amines: Anomerically Biased Species. *Chem. Rev.* **2005**, *105*, 827–856. [CrossRef] [PubMed]
- Liang, T.; Neumann, C.N.; Ritter, T. Introduction of Fluorine and Fluorine-Containing Functional Groups. *Angew. Chem. Int. Ed.* **2013**, *52*, 8214–8264. [CrossRef]
- Milcent, T.; Crousse, B. The main and recent syntheses of the N-CF₃ motif. *C. R. Chim.* **2018**, *21*, 771–781. [CrossRef]
- Logothetis, A.L. Aziridines from diazomethane and fluorine-substituted imines. *J. Org. Chem.* **1964**, *29*, 3049–3052. [CrossRef]
- Coe, P.L.; Holton, A.G. Some reactions of diazomethane with polyfluoroazolefins. *J. Fluor. Chem.* **1977**, *10*, 553–564. [CrossRef]

19. Kaupp, G.; Dengler, O.; Burger, K.; Rottegger, S. Stable triaziridines. *Angew. Chem.* **1985**, *97*, 341–342. [CrossRef]
20. Mitsch, R.A. Organic fluoronitrogens. X. Reductive defluorination-cyclization. *J. Org. Chem.* **1968**, *33*, 1847–1849. [CrossRef]
21. Chang, S.C.; Desmarteau, D.D. Perfluoromethanimine ion. *Polyhedron* **1982**, *1*, 129–130. [CrossRef]
22. Zheng, Y.Y.; Bauknight, C.W., Jr.; DesMarteau, D.D. Some novel reactions of N-chlorodifluoromethanimine. *J. Org. Chem.* **1984**, *49*, 3590–3595. [CrossRef]
23. Bauknight, C.W., Jr.; DesMarteau, D.D. Reactions of N-bromodifluoromethanimine. *J. Org. Chem.* **1988**, *53*, 4443–4447. [CrossRef]
24. Bauknight, C.W., Jr.; DesMarteau, D.D. Fluoride-promoted competitive reactions of cyanogen fluoride, perfluoromethanimine, and pentafluoro-2-azapropene. *J. Am. Chem. Soc.* **1990**, *112*, 728–733. [CrossRef]
25. Petrov, V.A.; Resnati, G. Polyfluorinated Oxaziridines: Synthesis and Reactivity. *Chem. Rev.* **1996**, *96*, 1809–1823. [CrossRef] [PubMed]
26. Falardeau, E.R.; DesMarteau, D.D. Direct synthesis of fluorinated peroxides. 6. The addition of fluorinated hydroperoxides to perfluoro-2-azapropene and the preparation of the first perfluorooxazirine. *J. Am. Chem. Soc.* **1976**, *98*, 3529–3532. [CrossRef]
27. Sekiya, A.; DesMarteau, D.D. Reaction of metal fluorides with $\text{CF}_3\text{OOCF}_2\text{N(H)CF}_3$. *Inorg. Chem.* **1979**, *18*, 919–920. [CrossRef]
28. Navarrini, W.; Desmarteau, D.D. Preparation of Perfluoroalkylaminooxaziridines as Monomers and Intermediates for Nitrons and Photopolymerization Initiators. U.S. Patent US4874875 A, 17 October 1989.
29. Ratcliffe, C.T. Epoxides. U.S. Patent US4287128 A, 1 September 1981.
30. Petrov, V.A.; DesMarteau, D.D. A new method for the synthesis of perfluorooxaziridines. Preparation of perfluoro-cis-2,3-dialkyloxaziridines. *J. Org. Chem.* **1993**, *58*, 4754–4755. [CrossRef]
31. Mlsna, T.E.; Young, J.A.; DesMarteau, D.D. Synthesis and chemistry of novel perhalogenated imines, oxaziridines, and oxazolines. *Z. Anorg. Allg. Chem.* **2002**, *628*, 1789–1793. [CrossRef]
32. Sekiya, A.; Desmarteau, D.D. The reaction of 2-(trifluoromethyl)-3,3-difluorooxaziridine with nucleophiles. *J. Fluor. Chem.* **1979**, *14*, 289–297. [CrossRef]
33. Sekiya, A.; DesMarteau, D.D. Reaction of 2-trifluoromethyl-3,3-difluorooxaziridine with some fluorinated nucleophiles. *J. Org. Chem.* **1979**, *44*, 1131–1133. [CrossRef]
34. Bragante, L.; Desmarteau, D.D. The chemistry of 3-(trifluoromethyl)perfluoroaza-2-butene and the synthesis of a new oxaziridine: 3,3-bis(trifluoromethyl)-2-(trifluoromethyl)oxaziridine. *J. Fluor. Chem.* **1991**, *53*, 181–197. [CrossRef]
35. Barr, D.A.; Haszeldine, R.N. Perfluoroalkyl derivatives of nitrogen. I. Perfluoro-2-methyl-1,2-oxazetidine and perfluoro (alkylene alkylamines). *J. Chem. Soc.* **1955**, 1881–1889. [CrossRef]
36. Barr, D.A.; Haszeldine, R.N. Perfluoroalkyl derivatives of nitrogen. III. Heptafluoronitrosopropane, perfluoro-2-n-propyl-1,2-oxazetidine, perfluoro(methylene-n-propylamine), and related compounds. *J. Chem. Soc.* **1956**, 3416–3428. [CrossRef]
37. Barr, D.A.; Haszeldine, R.N.; Willis, C.J. Perfluoroalkyl derivatives of nitrogen. IX. Reaction of trifluoronitrosomethane with some unsymmetrical olefins. *J. Chem. Soc.* **1961**, 1351–1362. [CrossRef]
38. Banks, R.E.; Haszeldine, R.N.; Sutcliffe, H.; Willis, C.J. Perfluoroalkyl derivatives of nitrogen. XV. The reaction of trifluoronitrosomethane with trifluoroethylene, vinylidene fluoride, vinyl fluoride, and ethylene. *J. Chem. Soc.* **1965**, 2506–2513. [CrossRef]
39. Banks, R.E.; Haszeldine, R.N.; Taylor, D.R. Polyhaloallenes. II. Reaction of tetrafluoroallene with trifluoronitrosomethane. *J. Chem. Soc.* **1965**, 5602–5612. [CrossRef]
40. Coy, D.H.; Haszeldine, R.N.; Newlands, M.J.; Tipping, A.E. Poly(bistrifluoromethylamino)-compounds. Synthesis of NN-bistrifluoromethylamino-substituted allenes and their reaction with trifluoronitrosomethane. *J. Chem. Soc. D* **1970**, 456–457. [CrossRef]
41. Coy, D.H.; Haszeldine, R.N.; Newlands, M.J.; Tipping, A.E. Polyfluoroalkyl derivatives of nitrogen. XL. Reaction of trifluoronitrosomethane with NN-bis(trifluoromethyl)amino-substituted allenes. *J. Chem. Soc. Perkin Trans. 1* **1973**, 1561–1564. [CrossRef]
42. Jaeger, U.; Schwab, M.; Sundermeyer, W. Fluorine-substituted 1,2-thiazetan-3-one 1-oxides by reaction of bis(trifluoromethyl)ketene and N-sulfinylamines. *Chem. Ber.* **1986**, *119*, 1127–1132. [CrossRef]
43. Ansorge, A.; Brauer, D.J.; Buerger, H.; Doerrenbach, F.; Hagen, T.; Pawelke, G.; Weuter, W. [2+2]-Cycloaddition reactions of (dialkylamino)bis(trifluoromethyl)boranes with isocyanates and isothiocyanates. Crystal structures of cyclic compounds $(\text{CF}_3)_2\text{BNMe}_2\text{CONtBu}$, $(\text{CF}_3)_2\text{BNMe}_2\text{CSNtBu}$, $(\text{CF}_3)_2\text{BNPhC(NMe}_2)_2\text{S}$ and $(\text{CF}_3)_2\text{BNMeC(NEt}_2)_2\text{OCONMe}$. *J. Organomet. Chem.* **1991**, *407*, 283–300. [CrossRef]
44. Meanwell, N.A. Fluorine and Fluorinated Motifs in the Design and Application of Bioisosteres for Drug Design. *J. Med. Chem.* **2018**, *61*, 5822–5880. [CrossRef]
45. Schiesser, S.; Chepliaka, H.; Kollback, J.; Quennesson, T.; Czechtizky, W.; Cox, R.J. N-Trifluoromethyl Amines and Azoles: An Underexplored Functional Group in the Medicinal Chemist’s Toolbox. *J. Med. Chem.* **2020**, *63*, 13076–13089. [CrossRef] [PubMed]
46. Kubo, O.; Takami, K.; Kamaura, M.; Watanabe, K.; Miyashita, H.; Abe, S.; Matsuda, K.; Tsujihata, Y.; Odani, T.; Iwasaki, S.; et al. Discovery of a novel series of GPR119 agonists: Design, synthesis, and biological evaluation of N-(Piperidin-4-yl)-N-(trifluoromethyl)pyrimidin-4-amine derivatives. *Bioorg. Med. Chem.* **2021**, *41*, 116208–116220. [CrossRef] [PubMed]

47. Yang, B.; Hird, A.W.; Russell, D.J.; Fauber, B.P.; Dakin, L.A.; Zheng, X.; Su, Q.; Godin, R.; Brassil, P.; Devereaux, E.; et al. Discovery of novel hedgehog antagonists from cell-based screening: Isosteric modification of p38 bisamides as potent inhibitors of SMO. *Bioorg. Med. Chem. Lett.* **2012**, *22*, 4907–4911. [CrossRef] [PubMed]
48. Dakin, L.; Fauber, B.; Hird, A.; Janetka, J.; Russell, D.J.; Su, Q.; Yang, B.; Zheng, X.L. Preparation of Amide Compounds Containing Heterocycle Moiety as Hedgehog Pathway Inhibitors. U.S. Patent WO2009027746 A1, 5 March 2009.
49. Schiffmann, R.; Neugebauer, A.; Klein, C.D. Metal-mediated inhibition of Escherichia coli methionine aminopeptidase: Structure-activity relationships and development of a novel scoring function for metal-ligand interactions. *J. Med. Chem.* **2006**, *49*, 511–522. [CrossRef]
50. Romero, D.; Robinson, S.; Greenwood, J.R. Preparation of IRAK Inhibitors and Their Uses in the Treatment of Diseases and Disorders. U.S. Patent WO2017004134 A1, 5 January 2017.
51. Goetz, G.H.; Farrell, W.; Shalaeva, M.; Sciabola, S.; Anderson, D.; Yan, J.; Philippe, L.; Shapiro, M.J. High Throughput Method for the Indirect Detection of Intramolecular Hydrogen Bonding. *J. Med. Chem.* **2014**, *57*, 2920–2929. [CrossRef]
52. Goetz, G.H.; Philippe, L.; Shapiro, M.J. EPSA: A Novel Supercritical Fluid Chromatography Technique Enabling the Design of Permeable Cyclic Peptides. *ACS Med. Chem. Lett.* **2014**, *5*, 1167–1172. [CrossRef]
53. Yagupolskii, L.M.; Fedyuk, D.V.; Petko, K.I.; Troitskaya, V.I.; Rudyk, V.I.; Rudyuk, V.V. N-Trihalomethyl derivatives of benzimidazole, benzotriazole and indazole. *J. Fluor. Chem.* **2000**, *106*, 181–187. [CrossRef]
54. Sokolenko, T.M.; Petko, K.I.; Yagupolskii, L.M. N-trifluoromethylazoles. *Chem. Heterocycl. Compd.* **2009**, *45*, 430–435. [CrossRef]
55. Morimoto, K.; Makino, K.; Yamamoto, S.; Sakata, G. Synthesis of fluoromethyl, difluoromethyl and trifluoromethyl analogs of pyrazosulfuron-ethyl as herbicides. *J. Heterocycl. Chem.* **1990**, *27*, 807–810. [CrossRef]
56. Burkholder, J.B.; Wilson, R.R.; Gierczak, T.; Talukdar, R.; McKeen, S.A.; Orlando, J.J.; Vaghjiani, G.L.; Ravishankara, A.R. Atmospheric fate of CF₃Br, CF₂Br₂, CF₂ClBr, and CF₂BrCF₂Br. *J. Geophys. Res. Atmos.* **1991**, *96*, 5025–5043. [CrossRef]
57. Dmowski, W.; Kaminski, M. Reaction of tertiary formamides with sulfur tetrafluoride. Direct synthesis of (trifluoromethyl)amines. *J. Fluor. Chem.* **1983**, *23*, 207–218. [CrossRef]
58. Boswell, G.A., Jr.; Ripka, W.C.; Scribner, R.M.; Tullock, C.W. Fluorination by sulfur tetrafluoride. *Org. React.* **1974**, *21*, 1–124.
59. Kuroboshi, M.; Hiyama, T. A facile synthesis of trifluoromethylamines by oxidative desulfurization-fluorination of dithiocarbamates. *Tetrahedron Lett.* **1992**, *33*, 4177–4178. [CrossRef]
60. Schaub, S.; Becker, J.; Schindler, S. A Facile and Inexpensive Way to Synthesize N-trifluoromethyl Compounds. *ChemistrySelect* **2022**, *7*, e202201803. [CrossRef]
61. Hagooly, Y.; Gatenyo, J.; Hagooly, A.; Rozen, S. Toward the Synthesis of the Rare N-(Trifluoromethyl)amides and the N-(Difluoromethylene)-N-(trifluoromethyl)amines [RN(CF₃)CF₂R'] Using BrF₃. *J. Org. Chem.* **2009**, *74*, 8578–8582. [CrossRef]
62. Scattolin, T.; Deckers, K.; Schoenebeck, F. Efficient Synthesis of Trifluoromethyl Amines through a Formal Umpolung Strategy from the Bench-Stable Precursor (Me₄N)SCF₃. *Angew. Chem. Int. Ed.* **2017**, *56*, 221–224. [CrossRef]
63. Yu, J.; Lin, J.-H.; Xiao, J.-C. Reaction of Thiocarbonyl Fluoride Generated from Difluorocarbene with Amines. *Angew. Chem. Int. Ed.* **2017**, *56*, 16669–16673. [CrossRef] [PubMed]
64. Liang, S.; Wei, J.; Jiang, L.; Liu, J.; Mumtaz, Y.; Yi, W. One-pot synthesis of trifluoromethyl amines and perfluoroalkyl amines with CF₃SO₂Na and RfSO₂Na. *Chem. Commun.* **2019**, *55*, 8536–8539. [CrossRef] [PubMed]
65. Miller, W.T., Jr.; Frass, W.; Resnick, P.R. Cesium fluoride catalyzed rearrangement of perfluorodienes to perfluorodialkylacetylenes. *J. Am. Chem. Soc.* **1961**, *83*, 1767–1768. [CrossRef]
66. Ogden, P.H.; Mitsch, R.A. Isomerization of perfluoro- α , ω -bisazomethines. *J. Am. Chem. Soc.* **1967**, *89*, 5007–5011. [CrossRef]
67. Scholl, H.J.; Klauke, E.; Lauerer, D. Azomethines. I. Fluorination of tetrachloroethane-1,2-bisocyanide dichloride. *J. Fluor. Chem.* **1973**, *2*, 203–204. [CrossRef]
68. Scholl, H.J.; Klauke, E.; Lauerer, D. Azomethines. II. New synthesis of perfluoro-2,5-diazahexa-2,4-diene and its dimerization. *J. Fluor. Chem.* **1973**, *2*, 205–206. [CrossRef]
69. Barnes, R.N.; Chambers, R.D.; Silvester, M.J.; Hewitt, C.D.; Klauke, E. Reactions involving fluoride ion. Part 28. Cyclization and formation of dimers from perfluoro-2,5-diazahexa-2,4-diene. *J. Fluor. Chem.* **1984**, *24*, 211–218. [CrossRef]
70. Barnes, R.N.; Chambers, R.D.; Hewitt, C.D.; Silvester, M.J.; Klauke, E. Reaction involving fluoride ion. Part 31. Cooligomers of perfluoro-1-methyl-1,3-diazacyclopent-2- and -3-ene. *J. Chem. Soc. Perkin Trans. 1* **1985**, 53–56. [CrossRef]
71. Chambers, R.D.; Hewitt, C.D.; Silvester, M.J.; Klauke, E. Reactions involving fluoride ion. Part 33. Perfluoroaza-alkylation of fluorinated heteroaromatics with perfluoro-1-methyl-1,3-diazacyclopent-2- and -3-ene. *J. Fluor. Chem.* **1986**, *32*, 389–402. [CrossRef]
72. Pawelke, G.; Buerger, H.; Brauer, D.J.; Wilke, J. Fluorination with concomitant cyclization of Cl₂C=NCCl₂CCl₂N=CCl₂ with antimony pentafluoride and molecular structure of a 2-imidazolidinone derivative. *J. Fluor. Chem.* **1987**, *36*, 185–194. [CrossRef]
73. Lam, W.Y.; DesMarteau, D.D. Unusual cycloaddition reactions with 2-(trifluoromethyl)-3,3-difluorooxaziridine. *J. Am. Chem. Soc.* **1982**, *104*, 4034–4035. [CrossRef]
74. O'Brien, B.A.; Lam, W.Y.; DesMarteau, D.D. Cycloaddition and oxygen-transfer reactions of 2-(trifluoromethyl)-3,3-difluorooxaziridine. *J. Org. Chem.* **1986**, *51*, 4466–4470. [CrossRef]
75. Zhang, Z.; Zhou, Q.; Ye, F.; Xia, Y.; Wu, G.; Hossain, M.L.; Zhang, Y.; Wang, J. Copper(I)-Catalyzed Three-Component Coupling of N-Tosylhydrazones, Alkynes and Azides: Synthesis of Trisubstituted 1,2,3-Triazoles. *Adv. Synth. Catal.* **2015**, *357*, 2277–2286. [CrossRef]

76. Blastik, Z.E.; Voltrova, S.; Matousek, V.; Jurasek, B.; Manley, D.W.; Klepetarova, B.; Beier, P. Azidoperfluoroalkanes: Synthesis and Application in Copper(I)-Catalyzed Azide-Alkyne Cycloaddition. *Angew. Chem. Int. Ed.* **2017**, *56*, 346–349. [CrossRef]
77. Blastik, Z.E.; Klepetarova, B.; Beier, P. Enamine-Mediated Azide-Ketone [3+2] Cycloaddition of Azidoperfluoroalkanes. *ChemistrySelect* **2018**, *3*, 7045–7048. [CrossRef]
78. Motornov, V.; Markos, A.; Beier, P. A rhodium-catalyzed transannulation of N-(per)fluoroalkyl-1,2,3-triazoles under microwave conditions—A general route to N-(per)fluoroalkyl-substituted five-membered heterocycles. *Chem. Commun.* **2018**, *54*, 3258–3261. [CrossRef] [PubMed]
79. Bakhanovich, O.; Khutorianskyi, V.; Motornov, V.; Beier, P. Synthesis of N-perfluoroalkyl-3,4-disubstituted pyrroles by rhodium-catalyzed transannulation of N-fluoroalkyl-1,2,3-triazoles with terminal alkynes. *Beilstein J. Org. Chem.* **2021**, *17*, 504–510. [CrossRef] [PubMed]
80. Zhang, R.Z.; Zhang, R.X.; Wang, S.; Xu, C.; Guan, W.; Wang, M. An N-Trifluoromethylation/Cyclization Strategy for Accessing Diverse N-Trifluoromethyl Azoles from Nitriles and 1,3-Dipoles. *Angew. Chem. Int. Ed.* **2022**, *61*, e202110749.
81. Zhang, R.Z.; Huang, W.; Zhang, R.X.; Xu, C.; Wang, M. Synthesis of N-CF₃ Amidines/Imidates/Thioimidates via N-CF₃ Nitrilium Ions. *Org. Lett.* **2022**, *24*, 2393–2398. [CrossRef]
82. Liu, X.; Wang, S.; Gao, C.; Guan, W.; Wang, M. Reassembly and functionalization of N-CF₃ pyridinium salts: Synthesis of nicotinaldehydes. *Org. Chem. Front.* **2022**, *9*, 4549–4553. [CrossRef]
83. Lutz, W.; Sundermeyer, W. Synthesis and reactions of trifluoromethyl isocyanate. *Chem. Ber.* **1979**, *112*, 2158–2166. [CrossRef]
84. Varwig, J.; Mews, R. Synthesis of a stable 1,3,4-dioxazolidine. *Angew. Chem.* **1977**, *89*, 675. [CrossRef]
85. Lentz, D.; Bruedgam, I.; Hartl, H. Trifluoromethyl isocyanide as a building block in synthesis. Reaction with trifluoroacetic acid and hexafluoroacetone. *Angew. Chem. Int. Ed. Engl.* **1987**, *99*, 921–923. [CrossRef]
86. Lentz, D.; Marschall, R. Cycloaddition reactions of trifluoromethyl isocyanide with diphosphenes. Synthesis and structure of the new 2-phosphinidene-1,3-azaphospholidine derivative Mes*P=CN(CF₃)C(=NCF₃)C(=NCF₃)-PMes*. *Z. Anorg. Allg. Chem.* **1992**, *617*, 53–58. [CrossRef]
87. Cao, T.; Retailleau, P.; Milcent, T.; Crousse, B. Synthesis of N-CF₃ hydrazines through radical trifluoromethylation of azodicarboxylates. *Chem. Commun.* **2021**, *57*, 10351–10354. [CrossRef]
88. Scattolin, T.; Bouayad-Gervais, S.; Schoenebeck, F. Straightforward access to N-trifluoromethyl amides, carbamates, thiocarbamates and ureas. *Nature* **2019**, *573*, 102–107. [CrossRef]
89. Bouayad-Gervais, S.; Scattolin, T.; Schoenebeck, F. N-Trifluoromethyl Hydrazines, Indoles and Their Derivatives. *Angew. Chem. Int. Ed.* **2020**, *59*, 11908–11912. [CrossRef] [PubMed]
90. Nielsen, C.D.T.; Zivkovic, F.G.; Schoenebeck, F. Synthesis of N-CF₃ Alkynamides and Derivatives Enabled by Ni-Catalyzed Alkynylation of N-CF₃ Carbamoyl Fluorides. *J. Am. Chem. Soc.* **2021**, *143*, 13029–13033. [CrossRef] [PubMed]
91. Bouayad-Gervais, S.; Nielsen, C.D.T.; Turksoy, A.; Sperger, T.; Deckers, K.; Schoenebeck, F. Access to Cyclic N-Trifluoromethyl Ureas through Photocatalytic Activation of Carbamoyl Azides. *J. Am. Chem. Soc.* **2022**, *144*, 6100–6106. [CrossRef]
92. Turksoy, A.; Bouayad-Gervais, S.; Schoenebeck, F. N-CF₃ Imidazolidin-2-one Derivatives via Photocatalytic and Silver-Catalyzed Cyclizations. *Chem.-Eur. J.* **2022**, *28*, e202201435. [CrossRef] [PubMed]
93. Liu, S.; Huang, Y.; Wang, J.; Qing, F.-L.; Xu, X.-H. General Synthesis of N-Trifluoromethyl Compounds with N-Trifluoromethyl Hydroxylamine Reagents. *J. Am. Chem. Soc.* **2022**, *144*, 1962–1970. [CrossRef] [PubMed]
94. Liu, S.; Huang, Y.; Qing, F.-L.; Xu, X.-H. Photoredox/Copper-Catalyzed Trifluoromethylamino-Cyanation of 1,3-Enynes. *Eur. J. Org. Chem.* **2023**, *26*, e202201061. [CrossRef]
95. Eisenberger, P.; Gischig, S.; Togni, A. Novel 10-I-3 hypervalent iodine-based compounds for electrophilic trifluoromethylation. *Chem.-Eur. J.* **2006**, *12*, 2579–2586. [CrossRef]
96. Eisenberger, P. The Development of New Hypervalent iodine Reagents for Electrophilic Trifluoromethylation. Ph.D. Thesis, Swiss Federal Institute of Technology, Zürich, Switzerland, 2007.
97. Niedermann, K.; Frueh, N.; Vinogradova, E.; Wiehn, M.S.; Moreno, A.; Togni, A. A Ritter-type reaction: Direct electrophilic trifluoromethylation at nitrogen atoms using hypervalent iodine reagents. *Angew. Chem. Int. Ed.* **2011**, *50*, 1059–1063. [CrossRef]
98. Niedermann, K.; Frueh, N.; Senn, R.; Czarniecki, B.; Verel, R.; Togni, A. Direct Electrophilic N-Trifluoromethylation of Azoles by a Hypervalent Iodine Reagent. *Angew. Chem. Int. Ed.* **2012**, *51*, 6511–6515. [CrossRef] [PubMed]
99. Umemoto, T.; Adachi, K.; Ishihara, S. CF₃ Oxonium Salts, O-(Trifluoromethyl)dibenzofuranium Salts: In Situ Synthesis, Properties, and Application as a Real CF₃⁺ Species Reagent. *J. Org. Chem.* **2007**, *72*, 6905–6917. [CrossRef] [PubMed]
100. Onida, K.; Vanoye, L.; Tlili, A. Direct Synthesis of Thiocarbamoyl Fluorides and Trifluoromethylamines Through Fluorinative Desulfurization. *Eur. J. Org. Chem.* **2019**, *2019*, 6106–6109. [CrossRef]
101. Debreczeni, N.; Hotzi, J.; Bege, M.; Lovas, M.; Mezo, E.; Bereczki, I.; Herczegh, P.; Kiss, L.; Borbas, A. N-Fluoroalkylated Morpholinos—A New Class of Nucleoside Analogues. *Chem.-Eur. J.* **2023**, *29*, e202203248. [CrossRef] [PubMed]
102. Banks, R.E.; Barlow, M.G.; Haszeldine, R.N. Perfluoroalkyl derivatives of nitrogen. XVIII. Reaction of trifluoronitrosomethane with perfluorobutadiene and 3,4-dichlorohexafluorobut-1-ene. *J. Chem. Soc.* **1965**, 6149–6163. [CrossRef]
103. Banks, R.E.; Barlow, M.G.; Haszeldine, R.N. Perfluoroalkyl derivatives of nitrogen. XVI. Reaction of trifluoronitrosomethane with butadiene and with isobutene. *J. Chem. Soc.* **1965**, 4714–4718. [CrossRef]
104. Banks, R.E.; Harrison, A.C.; Haszeldine, R.N.; Orrell, K.G. Polyfluorocyclopentadienes. III. Diels-Alder reactions of perfluorocyclopentadiene. *J. Chem. Soc. C* **1967**, 1608–1621. [CrossRef]

105. Haszeldine, R.N.; Banks, R.E.; Bridge, M.; Roberts, D.W.; Tucker, N.I. Polyfluorocyclopentadienes. VI. Synthesis of 1- and 5-chloropentafluorocyclopentadiene. *J. Chem. Soc. C* **1970**, 2531–2535. [CrossRef]
106. Barlow, M.G.; Haszeldine, R.N.; Murray, K.W. Polyfluoroalkyl derivatives of nitrogen. Part 49. Ene reactions of trifluoronitrosomethane: Formation of N-trifluoromethylhydroxylamines. *J. Chem. Soc. Perkin Trans. 1* **1980**, 1960–1964. [CrossRef]
107. Carson, P.A.; Roberts, D.W. Nucleophilic substitution reactions of the heterocyclic fluoro-olefin perfluoro-(3,6-dihydro-2-methyl-2H-1,2-oxazine). *Tetrahedron* **1986**, *42*, 6495–6510. [CrossRef]
108. Al'bekov, V.A.; Benda, A.F.; Gontar, A.F.; Sokol'skii, G.A.; Knunyants, I.L. [2+4]-Cycloaddition reactions of perfluoroazomethines. *Izv. Akad. Nauk SSSR Ser. Khim.* **1986**, 1437–1440. [CrossRef]
109. Jaeger, U.; Sundermeyer, W. [4+2]-Cycloaddition products of perfluoroorgano-N-sulfinylamines and their oxidation. *Chem. Ber.* **1986**, *119*, 3405–3410. [CrossRef]
110. Flowers, W.T.; Franklin, R.; Haszeldine, R.N.; Perry, R.J. Reaction of amines with perfluoroazapropene: Formation of the novel 4H-pyrido [1,2-a]-s-triazine system via unsymmetrical carbodi-imides. *J. Chem. Soc. Chem. Commun.* **1976**, 567–568. [CrossRef]
111. Tesky, F.M.; Mews, R. 1,1,3,3-Tetraoxo-2,4-bis(perfluoroalkyl)cyclodiazal- λ^6 -thianes (RfNSO₂)₂. *Chem.-Ztg.* **1987**, *111*, 345–346.
112. Lin, W.H.; Lagow, R.J. The synthesis of perfluoro highly branched heterocyclic fluorine compounds by direct fluorination. *J. Fluor. Chem.* **1990**, *50*, 15–30. [CrossRef]
113. Banks, R.E.; Eapen, K.C.; Haszeldine, R.N.; Holt, A.V.; Myerscough, T.; Smith, S. Nitroxide chemistry. VII. Synthesis and reactions of perfluoro-2,5-diazaheptane 2,5-dioxy. *J. Chem. Soc., Perkin Trans. 1* **1974**, 2532–2538. [CrossRef]
114. Banks, R.E.; Haszeldine, R.N.; Stevenson, M.J. Perfluoroalkyl derivatives of nitrogen. XXI. Some reactions of bis(trifluoromethyl) nitroxide. *J. Chem. Soc. C* **1966**, 901–904. [CrossRef]
115. Banks, R.E.; Eapen, K.C.; Haszeldine, R.N.; Mitra, P.; Myerscough, T.; Smith, S. Perfluoro-2,5-diazaheptane-2,5-dioxy and its use in polymer chemistry and in polymer cross-linking. *J. Chem. Soc. Chem. Commun.* **1972**, 833–834. [CrossRef]
116. Green, M.J.; Tipping, A.E. The reaction of perfluoro-2,5-diazaheptane 2,5-dioxy with alkenes. *J. Fluor. Chem.* **1993**, *65*, 115–125. [CrossRef]
117. Green, M.J.; Tipping, A.E. The reactions of mercury(II) perfluoro-2,5-diazaheptane-2,5-dioxy and perfluoro-2,5-diazaheptane-2,5-diol with haloalkanes, acid chlorides, and dichlorosilanes. *J. Fluor. Chem.* **1994**, *66*, 271–277. [CrossRef]
118. Booth, B.L.; Haszeldine, R.N.; Holmes, R.G.G. Some oxidative-addition reactions of the diradical, perfluoro-NN'-dimethylethane-1,2-bis(aminoxy), CF₃N(O)CF₂CF₂N(O)CF₃, with iridium(I) and platinum(0) complexes. *J. Chem. Soc. Dalton Trans.* **1982**, 671–672. [CrossRef]
119. Arfaei, A.; Smith, S. Reactions of perfluoronitroxides with sulfur dioxide. *J. Chem. Soc. Perkin Trans. 1* **1984**, 1791–1794. [CrossRef]
120. Motornov, V.; Beier, P. Chemoselective Aza-[4+3]-annulation of N-Perfluoroalkyl-1,2,3-triazoles with 1,3-Dienes: Access to N-Perfluoroalkyl-Substituted Azepines. *J. Org. Chem.* **2018**, *83*, 15195–15201. [CrossRef]
121. Ogden, P.H. Cyclizations via fluoride ion induced isomerizations. Novel perfluoroheterocyclic compounds. *J. Chem. Soc. C* **1971**, 2920–2926. [CrossRef]
122. Banks, R.E.; Cheng, W.M.; Haszeldine, R.N. Heterocyclic polyfluoro compounds. II. Reactions of undecafluoropiperidine. The preparation of perfluoro-2,3,4,5-tetrahydropyridine and perfluoro-(1-methylpyrrolidine). *J. Chem. Soc.* **1962**, 3407–3416. [CrossRef]
123. Banks, R.E.; Burling, E.D. Heterocyclic polyfluoro compounds. IX. Some reactions of perfluoro-N-fluoromorpholine. The preparation of perfluoro-5,6-dihydro-2H-1,4-oxazine and perfluoro-3-methyloxazolidine. *J. Chem. Soc.* **1965**, 6077–6083. [CrossRef]
124. Banks, R.E.; Haszeldine, R.N.; Matthews, V. Heterocyclic polyfluoro compounds. XIII. Thermal reactions of perfluorotetrahydro-2-methyl-2H-1,2-oxazine and perfluoro-3,6-dihydro-2-methyl-2H-1,2-oxazine. Synthesis and properties of perfluoro-1-methyl-2-pyrrolidone, perfluoro-1-methyl-2-oxo-3-pyrroline, and perfluoro-1-methylazetidine. *J. Chem. Soc. C* **1967**, 2263–2267. [CrossRef]
125. Plevy, R.G.; Rendell, R.W.; Tatlow, J.C. Fluorinations with complex metal fluorides. Part 7. Fluorinations of the methylpyridines with cesium tetrafluorocobaltate. *J. Fluor. Chem.* **1982**, *21*, 265–286. [CrossRef]
126. Zhang, X.-G.; Guo, P.; Han, J.-F.; Ye, K.-Y. Cobalt fluorides: Preparation, reactivity and applications in catalytic fluorination and C-F functionalization. *Chem. Commun.* **2020**, *56*, 8512–8523. [CrossRef]
127. Meinert, H.; Fackler, R.; Mader, J.; Reuter, P.; Roehlke, W. The electrochemical fluorination of derivatives of morpholine, piperidine and carbazole. *J. Fluor. Chem.* **1992**, *59*, 351–365. [CrossRef]
128. Abe, T.; Hayashi, E.; Baba, H.; Fukaya, H. The electrochemical fluorination of nitrogen-containing carboxylic acids. Fluorination of dimethylamino- or diethylamino-substituted carboxylic acid derivatives. *J. Fluor. Chem.* **1990**, *48*, 257–279. [CrossRef]
129. Abe, T.; Hayashi, E.; Fukaya, H.; Hayakawa, Y.; Baba, H.; Ishikawa, S.; Asahino, K. The electrochemical fluorination of nitrogen-containing carboxylic acids. Fluorination of methyl esters of 3-(dialkylamino)propionic acids. *J. Fluor. Chem.* **1992**, *57*, 101–111. [CrossRef]
130. Abe, T.; Baba, H.; Soloshonok, I. Electrochemical fluorination of 1-ethylpiperazine and 4-methyl- and/or 4-ethylpiperazinyl substituted carboxylic acid methyl esters. *J. Fluor. Chem.* **2001**, *108*, 21–35. [CrossRef]
131. Abe, T.; Baba, H.; Fukaya, H.; Tamura, M.; Sekiya, A. Simons electrochemical fluorination of substituted homopiperazines(hexahydro-1,4-diazepines) and piperazines. *J. Fluor. Chem.* **2003**, *119*, 27–38. [CrossRef]

132. Naito, Y.; Inoue, Y.; Ono, T.; Arakawa, Y.; Fukaya, C.; Yokoyama, K.; Kobayashi, Y.; Yamanouchi, K. Synthesis of per-fluorochemicals for use as blood substitutes, part I. Electrochemical fluorination of N-methyldecahydroquinoline and N-methyldecahydroisoquinoline. *J. Fluor. Chem.* **1984**, *26*, 485–497. [CrossRef]
133. Sartori, P.; Velayutham, D.; Ignat'ev, N.; Noel, M. Investigations on the product distribution pattern during the electrochemical fluorination of 2-fluoropyridine and pyridine. *J. Fluor. Chem.* **1998**, *87*, 31–36. [CrossRef]

Disclaimer/Publisher's Note: The statements, opinions and data contained in all publications are solely those of the individual author(s) and contributor(s) and not of MDPI and/or the editor(s). MDPI and/or the editor(s) disclaim responsibility for any injury to people or property resulting from any ideas, methods, instructions or products referred to in the content.

Review

Synthesis of Phosphorus(V)-Substituted Six-Membered N-Heterocycles: Recent Progress and Challenges

Yulia Volkova * and Igor Zavarzin

N. D. Zelinsky Institute of Organic Chemistry, Russian Academy of Sciences, 47 Leninsky Prosp., 119991 Moscow, Russia

* Correspondence: yavolkova@gmail.com

Abstract: Heterocycles functionalized with pentavalent phosphorus are of great importance since they include a great variety of biologically active compounds and pharmaceuticals, advanced materials, and valuable reactive intermediates for organic synthesis. Significant progress in synthesis of P(O)R₂-substituted six-membered heterocycles has been made in the past decade. This review covers the synthetic strategies towards aromatic monocyclic six-membered N-heterocycles, such as pyridines, pyridazines, pyrimidines, and pyrazines bearing phosphonates and phosphine oxides, which were reported from 2012 to 2022.

Keywords: heterocycles; pyridine; pyridazine; pyrimidine; pyrazine; organophosphorus compounds

1. Introduction

Pentavalent phosphorus-substituted heterocycles are organophosphorus compounds of great importance. In materials chemistry, they are used in design of dyes and polymers with outstanding characteristics [1]. They are of interest as Lewis acids and ligands in metal-catalyzed organic reactions [2–5]. Moreover, phosphorus(V)-substituted heterocycles exhibit a wide range of biological activities. In particular, pyridines were used to design anticancer [6–8], antidiabetic [9], and lusitropic agents [10], antioxidants [11], human glucokinase activators [12], NMDA receptor antagonists [13], and metalloprotein ligands [14]. Phosphorus-modified pyridazines are promising candidates as antimicrobial agents [15] and foliar herbicides [16]. Phosphorus-containing pyrimidines are used as inhibitors of dihydroorotate dehydrogenase and hepatitis C virus polymerase [17–19]. Pyrazines are of interest as modulators of the human glucagon-like peptide-1 receptor [20] and cyclin-dependent kinases [21].

A variety of methodologies for synthesis of pentavalent phosphorus-substituted heterocycles and their derivatives have been reported in past years. Meanwhile, development of novel methodologies is in continuous demand. Of particular interest are methods that provide a broad substrate scope and provide products with high atom economy, molecular complexity, and great efficiency under mild conditions. Among them, several eco-friendly approaches have been developed by us [22,23]. In general, the known methods for synthesis of phosphorus(V)-substituted aromatic heterocycle are classified into two synthetic strategies: (1) construction of a heterocyclic core using phosphorus-containing reagents and (2) functionalization of a pre-synthesized heterocyclic core with phosphorus reagents.

Several excellent reviews dealing with synthesis of phosphorus-containing heterocyclic compounds were published in the literature in recent years. A number of reviews highlighted phosphorylation as the most common approach [24,25] and specifically radical phosphorylation [26] and metal-catalyzed/promoted C–H bond phosphorylation [27]. Another array of reviews considered use of a specific kind of transformations, including photoredox-catalyzed reactions [28], electrocatalytic [29], and radical [30] C–P bond formation, multicomponent reactions [31], and functionalization of phosphorus-centered radicals [32]. Some reviews are focused on the type of P-functional groups [33] or type of

Citation: Volkova, Y.; Zavarzin, I. Synthesis of Phosphorus(V)-Substituted Six-Membered N-Heterocycles: Recent Progress and Challenges. *Molecules* **2023**, *28*, 2472. <https://doi.org/10.3390/molecules28062472>

Academic Editors: Alexey M. Starosotnikov, Maxim A. Bastrakov and Igor L. Dalinger

Received: 15 February 2023

Revised: 2 March 2023

Accepted: 2 March 2023

Published: 8 March 2023



Copyright: © 2023 by the authors. Licensee MDPI, Basel, Switzerland. This article is an open access article distributed under the terms and conditions of the Creative Commons Attribution (CC BY) license (<https://creativecommons.org/licenses/by/4.0/>).

heterocycles [34], e.g., phosphorylindoles [35,36], pyrazoles [37,38], or pyrrolidines [39]. However, systematic reviews of the published data on different methods for synthesis of most monocyclic phosphorus(V)-substituted six-membered *N*-heterocycles are lacking.

The main focus of this review is monocyclic six-membered aromatic P(O)R₂-substituted *N*-heterocycles, including pyridines, pyridazines, pyrimidines, and pyrazines. The review is an attempt to systematically consider and classify methods for synthesis of corresponding heterocyclic phosphonates and phosphine oxides. Phosphonic acids are excluded from consideration since most of them are available by saponification of phosphonates [40–45]. Synthesis of six-membered *N*-heterocyclic phosphinamides, phosphonamide, and phosphonamidate has also not been described in recent years. The review is organized in a classical way and includes classification according to type of *N*-heterocycles using the following criteria: (a) the number of nitrogen atoms in heterocycles, (b) the nature of synthetic precursors, and (c) the type of chemical transformations involving these heterocycles.

The review addresses the scientific advances made over the past decade, in the period from 2012 up to the end of 2022. However, some earlier pioneering studies are cited where necessary. In many cases, the reaction mechanisms are briefly discussed in order to more completely describe the synthetic approaches to phosphorus-substituted *N*-heterocycles. In order to avoid overloading of the text with names of semantically similar processes, the term “phosphorylation” in this review deals with introduction of any P(O)R₂ substituent, not only a phosphoryl moiety, into the heterocyclic core. To enhance the readability of the schemes, the following color coding of the reagents is used: the source of the nitrogen atom is shown in blue, the source of the phosphorus atom in red, and the extra components in green. In the case of intramolecular cyclizations of reagents containing both nitrogen and phosphorus, the nitrogen atom is marked in blue and the phosphorus moiety in red.

2. Pyridines

Phosphorus(V)-substituted pyridine was first synthesized by Plazek’s research group [46] in 1936 by a reaction of 2-dimethylaminopyridine with phosphorus trichloride under oxidative conditions. Later, related compounds were obtained by reactions of meta-lated pyridines with phosphorus-halogen compounds [47–49], of pyridinediazonium tetrafluoroborate with phosphorus trichloride [50], of *N*-alkoxy pyridines with sodium diethyl phosphite and phosphines [51–55], and of *N*-pyridylpyridines with phosphonic acid [56], by the Michaelis–Arbuzov reaction [57,58], Pd(II)-catalyzed phosphorylation of halopyridines [45,59,60], cyclization of phosphorus-containing 3-azatrienes [61], and the Diels–Alder reaction involving 3-phosphoryl-1-azadienes [62]. This section of the review considers recent examples of synthesis of POR₂-substituted pyridines, including the intramolecular cyclizations of Michael adducts, insertion of carbenoids, formal [2+2+2]-cycloaddition, and phosphorylation reactions (Figure 1).

2.1. Cyclizations Based on the Michael Reaction

In recent years, synthesis of pyridines via the Michael reaction using phosphoryl-substituted Michael acceptors and donors has gained significant attention. Allais et al. [63–65] described three-component condensation of 1,3-dicarbonyl compounds **3** with P(O)Et₂-bearing vinyl ketones **2** and ammonium acetate (**1**) in the presence of oxygen, leading to pyridine-2-phosphonates **4** (Scheme 1). The authors suggested that the reaction occurs through successive addition of compound **3** to Michael acceptors **2**, providing ketone **5** followed by enamination of the latter with ammonia (**1'**) to form intermediate **6**, which undergoes intramolecular cyclization into dihydropyridine **7**. Complete oxidation of intermediate **7** to pyridine **4** was achieved using oxygen in the presence of activated carbon. The reaction was general with respect to β-oxo esters and β-oxoamides, providing products in 49–80% yields.

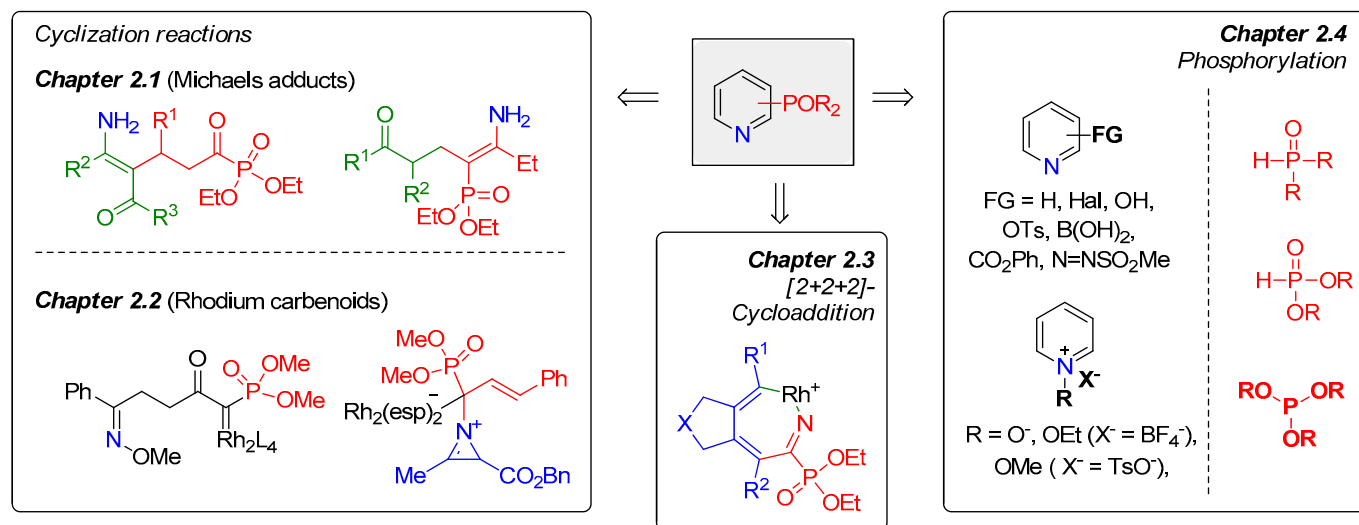
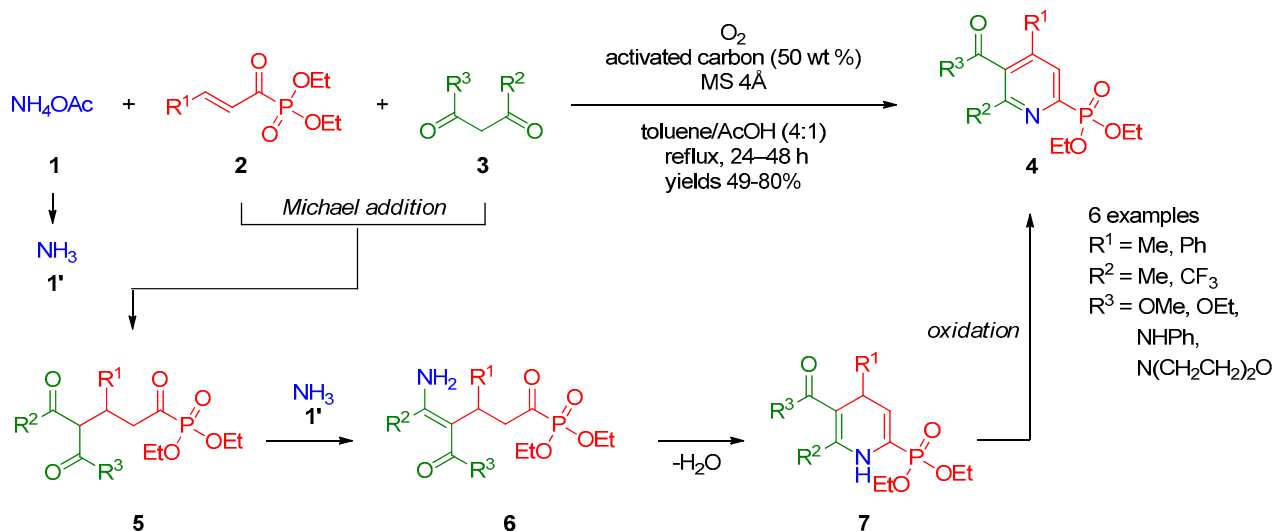
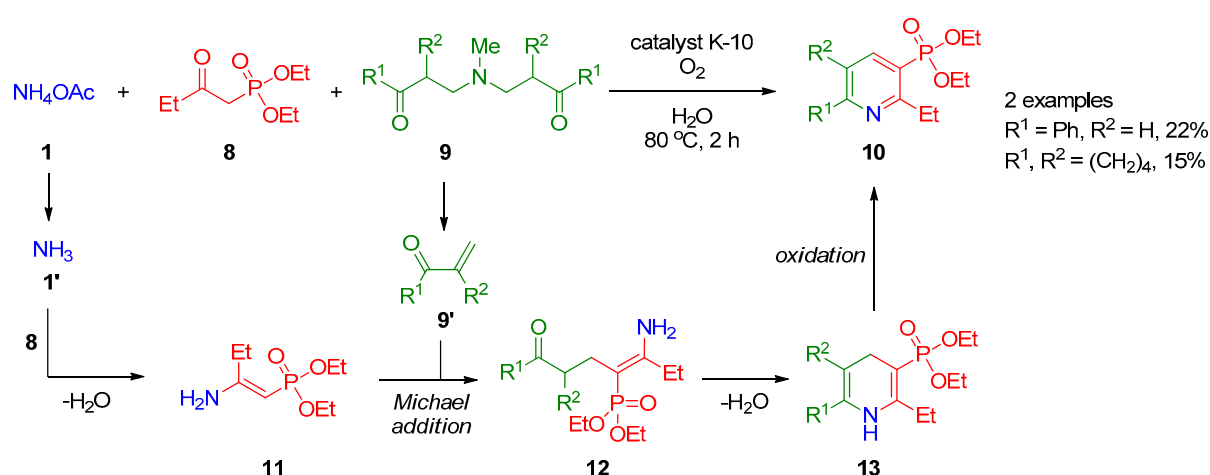


Figure 1. Approaches to synthesis of POR₂-containing pyridines.



Scheme 1. Synthesis of pyridine-2-phosphonates.

Hanashalshahaby and Unaleroglu [66] showed that pyridine-3-phosphonates **10** can be obtained by three-component oxidative coupling of diethyl (2-oxobutyl)phosphonate (**8**) with Mannich bases **9** and ammonium acetate (**1**) in the presence of catalyst K-10 (Scheme 2). The product yields are reasonable both for aryl- and alkyl-substituted Mannich bases. The authors hypothesized that β -keto phosphonate **8** reacts with ammonia **1'** generated in situ from ammonium acetate (**1**) to form enamine **11**, which is accompanied by thermal decomposition of Mannich base **9**, giving α,β -unsaturated carbonyl compound **9'**. These two intermediates are subjected to the Michael addition to form ketoamine **12**, which undergoes intramolecular cyclization to dihydropyridine **13**, followed by oxidation of the latter with atmospheric oxygen to provide final product **10**.

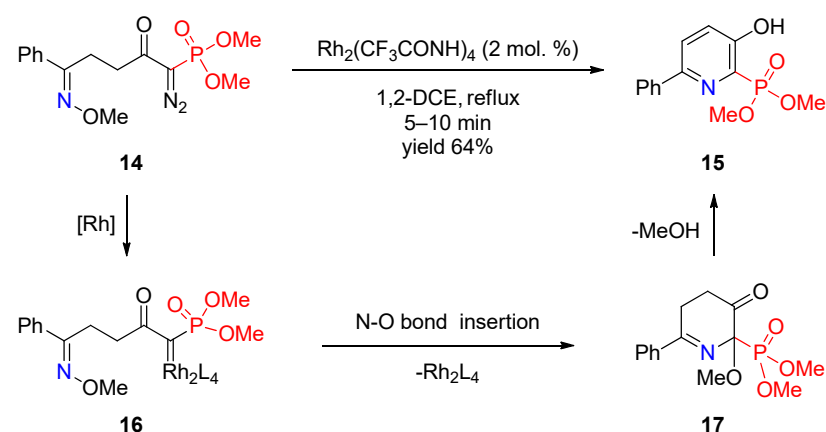


Scheme 2. Reaction of diethyl (2-oxobutyl)phosphonate with Mannich bases.

Further, Abdou et al. [67] found that diethyl (2-amino-2-thioxoethyl)phosphonate acts as an efficient Michael donor in the addition reaction with β -(dimethylamino)vinyl ketone, thus leading to 2-thioxopyridin-3-ylphosphonate. Liao et al. [68] described one example of the aza-Michael reaction between diethyl (3-phenyl-3-oxopropyn-1-yl)phosphonate with methyl 3-aminocrotonate, providing phosphonate-ester-containing pyridine moiety under mild conditions.

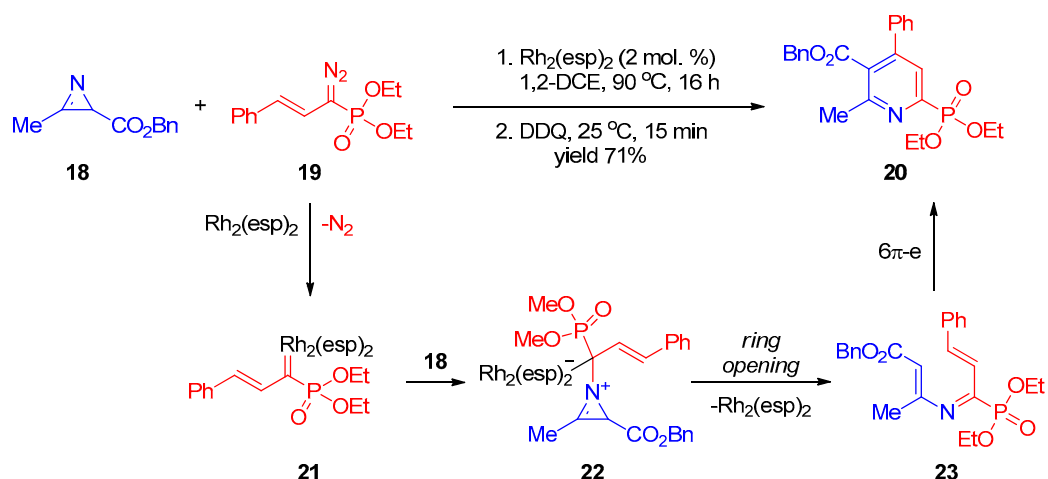
2.2. Carbenoid-Mediated Reactions

Recently, several studies by Park and co-workers demonstrated the prospects of using metal carbenoids in synthesis of phosphoryl-substituted pyridines. They described [69] Rh(II)-catalyzed intramolecular cyclization of δ -diazo oximes to pyridines and showed that this is a facile method for synthesis of pyridine-2-phosphonate **15** (Scheme 3). $\text{Rh}_2(\text{CF}_3\text{CONH})_4$ was used as the catalyst of choice. The authors proposed a mechanism that involves reaction of the diazo group of oxime **14** with Rh(II), providing rhodium carbenoid **16**, followed by insertion of the latter into the N–O bond to form dihydropyridinone **17**, which undergoes aromatization to final pyridine **15** via elimination of methanol.



Scheme 3. Rh(II)-catalyzed cyclization of δ -diazo oxime ether.

In another work by Park and co-workers [70], synthesis of pyridine-2-phosphonate **20** was accomplished using phosphorylated vinyl carbenoid **21** generated in situ from diazophosphonate **19** and dirhodium(II) catalyst $\text{Rh}_2(\text{esp})_2$ (Scheme 4). Addition of compound **21** to 2*H*-azirine **18** affords intermediate **22**. The latter undergoes three-membered ring opening accompanied by elimination of the Rh(II) catalyst to provide 3-azahexatriene **23**, followed by cyclization to yield pyridine **20**.



Scheme 4. Reaction of phosphorylated carbenoid with 2*H*-azirine.

2.3. Formal [2+2+2]-Cycloaddition

An approach towards phosphoryl-substituted pyridines, which is probably one of the most versatile, is based on the formal [2+2+2]-cycloaddition. Tanaka's research group [71,72] described synthesis of annulated pyridine-2-phosphonates **26** based on rhodium(I)/biaryl-bisphosphine-complex-catalyzed cycloaddition of 1,6- and 1,7-diyne **24** with diethyl phosphorocyanidate (**25**) (Scheme 5). The reaction has a broad scope with respect to diynes since quaternary carbon-, methylene-, nitrogen-, and oxygen-linked internal 1,6-diyne and terminal biaryl-linked 1,7-diyne can be involved in the heterocyclization. Steric and electronic variations in diynes had minimal impact on the efficacy of the reaction, but, in some cases, using unsymmetrically substituted diynes, the reactions afforded mixtures of regioisomers. The authors proposed rhodium cyclopentadiene **27** or rhodium azacyclopentadiene **28** as two possible key intermediates in the reaction (Scheme 5). Ring expansion of both cyclopentadienes can provide seven-membered intermediate **29**, and reductive elimination of Rh(I)⁺ from the latter accomplishes formation of the final product **26**. Based on the outcome of the enantioselective version of the reaction, the authors were inclined to believe that the main reaction pathway involves intermediate **28**.

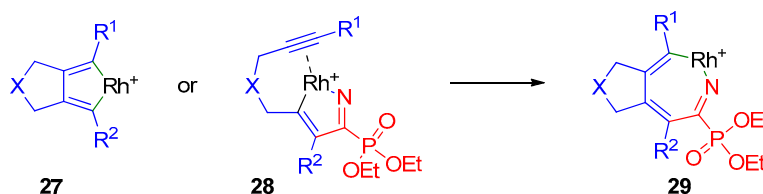


18 examples

X = CH₂, C(CO₂Me)₂, C(CO₂Bn)₂, CBz₂, C(CH₂OMe)₂, C(CH₂OBn)₂, C(CH₂OH)₂, NTs, O, [C(CO₂Et)₂]₂, biphenyl-2,2'-diyl, C(CO₂Me)Ph

R¹ = H, Me, Et, CO₂Me, 2-ClC₆H₄, R² = H, Me, Et

Proposed mechanism



Scheme 5. Formal [2+2+2]-cycloaddition of 1,6- and 1,7-diyne with diethyl phosphorocyanidate.

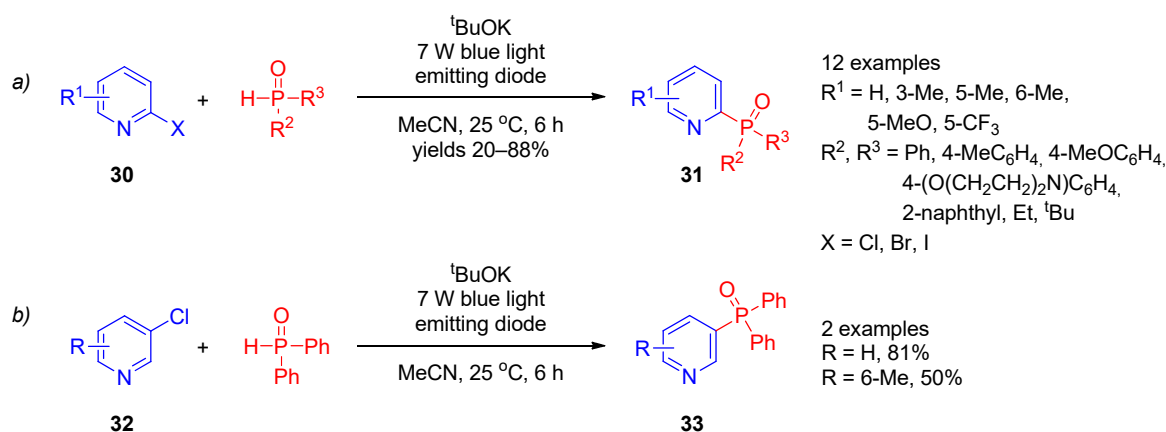
2.4. Phosphorylation of Pyridines

Phosphorylation is definitely the most general route to phosphorus-substituted pyridines. Due to a wide range of available phosphorylating agents and the possibility of perform-

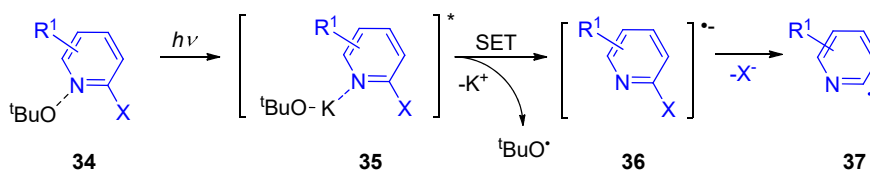
ing the reaction in a nucleophilic, electrophilic, or radical manner, phosphorylation has attracted great attention. Such methods as the Arbuzov reaction, Hirao coupling, palladium-catalyzed cross-coupling of diethyl phosphonate with halogen-substituted heterocycles, and C(sp²)H-phosphorylation of heterocycles with diethyl phosphonates promoted by one-electron oxidants were extensively developed in past decades. Their specific applications in recent years are discussed in more detail later in the text.

2.4.1. Radical Phosphorylation of Pyridines

P-centered radicals can easily be generated through hydrogen atom transfer or single-electron transfer using peroxides, metal salts, and photocatalysts. Thus, radical phosphorylation has become an efficient strategy for synthesis of structurally diverse phosphorus(V)-substituted pyridines. Due to environmental friendliness and potential industrial application, photocatalytic radical phosphorylation of the pyridine ring received extra attention. In 2018, Yuan et al. [73] reported synthesis of 2- and 3-phosphine oxide-substituted pyridines **31** and **33** (Scheme 6, lines a,b) from 2- and 3-halopyridines **30** and **32** by photocatalytic functionalization with secondary phosphine oxides in the presence of ^tBuOK. The reaction occurred under mild conditions using irradiation with a blue-light-emitting diode. The scope of this transformation is somewhat limited to pyridines with electron-donating substituents and their analogs with an extended π -system. The plausible reaction mechanism involves formation of a complex of halopyridine with potassium *tert*-butoxide **34**, absorption of a light quantum, transition to an excited state **35**, and electron transfer from *tert*-butoxide to a pyridine ring to form the *tert*-butoxy radical and halopyridine radical anion **36**. Elimination of halide from radical anion **36** affords aryl radical **37**. Simultaneously, the *tert*-butoxy radical causes the proton abstraction from secondary phosphine to form a phosphorus-containing radical. Recombination of the latter radical with an aryl radical affords the final product. Recently, the approach proposed by Yuan et al. was expanded [74,75], including electron-primed photoredox [76] and visible light-induced nickel-catalyzed photoredox [77] conditions for radical generation.



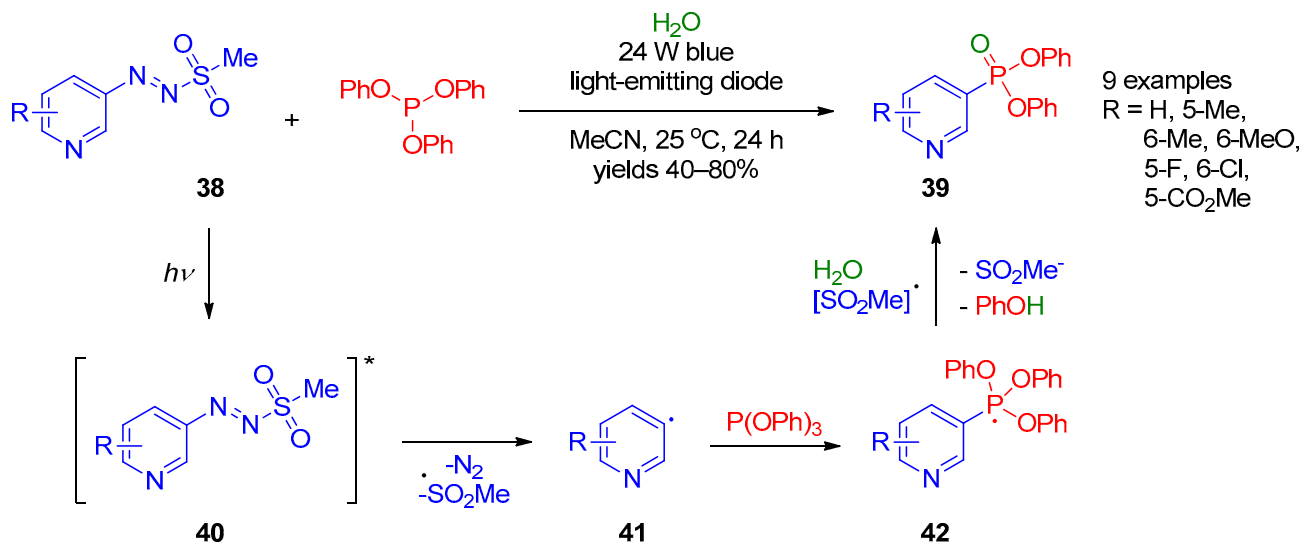
Intermediates



Scheme 6. Photocatalytic phosphorylation of halopyridines: (a) Synthesis of 2-phosphine oxide-substituted pyridines; (b) Synthesis of 3-phosphine oxide-substituted pyridines.

In 2019, the photocatalytic radical reaction of pyridylazo sulfones **38** with triphenyl phosphite giving pyridine-3-phosphonates **39** was described by Qiu et al. [78] (Scheme 7).

The reaction occurred in the presence of water. A variety of substituted pyridines can be efficiently employed in this reaction. The proposed mechanism for this transformation involves excitation of arylazo sulfone **38** under visible light to provide radical **40**, its decomposition into sulfonyl and aryl radicals, along with extrusion of a nitrogen molecule. Then, aryl radical **41** reacts with triphenyl phosphite to form phosphorus-centered radical **42**, followed by its oxidation with the sulfonyl radical and elimination of phenol to provide the final product **39**.

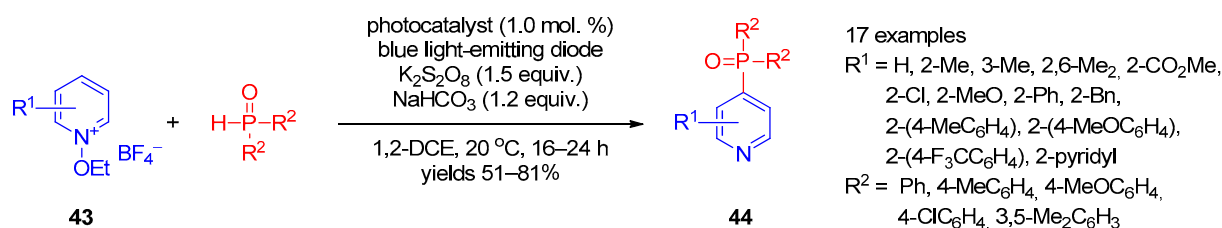


Scheme 7. Synthesis of pyridine-3- and pyridine-4-phosphonates from pyridylazo sulfones.

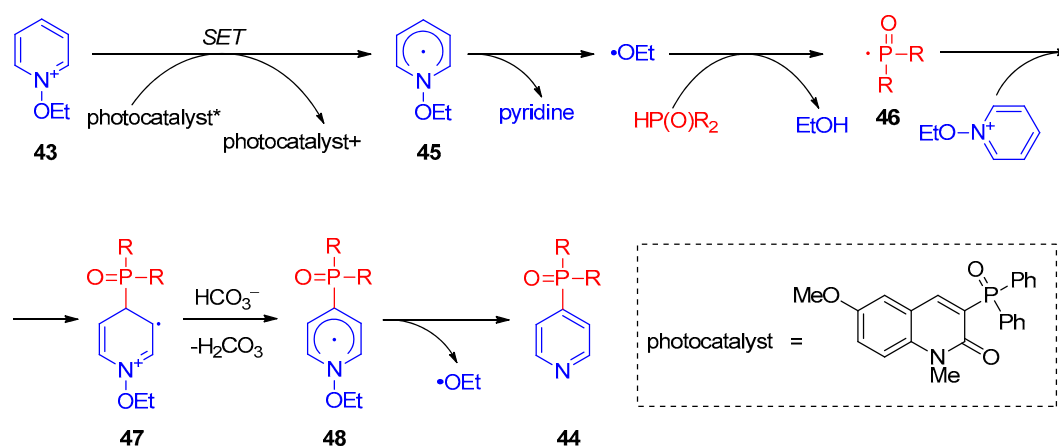
Independently, in 2019, Kim et al. [79] described site-selective synthesis of pyridines **44** bearing phosphine oxide moieties at C-4 using radical coupling of *N*-ethoxypyridinium salts **43** with secondary phosphine oxides under photocatalytic conditions (Scheme 8). Further, 3-Diphenylphosphoryl-6-methoxy-1-methyl-2(1*H*)-quinolinone under blue-light-emitting diode illumination was used as a photocatalyst and potassium persulfate as an oxidant. Examination of the reaction scope revealed that a variety of electron-withdrawing and electron-donating substituted pyridines, as well various aryl-substituted phosphine oxides, were tolerated. The plausible mechanism of this reaction involves single-electron transfer from the photocatalyst to *N*-ethoxypyridinium **43**, giving radical **45**, which undergoes decomposition accompanied by elimination of pyridine. The remaining ethoxy radical abstracts a proton from phosphine, followed by addition of the resulting phosphinoyl radical **46** to *N*-ethoxypyridinium **43**. The subsequent deprotonation of intermediate **47** and elimination of the new ethoxy radical from intermediate **48** afford target product **44**. The origin of reaction chemoselectivity was revealed by DFT calculations, showing that phosphinoyl radicals are too large for providing an electrostatic attraction between the its oxo functionality and the pyridine nitrogen crucial for *ortho* functionalization.

Apart from the approaches based on photocatalytic radical phosphorylation, several examples using metal salts for P-radical generation were described. Huang and co-workers [80] developed a CH-phosphorylation method for synthesis of pyridinyl-2-phosphonates **50** based on Ag(I)-catalyzed reaction of pyridines **49** with dialkyl phosphonates using potassium persulfate as an oxidant (Scheme 9). An interesting feature of this reaction is that it involves subsequent treatment of the reaction mixture with sodium thiosulfate, which makes it possible to significantly increase the product yield due to a reduction of pyridine *N*-oxide formed as a by-product. In the authors' opinion, this transformation proceeds through a radical pathway and begins with oxidation of Ag(I) to Ag(II) with persulfate, followed by oxidation of dialkyl phosphite with Ag(II) to form radical cation **5**. Addition of the latter at 2 position of the pyridine ring provides intermediate **52**. Subsequent abstraction of two protons accompanied by oxidation of radical **52** affords the

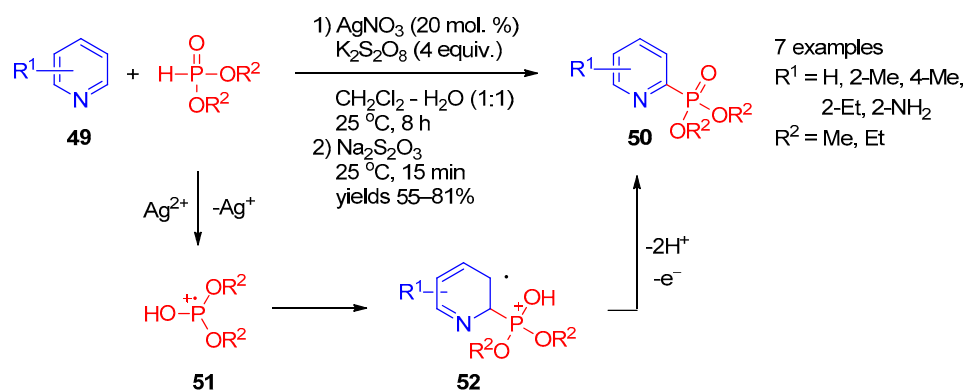
final product. Recently, Kittikool et al. [81] expanded the scope of this phosphorylation approach to 2-pyridones using $\text{Mn}(\text{OAc})_2$ as the catalyst.



Proposed mechanism



Scheme 8. Photocatalytic reaction of *N*-ethoxypyridinium salts with phosphine oxides.



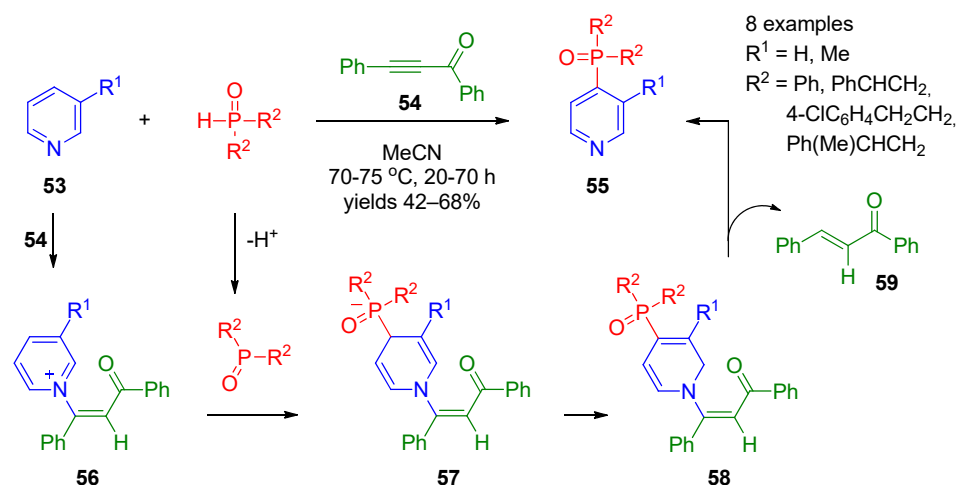
Scheme 9. Oxidative coupling of pyridines with dialkyl phosphites in the presence of $\text{Ag}(\text{I})$.

Noteworthy also is a one-pot three-step protocol for synthesis of diphenyl(pyridin-2-yl)phosphine oxide based on the KOH -promoted oxidative radical phosphorylation of 2-bromopyridine with diphenylphosphine developed by Chen et al. [82].

2.4.2. Nucleophilic Phosphorylation of Pyridines

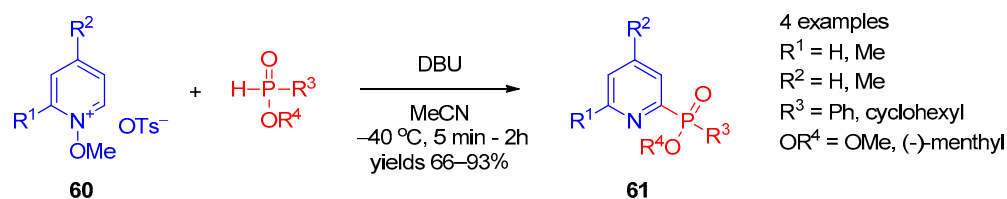
Studies by Trofimov's research group [83–85] have contributed to recent progress in nucleophilic phosphorylation of pyridines at the 4 position. They accomplished synthesis of 4-phosphine oxide-substituted pyridines **55** by coupling of pyridines **53** with secondary phosphine oxides using diphenyl ethynyl ketone (**54**) as the oxidant (Scheme 10). A variety of substituted aryl and alkyl phosphine oxides can efficiently be employed in this reaction. The proposed mechanism for this transformation involves aza-Michael reaction of pyridine **53** with acetylene **54**, providing intermediate **56**, and deprotonation of phosphine, resulting in formation of the anion. Subsequent addition of a phosphine

anion at the 4 position of the activated pyridine ring affords dihydropyridine **57**. The latter undergoes isomerization to intermediate **58**, followed by elimination of alkene **59** to form the final product. In this approach, 3-phenyl-2-propynenitrile can also be applied as an oxidant [84]. The reaction can be stopped at the step of 1,4-dihydropyridines **57** using terminal acylacetylenes [85]. It is interesting that 1,4-dihydropyridines are shown to be produced through 2-4 migration of the POR_2 group in 1,2-dihydro adducts during vinylation/phosphorylation of pyridines [85]. DFT calculations supported the hypotheses that 1,4-dihydropyridines are the thermodynamic products while their 1,2-regioisomers are the kinetic ones [85].



Scheme 10. Coupling of pyridines with secondary phosphine oxides in the presence of acetylenes.

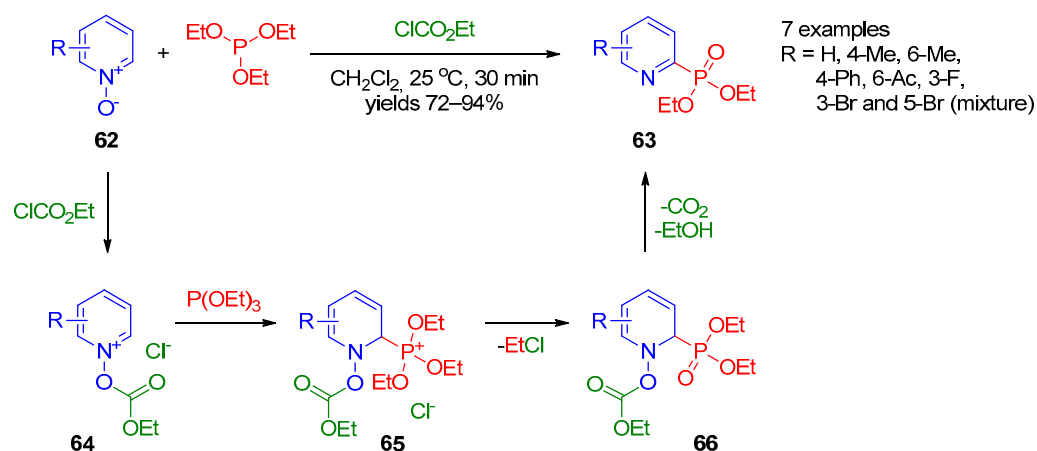
Direct nucleophilic phosphorylation at the 2 position of the pyridine ring was described in 2012 by Oka et al. [86]. A series of 2-phosphinate-substituted pyridines **61** were prepared from *N*-methoxypyridinium tosylates **60** by reaction with secondary phosphinates (Scheme 11). Presumably, the reaction proceeds via the $\text{S}_{\text{N}}\text{Ar}$ mechanism. Further, 1,8-Diazabicyclo[5.4.0]undec-7-ene (DBU) in acetonitrile at low temperature was found to be the optimal base for chemoselective transformation. The procedure was general for thiophosphinate, providing 2-pyridyl thiophosphinate. The 2-pyridyl phosphinate derivatives produced by this method are P-chiral, and the reaction can be accomplished with high diastereoselectivity using chiral phosphines.



Scheme 11. Reaction between *N*-methoxypyridinium tosylates and secondary phosphines.

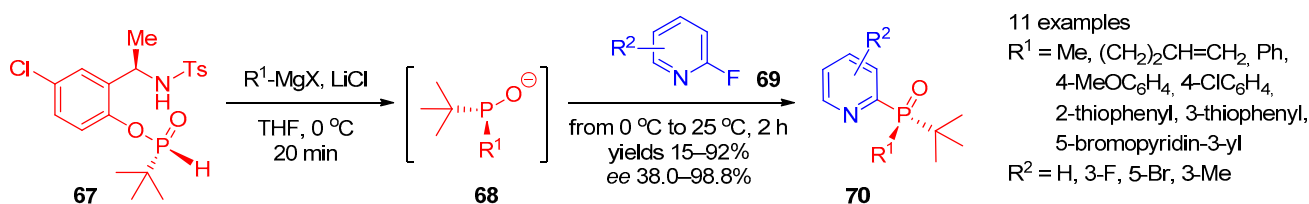
In 2014, Wang et al. [87] showed that synthesis of pyridine-2-phosphonates can be accomplished directly from pyridine *N*-oxides and dimethyl phosphate over long-term heating in toluene. Independently, Lee et al. [88] developed an approach to synthesize diethyl pyridine-2-phosphonates **63** by reaction of pyridine *N*-oxides **62** with triethyl phosphite in the presence of ethyl chloroformate (Scheme 12). This reaction presumably starts with activation of pyridine *N*-oxide **62** by chloroformate, followed by addition of triethyl phosphate to the resulting pyridinium salt **64** to form intermediate **65**. The nucleophilic attack of the chloride anion at the ethyl moiety followed by elimination of ethyl carbonate from 1,2-dihydropyridine **66** affords the final product. This approach is general for preparation of quinolin-2-ylphosphonates. An apparent limitation of this

approach is formation of phosphorylated isomeric mixtures in the case of 3-bromopyridine *N*-oxide.



Scheme 12. Reaction of pyridine *N*-oxides with triethyl phosphite.

Recently, Tsantrizos and co-workers [89] proposed a route to *P*-chiral 2-phosphine oxide-substituted pyridines (Scheme 13). Using the reaction of (*R*)-*N*-(1-(5-chloro-2-hydroxyphenyl)ethyl)-4-methylbenzenesulfonamide (**67**) with Grignard to generate chiral phosphorylating agent **68**, they accomplished enantioselective synthesis of products **70** from 2-fluoropyridines **69**.

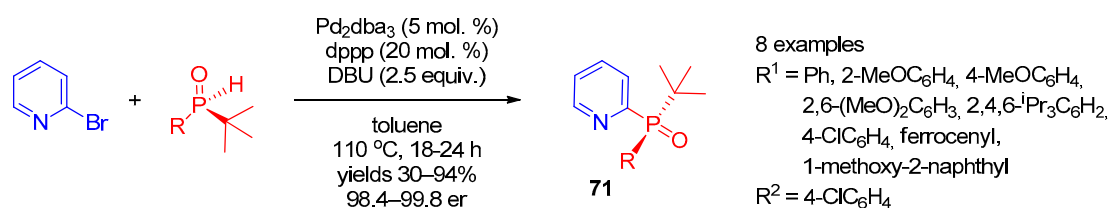


Scheme 13. Asymmetric synthesis of tertiary pyridine-containing phosphine oxides.

2.4.3. Transition-Metal-Catalyzed Phosphorylation of Pyridines

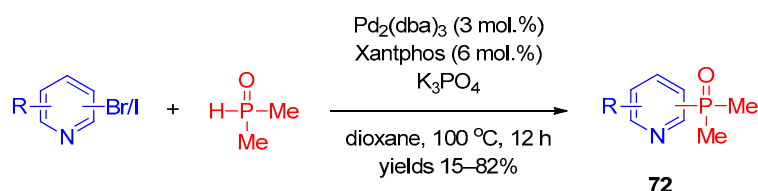
Transition metals are widely used to increase efficiency of conventional non-catalyzed phosphorylation of heterocycles [27]. In the past decade, significant progress in the field of phosphorylation of pyridines was made due to application of palladium and nickel catalysis, which enabled expansion of the range of substrates active in phosphorylation reactions to involve halogen-, hydroxyl-, boronic acid-, triflate-, nonaflate-, ester-substituted, trimethylammonium pyridines, etc. It was also shown that transition-metal-catalyzed phosphorylation with phosphine oxides, phosphates, and phosphites could be efficiently used for construction of functionalized pyridines, including chiral structures. Meanwhile, transition-metal-catalyzed C–H phosphorylation of pyridines still remains an unsolved challenge.

Halopyridines (Hal = Cl, Br, and I) are efficient precursors for synthesis of 2,3,4-POR₂-substituted pyridines under palladium catalysis conditions. In 2017, Han et al. [90] reported stereoselective palladium-catalyzed cross-coupling of 2-bromopyridine with chiral *tert*-butyl-containing phosphine oxides (Scheme 14). Use of Pd₂(dba)₃ with the dppe ligand enabled synthesis of tertiary pyridine-containing phosphine oxides **71** with excellent selectivity. In 2016, Dziuganowska et al. [13] used the same catalytic system to prepare a series of phosphonopyridinecarboxylic acid esters from appropriate bromides.



Scheme 14. Synthesis of chiral tertiary pyridine-containing phosphine oxides.

Mykhailiuk and co-workers [91] expanded the scope of this reaction using the $\text{Pd}_2(\text{dba})_3$ /Xantphos catalytic system in the reaction of bromo(iodo)pyridines with dimethylphosphine oxide (Scheme 15). The scope of this reaction was found to be quite general and enables facile preparation of 2-, 3-, and 4-dimethylphosphine-oxide-substituted pyridines **72** in up to good yields. A variety of electron-withdrawing and electron-donating aryl-substituted pyridines successfully participated in the reaction.



29 examples

2-phosphorylated products:

$\text{R} = \text{H}$, 3-NH₂, 4-NH₂, 5-NH₂, 6-NH₂, 5-CN, 4-CO₂Me, 5-CO₂Me, 4-CH(OMe)₂, 5-CH(OMe)₂

3-phosphorylated products:

$\text{R} = \text{H}$, 2-F, 5-F, 6-F, 5-Cl, 6-Cl, 2-NH₂, 4-NH₂, 5-NH₂, 6-NH₂, 2-CN, 5-CN, 6-CN, 5-CO₂Me

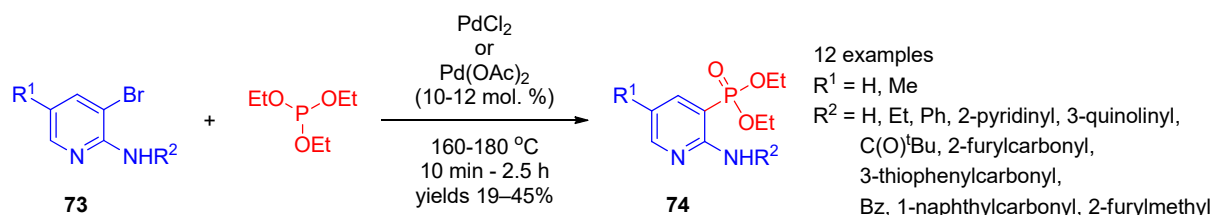
4-phosphorylated products:

$\text{R} = \text{H}$, 2-F, 2-Cl, 2-NH₂, 2-CN, 2-CO₂Me

Scheme 15. Cross-coupling of halopyridines with dimethylphosphine oxide.

Borisova and co-workers [92] accomplished synthesis of bis(phosphoryl)pyridines and 2,2'-bipyridines using palladium acetate/dppf-catalyzed cross-coupling of chloropyridines with secondary phosphine oxides. Ligand-free microwave-assisted $\text{Pd}(\text{OAc})_2$ -catalyzed phosphorylation of bromopyridines with diphenylphosphine oxide or diethyl phosphite was described by Henyecz et al. [93]. Catalyst $\text{Pd}(\text{OAc})_2$ in the presence of sodium iodide as the promoter was also shown to be an effective catalyst for ligand-free coupling of diphenylphosphine oxide with pyridinium nonaflate [94]. An example of $\text{Pd}(\text{PPh}_3)_4$ -catalyzed coupling of 2-bromo-6-pyrrolylpyridine with diethyl phosphite was recently reported by Ti et al. [95].

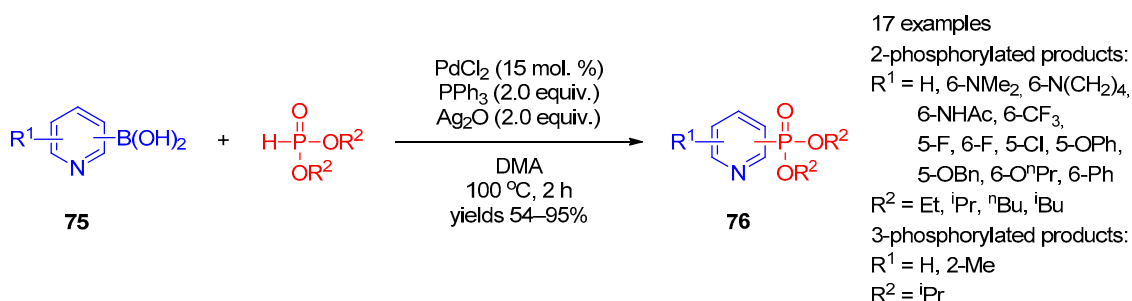
The palladium-catalyzed Hirao coupling of bromopyridines with triethyl phosphite enables preparation of pyridinephosphonates. Adam et al. [96] used the palladium-catalyzed cross-coupling of 3-bromopyridines **73** with triethyl phosphite to synthesize 2-aminopyridine-3-phosphonates **74** (Scheme 16). It is worth noting that the reaction was performed in the absence of the solvent during short-term heating to 160–180 °C.



Scheme 16. Pd(II)-catalyzed cross-coupling of 3-bromopyridines with triethyl phosphite.

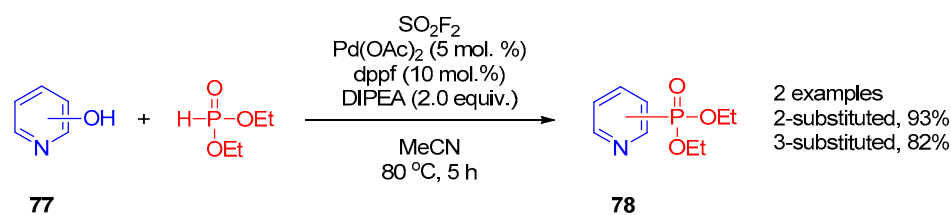
Apart from halopyridines, pyridine boronic acids and hydroxypyridines were involved in phosphorylation under palladium catalysis. Zou, Wu, and co-workers [97]

constructed a C–P bond by means of cross-coupling of pyridine boronic acids **75** with dialkyl phosphonates under PdCl₂ catalysis conditions (Scheme 17). The reaction requires the presence of Ag₂O as the oxidant. The method can be used to prepare structurally diverse pyridine-3- and pyridine-4-phosphonates **76**.



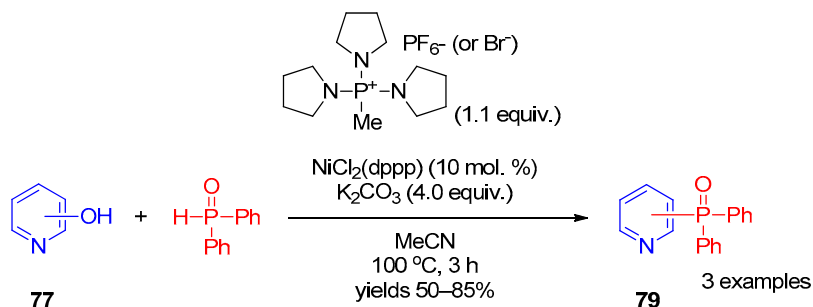
Scheme 17. Cross-coupling of pyridine carboxylic acids with dialkyl phosphites.

Recently, Ding and co-workers [98] described the general palladium-catalyzed one-pot procedure for synthesis of phosphonates, phosphinates, and phosphine oxides from phenols mediated by sulfonyl fluoride. The reaction was efficient for functionalization of 2- and 3-hydroxypyridines **77** with diethyl phosphonate (Scheme 18). According to the proposed mechanism, the fluorosulfates generated in situ are key intermediates in synthesis of pyridines **78**.



Scheme 18. Replacement of the OH group of hydroxypyridines mediated by sulfonyl fluoride.

Before these works, in 2012, direct replacement of an OH group of hydroxypyridines by a diphenylphosphoryl moiety was achieved by Zhao et al. [99] under Ni(II) catalysis. A C–O bond was activated using bromotripyrrolidinophosphonium hexafluorophosphate. The activated complex of hydroxypyridine **77** with this salt reacts with diphenylphosphine oxide in the presence of dichloro[1,3-bis(diphenylphosphino)propane]nickel salts as the catalyst to produce pyridines **79** (Scheme 19).

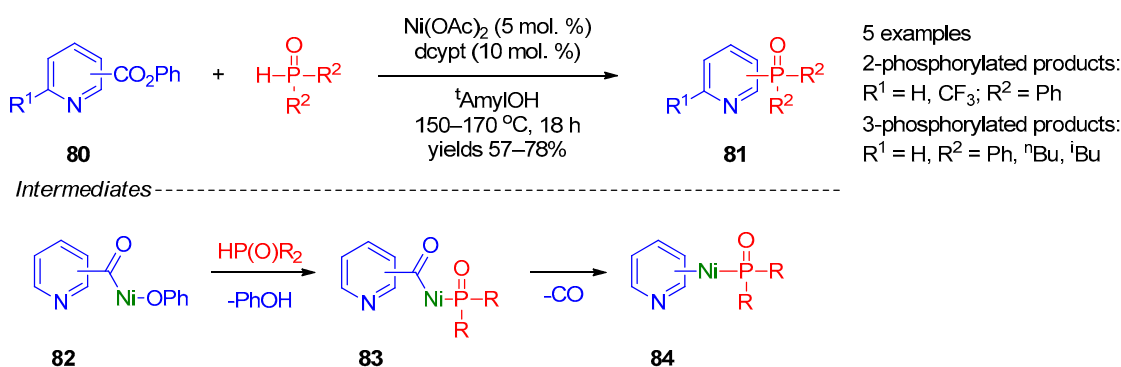


Scheme 19. Replacement of the OH group of hydroxypyridines by the diphenylphosphoryl moiety.

Later, the substrate scope of Ni-catalyzed phosphorylation of pyridines with phosphine oxides was expanded to pyridine carboxylic acid phenyl esters [100] and trimethylammonium triflate of pyridine [101]. Cross-coupling of pyridine tosylates [102] and aryltrimethylammonium tetrafluoroborate [103] with phosphites was also implemented.

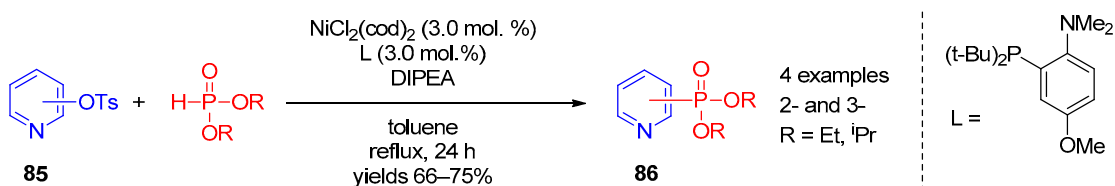
A relatively general method was proposed by Yamaguchi's research group [100]. They performed cross-coupling of pyridine carboxylic acid phenyl esters **80** with secondary

phosphine oxides accompanied by decarbonylation (Scheme 20). The reaction is catalyzed by nickel acetate and requires high temperatures (150–170 °C). This approach is applicable to synthesis of 2- and 3-phosphine-oxide-substituted pyridines **81**, the position of the POR₂ substituent in the product being defined by the position of the carbonyl group in the starting compound. The authors suggested that this transformation initially proceeds through oxidative insertion of Ni(0) into the C–O bond, providing intermediate **82**, and exchange of the phenoxide ligand by phosphine provides **83**. Subsequent decarbonylation of intermediate **83** and reductive elimination from intermediate **84** afford the final product.



Scheme 20. Cross-coupling of aryl carboxylic acid esters with phosphine oxides.

Of interest as well is Ni(II)-catalyzed reaction of tosylates **85** with H-phosphonate diesters proposed by Chun-Jing Li [102] as an approach to 2- and 3-phosphorylpyridines **86**; NiCl₂(cod)₂ was an optimal catalyst for this transformation (Scheme 21).



Scheme 21. Ni(II)-catalyzed replacement of the tosyl group in pyridines.

3. Pyridazines

Phosphorus(V)-substituted pyridazines are poorly described heterocycles. Therefore, all known methods for synthesis of these compounds, including isomerization of (diazomethyl)cyclopropenes and bis-azirine, intramolecular cyclization of γ,δ -unsaturated α -diazo- β -ketone and hydrazone, as well as phosphorylation of the pyridazine ring (Figure 2), are considered below.

3.1. Isomerization Reactions

Regitz and co-workers [104–107] reported the only method for synthesis of POR₂-containing pyridazines, the general character of which was demonstrated in relation to a representative series of compounds. The authors showed that (diazomethyl)cyclopropenes **89**, derived from cyclopropenyl cations **87** and phosphorus-containing diazomethanes **88**, undergo intramolecular isomerization to 3-P(O)R₂-substituted pyridazines **90** (Scheme 22). When using secondary amino-substituted cyclopropenyl cations as substrates, the reaction can be performed in a one-pot fashion [107]. The method tolerates substrates containing phosphine oxide moieties and can be used to synthesize POR₂-containing 4,5-diamino-substituted pyridazines in 16–68% yields. The authors suggested 3,4-diazabenzvalene **I**, product of the intramolecular 1,3-dipolar cycloaddition, or bicyclic zwitterions **II**, formed via intramolecular 1,5-dipolar cyclization, as two key intermediates in the isomerization reaction (Scheme 22). The results of the reactions with sterically hindered cyclopropenes inclined the authors to believe that the main reaction pathway involves intermediate **II**.

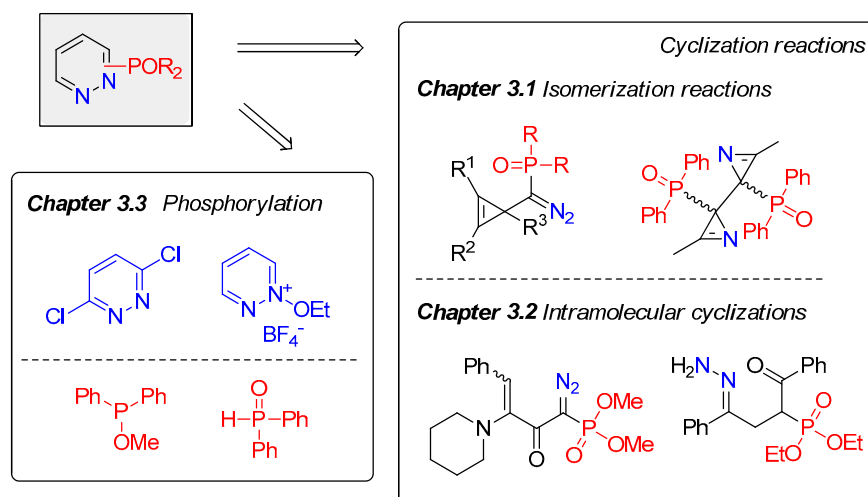
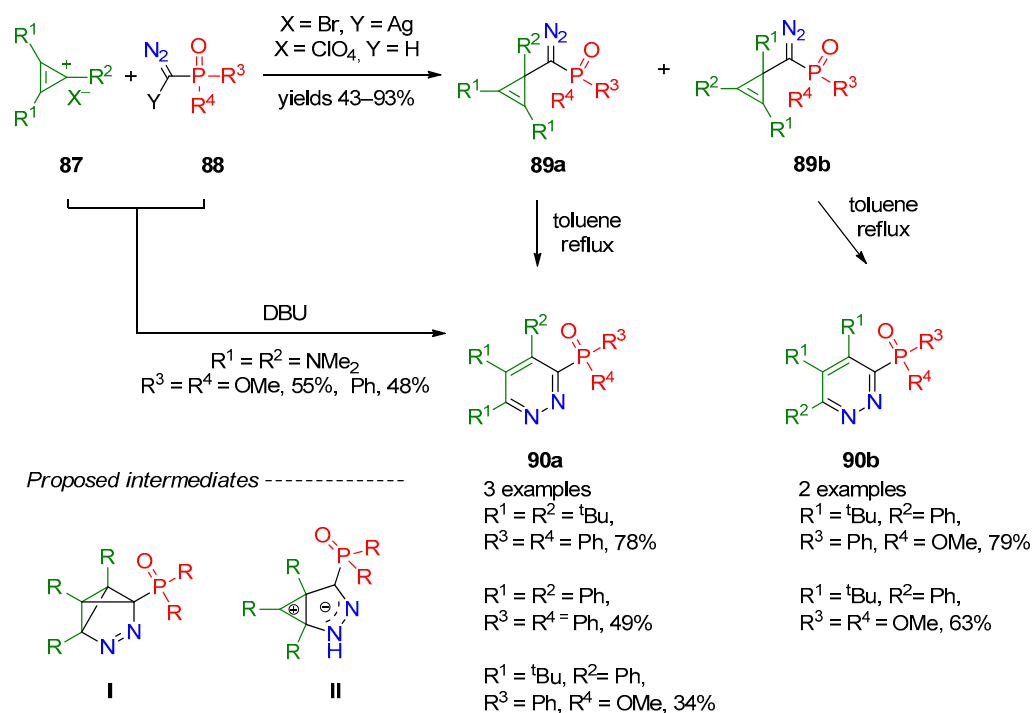
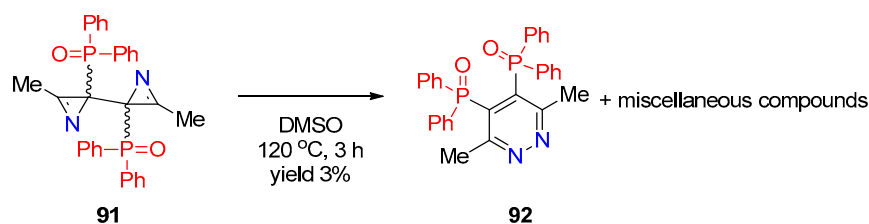


Figure 2. Approaches to synthesis of POR_2 -containing pyridazines.



Scheme 22. Reactions of cyclopropenyl salts with phosphorus-containing diazomethanes.

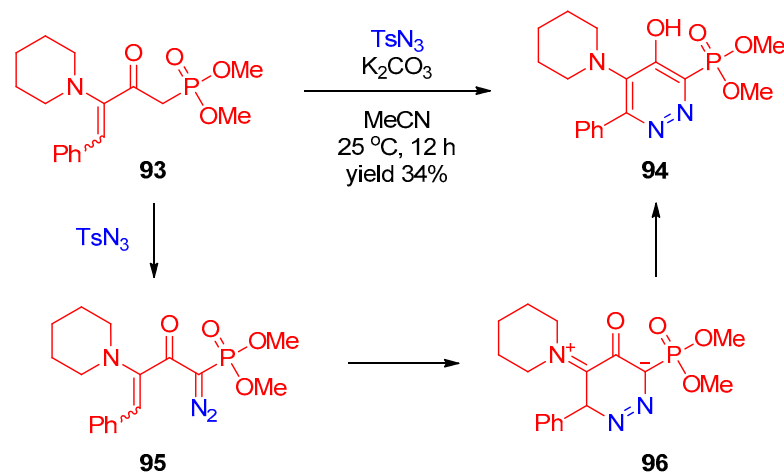
A single example of thermal rearrangement of phosphorus-substituted bis-azirine **91** into 4,5-bis(phosphine oxide)pyridazine **92** was reported by Banert et al. [108] (Scheme 23). Formation of pyridazine may be explained by multistep diradical pathways, supported by DFT calculations. However, this is one of several reaction pathways, and the yield of the target product was as low as 3%.



Scheme 23. Rearrangement of phosphorus-containing bis-azirine.

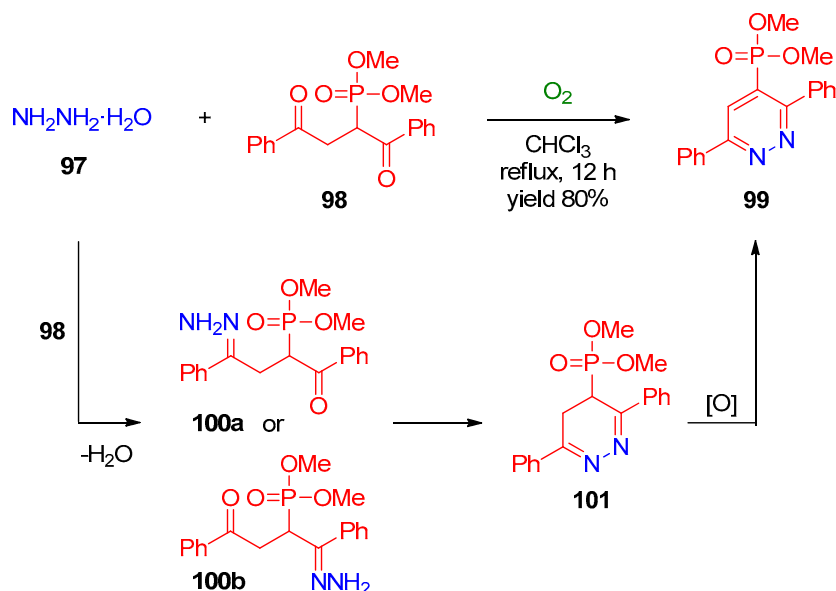
3.2. Intramolecular Cyclizations

Doutheau and co-workers [109] described one example of cyclization of γ,δ -unsaturated α -diazo- β -keto phosphonate **95** to pyridazine-2-phosphonate **94** (Scheme 24). This compound is generated in situ via diazo transfer from γ,δ -unsaturated β -keto phosphonate **93** in the presence of tosyl azide and immediately undergoes intramolecular electrophilic cyclization involving a diazo moiety and double bond to form intermediate **96**, followed by rearrangement of the latter into final product.



Scheme 24. Cyclization of γ,δ -unsaturated α -diazo- β -keto phosphonate.

Touil and Zantour [110] synthesized pyridazine-3-phosphonate **99** by reaction of phosphorylated 1,4-dicarbonyl compound **98** with hydrazine hydrate (**97**) under oxidative conditions (Scheme 25). The reaction presumably proceeds through intermediate hydrazones **100**, which undergo spontaneous intramolecular cyclization to 4,5-dihydropyridazine **101**. Oxidative aromatization of the latter with oxygen affords a product in high yield.

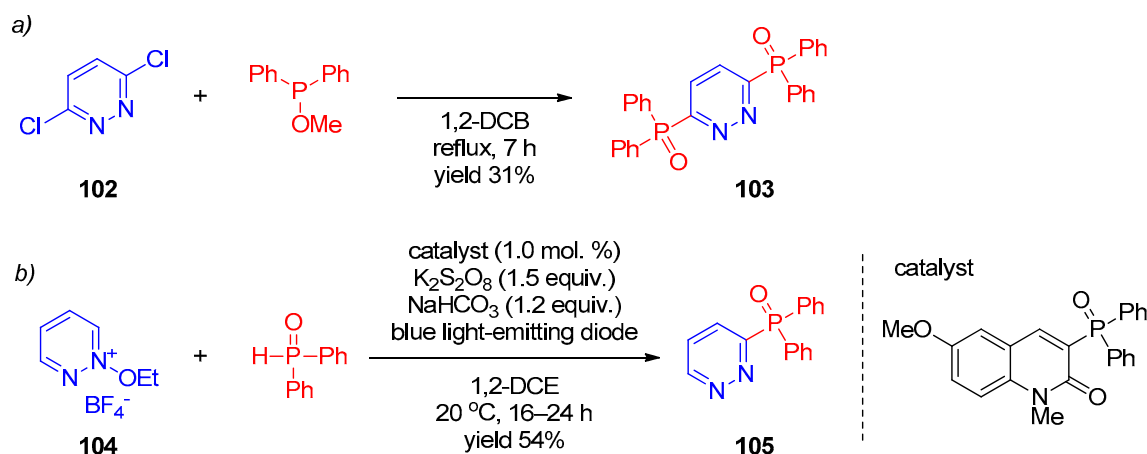


Scheme 25. Synthesis of dimethyl 3,6-diphenylpyridazine-3-phosphonate.

3.3. Phosphorylation of Pyridazines

There are only two known examples of phosphorylation of pyridazines. Thus, the Michaelis–Arbuzov reaction of 3,6-dichloropyridazine (**102**) with methoxydiphenylphosphine was proposed as an approach to synthesis of 3,6-bis(diphenylphosphine oxide)pyridazine

(103) in the patent by Mrowca [111] (Scheme 26, line a). An example of synthesis of 2-diphenyl(pyridazin-3-yl)phosphine oxide 105 from *N*-ethoxy-pyridazin-3-ium 104 and diphenylphosphine oxide via photocatalysis was presented by Kim et al. [79] (Scheme 26, line b). This process follows a radical mechanism, which is considered in more detail in Section 2.4.1 (Scheme 8). Therefore, the known phosphorylation reactions of pyridazines are limited to functionalization of the 3 and 6 positions of the heterocyclic core.



Scheme 26. Phosphorylation of pyridazines: (a) Mrowca et al., 1980 [111]; (b) Kim et al., 2019 [79].

4. Pyrimidines

Phosphorus(V)-substituted pyrimidines were first synthesized by Kosolapoff and Roy [112] in 1961 by reaction of chloropyrimidines with $\text{NaP}(\text{O})(\text{OEt})_2$. This method was also applied in many other studies [111,113]. Further, related compounds were prepared by reaction of bis-electrophiles with amidines [114–118], reaction of β -keto vinylphosphonates with amidines [119], reaction of metalated pyrimidines with P-Cl compounds [120], and palladium-catalyzed phosphorylation [45]. This section deals with recent examples of synthesis of phosphorus-containing pyrimidines, including the reactions of α, β -unsaturated β -phosphoryl carbonyl compounds with guanidine and phosphorylation of the pyrimidine core (Figure 3).

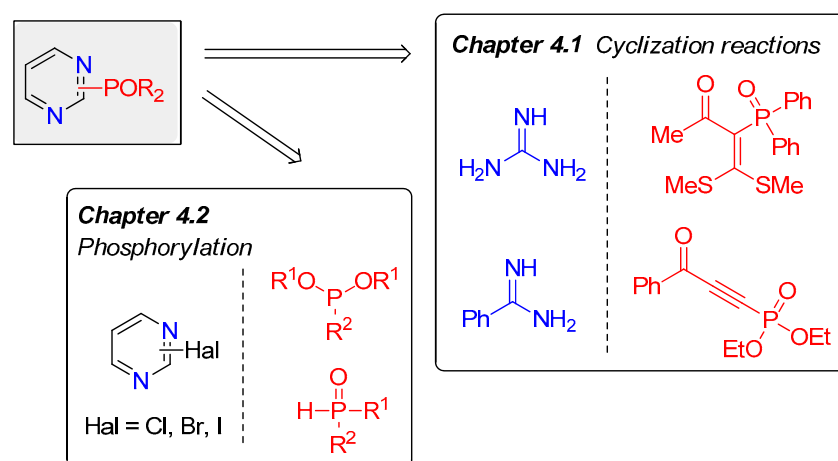
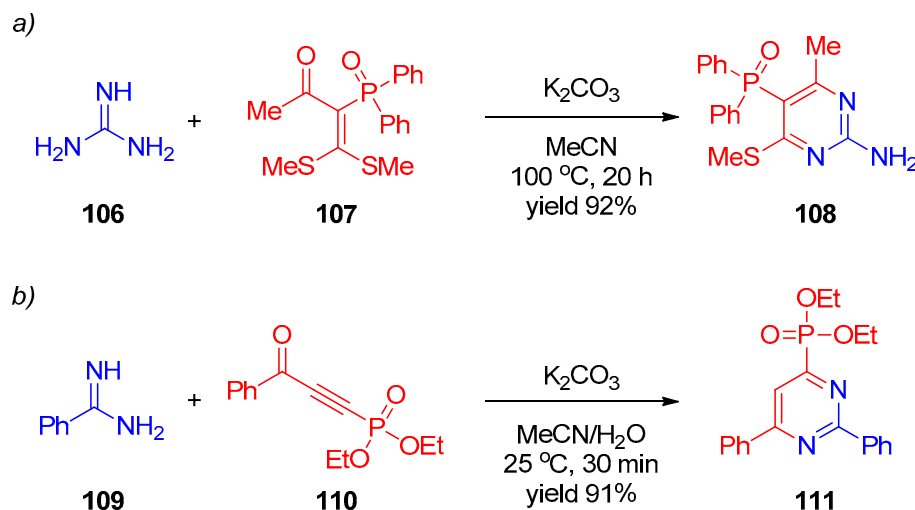


Figure 3. Approaches to synthesis of POR_2 -containing pyrimidines.

4.1. Cyclizations Using Guanidine and Amidines

In early works, synthesis of pyrimidines was accomplished by heterocyclization of guanidine and amidines with phosphorus-containing bis-electrophiles, such as 3-(methylthio)acrylonitriles [114,118], 3-(dimethylamino)propenones [115,116], and acrylonitrile acetal [117]. Recently, Zhu et al. [121] reported one example of the reaction of phosphine oxide-substituted

ketene dithioacetal **107** with guanidine (**106**) providing 5-phosphorus(V)-containing pyrimidine **108** (Scheme 27, line a). Liao et al. [68] described synthesis of pyrimidinyl-4-phosphonate **111** by a reaction between diethyl (3-phenyl-3-oxopropyn-1-yl)phosphonate **110** and benzamidine (**109**) (Scheme 27, line b).



Scheme 27. Cyclization reactions of guanidine (a) and amidine (b).

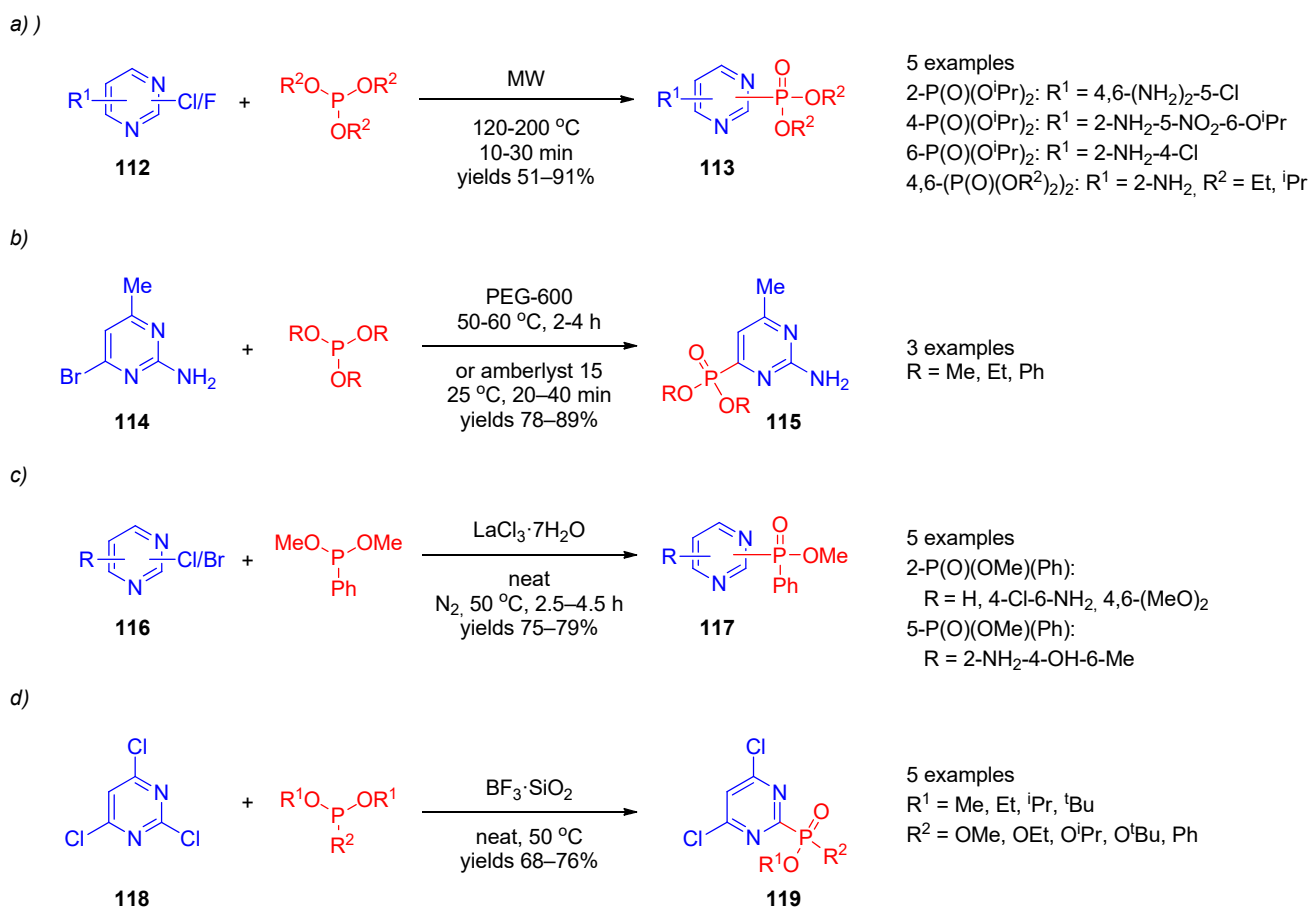
In addition, it may be noted that, recently, three-component acidic condensation of β -keto phosphonates with aldehydes and urea (Biginelli reaction) was shown to be efficient for synthesis of 1,4-dihydro-2-oxopyrimidine-5-phosphonates [122–124]. In this regard, it can be assumed that, in the future, a similar approach using amidines can also be implemented to obtain pentavalent phosphorus-substituted pyrimidines.

4.2. Phosphorylation of Pyrimidines

Due to the significant limitations of synthetic approaches to structurally diverse phosphorus-substituted pyrimidines from phosphorus-containing precursors, phosphorylation of pyrimidines has gained great attention in recent years. Pioneering studies of nucleophilic and electrophilic phosphorylation of pyrimidines [111–113,120] were completed by the Michaelis–Arbuzov reaction, radical, and transition-metal-complex-catalyzed phosphorylation, which are discussed below.

4.2.1. Michaelis–Arbuzov Reaction in Synthesis of Phosphorus-Substituted Pyrimidines

The Michaelis–Arbuzov reaction can probably be considered the most general method for synthesis of phosphorylpyrimidines known at the moment. Examples of use of the Michaelis–Arbuzov reaction in synthesis of pyrimidinylphosphonates (Scheme 28) were described in several studies [125–129]. Pyrimidines **113**, **115**, **117**, and **119** containing the phosphonate moiety at the 2, 4, 5, or 6 position were obtained by reaction of pyrimidinyl halides **112**, **114**, **116**, and **118**, respectively, with phosphites. Several procedures requiring either microwave activation (line a) or the presence of a catalyst, such as acidic ion-exchange resin (line b) or LaCl_3 (line c), were developed and shown to be tolerant to electron-donating and electron-withdrawing substituents on the pyrimidine ring. The chemoselective Michaelis–Arbuzov reaction was accomplished by Varalakshmi et al. [129], who prepared 2,6-dichloropyrimidine-2-phosphonates by coupling of 2,4,6-trichloropyrimidine using silica-gel-supported BF_3 as the catalyst (line d).

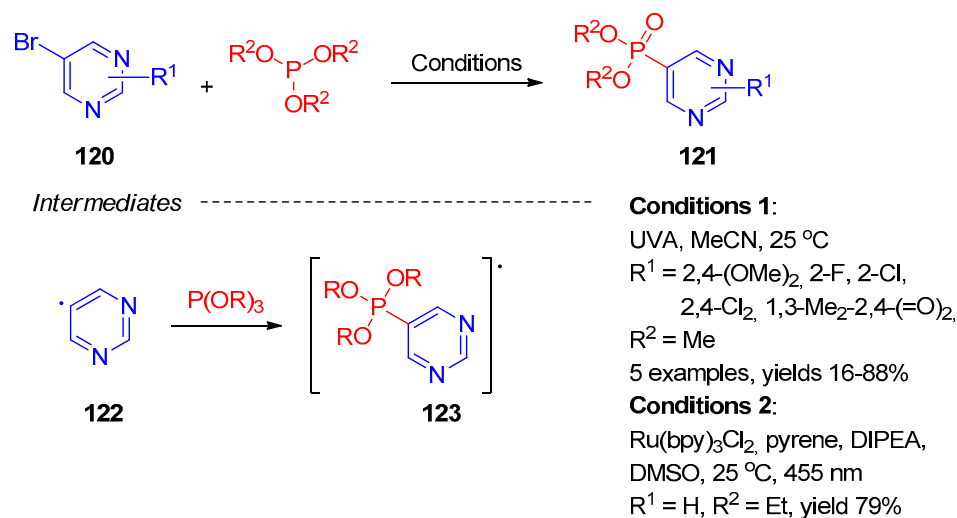


Scheme 28. Michaelis–Arbuzov reaction in synthesis of pyrimidine phosphonates: (a) Jansa et al., 2012 [125]; (b) Kunda et al., 2011 [126]; Mohan Naidu et al., 2011 [127]; (c) Golla et al., 2014 [128]; (d) Varalakshmi et al., 2015 [129].

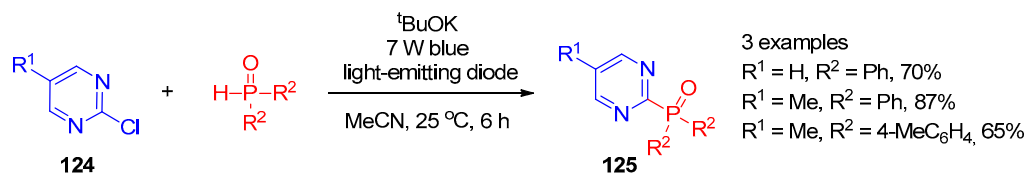
A photochemical version of the Arbuzov reaction was shown to be efficient for synthesis of pyrimidine-5-phosphonates **121** from 5-bromopyrimidines **120** and trialkyl phosphites (Scheme 29) [130,131]. This radical process can be accomplished either directly under mild UV activation or using the Ru(bpy)₃ pyrene dyad irradiated with blue light (455 nm). The plausible mechanism of this transformation involves formation of pyrimidinyl radical **122** either by action of an excited pyrene molecule or directly upon absorption of a light quantum. This radical attacks trialkyl phosphite, and the resulting radical **123** is decomposed to form the product accompanied by release of the alkyl radical.

4.2.2. Radical Phosphorylation of Pyrimidines

Radical functionalization of pyrimidines with phosphine oxides and phosphonates is poorly known. Only the photocatalytic radical reaction of 2-chloropyrimidines **124** with secondary phosphine oxides giving products **125** (Scheme 30) was recently described by Yuan et al. [73] The mechanism of this transformation is similar to that for chloropyrimidines and is considered in Section 2.4.1 (Scheme 6). As a distant example of the radical phosphorylation of pyrimidines, let us mention the work by Zhang et al. [132], who accomplished phosphorylation of pyrimidin-4-ones with dimethyl phosphite in the presence of Mn(OAc)₃.



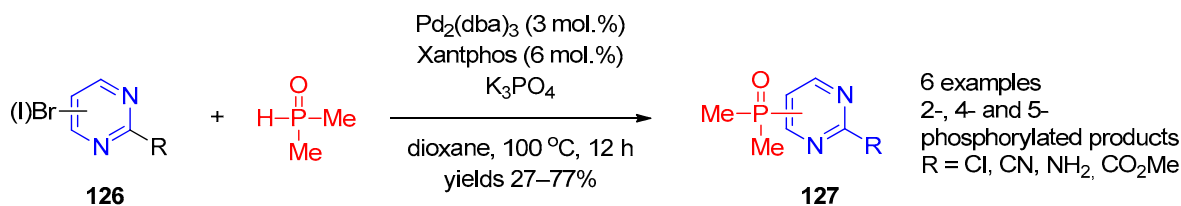
Scheme 29. Photo-Arbusov reaction in synthesis of pyrimidine-5-phosphonates.



Scheme 30. Photocatalytic phosphorylation of 2-chloropyrimidines.

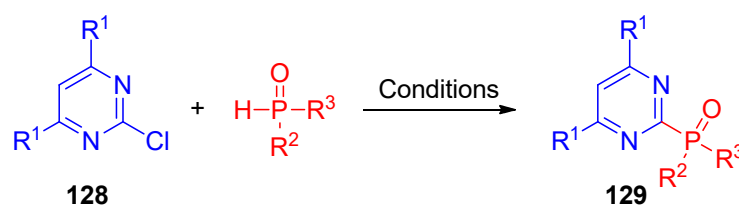
4.2.3. Transition-Metal-Catalyzed Phosphorylation of Pyrimidines

Since the first work on palladium-catalyzed phosphorylation of pyrimidines published in 2008 by Belabassi et al. [45], transition-metal-catalyzed cross-coupling of halopyrimidines with secondary phosphine oxides and phosphonates proved to be an efficient route to phosphorylpyrimidines. Mykhailiuk and co-workers [91] published a procedure for Pd(II)-catalyzed coupling of halo(Br/I)pyrimidines **126** with dimethylphosphine oxide, showing remarkable generality (Scheme 31). Synthesis of 2-, 4-, and 6-phosphine-oxide-substituted pyrimidines **127** bearing electron-donating and electron-withdrawing substituents on the heterocyclic moiety was accomplished using $Pd_2(dba)_3$ in the presence of the Xantphos ligand.



Scheme 31. $Pd_2(dba)_3$ -catalyzed cross-coupling of halopyrimidines with dimethylphosphine oxide.

Individual examples of metal-complex-catalyzed coupling of 2-chloropyrimidines **128** with phosphine oxides were published in studies by Montchamp, Yang, Montel, Zakirova, and their co-workers (Scheme 32) [133–136]. Catalysis was accomplished using Pd(II), Pd(0), or Ni(II) salts, providing 2-phosphorylated pyrimidines **129** in good yield.



Conditions 1: Pd(OAc)₂ (2 mol. %), xantphos (2 mol. %), DIPEA (1.3 equiv.), toluene/ethylene glycol 9:1, 110 °C, R¹ = H, R² = 4-C₈H₁₇, R³ = OEt, 52%

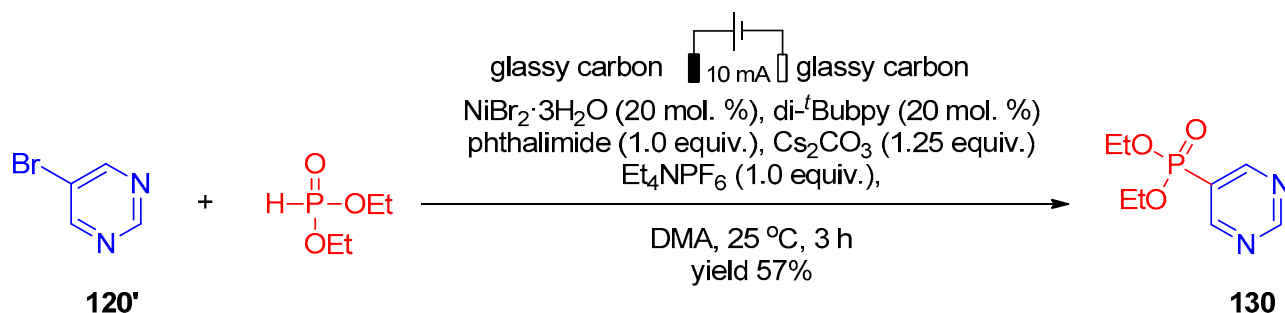
Conditions 2: Pd₂dba₃ (5 mol. %), dppf (10 mol. %), Et₃N (1.5 equiv.), toluene, 80 °C, R¹ = H, R² = OEt, R³ = (CH₂)₃P(O)(OEt)₂, 68%

Conditions 3: Pd(OAc)₂ (1 mol. %), dppf (2 mol. %), K₂CO₃ (1.5 equiv.), DMF, 120 °C, R¹ = H, R² = R³ = Ph, 68%

Conditions 4: NiCl₂(DME) (5 mol. %), ^tBuONa (1.5 equiv.), DMF, 90 °C, R¹ = H, R² = R³ = Ph, 79%

Scheme 32. Transition-metal-catalyzed cross-coupling of 2-chloropyrimidines with phosphine oxides.

Bai et al. [137] reported one example of electrochemical phosphorylation of 5-bromopyrimidine (120') with diethyl phosphonate in the presence of NiBr₂ (Scheme 33), giving diethylpyrimidine-5-phosphonate 130. The authors suggested that the reaction proceeds via a radical mechanism accompanied by anodic generation of a phosphorus-centered radical.



Scheme 33. NiBr₂-catalyzed electrochemical synthesis of 5-phosphorylpyrimidine.

5. Pyrazines

Phosphorus(V)-containing pyrazines are poorly studied six-membered *N*-heterocycles. Synthesis of phosphorylpyrazines was described or mentioned in just over a dozen publications, and, what is more important, most of them are fragmentary in scope. The group of Palacios in the 2000s [138–140], made the most significant contribution to the development of original synthetic approaches to POR₂-substituted pyrazines. The authors proposed self-dimerization of nitrile ylides and 4-dimethylamino-3-phosphoryl-2-azadienes and the formal [4+2]-cycloaddition of 1,2-diaza-1,3-butadienes with 1,2-diamines, which are considered below along with works on phosphorylation of the pyrazine ring (Figure 4).

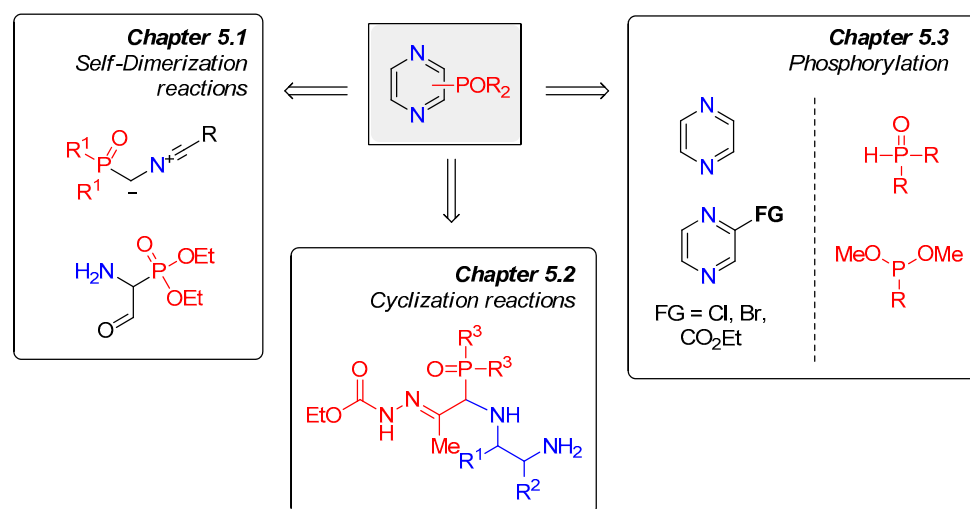
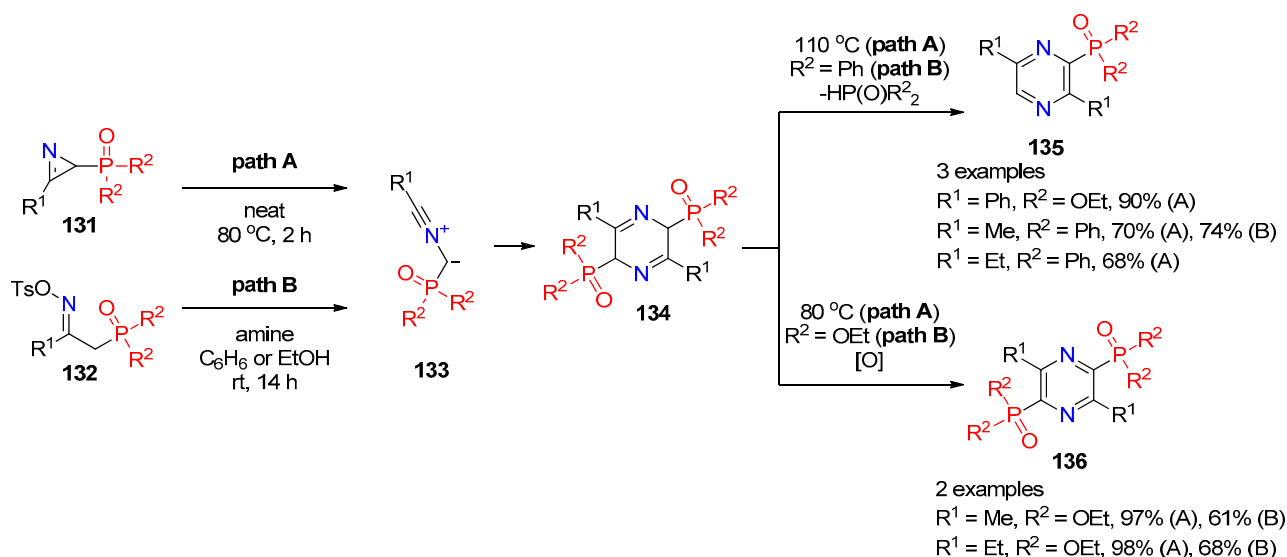


Figure 4. Approaches to synthesis of POR_2 -containing pyrazines.

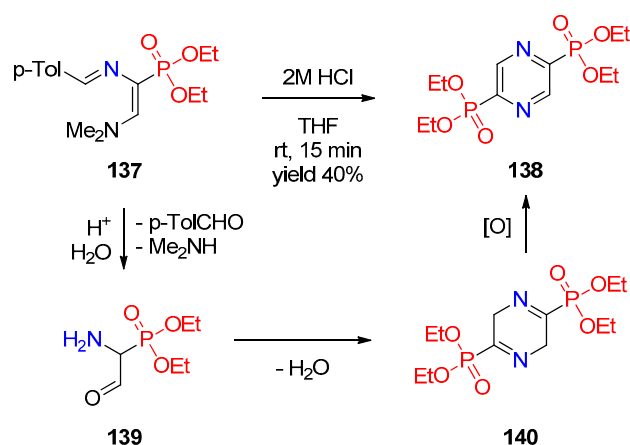
5.1. Dimerization Reactions

Palacios et al. [138] described synthesis of phosphorus-substituted pyrazines via dimerization of nitrile ylides **133** (Scheme 34), which can be generated in situ from POR_2 -bearing 2*H*-azirines **131** (pathway A) or tosylated 2-hydroxyiminophosphonates **132** (pathway B). According to the proposed mechanism, intermediate **133** undergoes self-dimerization to dihydropyrazine **134** followed by either oxidation of the latter compound or elimination of secondary phosphine oxide. An interesting feature of this transformation is that it allows targeted synthesis of either mono- or bisphosphorus(V)-substituted pyrazines **135** and **136**. Thus, synthesis via pathway A at 80 °C affords products **136**, whereas heating to 110 °C yields products **135**. The outcome of the reaction via pathway B is determined by substituents on the phosphorus(V) moiety. Thus, presence of a phenyl group results in formation of the monophosphorylated product, whereas the bisphosphorylated product is generated in the presence of the ethoxy group.



Scheme 34. Synthesis of phosphorus-containing pyrazines via dimerization of nitrile ylides.

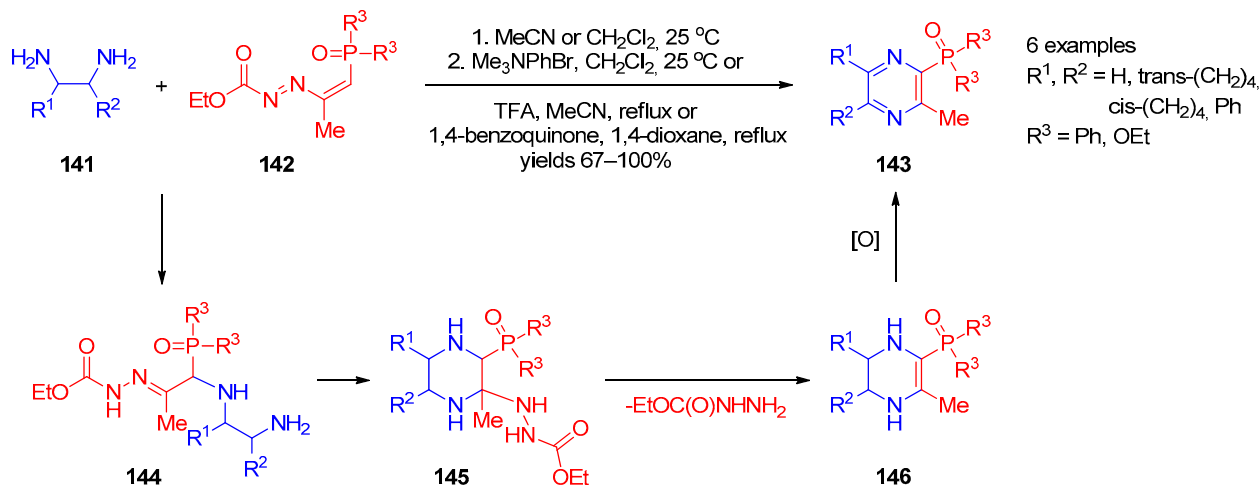
In another study, the same group [139] demonstrated that bis-2,5-phosphorylpyrazine **138** can be obtained via dimerization of aminoaldehyde **139** derived from 4-dimethylamino-3-phosphoryl-2-azadiene **137** via acid hydrolysis of both enamine and imine groups (Scheme 35). The reaction was proposed to occur through formation of dihydropyrazine **140**, the oxidation of which in the reaction medium provides the final pyrazine.



Scheme 35. Dimerization of 4-dimethylamino-3-phosphoryl-2-azadiene.

5.2. Formal [4+2]-Cycloaddition

In the subsequent study, Palacios and co-workers [140] used the reaction of phosphorus-containing 1,2-diaza-1,3-butadienes **142** with 1,2-diamines **141** as access to polysubstituted POR_2 -modified pyrazines **143** (Scheme 36). This formal [4+2]-cycloaddition is a general method for synthesis of alkyl- and arylpyrazines bearing phosphine oxides and phosphonates substituents. The plausible mechanism of this reaction involves the following steps: the Michael addition of diamine **141** to diazadiene system **142**, giving adduct **144**, intramolecular attack of the second amino group on the C=N double bond of hydrazone, and elimination of ethyl hydrazinecarboxylate from the resulting piperazine **145** followed by oxidation of 1,2,3,4-tetrahydropyrazine **146** to pyrazine.



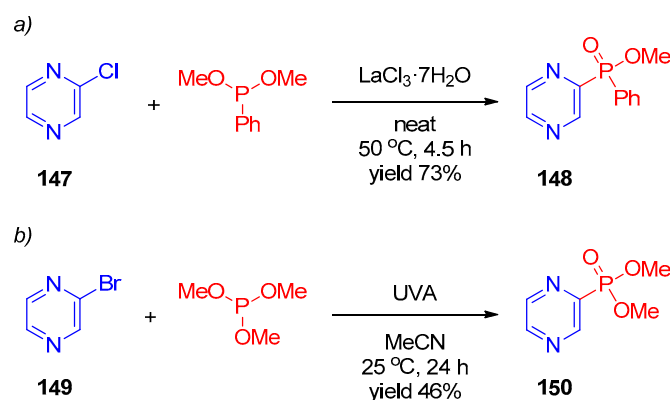
Scheme 36. Synthesis of 2- POR_2 -substituted pyrazines from 1,2-diaza-1,3-butadienes and 1,2-diamines.

5.3. Phosphorylation of Pyrazines

Synthesis of 2-phosphorus(V)-substituted pyrazine based on phosphorylation was first described by Seggio et al. [141] in 2007. They reported an efficient two-step procedure for preparation of (diphenylphosphino)pyrazine oxide based on deprotonation of pyrazine with a mixture of ZnCl_2 , TMEDA, and LiTMP followed by treatment of the resulting lithium complex of di(pyrazin-2-yl)zinc with chlorodiphenylphosphine. Most of the later studies are scattered and describe single examples of phosphorylation of the pyridazine core via the Michaelis–Arbuzov reaction, radical, and transition-metal-catalyzed phosphorylation reactions, which are discussed below.

5.3.1. Michaelis–Arbuzov Reaction in the Synthesis of Phosphorus-Substituted Pyrazines

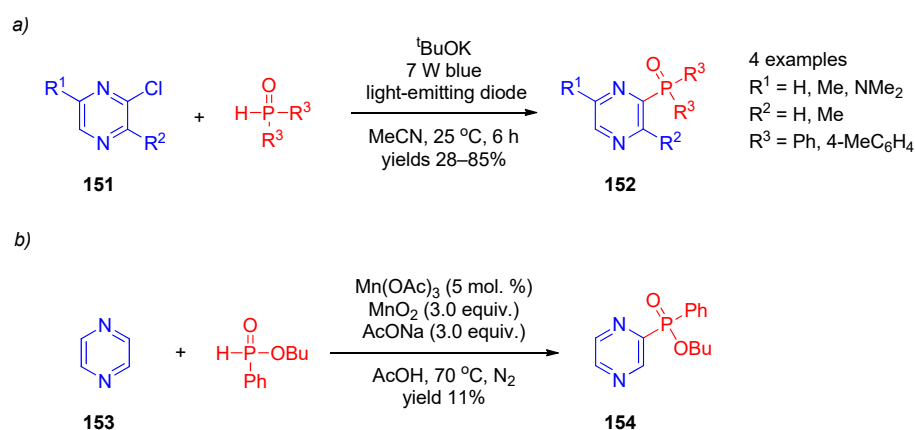
Despite more than a century of history, the Michaelis–Arbuzov reaction was relatively recently applied for phosphorylation of pyridazines. Thus, Golla et al. [128] synthesized 2-phosphorylpyrazine **148** from 2-chloropyrazine (**147**) and dimethyl phenylphosphonite using $\text{LaCl}_3 \cdot 7\text{H}_2\text{O}$ as the catalyst under neat conditions (Scheme 37, line a). Goddard and co-workers [131] reported an example of using the photo-Arbuzov reaction to prepare dimethyl pyrazine-2-phosphonate **150** from 2-bromopyrazine (**149**) and trimethyl phosphite under mild UVA irradiation (Scheme 37, line b).



Scheme 37. Synthesis of 2-phosphorylpyrazine by the Arbuzov reaction: (a) Golla et al., 2014 [128]; (b) Goddard et al., 2016 [131].

5.3.2. Radical Phosphorylation of Pyrazines

Recently, Yuan et al. [73] described three examples of photocatalytic radical phosphorylation of 2-chloropyrazines **151** with secondary phosphine oxides, giving 2-substituted pyrazines **152** (Scheme 38, line a). The reaction occurred in the presence of $^t\text{BuOK}$ under mild conditions using irradiation with a blue-light-emitting diode. The mechanism of transformation is similar to that discussed for pyridines in Chapter 2.4.1 (Scheme 6). Further, Berger and Montchamp [142] reported synthesis of single 2-phosphorylated pyrazine **154** by reaction of pyridazine (**153**) with phosphonite in the presence of MnO_2 and $\text{Mn}(\text{OAc})_3$ (Scheme 38, line b). The authors suggested that the reaction proceeds through formation of a phosphorus-centered radical that adds to pyrazine.

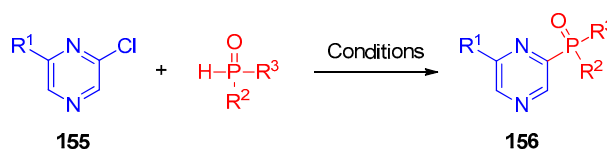


Scheme 38. Synthesis of 2-POR₂-substituted pyrazines by radical phosphorylation: (a) Yuan et al., 2018 [73]; (b) Berger and Montchamp, 2019 [142].

5.3.3. Transition-Metal-Catalyzed Phosphorylation of Pyrazines

It was shown that 2-chloropyrimidines **155** have good synthetic potential as precursors for synthesis of 2-phosphorus-substituted pyrazines **156** under conditions of metal-catalyzed phosphorylation (Scheme 39). The Pd(II)-catalyzed phosphorylation

of chloropyrazine was described in studies by Belabassi, Deal, Nikishin, and their co-workers [40,45,133,143] (conditions 1–3). The generality of the approach with respect to phosphine oxides and phosphonates was demonstrated using Pd(dppf)Cl₃ as the catalyst (condition 3). Note that Zhao et al. [144] performed this transformation in the presence of NiCl₂(dppp) complexes as the catalyst (condition 4). Further, Yamaguchi and co-workers [100] described one example of nickel(II)-acetate-catalyzed phosphorylation of phenyl pyrazine-2-carboxylate with diphenylphosphine oxide accompanied by decarbonylation.



Conditions 1: Pd(OAc)₂ (1 mol. %), dppf (1 mol. %), DIPEA (1.3 equiv.), MeCN, reflux, 19 h, R¹ = H, R² = R³ = O^tPr, 97%

Conditions 2: Pd(OAc)₂ (2 mol. %), xantphos (2 mol. %), DIPEA (1.3 equiv.), toluene/ethylene glycol 9:1, 110 °C, R¹ = H, R² = C₈H₁₇, R³ = OEt, 79%

Conditions 3: Pd(dppf)Cl₃ (1 mol. %), DIPEA or DBU (1.05 equiv.), MeCN, reflux, 3-20 h, R¹ = C(O)Me, C(O)N(CH₂CH₂)₂O, C(O)N(C₈H₁₇)₂, C(O)NH(CH₂)₃O(calix[4]arene), R² = R³ = O^tPr, Ph, 6 examples, 61-92%

Conditions 4: NiCl₂(dppp) (10 mol. %), K₃PO₄ (2.0 equiv.), 1,4-dioxane, 120 °C, R¹ = H, R² = R³ = OMe, 50%

Scheme 39. Synthesis of 2-phosphorylpyrazines under transition metal catalysis.

6. Conclusions

In conclusion, in the past decade, significant progress was made in synthesis of phosphorus-substituted six-membered aromatic heterocycles. Numerous interesting synthetic approaches were developed based on construction of a heterocyclic core using phosphoryl-containing reagents, mainly formal cycloaddition and intra(inter)molecular cyclization/isomerization, using the Michael reaction, carbenoid intermediates, and classical nucleophilic–electrophilic interactions. Their apparent advantages are structurally diverse products and high tolerance to functional groups. Further, phosphorylation represents the most general route to phosphorus-substituted pyridines, pyridazines, pyrimidines, and pyrazines. Halogen-substituent in six-membered *N*-heterocycles has proven to be a universal leaving group providing phosphorylation, and some functional groups (OH, OTs, B(OH)₂, CO₂Ph, N=NSO₂Me, etc.) were also efficient in this process. However, the necessity of finding conditions for each particular type of heterocycles, severe reaction conditions (high temperature, presence of strong bases and acids), and high cost of reagent/catalysts significantly limit practical application of this approach.

Evidently, development of synthetic methods based on phosphorylation of heterocycles and heterocyclization involving phosphorus-substituted reagents is of fundamental research interest. In point of fact, pyridines have received a great deal of attention among monocyclic six-membered *N*-heterocycles in the past decade, resulting in development of a number of approaches with good substrate scope and efficiency. Most of the methods proposed for pyridazines, pyrimidines, and pyrazines are fragmented and sporadic, while phosphorus-substituted triazines and tetrazines are not described. In this regard, further development of this research area is associated with the following issues: *design of new versatile multifunctional reagents for various chemical transformations* (detailed investigation of such new reagents would provide the basis for a new area in synthesis of nitrogen-containing heterocyclic compounds with different combinations of heteroatoms and also for preparation of new complex heterocyclic systems and assemblies); *transition-metal-catalyzed C–H phosphorylation of six-membered N-heterocycles* (transition-metal-catalyzed CH phosphorylation is a straightforward and attractive approach to construct C–P bonds; however, it is difficult to execute this approach in practice because of the strong propensity of phosphorus reagents to induce catalyst poisoning through coordination); *development of*

methods for synthesis of phosphorus-substituted six-membered *N*-heterocycles with more than two nitrogen atoms in the ring (no representatives of such compounds have been described to date). Since there are a few examples of synthesis of certain phosphorus(V)-substituted six-membered heterocycles while synthetic approaches to phosphorylated derivatives of a wide range of particular *N*-heterocycles are still absent, further research in this field is a long-term challenge.

Author Contributions: Conceptualization, writing, editing, and submitting, Y.V.; Conceptualization, I.Z. All authors have read and agreed to the published version of the manuscript.

Funding: This work was financially supported by the Russian Science Foundation (project No. 22-13-00161).

Institutional Review Board Statement: Not applicable.

Informed Consent Statement: Not applicable.

Data Availability Statement: Not applicable.

Acknowledgments: We also acknowledge Mikhail Kozlov for technical assistance in preparing the manuscript.

Conflicts of Interest: The authors declare no conflict of interest.

Sample Availability: Not applicable.

Abbreviations

N-methyl-D-aspartate (NMDA); dibenzylideneacetone (dba); 1,8-diazabicyclo [5.4.0]undec-7-ene (DBU); density functional theory (DFT); 1,1'-bis(diphenylphosphino)ferrocene (dppf); 1,3-bis(diphenylphosphino)propane (dppp); 4,4'-dipyridyl (dpy); lithium tetramethylpiperidide (LiTMP); tetramethylethylenediamine (TMEDA); ultraviolet radiation (UVA); 4,5-bis(diphenylphosphino)-9,9-dimethylxanthene (Xantphos).

References

- Duffy, M.P.; Delaunay, W.; Bouit, P.-A.; Hissler, M. π -Conjugated phospholes and their incorporation into devices: Components with a great deal of potential. *Chem. Soc. Rev.* **2016**, *45*, 5296–5310. [CrossRef] [PubMed]
- Tang, W.; Zhang, X. New chiral phosphorus ligands for enantioselective hydrogenation. *Chem. Rev.* **2003**, *103*, 3029–3070. [CrossRef] [PubMed]
- Surry, D.S.; Buchwald, S.L. Biaryl phosphane ligands in palladium-catalyzed amination. *Angew. Chem. Int. Ed.* **2008**, *47*, 6338–6361. [CrossRef] [PubMed]
- Bayne, J.; Stephan, D. Phosphorus Lewis acids: Emerging reactivity and applications in catalysis. *Chem. Soc. Rev.* **2016**, *45*, 765–774. [CrossRef] [PubMed]
- Nixon, T.D.; Gamble, A.J.; Thatcher, R.J.; Whitwood, A.C.; Lynam, J.M. Synthesis and coordination chemistry of pyrimidine-substituted phosphine ligands. *Inorg. Chim. Acta* **2012**, *380*, 252–260. [CrossRef]
- Cross, J.M.; Gallagher, N.; Gill, J.H.; Jain, M.; McNeillis, A.W.; Rockley, K.L.; Tscherny, F.H.; Wirszyocz, N.J.; Yufit, D.S.; Walton, J.W. Pyridylphosphinate metal complexes: Synthesis, structural characterisation and biological activity. *Dalton Trans.* **2016**, *45*, 12807–12813. [CrossRef]
- Artem'ev, A.V.; Eremina, J.A.; Lider, E.V.; Antonova, O.V.; Vorontsova, E.V.; Bagryanskaya, I.Y. Luminescent Ag (I) scorpionates based on tris(2-pyridyl)phosphine oxide: Synthesis and cytotoxic activity evaluation. *Polyhedron* **2017**, *138*, 218–224. [CrossRef]
- Shudo, N.; Mizoguchi, T.; Kiyosue, T.; Arita, M.; Yoshimura, A.; Seto, K.; Sakoda, R.; Akiyama, S.-I. Two pyridine analogues with more effective ability to reverse multidrug resistance and with lower calcium channel blocking activity than their dihydropyridine counterparts. *Cancer Res.* **1990**, *50*, 3055–3061.
- Pfefferkorn, J.A.; Guzman-Perez, A.; Litchfield, J.; Aiello, R.; Treadway, J.L.; Pettersen, J.; Minich, M.L.; Filipinski, K.J.; Jones, C.S.; Tu, M. Discovery of (S)-6-(3-cyclopentyl-2-(4-(trifluoromethyl)-1H-imidazol-1-yl)propanamido) nicotinic acid as a hepatoselective glucokinase activator clinical candidate for treating type 2 diabetes mellitus. *J. Med. Chem.* **2012**, *55*, 1318–1333. [CrossRef] [PubMed]
- Murray, K.J.; Porter, R.A.; Warrington, B.H.; Lahouratate, P. Phenol and Pyridinol Derivatives as Lusitropic Agents. Patent WO1993019754A1, 23 March 1993.

11. Ali, T.E.; Assiri, M.A.; El-Shaar, H.M.; Abed-Kariem, S.M.; Abdel-Monem, W.R.; El-Edfawy, S.M.; Hassanin, N.M.; Shati, A.A.; Alfaifi, M.Y.; Elbehairi, S.E.I. Synthesis and biological activities of some new phosphorus compounds containing pyranopyrazole moiety. *Heterocycles* **2021**, *102*, 1119–1137. [CrossRef]
12. de Assis, T.M.; Gajo, G.C.; de Assis, L.C.; Garcia, L.S.; Silva, D.R.; Ramalho, T.C.; da Cunha, E.F.F. QSAR models guided by molecular dynamics applied to human glucokinase activators. *Chem. Biol. Drug Des.* **2016**, *87*, 455–466. [CrossRef]
13. Dziuganowska, Z.A.; Slepokura, K.; Volle, J.-N.; Virieux, D.; Pirat, J.-L.; Kafarski, P. Structural analogues of Selfotel. *J. Org. Chem.* **2016**, *81*, 4947–4954. [CrossRef] [PubMed]
14. Khandelwal, A.; Lukacova, V.; Comez, D.; Kroll, D.M.; Raha, S.; Balaz, S. A combination of docking, QM/MM methods, and MD simulation for binding affinity estimation of metalloprotein ligands. *J. Med. Chem.* **2005**, *48*, 5437–5447. [CrossRef]
15. Venkata Ramana, K.; Venkata Subbaiah, K.; Lokanatha, V.; Naga Raju, C. Synthesis and antimicrobial activity evaluation of new dialkyl heteroarylphosphonates. *Der. Pharm. Chem.* **2011**, *3*, 181–188.
16. Gardner, G.; Steffens, J.J.; Grayson, B.T.; Kleier, D.A. 2-Methylcinnolinium herbicides: Effect of 2-methylcinnolinium-4-(O-methylphosphonate) on photosynthetic electron transport. *J. Agric. Food Chem.* **1992**, *40*, 318–321. [CrossRef]
17. DeFrees, S.A.; Sawick, D.P.; Cunningham, B.; Heinsteinst, P.F.; Morré, D.J.; Cassady, J.M. Structure-activity relationships of pyrimidines as dihydroorotate dehydrogenase inhibitors. *Biochem. Pharmacol.* **1988**, *37*, 3807–3816. [CrossRef] [PubMed]
18. Stansfield, I.; Avolio, S.; Colarusso, S.; Gennari, N.; Narjes, F.; Pacini, B.; Ponzi, S.; Harper, S. Active site inhibitors of HCV NS5B polymerase. The development and pharmacophore of 2-thienyl-5, 6-dihydroxypyrimidine-4-carboxylic acid. *Bioorganic Med. Chem. Lett.* **2004**, *14*, 5085–5088. [CrossRef] [PubMed]
19. Zhang, H.-w.; Zhou, L.; Coats, S.J.; McBrayer, T.R.; Tharnish, P.M.; Bondada, L.; Detorio, M.; Amichai, S.A.; Johns, M.D.; Whitaker, T. Synthesis of purine modified 2'-C-methyl nucleosides as potential anti-HCV agents. *Bioorganic Med. Chem. Lett.* **2011**, *21*, 6788–6792. [CrossRef] [PubMed]
20. Teng, M.; Johnson, M.D.; Thomas, C.; Kiel, D.; Lakis, J.N.; Kercher, T.; Aytes, S.; Kostrowicki, J.; Bhumralkar, D.; Truesdale, L. Small molecule ago-allosteric modulators of the human glucagon-like peptide-1 (hGLP-1) receptor. *Bioorganic Med. Chem. Lett.* **2007**, *17*, 5472–5478. [CrossRef]
21. Kumar, A.V.; Mohan, K. Insights into binding of potential antitumor quinoxaline analogues against cyclin dependent kinase 2 using docking studies. *J. Chem. Biol. Phys. Sci.* **2012**, *2*, 2419.
22. Kozlov, M.; Komkov, A.; Losev, T.; Tyurin, A.; Dmitrenok, A.; Zavarzin, I.; Volkova, Y. Flexible synthesis of phosphoryl-substituted imidazolines, tetrahydropyrimidines, and thioamides by sulfur-mediated processes. *J. Org. Chem.* **2019**, *84*, 11533–11541. [CrossRef] [PubMed]
23. Kozlov, M.; Kozlov, A.; Komkov, A.; Lyssenko, K.; Zavarzin, I.; Volkova, Y. Synthesis of phosphoryl thioamides via three-component reaction of phosphinic chlorides with amines and sulfur. *Adv. Synth. Catal.* **2019**, *361*, 2904–2915. [CrossRef]
24. Van der Jeught, S.; Stevens, C.V. Direct phosphorylation of aromatic azaheterocycles. *Chem. Rev.* **2009**, *109*, 2672–2702. [CrossRef] [PubMed]
25. Chen, L.; Liu, X.Y.; Zou, Y.X. Recent advances in the construction of phosphorus-substituted heterocycles, 2009–2019. *Adv. Synth. Catal.* **2020**, *362*, 1724–1818. [CrossRef]
26. Liu, J.; Xiao, H.-Z.; Fu, Q.; Yu, D.-G. Advances in radical phosphorylation from 2016 to 2021. *Chem. Synth.* **2021**, *1*, 9. [CrossRef]
27. Budnikova, Y.H.; Sinyashin, O.G.D. Phosphorylation of C–H bonds of aromatic compounds using metals and metal complexes. *Russ. Chem. Rev.* **2015**, *84*, 917–951. [CrossRef]
28. Luo, K.; Yang, W.C.; Wu, L. Photoredox catalysis in organophosphorus chemistry. *Asian J. Org. Chem.* **2017**, *6*, 350–367. [CrossRef]
29. Budnikova, Y.H.; Gryaznova, T.V.; Grinenko, V.V.; Dudkina, Y.B.; Khrizanforov, M.N. Eco-efficient electrocatalytic C–P bond formation. *Pure Appl. Chem.* **2017**, *89*, 311–330. [CrossRef]
30. Pan, X.-Q.; Zou, J.-P.; Yi, W.-B.; Zhang, W. Recent advances in sulfur- and phosphorus-centered radical reactions for the formation of S–C and P–C bonds. *Tetrahedron* **2015**, *40*, 7481–7529. [CrossRef]
31. Haji, M. Multicomponent reactions: A simple and efficient route to heterocyclic phosphonates. *Beilstein J. Org. Chem.* **2016**, *12*, 1269–1301. [CrossRef]
32. Gao, Y.; Tang, G.; Zhao, Y. Recent progress toward organophosphorus compounds based on phosphorus-centered radical difunctionalizations. *Phosphorus Sulfur Silicon Relat. Elem.* **2017**, *192*, 589–596. [CrossRef]
33. Demmer, C.S.; Krogsgaard-Larsen, N.; Bunch, L. Review on modern advances of chemical methods for the introduction of a phosphonic acid group. *Chem. Rev.* **2011**, *111*, 7981–8006. [CrossRef] [PubMed]
34. Volkova, Y.; Kozlov, M.; Zavarzin, I. Synthetic Routes to P(O)-Substituted Five-Membered Aromatic Heterocycles (2010–2021). *Targets Heterocycl. Syst. Chem. Prop.* **2022**, *26*, 18–45.
35. Egorova, A.V.; Svintitskaya, N.I.; Dogadina, A.V. Synthesis of phosphorylated indoles. *Russ. J. Gen. Chem.* **2018**, *88*, 2276–2289. [CrossRef]
36. Chen, L.; Zou, Y.X. Recent progress in the synthesis of phosphorus-containing indole derivatives. *Org. Biomol. Chem.* **2018**, *16*, 7544–7556. [CrossRef]
37. Baiju, T.; Namboothiri, I.N. Synthesis of functionalized pyrazoles via 1,3-dipolar cycloaddition of α -diazo- β -ketophosphonates, sulfones and esters with electron-deficient alkenes. *Chem. Rec.* **2017**, *17*, 939–955. [CrossRef]
38. Goulioukina, N.S.; Makukhin, N.N.; Beletskaya, I.P. Synthetic routes to 3(5)-phosphonylated pyrazoles. *Russ. Chem. Rev.* **2016**, *85*, 667–683. [CrossRef]

39. Gazizov, A.S.; Smolobochkin, A.V.; Turmanov, R.A.; Pudovik, M.A.; Burilov, A.R.; Sinyashin, O.G. Synthesis of phosphaproline derivatives: A short overview. *Synthesis* **2019**, *51*, 3397–3409. [CrossRef]
40. Nikishkin, N.I.; Huskens, J.; Assenmacher, J.; Wilden, A.; Modolo, G.; Verboom, W. Palladium-catalyzed cross-coupling of various phosphorus pronucleophiles with chloropyrazines: Synthesis of novel Am(III)-selective extractants. *Org. Biomol. Chem.* **2012**, *10*, 5443–5451. [CrossRef] [PubMed]
41. Deng, L.; Diao, J.; Chen, P.; Pujari, V.; Yao, Y.; Cheng, G.; Crick, D.C.; Prasad, B.V.; Song, Y. Inhibition of 1-deoxy-D-xylulose-5-phosphate reductoisomerase by lipophilic phosphonates: SAR, QSAR, and crystallographic studies. *J. Med. Chem.* **2011**, *54*, 4721–4734. [CrossRef] [PubMed]
42. Perry, H.; Zoń, J.; Law, J.; Clearfield, A. Structural variations of SnII pyridylphosphonates influenced by an uncommon Sn–N interaction. *J. Solid State Chem.* **2010**, *183*, 1165–1173. [CrossRef]
43. Zhang, J.; Wang, J.; Wei, C.; Wang, Y.; Xie, G.; Li, Y.; Li, M. Rapidly sequence-controlled electrosynthesis of organometallic polymers. *Nat. Commun.* **2020**, *11*, 2530. [CrossRef] [PubMed]
44. Barycki, J.; Gancarz, R.; Milewska, M.; Tyka, R.; Sawka-Dobrowolska, W. 1-Phthalazinephosphonic acid—An unexpected product of the reaction between diisopropylphosphite and *o*-phthalazine. *Phosphorus Sulfur Silicon Relat. Elem.* **1998**, *143*, 167–178. [CrossRef]
45. Belabassi, Y.; Alzghari, S.; Montchamp, J.-L. Revisiting the Hirao cross-coupling: Improved synthesis of aryl and heteroaryl phosphonates. *J. Organomet. Chem.* **2008**, *693*, 3171–3178. [CrossRef]
46. Plazek, S.; Sasyk, Z. Über einige phosphoe-pyridinverbindungen. *Chemisches Zent.* **1935**, *106*, 2177.
47. Collins, D.J.; Hetherington, J.W.; Swan, J.M. Organophosphorus compounds. XIV. A new synthesis of 3-pyridylphosphonic acid. *Aust. J. Chem.* **1974**, *27*, 1355–1360. [CrossRef]
48. Wu, J.; Chen, H.; Zhou, Z.-Y.; Yeung, C.H.; Chan, A.S.C. Synthesis and structural characterization of a highly effective chiral dipyridylphosphine ligand and its application in the Ru-catalyzed asymmetric hydrogenation of β -ketoesters. *Synlett* **2001**, *2001*, 1050–1054. [CrossRef]
49. Wu, J.; Chen, H.; Kwok, W.H.; Lam, K.H.; Zhou, Z.Y.; Yeung, C.H.; Chan, A.S.C. A new chiral dipyridylphosphine ligand Xyl-P-Phos and its application in the Ru-catalyzed asymmetric hydrogenation of β -ketoesters. *Tetrahedron Lett.* **2002**, *43*, 1539–1543. [CrossRef]
50. Bennett, R.; Burger, A.; Volk, W. Communications—3-Pyridylphosphonic acid. *J. Org. Chem.* **1958**, *23*, 940. [CrossRef]
51. Redmore, D. Phosphorus derivatives of nitrogen heterocycles. 2. Pyridinephosphonic acid derivatives. *J. Org. Chem.* **1970**, *35*, 4114–4117. [CrossRef]
52. Eliseenkov, V.N.; Bureva, N.V.; Ivanov, B.E. Some transformations in a number of (2-pyridyl)phosphonates. *Chem. Heterocycl. Compd.* **1974**, *10*, 1182–1184. [CrossRef]
53. Predvoditelev, D.A.; Chukbar, T.G.; Nifant'ev, E. Some new derivatives of pyridyl- and quinolylphosphonic acids. *Chem. Heterocycl. Compd.* **1975**, *11*, 330–333. [CrossRef]
54. Bulot, J.J.; Aboujaoude, E.E.; Collignon, N.; Savignac, P. Préparation d'aminophenyl-, nitrophenyl-, pyridyl-, et quinolylphosphonates sous photostimulation ou assistance métallique; acces aux acides aminophosphoniques correspondants. *Phosphorus Sulfur Relat. Elem.* **2006**, *21*, 197–204. [CrossRef]
55. Boduszek, B. Pyridine-2-phospho-carboxylic acids: Synthesis and properties. *J. Prakt. Chem. Chem. Ztg.* **1992**, *334*, 444–446. [CrossRef]
56. Boduszek, B.; Wieczorek, J.S. A new method for the preparation of pyridine-4-phosphonic acids. *Synthesis* **1979**, *1979*, 452–453. [CrossRef]
57. Markovskii, L.N.; Furin, G.G.; Shermolovich, Y.G.; Yakobson, G.G. Phosphorylation of polyfluoroaromatic compounds. *Bull. Acad. Sci. USSR Div. Chem. Sci.* **1981**, *30*, 646–648. [CrossRef]
58. Boenigk, W.; Fischer, U.; Hägele, G. Über die michaelis-arbuzov-reaktion perhalogenierter pyridine. II¹. *Phosphorus Sulfur Relat. Elem.* **2007**, *16*, 263–266. [CrossRef]
59. Penicaud, V.; Odobel, F.; Bujoli, B. Facile and efficient syntheses of 2,2'-bipyridine-based bis(phosphonic) acids. *Tetrahedron Lett.* **1998**, *39*, 3689–3692. [CrossRef]
60. Adam, M.S.S.; Kühl, O.; Kindermann, M.K.; Heinicke, J.W.; Jones, P.G. 3-Amino- and 3-acylamido-2-phosphonopyridines: Synthesis by Pd-catalyzed P–C coupling, structure and conversion to pyrido[*b*]-annelated P=C–N heterocycles. *Tetrahedron* **2008**, *64*, 7960–7967. [CrossRef]
61. Palacios, F.; Gil, M.J.; de Marigorta, E.M.; Rodríguez, M. Synthesis and reactivity of imines derived from bisphosphonates and 3-phosphorylated 2-aza-1,3-dienes. *Tetrahedron* **2000**, *56*, 6319–6330. [CrossRef]
62. Palacios, F.; Aparicio, D.; López, Y.; de los Santos, J.M.; Ezpeleta, J.M. Preparation and reactions of 3-phosphinyl-1-aza-1,3-butadienes. Synthesis of phosphorylated pyridine and pyrazole derivatives. *Tetrahedron* **2006**, *62*, 1095–1101. [CrossRef]
63. Allais, C.; Lieby-Muller, F.; Rodriguez, J.; Constantieux, T. Metal-free michael-addition-initiated three-component reaction for the regioselective synthesis of highly functionalized pyridines: Scope, mechanistic investigations and applications. *Eur. J. Org. Chem.* **2013**, *2013*, 4131–4145. [CrossRef]
64. Allais, C.; Constantieux, T.; Rodriguez, J. Use of beta,gamma-unsaturated alpha-ketocarboxyls for a totally regioselective oxidative multicomponent synthesis of polyfunctionalized pyridines. *Chemistry* **2009**, *15*, 12945–12948. [CrossRef] [PubMed]

65. Allais, C.; Liéby-Muller, F.; Constantieux, T.; Rodriguez, J. Dual heterogeneous catalysis for a regioselective three-component synthesis of bi- and tri(hetero)arylpyridines. *Adv. Synth. Catal.* **2012**, *354*, 2537–2544. [CrossRef]
66. Hanashalshahaby, E.H.; Unaleroglu, C. Mannich bases as enone precursors for water-mediated efficient synthesis of 2,3,6-trisubstituted pyridines and 5,6,7,8-tetrahydroquinolines. *ACS Comb. Sci.* **2015**, *17*, 374–380. [CrossRef]
67. Abdou, W.M.; Shaddy, A.A.; Kamel, A.A. Structure-based design and synthesis of acyclic and substituted heterocyclic phosphonates linearly linked to thiazolobenzimidazoles as potent hydrophilic antineoplastic agents. *Chem. Pap.* **2017**, *71*, 1961–1973. [CrossRef]
68. Liao, L.; Zhang, H.; Zhao, X. Selenium- π -acid catalyzed oxidative functionalization of alkynes: Facile access to ynones and multisubstituted oxazoles. *ACS Catal.* **2018**, *8*, 6745–6750. [CrossRef]
69. Qi, X.; Dai, L.; Park, C.M. Carbenoid-mediated N-O bond insertion and its application in the synthesis of pyridines. *Chem. Commun.* **2012**, *48*, 11244–11246. [CrossRef]
70. Loy, N.S.; Singh, A.; Xu, X.; Park, C.M. Synthesis of pyridines by carbenoid-mediated ring opening of 2H-azirines. *Angew. Chem. Int. Ed.* **2013**, *52*, 2212–2216. [CrossRef]
71. Kashima, K.; Ishii, M.; Tanaka, K. Synthesis of pyridylphosphonates by rhodium-catalyzed [2+2+2] cycloaddition of 1,6- and 1,7-diyne with diethyl phosphorocyanidate. *Eur. J. Org. Chem.* **2015**, *2015*, 1092–1099. [CrossRef]
72. Kashima, K.; Teraoka, K.; Uekusa, H.; Shibata, Y.; Tanaka, K. Rhodium-catalyzed atroposelective [2+2+2] cycloaddition of ortho-substituted phenyl diynes with nitriles: Effect of ortho substituents on regio- and enantioselectivity. *Org. Lett.* **2016**, *18*, 2170–2173. [CrossRef] [PubMed]
73. Yuan, J.; To, W.P.; Zhang, Z.Y.; Yue, C.D.; Meng, S.; Chen, J.; Liu, Y.; Yu, G.A.; Che, C.M. Visible-light-promoted transition-metal-free phosphinylation of heteroaryl halides in the presence of potassium *tert*-butoxide. *Org. Lett.* **2018**, *20*, 7816–7820. [CrossRef]
74. Zeng, H.; Dou, Q.; Li, C.-J. Photoinduced transition-metal-free cross-coupling of aryl halides with H-phosphonates. *Org. Lett.* **2019**, *21*, 1301–1305. [CrossRef] [PubMed]
75. Liu, Y.; Guo, W. Visible-light driven C-P bond formation with recyclable carbon nitride photocatalyst. *ChemCatChem* **2022**, *14*, e202200449. [CrossRef]
76. Cowper, N.G.; Chernowsky, C.P.; Williams, O.P.; Wickens, Z.K. Potent reductants *via* electron-primed photoredox catalysis: Unlocking aryl chlorides for radical coupling. *J. Am. Chem. Soc.* **2020**, *142*, 2093–2099. [CrossRef]
77. Zhu, D.-L.; Jiang, S.; Wu, Q.; Wang, H.; Chai, L.-L.; Li, H.-Y.; Li, H.-X. Visible-light-induced nickel-catalyzed P(O)-C(sp²) coupling using thioxanthen-9-one as a photoredox catalysis. *Org. Lett.* **2020**, *23*, 160–165. [CrossRef]
78. Qiu, D.; Lian, C.; Mao, J.; Ding, Y.; Liu, Z.; Wei, L.; Fagnoni, M.; Protti, S. Visible Light-Driven, Photocatalyst-free Arbuzov-like reaction *via* arylazo sulfones. *Adv. Synth. Catal.* **2019**, *361*, 5239–5244. [CrossRef]
79. Kim, I.; Kang, G.; Lee, K.; Park, B.; Kang, D.; Jung, H.; He, Y.T.; Baik, M.H.; Hong, S. Site-selective functionalization of pyridinium derivatives *via* visible-light-driven photocatalysis with quinolinone. *J. Am. Chem. Soc.* **2019**, *141*, 9239–9248. [CrossRef] [PubMed]
80. Xiang, C.B.; Bian, Y.J.; Mao, X.R.; Huang, Z.Z. Coupling reactions of heteroarenes with phosphites under silver catalysis. *J. Org. Chem.* **2012**, *77*, 7706–7710. [CrossRef]
81. Kittikool, T.; Phakdeeyothin, K.; Chantarojsiri, T.; Yotphan, S. Manganese-promoted regioselective direct C3-phosphinylation of 2-pyridones. *Eur. J. Org. Chem.* **2021**, *2021*, 3071–3078. [CrossRef]
82. Zhou, Y.; Liu, C.; Shen, Z.; Dai, B.; Chen, J. Efficient potassium hydroxide promoted P-arylation of aryl halides with diphenylphosphine. *J. Organomet. Chem.* **2021**, *949*, 121932. [CrossRef]
83. Trofimov, B.A.; Volkov, P.A.; Khrapova, K.O.; Telezhkin, A.A.; Ivanova, N.I.; Albanov, A.I.; Gusarova, N.K.; Chupakhin, O.N. Metal-free site selective cross-coupling of pyridines with secondary phosphine chalcogenides using acylacetylenes as oxidants. *Chem. Commun.* **2018**, *54*, 3371–3374. [CrossRef]
84. Volkov, P.A.; Gusarova, N.K.; Khrapova, K.O.; Telezhkin, A.A.; Albanov, A.I.; Vasilevskiy, S.F.; Trofimov, B.A. A mechanistic insight into the chemoselectivity of the reaction between 3-phenyl-2-propynenitrile, secondary phosphine oxides and pyridinoids. *Mendeleev Commun.* **2021**, *31*, 670–672. [CrossRef]
85. Volkov, P.A.; Telezhkin, A.A.; Khrapova, K.O.; Ivanova, N.I.; Albanov, A.I.; Gusarova, N.K.; Trofimov, B.A. Metal-free S HN cross-coupling of pyridines with phosphine chalcogenides: Polarization/deprotonation/oxidation effects of electron-deficient acetylenes. *New J. Chem.* **2021**, *45*, 6206–6219. [CrossRef]
86. Oka, N.; Ito, K.; Tomita, F.; Ando, K. Synthesis of 2-pyridylphosphinate and thiophosphinate derivatives by nucleophilic aromatic substitution of *N*-methoxypyridinium tosylates. *Chem. Lett.* **2012**, *41*, 1630–1632. [CrossRef]
87. Wang, H.; Cui, X.; Pei, Y.; Zhang, Q.; Bai, J.; Wei, D.; Wu, Y. Direct regioselective phosphonation of heteroaryl *N*-oxides with H-phosphonates under metal and external oxidant free conditions. *Chem. Commun.* **2014**, *50*, 14409–14411. [CrossRef] [PubMed]
88. Lee, S.-J.; Kim, H.-S.; Yang, H.-W.; Yoo, B.-W.; Yoon, C.M. Synthesis of diethyl pyridin-2-ylphosphonates and quinolin-2-ylphosphonates by deoxygenative phosphorylation of the corresponding *N*-oxides. *Bull. Korean Chem. Soc.* **2014**, *35*, 2155–2158. [CrossRef]
89. Li, S.G.; Yuan, M.; Topic, F.; Han, Z.S.; Senanayake, C.H.; Tsantrizos, Y.S. Asymmetric library synthesis of *P*-chiral *t*-butyl-substituted secondary and tertiary phosphine oxides. *J. Org. Chem.* **2019**, *84*, 7291–7302. [CrossRef] [PubMed]

90. Han, Z.S.; Wu, H.; Xu, Y.; Zhang, Y.; Qu, B.; Li, Z.; Caldwell, D.R.; Fandrick, K.R.; Zhang, L.; Roschangar, F.; et al. General and stereoselective method for the synthesis of sterically congested and structurally diverse P-stereogenic secondary phosphine oxides. *Org. Lett.* **2017**, *19*, 1796–1799. [CrossRef]
91. Stambirskiy, M.V.; Kostyuk, T.; Sirobaba, S.I.; Rudnichenko, A.; Titikaiev, D.L.; Dmytriv, Y.V.; Kuznietsova, H.; Pishel, I.; Borysko, P.; Mykhailiuk, P.K. Phosphine oxides (– POME₂) for medicinal chemistry: Synthesis, properties, and applications. *J. Org. Chem.* **2021**, *86*, 12783–12801. [CrossRef]
92. Zakirova, G.G.; Mladentsev, D.Y.; Borisova, N.E. Synthesis of chelating tertiary phosphine oxides *via* palladium-catalysed C–P bond formation. *Tetrahedron Lett.* **2017**, *58*, 3415–3417. [CrossRef]
93. Henyecz, R.; Oroszy, R.; Keglevich, G. Microwave-assisted Hirao reaction of heteroaryl bromides and >P(O)H reagents using Pd(OAc)₂ as the catalyst precursor in the absence of added P-ligands. *Curr. Org. Chem.* **2019**, *23*, 1151–1157. [CrossRef]
94. McErlain, H.; Riley, L.M.; Sutherland, A. Palladium-catalyzed C–P bond-forming reactions of aryl nonaflates accelerated by iodide. *J. Org. Chem.* **2021**, *86*, 17036–17049. [CrossRef]
95. Ma, F.; Zhang, T.-T.; Zhang, Z.-H.; Tong, H.-X.; Yi, X.-Y. Photorelease of nitric oxide in water-soluble diruthenium nitrosyl complexes with phosphonate substituted pyridylpyrrole. *Inorg. Chim. Acta* **2022**, *534*, 120826. [CrossRef]
96. Adam, M.S.S.; Kindermann, M.K.; Köckerling, M.; Heinicke, J.W. Phosphonylation of 2-amino- and 2-amido-3-bromopyridines and 2-amino-3-chloroquinoxalines with triethyl phosphite. *Eur. J. Org. Chem.* **2009**, *2009*, 4655–4665. [CrossRef]
97. Geng, Z.; Zhang, Y.; Zheng, L.; Li, J.; Zou, D.; Wu, Y.; Wu, Y. Pd-catalyzed C–P coupling of heteroaryl boronic acid with H-phosphonate diester. *Tetrahedron Lett.* **2016**, *57*, 3063–3066. [CrossRef]
98. Zhang, G.; Wang, J.; Guan, C.; Zhao, Y.; Ding, C. Nickel- and palladium-catalyzed cross-coupling of aryl fluorosulfonates and phosphites: Synthesis of aryl phosphonates. *Eur. J. Org. Chem.* **2021**, *2021*, 810–813. [CrossRef]
99. Zhao, Y.L.; Wu, G.J.; Han, F.S. Ni-catalyzed construction of C–P bonds from electron-deficient phenols *via* the in situ aryl C–O activation by PyBroP. *Chem. Commun.* **2012**, *48*, 5868–5870. [CrossRef]
100. Isshiki, R.; Muto, K.; Yamaguchi, J. Decarbonylative C–P bond formation using aromatic esters and organophosphorus compounds. *Org. Lett.* **2018**, *20*, 1150–1153. [CrossRef]
101. Yang, B.; Wang, Z.-X. Ni-Catalyzed C–P coupling of aryl, benzyl, or allyl ammonium salts with P(O)H compounds. *J. Org. Chem.* **2019**, *84*, 1500–1509. [CrossRef]
102. Li, C.-J. Nickel-catalyzed phosphorylation of tosylates. *Russ. J. Gen. Chem.* **2020**, *90*, 725–730. [CrossRef]
103. Li, C.J. Aryltrimethylammonium tetrafluoroborates in nickel-catalyzed C–P bond-forming reactions. *Russ. J. Org. Chem.* **2021**, *57*, 954–960. [CrossRef]
104. Regitz, M.; Heydt, A.; Weber, B. (Diazomethyl)cyclopropene—*Synthese*, isomerisierung und carbenreaktionen. *Angew. Chem.* **1979**, *91*, 566–568. [CrossRef]
105. Heydt, A.; Heydt, H.; Weber, B.; Regitz, M. Untersuchungen an diazoverbindungen und aziden, XLII. (Diazomethyl)cyclopropene durch elektrophile diazoalkan-substitution. *Chem. Ber.* **1982**, *115*, 2965–2980. [CrossRef]
106. Eisenbarth, P.; Regitz, M. Untersuchungen an diazoverbindungen und aziden, XLIII(1). 1,2-Dewarpyridazine—*Vorstufen* zur erzeugung von azacyclobutadienen? *Chem. Ber.* **1984**, *117*, 445–454. [CrossRef]
107. Heydt, H.; Eisenbarth, P.; Feith, K.; Regitz, M. Diaminopyridazine aus diaminocyclopropenylsalzen und (diazomethyl)-verbindungen. *J. Heterocycl. Chem.* **1986**, *23*, 385–391. [CrossRef]
108. Banert, K.; Kohler, F.; Melzer, A.; Scharf, I.; Rheinwald, G.; Ruffer, T.; Lang, H.; Herges, R.; Hess, K.; Ghavtadze, N.; et al. Experimental and theoretical characterization of the aromatization, epimerization, and fragmentation reactions of bi-2H-azirin-2-yls prepared from 1,4-diazidobuta-1,3-dienes. *Chemistry* **2011**, *17*, 10071–10080. [CrossRef]
109. Collomb, D.; Deshayes, C.; Doutheau, A. Synthesis of functionalized phenolic derivatives *via* the benzannulation of dienylketenes formed by a thermal wolff rearrangement of α -diazo- β -keto compounds. *Tetrahedron* **1996**, *52*, 6665–6684. [CrossRef]
110. Touil, S.; Zantour, H. Action des hydrazines sur les γ,β' -dicarbonylphosphonates et phosphineoxides: Synthèse de 4-phosphopyridazines et pyridazin-3-ones. *Phosphorus Sulfur Silicon Relat. Elem.* **1998**, *134*, 493–502. [CrossRef]
111. Mrowca, J.J. Phosphine Oxide-Substituted Pyrimidines. U.S. Patent 19790049481, 18 November 1980.
112. Kosolapoff, G.M.; Roy, C.H. Synthesis of some pyrimidylphosphonates. *J. Org. Chem.* **1961**, *26*, 1895–1898. [CrossRef]
113. Haas, A.; Lieb, M. Darstellung und eigenschaften trifluormethylmercapto-substituierter pyrimidine. *J. Heterocycl. Chem.* **1986**, *23*, 1079–1084. [CrossRef]
114. Günther, O.; Hartke, K. Heterocyclische *o*-amino-phosphonester. *Arch. Der Pharm.* **1975**, *308*, 693–700. [CrossRef]
115. Aboujaoude, E.E.; Collignon, N.; Savignac, P. Dialkyl formyl-1 methylphosphonates α -fonctionnels—II¹. *Tetrahedron* **1985**, *41*, 427–433. [CrossRef]
116. Aboujaoude, E.E.; Collignon, N.; Savignac, P. Synthèse d'hétérocycles α -phosphoniques. nouveaux développements. *Phosphorous Sulfur Relat. Elem.* **1987**, *31*, 231–243. [CrossRef]
117. Neidlein, R.; Eichinger, T. [(1,3-Dioxolan-2-yliden)methyl]phosphonate und -phosphinate als (einfache) Synthone in der Heterocyclensynthese. *Helv. Chim. Acta* **1992**, *75*, 124–136. [CrossRef]
118. Lu, R.; Yang, H. A novel approach to phosphonyl-substituted heterocyclic system(I). *Tetrahedron Lett.* **1997**, *38*, 5201–5204. [CrossRef]
119. Penz, G.; Zbiral, E. 3-Oxo-2-tosyloxy-1-alkenylphosphonsauredialkylester als synthone zum aufbau von hetarylphosphonsauredialkylestern. *Mon. Fur Chem. Chem. Mon.* **1985**, *116*, 1041–1049. [CrossRef]

120. Maruyama, T.; Taira, Z.; Horikawa, M.; Sato, Y.; Honjo, M. Synthesis of uracil-5- and adenine-8-phosphonic acids. *Tetrahedron Lett.* **1983**, *24*, 2571–2574. [CrossRef]
121. Zhu, L.; Yu, H.; Guo, Q.; Chen, Q.; Xu, Z.; Wang, R. C-H bonds phosphorylation of ketene dithioacetals. *Org. Lett.* **2015**, *17*, 1978–1981. [CrossRef]
122. Essid, I.; Lahbib, K.; Kaminsky, W.; Ben Nasr, C.; Touil, S. 5-Phosphonato-3,4-dihydropyrimidin-2(1H)-ones: Zinc triflate-catalyzed one-pot multi-component synthesis, X-ray crystal structure and anti-inflammatory activity. *J. Mol. Struct.* **2017**, *1142*, 130–138. [CrossRef]
123. Essid, I.; Touil, S. β -Ketophosphonates as substrates in the Biginelli multicomponent reaction: An efficient and straightforward synthesis of phosphorylated dihydropyrimidinones. *Arkivoc* **2013**, *4*, 98–106. [CrossRef]
124. Timoshenko, V.M.; Markitanov, Y.N.; Shermolovich, Y.G. Preparation of pyrimidine derivatives through three-component reactions of dialkyl(2-oxo-3,3,3-trifluoropropyl)phosphonates. *Chem. Heterocycl. Compd.* **2011**, *47*, 977–982. [CrossRef]
125. Jansa, P.; Hradil, O.; Baszczyński, O.; Dračinský, M.; Klepetářová, B.; Holý, A.; Balzarini, J.; Janeba, Z. An efficient microwave-assisted synthesis and biological properties of polysubstituted pyrimidinyl- and 1,3,5-triazinylphosphonic acids. *Tetrahedron* **2012**, *68*, 865–871. [CrossRef]
126. Kunda, U.M.R.; Mudumala, V.N.R.; Reddy Gangireddy, C.S.; Nemallapudi, B.R.; Sandip, K.N.; Cirandur, S.R. Amberlyst-15 catalyzed synthesis of alkyl/aryl/heterocyclic phosphonates. *Chin. Chem. Lett.* **2011**, *22*, 895–898. [CrossRef]
127. Mohan Naidu, K.R.; Dadapeer, E.; Reddy, C.B.; Rao, A.J.; Reddy, C.S.; Raju, C.N. Polyethylene glycol-promoted dialkyl, aryl/heteroaryl phosphonates. *Synth. Commun.* **2011**, *41*, 3462–3468. [CrossRef]
128. Golla, M.; Syed, R.; Katla, V.R.; Devineni, S.R.; Kondapalli, N.; Chamarthi, N.R. $\text{LaCl}_3 \cdot 7\text{H}_2\text{O}$: An efficient catalyst for the synthesis of phosphinates (Michaelis–Arbuzov reaction) under neat conditions and their potential antimicrobial activity. *J. Chem. Sci.* **2014**, *126*, 117–125. [CrossRef]
129. Varalakshmi, M.; Srinivasulu, D.; Kotakadi, V.S. Nano- $\text{BF}_3 \cdot \text{SiO}_2$ catalyst-promoted Michaelis–Arbuzov reaction: Solvent-free synthesis and antimicrobial evaluation. *Phosphorus Sulfur Silicon Relat. Elem.* **2015**, *190*, 1518–1524. [CrossRef]
130. Ghosh, I.; Shaikh, R.S.; Konig, B. Sensitization-initiated electron transfer for photoredox catalysis. *Angew. Chem. Int. Ed.* **2017**, *56*, 8544–8549. [CrossRef]
131. Erbland, G.; Ruch, J.; Goddard, J.-P. Photochemical functionalization of diazines: Metal-free vinylation and phosphorylation. *Tetrahedron* **2016**, *72*, 7826–7831. [CrossRef]
132. Zhang, W.; Zou, J.-P.; Sun, W.-B.; Ji, Y.-F.; Pan, X.-Q.; Zhou, S.-F.; Asekun, O. $\text{Mn}(\text{OAc})_3$ -mediated selective free radical phosphorylation of pyridinones and pyrimidinones. *Synthesis* **2013**, *45*, 1529–1533.
133. Deal, E.L.; Petit, C.; Montchamp, J.L. Palladium-catalyzed cross-coupling of H-phosphinate esters with chloroarenes. *Org. Lett.* **2011**, *13*, 3270–3273. [CrossRef] [PubMed]
134. Zhang, H.Y.; Sun, M.; Ma, Y.N.; Tian, Q.P.; Yang, S.D. Nickel-catalyzed C-P cross-coupling of diphenylphosphine oxide with aryl chlorides. *Org. Biomol. Chem.* **2012**, *10*, 9627–9633. [CrossRef]
135. Montel, S.; Midrier, C.; Volle, J.-N.; Braun, R.; Haaf, K.; Willms, L.; Pirat, J.-L.; Virieux, D. Functionalized phosphanyl-phosphonic acids as unusual complexing units as analogues of fosmidomycin. *Eur. J. Org. Chem.* **2012**, *2012*, 3237–3248. [CrossRef]
136. Zakirova, G.; Mladentsev, D.; Borisova, N. Palladium-catalyzed C-P cross-coupling between (het)aryl halides and secondary phosphine oxides. *Synthesis* **2019**, *51*, 2379–2386. [CrossRef]
137. Bai, Y.; Liu, N.; Wang, S.; Wang, S.; Ning, S.; Shi, L.; Cui, L.; Zhang, Z.; Xiang, J. Nickel-catalyzed electrochemical phosphorylation of aryl bromides. *Org. Lett.* **2019**, *21*, 6835–6838. [CrossRef]
138. Palacios, F.; Ochoa de Retana, A.M.; Gil, J.I.; Lopez de Munain, R. Synthesis of pyrazine-phosphonates and -phosphine oxides from 2H-azirines or oximes. *Org. Lett.* **2002**, *4*, 2405–2408. [CrossRef]
139. Palacios, F.; de Retana, A.M.a.O.; de Marigorta, E.M.n.; Rodriguez, M.; Pagalday, J. Aza-Wittig reaction of N-phosphorylalkyl phosphazenes with carbonyl compounds and phenylisocyanate. Synthesis of 4-amino-3-phosphoryl-2-azadienes and pyrazine-phosphonates. *Tetrahedron* **2003**, *59*, 2617–2623. [CrossRef]
140. Aparicio, D.; Attanasi, O.A.; Filippone, P.; Ignacio, R.; Lillini, S.; Mantellini, F.; Palacios, F.; de Los Santos, J.M. Straightforward access to pyrazines, piperazinones, and quinoxalines by reactions of 1,2-diaza-1,3-butadienes with 1,2-diamines under solution, solvent-free, or solid-phase conditions. *J. Org. Chem.* **2006**, *71*, 5897–5905. [CrossRef]
141. Seggio, A.; Chevallier, F.; Vaultier, M.; Mongin, F. Lithium-mediated zincation of pyrazine, pyridazine, pyrimidine, and quinoxaline. *J. Org. Chem.* **2007**, *72*, 6602–6605. [CrossRef]
142. Berger, O.; Montchamp, J.L. Manganese-catalyzed and mediated synthesis of arylphosphinates and related compounds. *J. Org. Chem.* **2019**, *84*, 9239–9256. [CrossRef] [PubMed]

143. Nikishkin, N.I.; Huskens, J.; Ansari, S.A.; Mohapatra, P.K.; Verboom, W. Pyrazine-functionalized calix[4]arenes: Synthesis by palladium-catalyzed cross-coupling with phosphorus pronucleophiles and metal ion extraction properties. *New J. Chem.* **2013**, *37*, 391–402. [CrossRef]
144. Zhao, Y.L.; Wu, G.J.; Li, Y.; Gao, L.X.; Han, F.S. [NiCl₂(dppp)]-catalyzed cross-coupling of aryl halides with dialkyl phosphite, diphenylphosphine oxide, and diphenylphosphine. *Chemistry* **2012**, *18*, 9622–9627. [CrossRef] [PubMed]

Disclaimer/Publisher’s Note: The statements, opinions and data contained in all publications are solely those of the individual author(s) and contributor(s) and not of MDPI and/or the editor(s). MDPI and/or the editor(s) disclaim responsibility for any injury to people or property resulting from any ideas, methods, instructions or products referred to in the content.

Review

Imidazole: Synthesis, Functionalization and Physicochemical Properties of a Privileged Structure in Medicinal Chemistry

Heber Victor Tolomeu ^{1,2} and Carlos Alberto Manssour Fraga ^{1,2,*}

¹ Laboratório de Avaliação e Síntese de Substâncias Bioativas (LASSBio), Instituto de Ciências Biomédicas, Universidade Federal do Rio de Janeiro, Rio de Janeiro 21941-909, Brazil

² Programa de Pós-Graduação em Farmacologia e Química Medicinal, Instituto de Ciências Biomédicas, Universidade Federal do Rio de Janeiro, Rio de Janeiro 21941-909, Brazil

* Correspondence: cmfraga@ccsdecania.ufrj.br; Tel.: +55-21-39386447

Abstract: Imidazole was first synthesized by Heinrich Debus in 1858 and was obtained by the reaction of glyoxal and formaldehyde in ammonia, initially called glyoxaline. The current literature provides much information about the synthesis, functionalization, physicochemical characteristics and biological role of imidazole. Imidazole is a structure that, despite being small, has a unique chemical complexity. It is a nucleus that is very practical and versatile in its construction/functionalization and can be considered a rich source of chemical diversity. Imidazole acts in extremely important processes for the maintenance of living organisms, such as catalysis in enzymatic processes. Imidazole-based compounds with antibacterial, anti-inflammatory, antidiabetic, antiparasitic, antituberculosis, anti-fungal, antioxidant, antitumor, antimalarial, anticancer, antidepressant and many others make up the therapeutic arsenal and new bioactive compounds proposed in the most diverse works. The interest and importance of imidazole-containing analogs in the field of medicinal chemistry is remarkable, and the understanding from the development of the first blockbuster drug cimetidine explores all the chemical and biological concepts of imidazole in the context of research and development of new drugs.

Keywords: imidazole; synthesis; medicinal chemistry; drug discovery

Citation: Tolomeu, H.V.; Fraga, C.A.M. Imidazole: Synthesis, Functionalization and Physicochemical Properties of a Privileged Structure in Medicinal Chemistry. *Molecules* **2023**, *28*, 838. <https://doi.org/10.3390/molecules28020838>

Academic Editor: Sreekantha B. Jonnalagadda

Received: 10 December 2022

Revised: 30 December 2022

Accepted: 1 January 2023

Published: 13 January 2023



Copyright: © 2023 by the authors. Licensee MDPI, Basel, Switzerland. This article is an open access article distributed under the terms and conditions of the Creative Commons Attribution (CC BY) license (<https://creativecommons.org/licenses/by/4.0/>).

1. The Chemistry of Imidazole

Imidazole **1** (Figure 1) was first synthesized by Heinrich Debus in 1858, but since the 1840s, several imidazole derivatives have been discovered. Its synthesis started from the use of glyoxal **2** and formaldehyde **3** in ammonia, producing imidazole **1** as a final product, which was initially called glyoxaline (Figure 2) [1,2]. This synthesis, despite producing relatively low yields, is still used to create C-substituted imidazoles.

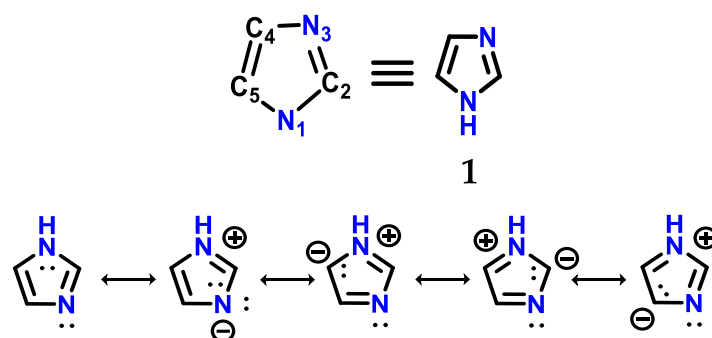


Figure 1. Structure of imidazole **1** with its respective numbering and resonance hybrids.

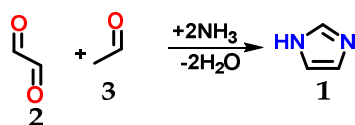


Figure 2. Scheme of the synthesis of imidazole **1** using glyoxal **2** and formaldehyde **3** in ammonia.

Among the nitrogen-based heterocyclic compounds, imidazole **1** plays an important role in humans. It is included in chemical sciences, biological sciences and materials science, and used as a catalyst in compound synthesis and the process of developing new drugs (Figure 3) [3–6].

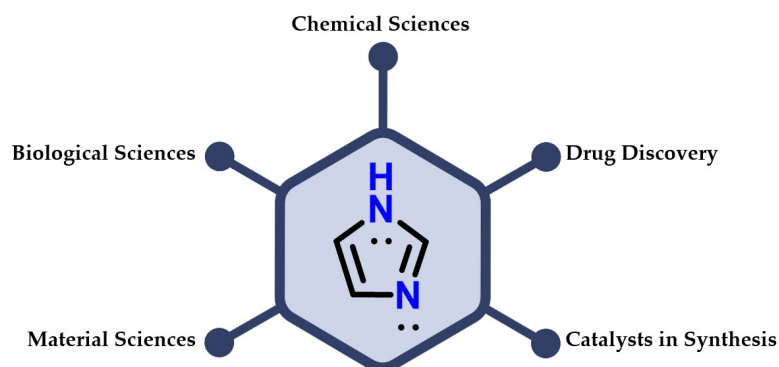


Figure 3. Applications of imidazole **1** in different areas of knowledge.

With a 5-membered planar ring, imidazole **1** exhibits solubility in water and other polar solvents. Two equivalent tautomeric forms are observed because the hydrogen atom can be located on either of the two nitrogen atoms [2]. Imidazole **1** is a highly polar compound, as seen by a calculated dipole of 3.61D, and is completely soluble in water [2,7]. Imidazole **1** is classified as an amphoteric compound, acting as both an acid and a base. The compound is classified as aromatic due to the presence of a sextet of π electrons, consisting of a pair of nonbonding electrons from the nitrogen *N*-1 atom and one from each of the four remaining ring atoms [2,7].

Imidazole **1** can form stable crystalline salts with strong acids through the protonation of the sp^2 nitrogen (*N*-3), known as imidazolium salts. Imidazole **1** has a pKaH of 7.1 (Figure 4), acting as a strong base [8]. The basicity of imidazole is above that of pyridine **4** (pKaH of 5.2) due to the amidine-like **5** resonance, which allows both nitrogens to participate equally in charge accommodation [7–9]. Comparatively, the basicity of imidazole **1** contrasts with the basicity of pyrrole **6** (pKaH of 0.4), which is an extremely weak base, because when pyrrole **6** is protonated, there is a loss of aromaticity which is built with the participation of the nonbonding electron pair of *N*-1 nitrogen [7].

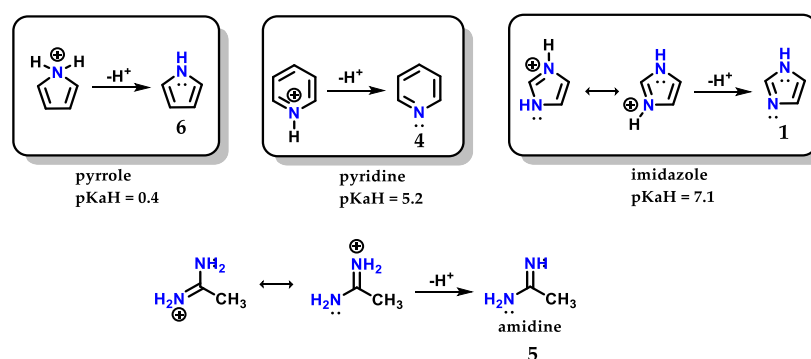


Figure 4. Protonated structures of pyrrole **6**, pyridine **4** and imidazole **1**, with their respective pKaH values and the structure of protonated amidine **5** compared to imidazole.

Imidazole **1** is a good donor and acceptor of hydrogen bond interactions; the sp^2 nitrogen ($N-3$) accepts a hydrogen interaction, while $N-1$ nitrogen, being relatively acidic, donates its hydrogen to an interaction (Figure 5A) [8]. This property is fundamental for the mode of action of several enzymes that use the imidazole ring, such as the histidine 7 amino acid residue, one of the 20 amino acids found in proteins [8]. These important interactions for living organisms are present not only in macromolecules but also in bioactive small molecules.

A recent study demonstrating this important effect was carried out by Movellan and collaborators [10], where it was possible to analyze the hydrogen residues in histidine residues 7 in the M2 tetramer of influenza A, important for the process of endocytosis and maintenance of the virus life cycle [1–4,11–15]. Using the M2 conduction domain construct in lipid bilayers, that the imidazole ring is hydrogen bonded even at a pH of 7.8 in the neutral charge state (Figure 5B). An intermolecular $^2hJ_{NN}$ hydrogen bond of 8.9 ± 0.3 Hz was observed between H37 $N\epsilon$ and $N\delta$. However, this $^2hJ_{NN}$ interaction could not be detected in the sample connected to the drug rimantadine (Rmt), with consequent modification in the proton chemical shifts value of 3 ppm for histidine residues [10].

Histamine **8** is an example of a small molecule with different actions in living organisms. It is biosynthesized from histidine **7** itself by the action of the enzyme histidine decarboxylase (Figure 5B) [16].

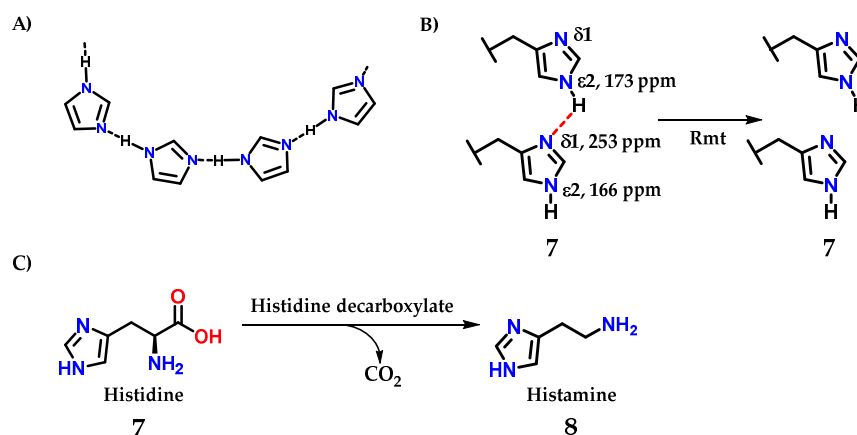


Figure 5. (A) Intermolecular interactions through the hydrogen interactions that imidazole-containing derivatives can perform. (B) Intermolecular interactions through the hydrogen interactions in histidine residues. (C) Structure of histidine **7**, precursor of histamine **8** biosynthesis.

The presence of the $N-1$ nitrogen in the imidazole **1** structure makes it tautomer, which becomes evident in non-symmetrically substituted compounds, such as methyl imidazole **9** (Figure 6) [9]. This curious feature of imidazole chemistry means that simply writing “4-methylimidazole” would be incorrect, considering the rapid tautomeric equilibrium with the 5-methylimidazole structure [9,17].

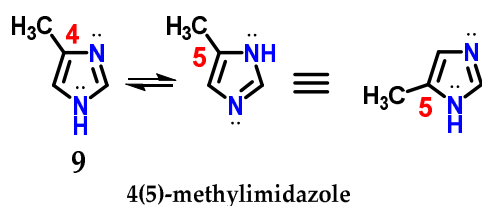


Figure 6. Representation of the tautomeric forms of methyl imidazole **9**.

Despite the existence of the tautomeric effect in imidazole **1**, the ratio in terms of proportion of these tautomers varies according to the substituent added to the ring. The tautomer ratio observed in the 4(5)-nitroimidazole **10** derivative is approximately 400:1 for

Imidazole **1** behaves as a π -deficient ligand (π -acceptor) similar to pyridine **4**, and its sp^2 nitrogen atoms mainly form $\eta^1(\sigma, N_{py})$ complexes (Figure 9), as does pyridine **4** [7].

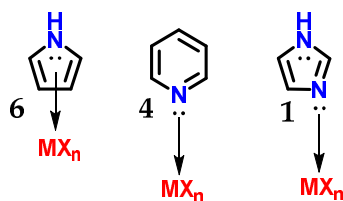


Figure 9. Complex with transition metals $\eta^5(\pi)$ carried out by pyrrole **6** and the complexes $\eta^1(\sigma, N_{py})$ carried out by imidazole **1** and pyridine **4**.

Imidazole **1** has a very exciting physicochemical complexity. This makes it a target nucleus for the most diverse applications, which employ synthetic methodologies for its obtention and functionalization.

2. Synthesis and Functionalization of Imidazole

The synthesis of substituted imidazole **1** using heterogeneous catalysis has been widely exploited. These functionalized structures are useful building blocks for the synthesis of molecules of biological and pharmaceutical interest.

2.1. Mono-Substituted Derivatives

One-pot reactions using iodobenzene **11** and imidazole **1** in the presence of K_3PO_4 as the base, CuI as the catalyst and DMF as the solvent at 35–40 °C for 40 h, give the corresponding *N*-arylimidazoles **12** in quantitative yields (Figure 10) [21].

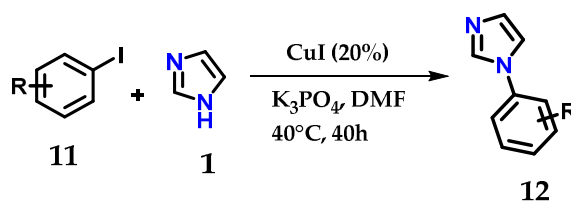


Figure 10. Catalytic *N*-arylation of imidazole **1** with aryl iodides and CuI.

Exploring the bifunctionalization of 1,2-disubstituted acetylenes **13** by ruthenium carbonyl to form *cis*-enediol diacetates **14**, followed by reaction with ammonium carbonate as a source of nitrogen and methanol for the C-2 carbon, permitted us to obtain monosubstituted imidazoles **15**, as shown below (Figure 11). In reactions where (R) were aromatic rings, both substituents, withdrawers (EWG) and donors (EDG) were tolerated under the applied conditions [22].

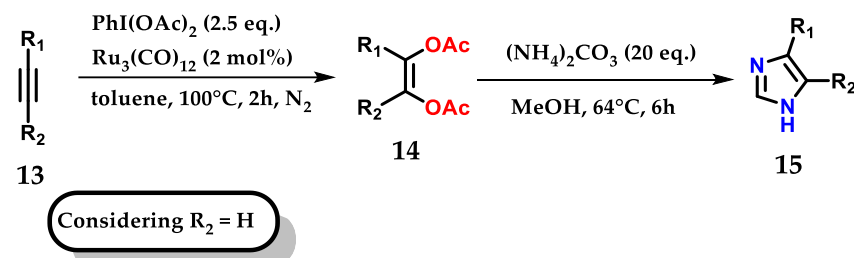


Figure 11. Ruthenium-catalyzed oxidation of alkynes for mono-substituted imidazole **15** synthesis.

2.2. Disubstituted Derivatives

The work below shows the development of an efficient methodology for the synthesis of novel 2-aryl-4-benzoyl-imidazoles **16** by structural modification of 2-aryl-imidazole-4-

carboxylic amide (AICA) **17** and 4-substituted methoxybenzoyl-aryl-thiazoles (SMART) **18**, presenting antiproliferative activity (Figure 12) [23].

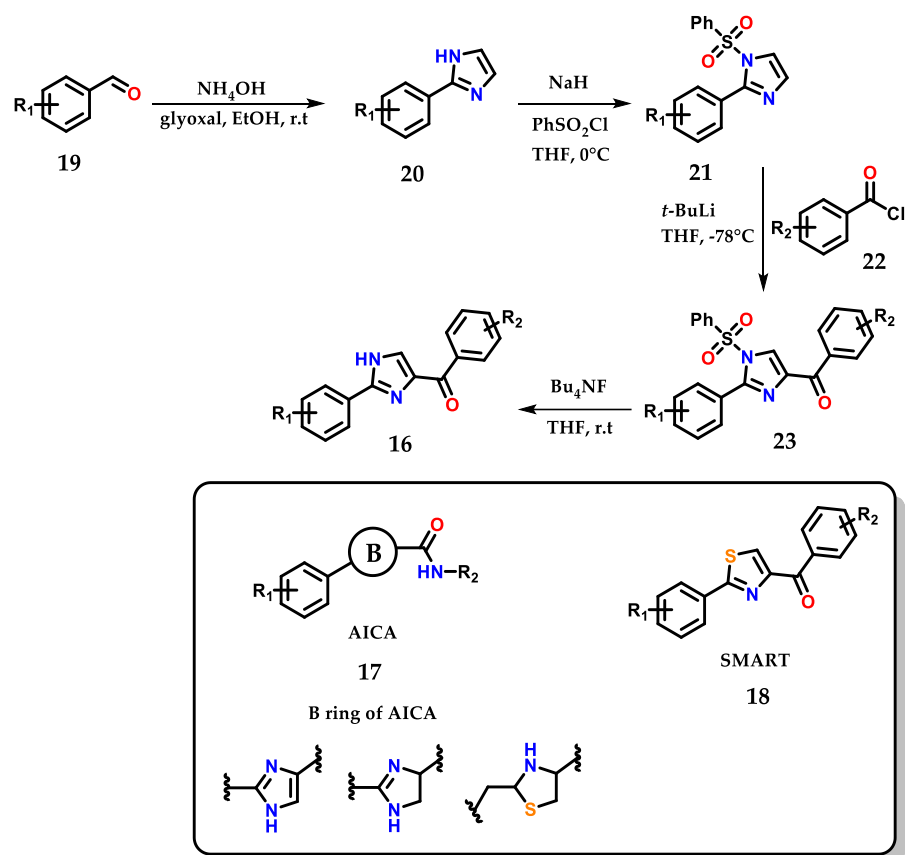


Figure 12. Obtaining 2-aryl-4-benzoyl-imidazoles **16** based on AICA **17** and SMART **18**.

Disubstituted imidazoles **24** could also be synthesized by cyclization of α -keto-aldehydes **25** obtained from the oxidation of aryl methyl-ketones **26** with selenium dioxide (SeO_2) after treatment with ammonium acetate and ethanol. The synthesized derivatives were used as fluorogenic sensors for detection, selectivity and sensitivity to Fe^{3+} ions (Figure 13) [24].

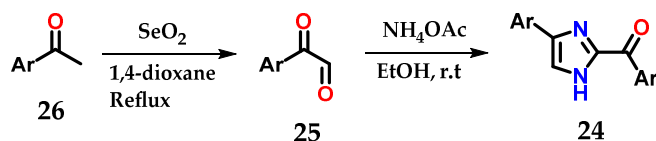


Figure 13. Obtaining disubstituted imidazoles **24** from aryl-methylketones **26**.

Another synthetic strategy used to construct disubstituted imidazole derivatives **27** from methyl ketones **28** consisted of exploiting its metal-free acid-catalyzed oxidation and coupling with aldehydes **29** and **30** in the presence of ammonium acetate (Figure 14) [25].

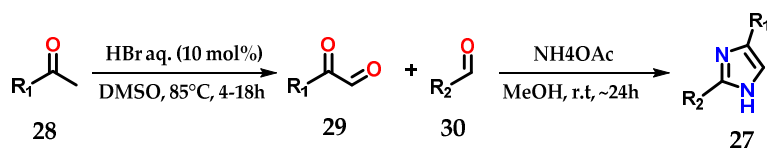


Figure 14. Synthesis of disubstituted imidazoles **27** starting from the acid-catalyzed oxidation of methylketones **28**.

Moreover, disubstituted imidazoles presenting a carbomethoxy group **31** at C-4 could be obtained from the coupling of functionalized amidoximes **32** and methyl propiolate **33** in the presence of a catalytic amount of 1,4-diazabicyclo[2.2]octane (DABCO) under microwave irradiation (Figure 15) [26].

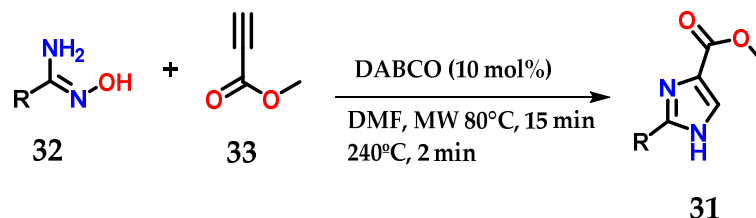


Figure 15. Disubstituted imidazoles **31** were obtained from the base-catalyzed condensation of amidoximes **32** and methyl propiolate **33**.

Amido-nitrile **34** cyclization mediated by functionalized boronic acids is also able to produce 2,4-disubstituted imidazoles **35**. It was possible to explore a considerable diversity of substituents, considering the reaction conditions reported below (Figure 16) [27].

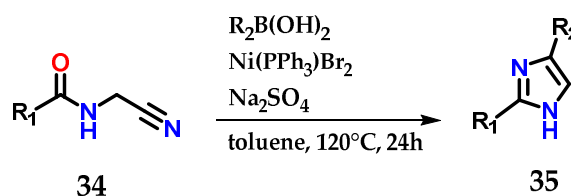


Figure 16. Nickel-catalyzed cyclization of amido-nitriles **34** to obtain disubstituted imidazoles **35**.

2.3. Trisubstituted Derivatives

On the other hand, 2,4,5-trisubstituted imidazoles **36** could be obtained by using 2,3-dioxo-3-substituted propanoates **37** as precursors after condensation using ammonium acetate and various aromatic aldehydes **38** in EtOH and AcOH as catalysts at room temperature (Figure 17) [28,29].

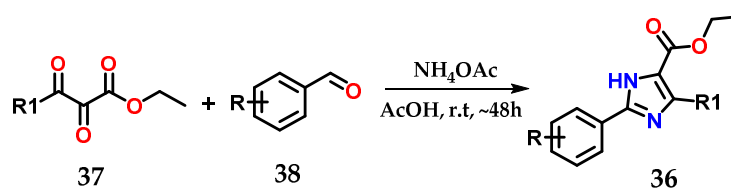


Figure 17. Obtaining 2,4,5-trisubstituted imidazoles **36** from 2,3-dioxo-3-substituted propanoates **37**.

2-Aryl-4,5-dicarbonitrile imidazole derivatives **39** could be obtained from the coupling of substituted aromatic aldehydes **40** and 2,3-diaminomaleonitriles **41** in the presence of a mixture of cerium (IV) ammonium nitrate/nitric acid (CAN: NA | 0.05: 0.4 eq.) at 120 °C for less than 1 h without using solvents (Figure 18) [30].

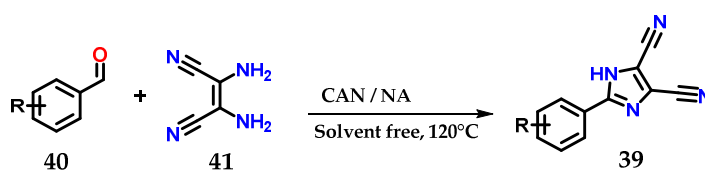


Figure 18. Obtaining 2-aryl-4,5-dicarbonitrile imidazole derivatives **39** using a mixture of CAN:NA as catalysts.

The efficient combination of α -aminoketones **42** with formamide **43** in THF at 180 °C for 8 h is also able to provide 1,4,5-trisubstituted imidazoles **44** [31] (Figure 19).

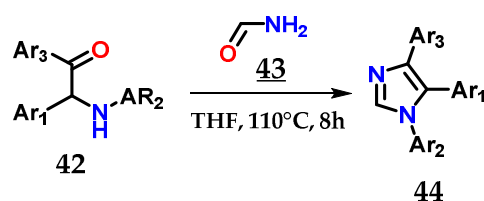


Figure 19. Obtaining 1,4,5-trisubstituted imidazoles **44** from the coupling of α -aminoketones **42** with formamide **43**.

Using the Van Leusen method, it was possible to synthesize 1,4,5-trisubstituted imidazoles containing a trifluoromethyl group **45**, exploiting the coupling of *N*-aryltrifluoroacetimidoyl chloride **46** and tosyl-methylisocyanate (TosMIC) **47** using sodium hydride as a base in dry THF at room temperature (Figure 20) [32].

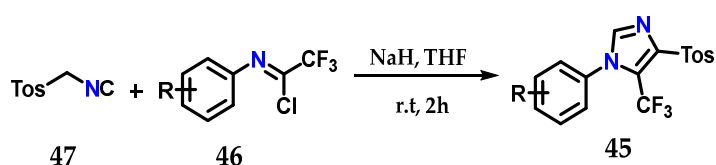


Figure 20. Obtaining 1,4,5-trisubstituted imidazoles **45** using the Van Leusen method.

Methodologies reported in the literature show the use of substituted 1,2-diphenylethane-1,2-dione (benzyl) **48**, substituted aldehydes **49** and ammonium acetate under various conditions, with the aim of optimizing the construction of 2,4,5-trisubstituted imidazole **50** with great structural diversity [33–40]. The reactions are simple and fast, as illustrated in the example below, which uses the system with EtOH and fluorinated graphene oxide (A-MFGO) as a catalyst at room temperature (Figure 21).

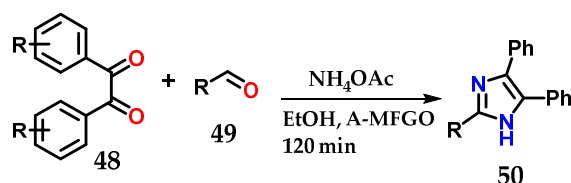


Figure 21. Obtaining 2,4,5-trisubstituted imidazoles **50** from the coupling of substituted 1,2-diphenylethane-1,2-dione (benzyl) **48**, substituted aldehydes **49** and NH_4OAc using A-MFGO as a catalyst.

More complex heterocycles presenting the imidazole ring in their structure are described in the literature, such as benzo[*d*]imidazo[2,1-*b*]thiazoles **51**, which could be synthesized by the condensation of aromatic ketones **52** and 5-(biphenyl-4-yl)-1,3,4-thiadiazol-2-amine **53** in the presence of *N*-bromosuccinimide **54**, PEG-400 and water as solvent under microwave irradiation at 85 °C in quantitative yields after a few minutes of reaction (Figure 22) [41].

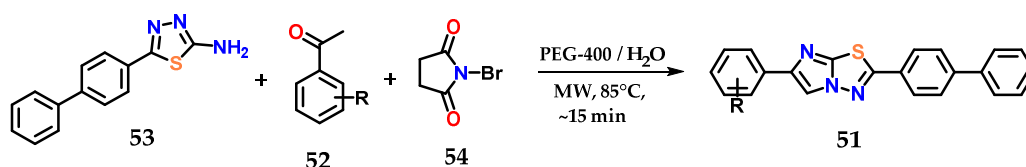


Figure 22. Obtaining benzo[*d*]imidazo[2,1-*b*]thiazoles **51** from the condensation of aromatic ketones **52** and 5-(biphenyl-4-yl)-1,3,4-thiadiazol-2-amine **53**.

2.4. Tetrasubstituted Derivatives

Using various aldehydes **55**, benzyl **56**, ammonium acetate and prop-2-ynylamine **57** in the presence of $\text{CuFe}_2\text{O}_4\text{NPs}$ as a catalyst in $\text{H}_2\text{O}:\text{EtOH}$ under reflux for approximately 50 min, it was possible to obtain several tetrasubstituted imidazole derivatives **58** in a multicomponent synthesis. It was possible to reuse the catalyst for six reactions without losing its efficiency (Figure 23) [42].

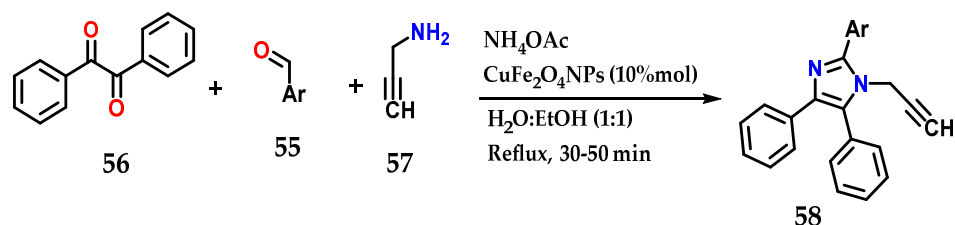


Figure 23. Tetrasubstituted imidazoles **58** were obtained by the coupling of benzyl **56**, functionalized aldehyde **55**, prop-2-ynylamine **57** and ammonium acetate using $\text{CuFe}_2\text{O}_4\text{NPs}$ as the catalyst.

In the presence of $\text{SO}_4^{2-}/\text{Y}_2\text{O}_3$ as a catalyst, the multicomponent condensation of benzyl **56**, aminoethylpiperazine **59**, various aldehydes **60** and ammonium acetate in ethanol at 80°C for 10 h was carried out to form tetrasubstituted 1,2,4,5-imidazole derivative **61**. The catalyst was reused up to five times with no significant loss in catalytic efficiency (Figure 24) [43].

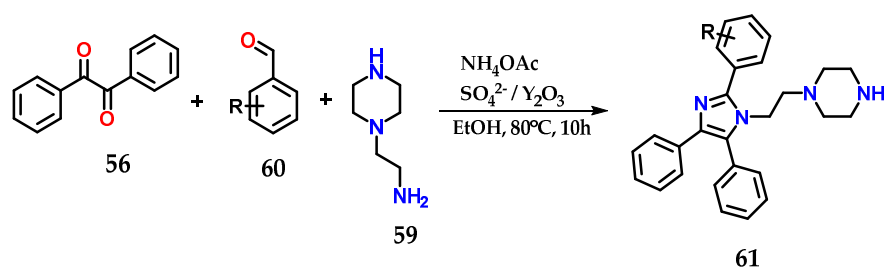


Figure 24. Tetrasubstituted imidazoles **61** were obtained from the multicomponent condensation of benzyl **56**, aminoethylpiperazine **59**, various aldehydes **60** and ammonium acetate using $\text{SO}_4^{2-}/\text{Y}_2\text{O}_3$ as a catalyst.

Alternatively, the synthesis of 1,2,4,5-tetrasubstituted imidazole derivatives **62** could be achieved through the condensation of benzyl **56**, aldehydes **63** and anilines **64** in the presence of ammonium acetate under the solvent-free catalysis of $\text{Fe}_3\text{O}_4@\text{SiO}_2/\text{bipyridinium}$ nanocomposite ($\text{Fe}_3\text{O}_4@\text{SiO}_2/\text{BNC}$) (Figure 25). The catalyst was reused until the fifth reaction without much change in catalytic efficiency. Methodologies using other catalysts and even solvents have also been reported [44–47].

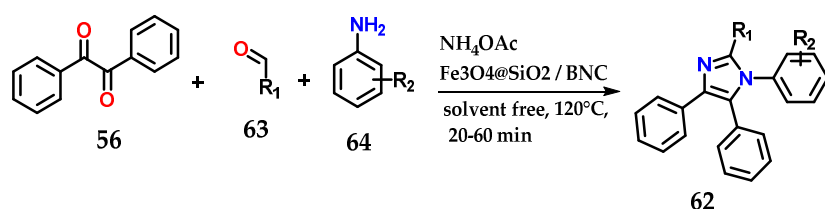


Figure 25. Tetrasubstituted imidazoles **62** were obtained through the condensation of benzyl **56**, aldehydes **63** and anilines **64** in the presence of ammonium acetate using $\text{Fe}_3\text{O}_4@\text{SiO}_2/\text{BNC}$ as a catalyst.

Another methodology used for obtaining hybrid imidazole derivatives was starting with hippuric acid **65** and 2-chloroquinoline-3-carbaldehyde **66** in acetic anhydride,

and 4-((2-chloroquinolin-3-yl)methylene)-2-phenyloxazol-5(4*H*)-ones **67** could be obtained through Perkin condensation in the presence of anhydrous sodium acetate under microwave irradiation. Subsequently, the previously obtained derivatives were condensed with *N*-aminoarylcarboxamides **68** in pyridine under reflux to furnish the final desired azaheterocyclic acylhydrazides **69**. For some derivatives of this series, antimicrobial properties were observed (Figure 26) [48].

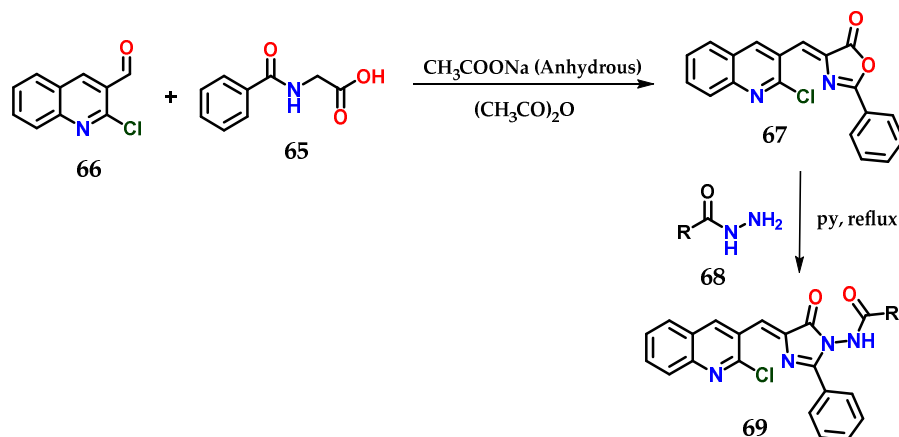


Figure 26. Synthesis of *N*-(4-((2-chloroquinolin-3-yl)methylene)-5-oxo-2-phenyl-4,5-dihydro-1*H*-imidazol-1-yl)(aryl)amides **69**.

Since its synthesis in 1858, the imidazole **1** ring has been exploited in different contexts, whether chemical or biological. The examples presented herein illustrate the more recent ways of obtaining this azaheterocyclic system through the use of a range of methodologies and chemical reagents, providing great chemical diversity.

3. Imidazole as a Privileged Structure in Medicinal Chemistry

As already mentioned, imidazole **1**, in biological systems, is found in the form of the amino acid histidine **7**, presenting an important role in the catalysis promoted by enzymatic systems [8]. Furthermore, the neurotransmitter histamine **8** induces immunological processes [8,16,49–51] and composes the structures of the guanine **70** and adenosine **71** bases of nucleic acids (Figure 27) [52].

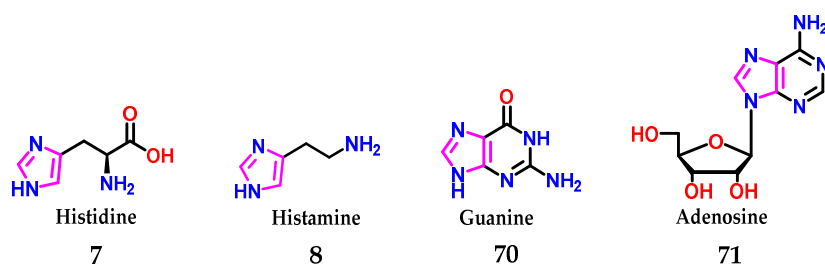


Figure 27. Presence of the imidazole **1** nucleus in several biologically active compounds.

3.1. The Catalytic Potential of Imidazole in Biological Systems

The breakage of the P-O and C-O bonds are biological events of extreme importance and are estimated to be on the order of 5 to 13 million years [53] in the absence of enzymes and can reach the order of billions of years for DNA [54]. Imidazole **1** stands out for constituting numerous enzymatic active sites in the form of the histidine **7** amino acid residue and acting in catalytic processes, accelerating such unfavorable reactions [55].

The imidazole **1** group in biological systems generally acts in acid–base and nucleophilic catalysis (Figure 28). As an acid catalyst, protonated imidazole **1** acts as an acid facilitating the exit of the RO- group through hydrogen transfer [56]. In the neutral form, imidazole **1** can act as a nucleophilic catalyst by attacking the electrophilic center, leading

to a phosphorylated or acylated intermediate, which is consecutively hydrolyzed, regenerating the imidazole 1 group [57]. Therefore, imidazole 1 catalyzes the cleavage of the X-O bond (for X = C or P). Finally, imidazole 1 can also act as a basic catalyst, assisting the attack of a nucleophile (Nu-H) on the electrophilic center of a substrate, abstracting a proton and thus increasing its nucleophilicity [58–61].

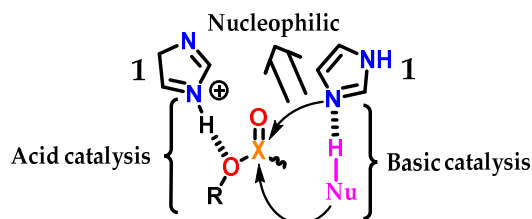


Figure 28. Acidic, basic and nucleophilic catalysis promoted by an imidazole 1 subunit.

The amino acid histidine 7 plays a fundamental role in several enzymatic active sites, including ribonucleases, phosphotriesterases, kinases, chymotrypsins and histone deacetylases [62–65]. As illustrated in Figure 29, histidine 7 residues (H573/H574) participate in the catalytic process of deacetylation of the lysine residue by histone deacetylase 6 (HDAC6). We can also see the residue (H614) acting on the triad of amino acids responsible for sustaining the zinc atom (through the interaction $\eta^1(\sigma, N_{py})$) present in the catalytic site of the enzyme [7,65].

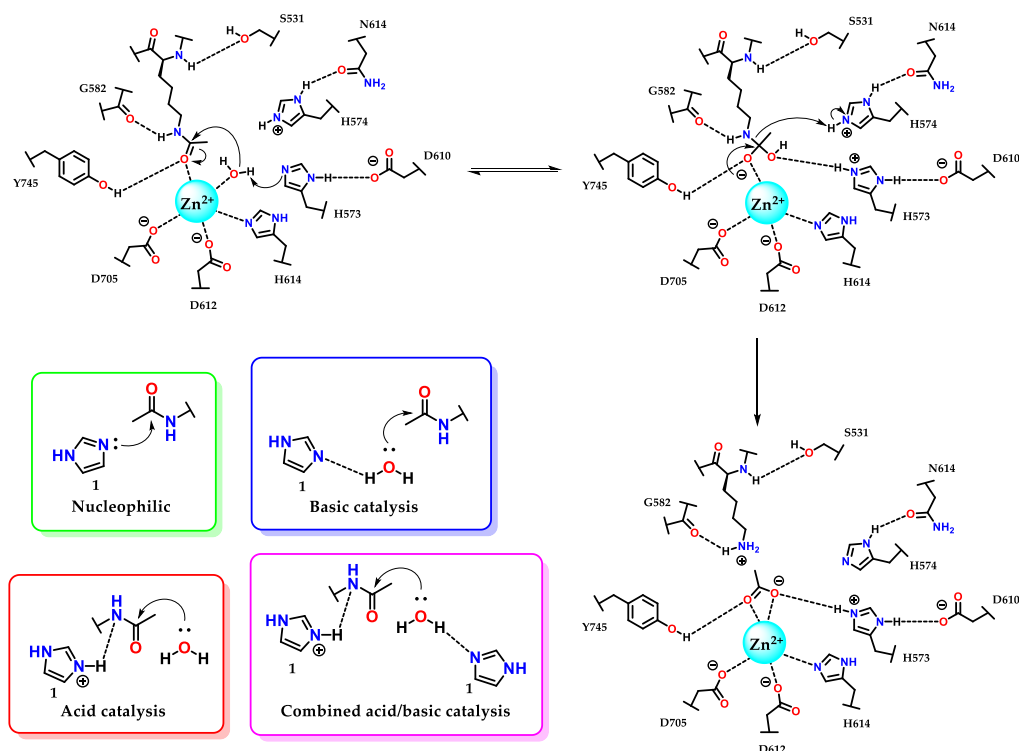


Figure 29. Participation of histidine 7 residues in the deacetylation reaction of lysine residues promoted by enzyme histone deacetylase 6 (HDAC6) and the kinetic profiles of imidazole catalysis.

It is interesting to analyze in more detail the kinetic profiles considering the pH for an acid, basic, bifunctional acid–base and nucleophilic catalysis for the cases of deacylation reactions [66,67], but which similarly follow the same profiles in dephosphorylation [68,69]. In some pH ranges (considered pH 5–9), imidazole 1 has pronounced activity, with prevalence at pH values (considering pH 8–10) above the pK_{aH} , for the neutral imidazole 1 species. This action makes it a basic and nucleophilic catalyst with similar kinetic profiles

for both cases, where the rate constant is directly proportional to the increase in pH, capable of presenting a level where the amount of neutral and reactive species remains constant (pH ~9) (Figure 29) [49]. At the plateau, it is common to observe that the rate constant in nucleophilic catalysis is higher than that in basic catalysis, considering that nucleophilic processes are faster [55]. For pH values below the pKaH, where protonated imidazole **1** predominates, the catalysis is preferably acidic. As with basic and nucleophilic catalysis, acid catalysis has the same effect at the plateau (pH ~5) (Figure 29) [55].

Considering the above remarks, we can conclude that histidine 7 residues present in the active site of HDAC6 participate in catalysis by a combined acid/base mechanism, as this hydrolyses assists with the aid of the tyrosine residue (Y745) and the metal itself (Zn^{2+}), which, when complexed with the carbonyl oxygen, further favors the reaction shown, considering the low reactivity of amide carbonyls (Figure 29).

3.2. Imidazole as a Building Block in the Structure of Bioactive Molecules and Drugs

Imidazole **1** is present in several chemical structures of pharmaceutical interest because its particular chemical properties could favor molecular recognition by different targets. Examples of the presence of imidazole **1** in the structure of bioactive substances include antibacterial [70–73], anti-inflammatory [74–76], antidiabetic [77], antiparasitic [78], antituberculosis [79], antifungal [80–82], antioxidant [83], antitumor [84–86], antimalarial [87,88], anticancer [89–91], antidepressant [92] and many other compounds (Figure 30).

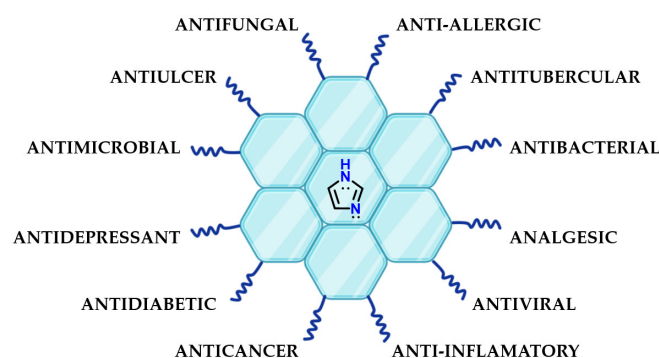


Figure 30. Presence of imidazole **1** in the most diverse classes of bioactive compounds.

Moreover, imidazole **1** is also present in several natural compounds with biological activity. As an example, pilocarpine **72** is used for the treatment of xerostomia and glaucoma [93], toposentin **73** shows anticancer activity [94] and isonaamine A **74** also shows anticancer activity through its action as an inhibitor of the epidermal growth factor receptor (EGFR) [95] (Figure 31).

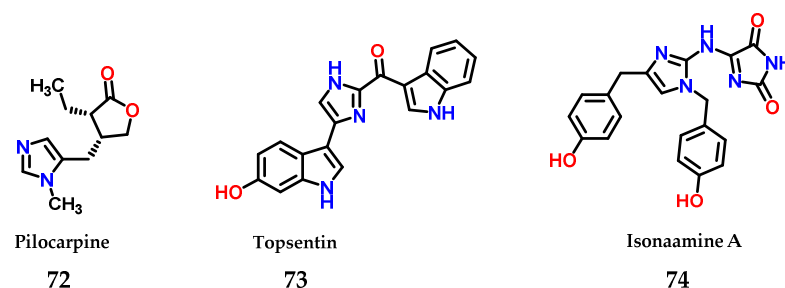


Figure 31. Structures of imidazole-containing natural products pilocarpine **72**, toposentin **73** and isonaamine A **74**.

To date, a great diversity of imidazole-containing compounds with biological activity is known, whether of natural or synthetic origin. Among the compounds with imidazole-containing activity, azomycin **75** can be considered the one with the simplest structural

complexity of all. The antibiotic azomycin was first isolated by Maeda in 1953 from a strain similar to *Mesenteric nocardia* [96]. In addition to azomycin 75, we can illustrate the structure of several more complex compounds that are even well known in current pharmacotherapy containing the imidazole nucleus, such as dacarbazine 76 [97], nafamidone 77 [98], flumizole 78 [99], cimetidine 79 [100], losartan 80 [101] and ketoconazole 81 [102] (Figure 32).

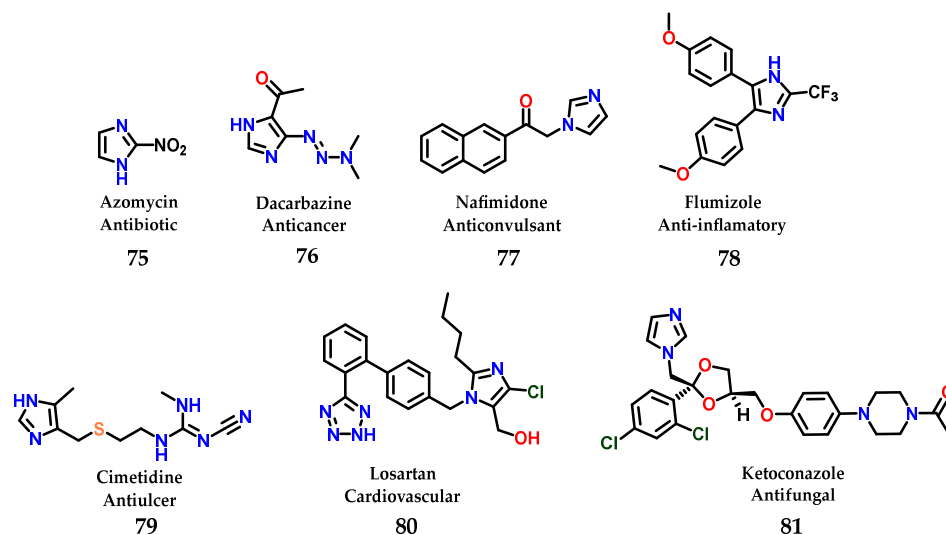


Figure 32. Structures of azomycin 75 and other imidazole-containing drugs currently used in pharmacotherapy.

Imidazole 1 proves to be a very versatile structure for medicinal chemistry, not only for its ability to act directly as a pharmacophoric group but also for being able to act as a “guide” to other groups, directing them and favoring correct auxophoric/pharmacophoric interactions, allowing the exploration of a large number of possible substitutions. Imidazole 1 is considered a bioisostere of a carboxamide unit. Thus, it can be interpreted as a peptide backbone unit isostere [103]. Depending on the substituents and their substitution pattern, small mimetic oligopeptides with *trans* and *cis* conformations can be evidenced (Figure 33) [103,104]. The isosteric exchange of amides for imidazole can be considered a good strategy to overcome problems resulting from metabolic instability promoted by amidases [105].

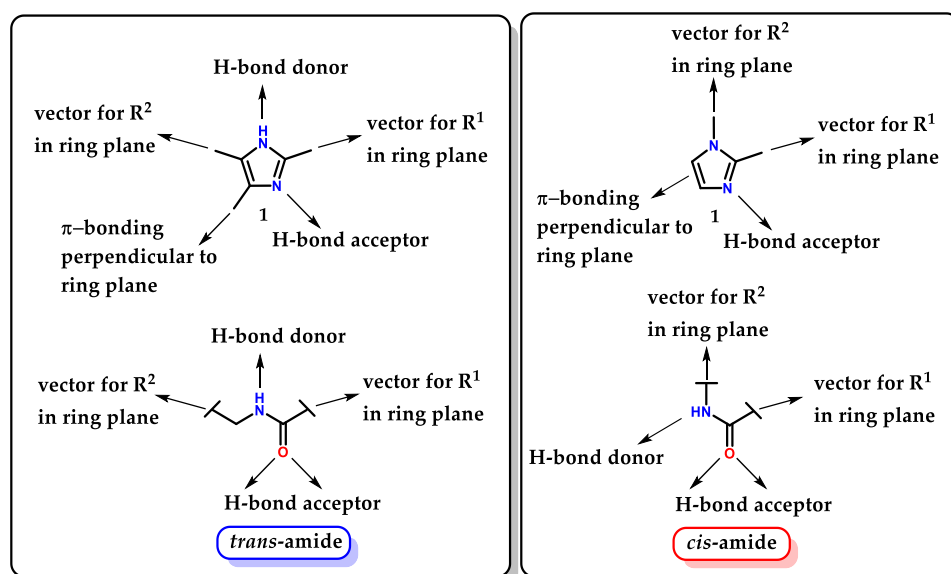


Figure 33. Isosteric relationship between imidazole 1 and *trans*/*cis*-amides.

In a more recent work by Heppner and collaborators [106], the importance of the imidazole nucleus in compounds containing biological activity was highlighted. The aim of the study was the modulation of the mutated epidermal growth factor receptor (EGFR) target, in the context of non-small-cell lung cancer, which presents acquired drug resistance. Compounds with nanomolar potency against EGFR (L858R/T790M/C797S) were obtained in a reversible binding mechanism [106].

Analysis of the X-ray crystallographic results shows how the imidazole nucleus acts as a hydrogen bond acceptor for the catalytic residue of lysine (K745) in the “ α C-helix out” inactive state of EGFR. Furthermore, selective *N*-methylation on the imidazole nucleus at the hydrogen bond acceptor position drastically reduces the potency, confirming the importance of the interaction of (K745) with the imidazole nucleus for modulating the EGFR variant (C797S) [106]. Additionally, it was observed that there is an intramolecular hydrogen interaction between the *N*-1 and the phenylacrylamide group **82** (Figure 34) [107]. The covalent bond with (C797) does not significantly change the mode of inhibitory interaction compared to the reversible compounds, indicating that the interaction of imidazole with (K757) is conserved in both covalent and non-covalent modes.

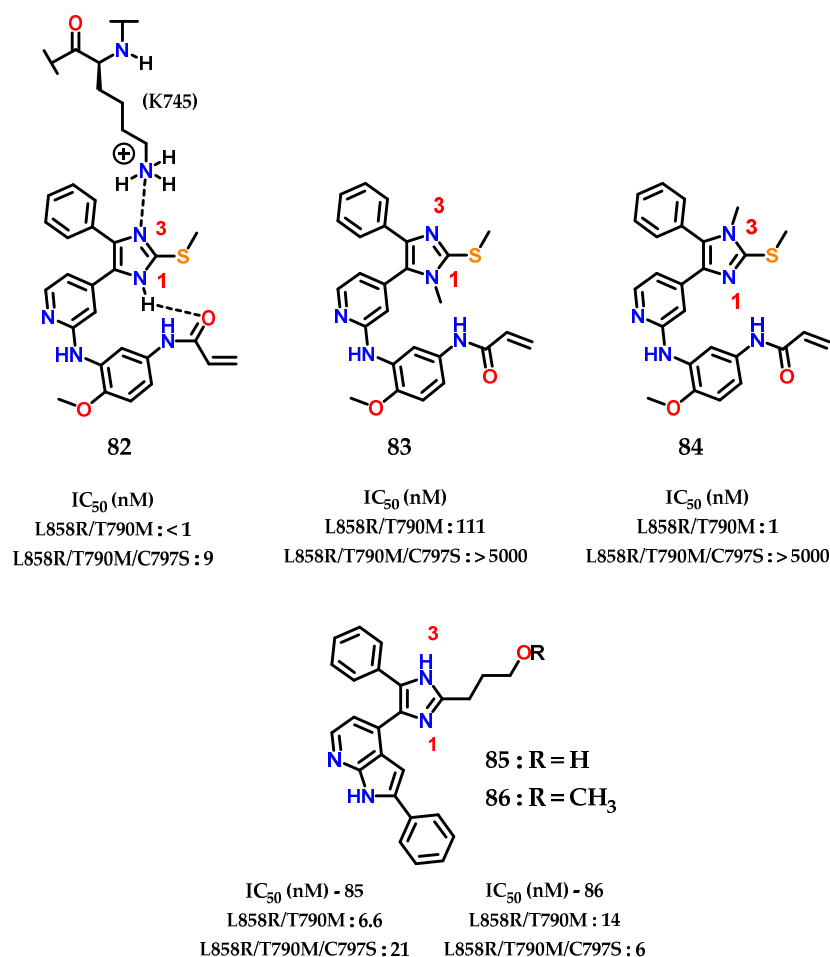


Figure 34. EGFR(L858R/T790M) and EGFR(L858R/T790M/C797S) imidazole inhibitors.

Analyzing the activity values for **82**, **83** and **84** (Figure 34), it was concluded that *N*-1 methylation **83** impacts activity against EGFR (L858R/T790M), indicating that the intramolecular interaction between imidazole and the phenylacrylamide group is required for the inhibitory mode of interaction. For *N*-3 methylation **84**, the nitrogen involved in the interaction with (K745) in the inactive form “ α C-helix out” of EGFR, does not significantly alter the inhibition activity towards EGFR (L858R/T790M), showing that the potency of **82**

does not depend on the interaction with the residue (K745) but more on the covalent bond with (C797).

Finally, it was observed that, for EGFR (L858R/T790M/C797S), the presence of both unsubstituted nitrogens in the imidazole nucleus are extremely important for activity against this mutated form. Confirmed through the data already presented by **83** and **84**, as well as the data for **85** and **86**, showing excellent IC_{50} values with this interaction pattern, and acting as reversible inhibitors.

This study shows us as an interesting practical example how imidazole may be able to act as an important auxophoric group and act directing other auxophoric and pharmacophoric groups.

Another example of imidazole application was described by Lee et al. [108], where the activity-based sensing (ABS) strategy for detecting copper in living cells was presented, which preserves spatial information through a copper-dependent bio-conjugation reaction. Copper-targeted acyl imidazole dyes were designed that operate through copper-mediated activation of acyl imidazole electrophiles for subsequent labeling of proximal proteins at sites of high labile copper to provide a permanent color that resists washing and fixation (Figure 35).

Labile pools have been characterized using this strategy in three main types of brain cells: neurons, astrocytes and microglia. Exposure of each of these cell types to physiologically relevant stimuli distinct changes in these labile copper pools. Neurons exhibit translocation of labile copper from somatic cell bodies to peripheral processes after activation, while astrocytes and microglia exhibit global decreases and increases in intracellular labile copper pools, respectively, after exposure to inflammatory stimuli [108].

This work provides fundamental information on cell-type-dependent copper homeostasis, an essential metal in the brain, as well as a starting point for the design of new activity-transmitted probes for metals and other signal analytes and dynamic stress in biology, in the context of poor regulation of copper in inflammation and neurodegenerative process [109–113]. In Figure 35 the imidazole **1** present in **87** as a metal chelator, in this case copper, is demonstrated through the $\eta^1(\sigma, Npy)$ interaction, as previously commented.

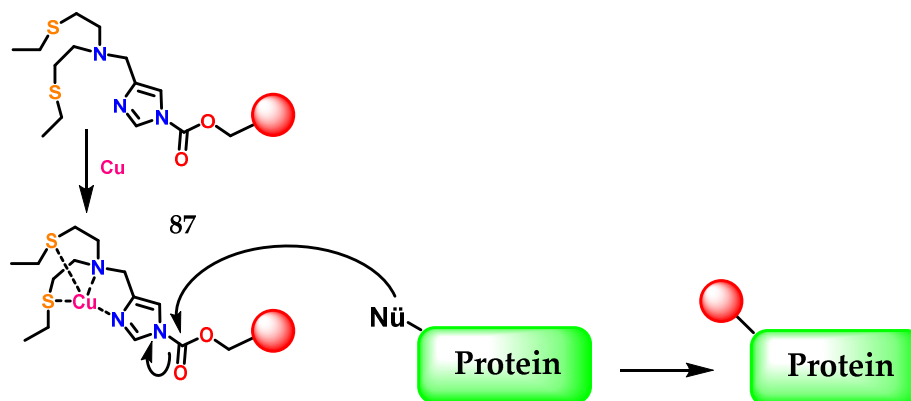


Figure 35. The activity-based sensing (ABS) strategy using acyl imidazole electrophiles **87** for subsequent labeling of proximal proteins at sites of high labile copper.

In a recent background of compounds containing imidazole for anti-proliferative activity, a large number of di/triaryl imidazole-based derivatives (Figure 36) have been reported with p38 α MAP and/or BRAF kinase inhibitory activities [114–117]. Considering these representatives, compound **88** (SB203580) was reported as a p38 α MAP kinase inhibitor with IC_{50} value of 48 nM [114,115]. Furthermore, compounds **89** and **90** exhibited their inhibitory activities against p38 α at IC_{50} values of 19 and 41 nM, respectively [116]. Compound **91** diaryl imidazole showed inhibitory activity against BRAF (IC_{50} = 900 nM) [117]. However, triaryl imidazole exhibited greater inhibitory activity against BRAF. In a series

of triaryl-substituted imidazole-based derivatives, compound **92** was the most potent in inhibiting mutant BRAF in vitro [118].

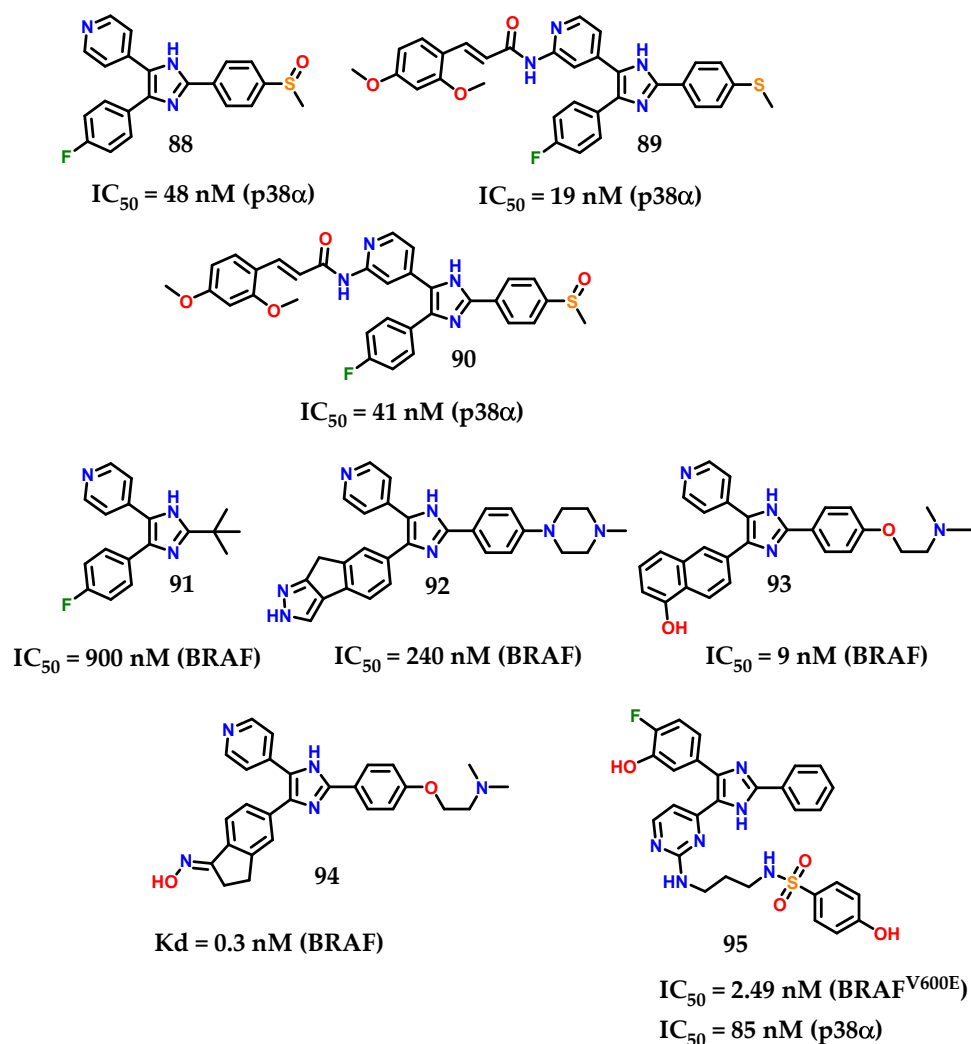


Figure 36. Di/triaryl imidazole-based derivatives with p38 α and/or BRAF inhibitory activity.

More studies about compound **92** show a weak inhibitory activity against mutant BRAF at the cellular level. Nevertheless, compound **93** showed potent BRAF inhibition ($IC_{50} = 9$ nM) and inhibited the growth of BRAF-dependent WM266.4 cells with GI_{50} of 0.22 μ M [119]. Takle and coworkers [117] reported on SB-590885 **94** among a series of derivatives based on triaryl imidazole with potent and selective inhibitory activity against BRAF kinase. The compound **94** was prepared to improve water solubility. Furthermore, it showed increased potency with more than 1000 times greater selectivity for p38 α , GSK3- β and Ick kinases compared to BRAF [117]. Recently, compound **95** (Figure 36) was reported as a derivative based on imidazol-5-yl-pyrimidine with BRAF^{V600E}/p38 α dual activity [120]. Compound **95** inhibited BRAF^{V600E} and p38 α MAP with IC_{50} values of 2.49 and 85 nM, respectively.

The designed compounds **96** and **97** were made by Youssif and collaborators [121] considering the proposed binding interactions of compound **95** with p38 α and BRAF^{V600E} (Figure 37). Investigation of compound **88**'s binding interactions in p38 α MAP revealed the presence of different types of binding interactions, including hydrogen bonding and hydrophobic interactions [121]. However, an unfavorable donor–donor interaction of the nitrogen N-1 on the imidazole ring of compound **88** with Lys53 at p38 α was reported. To avoid this unfavorable interaction, the imidazole N-1 was alkylated with the hexyl group.

Hexyl groups can also provide hydrophobic interactions with hydrophobic residues on p38 α . The structure of the compounds **96** and **97** was also extended by a four-atom linker connecting the 1,3-benzodioxolo **96** and 4-methoxybenzyl **97** ring substituents with the triaryl imidazole scaffold [121]. The ligand includes three hydrogen bond acceptor atoms (CO-O-N=) and a hydrogen bond donor group (NH₂) that can form hydrogen bonds with amino acids on the phosphate binding region at p38 α [121].

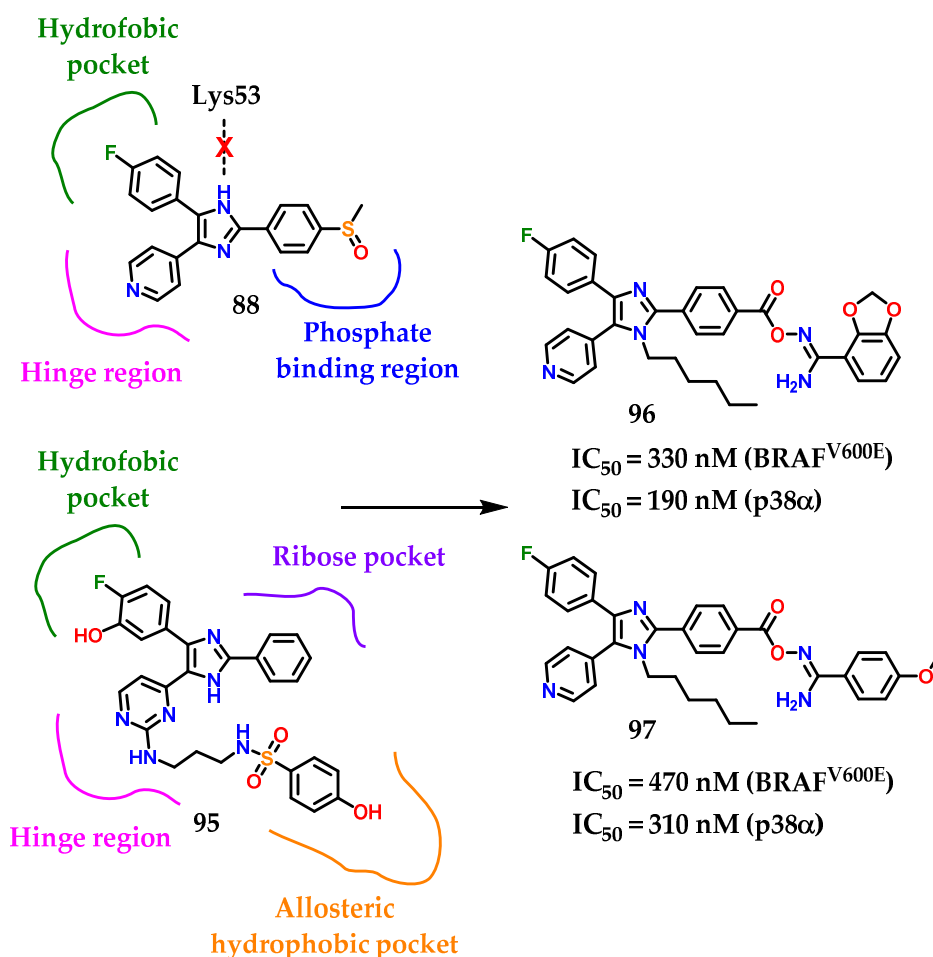


Figure 37. Rational design of compounds **96** and **97**.

Among the docking studies, compounds **96** and **97** were able to properly interact with Lys53 in the imidazole scaffold *N*-3. In conclusion, we can see that **96** and **97** are promising lead compounds with high potential for development as new dual p38 α /BRAFF^{V600E} inhibitors based on the good activity values.

With these recent examples from the literature, we can see that imidazole presents itself as a privileged structure, being widely explored as a nucleus capable of efficiently participating and assisting in the modulation of several molecular targets and acting in other areas, such as probes for biological assessment.

3.3. The Origin of Cimetidine as an Imidazole-Containing Drug

To the best of our knowledge, there are four types of histamine receptors that belong to the G-protein-coupled receptor family: histamine H₁ receptor, histamine H₂ receptor, histamine H₃ receptor and histamine H₄ receptor, which could be stimulated by the endogenous messenger histamine **8** without distinction [122,123]. However, properly designed antagonists must be able to distinguish between them [124]. In the 1960s–1970s, selective antagonists capable of inhibiting the histamine receptors involved in the allergic process

(H₁ receptors) and antagonists capable of inhibiting histamine receptors responsible for gastric acid secretion (H₂ receptors) were already known [124].

Variations were made in the structure of histamine **8** so that it was recognized by the receptor. Simultaneously, it was able to act as an antagonist. SAR studies on histamine analogs revealed that the requirements for histamine **8** to bind to the proposed H₁ and H₂ receptors were slightly different (Figure 38) [125]. On the H₁ receptors, the essential requirements are as follows:

The side chain must have a positively charged nitrogen atom with at least one hydrogen. Quaternary ammonium salts are not active.

There must be a flexible chain between the cation and the heteroaromatic ring.

The heteroaromatic ring does not have to be imidazole **1** but must have a nitrogen atom with a pair of electrons adjacent to the side chain.

On the other hand, the requirements for H₂ and H₁ receptors are the same, except that:

The heteroaromatic ring must have an amidine **5** unit (-HN-CH=N-) acting as a proton transfer agent.

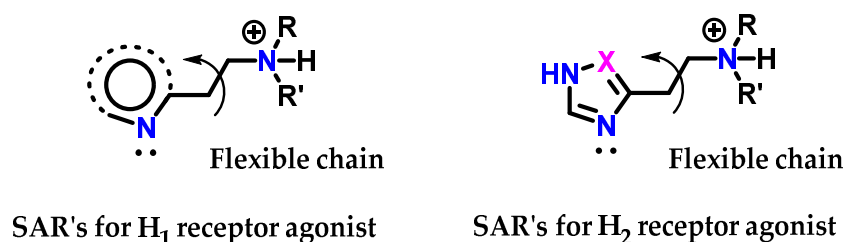


Figure 38. SAR for histamine H₁ and H₂ receptor agonists.

Based on this information, it appears that the terminal amino group being protonated is involved in an ionic interaction with both types of receptors, while the nitrogen atoms of the heteroaromatic ring are linked through hydrogen bonds, and for H₂ receptors, the ring participates in an extra interaction through proton transfer (Figure 39) [125].

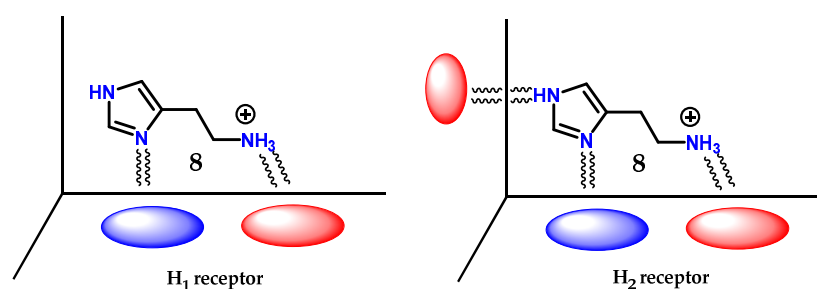


Figure 39. Scheme of the spatial arrangement for the interaction of histamine **8** on the H₁ and H₂ receptors.

Checking the changes in the structure of histamine **8**, it was noted that 4(5)-methylhistamine **98** is a highly selective H₂ receptor agonist, showing greater selectivity for H₂ than for H₁ [125,126]. 4(5)-Methylhistamine **98**, similar to histamine **8**, is a highly flexible molecule due to its side chain, but structural studies show that some of their conformations are less stable than others (Figure 40) [125,126]. In particular, conformation (A) is disadvantaged due to the steric interaction between the methyl group and the side ethylamine chain. The selectivity observed suggests that, for both receptors, 4(5)-methylhistamine **98** has to adopt two different conformations to bind to these receptors [125,126]. As 4(5)-methylhistamine **98** is more active as an agonist of the H₂ receptor, this suggests that the favorable conformation (B) is required for the interaction with the H₂ receptor, while the conformation required for the H₁ receptor would be the sterically unfavorable conformation (A) [125,126].

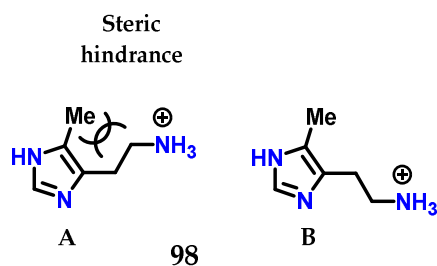


Figure 40. Conformations of 4(5)-methylhistamine **98**. Energetically unfavorable conformation **A** and the more stable conformation **B**.

In histamine **8**, the exocyclic amino group is protonated at physiological pH, exerting a strong electron-withdrawing effect on the imidazole ring. This effect is more pronounced for the nitrogen closest to this side chain, so the hydrogen atom in the nitrogen $N\pi$ will be more acidic than the one bound to the $N\tau$ [125–127]. For this reason, the last tautomer ($N\tau$) is more stable than π ($N\pi$) in histamine **8**, given that the favored ionization in the structure would lead to stabilization of the charge formed (Figure 41). On the other hand, the thiourea group of burimamide **99** exerts a less pronounced electron-donating effect, and therefore, the $N\pi$ tautomer is favored [125–127]. Thus, the idea would be to remove electrons from the burimamide **99** side chain instead of donating electrons through the introduction of an electron withdrawing atom in this chain. The use of an isosteric group of the methylene group was proposed [125–127]. The sulfur atom is considered a good classical isostere of the methylene group, as their van der Waals radii and bond angles are similar [125–128]. The substitution site was also chosen based on synthetic reasons (Figure 41).

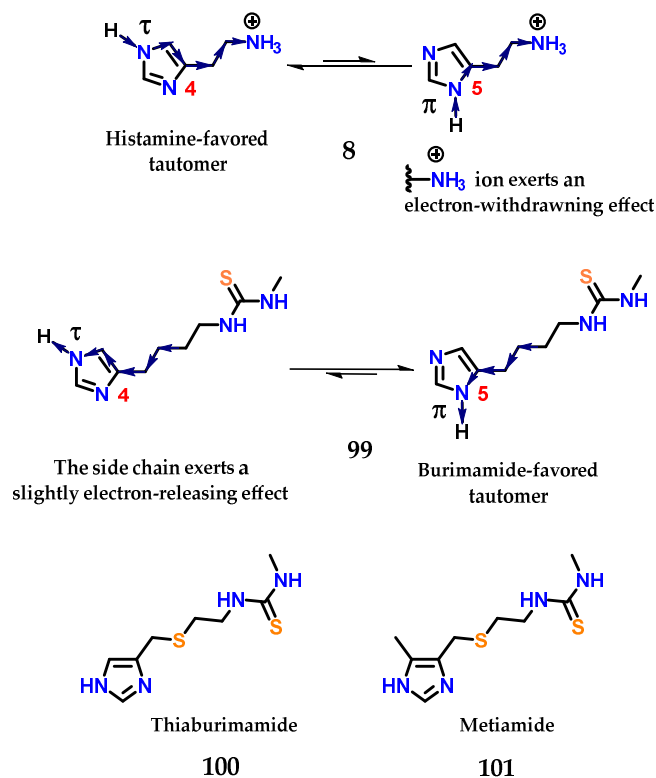


Figure 41. Preferred tautomeric forms of histamine **8** and burimamide **99**. Thiaburimamide **100** and metiamide **101** derivatives as H_2 receptor antagonists.

The sulfur atom present in the side chain of thiaburimamide **100** carried out the removal of electrons, favoring the *tau* tautomer (τ). Furthermore, a hypothesis has been raised about the possibility of increasing the favoring of this tautomer through the insertion of a group in position 5 of the imidazole **1** ring [125–127]. In this position, the inductive effect would have a more pronounced impact on the neighboring nitrogen atom ($N\tau$). The methyl group was chosen because it was known that (4)-methylhistamine **98** was highly selective against the H_2 receptor, in addition to influencing the pKa of hydrogen $N\tau$, with an electron donating effect [125–127,129]. Metiamide **101** was obtained, showing the highest antagonistic activity on H_2 receptors (Figure 41).

Metiamide **101** was shown to be 10 times more potent than burimamide **99** [130] and showed great promise as an antiulcer agent. Unfortunately, several patients suffered from kidney problems and granulocytopenia, a disease that leads to a reduction in leukocytes and makes patients more susceptible to infection due to the metabolism of thiourea, which led to metiamide **101** not being approved in stage I clinical trials [131,132].

After the study of metiamide **101**, several other studies were carried out with the objective of modifying the thiourea subunit, a region that is also responsible for important interactions with the target receptor, giving the compounds the profile of antagonists (region of binding of the antagonist). Figure 42 summarizes all the work and rationale used to design the first blockbuster drug cimetidine. Cimetidine, similar to other examples in the literature, is a drug that has an imidazole nucleus in its structure and is a beautiful and inspiring example of rational drug design carried out in the mid-1960s–1970s [133].

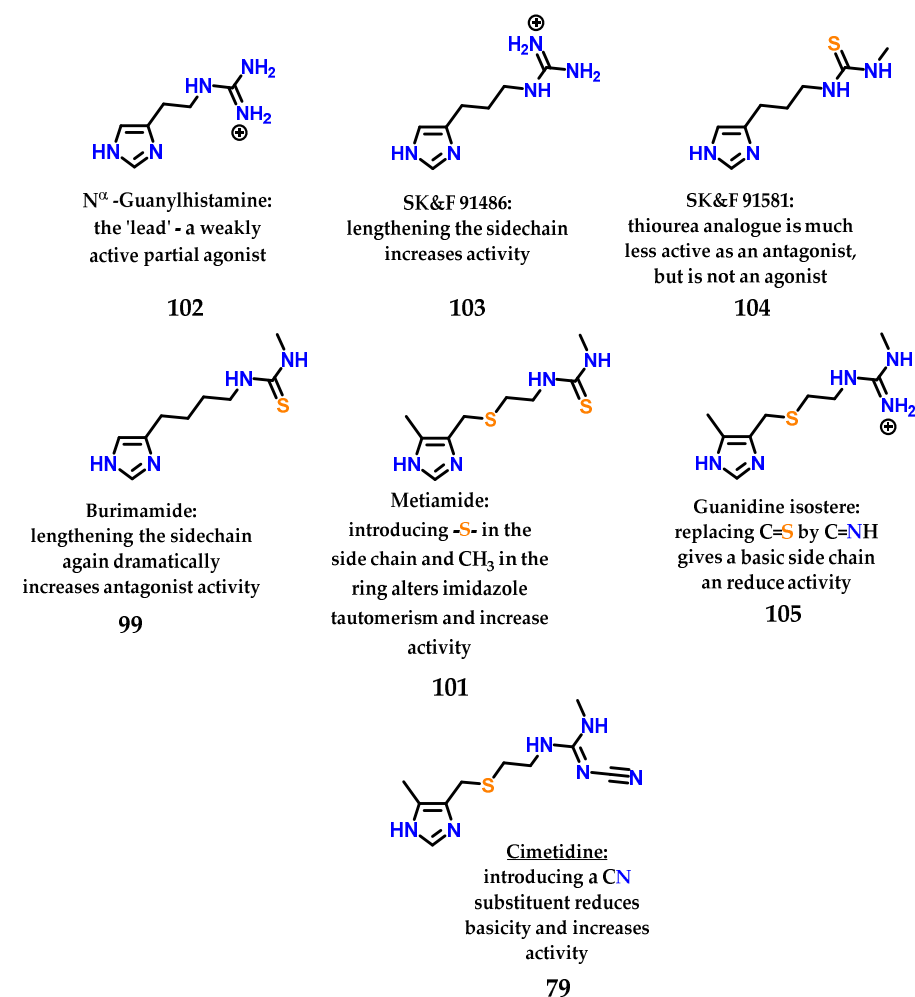


Figure 42. Sequential analogues described by Black, Ganellin and coworkers at SK&F until the discovery of cimetidine **79**.

Figueiredo and coworkers [134], who described the synthesis of methyl-imidazolyl *N*-acylhydrazone (NAH) derivatives showing antinociceptive activity, demonstrated another interesting study on imidazole **1** tautomerism, exploring the idea of cimetidine **79**. Using the AM1 Hamiltonian [135] with unsubstituted derivative **106**, the conformational behavior of the (NAH) motif around C-4 from the imidazole nucleus was investigated. Figueiredo and coworkers observed that the *S*-*cis*-like conformation (**A**) of the *N*-4 tautomer from compound **106** was ca. 6.0 kcal/mol more stable than the corresponding *S*-*trans* (**A'**) conformation (Figure 43) [134]. A five-member-like intramolecular hydrogen bond involving the hydrogen atom of the *N*-acylhydrazone moiety and the nitrogen atom *N*-3 of the imidazole **1** ring could be the reason for this favored conformation. Hydrogen bonding was also observed in the *N*-5 tautomer (**B'**) (Figure 43); however, in this case, a 3 kcal/mol decrease in stability was observed [134].

We observed in this study [134] that for structure (**A**), there are several favorable factors to maintain the (4)-tautomer, i.e., the withdrawing group (EWG) in the C-4 position and the methyl group at the C-5 position, in addition to the possible intramolecular interaction due to the presence of the NAH subunit. Additionally, the methyl group at the C-5 position may contribute slightly through steric effects to the formation of (**A**) instead (**A'**), given the steric hindrance caused by methyl and the NAH substituent. A similar effect was observed for 4(5)-methylhistamine **98**. Considering all the structures, (**B'**) demonstrates several unfavorable requirements to maintain (5)-tautomerism, even presenting an intramolecular interaction. Given that several of these structural factors play against the pKa value of *N*-1 present in the imidazole ring, its acidity is increased.

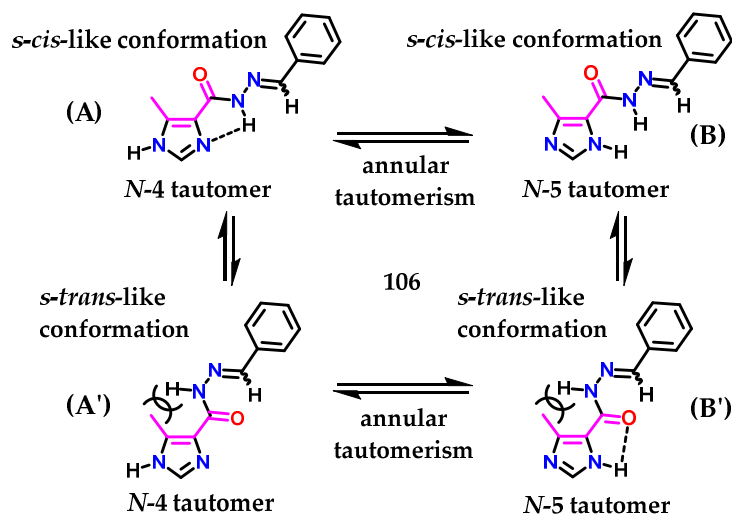


Figure 43. Ring isomerism and conformers of *N*-acylhydrazone derivative **90**.

4. Conclusions

To date, much work has been done on the synthesis, functionalization, description of physicochemical characteristics and biological application of imidazole heterocycles. This work highlighted the special interest and importance of imidazole-containing derivatives in the field of medicinal chemistry and drug discovery.

As demonstrated, imidazole **1** is a structure that, despite being small, presents unique chemical complexity. It is a nucleus that proves to be very practical and versatile in its construction/functionalization and can be considered a rich source of chemical diversity. The role and importance of imidazole **1** in processes for the maintenance of living organisms, such as catalytic participation in enzymatic processes, were also reported. We observed examples of imidazole-based compounds with antibacterial, anti-inflammatory, antidiabetic, antiparasitic, antituberculosis, antifungal, antioxidant, antitumor, antimalarial, anticancer, antidepressant and many other activities in the literature. Finally, the role of imidazole **1** in drug research and development was briefly demonstrated through the discussion of

the discovery of cimetidine **79**. It was possible to explore several chemical and biological phenomena of this important drug, which certainly served as a rich base for knowledge and inspiration for several other bioactive imidazole-based drug candidates. This was also demonstrated in the structure of methyl-imidazolyl *N*-acylhydrazone derivative **106**, which was produced after cimetidine and presented a nociceptive effect, and those that continue to currently be developed.

Author Contributions: All authors have written, read and agreed to the published version of the manuscript. All authors have read and agreed to the published version of the manuscript.

Funding: This study was financed in part by the Coordenação de Aperfeiçoamento de Pessoal de Nível Superior—Brasil (CAPES)—Finance Code 001. The authors would like to thank INCT-INOVAR (BR, grant number 465.249/2014-0), Fundação Carlos Chagas Filho de Amparo à Pesquisa do Estado do Rio de Janeiro (FAPERJ, grant numbers E-26/010.001273/2016 and SEI-260003/003613/2022, fellowship to CAMF), Conselho Nacional de Desenvolvimento Científico e Tecnológico (CNPq, grant number 304394/2017-3) and Departamento de Ciência e Tecnologia (DECIT, Ministry of Health, Brazil).

Institutional Review Board Statement: Not applicable.

Informed Consent Statement: Not applicable.

Data Availability Statement: Not applicable.

Acknowledgments: Not applicable.

Conflicts of Interest: The authors declare no conflict of interest.

References

1. Debus, H. Ueber Die Einwirkung Des Ammoniaks Auf Glyoxal. *Ann. Chem. Pharm.* **1858**, *107*, 199–208. [CrossRef]
2. Verma, A.; Joshi, S.; Singh, D. Imidazole: Having Versatile Biological Activities. *J. Chem.* **2013**, *1*, 1–12. [CrossRef]
3. Asif, M. A Mini Review: Biological Significances of Nitrogen Hetero Atom Containing Heterocyclic Compounds. *Int. J. Bioorg. Chem.* **2017**, *2*, 146–152.
4. Zhao, C.; Qiao, X.; Yi, Z.; Guan, Q.; Li, W. Active Centre and Reactivity Descriptor of a Green Single Component Imidazole Catalyst for Acetylene Hydrochlorination. *Phys. Chem. Chem. Phys.* **2020**, *22*, 2849–2857. [CrossRef] [PubMed]
5. Olofson, A.; Yakushijin, K.; Horne, D.A. Synthesis of Marine Sponge Alkaloids Oroidin, Clathrocin, and Dispacamides. Preparation and Transformation of 2-Amino-4, 5-Dialkoxy-4, 5-Dihydroimidazolines from 2-Aminoimidazoles. *J. Org. Chem.* **1998**, *63*, 1248–1253. [CrossRef]
6. Wan, Y.; Hur, W.; Cho, C.Y.; Liu, Y.; Adrian, F.J.; Lozach, O.; Bach, S.; Mayer, T.; Fabbro, D.; Meijer, L. Synthesis and Target Identification of Hymenialdisine Analogs. *Chem. Biol.* **2004**, *11*, 247–259. [CrossRef]
7. Richaud, A.; Barba-Behrens, N.; Méndez, F. Chemical Reactivity of the Imidazole: A Semblance of Pyridine and Pyrrole? *Org. Lett.* **2011**, *13*, 972–975. [CrossRef]
8. Mullins, R.J.; Azman, A.M. Imidazoles. In *Tetrahedron Organic Chemistry Series*; Elsevier: Amsterdam, The Netherlands, 2007; Volume 26, pp. 407–433. [CrossRef]
9. Stockman, R.A. Heterocyclic Chemistry. *Annu. Rep. Prog. Chem. Sect. B Org. Chem.* **2007**, *103*, 107–124. [CrossRef]
10. Movellan, K.T.; Wegstroth, M.; Overkamp, K.; Leonov, A.; Becker, S.; Andreas, L.B. Imidazole–Imidazole Hydrogen Bonding in the PH-Sensing Histidine Side Chains of Influenza A M2. *J. Am. Chem. Soc.* **2020**, *142*, 2704–2708. [CrossRef]
11. Kochendoerfer, G.G.; Salom, D.; Lear, J.D.; Wilk-Orescan, R.; Kent, S.B.H.; DeGrado, W.F. Total Chemical Synthesis of the Integral Membrane Protein Influenza A Virus M2: Role of Its C-Terminal Domain in Tetramer Assembly. *Biochemistry* **1999**, *38*, 11905–11913. [CrossRef]
12. Sakaguchi, T.; Tu, Q.; Pinto, L.H.; Lamb, R.A. The Active Oligomeric State of the Minimalistic Influenza Virus M2 Ion Channel Is a Tetramer. *Proc. Nat. Acad. Sci. USA* **1997**, *94*, 5000–5005. [CrossRef]
13. Sugrue, R.J.; Hay, A.J. Structural Characteristics of the M2 Protein of Influenza A Viruses: Evidence That It Forms a Tetrameric Channel. *Virology* **1991**, *180*, 617–624. [CrossRef]
14. Sugrue, R.J.; Bahadur, G.; Zambon, M.C.; Hall-Smith, M.; Douglas, A.R.; Hay, A.J. Specific Structural Alteration of the Influenza Haemagglutinin by Amantadine. *EMBO J.* **1990**, *9*, 3469–3476. [CrossRef]
15. Colvin, M.T.; Andreas, L.B.; Chou, J.J.; Griffin, R.G. Proton Association Constants of His 37 in the Influenza–A M218–60 Dimer-of-Dimers. *Biochemistry* **2014**, *53*, 5987–5994. [CrossRef]
16. Bylund, D.B. Histamine. In Reference Module in Biomedical Sciences. 2017. Available online: <https://scitechconnect.elsevier.com/resources/reference-module-biomedical-sciences/> (accessed on 31 December 2022). [CrossRef]

17. Arnau, N.; Arredondo, Y.; Moreno-Mañas, M.; Pleixats, R.; Villarroja, M. Palladium (0)-catalyzed Allylation of 4 (5)-substituted Imidazoles, 5 (6)-substituted Benzimidazoles, Benzotriazole and 5 (6)-methylbenzotriazole. *J. Heterocycl. Chem.* **1995**, *32*, 1325–1334. [CrossRef]
18. Kuzuya, M.; Noguchi, A.; Mano, E.; Okuda, T. The Structure–Reactivity–Chemoselectivity Relationship on the Reactions of 1–Unsubstituted Tautomeric 2–Pyridones with Benzyne. *Bull. Chem. Soc. Jpn.* **1985**, *58*, 1149–1155. [CrossRef]
19. Katritzky, A.R.; Lagowski, J.M. Prototropic Tautomerism of Heteroaromatic Compounds: IV. Five–Membered Rings with Two or More Hetero Atoms. *Adv. Heterocycl. Chem.* **1963**, *2*, 27–81.
20. Walba, H.; Isensee, R.W. Acidity Constants of Some Arylimidazoles and Their Cations. *J. Org. Chem.* **1961**, *26*, 2789–2791. [CrossRef]
21. Zhu, L.; Li, G.; Luo, L.; Guo, P.; Lan, J.; You, J. Highly Functional Group Tolerance in Copper-Catalyzed N-Arylation of Nitrogen-Containing Heterocycles under Mild Conditions. *J. Org. Chem.* **2009**, *74*, 2200–2202. [CrossRef]
22. Ruan, Y.; Chen, Y.; Gu, L.; Luo, Y.; Yang, Z.; He, L. Preparation of Imidazole Derivatives via Bisfunctionalization of Alkynes Catalyzed by Ruthenium Carbonyl. *Synthesis* **2019**, *51*, 3520–3528. [CrossRef]
23. Chen, J.; Wang, Z.; Li, C.-M.; Lu, Y.; Vaddady, P.K.; Meibohm, B.; Dalton, J.T.; Miller, D.D.; Li, W. Discovery of Novel 2-Aryl–4–Benzoyl–Imidazoles Targeting the Colchicines Binding Site in Tubulin as Potential Anticancer Agents. *J. Med. Chem.* **2010**, *53*, 7414–7427. [CrossRef] [PubMed]
24. Kuzu, B.; Tan, M.; Ekmekci, Z.; Menges, N. A Novel Fluorescent Sensor Based on Imidazole Derivative for Fe³⁺ Ions. *J. Lumin.* **2017**, *192*, 1096–1103. [CrossRef]
25. de Toledo, I.; Grigolo, T.A.; Bennett, J.M.; Elkins, J.M.; Pilli, R.A. Modular Synthesis of Di-and Trisubstituted Imidazoles from Ketones and Aldehydes: A Route to Kinase Inhibitors. *J. Org. Chem.* **2019**, *84*, 14187–14201. [CrossRef] [PubMed]
26. Shabalin, D.A.; Dunsford, J.J.; Ngwerume, S.; Saunders, A.R.; Gill, D.M.; Camp, J.E. Synthesis of 2, 4–Disubstituted Imidazoles via Nucleophilic Catalysis. *Synlett.* **2020**, *31*, 797–800.
27. Fang, S.; Yu, H.; Yang, X.; Li, J.; Shao, L. Nickel-Catalyzed Construction of 2, 4–Disubstituted Imidazoles via C–C Coupling and C–N Condensation Cascade Reactions. *Adv. Synth. Catal.* **2019**, *361*, 3312–3317. [CrossRef]
28. Wong, L.C.; Gehre, A.; Stanforth, S.P.; Tarbit, B. Convenient Synthesis of Highly Substituted Imidazole Derivatives. *Synth. Commun.* **2013**, *43*, 80–84. [CrossRef]
29. Noriega-Iribe, E.; Díaz-Rubio, L.; Estolano-Cobián, A.; Barajas-Carrillo, V.W.; Padrón, J.M.; Salazar-Aranda, R.; Díaz-Molina, R.; García-González, V.; Chávez-Santoscoy, R.A.; Chávez, D. In Vitro and in Silico Screening of 2, 4, 5–Trisubstituted Imidazole Derivatives as Potential Xanthine Oxidase and Acetylcholinesterase Inhibitors, Antioxidant, and Antiproliferative Agents. *Appl. Sci.* **2020**, *10*, 2889. [CrossRef]
30. Kalhor, M.; Seyedzade, Z.; Zarnegar, Z. (NH₄)₂Ce(NO₃)₆/HNO₃ as a High-Performance Oxidation Catalyst for the One-Step, Solvent-Free Synthesis of Dicyano Imidazoles. *Polycycl. Aromat. Compd.* **2021**, *41*, 1506–1514. [CrossRef]
31. Takashima, R.; Tsunekawa, K.; Shinozaki, M.; Suzuki, Y. Selective Synthesis of 1, 4, 5–Trisubstituted Imidazoles from α -Imino Ketones Prepared by N-Heterocyclic–Carbene–Catalyzed Aroylation. *Tetrahedron* **2018**, *74*, 2261–2267. [CrossRef]
32. Bunev, A.S.; Vasiliev, M.A.; Statsyuk, V.E.; Ostapenko, G.I.; Peregudov, A.S. Synthesis of 1–Aryl–4–Tosyl–5–(Trifluoromethyl)–1H–Imidazoles. *J. Fluor. Chem.* **2014**, *163*, 34–37. [CrossRef]
33. Hanoon, H.D.; Kowsari, E.; Abdouss, M.; Ghasemi, M.H.; Zandi, H. Highly Efficient and Simple Protocol for Synthesis of 2, 4, 5–Triarylimidazole Derivatives from Benzil Using Fluorinated Graphene Oxide as Effective and Reusable Catalyst. *Res. Chem. Intermed.* **2017**, *43*, 4023–4041. [CrossRef]
34. Tan, J.; Li, J.R.; Hu, Y.L. Novel and Efficient Multifunctional Periodic Mesoporous Organosilica Supported Benzotriazolium Ionic Liquids for Reusable Synthesis of 2, 4, 5–Trisubstituted Imidazoles. *J. Saudi Chem. Soc.* **2020**, *24*, 777–784. [CrossRef]
35. Hilal, D.A.; Hanoon, H.D. Bronsted Acidic Ionic Liquid Catalyzed an Eco-Friendly and Efficient Procedure for Synthesis of 2, 4, 5–Trisubstituted Imidazole Derivatives under Ultrasound Irradiation and Optimal Conditions. *Res. Chem. Intermed.* **2020**, *46*, 1521–1538. [CrossRef]
36. Alinezhad, H.; Tajbakhsh, M.; Maleki, B.; Pourshaban Oushibi, F. Acidic Ionic Liquid [H-NP] HSO₄ Promoted One-Pot Synthesis of Dihydro–1H–Indeno [1, 2–b] Pyridines and Polysubstituted Imidazoles. *Polycycl. Aromat. Compd.* **2020**, *40*, 1485–1500. [CrossRef]
37. Maleki, A.; Rahimi, J.; Valadi, K. Sulfonated Fe₃O₄@ PVA Superparamagnetic Nanostructure: Design, in-Situ Preparation, Characterization and Application in the Synthesis of Imidazoles as a Highly Efficient Organic–Inorganic Bronsted Acid Catalyst. *Nano-Struct. Nano-Objects.* **2019**, *18*, 100264. [CrossRef]
38. Gupta, S.; Lakshman, M. Magnetic Nano Cobalt Ferrite: An Efficient Recoverable Catalyst for Synthesis of 2, 4, 5–Trisubstituted Imidazoles. *J. Med. Chem. Sci.* **2019**, *2*, 51–54.
39. Kalhor, M.; Zarnegar, Z. Fe₃O₄/SO₃H@ Zeolite-Y as a Novel Multi-Functional and Magnetic Nanocatalyst for Clean and Soft Synthesis of Imidazole and Perimidine Derivatives. *RSC Adv.* **2019**, *9*, 19333–19346. [CrossRef]
40. Singh, H.; Rajput, J.K. Co (II) Anchored Glutaraldehyde Crosslinked Magnetic Chitosan Nanoparticles (MCS) for Synthesis of 2, 4, 5-trisubstituted and 1, 2, 4, 5-tetrasubstituted Imidazoles. *Appl. Organomet. Chem.* **2018**, *32*, e3989. [CrossRef]
41. Wagare, D.S.; Sonone, A.; Farooqui, M.; Durrani, A. An Efficient and Green Microwave-Assisted One Pot Synthesis of Imidazothiadiazoles in PEG–400 and Water. *Polycycl. Aromat. Compd.* **2021**, *41*, 1749–1754. [CrossRef]

42. Ali, M.A.E.A.A.; Abu-Dief, A.M. CuFe₂O₄ Nanoparticles: An Efficient Heterogeneous Magnetically Separable Catalyst for Synthesis of Some Novel Propynyl-1H-Imidazoles Derivatives. *Tetrahedron* **2015**, *71*, 2579–2584.
43. Rajkumar, R.; Kamaraj, A.; Krishnasamy, K. Multicomponent, One-Pot Synthesis and Spectroscopic Studies of 1-(2-(2, 4, 5-Triphenyl-1 H-Imidazol-1-Yl) Ethyl) Piperazine Derivatives. *J. Taibah Uni. Sci.* **2015**, *9*, 498–507. [CrossRef]
44. Wang, S.; Kirillova, K.; Lehto, X. Travelers' Food Experience Sharing on Social Network Sites. *J. Travel Tour. Mark.* **2017**, *34*, 680–693. [CrossRef]
45. Hosseini, S.; Kiasat, A.R.; Farhadi, A. Fe₃O₄@SiO₂/Bipyridinium Nanocomposite as a Magnetic and Recyclable Heterogeneous Catalyst for the Synthesis of Highly Substituted Imidazoles Via Multi-Component Condensation Strategy. *Polycycl. Aromat. Compd.* **2021**, *41*, 761–771. [CrossRef]
46. Davoodnia, A.; Heravi, M.M.; Safavi-Rad, Z.; Tavakoli-Hoseini, N. Green, One-Pot, Solvent-Free Synthesis of 1, 2, 4, 5-Tetrasubstituted Imidazoles Using a Brønsted Acidic Ionic Liquid as Novel and Reusable Catalyst. *Synth. Commun.* **2010**, *40*, 2588–2597. [CrossRef]
47. Safa, K.D.; Feyzi, A.; Allahvirdinesbat, M.; Sarchami, L.; Panahi, P.N. Synthesis of Novel Organosilicon Compounds Possessing Fully Substituted Imidazole Nucleus Sonocatalyzed by Fe–Cu/ZSM-5 Bimetallic Oxides. *Synth. Commun.* **2015**, *45*, 382–390. [CrossRef]
48. Desai, N.C.; Maheta, A.S.; Rajpara, K.M.; Joshi, V.; Vaghani, H.V.; Satodiya, H.M. Green Synthesis of Novel Quinoline Based Imidazole Derivatives and Evaluation of Their Antimicrobial Activity. *J. Saudi Chem. Soc.* **2014**, *18*, 963–971. [CrossRef]
49. Green, J.P.; Prell, G.D.; Khandelwal, J.K.; Blandina, P. Aspects of Histamine Metabolism. *Agents Actions* **1987**, *22*, 1–15. [CrossRef]
50. Haas, H.L.; Sergeeva, O.A.; Selbach, O. Histamine in the Nervous System. *Physiol. Rev.* **2008**, *88*, 1183–1241. [CrossRef]
51. Fox, S.W. Chemistry of the Biologically Important Imidazoles. *Chem. Rev.* **1943**, *32*, 47–71. [CrossRef]
52. Gupta, R.R.; Kumar, M.; Gupta, V. *Heterocyclic Chemistry: Volume II: Five-Membered Heterocycles*; Springer Science & Business Media: Berlin, German, 2013; ISBN 3662077574.
53. Wolfenden, R.; Snider, M.J. The Depth of Chemical Time and the Power of Enzymes as Catalysts. *Acc. Chem. Res.* **2001**, *34*, 938–945. [CrossRef]
54. Liu, C.; Wang, M.; Zhang, T.; Sun, H. DNA Hydrolysis Promoted by Di- and Multi-Nuclear Metal Complexes. *Coord. Chem. Rev.* **2004**, *248*, 147–168. [CrossRef]
55. Silva, V.B.; Orth, E.S. Imidazole and Catalysis: A Perfect Match. *Quim. Nova.* **2021**, *44*, 318–333.
56. Schowen, K.B.; Limbach, H.-H.; Denisov, G.S.; Schowen, R.L. Hydrogen Bonds and Proton Transfer in General-Catalytic Transition-State Stabilization in Enzyme Catalysis. *Biochim. Biophys. Bioenerg.* **2000**, *1458*, 43–62. [CrossRef]
57. Attwood, P.; Piggott, M.J.; Zu, X.L.; Besant, P.G. Focus on Phosphohistidine. *Amino Acids* **2007**, *32*, 145–156. [CrossRef]
58. Raines, R.T. Ribonuclease a. *Chem. Rev.* **1998**, *98*, 1045–1066. [CrossRef]
59. Anderson, V.E.; Ruzsyczky, M.W.; Harris, M.E. Activation of Oxygen Nucleophiles in Enzyme Catalysis. *Chem. Rev.* **2006**, *106*, 3236–3251. [CrossRef]
60. Matuszak, C.A.; Matuszak, A.J. Imidazole-Versatile Today, Prominent Tomorrow. *J. Chem. Educ.* **1976**, *53*, 280. [CrossRef]
61. Orth, E.S.; Brandao, T.A.S.; Milagre, H.M.S.; Eberlin, M.N.; Nome, F. Intramolecular Acid–Base Catalysis of a Phosphate Diester: Modeling the Ribonuclease Mechanism. *J. Am. Chem. Soc.* **2008**, *130*, 2436–2437. [CrossRef]
62. Raushel, F.M.; Holden, H.M. Phosphotriesterase: An Enzyme in Search of Its Natural Substrate. *Adv. Enzymol. Relat. Areas Mol. Biol.* **2000**, *74*, 51–93.
63. Yang, W. Nucleases: Diversity of Structure, Function and Mechanism. *Q. Rev. Biophys.* **2011**, *44*, 1–93. [CrossRef]
64. Lehninger, A.L.; Nelson, D.L.; Cox, M.M. *Overhead Transparency Set for Lehninger Principles of Biochemistry*, 4th ed.; Palgrave Mcmillan: London, UK, 2004; ISBN 071675956X.
65. Hai, Y.; Christianson, D.W. Histone Deacetylase 6 Structure and Molecular Basis of Catalysis and Inhibition. *Nat. Chem. Biol.* **2016**, *12*, 741–747. [CrossRef] [PubMed]
66. Lee, W.-S.; Ueno, A. A New Feature of Bifunctional Catalysis. Cyclodextrins Bearing Two Imidazole Moieties as Hydrolysis Enzyme Model. *Chem. Lett.* **2000**, *29*, 258–259. [CrossRef]
67. Brown, R.S.; Clewley, R.G. Intramolecular Imidazole-Promoted General-Base Catalysis of the Hydrolysis of an Acetylimidazole. *J. Org. Chem.* **1987**, *52*, 1216–1218. [CrossRef]
68. Orth, E.S.; Almeida, T.G.; Silva, V.B.; Oliveira, A.R.M.; Ocampos, F.M.M.; Barison, A. Mechanistic Insight on the Catalytic Detoxification of Paraoxon Mediated by Imidazole: Furnishing Optimum Scaffolds for Scavenging Organophosphorus Agents. *J. Mol. Catal. A Chem.* **2015**, *403*, 93–98. [CrossRef]
69. Campos, R.B.; Menezes, L.R.A.; Barison, A.; Tantillo, D.J.; Orth, E.S. The Importance of Methyl Positioning and Tautomeric Equilibria for Imidazole Nucleophilicity. *Eur. J. Chem.* **2016**, *22*, 15521–15528. [CrossRef]
70. Khabnadideh, S.; Rezaei, Z.; Khalafi-Nezhad, A.; Bahrinajafi, R.; Mohamadi, R.; Farrokhrooz, A.A. Synthesis of N-Alkylated Derivatives of Imidazole as Antibacterial Agents. *Bioorg. Med. Chem. Lett.* **2003**, *13*, 2863–2865. [CrossRef]
71. Kalaria, P.N.; Sataasia, S.P.; Avalani, J.R.; Raval, D.K. Ultrasound-Assisted One-Pot Four-Component Synthesis of Novel 2-Amino-3-Cyanopyridine Derivatives Bearing 5-Imidazopyrazole Scaffold and Their Biological Broadcast. *Eur. J. Med. Chem.* **2014**, *83*, 655–664. [CrossRef]
72. Moraski, G.C.; Thanassi, J.A.; Podos, S.D.; Pucci, M.J.; Miller, M.J. One-Step Syntheses of Nitrofuranyl Benzimidazoles That Are Active against Multidrug-Resistant Bacteria. *J. Antibiot.* **2011**, *64*, 667–671. [CrossRef]

73. Lu, B.; Lu, F.; Ran, L.; Yu, K.; Xiao, Y.; Li, Z.; Dai, F.; Wu, D.; Lan, G. Self-Assembly of Natural Protein and Imidazole Molecules on Gold Nanoparticles: Applications in Wound Healing against Multi-Drug Resistant Bacteria. *Int. J. Biol. Macromol.* **2018**, *119*, 505–516. [CrossRef]
74. Toja, E.; Selva, D.; Schiatti, P. 3-Alkyl-2-Aryl-3H-Naphth [1, 2-d] Imidazoles, a Novel Class of Nonacidic Antiinflammatory Agents. *J. Med. Chem.* **1984**, *27*, 610–616. [CrossRef]
75. Bender, P.E.; Hill, D.; Offen, P.H.; Razgaitis, K.; Lavanchy, P.; Stringer, O.D.; Sutton, B.M.; Griswold, D.E.; DiMartino, M. 5, 6-Diaryl-2, 3-Dihydroimidazo [2, 1-b] Thiazoles: A New Class of Immunoregulatory Antiinflammatory Agents. *J. Med. Chem.* **1985**, *28*, 1169–1177. [CrossRef]
76. de Gaetano, M.; Butler, E.; Gahan, K.; Zanetti, A.; Marai, M.; Chen, J.; Cacace, A.; Hams, E.; Maingot, C.; McLoughlin, A. Asymmetric Synthesis and Biological Evaluation of Imidazole-and Oxazole-Containing Synthetic Lipoxin A4 Mimetics (SLXms). *Eur. J. Med. Chem.* **2019**, *162*, 80–108. [CrossRef]
77. Koh, A.; Molinaro, A.; Ståhlman, M.; Khan, M.T.; Schmidt, C.; Mannerås-Holm, L.; Wu, H.; Carreras, A.; Jeong, H.; Olofsson, L.E. Microbially Produced Imidazole Propionate Impairs Insulin Signaling through MTORC1. *Cell* **2018**, *175*, 947–961. [CrossRef]
78. Adeyemi, O.S.; Eseola, A.O.; Plass, W.; Atolani, O.; Sugi, T.; Han, Y.; Batiha, G.E.; Kato, K.; Awakan, O.J.; Olaolu, T.D. Imidazole Derivatives as Antiparasitic Agents and Use of Molecular Modeling to Investigate the Structure–Activity Relationship. *Parasitol. Res.* **2020**, *119*, 1925–1941. [CrossRef]
79. Gupta, P.; Hameed, S.; Jain, R. Ring-Substituted Imidazoles as a New Class of Anti-Tuberculosis Agents. *Eur. J. Med. Chem.* **2004**, *39*, 805–814. [CrossRef]
80. Jeanmart, S.; Gagnepain, J.; Maity, P.; Lamberth, C.; Cederbaum, F.; Rajan, R.; Jacob, O.; Blum, M.; Bieri, S. Synthesis and Fungicidal Activity of Novel Imidazole-Based Ketene Dithioacetals. *Bioorg. Med. Chem.* **2018**, *26*, 2009–2016. [CrossRef]
81. B’bhatt, H.; Sharma, S. Synthesis, Characterization, and Biological Evaluation of Some Tri-Substituted Imidazole/Thiazole Derivatives. *J. Heterocycl. Chem.* **2015**, *52*, 1126–1131. [CrossRef]
82. Park, N. -H.; Shin, K.-H.; Kang, M.K. 34—Antifungal and Antiviral Agents. *Pharmacol. Ther.* **2017**, *10*, 488–503.
83. Hu, D.-C.; Chen, L.-W.; Yang, Y.-X.; Liu, J.-C. Syntheses, Structures and Antioxidant Activities of Two New Cu (II) Complexes with a Benzimidazole Schiff Base Ligand. *Inorg. Nano-Met. Chem.* **2017**. (just accepted). [CrossRef]
84. Keppler, B.K.; Wehe, D.; Endres, H.; Rupp, W. Synthesis, Antitumor Activity, and x-Ray Structure of Bis (Imidazolium)(Imidazole) Pentachlororuthenate (III),(ImH) 2 (RuImCl5). *Inorg. Chem.* **1987**, *26*, 844–846. [CrossRef]
85. Antonini, I.; Claudi, F.; Cristalli, G.; Franchetti, P.; Grifantini, M.; Martelli, S. Heterocyclic Quinones with Potential Antitumor Activity. 2. Synthesis and Antitumor Activity of Some Benzimidazole-4, 7-Dione Derivatives. *J. Med. Chem.* **1988**, *31*, 260–264. [CrossRef] [PubMed]
86. Inoue, T.; Shimozato, O.; Matsuo, N.; Mori, Y.; Shinozaki, Y.; Lin, J.; Watanabe, T.; Takatori, A.; Koshikawa, N.; Ozaki, T. Hydrophobic Structure of Hairpin Ten-Ring Pyrrole–Imidazole Polyamides Enhances Tumor Tissue Accumulation/Retention in Vivo. *Bioorg. Med. Chem.* **2018**, *26*, 2337–2344. [CrossRef] [PubMed]
87. Shalmali, N.; Ali, M.R.; Bawa, S. Imidazole: An Essential Edifice for the Identification of New Lead Compounds and Drug Development. *Mini Rev. Med. Chem.* **2017**, *18*. [CrossRef] [PubMed]
88. Kondaparla, S.; Manhas, A.; Dola, V.R.; Srivastava, K.; Puri, S.K.; Katti, S.B. Design, Synthesis and Antiplasmodial Activity of Novel Imidazole Derivatives Based on 7-Chloro-4-Aminoquinoline. *Bioorg. Chem.* **2018**, *80*, 204–211. [CrossRef] [PubMed]
89. James, D.A.; Koya, K.; Li, H.; Chen, S.; Xia, Z.; Ying, W.; Wu, Y.; Sun, L. Conjugated Indole-Imidazole Derivatives Displaying Cytotoxicity against Multidrug Resistant Cancer Cell Lines. *Bioorg. Med. Chem. Lett.* **2006**, *16*, 5164–5168. [CrossRef]
90. Özkay, Y.; Işıkdag, İ.; Incesu, Z.; Akalin, G. Synthesis of 2-Substituted-N-[4-(1-Methyl-4, 5-Diphenyl-1H-Imidazole-2-Yl) Phenyl] Acetamide Derivatives and Evaluation of Their Anticancer Activity. *Eur. J. Med. Chem.* **2010**, *45*, 3320–3328. [CrossRef]
91. Bellina, F.; Guazzelli, N.; Lessi, M.; Manzini, C. Imidazole Analogues of Resveratrol: Synthesis and Cancer Cell Growth Evaluation. *Tetrahedron* **2015**, *71*, 2298–2305. [CrossRef]
92. Seo, H.J.; Park, E.-J.; Kim, M.J.; Kang, S.Y.; Lee, S.H.; Kim, H.J.; Lee, K.N.; Jung, M.E.; Lee, M.; Kim, M.-S. Design and Synthesis of Novel Arylpiperazine Derivatives Containing the Imidazole Core Targeting 5-HT_{2A} Receptor and 5-HT Transporter. *J. Med. Chem.* **2011**, *54*, 6305–6318. [CrossRef]
93. Panarese, V.; Moshirfar, M. Pilocarpine. In *StatPearls*; StatPearls Publishing: Tampa, FL, USA, 2021.
94. Hwang, J.; Kim, D.; Park, J.S.; Park, H.J.; Shin, J.; Lee, S.K. Photoprotective Activity of Topsentin, A Bis (Indole) Alkaloid from the Marine Sponge Spongosorites Genitrix, by Regulation of COX-2 and Mir-4485 Expression in UVB-Irradiated Human Keratinocyte Cells. *Mar. Drugs.* **2020**, *18*, 87. [CrossRef]
95. Gibbons, J.B.; Salvant, J.M.; Vaden, R.M.; Kwon, K.-H.; Welm, B.E.; Looper, R.E. Synthesis of Naamidine A and Selective Access to N2-Acyl-2-Aminoimidazole Analogues. *J. Org. Chem.* **2015**, *80*, 10076–10085. [CrossRef]
96. Maeda, K. A New Antibiotic, Azomycin. *J. Antibiot.* **1953**, *6*, 182.
97. Al-Badr, A.A.; Alodhaib, M.M. Dacarbazine. *Profiles Drug Subst. Excip. Relat. Methodol.* **2016**, *41*, 323–377. [CrossRef]
98. Hempel, A.; Camerman, N.; Camerman, A.; Mastropaolo, D. Nafimidone Monohydrate: An Imidazole Anticonvulsant. *Acta Crystallogr. Sect. E Struct. Rep.* **2005**, *61*, 1387–1389. [CrossRef]
99. McIlhenny, H.M.; Bettis, J.W.; Wiseman, E.H. Flumizole, a New Nonsteroidal Anti-inflammatory Agent. *J. Pharm. Sci.* **1975**, *64*, 1469–1475. [CrossRef]
100. Finkelstein, W.; Isselbacher, K.J. Cimetidine. *N. Engl. J. Med.* **1978**, *299*, 992–996.

101. Goa, K.L.; Wagstaff, A.J. Losartan Potassium. *Drugs* **1996**, *51*, 820–845. [CrossRef]
102. Sohn, C.A. Evaluation of Ketoconazole. *Clin. Pharm.* **1982**, *1*, 217–224.
103. Petit, S.; Fruit, C.; Bischoff, L. New Family of Peptidomimetics Based on the Imidazole Motif. *Org. Lett.* **2010**, *12*, 4928–4931. [CrossRef]
104. Bräse, S. *Privileged Scaffolds in Medicinal Chemistry: Design, Synthesis, Evaluation*; Royal Society of Chemistry: London, UK, 2015; ISBN 1782622241.
105. Busby, R.W.; Cai, X.; Yang, S.; Ramos, L.; Venkatarangan, L.; Shen, H.; Wax, S.; Sadeque, A.J.M.; de Colle, C. Metopimazine Is Primarily Metabolized by a Liver Amidase in Humans. *Pharmacol. Res. Perspect.* **2022**, *10*, 00903. [CrossRef]
106. Heppner, D.E.; Günther, M.; Wittlinger, F.; Laufer, S.A.; Eck, M.J. Structural Basis for EGFR Mutant Inhibition by Trisubstituted Imidazole Inhibitors. *J. Med. Chem.* **2020**, *63*, 4293–4305. [CrossRef]
107. Günther, M.; Juchum, M.; Kelter, G.; Fiebig, H.; Laufer, S. Lung Cancer: EGFR Inhibitors with Low Nanomolar Activity against a Therapy-resistant L858R/T790M/C797S Mutant. *Angew. Chem. Int. Ed.* **2016**, *55*, 10890–10894. [CrossRef] [PubMed]
108. Lee, S.; Chung, C.Y.S.; Liu, P.; Craciun, L.; Nishikawa, Y.; Bruemmer, K.J.; Hamachi, I.; Saijo, K.; Miller, E.W.; Chang, C.J. Activity-Based Sensing with a Metal-Directed Acyl Imidazole Strategy Reveals Cell Type-Dependent Pools of Labile Brain Copper. *J. Am. Chem. Soc.* **2020**, *142*, 14993–15003. [CrossRef] [PubMed]
109. Hare, D.J.; New, E.J.; de Jonge, M.D.; McColl, G. Imaging Metals in Biology: Balancing Sensitivity, Selectivity and Spatial Resolution. *Chem. Soc. Rev.* **2015**, *44*, 5941–5958. [CrossRef] [PubMed]
110. Xiao, G.; Fan, Q.; Wang, X.; Zhou, B. Huntington Disease Arises from a Combinatory Toxicity of Polyglutamine and Copper Binding. *Proc. Natl. Acad. Sci. USA* **2013**, *110*, 14995–15000. [CrossRef]
111. Fox, J.H.; Kama, J.A.; Lieberman, G.; Chopra, R.; Dorsey, K.; Chopra, V.; Volitakis, I.; Cherny, R.A.; Bush, A.I.; Hersch, S. Mechanisms of Copper Ion Mediated Huntington’s Disease Progression. *PLoS ONE* **2007**, *2*, e334. [CrossRef] [PubMed]
112. Desai, V.; Kaler, S.G. Role of Copper in Human Neurological Disorders. *Am. J. Clin. Nutr.* **2008**, *88*, 855S–858S. [CrossRef]
113. Savelieff, M.G.; Nam, G.; Kang, J.; Lee, H.J.; Lee, M.; Lim, M.H. Development of Multifunctional Molecules as Potential Therapeutic Candidates for Alzheimer’s Disease, Parkinson’s Disease, and Amyotrophic Lateral Sclerosis in the Last Decade. *Chem. Rev.* **2019**, *119*, 1221–1322. [CrossRef]
114. Tong, L.; Pav, S.; White, D.M.; Rogers, S.; Crane, K.M.; Cywin, C.L.; Brown, M.L.; Pargellis, C.A. A Highly Specific Inhibitor of Human P38 MAP Kinase Binds in the ATP Pocket. *Nat. Struct. Biol.* **1997**, *4*, 311–316. [CrossRef]
115. Wang, Z.; Canagarajah, B.J.; Boehm, J.C.; Kassisà, S.; Cobb, M.H.; Young, P.R.; Abdel-Meguid, S.; Adams, J.L.; Goldsmith, E.J. Structural Basis of Inhibitor Selectivity in MAP Kinases. *Structure* **1998**, *6*, 1117–1128. [CrossRef]
116. Peifer, C.; Abadleh, M.; Bischof, J.; Hauser, D.; Schattel, V.; Hirner, H.; Knippschild, U.; Laufer, S. 3, 4-Diaryl-Isoxazoles and-Imidazoles as Potent Dual Inhibitors of P38 α Mitogen Activated Protein Kinase and Casein Kinase 1 δ . *J. Med. Chem.* **2009**, *52*, 7618–7630. [CrossRef]
117. Takle, A.K.; Brown, M.J.B.; Davies, S.; Dean, D.K.; Francis, G.; Gaiba, A.; Hird, A.W.; King, F.D.; Lovell, P.J.; Naylor, A. The Identification of Potent and Selective Imidazole-Based Inhibitors of B-Raf Kinase. *Bioorg. Med. Chem. Lett.* **2006**, *16*, 378–381. [CrossRef]
118. Niculescu-Duvaz, D.; Niculescu-Duvaz, I.; Suijkerbuijk, B.M.J.M.; Ménard, D.; Zambon, A.; Nourry, A.; Davies, L.; Manne, H.A.; Friedlos, F.; Ogilvie, L. Novel Tricyclic Pyrazole BRAF Inhibitors with Imidazole or Furan Central Scaffolds. *Bioorg. Med. Chem.* **2010**, *18*, 6934–6952. [CrossRef]
119. Niculescu-Duvaz, D.; Niculescu-Duvaz, I.; Suijkerbuijk, B.M.J.M.; Ménard, D.; Zambon, A.; Davies, L.; Pons, J.-F.; Whittaker, S.; Marais, R.; Springer, C.J. Potent BRAF Kinase Inhibitors Based on 2, 4, 5-Trisubstituted Imidazole with Naphthyl and Benzothio-phenone 4-Substituents. *Bioorg. Med. Chem.* **2013**, *21*, 1284–1304. [CrossRef]
120. Ali, E.M.H.; El-Telbany, R.F.A.; Abdel-Maksoud, M.S.; Ammar, U.M.; Mersal, K.I.; Zarai, S.-O.; El-Gamal, M.I.; Choi, S.-I.; Lee, K.-T.; Kim, H.-K. Design, Synthesis, Biological Evaluation, and Docking Studies of Novel (Imidazol-5-Yl) Pyrimidine-Based Derivatives as Dual BRAFV600E/P38 α Inhibitors. *Eur. J. Med. Chem.* **2021**, *215*, 113277. [CrossRef]
121. Youssif, B.G.M.; Gouda, A.M.; Moustafa, A.H.; Abdelhamid, A.A.; Gomaa, H.A.M.; Kamal, I.; Marzouk, A.A. Design and Synthesis of New Triarylimidazole Derivatives as Dual Inhibitors of BRAFV600E/P38 α with Potential Antiproliferative Activity. *J. Mol. Struct.* **2022**, *1253*, 132218. [CrossRef]
122. Akdis, C.A.; Simons, F.E.R. Histamine Receptors Are Hot in Immunopharmacology. *Eur. J. Pharmacol.* **2006**, *533*, 69–76. [CrossRef]
123. Thangam, E.B.; Jemima, E.A.; Singh, H.; Baig, M.S.; Khan, M.; Mathias, C.B.; Church, M.K.; Saluja, R. The Role of Histamine and Histamine Receptors in Mast Cell-Mediated Allergy and Inflammation: The Hunt for New Therapeutic Targets. *Front. Immunol.* **2018**, *9*, 1873. [CrossRef]
124. Hill, S.J.; Ganellin, C.R.; Timmerman, H.; Schwartz, J.C.; Shankley, N.P.; Young, J.M.; Schunack, W.; Levi, R.; Haas, H.L. International Union of Pharmacology. XIII. Classification of Histamine Receptors. *Pharmacol. Rev.* **1997**, *49*, 253–278.
125. Durant, G.J.; Ganellin, C.R.; Parsons, M.E. Chemical Differentiation of Histamine H1- and H2-Receptor Agonists. *J. Med. Chem.* **1975**, *18*, 905–909. [CrossRef]
126. Reggio, P.; Topiol, S.; Weinstein, H. Molecular Determinants for the Agonist Activity of 2-Methylhistamine and 4-Methylhistamine at H2-Receptors. *J. Med. Chem.* **1986**, *29*, 2412–2415. [CrossRef]
127. Ganellin, R. 1980 Award in medicinal chemistry. Medicinal chemistry and dynamic structure-activity analysis in the discovery of drugs acting at histamine H2 receptors. *J. Med. Chem.* **1981**, *24*, 913–920. [CrossRef] [PubMed]

128. Lima, L.M.; Barreiro, E.J. Bioisosterism: A Useful Strategy for Molecular Modification and Drug Design. *Curr. Med. Chem.* **2005**, *12*, 23–49. [CrossRef] [PubMed]
129. Barreiro, E.J.; Kümmerle, A.E.; Fraga, C.A.M. The Methylation Effect in Medicinal Chemistry. *Chem. Rev.* **2011**, *111*, 5215–5246. [CrossRef] [PubMed]
130. Prout, K.; Critchley, S.R.; Ganellin, C.R.; Mitchell, R.C. Crystal and Molecular Structure of the Histamine H₂-Receptor Antagonists, N-Methyl-N'-[2-[(5-Methylimidazol-4-Yl) Methylthio] Ethyl] Thiourea (Metiamide) and N-[2-[(Imidazol-4-Yl) Methylthio] Ethyl]-N'-Methylthiourea (Thiaborimamide). *J. Chem. Soc. Perkin. Trans. 2* **1977**, 68–75. [CrossRef]
131. Wermuth, C.G. *The Practice of Medicinal Chemistry*; Academic Press: Cambridge, MA, USA, 2011; ISBN 0080568777.
132. Patrick, G.L. *An Introduction to Medicinal Chemistry*; Oxford University Press: New York, NY, USA, 2013; ISBN 0199697396.
133. Brimblecombe, R.W.; Duncan, W.A.M.; Durant, G.J.; Emmett, J.C.; Ganellin, C.R.; Leslie, G.B.; Parsons, M.E. Characterization and Development of Cimetidine as a Histamine H₂-Receptor Antagonist. *Gastroenterology* **1978**, *74*, 339–347. [CrossRef]
134. Figueiredo, J.M.; de A Câmara, C.; Amarante, E.G.; Miranda, A.L.P.; Santos, F.M.; Rodrigues, C.R.; Fraga, C.A.M.; Barreiro, E.J. Design and Synthesis of Novel Potent Antinociceptive Agents: Methyl-Imidazolyl N-Acylhydrazone Derivatives. *Bioorg. Med. Chem.* **2000**, *8*, 2243–2248. [CrossRef]
135. Dewar, M.J.S.; Zoebisch, E.G.; Healy, E.F.; Stewart, J.J.P. Development and Use of Quantum Mechanical Molecular Models. 76. AM1: A New General Purpose Quantum Mechanical Molecular Model. *J. Am. Chem. Soc.* **1985**, *107*, 3902–3909. [CrossRef]

Disclaimer/Publisher's Note: The statements, opinions and data contained in all publications are solely those of the individual author(s) and contributor(s) and not of MDPI and/or the editor(s). MDPI and/or the editor(s) disclaim responsibility for any injury to people or property resulting from any ideas, methods, instructions or products referred to in the content.

Review

Azomethine Ylides—Versatile Synthons for Pyrrolidinyl-Heterocyclic Compounds

Siva S. Panda ^{1,*}, Marian N. Aziz ², Jacek Stawinski ^{3,4} and Adel S. Girgis ^{2,*}

¹ Department of Chemistry and Physics, Augusta University, Augusta, GA 30912, USA

² Department of Pesticide Chemistry, National Research Centre, Dokki, Giza 12622, Egypt

³ Institute of Bioorganic Chemistry, Polish Academy of Sciences, Noskowskiego 12/14, 61-704 Poznan, Poland

⁴ Department of Organic Chemistry, Arrhenius Laboratory, Stockholm University, S-106 91 Stockholm, Sweden

* Correspondence: sipanda@augusta.edu or sspanda12@gmail.com (S.S.P.);

girgisas10@yahoo.com or as.girgis@nrc.sci.eg (A.S.G.)

Abstract: Azomethine ylides are nitrogen-based three-atom components commonly used in [3+2]-cycloaddition reactions with various unsaturated 2π -electron components. These reactions are highly regio- and stereoselective and have attracted the attention of organic chemists with respect to the construction of diverse heterocycles potentially bearing four new contiguous stereogenic centers. This review article compiles the most important [3+2]-cycloaddition reactions of azomethine ylides with various olefinic, unsaturated 2π -electron components (acyclic, alicyclic, heterocyclic, and exocyclic ones) reported over the past two decades.

Keywords: cycloaddition; azomethine ylide; pyrrolidine; spiro-compound

Citation: Panda, S.S.; Aziz, M.N.; Stawinski, J.; Girgis, A.S. Azomethine Ylides—Versatile Synthons for Pyrrolidinyl-Heterocyclic Compounds. *Molecules* **2023**, *28*, 668. <https://doi.org/10.3390/molecules28020668>

Academic Editors: Alexey M. Starostnikov, Maxim A. Bastrakov and Igor L. Dalinger

Received: 8 December 2022

Revised: 3 January 2023

Accepted: 4 January 2023

Published: 9 January 2023



Copyright: © 2023 by the authors. Licensee MDPI, Basel, Switzerland. This article is an open access article distributed under the terms and conditions of the Creative Commons Attribution (CC BY) license (<https://creativecommons.org/licenses/by/4.0/>).

1. Introduction

The three-atom component (TAC) is an organic species that is represented by zwitterionic octet structures and undergoes [3+2]-cycloadditions with an unsaturated 2π -electron component in a one-step reaction, often in an asynchronous and symmetry-conductive fashion, via a thermal six-electron Hückel aromatic transition state. The formal charges are lost in the [3+2→5] cycloaddition (Figure 1) [1]. Recently, studies based on molecular electron density theory (MEDT) have suggested that the compounds involved in these reactions do not have a polar nature but a diradical, pseudoradical, or carbenoid nature. Therefore, the use of the term “1,3-dipole” is unjustified and should be replaced with “three-atom component”. It was also recommend that the designation of “dipolarophile” should be replaced with “unsaturated 2π -electron component”, and “1,3-dipolar cycloaddition” with “[3+2]-cycloaddition” [2].

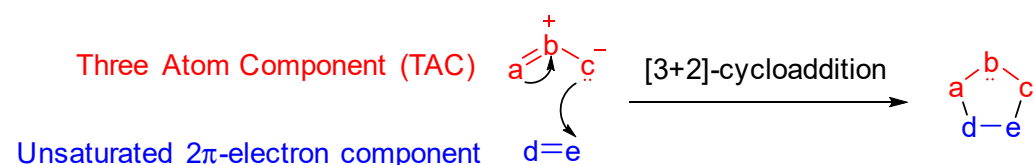


Figure 1. Historical Huisgen’s view on the [3+2]-cycloaddition reaction.

While there is a mechanistic spectrum of this reaction from a synchronous one-step process to a stepwise overall transformation (including radical pathways), to avoid mechanistic digressions that may not have chemical or stereochemical consequences, in this synthetic review article, we will refer to the azomethine ylide reaction as a pericyclic cycloaddition. [3+2]-Cycloadditions of azomethine ylide with homomultiple and heteromultiple unsaturated 2π -electron components have been extensively used to produce a wide range of

heterocycles [3]. There are several methods for the formation of azomethine ylides, including the thermolysis or photolysis of readily prepared aziridines, the dehydrohalogenation of immonium salts, and proton abstraction from imine derivatives of α -amino acids [3]. They are often generated in situ because of their high reactivity and/or transient existence; however, in some cases, stabilized ylides have been isolated and used further [4–6].

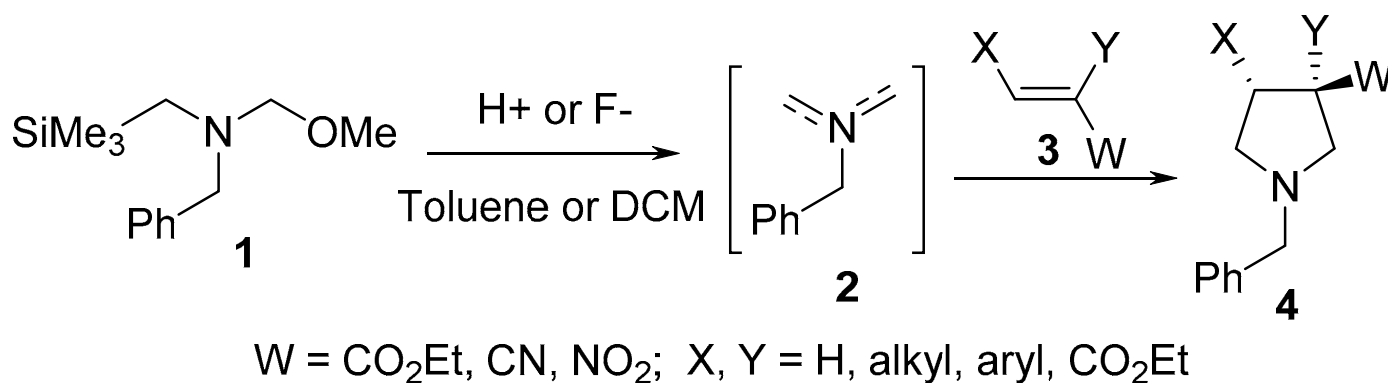
The synthesis of five-membered heterocyclic systems through azomethine ylides is one of the most adopted, efficient, and powerful approaches. Since the first report of successful the enantioselective [3+2]-cycloaddition of an azomethine ylide in 1991 [7], there has been tremendous progress in the chemistry regarding azomethine ylides. Azomethine ylides are extensively used in the synthesis of various heterocyclic systems such as pyrrolidines, pyrrolizidines, indolizidines, piperidines, oxazolidines, spiroindoles, spiropyrrolidines, and spiropiperidines, but they are also used for the total synthesis of complex natural products as well as bioactive compounds [8–15]. In recent years, the [3+2]-cycloaddition reaction has been extensively studied for the synthesis of heterocycles using different synthetic strategies [16,17]. In addition, the reaction is also investigated to understand the related reactivity, reaction conditions, intermediates, etc. [18,19].

This review article deals with the [3+2]-cycloaddition reaction of azomethine ylides with an unsaturated carbon–carbon bond (in either acyclic, alicyclic, heterocyclic, or exocyclic systems) that leads to the formation of pyrrolidinyl-containing analogs reported in the last two decades and their biological applications. This review article is intended to be a critical resource for the researchers involved or interested in azomethine ylides-mediated heterocyclic synthesis. It is also hoped that this review article will inspire chemists in this area of research.

2. Acyclic Unsaturated 2π -Electron Components

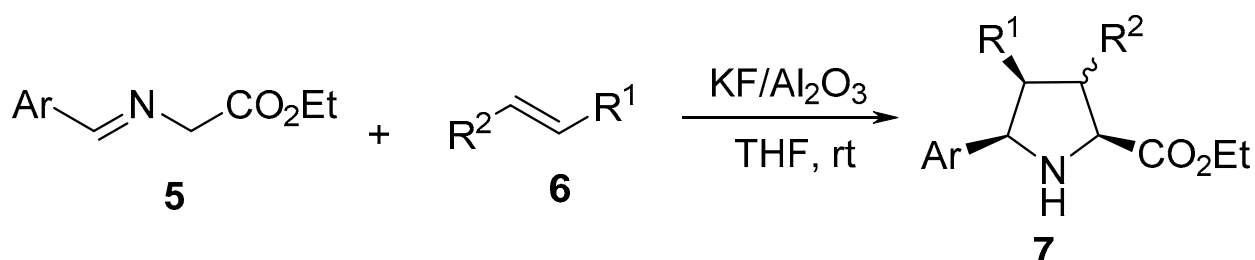
2.1. Intermolecular Cycloaddition Reaction of Azomethine Ylides to Acyclic Unsaturated 2π -Electron Components (Alkenes)

Unstabilized azomethine ylide **2** derived from benzyl(methoxymethyl)(trimethylsilylmethyl) amine **1** undergoes a [3+2]-cycloaddition reaction with electron-deficient alkenes **3** under continuous flow conditions in the presence of catalytic trifluoroacetic acid, thereby affording the corresponding pyrrolidines **4** (Scheme 1) [20].



Scheme 1. Synthesis of pyrrolidines **4**.

Azomethine ylides generated via the deprotonation of α -imino-esters **5** undergo a [3+2]-cycloaddition reaction with unsaturated 2π -electron components **6** in the presence of the eco-friendly supported solid-base catalyst KF/Al₂O₃ to yield the corresponding pyrrolidines **7** with high regio- and diastereoselectivity (Scheme 2) [21].

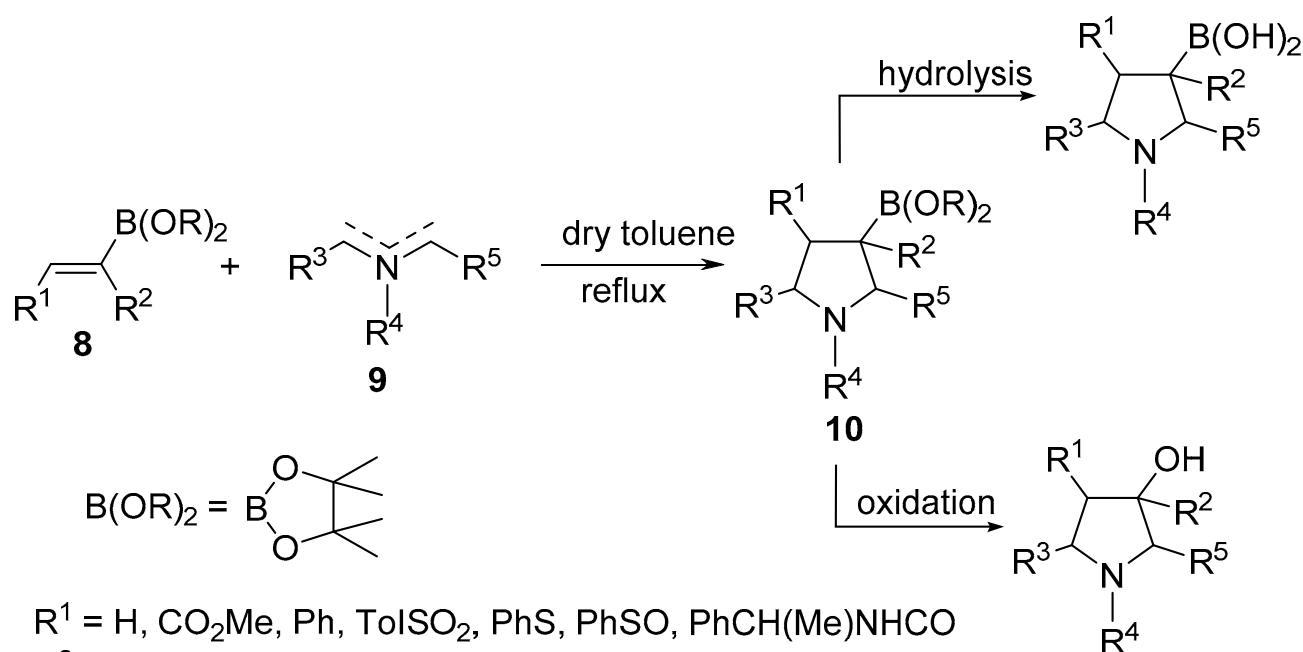


Ar = Ph, 4-ClC₆H₄, 4-MeC₆H₄, 4-MeOC₆H₄, 4-NO₂C₆H₄

R¹/R² = CO₂Me/H, CN/H, COCH₃/H, Ph/CO₂Et, CO₂Me, N-phenylmaleimide

Scheme 2. Synthesis of pyrrolidines 7.

Belfaitah et al. reported the cycloaddition reaction of azomethine ylides 9 with alkenyl boronates 8 to obtain the 3-boronic-ester-substituted pyrrolidines 10 (Scheme 3) [22].



R¹ = H, CO₂Me, Ph, TolSO₂, PhS, PhSO, PhCH(Me)NHCO

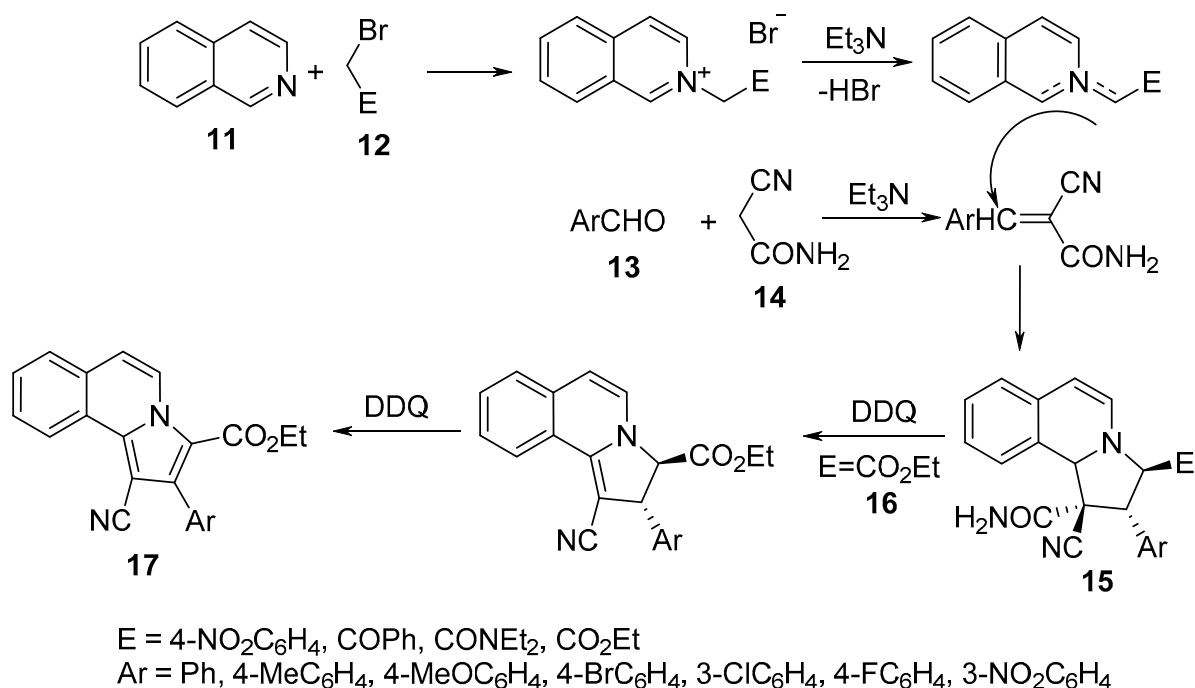
R² = H, Me

R³/R⁴ = H/Me, H/PhCH₂, (CH₂)₃

R⁵ = H, CO₂Me

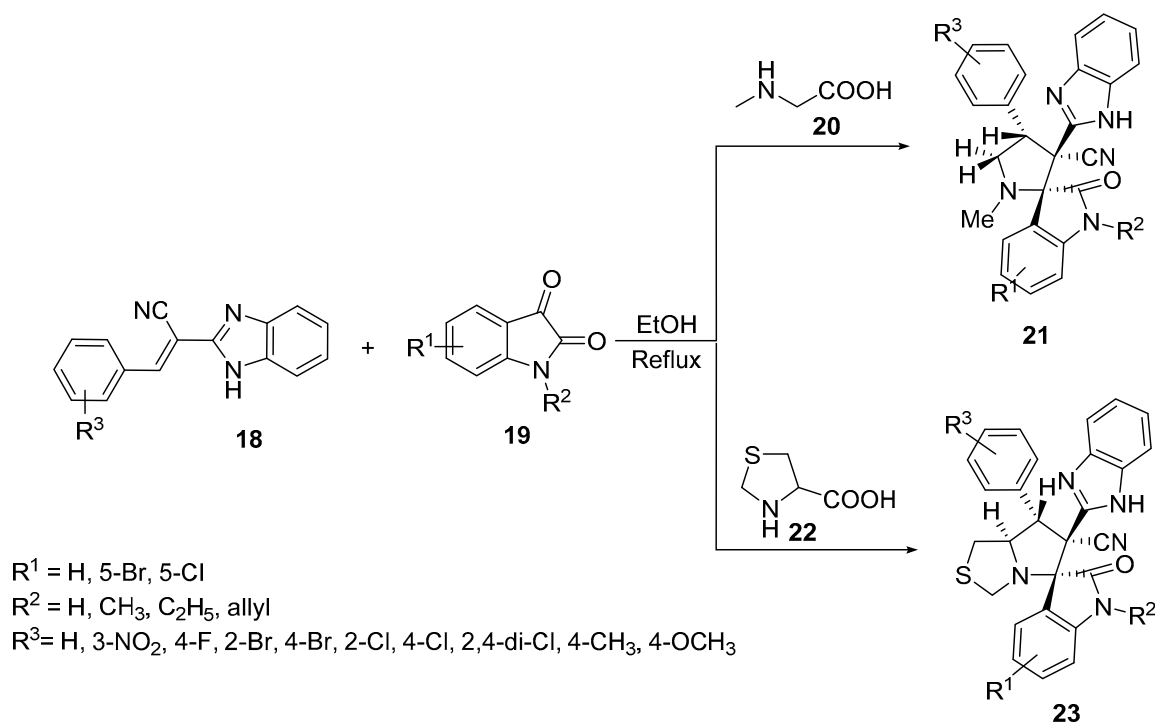
Scheme 3. Synthesis of 3-boronate pyrrolidines 10.

Pyrrolo[2,1-*a*]isoquinolines 15 were obtained through a sequential one-pot, two-step tandem reaction of isoquinoline 11, α -halogenated methylenes 12, aromatic aldehydes 13, and cyanoacetamide 14 in the presence of triethylamine as a basic catalyst and 2,4-dichloro-5,6-dicyano-1,4-benzoquinone (DDQ) as an oxidizing agent. The transformation was assumed to take place through [3+2]-cycloaddition of *N*-substituted carbonylmethyleneisoquinolinium bromide (formed via the reaction of isoquinoline 11 and 12) with arylidene cyanoacetamide (formed via the condensation of cyanoacetamide 14 with aromatic aldehyde 13) [23]. In the case of the ethyl bromoacetate 16 derivative, the formation of pyrrolo[2,1-*a*]isoquinolines 17 was observed probably due to DDQ oxidation (Scheme 4) [23].



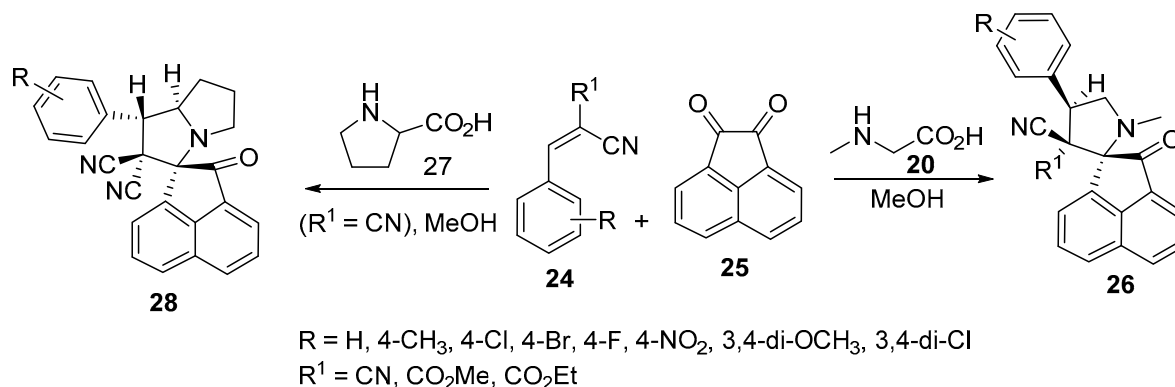
Scheme 4. Synthesis of pyrrolo[2,1-*a*]isoquinolines 15/17.

Spiro[indoline-3,2'-pyrrolidines] **21** were prepared by the [3+2]-cycloaddition reaction of benzoimidazol-2-yl-3-phenylacrylonitriles **18** with azomethine ylides, which was generated in situ from the condensation of isatin **19** and sarcosine **20** in refluxing ethanol. Similarly, spiro[indoline-3,5'-pyrrolo[1,2-*c*]thiazoles] **23** were formed by using thioproline **22** as a secondary amino acid (Scheme 5) [24].



Scheme 5. Synthesis of spiro[indoline-3,2'-pyrrolidines] **21** and spiro[indoline-3,5'-pyrrolo[1,2-*c*]thiazoles] **23**.

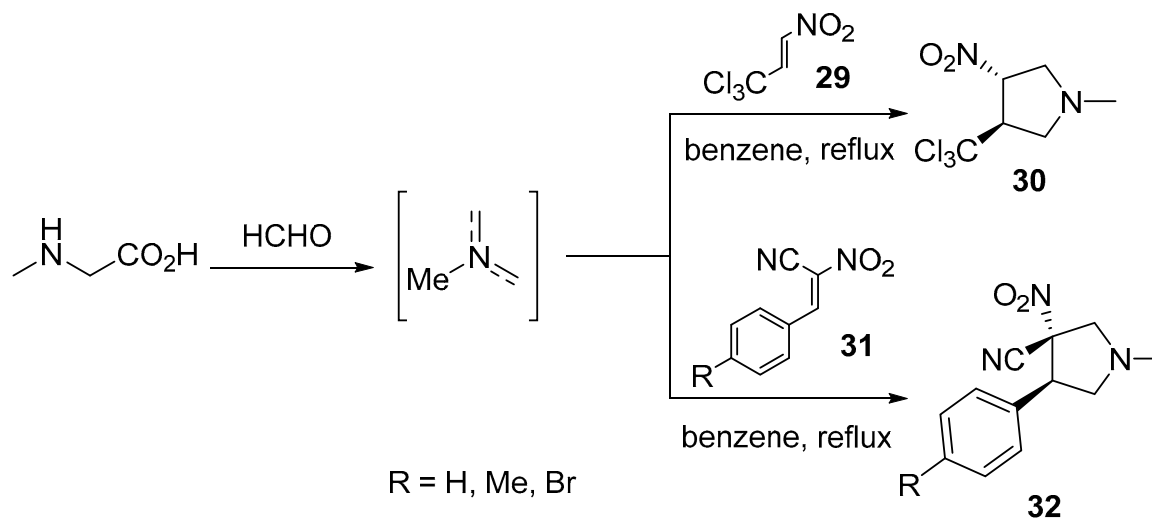
The chemistry was extended further to obtain spiro[acenaphthylene-1,2'-pyrrolidines] **26** and spiro[acenaphthylene-1,2'-pyrrolizidines] **28** possessing a cyano group from the azomethine ylides (generated from acenaphthenequinone **25**) with α -amino acids (sarcosine **20** and proline **27**) and Knoevenagel adducts **24** (Scheme 6) [25].



Scheme 6. Synthesis of spiro[acenaphthylene-1,2'-pyrrolidines] **26** and spiro[acenaphthylene-1,2'-pyrrolizidines] **28**.

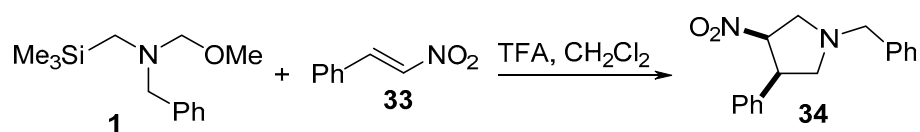
2.2. Nitroalkenes

Nitroalkenes are reactive, unsaturated 2π -electron components that are intensively used in cycloaddition reactions by various researchers [26]. 3-Nitro-4-(trichloromethyl)pyrrolidine **30** was obtained through the cycloaddition of *trans*-3,3,3-trichloro-1-nitroprop-1-ene **29** with azomethine ylide (obtained from the condensation of paraformaldehyde and sarcosine in refluxing benzene). Quantum chemical calculations (DFT, M062X/6-311G(d)) explained the reaction pathway [27]. Analogously, 3-nitro-4-arylpyrrolidine-3-carbonitriles **32** were obtained through the cycloaddition of the azomethine ylide with (*E*)-3-phenyl-2-nitroprop-2-enenitriles **31** [28] (Scheme 7).



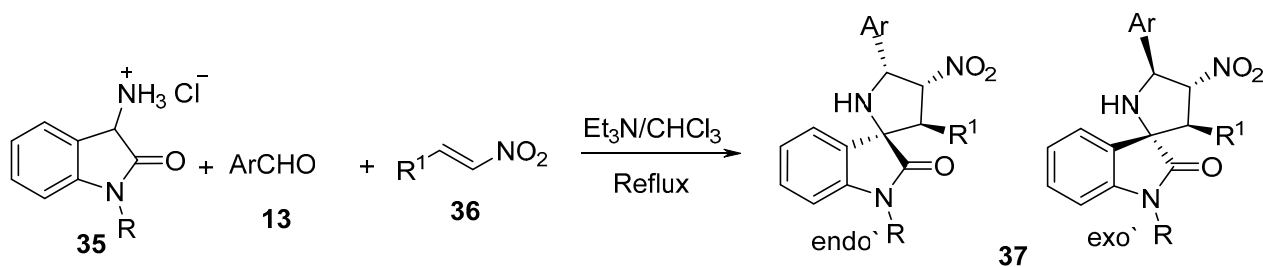
Scheme 7. Synthesis of 3-nitro-4-(trichloromethyl)pyrrolidine **30** and 3-nitro-4-arylpyrrolidine-3-carbonitriles **32**.

Trans-3-nitropyrrolidine **34** was prepared by reacting *trans*-1-nitro-2-phenylethylene **33** with *N*-(methoxymethyl)-*N*-[(trimethylsilyl)methyl]benzylamine **1**, which is an azomethine ylide equivalent, in the presence of trifluoroacetic acid in dichloromethane. Some of the synthesized **34** revealed promising inhibitory properties as Na^+ channel blockers, which are useful in the treatment of ischemic stroke (Scheme 8) [29].



Scheme 8. Synthesis of *trans*-3-nitropyrrolidine **34**.

Another set of spiro compounds, spiro[pyrrolidine-2,3'-oxindoles] **37**, were regioselectively synthesized by a multicomponent reaction of azomethine ylides, generated in situ from 3-aminoindoline-2-ones hydrochloride **35**, with aldehydes **13** and (*E*)-nitroalkenes **36** (Scheme 9) [30].

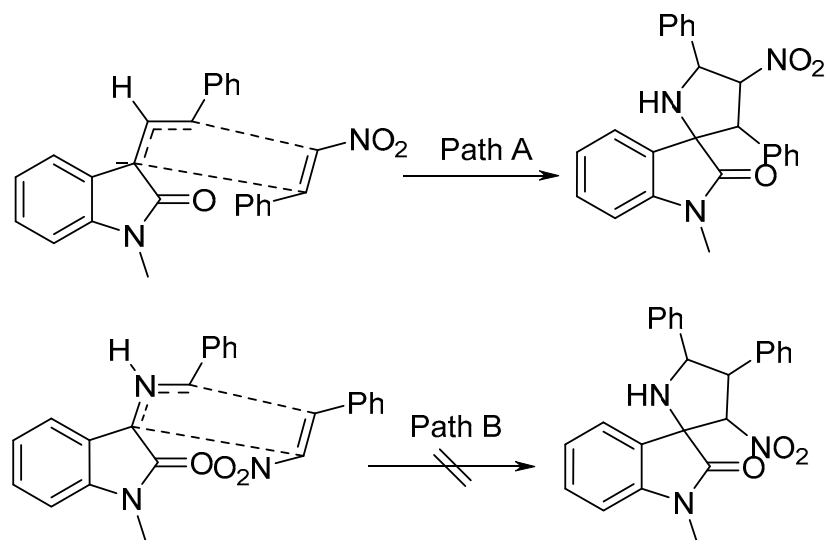


R = H, Me, Bn; Ar = Ph, 2-FC₆H₄, 3-FC₆H₄, 4-FC₆H₄, 4-ClC₆H₄, 4-MeC₆H₄, 4-MeOC₆H₄, 3-F₃CC₆H₄, 1-naphthyl, 2-thienyl, CH₃(CH₂)₂, cyclohexyl;

R¹ = Ph, 2-FC₆H₄, 3-FC₆H₄, 4-FC₆H₄, 3-ClC₆H₄, 4-MeC₆H₄, 4-MeOC₆H₄, 3-F₃CC₆H₄, 2-naphthyl, 2-thienyl

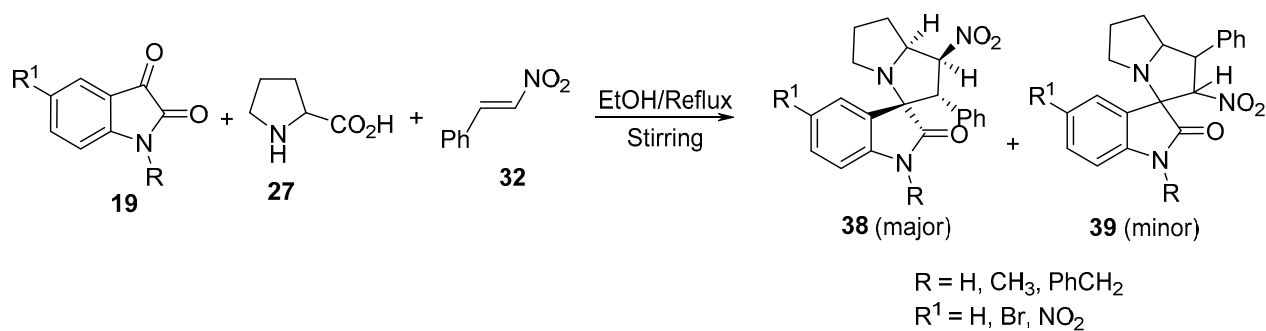
Scheme 9. Synthesis of spiro[pyrrolidin-2,3'-oxindoles] **37**.

It was assumed that, based on the secondary orbital interaction (SOI) of the electron-poor nitroalkenes **36** with the azomethine ylide, Path A was exclusively followed, as the *endo*-transition state in the reaction sequence was more energetically favorable (Scheme 10) [30].



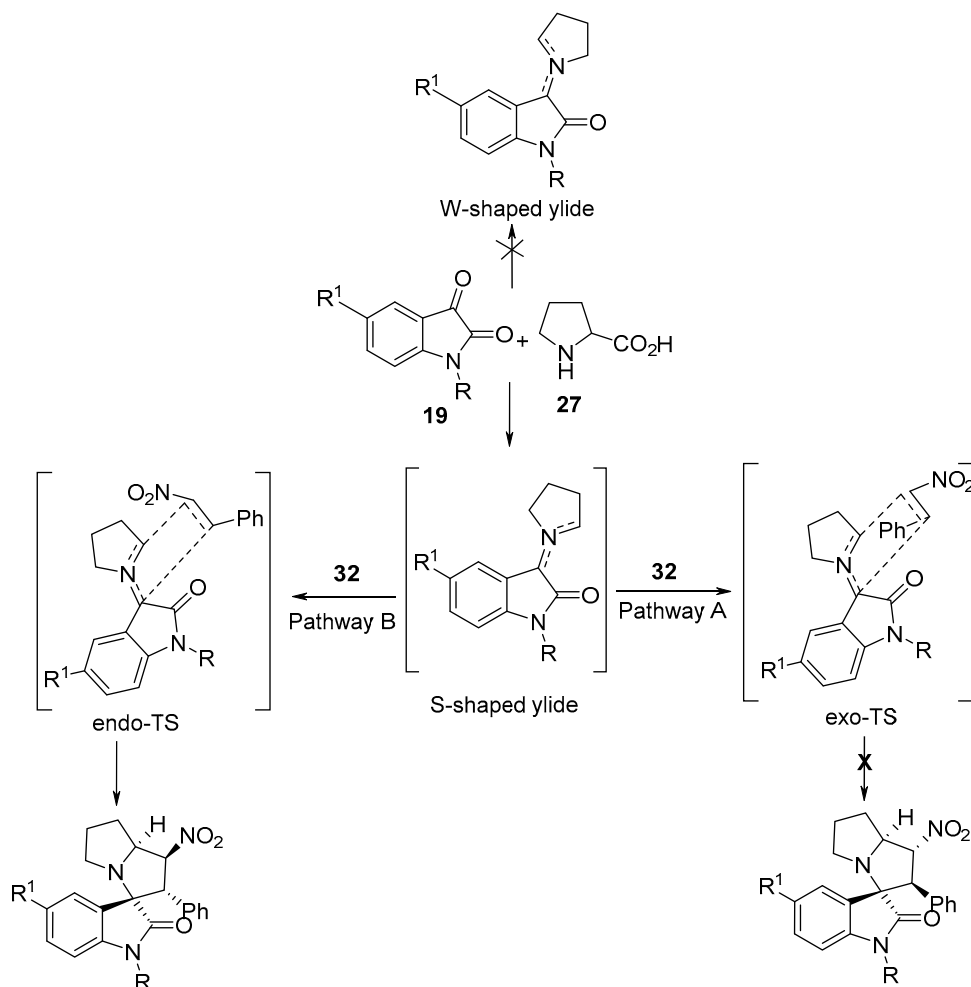
Scheme 10. Proposed mechanism for the cycloaddition of azomethine ylide (via *endo*'-transition state).

Spirooxindolo-nitropyrrolizines **38** (major product) and **39** (minor product) were obtained from the cycloaddition reaction of azomethine ylides, generated in situ from isatin **19**, with proline **27** and (*E*)- β -nitrostyrene **32** (Scheme 11) [31]. A significant inversion in the regioselectivity was observed when the polar [3+2]-cycloaddition of the azomethine ylides was attempted with *trans*- β -nitrostyrene instead of (*E*)-1-phenyl-2-nitropropene.



Scheme 11. Synthesis of spirooxindolo-nitropyrrolizines **38** and **39**.

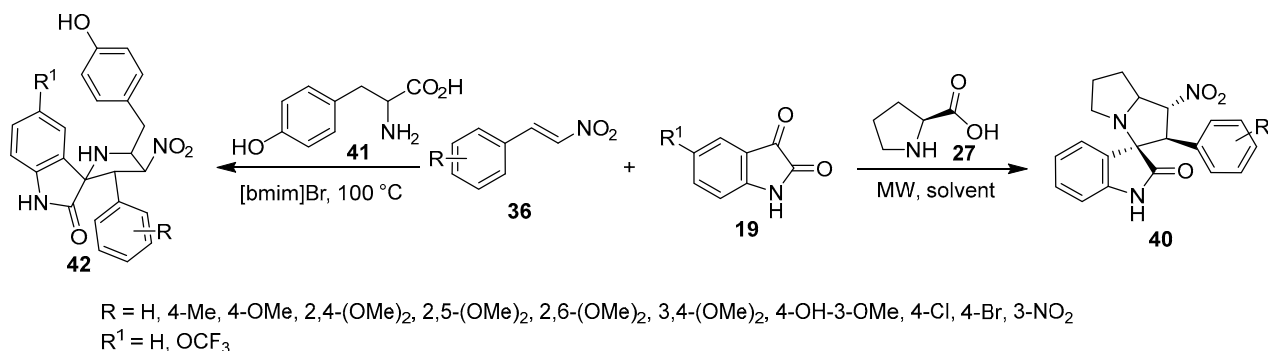
It was assumed that the reaction proceeds through *S*-shaped ylide with a cycloaddition via the endo-transition state (pathway B), yielding cycloadducts **38**, and not the exo-transition state (pathway A). Computational studies (Gaussian 03) of the transition states (Density Functional Theory (DFT), B3LYP, and 6-31G(d,p) basis set) confirmed these assumptions (Scheme 12) [31].



Scheme 12. Proposed mechanism for the cycloaddition of the azomethine ylides with nitrostyrene.

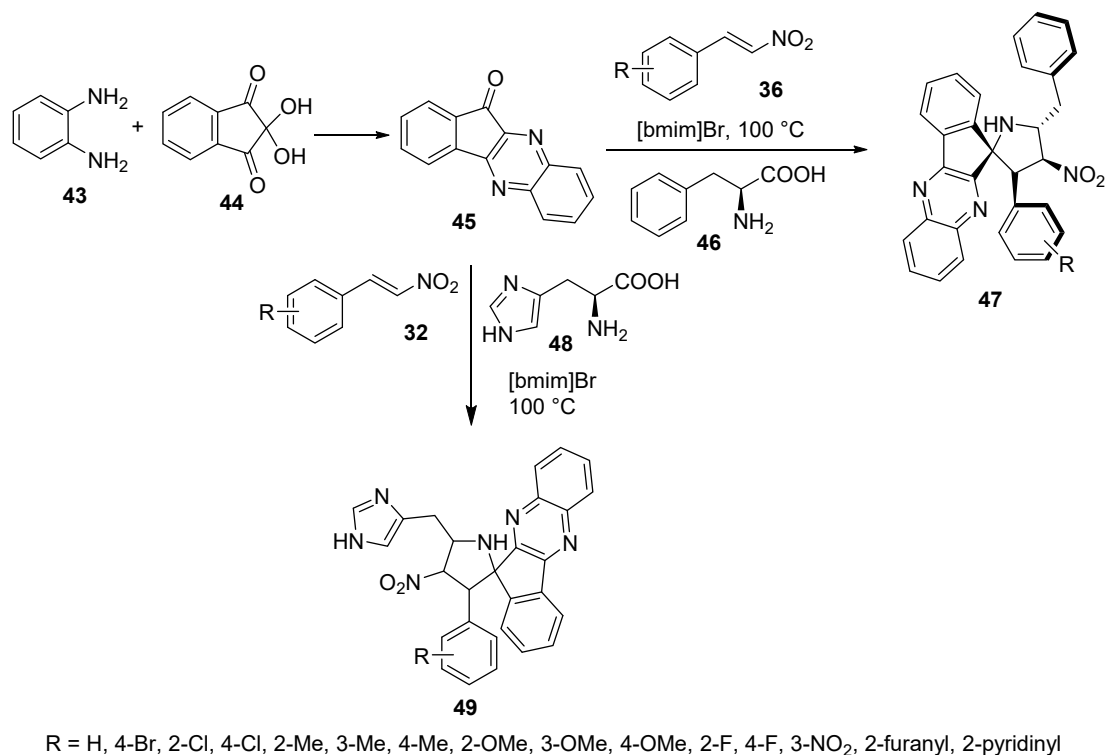
A series of spiro[indoline-3,3'-pyrrolizin]-2-ones **40** with potential anti-amyloidogenic properties useful against Alzheimer's disease were obtained by the microwave-assisted cycloaddition of nitroalkenes **36** and azomethine ylides (generated from isatin **19** and *L*-proline **27**) [32]. Analogously, spirooxindole-pyrrolidines **42** were obtained by the reaction of tyrosine **41** in an ionic liquid [bmim]Br at 100 °C. Promising antiproliferation

properties were observed for some of the synthesized compounds (**42**) against human A549 (adenocarcinoma basal epithelial) and Jurkat (*T*-cell lymphoma) cell lines (MTT assay) using Camptothecin as a positive control; the compounds exhibited a safe response against the non-cancer cell lines MCF-10 (normal breast) and PCS-130-010 (lung smooth muscle). Caspase-dependent apoptosis (especially caspase-3) was mentioned as the mode of action for the observed antiproliferative activity (Scheme 13) [33].



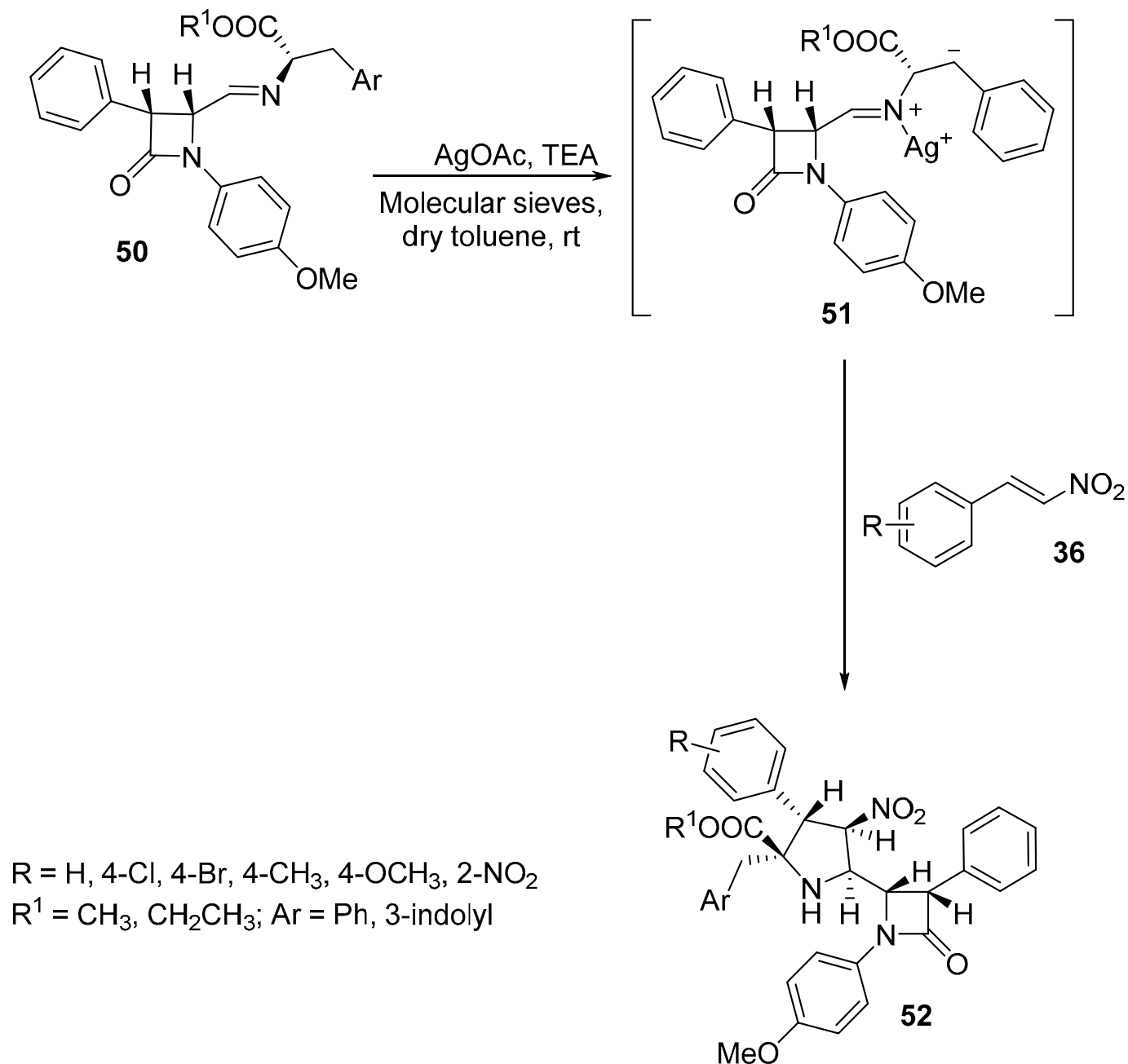
Scheme 13. Synthesis of spiro-indolines **40**, **42**.

Ionic liquid chemistry was utilized to prepare 4'-nitrospiro[indeno[1,2-*b*]quinoxaline-11,2'-pyrrolidines] **47** by the cycloaddition reaction of nitroalkenes **36** with azomethine ylide (generated from indenoquinoxalinone **45** and *L*-phenylalanine **46**) in an ionic liquid [bmim]Br. Some of the synthesized agents revealed antimycobacterial properties (*Mycobacterium tuberculosis* H37Rv) with an efficacy comparable to that of ethambutol (reference standard) [34]. Similarly, spiro compounds **49** were obtained by using *L*-histidine **48** instead of *L*-phenylalanine **46** in this reaction. Some of the synthesized compounds revealed cholinesterase (acetylcholinesterase and butyrylcholinesterase)-inhibitory properties with considerable efficiencies relative to Galantamine (Scheme 14) [35].



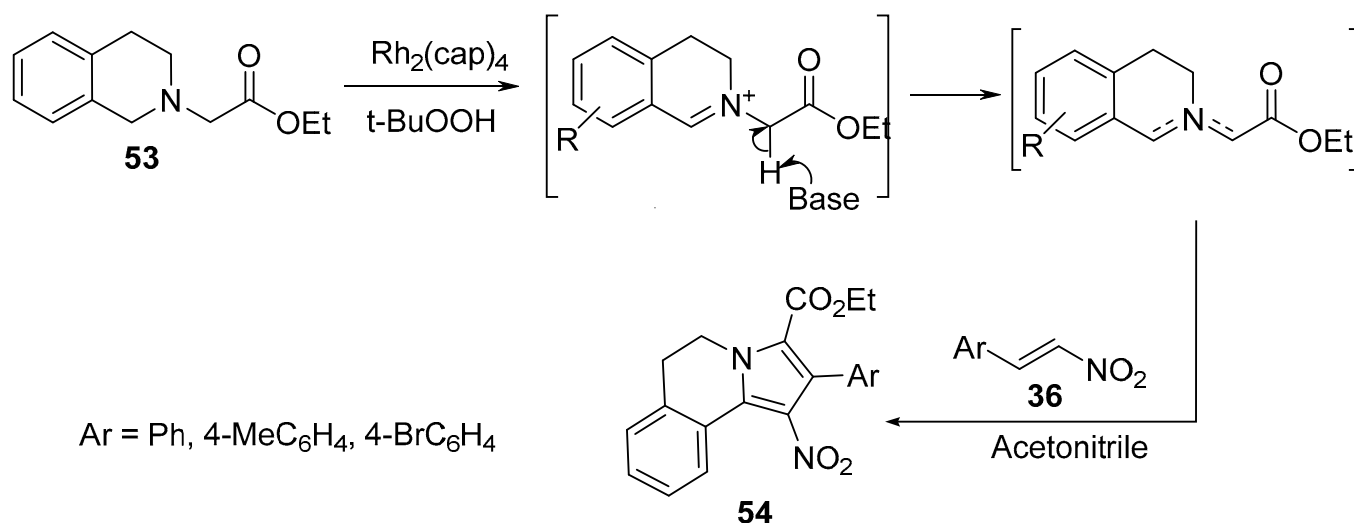
Scheme 14. Synthesis of 4'-nitrospiro[indeno[1,2-*b*]quinoxaline-11,2'-pyrrolidines] **47**, **49**.

Pyrrolidinyll β -lactams **52** were prepared as single diastereomers by the reaction of azomethine ylides **51**, generated from β -lactam imines of α -amino ester **50**, with nitrostyrenes **36** in the presence of silver acetate and triethylamine (Scheme 15). This reaction is an example of [3+2]-cycloaddition reaction via *N*-metallo azomethine ylide [36].



Scheme 15. Synthesis of pyrrolidinyll β -lactams **52**.

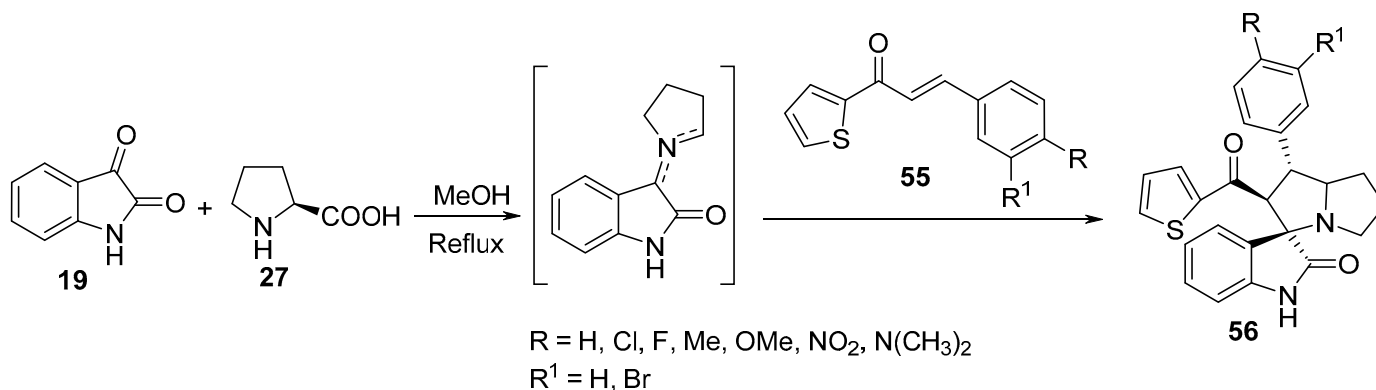
3,4-Dihydropyrrolo[2,1-*a*]isoquinolines **54** were obtained by the [3+2]-cycloaddition reaction of nitroalkenes **36** with an azomethine ylide that was efficiently generated via the dirhodium(II)caprolactamate $[\text{Rh}_2(\text{cap})_4]$ catalyzed oxidation of tetrahydroisoquinoline **53** (Scheme 16). Doyle's oxidative protocol was used to generate azomethine ylides, which were further trapped in situ via [3+2]-cycloaddition [37].



Scheme 16. Synthesis of pyrrolo[2,1-*a*]isoquinolines **54**.

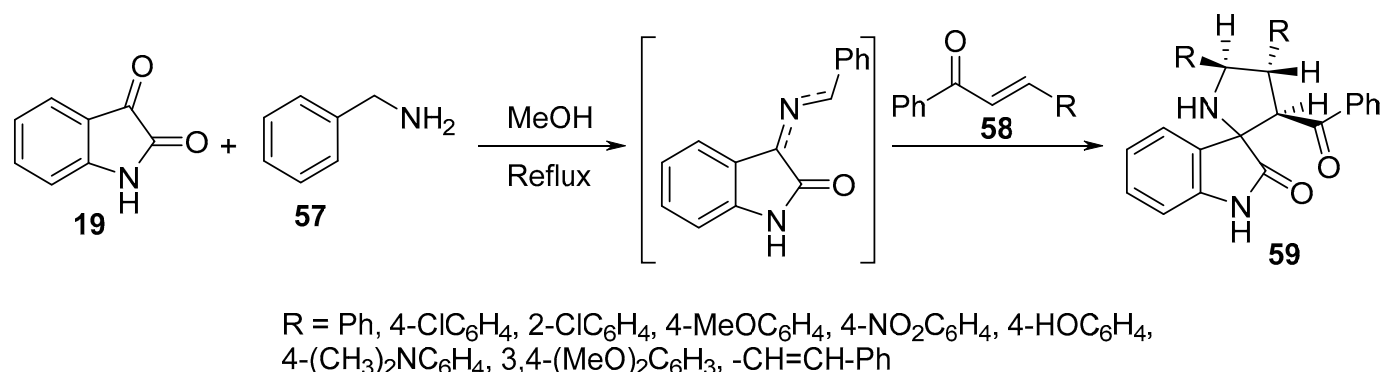
2.3. α,β -Unsaturated Polarophiles

Spiro[3H-indole-3,3'-[3H]pyrrolizin]-2-ones **56** were synthesized by the cycloaddition reaction of (*E*)-3-aryl-1-(thiophen-2-yl)-prop-2-en-1-ones **55** with azomethine ylide generated in situ from the condensation of isatin **19** with *L*-proline **27** (Scheme 17). Some of the synthesized spiroindoles **56** showed potential antibacterial activity against *Staphylococcus aureus* and *Salmonella typhi* (relative to Streptomycin) and antifungal activity against *Candida albicans* (relative to Amphotericin B) [38].



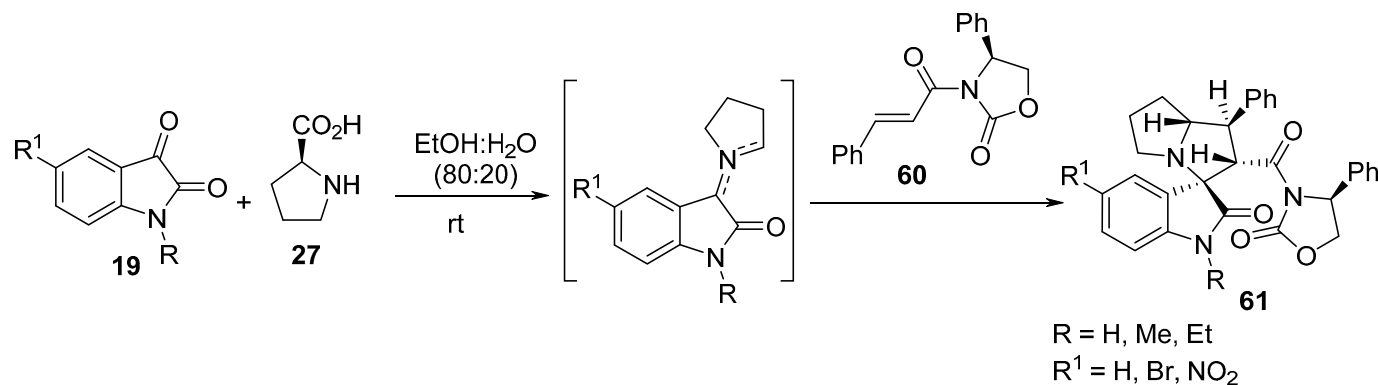
Scheme 17. Synthesis of spiro[3H-indole-3,3'-[3H]pyrrolizin]-2-ones **56**.

Spiro[pyrrolidine-2,3'-indolin]-2'-ones **59** were synthesized by the multi-component cycloaddition reaction of chalcones **58** and an azomethine ylide formed from the condensation of isatin **19** and benzylaminemine **57**. Few of the synthesized spiro-analogs **59** revealed potent inhibitory advanced glycation end (AGE) product formation in a bovine serum albumin (BSA)-glucose assay that was higher than that of aminoguanidine (standard reference). The occurrence of AGE is related to hyperglycemia observed as a complication of diabetes (Scheme 18) [39].



Scheme 18. Synthesis of spiro[pyrrolidine-2,3'-indolin]-2'-ones **59**.

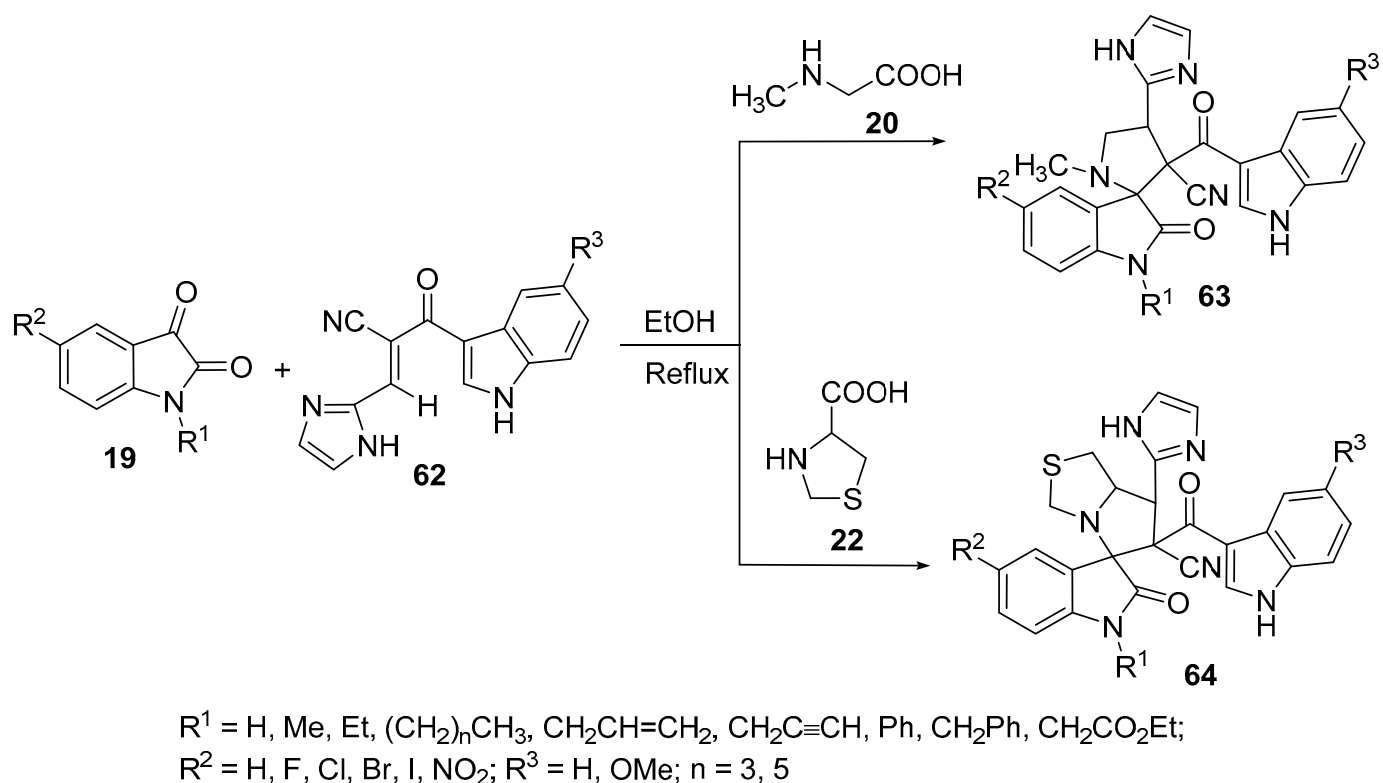
Taghizadeh et al. reported an efficient and greener multicomponent protocol for the synthesis of regio-, diastereo-, and enantioselective spiro-oxindolopyrrolizidines **61** from optically active cinnamoyl oxazolidinone **60** and azomethine ylides that were formed from the condensation reaction of isatin **19** and *S*-proline **27** (Scheme 19) [40].



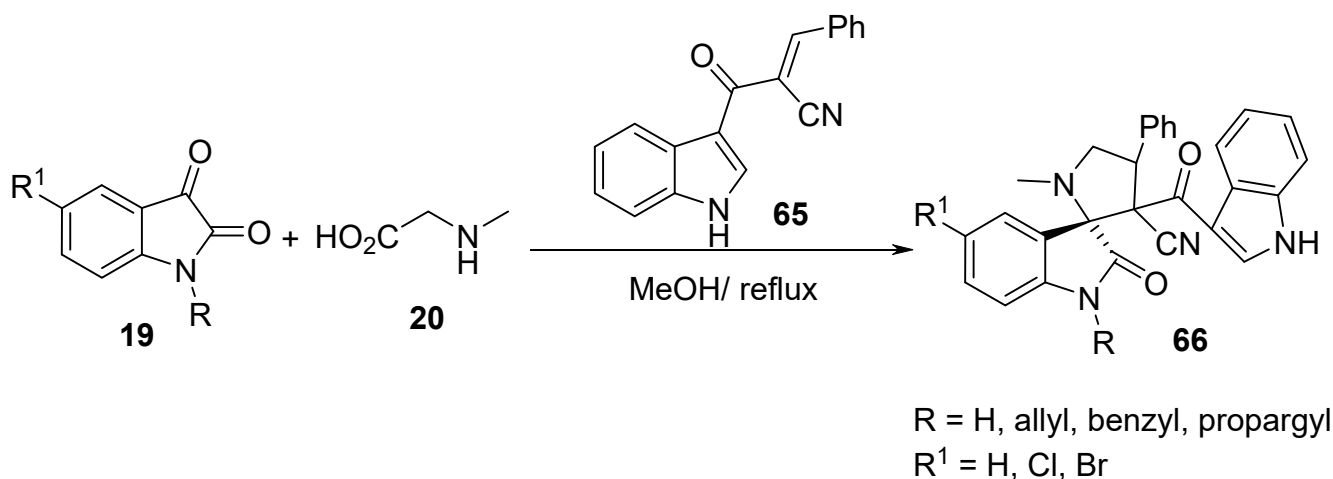
Scheme 19. Synthesis of the spiro-oxindolopyrrolizidines **61**.

Spiro[indoline-3,2'-pyrrolidines] **63** were prepared by the reaction of compound **62** containing an α,β -unsaturated ketone function with azomethine ylides obtained from isatin **19** and sarcosine **20**, while spiro[indoline-3,5'-pyrrolo[1,2-*c*]thiazoles] **64** was obtained from a similar reaction that involved thioproline **22** instead of sarcosine **20** (Scheme 20). Some of the synthesized spiro-compounds, **63** and **64**, revealed anticancer properties against the A549 lung cancer cell line (MTT assay) [41,42] and spiro-compound **63** also showed antimicrobial activity against Gram-positive (*Micrococcus luteus*, *Enterobacter aerogenes*, *Staphylococcus aureus* and *Staphylococcus aureus* "MRSA-methicillin resistant") and Gram-negative (*Salmonella typhimurium*, *Klebsiella pneumoniae*, *Proteus vulgaris*, and *Shigella flexneri*) bacterial strains and fungi (*Malassesia pachydermatis*, *Candida albicans*) relative to Streptomycin and Ketoconazole (used as antibacterial and antifungal standard references, respectively) [42].

Spiropyrrrolidine-oxindoles **66** were prepared in appreciable yields by the cycloaddition reaction of the unsaturated 2π -electron component (*E*)-2-(1*H*-indole-3-carbonyl)-3-phenylacrylonitrile **65** and azomethine ylides obtained from the condensation of isatin **19** and sarcosine **20** (Scheme 21) [43].

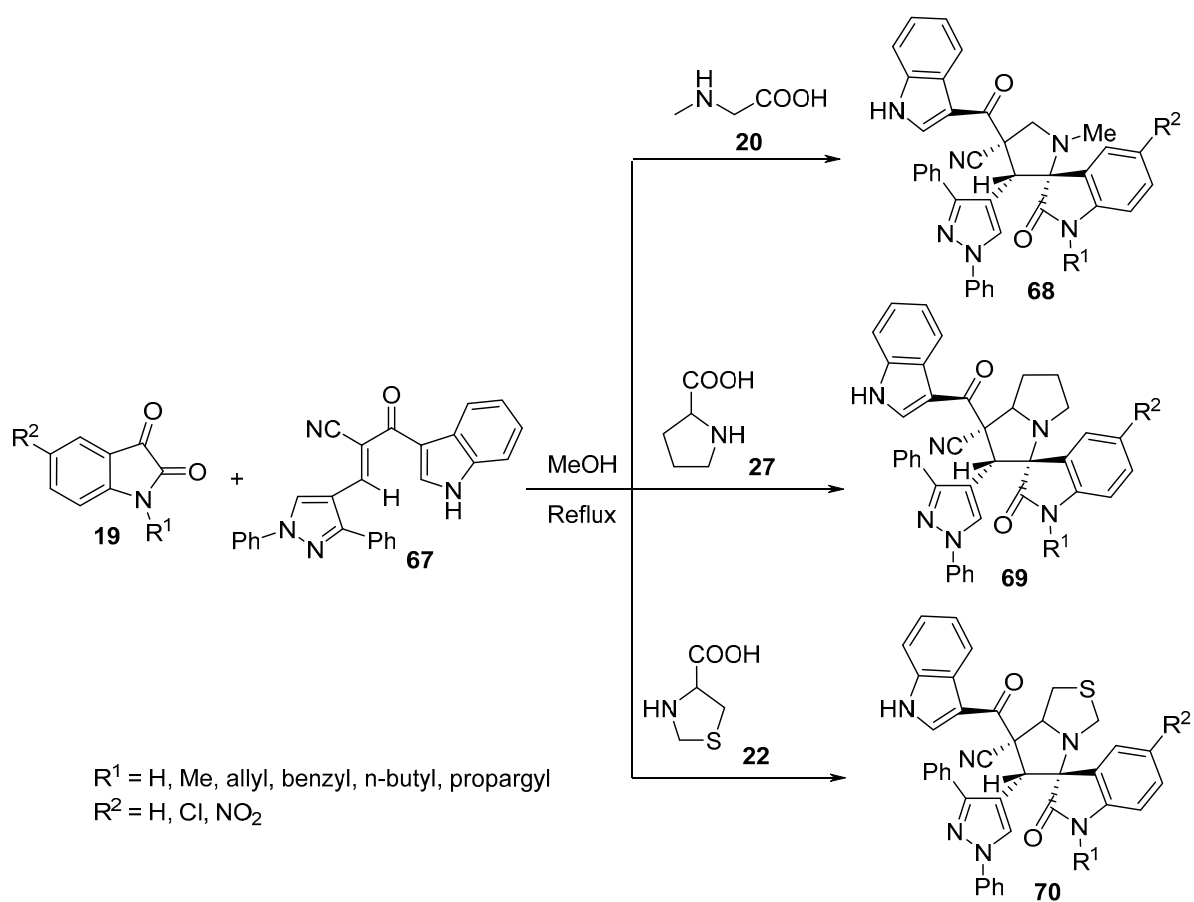


Scheme 20. Synthesis of spiro[indoline-3,2'-pyrrolidines] **63** and spiro[indoline-3,5'-pyrrolo[1,2-c]thiazoles] **64**.



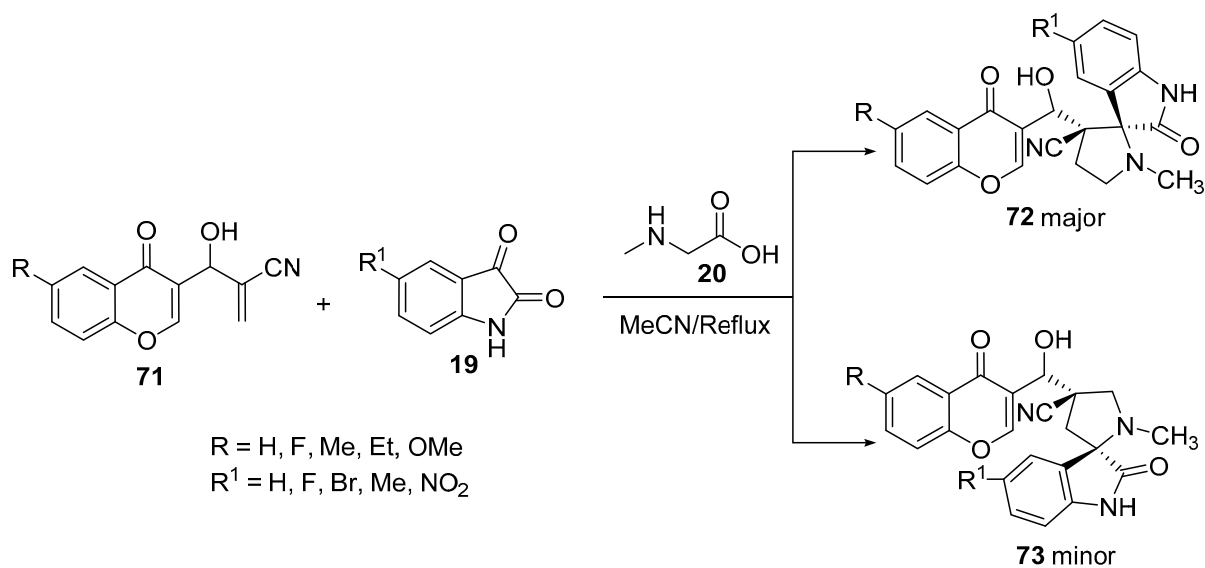
Scheme 21. Synthesis of spiropyrrolidine-oxindoles **66**.

Similarly, spiropyrrolidine-oxindoles **68–70** were obtained from the reaction of enone **67** with azomethine ylides derived from isatin **19** and α -amino acids (sarcosine **20**, proline **27** or thioproline **22**). Among all the synthesized compounds, some showed antimicrobial properties against Gram-positive and Gram-negative bacterial as well as fungal strains using Streptomycin and Ketconazole as standard references (Scheme 22) [44].



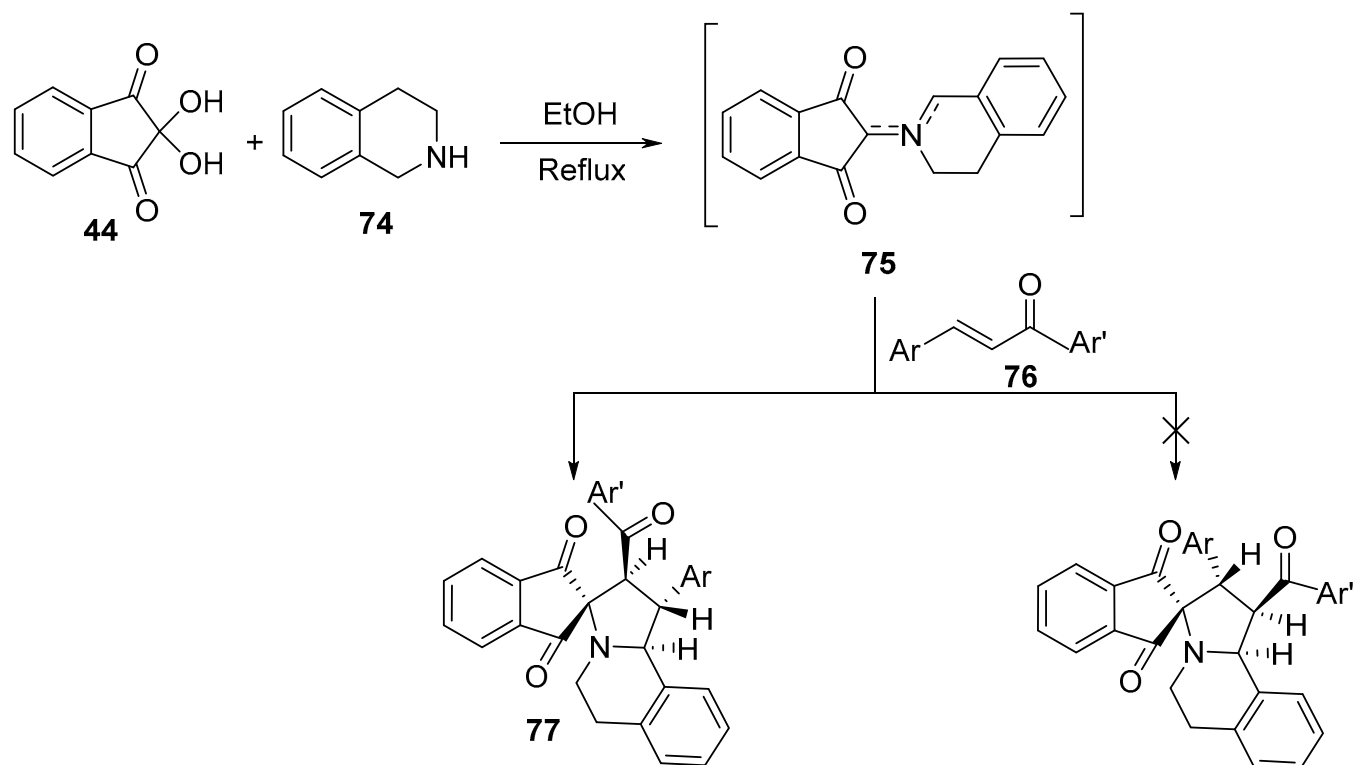
Scheme 22. Synthesis of spiro[pyrrolidine-oxindoles] 68–70.

The unsaturated 2π -electron component, 2-[hydroxyl(4-oxo-4*H*-chromen-3-yl)methyl]acrylonitrile **71**, was synthesized by the Baylis–Hillman reaction of chromene-3-aldehyde, treated with the azomethine ylides (from isatin **19** and sarcosine **20**), which afforded the corresponding regioselective spiro[pyrrolidine-oxindoles] **72** and **73** as major and minor products, respectively (Scheme 23) [45].



Scheme 23. Synthesis of spiro[pyrrolidine-oxindoles] **72**, **73**.

A convenient method for the selective construction of spiroindane-1,3-diones **77** relies upon the generation of unstabilized azomethine ylides from the initial condensation between ninhydrin **44** and 1,2,3,4-tetrahydroisoquinoline **74**. Subsequent azomethine ylide cycloaddition onto the conjugated double bond of chalcone **76** was exploited, giving target cycloadducts with good yields (77–94%) and diastereoselectivity (Scheme 24) [46].

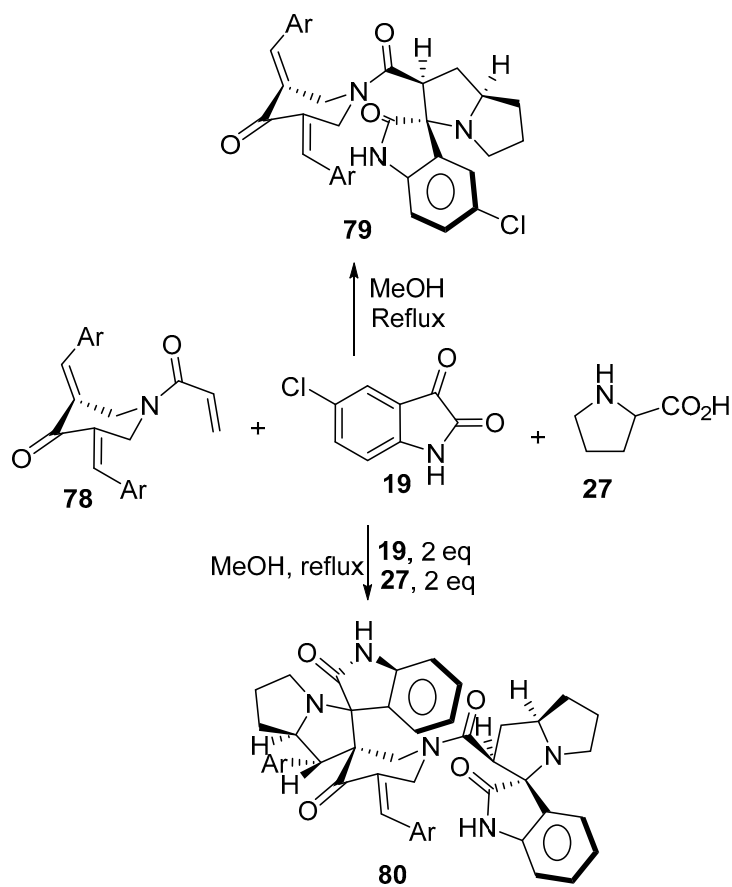


Ar = Ph, 4-CNC₆H₄, 4-MeC₆H₄, 2-ClC₆H₄, 4-ClC₆H₄, 4-BrC₆H₄, 4-FC₆H₄, 2-NO₂C₆H₄, 4-NO₂C₆H₄,
4-MeOC₆H₄, 3-MeOC₆H₄
Ar' = Ph, 4-ClC₆H₄, 3-ClC₆H₄, 2-NO₂C₆H₄, 4-MeOC₆H₄

Scheme 24. Synthesis of spiroindane-1,3-diones **77**.

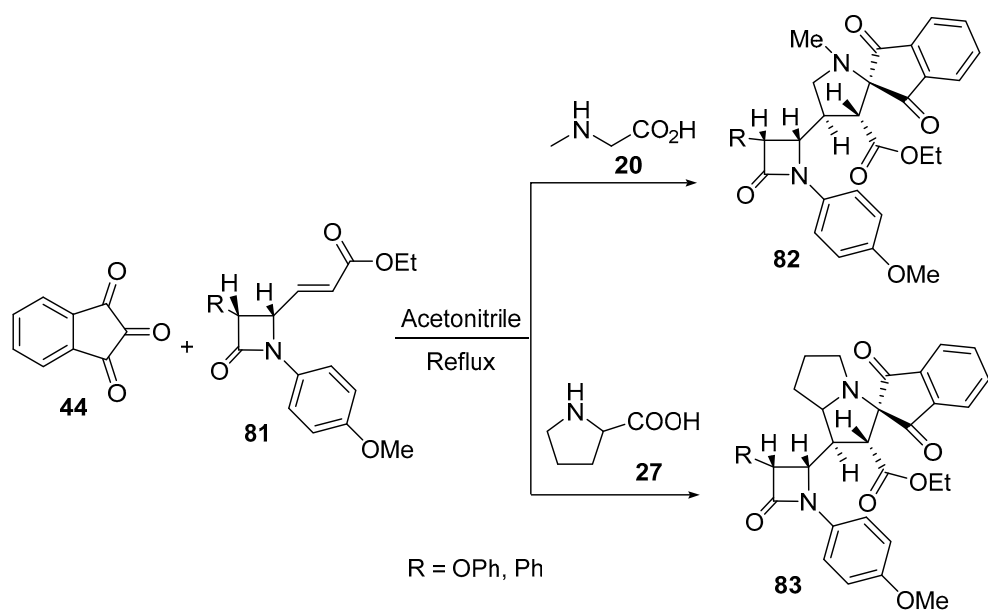
The reaction of azomethine ylide generated from 5-chloroisatin **19** and *L*-proline **27** as well as 1-acryloyl-4-piperidinones **78** yielded the corresponding spirooxindole-pyrrolizines **79** (yield 62–84%). Some of the synthesized cycloadducts **79** displayed cholinesterase-inhibitory properties (acetylcholinesterase and butyrylcholinesterase) with potency relative to Galantamine [47]. When the reaction was conducted in a 1:2:2 molar ratio of 1-acryloyl-4-piperidinones **78**, isatin **19**, and *L*-proline **27**, respectively, the bispiropyrrolizines **80** were formed instead (yield 53–74%). It was found that most of the mono-spiropyrrolizines **79** (obtained using a 1:1:1 molar ratio of the reactants in yields of 73–84%) revealed higher cholinesterase enzyme (acetylcholinesterase and butyrylcholinesterase)-inhibitory activity than the bispiropyrrolizine derivatives **80** (Scheme 25) [48].

The reaction of 3-(3-phenylazetididin-2-yl) acrylates **81** with azomethine ylide formed by the condensation of ninhydrin **44** and amino acids (sarcosine **20**/*L*-proline **27**) afforded the corresponding spiroindanopyrrolidines **82** and spiroindanopyrrolizines **83** (Scheme 26). The synthesized cycloadducts **82** and **83** showed antibacterial properties against *Proteus mirabilis*, *Proteus vulgaris*, *Salmonella typhi*, and *Staphylococcus aureus* relative to Tetracycline (standard reference drug) [49].



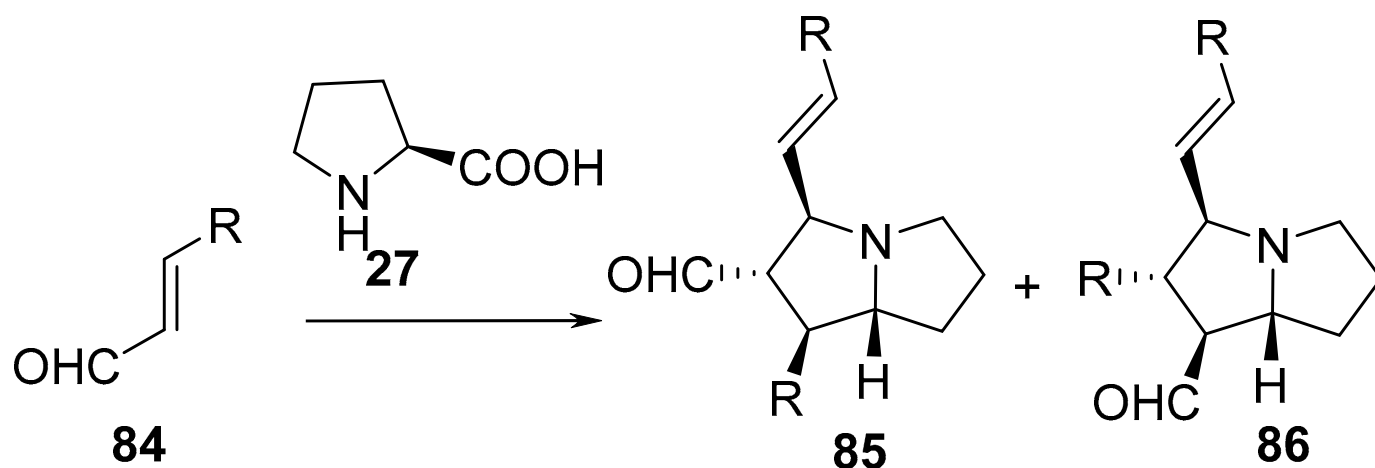
Ar = Ph, 2-MeC₆H₄, 2-MeOC₆H₄, 2-ClC₆H₄, 2-FC₆H₄, 3-NO₂C₆H₄, 2,4-Cl₂C₆H₃, 4-MeC₆H₄, 4-ClC₆H₄, 4-FC₆H₄, 1-naphthyl

Scheme 25. Synthesis of mono-spiropyrrrolizines **79** and bis-spiropyrrrolizines **80**.



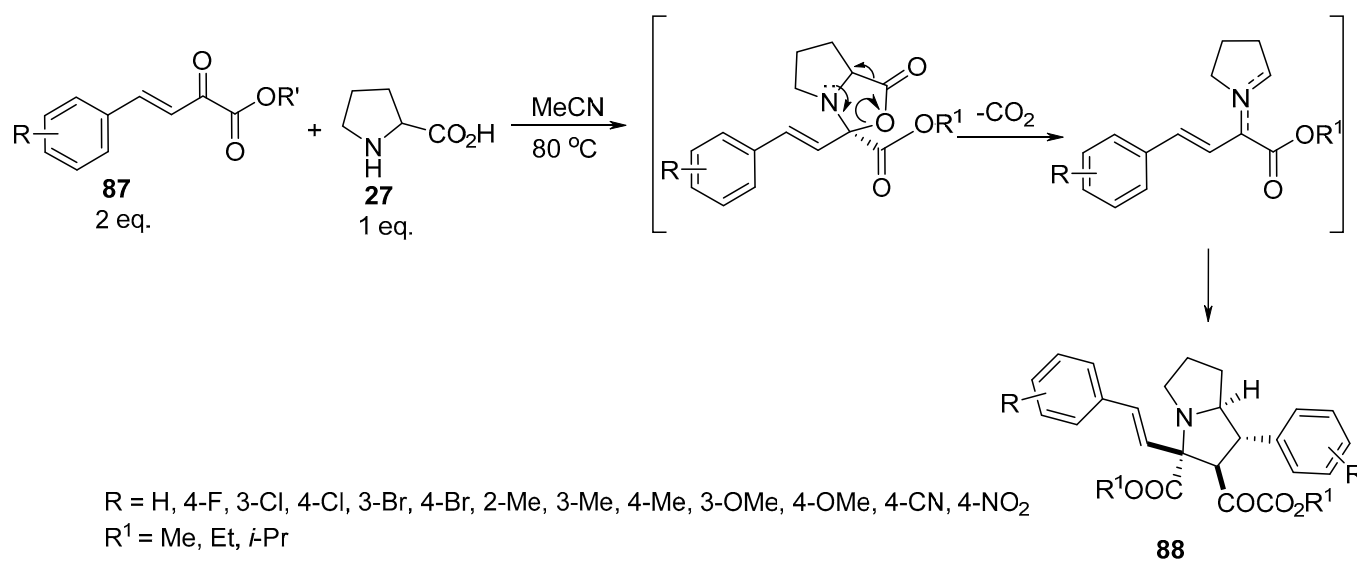
Scheme 26. Synthesis of spiroindanopyrrolidines **82** and spiroindanopyrrolizines **83**.

Cycloaddition of cinnamaldehydes **84** with azomethine ylides, generated from another cinnamaldehyde molecule **84** and *L*-proline **27**, afforded hexahydro-1*H*-pyrrolizines **85** and **86** in different ratios depending on the heating method (conventional heating, 25–80 °C vs. with microwave technique) and the solvent used (MeCN, DMF, toluene, CH₂Cl₂, DMSO) (Scheme 27) [50].



Scheme 27. Synthesis of hexahydro-1*H*-pyrrolizines **85** and **86**.

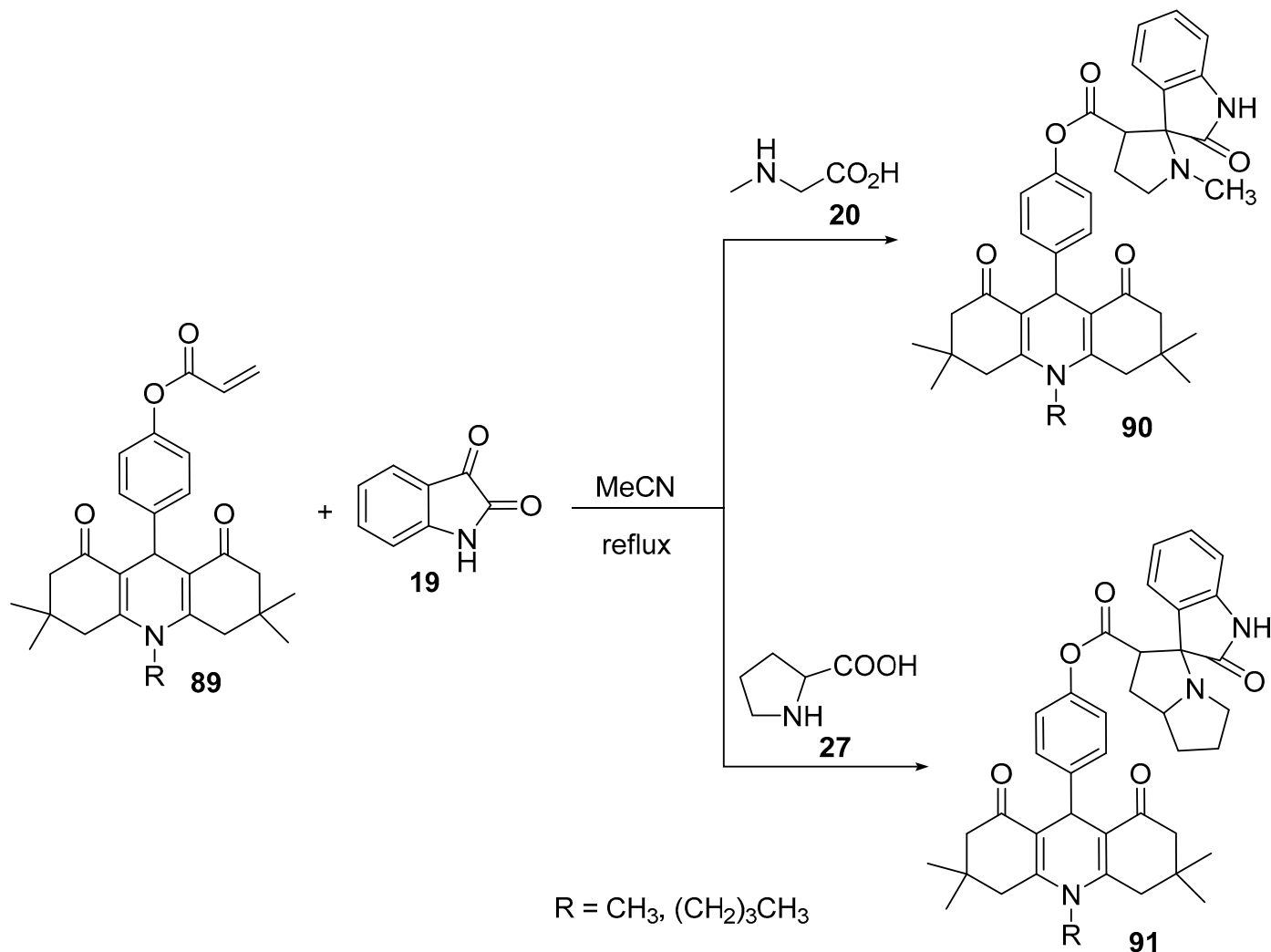
Pyrrrolizidines of type **88** were obtained by reacting β,γ -unsaturated α -keto esters of type **87** with proline **27** in a 2:1 molar ratio. The reaction was assumed to proceed via the formation of azomethine ylides by the condensation of the starting unsaturated esters of type **87** with amino acid **27**, which, in turn, interacted with another molecule of **87** to ultimately yield pyrrolizidines of type **88** (Scheme 28) [51].



Scheme 28. Synthesis of pyrrolizidines **88**.

2.4. Acrylates

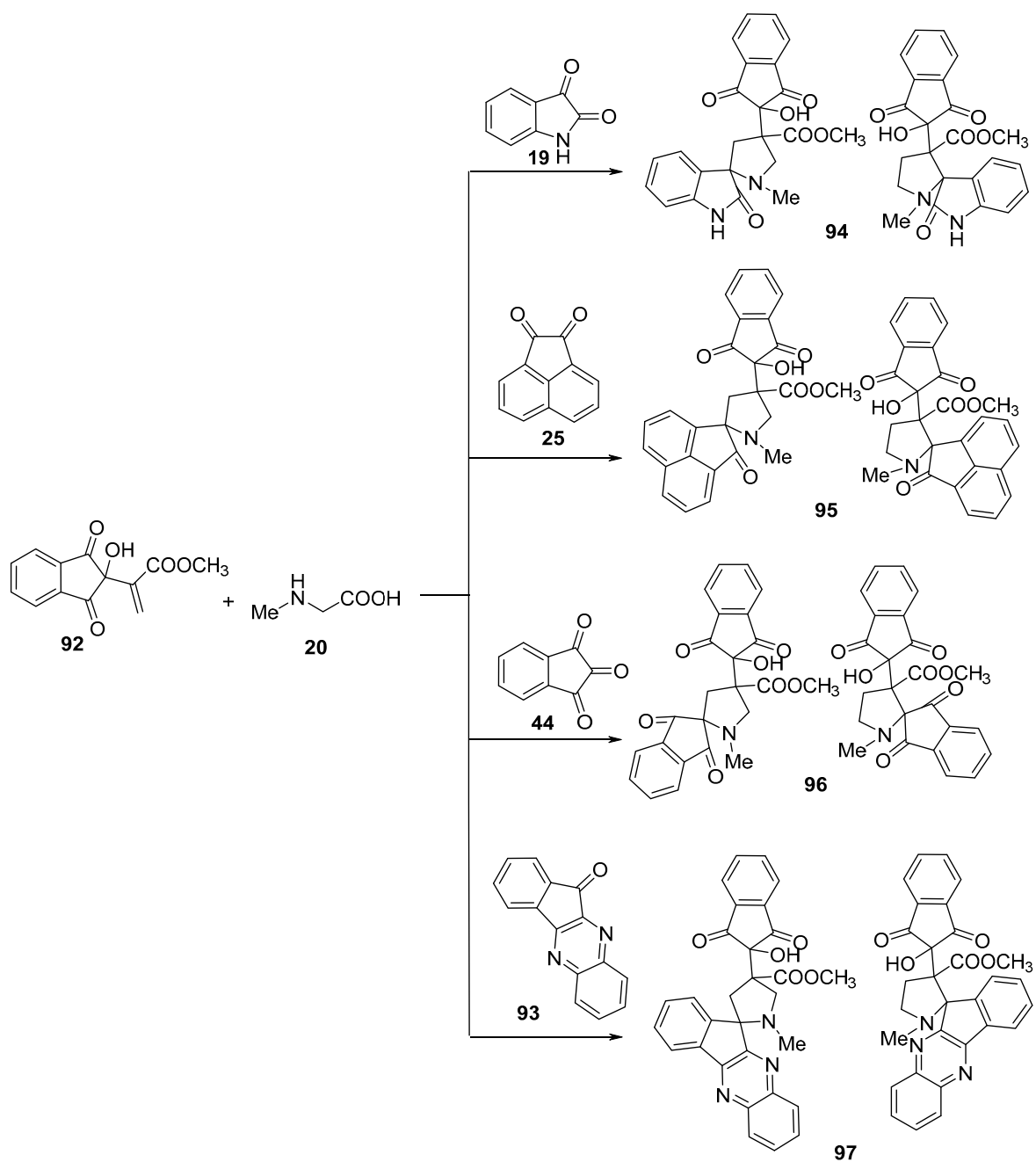
The reaction of *O*-acryloylacridinediones **89** with azomethine ylides, generated from isatin **19** and secondary amino acids (sarcosine **20**/proline **27**), afforded the corresponding spiro-pyrrolidines **90** and spiro-pyrrolizidines **91** (Scheme 29) [52].



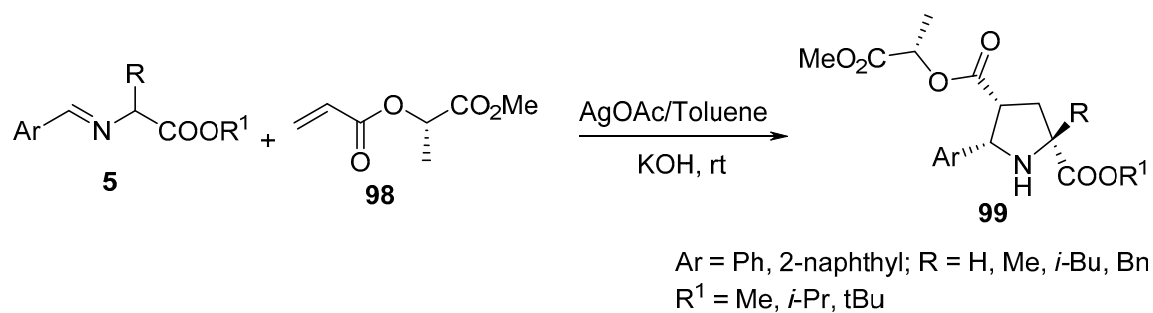
Scheme 29. Synthesis of spiro-pyrrolidines/pyrrolizidines **90/91**.

Spiropyrrolidines **94–97** were obtained via the reaction of methyl 2-(1*H*-inden-2-yl)acrylate **92** with azomethine ylides generated in situ by reacting ketones (isatin **19**, acenaphthenequinone **25**, ninhydrin **44**, or 11*H*-indeno[1,2-*b*]quinoxaline-11-one **93**) with sarcosine **20** (Scheme 30) [53].

The reaction of methyl lactate acrylates of type **98** with azomethine ylides, generated from imino-esters **5** in the presence of silver acetate and KOH, gave chiral proline derivatives of type **99** (Scheme 31) [54].

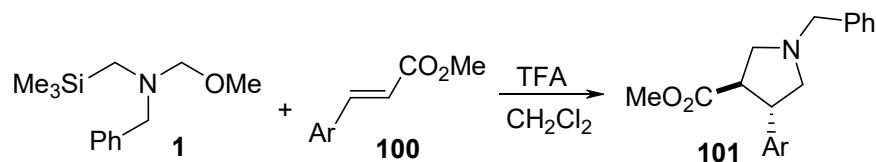


Scheme 30. Synthesis of spiropyrrolidines 94–97.



Scheme 31. Synthesis of chiral prolines 99.

The reaction of *trans* arylacrylates **100** with the azomethine ylide, formed from benzyl-(methoxymethyl)[(trimethylsilyl)methyl]amine **1** in the presence of a catalytic amount of trifluoroacetic acid, afforded the corresponding *trans* pyrrolidine derivatives **101** (Scheme 32) [55].



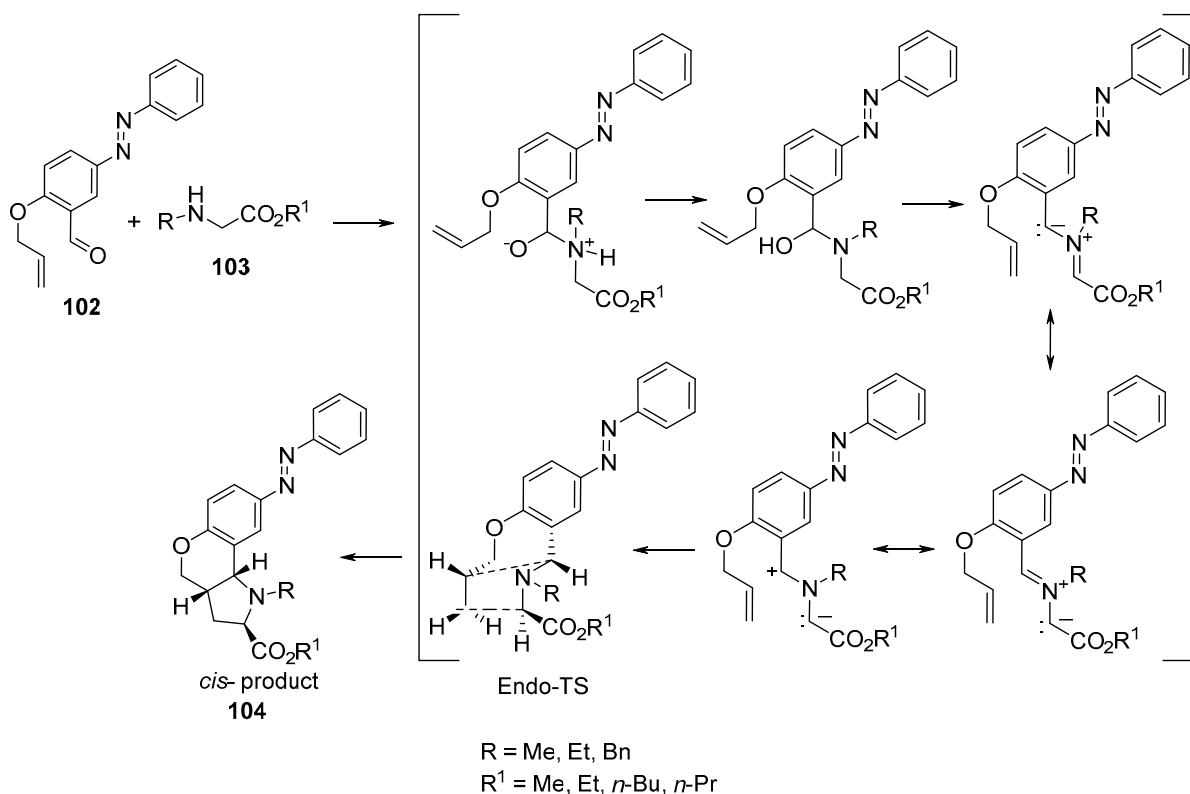
Ar = Ph, 2-FC₆H₄, 4-FC₆H₄, 2,4-F₂C₆H₃, 4-ClC₆H₄, 4-MeC₆H₄, 4-MeOC₆H₄

Scheme 32. Synthesis of *trans* pyrrolidines **101**.

2.5. Intramolecular Cycloaddition Reaction of Azomethine Ylides with Acyclic Unsaturated 2π-Electron Components

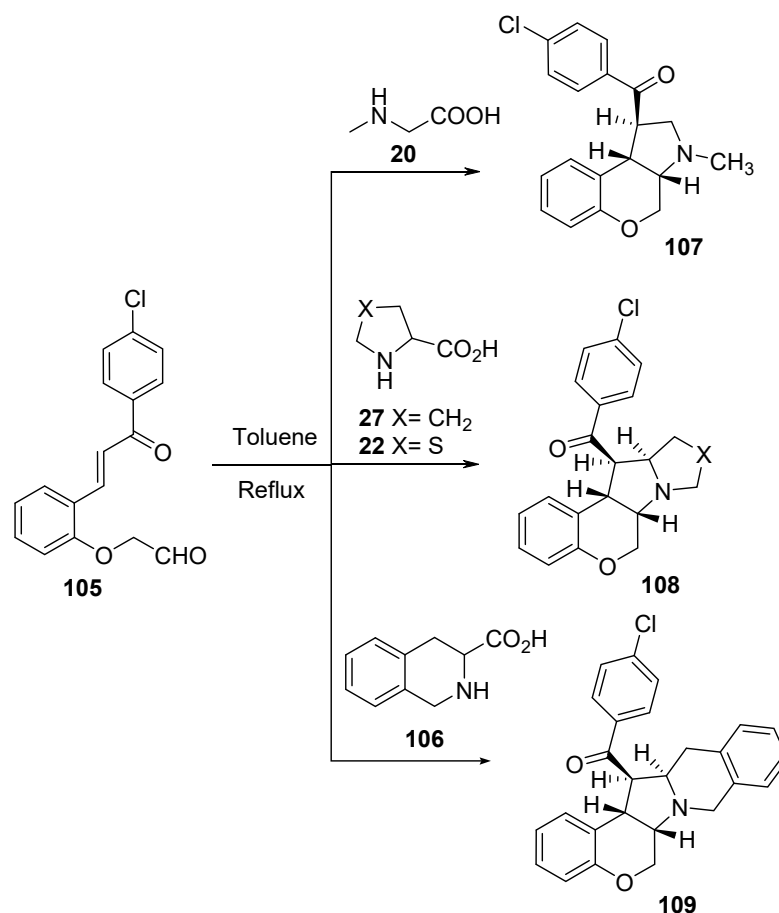
2.5.1. Acyclicunsaturated 2π-Electron Components Containing Olefinic and Aldehyde Groups

Azomethine ylides (formed via the reaction of α-amino esters **103** with *O*-allyl-5-phenyldiazenylsalicylaldehyde **102**) underwent intramolecular [3+2]-cycloaddition under microwave conditions, affording the 8-phenyldiazenylchromeno[4,3-*b*]pyrrolidines **104** (Scheme 33). The synthesized compounds showed antibacterial activity against Gram-positive (*Streptococcus pneumoniae*, *Clostridium tetani*, and *Bacillus subtilis*) and Gram-negative bacteria (*Salmonella typhi*, *Vibrio cholerae*, and *Escherichia coli*), fungi (*Aspergillus fumigatus* and *Candida albicans*), and mycobacteria (*M. Tuberculosis* H37RV) relative to the antibacterial (Ampicillin, Norfloxacin, Chloramphenicol, Ciprofloxacin), antifungal (Griseofulvin, Nystatin), and antimycobacterial (Metronidazole) standard references used [56].



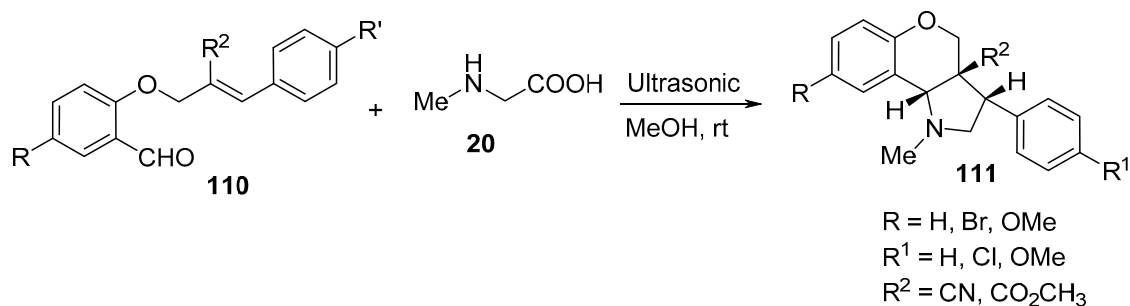
Scheme 33. Synthesis of 8-phenyldiazenylchromeno[4,3-*b*]pyrrolidines **104**.

The intramolecular cycloaddition reaction of azomethine ylides, formed from alkenyl aldehyde **105** and secondary amino acids (sarcosine **20**, *L*-proline **27**, thioproline **22**, and tetrahydroisoquinoline-3-carboxylic acid **106**), afforded the corresponding chromenopyrrole derivatives **107–109** (Scheme 34). The synthesized compounds showed promising antibacterial (against *S. aureus*, *B. subtilis* “Gram-positive”; *S. pneumoniae*, *E. coli*, and *Shigella* sp., *S. typhi* “Gram-negative”) and antifungal (against *Trichoderma* sp., *Aspergillus* sp. and *C. albicans*) activities against the references Tetracycline and Carbendazim (antibacterial and antifungal standard references, respectively) [57].



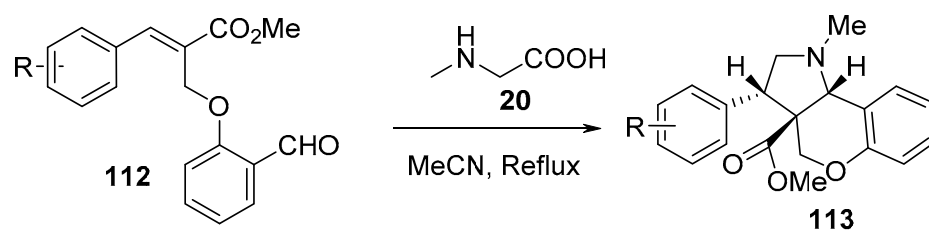
Scheme 34. Synthesis of chromenopyrrole-containing compounds **107–109**.

The intramolecular cycloaddition of *O*-allyl salicylaldehydes **110** and sarcosine **20** under ultrasonic irradiation in methanol at room temperature yielded the corresponding chromeno[4,3-*b*]pyrroles **111** (Scheme 35) [58].



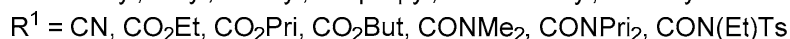
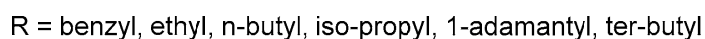
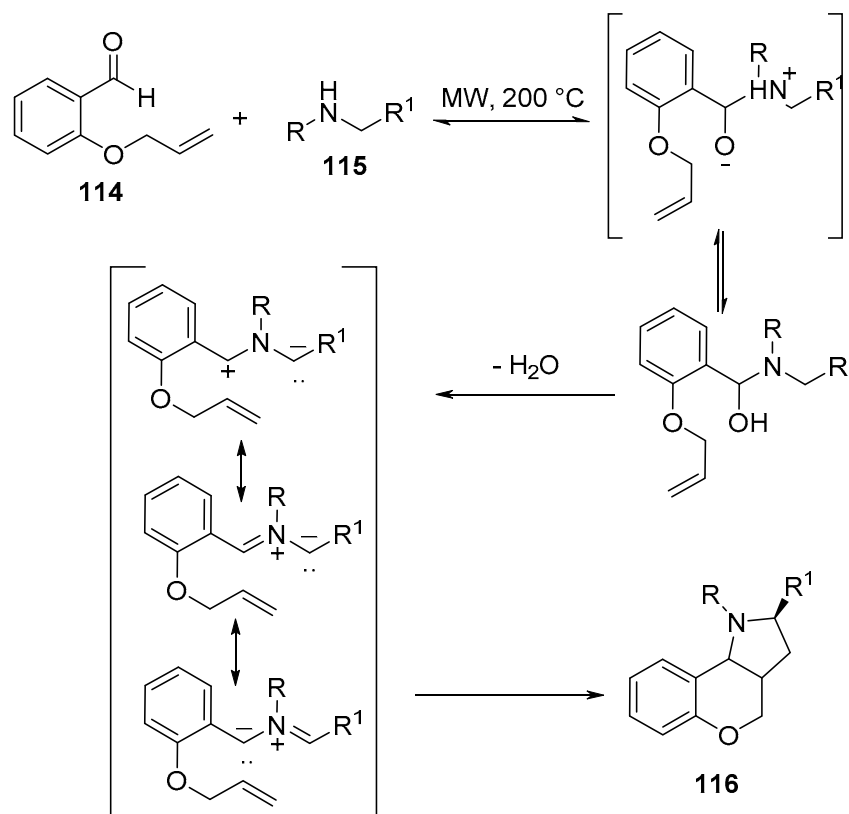
Scheme 35. Synthesis of chromeno[4,3-*b*]pyrroles **111**.

Chromeno[4,3-*b*]pyrrolidines **113** were obtained in a highly regio- and stereoselective manner by the intramolecular cycloaddition of *O*-allylic salicylaldehydes **112** and sarcosine **20** (Scheme 36) [59].



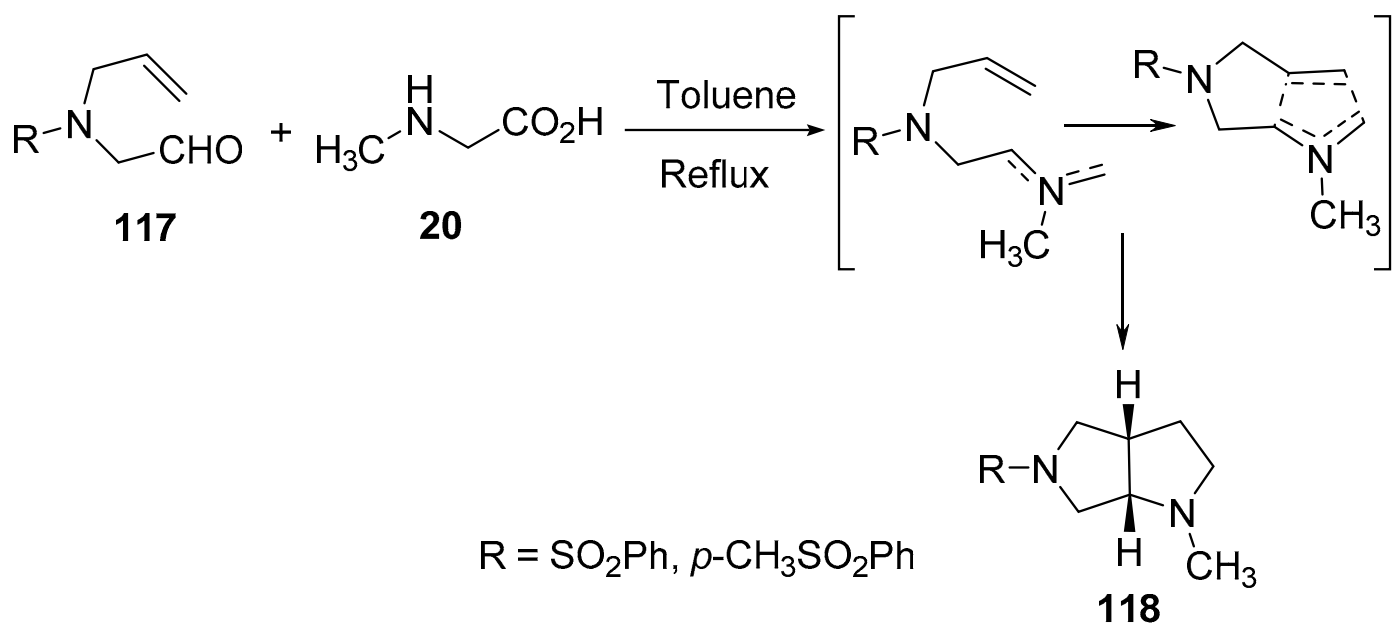
Scheme 36. Synthesis of chromeno[4,3-*b*]pyrrolidines **113**.

Similarly, hexahydrochromeno[4,3-*b*]pyrroles **116** were obtained via intramolecular [3+2]-cycloaddition of *O*-allylic salicylaldehyde **114** and amines **115** under microwave conditions (Scheme 37) [60].



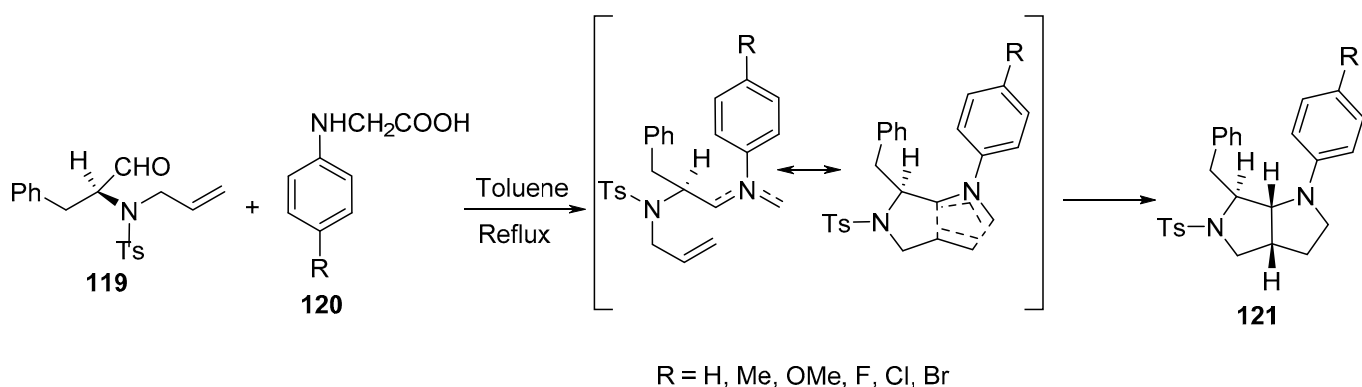
Scheme 37. Synthesis of hexahydrochromeno[4,3-*b*]pyrroles **116**.

Bicyclic pyrrolo[3,4-*b*]pyrroles **118** were obtained by the intramolecular cyclization of the generated azomethine ylides from aldehydes **117** and sarcosine **20** under refluxing conditions in toluene (Scheme 38) [61].



Scheme 38. Synthesis of pyrrolo[3,4-*b*]pyrroles **118**.

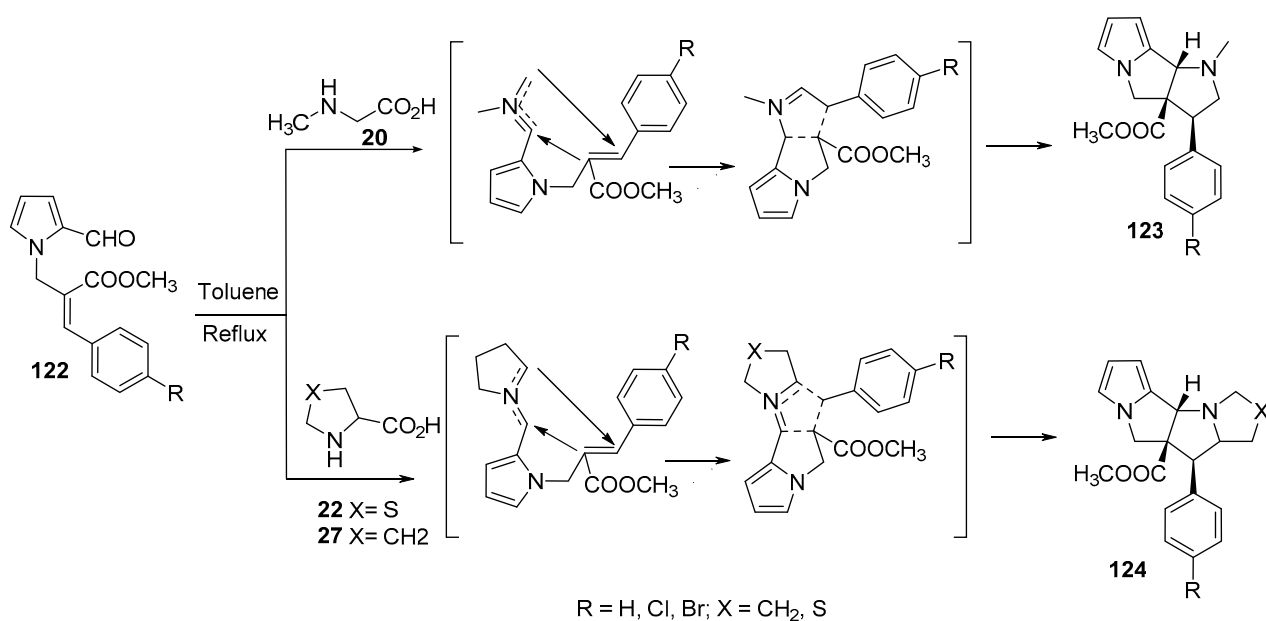
Octahydropyrrolo[3,4-*b*]pyrroles **121** with various substituents in their aromatic rings were synthesized by the intramolecular cycloaddition of azomethine ylides, which was formed from the reaction of alkenyl aldehyde **119** with *N*-aryl glycines **120** (Scheme 39) [62].



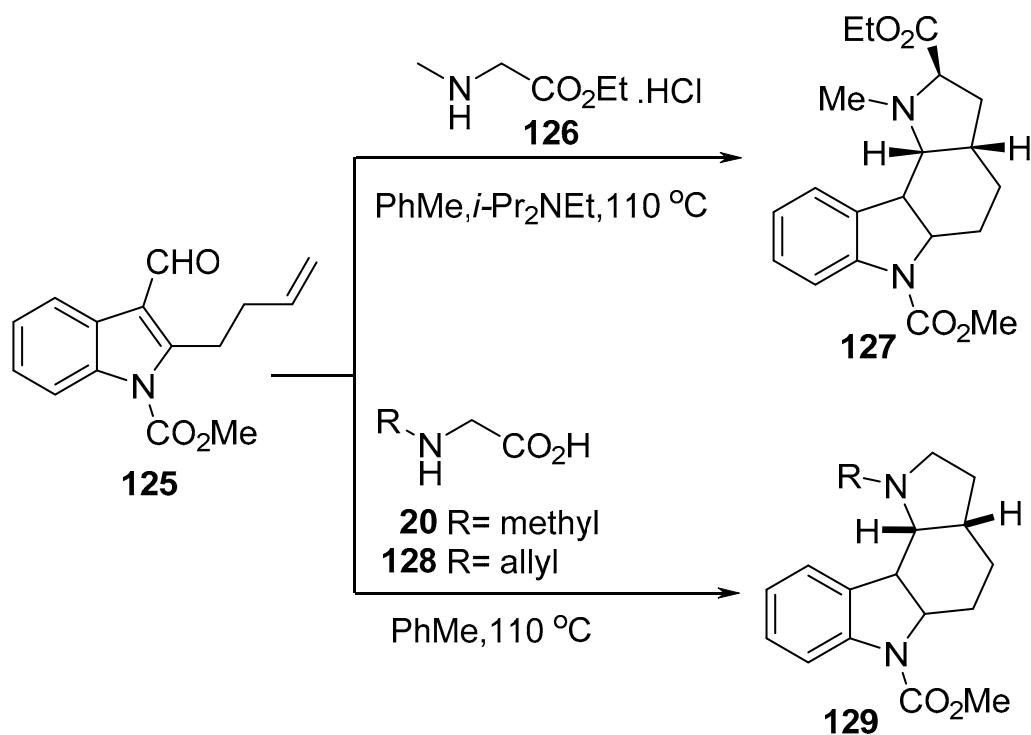
Scheme 39. Synthesis of octahydropyrrolo[3,4-*b*]pyrroles **121**.

The condensation of *N*-alkenyl aldehydes **122** with α -amino acids (sarcosine **20**, thio-proline **22** and proline **27**) generated azomethine ylides, which underwent an intramolecular cycloaddition reaction yielding the corresponding polycyclic compounds **123** and **124** (Scheme 40) [63].

Similarly, the intramolecular reaction of azomethine ylide obtained from 2-butenylindole-3-carboxaldehyde **125** with *N*-methyl glycine ethyl ester hydrochloride **126** gave the indole-containing alkaloid **127**. Whereas its reaction with *N*-methyl glycine **20** or *N*-allyl glycine **128** gave the corresponding indole heterocycles of type **129** (Scheme 41) [64].

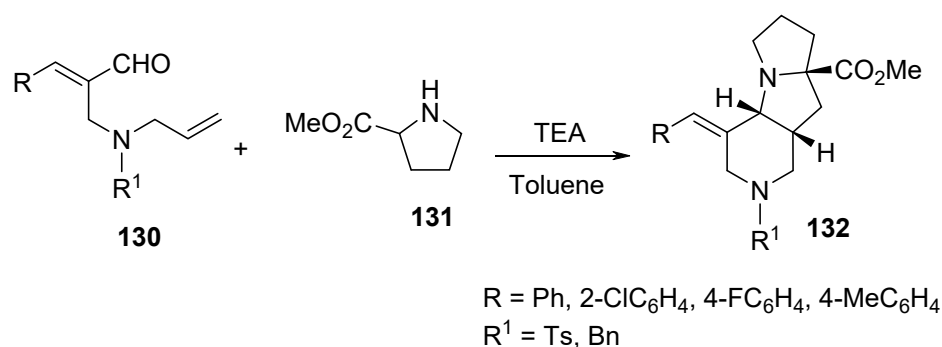


Scheme 40. Synthesis of polycyclic compounds 123 and 124.



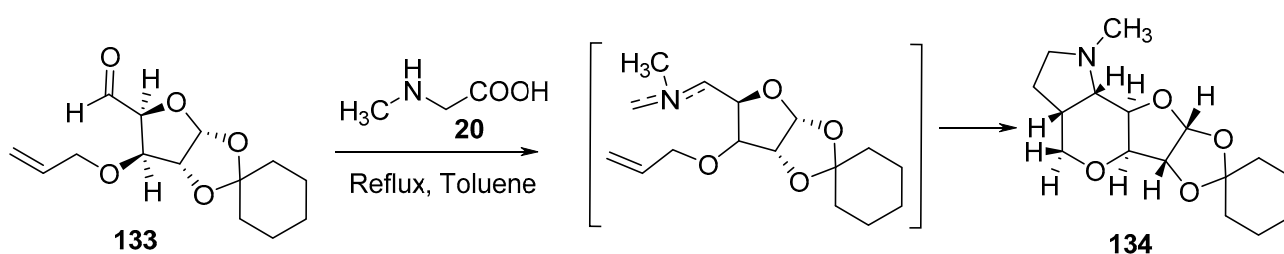
Scheme 41. Synthesis of indole-containing heterocycles 127 and 129.

Another example of intramolecular cycloaddition was the reaction of (*E*)-2-[[allyl(benzyl) amino]methyl] cinnamaldehydes **130** with proline methyl ester hydrochloride **131** under microwave conditions, which afforded the pyrido[3,4-*b*]pyrrolizines **132** (Scheme 42) [65].



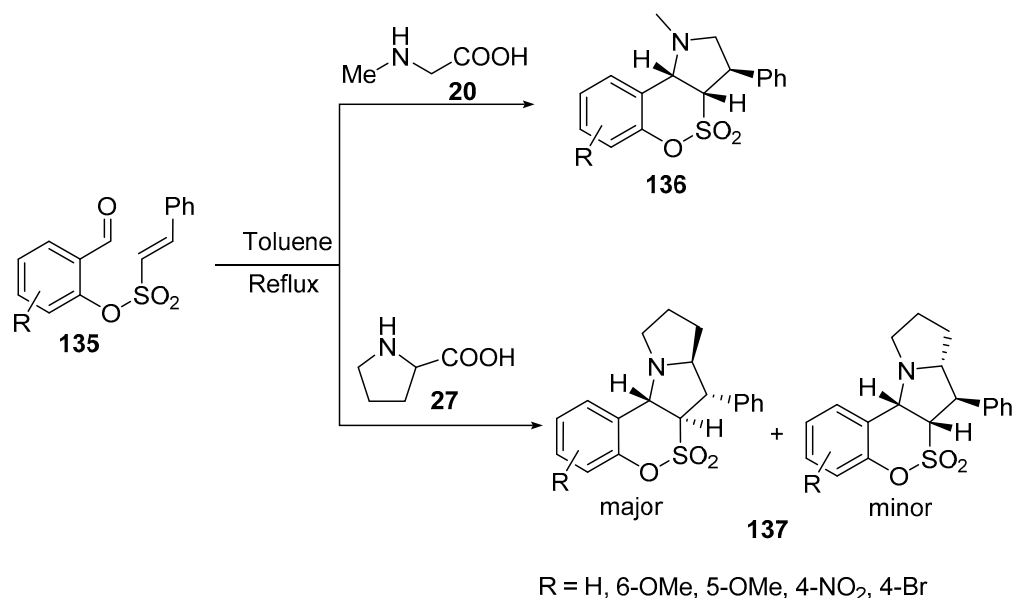
Scheme 42. Synthesis of pyrido[3,4-*b*]pyrrolizines **132**.

By using 1,2-*O*-cyclohexylidene-3-*O*-allyl- α -*D*-xylopentodialdo-1,4-furanose **133** (sugar-derived aldehyde) in a reaction with sarcosine **20**, furopyranopyrrolidine of type **134** was formed with high diastereoselectivity (Scheme 43) [66].



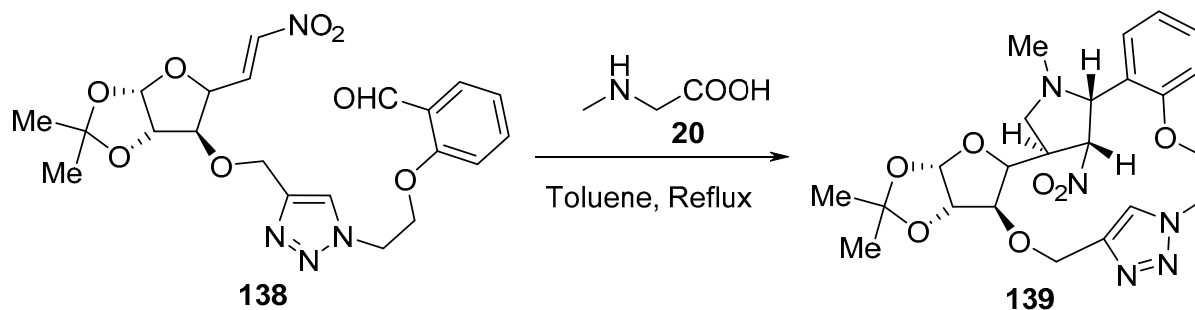
Scheme 43. Synthesis of furopyranopyrrolidine **134**.

The intramolecular [3+2]-cycloaddition of azomethine ylides, generated from 2-formylphenyl-(*E*)-2-phenylethanesulfonates **135** and sarcosine **20**, afforded the corresponding [1,2]oxathiino[4,3-*b*]pyrroles **136**. However, the reaction of derivative **135** with *L*-proline **27** gave the corresponding [1,2]oxathiino[3,4-*b*]pyrrolizines **137** as *trans-trans* (major) and *cis-trans* (minor) isomers (Scheme 44) [67].



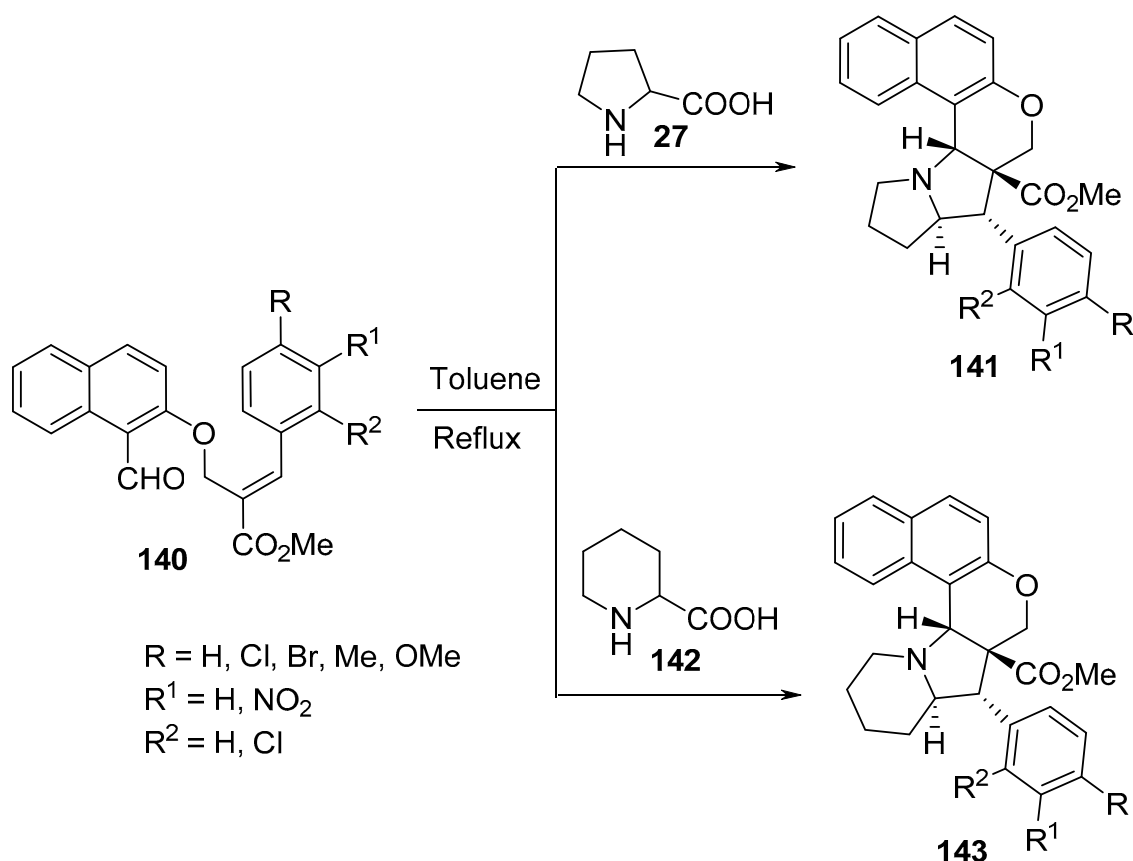
Scheme 44. Synthesis of benzo[*e*][1,2]oxathiino[4,3-*b*]pyrrole-4,4-dioxides **136** and benzo[*e*][1,2]oxathiino[3,4-*b*]pyrrolizine-6,6-dioxides **137**.

Scheme 45 shows an interesting example of a macrocycle of type **139** formation via the intramolecular cycloaddition of an azomethine ylide generated from a triazole-linked glycol-nitroalkenyl aldehyde derivative **138** and sarcosine **20** [68].



Scheme 45. Synthesis of macrocycle **139**.

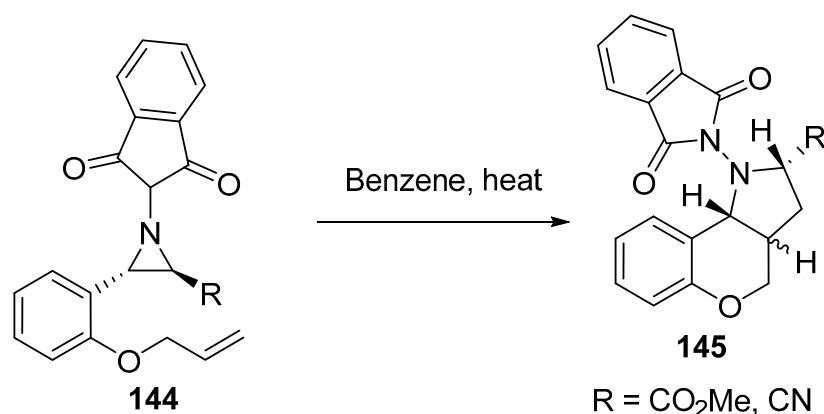
Polycyclic naphtho[2,1-*b*]pyrano-pyrrolizidine and indolizidine derivatives **141** and **143** were synthesized by the intramolecular [3+2]-cycloaddition of azomethine ylides generated from naphtho-*O*-alkenyl aldehydes **140** and α -amino acids (*L*-proline **27** or *DL*-pipercolinic acid **142**) (Scheme 46) [69].



Scheme 46. Synthesis of naphtho-pyrano-pyrrolizidines/indolizidines **141** and **143**.

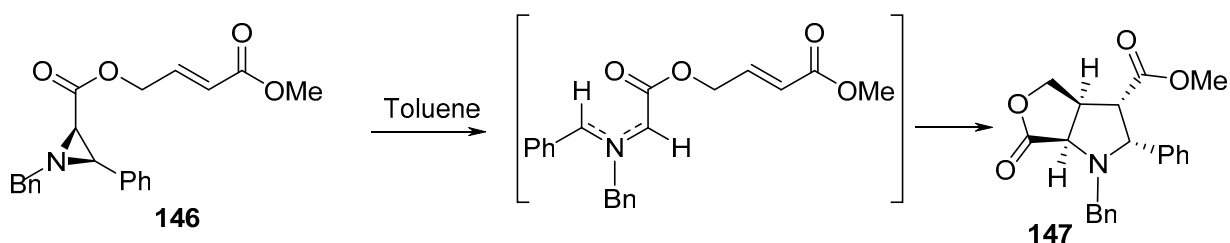
2.5.2. Acyclic Unsaturated 2π -Electron Components Containing Olefinic Linkage and Aziridine

Scheme 47 shows the thermolysis of aziridines **144** that led to the in situ formation of azomethine ylides, which underwent intramolecular cycloaddition, thus affording *N*-phthalimidopyrrolidine derivatives **145** as a mixture of two diastereoisomers [70].



Scheme 47. Synthesis of *N*-phthalimidopyrrolidines **145**.

Another bicyclic system of γ -lactone **147** was created by the intramolecular [3+2]-cycloaddition of azomethine ylide generated via the thermolysis of aziridine derivative **146** in refluxing toluene (Scheme 48) [71].

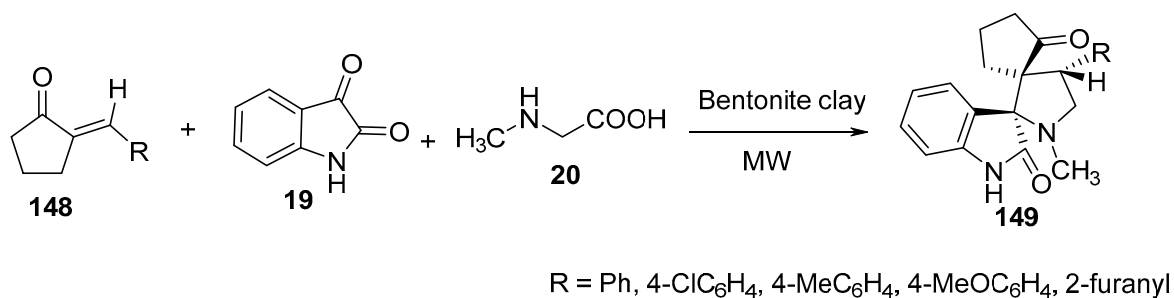


Scheme 48. Synthesis of bicyclic γ -lactone **147**.

3. Exocyclic, Unsaturated 2π -Electron Components

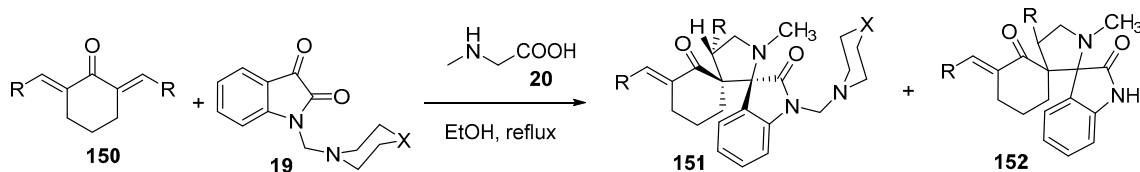
3.1. Cycloalkanones

The exocyclic olefinic linkage is a reactive, unsaturated 2π -electron component intensively used in [3+2]-cycloaddition reactions forming various heterocycles [72–76]. For example, the cycloaddition of azomethine ylide (formed from isatin **19** and sarcosine **20**) with 2-arylidene-1-cyclopentanones **148** in the presence of bentonite clay under microwave conditions afforded dispiropyrrolidinyl-oxindoles **149** (Scheme 49) [77].



Scheme 49. Synthesis of dispiropyrrolidinyl-oxindoles **149**.

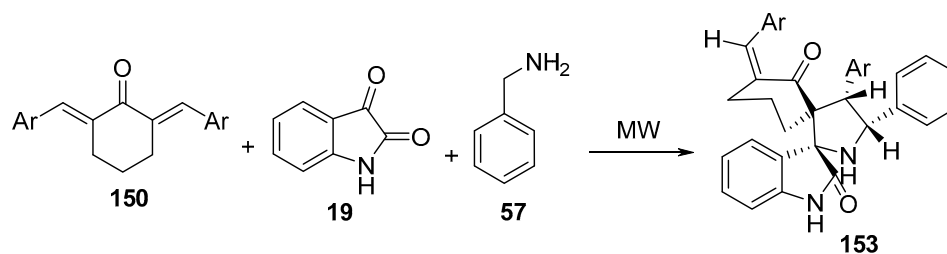
Similarly, dispiro[cyclohexane-1,3'-pyrrolidine-2',3''-[3*H*]indoles] **151** and **152** were obtained by the cycloaddition reaction of azomethine ylides (generated from isatin derivative **19** and sarcosine **20**) with 2*E*,6*E*-bis(arylidene)-1-cyclohexanones **150** (Scheme 50). Some of the synthesized compounds demonstrated antitumor properties against liver (HEPG2), cervical (HELA), and prostate (PC3) cancer cell lines while using Doxorubicin as a standard reference in an SRB assay [78].



R = Ph, 4-ClC₆H₄, 2,4-Cl₂C₆H₃, 4-FC₆H₄, 4-CH₃C₆H₄, 4-MeOC₆H₄, 3,4-(MeO)₂C₆H₃, 2-thienyl, 5-methyl-2-furanyl
X = CH₂, O, NCH₃

Scheme 50. Synthesis of dispiro[cyclohexane-1,3'-pyrrolidine-2',3''-[3H]indoles] **151** and **152**.

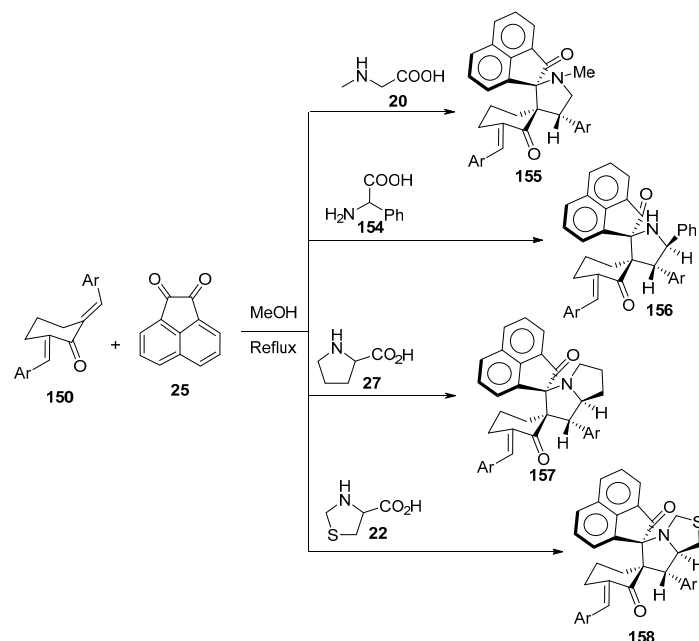
Azomethine ylide formed from the condensation of benzylamine **57** and isatin **19** also underwent a cycloaddition reaction with 2,6-bis(ylidene)cyclohexanones **150** under solvent-free conditions using microwave irradiation, thereby affording the dispiro-oxindole **153** with high regioselectivity (Scheme 51) [79].



Ar = Ph, 4-ClC₆H₄, 4-MeC₆H₄, 4-MeOC₆H₄, 4-NO₂C₆H₄

Scheme 51. Synthesis of dispiro-oxindoles **153**.

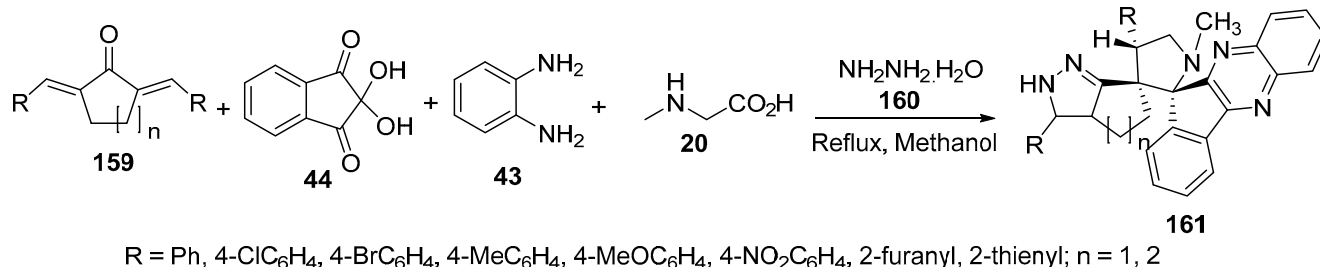
Azomethine ylides derived from acenaphthenequinone **25** and α -amino acids (sarcosine **20**, phenylglycine **154**, proline **27**, or thioproline **22**) afforded the corresponding spirocyclohexanones **155–158** upon reaction with 2,6-bis(ylidene)cyclohexanones **150** in refluxing methanol [80] (Scheme 52). Some of the synthesized spiro compounds revealed activity against *Mycobacterium tuberculosis* H37Rv (MTB) relative to Ethambutol and Pyrazinamide [80].



Ar = Ph, 4-ClC₆H₄, 4-MeC₆H₄, 4-MeOC₆H₄, 4-FC₆H₄, 2-ClC₆H₄, 2-MeC₆H₄, 3-FC₆H₄, 2,4-Cl₂C₆H₃, 1-naphthyl

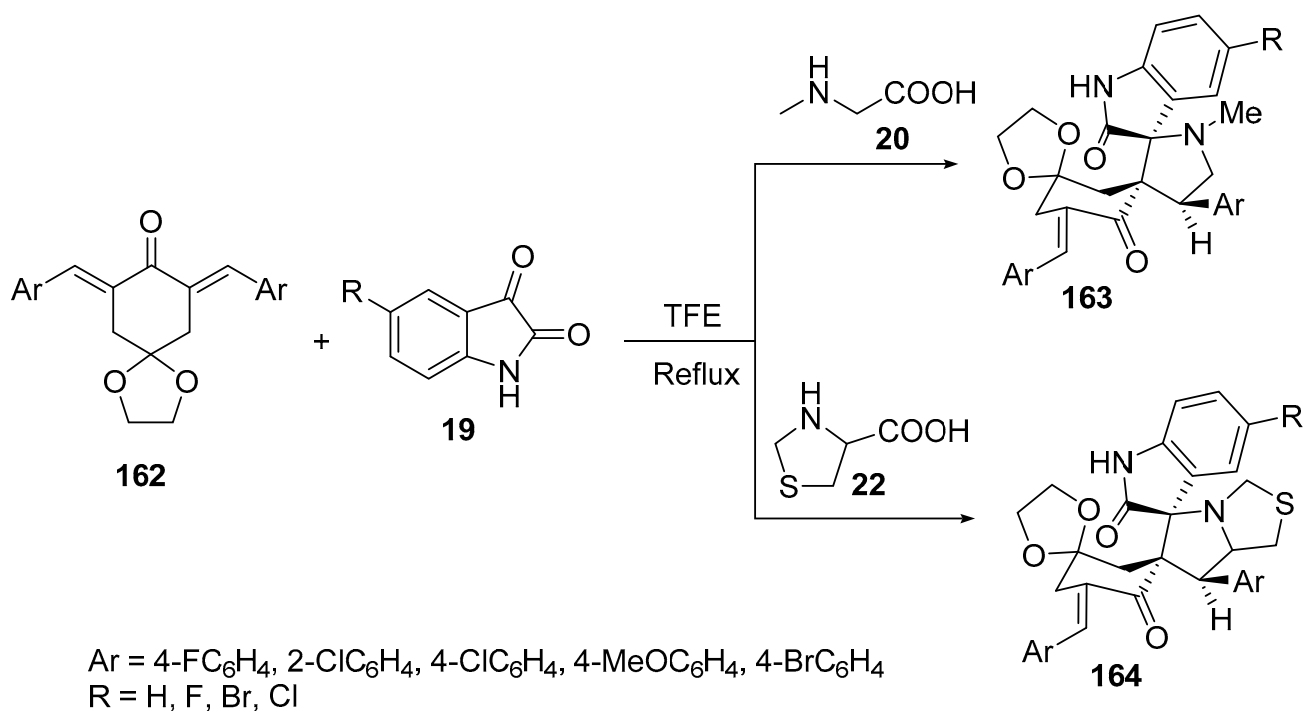
Scheme 52. Synthesis of spirocyclohexanone **155–158**.

A one-pot, five-component reaction of azomethine ylide (formed from ninhydrin **44**, *o*-phenylenediammine **43**, and sarcosine **20**) with bis(ylidene)cycloalkanones **159** in the presence of hydrazine hydrate **160** in refluxing methanol regioselectively afforded the corresponding spiro-indenoquinoxaline-pyrrolidines **161** at a high yield (Scheme 53) [81].



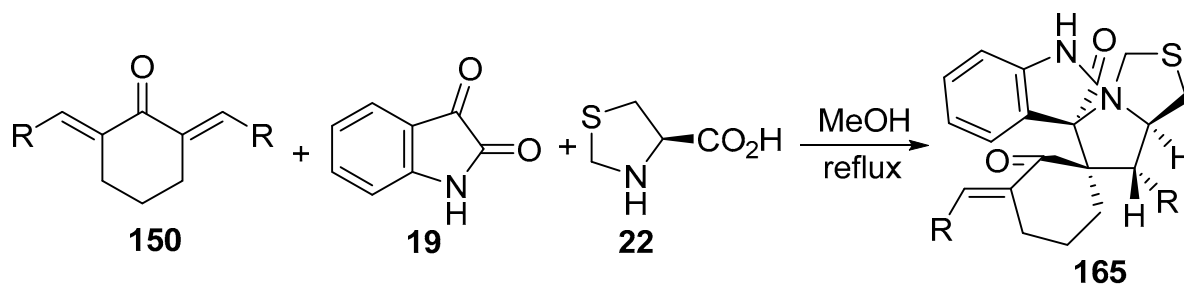
Scheme 53. Synthesis of spiro-indenoquinoxaline pyrrolidines **161**.

Trispiropyrrolidines/thiapyrrolizidines **163** and **164** were synthesized through the reaction of 7,9-bis[(*E*)-ylidene]-1,4-dioxo-spiro[4,5]decane-8-ones **162** and azomethine ylides (formed from isatin **19** and sarcosine **20** or thioproline **22**) in 2,2,2-trifluoroethanol (TFE) (Scheme 54). Some of the products showed anti-fungal properties (against *Candida albicans* MTCC 227, *Aspergillus niger* MTCC 282, and *Aspergillus clavatus* MTCC 1323) and antimycobacterial properties against *M. tuberculosis* H37Rv relative to the standard references Nysyatin, Greseofulvin (antifungal), and Isoniazid (antimycobacterial) [82].



Scheme 54. Synthesis of trispiropyrrolidines/thiapyrrolizidines **163**, **164**.

Analogously, dispiro compounds of type **165** were synthesized by the reaction of 2,6-bis(ylidene)cyclohexanones **150** with azomethine ylide (formed from *L*-thiopropine **22** and isatin **19**) in refluxing methanol. Some of the synthesized derivatives revealed promising antiproliferative properties (apoptotic mechanism) against the MCF7 (breast) and K562 (leukemia) cell lines (WST-1 assay) relative to 5-Fluorouracil (standard reference drug) (Scheme 55) [83].

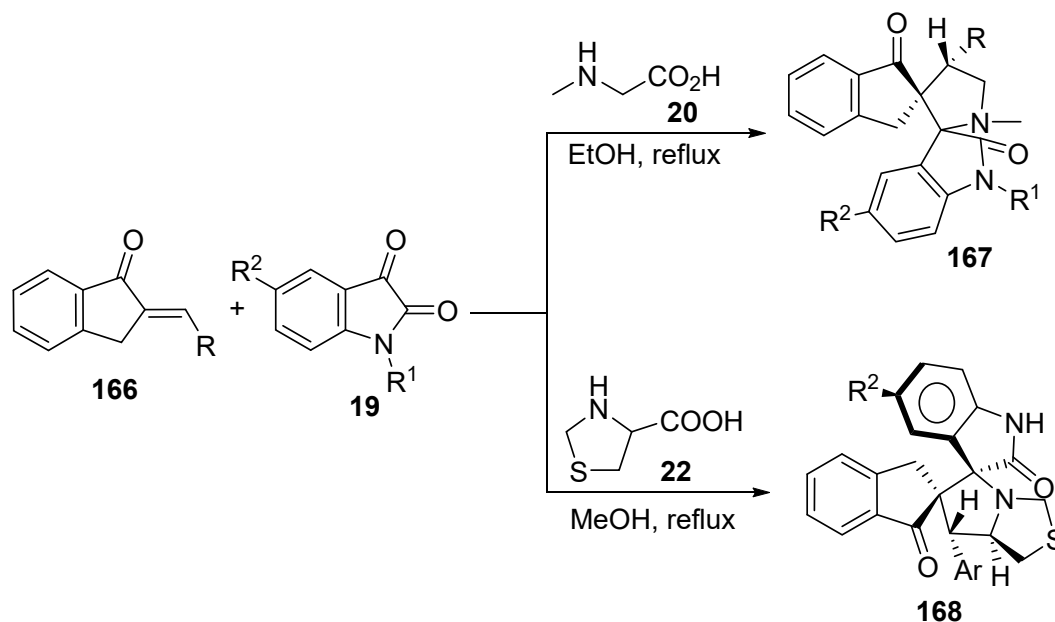


R = Ph, 4-MeC₆H₄, 4-ClC₆H₄, 4-F₃CC₆H₄, 3-MeC₆H₄, 3-FC₆H₄, 3-BrC₆H₄, 2,4-Cl₂C₆H₃, 4-MeC₆H₄, 3-NO₂C₆H₄, 4-BrC₆H₄, 4-FC₆H₄, 2-thienyl, 2-naphthyl

Scheme 55. Synthetic route towards dispiro[cyclohexane-1,6'-pyrrolo[1,2-c].thiazole-5',3''-indoline]-2,2''-diones **165**.

3.2. Indanones and Indanediones

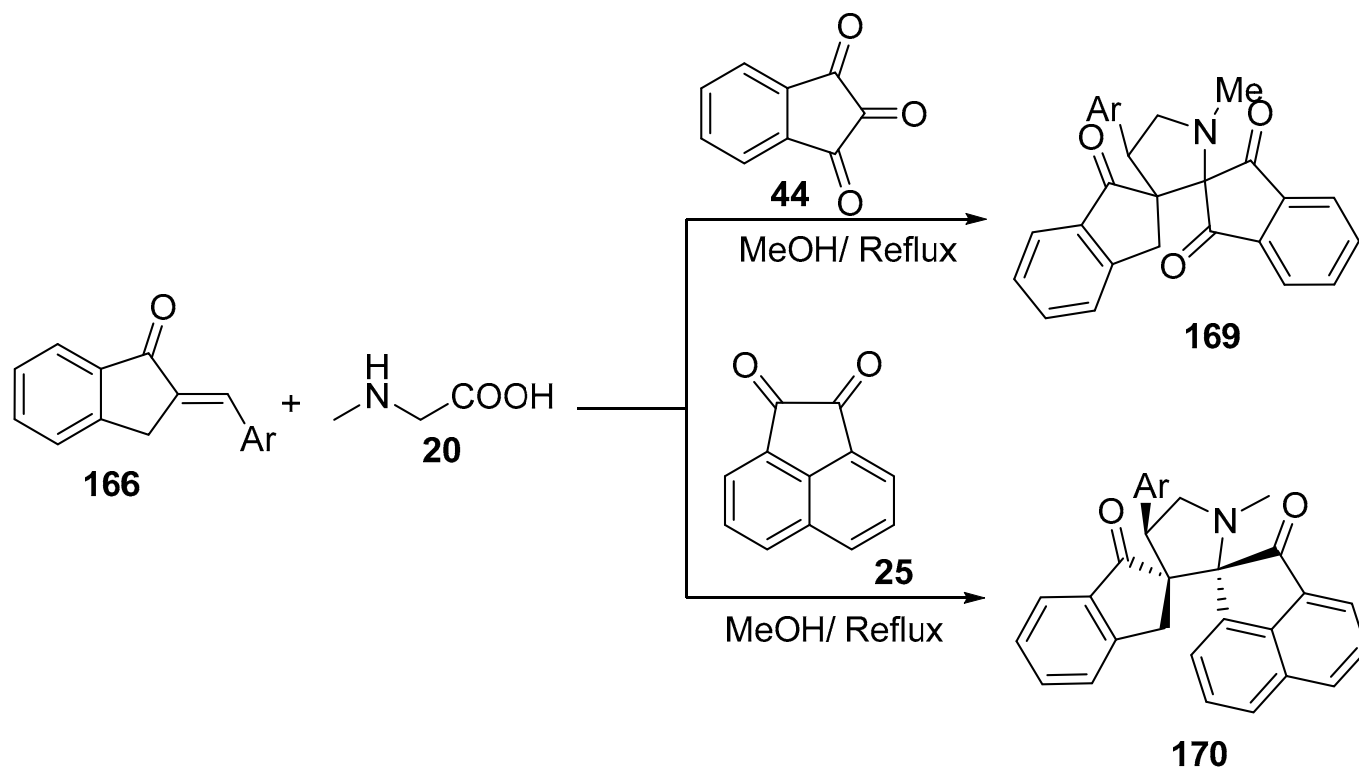
A series of dispiro compounds of type **167** were regioselectively synthesized by the cycloaddition of 2-(ylidene)-1-indanones **166** with azomethine ylides (formed from isatin derivatives **19** with sarcosine **20**) in refluxing ethanol. Promising anti-inflammatory properties were exhibited by the synthesized compounds (via a rat carrageenan paw edema assay) relative to Indomethacin (standard reference drug) [84]. Antiproliferative properties were also revealed by some of the synthesized derivatives against human metastatic melanoma cells (GaLa, LuPiCi, and LuCa), with a potency relative to that of Doxorubicin (SRB assay) (Scheme 56) [85]. In an analogous reaction, by using *L*-thioprosine **22** instead of sarcosine **20**, spiro-pyrrolothiazolyloxindole derivatives of type **168** were obtained. Some of these compounds showed activities against *Mycobacterium tuberculosis* H37Rv relative to Ethambutol (standard reference) [86].



R = Ph, 4-FC₆H₄, 2-ClC₆H₄, 4-ClC₆H₄, 4-BrC₆H₄, 2,3-Cl₂C₆H₃, 2,4-Cl₂C₆H₃, 2-MeC₆H₄, 4-MeC₆H₄, 4-MeOC₆H₄, 3,4,5-(MeO)₃C₆H₂, 4-Me₂NC₆H₄, 4-NO₂C₆H₄, 2-thienyl, 2-furanyl
 R¹ = H, Me, CH₂(1-piperidinyl), CH₂(4-morpholinyl)
 R² = H, Cl, NO₂

Scheme 56. Synthetic route towards dispiro compounds **167** and **168**.

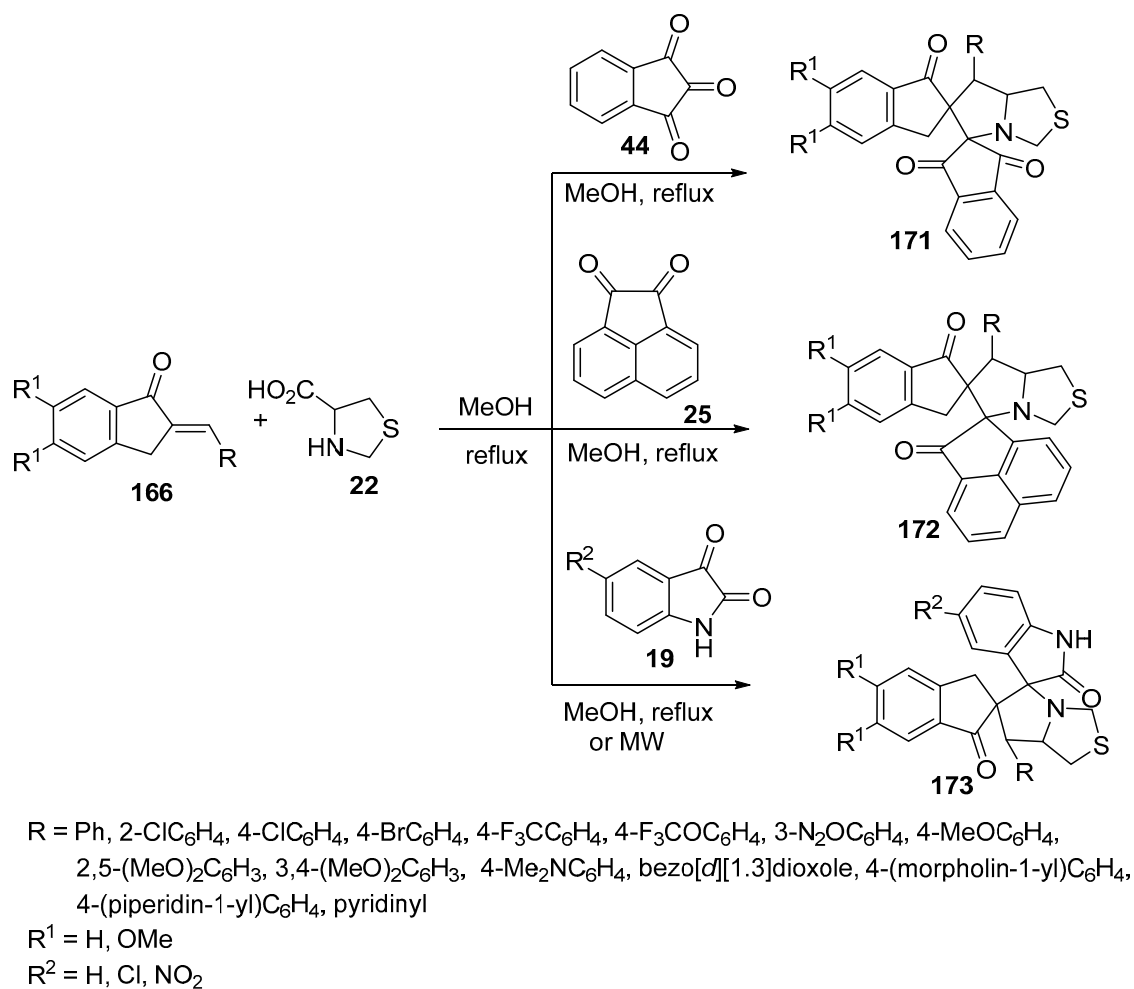
Other dispiropyrrolidines of type **169** were synthesized by the cycloaddition of azomethine ylide (formed from ninhydrin **44** and sarcosine **20**) with 2-(arylidene)-1-indanones **166** (Scheme 57). When acenaphthenequinone **25** was used instead of ninhydrin **44** in this reaction, dispiropyrrolidines of type **170** were formed in a highly regio- and stereoselective manner. Some of the synthesized derivatives—**169** and **170** showed antimycobacterial properties against *M. tuberculosis* H37Rv and INH resistant *M. tuberculosis* strains relative to Isoniazid and Ethambutol (standard reference drugs) [87,88].



Ar = Ph, 5-(4-fluorophenyl)pyridinyl, 4-chlorophenyl, 4-bromophenyl, 4-carboxyphenyl, 3-nitrophenyl, 4-trifluoromethylphenyl, 4-trifluoromethoxyphenyl, 4-methoxyphenyl, 4-carboxyphenyl, 3-nitrophenyl, benzo[*d*][1,3]dioxolyl, 4-dimethylaminophenyl, 2,5-dimethoxyphenyl, 1-[4-(piperidine-1-yl)phenyl], 1-[4-(morpholine-1-yl)phenyl]

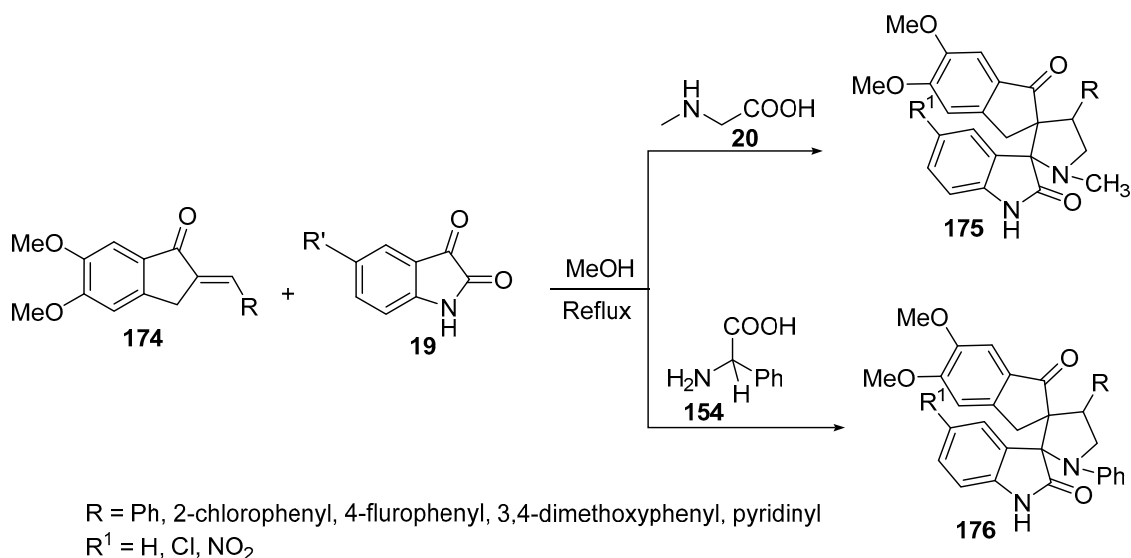
Scheme 57. Synthesis of dispiropyrrolidines **166** and **167**.

Dispiropyrrolidines **171** and **172** were obtained by the cycloaddition of 2-(ylidene)-1-indanones **166** with azomethine ylides (obtained through the condensation of *L*-thiopropine **22** with ninhydrin/acenaphthenequinone **44/25**) in refluxing methanol. Some of the synthesized compounds showed promising in-vitro antimycobacterial properties against *M. tuberculosis* H37RV relative to Cycloserine [89]. Analogously, pyrrolothiazolyloxindoles of type **173** were obtained when isatin **19** was used instead of ninhydrin **44** or acenaphthenequinone **25** in this reaction. Some of the isatin-derived compounds of type **173** exhibited inhibitory properties toward acetylcholinesterase that could be useful for Alzheimer's disease therapy (Scheme 58) [90].



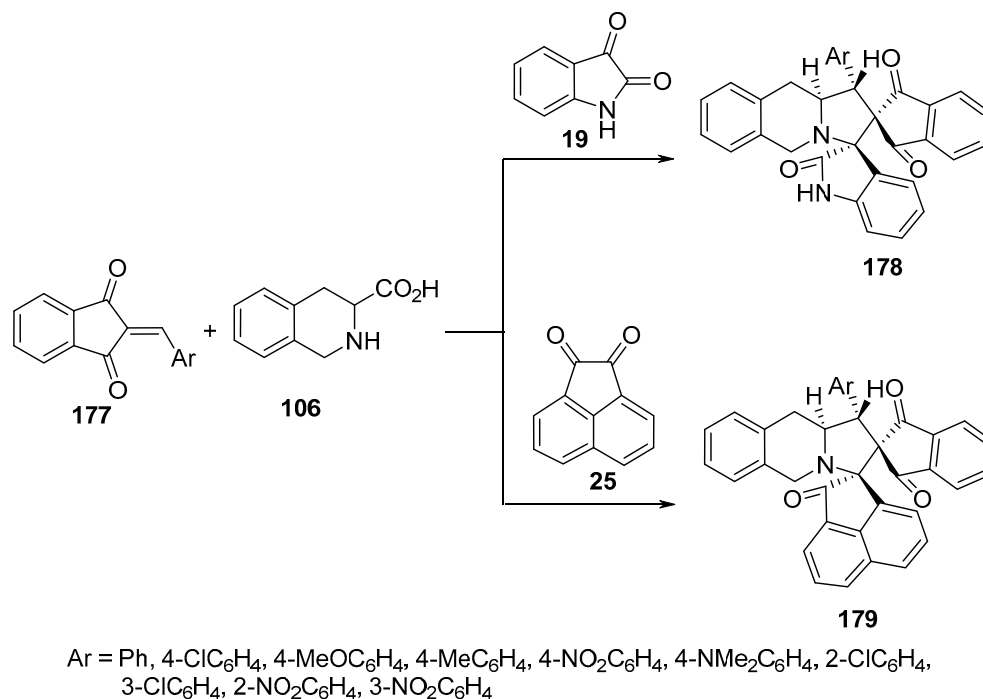
Scheme 58. Synthetic route towards dispiro compounds 171–173.

By reacting 5,6-dimethoxy-2-(arylidene)-1-indanone **174** and isatin **19** with sarcosine **20** or phenylglycine **154**, spiropyrrolidines **175** and **176**, respectively, were obtained (Scheme 59). Some of these compounds showed inhibitory activities toward acetylcholinesterase [91].



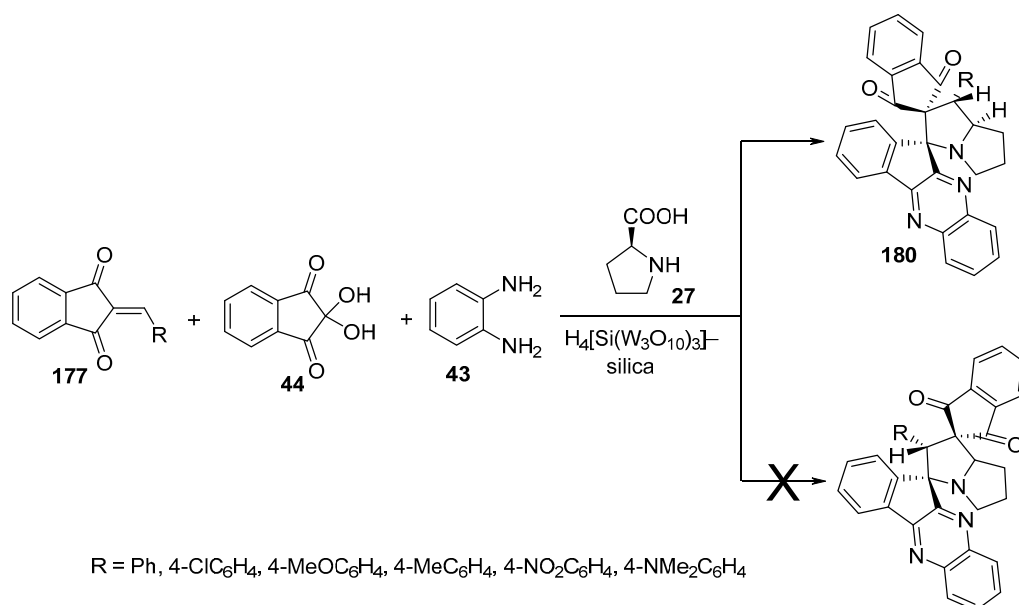
Scheme 59. Synthesis of spiropyrrolidines 175 and 176.

TiO₂-silica was used as an efficient solid-supported catalyst for the cycloaddition reaction of 2-arylidene-1,3-indanediones **177** with the corresponding azomethine ylides generated from tetrahydroisoquinoline-3-carboxylic acid **106** and isatin derivative **19** or acenaphthenequinone **25** to afford the corresponding dispiropyrroloisoquinolines **178** and **179** (Scheme 60) [92].



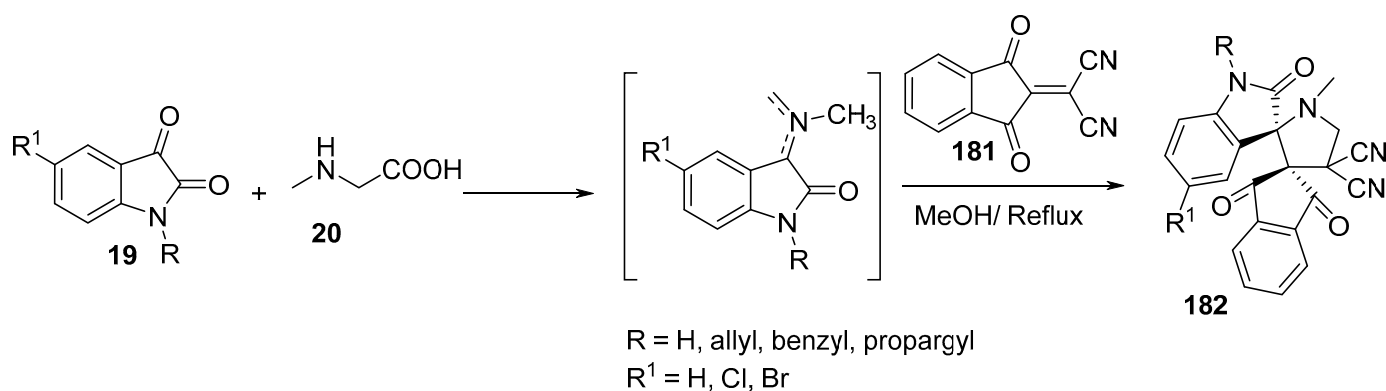
Scheme 60. Synthesis of dispiropyrroloisoquinolines **178** and **179**.

The four-component reaction of 2-arylidene-1,3-indanediones **177**, ninhydrin **44**, *o*-phenylenediamine **43**, and *L*-proline **27**, proceeding via an azomethine intermediate and in the presence of heteropolyacid H₄[Si(W₃O₁₀)₃]-silica as a catalyst in refluxing acetonitrile, afforded the dispiroindenoquinoxaline-pyrrolizidines **180** (Scheme 61) [93].



Scheme 61. Synthesis of dispiroindenoquinoxaline-pyrrolizidine **180**.

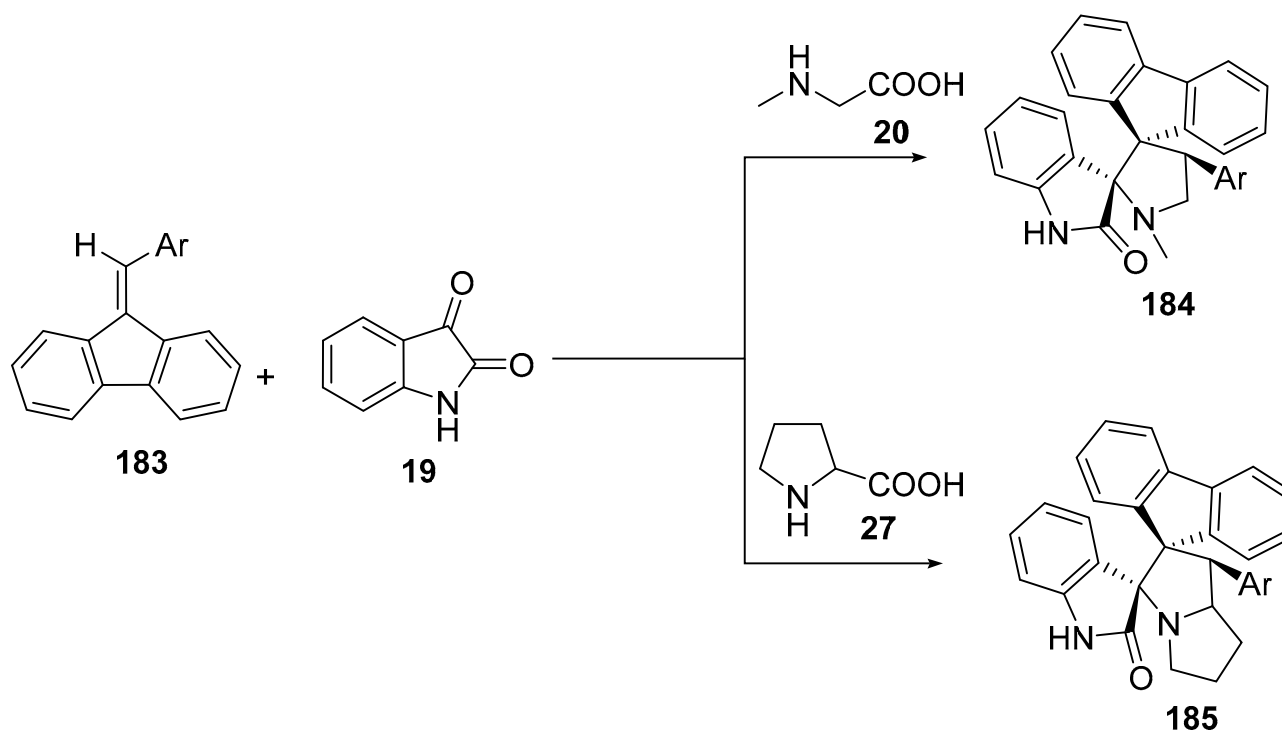
Dispiro compounds of type **182** were synthesized by the reaction of the generated azomethine ylides (from isatin **19** and sarcosine **20**) with 2-(1,3-dioxo-indan-2-ylidene) malononitrile **181** (Scheme 62) [43].



Scheme 62. Synthesis of spiroindane-1,3-diones **182**.

3.3. Fluorenes

The solvent-free reaction of (*E*)-arylidene fluorenes **183** with isatin **19** and sarcosine **20** or proline **27**, under microwave conditions, afforded the corresponding dispiro-oxindoles **184** and **185**, respectively (Scheme 63) [94].

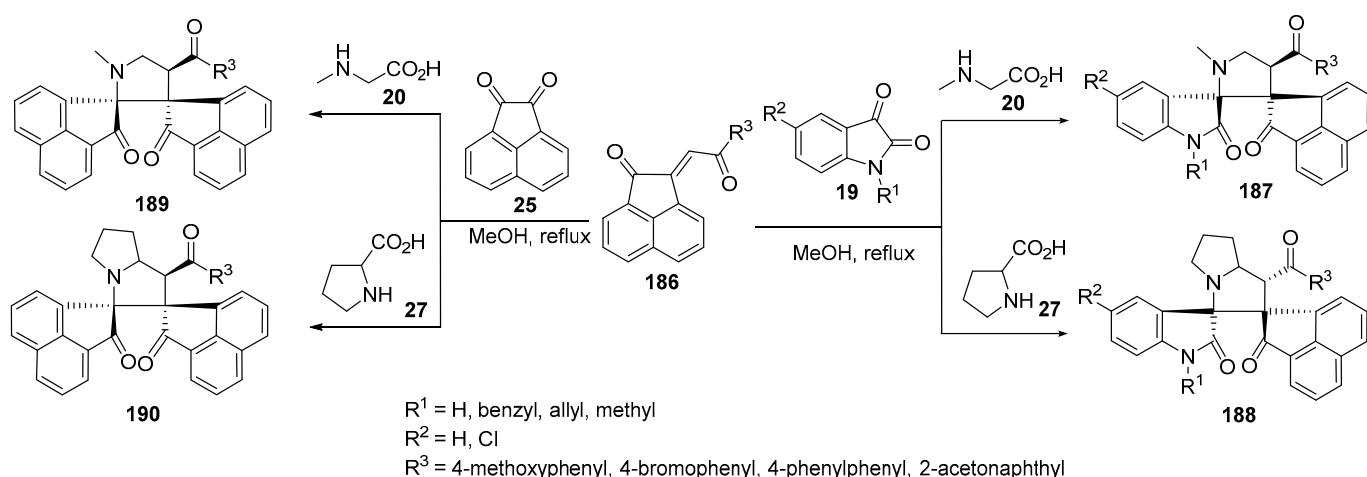


Ar = Ph, 4-MeC₆H₄, 4-MeOC₆H₄, 4-ClC₆H₄, 4-NO₂C₆H₄, 4-Me₂NC₆H₄

Scheme 63. Synthesis of dispiro-oxindoles **184** and **185**.

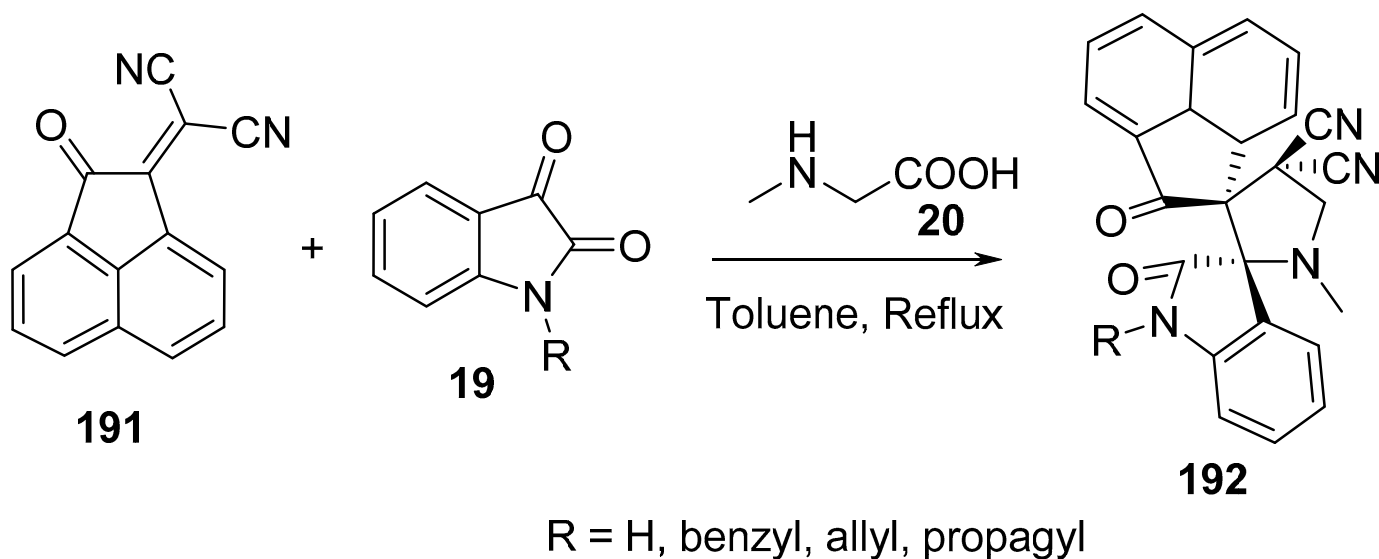
3.4. Acenaphthenes

The reaction of acenaphthenone-2-ylidene ketones of type **186** with azomethine ylides formed from the condensation of isatin **19** or acenaphthenequinone **25** and secondary amino acids (sarcosine **20** or *L*-proline **27**) in refluxing methanol afforded the corresponding spirooxindoles **187–190** (Scheme 64) [95].



Scheme 64. Synthesis of spirooxindoles 187–190.

Similarly, 2-oxo-(2*H*)-acenaphthylen-1-ylidene-malononitrile **191** afforded the corresponding dispiropyrrolidine-oxindoles **192** by its reaction with isatin **19** and sarcosine **20** in refluxing toluene (Scheme 65) [96].

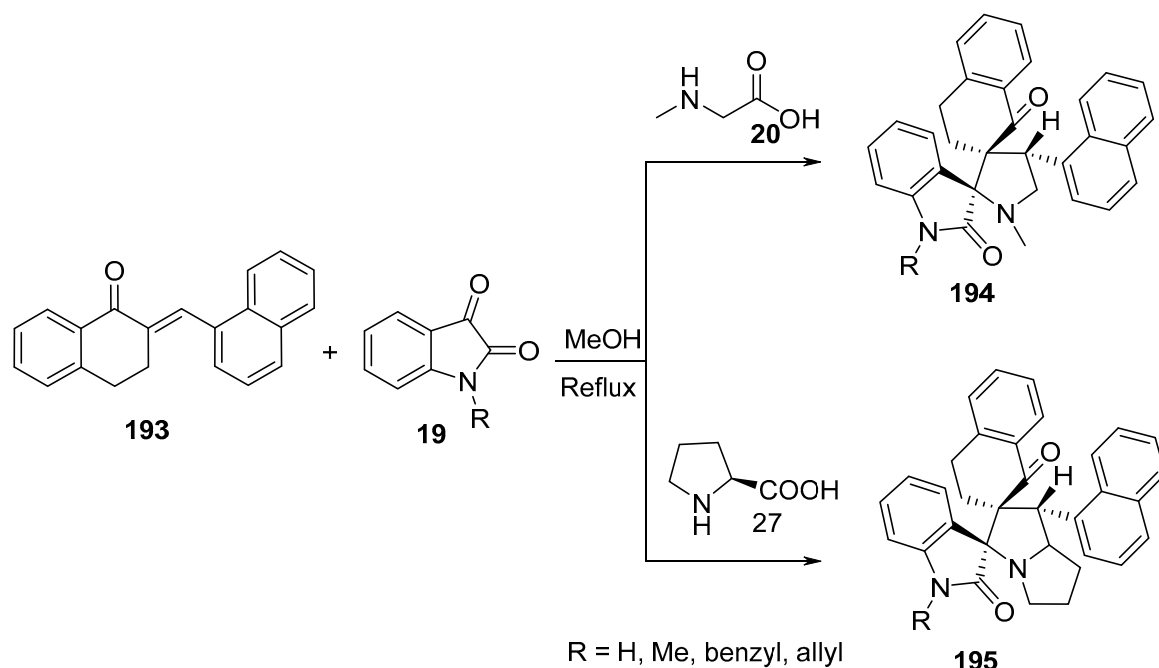
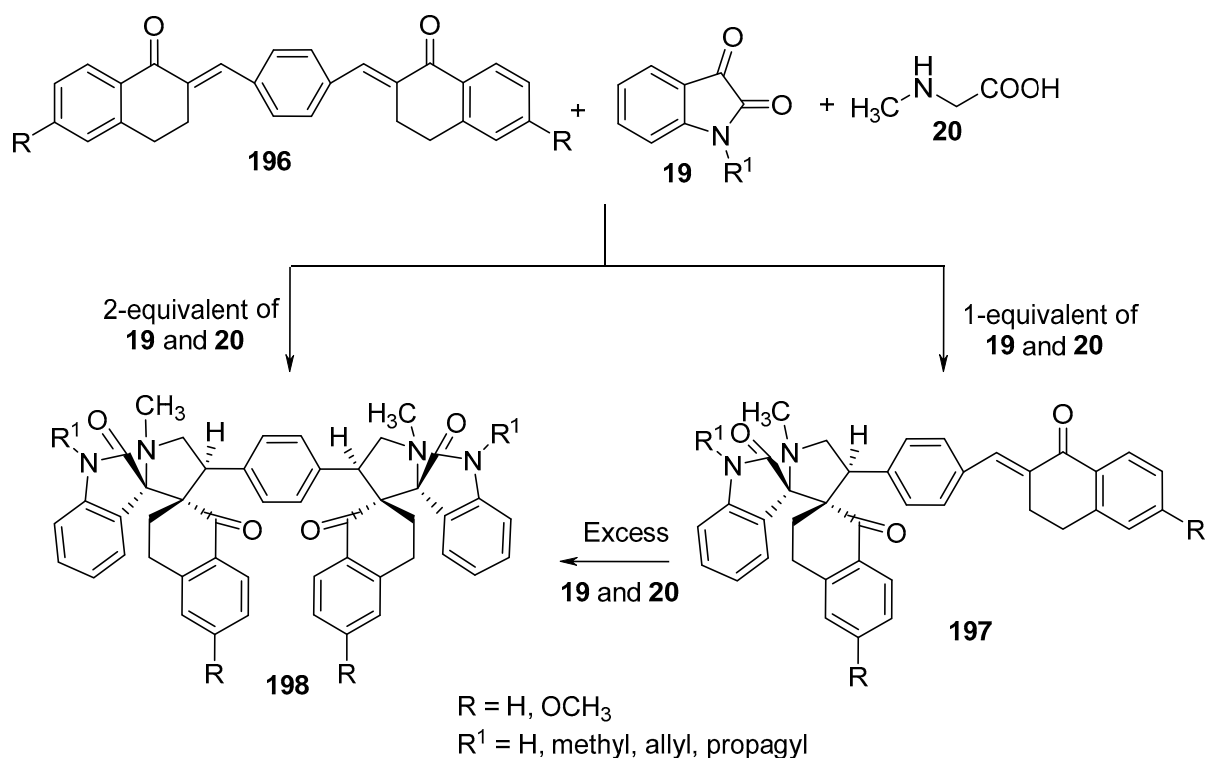


Scheme 65. Synthesis of dispiropyrrolidine-oxindoles **192**.

3.5. Tetralones

Dispiro-oxindolopyrrolidine/pyrrolizidines **194** and **195** were synthesized via the cycloaddition of (*E*)-1-naphthylidene-1-tetralone **193** with the corresponding azomethine ylides generated from isatin **19** and sarcosine **20** or *L*-proline **27** (Scheme 66) [97].

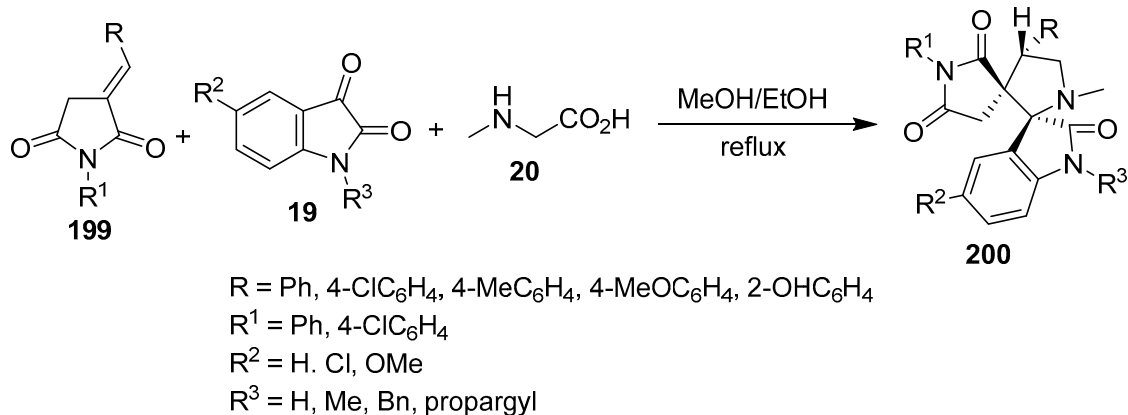
Further, the cycloaddition of 1,4-bis(3',4'-dihydro-1'-oxonaphthalen-2'-ylidene)benzene derivative **196** with azomethine ylides (from isatin **19** and sarcosine **20**) in a 1:2 molar ratio afforded the corresponding tetraspiro-bisoxindolopyrrolidine **198**. With a 1:1 ratio of the reactants, mono derivatives of type **197** were formed, which, in the presence of an excess of isatin **19** and sarcosine **20**, afforded bisoxindolopyrrolidines **198** [98] (Scheme 67).

Scheme 66. Synthesis of dispiro-oxindolopyrrolidine/pyrrolizidines **194** and **195**.Scheme 67. Synthesis of tetraspiro-bisoxindolopyrrolidines **198**.

3.6. Pyrrolidine-2,5-diones

Dispiropyrrolidines of type **200** were prepared regioselectively by the cycloaddition of 3-(ylidene)pyrrolidine-2,5-diones **199** with azomethine ylide (formed from condensation of sarcosine **20** and isatin **19**) in refluxing alcohol. Promising cholinesterase (acetylcholinesterase and butyrylcholinesterase) inhibitory properties were observed for some of the synthesized compounds (relative to Donepezil, used as the standard reference) that

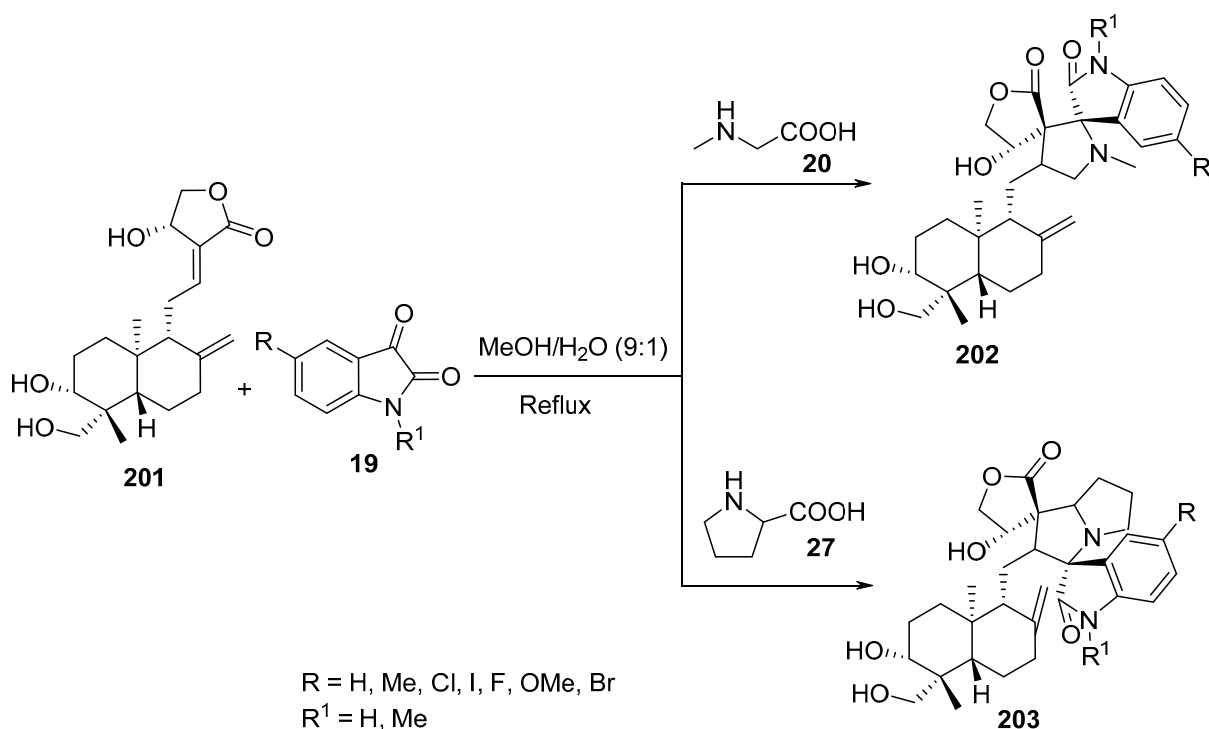
are of potential importance for fighting Alzheimer's disease (Scheme 68) [99]. Some of the synthesized **200** also revealed antibacterial activities against *Bacillus subtilis* NCIM 2718, *Staphylococcus aureus* NCIM5021, *Salmonella typhi* NCIM2501, *Pseudomonas aeruginosa* NCIM 5029, and *Proteus vulgaris* NCIM2813 relative to Ampicillin [100].



Scheme 68. Synthetic route towards dispiro[indoline-3,2'-pyrrolidine-3',3''-pyrrolidines] **200**.

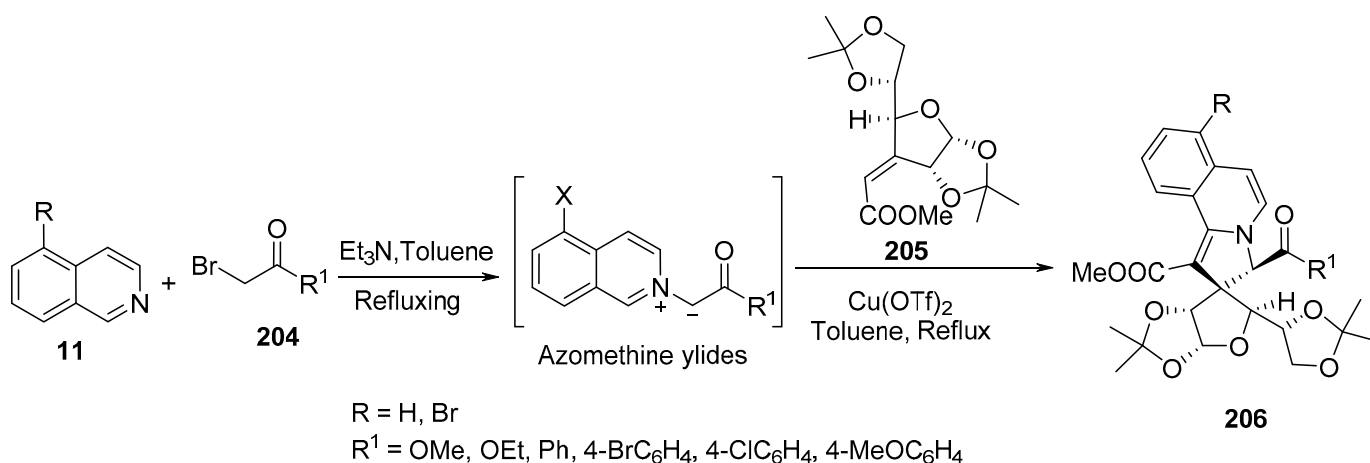
3.7. Lactones

Dispiropyrrolidino/pyrrolizidino-oxindoles **202** and **203** were obtained through the cycloaddition of α,β -unsaturated- γ -lactone **201** with isatin **19**/sarcosine **20** or isatin **19**/proline **27** reagent systems (Scheme 69) [101].



Scheme 69. Synthesis of dispiropyrrolidino/pyrrolizidino-oxindoles **202** and **203**.

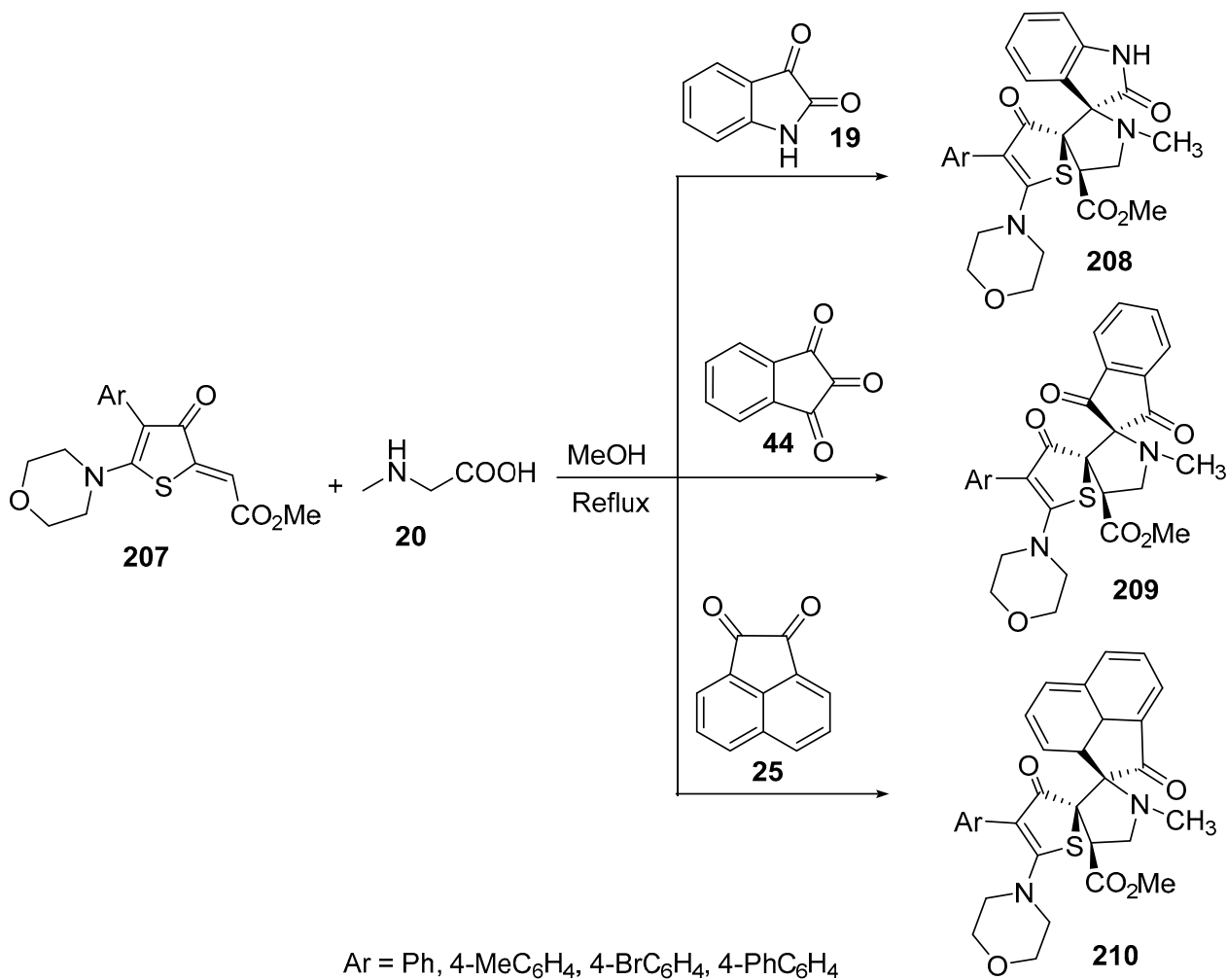
Glycospiro-2,3-dihydropyrrolo[2,1-*a*]isoquinolines **206** were synthesized by the reaction of 3-deoxy-3-*C*-[(*Z*)-(methoxycarbonyl)methylene]-1,2:5,6-di-*O*-isopropylidene- α -*D*-glucofuranose **205** with isoquinoline-based azomethine ylide formed from isoquinolines **11** and alkyl bromoacetates or 2-bromoacetophenones **204** in the presence of $\text{Cu}(\text{OTf})_2\text{-Et}_3\text{N}$ as a catalyst (Scheme 70) [102].



Scheme 70. Synthesis of glycospiro-2,3-dihydropyrrolo[2,1-*a*]isoquinolines **206**.

3.8. Thiophenones

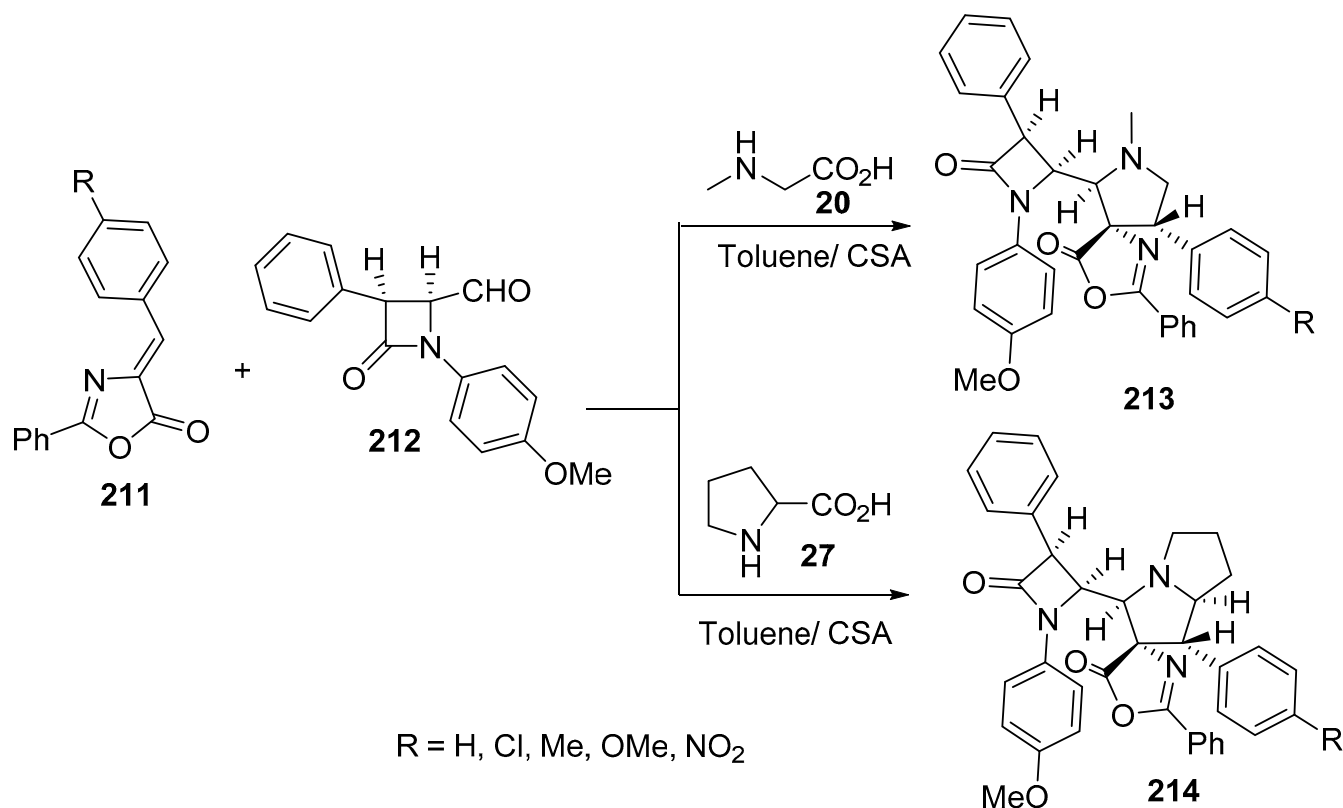
The reaction of 2-(ylidene)thiophen-3-ones **207** with various azomethine ylides generated from sarcosine **20** and different ketones (isatin **19**, ninhydrin **44** or acenaphthoquinone **25**) afforded the corresponding dispiropyrrolidine containing-thiophenones **208–210** in good yields (Scheme 71) [103].



Scheme 71. Synthesis of dispiropyrrolidine containing-thiophenones **208–210**.

3.9. Oxazolones

The reaction of 4-ylidene-5-(4*H*)-oxazolones **211** with azomethine ylide derived from *cis*-4-formyl-2-azetidinone **212** and sarcosine **20** or pyrrolidine **27**, in the presence of camphor sulphonic acid (CSA) as a catalyst, afforded the corresponding spiro[3.4']-(oxazol-5'-one)-pyrrolidines **213** and spiro[3.4']-(oxazol-5'-one)-pyrrolizidines **214**, respectively (Scheme 72) [104].

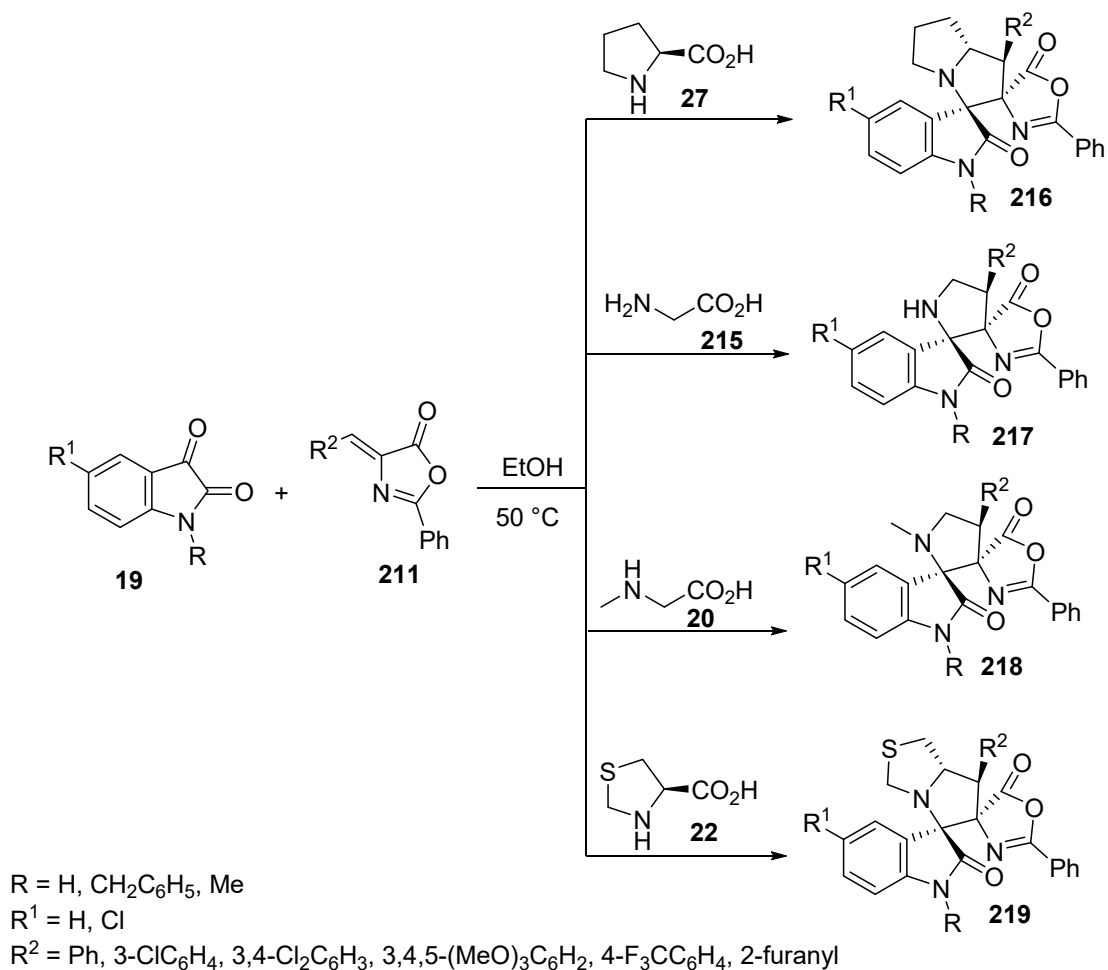


Scheme 72. Synthesis of spiro[3.4']-(oxazol-5'-one)-pyrrolidines **213** and spiro[3.4']-(oxazol-5'-one)-pyrrolizidines **214**.

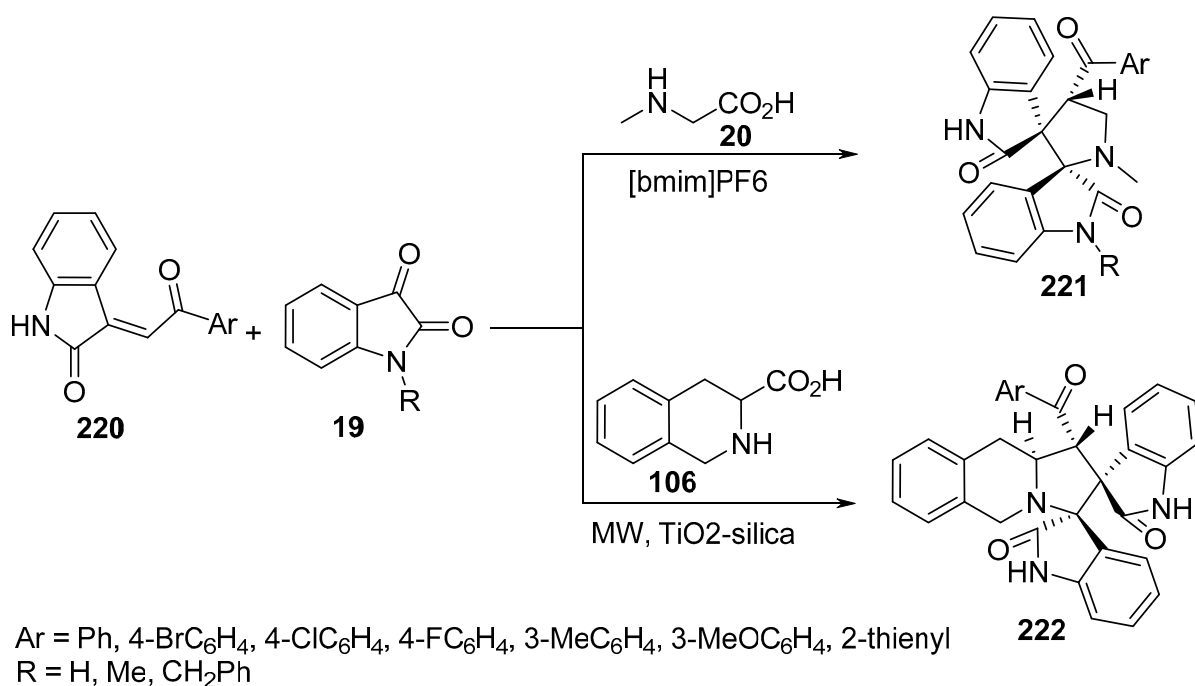
Spiro-compounds of types **216–219** were obtained via the cycloaddition reaction of 4-ylidene-5-oxazolones **211** and azomethine ylides (generated from isatin **19** and the appropriate α -amino acids). Some of the synthesized compounds showed considerable antitumor properties against breast cancer (MCF7, MDA-MB-231, and MDA-MB-468) and hepatocellular (HepG2, HCCC-9810, and HuH7) cell lines (MTT assay) relative to Gefitinib and Sorafenib (standard references) (Scheme 73) [105].

3.10. Indoles

The azomethine ylide (formed from isatin **19** and sarcosine **20**) underwent cycloaddition with 3-arylmethyleneindol-2-ones **220** under green chemistry conditions in an ionic liquid ([bmim]PF₆, 1-butyl-3-methylimidazolium hexafluorophosphate) to afford the corresponding dispiropyrrrolidine-bisoxindoles **221** [106]. TiO₂-silica was also used as a solid-supported catalyst under microwave conditions for the synthesis of dispiropyrrroloisoquinolines **222** via the three-atom component cycloaddition reaction of azomethine ylide (generated from tetrahydroisoquinoline-3-carboxylic acid **106** and isatin **19**) with **220** [92] (Scheme 74).

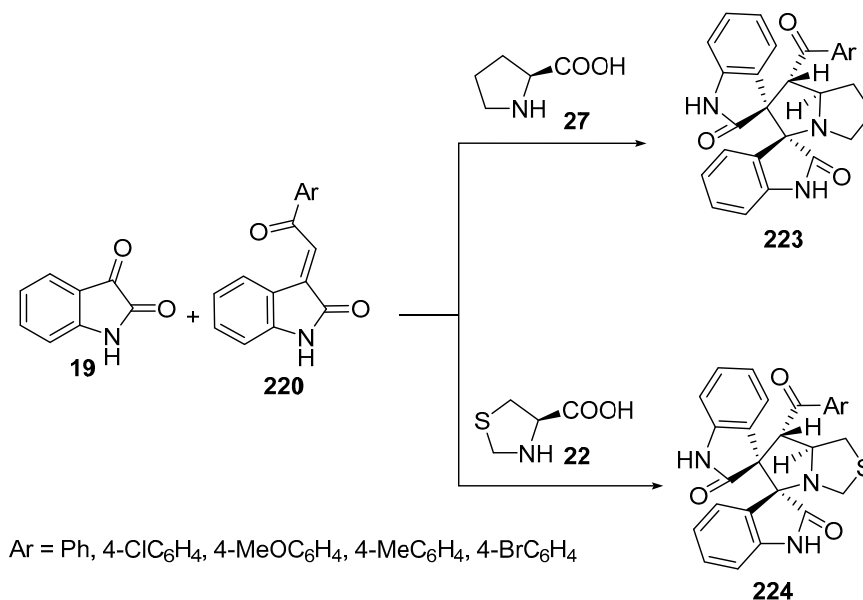


Scheme 73. Synthetic route towards spiro-compounds 216–219.



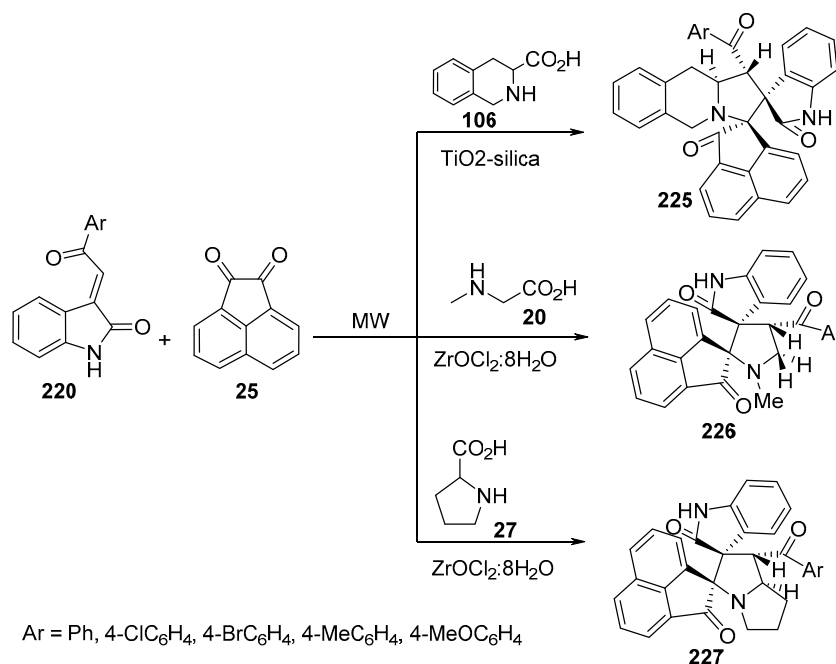
Scheme 74. Synthesis of dispiropyrrolidines 221 and 222.

Dispiro-oxindolopyrrolizidines **223** and dispiro-oxindolothienopyrroles **224** could also be obtained by the reaction of azomethine ylides (generated from isatin **19** with *L*-proline **27** or *R*-thioprolinone **22**) with 3-arylmethyleneindol-2-ones **220** under ultrasonication conditions in the presence of silica as a catalyst (Scheme 75) [107].



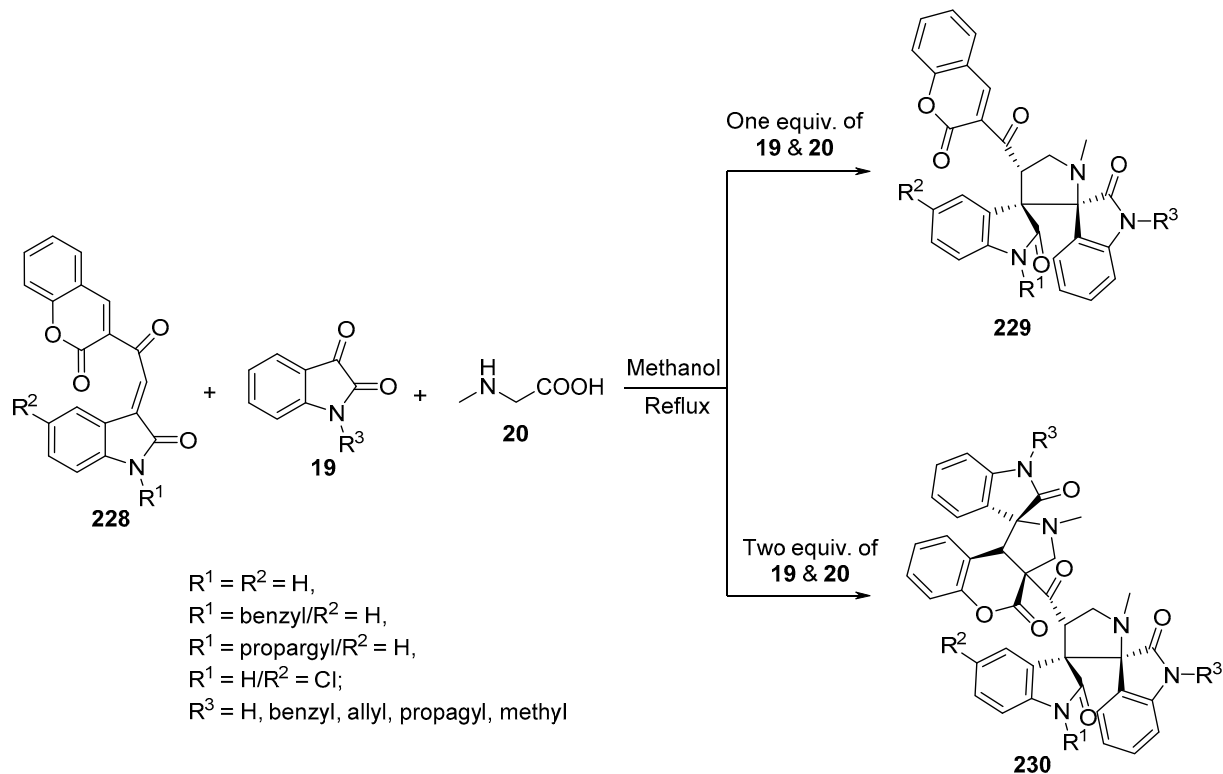
Scheme 75. Synthesis of dispiro-oxindolopyrrolizidines **223** and dispiro-oxindolothienopyrroles **224**.

Similarly, the cycloaddition reaction of 3-arylmethyleneindol-2-ones **220** with azomethine ylide (formed from tetrahydroisoquinoline-3-carboxylic acid **106** and acenaphthenequinone **25**) using TiO₂-silica as a solid-supported catalyst under microwave conditions yielded dispiropyrrroloisoquinoline **225** [92]. Ball-clay-supported zirconium oxychloride octahydrate was also used as a catalyst in the cycloaddition reaction of azomethine ylides (generated from acenaphthenequinone **25** and sarcosine **20** or *L*-proline **27**) to produce spiro-oxindolopyrrolidine **226** and spiro-oxindolopyrrolizidine **227**, respectively (Scheme 76) [108].



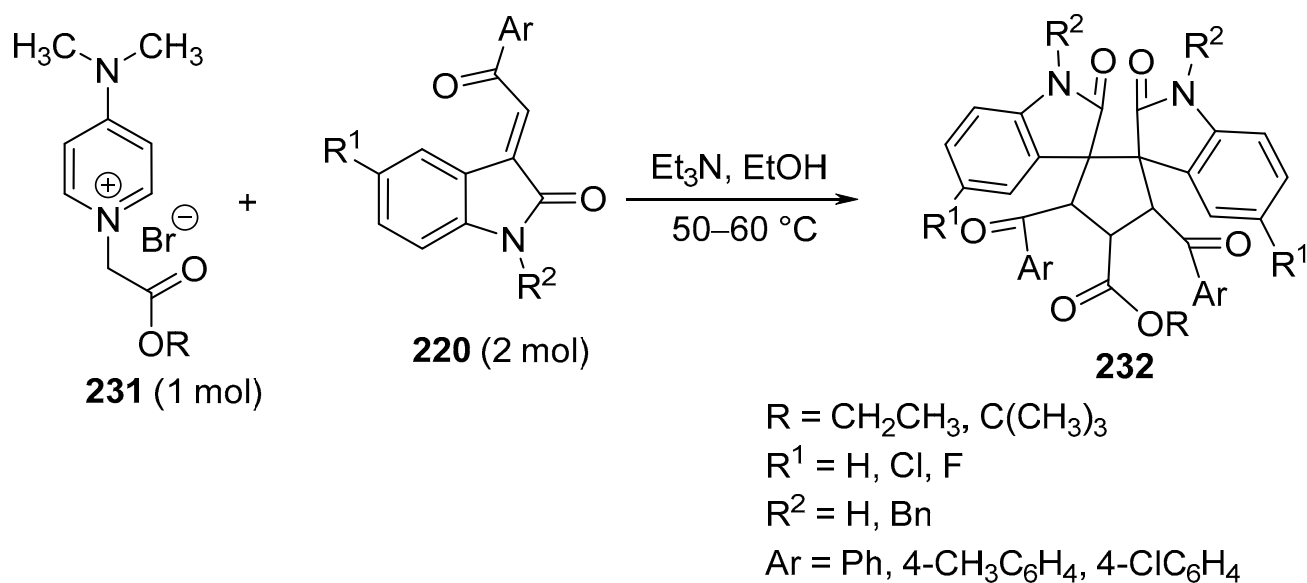
Scheme 76. Synthesis of spiro-pyrrolidines **225**–**227**.

Spiro-oxindoles of type **229** were obtained by reacting isatin **19**, sarcosine **20**, and 3-[2-oxo-ethylidene]indolin-2-one **228** in equimolar quantities whereas spiro-oxindole derivatives of type **230** were formed when isatin **19** and sarcosine **20** were used at a two-fold degree of molar excess over acceptor **228** (Scheme 77) [109].



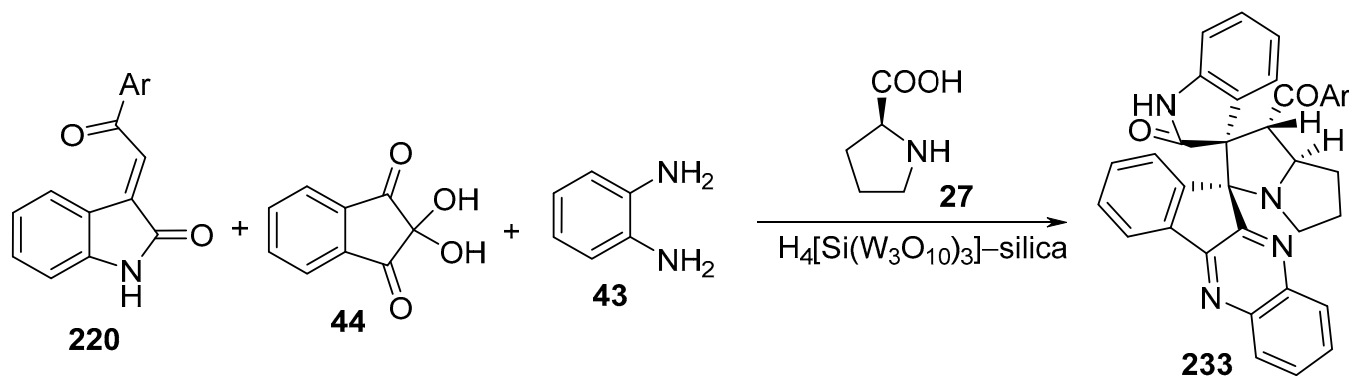
Scheme 77. Synthesis of spiropyrrolidinyl-oxindoles **229** and **230**.

Another dispirocyclopentanebisoxindole **232** can be obtained by the cycloaddition of azomethine ylides generated from 4-dimethylamino-1-alkoxycarbonylmethylpyridinium bromide **231** and aroylmethyleneindol-2-one **220** (Scheme 78) [110].



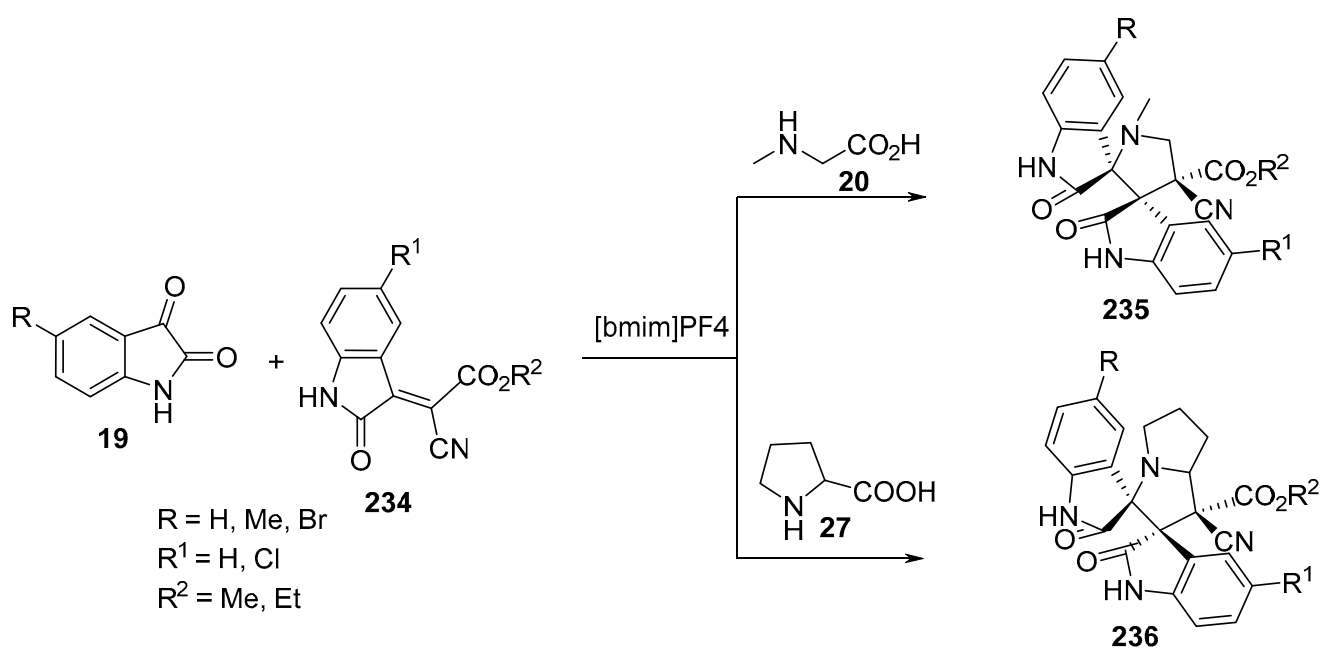
Scheme 78. Synthesis of dispirocyclopentanebisoxindole **232**.

The cycloaddition of aroylmethyleneindol-2-one **220** with azomethine ylide formed from indenoquinoline-11-one (generated in situ from ninhydrin **44** and *o*-phenylenediamine **43**) and *L*-proline **27** was catalyzed by eteropolyacid $H_4[Si(W_3O_{10})_3]$ -silica and afforded the corresponding dispiroindenoquinoline-pyrrolizidine **233** (Scheme 79) [91].



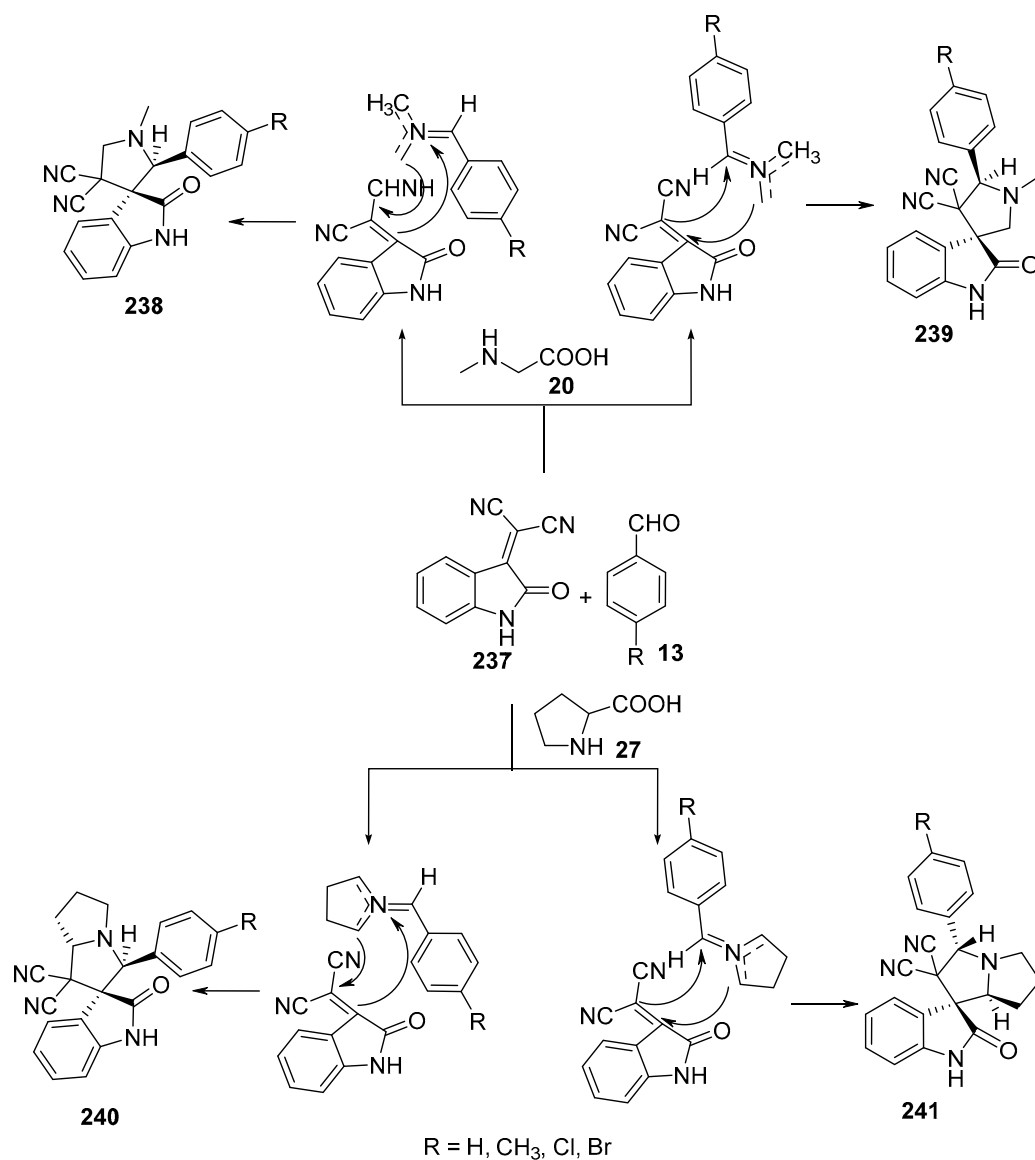
Scheme 79. Synthesis of dispiroindenoquinoline-pyrrolizidine **233**.

The reaction of azomethine ylides—formed from the condensation of isatin **19** and sarcosine **20** or proline **27** in an ionic liquid [bmim] BF₄ (without using any catalyst)—with 2-cyano-2-(2-oxoindolin-3-ylidene)acetate **234** yielded the corresponding dispiropyrrrolidine-bisoxindole **235** and dispiropyrrrolizidine-bisoxindole **236**, respectively (Scheme 80) [111].



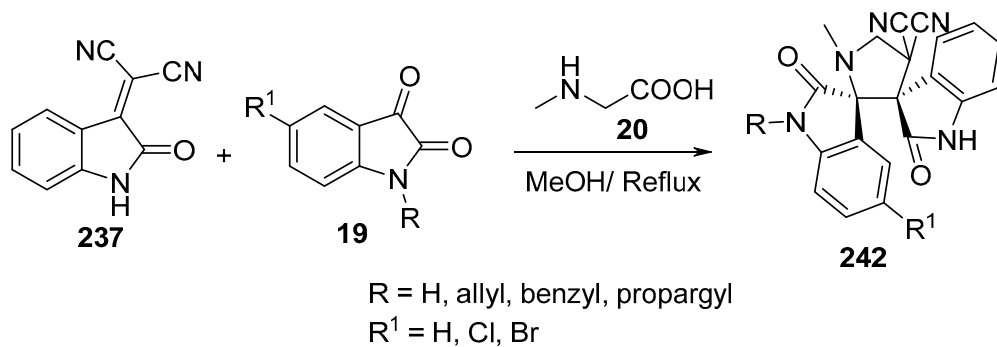
Scheme 80. Synthesis of dispiropyrrrolidine-bisoxindoles/dispiropyrrrolizidine-bisoxindoles **235/236**.

Spiropyrrrolidine/spiropyrrrolizine-oxindoles **238–241** were synthesized by a multi-component cycloaddition reaction of 2-oxo-(3*H*)-indol-3-ylidene-malononitrile **237** with azomethine ylides (generated from aromatic aldehyde **13** and sarcosine **20** or *L*-proline **27**) in refluxing toluene containing molecular sieves (3 Å) (Scheme 81) [112].



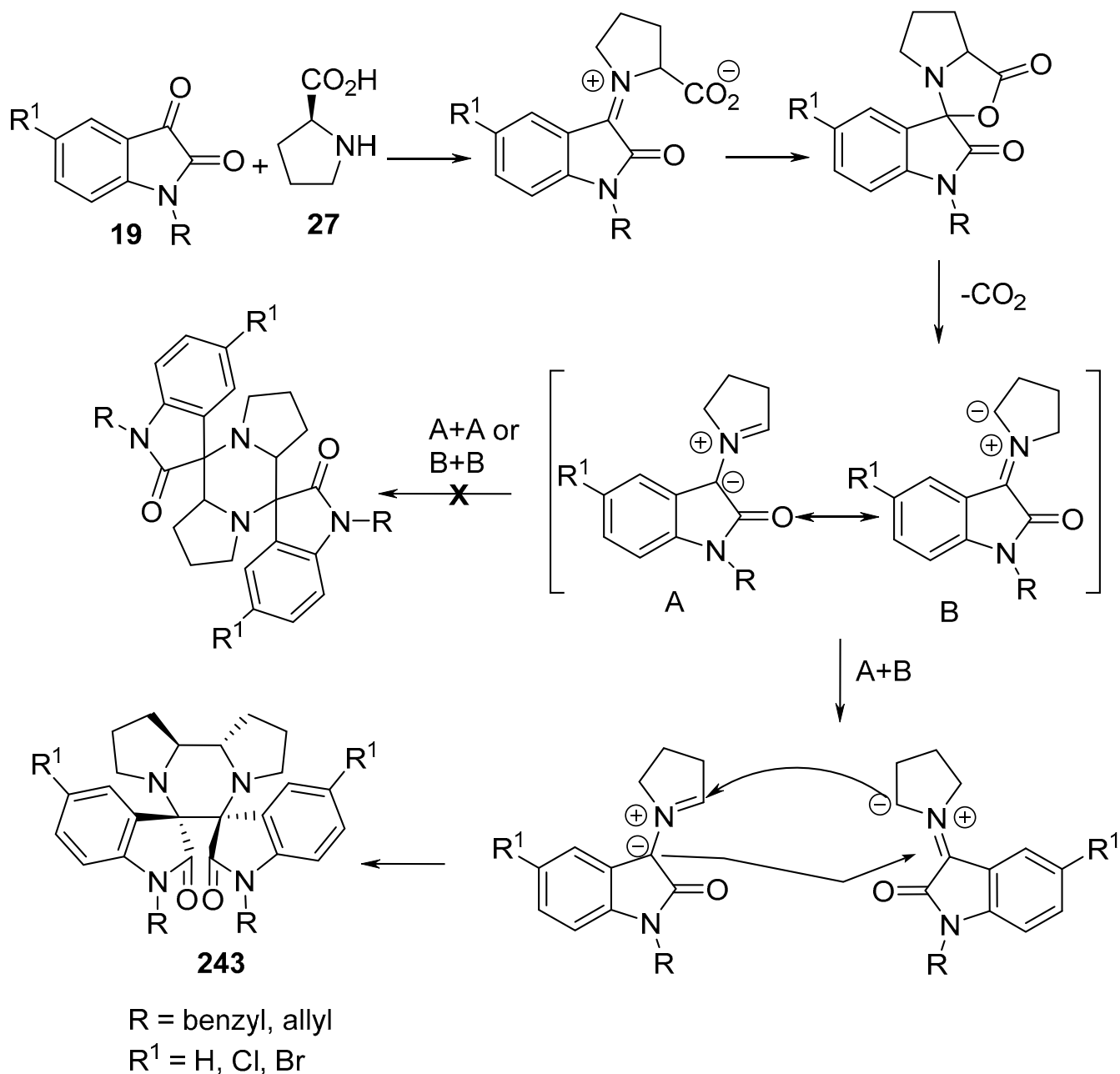
Scheme 81. Synthesis of spiroindole derivatives 238–241.

In addition, dispiroindole-bisoxindole derivatives of type 242 were obtained from a three-atom component reaction of isatin 19, sarcosine 20, and isatylydene malononitrile 237 with high regioselectivity (Scheme 82) [43].



Scheme 82. Synthesis of dispiroindole-bisoxindole 242.

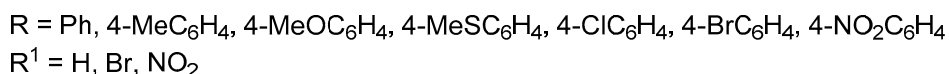
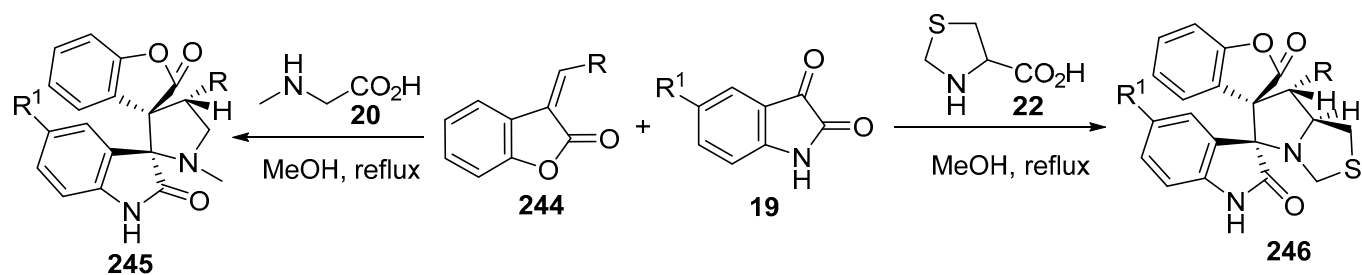
Dispiro-oxindoles of type **243** were obtained by the dimerization of in situ generated azomethine ylides (A and B) via A+B pathways. X-Ray studies supported the postulated structures of type **243** (Scheme 83) [113].



Scheme 83. Synthesis of dispiro-oxindole **243**.

3.11. Benzofuran-2-ones

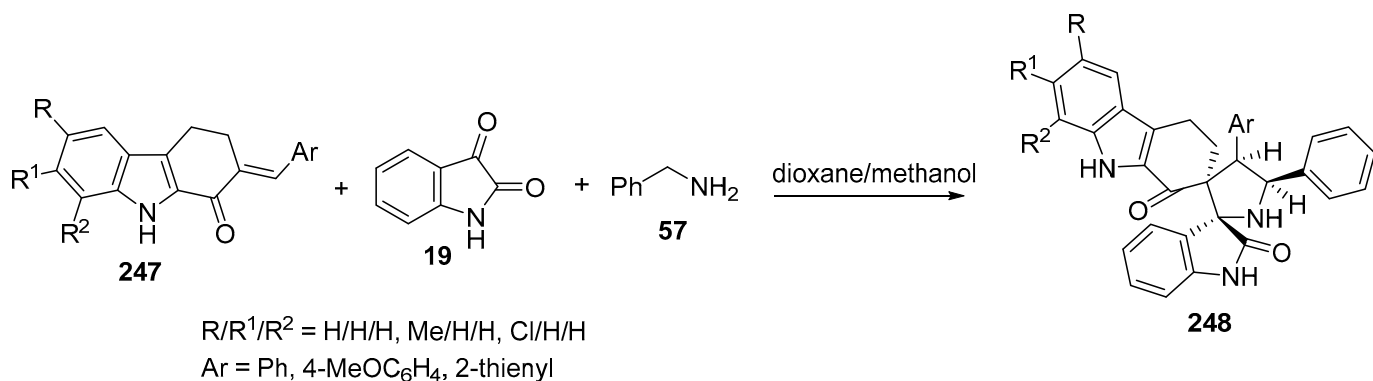
Dispiro-oxindolopyrrolidine **245** and dispiro-oxindolopyrrolthiazole **246** were obtained by a multi-component reaction of 3-(ylidene)benzofuran-2-one **244** with isatin **19** and the appropriate α -amino acid (sarcosine **20** or thioproline **22**, respectively) in refluxing methanol. Some of the synthesized compounds revealed promising antimycobacterial (*M. tuberculosis* H37Rv) properties relative to pyrazinamide (standard reference) (Scheme 84) [114].



Scheme 84. Synthetic route towards dispiro-oxindolopyrrolidine **245** and dispiro-oxindolopyrrolothiazole **246**.

3.12. Keto-Carbazoles

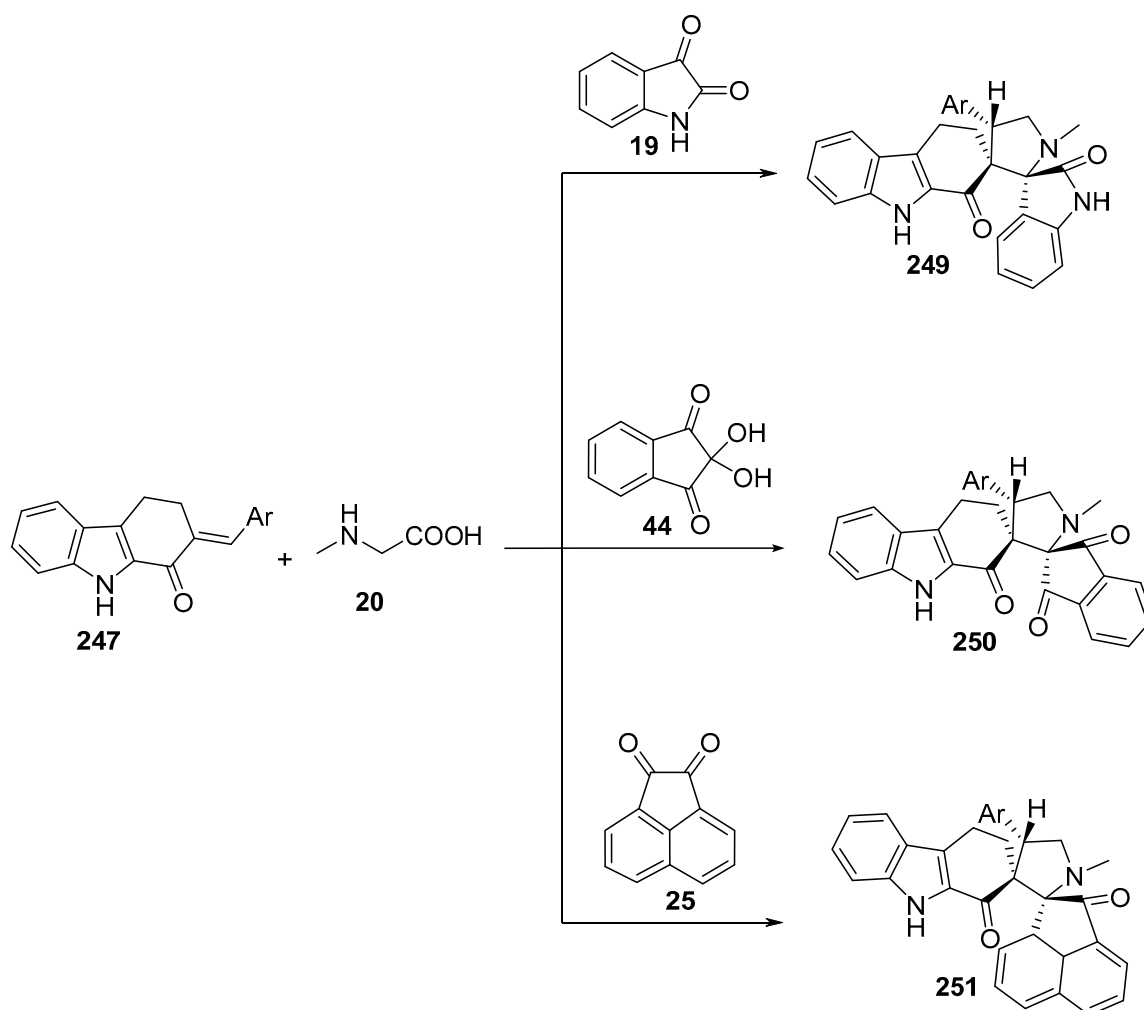
Dispiro[carbazole-2,3'-pyrrolo-2',3''-indole] derivatives of type **248** were synthesized regio- and stereoselectively by the reaction of 2-ylidene-1*H*-carbazol-1-one **247** and in situ-generated azomethine ylide (formed from isatin **19** and benzylamine **57**). Some of the obtained compounds revealed antiproliferative properties (MTT assay) via apoptosis induction against MCF7 (breast) and A-549 (lung) cancer cell lines relative to Cisplatin (Scheme 85) [115].



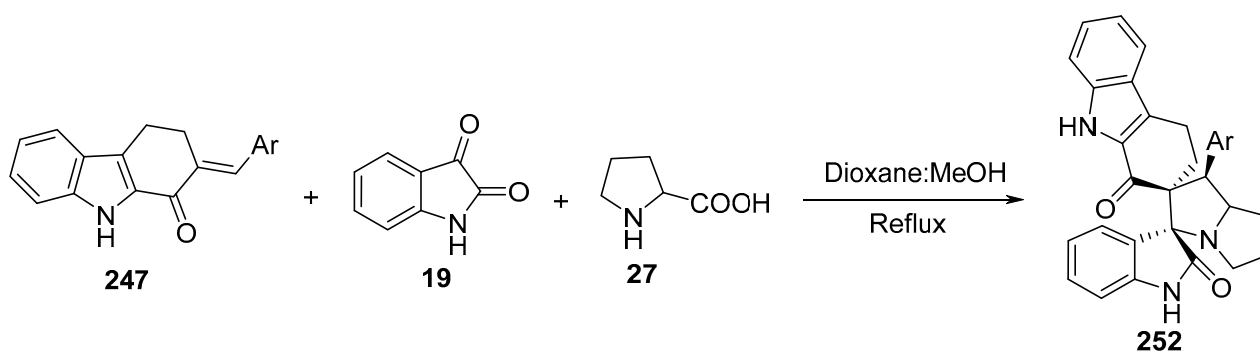
Scheme 85. Synthesis of dispiro[carbazole-2,3'-pyrrolo-2',3''-indoles] **248**.

The reaction of (*E*)-2-arylidene-1-ketocarbazole **247** with various azomethine ylides generated from sarcosine **20** and di/tri ketone (isatin **19**, ninhydrin **44**, acenathenequinone **25**) under microwave irradiation afforded the corresponding ketocarbazolodispiropyrrrolidines **249–251** (Scheme 86). Some of the synthesized compounds showed antimicrobial properties against *Proteus vulgaris*, *Proteus mirabilis*, *Staphylococcus aureus*, and *Salmonella typhi* relative to Tetracycline [116].

Similarly, dispiro-oxindolopyrrolizidines of type **252** were prepared by reacting (*E*)-2-arylidene-1-ketocarbazole **247** with the azomethine ylide formed from isatin **19** and proline **27** (Scheme 87). Some of the products showed antimicrobial activities against human pathogens (*Proteus vulgaris*, *Proteus mirabilis*, *Staphylococcus aureus*, and *Salmonella typhi*) relative to Tetracycline and acted as inhibitors of plant fungal pathogen mycelial growth (*Fusarium oxysporum* and *Macrophomena phaseolina*) relative to the standard reference—Carbendazim [117].



Scheme 86. Synthesis of ketocarbazolodispiropyrrolidines 249–251.

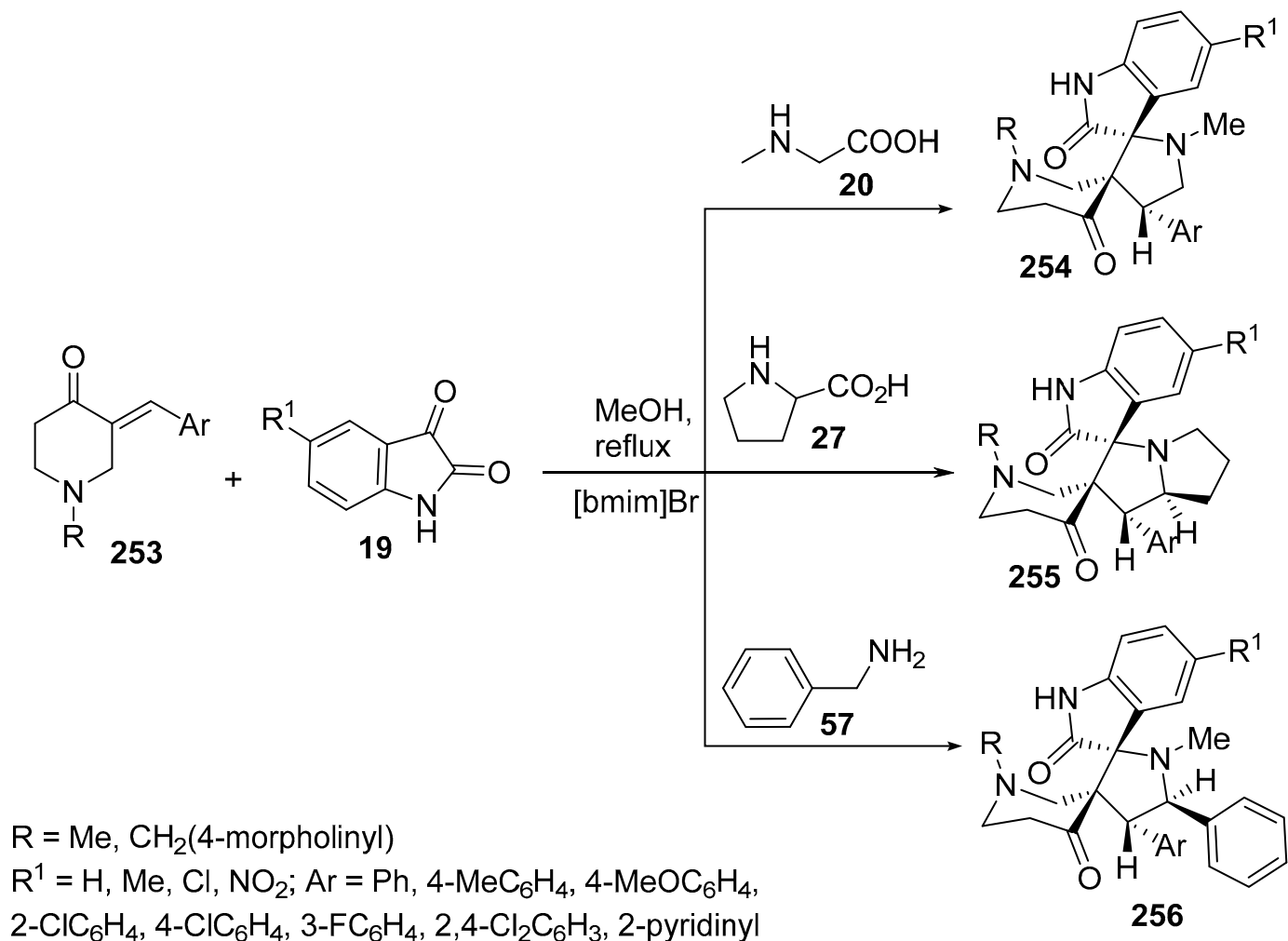


Scheme 87. Synthesis of dispiro-oxindolopyrrolizidines 252.

3.13. Piperidones

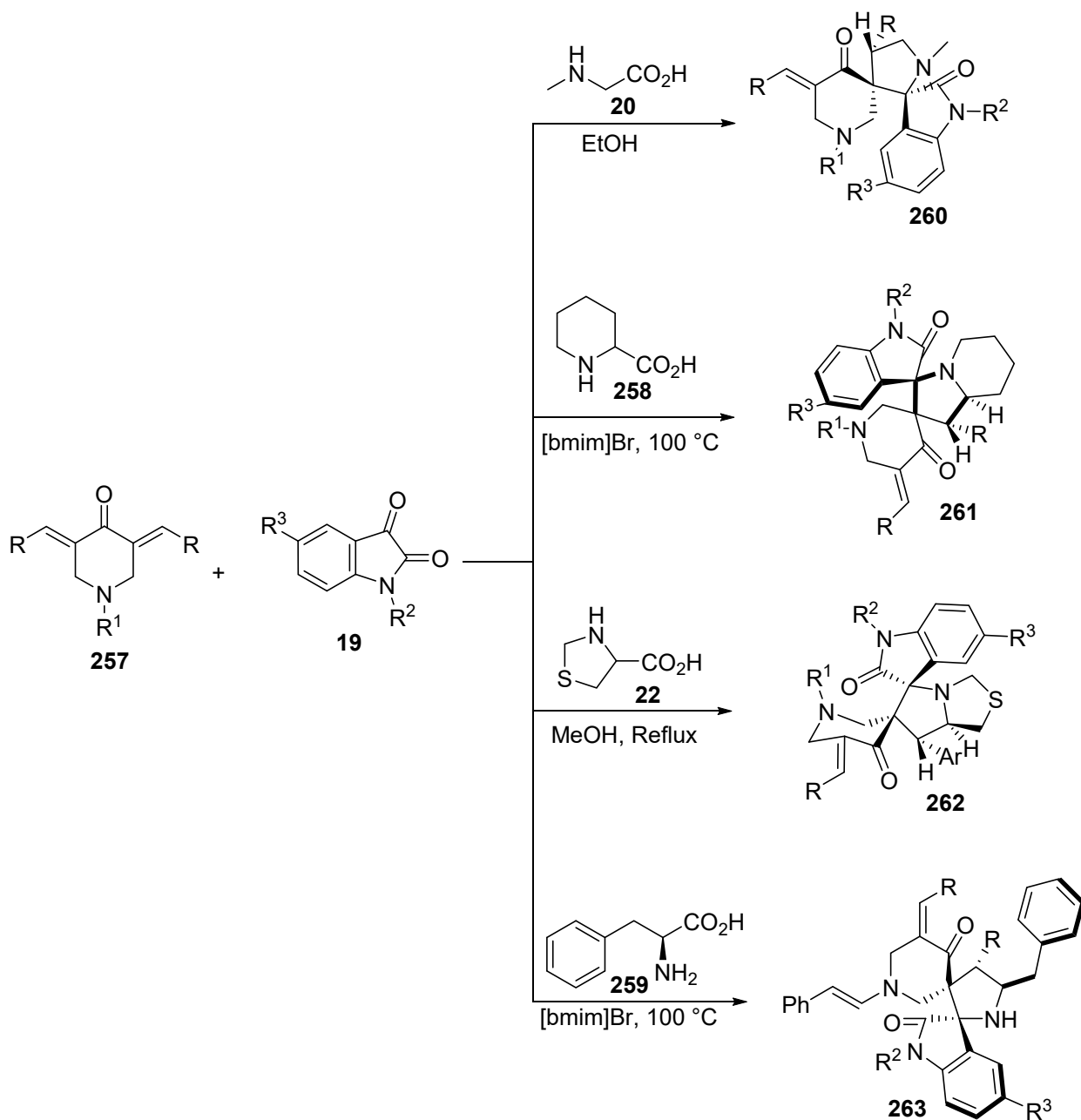
The reaction of isatin **19** with various amines (sarcosine **20**, proline **27**, and benzylamine **57**) in refluxing methanol or in ionic liquid [bmim]Br generated the corresponding azomethine ylides that was added to 3-(arylidene)-4-piperidones **253** to form the corresponding spiro-piperido-pyrrolizines/pyrrolidines **254–256** (Scheme 88). Some of the products showed activities against *Mycobacterium tuberculosis* H37Rv (MTB), multi-drug

resistant *M. tuberculosis* (MDR-TB), and *Mycobacterium smegmatis* (MC2) relative to ethambutol and pyrazinamide (standard references) [118], and also had acetyl- and butyrylcholinesterase inhibitory properties (of potential use against Alzheimer's disease) relative to galantamine [119].



Scheme 88. Synthesis of spiro-piperido-pyrrolizines/pyrrolidines 254–256.

A variety of dispiro-heterocycles of types 260–263 were obtained via azomethine ylide intermediates (formed from isatin 19 and sarcosine 20, piperidine-2-carboxylic acid 258, thioproline 22, or 2-amino-3-phenylpropanoic acid 259) in a reaction with 3,5-bis(ylidene)-4-piperidone 257 (Scheme 89). Some of the synthesized analogs revealed considerable antiproliferation properties against a variety of tumor cell lines [120–123]. Promising anti-inflammatory properties were also exhibited by some of the synthesized compounds (50 mg/kg) in a rat model of carrageenan-induced paw edema (anti-edematous test) relative to indomethacin (10 mg/kg) [120,124]. Some derivatives of compound 262 showed activities against *Mycobacterium tuberculosis* H37Rv (MTB) and multi-drug resistant *M. tuberculosis* (MDR-TB) relative to ethambutol and pyrazinamide (standard references) [125], and had antifungal properties against *Candida albicans* ATCC 10231 with high inhibition of the fungal hyphae relative to fluconazole (standard reference drug) [126].



R = Ph, 2-BrC₆H₄, 4-BrC₆H₄, 2-ClC₆H₄, 4-ClC₆H₄, 2-FC₆H₄, 4-FC₆H₄, 2,4-Cl₂C₆H₃, 2-MeC₆H₄, 3-MeC₆H₄, 4-MeC₆H₄, 4-ⁱPrC₆H₄, 2-MeOC₆H₄, 3-MeOC₆H₄, 4-MeOC₆H₄, 2,4-MeO₂C₆H₃, 3-NO₂C₆H₄, 2-thienyl, 5-methyl-2-furanyl, 3-pyridinyl

R¹ = Me, Et

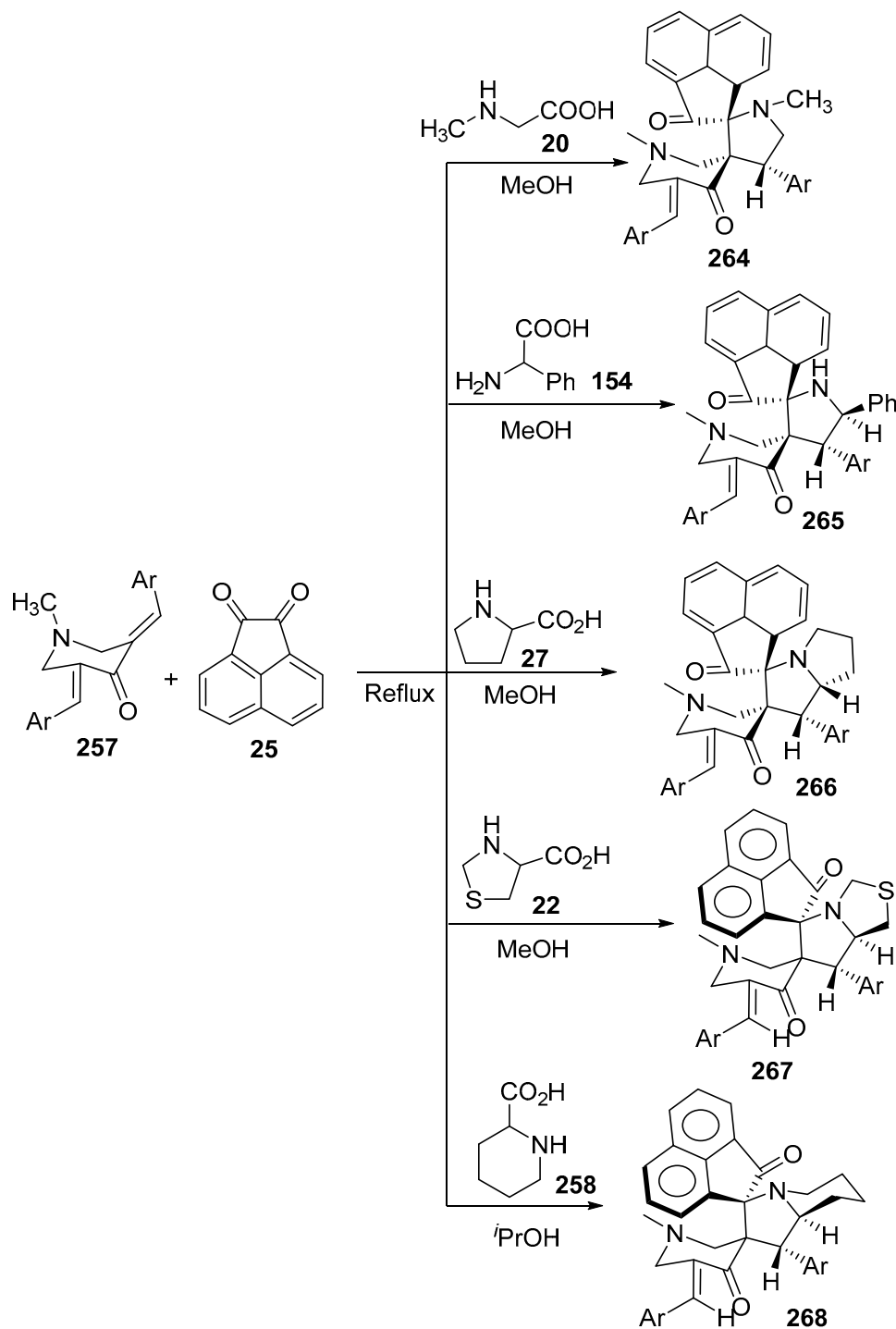
R² = H, Me, CH₂(1-piperidinyl), CH₂(4-morpholinyl)

R³ = H, Cl, OMe, OCF₃

Scheme 89. Synthesis of spiropyrrolidines 260–263.

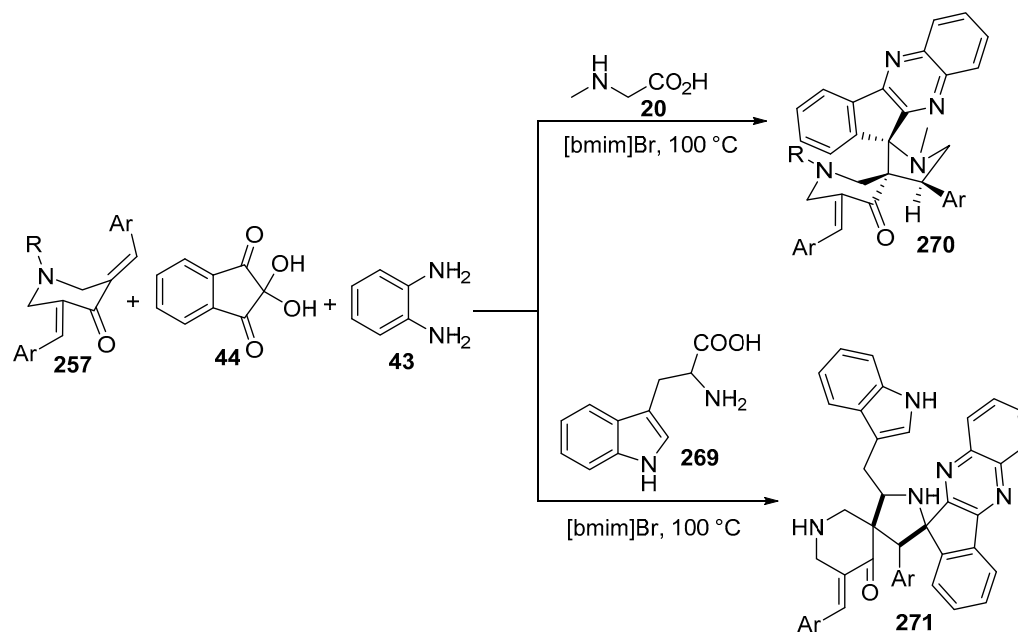
Similarly, the reaction of 3,5-bis(ylidene)-4-piperidone **257** with a series of azomethine ylides generated from acenaphthenequinone **25** and α -amino acids (sarcosine **20**, phenylglycine **154**, proline **27**, thioproline **22**, or piperidine-2-carboxylic acid **258**) afforded the corresponding spiro-piperidone-containing compounds **264–268** (Scheme 90). Some of these derivatives revealed promising activities against *Mycobacterium tuberculosis* H37Rv (MTB),

multi-drug resistant *Mycobacterium tuberculosis* (MDR-TB), and *Mycobacterium smegmatis* relative to Isoniazid [127]. Another group of the synthesized spiro-heterocycles **267** and **268** showed acetylcholine (AChE)-inhibitory properties relative to Donepezil HCl [128].



Scheme 90. Synthesis of spiro-piperidone-containing compounds **264–268**.

A multicomponent reaction of 3,5-bis[(*E*)-ylidene]-4-piperidone **257**, ninhydrin **44**, *o*-phenylenediamine **43**, and α -amino acid (sarcosine **20** or *L*-tryptophan **269**) in 1-butyl-3-methylimidazoliumbromide ([BMIm]Br) used as an ionic liquid produced the corresponding dispiro compounds **270** and **271** [129,130] (Scheme 91). Significant acetylcholinesterase (AChE) and butyrylcholinesterase (BChE)-inhibitory properties were shown by some of the synthesized compounds relative to galantamine (standard reference) [130].

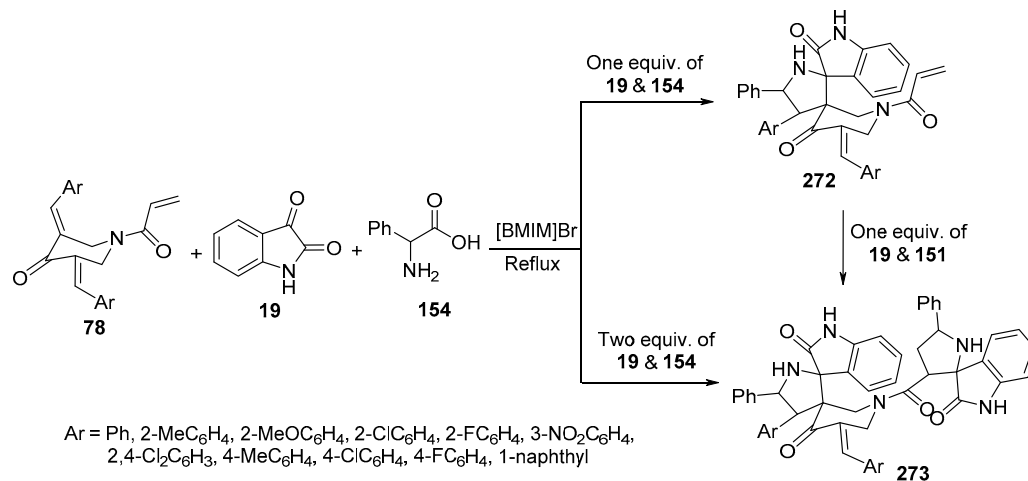


R = H, Me, CH₂C₆H₅

Ar = H, Ph, 2-ClC₆H₄, 4-ClC₆H₄, 2,4-Cl₂C₆H₃, 2-BrC₆H₄, 3-BrC₆H₄, 4-BrC₆H₄, 2-MeC₆H₄, 3-MeC₆H₄, 4-MeC₆H₄, 3-MeOC₆H₄, 4-MeOC₆H₄, 4-ⁱPrC₆H₄, 4-Me₂NC₆H₄, 3-NO₂C₆H₄, 2-thienyl, 1-naphthyl

Scheme 91. Synthesis of dispiro compounds **270** and **271**.

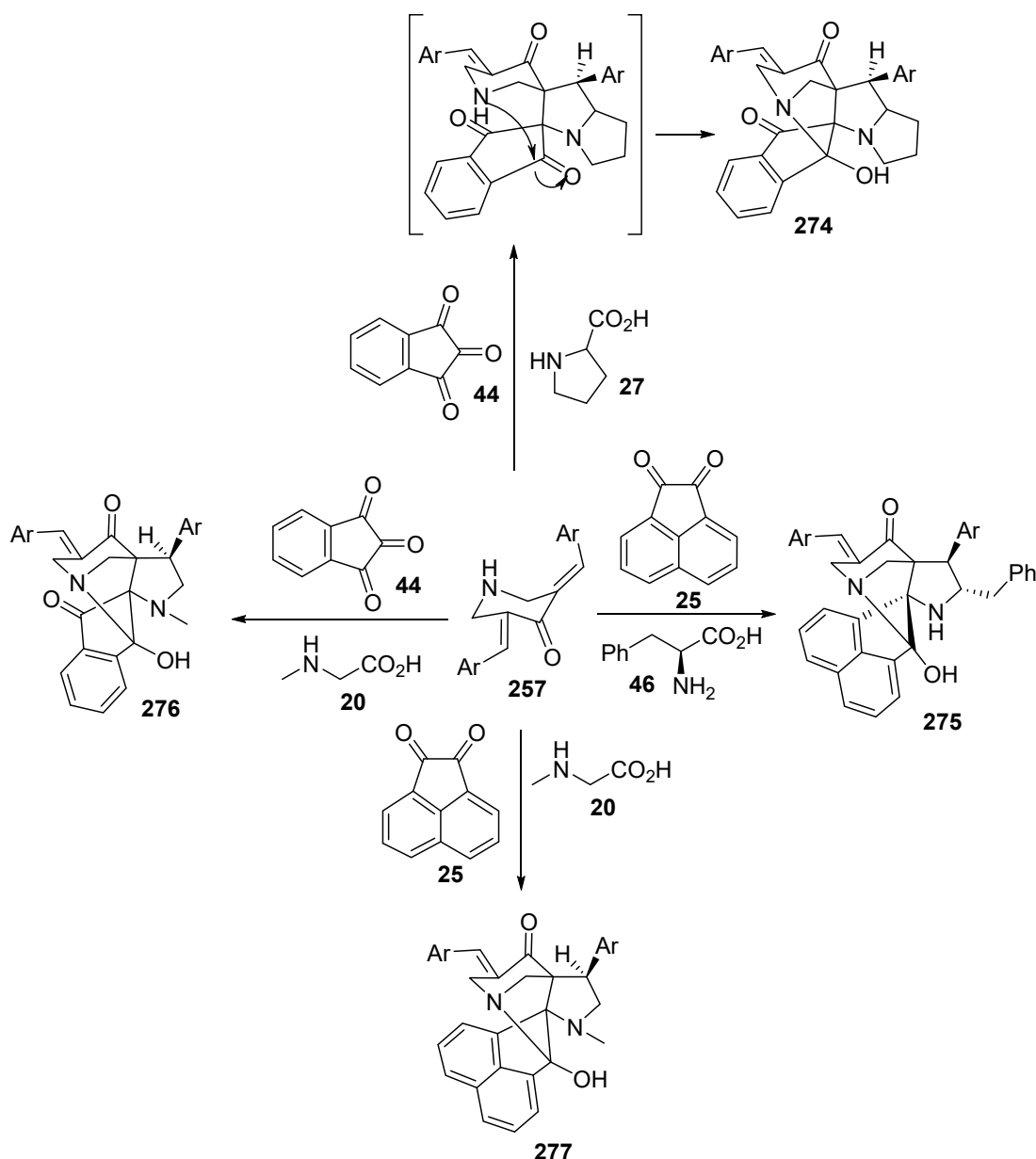
Mono-spiropyrrolidines of type **272** were synthesized by the reaction of 1-acryloyl-3,5-bis(ylidene)-4-piperidinone **78** with azomethine ylide generated from isatin **19** and phenylglycine **154** from equimolar amounts of the reactants. Meanwhile, bispiropyrrolidine derivatives of type **273** were formed using two equivalents, namely, isatin **19** and phenylglycine **154** (Scheme 92). Some of the synthesized compounds showed promising AChE- and BChE-inhibitory properties relative to Galanthamine [131].



Ar = Ph, 2-MeC₆H₄, 2-MeOC₆H₄, 2-ClC₆H₄, 2-FC₆H₄, 3-NO₂C₆H₄, 2,4-Cl₂C₆H₃, 4-MeC₆H₄, 4-ClC₆H₄, 4-FC₆H₄, 1-naphthyl

Scheme 92. Synthesis of mono-spiropyrrolidines **272** and bispiropyrrolidines **273**.

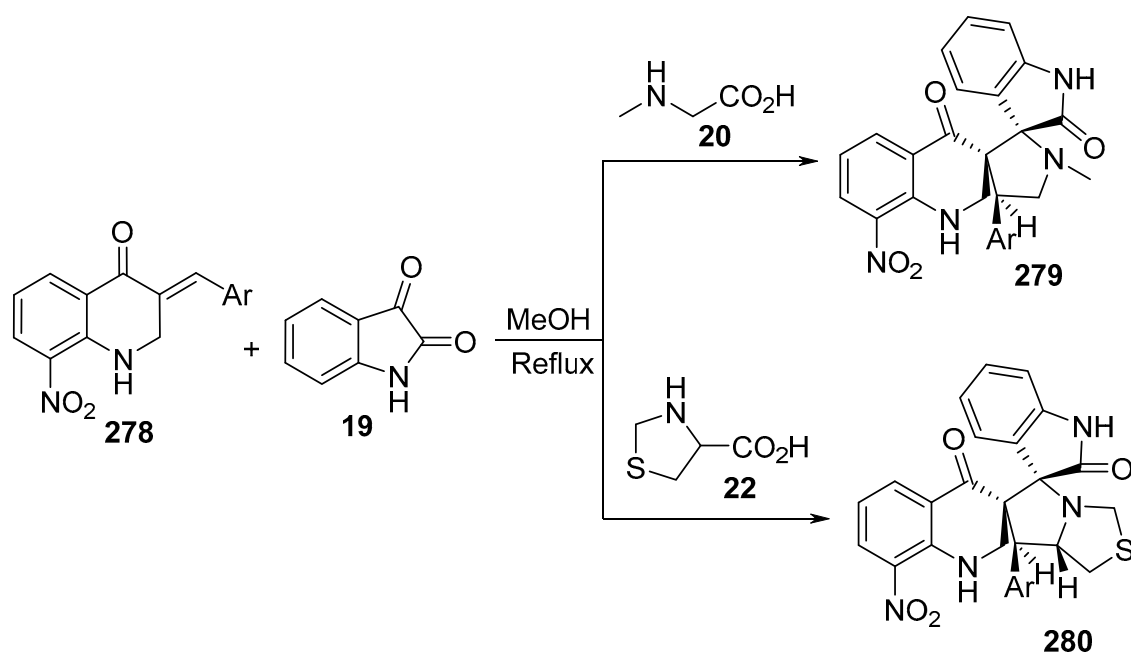
Finally, the reaction of 3,5-bis(ylidene)-4-piperidone **257** with azomethine ylide formed from ninhydrin **44** and proline **27** in refluxing methanol afforded diazahexacycle **274** [132]. Similarly, **275–277** were obtained by the reaction of **257** with another azomethine ylides generated from ninhydrin **44** or acenaphthenequinone **25** with sarcosine **20** or *L*-phenylalanine **46** (Scheme 93) [133,134]. Some of the derivatives of type **274** exhibited inhibitory activities toward AChE relative to Donepezil HCl [132].



Scheme 93. Synthesis of diazahexacycles **274–277**.

3.14. Quinolones

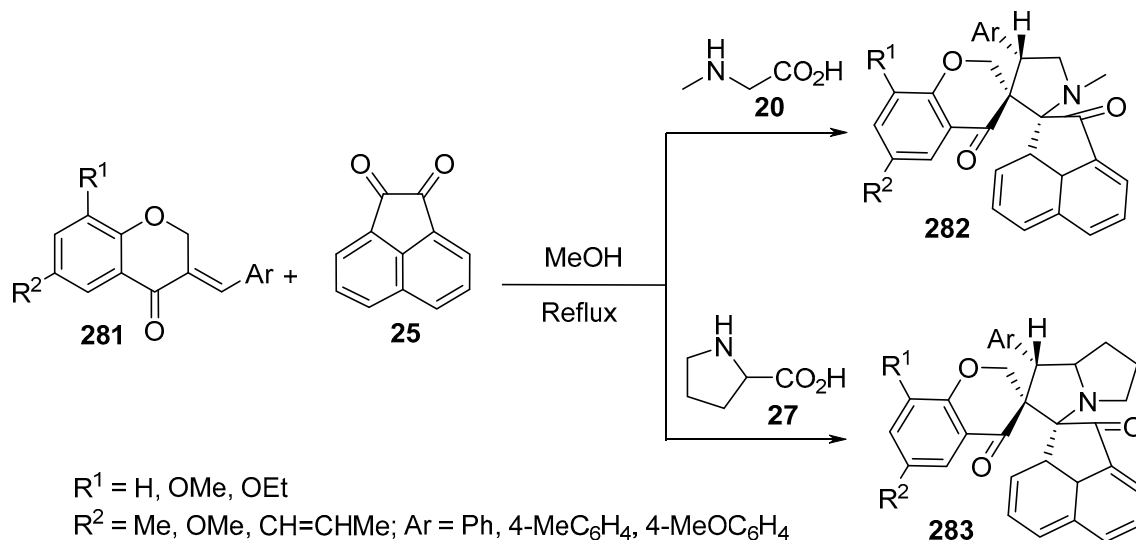
Spiropyrrolidines **279** and **280** were synthesized by the reaction of (*E*)-3-(ylidene)-4-quinolone **278** with azomethine ylides formed from isatin **19** and sarcosine **20** or thioproline **22** (Scheme 94) [135].



Scheme 94. Synthesis of spiropyrrolidines **279** and **280**.

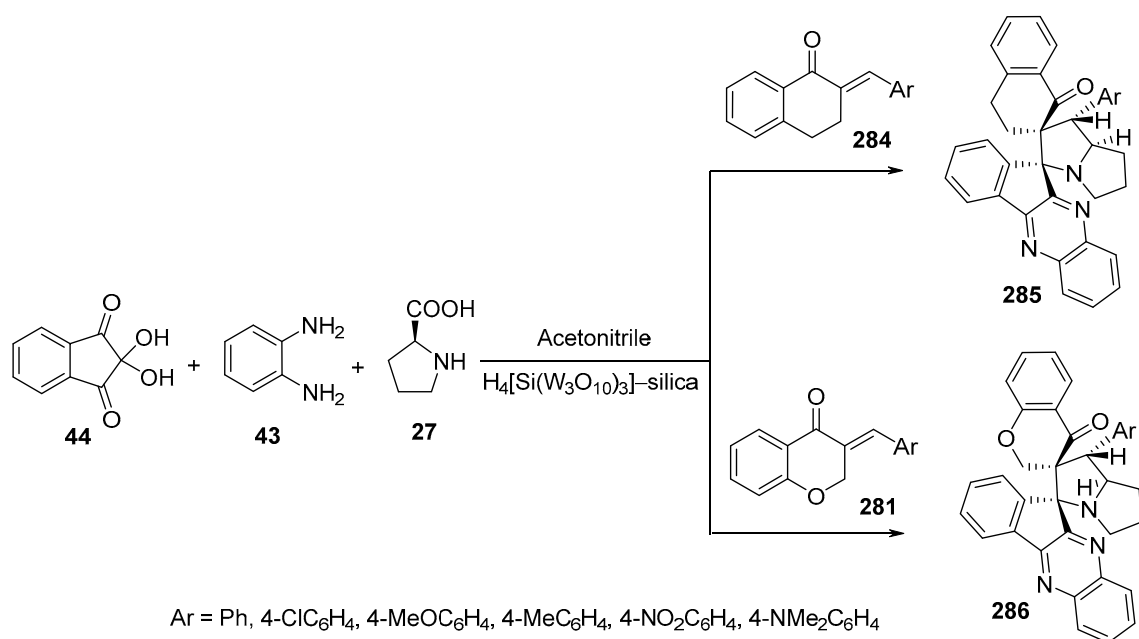
3.15. Chromanones

The reaction of (*E*)-3-arylidene-4-chromanone of type **281** with azomethine ylides formed from acenaphthenequinone **25** and sarcosine **20** or proline **27** afforded spiropyrrolidines **282** and **283**, respectively, with high regioselectivity (Scheme 95) [136].



Scheme 95. Synthesis of spiropyrrolidines **282** and **283**.

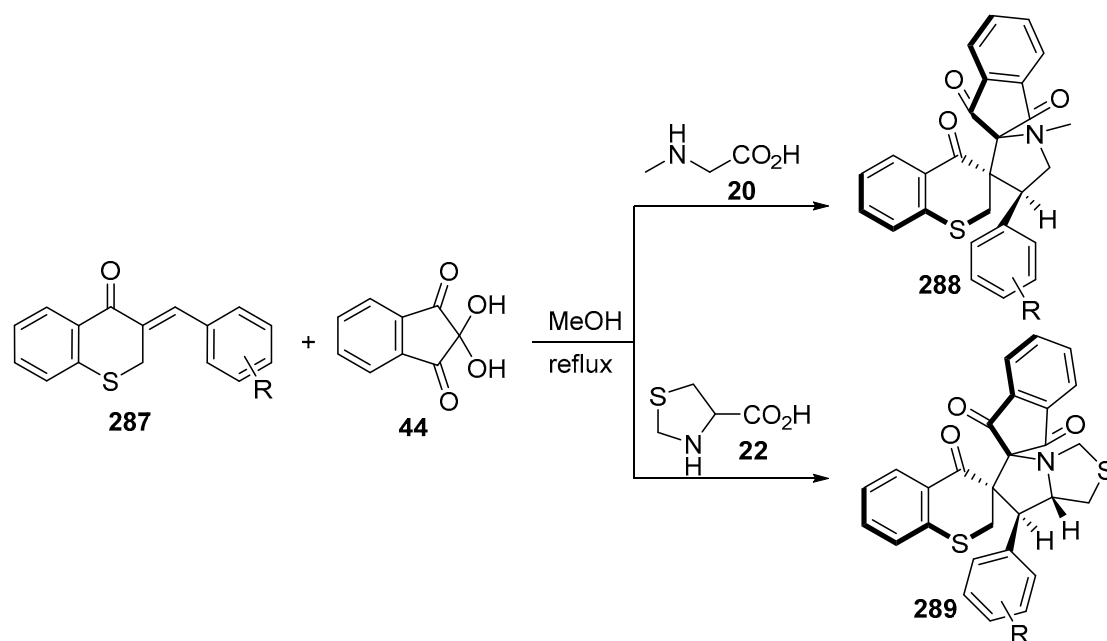
A multi-component reaction of 2-ylidene-tetrahydronaphthalene-1-one **284** or (*E*)-3-ylidene-4-chromanone **281** with azomethine ylide formed from indenoquinoline-11-one (generated from ninhydrin **44** and *o*-phenylenediamine **43**) and *L*-proline **27** afforded, in the presence of heteropolyacid H₄[Si(W₃O₁₀)₃]-silica as a catalyst in refluxing acetonitrile, the corresponding dispiroindenoquinoline-pyrrolizidines **285** and **286**, respectively (Scheme 96) [93].



Scheme 96. Synthesis of dispiroindenoquininoxaline-pyrrolizidines **285** and **286**.

3.16. Thiochromanones

Dispiro[indene-2,2'-pyrrolidine-3',3''-thiochromanes] **288** were obtained by reacting 3-arylidene-thiochroman-4-one **287** with azomethine ylide (obtained from ninhydrin **44** and sarcosine **20**) in refluxing methanol. When thioproline **22** was used instead of sarcosine **20**, the corresponding dispiro derivatives of type **289** were obtained. Some of the synthesized pyrrolizidines revealed antimycobacterial properties (*Mycobacterium tuberculosis* H37Rv) relative to Cycloserine and Pyrimethamine (standard references). Additionally, mild antiproliferative properties against CCRF-CEM (leukemia), HT29 (ovarian), and MCF7 (breast) cancer cell lines relative to Doxorubicin (MTT assay) were observed (Scheme 97) [137].

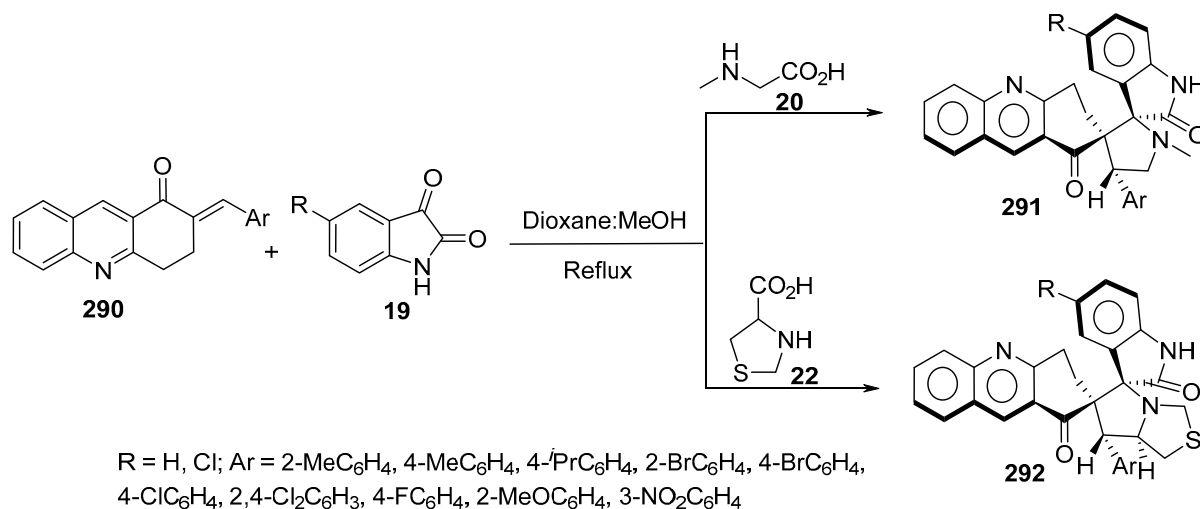


R = H, 3-F, 4-F, 2-Cl, 4-Cl, 2,4-Cl₂, 2-Br, 3-Br, 4-Br, 4-Me, 4-*i*-Pr, 4-OMe, 1-naphthyl, 2-thienyl

Scheme 97. Synthetic route towards dispiro-containing compounds **288** and **289**.

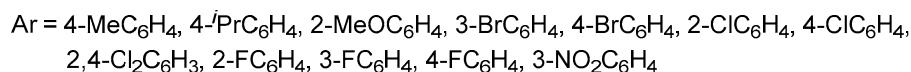
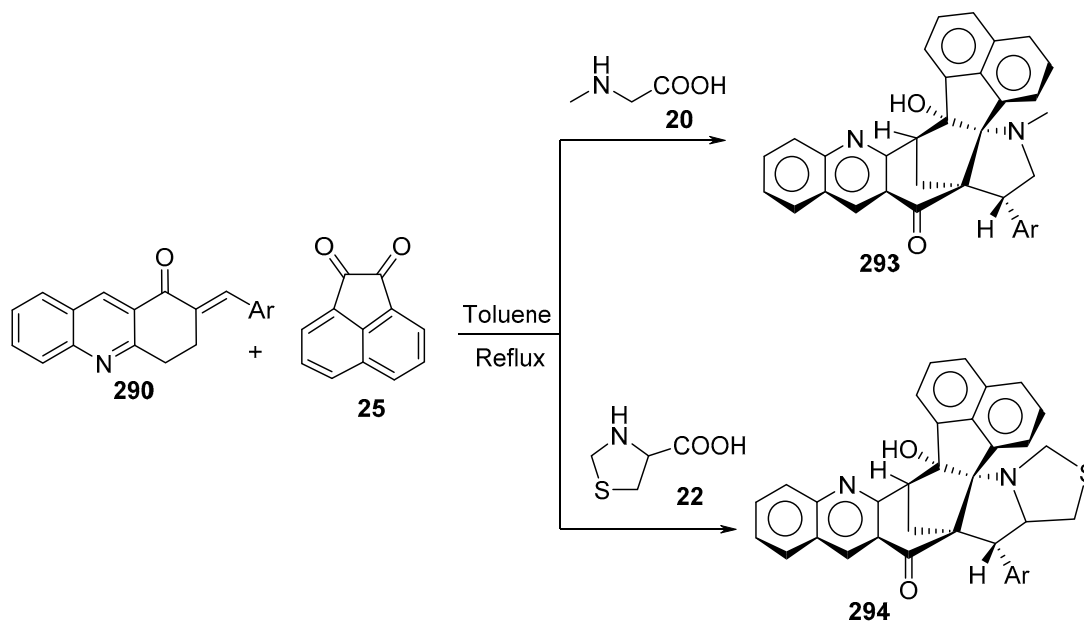
3.17. Acridinones

The reaction of (*E*)-2-(arylidene)-3,4-dihydro-1(2*H*)-acridinones **290** with azomethine ylides formed from the condensation of isatin **19** and sarcosine **20** or thioproline **22** in refluxing dioxane/methanol afforded the corresponding dispirooxindolyl-[acridine-2',3-pyrrolidine/thiapyrrolizidine]-1'-ones **291** and **292**, respectively (Scheme 98) [138].



Scheme 98. Synthesis of dispirooxindolyl-[acridine-2',3-pyrrolidine/thiapyrrolizidine]-1'-ones **291** and **292**.

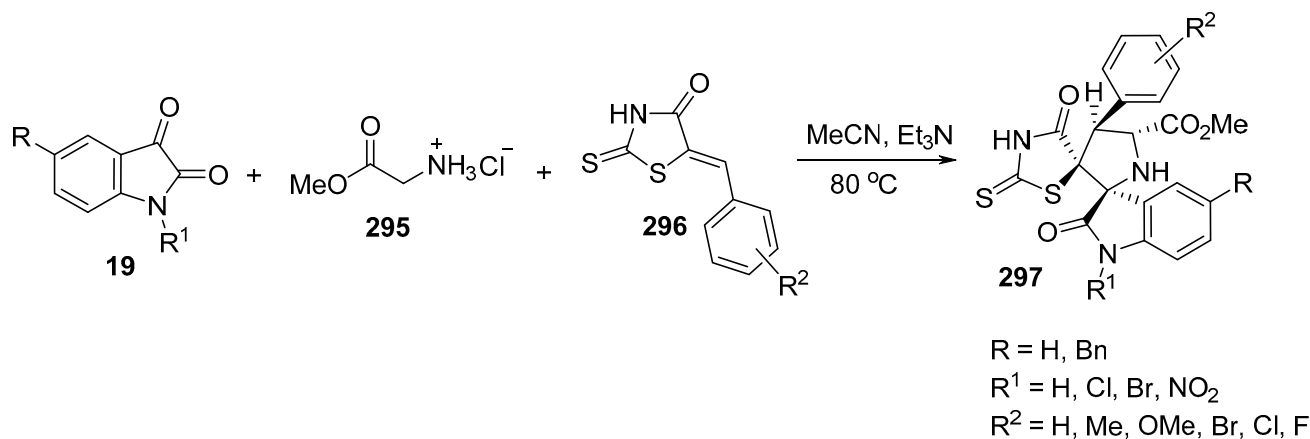
Naphtho[1',8':1,2,3]pyrrolo[3',2':8,8*a*]azuleno[5,6-*b*]quinolin-14-one **293** and naphtho[1',8':1,2,3]thiazolo[3'',4'':1',5']pyrrolo[3',2':8]-azuleno-[5,6-*b*]quinolin-18-one **294** were obtained by reacting (*E*)-2-(arylidene)-3,4-dihydro-1(2*H*)-acridinone **290** with azomethine ylides generated from acenaphthoquinone **25** with sarcosine **20** or thioproline **22** in refluxing toluene, respectively (Scheme 99) [139].



Scheme 99. Synthesis of naphtho[1',8':1,2,3]pyrrolo[3',2':8,8*a*]azuleno[5,6-*b*]quinolin-14-ones **293** and naphtho[1',8':1,2,3]thiazolo[3'',4'':1',5']pyrrolo[3',2':8]-azuleno-[5,6-*b*]quinolin-18-ones **294**.

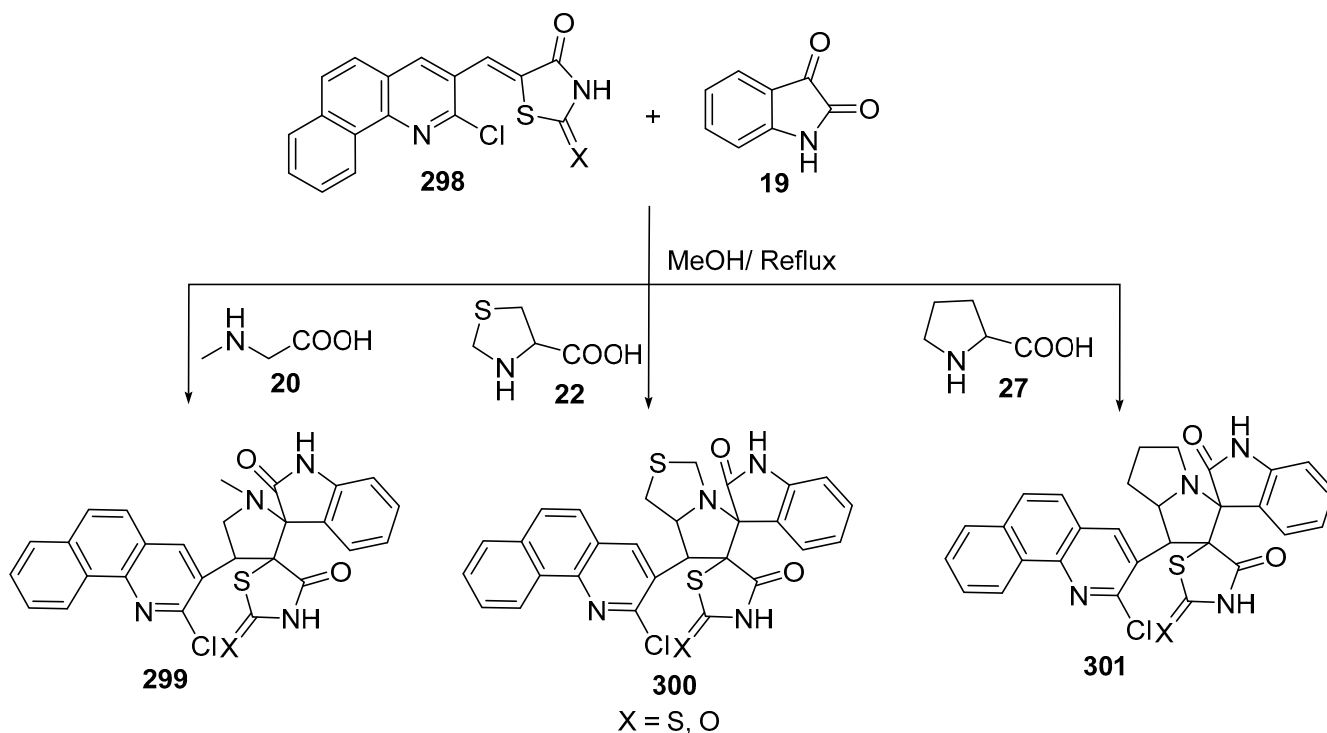
3.18. Thiazolidinones

A series of dispiro[indoline-3,2'-pyrrolidine-3',5''-thiazolidines] of type **297**, which are potential α -amylase inhibitors (useful for type-2 diabetes mellitus), were obtained through the cycloaddition of azomethine ylide (generated from glycine methyl ester **295** and isatin **19**) and 5-arylidene-2-thioxothiazolidin-4-one **296** (Scheme 100) [140].



Scheme 100. Synthesis of dispiro[indoline-3,2'-pyrrolidine-3',5''-thiazolidines] **297**.

Another group of benzo[*h*]quinoliny dispiro-compounds **299–301** was obtained by reacting [5-(2'-chlorobenzo[*h*]quinolin-3'-yl)methylidene]-thiazolidin-2,4-dione/2-thioxothiazolidin-4-one **298** with various azomethine ylides formed from isatin **19** and different amino acids (sarcosine **20**, thioproline **22**, or *L*-proline **27**) (Scheme 101) [141].

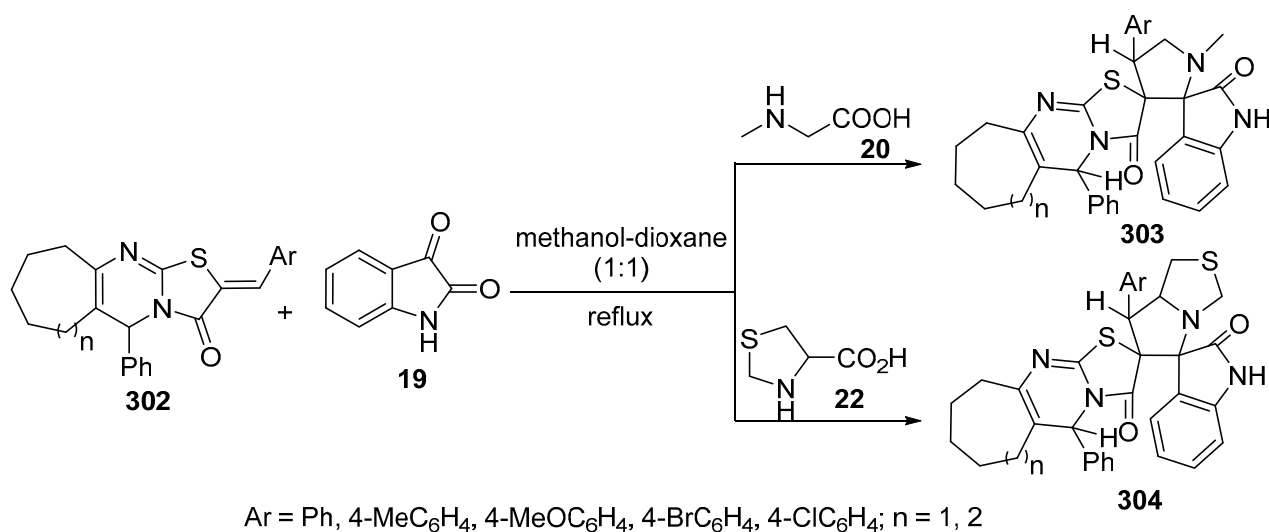


Scheme 101. Synthesis of benzo[*h*]quinoliny dispiro-compounds **299–301**.

3.19. Thiazolo[3,2-*a*]pyrimidine-3-ones

Various (*E*)-arylmethylene-octahydro/decahydro cycloalka[*d*]thiazolo[3,2-*a*]pyrimidine-3-ones of type **302** reacted smoothly with azomethine ylides formed from isatin **19** and

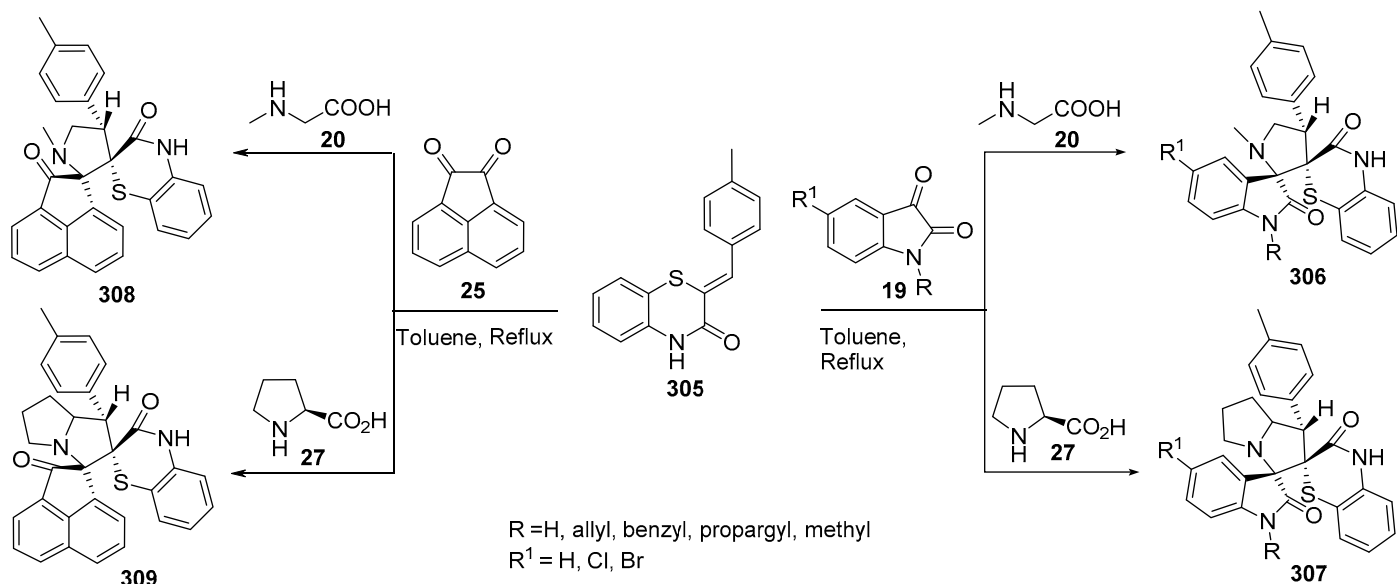
sarcosine **20** or thioproline **22** in a refluxing methanol-dioxane (1:1) mixture, thereby affording the corresponding spiro-oxindoles **303** and **304**, respectively (Scheme 102) [142].



Scheme 102. Synthesis of spiro-oxindoles **303** and **304**.

3.20. Benzo[1,4]thiazines

Spiro-oxindoles **306** and **307** and spiro-acenaphthylen-1-ones **308** and **309** were synthesized via a multicomponent reaction of 2-(4-methylbenzylidene)-4*H*-benzo[1,4]thiazin-3-one **305** and azomethine ylides derived from isatin **19** or acenaphthenequinone **25** with sarcosine **20** or *L*-proline **27** in refluxing toluene (Scheme 103) [143].



Scheme 103. Synthesis of spiro-oxindoles and spiro-acenaphthylen-1-ones **306**–**309**.

4. Cyclic Unsaturated 2π-Electron Components

4.1. Non-Aromatic Cyclc 2π-Electron Components

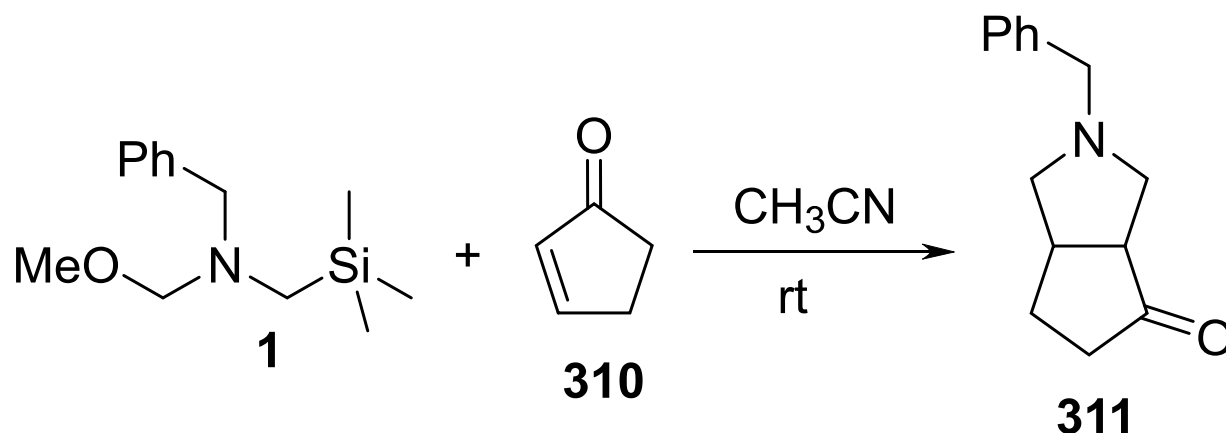
4.1.1. Alicyclic Unsaturated 2π-Electron Components

Intermolecular Cycloaddition Reactions

- Cyclopentenone

The reaction of azomethine ylide generated from benzyl(methoxymethyl)(trimethylsilyl)methylamine **1** with cyclopentenone **310** afforded bicyclic ketone **311** via an addition to

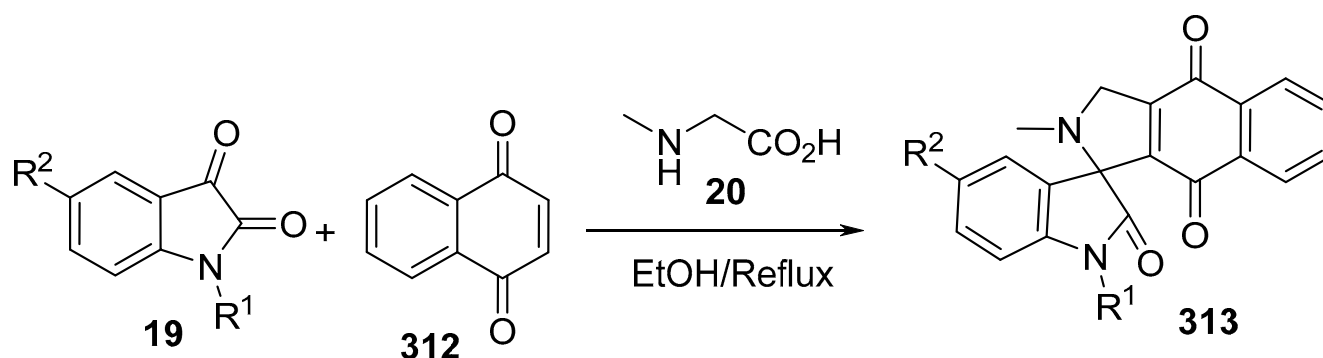
the C2-C3 unsaturated linkage. Some analogs of **307** exhibited histamine H₃ receptor antagonists that are responsible for the production and regulation of histamine and other neurotransmitters (Scheme 104) [144].



Scheme 104. Synthesis of bicyclic ketone **311**.

- 1,4-Naphthoquinone

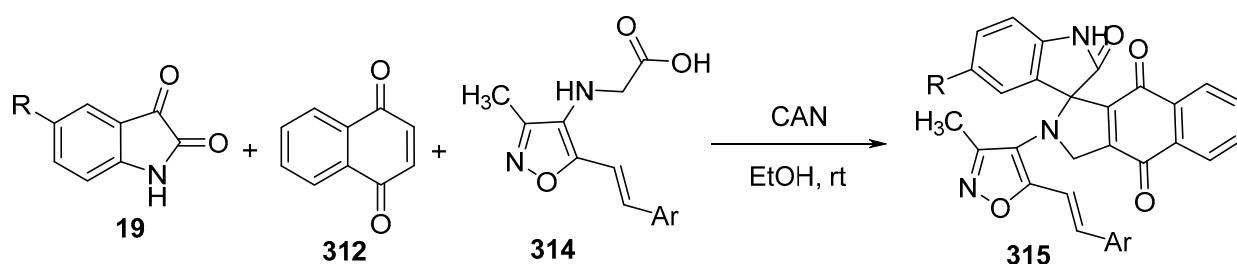
Spirooxindoles of type **313** were obtained by the cycloaddition of azomethine ylides, formed from isatin **19** and sarcosine **20**, with 1,4-naphthoquinone **312** in refluxing ethanol (Scheme 105). Some of the synthesized compounds showed antibacterial activities against *Staphylococcus aureus*, *S. aureus* (MRSA), *Enterobacter aerogens*, *Micrococcus luteus*, *Proteus vulgaris*, *Klebsiella pneumonia*, *Salmonella typhimurium*, and *Salmonella paratyphi-B*, and antifungal activities against *Malassezia pachydermatis*, *Candida albicans*, and *Botrytis cinerea* relative to Streptomycin and Ketoconazole (standard references) [145].



R¹ = H, Me, Et, propargyl, propenyl, benzyl, butyl, hexyl, acetyl
R² = H, Me, Cl, Br, I

Scheme 105. Synthesis of spiro-indoles **313**.

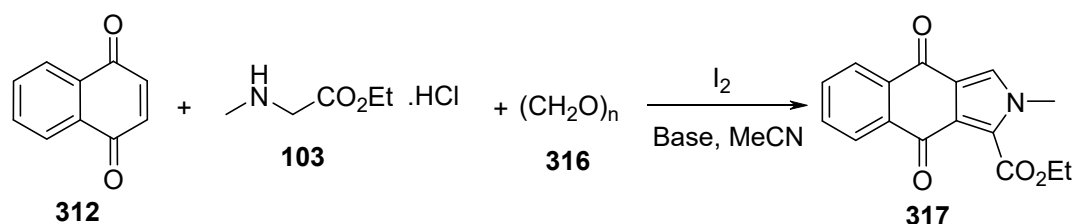
Further spiro[benzo[*f*]isoindole-1,3'-indolines] of type **315** were synthesized by the cycloaddition of azomethine ylides (formed from isatin **19** and 2-(3-methyl-5-styrylisoxazol-4-ylamino)acetic acids **314**) and 1,4-naphthoquinone **312** using ceric ammonium nitrate (CAN) as a catalyst (Scheme 106). Some of the products showed anti-inflammatory (determined via rat carrageen paw edema assay) and analgesic (determined via acetic acid writhing protocol) properties relative to Ibuprofen and Diclofenac as references, respectively [146].



Ar = Ph, 4-MeC₆H₄, 4-MeOC₆H₄, 4-ClC₆H₄, 2,4-Cl₂C₆H₃, 2,6-Cl₂C₆H₃, 2-OHC₆H₄
 R = H, Cl, OMe, Me

Scheme 106. Synthesis of spiro[benzo[*f*]isoindole-1,3'-indolines] **315**.

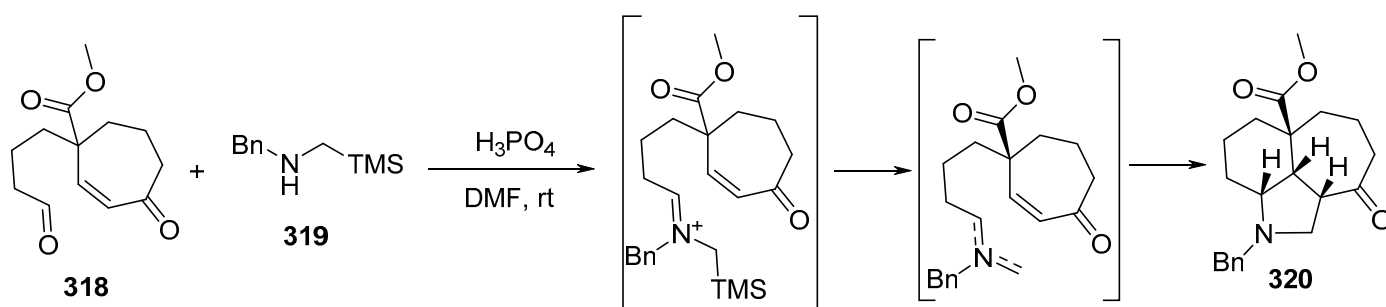
Tricyclic benzo[*f*]isoindole-4,9-dione-1-carboxylate **317** was obtained by reacting 1,4-naphthoquinone **312** with azomethine ylide generated from sarcosine ethyl ester hydrochloride **103** and paraformaldehyde **316** in the presence of iodine and sodium bicarbonate as a base in refluxing acetonitrile (Scheme 107) [147].



Scheme 107. Synthesis of benzo[*f*]isoindole-4,9-dione-1-carboxylate **317**.

Intramolecular Cycloaddition Reactions

The azatricyclic [6-5-7] ring system **320** was created via the intramolecular [3+2]-cycloaddition reaction of azomethine ylide generated from aldehyde **318** and *N*-(trimethylsilyl) methyl iminium salt **319** in the presence of a catalytic amount of phosphoric acid in DMF as a solvent (Scheme 108) [148].

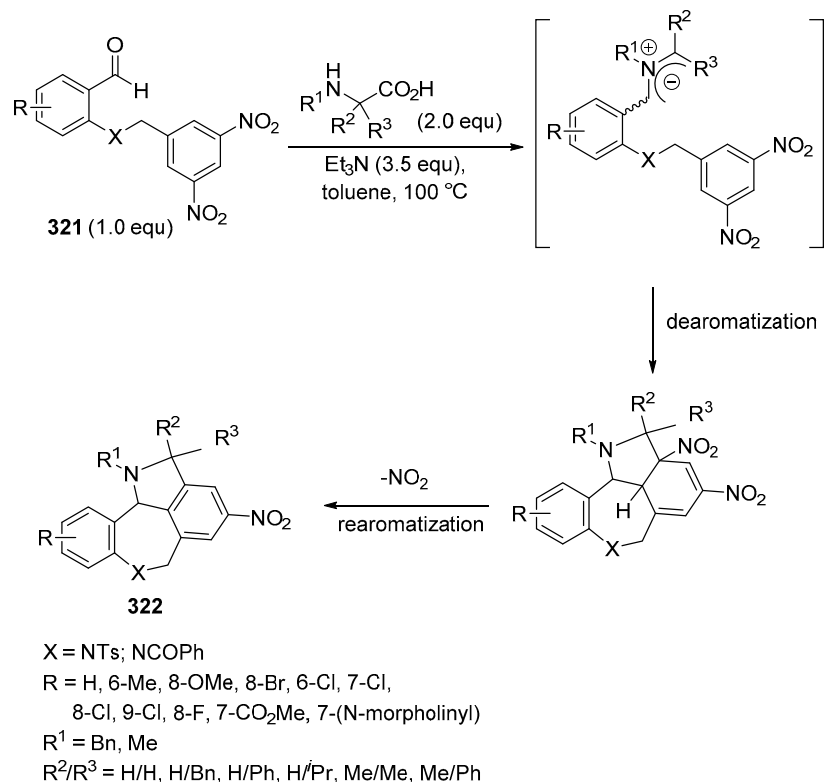


Scheme 108. Synthesis of azatricyclic [6-5-7] ring system **320**.

4.2. Aromatic Cyclic Unsaturated 2π-Electron Components

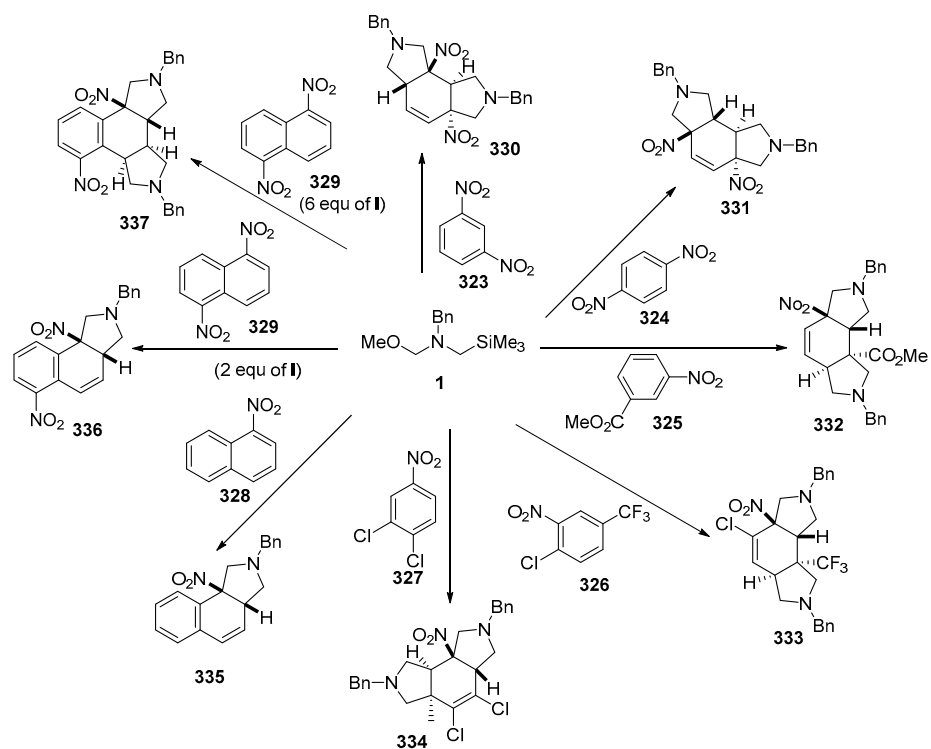
Azomethine ylide's cycloaddition to aromatic 2π-electron components (aromatic or heteroaromatic) was reviewed in [149].

A series of benzoazepine-fused isoindolines of type **322** were obtained through thermal azomethine ylide-based cycloaddition of benzaldehydes bearing 3,5-dinitrophenyl **321** and *N*-substituted α-amino acids. The reaction was assumed to proceed through a regioselective dearomatizing [3+2] cycloaddition with the removal of HNO₂, thus yielding the aromatic final product **322** (Scheme 109) [150].



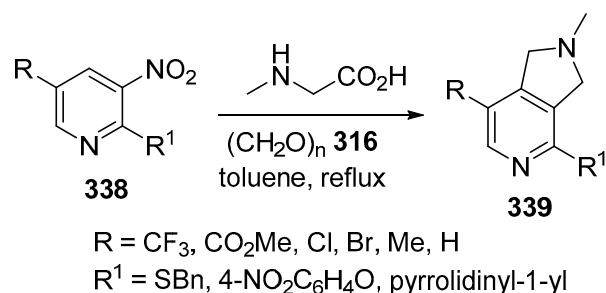
Scheme 109. Synthesis of benzoazepine-fused isoindolines **322**.

Nitro-substituted benzenes **323–329** underwent [3+2] cycloaddition of azomethine ylide derived from (*N*-(methoxymethyl)-*N*-(trimethylsilyl-methyl)-benzylamine) **1**, affording the pyrrolidinyl cycloadducts **330–337** (Scheme 110) [151].



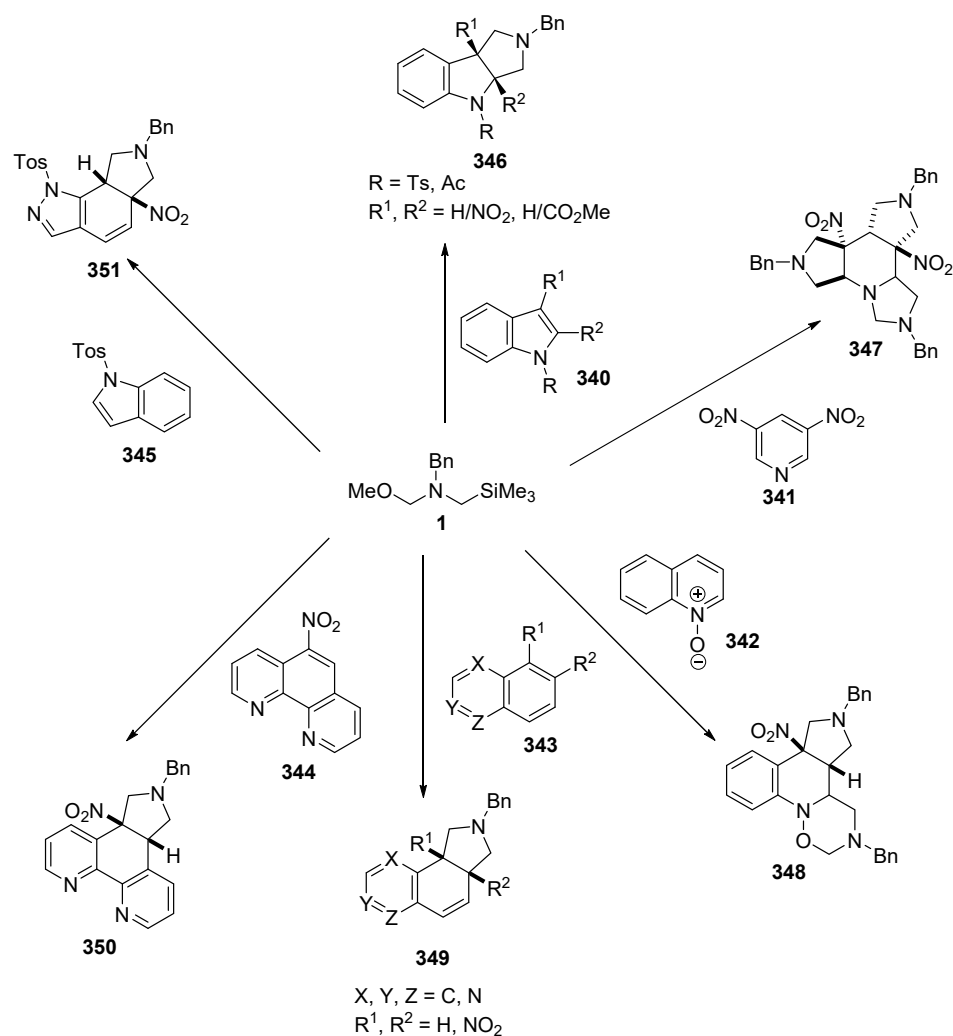
Scheme 110. Synthesis of pyrrolidinyl cycloadducts **330–337**.

Pyrrolo[3,4-*c*]pyridines **339** were obtained through azomethine ylide's (formed from sarcosine and paraformaldehyde **316**) cycloaddition with 3-nitropyridines **338** in refluxing toluene (Scheme 111) [152].

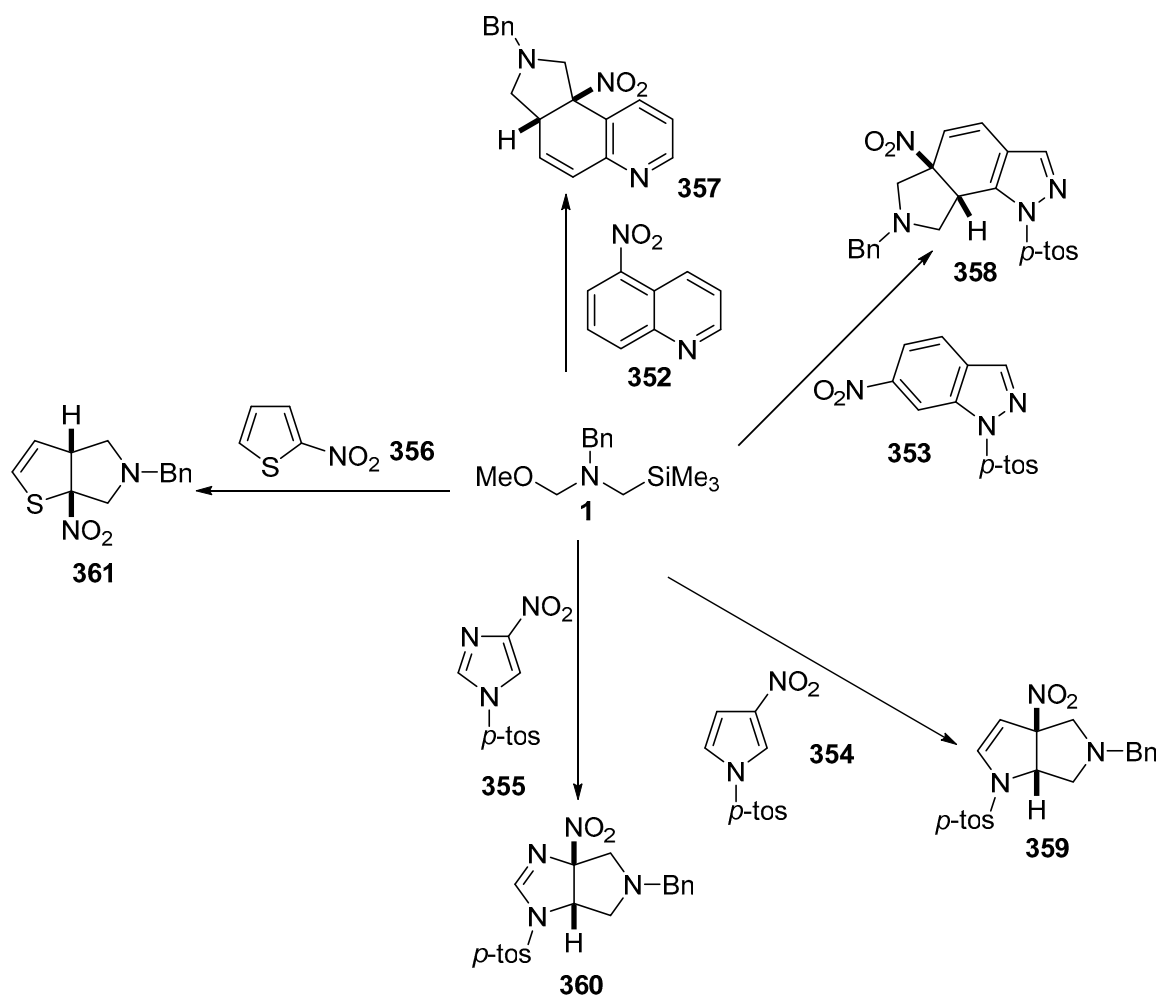


Scheme 111. Synthesis of pyrrolo[3,4-*c*]pyridines **339**.

Analogously, heterocyclic compounds bearing nitro groups **340–345** and **352–356** underwent a cycloaddition reaction with azomethine ylide derived from *N*-(methoxymethyl)-*N*-(trimethylsilyl-methyl)-benzylamine **1**, affording the pyrrolidinyl-containing analogs **346–351** and **357–361** (Schemes 112 and 113) [151,153].

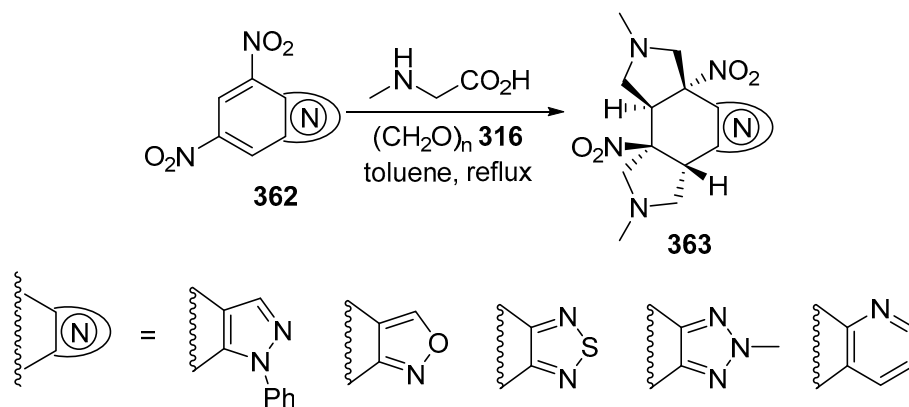


Scheme 112. pyrrolidinyl-fused heterocycles **346–351**.



Scheme 113. pyrrolidiny-fused heterocycles 357–361.

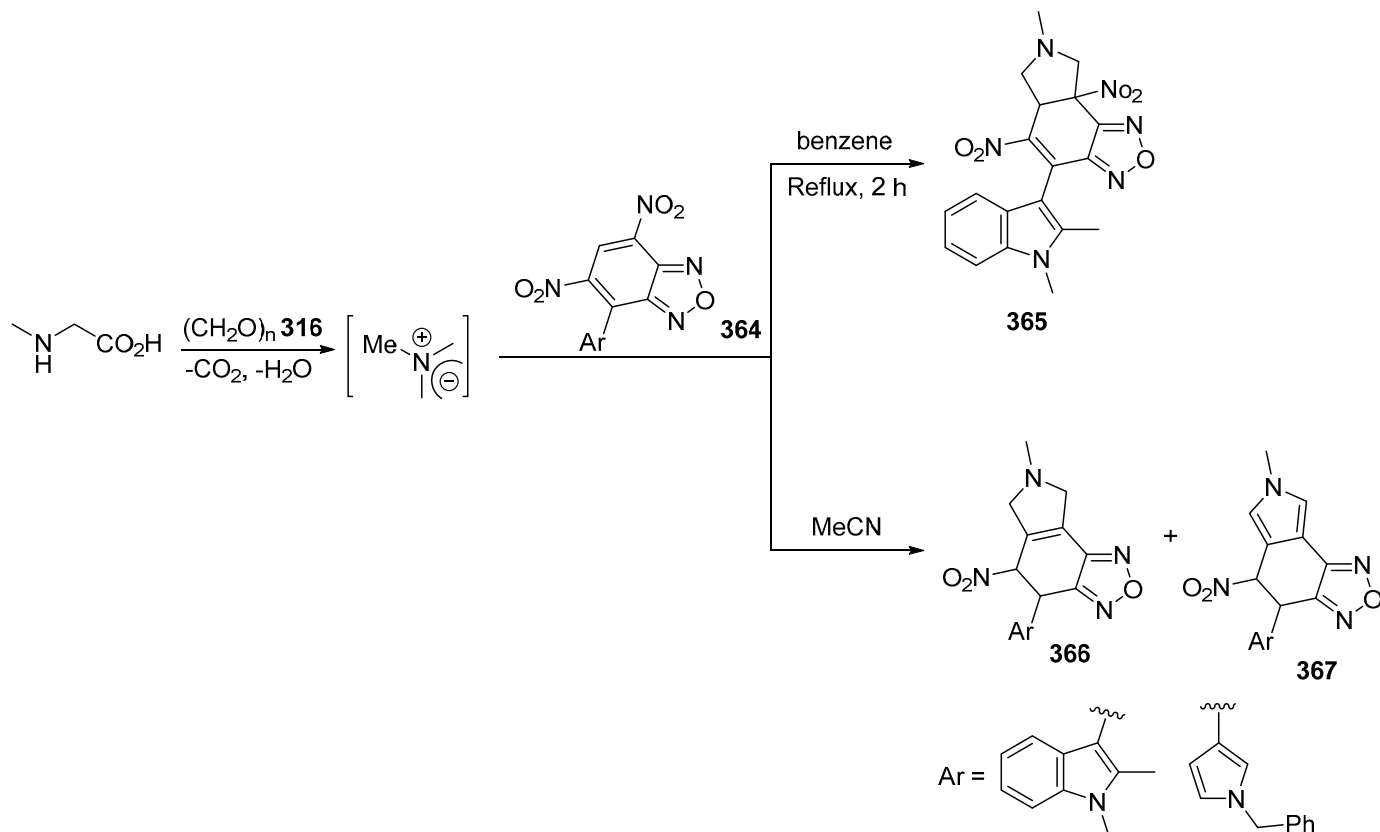
Double cycloadducts of type 363 were obtained through azomethine ylide (formed from sarcosine and paraformaldehyde 316) with meta-dinitro-containing nitrogenous heterocycles 362 in refluxing toluene (Scheme 114) [154].



Scheme 114. Synthesis of double cycloadducts 363 from meta-dinitro-containing nitrogenous heterocycles of type 362.

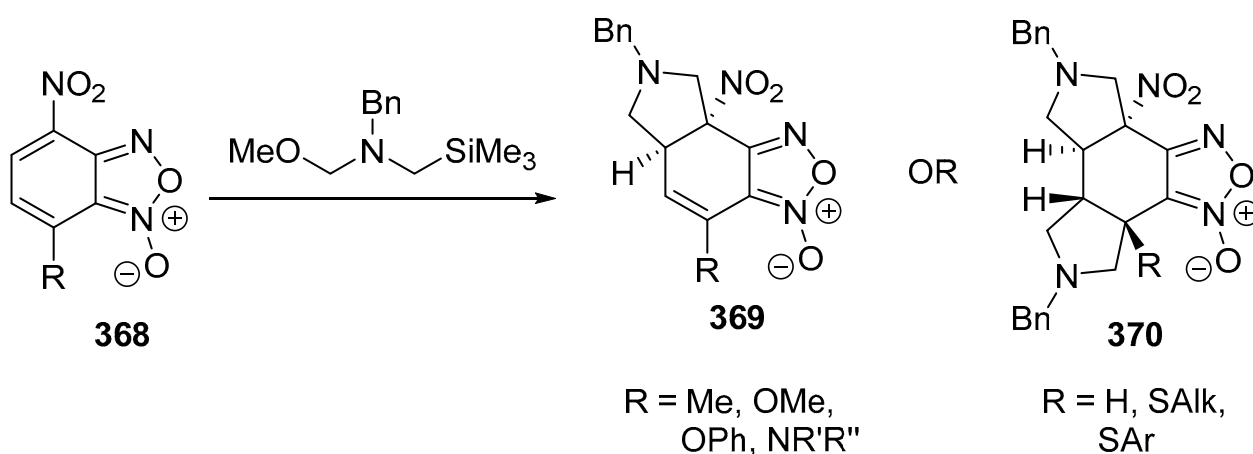
4-Chloro-5,7-dinitro-4-benzofurazan bearing indolyl heterocycle 364 underwent azomethine ylide (formed from the condensation of sarcosine and paraformaldehyde 316) cycloaddition in refluxing benzene, affording the corresponding tetrahydro-5aH-[1,2,5]oxa-diazolo[3,4-

e]isoindole **365**. Alternatively, conducting the reaction in refluxing MeCN afforded a mixture of **366** and **367**. Similarly, analogs with a pyrrolidinyl function (**366** and **367**) were obtained upon reacting the appropriate analog of **365** in MeCN at room temperature (in the darkness) (Scheme 115) [155].



Scheme 115. Synthesis of [1,2,5]oxa-diazolo[3,4-*e*]isoindole **365**–**367**.

The cycloaddition reaction of azomethine ylide derived from (*N*-(methoxymethyl)-*N*-(trimethylsilyl-methyl)-benzylamine) with 4-nitrobenzofuroxan **368** afforded either mono **369** or bis **370** cycloadducts based via the substitution of the starting benzofuroxan at the 7-position (Scheme 116) [156].

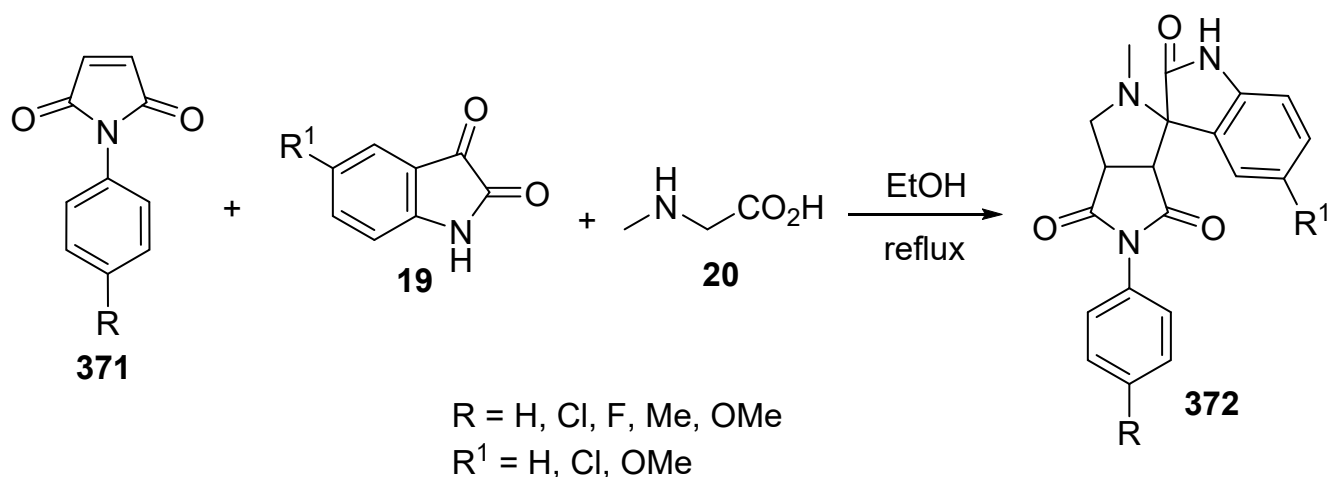


Scheme 116. Synthesis of mono-**369** or biscycloadducts **370** of 4-nitrobenzofuroxans.

4.3. Heterocyclic Unsaturated 2 π -Electron Components

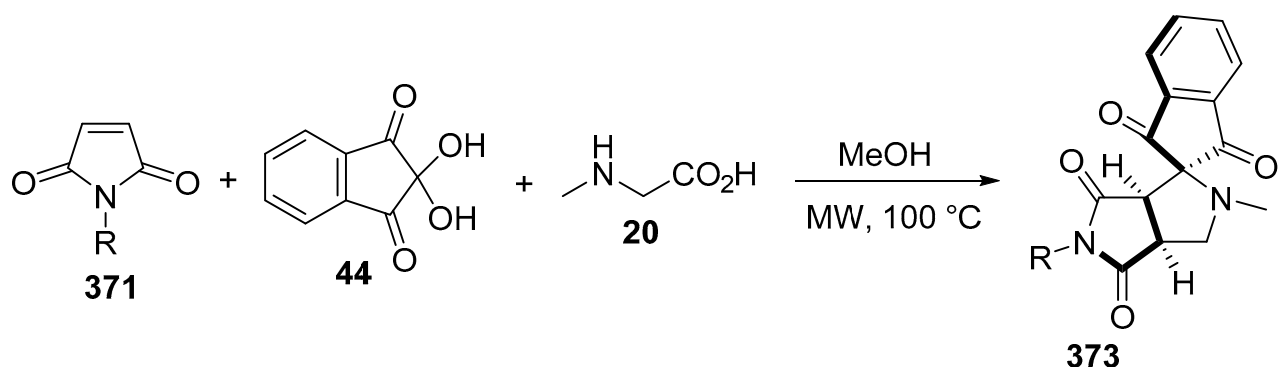
4.3.1. Maleimides

Spiro[3*H*-indole-3,2'(1'*H*)-pyrrolo[3,4-*c*]pyrroles] of type **372** were obtained in good yields by the cycloaddition of azomethine ylide (formed from sarcosine **20** and isatin **19**) to the C3-C4 unsaturated bond of maleimide **371**. Some of the synthesized compounds revealed promising to moderate antiproliferative properties against HEPG2 (liver), HCT116 (colon), and MCF7 (breast) cancer cell lines (SRB technique) relative to Doxorubicin (standard reference drug) (Scheme 117) [157].



Scheme 117. Synthetic route towards spiro[3*H*-indole-3,2'(1'*H*)-pyrrolo[3,4-*c*]pyrroles] **372**.

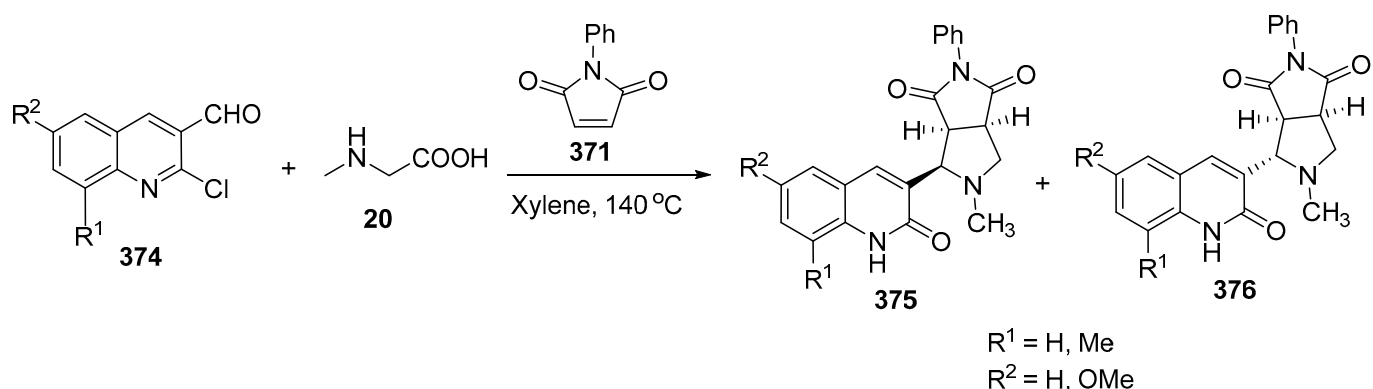
A microwave-assisted multi-component reaction of maleimide **371** with azomethine ylide produced from sarcosine **20** and ninhydrin **44** stereoselectively afforded spiro[indene-2,1'-pyrrolo[3,4-*c*]pyrroles] **373**. Some of the products showed promising antimycobacterial (*M. tuberculosis* H37Rv) properties relative to Cycloserine (Scheme 118) [158].



R = Ph, Me, CH₂Ph, cyclohexyl, 4-FC₆H₄, 3-FC₆H₄, 4-ClC₆H₄, 4-BrC₆H₄, 4-MeC₆H₄, 4-EtC₆H₄, 4-*i*-PrC₆H₄, 4-MeOC₆H₄, 2-MeOC₆H₄, 4-NO₂C₆H₄

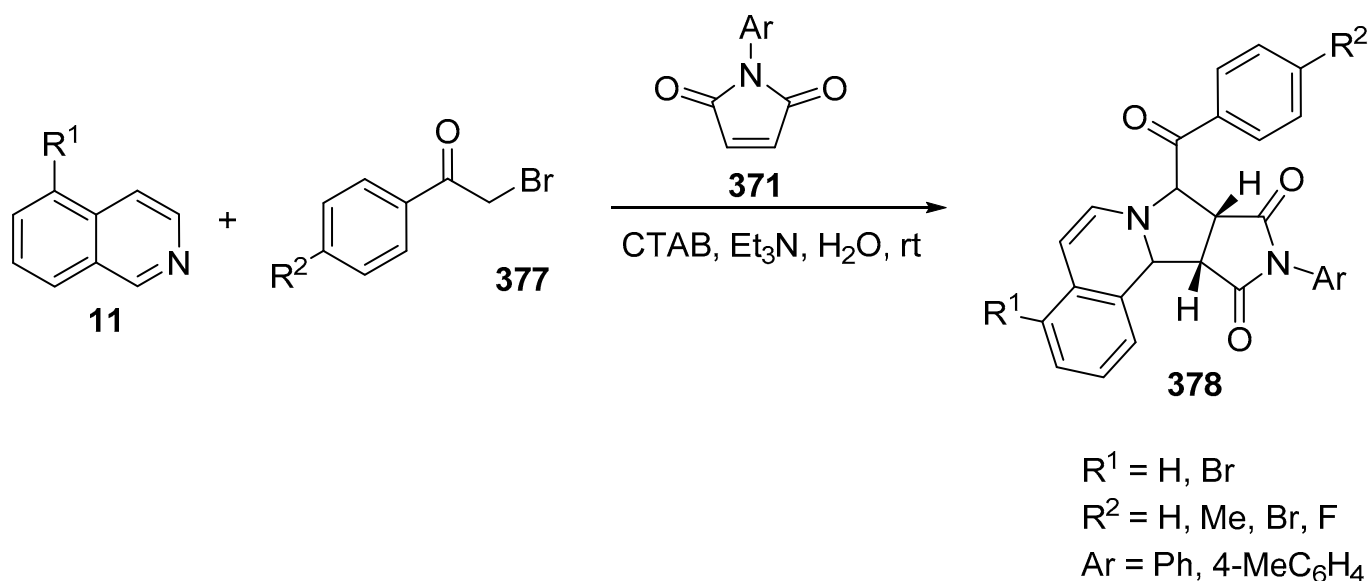
Scheme 118. Synthetic route towards spiro[indene-2,1'-pyrrolo[3,4-*c*]pyrroles] **373**.

In another reaction of *N*-phenylmaleimide **371** with azomethine ylides generated from 2-chloro-quinoline-3-carbaldehydes **374** and sarcosine **20**, two isomeric cycloadducts, namely, 1,4-diaza-bicyclo[3.3.0]octanes **375** and **376**, were formed (Scheme 119) [159].



Scheme 119. Synthesis of the two isomeric cycloadducts 5-(2-chloroquinolin-3-yl)-1,4-diaza-2,6-dioxo-4-methyl-1-phenyl-bicyclo[3.3.0]octanes **375** and **376**.

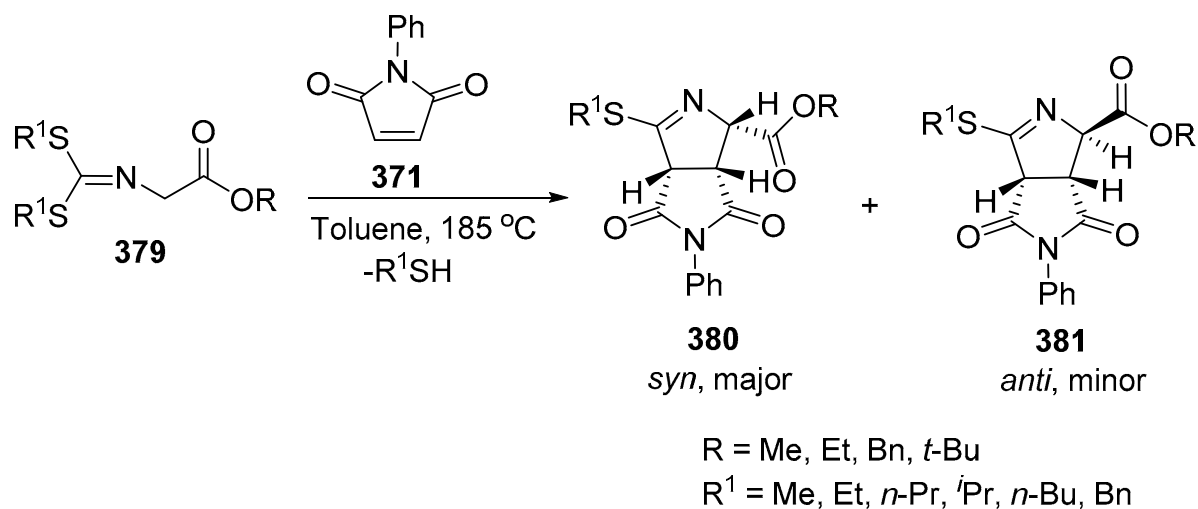
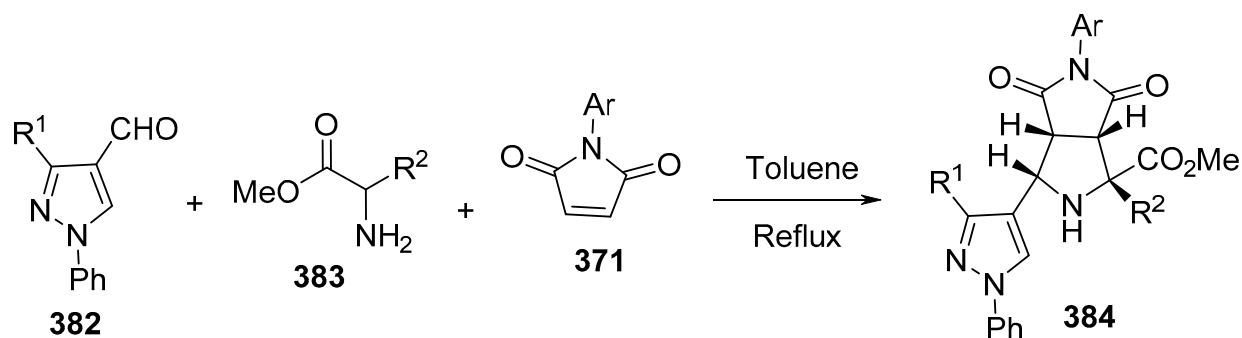
Tetracyclic pyrroloisoquinolines of type **378** were synthesized by the reaction of azomethine ylides, formed from isoquinolines **11** and phenacyl bromide **377**, with *N*-arylmaleimides **371** in the presence of cetyl trimethyl ammonium bromide (CTAB) (Scheme 120) [160].



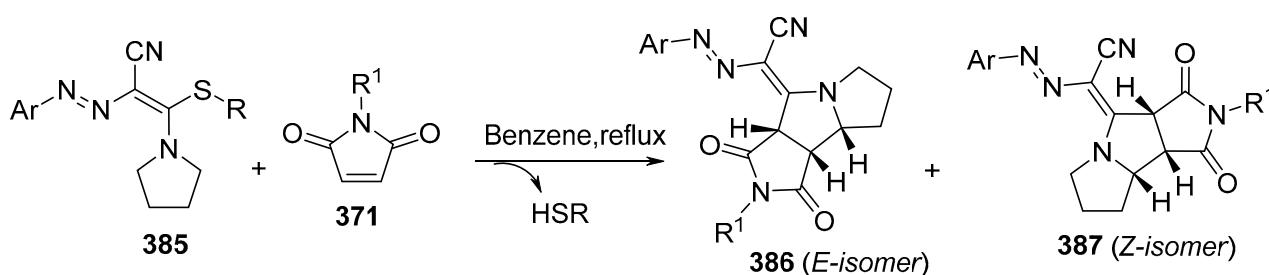
Scheme 120. Synthesis of pyrroloisoquinolines **378**.

Bicyclic hexahydropyrrolo[3,4-*c*]pyrrole-1-carboxylates **380** and **381** were obtained by reacting *N*-phenylmaleimide **371** with a series of azomethine ylides generated in situ from sulfanyl-substituted imines of glycine esters **379** (Scheme 121) [161]. Some of the synthesized diastereomeric compounds showed antioxidant activity relative to Nordihydroguaiaretic acid and Trolox [161].

Another reaction of maleimide **371** with pyrazole-4-carbaldehyde **382** and α -amino acid ester **383**, proceeding via azomethine intermediates in refluxing toluene, afforded the corresponding pyrazolylpyrrolopyrrole **384** (Scheme 122) [162].

Scheme 121. Synthesis of hexahydropyrrolo[3,4-*c*]pyrrole-1-carboxylates **380** and **381**.Scheme 122. Synthesis of pyrazolylpyrrolopyrroles **384**.

Isomeric pyrrolo[3,4-*a*]pyrrolizines **386** and **387** were synthesized by the cycloaddition of maleimide **371** with azomethine ylides formed from 3-alkylsulfanyl-2-arylazo-3-(pyrrolidin-1-yl)acrylonitriles of type **385** in refluxing benzene (Scheme 123) [163].



R = Me, allyl

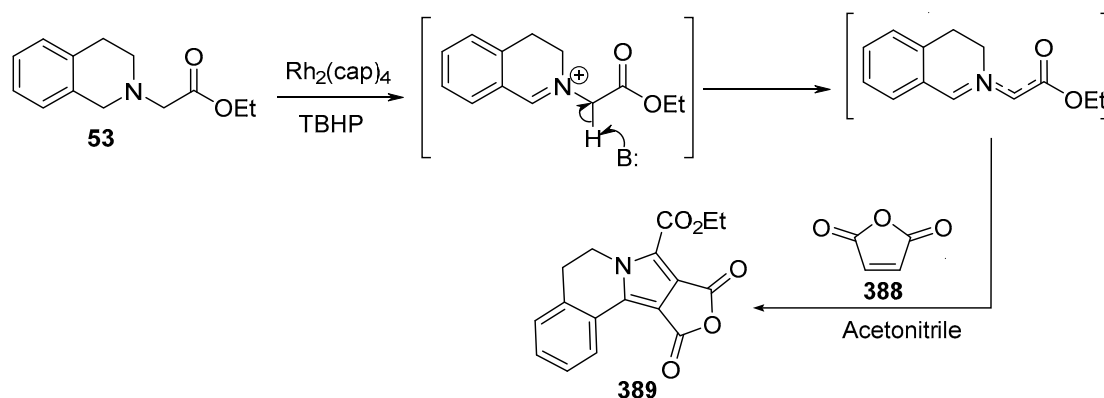
R¹ = Me, Ph

Ar = Ph, 4-NO₂C₆H₄, 2-CF₃C₆H₄, 4-CF₃C₆H₄, 4-EtO₂CC₆H₄, 4-ClC₆H₄, 2,4-Cl₂C₆H₃, 2-Cl-4-MeC₆H₃, 4-MeC₆H₄, 4-MeOC₆H₄, 4-EtOC₆H₄

Scheme 123. Synthesis of pyrrolo[3,4-*a*]pyrrolizines **386**, **387**.

4.3.2. Maleic Anhydride

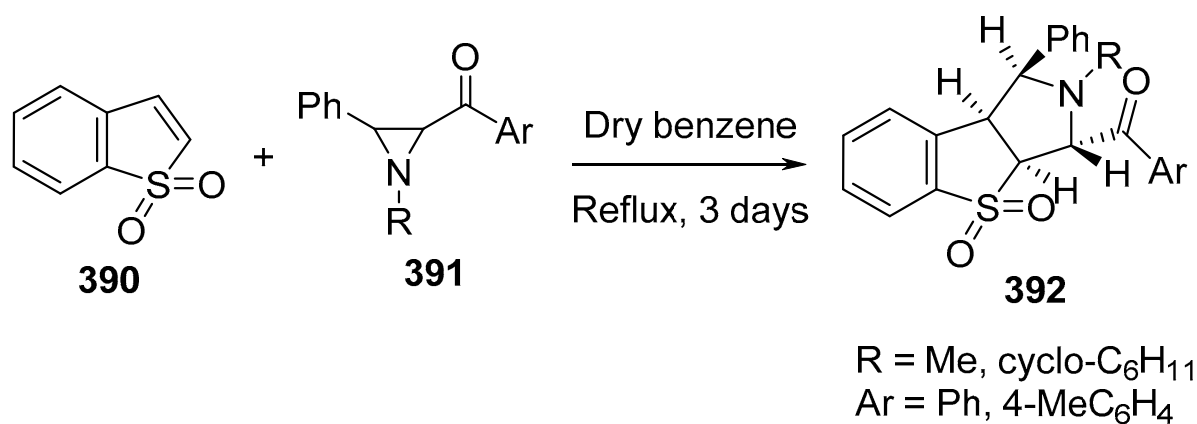
3,4-Dihydropyrrolo[2,1-*a*]isoquinoline **389** was obtained through the reaction of maleic anhydride **388** with azomethine ylide formed via the oxidation of tetrahydroisoquinoline **53** by dirhodium(II)caprolactamate [Rh₂(cap)₄] in the presence of *tert*-butyl hydroperoxide (TBHP) (Scheme 124) [37].



Scheme 124. Synthesis of 3,4-dihydropyrrolo[2,1-*a*]isoquinoline **389**.

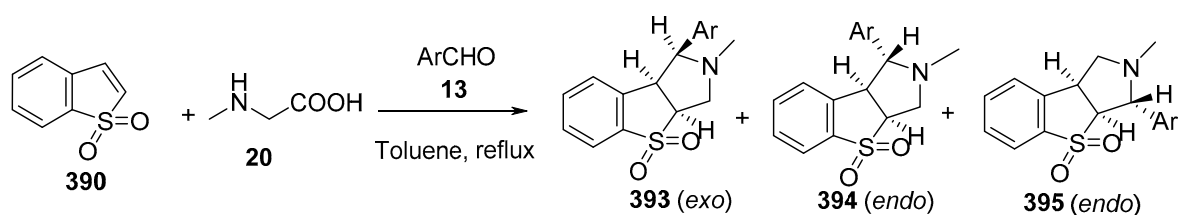
4.3.3. Benzo[*b*]thiophene-1,1-dioxide

The reaction of benzo[*b*]thiophene-1,1-dioxide **390** with a thermally generated azomethine ylide from aziridines **391** in refluxing dry benzene afforded the cycloadducts of type **392** (Scheme 125) [164].



Scheme 125. Synthesis of cycloadducts **392**.

Three isomeric cycloadducts, **393**–**395**, were obtained by reacting benzo[*b*]thiophene-1,1-dioxide **390** with azomethine ylides generated from sarcosine **20** and aldehydes **13** in refluxing toluene (Scheme 126) [164].

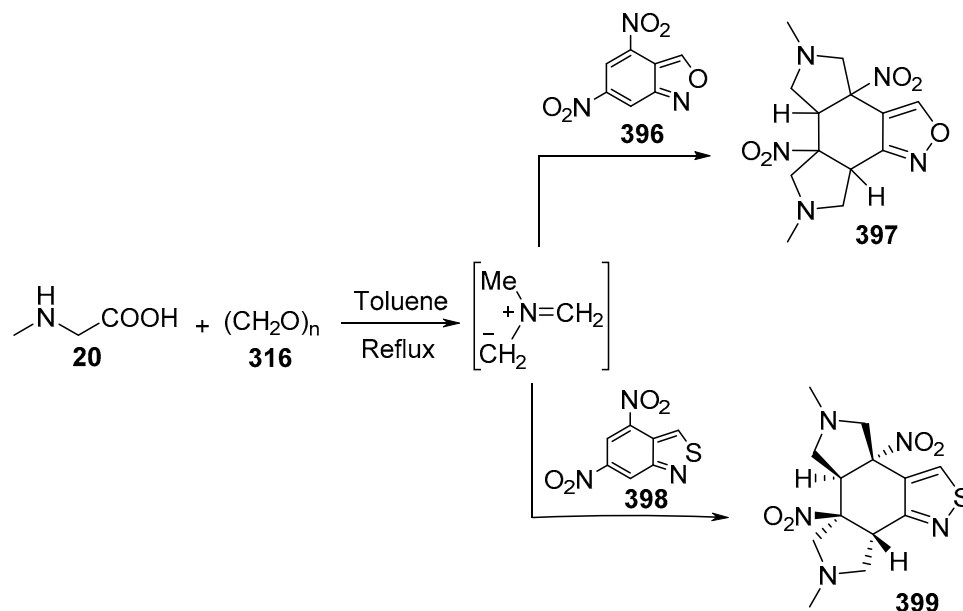


Ar = Ph, 4-NO₂C₆H₄, 4-MeOC₆H₄, 3,5-(MeO)₂C₆H₃, 4-BrC₆H₄

Scheme 126. Synthesis of cycloadducts **393**–**395**.

4.3.4. Benzo[*c*]isoxazole and Benzo[*c*]isothiazole

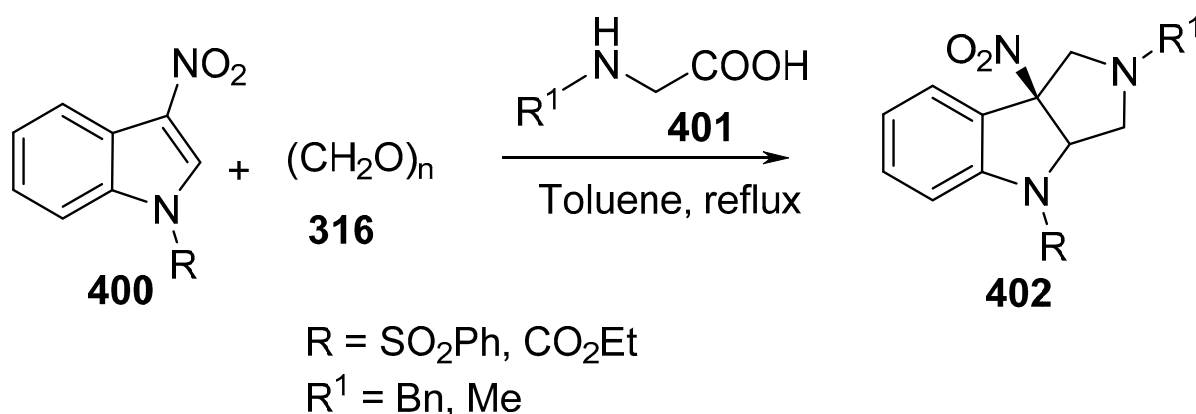
Decahydroisoxazolo[3,4-*e*]pyrrolo[3,4-*g*]isoindole **397** and its isothiazolo-derivative **399** were synthesized by the [3+2]-cycloaddition of benzo[*c*]isoxazole **396** and benzo[*c*]isothiazole **398**, respectively, to azomethine ylide generated from sarcosine **20** and paraformaldehyde **316** in toluene under reflux conditions (Scheme 127) [165].



Scheme 127. Synthesis of decahydroisoxazolo[3,4-*e*]pyrrolo[3,4-*g*]isoindole **397** and decahydroisothiazolo[3,4-*e*]pyrrolo[3,4-*g*]isoindole **399**.

4.3.5. Indoles

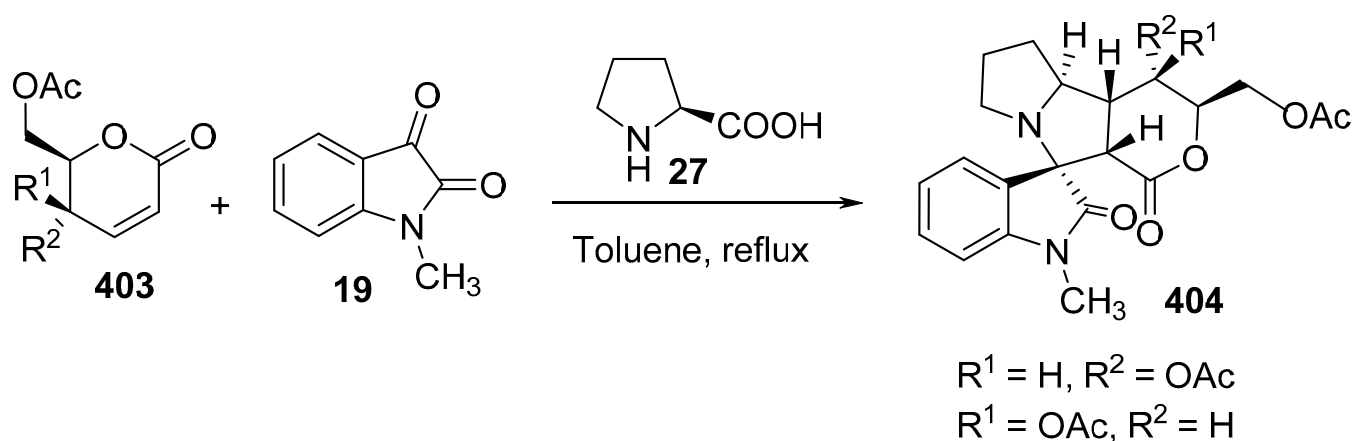
Hexahydropyrrolo[3,4-*b*]indoles of type **402** were synthesized by reacting 3-nitroindoles of type **400** with azomethine ylides formed from α -amino acids (sarcosine **20** or *N*-benzylglycine **401**) and paraformaldehyde **316** (Scheme 128) [166].



Scheme 128. Synthesis of hexahydropyrrolo[3,4-*b*]indoles **402**.

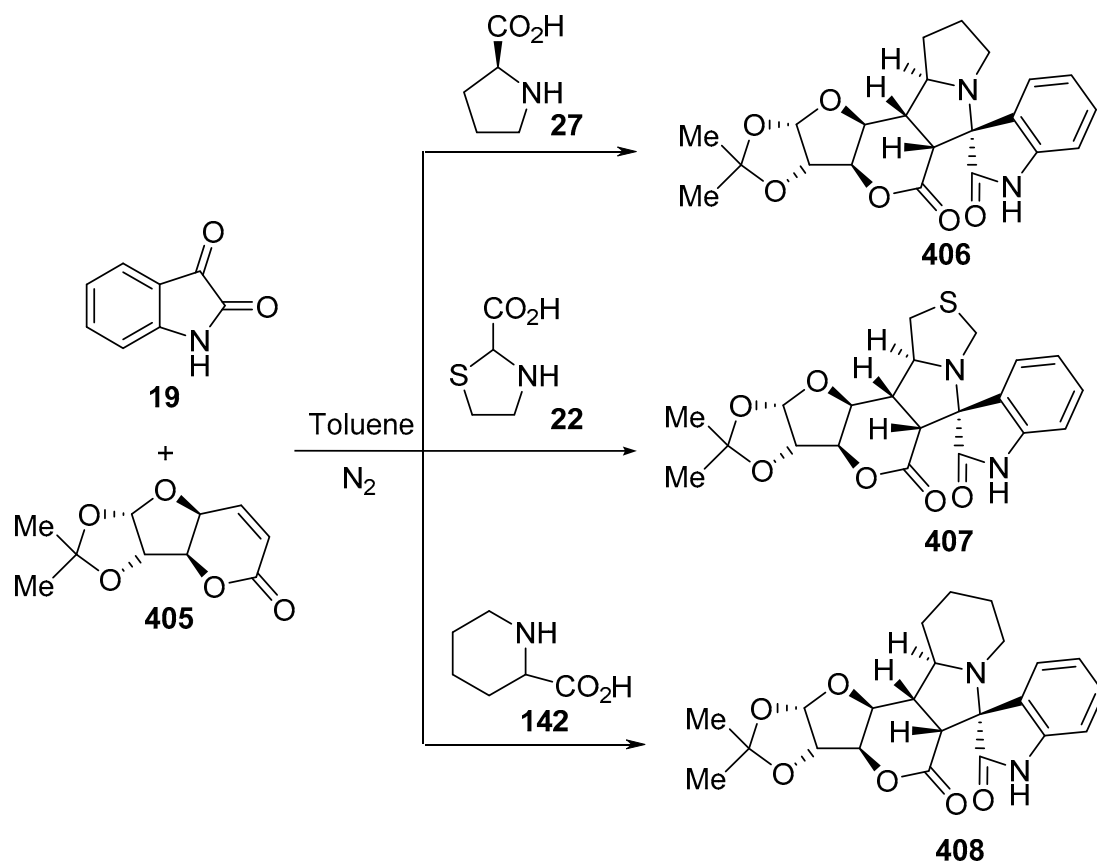
4.3.6. Lactones

The reaction of α,β -unsaturated lactones of type **403** with azomethine ylide formed from *N*-methyl isatin **19** and proline **27** in refluxing toluene afforded the corresponding pyrrolidinyloxyindole lactones of type **404** in high yield (Scheme 129) [167].



Scheme 129. Synthesis of pyrrolidinyl-spirooxindole lactones **404**.

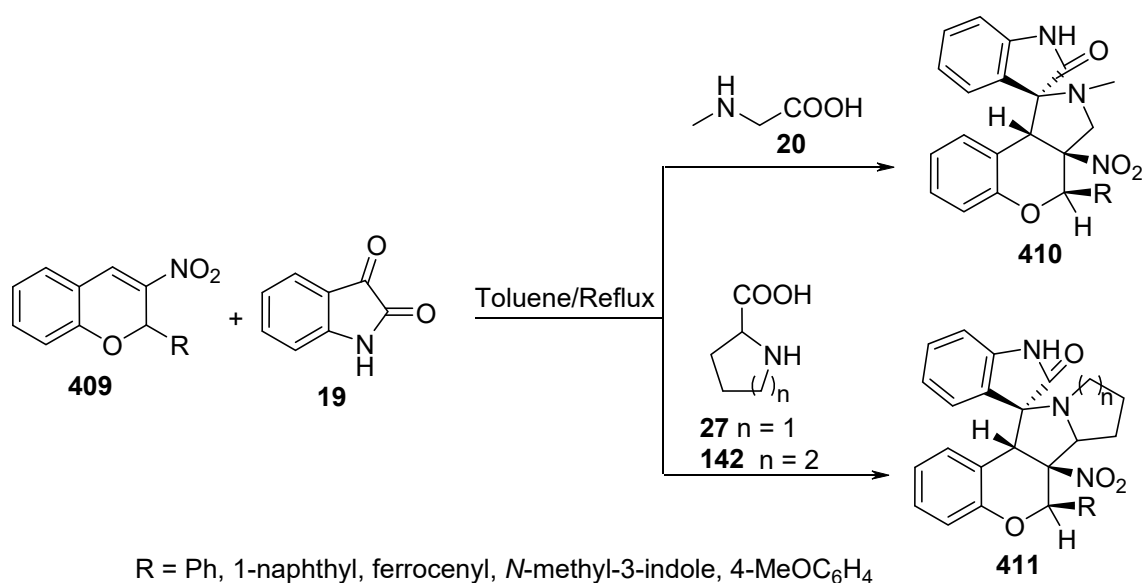
Another glucosyl α,β -unsaturated-7,3-lactone **405** reacted with azomethine ylides generated from isatin **19** and secondary amino acids (proline **27**, thioproline **22** or pipacolinic acid **142**) in refluxing dry toluene under N_2 (inert atmosphere) to produce glucosylspirooxindoles **406–408** in a highly regio- and stereoselective manner (Scheme 130) [168].



Scheme 130. Synthesis of glucosyl-spirooxindoles **406–408**.

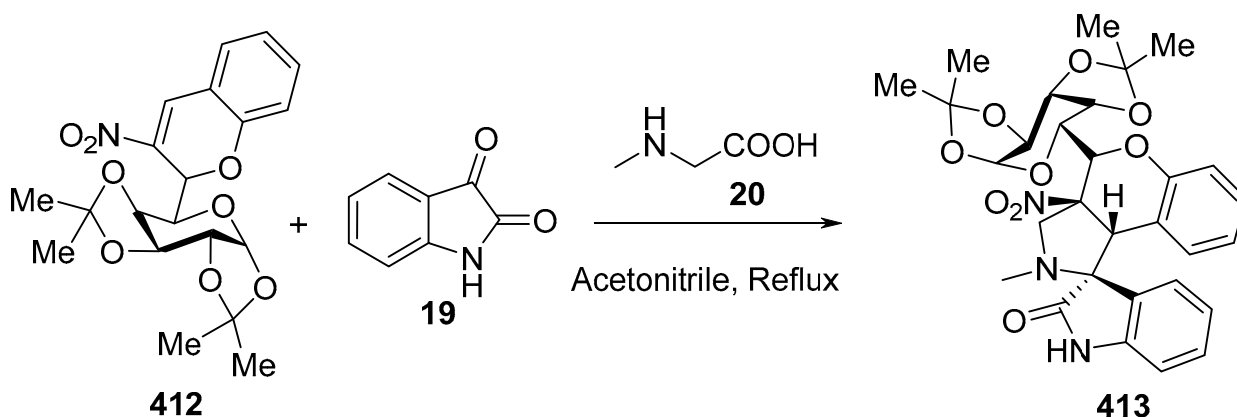
4.3.7. Chromenes

3-Nitrochromenes of type **409** underwent a reaction with azomethine ylides formed from isatin **19** and amino acids (sarcosine **20**, proline **27**, or pipacolinic acid **142**) in refluxing toluene to afford the corresponding spiropyrrolidine/spiro-pyrrolizidine/spiroindolizidine-oxindoles **410** and **411** (Scheme 131) [169].



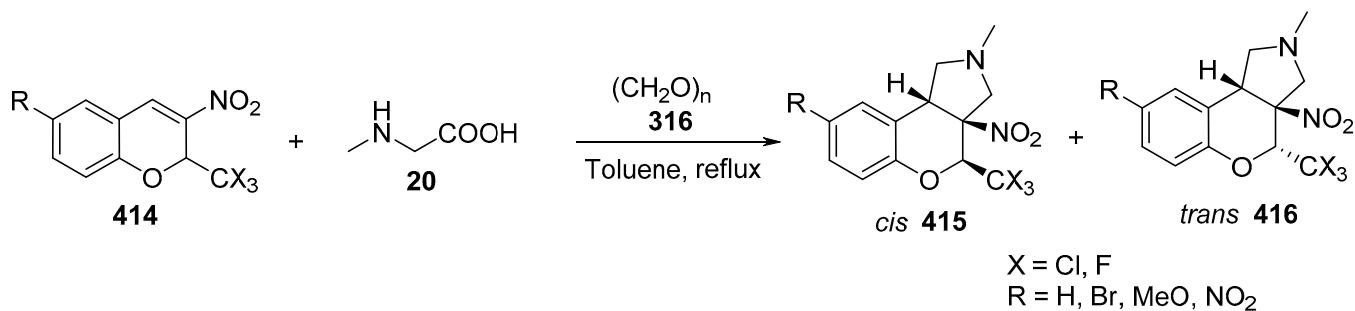
Scheme 131. Synthesis of spiropyrrolidine/spiropyrrrolizidine/spiroidolizidine-oxindoles **410** and **411**.

Spiropyrrrolidine-oxindole carbohydrate **413** was synthesized by the reaction of glycol 3-nitrochromene **412** with azomethine ylide formed from isatin **19** and sarcosine **20** in refluxing acetonitrile (Scheme 132) [170].



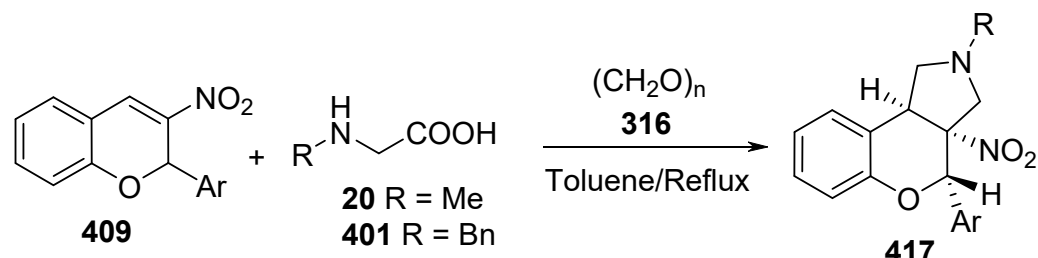
Scheme 132. Synthesis of spiropyrrolidine-oxindole carbohydrate **413**.

Isomeric benzopyrano[3,4-*c*]pyrrolidines **415** and **416** were obtained via the cycloaddition of 3-nitro-2-trihalomethyl-2*H*-chromenes **414** to azomethine ylide generated from sarcosine **20** and paraformaldehyde **316** in refluxing toluene (Scheme 133) [171].



Scheme 133. Synthesis of benzopyrano[3,4-*c*]pyrrolidines **415** and **416**.

However, the reaction of 2-aryl-3-nitrochromenes **409** with azomethine ylides formed from paraformaldehyde **316** and sarcosine **20** or *N*-benzyl-glycine **401** in toluene under refluxing conditions afforded the corresponding 3*a*-nitro-4-aryl benzopyrano[3,4-*c*]pyrrolidines of type **417** in high yields. Further, ^1H , ^1H -NOE spectroscopic studies supported the structure of **417** (Scheme 134) [172].

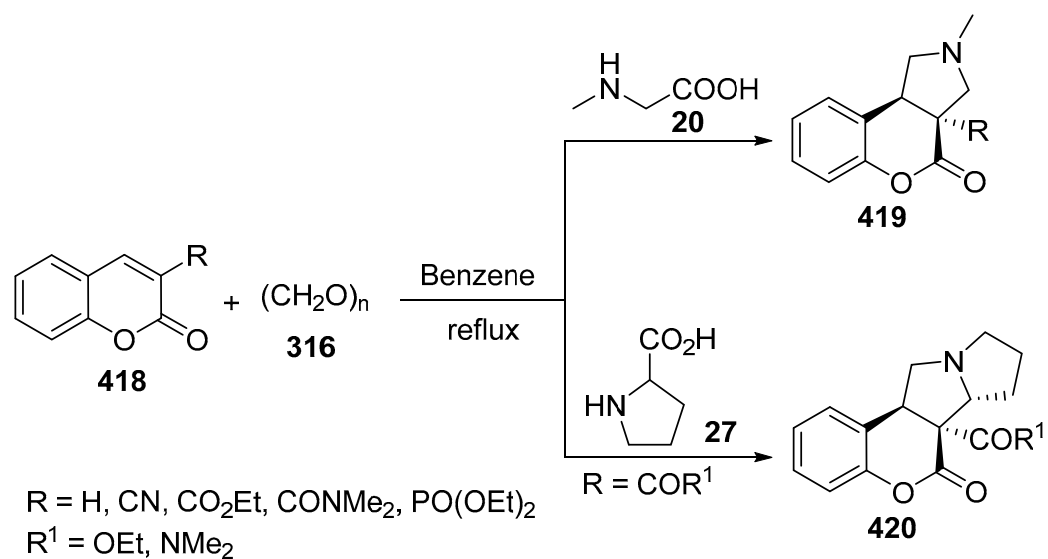


Ar = Ph, 4-ClC₆H₄, 2-ClC₆H₄, 4-MeOC₆H₄, 3-NO₂C₆H₄, 3,4-(MeO)₂C₆H₃

Scheme 134. Synthesis of 3*a*-nitro-4-aryl benzopyrano[3,4-*c*]pyrrolidines **417**.

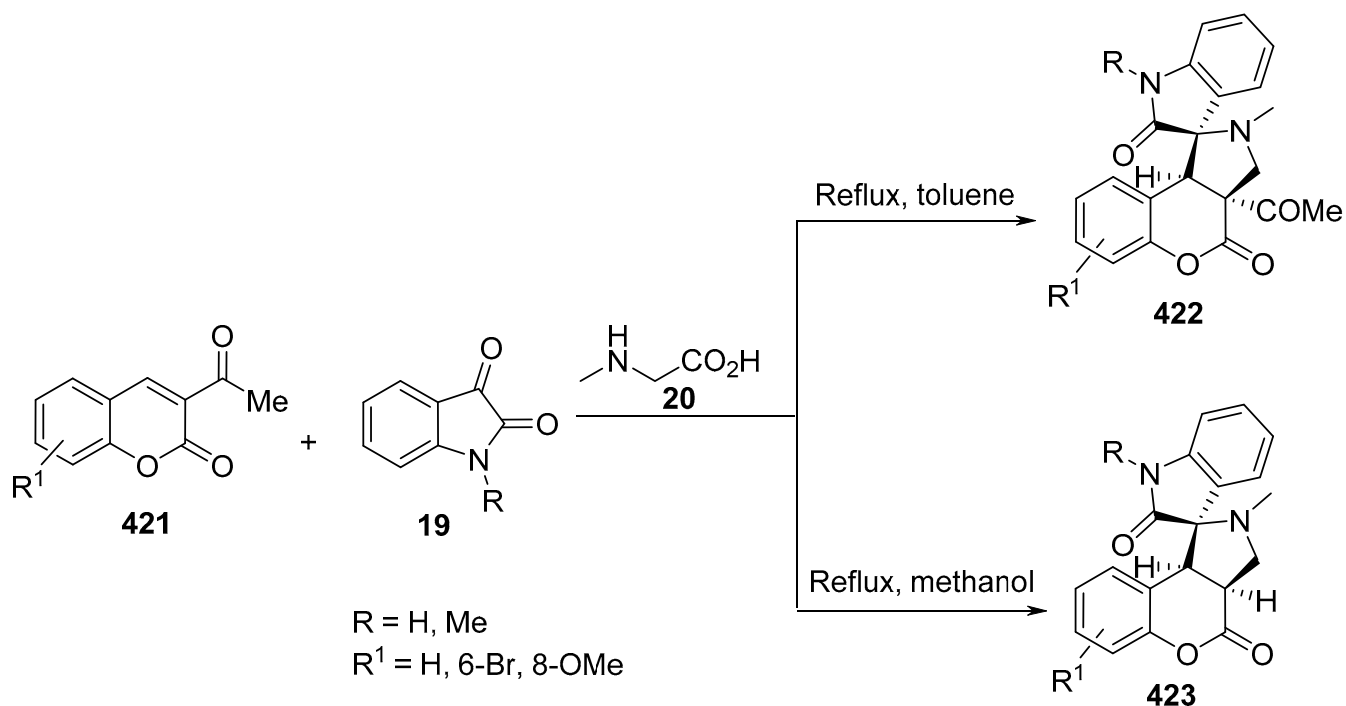
4.3.8. Coumarins

A cycloaddition strategy for the synthesis of [1]-benzopyrano[3,4-*c*]pyrrolidines **419** and **420** was based on the reaction of 3-substituted coumarins of type **418** and in situ-generated azomethine ylides formed from sarcosine **20** or proline **27** with paraformaldehyde **316** in refluxing benzene (Scheme 135) [173,174].



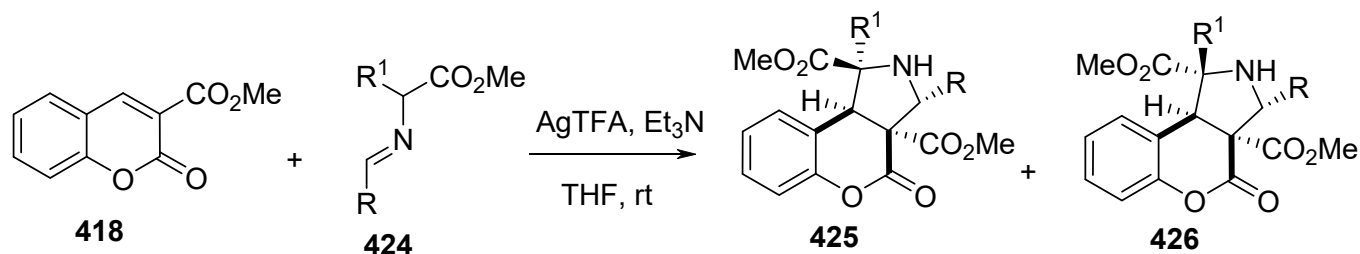
Scheme 135. Synthesis of [1]-benzopyrano[3,4-*c*]pyrrolidines **419**, **420**.

The reaction of 3-acetyl-2*H*-chromen-2-one **421** with azomethine ylides generated from isatin **19** and sarcosine **20** in refluxing toluene afforded the corresponding chromeno[3,4-*c*]spiropyrrrolidine-oxindoles of type **422**, while the analogous reaction in methanol gave chromeno[3,4-*c*]spiropyrrrolidine-oxindole derivatives of type **423** (Scheme 136) [175].



Scheme 136. Synthesis of chromeno[3,4-*c*]spiropyrrolidine-oxindoles **422** and **423**.

Mixtures of isomeric benzopyrano[3,4-*c*]pyrrolidines **425** and **426** were obtained from the reaction of coumarin **418** with azomethine ylides formed from α -iminoester **424** in the presence of silver(I)-trifluoroacetate (AgTFA) in tetrahydrofuran at room temperature (Scheme 137) [176].

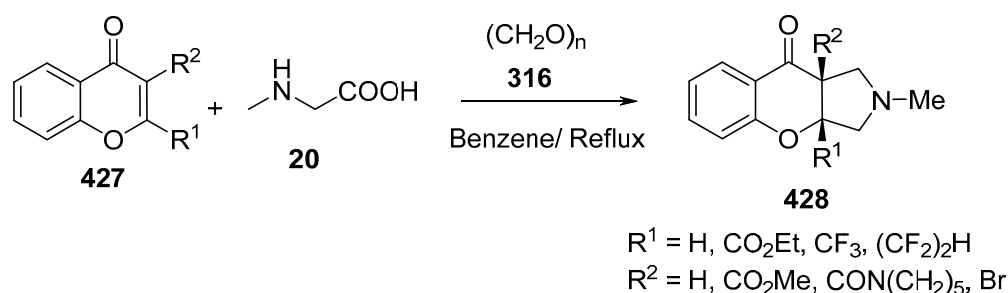


$\text{R} = \text{Ph, 4-BrC}_6\text{H}_4, 4\text{-FC}_6\text{H}_4, 3\text{-FC}_6\text{H}_4, 2\text{-FC}_6\text{H}_4, 4\text{-CF}_3\text{C}_6\text{H}_4, 3,5\text{-(CF}_3)_2\text{C}_6\text{H}_3, 4\text{-MeC}_6\text{H}_4,$
 $3\text{-MeC}_6\text{H}_4, 2\text{-MeC}_6\text{H}_4, 4\text{-MeOC}_6\text{H}_4, 2\text{-naphthyl, 3-MeO-4-benzyloxyC}_6\text{H}_3,$
 $2\text{-furanyl, 5-benzodioxole, }^t\text{Bu, pentanyl}$
 $\text{R}^1 = \text{H, Me, }^i\text{Pr, Ph}$

Scheme 137. Synthesis of benzopyrano[3,4-*c*]pyrrolidines **425** and **426**.

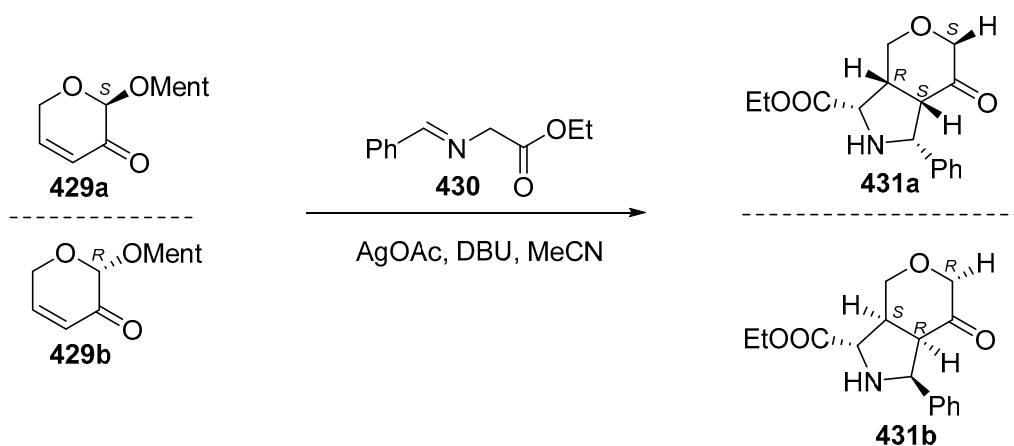
4.3.9. Chromones

Benzopyranopyrrolidine derivatives of type **428** were synthesized by the cycloaddition of 3-substituted chromones of type **427** with azomethine ylide generated from sarcosine **20** and paraformaldehyde **316** in benzene under refluxing conditions (Scheme 138) [177].



Scheme 138. Synthesis of benzopyranopyrrolidines **428**.

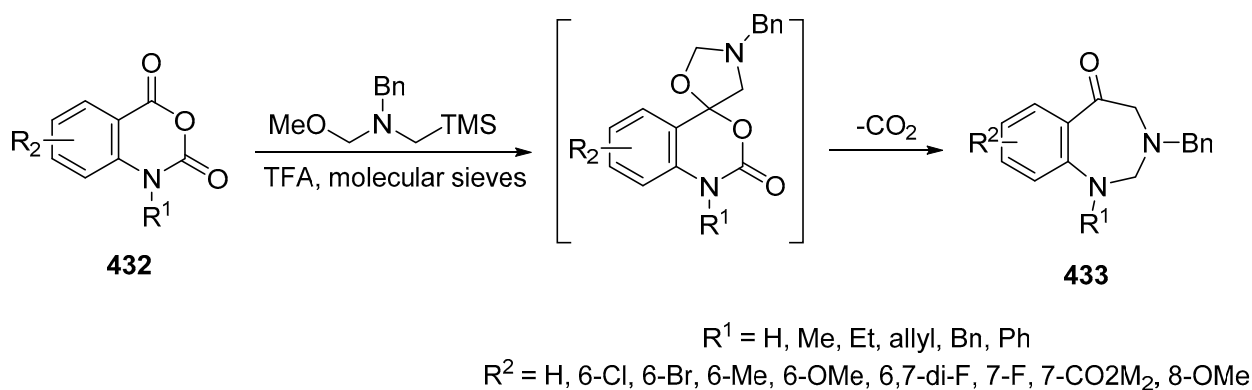
Udry et al. described the synthesis of enantiomerically pure cycloadducts (**431a**, **431b**) from stabilized azomethine ylides of type **430** and sugar-derived enones (**429a** and **429b**) through the [3+2]-cycloaddition reaction in the presence of silver acetate (AgOAc) and DBU in acetonitrile. The cycloadducts were further used to synthesize enantiomeric polyhydroxyalkylpyrrolidines as potential β -galactofuranosidase inhibitors (Scheme 139) [178].



Scheme 139. Synthesis of enantiomeric pyrrolidines **431**.

4.3.10. Isatoic Anhydride

1,3-Benzodiazepin-5-ones of type **433** were obtained through azomethine ylide (formed from (*N*-(methoxymethyl)-*N*-(trimethylsilyl-methyl)-benzylamine) **1** cycloaddition to isatoic anhydride **432** in trifluoroacetic acid in the presence of molecular sieves (4 Å) (Scheme 140) [179].



Scheme 140. Synthesis of 1,3-benzodiazepin-5-one **433**.

5. Conclusions and Outlook

Among various methods, the [3+2]-cycloaddition reaction of azomethine ylides is one of the most adopted protocols for the formation of pyrrolidine and pyrrole systems. The chemistry of azomethine ylides has progressed significantly in the last two decades. Azomethine ylides have been used for the synthesis of many stereoselective natural products, core ring systems of natural products, and several bioactive molecules containing multiple chiral centers. The cycloaddition of a three-atom component to an appropriate unsaturated substrate, namely, the unsaturated 2π -electron component, is the most embraced approach to the synthesis of five-membered heterocyclic compounds. By using various unsaturated 2π -electron components in reaction with in situ-generated azomethine ylides, a plethora of pyrrolidinyll-containing heterocycles can be obtained in a highly regio- and stereoselective manner. As a result of intermolecular cycloadditions, one new ring with a defined stereochemistry is formed; however, when the three-atom component and the substrate are part of the same molecule, the cycloaddition is intramolecular and leads to a more complex molecular architecture that is difficult to access by other routes, namely, through the use of new bicyclic systems.

This review summarizes the synthesis of some of the most important compounds resulting from the [3+2]-cycloaddition reactions of azomethine ylides with various olefinic (acyclic, alicyclic/heterocyclic, and exocyclic) unsaturated 2π -electron components and highlights their potential therapeutic significance. We believe the compiled subject will develop interest within this field among the research community and encourage them to develop a wider variety of asymmetric [3+2]-cycloaddition reaction strategies for the synthesis of complex molecules.

Funding: This work was supported financially by National Research Centre, Egypt, project ID: 12060101.

Institutional Review Board Statement: Not applicable.

Informed Consent Statement: Not applicable.

Data Availability Statement: Not applicable.

Acknowledgments: We thank the Department of Chemistry and Physics at Augusta University for its support.

Conflicts of Interest: The authors declare no conflict of interest.

References

- Huisgen, R. *1,3-Dipolar Cycloaddition Chemistry*; Padwa, A., Ed.; John Wiley & Sons: Hoboken, NJ, USA, 1984; Volume 1, Chapter 1; pp. 3–5.
- Rios-Gutierrez, M.; Domingo, L.R. Unravelling the mysteries of the [3+2] cycloaddition reactions. *Eur. J. Org. Chem.* **2019**, *2019*, 267–282. [CrossRef]
- William Lown, J. *1,3-Dipolar Cycloaddition Chemistry*; Padwa, A., Ed.; John Wiley & Sons: Hoboken, NJ, USA, 1984; Volume 1, Chapter 6; pp. 657, 726.
- Coldham, I.; Hufton, R. Intramolecular Dipolar Cycloaddition Reactions of Azomethine Ylides. *Chem. Rev.* **2005**, *105*, 2765–2809. [CrossRef] [PubMed]
- Song, G.; Chen, D.; Su, Y.; Han, K.; Pan, C.-L.; Jia, A.; Li, X. Isolation of Azomethine Ylides and Their Complexes: Iridium(III)-Mediated Cyclization of Nitron Substrates Containing Alkynes. *Angew. Chem. Int. Ed.* **2011**, *50*, 7791–7796. [CrossRef] [PubMed]
- Lee, D.J.; Han, H.S.; Shin, J.; Yoo, E.J. Multicomponent [5+2] Cycloaddition Reaction for the Synthesis of 1,4-Diazepines: Isolation and Reactivity of Azomethine Ylides. *J. Am. Chem. Soc.* **2014**, *136*, 11606–11609. [CrossRef]
- Molteni, G.; Silvani, A. Spiro-2-oxindoles via 1,3-dipolar cycloadditions. A decade update. *Eur. J. Org. Chem.* **2021**, *2021*, 1653–1675. [CrossRef]
- Adrio, J.; Carretero, J.C. Stereochemical diversity in pyrrolidine synthesis by catalytic asymmetric 1,3-dipolar cycloaddition of azomethine ylides. *Chem. Comm.* **2019**, *55*, 11979–11991. [CrossRef]
- Bdiri, B.; Zhao, B.-J.; Zhou, Z.-M. Recent advances in the enantioselective 1,3-dipolar cycloaddition of azomethine ylides and dipolarophiles. *Tetrahedron Asymm.* **2017**, *28*, 876–899. [CrossRef]
- Tang, S.; Zhang, X.; Sun, J.; Niu, D.; Chruma, J.J. 2-Azaallyl Anions, 2-Azaallyl Cations, 2-Azaallyl Radicals, and Azomethine Ylides. *Chem. Rev.* **2018**, *118*, 10393–10457. [CrossRef]

11. Dondas, H.A.; de Gracia Retamosa, M.; Sansano, J.M. Current Trends towards the Synthesis of Bioactive Heterocycles and Natural Products Using 1,3-Dipolar Cycloadditions (1,3-DC) with Azomethine Ylides. *Synthesis* **2017**, *49*, 2819–2851. [CrossRef]
12. Meyer, A.G.; Ryan, J.H. 1,3-Dipolar Cycloaddition Reactions of Azomethine Ylides with Carbonyl Dipolarophiles Yielding Oxazolidine Derivatives. *Molecules* **2016**, *21*, 935. [CrossRef]
13. Fang, X.; Wang, C.-J. Catalytic asymmetric construction of spiropyrrolidines via 1,3-dipolar cycloaddition of azomethine ylides. *Org. Biomol. Chem.* **2018**, *16*, 2591–2601. [CrossRef] [PubMed]
14. Arrastia, I.; Arrieta, A.; Cossio, F.P. Application of 1,3-Dipolar Reactions between Azomethine Ylides and Alkenes to the Synthesis of Catalysts and Biologically Active Compounds. *Eur. J. Org. Chem.* **2018**, *2018*, 5889–5904. [CrossRef] [PubMed]
15. Wei, L.; Chang, X.; Wang, C.-J. Catalytic Asymmetric Reactions with N-Metallated Azomethine Ylides. *Acc. Chem. Res.* **2020**, *53*, 1084–1100. [CrossRef] [PubMed]
16. Verma, S.; George, J.; Singh, S.; Pardasani, P.; Pardasani, R. [3+2] Cycloaddition reactions of thioisatin with thiazolidine-2-carboxylic acid: A versatile route to new heterocyclic scaffolds. *Org. Med. Chem. Lett.* **2011**, *1*, 6. [CrossRef] [PubMed]
17. Lashgari, N.; Ziarani, G.M. Synthesis of heterocyclic compounds based on isatin through 1,3-dipolar cycloaddition reactions. *ARKIVOC* **2012**, *2012*, 277–320. [CrossRef]
18. Padwa, A.; Pearson, W.H. (Eds.) The chemistry of heterocyclic compounds. In *Synthetic Applications of 1,3-Dipolar Cycloaddition Chemistry toward Heterocycles and Natural Products*; John Wiley & Sons: Hoboken, NJ, USA, 2002; Volume 59.
19. Martina, K.; Tagliapietra, S.; Veselov, V.V.; Cravotto, G. Green protocols in heterocycle syntheses via 1,3-dipolar cycloadditions. *Front. Chem.* **2019**, *7*, 95. [CrossRef]
20. Grafton, M.; Mansfield, A.C.; Fray, M.J. [3+2] Dipolar cycloadditions of an unstabilised azomethine ylide under continuous flow conditions. *Tetrahedron Lett.* **2010**, *51*, 1026–1029. [CrossRef]
21. Boruah, M.; Konwar, D.; Sharma, S.D. KF/Al₂O₃ mediated 1,3-dipolar cycloaddition of azomethine ylides: A novel and convenient procedure for the synthesis of highly substituted pyrrolidines. *Tetrahedron Lett.* **2007**, *48*, 4535–4537. [CrossRef]
22. Belfaitah, A.; Isly, M.; Carboni, B. 1,3-Dipolar cycloadditions of azomethine ylides to alkenylboronic esters. Access to substituted boron analogues of β -proline and 3-hydroxypyrrolidines. *Tetrahedron Lett.* **2004**, *45*, 1969–1972. [CrossRef]
23. Han, Y.; Hou, H.; Fu, Q.; Yan, C.-G. One-pot two-step tandem reactions for selective synthesis of pyrrolo[2,1-a]isoquinolines and dihydro-, tetrahydro-derivatives. *Tetrahedron* **2011**, *67*, 2313–2322. [CrossRef]
24. Poomathi, N.; Mayakrishnan, S.; Muralidharan, D.; Perumal, P.T. A facile access to novel spiroxindole fused pyrrolidine and thiazolo pyrrolidine benzimidazole derivatives via 1,3-dipolar cycloaddition reaction. *Tetrahedron Lett.* **2015**, *56*, 721–726. [CrossRef]
25. Dandia, A.; Jain, A.K.; Laxkar, A.K.; Bhati, D.S. A highly efficient protocol for the regio- and stereo-selective synthesis of spiro pyrrolidine and pyrrolizidine derivatives by multicomponent reaction. *Tetrahedron Lett.* **2013**, *54*, 3180–3184. [CrossRef]
26. Aksenov, A.V.; Aksenov, D.A.; Arutiunov, N.A.; Aksenov, N.A.; Aleksandrova, E.V.; Zhao, Z.; Du, L.; Kornienko, A.; Rubin, M. Synthesis of Spiro [indole-3, 5'-isoxazoles] with Anticancer Activity via a Formal [4+1]-Spirocyclization of Nitroalkenes to Indoles. *J. Org. Chem.* **2019**, *84*, 7123–7137. [CrossRef] [PubMed]
27. Żmigrodzka, M.; Sadowski, M.; Kras, J.; Dresler, E.; Demchuk, O.M.; Kula, K. Polar [3+2] cycloaddition between N-methyl azomethine ylide and trans-3, 3, 3-trichloro-1-nitroprop-1-ene. *Sci. Radices* **2022**, *1*, 26–35. [CrossRef]
28. Żmigrodzka, M.; Dresler, E.; Hordyjewicz-Baran, Z.; Kulesza, R.; Jasiński, R. Synthesis and chemical properties of 3-alkoxycarbonylchromones and 3-alkoxalylchromones. *Chem. Heter. Comp.* **2017**, *53*, 1161–1162. [CrossRef]
29. Seki, M.; Tsuruta, O.; Tatsumi, R.; Soejima, A. Synthesis and biological evaluation of pyrrolidine derivatives as novel and potent sodium channel blockers for the treatment of ischemic stroke. *Bioorg. Med. Chem. Lett.* **2013**, *23*, 4230–4234. [CrossRef]
30. Sun, H.; Wang, X.; Chen, Y.; Ouyang, L.; Liu, J.; Zhang, Y. Efficient construction of highly functionalized endo'-selective spiro[pyrrolidin-2,3'-oxindoles] via a regioselective 1,3-dipolar cycloaddition reaction between 3-amino oxindoles as azomethine ylide precursors and nitroalkenes. *Tetrahedron Lett.* **2014**, *55*, 5434–5438. [CrossRef]
31. Alimohammadi, K.; Sarrafi, Y.; Tajbakhsh, M.; Yeganegi, S.; Hamzehloueian, M. An experimental and theoretical investigation of the regio- and stereoselectivity of the polar [3+2] cycloaddition of azomethine ylides to nitrostyrenes. *Tetrahedron* **2011**, *67*, 1589–1597. [CrossRef]
32. De Silva, N.H.; Pyreddy, S.; Blanch, E.W.; Hügel, H.M.; Maniam, S. Microwave-assisted rapid synthesis of spirooxindole-pyrrolizidine analogues and their activity as anti-amyloidogenic agents. *Bioorg. Chem.* **2021**, *114*, 105128. [CrossRef]
33. Kumar, R.S.; Almansour, A.I.; Arumugam, N.; Mohammad, F.; Kotresha, D.; Menéndez, J.C. Spirooxindole-pyrrolidine heterocyclic hybrids promotes apoptosis through activation of caspase-3. *Bioorg. Med. Chem.* **2019**, *27*, 2487–2498. [CrossRef]
34. Arumugam, N.; Almansour, A.I.; Kumar, R.S.; Alaqeel, S.I.; Krishna, V.S.; Sriram, D. Anti-tubercular activity of novel class of spiropyrrolidine tethered indenoquinoline heterocyclic hybrids. *Bioorg. Chem.* **2020**, *99*, 103799. [CrossRef] [PubMed]
35. Almansour, A.I.; Arumugam, N.; Kumar, R.S.; Kotresha, D.; Manohar, T.S.; Venketesh, S. Design, synthesis and cholinesterase inhibitory activity of novel spiropyrrolidine tethered imidazole heterocyclic hybrids. *Bioorg. Med. Chem. Lett.* **2020**, *30*, 126789. [CrossRef] [PubMed]
36. Arumugam, N.; Raghunathan, R. Synthesis of highly functionalized β -lactam substituted pyrroloisoquinoline and indolizinoindole system by sequential intermolecular 1,3-dipolar cycloaddition reaction and Pictet-Spengler cyclization. *Tetrahedron* **2010**, *66*, 969–975. [CrossRef]

37. Wang, H.-T.; Lu, C.-D. Synthesis of 3,4-dihydropyrrolo[2,1-a]isoquinolines based on [3+2] cycloaddition initiated by Rh₂(cap)₄-catalyzed oxidation. *Tetrahedron Lett.* **2013**, *54*, 3015–3018. [CrossRef]
38. Thangamani, A. Regiospecific synthesis and biological evaluation of spirooxindolopyrrolizidines via [3+2] cycloaddition of azomethine ylide. *Eur. J. Med. Chem.* **2010**, *45*, 6120–6126. [CrossRef]
39. Kaur, A.; Singh, B.; Vyas, B.; Silakari, O. Synthesis and biological activity of 4-aryl-3-benzoyl-5-phenylspiro[pyrrolidine-2,3'-indolin]-2'-one derivatives as novel potent inhibitors of advanced glycation end product. *Eur. J. Med. Chem.* **2014**, *79*, 282–289. [CrossRef]
40. Taghizadeh, M.J.; Arvinnezhad, H.; Samadi, S.; Jadidi, K.; Javidan, A.; Notash, B. Synthesis of new enantiomerically pure spirooxindolopyrrolizidines via a three-component asymmetric 1,3-dipolar cycloaddition reaction of azomethine ylides derived from isatin. *Tetrahedron Lett.* **2012**, *53*, 5148–5150. [CrossRef]
41. Arun, Y.; Saranraj, K.; Balachandran, C.; Perumal, P.T. Novel spirooxindole-pyrrolidine compounds: Synthesis, anticancer and molecular docking studies. *Eur. J. Med. Chem.* **2014**, *74*, 50–64. [CrossRef]
42. Arun, Y.; Bhaskar, G.; Balachandran, C.; Ignacimuthu, S.; Perumal, P.T. Facile one-pot synthesis of novel dispirooxindole-pyrrolidine derivatives and their antimicrobial and anticancer activity against A549 human lung adenocarcinoma cancer cell line. *Bioorg. Med. Chem. Lett.* **2013**, *23*, 1839–1845. [CrossRef]
43. Lakshmi, N.V.; Thirumurugan, P.; Perumal, P.T. An expedient approach for the synthesis of dispiropyrrrolidine bisoxindoles, spiropyrrrolidine oxindoles and spiroindane-1,3-diones through 1,3-dipolar cycloaddition reactions. *Tetrahedron Lett.* **2010**, *51*, 1064–1068. [CrossRef]
44. Kathirvelan, D.; Haribabu, J.; Reddy, B.S.R.; Balachandran, C.; Duraipandiyar, V. Facile and diastereoselective synthesis of 3,2'-spiropyrrrolidineoxindoles derivatives, their molecular docking and antiproliferative activities. *Bioorg. Med. Chem. Lett.* **2015**, *25*, 389–399. [CrossRef] [PubMed]
45. Yuvaraj, P.; Reddy, B.S.R. Synthesis of 3-spiropyrrrolidine-3-spirooxindoles from Baylis–Hillman adducts of chromone with azomethine ylides via [3+2] cycloaddition reaction. *Tetrahedron Lett.* **2013**, *54*, 821–827. [CrossRef]
46. Sarrafi, Y.; Hamzehlouian, M.; Alimohammadi, K.; Khavasi, H.R. Regioselective synthesis of novel spiroindane-1,3-diones through 1,3-dipolar cycloaddition reactions. *Tetrahedron Lett.* **2010**, *51*, 4734–4737. [CrossRef]
47. Kia, Y.; Osman, H.; Kumar, R.S.; Murugaiyah, V.; Basiri, A.; Perumal, S.; Razak, I.A. A facile chemo-, regio- and stereoselective synthesis and cholinesterase inhibitory activity of spirooxindole-pyrrolizine-piperidine hybrids. *Bioorg. Med. Chem. Lett.* **2013**, *23*, 2979–2983. [CrossRef] [PubMed]
48. Kia, Y.; Osman, H.; Kumar, R.S.; Murugaiyah, V.; Basiri, A.; Perumal, S.; Wahab, H.A.; Bing, C.S. Synthesis and discovery of novel piperidone-grafted mono- and bis-spirooxindole-hexahydropyrrolizines as potent cholinesterase inhibitors. *Bioorg. Med. Chem.* **2013**, *21*, 1696–1707. [CrossRef] [PubMed]
49. Arumugam, N.; Periyasami, G.; Raghunathan, R.; Kamalraj, S.; Muthumary, J. Synthesis and antimicrobial activity of highly functionalised novel β -lactam grafted spiropyrrrolidines and pyrrolizidines. *Eur. J. Med. Chem.* **2011**, *46*, 600–607. [CrossRef]
50. Hong, B.-C.; Liu, K.-L.; Tsai, C.-W.; Liao, J.-H. Proline-mediated dimerization of cinnamaldehydes via 1,3-dipolar cycloaddition reaction with azomethine ylides. A rapid access to highly functionalized hexahydro-1H-pyrrolizine. *Tetrahedron Lett.* **2008**, *49*, 5480–5483. [CrossRef]
51. Kang, T.-R.; Cheng, Y.; He, L.; Ye, J.; Liu, Q.-Z. Facile synthesis of highly functional pyrrolizidine derivatives from β,γ -unsaturated α -keto esters and proline via a tandem cycloaddition. *Tetrahedron Lett.* **2012**, *53*, 2552–2555. [CrossRef]
52. Rajesh, R.; Suresh, M.; Selvam, R.; Raghunathan, R. Synthesis of acridinedione derived mono spiro-pyrrolidine/pyrrolizidine derivatives—a facile approach via intermolecular [3+2] cycloaddition reaction. *Tetrahedron Lett.* **2014**, *55*, 4047–4053. [CrossRef]
53. Ramesh, E.; Kathiresan, M.; Raghunathan, R. Solvent-free microwave-assisted conversion of Baylis–Hillman adducts of ninhydrin into functionalized spiropyrrrolidines/pyrrolizidines through 1,3-dipolar cycloaddition. *Tetrahedron Lett.* **2007**, *48*, 1835–1839. [CrossRef]
54. Nájera, C.; de Gracia Retamosa, M.; Sansano, J.M. 1,3-Dipolar cycloadditions of azomethine ylides with chiral acrylates derived from methyl (S)- and (R)-lactate: Diastereo- and enantioselective synthesis of polysubstituted prolines. *Tetrahedron Asymmetry* **2006**, *17*, 1985–1989. [CrossRef]
55. Ujjainwalla, F.; Warner, D.; Snedden, C.; Grisson, R.D.; Walsh, T.F.; Wyvratt, M.J.; Kalyani, R.N.; MacNeil, T.; Tang, R.; Weinberg, D.H.; et al. Design and syntheses of melanocortin subtype-4 receptor agonists. Part 2: Discovery of the dihydropyridazinone motif. *Bioorg. Med. Chem. Lett.* **2005**, *15*, 4023–4028. [CrossRef] [PubMed]
56. Parmar, N.J.; Pansuriya, B.R.; Barad, H.A.; Kant, R.; Gupta, V.K. An improved microwave assisted one-pot synthesis, and biological investigations of some novel aryldiazanyl chromeno fused pyrrolidines. *Bioorg. Med. Chem. Lett.* **2012**, *22*, 4075–4079. [CrossRef] [PubMed]
57. Purushothaman, S.; Prasanna, R.; Niranjana, P.; Raghunathan, R.; Nagaraj, S.; Rengasamy, R. Stereoselective synthesis of hexahydro-3-methyl-1-arylchromeno[3,4-b]pyrrole and its annulated heterocycles as potent antimicrobial agents for human pathogens. *Bioorg. Med. Chem. Lett.* **2010**, *20*, 7288–7291. [CrossRef] [PubMed]
58. Ramesh, E.; Raghunathan, R. A facile synthesis of chromeno[4,3-b]pyrroles derived from allyl derivatives of Baylis–Hillman adducts through intramolecular 1,3-dipolar cycloaddition using ultrasonication. *Tetrahedron Lett.* **2008**, *49*, 1125–1128. [CrossRef]
59. Bakthadoss, M.; Sivakumar, N.; Sivakumar, G.; Murugan, G. Highly regio- and stereoselective synthesis of tricyclic frameworks using Baylis–Hillman derivatives. *Tetrahedron Lett.* **2008**, *49*, 820–823. [CrossRef]

60. Pospíšil, J.; Potáček, M. Microwave-assisted solvent-free intramolecular 1,3-dipolar cycloaddition reactions leading to hexahydrochromeno[4,3-b]pyrroles: Scope and limitations. *Tetrahedron* **2007**, *63*, 337–346. [CrossRef]
61. Poornachandran, M.; Raghunathan, R. Synthesis of pyrrolo[3,4-b]pyrroles and perhydrothiazolo[3',4'-2,3]pyrrolo[4,5-c]pyrroles. *Tetrahedron* **2008**, *64*, 6461–6474. [CrossRef]
62. Poornachandran, M.; Raghunathan, R. A novel diastereoselective 1,3-dipolar cycloaddition approach to cis-fused bispyrrolidines. *Tetrahedron Asymmetry* **2008**, *19*, 2177–2183. [CrossRef]
63. Kathiravan, S.; Ramesh, E.; Raghunathan, R. Synthesis of pyrrolo[2,3-a]pyrrolizine and pyrrolizine[2,3-a]pyrrolizine derived from allyl derivatives of Baylis–Hillman adducts through intramolecular 1,3-dipolar cycloaddition. *Tetrahedron Lett.* **2009**, *50*, 2389–2391. [CrossRef]
64. Coldham, I.; Dobson, B.C.; Franklina, A.I.; Fletcher, S.R. Synthesis of tetracyclic indole-containing ring systems by intramolecular cycloadditions of azomethine ylides. *Tetrahedron Lett.* **2007**, *48*, 873–875. [CrossRef]
65. Mishra, A.; Rastogi, N.; Batra, S. 2-(N-Allylaminomethyl)cinnamaldehydes as substrates for syntheses of aza-polycycles via intramolecular cycloaddition reactions. *Tetrahedron* **2012**, *68*, 2146–2154. [CrossRef]
66. Sirisha, N.; Raghunathan, R. Stereoselective synthesis of novel glyco-pyrano pyrrolidines/pyrrolizidines/indolizidines through intramolecular [3+2] cycloaddition approach. *Tetrahedron Lett.* **2010**, *51*, 2515–2518. [CrossRef]
67. Ghandi, M.; Taheri, A.; Bozcheloei, A.H.; Abbasi, A.; Kia, R. Synthesis of novel tricyclic and tetracyclic sultone scaffolds via intramolecular 1,3-dipolar cycloaddition reactions. *Tetrahedron* **2012**, *68*, 3641–3648. [CrossRef]
68. Rao, J.N.S.; Raghunathan, R. One-pot sequential azide–alkyne/intramolecular azomethine ylide 1,3-dipolar cycloaddition strategy for the synthesis of carbohydrate grafted macrocycles. *Tetrahedron Lett.* **2015**, *56*, 2669–2673. [CrossRef]
69. Kathiravan, S.; Vijayarajan, D.; Raghunathan, R. Novel synthesis of naphtho[2,1-b]pyrano pyrrolizidines and indolizidines through intramolecular 1,3-dipolar cycloaddition reaction. *Tetrahedron Lett.* **2010**, *51*, 3065–3070. [CrossRef]
70. Pankova, A.S.; Voronin, V.V.; Kuznetsov, M.A. Intramolecular cycloaddition of N-phthalimidoaziridines to double and triple carbon–carbon bonds. *Tetrahedron Lett.* **2009**, *50*, 5990–5993. [CrossRef]
71. Shishido, Y.; Ito, F.; Morita, H.; Ikunaka, M. Stereoselective synthesis of a novel 2-aza-7-oxabicyclo[3.3.0]octane as neurokinin-1 receptor antagonist. *Bioorg. Med. Chem. Lett.* **2007**, *17*, 6887–6890. [CrossRef]
72. Girgis, A.S.; Farag, H.; Ismail, N.S.M.; George, R.F. Synthesis, hypnotic properties and molecular modeling studies of 1,2,7,9-tetraaza-spiro[4.5]dec-2-ene-6,8,10-triones. *Eur. J. Med. Chem.* **2011**, *46*, 4964–4969. [CrossRef]
73. Girgis, A.S.; Ismail, N.S.M.; Farag, H.; El-Eraky, W.I.; Saleh, D.O.; Tala, S.R.; Katritzky, A.R. Regioselective synthesis and molecular modeling study of vasorelaxant active 7,9-dioxo-1,2-diaza-spiro[4.5]dec-2-ene-6,10-diones. *Eur. J. Med. Chem.* **2010**, *45*, 4229–4238. [CrossRef]
74. Girgis, A.S.; Barsoum, F.F.; Samir, A. Regioselective synthetic approaches towards 1,2,8,9-tetraazadispiro[4.1.4.2]trideca-2,9-dien-6-ones of potential antimicrobial properties. *Eur. J. Med. Chem.* **2009**, *44*, 2447–2451. [CrossRef] [PubMed]
75. Mishriky, N.; Girgis, A.S.; Hosni, H.M.; Farag, H. Regio- and stereoselective synthesis of spiro[1-benzothiepine-4(5H),3'(3H)-pyrazol]-5-ones. *J. Heterocycl. Chem.* **2006**, *43*, 1549–1556. [CrossRef]
76. Hegab, M.I.; Girgis, A.S.; Ahmed-Farag, I.S. Novel regioselective synthesis of 3'H, 4H-spiro[chromene-3,2'-[1,3,4]thiadiazol]-4-one containing compounds. *J. Heterocycl. Chem.* **2006**, *43*, 1237–1242. [CrossRef]
77. Sridhar, G.; Gunasundari, T.; Raghunathan, R. A greener approach for the synthesis of 1-N-methyl-(spiro[2.3']oxindolespiro[3.2']/spiro[2.3']indan-1,3-dionespiro[2.2'])cyclopentanone-4-aryl pyrrolidines. *Tetrahedron Lett.* **2007**, *48*, 319–322. [CrossRef]
78. George, R.F.; Ismail, N.S.M.; Stawinski, J.; Girgis, A.S. Design, synthesis and QSAR studies of dispiroindole derivatives as new anti-proliferative agents. *Eur. J. Med. Chem.* **2013**, *68*, 339–351. [CrossRef]
79. Jayashankaran, J.; Manian, R.D.R.S.; Venkatesan, R.; Raghunathan, R. A regioselective synthesis of dispiro[oxindole-cyclohexanone]pyrrolidines and dispiro[oxindole-hexahydroindazole]pyrrolidines by sequential 1,3-dipolar cycloaddition and annulation through a microwave induced solvent-free approach. *Tetrahedron* **2005**, *61*, 5595–5598. [CrossRef]
80. Kumar, R.R.; Perumal, S.; Manju, S.C.; Bhatt, P.; Yogeewari, P.; Sriram, D. An atom economic synthesis and antitubercular evaluation of novel spiro-cyclohexanones. *Bioorg. Med. Chem. Lett.* **2009**, *19*, 3461–3465. [CrossRef]
81. Gavaskar, D.; Raghunathan, R.; Babu, A.R.S. An expedient one-pot sequential five-component synthesis of highly substituted spiro-pyrrolidine heterocycles. *Tetrahedron Lett.* **2014**, *55*, 2217–2220. [CrossRef]
82. Dandia, A.; Singh, R.; Joshi, J.; Kumari, S. An eco-compatible synthesis of medicinally important novel class of trispiroheterocyclic framework using 2,2,2-trifluoroethanol as a reusable medium. *J. Fluor. Chem.* **2013**, *156*, 283–289. [CrossRef]
83. Lotfy, G.; Said, M.M.; El Ashry, E.H.; El Tamany, E.H.; Al-Dhfyhan, A.; Abdel Aziz, Y.M.; Barakat, A. Synthesis of new spirooxindole-pyrrolothiazole derivatives: Anti-cancer activity and molecular docking. *Bioorg. Med. Chem.* **2017**, *25*, 1514–1523. [CrossRef]
84. Girgis, A.S. Regioselective synthesis of dispiro[1H-indene-2,3'-pyrrolidine-2',3''-[3H]indole]-1,2''(1''H)-diones of potential anti-tumor properties. *Eur. J. Med. Chem.* **2009**, *44*, 91–100. [CrossRef] [PubMed]
85. Girgis, A.S.; Panda, S.S.; Srour, A.M.; Farag, H.; Ismail, N.S.M.; Elgendy, M.; Abdel-Aziz, A.K.; Katritzky, A.R. Rational design, synthesis and molecular modeling studies of novel anti-oncological alkaloids against melanoma. *Org. Biomol. Chem.* **2015**, *13*, 6619–6633. [CrossRef] [PubMed]
86. Prasanna, P.; Balamurugan, K.; Perumal, S.; Yogeewari, P.; Sriram, D. A regio- and stereoselective 1,3-dipolar cycloaddition for the synthesis of novel spiro-pyrrolothiazolyloxindoles and their antitubercular evaluation. *Eur. J. Med. Chem.* **2010**, *45*, 5653–5661. [CrossRef] [PubMed]

87. Wei, A.C.; Ali, M.A.; Yoon, Y.K.; Ismail, R.; Choon, T.S.; Kumar, R.S.; Arumugam, N.; Almansour, A.I.; Osman, H. Antimycobacterial activity: A facile three-component [3+2]-cycloaddition for the regioselective synthesis of highly functionalised dispiropyrrolidines. *Bioorg. Med. Chem. Lett.* **2012**, *22*, 4930–4933. [CrossRef]
88. Wei, A.C.; Ali, M.A.; Yoon, Y.K.; Ismail, R.; Choon, T.S.; Kumar, R.S. A facile three-component [3+2]-cycloaddition for the regioselective synthesis of highly functionalised dispiropyrrolidines acting as antimycobacterial agents. *Bioorg. Med. Chem. Lett.* **2013**, *23*, 1383–1386. [CrossRef] [PubMed]
89. Wei, A.C.; Ali, M.A.; Yoon, Y.K.; Choi, S.B.; Osman, H.; Masand, V.H.; Choon, T.S. Antimycobacterial activity and in silico study of highly functionalised dispiropyrrolidines. *Med. Chem. Res.* **2015**, *24*, 818–828. [CrossRef]
90. Ali, M.A.; Ismail, R.; Choon, T.S.; Kumar, R.S.; Osman, H.; Arumugam, N.; Almansour, A.I.; Elumalai, K.; Singh, A. AChE inhibitor: A regio- and stereo-selective 1,3-dipolar cycloaddition for the synthesis of novel substituted 5,6-dimethoxy spiro[5.3']-oxindolespiro-[6.3'']-2,3-dihydro-1H-inden-1''-one-7-(substituted aryl)-tetrahydro-1H-pyrrolo[1,2-c][1,3]thiazole. *Bioorg. Med. Chem. Lett.* **2012**, *22*, 508–511. [CrossRef]
91. Ali, M.A.; Ismail, R.; Choon, T.S.; Yoon, Y.K.; Wei, A.C.; Pandian, S.; Kumar, R.S.; Osman, H.; Manogaran, E. Substituted spiro [2.3']oxindolespiro[3.2'']-5,6-dimethoxy-indane-1''-one-pyrrolidine analogue as inhibitors of acetylcholinesterase. *Bioorg. Med. Chem. Lett.* **2010**, *20*, 7064–7066. [CrossRef]
92. Babu, A.R.S.; Raghunathan, R. TiO₂-silica mediated one pot three component 1,3-dipolar cycloaddition reaction: A facile and rapid synthesis of dispiro acenaphthenone/oxindole [indanedione/oxindole] pyrroloisoquinoline ring systems. *Tetrahedron* **2007**, *63*, 8010–8016. [CrossRef]
93. Babu, A.R.S.; Raghunathan, R. Heteropolyacid-silica mediated [3+2] cycloaddition of azomethine ylides—a facile multicomponent one-pot synthesis of novel dispiroheterocycles. *Tetrahedron Lett.* **2006**, *47*, 9221–9225. [CrossRef]
94. Jayashankaran, J.; Manian, R.D.R.S.; Raghunathan, R. A facile synthesis of novel dispiroheterocycles through solvent-free microwave-assisted [3+2] cycloaddition of azomethine ylides. *Tetrahedron Lett.* **2004**, *45*, 7303–7305. [CrossRef]
95. Lanka, S.; Thennarasu, S.; Perumal, P.T. Facile synthesis of novel dispiroheterocyclic derivatives through cycloaddition of azomethine ylides with acenaphthenone-2-ylidene ketones. *Tetrahedron Lett.* **2012**, *53*, 7052–7055. [CrossRef]
96. Dandia, A.; Jain, A.K.; Bhati, D.S. Direct construction of novel dispiro heterocycles through 1,3-dipolar cycloaddition of azomethine ylides. *Tetrahedron Lett.* **2011**, *52*, 5333–5337. [CrossRef]
97. Saravanan, P.; Pushparaj, S.; Raghunathan, R. An expedient approach for the synthesis of naphthyl dispiro pyrrolidine/pyrrolizidine through 1,3-dipolar cycloaddition reaction. *Tetrahedron Lett.* **2013**, *54*, 3449–3452. [CrossRef]
98. Rajesh, R.; Raghunathan, R. Regio- and stereoselective synthesis of novel tetraspiro-bispyrrolidine and bisoxindolopyrrolidine derivatives through 1,3-dipolar cycloaddition reaction. *Tetrahedron Lett.* **2010**, *51*, 5845–5848. [CrossRef]
99. Youssef, M.A.; Panda, S.S.; El-Shiekh, R.A.; Shalaby, E.M.; Aboshouk, D.R.; Fayad, W.; Fawzy, N.G.; Girgis, A.S. Synthesis and molecular modeling studies of cholinesterase inhibitor dispiro[indoline-3,2'-pyrrolidine-3',3''-pyrrolidines]. *RSC Adv.* **2020**, *10*, 21830–21838. [CrossRef]
100. Karthikeyan, K.; Kumar, P.M.S.; Doble, M.; Perumal, P.T. Synthesis, antibacterial activity evaluation and QSAR studies of novel dispiropyrrolidines. *Eur. J. Med. Chem.* **2010**, *45*, 3446–3452. [CrossRef]
101. Hazra, A.; Paira, P.; Sahu, K.B.; Naskar, S.; Saha, P.; Paira, R.; Mondal, S.; Maity, A.; Luger, P.; Weber, M.; et al. Chemistry of andrographolide: Formation of novel di-spiropyrrolidino and di-spiropyrrolizidino-oxindole adducts via one-pot three-component [3+2] azomethine ylide cycloaddition. *Tetrahedron Lett.* **2010**, *51*, 1585–1588. [CrossRef]
102. Barman, P.D.; Sanyal, I.; Mandal, S.B.; Banerjee, A.K. Cu(OTf)₂-promoted efficient synthetic route towards glycospiro-pyrrolo[2,1-a]isoquinolines. *Tetrahedron Lett.* **2014**, *55*, 5648–5651. [CrossRef]
103. Moghaddam, F.M.; Khodabakhshi, M.R.; Ghahremanjad, Z.; Foroushani, B.K.; Ng, S.W. A one-pot, three-component regioselective synthesis of dispiropyrrolidines containing a thiophenone ring via 1,3-dipolar cycloaddition reactions of azomethine ylides. *Tetrahedron Lett.* **2013**, *54*, 2520–2524. [CrossRef]
104. Arumugam, N.; Jayashankaran, J.; Manian, R.D.R.S.; Raghunathan, R. A novel access to highly functionalised β-lactams by regio- and stereoselective 1,3-dipolar cycloaddition reaction. *Tetrahedron* **2005**, *61*, 8512–8516. [CrossRef]
105. Dong, H.; Song, S.; Li, J.; Xu, C.; Zhang, H.; Ouyang, L. The discovery of oxazolones-grafted spirooxindoles via three-component diversity oriented synthesis and their preliminary biological evaluation. *Bioorg. Med. Chem. Lett.* **2015**, *25*, 3585–3591. [CrossRef] [PubMed]
106. Jain, R.; Sharma, K.; Kumar, D. Ionic liquid mediated 1,3-dipolar cycloaddition of azomethine ylides: A facile and green synthesis of novel dispiro heterocycles. *Tetrahedron Lett.* **2012**, *53*, 1993–1997. [CrossRef]
107. Babu, A.R.S.; Raghunathan, R. Ultrasonic assisted-silica mediated [3+2] cycloaddition of azomethine ylides—a facile multicomponent one-pot synthesis of novel dispiroheterocycles. *Tetrahedron Lett.* **2007**, *48*, 6809–6813. [CrossRef]
108. Babu, A.R.S.; Raghunathan, R. ZrOCl₂·8H₂O mediated microwave induced [3+2] cycloaddition of azomethine ylides—a facile one-pot synthesis of novel dispiroheterocycles. *Tetrahedron Lett.* **2007**, *48*, 305–308. [CrossRef]
109. Lanka, S.; Thennarasu, S.; Perumal, P.T. Stoichiometry-controlled cycloaddition of azomethine ylide with dipolarophiles: Chemoselective and regioselective synthesis of bis- and tris-spirooxindole derivatives. *Tetrahedron Lett.* **2014**, *55*, 2585–2588. [CrossRef]

110. Lu, L.-J.; Fu, Q.; Sun, J.; Yan, C.-G. Synthesis of complex dispirocyclopentanebisoxindoles via cycloaddition reactions of 4-dimethylamino-1-alkoxycarbonylmethylpyridinium bromides with 2-oxindolin-3-ylidene derivatives. *Tetrahedron* **2014**, *70*, 2537–2545. [CrossRef]
111. Dandia, A.; Jain, A.K.; Laxkar, A.K.; Bhati, D.S. Synthesis and stereochemical investigation of highly functionalized novel dispirobisoxindole derivatives via [3+2] cycloaddition reaction in ionic liquid. *Tetrahedron* **2013**, *69*, 2062–2069. [CrossRef]
112. Ghandi, M.; Yari, A.; Rezaei, S.J.T.; Taheri, A. Synthesis of novel spiro-pyrrolidine/pyrrolizine-oxindole scaffolds through 1,3-dipolar cycloadditions. *Tetrahedron Lett.* **2009**, *50*, 4724–4726. [CrossRef]
113. Mamari, K.A.; Ennajih, H.; Zouihri, H.; Bouhfid, R.; Ng, S.W.; Essassi, E.M. Synthesis of novel dispiro-oxindoles via 1,3-dipolar cycloaddition reactions of azomethine ylides. *Tetrahedron Lett.* **2012**, *53*, 2328–2331. [CrossRef]
114. Mhiri, C.; Boudriga, S.; Askri, M.; Knorr, M.; Sriram, D.; Yogeewari, P.; Nana, F.; Golz, C.; Strohmman, C. Design of novel dispirooxindolopyrrolidine and dispirooxindolopyrrolothiazole derivatives as potential antitubercular agents. *Bioorg. Med. Chem. Lett.* **2015**, *25*, 4308–4313. [CrossRef] [PubMed]
115. Murali, K.; Sparkes, H.A.; Prasad, K.J.R. Regio- and stereoselective synthesis of dispirooxindole-pyrrolocarbazole hybrids via 1,3-dipolar cycloaddition reactions: Cytotoxic activity and SAR studies. *Eur. J. Med. Chem.* **2018**, *143*, 292–305. [CrossRef] [PubMed]
116. Periyasami, G.; Raghunathan, R.; Surendiran, G.; Mathivanan, N. Regioselective synthesis and antimicrobial screening of novel ketocarbazolodispiropyrrrolidine derivatives. *Eur. J. Med. Chem.* **2009**, *44*, 959–966. [CrossRef]
117. Periyasami, G.; Raghunathan, R.; Surendiran, G.; Mathivanan, N. Synthesis of novel spiro-pyrrolizidines as potent antimicrobial agents for human and plant pathogens. *Bioorg. Med. Chem. Lett.* **2008**, *18*, 2342–2345. [CrossRef] [PubMed]
118. Kumar, R.R.; Perumal, S.; Senthilkumar, P.; Yogeewari, P.; Sriram, D. A facile synthesis and antimycobacterial evaluation of novel spiro-pyrido-pyrrolizines and pyrrolidines. *Eur. J. Med. Chem.* **2009**, *44*, 3821–3829. [CrossRef] [PubMed]
119. Basiri, A.; Abd Razik, B.M.; Ezzat, M.O.; Kia, Y.; Kumar, R.S.; Almansour, A.I.; Arumugam, N.; Murugaiyah, V. Synthesis and cholinesterase inhibitory activity study of new piperidone grafted spiro-pyrrolidines. *Bioorg. Chem.* **2017**, *75*, 210–216. [CrossRef] [PubMed]
120. Girgis, A.S. Regioselective synthesis and stereochemical structure of anti-tumor active dispiro[3H-indole-3,2'-pyrrolidine-3',3''-piperidine]-2(1H),4''-diones. *Eur. J. Med. Chem.* **2009**, *44*, 1257–1264. [CrossRef]
121. Girgis, A.S.; Panda, S.S.; Shalaby, E.M.; Mabied, A.F.; Steel, P.J.; Hall, C.D.; Katritzky, A.R. Regioselective synthesis and theoretical studies of an anti-neoplastic fluoro-substituted dispirooxindole. *RSC Adv.* **2015**, *5*, 14780–14787. [CrossRef]
122. George, R.F.; Panda, S.S.; Shalaby, E.M.; Srour, A.M.; Ahmed Farag, I.S.; Girgis, A.S. Synthesis and molecular modeling studies of indole-based antitumor agents. *RSC Adv.* **2016**, *6*, 45434–45451. [CrossRef]
123. Girgis, A.S.; Panda, S.S.; Aziz, M.N.; Steel, P.J.; Hall, C.D.; Katritzky, A.R. Rational design, synthesis, and 2D-QSAR study of anti-oncological alkaloids against hepatoma and cervical carcinoma. *RSC Adv.* **2015**, *5*, 28554–28569. [CrossRef]
124. Kumar, R.S.; Antonisamy, P.; Almansour, A.I.; Arumugam, N.; Periyasami, G.; Altaf, M.; Kim, H.-R.; Kwon, K.-B. Functionalized spirooxindole-indolizine hybrids: Stereoselective green synthesis and evaluation of anti-inflammatory effect involving TNF- α and nitrite inhibition. *Eur. J. Med. Chem.* **2018**, *152*, 417–423. [CrossRef] [PubMed]
125. Karthikeyan, S.V.; Bala, B.D.; Raja, V.P.A.; Perumal, S.; Yogeewari, P.; Sriram, D. A highly atom economic, chemo-, regio- and stereoselective synthesis and evaluation of spiro-pyrrolothiazoles as antitubercular agents. *Bioorg. Med. Chem. Lett.* **2010**, *20*, 350–353. [CrossRef] [PubMed]
126. Lawson, S.; Arumugam, N.; Almansour, A.I.; Kumar, R.S.; Thangamani, S. Dispiropyrrrolidine tethered piperidone heterocyclic hybrids with broad-spectrum antifungal activity against *Candida albicans* and *Cryptococcus neoformans*. *Bioorg. Chem.* **2020**, *100*, 103865. [CrossRef] [PubMed]
127. Kumar, R.R.; Perumal, S.; Senthilkumar, P.; Yogeewari, P.; Sriram, D. A highly atom economic, chemo-, regio- and stereoselective synthesis, and discovery of spiro-pyrido-pyrrolizines and pyrrolidines as antimycobacterial agents. *Tetrahedron* **2008**, *64*, 2962–2971. [CrossRef]
128. Sivakumar, S.; Kumar, R.R.; Ali, M.A.; Choon, T.S. An atom economic synthesis and AChE inhibitory activity of novel dispiro 7-aryltetrahydro-1H-pyrrolo[1,2-c][1,3]thiazole and 4-aryloctahydroindolizine N-methylpiperidin-4-one hybrid heterocycles. *Eur. J. Med. Chem.* **2013**, *65*, 240–248. [CrossRef]
129. Rajesh, S.M.; Bala, B.D.; Perumal, S. Multi-component, 1,3-dipolar cycloaddition reactions for the chemo-, regio- and stereoselective synthesis of novel hybrid spiroheterocycles in ionic liquid. *Tetrahedron Lett.* **2012**, *53*, 5367–5371. [CrossRef]
130. Arumugam, N.; Almansour, A.I.; Kumar, R.S.; Kotresha, D.; Saiswaroop, R.; Venketesh, S. Dispiropyrrrolidinyl-piperidone embedded indeno[1,2-b]quinoxaline heterocyclic hybrids: Synthesis, cholinesterase inhibitory activity and their molecular docking simulation. *Bioorg. Med. Chem.* **2019**, *27*, 2621–2628. [CrossRef]
131. Kia, Y.; Osman, H.; Kumar, R.S.; Basiri, A.; Murugaiyah, V. Synthesis and discovery of highly functionalized mono- and bis-spiro-pyrrolidines as potent cholinesterase enzyme inhibitors. *Bioorg. Med. Chem. Lett.* **2014**, *24*, 1815–1819. [CrossRef]
132. Kumar, R.S.; Ali, M.A.; Osman, H.; Ismail, R.; Choon, T.S.; Yoon, Y.K.; Wei, A.C.; Pandian, S.; Manogaran, E. Synthesis and discovery of novel hexacyclic cage compounds as inhibitors of acetylcholinesterase. *Bioorg. Med. Chem. Lett.* **2011**, *21*, 3997–4000. [CrossRef]

133. Arumugam, N.; Almansour, A.I.; Kumar, R.S.; Perumal, S.; Ghabbour, H.A.; Fun, H.-K. A 1,3-dipolar cycloaddition-annulation protocol for the expedient regio-, stereo- and product-selective construction of novel hybrid heterocycles comprising seven rings and seven contiguous stereocentres. *Tetrahedron Lett.* **2013**, *54*, 2515–2519. [CrossRef]
134. Kumar, R.S.; Osman, H.; Perumal, S.; Menéndez, J.C.; Ali, M.A.; Ismail, R.; Choon, T.S. A facile three-component [3+2]-cycloaddition/annulation domino protocol for the regio- and diastereoselective synthesis of novel penta- and hexacyclic cage systems, involving the generation of two heterocyclic rings and five contiguous stereocenters. *Tetrahedron* **2011**, *67*, 3132–3139. [CrossRef]
135. Chandraprakash, K.; Sankaran, M.; Uvarani, C.; Shankar, R.; Ata, A.; Dallemer, F.; Mohan, P.S. A strategic approach to the synthesis of novel class of dispiroheterocyclic derivatives through 1,3 dipolar cycloaddition of azomethine ylide with (E)-3-arylidene-2,3-dihydro-8-nitro-4-quinolone. *Tetrahedron Lett.* **2013**, *2011*, 3896–3901. [CrossRef]
136. Augustine, T.; Kanakam, C.C.; Vithiya, S.M.; Ramkumar, V. A facile entry into a novel class of dispiroheterocyclic framework through 1,3-dipolar cycloaddition of azomethine ylides with 3-arylidene-4-chromanones as dipolarophiles. *Tetrahedron Lett.* **2009**, *50*, 5906–5909. [CrossRef]
137. Bharkavi, C.; Kumar, S.V.; Ali, M.A.; Osman, H.; Muthusubramanian, S.; Perumal, S. A facile stereoselective synthesis of dispiro-indeno pyrrolidine/pyrrolothiazole-thiochroman hybrids and evaluation of their antimycobacterial, anticancer and AchE inhibitory activities. *Bioorg. Med. Chem.* **2016**, *24*, 5873–5883. [CrossRef] [PubMed]
138. Maheswari, S.U.; Perumal, S.; Almansour, A.I. A facile regio- and stereoselective synthesis of novel dispirooxindolyl[acridine-2',3-pyrrolidine/thiapyrrolizidine]-1'-ones via 1,3-dipolar cycloaddition of azomethine ylides. *Tetrahedron Lett.* **2012**, *53*, 349–353. [CrossRef]
139. Maheswari, S.U.; Perumal, S. An expedient domino three-component [3+2]-cycloaddition/annulation protocol: Regio- and stereoselective assembly of novel polycyclic hybrid heterocycles with five contiguous stereocentres. *Tetrahedron Lett.* **2013**, *54*, 7044–7048. [CrossRef]
140. Toumi, A.; Boudriga, S.; Hamden, K.; Sobeh, M.; Cheurfa, M.; Askri, M.; Knorr, M.; Strohmman, C.; Brieger, L. Synthesis, antidiabetic activity and molecular docking study of rhodanine-substituted spirooxindole pyrrolidine derivatives as novel α -amylase inhibitors. *Bioorg. Chem.* **2021**, *106*, 104507. [CrossRef]
141. Kumar, G.S.; Satheeshkumar, R.; Kaminsky, W.; Platts, J.; Prasad, K.J.R. A facile regioselective 1,3-dipolar cycloaddition protocol for the synthesis of new class of quinolinyl dispiro heterocycles. *Tetrahedron Lett.* **2014**, *55*, 5475–5480. [CrossRef]
142. Poornachandran, M.; Raghunathan, R. Synthesis of dispirooxindolecycloalka[d]pyrimidino[2,3-b]thiazole pyrrolidine/thiapyrrolizidine ring systems. *Tetrahedron* **2006**, *62*, 11274–11281. [CrossRef]
143. Lakshmi, N.V.; Tamilsai, R.; Perumal, P.T. A facile synthetic approach to novel spiro-oxindoles/acenaphthylen-1-ones containing benzo[1,4]thiazin-3-one ring via 1,3-dipolar cycloaddition. *Tetrahedron Lett.* **2011**, *52*, 5301–5307. [CrossRef]
144. Santora, V.J.; Covell, J.A.; Hayashi, R.; Hofilena, B.J.; Ibarra, J.B.; Pulley, M.D.; Weinhouse, M.I.; Sengupta, D.; Duffield, J.J.; Semple, G.; et al. A new family of H3 receptor antagonists based on the natural product Conessine. *Bioorg. Med. Chem. Lett.* **2008**, *18*, 1490–1494. [CrossRef] [PubMed]
145. Bhaskar, G.; Arun, Y.; Balachandran, C.; Saikumar, C.; Perumal, P.T. Synthesis of novel spirooxindole derivatives by one pot multicomponent reaction and their antimicrobial activity. *Eur. J. Med. Chem.* **2012**, *51*, 79–91. [CrossRef] [PubMed]
146. Rajanarendar, E.; Ramakrishna, S.; Reddy, K.G.; Nagaraju, D.; Reddy, Y.N. A facile synthesis, anti-inflammatory and analgesic activity of isoxazolyl-2,3-dihydrospiro[benzo[f]isoindole-1,3'-indoline]-2',4,9-triones. *Bioorg. Med. Chem. Lett.* **2013**, *23*, 3954–3958. [CrossRef]
147. Huang, H.-M.; Gao, J.-R.; Hou, L.-F.; Jia, J.-H.; Han, L.; Ye, Q.; Li, Y.-J. The first iodine improved 1,3-dipolar cycloaddition: Facile and novel synthesis of 2-substituted benzo[f]isoindole-4,9-diones. *Tetrahedron* **2013**, *69*, 9033–9037. [CrossRef]
148. Ma, D.; Cheng, H.; Huang, C.; Xu, L. Synthesis of the azatricyclic ACD ring system of calyciphylline A-type Daphniphyllum alkaloids via a nonstabilized azomethine ylide generated by desilylation. *Tetrahedron Lett.* **2015**, *56*, 2492–2495. [CrossRef]
149. Ryan, J.H. 1,3-Dipolar cycloaddition reactions of azomethine ylides with aromatic dipolarophiles. *ARKIVOC* **2015**, *46*, 160–183. [CrossRef]
150. Wales, S.M.; Rivinoja, D.J.; Gardiner, M.G.; Bird, M.J.; Meyer, A.G.; Ryan, J.H.; Hyland, C.J.T. Benzoazepine-fused isoindolines via intramolecular (3+2)-cycloadditions of azomethine ylides with dinitroarenes. *Org. Lett.* **2019**, *21*, 4703–4708. [CrossRef]
151. Lee, S.; Chataigner, I.; Piettre, S.R. Facile dearomatization of nitrobenzene derivatives and other nitroarenes with *N*-benzyl azomethine ylide. *Angew. Chem. Int. Ed.* **2011**, *50*, 472–476. [CrossRef]
152. Bastrakov, M.A.; Fedorenko, A.K.; Starosotnikov, A.M.; Shakhnes, A.K. Nitropyridines as 2π -partners in 1,3-dipolar cycloadditions with *N*-methyl azomethine ylide: An easy access to condensed pyrrolines. *Molecules* **2021**, *26*, 5547. [CrossRef]
153. Lee, S.; Diab, S.; Queval, P.; Sebban, M.; Chataigner, I.; Piettre, S.R. Aromatic C=C bonds as dipolarophiles: Facile reactions of uncomplexed electron-deficient benzene derivatives and other aromatic rings with a non-stabilized azomethine ylide. *Chem. Eur. J.* **2013**, *19*, 7181–7192. [CrossRef]

154. Bastrakov, M.A.; Starosotnikov, A.M.; Pechenkin, S.Y.; Kachala, V.V.; Glukhov, I.V.; Shevelev, S.A. Double 1,3-dipolar cycloaddition of N-methyl azomethine ylide to meta-dinitrobenzene annelated with nitrogen aromatic heterocycles. *J. Heterocycl. Chem.* **2010**, *47*, 893–896. [CrossRef]
155. Semenyuk, Y.P.; Kochubei, A.S.; Morozov, P.G.; Burov, O.N.; Kletsii, M.E.; Kurbatov, S.V. [3+2] Cycloaddition reactions to indolyl- and pyrrolyl derivatives of dinitrobenzofurazan. *Chem. Heterocycl. Compd.* **2015**, *50*, 1731–1740. [CrossRef]
156. Starosotnikov, A.M.; Bastrakov, M.A.; Kachala, V.V.; Fedyanin, I.V.; Shevelev, S.A.; Dalinger, I.L. Unusual pericyclic reactivity of 4-nitrobenzofuroxans in 1,3-dipolar cycloaddition with N-benzyl azomethine ylide—A new example of multiple C–C bond forming transformations. *ChemistrySelect* **2018**, *3*, 9773–9777. [CrossRef]
157. Girgis, A.S.; Stawinski, J.; Ismail, N.S.M.; Farag, H. Synthesis and QSAR study of novel cytotoxic spiro[3H-indole-3,2'(1'H)-pyrrolo[3,4-c]pyrrole]-2,3',5'(1H,2'aH,4'H)-triones. *Eur. J. Med. Chem.* **2012**, *47*, 312–322. [CrossRef] [PubMed]
158. Bharkavi, C.; Kumar, S.V.; Ali, M.A.; Osman, H.; Muthusubramanian, S.; Perumal, S. One-pot microwave assisted stereoselective synthesis of novel dihydro-2'H-spiro[indene-2,1'-pyrrolo[3,4-c]pyrrole]-tetraones and evaluation of their antimycobacterial activity and inhibition of AChE. *Bioorg. Med. Chem. Lett.* **2017**, *27*, 3071–3075. [CrossRef]
159. Nyerges, M.; Pintér, Á.; Virányi, A.; Blaskó, G.; Tőke, L. Synthesis of pyrrolo[3,4-c]quinolines by 1,5-electrocyclisation of non-stabilised azomethine ylides. *Tetrahedron* **2005**, *61*, 8199–8205. [CrossRef]
160. Mondal, S.; Maity, A.; Paira, R.; Banerjee, M.; Bharitkar, Y.P.; Hazra, A.; Banerjee, S.; Mondal, N.B. Efficient synthesis of novel tetrahydropyrrolo[3',4':3,4]pyrrolo[2,1-a]isoquinoline derivatives via a simple and convenient MCR in aqueous micellar system. *Tetrahedron Lett.* **2012**, *53*, 6288–6291. [CrossRef]
161. Georgiou, D.; Toutountzoglou, V.; Muir, K.W.; Hadjipavlou-Litina, D.; Elemen, Y. Synthesis of sulfur containing dihydro-pyrrolo derivatives and their biological evaluation as antioxidants. *Bioorg. Med. Chem.* **2012**, *20*, 5103–5109. [CrossRef]
162. Quiroga, J.; Gálvez, J.; Pérez, A.; Valencia, A.; Abonia, R.; Insuasty, B. Catalyst free three-component synthesis of (±)-pyrazolylpyrrolopyrroles by 1,3-dipolar cycloaddition reaction. *Tetrahedron Lett.* **2011**, *52*, 5471–5473. [CrossRef]
163. Belskaya, N.P.; Bakulev, V.A.; Deryabina, T.G.; Subbotina, J.O.; Kodess, M.I.; Dehaen, W.; Toppet, S.; Robeyns, K.; Meervelt, L.V. 3-Alkylsulfanyl-2-aryloxy-3-(pyrrolidin-1-yl)-acrylonitriles as masked 1,3-dipoles. *Tetrahedron* **2009**, *65*, 7662–7672. [CrossRef]
164. Malatesti, N.; Boa, A.N.; Clark, S.; Westwood, R. 1,3-Dipolar cycloaddition reactions of benzo[b]thiophene 1,1-dioxide with azomethine ylides. *Tetrahedron Lett.* **2006**, *47*, 5139–5142. [CrossRef]
165. Konstantinova, L.S.; Bastrakov, M.A.; Starosotnikov, A.M.; Glukhov, I.V.; Lysov, K.A.; Rakitin, O.A.; Shevelev, S.A. 4,6-Dinitrobenzo[c]isothiazole: Synthesis and 1,3-dipolar cycloaddition to azomethine ylide. *Mendeleev Commun.* **2010**, *20*, 353–354. [CrossRef]
166. Roy, S.; Kishbaugh, T.L.S.; Jasinski, J.P.; Gribble, G.W. 1,3-Dipolar cycloaddition of 2- and 3-nitroindoles with azomethine ylides. A new approach to pyrrolo[3,4-b]indoles. *Tetrahedron Lett.* **2007**, *48*, 1313–1316. [CrossRef]
167. Rao, J.N.S.; Raghunathan, R. An expedient diastereoselective synthesis of pyrrolidinyl spirooxindoles fused to sugar lactone via [3+2] cycloaddition of azomethine ylides. *Tetrahedron Lett.* **2012**, *53*, 854–858. [CrossRef]
168. Prasanna, R.; Purushothaman, S.; Raghunathan, R. Synthesis of glucosylspiro-oxindole derivatives via one-pot three-component cycloaddition of azomethine ylides. *Tetrahedron Lett.* **2014**, *55*, 6631–6634. [CrossRef]
169. Rao, J.N.S.; Raghunathan, R. An expedient synthesis of pyrrolidinyl spirooxindole grafted 3-nitrochromanes through 1,3-dipolar cycloaddition reaction of azomethine ylides. *Tetrahedron Lett.* **2013**, *54*, 6568–6573. [CrossRef]
170. Rao, J.N.S.; Raghunathan, R. A facile synthesis of glyco 3-nitrochromane hybrid pyrrolidinyl spiro heterocycles via [3+2] cycloaddition of azomethine ylides. *Tetrahedron Lett.* **2015**, *56*, 2276–2279. [CrossRef]
171. Korotaev, V.Y.; Barkov, A.Y.; Moshkin, V.S.; Matochkina, E.G.; Kodess, M.I.; Sosnovskikh, V. Ya. Highly diastereoselective 1,3-dipolar cycloaddition of nonstabilized azomethine ylides to 3-nitro-2-trihalomethyl-2H-chromenes: Synthesis of 1-benzopyrano[3,4-c]pyrrolidines. *Tetrahedron* **2013**, *69*, 8602–8608. [CrossRef]
172. Virányi, A.; Marth, G.; Dancsó, A.; Blaskó, G.; Tőke, L.; Nyerges, M. 3-Nitrochromene derivatives as 2π components in 1,3-dipolar cycloadditions of azomethine ylides. *Tetrahedron* **2006**, *62*, 8720–8730. [CrossRef]
173. Moshkin, V.S.; Sosnovskikh, V.Y.; Röschenhaler, G.-V. Synthesis of benzopyranopyrrolidines via 1,3-dipolar cycloaddition of nonstabilized azomethine ylides with 3-substituted coumarins. *Tetrahedron* **2013**, *69*, 5884–5892. [CrossRef]
174. Moshkin, V.S.; Sosnovskikh, V.Y.; Slepukhin, P.A.; Röschenhaler, G.-V. 1,3-Dipolar cycloadditions of nonstabilised azomethine ylides at 3-substituted coumarins: Synthesis of 1-benzopyrano[3,4-c]pyrrolidines. *Mendeleev Commun.* **2012**, *22*, 29–31. [CrossRef]
175. Ghandi, M.; Taheri, A.; Abbasi, A. A facile synthesis of chromeno[3,4-c]spiropyrrolidine-oxindoles via 1,3-dipolar cycloadditions. *Tetrahedron* **2010**, *66*, 6744–6748. [CrossRef]
176. Potowski, M.; Golz, C.; Strohmman, C.; Antonchick, A.P.; Waldmann, H. Biology-oriented synthesis of benzopyrano[3,4-c]pyrrolidines. *Bioorg. Med. Chem.* **2015**, *23*, 2895–2903. [CrossRef]
177. Sosnovskikh, V.Y.; Kornev, M.Y.; Moshkin, V.S.; Buev, E.M. Substituted chromones in [3+2] cycloadditions with nonstabilized azomethine ylides: Synthesis of 1-benzopyrano[2,3-c]pyrrolidines and 1-benzopyrano[2,3-c:3,4-c']dipyrrolidines. *Tetrahedron* **2014**, *70*, 9253–9261. [CrossRef]

178. Oliveira, U.; Guillermo, A.; Repetto, E.; Vega, D.R.; Varela, O. Synthesis of Enantiomeric Polyhydroxyalkylpyrrolidines from 1,3-Dipolar Cycloadducts. Evaluation as Inhibitors of a β -Galactofuranosidase. *J. Org. Chem.* **2016**, *81*, 4179–4189. [CrossRef] [PubMed]
179. D'Souza, A.M.; Spiccia, N.; Basutto, J.; Jokisz, P.; Wong, L.S.-M.; Meyer, A.G.; Holmes, A.B.; White, J.M.; Ryan, J.H. 1,3-Dipolar cycloaddition-decarboxylation reactions of an azomethine ylide with isatoic anhydrides: Formation of novel benzodiazepinones. *Org. Lett.* **2011**, *13*, 486–489. [CrossRef] [PubMed]

Disclaimer/Publisher's Note: The statements, opinions and data contained in all publications are solely those of the individual author(s) and contributor(s) and not of MDPI and/or the editor(s). MDPI and/or the editor(s) disclaim responsibility for any injury to people or property resulting from any ideas, methods, instructions or products referred to in the content.

Review

Folic Acid Antimetabolites (Antifolates): A Brief Review on Synthetic Strategies and Application Opportunities

Igor S. Kovalev¹, Grigory V. Zyryanov^{1,2,*}, Sougata Santra¹, Adinath Majee^{3,*}, Mikhail V. Varaksin^{1,2} and Valery N. Charushin^{1,2}

¹ Department of Organic & Biomolecular Chemistry, Ural Federal University, 620002 Yekaterinburg, Russia

² I. Ya. Postovskiy Institute of Organic Synthesis, Ural Branch, Russian Academy of Sciences, 620219 Yekaterinburg, Russia

³ Department of Chemistry, Visva-Bharati (A Central University), Santiniketan 731235, India

* Correspondence: gvzyryanov@gmail.com or g.v.zyryanov@urfu.ru (G.V.Z.);

adinath.majee@visva-bharati.ac.in (A.M.)

Abstract: Antimetabolites of folic acid represent a large group of drugs and drug candidates, including those for cancer chemotherapy. In this current review, the most common methods and approaches are presented for the synthesis of therapeutically significant antimetabolites of folic acid, which are Methotrexate (MTX), Raltitrexed (Tomudex, ZD1694), Pralatrexate, Pemetrexed, TNP-351, and Lometrexol. In addition, the applications or uses of these folic acid antimetabolites are also discussed.

Keywords: antifolates; folic acids; synthesis; applications; drugs

Citation: Kovalev, I.S.;

Zyryanov, G.V.; Santra, S.; Majee, A.; Varaksin, M.V.; Charushin, V.N. Folic Acid Antimetabolites (Antifolates): A Brief Review on Synthetic Strategies and Application Opportunities.

Molecules **2022**, *27*, 6229. <https://doi.org/10.3390/molecules27196229>

Academic Editors: Alexey

M. Starosotnikov, Maxim

A. Bastrakov and Igor L. Dalinger

Received: 29 August 2022

Accepted: 19 September 2022

Published: 22 September 2022

Publisher's Note: MDPI stays neutral with regard to jurisdictional claims in published maps and institutional affiliations.



Copyright: © 2022 by the authors. Licensee MDPI, Basel, Switzerland. This article is an open access article distributed under the terms and conditions of the Creative Commons Attribution (CC BY) license (<https://creativecommons.org/licenses/by/4.0/>).

1. Introduction

Antimetabolites, which are antagonists of natural metabolites, belong to a group of highly efficient anticancer drugs. Based on the chemical structure, these groups can be divided into several sub-groups, such as non-natural amino-acids [1] or peptides [2,3], including phospho-analogues [4], analogues of purine and pyrimidine bases, such as competitors in the synthesis of the nucleic acids [5,6], as well as vitamin actions including folic acid [7], hormones [8], coenzymes [9], and other substrates responsible for the normal functioning of cells and tissues of the human body.

The mechanism of antimetabolites action is based on their ability to enter into competitive relationships with structurally similar metabolites of the living, which leads to a lack of the corresponding metabolite and a decrease in the activity of vital biochemical processes in the cell. In order to interfere with the synthesis of the DNA constituents, the most common antimetabolites should be structural analogues of purine and pyrimidine bases/nucleosides, or of folate cofactors [10].

In this current review, we analyze the most common approaches for the synthesis of therapeutically significant antimetabolites of folic acid [11–13], such as Methotrexate (MTX), Raltitrexed (Tomudex, ZD1694), Pralatrexate, Pemetrexed, TNP-351, and Lometrexol.

2. Discussion

2.1. Mechanism of Antifolates Action

Folic acid (**1**) first has to be reduced to THFA (**2**) by dihydrofolate reductase (Figure 1), after which it can attach various one-carbon groups and transfer them to other molecules. In the reaction, once catalyzed by thymidylate synthase, deoxyuridine monophosphate (deoxy-UMP or dUMP) is converted to deoxythymidine monophosphate (deoxy-TMP or dTMP), producing a methylene group from 5,10-methylene-THFA; the latter is oxidized into dihydrofolic acid and must be reduced again to participate in further reactions. Methotrexate (MTX) and other folic acid antagonists with a high affinity for dihydrofolate reductase (K, 0.01–0.2 nmol/L) disrupt the formation of THFA, causing a deficiency of

reduced folates and an accumulation of toxic dihydrofolic acid polyglutamates. At the same time, the transfer reactions of one-carbon groups, which are necessary for the synthesis of purines and dTMP, are inhibited; as a result, the synthesis of nucleic acids and other metabolic processes are disrupted. The toxic action of methotrexate is prevented by calcium folinate (the calcium salt of 5-formyl-THFA), which enters the cell via a reduced folate transporter and is converted into the other THFA derivatives [14] (Scheme 1).

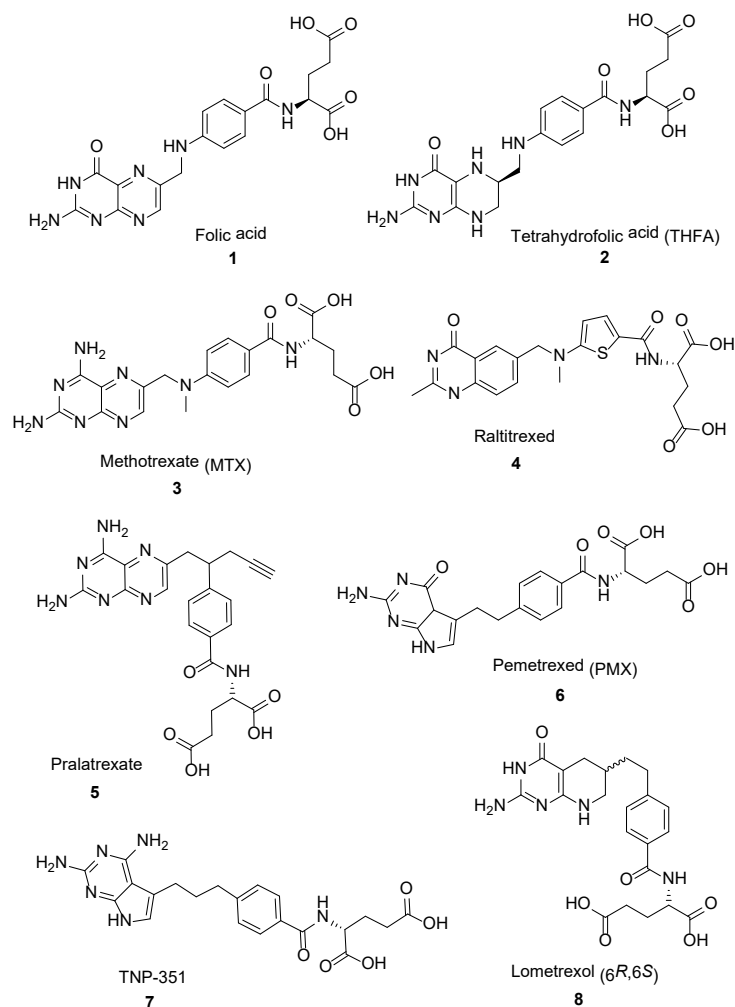
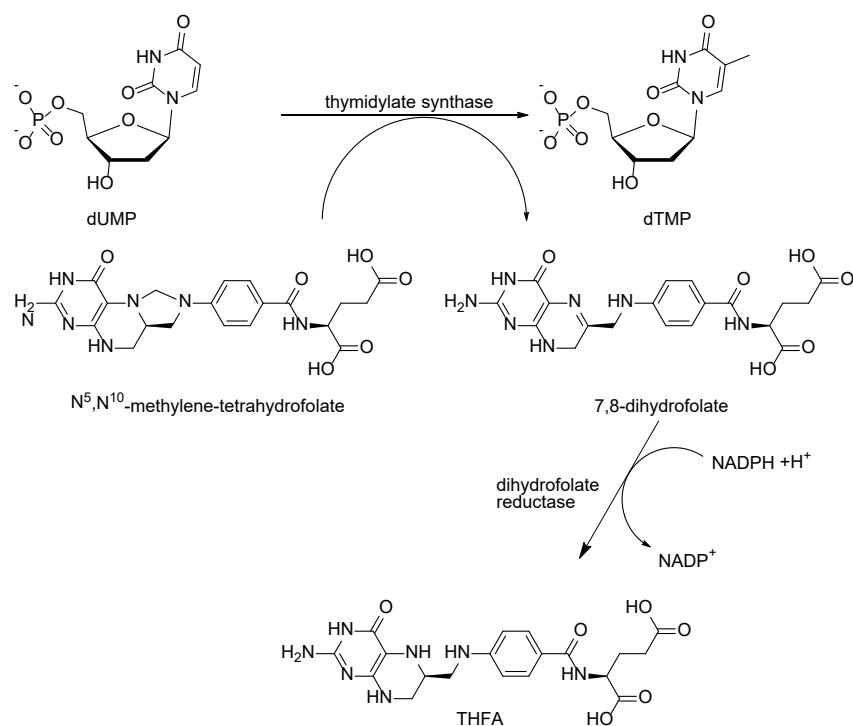


Figure 1. Structure of folic acid (1) and tetrahydrofolic acid (THFA) (2) and their antimetabolites.

Once it became clear that methotrexate directly inhibits not only dihydrofolate reductase but also the enzymes for the synthesis of purines and thymidylate synthase, the coenzymes of which are reduced folates, a search commenced for folic acid antagonists that selectively inhibit these enzymes. By replacing the N-5, N-8 and N-10 atoms and modifying the side chains of the methotrexate molecule, it was possible to synthesize drugs that retain their inherent ability to form stable polyglutamates inside the cell, but better penetrate the tumor [15], such as the following: raltitrexed, a thymidylate synthase inhibitor; lometrexol, a purine synthesis inhibitor; and pemetrexed, which combines both mechanisms of action [16].

Most folic acid antimetabolites are only partially selective for tumor cells and affect rapidly proliferating normal cells, including bone marrow and gastrointestinal mucosa. Folic acid antagonists act in the S-period and are most active against cells in the logarithmic growth phase [17].

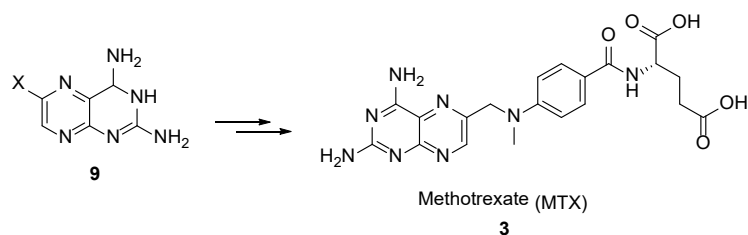


Scheme 1. Main target processes for antifolates in living cells.

2.2. Methotrexate: (*S*)-2-(4-(((2,4-Diaminopteridin-6-yl)Methyl)(Methyl)Amino)benzamido)Pentanedioic Acid (MTX, Rheumatrex, Amethopterin, Abitrexate, Trexall, Methylaminopterin, Mexate, Metatrexan)

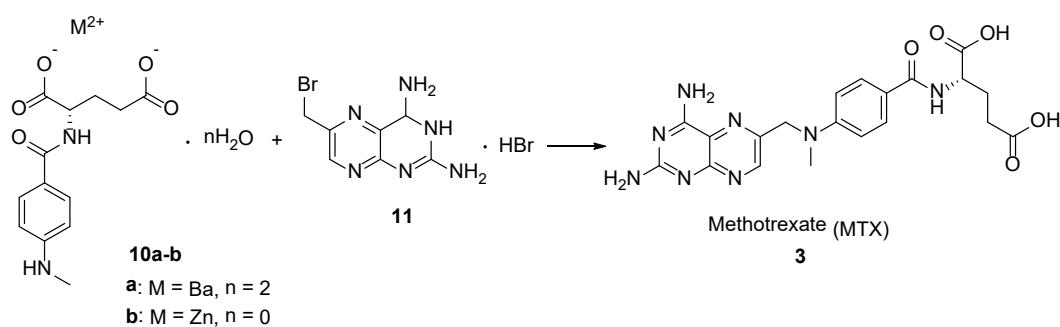
The discovery of the first folic acid antagonist, methotrexate (MTX), with its promising activity for the treatment of a variety of human cancers, prompted the search for other folate analogs [18]. As a structural analogue of folic acid, methotrexate inhibits the activity of the enzyme folate reductase, which prevents the conversion of folic acid into tetrahydrofolic acid, which is involved in cell metabolism and reproduction. Methotrexate is recommended for acute childhood leukemia; chorionepithelioma of the uterus; cancer of the breast, lungs, testicles, and other malignant tumors in adults (in combination with other antitumor drugs); and is also used as an immunosuppressive agent.

The most common synthetic strategy for the preparation of MTX **3** involves the post-modification of 3,4-dihydropteridine-2,4-diamines **9**, as depicted in Scheme 2.



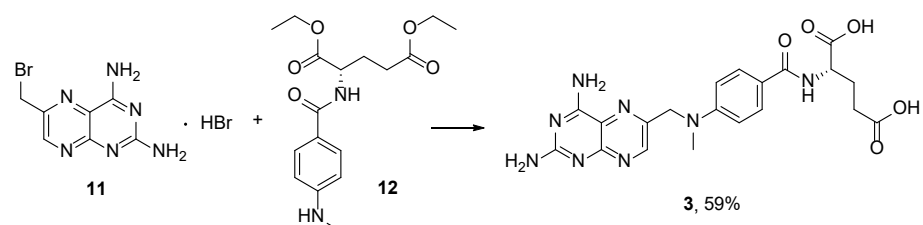
Scheme 2. Synthetic strategy towards MTX by the post-modification of 3,4-dihydropteridine-2,4-diamines **9**.

Thus, MTX was obtained by the reaction of 2,4-diamino-6-bromomethylpteridine hydrobromide **11** with barium salt dehydrate [19] or Zn²⁺ salt [20] of *p*-(*N*-methyl)-aminobenzoyl-*L*-glutamic acid **10** in 87.5% and 56.1% yields, accordingly (Scheme 3).



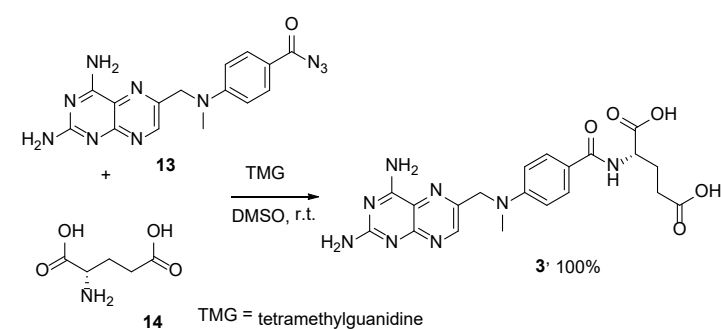
Scheme 3. Synthesis of MTX by the reaction between metal salt of *p*-(*N*-methyl)-aminobenzoyl-*L*-glutamic acid and 2,4-diamino-6-bromomethylpteridine hydrobromide.

The reaction of **11** with the diethyl *p*-(*N*-methyl)-aminobenzoyl-*L*-glutamate **12** followed by basic saponification (Scheme 4) provided lower yields of the target product [21].



Scheme 4. Synthesis of MTX by the reaction of 2,4-diamino-6-bromomethylpteridine hydrobromide **11** with diethyl *p*-(*N*-methyl)-aminobenzoyl-*L*-glutamate **12**.

Another approach involves the substitution of the azide group in 4-(*N*-methyl-*N'*-(6''-aminopteroil-methylene)aminobenzoic acid derivative **13** in a reaction with *L*-glutamic acid **14** in DMSO at room temperature in the presence of tetramethylguanidine (TMG) as the base (Scheme 5) [22]. The reaction resulted in the corresponding desired MTX in a quantitative yield, which is the main advantage of this method.

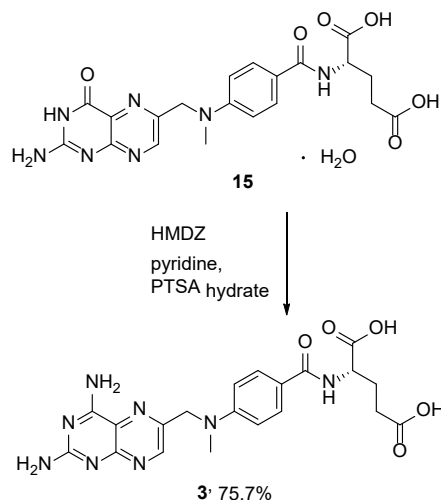


Scheme 5. Quantitative synthesis of MTX by the reaction of 4-(*N*-methyl-*N'*-(6''-aminopteroil-methylene)aminobenzoic acid derivative **13** with *L*-glutamic acid **14**.

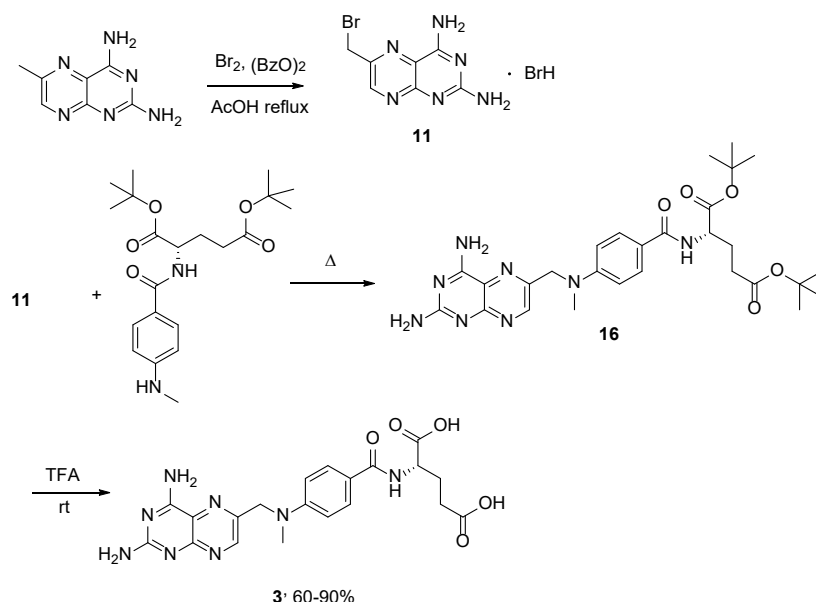
In addition, MTX was obtained in a 75.7% yield by means of the transformation of its more stable and synthetically available 4-oxoderivative (methopterin hydrate) (**15**) in the presence of pyridine, *p*-toluenesulfonic acid monohydrate and 1,1,1,3,3,3-hexamethyl-disilazane (HMDZ) (Scheme 6) [23].

Along with MTX, its ^{13}C -multilabelled forms with ^{13}C -enrichment at 2, 7, 9, 4, 7, 8a, 9 and 2, 4a,b positions were synthesized from the di-*tert*-butyl ester of MTX **16** for the NMR study of the mechanisms of drug–enzyme interactions (Scheme 7) [24]. The reaction was carried out by performing 'benzylic' bromination, followed by the substitution of the bromine atom by the di-*t*-butyl *N*-(*p*-methylaminobenzoyl)-*L*-glutamate. The acid treatment of each of the formed methotrexate di-*t*-butyl esters yielded the corresponding

^{13}C -enriched methotrexate in 60–90% yields. So far, this is the only method reported for the synthesis of C^{13} -MTX.



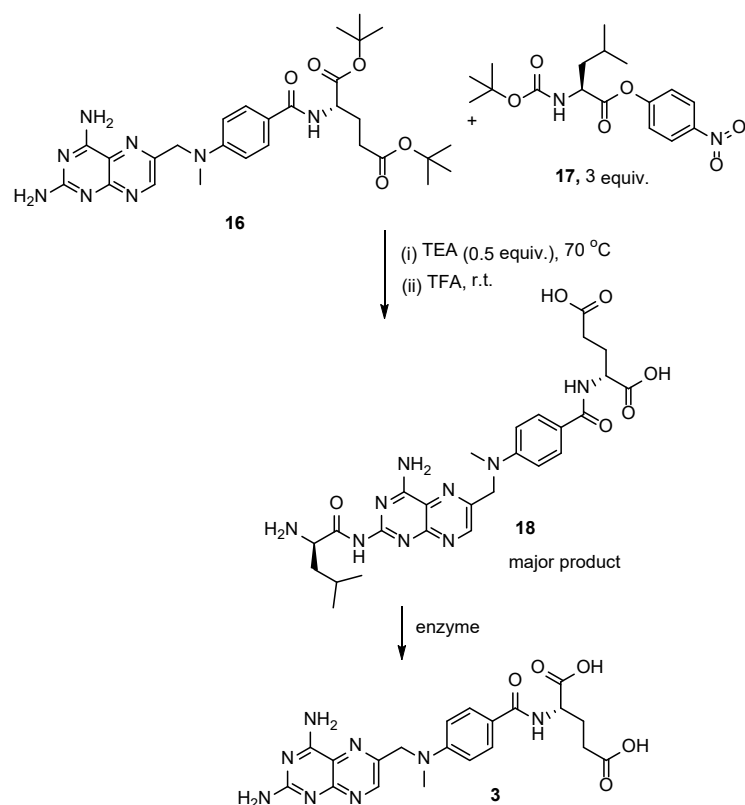
Scheme 6. Synthesis of MTX from 4-oxoderivative of MTX (methopterin hydrate) (15).



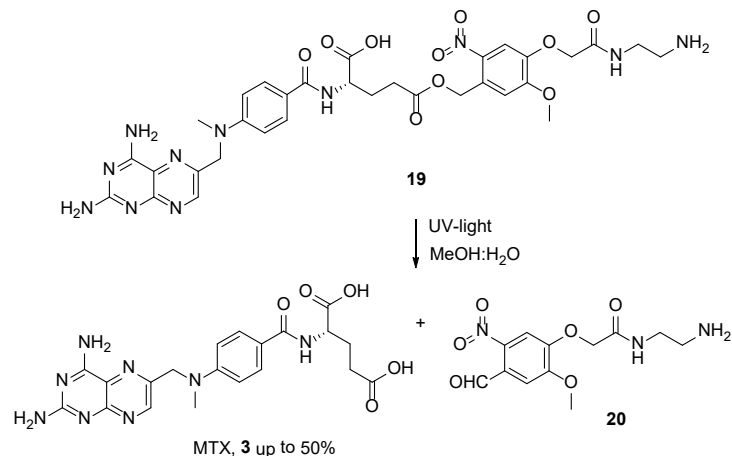
Scheme 7. Multistep synthesis of MTX.

In another method for the synthesis of MTX 3, the pro-drug of MTX, *N*-(*L*- α -aminoacyl)-derivative of methotrexate 18, was initially prepared by a reaction between the di-*tert*-butyl ester of MTX 16 and *N*-*tert*-butyloxycarbonyl-*L*-leucine derivative 17, followed by the acidic deprotection of protective groups [25]. Subsequently, the obtained pro-drug 18 was successfully converted into MTX via the enzymatic cleavage by porcine microsomal leucine aminopeptidase (Scheme 8). Unfortunately, the authors did not provide any yields due to the format of the publication.

Free-form MTX was obtained from the conjugate of the *o*-nitrobenzyl alcohol derivative and MTX 19 during a photolysis experiment in aqueous methanol under UV-light irradiation [26]. This technique was considered by the authors as a possible way to transport the MTX to the cancer cells with the release of MTX free form at up to 50% at a pH level of 7.4 (Scheme 9).

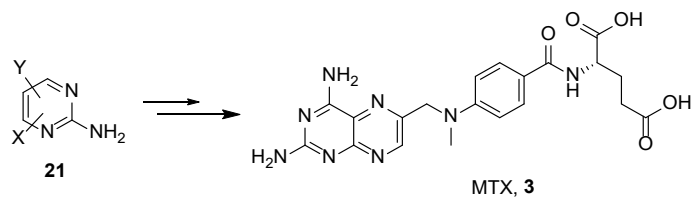


Scheme 8. Three-step synthesis of MTX starting from di-*tert*-butyl ester of MTX **16** and *N*-*tert*-butyloxycarbonyl-*L*-leucine derivative **17**.



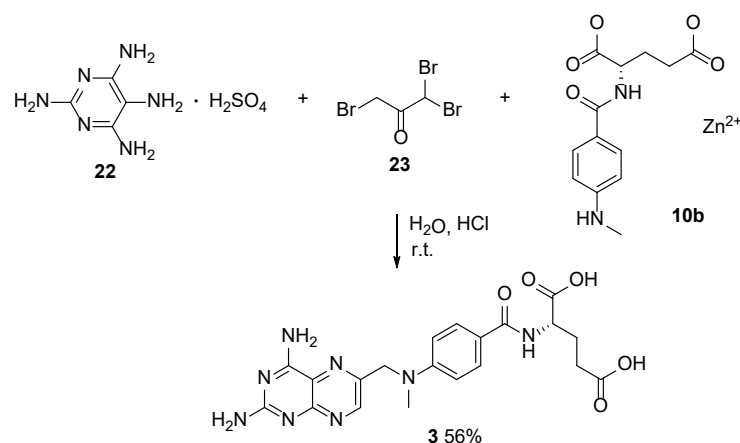
Scheme 9. UV-light promoted synthesis of MTX from **19**. Reproduced with the permission of reference [26]. Copyright © 2011, Elsevier Ltd.

In the literature, there are less common synthetic approaches available that involve the construction of a 3,4-dihydropteridine core starting from aminopyrimidines **21** (Scheme 10).



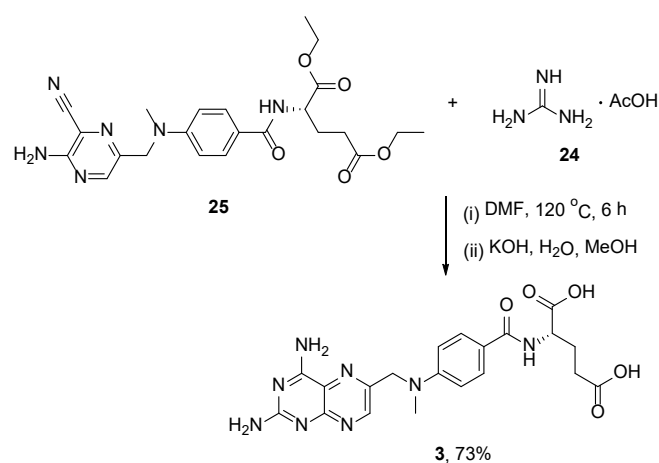
Scheme 10. Synthetic strategy towards MTX by the post-modification of aminopyrimidines **21**.

In this context, MTX was obtained by the tandem multicomponent reaction between Zn^{2+} salt of *N*-(4-*N*-methylaminobenzoyl)-*L*-glutamic acid **10b**, 1,1,3-tribromoacetone **23** and 2,2,5,6-tetraaminopyrimidine sulfate **22** under mild conditions (Scheme 11) [27]. This method has a noticeable advantage, such as the possibility to carry out several reactions in one step without the isolation of intermediates during each step.



Scheme 11. Multicomponent synthesis of MTX under mild reaction conditions.

In another method, the MTX core was constructed by means of a heterocyclization reaction between commercially available guanidine acetate **24** and easily derived diethyl (4-(((5-amino-6-cyanopyrazin-2-yl)methyl)(methyl)amino)benzoyl)glutamate **25** under heating conditions, followed by basic hydrolysis (Scheme 12) [28].

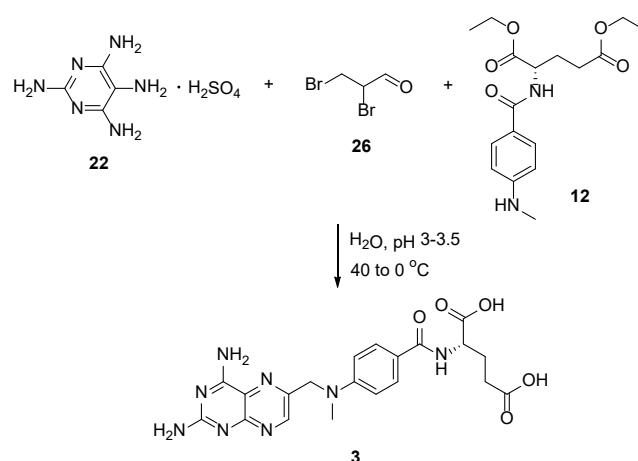


Scheme 12. Synthesis of MTX by the reaction between guanidine acetate **24** and diethyl (4-(((5-amino-6-cyanopyrazin-2-yl)methyl)(methyl)amino)benzoyl)glutamate **25**.

Lastly, the approach for MTX **3** involves a reaction between 2,4,5,6-tetraaminopyrimidine hydrosulphate **22**, 2,3-dibromopropionaldehyde **26**, and *N*-4-(methylamino)benzoyl)-*L*-glutamic acid **12** disodium salt under oxidative conditions (iodine in the presence of KI) (Scheme 13) [29]. In this article, the authors were more concerned about the purity of the obtained compounds than their yields.

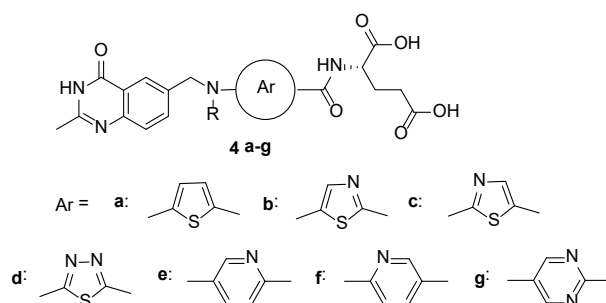
2.3. Raltitrexed: (2*S*)-2-[[[5-[Methyl-[(2-Methyl-4-oxo-3*H*-Quinazolin-6-yl)Methyl]Amino]Thiophene-2-Carbonyl]Amino]Pentanedioic Acid (Tomudex, ZD1694)

Raltitrexed (Tomudex) is a more recent, specific, mixed, and non-competitive inhibitor of thymidylate synthase indicated for use in cancer therapy, especially colorectal cancer [30–32].



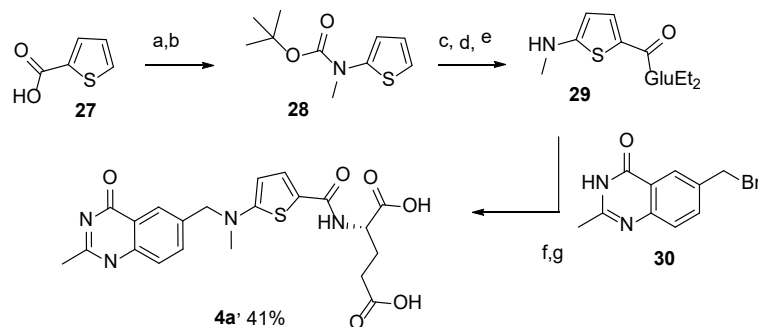
Scheme 13. Synthesis of MTX by the reaction between 2,4,5,6-tetraaminopyrimidine hydrosulphate **22**, 2,3-dibromopropionaldehyde **26**, and *N*-4-(methylamino)benzoyl-*L*-glutamic acid **12** disodium salt under oxidative conditions.

In 1991, Marsham et al. reported the synthesis of a series of C2-methyl-N10-alkylquinazoline-based antifolates, in which the benzene ring was replaced by the heterocycles, i.e., thiophene, thiazole, thiadiazole, pyridine, and pyrimidine (Scheme 14) [33].



Scheme 14. Structures of a series of C2-methyl-N10-alkylquinazoline-based antifolates. Reproduced with the permission of reference [33]. Copyright © 1991, American Chemical Society.

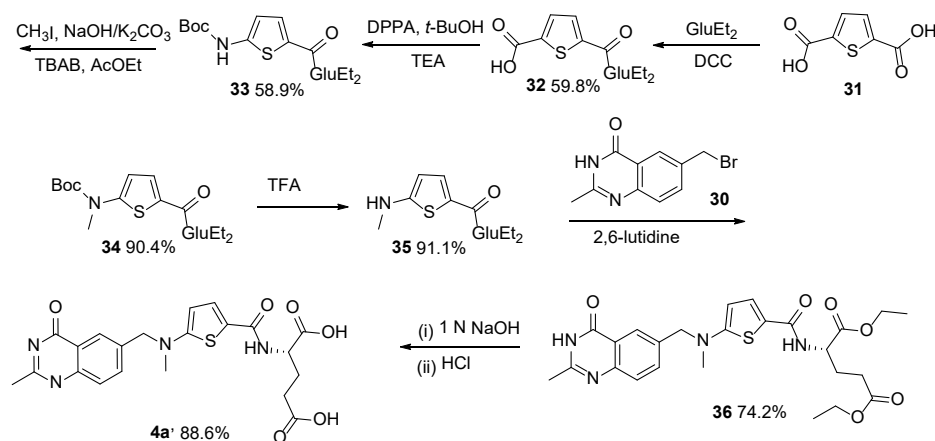
The thiophene system **4a** and its related thiazole **4b** yielded analogues that were considerably more efficient than the parent benzene series as inhibitors of L1210 cell growth. Although, in general, these heterocycles were somewhat poorer inhibitors of the isolated TS enzyme. Raltitrexed **4a** (R = CH₃) was synthesized in a 41% yield starting with the thiophene-2-carboxylic acid, as shown in Scheme 15.



Reagents and conditions: (a) Diphenyl phosphorazidate, Et₃N, *t*-BuOH, reflux; (b) sodium hydride, iodomethane, DMF; (c) (i) *n*-BuLi, (ii) CO₂; (d) (i) oxalyl chloride, DMF, (ii) diethyl glutamate, Et₃N, CH₂Cl₂; (e) trifluoroacetic acid; (f) 2,6-lutidine, DMF, Ar; (g) 1 N aq. NaOH, Ar.

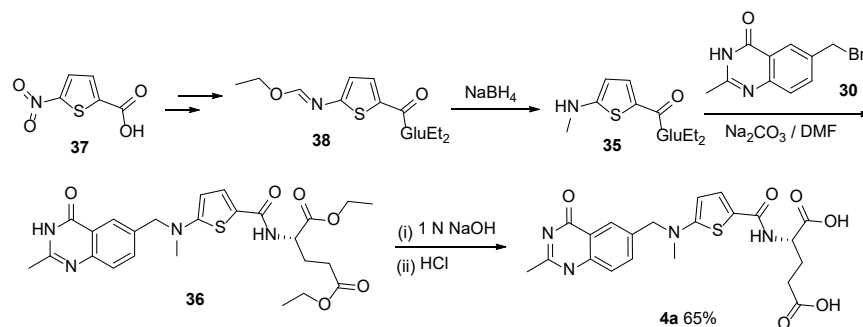
Scheme 15. Multistep synthesis of Raltitrexed **4a** starting from thiophene-2-carboxylic acid **27**.

Another route to Raltitrexed was reported that started with thiophene-2,5-dicarboxylic acid **31**, which was then converted in four steps to diethyl (5-(methylamino)thiophene-2-carbonyl)-*L*-glutamate **35**. This was followed by an alkylation reaction of the last one with 6-bromomethyl-2-methyl-4-quinazolinone **30** and basic hydrolysis, which resulted in the target product **4a** (Scheme 16) [34].



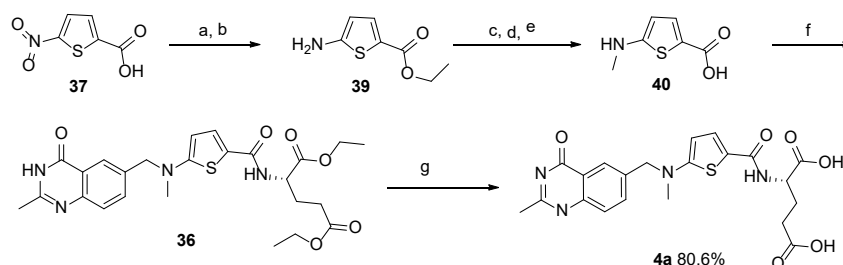
Scheme 16. Multistep synthesis of Raltitrexed starting from thiophene-2,5-dicarboxylic acid **31**.

A similar route to Raltitrexed was reported by Yao et al. starting with 5-nitrothiophene-2-carboxylic acid **37** via the sequence of NaBH_4 reduction, alkylation, and saponification (Scheme 17) [35]. The target product was isolated in a lower yield.



Scheme 17. Multistep synthesis of Raltitrexed starting from 5-nitrothiophene-2-carboxylic acid **37**.

Raltitrexed was also prepared by using the same compound in less reaction steps as reported by Xiqun et al. (Scheme 18) [36].

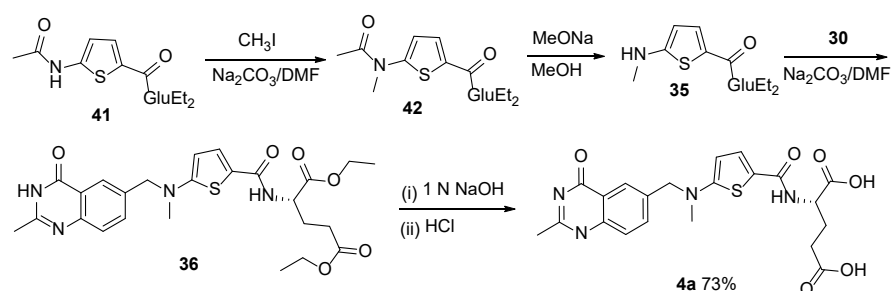


Reagents and conditions: (a) EtOH, H^+ ; (b) $\text{H}_2/\text{Pd}/\text{C}/\text{NH}_4\text{COOH}$; (c) $\text{CH}(\text{OMe})_3$; (d) NaBH_4 ; (e) NaOH; (f) (i) SOCl_2 , (ii) L-GluEt₂, (iii) **30**; (g) (i) 1 N NaOH, (ii) HCl.

Scheme 18. Multistep synthesis of Raltitrexed starting from 5-nitrothiophene-2-carboxylic acid **37**.

Moreover, the most recent and—in our opinion—easiest approach was reported in the work of H. Shaojie et al. regarding Raltitrexed, which involves a four-step sequence

using diethyl (5-(*N*-methylacetamido)thiophene-2-carbonyl)-*L*-glutamate **41** as the starting material (Scheme 19) [37].



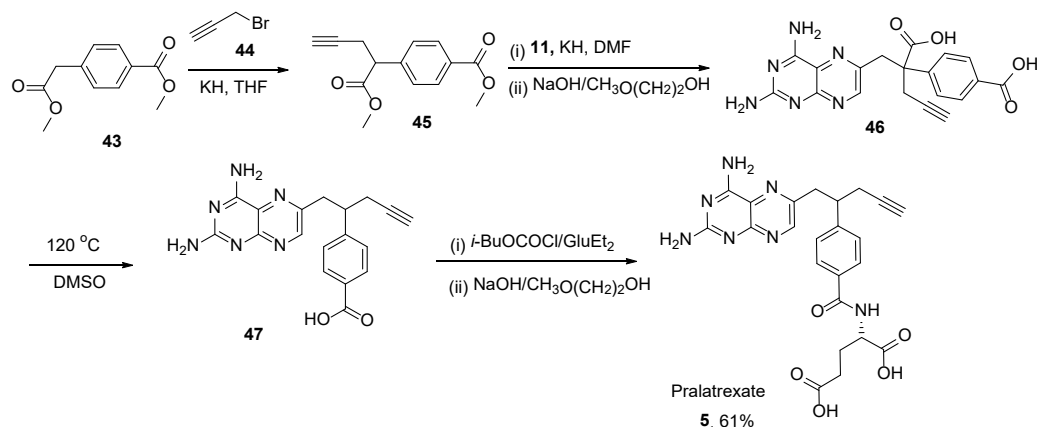
Scheme 19. Synthesis of Raltitrexed by diethyl (5-(*N*-methylacetamido)thiophene-2-carbonyl)-*L*-glutamate **41** as the starting material.

2.4. Pralatrexate (Folotyn):

N-4-[1-(2,4-Diaminopteridin-6-yl)Pent-4-yn-2-yl]Benzoyl-*L*-Glutamic Acid

Pralatrexate **25** is another folate antagonist and antineoplastic agent with confirmed activity for the treatment of relapsed or refractory peripheral T-cell lymphoma (PTCL). Pralatrexate was approved for medical use in the United States in September 2009, as the first treatment for Peripheral T-cell Lymphoma (PTCL) [38,39], an often-aggressive type of non-Hodgkins lymphoma [40].

Successive alkylation of dimethyl homoterephthalate **43** with propargyl bromide **44** and 2,4-diamino-6-(bromomethyl)pteridine **11** followed by ester saponification at room temperature resulted in 2,4-diamino-4-deoxy-10-carboxy-10-propargyl-10-deazapteroic acid **46**. Subsequently, compound **46** was readily decarboxylated by heating in DMSO at 120 °C to yield diamino-10-propargyl-10-deazapteroic acid **47** as a precursor of Pralatrexate **5**. Additionally, the coupling of **47** with diethyl *L*-glutamate followed by ester hydrolysis, yielded Pralatrexate **5** (Scheme 20) [41].

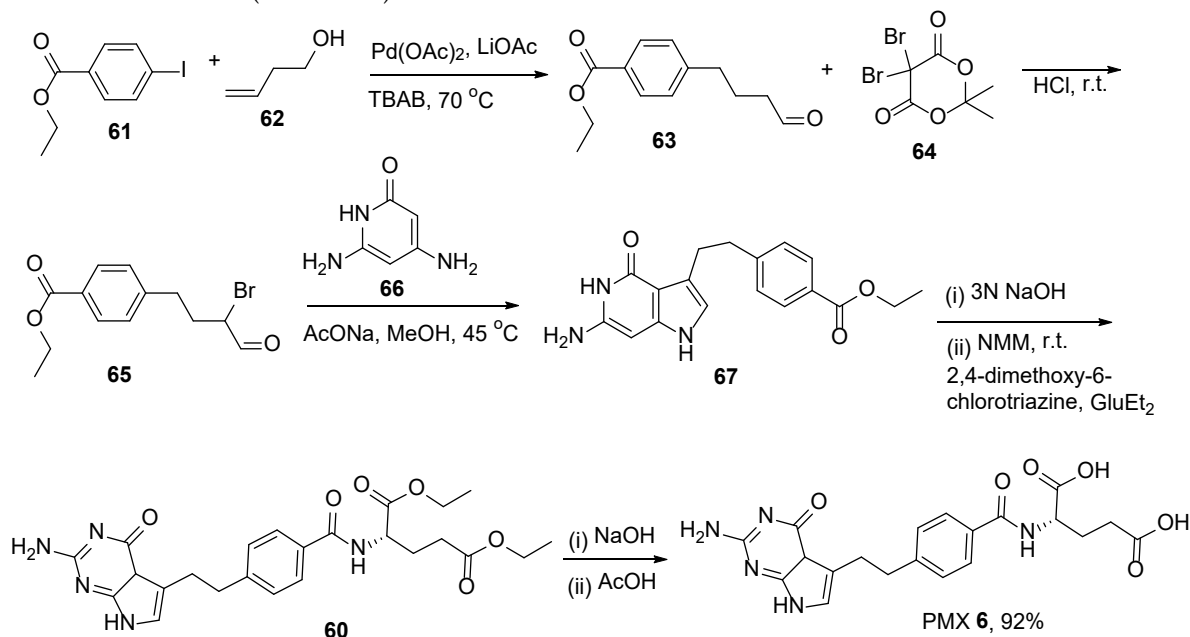


Scheme 20. Synthesis of Pralatrexate starting from the reaction between dimethyl homoterephthalate **43** and propargyl bromide. Reproduced with the permission of reference [41]. Copyright © 1993, American Chemical Society.

After the abovementioned publication, many improved procedures were reported for the preparation of Pralatrexate [42–48]. The synthesis of optically pure diastereomers of Pralatrexate has also been reported [49].

Another approach to producing Pralatrexate was developed by Alla et al. (2013), starting with ethyl 4-formylbenzoate **48**; however, the yield was not specified (Scheme 21) [50].

Mitchell-Ryan et al. reported the synthesis of 5-substituted pyrrolo[2,3-*d*]pyrimidine antifolates with one-to-six bridge carbons and a benzoyl ring in the side chain as antitumor agents [58]. The compound with a 4-carbon bridge was the most active analogue and it potentially inhibited the proliferation of the folate receptor (FR) α -expressing Chinese hamster ovary and KB human tumor cells. PMX was synthesized from ethyl 4-iodobenzoate **61**, and 1-butene-4-ol **62** using a Heck cross-coupling reaction followed by bromination of the aldehyde at alpha-position. Further heterocyclization with basic hydrolysis and the formation of amide from diethyl-*L*-glutamate resulted in acid derivative **60**. In the final step, PMX **6** was obtained by the basic hydrolysis of the ester groups in a glutamate moiety (Scheme 23).



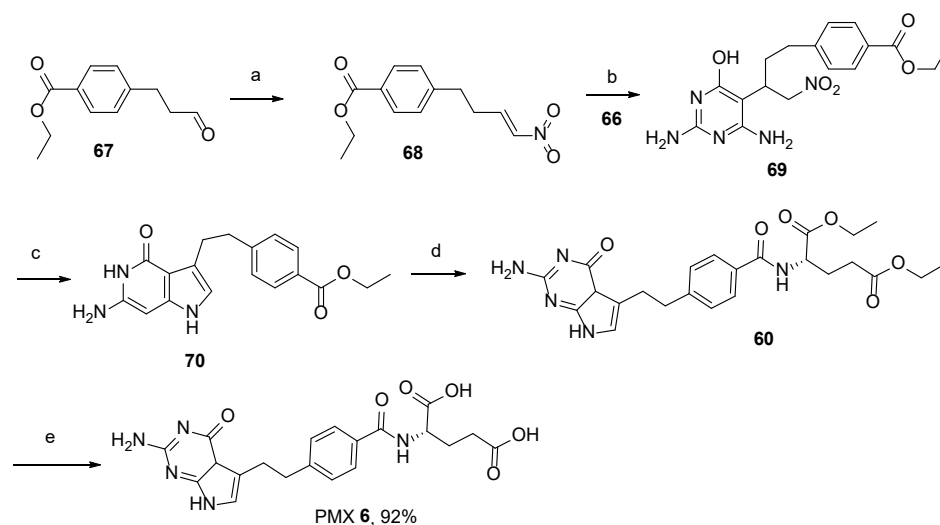
Scheme 23. Synthesis of Pemetrexed starting from ethyl 4-iodobenzoate **61**, and 1-butene-4-ol **62** through Heck cross-coupling reaction. Reproduced with the permission of reference [58]. Copyright © 2013, American Chemical Society.

As an improvement to the abovementioned method, the preparation of lysin salt of PMX was reported [59].

Michalak et al. reported the synthesis of PMX along with its common impurities/side products, starting with 4-[2-(2-amino-4-oxo-4,7-dihydro-1*H*-pyrrolo[2,3-*d*]pyrimidin-5-yl)ethyl]benzoic acid **28** [60].

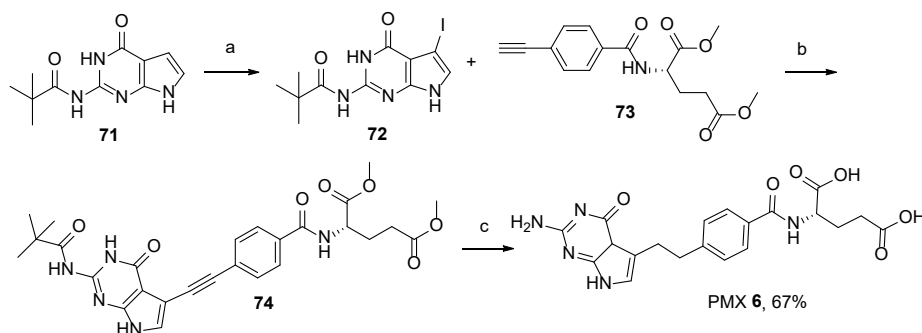
In the method reported by Taylor et al. for the synthesis of PMX, ethyl-4-(3-oxopropyl)benzoate **67** was used as a starting compound [61–63]. After the Henry reaction with nitromethane, the product was converted to the semi-product with 2,6-diaminopyrimidin-4-ol **69**. The heterocyclization of this semi-product resulted in pyrrolo[2,3-*d*]pyrimidine derivative **70**, which, followed by its functionalization with diethyl-*L*-glutamate and basic hydrolysis, resulted in the desired product **6** in a 92% yield (Scheme 24).

The same research group reported an improved synthesis of PMX, starting from dimethyl (4-ethynylbenzoyl)-*L*-glutamate **73** and *N*-(4-oxo-4,7-dihydro-3*H*-pyrrolo[2,3-*d*]pyrimidin-2-yl)pivalamide **71** [64]. The sequence of iodination, reduction, Sonogashira cross-coupling, reduction reactions, and basic hydrolysis in the last step, resulted in the final product, PMX, in a 67% yield (Scheme 25).



Reagents and conditions: (a) (i) $\text{CH}_3\text{NO}_2/\text{NaOH}/\text{EtOH}$; (ii) $\text{CH}_3\text{SO}_2\text{Cl}/\text{Et}_3\text{N}$; (b) $\text{EtOAc}/\text{H}_2\text{O}$ 1:1, 50°C , 24 h; (c) (i) aq. NaOH , rt, 2 h; (ii) add to aq. H_2SO_4 at 0°C , 3 h; (iii) aq. NaOH to pH 7, rt, 1 h; HOAc , then filter; (d) NMM , 2,4-dimethoxy-6-chlorotriazine, DMF , rt; (e) NaOH , $\text{THF}/\text{H}_2\text{O}$

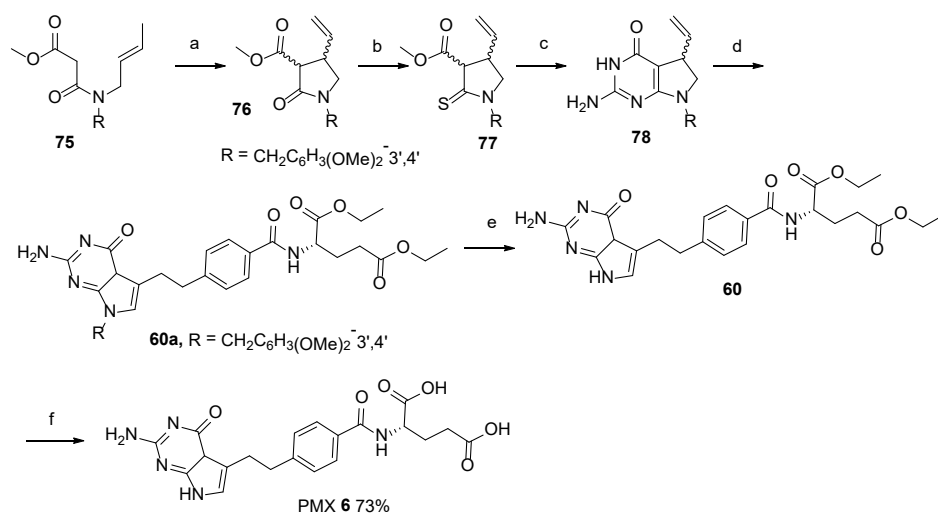
Scheme 24. Synthesis of Pemetrexed starting from ethyl-4-(3-oxopropyl)benzoate 67.



Reagents and conditions: (a) (i) NIS , DMF , rt; (ii) Zn dust, AcOH (b) CuI , TEA , $\text{Pd}(\text{PPh}_3)_4$, rt; (c) (i) H_2 50 psi Pd/C (ii) 1N NaOH , AcOH , 3 d, rt.

Scheme 25. Synthesis of Pemetrexed starting from dimethyl (4-ethynylbenzoyl)-*L*-glutamate 73 and *N*-(4-oxo-4,7-dihydro-3*H*-pyrrolo[2,3-*d*]pyrimidin-2-yl)pivalamide 71.

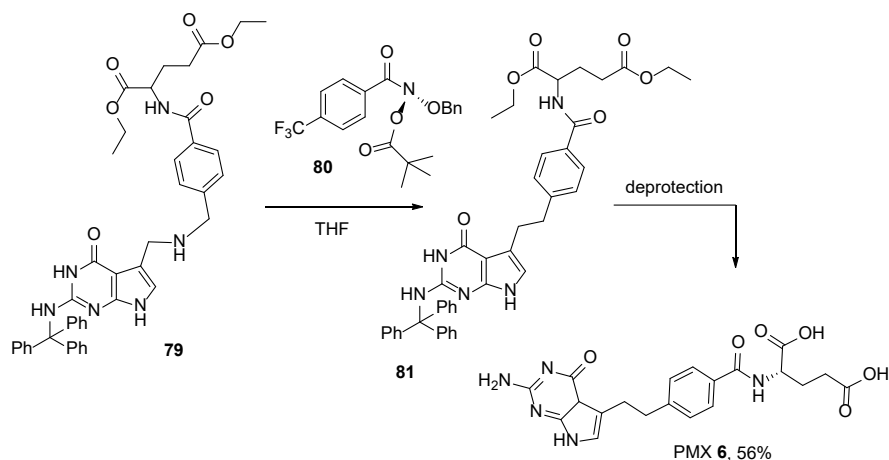
The same authors also reported the synthesis of PMX starting from methyl (*E*)-3-(but-2-en-1-yl(3,4-dimethoxybenzyl)amino)-3-oxopropanoate [65]. The last one was cyclized to methyl-1-(3,4-dimethoxybenzyl)-2-oxo-4-vinylpyrrolidine-3-carboxylate by the reaction of $\text{Mn}(\text{III})$ and $\text{Cu}(\text{II})$ acetates. The oxo-group was then converted to the thioxo-group upon treatment with P_2S_5 . After the heterocyclization reaction, the obtained 2-amino-7-(3,4-dimethoxybenzyl)-5-vinyl-4*a*,5,6,7-tetrahydro-4*H*-pyrrolo[2,3-*d*]pyrimidin-4-one was subjected to a Heck cross-coupling reaction with diethyl 4-iodobenzoylglutamate. Additionally, the coupling product was identified as one with unexpected double bond migration products in vinyl-bridged pyrrolinopyrimidine to form the ethano-bridged pyrrolopyrimidine. Thus, the authors avoided the reduction of the unsaturated bridge and the subsequent oxidation of the pyrroline ring at the same time. According to the authors, the protection of the N-7 position eliminates the PMX cell growth's inhibitory activity. In addition, deprotection of the N-7 position was finally achieved upon treatment with a $\text{H}_2\text{SO}_4/\text{TFA}$ mixture to facilitate the PMX precursor in a 30% yield, which resulted in the target product after saponification (Scheme 26).



Reagents and conditions: (a) $\text{Mn}(\text{OAc})_3 \cdot 2\text{H}_2\text{O}$, $\text{Cu}(\text{OAc})_2 \cdot \text{H}_2\text{O}$; (b) P_2S_5 ; (c) guanidine; (d) diethyl 4-iodobenzoyl-L-glutamate, $\text{Pd}(\text{OAc})_2$; (e) $\text{H}_2\text{SO}_4/\text{TFA}$; (f) NaOH .

Scheme 26. Synthesis of Pemetrexed starting from methyl (*E*)-3-(but-2-en-1-yl)(3,4-dimethoxybenzyl)amino)-3-oxopropanoate 75.

Finally, very recently, a method for PMX synthesis was developed by means of the reaction of an anomeric amide agent with a secondary amine precursor followed by the deprotection of protective groups (Scheme 27) [66].



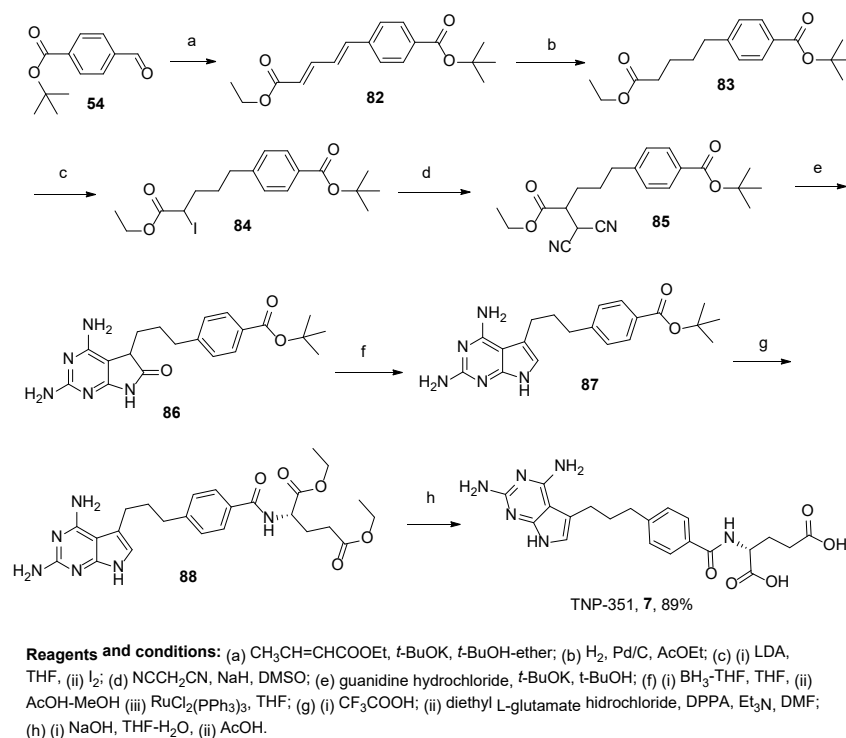
Scheme 27. Synthesis of Pemetrexed by the reaction of anomeric amide agent with secondary amine precursor followed by the deprotection of protective groups.

2.6. TNP-351: (2*S*)-2-[[4-[3-(2,4-Diamino-7*H*-Pyrrolo[2,3-*d*]Pyrimidin-5-yl)Propyl]benzoyl]Amino]Pentanedioic Acid (HY-19095)

TNP-351 is another antifolate from the same family as PMX. As a dihydrofolate reductase (DHFR) inhibitor, TNP-351 has good potential for the treatment of not only leukemia cells but also solid tumor cells, both *in vitro* and *in vivo* [67]. The structure of TNP-351 contains three methylene bridges instead of two as in PMX and two amino groups in pyrimidine core.

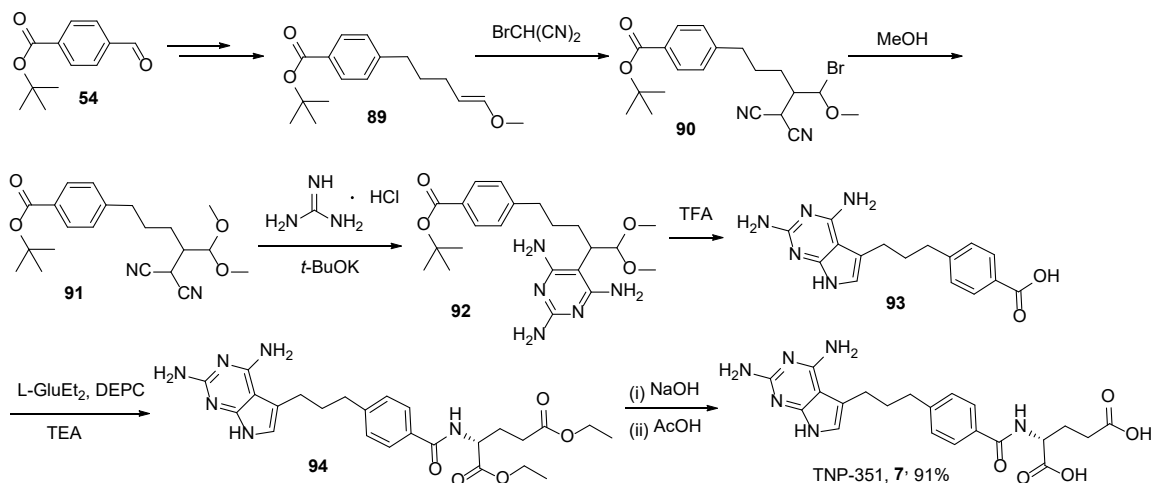
So far, only two synthetic approaches to TNP-351 7 have been reported; the first one includes construction of the key intermediary acyclic skeleton, 5-[4-(*tert*-butoxycarbonyl)phenyl]-2-(dicyanomethyl)pentanoate 85, cyclization with guanidine, followed by reduction to pyrrolo[2,3-*d*]pyrimidine derivatives 87, and subsequent glutamate coupling and saponification. These antifolates were more growth-inhibitory by approximately one order of

magnitude than methotrexate (MTX) against KB human epidermoid carcinoma cells and A549 human non-small cell lung carcinoma cells with in vitro culture (Scheme 28) [68].



Scheme 28. Multistep synthesis of TNP-351.

The second method belongs to the same article, where the synthesis of TNP-351 has been reported along with PMX synthesis (Scheme 29) [57].



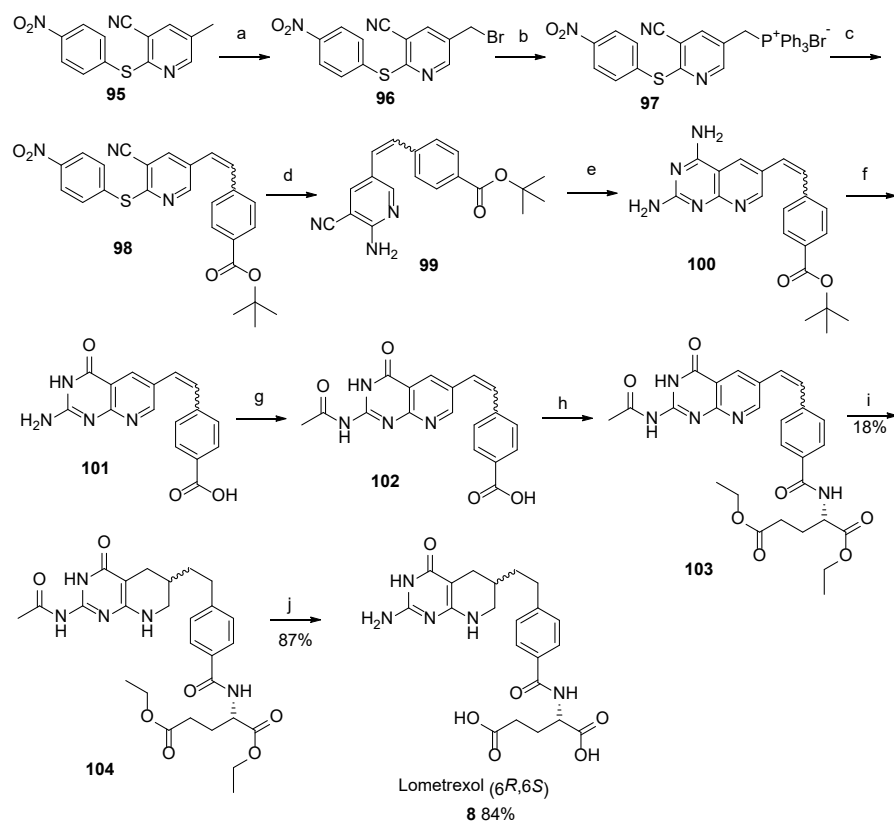
Scheme 29. Multistep synthesis of TNP-351.

2.7. Lometrexol: (2S)-2-[[4-[2-[(6R)-2-Amino-4-oxo-5,6,7,8-Tetrahydro-1H-Pyrido[2,3-d]Pyrimidin-6-yl]Ethyl]Benzoyl]Amino]Pentanedioic Acid (LY 264618, DDATHF-B, Lometrexolum)

Lometrexol (6R)-**8** is a folate analogue antimetabolite with antineoplastic activity [69–71]. As the 6R diastereomer of 5,10-dideazatetrahydrofolate, lometrexol inhibits glycinamide ribonucleotide formyltransferase (GARFT), the enzyme that catalyzes the first step in the de novo purine biosynthetic pathway, thereby inhibiting DNA synthesis, arresting cells in the S phase of the cell cycle, and inhibiting tumor cell proliferation. The agent is active against tumors that are resistant to the folate antagonist methotrexate.

Lometrexol has been used in trials for the treatment of lung cancer, drug/agent toxicity by tissues/organs, as well as for the treatment of unspecified adult solid tumors.

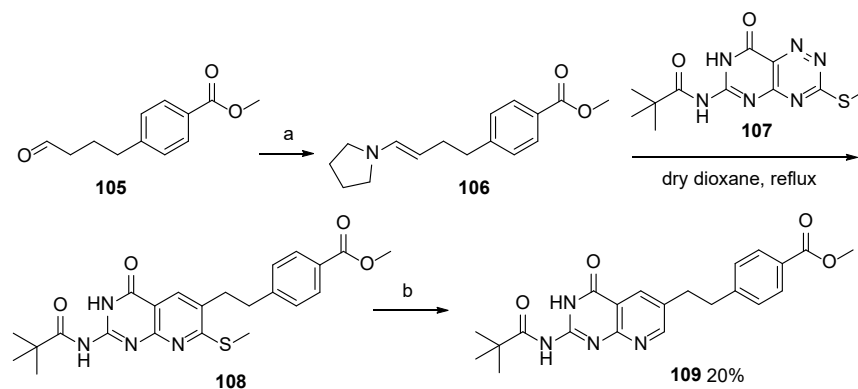
Taylor et al. reported several approaches to Lometrexol. The first of their approaches relates to the synthesis of (mixture of diastereomers) (6*S*,6*R*)-Lometrexol **8** with a satisfactory yield starting from 5-methyl-2-((4-nitrophenyl)thio)nicotinonitrile **95** (Scheme 30) [72].



Reagents and conditions: (a) NBS, 1 h; (b) PPh₃; (c) **54**; (d) NH₃, CuBr₂; (e) guanidine; (f) 88% HCOOH, rt; (g) (i) Ac₂O, 120 °C; (ii) 1N NaOH; (iii) AcOH; (h) phenyl *N*-phenylphosphoramidochloridate, *N*⁻methylmorpholine, L-Glu, *N*-methylpyrrolidone; (i) H₂ 55 psi / 5% Pd/C, TFA, rt (j) NaOH, MeOH, rt.

Scheme 30. Synthesis of Lometrexol starting from 5-methyl-2-((4-nitrophenyl)thio)nicotinonitrile **95**.

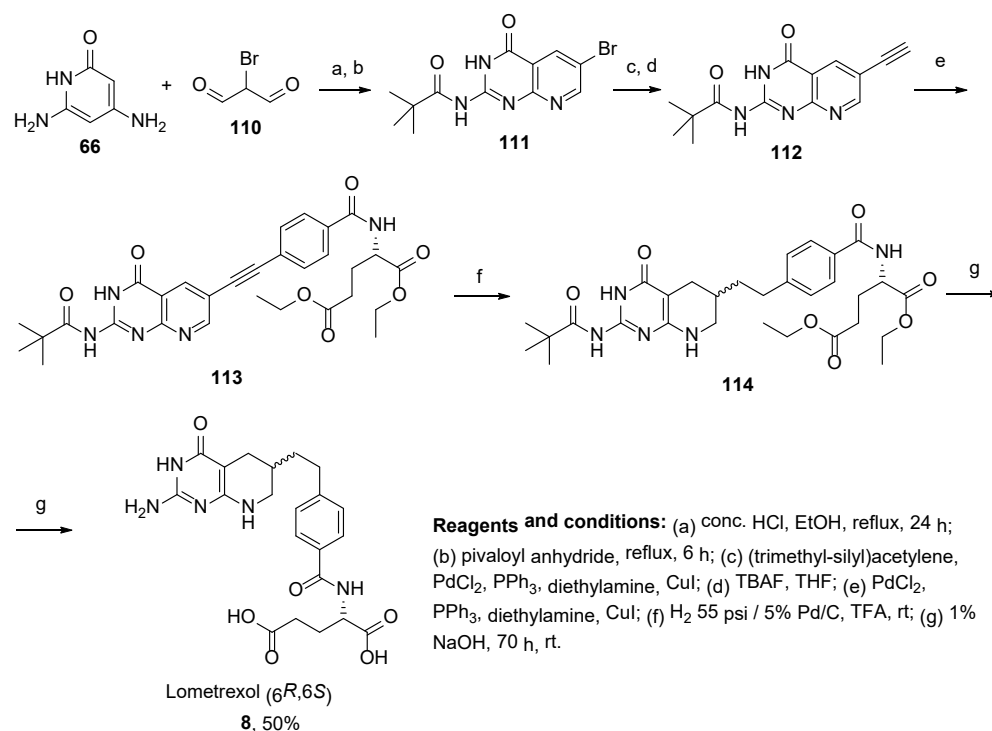
A key intermediate **109** for the subsequent synthesis of (6*S*,6*R*)-Lometrexol was also prepared by Taylor et al. via a regioselective intermolecular inverse electron demand Diels-Alder reaction between fused 1,2,4-triazines, 2-*N*-pivaloyl-7-substituted-6-azapterins, and enamine (Scheme 31) [73].



Reagents and conditions: (a) dry MgSO₄, dry THF; (b) Raney Ni, EtOH, rt, 5 d.

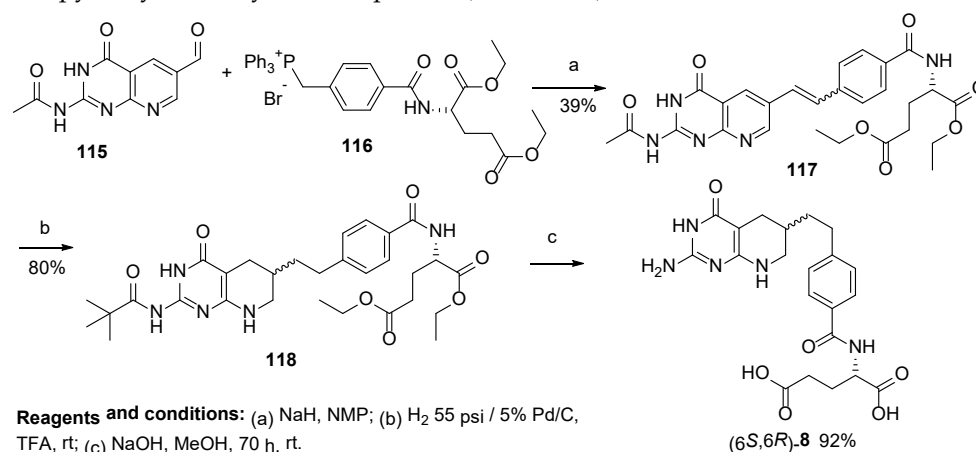
Scheme 31. Synthesis of key intermediate **109**.

In another work, Taylor et al. developed a convenient method for the synthesis of (6*S*,6*R*)-Lometrexol **8** with good yield via *N*-(6-bromo-4-oxo-3,4-dihydropyrido[2,3-*d*]pyrimidin-2-yl)pivalamide starting with 2,6-diaminopyrimidin-4(3*H*)-one (Scheme 32) [74].



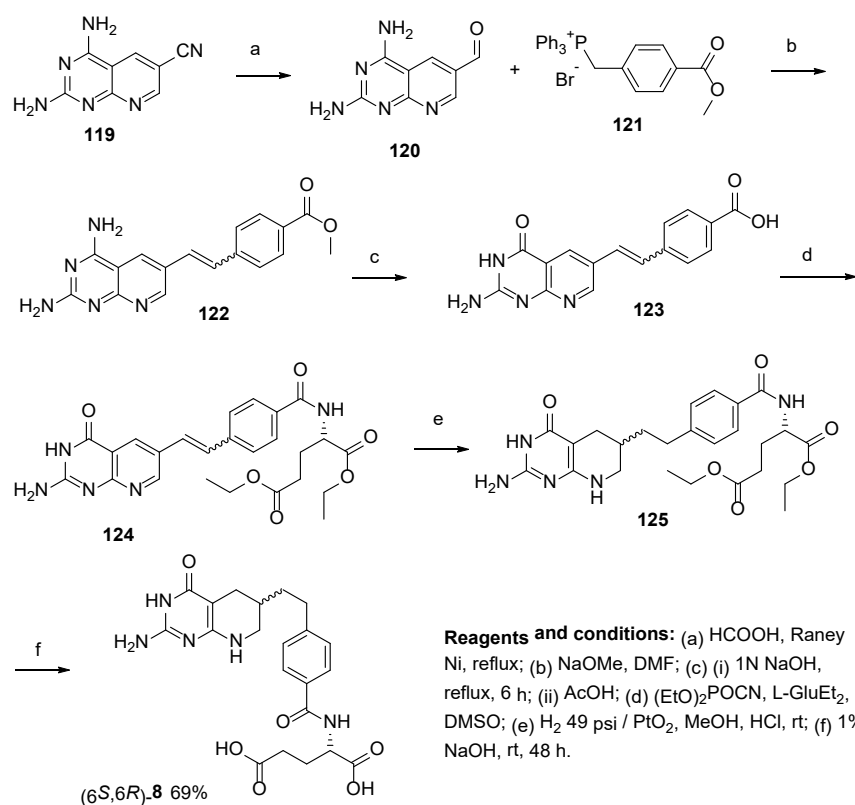
Scheme 32. Synthesis of (6*S*,6*R*)-Lometrexol **8** via *N*-(6-bromo-4-oxo-3,4-dihydropyrido[2,3-*d*]pyrimidin-2-yl)pivalamide starting from 2,6-diaminopyrimidin-4(3*H*)-one.

Boschelli et al. performed Wittig olefination of 2-acetyl-6-formyl-5-deazapterine to prepare (6*S*,6*R*)-Lometrexol in three synthetic steps instead of Sonogashira cross-coupling of 2-pivaloyl-6-formyl-5-deazapterine (Scheme 33) [75].



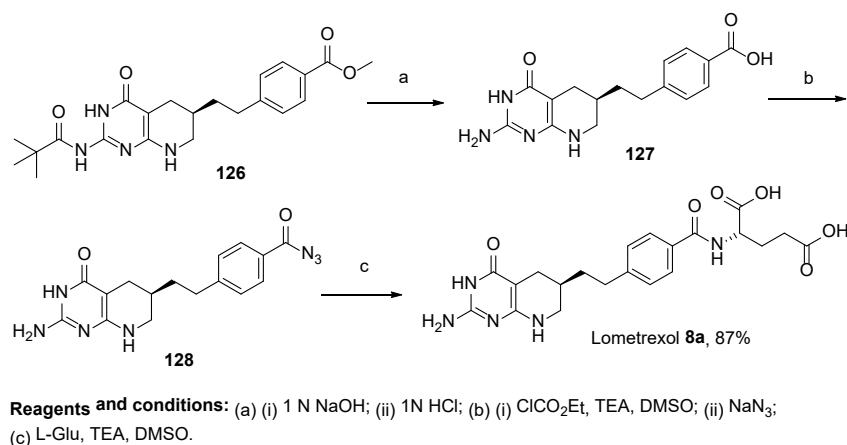
Scheme 33. Synthesis of (6*S*,6*R*)-Lometrexol **8** by the Wittig olefination of 2-acetyl-6-formyl-5-deazapterine.

Similarly, Wittig olefination was used by Piper et al. for the synthesis of (6*S*,6*R*)-Lometrexol starting from 2,4-diaminopyrido[2,3-*d*]pyrimidine-6-carboxaldehyde **120**, derived from 6-carbonyltrile, and [4-(methoxycarbonyl)benzylidene]triphenylphosphorane to yield 9,10-ethenyl precursor **122** [76]. Standard hydrolytic deamination produced 5,10-dideazafolic acid **123**, which was further converted to 5,10-dideazaaminopterin via a coupling reaction with dimethyl *L*-glutamate by using (EtO)₂POCN, followed by hydrogenation and ester hydrolysis which led to the final product **8** (Scheme 34).



Scheme 34. Synthesis of (6*S*,6*R*)-Lometrexol starting from 2,4-diaminopyrido[2,3-*d*]pyrimidine-6-carboxaldehyde.

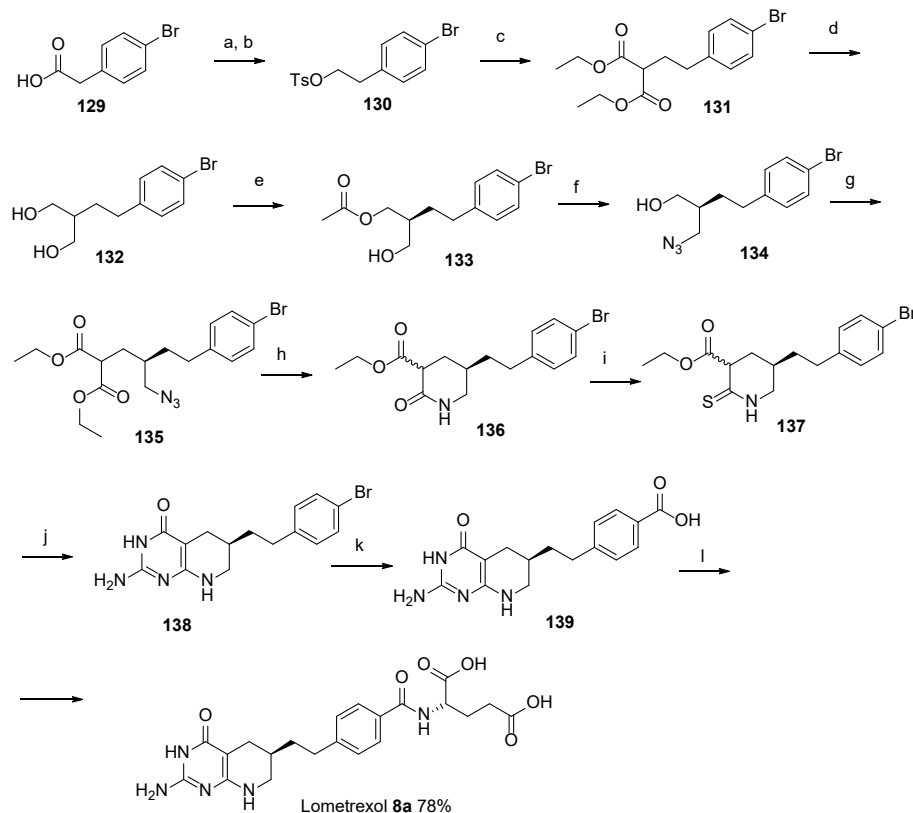
Currently, only two synthetic approaches toward diastereometrically pure 6*R*-Lometrexol are reported in the literature. In this context, the synthesis of 6*R*-Lometrexol was carried out starting from a double deprotected DDAH₄Pte-OH **126**, which was obtained with preparative chiral-HPLC in a mixture of diastereomers derived from the route based on the work of Taylor et al. [77]. After the transformation of the benzoic acid residue to a derivative which includes azides, the azide derivative was converted to the final product by the reaction of *L*-glutamic acid in DMSO in the presence of TEA (Scheme 35) [78].



Scheme 35. Synthesis of 6*R*-Lometrexol starting from a double deprotected DDAH₄Pte-OH **126**.

In another approach, the lipase-catalyzed enantioselective esterification of 2-(4-bromophenethyl) propane-1,3-diol, derived in several steps from 2-(4-bromophenyl)acetic acid, was utilized in the asymmetric synthesis of key (*R*)-2-amino-6-(4-bromophenethyl)-5,6,7,8-tetrahydropyrido

pyrimidin-4(3*H*)-one, which resulted in the target product in two synthetic steps (Scheme 36) [79,80].



Reagents and conditions: (a) BH₃·THF; (b) TsCl, Et₃N; (c) NaH, diethyl malonate; (d) LiAlH₄, Et₂O; (e) PPL-porcine pancreatic lipase (Sigma type II) immobilized on Hyflo Super Cel, MeOAc; (f) (i) MsCl, Et₃N; (ii) NaN₃, DMF; (iii) HCl, MeOH; (g) (i) TsCl, Et₃N; (ii) NaH, diethyl malonate, NaI; (h) Bu₃P, THF; (i) P₂S₅; (j) guanidine; (k) CuCN, NMP, reflux; (l) (i) H₂N-L-Glu(OEt)₂; (ii) 6M HCl, reflux.

Scheme 36. Multistep synthesis of Lometrexol starting from 2-(4-bromophenyl)acetic acid. Reproduced with the permission of references [79]. Copyright © 1989, Elsevier Ltd.

3. Conclusions and Future Perspectives

In summary, this review represents the analysis of the most up-to-date synthetic approaches for the synthesis of therapeutically significant analogues of folic acid, such as Lometrexol, Methotrexate, Pemetrexed, Pralatrexate, Raltitrexed, and TNP-351. Among the other folic acid analogues exhibiting antimalarial/antiprotozoal [81] and broad-spectrum antimicrobial activity [82–84], the importance and effectiveness of the abovementioned six analogues of folic acid as drugs or drug candidates for the treatment of diseases with a social significance, such as various types of cancers, severe psoriasis, and rheumatoid arthritis, were reported in a large number of original research publications and review articles [18,30–32,40,51–55,67,69–71]. Even though folates were reported to be somehow connected with the severeness of COVID-19 [85–87], several recent studies suggested the effectiveness of antifolates for the therapy of patients with coronavirus SARS-CoV-2 [85,88,89], along with the enhancement of the antiviral efficacy of remdesivir [88], treatment of fungal infections with COVID-19-like symptoms [90], as well as treatment of fungal infections among COVID-19 patients [90].

Most of the synthetic strategies for these important scaffolds presented in research articles and patents are based on similar approaches and have only minor differences from each other. So far, no attention has been paid to methods based on transitional metal (TM)-catalyzed or the TM-free direct C-H-activation/C-H-functionalization of

aza-aromatic rings as the most atom- and step-efficient approaches. We hope that our review will encourage future interest in this research area.

Author Contributions: Conceptualization, I.S.K., G.V.Z. and A.M.; methodology, I.S.K. and S.S.; software, S.S. and M.V.V.; validation, G.V.Z., A.M. and V.N.C.; formal analysis, G.V.Z., A.M. and V.N.C.; investigation, G.V.Z. and A.M.; resources, I.S.K. and G.V.Z.; data curation, I.S.K. and S.S.; writing—original draft preparation, I.S.K., G.V.Z. and S.S.; writing—review and editing, G.V.Z. and S.S.; visualization, A.M. and M.V.V.; supervision, G.V.Z., A.M. and V.N.C.; project administration, G.V.Z. and S.S.; funding acquisition, G.V.Z. and S.S. All authors have read and agreed to the published version of the manuscript.

Funding: The analysis of synthetic approaches to antifolates was supported by the Russian Science Foundation (Project # 20-43-01004). The analysis of biological activity of antifolates was supported by the Ministry of Science and the Higher Education of RF (Ref. # 075-15-2022-1118, dated 29 June 2022).

Institutional Review Board Statement: Not applicable.

Informed Consent Statement: Not applicable.

Data Availability Statement: Not applicable.

Conflicts of Interest: The authors declare no conflict of interest.

References

- Ahluwalia, G.S.; Grem, J.L.; Hao, Z.; Cooney, D.A. Metabolism and action of amino acid analog anti-cancer agents. *Pharmacol. Ther.* **1990**, *46*, 243–271. [CrossRef]
- Xie, M.; Liu, D.; Yang, Y. Anti-cancer peptides: Classification, mechanism of action, reconstruction and modification. *Open Biol.* **2020**, *10*, 200004. [CrossRef]
- Chiangjong, W.; Chutipongtanate, S.; Hongeng, S. Anticancer peptide: Physicochemical property, functional aspect and trend in clinical application (Review). *Int. J. Oncol.* **2020**, *57*, 678–696. [CrossRef]
- Mandal, P.K.; Gao, F.; Lu, Z.; Ren, Z.; Ramesh, R.; Birtwistle, J.S.; Kaluarachchi, K.K.; Chen, X.; Bast, R.C., Jr.; Liao, W.S.; et al. Potent and selective phosphopeptide mimetic prodrugs targeted to the Src homology 2 (SH2) domain of signal transducer and activator of transcription 3. *J. Med. Chem.* **2011**, *54*, 3549–3563. [CrossRef] [PubMed]
- Gut, J. Aza Analogs of Pyrimidine and Purine Bases of Nucleic Acids. *Adv. Heterocycl. Chem.* **1963**, *1*, 189–251. [CrossRef]
- Gojkovic, Z.; Karlsson, A. Purine and Pyrimidine-Based Analogs and Suicide Gene Therapy. In *Deoxynucleoside Analogs in Cancer Therapy*; Humana Press: Totowa, NJ, USA, 2007; pp. 403–439. [CrossRef]
- Zelder, F.; Sonnay, M.; Prieto, L. Antivitamins for medicinal applications. *ChemBioChem* **2015**, *16*, 1264–1278. [CrossRef] [PubMed]
- Howell, A. *The Role of Antihormones*; CRC Press: Boca Raton, FL, USA, 1990.
- Albert, A. Antimetabolites: Antagonistic analogues of coenzymes and enzyme substrates. In *Selective Toxicity*; Albert, A., Ed.; Springer: Dordrecht, The Netherlands, 1985; pp. 323–378.
- Lansiaux, A. Les antimétabolites. *Bull. Cancer* **2011**, *98*, 1263–1274. [CrossRef] [PubMed]
- Petering, H.G. Folic acid antagonists. *Physiol. Rev.* **1952**, *32*, 197–213. [CrossRef]
- Ellison, R.R. Treating Cancer with Antimetabolites. *Am. J. Nurs.* **1962**, *62*, 79. [CrossRef]
- Panderi, I.; Koufopantelis, P. Methotrexate, an antimetabolite of folic acid, a brief throwback. *Pharmakeftiki* **2014**, *26*, 45–56.
- Chu, E.; Drake, J.C.; Boarman, D.; Baram, J.; Allegra, C.J. Mechanism of thymidylate synthase inhibition by methotrexate in human neoplastic cell lines and normal human myeloid progenitor cells. *J. Biol. Chem.* **1990**, *265*, 8470–8478. [CrossRef]
- Messmann, R.; Allegra, C. Antifolates. In *Cancer Chemotherapy and Biotherapy*; Chabner, B., Longo, D., Eds.; L. Williams & W: Philadelphia, PA, USA, 2001; pp. 139–184.
- Shih, C.; Chen, V.J.; Gossett, L.S.; Gates, S.B.; MacKellar, W.C.; Habeck, L.L.; Shackelford, K.A.; Mendelsohn, L.G.; Soose, D.J.; Patel, V.F.; et al. Ly231514, a pyrrolo [2,3-d]pyrimidine-based antifolate that inhibits multiple folate-requiring enzymes. *Cancer Res.* **1997**, *57*, 1116–1123. [PubMed]
- Avendaño, C.; Menéndez, J.C. (Eds.) Antimetabolites. In *Medicinal Chemistry of Anticancer Drugs*; Elsevier: Amsterdam, The Netherlands, 2008; pp. 9–52.
- Moran, R.G. Folate antimetabolites inhibitory to de novo purine synthesis. In *New Drugs, Concepts and Results in Cancer Chemotherapy. Cancer Treatment and Research*; Muggia, F.M., Ed.; Springer: Boston, MA, USA, 1991; Volume 58, pp. 65–87.
- Catalucci, E. Process for the Production of Methotrexate. U.S. Patent US4224446A, 23 September 1991.
- Bin, Y.; Shubin, W.; Zhichao, M.; Quansheng, S.; Yanjiao, X.; Lilian, L. A Kind of Preparation Method of Methotrexate (MTX). U.S. Patent CN109553619A, 2 April 2019.
- Piper, J.R.; Montgomery, J.A. 6-(Bromomethyl)-2,4-diaminopteridine Hydrobromide. U.S. Patent US4077957A, 11 April 1978.
- Luo, J.; Smith, M.D.; Lantrip, D.A.; Wang, S.; Fuchs, P.L. Efficient syntheses of pyrofolate and pteroyl azide, reagents for the production of carboxyl-differentiated derivatives of folic acid. *J. Am. Chem. Soc.* **1997**, *119*, 10004–10013. [CrossRef]

23. Attoline, E.; Michieletti, M.; Rossi, D.; Allegrini, P. Process for the Preparation of Pteridine Derivatives. U.S. Patent US4767859, 17 November 1988.
24. Cheung, A.H.T.; Smal, M.; Chau, D.D. Synthesis of multi-¹³C-enriched methotrexate for NMR studies of drug-Enzyme interactions. *Heterocycles* **1987**, *25*, 507–514. [CrossRef]
25. Cheung, A.H.T.; Boadle, D.K.; Tran, T.Q. N-(L- α -aminoacyl) derivatives of methotrexate. *Heterocycles* **1989**, *28*, 751–758. [CrossRef]
26. Choi, S.K.; Verma, M.; Silpe, J.; Moody, R.E.; Tang, K.; Hanson, J.J.; Baker, J.R., Jr. A photochemical approach for controlled drug release in targeted drug delivery. *Bioorg. Med. Chem.* **2012**, *20*, 1281–1290. [CrossRef]
27. Lei, T.; Yi, Z.; Jianta, W.; Gaofeng, Z.; Xing, C. Synthesis Process of Methotrexate. U.S. Patent CN112851676A, 28 May 2021.
28. Wiecko, J. Process for Preparing Methotrexate or an N-Substituted Derivative Thereof and/or a di (lower) Alkyl Ester Thereof and Precursor Therefor. U.S. Patent US4057548A, 30 March 1976.
29. Seeger, D.R.; Cosulich, D.B.; Smith, J.M.; Hultquist, M.E. Analogs of Pteroylglutamic Acid. III. 4-Amino Derivatives. *J. Am. Chem. Soc.* **1949**, *71*, 1753–1758. [CrossRef]
30. Widemann, B.C.; Balis, F.M.; Godwin, K.S.; McCully, C.; Adamson, P.C. The plasma pharmacokinetics and cerebrospinal fluid penetration of the thymidylate synthase inhibitor raltitrexed (Tomudex(TM)) in a nonhuman primate model. *Cancer Chemother. Pharmacol.* **1999**, *44*, 439–443. [CrossRef] [PubMed]
31. Liu, Y.; Wu, W.; Hong, W.; Sun, X.; Wu, J.; Huang, Q. Raltitrexed-based chemotherapy for advanced colorectal cancer. *Clin. Res. Hepatol. Gastroenterol.* **2014**, *38*, 219–225. [CrossRef]
32. Cocconi, G.; Cunningham, D.; Van Cutsem, E.; Francois, E.; Gustavsson, B.; van HazelD Kerr, G.; Possinger, K.; Hietschold, S.M. Open, randomized, multicenter trial of raltitrexed versus fluorouracil plus high-dose leucovorin in patients with advanced colorectal cancer. Tomudex Colorectal Cancer Study Group. *J. Clin. Oncol.* **2016**, *16*, 2943–2952. [CrossRef]
33. Marsham, P.R.; Hughes, L.R.; Jackman, A.L.; Hayter, A.J.; Oldfield, J.; Wardleworth, J.M.; Bishop, J.A.M.; O'Connor, B.M.; Calvert, A.H. Quinazoline Antifolate Thymidylate Synthase Inhibitors: Heterocyclic Benzoyl Ring Modifications. *J. Med. Chem.* **1991**, *34*, 1594–1605. [CrossRef] [PubMed]
34. Cao, S.L.; Wan, R.; Feng, Y.P. New synthesis of thymidylate synthase inhibitor raltitrexed. *Synth. Commun.* **2003**, *33*, 3519–3526. [CrossRef]
35. Yao, T.; Zubing, W.; Shuwang, G.; Jian, W.; Yuzhu, C.; Feng, L.; Dan, X.; Chunxia, Z.; Zhoushan, T. The Formoxyl of 5-((Alkoxy methylene)amino)thienyl-2-formyl Group)-L-glutamic Acid Dialkyl Ester and Preparation Method Thereof. U.S. Patent CN106957296A, 18 July 2017.
36. Xiqun, J.; Wei, W.; Zhoushan, T.; Jun, H.; Jing, W.; Yuzhu, C.; Huaping, W.; Dan, X.; Chunxia, Z.; Chuanjun, W. A kind of Pharmaceutical Composition of Raltitrexed Pharmaceutical Composition and Preparation Method Thereof. U.S. Patent CN107616976A, 23 January 2018.
37. Shaojie, H.; Wei, S.; Zhaobai, Z.; Xu, S. Preparation Method of Raltitrexed. U.S. Patent CN11055114A, 10 December 2019.
38. O'Connor, O.A.; Pro, B.; Pinter-Brown, L.; Bartlett, N.; Popplewell, L.; Coiffier, B.; Lechowicz, M.J.; Savage, K.J.; Shustov, A.R.; Gisselbrecht, C.; et al. Pralatrexate in patients with relapsed or refractory peripheral T-cell lymphoma: Results from the pivotal PROPEL study. *J. Clin. Oncol.* **2011**, *29*, 1182–1189. [CrossRef] [PubMed]
39. Amengual, J.E.; Lichtenstein, R.; Lue, J.; Sawas, A.; Deng, C.; Lichtenstein, E.; Khan, K.; Atkins, L.; Rada, A.; Kim, H.A.; et al. A phase 1 study of romidepsin and pralatrexate reveals marked activity in relapsed and refractory T-cell lymphoma. *Blood* **2018**, *131*, 397–407. [CrossRef] [PubMed]
40. Parker, T.; Barbarotta, L.; Foss, F. Pralatrexate: Treatment of T-cell non-Hodgkin's lymphoma. *Future Oncol.* **2012**, *9*, 21–29. [CrossRef] [PubMed]
41. DeGraw, J.I.; Colwell, W.T.; Piper, J.R.; Sirotnak, F.M. Synthesis and Antitumor Activity of 10-Propargyl-10-deazaaminopterin. *J. Med. Chem.* **1993**, *36*, 2228–2231. [CrossRef]
42. Guimin, Z.; Chengfu, C.; Chuanbing, W. A Kind of Preparation Method of Pralatrexate. U.S. Patent CN108069970, 02 June 2020.
43. Giust, W.; Burton, R.; Gorin, B.; Clayton, J. Process for Preparation of an Antifolate Agent. U.S. Patent WO2013/177713A1, 5 December 2013.
44. O'Connor, O.A.; Sirotnak, F.M. Treatment of T-Cell Lymphoma Using 10-Propargyl-10-Deazaaminopterin. U.S. Patent US2005/267117A1, 1 December 2005.
45. Lahiri, S.; Gupta, N.; Singh, H.K.; Panda, N.; Handa, V.; Abul, A.; Gupta, C.K.; Sanghani, S.; Sonavane, G.M. Process for the Preparation of Pralatrexate. U.S. Patent US9440979B2, 13 September 2016.
46. Lahiri, S.; Gupta, N.; Singh, H.K. Salts of Pralatrexate. U.S. Patent WO2014/20553A1, 6 February 2014.
47. Lahiri, S.; Gupta, N.; Singh, H.K.; Panda, N.; Handa, V.; Abul, A.; Gupta, C.K.; Sanghani, S.; Sonavane, G.M. Improved Process for the Preparation of Pralatrexate. U.S. Patent WO2014016740A2, 30 January 2014.
48. Tiseni, P.S.; Galluzzo, C.; Canavesi, A.; Biljan, T. Processes and Intermediates for Preparing Pralatrexate. U.S. Patent EP2794610B1, 27 June 2013.
49. Pronk, G.J. Optically Pure Diastereomers of 10-Propargyl-10-Deazaaminopterin and Methods of Using Same. U.S. Patent US8835433B2, 4 August 2011.
50. Alla, R.R.V.; Ramarao, C.; Michel, P.T.; Nitlikar, L.H.; Kalam, B.R.; Duduka, R. A Process for Preparing Intermediates of 10-propargyl-10-deazaaminopterin (pralatrexate) Synthesis and the Intermediates Thereof. U.S. Patent WO2013164856A1, 7 November 2013.

51. Cohen, M.H.; Justice, R.; Pazdur, R. Approval Summary: Pemetrexed in the Initial Treatment of Advanced/Metastatic Non-Small Cell Lung Cancer. *Oncologist* **2009**, *14*, 930–935. [CrossRef] [PubMed]
52. Rossi, A.; Ricciardi, S.; Maione, P.; de Marinis, F.; Gridelli, C. Pemetrexed in the treatment of advanced non-squamous lung cancer. *Lung Cancer* **2009**, *66*, 141–149. [CrossRef]
53. Gandhi, L.; Rodríguez-Abreu, D.; Gadgeel, S.; Esteban, E.; Felip, E.; De Angelis, F.; Domine, M.; Clingan, P.; Hochmair, M.J.; Powell, S.F.; et al. Pembrolizumab plus Chemotherapy in Metastatic Non-Small-Cell Lung Cancer. *N. Engl. J. Med.* **2018**, *378*, 2078–2092. [CrossRef] [PubMed]
54. Azzoli, C.G.; Kris, M.G.; Pfister, D.G. Cisplatin versus carboplatin for patients with metastatic non-small-cell lung cancer—an old rivalry renewed. *J. Natl. Cancer Inst.* **2007**, *99*, 828–829. [CrossRef]
55. Manegold, C. Pemetrexed (alimta, MTA, multitargeted antifolate, LY231514) for malignant pleural mesothelioma. *Semin. Oncol.* **2003**, *30*, 32–36. [CrossRef] [PubMed]
56. McLeod, H.L.; Cassidy, J.; Powrie, R.H.; Priest, D.G.; Zorbas, M.A.; Synold, T.W.; Shibata, S.; Spicer, D.; Bissett, D.; Pithavala, Y.K.; et al. Pharmacokinetic and Pharmacodynamic Evaluation of the Glycinamide Ribonucleotide Formyltransferase Inhibitor AG20341. *Clin. Cancer Res.* **2000**, *6*, 2677–2684. [PubMed]
57. Miwa, T.; Hitaka, T.; Akimoto, H. A Novel Synthetic Approach to Pyrrolo [2,3-d]pyrimidine Antifolates. *J. Org. Chem.* **1993**, *58*, 1696–1701. [CrossRef]
58. Mitchell-Ryan, S.; Wang, Y.; Raghavan, S.; Ravindra, M.P.; Hales, E.; Orr, S.; Cherian, C.; Hou, Z.; Matherly, L.H.; Gangjee, A. Discovery of 5-substituted pyrrolo[2,3-d]pyrimidine antifolates as dual-acting inhibitors of glycinamide ribonucleotide formyltransferase and 5-aminoimidazole-4-carboxamide ribonucleotide formyltransferase in de novo purine nucleotide biosynthesis. *J. Med. Chem.* **2013**, *56*, 10016–10032. [CrossRef]
59. Bonaccorsi, F.; Calvani, F.; Pasqui, F. Process for the Preparation of Pemetrexed and Lysin Salt Thereof. U.S. Patent EP2882753B1, 13 February 2014.
60. Michalak, O.; Gruza, M.M.; Witkowska, A.; Bujak, I.; Cmoch, P. Synthesis and physicochemical characterization of the impurities of pemetrexed disodium, an anticancer drug. *Molecules* **2015**, *20*, 10004–10031. [CrossRef]
61. Taylor, E.C.; Liu, B. A simple and concise synthesis of LY231514 (MTA). *Tetrahedron Lett.* **1999**, *40*, 4023–4026. [CrossRef]
62. Taylor, E.C.; Liu, B. A New and Efficient Synthesis of Pyrrolo[2,3-d]pyrimidine Anticancer Agents: Alimta (LY231514, MTA), Homo-Alimta, TNP-351, and Some Aryl 5-Substituted Pyrrolo[2,3-d]pyrimidines. *J. Org. Chem.* **2003**, *68*, 9938–9947. [CrossRef]
63. Taylor, E.C.; Liu, B. Process for the Preparation of pyrrolo[2,3-d]pyrimidines. U.S. Patent US6066732 A, 23 May 2000.
64. Taylor, E.C.; Kuhnt, D.; Shih, C.; Rinzel, S.M.; Grindey, G.B.; Barredo, J.; Jannatipour, M.; Moran, R.G. A Dideazatetrahydrofolate Analogue Lacking a Chiral Center at C-6, N-[4-[2-(2-Amino-3,4-dihydro-4-oxo-7H-pyrrolo[2,3-d]pyrimidin-5yl)ethyl]benzoyl]-l-glutamic Acid is an Inhibitor of Thymidylate Synthase. *J. Med. Chem.* **1992**, *35*, 4450–4454. [CrossRef]
65. Taylor, E.C.; Liu, B. A novel synthetic route to 7-substituted derivatives of the antitumor agent LY231514 (MTA). *Tetrahedron Lett.* **1999**, *40*, 5291–5294. [CrossRef]
66. Kennedy, S.H.; Dherange, B.D.; Berger, K.J.; Levin, M.D. Skeletal editing through direct nitrogen deletion of secondary amines. *Nature* **2021**, *593*, 223–227. [CrossRef]
67. Itoh, F.; Russello, O.; Akimoto, H.; Beardsley, G.P. Novel pyrrolo[2,3-d]pyrimidine antifolate TNP-351: Cytotoxic effect on methotrexate-resistant CCRF-CEM cells and inhibition of transformylases of de novo purine biosynthesis. *Cancer Chemother. Pharmacol.* **1994**, *34*, 273–279. [CrossRef] [PubMed]
68. Miwa, T.; Hitaka, T.; Akimoto, H.; Nomura, H.J. Novel pyrrolo [2, 3-d] pyrimidine antifolates: Synthesis and antitumor activities. *Med. Chem.* **1991**, *34*, 555–560.
69. Adams, J.; Elliott, P.J. New agents in cancer clinical trials. *Oncogene* **2000**, *19*, 6687–6692. [CrossRef] [PubMed]
70. Newell, D.R. Clinical pharmacokinetics of antitumor antifolates. *Semin. Oncol.* **1999**, *26*, 74–81.
71. Bronder, J.L.; Moran, R.G. Antifolates targeting purine synthesis allow entry of tumor cells into S phase regardless of p53 function. *Cancer Res.* **2002**, *62*, 5236–5241. [PubMed]
72. Taylor, E.C.; Harrington, P.J.; Fletcher, S.R.; Beardsley, G.P.; Moran, R.G. Synthesis of the Antileukemic Agents 5, 10-Dideazaaminopterin and 5, 10-Dideaza-5, 6, 7, 8-tetrahydroaminopterin. *J. Med. Chem.* **1985**, *28*, 914–921. [CrossRef] [PubMed]
73. Taylor, E.C.; Harrington, P.M.; Warner, J.C. Diels-Alder reactions of 6-azapterins. An alternative strategy for the synthesis of 5,10-dideaza-5,6,7,8-tetrahydrofolic acid (DDATHF). *Heterocycles* **1988**, *27*, 1925–1928. [CrossRef]
74. Taylor, E.C.; Wong, G.S.K. Convergent and Efficient Palladium-Effected Synthesis of 5,10-Dideaza-5,6,7,8-tetrahydrofolic Acid (DDATHF). *J. Org. Chem.* **1989**, *54*, 3618–3624. [CrossRef]
75. Boschelli, D.H.; Webber, S.; Whiteley, J.M.; Oronsky, A.L.; Kerwar, S.S. Synthesis and biological properties of 5,10-dideaza-5,6,7,8-tetrahydrofolic acid. *Arch. Biochem. Biophys.* **1988**, *265*, 43–49. [CrossRef]
76. Piper, J.R.; McCaleb, G.S.; Montgomery, J.A.; Kisliuk, R.L.; Gaumont, Y.; Thorndike, J.; Sirotnak, F.M. Synthesis and Antifolate Activity of 5-Methyl-5,10-dideaza Analogues of Aminopterin and Folic Acid and an Alternative Synthesis of 5,10-Dideazatetrahydrofolic Acid, a Potent Inhibitor of Glycinamide Ribonucleotide Formyltransferase. *J. Med. Chem.* **1988**, *31*, 2164–2169. [CrossRef] [PubMed]
77. Taylor, E.C.; Chaudhari, R.; Lee, K. A simplified and efficient synthesis of 5,10-dideaza-5,6,7,8-tetrahydrofolic acid (DDATHF). *Investig. New Drugs* **1996**, *14*, 281–285. [CrossRef] [PubMed]

78. Tomsho, J.W.; McGuire, J.J.; Coward, J.K. Synthesis of (6R)- and (6S)-5,10-dideazatetrahydrofolate oligo- γ -glutamates: Kinetics of multiple glutamate ligations catalyzed by polyglutamate synthetase. *Org. Biomol. Chem.* **2005**, *3*, 3388–3398. [CrossRef]
79. Barnett, C.J.; Wilson, T.M. Asymmetric synthesis and absolute configuration of 5,10-dideaza-5,6,7,8-tetrahydroptericoic acid and 5,10-dideaza-5,6,7,8-tetrahydrofolic acid (DDATHF). *Tetrahedron Lett.* **1989**, *30*, 6291–6294. [CrossRef]
80. Barnett, C.J.; Wilson, T.M.; Wendel, S.R.; Winningham, M.J.; Deeter, J.B. Asymmetric Synthesis of Lometrexol ((6R)-5,10-Dideaza-5,6,7,8-tetrahydrofolic Acid). *J. Org. Chem.* **1994**, *59*, 7038–7045. [CrossRef]
81. Sirichaiwat, C.; Intaraudom, C.; Kamchonwongpaisan, S.; Vanichtanankul, J.; Thebtaranonth, Y.; Yuthavong, Y. Target Guided Synthesis of 5-Benzyl-2,4-diamonopyrimidines: Their Antimalarial Activities and Binding Affinities to Wild Type and Mutant Dihydrofolate Reductases from Plasmodium falciparum. *J. Med. Chem.* **2004**, *47*, 345–354. [CrossRef] [PubMed]
82. Kimmitt, P.T.; Harwood, C.R.; Barer, M.R. Toxin gene expression by Shiga toxin-producing Escherichia coli: The role of antibiotics and the bacterial SOS response. *Emerg. Infect. Dis.* **2000**, *6*, 458–465. [CrossRef] [PubMed]
83. Heaslet, H.; Harris, M.; Fahnoe, K.; Sarver, R.; Putz, H.; Chang, J.; Subramanyam, C.; Barreiro, G.; Miller, J.R. Structural comparison of chromosomal and exogenous dihydrofolate reductase from Staphylococcus aureus in complex with the potent inhibitor trimethoprim. *Proteins Struct. Funct. Bioinforma.* **2009**, *76*, 706–717. [CrossRef]
84. Brogden, R.N.; Carmine, A.A.; Heel, R.C.; Speight, T.M.; Avery, G.S. Trimethoprim: A Review of its Antibacterial Activity, Pharmacokinetics and Therapeutic Use in Urinary Tract Infections. *Drugs* **1982**, *23*, 405–430. [CrossRef]
85. Topless, R.K.; Green, R.; Morgan, S.L.; Robinson, P.C.; Merriman, T.R.; Gaffo, A.L. Folic acid and methotrexate use and their association with COVID-19 diagnosis and mortality: An analysis from the UK Biobank. *medRxiv* **2022**. [CrossRef]
86. Sheybani, Z.; Dokoohaki, M.H.; Negahdaripour, M.; Dehdashti, M.; Zolghadr, H.; Moghadami, M.; Masoompour, S.M.; Zolghadr, A.R. The Role of Folic Acid in the Management of Respiratory Disease Caused by COVID-19. *ChemRxiv Camb. Camb. Open Engag.* **2020**. [CrossRef]
87. Meisel, E.; Efros, O.; Bleier, J.; Halevi, T.B.; Segal, G.; Rahav, G.; Leibowitz, A.; Grossman, E. Folate Levels in Patients Hospitalized with Coronavirus Disease 2019. *Nutrients* **2021**, *13*, 812. [CrossRef] [PubMed]
88. Stegmann, K.M.; Dickmanns, A.; Gerber, S.; Nikolova, V.; Klemke, L.; Manzini, V.; Schlösser, D.; Bierwirth, C.; Freund, J.; Sitte, M.; et al. The folate antagonist methotrexate diminishes replication of the coronavirus SARS-CoV-2 and enhances the antiviral efficacy of remdesivir in cell culture models. *Virus Res.* **2021**, *302*, 198469. [CrossRef] [PubMed]
89. Zhang, Y.; Guo, R.; Kim, S.H.; Shah, H.; Zhang, S.; Liang, J.H.; Fang, Y.; Gentili, M.; O' Leary, C.N.; Elledge, S.J.; et al. SARS-CoV-2 hijacks folate and one-carbon metabolism for viral replication. *Nat. Commun.* **2021**, *12*, 1676. [CrossRef]
90. Mujwar, S.; Tripathi, A. Repurposing benzbromarone as antifolate to develop novel antifungal therapy for Candida albicans. *J. Mol. Model.* **2022**, *28*, 193. [CrossRef] [PubMed]

Review

Heterocyclic Compounds as Dipeptidyl Peptidase-IV Inhibitors with Special Emphasis on Oxadiazoles as Potent Anti-Diabetic Agents

Badrud Duza Mohammad ¹, Mirza Shahed Baig ², Neeraj Bhandari ³, Falak A. Siddiqui ⁴, Sharuk L. Khan ^{4,*}, Zubair Ahmad ^{5,6}, Farhat S. Khan ⁶, Priti Tagde ⁷ and Philippe Jeandet ^{8,*}

¹ Department of Pharmaceutical Chemistry, G R T Institute of Pharmaceutical Education and Research, GRT Mahalakshmi Nagar, Tiruttani 631209, Tamil Nadu, India

² Department of Pharmaceutical Chemistry, Y. B. Chavan College of Pharmacy, Aurangabad 431001, Maharashtra, India

³ Arni School of Pharmacy, Arni University, Kathgarh, Indora 176401, Himachal Pradesh, India

⁴ Department of Pharmaceutical Chemistry, N.B.S. Institute of Pharmacy, AUSA 413520, Maharashtra, India

⁵ Unit of Bee Research and Honey Production, Faculty of Science, King Khalid University, P.O. Box 9004, Abha 61413, Saudi Arabia

⁶ Biology Department, College of Arts and Sciences, Dehnan Al-Junub, King Khalid University, P.O. Box 9004, Abha 61413, Saudi Arabia

⁷ Patel College of Pharmacy, Madhyanchal Professional University, Bhopal 462044, Madhya Pradesh, India

⁸ Research Unit Induced Resistance and Plant Bioprotection, University of Reims, USC INRAE 1488, SFR Condorcet FR CNRS 3417, 51687 Reims, France

* Correspondence: sharique.4u4@gmail.com (S.L.K.); philippe.jeandet@univ-reims.fr (P.J.)

Citation: Mohammad, B.D.; Baig, M.S.; Bhandari, N.; Siddiqui, F.A.; Khan, S.L.; Ahmad, Z.; Khan, F.S.; Tagde, P.; Jeandet, P. Heterocyclic Compounds as Dipeptidyl Peptidase-IV Inhibitors with Special Emphasis on Oxadiazoles as Potent Anti-Diabetic Agents. *Molecules* **2022**, *27*, 6001. <https://doi.org/10.3390/molecules27186001>

Academic Editors: Alexey M. Starosotnikov, Maxim A. Bastrakov and Igor L. Dalinger

Received: 8 August 2022

Accepted: 12 September 2022

Published: 15 September 2022

Publisher's Note: MDPI stays neutral with regard to jurisdictional claims in published maps and institutional affiliations.



Copyright: © 2022 by the authors. Licensee MDPI, Basel, Switzerland. This article is an open access article distributed under the terms and conditions of the Creative Commons Attribution (CC BY) license (<https://creativecommons.org/licenses/by/4.0/>).

Abstract: Dipeptidyl peptidase-IV (DPP-IV) inhibitors, often known as gliptins, have been used to treat type 2 diabetes mellitus (T2DM). They may be combined with other medications as an additional treatment or used alone as a monotherapy. In addition to insulin, sulfonylureas, thiazolidinediones, and metformin, these molecules appear as possible therapeutic options. Oxadiazole rings have been employed in numerous different ways during drug development efforts. It has been shown that including them in the pharmacophore increases the amount of ligand that may be bound. The exceptional hydrogen bond acceptor properties of oxadiazoles and the distinct hydrocarbon bonding potential of their regioisomers have been established. Beside their anti-diabetic effects, oxadiazoles display a wide range of pharmacological properties. In this study, we made the assumption that molecules containing oxadiazole rings may afford a different approach to the treatment of diabetes, not only for controlling glycemic levels but also for preventing atherosclerosis progression and other complications associated with diabetes. It was observed that oxadiazole fusion with benzothiazole, 5-(2,5,2-trifluoroethoxy) phenyl, β -homophenylalanine, 2-methyl-2-(5-(4-chlorophenyl), diamine-bridged bis-coumarinyl, 5-aryl-2-(6'-nitrobenzofuran-2'-yl), nitrobenzofuran, and/or oxindole leads to potential anti-diabetic activity.

Keywords: oxadiazole; sulfonylureas; DPP-IV inhibitors; diabetes mellitus; peptidomimetics

1. Introduction

Dipeptidyl peptidase-IV (DPP-IV) inhibitors, often known as gliptins, are a class of oral anti-diabetic medications that have been given approval by the Food and Drug Administration (FDA) to treat individuals with type 2 diabetes mellitus (T2DM) [1]. Following oral ingestion of food, the production of incretin hormones, which are hormones that are vital for maintaining glucose homeostasis, occurs in the gut. These hormones are the targets through which these drugs act [2]. Independent of the incretin pathway, in addition to their antihyperglycemic activities, this family of drugs also displays antihypertensive properties [3], anti-inflammatory effects [4], and antiapoptotic effects [5], as well as immunomodulatory effects [6,7] on the heart, kidneys, and blood vessels. A number of studies

have demonstrated that this class of molecules may also be useful for treating transplant patients who have acquired new-onset diabetes after their transplantation (NODAT). These molecules may be combined with other medications as an additional treatment or used alone as a monotherapy. Sulfonylureas, thiazolidinediones, and metformin are also possible therapeutic options in addition to insulin [8,9]. Iminosugars represent a kind of polyhydroxylated secondary or tertiary amines that mimic monosaccharide sugars, but which contain nitrogen in lieu of oxygen in the ring. Iminosugars constitute a wide variety of different types of small organic molecules. These molecules belong to the class of pyrrolidines, piperidines, azepanes, nortropanes, pyrrolizidines, and indolizidines. The capacity of iminosugars to function as inhibitors of glycosidases and glycosyltransferases constituted the first role they were utilized in. These inhibitors work mostly through competitive inhibition and are mainly used to treat diabetes [10–14].

The glucagon-like peptide-1 (GLP-1) has recently emerged as a possible target for T2DM treatment. GLP-1 is produced by the gut after a meal, enhancing insulin output. It has been demonstrated that increased levels of GLP-1 may contribute to a better glycemic control in T2DM individuals. DPP-IV controls the activity of GLP-1 by cleaving the *N*-terminus of GLP-1 [7–36]-amide to generate inert GLP-1 [9–36]-amide. The quantity of GLP-1 in the circulation may be increased by inhibiting DPP-IV [15]. As a result, a significant amount of time and effort has been dedicated to the research of DPP-IV inhibitors as potential treatments of T2DM. Sitagliptin [16] is one of these drugs, and it has been available in the United States since 2006 as the first FDA-approved DPP-IV inhibitor. Saxagliptin [17,18], vildagliptin [19], alogliptin [20], and linagliptin [21] (Figure 1) are all medications that have either been studied in diabetic patients or approved for sale in some countries. Based on structural similarities or differences with the DPP-IV molecule, DPP-IV inhibitors may be classified as either peptidomimetics (vildagliptin and saxagliptin) or non-peptidomimetics (sitagliptin, alogliptin, linagliptin). They are reversible competitive inhibitors of the DPP-IV substrates. These compounds have various degrees of affinity with DPP-IV substrates. The selectivity of the peptidomimetics toward DPP-IV is often lower as compared to DPP8/9. The greater the relative inhibition of DPP8/9 and the lower the relative selectivity toward DPP-IV, the greater the risk of adverse consequences (allergic skin manifestations, etc.) [22,23]. When compared to non-peptidomimetics, peptidomimetics display a distinct DPP-IV inhibition mechanism. Because non-peptidomimetics generate non-covalent extra-cellular interactions with residues in the catalytic region of the DPP-IV substrate, their inhibiting activity is powerful and rapid. In contrast, inhibition of the DPP-IV substrate by peptidomimetics takes place in a mode that includes the development of a reversible covalent enzyme-inhibitor complex. This complex may be broken down again. This complex binds to and dissociates from the catalytic site of the DPP-IV substrate in a very slow manner, resulting in the persistent inhibition of the DPP-IV enzyme a long time after the medication has been rendered ineffective. Because of this, the catalytic activity is hindered long after the free drug has been eliminated from circulation. In fact, vildagliptin and saxagliptin may be able to suppress DPP-IV activity for a longer period while having relatively short half-lives [24,25].

The usage of gliptin has been proven to be equally effective as compared to metformin, sulfonylureas (glimepiride, glipizide), thiazolidinediones (rosiglitazone, pioglitazone), and alfa-glucosidase inhibitors (voglibose). Compared to sulfonylureas, this therapy almost never causes hypoglycemia or affects body weight [26–28]. According to the findings of a meta-analysis that compared the effectiveness of sitagliptin and vildagliptin, the reported total HbA1c decrease was ~0.74% and 0.73%, respectively. If the starting HbA1c was superior to 9% instead of 8%, the glycemic results were shown to be more favorable [22]. According to a recent meta-analysis, the use of a gliptin was associated with a larger percentage of patients reaching the HbA1c target of <7% without any weight gain or hypoglycemia [29]. We have thus reviewed here the possible utilization of heterocyclic compounds as DPP-IV inhibitors, with special emphasis on oxadiazoles as potent anti-diabetic agents.

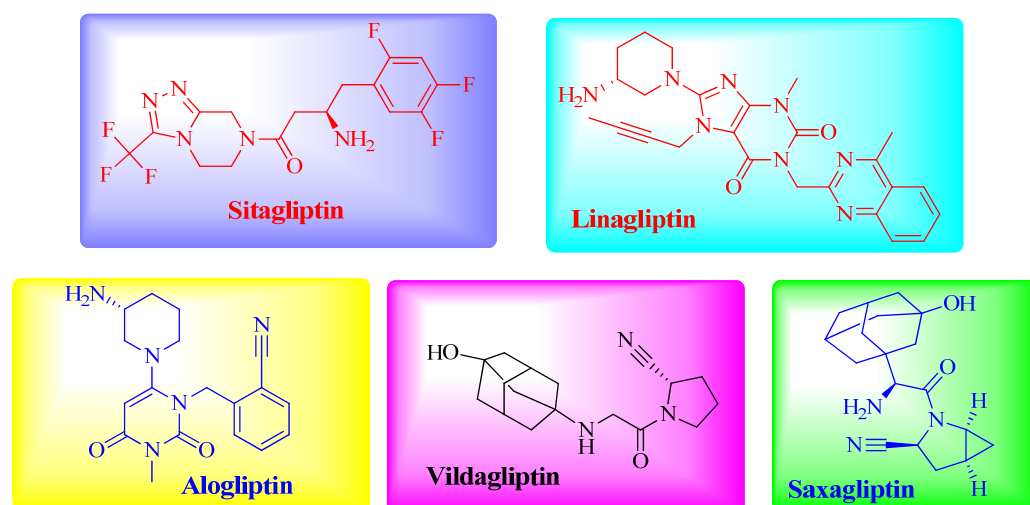


Figure 1. Structures of clinically-approved DPP-IV inhibitors.

2. Review of Different Heterocyclic Compounds as Potent DPP-IV Inhibitors

Yasufumi Miyamoto et al. [15] used structure-based drug design (SBDD) to modify compound 1 to generate a novel and strong DPP-IV inhibitor for the treatment of T2DM. Using the results of X-ray co-crystallography studies on compound 1 revealed that Arg125 might be a suitable target amino acid residue for obtaining a stronger inhibitory activity. According to the theory, the guanidino group of Arg125 may engage bidentately with two separate hydrogen bond acceptors at the same time. As a result, scientists have synthesized a number of 3-pyridylacetamide derivatives that each include an extra hydrogen bond acceptor and have the potential to take part in bidentate interactions with Arg125. Compound 2 was shown to bind in a bivalent manner with the guanidino group of Arg125, which is a powerful and selective DPP-IV inhibitor. The structures of compounds 1 and 2 are illustrated in Figure 2.

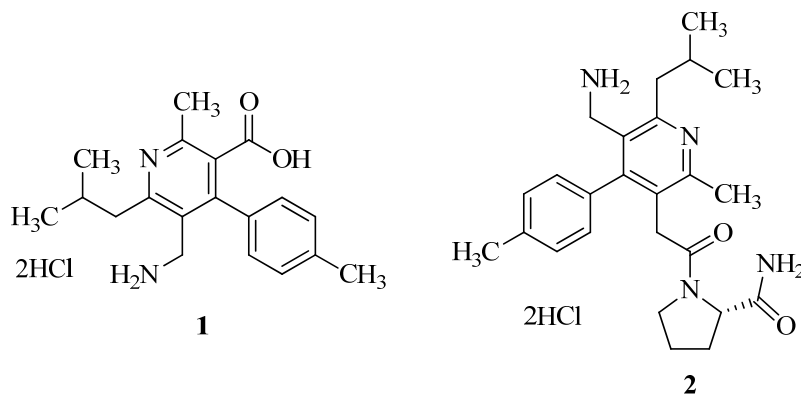


Figure 2. 3-Pyridylacetamide derivatives as DPP-IV inhibitors.

Utilizing the SAR of pyrrole-2-carbonitrile inhibitors, a variety of new hetero-aromatic moiety-substituted amino pyrrole-2-carbonitrile derivatives were synthesized. IC_{50} values ranged from 0.004 to 113.6 μ M for all drugs, indicating that they were effective DPP-IV inhibitors. Compounds 3 ($IC_{50} = 0.004 \mu$ M) and 4 ($IC_{50} = 0.01 \mu$ M) were found to have excellent inhibitory activities against DPP-IV and a good efficacy in an oral glucose tolerance test (OGTT) in mice. Moreover, compounds 3 and 4 exhibited intermediate pharmacokinetic characteristics (3, $F\% = 37.8\%$, $t_{1/2} = 1.45$ h; 4, $F\% = 16.8\%$, $t_{1/2} = 3.64$ h). The structures of compounds 3 and 4 are displayed in Figure 3 [30].

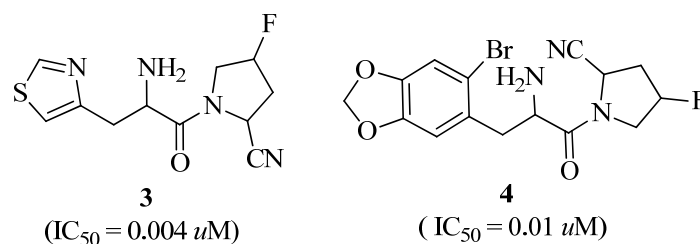


Figure 3. Pyrrole-2-carbonitrile has been shown to be effective as a DPP-IV inhibitor.

New beta-amino pyrrole-2-carbonitrile derivatives have been discovered and developed using the rational drug design approach. Compounds **5** and **6** (Figure 4) were reported to be powerful and specific DPP-IV inhibitors *in vivo*, leading to a reduction in glucose amounts in the blood. Compound **5** significantly inhibited DPP-IV ($IC_{50} = 0.05 \mu M$), and also displayed a high oral bioavailability ($F = 53.2\%$). Compound **6** demonstrated strong DPP-IV inhibitory action ($IC_{50} = 0.01 \mu M$), high selectivity against related peptidases, good effectiveness during the oral glucose tolerance test (OGTT) in ICR mice, and a moderate pharmacokinetic profile [31].

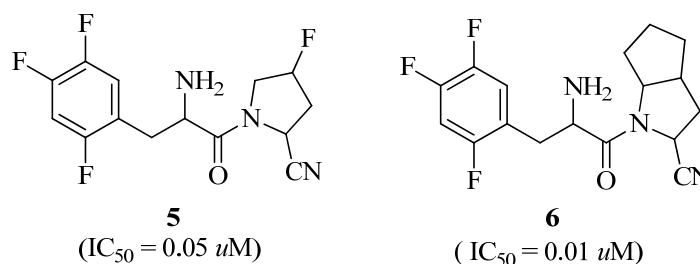


Figure 4. β -amino pyrrole-2-carbonitrile analogues.

A novel family of 1,2,3-Triazole-4-carboximidamide compounds was successfully developed for their DPP-IV inhibitory activity. When compared to the other drugs examined, compounds **7**, **8**, and **9** (Figure 5) displayed excellent inhibitory effects against DPP-IV, with IC_{50} values of 14.75, 6.75, and 6.57 nM, respectively. Compound **7**, at a dose of 10 mg/kg, enhanced glucose tolerance during OGTT in mice. Chronic treatment with compound **7** for 14 days in diabetic Wistar rats resulted in a significant drop in blood glucose levels, equivalent to the impact of Sitagliptin employed as a conventional treatment [32].

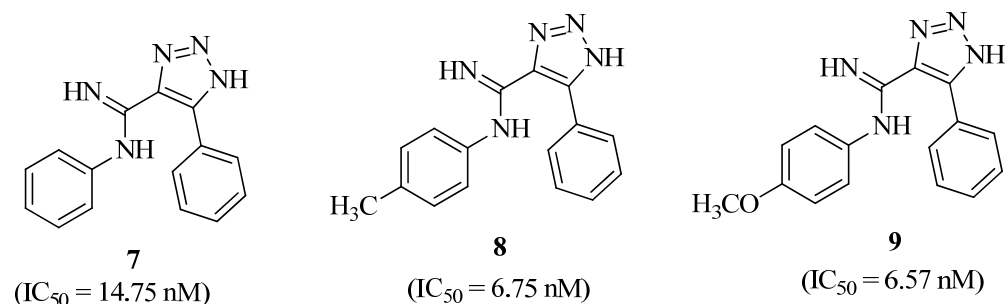


Figure 5. 1,2,3-Triazole-4-carboximidamide derivatives.

Six viable compounds were found using SBDD methods, and it was determined that compound **10** (Figure 6) had the highest docking score, i.e., $-10.463 \text{ K.cal/mol}$ with the DPP-IV enzyme (PDB ID-2ONC). Molecular dynamics (MD) simulations were also used to confirm the protein–ligand complex’s stability. Alogliptin and compound **10** were revealed to have a root-mean-square deviation (RMSD) smaller than 2.0 \AA [33].

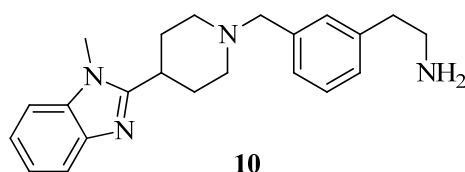


Figure 6. Benzimidazole derivative.

To interact with Try629 and Lys554 at the S2' position, novel uracil analogues with benzoic acid moieties at the N3 position were synthesized and tested for their DPP-IV inhibitory efficacy. From SAR studies, compound 11 was selected as the best candidate as a strong and selective DPP-IV inhibitor ($IC_{50} = 1.7$ nM). Based on docking data, it seems that additional salt bridging between the carboxylic acid group and the primary amine group of Lys554 plays a crucial role in increasing activity. According to the findings, compound 11 (Figure 7) showed no cytotoxicity in human hepatocyte L-O2 cells at doses up to 50 μ M. Later, in vivo testing revealed that the ester of compound 11 considerably enhanced normal mice's glucose tolerance. According to the study's results, compound 11 has the potential to be a safe and effective medication for T2DM [34].

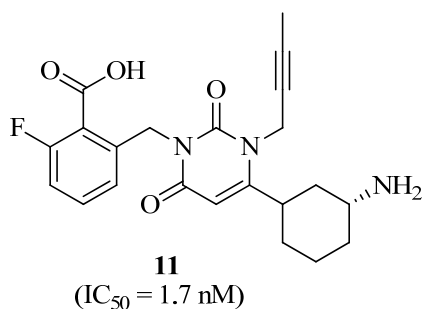


Figure 7. Uracil derivative containing benzoic acid as DPP-IV inhibitor.

Qing Li et al. [35] reported another DPP-IV inhibitor with minor modifications in compound 11 [12, methyl 3-((4-((R)-3-aminopiperidin-1-yl)-3-(but-2-ynyl)), Figure 8] displaying excellent results in vivo.

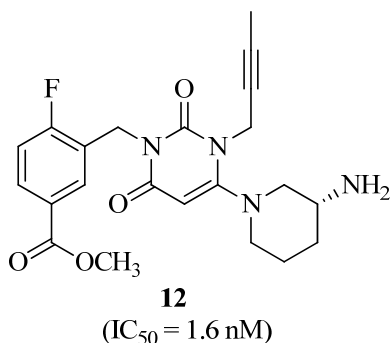


Figure 8. Aminopiperidin-dioxypyrimidin derivative as DPP-IV inhibitor.

From the above investigations, it was observed that oxygen and nitrogen heteroatoms play an important role in binding with receptors, resulting in significant conformational changes leading to potential biological activities. This led us to review the literature concerning the anti-diabetic activity of oxadiazoles.

3. Oxadiazoles as Potential Nuclei

Owing to their unique properties, oxadiazoles have attracted the attention of scientists in the disciplines of polymer and material science. These compounds feature five-membered rings comprised of two carbons, two nitrogens, and one oxygen atom

(Figure 9). The number of patent applications for oxadiazoles has climbed to a total of 646 over the last nine years. This suggests that the scientific community has attached great importance to this class of chemicals [36]. Zibotentan, a potential anticancer agent, and ataluren (Figure 10), a potential therapeutic for cystic fibrosis, are two examples of oxadiazole-containing compounds that are now participating in late-stage clinical studies [37]. The only compound available on the market that currently contains oxadiazole is an antiviral drug called raltegravir (Figure 10), which is used to treat HIV infection [38]. Oxadiazoles are now being included in an increasing number of therapeutic approaches in a wide range of disease areas, including but not limited to diabetes [39], obesity [40], inflammation [41], cancer [42], and infection [43].

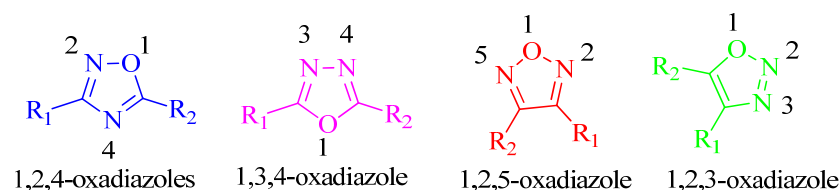


Figure 9. Several regioisomeric forms of oxadiazole rings.

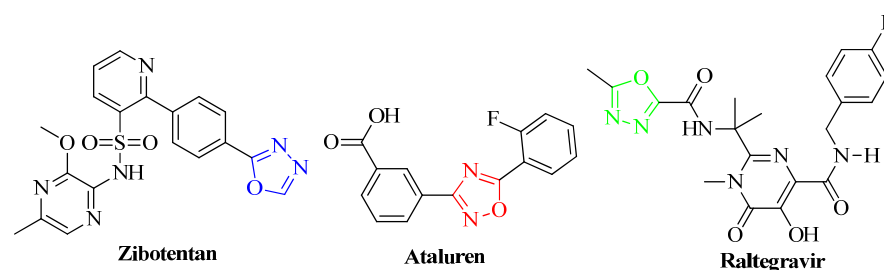


Figure 10. Oxadiazole structure-containing drugs.

A wide array of applications have been found for oxadiazole rings in drug development projects. It has been shown that including them in the pharmacophore improves ligand binding in various ways. The carbonyl groups of molecules such as esters, amides, carbamates, and hydrogenated hydroxamic esters may be replaced with oxadiazoles, constituting another use for these types of molecules [44–46].

Oxadiazole rings exist in form of numerous regioisomers, including 1,2,4-, 1,3,4-, and 1,2,5-isomers (Figure 9). Because the side chains R1 and R2 of the 1,2,5-regioisomer are orientated in a different way compared to that of the side chains in the other two isomers, this isomer is found less often. Oxadiazoles may display different regioisomeric configurations, but they always contain the same R1 and R2 side chains. As a consequence, the positions of these side chains are quite similar. It is envisaged that matching pairings would have identical overall molecular structures and, as a result, would form bonds in the same way. The exceptional hydrogen bond acceptor properties of oxadiazoles and the distinct hydrocarbon bonding potentials of their regioisomers have been established [47–49]. We will now investigate how oxadiazoles may help in treating diabetes.

3. An Overview of the Potential Use of Oxadiazole Derivatives as Anti-Diabetic Drugs

1,3,4-Oxadiazole and 1,2,4-oxadiazole have the potential to be used for many therapeutic applications [50–56].

Omarigliptin is a sulfonamide-containing moiety that inhibits the DPP-IV enzyme to achieve its antihyperglycemic activity [57]. Investigations into its pharmacokinetic properties have shown that it may be given on a once-weekly basis, which distinguishes it from all other DPP-IV inhibitors. The derivatives of 2-cyanopyrrolidine are classified as glycine-based inhibitors, which fall within the larger category of peptidomimetic inhibitors [58,59]. The presence of a nitrile group on the five-membered pyrrolidine ring in 2-cyanopyrrolidine derivatives is indicative of their capacity to exert reversible nanomolar

inhibition of the DPP-IV enzyme [60]. We reasoned that compounds based on oxadiazoles would be able to provide an alternative therapy for diabetes for not only controlling glucose levels but also preventing the progression of atherosclerosis and other complications associated with diabetes.

Kumar et al. [61] discovered that some 2-((benzothiazol-2-ylthio) methyl)-5-phenyl-1,3,4-oxadiazole derivatives have the potential to act as anti-diabetic compounds. Using glibenclamide as the reference, each of the synthetic compounds were evaluated for their capacity to combat diabetes in an animal model. At a dose of 350 mg/kg p.o., compound **13** (Figure 11) displayed the most noticeable effect of all molecules, even though all showed a significant activity (orally).

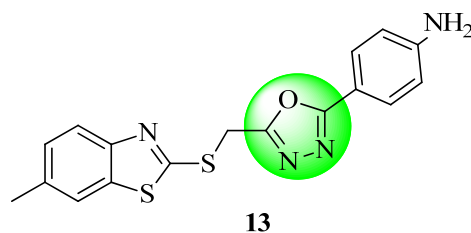


Figure 11. Benzothiazole tethered with 1,3,4-oxadiazole derivatives as an anti-diabetic oxadiazole derivative.

Benzothiazole-1,3,4-oxadiazole-4-thiazolidinone hybrid derivatives were synthesized by Bhutani et al. [62]. OGTT in non-diabetic rats and streptozotocin-induced diabetic rat models were used to evaluate seven compounds with the highest docking scores. The blood glucose levels were significantly reduced with all of the studied compounds, ranging from good to moderate. The anti-diabetic effects of the three compounds (**14**, **15** and **16**, Figure 12) were superior to those of the conventional medicine pioglitazone, showing a glucose concentration of 178.32 ± 1.88 mg/dL, compared to the lower concentrations of glucose of 157.15 ± 1.79 mg/dL, 154.39 ± 1.71 mg/dL, and 167.36 ± 2.45 mg/dL reported for **14–16**. Acarbose ($IC_{50} = 18.5 \pm 0.20$ μ M) was found to be the most potent inhibitor of alpha-glucosidase among the seven derivatives examined. However, three of its derivatives, compounds **14**, **17**, and **18** (Figure 12), displayed lower IC_{50} values (0.21 ± 0.01 μ M, 9.03 ± 0.12 μ M and 11.96 ± 0.40 μ M, respectively), suggesting that they were less effective than the ordinary acarbose. In other words, these innovative hybrids could be used as a basis for the development of novel agents [62].

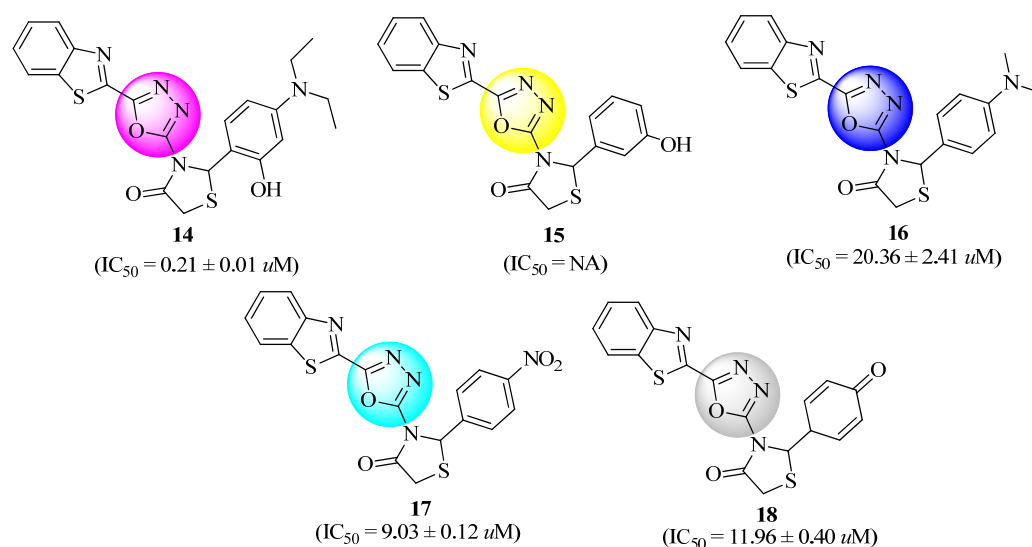


Figure 12. Synthetic analogues of benzothiazole-1,3,4-Oxadiazole-4-thiazolidinone.

New 5-(2,2,2-trifluoroethoxy)phenyl-1,3,4-oxadiazol-2-thiol derivatives have been synthesized and analyzed for their biological activities in vitro and in vivo. In comparison to acarbose ($IC_{50} = 34.71 \mu\text{g/mL}$), these compounds showed α -amylase inhibitory activities in the IC_{50} range of 40.00–80.00 $\mu\text{g/mL}$. Compounds **19** and **20** were the ones that exhibited the highest levels of activity in vitro compared to the other synthesized compounds. Animal experiments showed that compounds **19**, **20**, and **21** (Figure 13) were able to reduce glucose levels in *Drosophila*, but displayed a 17–30% lower capacity than acarbose. It was shown that compounds **19** and **20** exhibited the highest activity among the produced compounds. In this study, compounds **19**, **20**, and **21** were revealed to be good candidates for further research as possible anti-diabetes drugs [63].

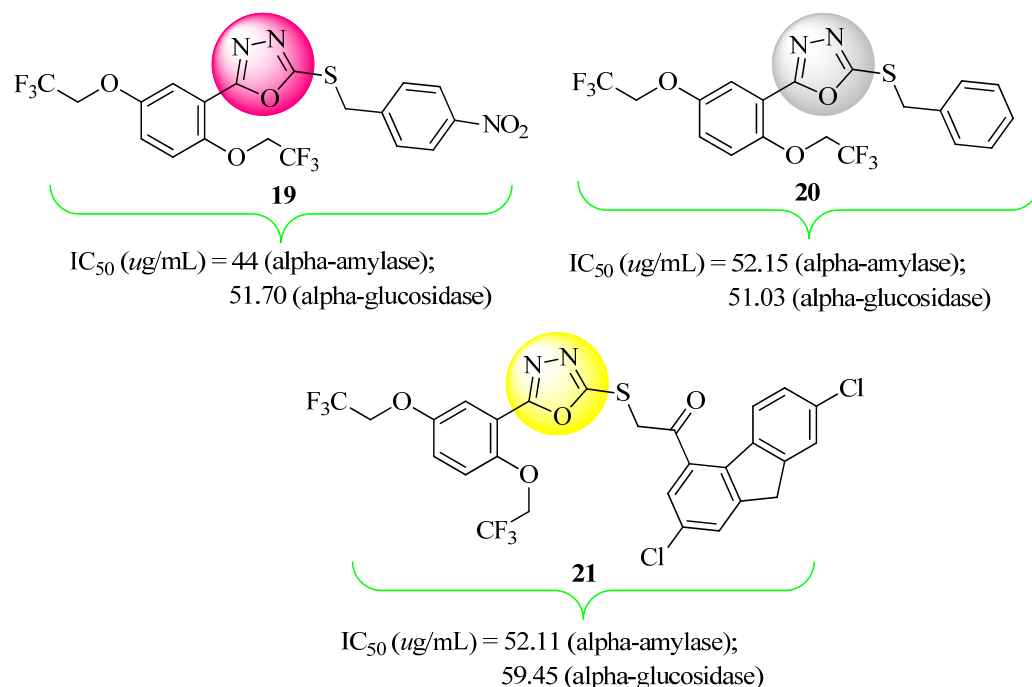


Figure 13. 1,3,4-Oxadiazole-2-thiol derivatives.

New benzothiazoles clubbed oxadiazole-Mannich bases (M-1 to M-22) synthesized by Bhutani et al. were evaluated using OGTT and STZ-induced diabetes in normal rats. Glucose levels were reduced with compound M-14 (**22**, Figure 14) ($161.39 \pm 4.38 \text{ mg/dL}$) in the STZ model, which was equivalent to treatment with glibenclamide ($140.29 \pm 1.24 \text{ mg/dL}$). The antihyperglycemic efficacy of the other substances tested ranged from fair to excellent [64].

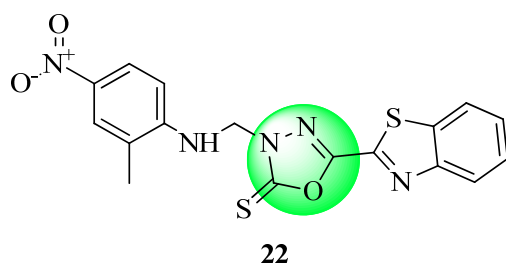


Figure 14. Benzothiazole clubbed oxadiazole-Mannich base.

Nordhoff et al. [65] demonstrated that amide substitutions enhanced the absorption, distribution, metabolism, and excretion (ADME) characteristics of a series of β -homophenylalanine-based inhibitors of DPP-IV. Thanks to the efforts of this group, a new class of powerful and selective DPP-IV inhibitors with an appealing pharmacokinetic profile and good performance was synthesized and evaluated in an animal model of diabetes.

Compounds **23** and **24** (Figure 15) from this new series of compounds were shown to display interesting pharmacokinetic properties and to work very well in animal models of diabetes.

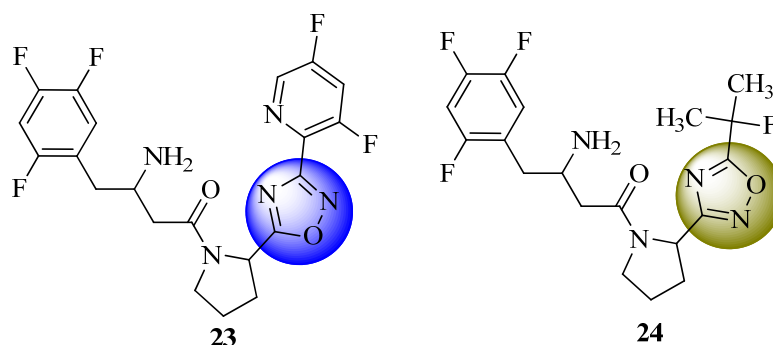


Figure 15. β -homophenylalanine-based inhibitors of DPP-IV.

A new class of powerful, selective, and orally accessible DPP-IV inhibitors has been discovered by Xu et al. [66] Without an electrophilic trap, they are among the most powerful chemicals known to date. Regarding DPP-IV homologs, compound **25** (Figure 16) was shown to have a higher selectivity. However, their short half-life, observed after oral treatment in rats and dogs, led to further research being stopped on these compounds.

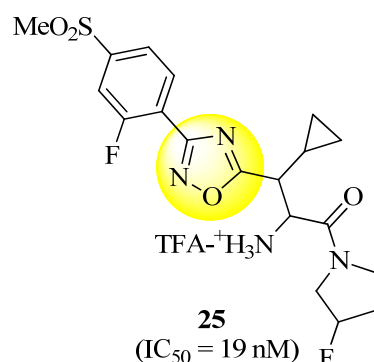


Figure 16. 1,2,4-Oxadiazole derivative as a potent DPP-IV inhibitor.

N-aryl/aralkyl derivatives of 2-methyl-2-[5-(4-chlorophenyl)-1,3,4-oxadiazole-2-ylthio] acetamides were synthesized and the α -glucosidase inhibitory potential of each drug was examined. Compounds **26–31** (Figure 17) displayed a strong α -glucosidase inhibitory activity (IC_{50} of 81.72 ± 1.18 , 52.73 ± 1.16 , 62.62 ± 1.15 , 56.34 ± 1.17 , 86.35 ± 1.17 , 52.63 ± 1.16 μ M, respectively). These results were validated by molecular modelling and ADME predictions. It was then possible to synthesize a library of compounds using ordinary basic materials possibly leading to the development of new medicines [67].

One-pot multicomponent design and synthesis of three series of diamine-bridged *bis*-coumarinyl oxadiazole conjugates were reported by Kazmi et al. [68]. The conjugates produced were tested for their ability to inhibit glucosidases. With an IC_{50} value of only 0.07 ± 0.001 μ M (acarbose: 38.2 ± 0.12 μ M), compound **32** (Figure 18), including the 4,4'-oxydianiline linker, was shown to be the primary and selective inhibitor of alpha-glucosidase enzymes. Its inhibitory activity was about 545 times higher compared to conventional drugs. Compound **32** was also shown to be a strong inhibitor of intestinal maltase-glucoamylase ($IC_{50} = 0.04 \pm 0.02$ μ M) compared to acarbose ($IC_{50} = 0.06 \pm 0.01$ μ M). With an IC_{50} value of 0.08 ± 0.002 μ M, this compound was reported to be the primary inhibitor of the β -glucosidase enzyme. The mechanism of the inhibition was investigated using Michaelis–Menten kinetic studies. All the generated molecules were docked against the glucosidase enzyme. According to the obtained results, numerous interactions were observed with catalytic residues in a coordinated manner, which might stabilize inhibitors in

the active site. In addition, β -glucosidase inhibitors were successfully identified via the use of molecules having strong binding interactions with amino acid residues.

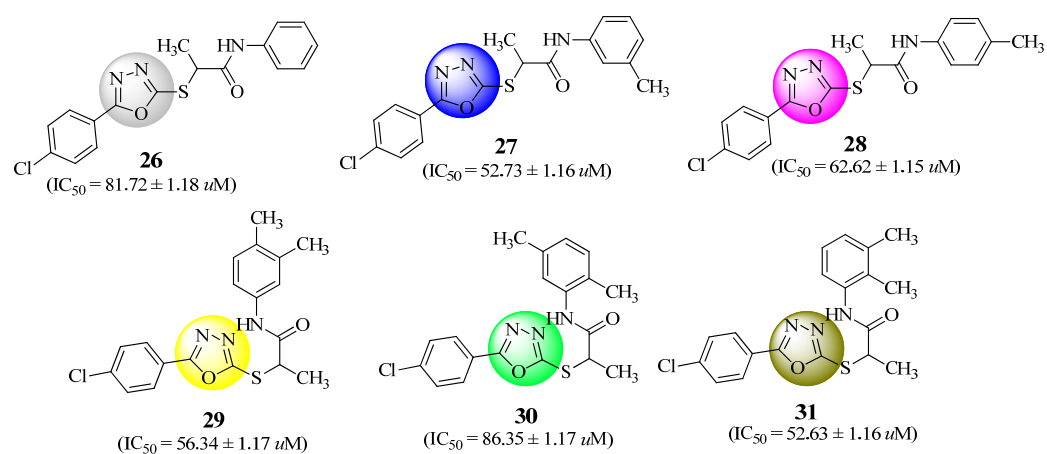


Figure 17. Oxadiazole derivatives with strong α -glucosidase inhibitory activity.

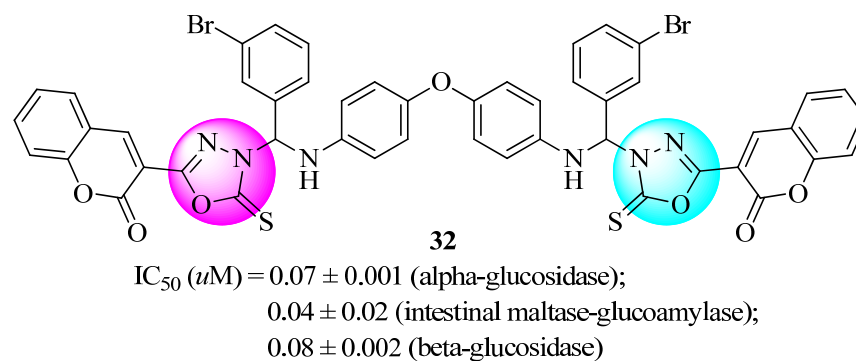


Figure 18. Anti-diabetic drugs derived from diamine-bridged coumarinyl oxadiazoles.

Taha et al. [69] designed and synthesized twenty 5-aryl-2-(6'-nitrobenzofuran-2'-yl)-1,3,4-oxadiazole derivatives and tested them for their ability to inhibit α -glucosidase. Compared to acarbose ($IC_{50} = 856.45 \pm 5.60 \mu M$), compounds with hydroxyl groups and halogens (compounds **33–38**, Figure 19) were shown to be five to seventy times more active, with IC_{50} values in the range of 12.75 ± 0.10 to $162.05 \pm 1.65 \mu M$. A hybrid family of oxadiazole and benzofuran compounds is now being studied for its ability to block α -glucosidase. Researchers may be prompted to use these results for the treatment of hyperglycemia. Within docking studies, hydrogen bonds and arene–arene interactions were shown to be the primary means of interactions with Glu 276, Asp 214, and Phe 177.

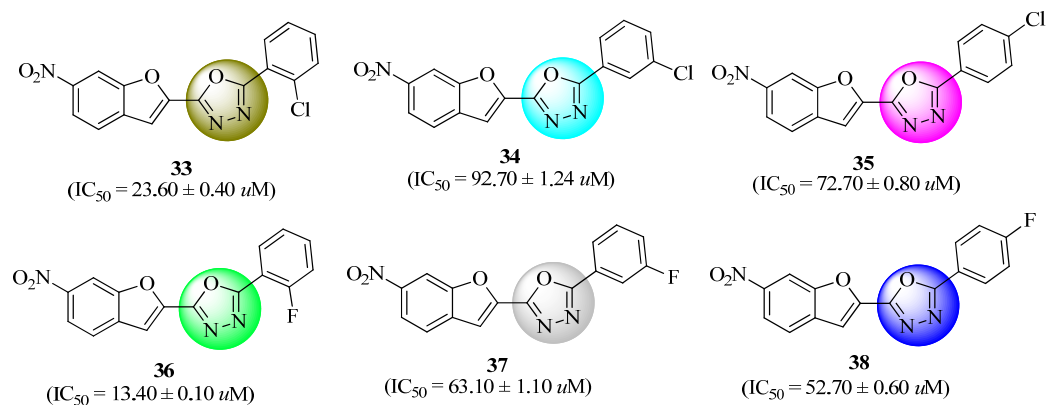


Figure 19. Nitrobenzofuran-1,3,4-Oxadiazoles derivatives.

Anti-diabetic drugs derived from 1,3,4-oxadiazoles have been discovered by Ullah et al. [70]. The ability of these newly synthesized compounds to inhibit α -glucosidase activity was investigated. As compared to acarbose ($38.45 \pm 0.80 \mu\text{M}$), all compounds showed strong inhibitory activities with IC_{50} values ranging from 0.80 ± 0.1 to $45.1 \pm 1.7 \mu\text{M}$. Thirteen compounds revealed potential inhibitory actions, though only one molecule ($\text{IC}_{50} = 45.1 \pm 1.7 \mu\text{M}$) was found to be less active. Among all the synthesized derivatives, one compound ($\text{IC}_{50} = 0.80 \pm 0.1 \mu\text{M}$) demonstrated the most promising inhibitory efficacy.

Taha et al. [71] discovered hybrid analogues of oxindole-based oxadiazoles (based on the structure of compound **39**, Figure 20) as potential α -glucosidase inhibitors. As compared to acarbose ($\text{IC}_{50} = 895.09 \pm 2.04 \mu\text{M}$), all compounds were shown to be powerful inhibitors of this enzyme, with IC_{50} values ranging from 1.25 ± 0.05 to $268.36 \pm 4.22 \mu\text{M}$. In this work, a new series of powerful α -glucosidase inhibitors have been discovered, suggesting further investigations.

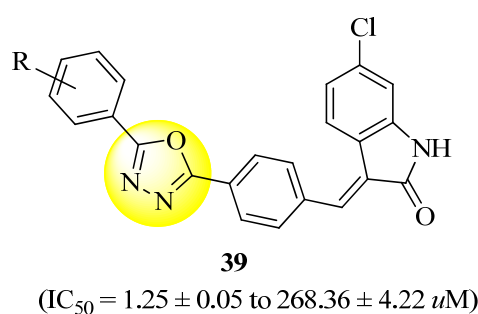
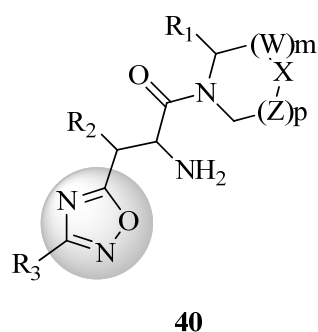


Figure 20. α -Glucosidase inhibitors based on oxadiazole hybrids.

New 1,2,4-oxadiazole derivatives, whose structures were reported in the US patent issued by Xu et al. [72] (compound **40**, Figure 21), are DPP-IV enzyme inhibitors and may be used to treat or prevent disorders involving this enzyme, such as diabetes, and more specifically type 2 diabetes. A pharmaceutical composition including these compounds and their application in the prevention or treatment of illnesses involving the DPP-IV enzyme are also contemplated by this invention.



Where,

m and p are each independently 0 or 1;

X is CH_2 , S , CHF , or CF_2 ;

W and Z are each independently CH_2 , CHF , or CF_2

Figure 21. DPP-IV inhibitors derived from 1,2,4-oxadiazole.

Hamdani et al. [73] synthesized three 1,3,4-oxadiazole derivatives (compounds **41**, **42**, and **43**, Figure 22) and used X-ray diffraction, density functional theory (DFT), and other methods to demonstrate their inhibitory potential of α -amylase. X-ray diffraction and other spectro-analytical methods were employed to validate the structures of the obtained compounds, which were prepared in excellent yields (70–83%). In addition to validating X-ray data, DFT calculations also examined charge dispersion and reactivity,

utilizing frontier molecular orbitals and molecular electrostatic potential (MEP) approaches. α -amylase inhibition experiments were used to determine the enzymatic inhibitory capacity of the produced compounds (**41**, **42**, and **43**). Compound **42** displayed a low IC_{50} value of $86.83 \pm 0.23 \mu\text{g/mL}$, which indicates its strong ability to inhibit α -amylase.

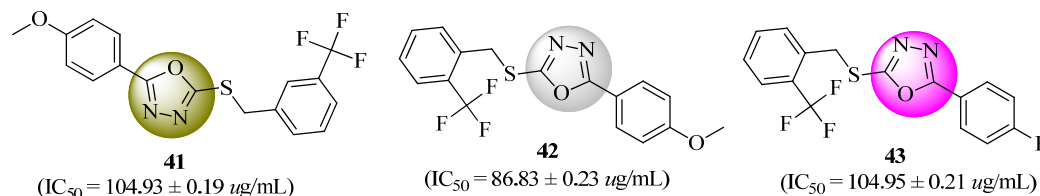


Figure 22. Inhibitors of alfa-amylase activity based on 1,3,4-oxadiazole derivatives.

The anti-diabetic properties of oxadiazole derivatives were studied *in silico* using the DFT approach, employing the B3LYP version with compounds set by Ibrahim et al. [74]. Four models were generated using the Genetic Function Algorithm (GFA). Based on the obtained results, researchers determined that Model 1 had the highest LOF (0.030552), R2 (0.09681), R2adj (0.09567), Q2CV (0.09364), and R2 (0.06969) values. Findings from molecular docking indicated that few ligands had the greatest docking scores of -9.9 kcal/mol among the co-ligands. The docking ratings produced here were shown to be in concordance with findings from previous studies. As a result of this work, anti-diabetic drugs with improved inhibitory action against α -glucosidase could potentially be developed.

In order to investigate the sequential conversion of indolyl butanoic acid into 1,3,4-oxadiazole-2-thiols, Nazir et al. [75] employed several chemical transformations. Several different amine derivatives were reacted with 2-bromoacetyl bromide to serve as an electrophile, leading to the production of 2-bromo-*N*-phenyl/arylacetyl bromides in a series of operations that ran in parallel with one another. A nucleophilic 1,3,4-oxadiazole-2-thiol analogue was then applied to the electrophilic compounds to produce a variety of *N*-substituted derivatives (compounds **44a** and **44b**, Figure 23). In this study, the anti-diabetic potential of all produced compounds was first examined through the inhibition of the α -glucosidase enzyme, and then by studying them *in silico*. In addition, their hemolytic activity was used to determine their cytotoxicity profile, and all of the compounds were shown to display minimal cytotoxicity. The most active compounds (**44a** and **44b**) had IC_{50} values of $9.46 \pm 0.03 \mu\text{M}$ and $9.37 \pm 0.03 \mu\text{M}$, respectively. As a result, they may serve in future studies to develop more efficient anti-diabetic drugs, as they showed excellent to moderate inhibitory potentials ($IC_{50} = 12.68 \pm 0.04$ to $37.82 \pm 0.07 \mu\text{M}$, respectively).

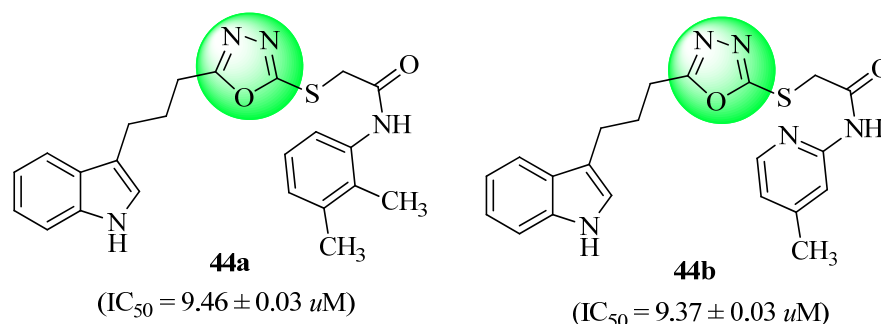


Figure 23. Derivatives of the 1,3,4-oxadiazole-2-thiol compound.

4. Structural Activity Relationship (SAR)

A brief structural activity relationship (SAR) is depicted in Figure 24. It was observed that almost all the potent derivatives were found to hold substitutions with different heterocyclic compounds or alkyl groups. Substitution with benzothiazoles and thiazolidinones leads to potent *in vivo* activity and displays significant overall anti-diabetic activities. The transformation of oxadiazole into the acetamido functional group has led to the devel-

opment of potential anti-diabetic agents, which were revealed as excellent DPP-IV inhibitors. However, many more substitutions, such as aminophenyl, β -homophenylalanine, coumarinyl, nitrobenzofuran, oxindole, trifluorophenyl-thiol, etc., could act as potential anti-diabetic agents, and especially as potential DPP-IV inhibitors.

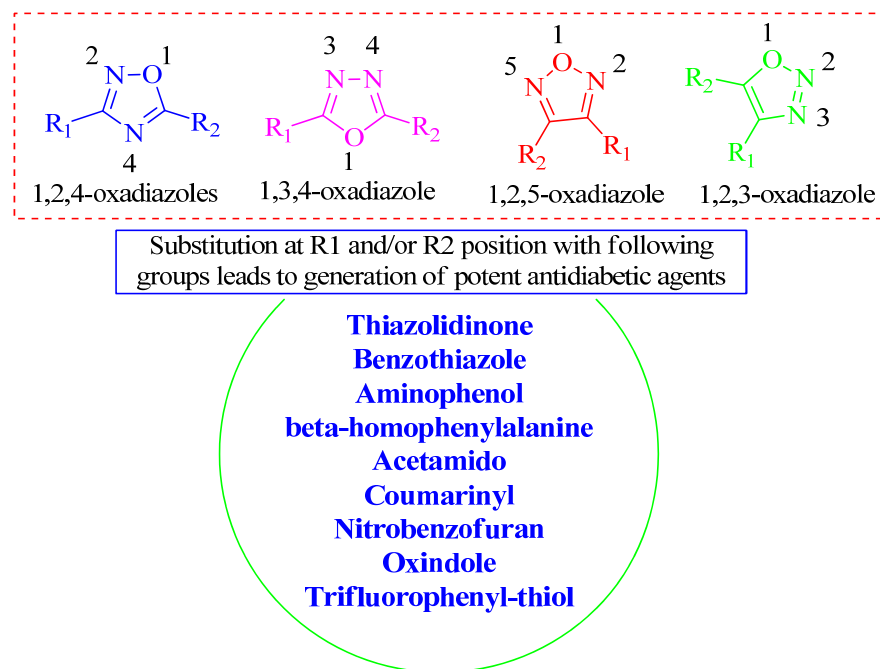


Figure 24. Predicted SAR of oxadiazoles.

5. Conclusion

1,3,4-Oxadiazole and 1,2,4-oxadiazole derivatives can be used in a variety of ways within the medical sector. Oxadiazoles possess diverse pharmacological activities, including anti-diabetic potential, and specifically acting as DPP-IV inhibitors. It has been reported that oxadiazoles fused with benzothiazoles, 5-(2,2,2-trifluoroethoxy)phenyl, β -homophenylalanine, 2-methyl-2-[5-(4-chlorophenyl)], diamine-bridged *bis*-coumarinyl, 5-aryl-2-(6'-nitrobenzofuran-2'-yl), nitrobenzofuran, and/or oxindoles demonstrate potential anti-diabetic activities. Furthermore, the most potent derivatives were obtained by substituting sulfur-containing heterocyclic compounds, as the sulfur atom has the potential to form interactions with the target enzymes. It was observed that almost all the potent derivatives were found to possess substitutions with different heterocyclic compounds or alkyl groups. Many of these derivatives induced strong conformational changes to the DPP-IV enzyme, resulting in excellent anti-diabetic activity. From this analysis, we came to the conclusion that oxadiazoles have properties that make them potent drugs. Further research is needed to consider them as valuable drugs to treat diabetes, especially as DPP-IV inhibitors. As discussed above, substitutions at the R1 and R2 positions leads to more potent and effective DPP-IV inhibitors. It may be possible to design some potent derivatives in future by appending different heterocyclic and alkyl groups at the R1 and R2 positions. It is a great challenge to maintain the binding mode of the derivatives following substitutions. After substitution, each derivative can be screened through molecular docking studies to determine its ability to cause conformational changes in the DPP-IV enzyme.

Author Contributions: Conceptualization, B.D.M. and S.L.K.; software, F.A.S., Z.A., F.S.K. and P.T.; validation, B.D.M., M.S.B. and S.L.K.; investigation, N.B. and F.A.S.; resources, B.D.M.; data curation, Z.A., F.S.K., M.S.B. and F.A.S.; writing—original draft preparation, B.D.M., M.S.B., N.B., F.A.S., S.L.K. and P.J.; writing—review and editing, B.D.M., M.S.B., N.B., F.A.S., S.L.K. and P.J.; visualization, S.L.K. and P.T.; supervision, S.L.K.; project administration, P.T., S.L.K. and P.J. All authors have read and agreed to the published version of the manuscript.

Funding: This research received no external funding.

Institutional Review Board Statement: Not applicable.

Informed Consent Statement: Not applicable.

Data Availability Statement: Not applicable.

Acknowledgments: The authors from King Khalid University extend their appreciation to the Deanship of Scientific Research at King Khalid University for funding this work through the Research Groups Program under Grant No. RGP.2/229/43.

Conflicts of Interest: The authors declare no conflict of interest.

References

- Jao, C.L.; Hung, C.C.; Tung, Y.S.; Lin, P.Y.; Chen, M.C.; Hsu, K.C. The Development of Bioactive Peptides from Dietary Proteins as a Dipeptidyl Peptidase IV Inhibitor for the Management of Type 2 Diabetes. *Biomedicine* **2015**, *5*, 9–15. [CrossRef]
- Green, B.D.; Flatt, P.R.; Bailey, C.J. Dipeptidyl Peptidase IV (DPP IV) Inhibitors: A Newly Emerging Drug Class for the Treatment of Type 2 Diabetes. *Diabetes Vasc. Dis. Res.* **2006**, *3*, 159–165. [CrossRef] [PubMed]
- Lovshin, J.A.; Zinman, B. Blood Pressure-Lowering Effects of Incretin-Based Diabetes Therapies. *Can. J. Diabetes* **2014**, *38*, 364–371. [CrossRef]
- Tomovic, K.; Lazarevic, J.; Kocic, G.; Deljanin-Ilic, M.; Anderluh, M.; Smelcerovic, A. Mechanisms and Pathways of Anti-Inflammatory Activity of DPP-4 Inhibitors in Cardiovascular and Renal Protection. *Med. Res. Rev.* **2019**, *39*, 404–422. [CrossRef] [PubMed]
- Nagamine, A.; Hasegawa, H.; Hashimoto, N.; Yamada-Inagawa, T.; Hirose, M.; Kobara, Y.; Tadokoro, H.; Kobayashi, Y.; Takano, H. The Effects of DPP-4 Inhibitor on Hypoxia-Induced Apoptosis in Human Umbilical Vein Endothelial Cells. *J. Pharmacol. Sci.* **2017**, *133*, 42–48. [CrossRef]
- Fadini, G.P.; Avogaro, A. Cardiovascular Effects of DPP-4 Inhibition: Beyond GLP-1. *Vascul. Pharmacol.* **2011**, *55*, 10–16. [CrossRef]
- Steven, S.; Frenis, K.; Oelze, M.; Kalinovic, S.; Kuntic, M.; Jimenez, M.T.B.; Vujacic-Mirski, K.; Helmstädter, J.; Kröller-Schön, S.; Münzel, T.; et al. Vascular Inflammation and Oxidative Stress: Major Triggers for Cardiovascular Disease. *Oxid. Med. Cell. Longev.* **2019**, *2019*, 7092151. [CrossRef]
- Singh, A.K.; Yadav, D.; Sharma, N.; Jin, J.O. Dipeptidyl Peptidase (Dpp)-iv Inhibitors with Antioxidant Potential Isolated from Natural Sources: A Novel Approach for the Management of Diabetes. *Pharmaceuticals* **2021**, *14*, 586. [CrossRef] [PubMed]
- Singh, A.K.; Jatwa, R.; Purohit, A.; Ram, H. Synthetic and Phytocompounds Based Dipeptidyl Peptidase-IV (DPP-IV) Inhibitors for Therapeutics of Diabetes. *J. Asian Nat. Prod. Res.* **2017**, *19*, 1036–1045. [CrossRef] [PubMed]
- Nash, R.J.; Kato, A.; Yu, C.Y.; Fleet, G.W. Iminosugars as Therapeutic Agents: Recent Advances and Promising Trends. *Future Med. Chem.* **2011**, *3*, 1513–1521. [CrossRef] [PubMed]
- Horne, G.; Wilson, F.X.; Tinsley, J.; Williams, D.H.; Storer, R. Iminosugars Past, Present and Future: Medicines for Tomorrow. *Drug Discov. Today* **2011**, *16*, 107–118. [CrossRef] [PubMed]
- Verma, A.K.; Dubbu, S.; Chennaiah, A.; Vankar, Y.D. Synthesis of Di- and Trihydroxy Proline Derivatives from D-Glycals: Application in the Synthesis of Polysubstituted Pyrrolizidines and Bioactive 1C-Aryl/Alkyl Pyrrolidines. *Carbohydr. Res.* **2019**, *475*, 48–55. [CrossRef] [PubMed]
- Chennaiah, A.; Bhowmick, S.; Vankar, Y.D. Conversion of Glycals into Vicinal-1,2-Diazides and 1,2-(or 2,1)-Azidoacetates Using Hypervalent Iodine Reagents and Me₃SiN₃. Application in the Synthesis of: N-Glycopeptides, Pseudo-Trisaccharides and an Iminosugar. *RSC Adv.* **2017**, *7*, 41755–41762. [CrossRef]
- Chennaiah, A.; Dahiya, A.; Dubbu, S.; Vankar, Y.D. A Stereoselective Synthesis of an Imino Glycal: Application in the Synthesis of (–)-1-Epi-Adenophorine and a Homoiminosugar. *Eur. J. Org. Chem.* **2018**, *2018*, 6574–6581. [CrossRef]
- Miyamoto, Y.; Banno, Y.; Yamashita, T.; Fujimoto, T.; Oi, S.; Moritoh, Y.; Asakawa, T.; Kataoka, O.; Takeuchi, K.; Suzuki, N.; et al. Design and Synthesis of 3-Pyridylacetamide Derivatives as Dipeptidyl Peptidase IV (DPP-4) Inhibitors Targeting a Bidentate Interaction with Arg125. *Bioorg. Med. Chem.* **2011**, *19*, 172–185. [CrossRef]
- Juang, J.H.; Kuo, C.H.; Liu, Y.H.; Chang, H.Y.; Chen, C.T. Effects of Dipeptidyl Peptidase-4 Inhibition with MK-0431 on Syngeneic Mouse Islet Transplantation. *Int. J. Endocrinol.* **2014**, *2014*, 795283. [CrossRef]
- Borja-Hart, N.L.; Whalen, K.L. Saxagliptin: A New Dipeptidyl Peptidase 4 Inhibitor for Type 2 Diabetes. *Ann. Pharmacother.* **2010**, *44*, 1046–1053. [CrossRef]
- Augeri, D.J.; Robl, J.A.; Betebenner, D.A.; Magnin, D.R.; Khanna, A.; Robertson, J.G.; Wang, A.; Simpkins, L.M.; Taunk, P.; Huang, Q.; et al. Discovery and Preclinical Profile of Saxagliptin (BMS-477118): A Highly Potent, Long-Acting, Orally Active Dipeptidyl Peptidase IV Inhibitor for the Treatment of Type 2 Diabetes. *J. Med. Chem.* **2005**, *48*, 5025–5037. [CrossRef]
- Barnett, A. DPP-4 Inhibitors and Their Potential Role in the Management of Type 2 Diabetes. *Int. J. Clin. Pract.* **2006**, *60*, 1454–1470. [CrossRef]

20. Inagaki, N.; Onouchi, H.; Sano, H.; Funao, N.; Kuroda, S.; Kaku, K. SYR-472, a Novel Once-Weekly Dipeptidyl Peptidase-4 (DPP-4) Inhibitor, in Type 2 Diabetes Mellitus: A Phase 2, Randomised, Double-Blind, Placebo-Controlled Trial. *Lancet Diabetes Endocrinol.* **2014**, *2*, 125–132. [CrossRef]
21. Gomes, G.K.A.; Pereira, M.L.; Sanches, C.; Baldoni, A.O. Post-Marketing Study of Linagliptin: A Pilot Study. *Front. Pharmacol.* **2019**, *10*. [CrossRef]
22. Amori, R.E.; Lau, J.; Pittas, A.G. Efficacy and Safety of Incretin Therapy in Type 2 Diabetes: Systematic Review and Meta-Analysis. *J. Am. Med. Assoc.* **2007**, *298*, 194–206. [CrossRef]
23. Cao, G.Y.; Li, X.C.; Zhao, N.; Liu, Q.; Hu, X. Dipeptidyl Peptidase IV Inhibitors for the Treatment of Type 2 Diabetes. *Chin. J. New Drugs* **2011**, *20*, 497–502. [CrossRef]
24. Drucker, D.J. The Biology of Incretin Hormones. *Cell Metab.* **2006**, *3*, 153–165. [CrossRef]
25. Holst, J.J. The Physiology and Pharmacology of Incretins in Type 2 Diabetes Mellitus. *Diabetes Obes. Metab.* **2008**, *10*, 14–21. [CrossRef]
26. Saisho, Y. Alogliptin Benzoate for Management of Type 2 Diabetes. *Vasc. Health Risk Manag.* **2015**, *11*, 229–243. [CrossRef]
27. Pratley, R.E. Alogliptin: A New, Highly Selective Dipeptidyl Peptidase-4 Inhibitor for the Treatment of Type 2 Diabetes. *Expert Opin. Pharmacother.* **2009**, *10*, 503–512. [CrossRef]
28. Mohan, V.; Yang, W.; Son, H.Y.; Xu, L.; Noble, L.; Langdon, R.B.; Amatruda, J.M.; Stein, P.P.; Kaufman, K.D. Efficacy and Safety of Sitagliptin in the Treatment of Patients with Type 2 Diabetes in China, India, and Korea. *Diabetes Res. Clin. Pract.* **2009**, *83*, 106–116. [CrossRef]
29. Esposito, K.; Cozzolino, D.; Bellastella, G.; Maiorino, M.I.; Chiodini, P.; Ceriello, A.; Giugliano, D. Dipeptidyl Peptidase-4 Inhibitors and HbA1c Target of <7% in Type 2 Diabetes: Meta-Analysis of Randomized Controlled Trials. *Diabetes Obes. Metab.* **2011**, *13*, 594–603. [CrossRef] [PubMed]
30. Ji, X.; Su, M.; Wang, J.; Deng, G.; Deng, S.; Li, Z.; Tang, C.; Li, J.; Li, J.; Zhao, L.; et al. Design, Synthesis and Biological Evaluation of Hetero-Aromatic Moieties Substituted Pyrrole-2-Carbonitrile Derivatives as Dipeptidyl Peptidase IV Inhibitors. *Eur. J. Med. Chem.* **2014**, *75*, 111–122. [CrossRef] [PubMed]
31. Li, J.; Ji, X.; Xia, C.; Wang, J.; Su, M.; Zhang, L.; Dong, T.; Li, Z.; Wan, X.; Li, J.; et al. Design, Synthesis and Biological Evaluation of 4-Fluoropyrrolidine-2-Carbonitrile and Octahydrocyclopenta[b]Pyrrole-2-Carbonitrile Derivatives as Dipeptidyl Peptidase IV Inhibitors. *Eur. J. Med. Chem.* **2014**, *86*, 242–256. [CrossRef]
32. Dastjerdi, H.F.; Naderi, N.; Nematpour, M.; Rezaee, E.; Mahboubi-Rabbani, M.; Ebrahimi, M.; Hosseinipoor, S.; Hosseini, O.; Tabatabai, S.A. Design, Synthesis and Anti-Diabetic Activity of Novel 1, 2, 3-Triazole-5-Carboximidamide Derivatives as Dipeptidyl Peptidase-4 Inhibitors. *J. Mol. Struct.* **2020**, *1221*. [CrossRef]
33. Nath, V.; Ramchandani, M.; Kumar, N.; Agrawal, R.; Kumar, V. Computational Identification of Potential Dipeptidyl Peptidase (DPP)-IV Inhibitors: Structure Based Virtual Screening, Molecular Dynamics Simulation and Knowledge Based SAR Studies. *J. Mol. Struct.* **2021**, *1224*, 129006. [CrossRef]
34. Huang, J.; Deng, X.; Zhou, S.; Wang, N.; Qin, Y.; Meng, L.; Li, G.; Xiong, Y.; Fan, Y.; Guo, L.; et al. Identification of Novel Uracil Derivatives Incorporating Benzoic Acid Moieties as Highly Potent Dipeptidyl Peptidase-IV Inhibitors. *Bioorg. Med. Chem.* **2019**, *27*, 644–654. [CrossRef] [PubMed]
35. Li, Q.; Deng, X.; Jiang, N.; Meng, L.; Xing, J.; Jiang, W.; Xu, Y. Identification and Structure–Activity Relationship Exploration of Uracil-Based Benzoic Acid and Ester Derivatives as Novel Dipeptidyl Peptidase-4 Inhibitors for the Treatment of Type 2 Diabetes Mellitus. *Eur. J. Med. Chem.* **2021**, *225*, 113765. [CrossRef] [PubMed]
36. Pace, A.; Pierro, P. The New Era of 1,2,4-Oxadiazoles. *Org. Biomol. Chem.* **2009**, *7*, 4337–4348. [CrossRef] [PubMed]
37. Jones, A.M.; Helm, J.M. Emerging Treatments in Cystic Fibrosis. *Drugs* **2009**, *69*, 1903–1910. [CrossRef]
38. Summa, V.; Petrocchi, A.; Bonelli, F.; Crescenzi, B.; Donghi, M.; Ferrara, M.; Fiore, F.; Gardelli, C.; Paz, O.G.; Hazuda, D.J.; et al. Discovery of Raltegravir, a Potent, Selective Orally Bioavailable HIV-Integrase Inhibitor for the Treatment of HIV-AIDS Infection. *J. Med. Chem.* **2008**, *51*, 5843–5855. [CrossRef]
39. Jones, R.M.; Leonard, J.N.; Buzard, D.J.; Lehmann, J. GPR119 Agonists for the Treatment of Type 2 Diabetes. *Expert Opin. Ther. Pat.* **2009**, *19*, 1339–1359. [CrossRef]
40. Suk, H.L.; Hee, J.S.; Lee, S.H.; Myung, E.J.; Park, J.H.; Park, H.J.; Yoo, J.; Yun, H.; Na, J.; Suk, Y.K.; et al. Biarylpyrazolyl Oxadiazole as Potent, Selective, Orally Bioavailable Cannabinoid-1 Receptor Antagonists for the Treatment of Obesity. *J. Med. Chem.* **2008**, *51*, 7216–7233. [CrossRef]
41. Unangst, P.C.; Shrum, G.P.; Connor, D.T.; Dyer, R.D.; Schrier, D.J. Novel 1,2,4-Oxadiazoles and 1,2,4-Thiadiazoles as Dual 5-Lipoxygenase and Cyclooxygenase Inhibitors. *J. Med. Chem.* **1992**, *35*, 3691–3698. [CrossRef]
42. Zhang, H.Z.; Kasibhatla, S.; Kuemmerle, J.; Kemnitzer, W.; Ollis-Mason, K.; Qiu, L.; Crogan-Grundy, C.; Tseng, B.; Drewe, J.; Cai, S.X. Discovery and Structure-Activity Relationship of 3-Aryl-5-Aryl-1,2,4-Oxadiazoles as a New Series of Apoptosis Inducers and Potential Anticancer Agents. *J. Med. Chem.* **2005**, *48*, 5215–5223. [CrossRef]
43. Cottrell, D.M.; Capers, J.; Salem, M.M.; DeLuca-Fradley, K.; Croft, S.L.; Werbovets, K.A. Antikinetoplastid Activity of 3-Aryl-5-Thiocyanatomethyl-1,2,4-Oxadiazoles. *Bioorg. Med. Chem.* **2004**, *12*, 2815–2824. [CrossRef]
44. Ohmoto, K.; Okuma, M.; Yamamoto, T.; Kijima, H.; Sekioka, T.; Kitagawa, K.; Yamamoto, S.; Tanaka, K.; Kawabata, K.; Sakata, A.; et al. Design and Synthesis of New Orally Active Inhibitors of Human Neutrophil Elastase. *Bioorg. Med. Chem.* **2001**, *9*, 1307–1323. [CrossRef]

45. Ono, M.; Haratake, M.; Saji, H.; Nakayama, M. Development of Novel β -Amyloid Probes Based on 3,5-Diphenyl-1,2,4-Oxadiazole. *Bioorg. Med. Chem.* **2008**, *16*, 6867–6872. [CrossRef]
46. Orlek, B.S.; Blaney, F.E.; Brown, F.; Clark, M.S.G.; Hadley, M.S.; Hatcher, J.; Riley, G.J.; Rosenberg, H.E.; Wadsworth, H.J.; Wyman, P. Comparison of Azabicyclic Esters and Oxadiazoles as Ligands for the Muscarinic Receptor. *J. Med. Chem.* **1991**, *34*, 2726–2735. [CrossRef] [PubMed]
47. Boström, J.; Hogner, A.; Schmitt, S. Do Structurally Similar Ligands Bind in a Similar Fashion? *J. Med. Chem.* **2006**, *49*, 6716–6725. [CrossRef]
48. McBriar, M.D.; Clader, J.W.; Chu, I.; Del Vecchio, R.A.; Favreau, L.; Greenlee, W.J.; Hyde, L.A.; Nomeir, A.A.; Parker, E.M.; Pissarnitski, D.A.; et al. Discovery of Amide and Heteroaryl Isosteres as Carbamate Replacements in a Series of Orally Active γ -Secretase Inhibitors. *Bioorg. Med. Chem. Lett.* **2008**, *18*, 215–219. [CrossRef]
49. Ladbury, J.E.; Klebe, G.; Freire, E. Adding Calorimetric Data to Decision Making in Lead Discovery: A Hot Tip. *Nat. Rev. Drug Discov.* **2010**, *9*, 23–27. [CrossRef]
50. Khan, I.; Ibrar, A.; Abbas, N. Oxadiazoles as Privileged Motifs for Promising Anticancer Leads: Recent Advances and Future Prospects. *Arch. Pharm.* **2014**, *347*, 1–20. [CrossRef]
51. Zhu, L.; Zeng, H.; Liu, D.; Fu, Y.; Wu, Q.; Song, B.; Gan, X. Design, Synthesis, and Biological Activity of Novel 1,2,4-Oxadiazole Derivatives. *BMC Chem.* **2020**, *14*, 68. [CrossRef] [PubMed]
52. Pitasse-Santos, P.; Suetth-Santiago, V.; Lima, M.E.F. 1,2,4- and 1,3,4-Oxadiazoles as Scaffolds in the Development of Antiparasitic Agents. *J. Braz. Chem. Soc.* **2018**, *29*, 435–456. [CrossRef]
53. Sonawane, A.D.; Rode, N.D.; Nawale, L.; Joshi, R.R.; Joshi, R.A.; Likhite, A.P.; Sarkar, D. Synthesis and Biological Evaluation of 1,2,4-Triazole-3-Thione and 1,3,4-Oxadiazole-2-Thione as Antimycobacterial Agents. *Chem. Biol. Drug Des.* **2017**, *90*, 200–209. [CrossRef] [PubMed]
54. Nazari, M.; Rezaee, E.; Hariri, R.; Akbarzadeh, T.; Tabatabai, S.A. Novel 1,2,4-Oxadiazole Derivatives as Selective Butyrylcholinesterase Inhibitors: Design, Synthesis, and Biological Evaluation. *EXCLI J.* **2021**, *20*, 907–921. [CrossRef]
55. Shukla, C.; Srivastava, S. Biologically Active Oxadiazole. *J. Drug Deliv. Ther.* **2015**, *5*, 8–13. [CrossRef]
56. Arshad, M.; Khan, T.A.; Khan, M.A. 1,2,4-Oxadiazole Nucleus With Versatile Biological Applications. *Int. J. Pharm. Sci. Res.* **2014**, *5*, 303–316.
57. Stoimenis, D.; Karagiannis, T.; Katsoula, A.; Athanasiadou, E.; Kazakos, K.; Bekiari, E.; Matthews, D.R.; Tsapas, A. Once-Weekly Dipeptidyl Peptidase-4 Inhibitors for Type 2 Diabetes: A Systematic Review and Meta-Analysis. *Expert Opin. Pharmacother.* **2017**, *18*, 843–851. [CrossRef]
58. Kato, N.; Oka, M.; Murase, T.; Yoshida, M.; Sakairi, M.; Yakufu, M.; Yamashita, S.; Yasuda, Y.; Yoshikawa, A.; Hayashi, Y.; et al. Synthesis and Pharmacological Characterization of Potent, Selective, and Orally Bioavailable Isoindoline Class Dipeptidyl Peptidase IV Inhibitors. *Org. Med. Chem. Lett.* **2011**, *1*, 7. [CrossRef]
59. Dalgaard, K.; Landgraf, K.; Heyne, S.; Lempradl, A.; Longinotto, J.; Gossens, K.; Ruf, M.; Orthofer, M.; Strogantsev, R.; Selvaraj, M.; et al. Trim28 Haploinsufficiency Triggers Bi-Stable Epigenetic Obesity. *Cell* **2016**, *164*, 353–364. [CrossRef]
60. Srivastava, J.K.; Dubey, P.; Singh, S.; Bhat, H.R.; Kumawat, M.K.; Singh, U.P. Discovery of Novel 1,3,5-Triazine-Thiazolidine-2,4-Diones as Dipeptidyl Peptidase-4 Inhibitors with Antibacterial Activity Targeting the S1 Pocket for the Treatment of Type 2 Diabetes. *RSC Adv.* **2015**, *5*, 14095–14102. [CrossRef]
61. Kumar, S.; Rathore, D.S.; Garg, G.; Khatri, K.; Saxena, R.; Sahu, S.K. Synthesis and Evaluation of Some 2-((Benzothiazol-2-Ylthio) Methyl)-5-Phenyl-1, 3, 4-Oxadiazole Derivatives as Antidiabetic Agents. *Asian Pacific J. Health Sci.* **2016**, *3*, 65–74. [CrossRef]
62. Bhutani, R.; Pathak, D.P.; Kapoor, G.; Husain, A.; Iqbal, M.A. Novel Hybrids of Benzothiazole-1,3,4-Oxadiazole-4-Thiazolidinone: Synthesis, in Silico ADME Study, Molecular Docking and in Vivo Anti-Diabetic Assessment. *Bioorg. Chem.* **2019**, *83*, 6–19. [CrossRef] [PubMed]
63. Gani, R.S.; Kudva, A.K.; Timanagouda, K.; Raghuvveer; Mujawar, S.B.H.; Joshi, S.D.; Raghu, S.V. Synthesis of Novel 5-(2,5-Bis(2,2,2-Trifluoroethoxy)Phenyl)-1,3,4-Oxadiazole-2-Thiol Derivatives as Potential Glucosidase Inhibitors. *Bioorg. Chem.* **2021**, *114*, 105046. [CrossRef]
64. Bhutani, R.; Pathak, D.P.; Kapoor, G.; Husain, A.; Kant, R.; Iqbal, M.A. Synthesis, Molecular Modelling Studies and ADME Prediction of Benzothiazole Clubbed Oxadiazole-Mannich Bases, and Evaluation of Their Anti-Diabetic Activity through in Vivo Model. *Bioorg. Chem.* **2018**, *77*, 6–15. [CrossRef] [PubMed]
65. Nordhoff, S.; Bulat, S.; Cerezo-Gálvez, S.; Hill, O.; Hoffmann-Enger, B.; López-Canet, M.; Rosenbaum, C.; Rummey, C.; Thiemann, M.; Matassa, V.G.; et al. The Design of Potent and Selective Inhibitors of DPP-4: Optimization of ADME Properties by Amide Replacements. *Bioorg. Med. Chem. Lett.* **2009**, *19*, 6340–6345. [CrossRef]
66. Xu, J.; Wei, L.; Mathvink, R.J.; Edmondson, S.D.; Eiermann, G.J.; He, H.; Leone, J.F.; Leiting, B.; Lyons, K.A.; Marsilio, F.; et al. Discovery of Potent, Selective, and Orally Bioavailable Oxadiazole-Based Dipeptidyl Peptidase IV Inhibitors. *Bioorg. Med. Chem. Lett.* **2006**, *16*, 5373–5377. [CrossRef] [PubMed]
67. Iftikhar, M.; Saleem, M.; Riaz, N.; Aziz-ur-Rehman; Ahmed, I.; Rahman, J.; Ashraf, M.; Sharif, M.S.; Khan, S.U.; Htar, T.T. A Novel Five-Step Synthetic Route to 1,3,4-Oxadiazole Derivatives with Potent α -Glucosidase Inhibitory Potential and Their in Silico Studies. *Arch. Pharm.* **2019**, *352*, 1900095. [CrossRef]

68. Kazmi, M.; Zaib, S.; Ibrar, A.; Amjad, S.T.; Shafique, Z.; Mehsud, S.; Saeed, A.; Iqbal, J.; Khan, I. A New Entry into the Portfolio of α -Glucosidase Inhibitors as Potent Therapeutics for Type 2 Diabetes: Design, Bioevaluation and One-Pot Multi-Component Synthesis of Diamine-Bridged Coumarinyl Oxadiazole Conjugates. *Bioorg. Chem.* **2018**, *77*, 190–202. [CrossRef]
69. Taha, M.; Ismail, N.H.; Imran, S.; Wadood, A.; Rahim, F.; Saad, S.M.; Khan, K.M.; Nasir, A. Synthesis, Molecular Docking and α -Glucosidase Inhibition of 5-Aryl-2-(6'-Nitrobenzofuran-2'-yl)-1,3,4-Oxadiazoles. *Bioorg. Chem.* **2016**, *66*, 117–123. [CrossRef]
70. Ullah, H.; Rahim, F.; Taha, M.; Hussain, R.; Wadood, A.; Nawaz, M.; Wahab, Z.; Kanwal; Khan, K.M. Synthesis, In Vitro α -Glucosidase Inhibitory Potential and Molecular Docking Studies of 2-Amino-1,3,4-Oxadiazole Derivatives. *Med. Chem.* **2019**, *16*, 724–734. [CrossRef]
71. Taha, M.; Imran, S.; Rahim, F.; Wadood, A.; Khan, K.M. Oxindole Based Oxadiazole Hybrid Analogs: Novel α -Glucosidase Inhibitors. *Bioorg. Chem.* **2018**, *76*, 273–280. [CrossRef]
72. Xu, J.; Wei, L.; Mastracchio, A.; Edmondson, S. (12) Patent Application Publication (10). U.S. Patent 2008/0225123. A1 Patent Application Publication. *Priv. Point Contain. Sm. Card* **2008**, *1*, 11–14.
73. Hamdani, S.S.; Khan, B.A.; Ahmed, M.N.; Hameed, S.; Akhter, K.; Ayub, K.; Mahmood, T. Synthesis, Crystal Structures, Computational Studies and α -Amylase Inhibition of Three Novel 1,3,4-Oxadiazole Derivatives. *J. Mol. Struct.* **2020**, *1200*, 127085. [CrossRef]
74. Ibrahim, M.T.; Uzairu, A.; Shallangwa, G.A.; Ibrahim, A. In-Silico Studies of Some Oxadiazoles Derivatives as Anti-Diabetic Compounds. *J. King Saud Univ. Sci.* **2020**, *32*, 423–432. [CrossRef]
75. Nazir, M.; Abbasi, M.A.; Aziz-ur-Rehman; Siddiqui, S.Z.; Khan, K.M.; Kanwal; Salar, U.; Shahid, M.; Ashraf, M. New Indole Based Hybrid Oxadiazole Scaffolds with N-Substituted Acetamides: As Potent Anti-Diabetic Agents. *Bioorg. Chem.* **2018**, *81*, 253–263. [CrossRef]

Review

Recent Strategies in Transition-Metal-Catalyzed Sequential C–H Activation/Annulation for One-Step Construction of Functionalized Indazole Derivatives

Pezhman Shiri ^{1,2,*}, Atefeh Roosta ³, Wim Dehaen ^{4,*} and Ali Mohammad Amani ^{1,2}

¹ Department of Medical Nanotechnology, School of Advanced Medical Sciences and Technologies, Shiraz University of Medical Sciences, Shiraz 7133654361, Iran; amani_a@sums.ac.ir

² Pharmaceutical Sciences Research Center, Shiraz University of Medical Sciences, Shiraz 7133654361, Iran

³ Department of Chemistry, Tarbiat Modares University, Tehran 1411713116, Iran; atefehroosta862@gmail.com

⁴ Molecular Design and Synthesis, Department of Chemistry, KU Leuven, 3001 Leuven, Belgium

* Correspondence: pezhmanshiri@yahoo.com (P.S.); wim.dehaen@kuleuven.be (W.D.)

Abstract: Designing new synthetic strategies for indazoles is a prominent topic in contemporary research. The transition-metal-catalyzed C–H activation/annulation sequence has arisen as a favorable tool to construct functionalized indazole derivatives with improved tolerance in medicinal applications, functional flexibility, and structural complexity. In the current review article, we aim to outline and summarize the most common synthetic protocols to use in the synthesis of target indazoles via a transition-metal-catalyzed C–H activation/annulation sequence for the one-step synthesis of functionalized indazole derivatives. We categorized the text according to the metal salts used in the reactions. Some metal salts were used as catalysts, and others may have been used as oxidants and/or for the activation of precatalysts. The roles of some metal salts in the corresponding reaction mechanisms have not been identified. It can be expected that the current synopsis will provide accessible practical guidance to colleagues interested in the subject.

Keywords: C–H functionalization; cyclization; indazole products; transition metals catalysis

Citation: Shiri, P.; Roosta, A.; Dehaen, W.; Amani, A.M. Recent Strategies in Transition-Metal-Catalyzed Sequential C–H Activation/Annulation for One-Step Construction of Functionalized Indazole Derivatives. *Molecules* **2022**, *27*, 4942. <https://doi.org/10.3390/molecules27154942>

Academic Editors: Alexey M. Starosotnikov, Maxim A. Bastrakov and Igor L. Dalinger

Received: 6 July 2022

Accepted: 29 July 2022

Published: 3 August 2022

Publisher's Note: MDPI stays neutral with regard to jurisdictional claims in published maps and institutional affiliations.



Copyright: © 2022 by the authors. Licensee MDPI, Basel, Switzerland. This article is an open access article distributed under the terms and conditions of the Creative Commons Attribution (CC BY) license (<https://creativecommons.org/licenses/by/4.0/>).

1. Introduction

Nitrogen-based heterocyclic systems are commonly found in pharmaceutical agents and natural products, and they have been intensively explored as new bioactive products [1–10]. Among them, the indazoles [11–16] are favored by synthetic and medicinal chemists, as evidenced by their widespread abundance in pharmaceuticals and natural products. In fact, products bearing the indazole segment have been found to show diverse biological activities, including analgesic, anticancer, anesthetic, anti-inflammatory, antifungal, anti-HIV, antiarrhythmic, and anti-emetic properties and high binding affinity for estrogen receptors (Figure 1) [11,17–24]. Pazopanib with an indazole scaffold has been proven to be a potent and selective multitargeted receptor tyrosine kinase inhibitor that inhibits tumor growth [25]. Moreover, derivatives of indazole have been used as electronically active and agricultural materials [26,27]. Indazoles are found in nature as well, and the structures of three natural products containing the indazole scaffold, named nigellicine, nigellidine, and nigeplanine, are illustrated in Figure 1 [11,28–31].

Notably, the known synthetic procedures toward indazoles may suffer from multistep routes, severe conditions, and relatively low substrate diversity [32–34]. Therefore, considerable attempts have been devoted to constructing these biologically critical scaffolds more efficiently, although the exploration of novel atom-economical strategies to produce these unique scaffolds is still a challenging topic. Recently, a transition-metal-catalyzed C–H bond activation and cyclization sequence [35–40] has received significant attention to provide these structures.

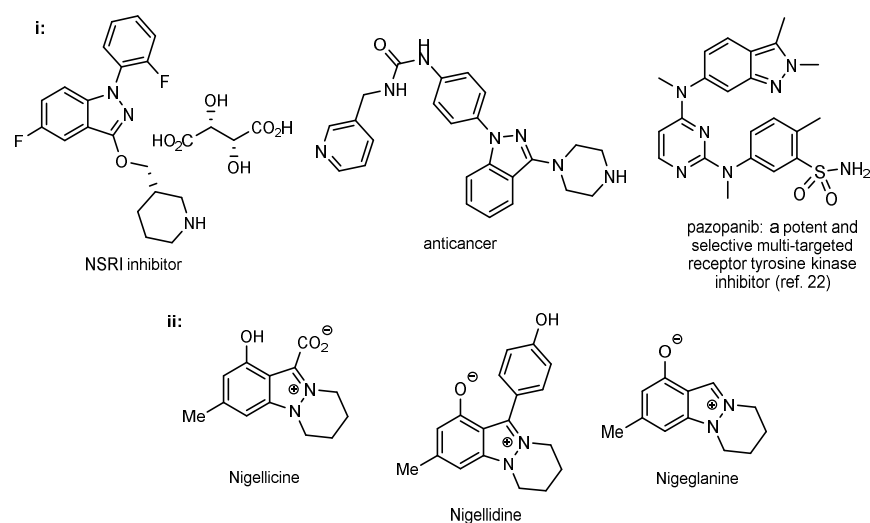


Figure 1. (i) Indazole derivatives with biological activity; (ii) Natural products of indazole alkaloids.

Transition-metal-catalyzed C–H activation [41] and annulation sequences [37,42–48] are powerful and reliable tools for the formation of complex molecular structures in an efficient, economical, practicable, and straightforward manner [37,49]. These synthetic strategies provide highly atom- and step-economic transformations for the development of efficient synthetic procedures with high functional-group tolerance while avoiding the excessive prefunctionalization of reactive centers. One major issue for these protocols is the intrinsic inferior reactivity of C–H bonds, requiring harsh conditions to convert substrates to the target products in satisfactory yields and resulting in low selectivities [50]. To solve this, the C–H activation of inactive arenes via a pendent chelating activator is an efficient route that is additionally incurring site selectivity in C–H activation. Metal salts or metal complexes have commonly been applied for these transformations. Thus, transition-metal-catalyzed sequential C–H activation/annulation reactions of suitable substrates with a variety of coupling partners have been applied to assemble complex indazole-based architectures.

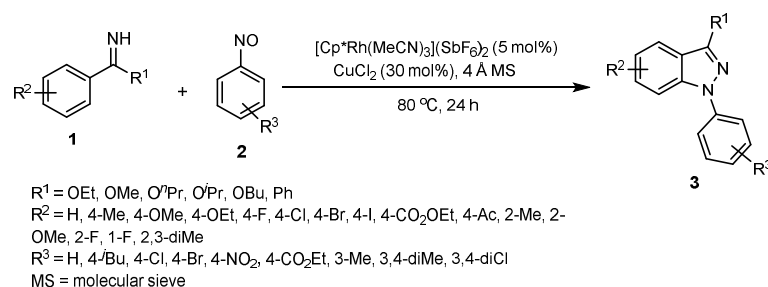
In 2018, a general review appeared on recent advances in various methods for the synthesis of indazole derivatives, focusing on their biological activities [12]. Meanwhile, Li et al. outlined the anticancer activity of indazole derivatives [51] while also summarizing the synthetic protocols and structure–activity relationships of target products [51]. In 2021, Babu et al. comprehensively covered the recent developments in the transition-metal-catalyzed synthesis of indazoles [52]. An overview of the development of novel and green electrochemical approaches in the functionalization of indazole derivatives was reported by Hajra in 2021 [53]. Moreover, a review article for approved marketed drugs containing indazole scaffolds as valid preclinical/clinical drug compounds was published by Wu et al. in 2021 [54]. Because of the significance of indazole heterocyclic systems as well as the rapid development of strategies based on transition-metal-catalyzed sequential C–H activation/annulation for the one-step synthesis of functionalized indazole derivatives, a dedicated comprehensive overview would be timely and beneficial for future drug discovery.

Consequently, we aim to present a review arranged according to the various sorts of metal salts or metal complexes applied in such transition-metal-catalyzed C–H activation and annulation sequences. The purpose of the current overview is to report the recent exploration in this area based on different transition metal catalysts derived from rhodium, cobalt, palladium, rhenium, and copper. While covering the subject, a variety of examples and selected mechanisms of reactions are discussed.

2. Different Synthesis Routes for the Construction of Indazoles via Transition-Metal-Catalyzed Sequential C–H Activation/Annulation

2.1. Synthesis of Indazoles Using Rhodium and Copper Salts

In 2016, a facile and efficient access to 1*H*-indazoles **3** was established through Rh(III)/Cu(II)-catalyzed sequential C–H bond activation and intramolecular cascade annulation. The reaction occurs at 80 °C within 24 h in PhCF₃ as a solvent. A comprehensive examination of this process was conducted using ethyl benzimidates **1** and nitrosobenzenes **2**. A control experiment without adding Rh or Cu catalysts was then run to demonstrate that this transformation could not proceed without either one of these catalysts. The authors proposed a significant facilitation role of the bridging acetate ligand in the Rh₂(OAc)₄ structure for the C–H activation. Benzimidate scaffolds **1** with both electron-withdrawing and electron-donating functional groups as well as halogens all worked well to afford the desired products with moderate to high yields. Furthermore, imidate substrates **1** that bear other alkyl esters as well as aryl substitution were transformed into the corresponding products **3** smoothly. Subsequently, a diverse range of nitrosobenzenes **2** with electron-donating and -withdrawing groups at different positions of the aryl ring were also proven to be viable substrates. Significantly, this transformation features satisfactory functional-group tolerance with good to high yields (Scheme 1) [55].

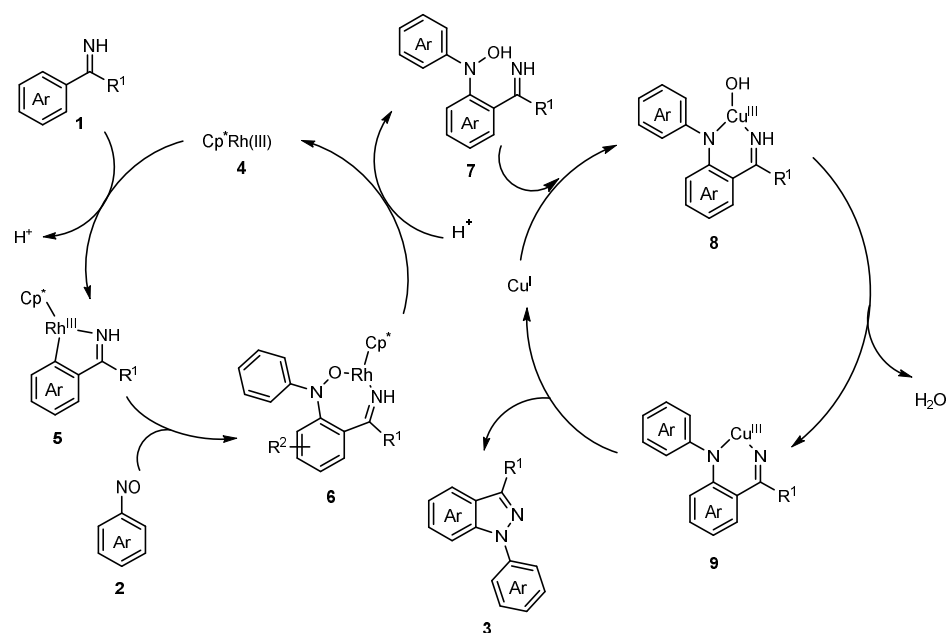


Scheme 1. A synthetic route for the preparation of 1*H*-indazole derivatives **3** from the reaction between imidates **1** and nitrosobenzenes **2** in the presence of a rhodium/copper catalyst.

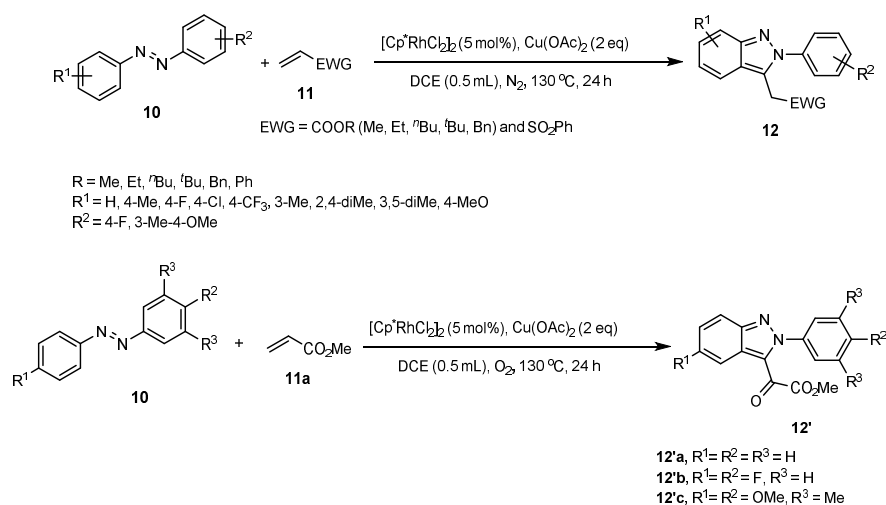
The mechanism for the formation of 1*H*-indazoles **3** through the reaction of imidates **1** with nitrosobenzenes **2** catalyzed by a rhodium/copper catalyst is given in Scheme 2. A rhodacycle **5** is generated by the coordination of an imidate **1** to a catalyst **4** and C–H activation. Subsequently, the migratory insertion of the Rh–C bond into the N=O group yields a six-membered rhodacycle **6**. In the next step, the protonolysis of the intermediate **6** delivers a hydroxylamine **7** along with a regenerated Rh(III) catalyst **4**. In another cycle, N–O oxidative addition is carried out using the Cu(I) catalyst to deliver a Cu(III) organocupracycle **8**. Finally, the dehydration of **8** and the reductive elimination of **9** take place to form the N–N bond [55]. Although the authors reported intermediates **8** and **9**, it seems Cu(III) would involve a chloride or another negatively charged ligand attached to copper in intermediates **8** and **9**.

A Rh(III)-mediated substrate-controlled conversion of azobenzenes **10** and alkenes **11** to indazoles **12** was described via C–H functionalization and cyclization (Scheme 3). First, 5 mol% of [Cp*RhCl₂]₂ and 200 mol% of Cu(OAc)₂ as oxidant and DCE as solvent were utilized to transfer azobenzenes **10** to indazoles **12** under nitrogen atmosphere in good to excellent yields. To highlight the importance of having both metals present, no desired compound was formed when either the Rh(III) as catalyst or Cu(II) as oxidant were removed. The scope of this C–H functionalization/cyclization reaction with regard to both azobenzenes **10** and alkenes **11** was screened. Acrylates **11** with different substitutions efficiently proceeded to afford final products in satisfactory yields. However, phenyl vinyl sulfone and dimethyl vinyl phosphonate did not react with its azobenzene partner under optimized conditions. Azobenzene substrates possessing both electron-donating and electron-withdrawing functional groups were well-tolerated, as evidenced by the isolation of the desired products in moderate to good yields. The product with a stronger

electron-withdrawing substituent (CF₃) was formed only in a trace amount. Next, this coupling reaction was applied to *m*- or *o*-substituted azobenzenes. The *m*-Me azobenzene **10** regioselectively resulted in the generation of the corresponding product **12** after reacting at the less hindered position. However, the *m*-MeO azobenzene **10** led to a mixture of two regioisomers **12**. The treatment of symmetrical disubstituted azobenzenes **10** with alkenes **11** enabled the C–H functionalization/cyclization sequence in good to moderate yields, while unsymmetrically substituted azobenzene **10** afforded the corresponding product **12**, after reaction at the less hindered position, in a good yield. Surprisingly, 3-acyl indazole products **12'** were achieved by performing the reactions under oxygen atmosphere. The subsequent utilization of the present strategy could be a rapid and straightforward approach for the synthesis of new functional and biologically active molecules [56].



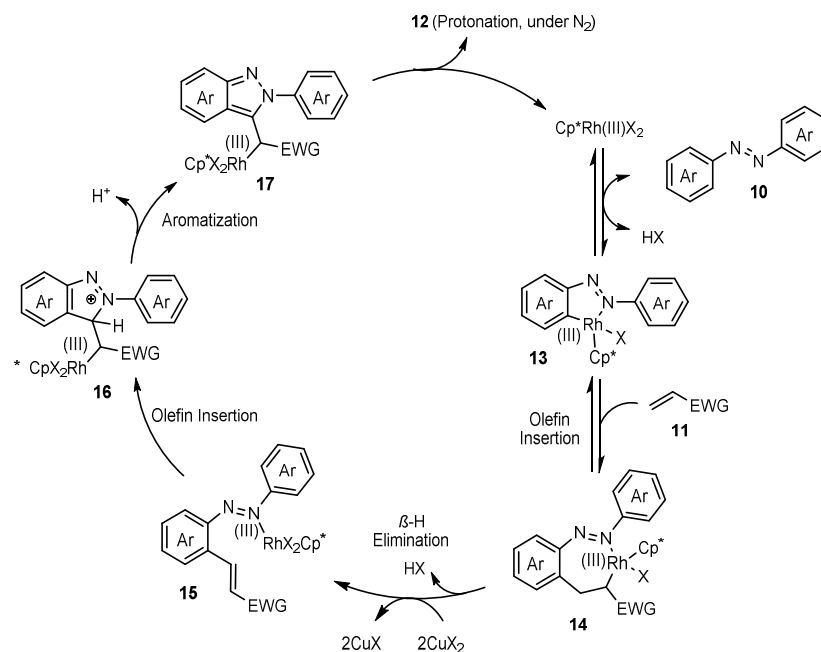
Scheme 2. A rational mechanism for the synthesis of 1*H*-indazole derivatives **3** from the reaction between imidates **1** and nitrosobenzenes **2** in the presence of a rhodium/copper catalyst.



Scheme 3. A synthetic route for the transformation of azobenzene substrates **10** to indazole derivatives **12** in the presence of a Rh(III) catalyst.

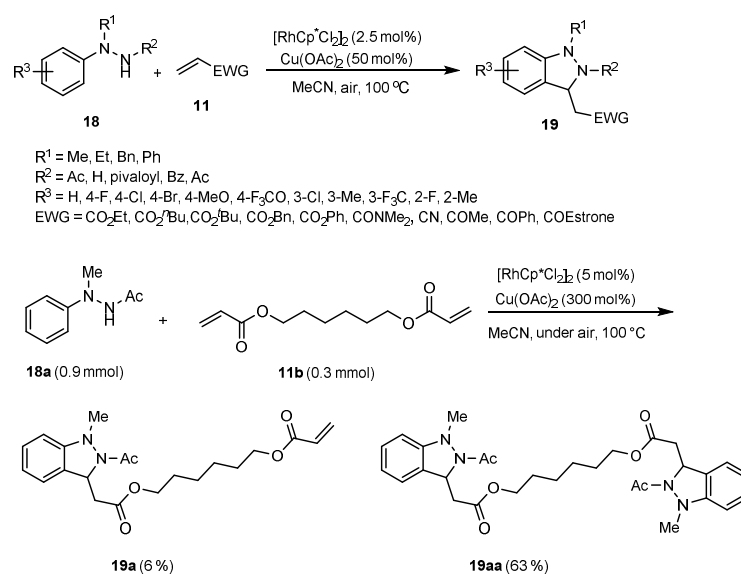
The mechanism for the synthesis of indazoles **12** from azobenzenes **10** is exhibited in Scheme 4, which involves coordination, C–H activation, alkene coordination and insertion,

β -hydride elimination, the insertion of a C=C bond into the Rh-N bond, and then aromatization to produce indazoles. It was proposed that copper acetate plays its role in the step of the β -hydride elimination to give indazoles [56].



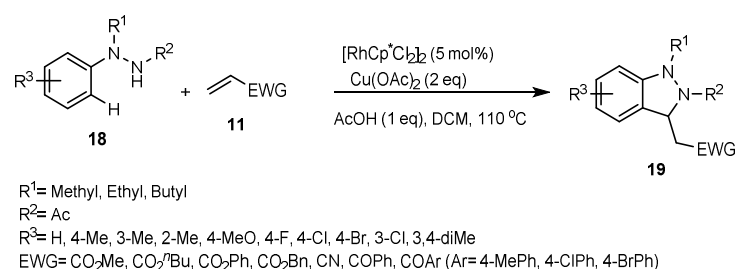
Scheme 4. A possible mechanism for the transformation of azobenzene substrates **10** to indazole derivatives **12** in the presence of a Rh(III) catalyst.

A novel methodology for the synthesis of 2,3-dihydro-1*H*-indazoles **19** via the oxidative olefination of 1,2-disubstituted arylhydrazines **18** with alkenes **11** through C(sp²)-H bond functionalization pursued by an intramolecular aza-Michael transformation was reported by Kim et al. A series of highly substituted 2,3-dihydro-1*H*-indazoles **19** with different substituents were obtained in low to high yields in the presence of [RhCp*Cl₂]₂ as a catalyst and Cu(OAc)₂ as an oxidant in MeCN under air atmosphere at 100 °C for 20 h in pressure tubes. The substrate scope was subsequently explored under this catalytic system, as illustrated in Scheme 5. Various acrylates **11** and *N'*-methyl-*N'*-arylacetohydrazides **18** with both electron-donating and -withdrawing substituents at the para-site of the aromatic ring were explored, giving the desired products **19** via oxidative olefination and the subsequent intramolecular cyclization in moderate to good yields. The functional-group tolerance, especially to the bromo and chloro groups, provides a versatile synthetic protocol for the further functionalization of the 2,3-dihydro-1*H*-indazoles **19**. Interestingly, when meta-substituted arylacetohydrazides **18** were used as the reaction substrates, Rh(III)-catalyzed oxidative coupling preferentially occurred at the less hindered site, providing the corresponding products **19** in a regioselective manner. Moreover, ortho-substituted compounds **18** afforded the desired products with slightly decreased effectivity, which is presumably attributed to the steric effect of a substituent at the ortho-position. The corresponding products **19** were further produced in low to high yields by the utilization of diverse olefins **11**. For acrylates containing -CO₂Me, -CO₂^{*n*}Bu, -CO₂^{*t*}Bu, -Bn, and -CO₂Ph as EWGs and acrylamide (containing -CONMe₂ as an EWG), 2,3-dihydro-1*H*-indazoles **19** were generated in high yields, while acrylonitrile **11** (containing -CN as an EWG) and but-3-en-2-one **11** (containing -COMe as an EWG) were reacted with *N'*-methyl-*N'*-phenylacetohydrazide with significantly decreased yield under the standard conditions. In the case of acrylate containing an estrogen scaffold, the desired product **19** was obtained in the reaction with *N'*-methyl-*N'*-phenylacetohydrazide. The bis-indazole **19aa** was then achieved in 63% yield by increasing the amounts of hydrazide, rhodium as a catalyst, and copper as an oxidant [57].



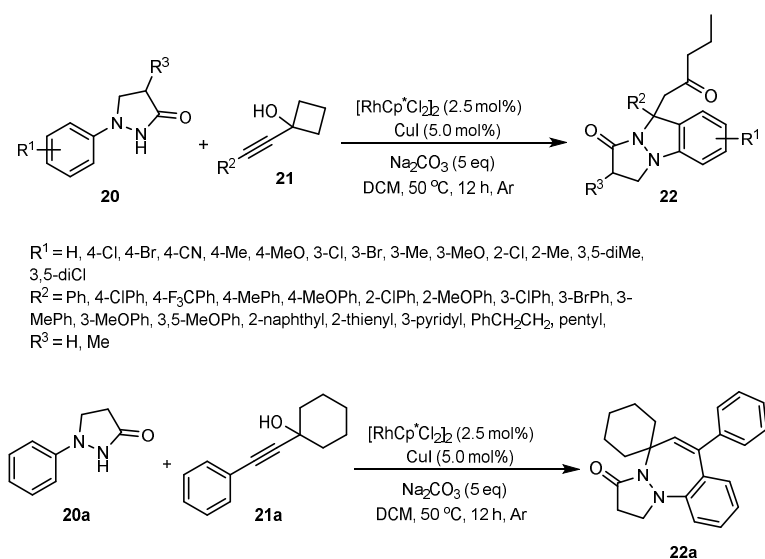
Scheme 5. A synthetic route for the preparation of 2,3-dihydro-1H-indazole derivatives **19** from the reaction between 1,2-disubstituted arylhydrazines **18** and electron-poor alkenes **11** in the presence of a Rh(III) catalyst.

The C–H bond activation of *N'*-alkyl-*N'*-arylaceto-hydrazide **18**, followed by cyclization with a variety of acrylates, ethyl acrylate, methyl acrylate, *n*-butyl acrylate, *t*-butyl acrylate, phenyl acrylate, and benzyl acrylate **11**, has been performed for the preparation of 2,3-dihydro-1H-indazoles **19** using a catalytic amount of $[\text{Cp}^*\text{RhCl}_2]_2$ in the presence of $\text{Cu}(\text{OAc})_2$ and AcOH in DCE at 110°C within 24 h under N_2 atmosphere. As illustrated in Scheme 6, the structurally diverse alkenes **19** reacted with *N'*-methyl-*N'*-phenylaceto-hydrazide to afford indazole derivatives **19** in good to high yields. A series of the *N'*-alkyl-*N'*-arylaceto-hydrazide derivatives **18** can smoothly be converted into corresponding products **19** with moderate to good yields as well. Disubstituted *N'*-alkyl-*N'*-arylaceto-hydrazides and *N'*-alkyl-*N'*-arylaceto-hydrazides **18** bearing both electron-rich and electron-deficient groups including methyl, methoxy, fluoro, chloro, and bromo on the aryl ring all displayed moderate to good reactivities in the sequence smoothly furnishing the desired indazoles **19**. In the case of meta-substituted *N'*-alkyl-*N'*-arylaceto-hydrazides, the reaction proceeded successfully at the less steric side of the arenes. Moreover, **18** containing an ortho-substituent also participated in this reaction to afford the corresponding product, although the yield greatly decreased. By having ethyl and *n*-butyl instead of methyl at the *N*-atom, the corresponding products **19** were obtained in moderate yields. This transformation provided a practical procedure to achieve useful target products **19** through C–H bond activation, featuring good to excellent yields with excellent regioselectivity, high atom economy, and versatile derivatization [58].



Scheme 6. A synthetic route for the preparation of 2,3-dihydro-1H-indazoles **19** via the C–H cleavage of arylhydrazines **18** in the presence of a Rh(III) catalyst.

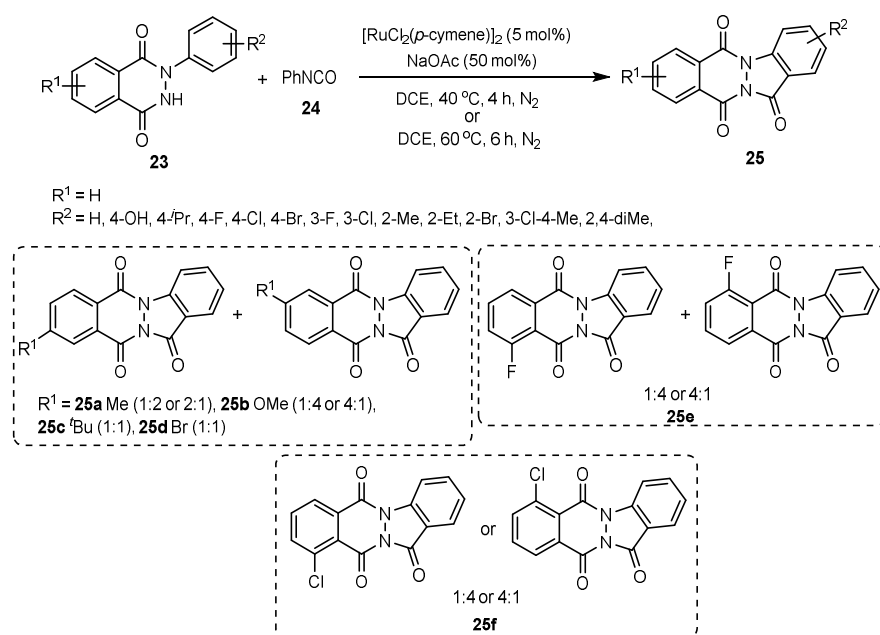
A catalytic reaction of 1-alkynylcyclobutanols **20** with pyrazolidinones **21** toward pyrazolo [1,2-*a*] indazoles **22** bearing a quaternary carbon was developed by Yu et al. in 2020. The reaction proceeds through Rh(III)-catalyzed sequential C–H/N–H activation and ring opening, followed by cyclization transformation in a one-pot process. This protocol provides an efficient and atom-economical approach for the direct synthesis of pyrazolo[1,2-*a*] indazoles **22** in high yields with exclusive regioselectivity under the optimized conditions (using catalytic amounts of $[\text{Cp}^*\text{RhCl}_2]_2$ and CuI in the presence of Na_2CO_3 in DCE at 50 °C within 12 h under Ar atmosphere) (Scheme 7). First, the reaction between 1-phenylpyrazolidin-3-one **20** and 1-alkynylcyclobutanols **21** bearing several electron-rich and electron-poor substituents at different positions on the phenyl ring was explored, affording the desired products in good to high yields. When the standard reaction conditions were applied to 1-alkynylcyclobutanols **21** with para- and meta-substituted phenyl groups, high yields of products were obtained. The usage of 1-(phenylethynyl) cyclobutanols **20** containing an electron-poor or electron-rich group, including halide or methoxy at the ortho-position of the benzene had little effect, and pyrazolo[1,2-*a*] indazole derivatives were achieved with good yields. Even the substrates substituted with heterocyclic naphthyl, thienyl, and pyridyl groups or alkyl groups could be used in the coupling reaction with satisfactory yields. Surprisingly, by the replacement of the cyclobutanol moiety of 1-(phenylethynyl) cyclobutanol with cyclohexanol, a seven-membered ring product **22a** was obtained with good yield. In order to better understand the substrate scope of this [4 + 1] cyclization and ring opening, a series of *N*-arylpyrazolidinones **20** were further tested under standard conditions. The coupling transformations proceeded successfully to form the desired indazoles **22** in moderate and high yields by the introduction of substituents such as -Cl, -Br, -CN, -Me, or -OMe at the para-site and -Cl, -Br, -Me, -OMe at the meta-site of the aryl ring. The *m*-OMe-substituted pyrazolidinone **20** displayed slightly lower regioselectivity for this reaction. Two pyrazolidinones substituted at the 3- and 5-positions were examined, and these delivered the desired products in reasonable yields. However, the [4 + 1] annulation and ring opening failed to form the corresponding products **22** when the ortho-substituted pyrazolidinones **20** possessing steric hindrance were exploited. No product was formed by the replacement of the phenyl moiety of pyrazolidinone **20** with a pyridyl group. The current procedure showed high functional-group tolerance and great efficiency, providing a variety of corresponding compounds **22** in moderate to good yields under mild conditions [59].



Scheme 7. A synthetic route for the preparation of pyrazolo[1,2-*a*] indazoles **22** containing a quaternary carbon in the presence of a Rh(III) catalyst.

2.2. Synthesis of Indazoles Using Ruthenium Salt in the Presence of Sodium Acetate

Ru(II)-catalyzed tandem ortho-carbonylation/amidation/cyclization of 2-aryl-2,3-dihydrophthalazine-1,4-diones **23** has been developed towards the direct assembly of substituted indazolo[1,2-*b*]phthalazine-triones **25**. The reaction conditions involve $[\text{RuCl}_2(p\text{-cymene})]_2$ (5 mol%) and NaOAc (50 mol%) in DCE as a solvent at 40 °C within 4 h under N_2 atmosphere (Scheme 8). The scope and limitations of this tandem ortho-carbonylation/amidation/cyclization strategy with respect to 2-aryl-2,3-dihydrophthalazine-1,4-diones **23** have been explored. In general, good to high yields of the corresponding products were achieved by using meta- and para-substituted substrates **23** with both electron-rich, electron-poor, and halogen functional groups. However, the substrates **23** substituted at the ortho site underwent this tandem reaction only under harsh reaction conditions (DCE at 120 °C for 6 h) to afford the products in moderate to high yields. Plus, disubstituted substrates **23** with substituents located at the meta- and para-sites were amenable to give the desired products in DCE at 40 °C within 4 h, although the substrate with substituents located at the ortho- and para-sites gave the targeted product in DCE only after heating at 120 °C for 6 h. In the case of 6/7-substituted phthalazine derivatives (phthalazine scaffold with 6/7-Me, 6/7-MeO, 6/7-*t*-butyl, 6/7-Br, 6/7-F, and 6/7-Cl), mostly inseparable mixtures of the corresponding products **25a–f** were obtained. Indeed, a mixture of products was obtained, as a mixture of the starting materials was applied in the reaction.

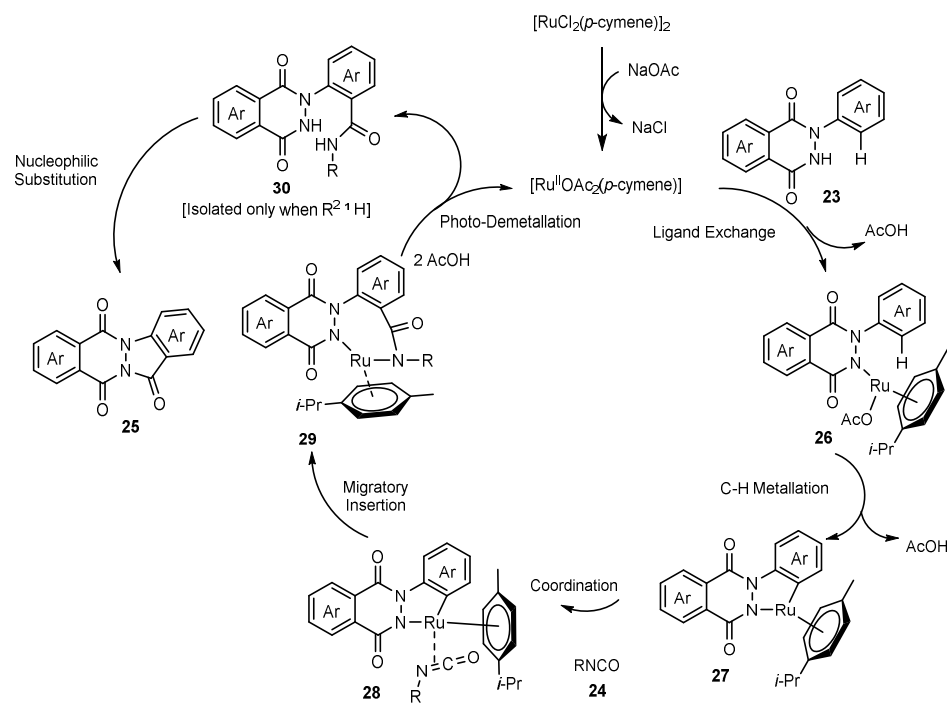


Scheme 8. A synthetic route for the preparation of indazolo[1,2-*b*]phthalazine-trione derivatives **25** from the reaction between 2-aryl-2,3-dihydrophthalazine-1,4-diones **23** and isocyanates **24** under ruthenium catalysis.

Phenylhydrazines containing 5-methyl, 5-methoxy, 5-*t*-butyl, 5-bromo, and 4-fluorophthalic anhydrides provided inseparable mixtures of 6/7-methyl, 6/7-methoxy, 6/7-*t*-butyl, 6/7-bromo, and 5/8-fluoro-2-phenyl-2,3-dihydrophthalazine-1,4-diones **25a–e**, while phenylhydrazine condensation products with 4-chlorophthalic anhydrides provided 5/8-chloro-2-phenyl-2,3-dihydrophthalazine-1,4-dione **25f** as a single regioisomer. The amino, nitro, trifluoromethyl, or cyano functional groups on aryl/phthalazinone moieties did not work under the optimized reaction conditions [21].

A plausible mechanism for this reaction is illustrated in Scheme 9. Initially, an active catalyst was formed in situ from $[\text{RuCl}_2(p\text{-cymene})]_2$ using NaOAc. The monomeric $[\text{Ru}^{\text{II}}\text{OAc}_2(p\text{-cymene})]$ species transferred to **26** via a ligand exchange with N-H of **23**, followed by C–H metalation to deliver a five-membered ruthenacyclic complex **27**. The

catalytic center was then coordinated by the C=N double bond of aryl isocyanate **24**. Next, the migratory insertion of –C=N into a Ru–Ar bond gives a seven-membered ruthenacyclic complex **29**. The protonolysis of the two nitrogens in intermediate **29**, followed by an intramolecular nucleophilic substitution, provided a tetracyclic carbocyclized product **25** [21].

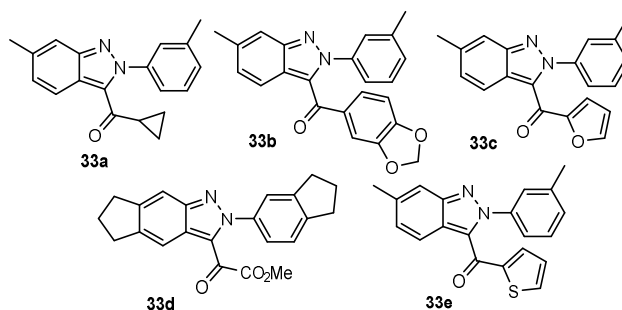
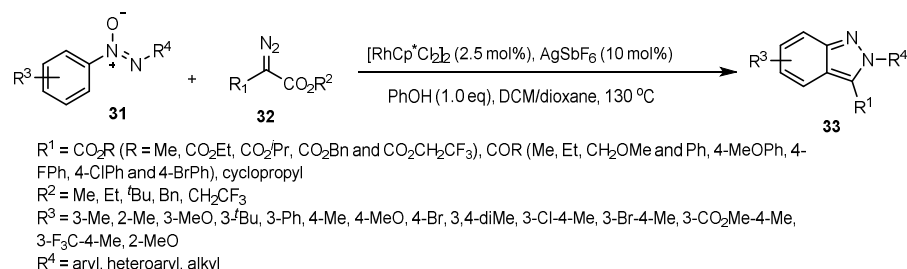


Scheme 9. A rational mechanism for the synthesis of indazolo[1,2-*b*]phthalazine-trione derivatives **25** from the reaction between 2-aryl-2,3-dihydropthalazine-1,4-diones **23** and isocyanates **24** under ruthenium catalysis.

2.3. Synthesis of Indazoles Using Rhodium Complexes and Silver Salts

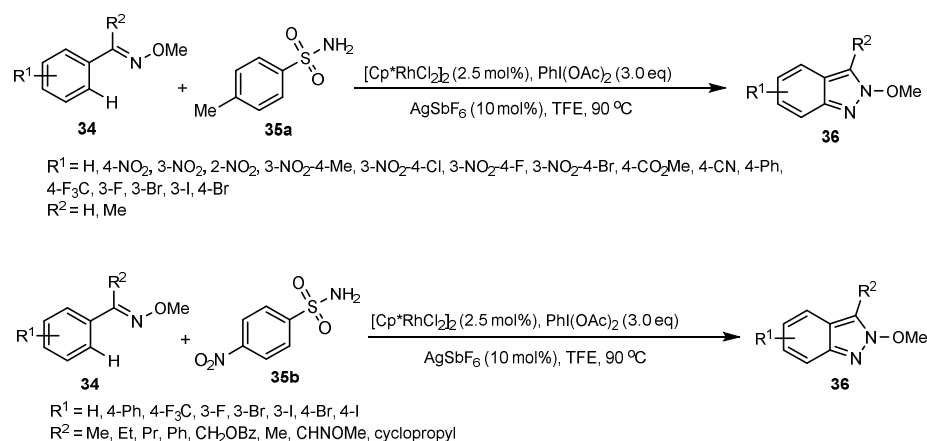
An interesting methodology for the synthesis of 3-acyl-2*H*-indazoles **33** was performed using a Rh(III)-catalyzed tandem C–H alkylation/intramolecular decarboxylative cyclization of azoxy compounds **31** with diazoesters **32**. The combination of catalytic amounts of [Cp*RhCl₂]₂/AgSbF₆ in the presence of PivOH in DCE/dioxane plays a crucial role to afford the corresponding products at 130 °C within 24 h. In this research, azoxy scaffold **31** was introduced as an incorporated directing group for regio- and chemoselective [4 + 1] cyclization, which could be promoted by diverse symmetrical and unsymmetrical di- and mono-aryldiazene oxides. The feasibility of the coupling of symmetrical and unsymmetrical di- and mono-aryldiazene oxides with diazoesters **32** was explored under standard conditions. First, several diazoesters **32** were investigated, affording *H*-indazoles. While the diisopropyl 2-diazomalonate led to a high yield, diazoester containing *t*-Bu led to a moderate yield, assumably owing to the easy hydrolysis of this functional group under the optimized reaction conditions. Moreover, α -diazo- β -keto esters participated in this annulation to the corresponding products in good to high yields. Generally, a wide range of functional-group tolerance for both α -diazo- β -alkyl keto esters and α -diazo- β -(hetero)aryl keto esters highlights this strategy for the regio- and chemoselective synthesis of 2*H*-indazoles. However, when diazoesters with *N*-heterocycles, including methyl 2-diazo-3-oxo-3-(pyridin-2-yl)propanoate, methyl 2-diazo-2-(pyridin-2-yl)acetate, and methyl 2-(benzo[d]thiazol-2-yl)-2-diazoacetate, were used under optimized reaction conditions, no product was formed. The diazo reagents including EtO₂C-CHN₂, EtO₂C-C(CH₃)N₂, EtO₂C-CPhN₂, and EtO₂C-C(CF₃)N₂ also did not work with this catalytic system. While symmetrical azoxybenzenes substituted at the ortho, meta, and para-positions of aryl rings could be applicable in this reaction, azoxybenzenes substituted at the meta-position of aryl rings delivered a fairly low yield, conceivably

because of steric congestion. The azoxybenzenes substituted at the ortho-position could be exploited as coupling partners, with coupling occurring exclusively in the sterically less hindered site. Some more complex molecules **33a–e** are shown in Scheme 10. The advantages and benefits of this transformation are regioselectivity for unsymmetrical azoxybenzenes and the compatibility of monoaryldiazeno oxides [60].



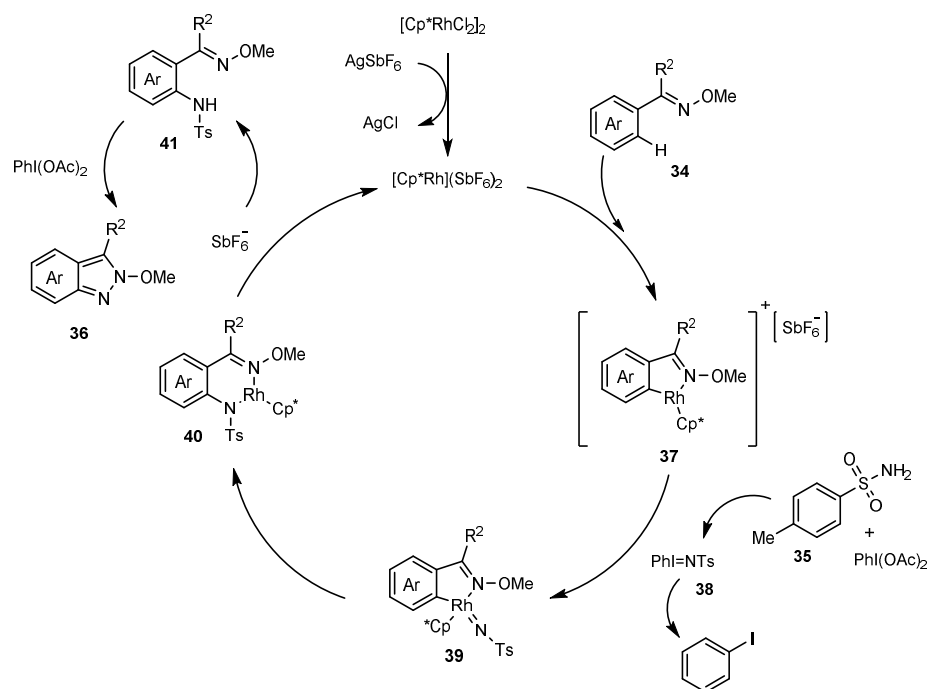
Scheme 10. A synthetic route for the preparation of 2H-indazoles derivatives **33** via the regio- and chemoselective [4 + 1] annulation of azoxy compounds **31** with diazoesters **32** under rhodium catalysis.

The rhodium(III)-catalyzed synthesis of indazole derivatives **36** has been realized through an intermolecular C–H amination and N–N bond formation sequence starting from readily available ketoxime ethers **34** and 4-toluenesulfonamide **35a** (Scheme 11). All reactions were carried out using 2.5 mol% of [Cp**RhCl*₂]₂ as a catalyst, 0.6 mmol PhI(OAc)₂, and 10 mol% of AgSbF₆ in trifluoroethanol (TFE) at 90 °C for 24 h. First, the functional-group tolerance of the ketoxime derivatives **34** was explored under optimized reaction conditions. Although the reaction of meta- or para-nitro-substituted acetophenone oxime derivatives was successfully carried out to afford moderate to good yields of desired products, the 2-nitrobenzaldehyde oxime methyl ether only gave the corresponding indazole **36** in a moderate yield due to steric effects on the aryl ring. The unsubstituted acetophenone oxime derivatives were all suitable for this system, leading to desired indazoles in satisfactory yields. In the next step, both *p*-ester- and cyano-substituted acetophenone oxime ethers were proven to be appropriate substrates for this transformation as well. The acetophenone oxime derivative exhibited less efficacy in this oxidative annulation, affording the expected indazole in a 15% yield. Afterward, the authors investigated more amides to address the low reactivity of 4-toluenesulfonamide **35a** in this reaction. The results showed that phenylsulfonamides **35b** containing electron-deficient substituents produced better yields of the target indazoles **36**. Several substituted acetophenone oxime ethers **34** derived from propiophenone, *n*-butyrophenone, cyclopropyl phenyl ketone, and diphenylketone exhibited good compatibility for the reaction with 4-nitrobenzenesulfonamide **35b**. Notably, substituents such as F, Br, I, and CF₃ on the aromatic ring of the acetophenone oxime ethers all survived the reaction conditions, affording the desired products **36** in good yields. To sum up, a broad range of substituents were possible with this catalytic system, producing different functionalized indazoles with acceptable yields [61].



Scheme 11. A synthetic route for the preparation of indazoles derivatives **36** via the oxidative annulation of ketoxime methyl ethers **34** with sulfonamide **35a–b** under rhodium catalysis.

The mechanism involves (Scheme 12) the electrophilic activation of Rh by chloride removal with the silver salt, the coordination of ketoxime ether **34** with an active catalyst, and C–H activation, respectively, to form the complex **37**. This complex is oxidized in the presence of in situ-generated iodonium **38** to give the complex **39**. In the next step, migratory insertion and releasing $[\text{Cp}^*\text{Rh}](\text{SbF}_6)_2$ as the active complex occurs to form **41**. Finally, target product **36** is obtained via the reaction with iodobenzene diacetate [61].

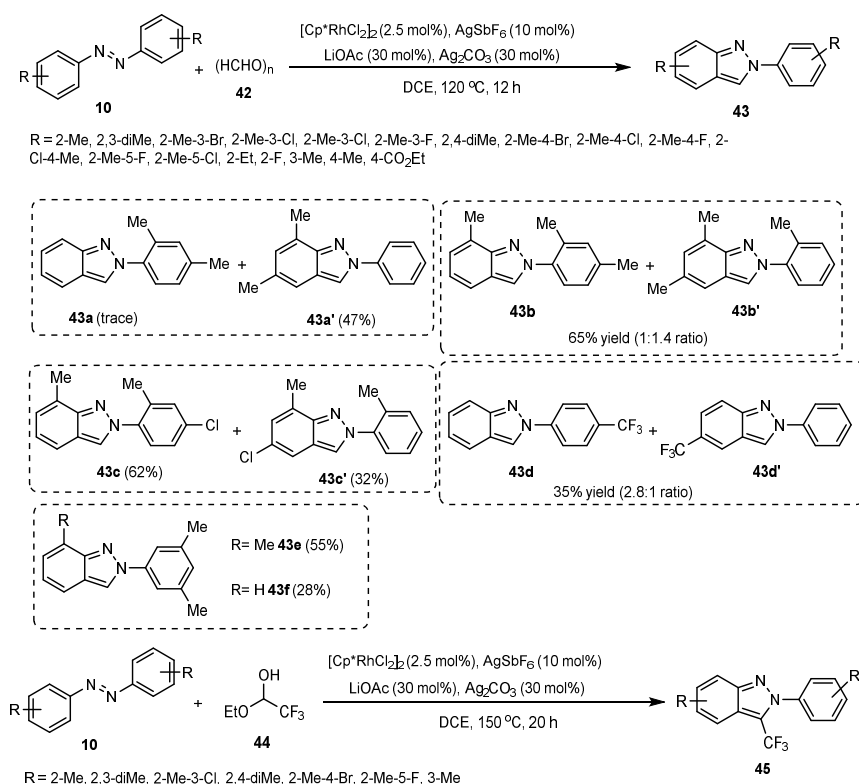


Scheme 12. A possible mechanism for the synthesis of indazole derivatives **36** via the oxidative annulation of ketoxime ethers **34** with sulfonamide **35** under rhodium catalysis.

2.4. Synthesis of Indazoles Using Rhodium and Silver Salts in the Presence of Lithium Acetate

The synthesis of C3-unsubstituted and C3-trifluoromethylated (2*H*)-indazoles starting from azobenzenes **10** and paraformaldehyde **42** as a useful C1-feedstock under rhodium catalysis was reported by Kim et al. in 2019. The strategy was also successfully expanded to C–H activation/annulation reactions of azobenzenes **10** with trifluoroacetaldehyde hemiacetal **44**. The optimized conditions for the synthesis of (2*H*)-indazoles **43** and **45** from azobenzenes **10** included 2.5 mol% of $[\text{RhCp}^*\text{Cl}_2]_2$, 10 mol% of AgSbF_6 , 30 mol% of LiOAc ,

and 30 mol% of Ag_2CO_3 in DCE as a solvent at 120 °C for 12 h (or 150 °C for 20 h) under air atmosphere in sealed reaction tubes. LiOAc and AgSbF_6 were used to activate the Rh catalyst by forming $[\text{Cp}^*\text{Rh(III)(OAc)}]\text{SbF}_6$. Various symmetrical ortho-, meta-, and para-substituted azobenzenes underwent coupling, with paraformaldehyde **42** showing good functional-group tolerance. While symmetrical 2,5-disubstituted azobenzenes (5-fluoro-2-methyl azobenzene and 5-chloro-2-methyl azobenzene) were well-tolerated and the desired products were obtained in 58% and 12% yields, respectively, sterically congested 2,5-dimethyl azobenzene failed to afford the corresponding product. In the next step, several unsymmetrical azobenzenes were screened as substrates, and the products **43a–d** and **43a'–43d'** were obtained (Scheme 13). Notably, the steric environment of the azobenzene orients the formation of desired products **43e–f**. The substrate scope of this reaction was further expanded to trifluoroacetaldehyde ethyl hemiacetal **44** to produce a range of C3- CF_3 -substituted (2*H*)-indazoles **45** in moderate to high yields. This conversion efficiently afforded several C3-unsubstituted and C3-trifluoromethylated (2*H*)-indazoles **43** and **45**, which are important molecules in organic chemistry and pharmaceutical sciences. The practicability of this approach is highlighted by its chemoselectivity, functional-group tolerance, and wide substrate scope [62].



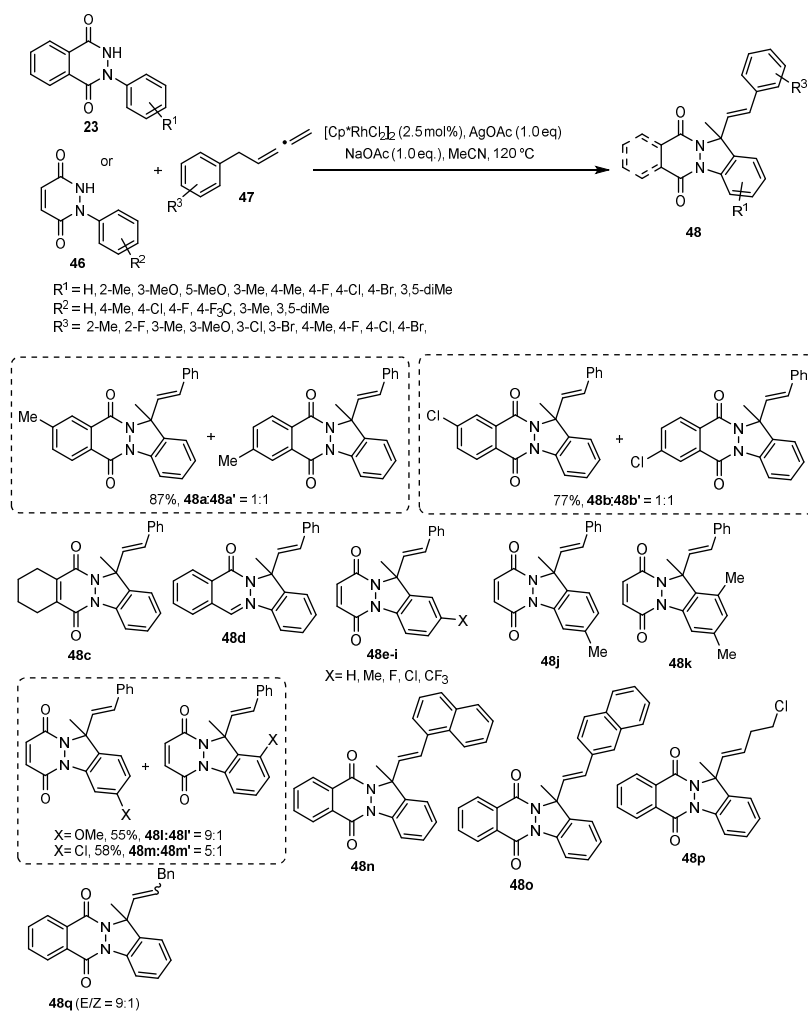
Scheme 13. A synthetic route for the preparation of 1*H*-indazole derivatives **43** and **45** from azobenzenes **10** using paraformaldehyde **42** as a one-carbon synthon or trifluoroacetaldehyde ethyl hemiacetal **44**.

2.5. Synthesis of Indazoles Using Rhodium and Silver Salts in the Presence of Sodium Acetate

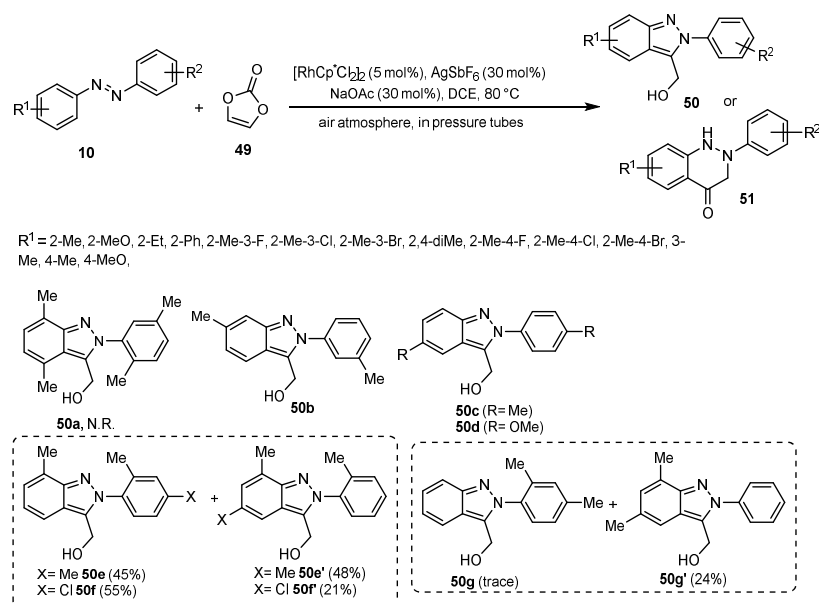
Yu's group developed an efficient and novel Rh(III)-catalyzed annulation transformation between phthalazinones/pyridazinones **23** and **46** and different allenes **47** into indazole derivatives **48** containing a quaternary carbon (Scheme 14). A C–H activation and olefin insertion sequence, followed by β -hydride elimination and intramolecular annulation occurs to produce indazole derivatives **48** using a catalytic amount of $[\text{Cp}^*\text{RhCl}_2]_2$ in the presence of AgOAc in MeCN at 100 °C within 12 h under air atmosphere. The active Rh catalyst is formed in situ by the ion exchange of chloride to acetate involving $[\text{Cp}^*\text{RhCl}_2]_2$ and $\text{AgOAc}/\text{NaOAc}$. In other words, acetate ions replace chloride ligands to give $[\text{Cp}^*\text{Rh(OAc)}_2]_2$. *N*-Aryl phthalazinone and pyridazinone substrates bearing a

range of electron-rich electron-poor substituents at different positions could deliver the corresponding products in satisfactory yields. The [4 + 1] cyclization of the substrate substituted by methyl at the ortho-position of the *N*-aryl affords the desired product in only a 26% yield because of steric hindrance. On the other hand, the reaction of the *N*-aryl substrate with methyl at the meta-position demonstrated remarkable reactivity and excellent chemoselectivity, while the corresponding meta-methoxy analogs gave an isomeric mixture in a 9:1 ratio. Para-substituted *N*-aryl phthalazinone substrates **23** with a variety of electron-rich and electron-poor functional groups can be easily transformed into the desired indazoles **48** in good to high yields under standard reaction conditions. It is worth noting that the substrate substituted by two methyl groups at the 3 and 5 positions of the *N*-aryl segment worked well to give the corresponding product in a good yield. The products **48a** and **48b** could be formed with moderate selectivity (1:1). The products **48c** and **48d** were also obtained under standard conditions. The target compounds **48e–m** were also achieved via this [4 + 1] cyclization in good yields. The substrate scope of a variety of allenes **47** substituted by several electron-donating or electron-deficient groups at different positions gave the corresponding products in acceptable to high yields. 1-Naphthyl- or 2-naphthyl-group-substituted allenes and aliphatic allene were also well-tolerated under these reaction conditions, thus producing the corresponding indazoles **48n–q** in good to high yields. Notably, a long-chain aryl-substituted substrate yielded the desired product **48q** with good selectivity (*E/Z* = 9:1) in a high yield. Finally, 1,1,4-trisubstituted and simple aliphatic allenes containing an ester group did not work under optimized reaction conditions. The approach successfully tolerates different substituents on the starting phthalazinones/pyridazinones and allenes and features practicability, high atom efficiency, and high *Z*-selectivity [63].

The synthesis of C3-hydroxymethylated (*2H*)-indazoles **50** can be achieved through a subsequent Rh(III)-catalyzed C–H functionalization/intramolecular cyclization between azobenzenes **10** and vinylene carbonate **49** using catalytic amounts of [RhCp*Cl₂]₂, AgSbF₆, and NaOAc in DCE at 80 °C within 14 h under air atmosphere in pressure tubes (Scheme 15). The electronic properties of the azobenzene rings can orient towards the construction of (*2H*)-indazoles **50** or the isomeric dihydrocinnolin-4-ones **51**. It is worth noting that the vinylene carbonate substrate plays a significant role in the promotion of the [4 + 1] or [4 + 2] cyclization. The substrate scope and limitations of the azobenzenes **10** were tested under optimized reaction conditions. The coupling transformations were successful for ortho-substituted azobenzenes containing electron-donating substituents, obtaining moderate to high yields of C3-hydroxymethylated (*2H*)-indazoles. This catalytic system allows moderate functional-group tolerance, particularly for –F, –Cl, and –Br substituents. No corresponding product **50a** was formed by the utilization of sterically congested 2,5-dimethyl-substituted azobenzene. Meta- and para-methyl substituted azobenzenes were also applicable using this catalytic system, although the desired products **50b** and **50c** were obtained with relatively low yields. Moreover, para-OMe azobenzene was proven to be an efficient substrate, producing **50d** in good yield. This exploration was further extended to the coupling of unsymmetrical azobenzenes with vinylene carbonate **49**. For example, azobenzenes containing electron-donating substituents on both aryl rings afforded almost equimolar ratios of **50e** and **50e'** under standard conditions. In the case of other unsymmetrical azobenzenes, the transformation mainly occurred on the more electron-donating aromatic ring, as for **50f** (**50f'**) and **50g** (**50g'**). Furthermore, it was shown that no C3-hydroxymethylated (*2H*)-indazole was obtained using azobenzenes containing electron-poor substituents, and only 2,3-dihydrocinnolin-4-ones **51** were formed via [4 + 2] annulation transformation. When unsubstituted azobenzene was used as a substrate in the reaction, a mixture of both (*2H*)-indazole and 2,3-dihydrocinnolin-4-one was produced. The notable benefits of this methodology are mild reaction conditions and excellent functional group compatibility, thus furnishing easy access to a series of indazoles of interest in organic chemistry and pharmacy [64].

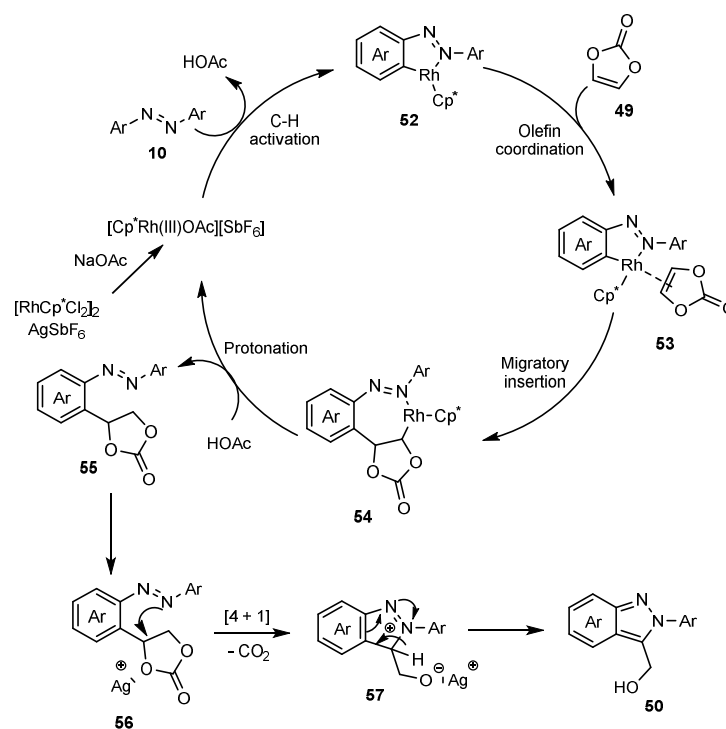


Scheme 14. A synthetic route for the preparation of indazole derivatives **48** through the C–H activation of phthalazinones **23** or pyridazinones **46** and allenes **47** under Rh(III) catalysis.



Scheme 15. A synthetic route for the preparation of 2H-indazole derivatives **50** via the annulation of azobenzenes **10** with vinylene carbonate **49** under Rh(III) catalysis.

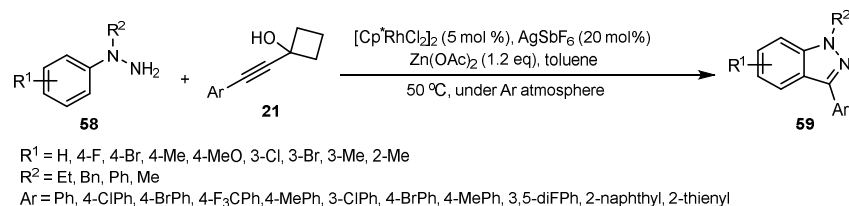
The mechanism for the synthesis of (2*H*)-indazoles **50** via the annulation of azobenzenes **10** with vinylene carbonate **49** under Rh(III) catalysis is illustrated in Scheme 16. First, the active catalyst is formed from $[\text{RhCp}^*\text{Cl}_2]_2$ and AgSbF_6 in the presence of NaOAc . The C–H bond of azobenzene **10** is activated to deliver a five-membered rhodacycle intermediate **52**. Subsequently, complex **52** undergoes olefin coordination, migratory insertion, and protonation to afford the ortho-alkylated compound **55**. In the next step, Ag^+ acts as a Lewis acid to activate the nucleophilic substitution of an azo group at the α -position on the dioxolan-2-one scaffold, followed by an aromatization transformation to produce (2*H*)-indazole **50** [64].



Scheme 16. A possible mechanism for the synthesis of 2*H*-indazole derivatives **50** via the annulation of azobenzenes **10** with vinylene carbonate **49** under Rh(III) catalysis.

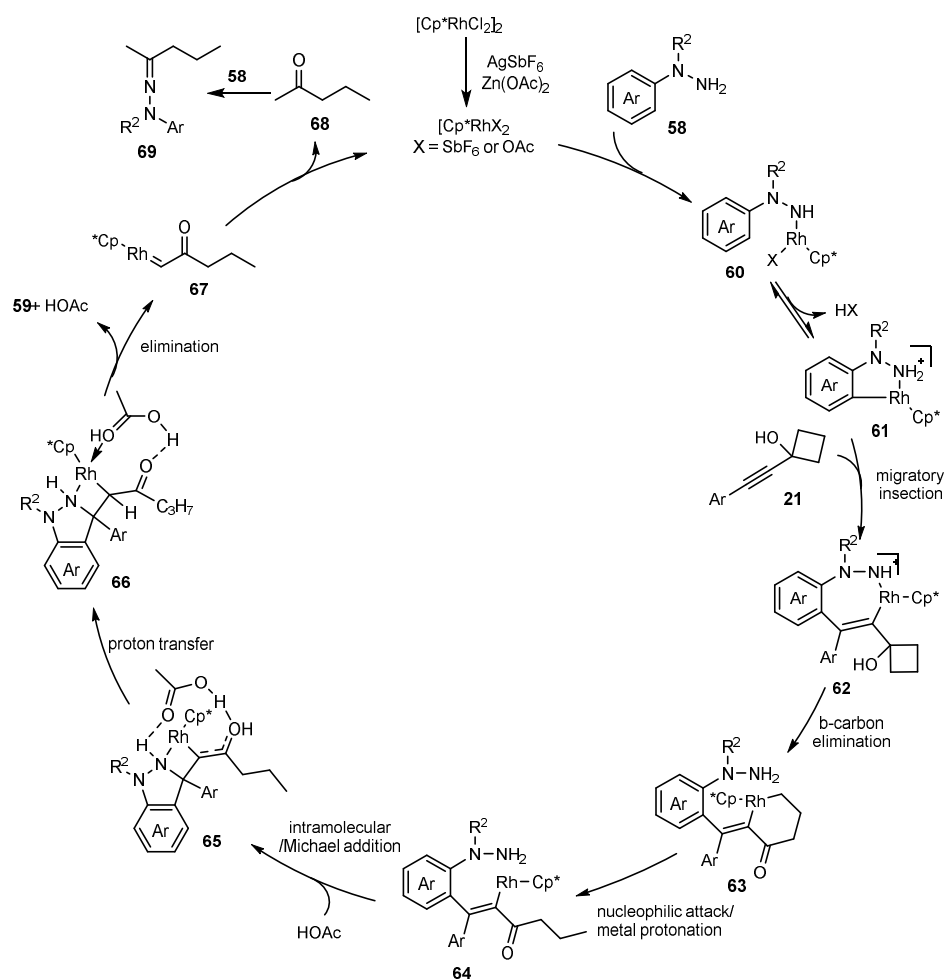
2.6. Synthesis of Indazoles Using Rhodium and Silver Salts in the Presence of Zinc Acetate

The commercially available $[\text{Cp}^*\text{RhCl}_2]_2$ has been exploited as a catalyst for the reaction of phenylhydrazines **58** with 1-alkynylcyclobutanols **21** in the presence of SbF_6 and $\text{Zn}(\text{OAc})_2$ in toluene at 50 °C for 24 h under Ar atmosphere (Scheme 17). Apparently, the reaction proceeds via a hydrazine-directed C–H functionalization process. This catalytic system provided an efficient protocol to produce 1*H*-indazole derivatives **59** via [4 + 1] annulation based on the cleavage of an alkyne bond with good functional group compatibility and moderate to good yields. First, the substrate scope of 1-arylethynyl cyclobutanols **21** was investigated, and all the results showed that 1-arylethynyl cyclobutanol derivatives containing both electron-deficient and electron-rich substituents on the para- or meta-sites of the benzene ring could afford the corresponding indazoles **59** in acceptable yields. It was found that di-fluoro or 2-thienyl substituted substrates could deliver the corresponding indazole in satisfactory yields using AgNO_3 instead of AgSbF_6 . In the next step, several arylhydrazines substituted at the position of the aryl-linked nitrogen were screened. While 1-ethyl and 1-benzyl phenylhydrazines delivered the corresponding indazoles **59** in good yields, the *N*-phenyl substituted substrate did not work in this reaction, presumably because of its higher steric hindrance. Arylhydrazines containing halides such as F, Cl, and Br as well as electron-rich substituents such as Me and OMe provided the desired products in satisfactory yields. Notably, 1-alkyl-1-phenylhydrazines substituted at the ortho-position were compatible under optimized reaction conditions [65].



Scheme 17. A synthetic route for the preparation of 1*H*-indazoles **59** via hydrazine-directed C–H functionalization with 1-alkynylcyclobutanols **21**.

The first step of the mechanism comprises the activation of a rhodium catalyst using $\text{AgSbF}_6/\text{Zn}(\text{OAc})_2$. In the case of $\text{Zn}(\text{OAc})_2$, apparently the zinc ion itself plays no role, and only the acetate ion activates the Rh catalyst (Scheme 18). Then, the hydrazine group of **58** coordinates to the metal center of this active complex. Next, C(aryl)–H activation, regioselective migratory insertion, and β -carbon elimination happen to form a six-membered rhodacycle intermediate **63**. In the next step, an intramolecular nucleophilic attack of phenyl hydrazine nitrogen on rhodium(III) ion affords intermediate **64**. Finally, the target molecule **59** is formed via an intramolecular Michael addition, a proton transfer, and releasing a rhodium-carbene **67** [65].

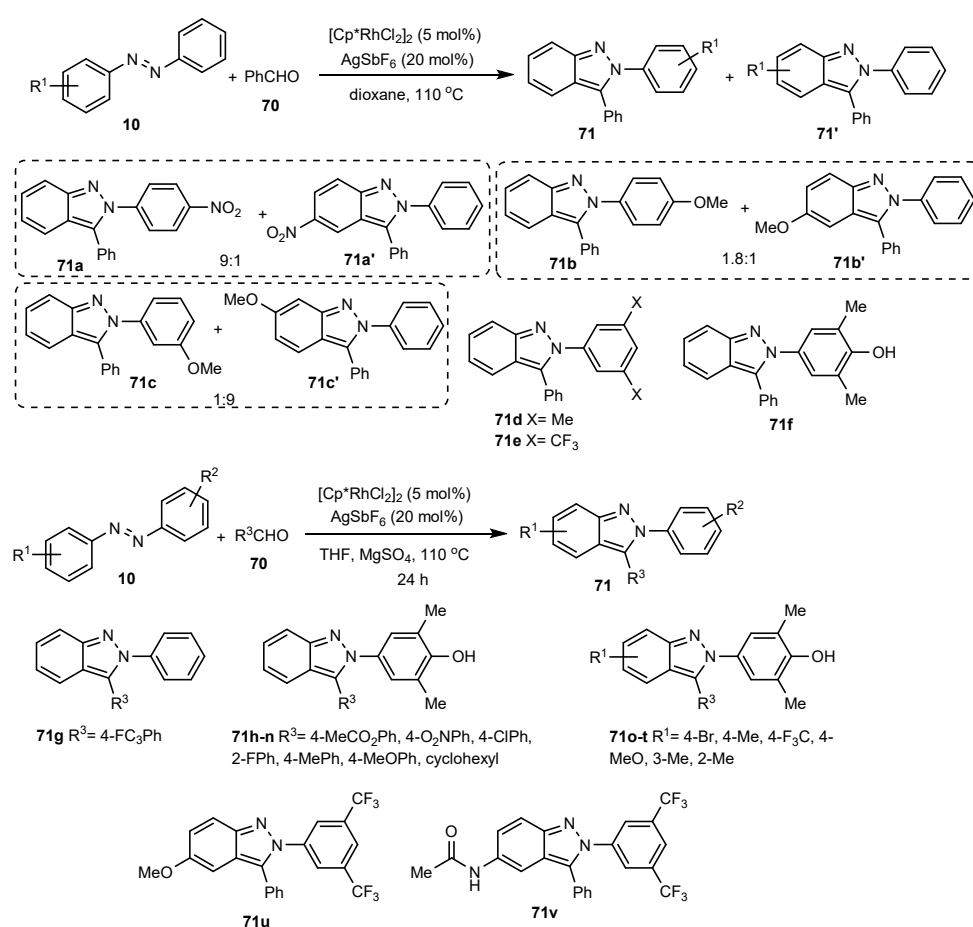


Scheme 18. A plausible mechanism for the synthesis of 1*H*-indazoles **59** via hydrazine-directed C–H functionalization with 1-alkynylcyclobutanols **58**.

2.7. Synthesis of Indazoles Using Rhodium and Silver Salts in the Presence of Magnesium Sulfate

A convenient transformation for the construction of substituted *N*-aryl-2*H*-indazole derivatives **71** through the reaction of azobenzenes **10** with aldehydes **70** in a simple, effi-

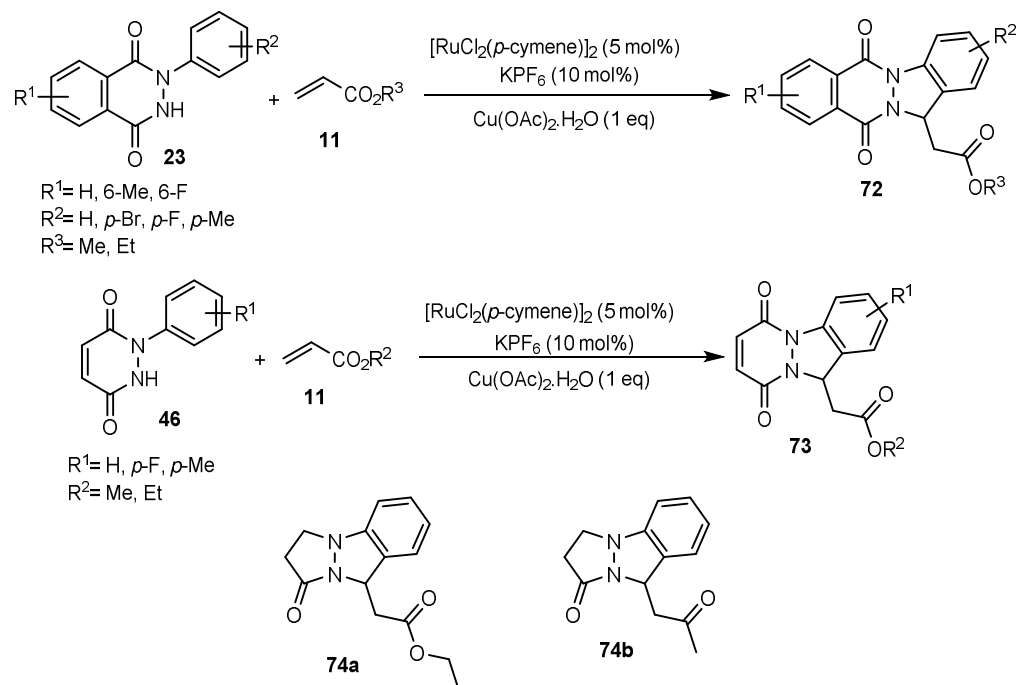
cient, and one-step process was reported by Ellman et al. in 2013 (Scheme 19). The reactions proceeded well to give the corresponding indazoles **71** by Rh(III)-catalyzed C–H bond functionalization and cyclative capture. The reaction of azobenzene with benzaldehyde was promoted by 5 mol% (Cp^*RhCl_2)₂ and 20 mol% AgSbF_6 in dioxane at 80 °C for 24 h. Whereas the unsymmetrical para-nitro azobenzene provided major product **71a** by annulation on the more electron-rich phenyl ring of the azobenzene, 4-methoxy-substituted azobenzene produced a mixture of products **71b** and **71b'** in low selectivity in which a C–H activation/annulation sequence occurred on the less electron-donating phenyl ring of the azobenzene. In contrast to para-nitro substituted azobenzene, the 3-methoxy substituted substrate afforded a mixture of products with 9:1 regioselectivity, favoring **71c'** with C–H activation on the more electron-donating phenyl ring. This fact displayed the capacity of meta-MeO for supplying resonance stabilization. The high regioselectivity observed for the synthesis of products **71d–f** indicated that steric effects are important. In the case of hydroxy-substituted azobenzene, the yield of product **71f** could be improved by the utilization of MgSO_4 as a drying agent and THF as a solvent. Next, aromatic aldehydes bearing both electron-deficient and electron-donating substituents proved to be suitable in the reaction with a 4-hydroxy-3,5-dimethylphenyl azobenzene substrate, leading to good to high yields of products **71h–v**. Notably, aliphatic aldehyde provided the desired indazole **71n** in a low yield. This reaction offers remarkable advantages, including the simplicity of the reaction, excellent regioselectivity, good functional-group tolerance, and the exploitation of commercially available materials [66].



Scheme 19. A synthetic route for the preparation of indazole derivatives **71** via C–H bond functionalization and cyclative capture.

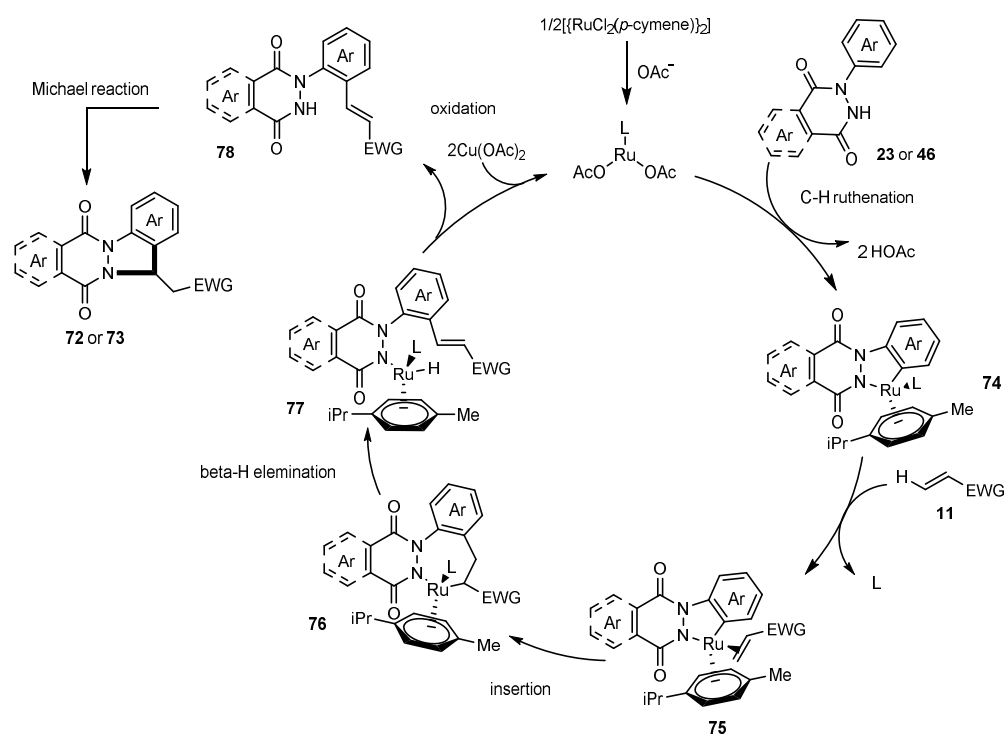
2.8. Synthesis of Indazoles Using Ruthenium and Copper Salts in the Presence of Potassium Hexafluorophosphate

A Ru-catalyzed cascade reaction between *N*-aryl phthalazinediones **23** or *N*-aryl pyridazinediones **46** with acrylates proceeded through a subsequential oxidative alkenylation/intramolecular cyclization in aqueous media as a green solvent (Scheme 20). All reactions proceeded successfully in the presence of $[\text{RuCl}_2(\textit{p}\text{-cymene})]_2$ (5 mol%) as a catalyst, KPF_6 (10 mol%) as an additive, and $\text{Cu}(\text{OAc})_2 \cdot \text{H}_2\text{O}$ (1 eq) as an oxidant to provide moderate to high yields of products. The limitations and diversity of this alkenylation–annulation via C–H bond activation were explored with respect to *N*-aryl phthalazinedione **23** and *N*-aryl pyridazinediones **46** derivatives. *N*-Aryl phthalazinediones **23** and *N*-aryl pyridazinediones **46** containing electron-deficient or electron-rich substitutions on the aromatic rings afforded the desired indazole derivatives **72** with moderate to excellent yields. The reaction conditions did not work for methyl methacrylate. Moderate yields of desired products **74a** and **74b** were achieved by using substrates bearing a pyrazolidinone scaffold [67].



Scheme 20. A synthetic route for the preparation of indazole derivatives **72**, **73**, and **74** via an alkenylation–annulation approach.

Subsequent oxidative vinylation and annulation are the key steps for this transformation. A possible mechanism for the reaction is shown in Scheme 21. The transformation is initiated by N–H assisted C–H bond ruthenation of compound **23** or **46** to construct a ruthenacycle complex **74**. Next, migratory insertion, β -hydride-elimination, and reductive elimination occurred to form alkenylated product **78**. Eventually, an intramolecular aza-Michael addition reaction took place to produce the target indazoles **72** or **73** [67].



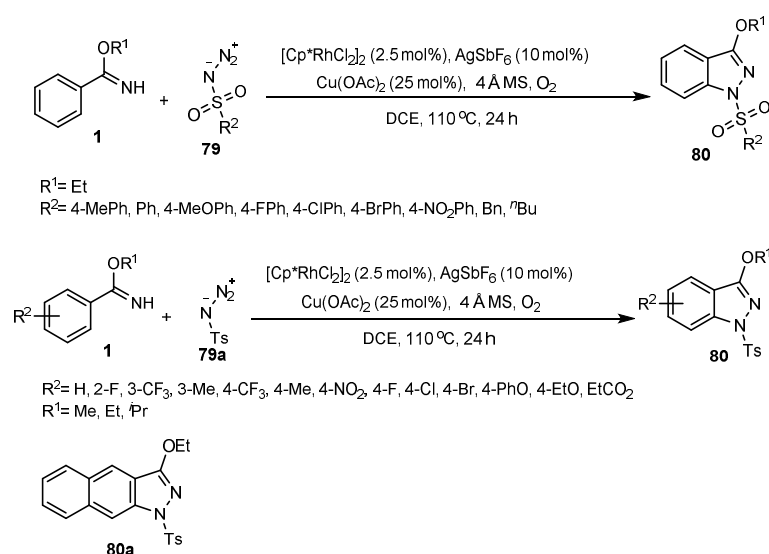
Scheme 21. A plausible mechanism for the synthesis of indazole derivatives **72** or **73** via an alkenylation–annulation approach.

2.9. Synthesis of Indazoles Using Rhodium, Copper, and Silver Salts

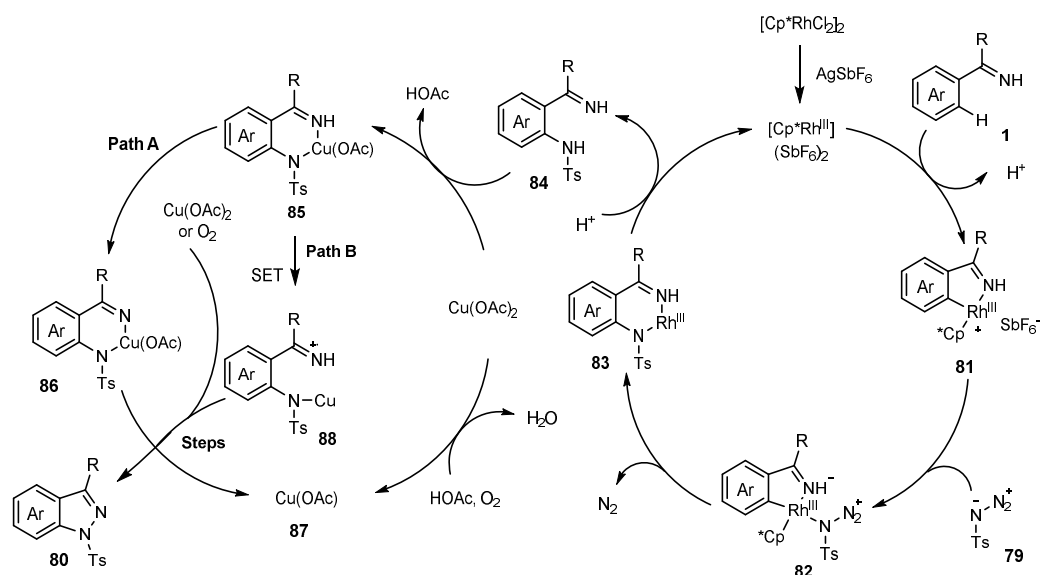
In 2013, Glorius and co-workers developed a process involving Rh(III)-catalyzed C–H activation/C–N bond formation and Cu-catalyzed N–N bond formation under mild reaction conditions for the synthesis of substituted 1*H*-indazoles **80** using $[\text{Cp}^*\text{RhCl}_2]_2$, $\text{Cu}(\text{OAc})_2$, and AgSbF_6 catalysts and molecular oxygen as the oxidant (Scheme 22). For the first time, in this study, it was possible to perform the transformation of N-H-imidates **1** to corresponding compounds **80**. Diverse arylsulfonyl azide derivatives **79** with 4-Me, 4-OMe, 4-NO₂, 4-F, 4-Cl, and 4-Br as substituents as well as alkylsulfonyl azides **79** ($\text{R}_2 = \text{Bn}, \text{Bu}$) demonstrated moderate to high reactivity in this conversion. Several arylimidates were exploited to explore the reactivity of different substituents in the alkoxy and arene parts. The ethylimidate **1** ($\text{R}_4 = \text{OEt}$) revealed a more satisfactory yield than methyl **1** ($\text{R}_4 = \text{OMe}$) and isopropyl **1** ($\text{R}_4 = \text{O-}i\text{-Pr}$) derivatives. Contrary to the electron-donating arylimidates, the electron-withdrawing imidates afforded better yields for this transformation. This cascade reaction is practical, scalable, and green, using O₂ as the stoichiometric oxidant. In addition, only N₂ and H₂O are the byproducts of this reaction. It is worth noting that indazole was formed with a <5% yield when omitting either of the Rh or Cu catalysts for the model reaction, denoting the important role of these two catalysts in the mechanism cycle [68].

Mechanistically, the construction of indazoles **80** comprises the steps shown below in Scheme 23. First, the active catalyst (cationic $[\text{Cp}^*\text{Rh}^{\text{III}}]$) is obtained in situ using AgSbF_6 to remove the chloride. Subsequently, coordination to imidate **1** and C–H activation are performed by the active catalyst to give rhodacyclic complex **81**. The coordination of azide substrate **79** to the catalyst followed by nitrogen loss and migratory insertion yields Rh^{III} amido species **83**. The resulting intermediate **83** is protonated to regenerate the active catalyst and provide the amidated compound **84**. In the next step, the resulting compound may coordinate to the copper source to form intermediate **85**. The authors considered two paths for the continuation of the mechanism. In route A, the Cu^{II} complex is transferred to a higher valent Cu^{III} complex in the presence of another molecule of $\text{Cu}(\text{OAc})_2$ or O₂. Next, the construction of the N–N bond via reductive elimination formed the target compound **80**. In the final step, Cu^I complex **87** is transformed to $\text{Cu}(\text{OAc})_2$ in the presence of O₂.

As shown in Scheme 23, the alternative route **B** is able to produce a N–N bond through double single-electron transfer [68].



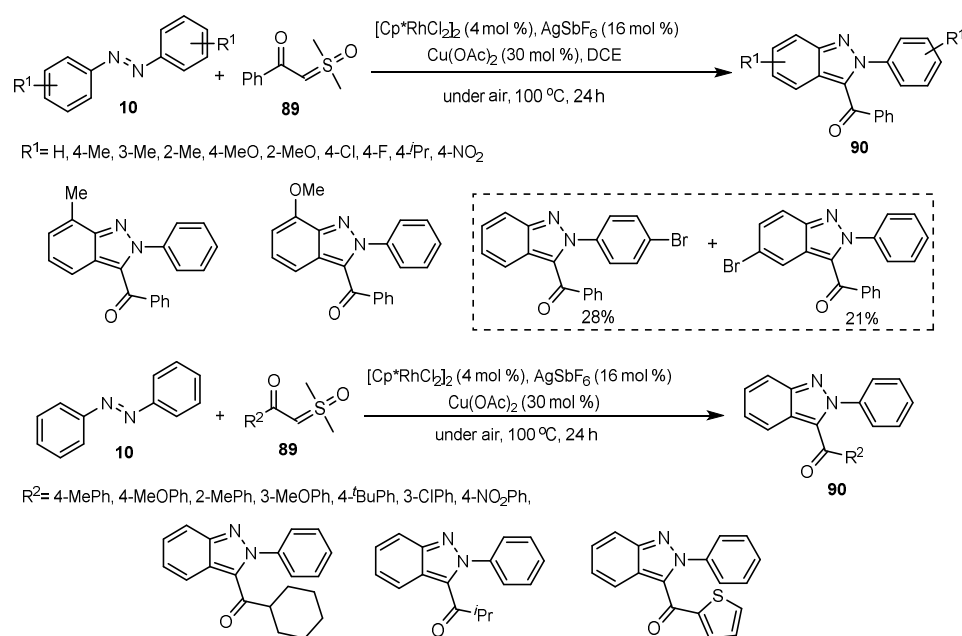
Scheme 22. A synthetic route for the preparation of 1*H*-indazole derivatives **80** via C–H amidation and N–N bond formation.



Scheme 23. A rational mechanism for the synthesis of 1*H*-indazole derivatives **80** via C–H amidation and N–N bond formation.

An efficient strategy for the synthesis of 3-acyl-(2*H*)-indazoles **90** via an Rh(III)/Cu(II)-catalyzed [4 + 1] annulation of azobenzenes **10** with α -carbonyl sulfoxonium ylides **89** has been developed by Cheng et al. (Scheme 24). The sequential catalytic aromatic C–H bond activation and cyclization steps in which sulfoxonium ylides **89** served as efficient and stable carbene precursors are highly important in the chemical synthesis of the corresponding indazoles **90**. The model reaction produced 3-acyl-(2*H*)-indazole in a 20% yield in the absence of $\text{Cu}(\text{OAc})_2$ in DCE under air at 100 °C within 24 h. The scope and limitation of azobenzene derivatives **10** and α -carbonyl sulfoxonium ylide derivatives **89** as starting materials were explored, as illustrated in Scheme 24. Some functional groups on azobenzene rings, such as methyl, methoxy, Cl, F, *i*-Pr, and Br, were very compatible under the optimized reaction conditions with moderate to high yields. The reaction progressed efficiently

by using sterically hindering substituents on the azobenzene ring under standard reaction conditions. As expected, with *m*-substituted substrates, the corresponding indazole derivatives were produced at the less hindered position. Unfortunately, the 4-nitro analogue of azobenzene failed to work. Unsymmetrical azobenzenes with Me and MeO groups were also explored, indicating the orientation of electron-rich aryl rings for the C–H activation and cyclization transformations. Next, sulfoxonium ylides with both electron-donating and electron-withdrawing substitutions were investigated. Several substitutions such as Me, MeO, Cl, NO₂, and *t*-Bu as well as alkyl- and heteroaryl-substituted analogues were found to be appropriate under standard reaction conditions. The reaction displayed a broad substrate scope, moderate to excellent yields, and tolerance to various substituents [69].

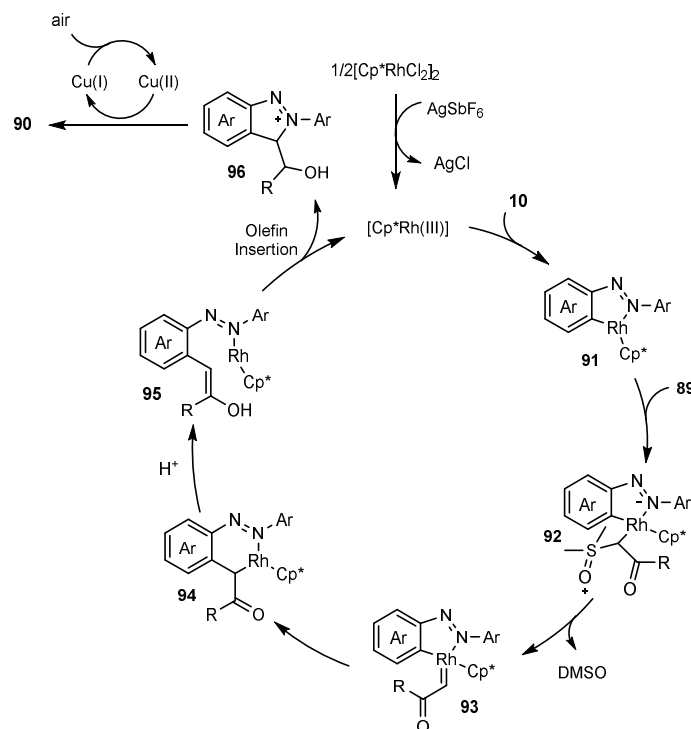


Scheme 24. A synthetic route for the preparation of 3-Acyl-(2H)-indazoles **90** via the [4 + 1] annulation of azobenzenes **10** with α -carbonyl sulfoxonium ylides **89**.

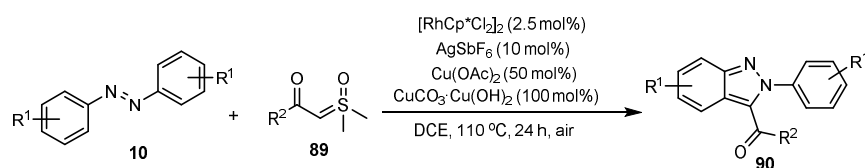
Initially, the catalyst is activated in the presence of AgSbF₆. Next, the Rh(III) catalyst activates the C–H bond of azobenzenes **10** to deliver five-membered cyclorhodium species **91**. Rh(III) intermediates **92** are generated by the insertion of sulfoxonium ylides **89** to the rhodium species. Six-membered rhodacycle species **94** are obtained via the α -elimination of DMSO followed by the migratory insertion of carbene complex **93**. The sequence of keto-enol tautomerization, the insertion of a C=C bond into the Rh–N bond, and the oxidation/aromatization in the presence of a copper catalyst produces **95**, **96**, and final products **90**, respectively (Scheme 25) [69].

The Rh(III)-catalyzed ortho-C–H bond activation of azobenzenes **10**, followed by the intramolecular annulation transformation of azobenzenes **10** between sulfoxonium ylides **89**, has been reported for the synthesis of 2H-indazole derivatives **90** in good to excellent yields with broad substrate scope, good selectivity, and good functional-group tolerance (Scheme 26). The combination of [RhCp*Cl₂]₂, AgSbF₆, Cu(OAc)₂, CuCO₃·Cu(OH)₂, and DCE at 110 °C for 24 h under air atmosphere in reaction tubes was found to be effective for this transformation. Next, the scope of these annulation reactions was examined, and the results are summarized in Scheme 26. The reactions using electron-rich para-substituted azobenzenes (such as Me, Et, and *t*-Bu) afforded the expected indazoles in excellent yields. Furthermore, the electron-rich meta- and ortho-substituted azobenzenes (such as OMe and Br at the meta-position or OMe, Me, and Et at the ortho-position) were explored, and a variety of indazoles were successfully produced in good to excellent yields. An electron-deficient azobenzene (CO₂Et at the para-position) was also applicable to this

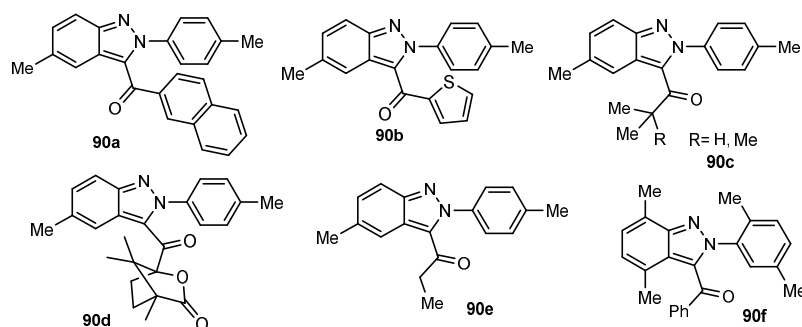
reaction, which afforded the corresponding product in a moderate yield, while electron-deficient meta-substituted azobenzenes (Br and F in the meta-position) were proven to be relatively less efficient for this transformation. Although a sterically congested disubstituted azobenzene (two methyl groups at the 2- and 5-positions) did not give the desired product, by employing disubstituted azobenzenes (two methyl groups at the 2- and 4-positions or two methyl groups at the 2- and 3-positions) as substrates, the corresponding products were achieved in good yields. The steric congestion of product **90f** may be the reason of why 2,5-disubstituted azobenzene did not work in the reaction [70].



Scheme 25. A plausible mechanism for the synthesis of 3-acyl-(2H)-indazoles **90** via the [4 + 1] annulation of azobenzenes **10** with α -carbonyl sulfoxonium ylides **89**.

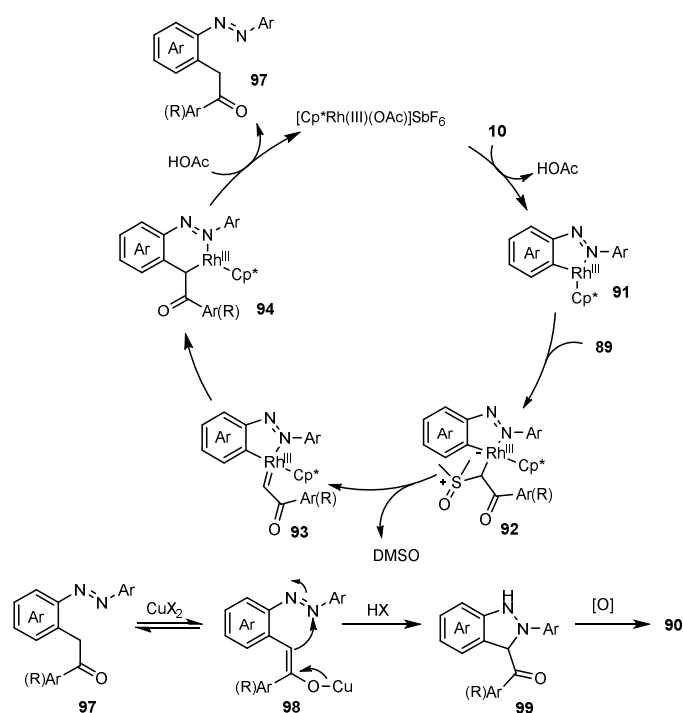


R¹= H, 4-Me, 4-Et, 4-CO₂Et, 3-MeO, 3-Me, 3-Br, 3-F, 2-MeO, 2-Et, 2-Me, 2,4-diMe, 2,3-diMe,
R²= Ph, 4-Me, 4-MeO, 4^tBu, 4-Ph, 3-F, 3-Cl, 3-Br, 3-CF₃, 2-Me, 2-MeO, 2-F, 2-Cl, 2-Br



Scheme 26. A synthetic route for the preparation of 2H-indazoles **90** through the annulation reaction of azobenzenes **10** with sulfoxonium ylides **89**.

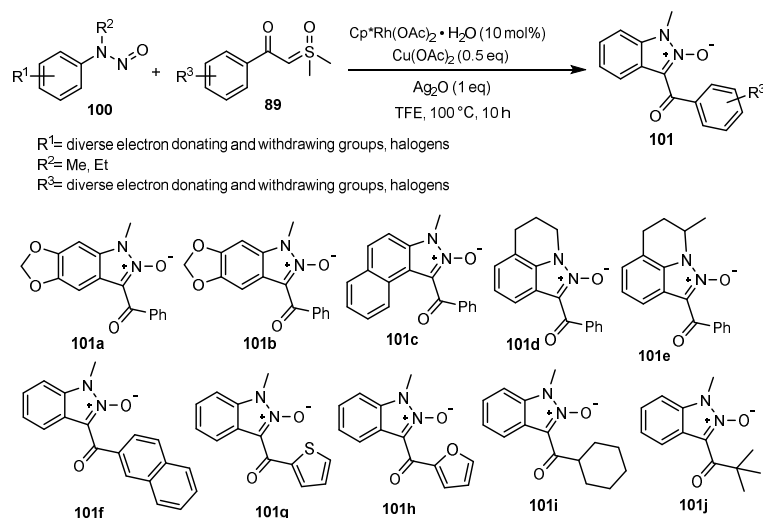
A plausible reaction mechanism for the Rh(III)/Cu(II) catalyzed synthesis of indazoles **90** is shown in Scheme 27. The mechanism comprises the coordination of the azo group to the Rh(III) catalyst, C–H bond activation, the coordination of sulfoxonium ylides **89**, and the α -elimination of DMSO to give a reactive α -oxo Rh-carbene species **93**. In the next step, migratory insertion and, subsequently, protonation occur to provide **97**. Base-mediated intramolecular annulation and oxidation by copper or O₂ take place to afford 3-acyl (2*H*)-indazoles **90** [70].



Scheme 27. A possible mechanism for the synthesis of 2*H*-indazoles **90** through the annulation reaction of azobenzenes **10** with sulfoxonium ylides **89**.

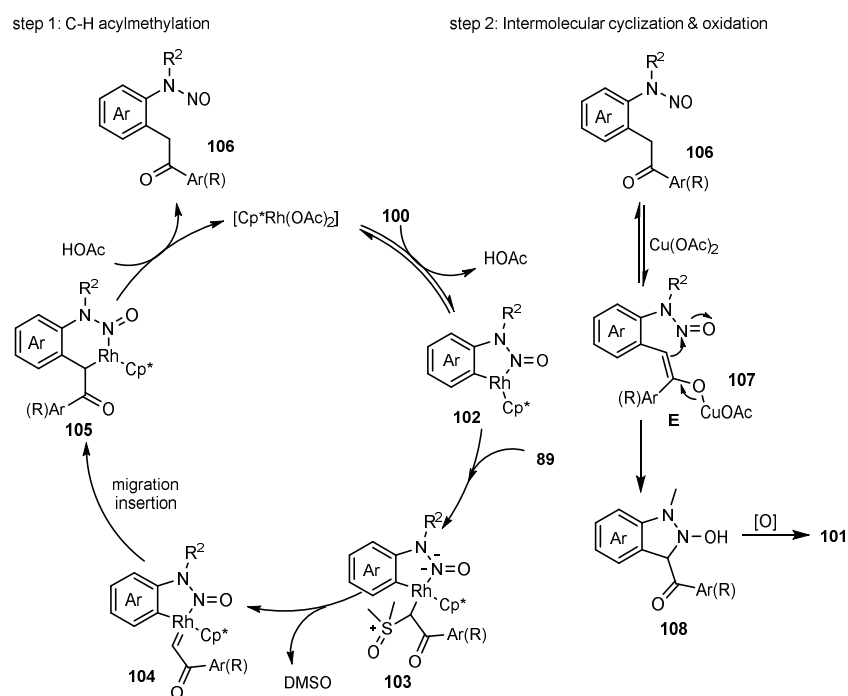
The successful use of *N*-nitrosoanilines **100** in which the *N*-nitroso group plays a dual role as a traceless directing group and an internal nitrosation reagent in the reaction with several sulfoxonium ylides **89** through the Rh(III)/Cu(II)-catalyzed C–H activation and cyclization reaction was demonstrated by Huang et al. in 2020 (Scheme 28). Thus, the subsequent oxidative [4 + 1] annulation reactions of various *N*-nitrosoanilines **100** with sulfoxonium ylides **89** were conducted using $\text{Cp}^*\text{Rh}(\text{OAc})_2 \cdot \text{H}_2\text{O}$ (10 mol%), $\text{Cu}(\text{OAc})_2$ (0.5 eq), and Ag_2O (1 eq) in TFE at 100 °C for 10 h. This simple and efficient strategy could be utilized for the synthesis of diverse substituted indazole *N*-oxides **101** with powerful reactivity, good functional-group tolerance, moderate to good yields, and atom- and step-economic reactions under mild conditions. Notably, this unique annulation approach indicates a previously unobserved reactivity model for the *N*-nitroso functional group. The scope and limitations of this cascade acylmethylation/annulation transformation were tested using the reaction of a variety of *N*-nitrosoanilines **100** and sulfoxonium ylides **89**. In general, a diverse array of functional groups (various electron-donating groups and halides) on the *o*-, *m*-, and *p*- positions of *N*-nitrosoaniline rings were possible under these conditions. In the case of *m*-Cl-substituted *N*-nitrosoanilines, a mixture of regioisomers was obtained. *N*-nitrosoanilines bearing two substituents exhibited moderate performances, providing desired products **101a** and **101b**. *N*-alkyl-*N*-nitrosophthylamines with different alkyls substituted on the amino group and substituted *N*-nitroso-tetrahydroquinoline were also tolerated, furnishing good to high yields of products **101c–e**. It is noteworthy that sulfoxonium ylides with one or two substitutions on different positions of the aryl ring were very good partners under the standard conditions, achieving moderate to high yields.

The naphthyl-derived substrates heterocyclic and alkyl ylides were next examined using this catalytic system, showing moderate yields of **101f–j** [71].



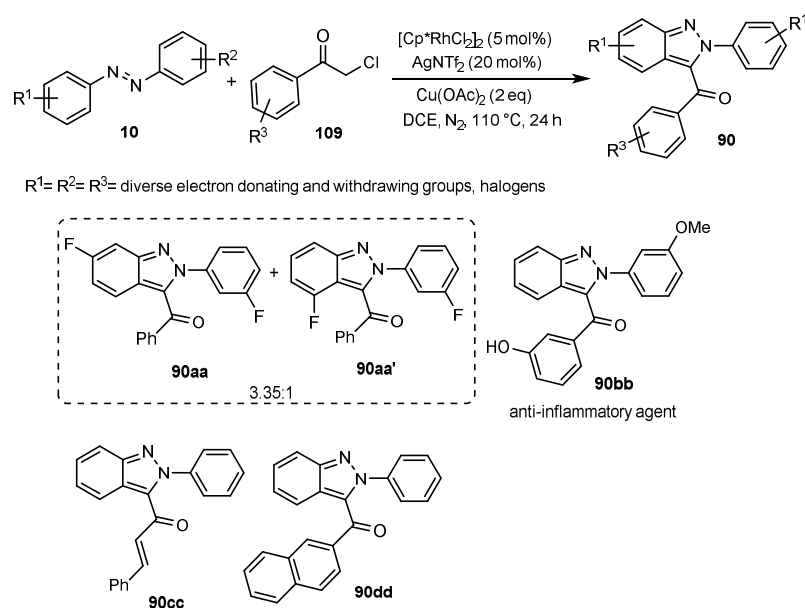
Scheme 28. A synthetic route for the preparation of substituted indazole *N*-oxides **101** via the tandem acylmethylation/annulation of *N*-nitrosoanilines **100** with sulfoxonium ylides **89**.

A reasonable mechanism is illustrated in Scheme 29. In the first step, coordination/*C–H* activation with a Rh catalyst affords complex **102**. The insertion of sulfoxonium ylide to the metal center of the previous complex produces a Rh(III) intermediate **103**, followed by releasing a DMSO molecule from **103**. Subsequently, the resulting rhodium α -oxo carbene species **104** carry out the migratory insertion of the Rh–C bond to provide a six-membered rhodacyclic intermediate **105**. In the next step, the acylmethylated intermediate **106** is obtained by the protonolysis of the Rh–N and Rh–C bonds. Subsequently, the final product **101** is generated from **106** by $\text{Cu}(\text{OAc})_2$ -mediated intramolecular annulation and oxidation in the presence of either Ag_2O or $\text{Cu}(\text{II})$ additives [71].



Scheme 29. A rational mechanism for the synthesis of substituted indazole *N*-oxides **101** via the tandem acylmethylation/annulation of *N*-nitrosoanilines **100** with sulfoxonium ylides **89**.

Interesting molecular architectures were achieved by the Rh(III)/Cu(II)-catalyzed [4 + 1] cyclization of azobenzenes **10** with α -Cl ketones **109** in excellent yields for more than 30 examples (Scheme 30). The generality and scope of 3-acyl-2*H*-indazoles synthesis by performing the annulation of azobenzenes **10** with α -Cl ketones **109** were screened. It was shown that this transformation could tolerate diverse starting materials bearing a variety of functional groups in both azobenzenes **10** and α -Cl ketones **109** and provided the desired products **90** in good to excellent yields. Generally, azobenzenes **10** with both electron-donating and -withdrawing functional groups at the *o*, *m*, and *p* positions as well as alkyl-, alkoxy-, or halogen-substituted azobenzenes afforded the desired products in moderate to good yields. It was observed that *m*-F substitution led to a mixture of two regioisomers, **90aa** and **90aa'**, in which the less hindered position was favored. Meanwhile, an unsymmetrical azobenzene-containing methoxy group was annulated with α -Cl ketone containing hydroxy at the *m* position to form an anti-inflammatory agent **90bb** with a high yield in a regioselective manner. Alkyl or heterocyclic azo compounds as substrates have not been applicable in this catalytic system. Various monosubstituted α -Cl ketones and disubstituted α -Cl ketones were able to undergo this cascade C–H activation/annulation reaction smoothly with azobenzenes to afford the corresponding products in moderate to excellent yields. As a result, substituent effects have no large effect on the yields, although strong electron-withdrawing groups on the α -Cl acetophenone aryl ring seem to be more practical for this cascade reaction. Moreover, alkenyl- and naphthyl-substituted scaffolds **90cc–dd** were also successfully used in the reaction to afford the corresponding products in moderate to good yields.

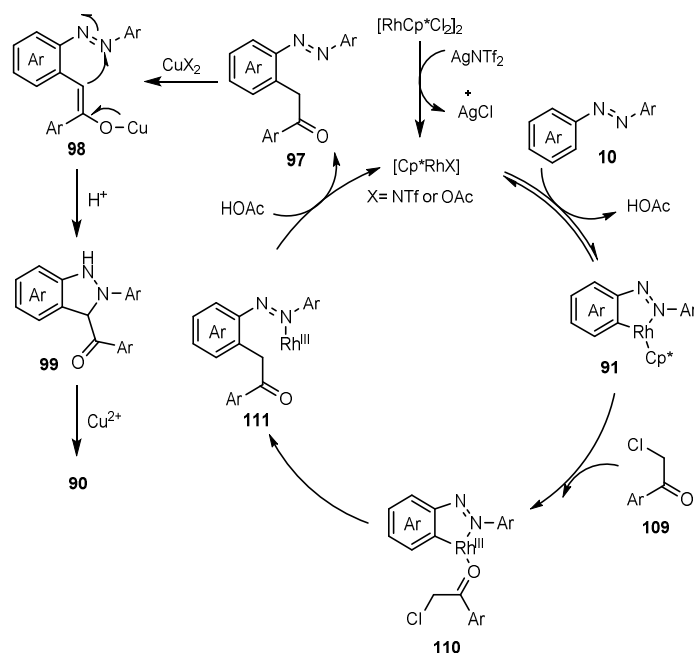


Scheme 30. A synthetic route for the preparation of 3-acyl-2*H*-indazoles **90** via the annulation of azobenzenes **10** with α -Cl ketones **109**.

Reactions occurred with high efficiency and with extensive functional-group tolerance under mild reaction conditions. It is worth noting that the efficient production of 3-acyl-2*H*-indazole **90bb** with anti-inflammatory activity in one step ensures the practicability of this approach [72].

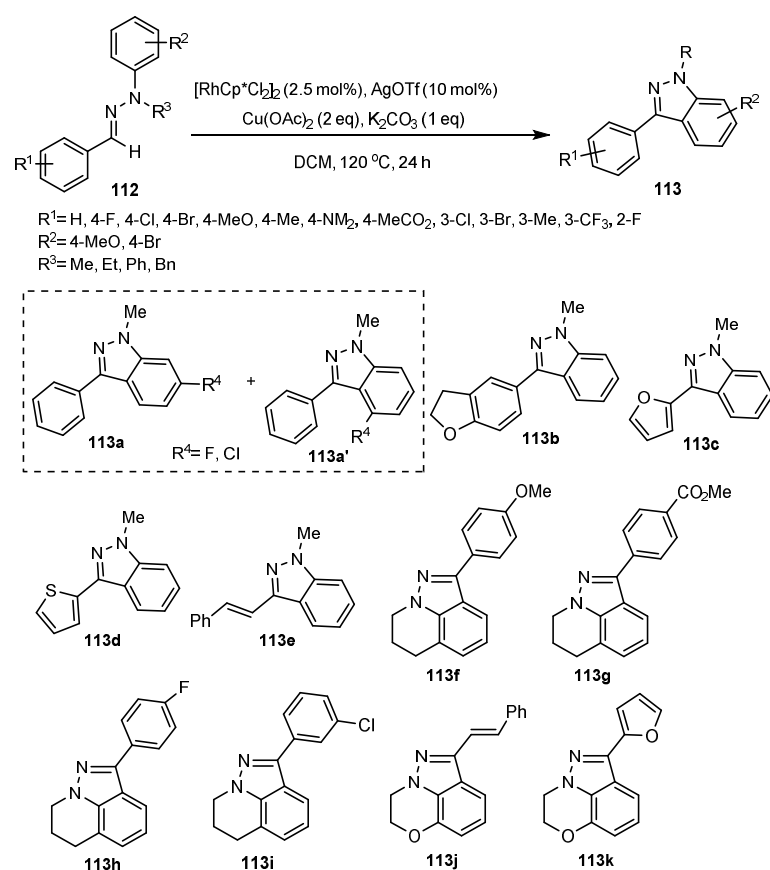
A reasonable mechanistic pathway is shown in Scheme 31. The subsequent coordination of azobenzenes **10** with the Rh(III) catalyst and C–H bond activation give a five-membered rhodacyclic intermediate **91**. The α -Cl acetophenones **109** coordinate to Rh(III), followed by C–C bond formation. *N*-protonation takes place to produce α -arylketone species **97** along with the regeneration of the Rh(III) catalyst. Enol-tautomerization,

intramolecular annulation, and oxidation transformations occur in the presence of Cu(II) species to produce target molecules **90** [72].



Scheme 31. A rational mechanism for the synthesis of 3-acyl-2-*H*-indazoles **90** via the annulation of azobenzenes **10** with α -Cl ketones **109**.

An efficient and novel C–H activation and C–H/C–H cross-coupling strategy has been developed to realize the synthesis of functionalized 1*H*-indazoles **113** from easily accessible aldehyde phenylhydrazones **112** (Scheme 32). Optimization studies showed that the best yields could be achieved by performing the reaction using a catalytic amount of $(\text{RhCp}^*\text{Cl}_2)_2/\text{AgOTf}$, with $\text{Cu}(\text{OAc})_2$ as the oxidant and K_2CO_3 as the base at 120 °C in 1,2-dichloroethane. Initially, the scope of the substrates with respect to different *N*-alkyl (Me, Et, and Bn) or aryl groups was tested. It was observed that these functional groups had only a moderate effect on the reaction, generating the desired compounds in very good to high yields. Whereas benzaldehyde derivatives **112** containing different electron-rich and electron-poor functional groups on the para- or meta-positions of the aryl ring yielded good to high yields of the corresponding indazoles, ortho-substituted benzaldehyde derivatives displayed less efficacy in this reaction, delivering the corresponding indazole **113** in a low yield. Heteroaromatics such as furan- and thiophene-aldehyde starting materials were also well-tolerated under this catalytic strategy, leading to the expected indazoles in acceptable yields. In the case of substrates substituted at the meta-position of the *N*-aryl ring, the regioselectivity was moderate, showing a mixture of products **113a** and **113a'** that had reacted at both positions. Some complex products **113b–k** synthesized by this methodology are illustrated in Scheme 32. In order to highlight the importance of this strategy, the authors extended the procedure to an easy preparation of certain important and bioactive products. These significant products displayed good 5-HT₄/5-HT₃ receptor antagonist activity. This transition metal strategy reveals good scalability, good functional-group compatibility, wide substrate scope, and moderate to high yields under mild reaction conditions. The combination of mechanistic experiments and DFT calculations indicates C(aryl)-H bond activation followed by a C(aldehyde)-H bond activation, and the reductive elimination process occurs to form a variety of targeted products **113** [73].

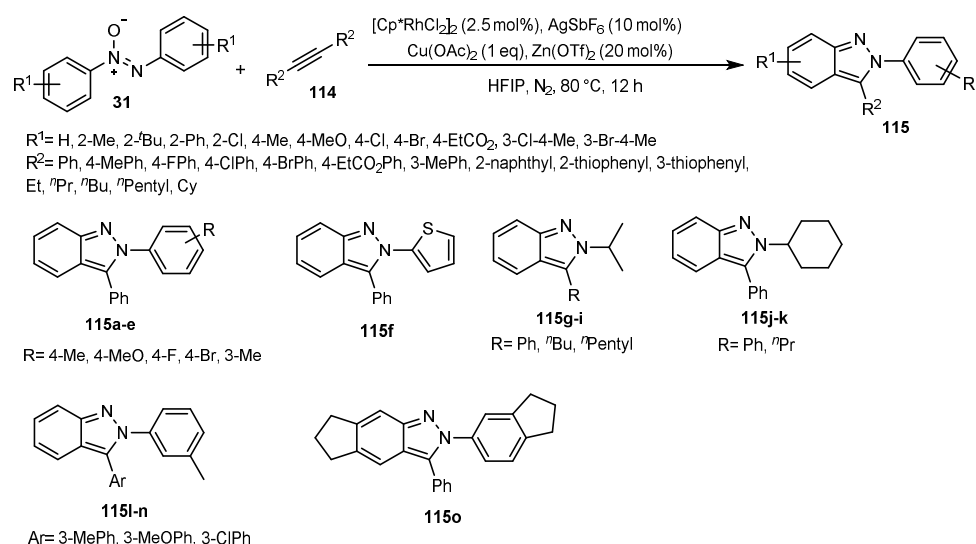


Scheme 32. A synthetic route for the preparation of functionalized 1*H*-indazole **113** via the double C–H activation of aldehyde hydrazones **112**.

2.10. Synthesis of Indazoles Using Rhodium, Silver, Copper, and Zinc Salts

Efficient rhodium(III)-catalyzed regioselective C–H activation/cyclization of an azoxy compound **31** with an alkyne **114** as the coupling partner has been realized via a [4 + 1] cycloaddition rather than a normal [4 + 2] mode (Scheme 33). The processes of cyclative capture, oxygen-atom transfer, and C≡C triple bond cleavage are the key steps of this reaction. The coupling of azoxy compounds **31** with alkynes **114** was conducted using [Cp*RhCl₂]₂ (2.5 mol%) as a precatalyst, AgSbF₆ (10 mol%), Cu(OAc)₂ (1.0 equiv), Zn(OTf)₂ (20 mol%), and HFIP (1.0 mL) under N₂ at 80 °C for 12 h. It seems AgSbF₆ and Cu(OAc)₂ are exploited to activate the Ru catalyst before or during the catalytic cycle. The authors mentioned no exact role for the Lewis acid Zn(OTf)₂. Initially, the generality of this catalytic system was studied with respect to the azoxy substrates **31**. The reactions with symmetrical azoxybenzenes containing electron-rich substituents including Me, *t*-Bu, and OMe as well as electron-withdrawing substituents such as F, Cl, Br, and COOEt proceeded smoothly to give indazoles **115** in moderate to excellent yields. It is worth noting that a variety of meta-substituted azoxybenzenes were used in the reaction to produce the corresponding products **115** in good to high yields while reacting at the less sterically hindered position. The strategy could also be extended to unsymmetrically substituted diaryldiazeno oxide substrates **31** (leading to **115a–n**). Even the monoaryldiazeno oxide substrates were well-tolerated and successfully reacted with diphenylacetylene to produce the expected indazoles **115g–k** in satisfactory yields. While the reaction was compatible with a wide range of azoxybenzenes, substrates functionalized by substituents such as Me, OMe, Cl, and Br at the ortho-position of the NO-phenyl ring failed to give corresponding products, probably due to steric congestion. Furthermore, the scope and limitations of the reaction were tested by the exploitation of alkyne substrates. As summarized in Scheme 33, different symmetrical diarylalkynes with both electron-rich and electron-poor substituents were successfully

utilized under the optimized reaction conditions, which gave indazoles **115** in moderate to good yields. It is noteworthy that this catalytic system showed complete compatibility with diarylacetylene substrates bearing 2-naphthyl, 2-thienyl, or 3-pyridyl scaffolds as well as dialkylalkyne substrates. Bis(trimethylsilyl)acetylene or monosubstituted alkyne substrates failed in this [4 + 1] annulation reaction. This strategy demonstrates various outstanding features, such as broad substrate scope, good functional-group tolerance, and operational convenience, which enable regioselective access to different 2*H*-indazoles **115** in moderate to high yields [74].



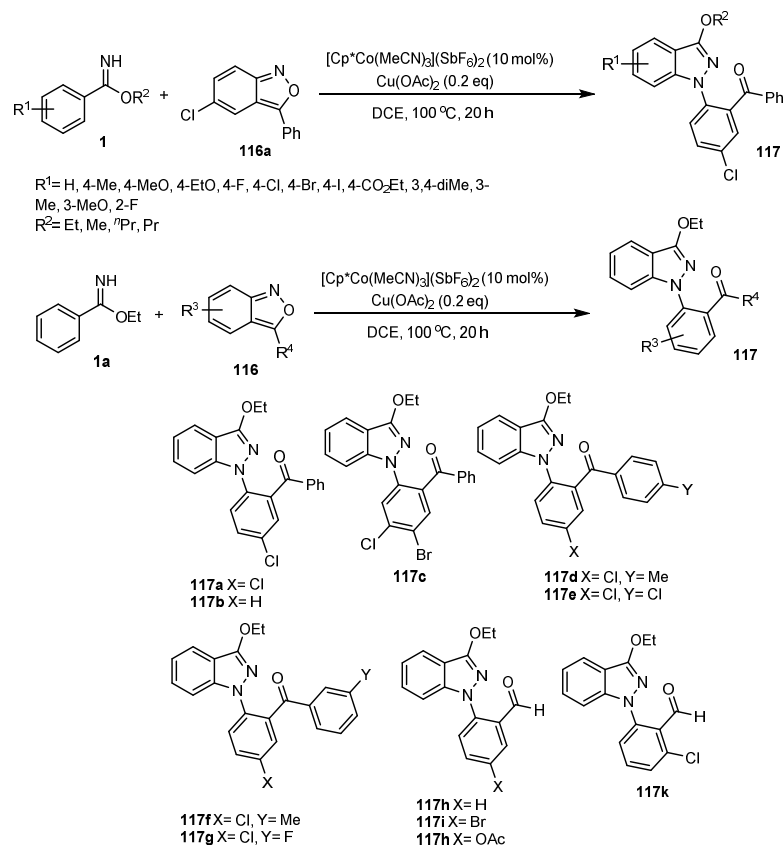
Scheme 33. A synthetic route for the preparation of 2*H*-indazole derivatives **115** via the [4 + 1] annulation of azoxy compounds **31** with alkynes **114**.

2.11. Synthesis of Indazoles Using Cobalt and Copper Salts

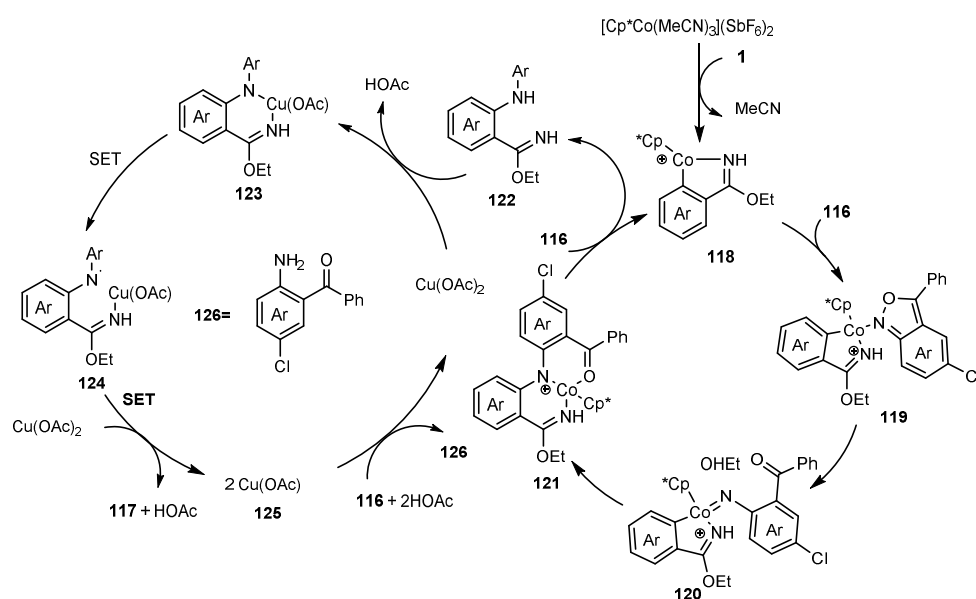
A Co/Cu-catalyzed C–H activation/oxidative coupling of imidate esters **1** with anthranils **116** in DCE at 100 °C (sealed tube) under N_2 atmosphere within 20 h for the synthesis of 1*H*-indazole derivatives **117** was described by Li et al. (Scheme 34). In this paper, anthranils **116** were exploited as novel bifunctional aminating reagents and organic oxidants under Co/Cu catalysis, affording a broad range of 1*H*-indazoles **117** in high yields (up to 99% yield) with excellent selectivity. It seems that the formation of the N–N bond involves Cu catalysis. Initially, anthranil **116a** was reacted with a range of imidates **1** containing both electron-donating and -withdrawing functional groups at the para-site of the phenyl ring. The results summarized in Scheme 34 demonstrate that this methodology is useful for the coupling of **116a** with a range of functionalized imidates **1**. The meta-substituted imidates were examined for the synthesis of the product **117** under standard conditions, with the C–N/N–N coupling of imidates **1** with anthranil **116a** taking place at the less hindered position. In the next step, the substrate scope of anthranil derivatives **116** under standard reaction conditions was investigated. Various substituents, including halogens and phenyl on different positions of the anthranil ring and a phenyl group substituted into the 3-position of the anthranil ring, were all applicable, leading to the desired indazole derivatives in satisfactory yields. Although unsubstituted anthranil was an effective substrate, the reaction rate was decreased. In this case, the utilization of pivalic acid additive facilitated the C–H activation transformation. When the reaction was carried out with 2-azidobenzaldehyde precursors instead of anthranils, poor results were obtained [75].

A plausible reaction mechanism for the Co(III)/Cu(II)-catalyzed synthesis of 1*H*-indazoles **117** from the coupling of imidates **1** with anthranils **116** is shown in Scheme 35. The mechanism comprises the cyclometalation of the imidate **1**, the coordination of anthranil to intermediate **118**, intramolecular N–O bond cleavage forming **120**, the migratory

insertion of the Co–aryl bond of **122** into the nitrene, and the coordination of an imidate to **121**, along with releasing the aminated intermediate **122**. In a successive catalytic cycle, the coordination of Cu(OAc)₂ to **122** and a double single-electron transfer occur to form target indazole **117** [75].



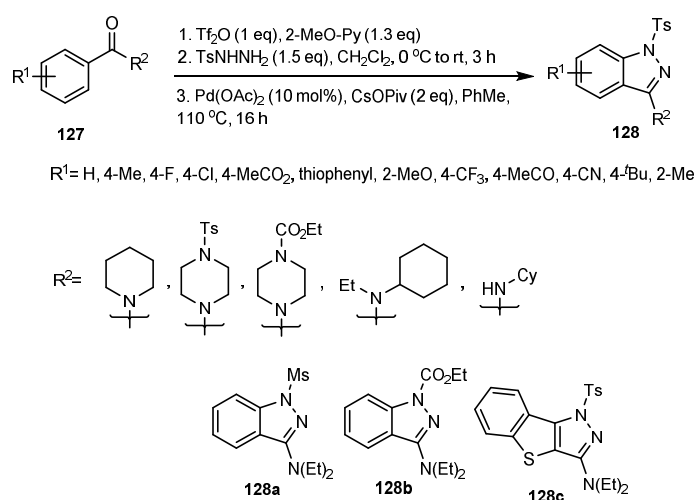
Scheme 34. A synthetic route for the preparation of *H*-indazoles **117** via the C–N/N–N coupling of imidates **1** with anthranils **116**.



Scheme 35. A rational mechanism for the synthesis of *H*-indazoles **117** via the C–N/N–N coupling of imidates **1** with anthranils **116**.

2.12. Synthesis of Indazoles Using Palladium Salts

The Pd-catalyzed C–H activation/annulation of substrates **127** was achieved by Charette in 2015. A series of 3-aminoindazoles **128** was produced with moderate to high yields (Scheme 36). In this reaction, the intermediate amidrazones were initially synthesized using an easy route from amide substrates **129** via (1) triflic anhydride activation and (2) condensation with hydrazines, to then (3) undergo a Pd-catalyzed C–H amination reaction. Structurally diverse amidrazones bearing various functional groups on the arene or nitrogen substituents revealed acceptable reactivity, yielding the expected indazoles **128**. As illustrated in Scheme 36, starting substrates with several cyclic and acyclic amine scaffolds can be applicable in the reaction. Various types of para-substituted substrates were investigated, delivering the desired indazoles **128** in yields of 15%–70%. In the case of a meta-substituted substrate (**127** substituted with OMe at the meta-position), a 4:1 mixture of regioisomers was obtained. Unfortunately, ortho-substituted substrates did not work in the reaction. Notably, the reaction was also effective using a substrate containing a 2-benzothienyl scaffold, achieving 3-aminoindazole fused heterocycle **128c**. The author offered no mechanistic explanation, but this may likely involve classical Pd-catalyzed C–H activation followed by cyclization. The current strategy offers an efficient procedure for the synthesis of 3-aminoindazoles **128**, which are easily synthesized from amide substrates in two steps [24].



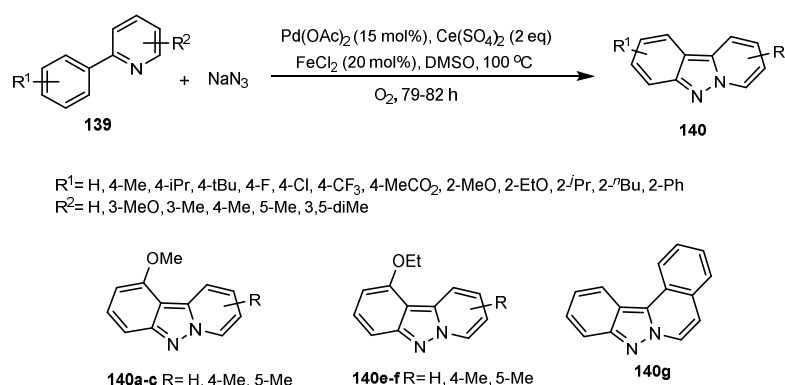
Scheme 36. A synthetic route for the preparation of 3-aminoindazoles **128** from tertiary amides **127**.

2.13. Synthesis of Indazoles Using Palladium Salt in the Presence of Cobalt Salts

An efficient Pd-catalyzed C–H functionalization/nitration/cyclization sequence for the synthesis of 3-nitro-1-(phenylsulfonyl)-1*H*-indazole derivatives **130** under mild reaction conditions was reported for the first time by Xia et al. (Scheme 37). The chelate-assisted cleavage of two C–H bonds is the key step in this transformation. The reaction was conducted using substrates **129** in the presence of 20 mol% Pd(OAc)₂ and 1.5 eq Co(NO₃)₂ · 6H₂O in DCE in a sealed tube at 110 °C for 4 h. Co(NO₃)₂ · 6H₂O has been used as an efficient nitration agent. A variety of functional groups on the para- and meta-positions of the benzylidene part were well-tolerated with little electronic dependence, providing, in most cases, 3-nitro-1-(phenylsulfonyl)-1*H*-indazoles **130** in excellent yields with high selectivity. The substrates substituted at the ortho-positions of the benzylidene scaffold underwent the C–H nitration and intramolecular C–H activation sequence uneventfully to give the target indazoles in more than 80% yields. As shown in Scheme 37, disubstituted substrates could also be successfully employed to deliver the indazoles **130a–e**. However, the di-MeO substrate failed to provide the desired product under the optimized reaction conditions. It was also found that various substrates containing substitutions at different positions of the phenylsulfonyl group were all tolerated to provide the desired 3-nitro-1-(phenylsulfonyl)-1*H*-indazole derivatives **130** with

2.14. Synthesis of Indazoles Using Palladium, Cerium, and Iron Salts

A novel, efficient, rapid, and versatile protocol to generate pyrido[1,2-*b*]indazole derivatives **140** through the C–H activation/azidation of arylpyridines **139** has been developed by Jiao et al. (Scheme 39). The synthetic approach involves C–H azidation and N–N bond formation, which was carried out at 100 °C using 15 mol% Pd(OAc)₂, 20 mol% FeCl₂, and Ce(SO₄)₂ in DMSO at 100 °C under O₂ atmosphere for 79–82 h. The scope of this reaction was first studied using the 3-methoxy-2-arylpyridine substrate and its derivatives. The substituent effect (electron-rich or electron-poor substituents) on the 3-methoxy-2-arylpyridine substrate was checked, showing a moderate effect on the yields. The 3-methyl-2-phenylpyridine substrate was explored as a further substrate, affording a satisfactory yield of the desired product. 4-Methyl, 5-methyl, or 3,5-dimethyl-substituted-2-phenylpyridines could also be successfully employed to provide the desired pyrido[1,2-*b*]indazoles in acceptable yields. It is worth noting that sterically hindered substrates could also be utilized, only providing the corresponding pyrido[1,2-*b*]indazoles **140a–f** in moderate yields. As expected, substrates with either electron-rich substituents such as Me and *t*-Bu or electron-poor substituents such as F and Cl at the para-position of the phenyl ring also proved to be suitable for this Pd-catalyzed tandem C–H azidation and N–N bond formation. Finally, 1-phenylisoquinoline yielded the corresponding product **140g** under optimized reaction conditions in a good yield. Involving direct C–N (via 2-pyridyl-directed Pd-catalyzed azidation) and N–N (via concerted nitrogen loss/ring closure) formations, this procedure proceeds under mild conditions, thus demonstrating a methodology for the synthesis of [*b*]fused indazoles in a single step [77].

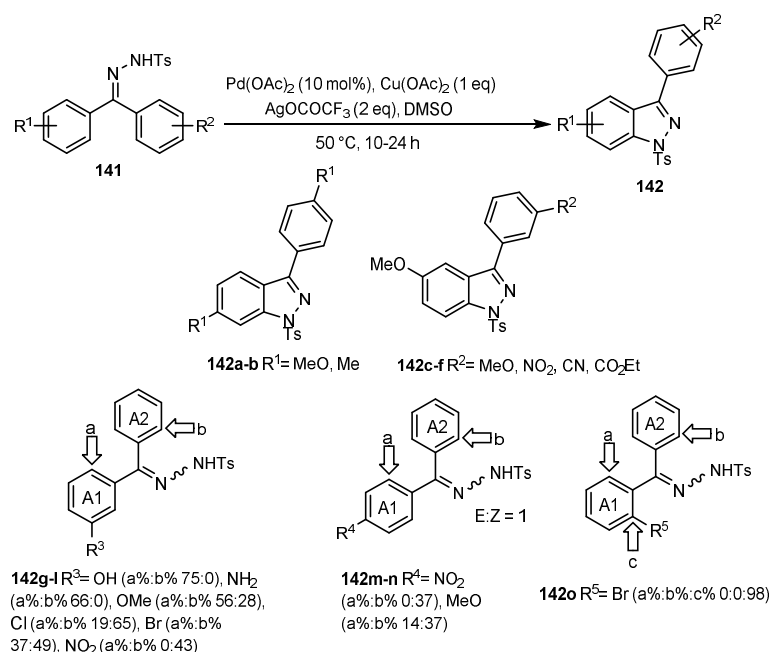


Scheme 39. A synthetic route for the preparation of pyrido[1,2-*b*]indazoles **140** via the tandem C–H azidation and N–N bond formation of arylpyridines **139**.

2.15. Synthesis of Indazoles Using Palladium, Copper, and Silver Salts

An efficient procedure for the mild synthesis of 3-aryl/alkylindazoles **142** catalyzed by palladium via a direct C–H activation/intramolecular amination sequence of hydrazone substrates **141** was presented by Hiroya (Scheme 40). This catalytic C–H activation/intramolecular amination reaction was performed involving 10 mol% Pd(OAc)₂, 1 equiv Cu(OAc)₂, and 2 equiv AgOCOCF₃ in DMSO at 50 °C for 10–24 h using hydrazone substrates **141**. This reaction was investigated using different substrates containing both electron-donating and -withdrawing functional groups on the benzene rings. As illustrated in Scheme 40, the transformation with two para-methoxy substituents gave only a 13% yield of product **142a**. In contrast, the compound containing two para-methyl substituents provided the expected product **142b** with a 73% yield. Surprisingly, the compound containing two meta-methoxy substituents proceeded successfully to afford only one product in a regioselective manner. Next, the starting materials containing two different groups at the meta-position reacted only at the 6-position on the more electron-donating aromatic ring, evidencing that both steric and electronic factors affect the outcome (see the products **142d–f**). The products **142** were achieved in acceptable yields using diverse monosubstituted substrates. As expected,

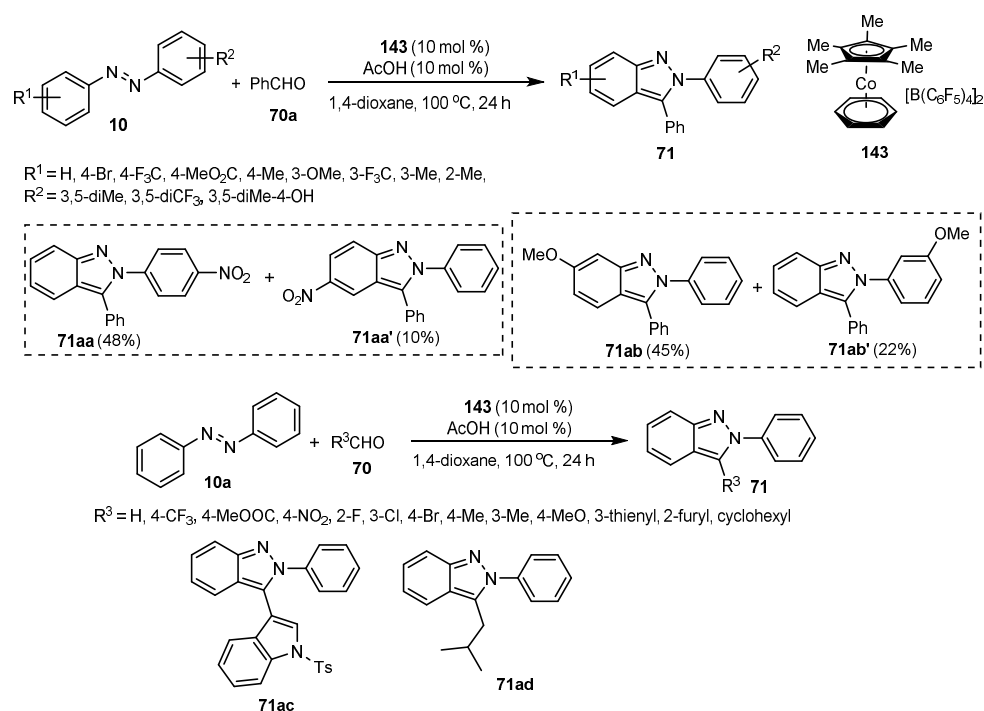
the reaction pathway was completely dependent on the nature of the functional groups on the benzene rings. The electron-rich donating substituents mainly oriented the reaction towards the A1 arene **142g–h**, whereas hydrazones containing an electron-poor substituent on the arene produced the corresponding indazoles on the nonsubstituted A2 arene **142d–f**. Notably, a C–H activation/intramolecular amination sequence took place preferentially on the A2 arene when para-substituted hydrazones containing electron-rich or -poor substituents were explored **142m–n** [78].



Scheme 40. A synthetic route for the preparation of 3-aryl/alkylindazoles **142** via the C–H activation/intramolecular amination reaction.

2.16. Synthesis of Indazoles Using Cobalt Salts

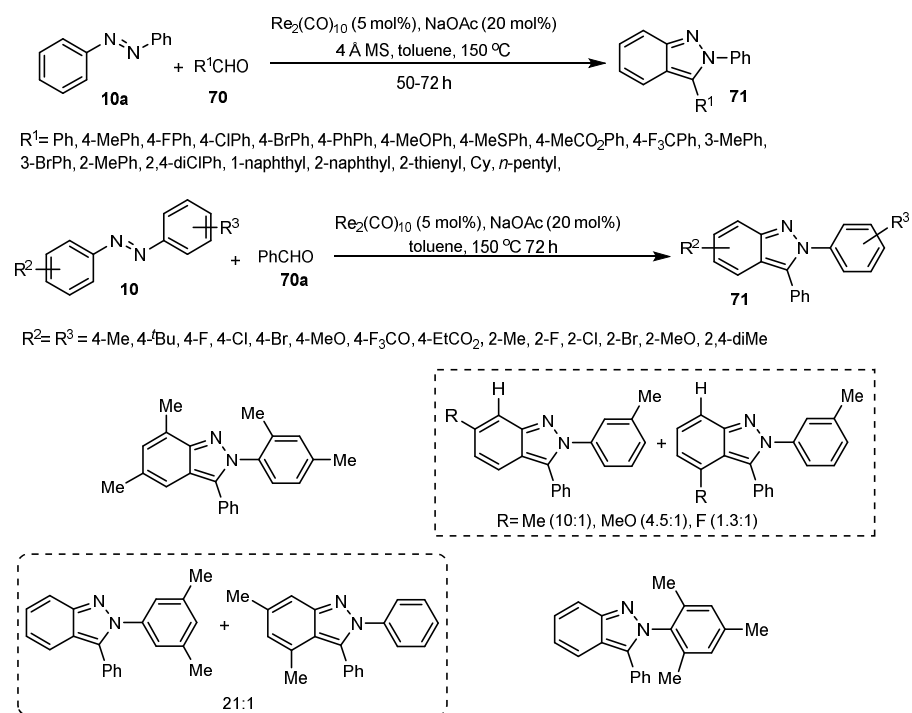
A novel efficient synthesis of indazoles **71** via sequential C–H bond functionalization/addition/cyclization was reported by Ellman (Scheme 41). The target products **71** were synthesized via a convergent one-step route using a novel air-stable cationic Co(III) catalyst. The reaction has been previously performed using 5 mol% (Cp*₂RhCl₂)₂ and 20 mol% AgSbF₆ in dioxane at 80 °C for 24 h. Although this system is efficient for the synthesis of indazoles, this chemistry displays some disadvantages, especially using an expensive Rh catalyst as well as the availability of Rh in the nature [66]. The reaction was carried out in the presence of 10 mol% co-catalyst **143** and 10 mol% AcOH in 1,4-dioxane (2.0 M) at 100 °C for 24 h and afforded the desired products **71** mostly with acceptable yields. First, the substrate scope of azobenzenes **10** was explored. Here, several symmetric and unsymmetrical azobenzenes containing electron-rich and electron-poor substituents were all well-tolerated and delivered the desired compounds in a regioselective manner. However, in the case of the para-nitro or meta-methoxy substituted azobenzene, a mixture of products **71aa**, **71aa'**, **71ab**, and **71ab'** was obtained. Different 3,5-disubstituted azobenzene substrates bearing a variety of substituents with donating or deficient natures were proven to afford satisfactory yields involving the less sterically hindered ring in the cyclization. Moreover, aromatic aldehydes containing electron-rich and electron-poor substituents as well as heteroaromatic aldehydes successfully reacted with azobenzene to form the corresponding indazoles in acceptable yields. The results of this study are illustrated in Scheme 41 [79].



Scheme 41. A synthetic route for the preparation of indazoles **71** via C–H bond functionalization/addition/cyclization cascades.

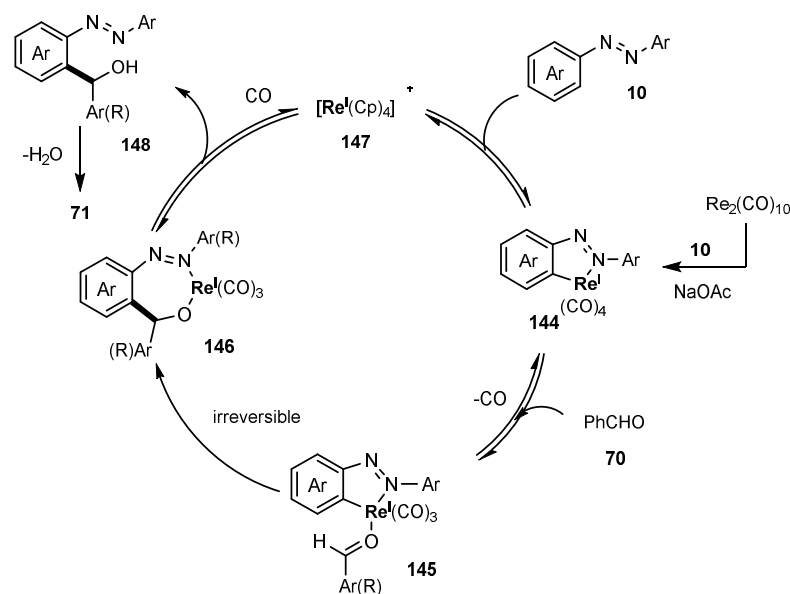
2.17. Synthesis of Indazoles Using Rhenium Salt in the Presence of Sodium Acetate

Wang and co-workers employed the first Re catalysis for the [4 + 1] annulation of azobenzenes **10** with aldehydes **70** to furnish 2*H*-indazoles **71** using catalytic amounts of $\text{Re}_2(\text{CO})_{10}$ and NaOAc in toluene at 150 °C within 50–72 h in an oven-dried Schlenk tube (Scheme 42). In comparison to similar works performed by Rh [66] and Co [79] catalysts, Re is less expensive than Rh but more expensive than a Co catalyst. It should be noted that Co and Rh catalysts could provide milder conditions for the reaction. The acetate could potentially enable an acceleration effect in the Re-catalyzed C–H activation of azobenzenes **10**. Initially, the scope of aldehyde substrates **70** was tested with both electron-rich and -poor functional groups on the aromatic ring, producing the target products in moderate to high yields. A wide variety of aldehydes **70** with substituents such as F, Cl, Br, MeS, CO_2Me , and CF_3 also coupled with different azobenzenes **10** to give corresponding products **71** in satisfactory yields. The reaction progressed smoothly using naphthaldehyde and thiophene-2-carbaldehyde to afford indazole derivatives **71** in good yields. When aliphatic aldehydes were introduced into this reaction, the yield was decreased. The scope and limitations of the reaction were screened by focusing on azobenzene derivatives **10**. The reaction proceeded smoothly with a variety of para-substituted azobenzenes, giving the corresponding indazoles **71** in good to high yields. Moreover, a variety of substituents on the ortho-position of azobenzenes were well-tolerated under standard conditions. In the case of disubstituted azobenzene (two methyl groups at the 2- and 4-positions of both rings), the reaction efficiently underwent the C–H functionalization/[4 + 1] annulation and generated the expected product in a high yield. Meanwhile, meta-methyl azobenzene produced a moderate yield of the corresponding product with high regioselectivity. The structures of some target products are shown in Scheme 42. No significant effect on the yield was observed when azobenzene was replaced with a bulky (mesityl) analog [80].



Scheme 42. A synthetic route for the preparation of indazole derivatives **71** via the [4 + 1] annulation of azobenzenes **10** with aldehydes **70**.

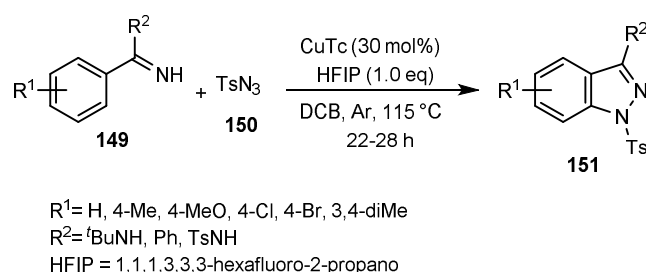
A reasonable reaction mechanism for the rhenium-catalyzed [4 + 1] annulation of azobenzenes **10** with aldehydes **70** is shown in Scheme 43. First, C–H is activated in the presence of $\text{Re}_2(\text{CO})_{10}/\text{NaOAc}$ to afford a cyclic Re(I)-complex **144**. In the next step, complex **145** bearing aldehyde is generated via an exchange between a CO ligand and an aldehyde. Finally, an irreversible aldehyde insertion to the Re–aryl bond, protonation, and an intramolecular nucleophilic substitution transformation followed by rearomatization produce the final product **71** [80].



Scheme 43. A rational mechanism for the synthesis of indazole derivatives **71** via the [4 + 1] annulation of azobenzenes **10** with aldehydes **70**.

2.18. Synthesis of Indazoles Using Copper Salts

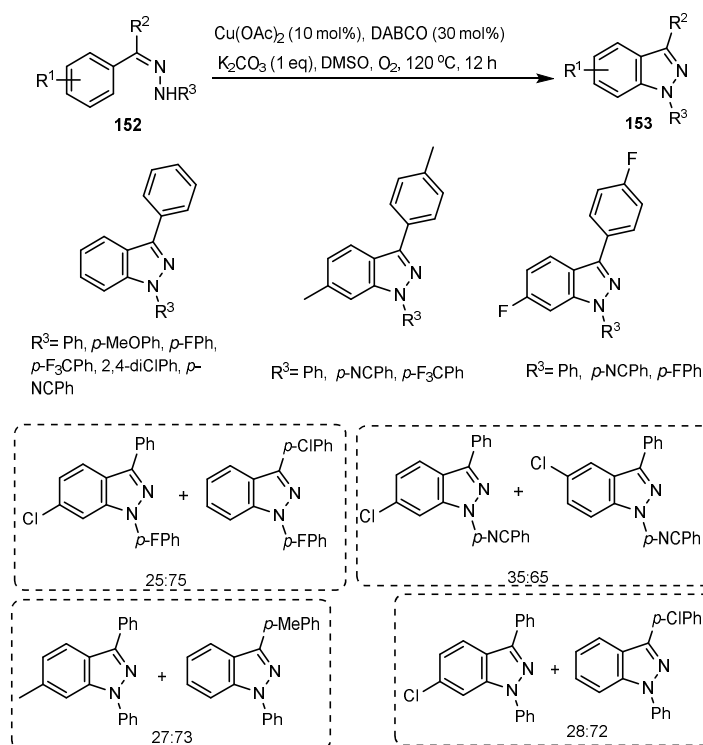
A highly regioselective synthesis of indazoles **151** was reported by Glorius via a copper-catalyzed C–H amidation process transformation. In this reaction, azides **150** were used as amino sources, and no oxidizing agent was used. The reaction exploited amidines or imine **149** to perform a tandem C–N/N–N bond-forming transformation for the production of indazole derivatives **151** in one pot (Scheme 44). All annulation reactions were carried out in 1,2-dichlorobenzene (DCB) at 115 °C using copper(I) thiophene-2-carboxylate (CuTc) (30 mol%) and 1,1,1,3,3,3-hexafluoro-2-propanol (HFIP) (1.0 eq) under Ar in a sealed tube. The *N*-tert-butylarylamidine substrates **149** bearing Me, MeO, Cl, or Br have been successfully employed in the Cu-catalyzed synthesis of *N*-tert-butyl-3-aminoindazoles using coupling with TsN₃ via a tandem C–N/N–N bond-forming reaction. A more detailed explanation of the mechanism includes a Cu-metallacycle, then nitrene coordination, migratory insertion, and reductive amination. The reaction of both tosyl-protected and free benzimidamide failed to form the corresponding products under optimized conditions. In addition, diphenylmethanimine as the starting material was examined, showing the expected indazole formation [81].



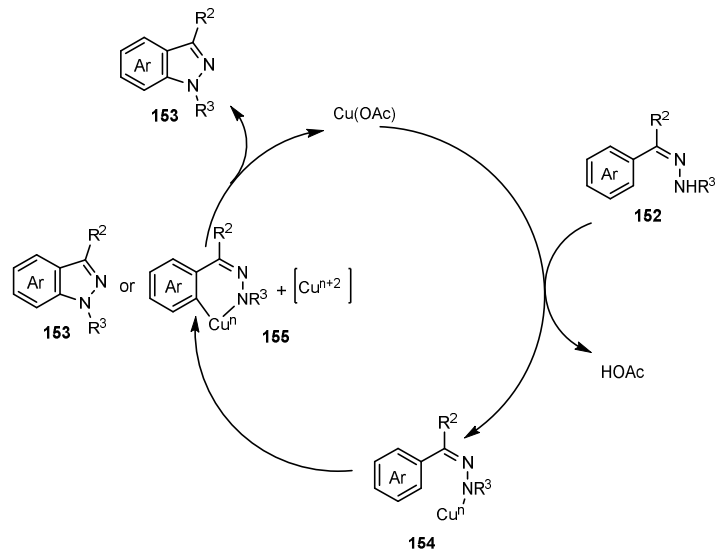
Scheme 44. A synthetic route for the preparation of indazole derivatives **151** via C(sp²)–H amidation **149** with azides **150** as amino sources.

An atom-economical protocol for the practical preparation of indazoles **153** through the Cu-catalyzed direct aerobic oxidative C(sp²)–H amination of benzophenone hydrazones **152** has been illustrated by Jiang et al. (Scheme 45). The synthesis of indazoles **153** was carried out successfully through an aerobic C(sp²)–H activation for C–N bond formation in the presence of catalytic amounts of Cu(OAc)₂ and DABCO in DMSO within 12 h in 70–86% yields. The substrate scope of the reaction was then tested. As shown in Scheme 45, the reactions of substrates **152** with substituents such as F, Cl, CF₃, and CN were then explored. These cascade reactions proceeded smoothly and afforded the corresponding indazoles **153** in moderate to good yields under standard conditions. Notably, substrates **152** containing an electron-rich substituent produced the desired indazoles in relatively higher yields than those with electron-poor substituents. It is worth noting that by using benzophenone hydrazone **152** containing two electronically unsymmetrical aromatic groups, a mixture of isomers was obtained, indicating that the reaction does not proceed in a regioselective manner. Some complex products synthesized by this Cu-catalyzed direct aerobic oxidative C(sp²)–H amination are illustrated in Scheme 45. The procedure has the privilege of good to high yields and tolerates a variety of substituents.

First, the Cu(OAc)₂ is probably coordinated with substrate **152**, resulting in a Cu–N adduct **154**. Subsequently, the C–H activation and C–N bond-forming transformation take place to afford the target molecules **153** (Scheme 46) [23].



Scheme 45. A synthetic route for the preparation of indazole derivatives **153** via aerobic $\text{C(sp}^2\text{)}\text{-H}$ functionalization/ C-N bond formation.



Scheme 46. A rational mechanism for the synthesis of indazole derivatives **153** via aerobic $\text{C(sp}^2\text{)}\text{-H}$ functionalization/ C-N bond formation.

3. Conclusions

The *N*-heterocycles show a wide structural variety that is beneficial for the investigation of further therapeutic agents for enhancing the pharmacokinetics and other physicochemical properties. Indazole derivatives are a significant category of *N*-heterocyclic five-membered systems that display a broad range of applications in biology, chemistry, and materials science. The investigation of indazole derivatives has become a rapidly evolving and increasingly active subject in therapeutic science. Meanwhile, transition-metal-catalyzed C-H activation/annulation strategies for the one-pot synthesis of indazoles has been growing steadily in synthetic organic chemistry. They are a superior class of trans-

formations that serve as powerful tools to access a wide range of indazoles. Numerous outstanding results have been reported for the synthesis of these structurally diverse indazole frames via transition-metal-catalyzed C–H activation/annulation reactions. The results of these articles have not previously been thoroughly studied or reviewed. This review article presents several atom-economical strategies for synthesizing indazole derivatives from accessible substrates through metal-catalyzed C–H functionalization and annulation transformations. The mentioned reactions feature easily available substrates, relatively good to high yields, large functional-group tolerance, diversity, and a high complexity of products under mild reaction conditions, furnishing practically useful methods to access structurally diverse indazoles.

Author Contributions: Conceptualization, W.D. and P.S.; writing, W.D., P.S. and A.R.; review and editing, W.D., P.S., A.R. and A.M.A. All authors have read and agreed to the published version of the manuscript.

Funding: This research received no external funding.

Institutional Review Board Statement: Not applicable.

Informed Consent Statement: Not applicable.

Data Availability Statement: The data presented in this study are available on request from the corresponding author.

Conflicts of Interest: The authors declare no conflict of interest.

References

- Kerru, N.; Gummidi, L.; Maddila, S.; Gangu, K.K.; Jonnalagadda, S.B. A Review on Recent Advances in Nitrogen-containing Molecules and Their Biological Applications. *Molecules* **2020**, *25*, 1909. [CrossRef] [PubMed]
- Santana, A.C.; Silva Filho, R.C.; Menezes, J.C.; Allonso, D.; Campos, V.R. Nitrogen-based Heterocyclic Compounds: A Promising Class of Antiviral Agents Against Chikungunya Virus. *Life* **2020**, *11*, 16. [CrossRef] [PubMed]
- Shiri, P. An Overview on The Copper-promoted Synthesis of Five-membered Heterocyclic Systems. *Appl. Organomet. Chem.* **2020**, *34*, e5600. [CrossRef]
- Shiri, P. Novel Hybrid Molecules Based on Triazole- β -lactam as Potential Biological Agents. *Mini-Rev. Med. Chem.* **2021**, *21*, 536–553. [CrossRef]
- Alizadeh, A.; Roosta, A.; Rezaiyehraad, R. Efficient Access to Pyrido[1, 2-*a*]pyrimidines and Imidazo[1, 2-*a*]pyridines Through Knoevenagel Reaction/aza-ene Addition/Intramolecular Cyclization. *J. Iran. Chem. Soc.* **2020**, *17*, 1123–1130. [CrossRef]
- Alizadeh, A.; Roosta, A. An Efficient Regioselective Access to (1*Z*)-11-(3-Aryl-5, 6-dihydropyrazin-2 (1*H*)-ylidene)-11*H*-indeno[1, 2-*b*]quinoxaline Derivatives via One-Pot Three-Component Reaction. *ChemistrySelect* **2019**, *4*, 13503–13505. [CrossRef]
- Khalafi-Nezhad, A.; Panahi, F. Ruthenium-catalyzed Synthesis of Benzoxazoles Using Acceptorless Dehydrogenative Coupling Reaction of Primary Alcohols with 2-Aminophenol under Heterogeneous Conditions. *ACS Catal.* **2014**, *4*, 1686–1692. [CrossRef]
- Jeong, T.; Han, S.H.; Han, S.; Sharma, S.; Park, J.; Lee, J.S.; Kwak, J.H.; Jung, Y.H.; Kim, I.S. Access to 3-acyl-(2*H*)-indazoles via Rh (III)-Catalyzed C–H Addition and Cyclization of Azobenzenes with α -Keto Aldehydes. *Org. Lett.* **2016**, *18*, 232–235. [CrossRef]
- Aboonajmi, J.; Panahi, F.; Sharghi, H. One-Pot Multicomponent Coupling Reaction of Catechols, Benzyl Alcohols/Benzyl Methyl Ethers, and Ammonium Acetate toward Synthesis of Benzoxazoles. *ACS Omega* **2021**, *6*, 22395–22399. [CrossRef]
- Mohtat, B.; Siadati, S.A.; Khalilzadeh, M.A.; Zareyee, D. The Concern of Emergence of Multi-station Reaction Pathways That Might Make Stepwise the Mechanism of the 1, 3-Dipolar Cycloadditions of Azides and Alkynes. *J. Mol. Struct.* **2018**, *1155*, 58–64. [CrossRef]
- Schmidt, A.; Beutler, A.; Snovydyvych, B. Recent Advances in the Chemistry of Indazoles. *Eur. J. Org. Chem.* **2008**, *2008*, 4073–4095. [CrossRef]
- Zhang, S.-G.; Liang, C.-G.; Zhang, W.-H. Recent Advances in Indazole-containing Derivatives: Synthesis and Biological Perspectives. *Molecules* **2018**, *23*, 2783. [CrossRef] [PubMed]
- Thangadurai, A.; Minu, M.; Wakode, S.; Agrawal, S.; Narasimhan, B. Indazole: A Medicinally Important Heterocyclic Moiety. *Med. Chem. Res.* **2012**, *21*, 1509–1523. [CrossRef]
- Khalifeh, R.; Karimzadeh, F. Copper Nanoparticles Supported on Charcoal Mediated One-pot Three-component Synthesis of *N*-Substituted-2*H*-indazoles via Consecutive Condensation C–N and N–N Bond Formation. *Can. J. Chem.* **2019**, *97*, 303–309. [CrossRef]
- Khalifeh, R.; Naseri, V.; Rajabzadeh, M. Synthesis of Imidazolium-Based Ionic Liquid on Modified Magnetic Nanoparticles for Application in One-Pot Synthesis of Trisubstituted Imidazoles. *ChemistrySelect* **2020**, *5*, 11453–11462. [CrossRef]

16. Khalili, D.; Evazi, R.; Neshat, A.; Aboonajmi, J. Copper (I) Complex of Dihydro Bis (2-Mercapto Benzimidazolyl) Borate as an Efficient Homogeneous Catalyst for the Synthesis of 2H-Indazoles and 5-Substituted 1H-Tetrazoles. *ChemistrySelect* **2021**, *6*, 746–753. [CrossRef]
17. Sharghi, H.; Aberi, M.; Shiri, P. Silica-supported Cu (II)–quinoline Complex: Efficient and Recyclable Nanocatalyst for One-pot Synthesis of Benzimidazolquinoline Derivatives and 2H-Indazoles. *Appl. Organomet. Chem.* **2019**, *33*, e4974. [CrossRef]
18. Kumar, A.; Verma, S.; Pathak, D.D. Synthesis and Characterization of A Recyclable Graphene Oxide-surface-engineered Copper(II) Schiff Base Complex: Catalytic Application in Synthesis of 1, 2, 3-Triazoles and 2H-Indazoles. *J. Environ. Chem. Eng.* **2021**, *9*, 105791. [CrossRef]
19. Sharghi, H.; Aberi, M.; Shiri, P. Highly Reusable Support-free Copper(II) Complex of Para-hydroxy-substituted Salen: Novel, Efficient and Versatile Catalyst for C–N Bond Forming Reactions. *Appl. Organomet. Chem.* **2017**, *31*, e3761. [CrossRef]
20. Magano, J.; Waldo, M.; Greene, D.; Nord, E. The Synthesis of (S)-5-Fluoro-1-(2-fluorophenyl)-3-(piperidin-3-ylmethoxy)-1H-Indazole, A Norepinephrine/Serotonin Reuptake Inhibitor for the Treatment of Fibromyalgia. *Org. Process Res. Dev.* **2008**, *12*, 877–883. [CrossRef]
21. Karishma, P.; Gogia, A.; Mandal, S.K.; Sakhuja, R. Ruthenium Catalyzed C–H Amidation and Carbocyclization using Isocyanates: An Access to Amidated 2-Phenylphthalazine-1, 4-diones and Indazolo [1, 2-b] Phthalazine-triones. *Adv. Synth. Catal.* **2021**, *363*, 762–775. [CrossRef]
22. Rhee, H.-K.; Yoo, J.H.; Lee, E.; Kwon, Y.J.; Seo, H.-R.; Lee, Y.-S.; Choo, H.-Y.P. Synthesis and Cytotoxicity of 2-Phenylquinazolin-4(3H)-one Derivatives. *Eur. J. Med. Chem.* **2011**, *46*, 3900–3908. [CrossRef] [PubMed]
23. Li, X.; He, L.; Chen, H.; Wu, W.; Jiang, H. Copper-catalyzed Aerobic C (sp²)–H Functionalization for C–N Bond Formation: Synthesis of Pyrazoles and Indazoles. *J. Org. Chem. Res.* **2013**, *78*, 3636–3646. [CrossRef]
24. Cyr, P.; Regnier, S.; Bechara, W.S.; Charette, A.B. Rapid Access to 3-Aminoindazoles from Tertiary Amides. *Org. Lett.* **2015**, *17*, 3386–3389. [CrossRef] [PubMed]
25. Shiri, P.; Ramezanpour, S.; Amani, A.M.; Dehaen, W. A Patent Review on Efficient Strategies for the Total Synthesis of Pazopanib, Regorafenib and Lenvatinib as Novel Anti-angiogenesis Receptor Tyrosine Kinase Inhibitors for Cancer Therapy. *Mol. Divers.* **2022**. [CrossRef] [PubMed]
26. Cekaviciute, M.; Simokaitiene, J.; Grazulevicius, J.; Buika, G.; Jankauskas, V. New Derivatives of Indazole as Electronically Active Materials. *Dye. Pigment.* **2012**, *92*, 654–658. [CrossRef]
27. Sharghi, H.; Aberi, M. Ligand-free Copper (I) Oxide Nanoparticle Catalyzed Three-component Synthesis of 2H-Indazole Derivatives from 2-Halobenzaldehydes, Amines and Sodium Azide in Polyethylene Glycol as a Green Solvent. *Synlett* **2014**, *25*, 1111–1115. [CrossRef]
28. Gaikwad, D.D.; Chapolikar, A.D.; Devkate, C.G.; Warad, K.D.; Tayade, A.P.; Pawar, R.P.; Domb, A.J. Synthesis of Indazole Motifs and Their Medicinal Importance: An Overview. *Eur. J. Med. Chem.* **2015**, *90*, 707–731. [CrossRef] [PubMed]
29. Malik, S.; Hasan, S.S.; Choudhary, M.I.; Ni, C.-Z.; Clardy, J. Nigellidine—A New Indazole Alkaloid from The Seeds of *Nigella Sativa*. *Tetrahedron Lett.* **1995**, *36*, 1993–1996.
30. Boubertakh, B.; Liu, X.-G.; Cheng, X.-L.; Li, P. A Spotlight on Chemical Constituents and Pharmacological Activities of *Nigella Glandulifera* Freyn et Sint seeds. *J. Chem.* **2013**, *2013*, 1–22. [CrossRef]
31. Inamoto, K.; Katsuno, M.; Yoshino, T.; Arai, Y.; Hiroya, K.; Sakamoto, T. Synthesis of 3-Substituted Indazoles and Benzoisoxazoles via Pd-Catalyzed Cyclization Reactions: Application to the Synthesis of Nigellidine. *Tetrahedron* **2007**, *63*, 2695–2711. [CrossRef]
32. Raut, S.; Hadi, A.; Pathan, M.A. The Efficient Synthesis of 3-[6-(Substituted)-[1, 2, 4] Triazol-3-yl]-1H-Indazole. *J. Heterocycl. Chem.* **2020**, *57*, 1291–1305. [CrossRef]
33. Rafique, R.; Khan, K.M.; Chigurupati, S.; Wadood, A.; Rehman, A.U.; Karunanidhi, A.; Hameed, S.; Taha, M.; Al-Rashida, M. Synthesis of New Indazole Based Dual Inhibitors of α -Glucosidase and α -Amylase Enzymes, Their In vitro, In silico and Kinetics Studies. *Bioorg. Chem.* **2020**, *94*, 103195. [CrossRef]
34. Rudavath, D.; Sreenivasulu, R.; Pinapati, S.R.; Raju, R.R. Synthesis and Anticancer Evaluation of Indazole-aryl Hydrazide-hydrazone Derivatives. *J. Indian Chem. Soc.* **2018**, *95*, 433–438.
35. Nie, B.; Wu, W.; Zhang, Y.; Jiang, H.; Zhang, J. Recent Advances in the Synthesis of Bridgehead (or ring-junction) Nitrogen Heterocycles via Transition Metal-catalyzed C–H Bond Activation and Functionalization. *Org. Chem. Front.* **2020**, *7*, 3067–3099. [CrossRef]
36. Kumar, A.; Sherikar, M.S.; Hanchate, V.; Prabhu, K.R. Application of Sulfoxonium Ylide in Transition-metal-catalyzed C–H Bond Activation and Functionalization Reactions. *Tetrahedron* **2021**, *101*, 132478. [CrossRef]
37. Xiang, Y.; Wang, C.; Ding, Q.; Peng, Y. Diazo Compounds: Versatile Synthons for the Synthesis of Nitrogen Heterocycles via Transition Metal-Catalyzed Cascade C–H Activation/Carbene Insertion/Annulation Reactions. *Adv. Synth. Catal.* **2019**, *361*, 919–944. [CrossRef]
38. Zhang, M. Construction of Heterocycle Scaffolds via Transition Metal-Catalyzed sp² C–H Functionalization. *Adv. Synth. Catal.* **2009**, *351*, 2243–2270. [CrossRef]
39. Kumar, G.R.; Rajesh, M.; Lin, S.; Liu, S. Propargylic Alcohols as Coupling Partners in Transition-Metal-Catalyzed Arene C–H Activation. *Adv. Synth. Catal.* **2020**, *362*, 5238–5256. [CrossRef]
40. Zhang, G.; Fan, Q.; Zhao, Y.; Ding, C. Copper-Promoted Oxidative Intramolecular C–H Amination of Hydrazones to Synthesize 1H-Indazoles and 1H-Pyrazoles Using a Cleavable Directing Group. *Eur. J. Org. Chem.* **2019**, *2019*, 5801–5806. [CrossRef]

41. Verbelen, B.; Leen, V.; Wang, L.; Boens, N.; Dehaen, W. Direct palladium-catalysed C–H arylation of BODIPY dyes at the 3- and 5-positions. *Chem. Commun.* **2012**, *48*, 9129–9131. [CrossRef] [PubMed]
42. Han, X.-L.; Lin, P.-P.; Li, Q. Recent Advances of Allenes in the First-row Transition Metals Catalyzed C–H Activation Reactions. *Chin. Chem. Lett.* **2019**, *30*, 1495–1502. [CrossRef]
43. Karak, P.; Rana, S.S.; Choudhury, J. Cationic π -extended Heteroaromatics via a Catalytic C–H Activation Annulative Alkyne-insertion Sequence. *Chem. Commun.* **2022**, *58*, 133–154. [CrossRef]
44. Mo, J.; Müller, T.; Oliveira, J.C.; Ackermann, L. 1, 4-Iron Migration for Expedient Allene Annulations through Iron-Catalyzed C–H/N–H/C–O/C–H Functionalizations. *Angew. Chem. Int. Ed. Engl.* **2018**, *57*, 7719–7723. [CrossRef] [PubMed]
45. Tang, J.; Tang, Y.; Wang, X.; Wang, Y.; Huang, X.; Xu, S.; Li, Y. Regioselective Cascade Annulation of Indoles with Alkynediones for Construction of Functionalized Tetrahydrocarbazoles Triggered by Cp*Rh^{III}-catalyzed C–H activation. *Org. Chem. Front.* **2021**, *8*, 3809–3814. [CrossRef]
46. Kalyani, A.; Tulichala, R.P.; Chauhan, S.; Swamy, K.K. Palladium Catalyzed Nitrile Insertion and Cyanation of Biindoles: Synthesis of Indole Fused α -Carboline Scaffolds via Double C–H Activation. *Tetrahedron Lett.* **2022**, *89*, 153600. [CrossRef]
47. Song, X.; Han, X.; Zhang, R.; Liu, H.; Wang, J. Rhodium (III)-catalyzed [4 + 2] Annulation via C–H Activation: Synthesis of Multi-substituted Naphthalenone Sulfoxonium Ylides. *Molecules* **2019**, *24*, 1884. [CrossRef] [PubMed]
48. Hosseini-Sarvari, M.; Roosta, A. Synthesis of 2-Amino-4H-Chromen-4-yl phosphonates via C–P Bond Formation Catalyzed by Nano-rods ZnO under Solvent-free Condition. *Comb. Chem. High Throughput Screen.* **2014**, *17*, 47–52. [CrossRef] [PubMed]
49. Song, L.; Van der Eycken, E.V. Transition Metal-Catalyzed Intermolecular Cascade C–H Activation/Annulation Processes for the Synthesis of Polycycles. *Chem. Eur. J.* **2021**, *27*, 121–144. [CrossRef]
50. Duarah, G.; Kaishap, P.; Begum, T.; Gogoi, S. Recent Advances in Ruthenium (II)-Catalyzed C–H Bond Activation and Alkyne Annulation Reactions. *Adv. Synth. Catal.* **2019**, *361*, 654–672. [CrossRef]
51. Dong, J.; Zhang, Q.; Wang, Z.; Huang, G.; Li, S. Recent Advances in the Development of Indazole-based Anticancer Agents. *ChemMedChem* **2018**, *13*, 1490–1507. [CrossRef] [PubMed]
52. Janardhanan, J.C.; Bhaskaran, R.P.; Praveen, V.K.; Manoj, N.; Babu, B.P. Transition-Metal-Catalyzed Syntheses of Indazoles. *Asian J. Org. Chem.* **2020**, *9*, 1410–1431. [CrossRef]
53. Ghosh, D.; Ghosh, S.; Hajra, A. Electrochemical Functionalization of Imidazopyridine and Indazole: An Overview. *Adv. Synth. Catal.* **2021**, *363*, 5047–5071. [CrossRef]
54. Cao, Y.; Luo, C.; Yang, P.; Li, P.; Wu, C. Indazole Scaffold: A Generalist for Marketed and Clinical Drugs. *Med. Chem. Res.* **2021**, *30*, 501–518. [CrossRef]
55. Wang, Q.; Li, X. Synthesis of 1H-indazoles from Imidates and Nitrosobenzenes via Synergistic Rhodium/copper catalysis. *Org. Lett.* **2016**, *18*, 2102–2105. [CrossRef]
56. Cai, S.; Lin, S.; Yi, X.; Xi, C. Substrate-controlled Transformation of Azobenzenes to Indazoles and Indoles via Rh (III)-catalysis. *J. Org. Chem. Res.* **2017**, *82*, 512–520. [CrossRef]
57. Han, S.; Shin, Y.; Sharma, S.; Mishra, N.K.; Park, J.; Kim, M.; Kim, M.; Jang, J.; Kim, I.S. Rh (III)-Catalyzed Oxidative Coupling of 1, 2-Disubstituted Arylhydrazines and Olefins: A New Strategy for 2, 3-Dihydro-1H-Indazoles. *Org. Lett.* **2014**, *16*, 2494–2497. [CrossRef]
58. Yao, J.; Feng, R.; Lin, C.; Liu, Z.; Zhang, Y. Synthesis of 2, 3-Dihydro-1H-indazoles by Rh (III)-catalyzed C–H Cleavage of Arylhydrazines. *Org. Biomol. Chem.* **2014**, *12*, 5469–5476. [CrossRef]
59. Zhou, J.; Zhang, L.; Chen, J.; Chen, J.; Yin, C.; Yu, C. Rh (III)-Catalyzed [4 + 1] Annulation and Ring Opening for the Synthesis of Pyrazolo [1, 2-a] Indazole Bearing a Quaternary Carbon. *Tetrahedron Lett.* **2020**, *61*, 152350. [CrossRef]
60. Long, Z.; Wang, Z.; Zhou, D.; Wan, D.; You, J. Rh (III)-Catalyzed Regio- and Chemoselective [4 + 1]-Annulation of Azoxy Compounds with Diazoesters for the Synthesis of 2H-Indazoles: Roles of the Azoxy Oxygen Atom. *Org. Lett.* **2017**, *19*, 2777–2780. [CrossRef] [PubMed]
61. Wang, N.; Liu, L.; Xu, W.; Zhang, M.; Huang, Z.; Shi, D.; Zhao, Y. Rhodium (III)-Catalyzed Oxidative Annulation of Ketoximes with Sulfonamide: A Direct Approach to Indazoles. *Org. Lett.* **2019**, *21*, 365–368. [CrossRef] [PubMed]
62. Chun, R.; Kim, S.; Han, S.H.; Han, S.; Lee, S.H.; Mishra, N.K.; Jung, Y.H.; Kim, H.S.; Kim, I.S. Synthesis of (2H)-Indazoles from Azobenzenes Using Paraformaldehyde as a One-Carbon Synthone. *Adv. Synth. Catal.* **2019**, *361*, 1617–1626. [CrossRef]
63. Yin, C.; Zhong, T.; Zheng, X.; Li, L.; Zhou, J.; Yu, C. Direct Synthesis of Indazole Derivatives via Rh (III)-catalyzed C–H Activation of Phthalazinones and Allenes. *Org. Biomol. Chem.* **2021**, *19*, 7701–7705. [CrossRef]
64. Park, M.S.; Moon, K.; Oh, H.; Lee, J.Y.; Ghosh, P.; Kang, J.Y.; Park, J.S.; Mishra, N.K.; Kim, I.S. Synthesis of (2H)-Indazoles and Dihydrocinnolinones through Annulation of Azobenzenes with Vinylene Carbonate under Rh (III) Catalysis. *Org. Lett.* **2021**, *23*, 5518–5522. [CrossRef] [PubMed]
65. Zhang, L.; Chen, J.; Chen, X.; Zheng, X.; Zhou, J.; Zhong, T.; Chen, Z.; Yang, Y.-F.; Jiang, X.; She, Y.-B. Rh (III)-catalyzed, Hydrazine-directed C–H Functionalization with 1-Alkynylcyclobutanols: A New strategy for 1H-Indazoles. *Chem. Commun.* **2020**, *56*, 7415–7418. [CrossRef]
66. Lian, Y.; Bergman, R.G.; Lavis, L.D.; Ellman, J.A. Rhodium (III)-catalyzed Indazole Synthesis by C–H Bond Functionalization and Cyclative Capture. *J. Am. Chem. Soc.* **2013**, *135*, 7122–7125. [CrossRef] [PubMed]
67. Gholamhosseini, M.; Kianmehr, E. A Ruthenium-catalyzed Alkenylation–annulation Approach for the Synthesis of Indazole Derivatives via C–H Bond Activation. *Org. Biomol. Chem.* **2018**, *16*, 5973–5978. [CrossRef]

68. Yu, D.-G.; Suri, M.; Glorius, F. Rh (III)/Cu (II)-Cocatalyzed Synthesis of 1*H*-Indazoles Through C–H Amidation and N–N Bond Formation. *J. Am. Chem. Soc.* **2013**, *135*, 8802–8805. [CrossRef] [PubMed]
69. Zhu, J.; Sun, S.; Cheng, J. Rh (III)-catalyzed [4 + 1]-Annulation of Azobenzenes with α -Carbonyl Sulfoxonium Ylides Toward 3-acyl-(2*H*)-Indazoles. *Tetrahedron Lett.* **2018**, *59*, 2284–2287. [CrossRef]
70. Oh, H.; Han, S.; Pandey, A.K.; Han, S.H.; Mishra, N.K.; Kim, S.; Chun, R.; Kim, H.S.; Park, J.; Kim, I.S. Synthesis of (2*H*)-Indazoles through Rh (III)-Catalyzed Annulation Reaction of Azobenzenes with Sulfoxonium Ylides. *J. Org. Chem. Res.* **2018**, *83*, 4070–4077. [CrossRef] [PubMed]
71. Cui, X.-F.; Huang, G.-S. Rhodium-catalyzed Tandem Acylmethylation/annulation of *N*-Nitrosoanilines with Sulfoxonium Ylides for the Synthesis of Substituted Indazole *N*-Oxides. *Org. Biomol. Chem.* **2020**, *18*, 4014–4018. [CrossRef] [PubMed]
72. Li, H.; Han, Y.; Yang, Z.; Yao, Z.; Wang, L.; Cui, X. Rh (III)-catalyzed Annulation of Azobenzenes and α -Cl Ketones toward 3-Acyl-2*H*-indazoles. *Chin. Chem. Lett.* **2021**, *32*, 1709–1712. [CrossRef]
73. Xu, P.; Wang, G.; Wu, Z.; Zhu, C. Rh (III)-Catalyzed Double C–H Activation of Aldehyde Hydrazones: A Route for Functionalized 1*H*-Indazole Synthesis. *Chem. Sci.* **2017**, *8*, 1303–1308. [CrossRef]
74. Long, Z.; Yang, Y.; You, J. Rh (III)-Catalyzed [4 + 1]-annulation of Azoxy Compounds with Alkynes: A Regioselective Approach to 2*H*-Indazoles. *Org. Lett.* **2017**, *19*, 2781–2784. [CrossRef]
75. Li, L.; Wang, H.; Yu, S.; Yang, X.; Li, X. Cooperative Co (III)/Cu (II)-Catalyzed C–N/N–N Coupling of Imidates with Anthranils: Access to 1*H*-Indazoles via C–H Activation. *Org. Lett.* **2016**, *18*, 3662–3665. [CrossRef]
76. Wang, G.; Sun, J.; Wang, K.; Han, J.; Li, H.; Duan, G.; You, G.; Li, F.; Xia, C. Palladium-catalyzed Direct C–H Nitration and Intramolecular C–H Functionalization for the Synthesis of 3-Nitro-1-(phenylsulfonyl)-1*H*-indazole Derivatives. *Org. Chem. Front.* **2019**, *6*, 1608–1612. [CrossRef]
77. Zheng, Q.-Z.; Feng, P.; Liang, Y.-F.; Jiao, N. Pd-Catalyzed Tandem C–H Azidation and N–N Bond Formation of Arylpyridines: A Direct Approach to Pyrido [1, 2-*b*] Indazoles. *Org. Lett.* **2013**, *15*, 4262–4265. [CrossRef] [PubMed]
78. Inamoto, K.; Saito, T.; Katsuno, M.; Sakamoto, T.; Hiroya, K. Palladium-catalyzed C–H Activation/intramolecular Amination Reaction: A New Route to 3-Aryl/alkylindazoles. *Org. Lett.* **2007**, *9*, 2931–2934. [CrossRef]
79. Hummel, J.R.; Ellman, J.A. Cobalt (III)-catalyzed Synthesis of Indazoles and Furans by C–H Bond Functionalization/addition/cyclization Cascades. *J. Am. Chem. Soc.* **2015**, *137*, 490–498. [CrossRef] [PubMed]
80. Geng, X.; Wang, C. Rhenium-catalyzed [4+1] Annulation of Azobenzenes and Aldehydes via Isolable Cyclic Rhenium(I) Complexes. *Org. Lett.* **2015**, *17*, 2434–2437. [CrossRef]
81. Peng, J.; Xie, Z.; Chen, M.; Wang, J.; Zhu, Q. Copper-catalyzed C (sp²)-H Amidation with Azides as Amino Sources. *Org. Lett.* **2014**, *16*, 4702–4705. [CrossRef]

MDPI AG
Grosspeteranlage 5
4052 Basel
Switzerland
Tel.: +41 61 683 77 34

Molecules Editorial Office
E-mail: molecules@mdpi.com
www.mdpi.com/journal/molecules



Disclaimer/Publisher's Note: The statements, opinions and data contained in all publications are solely those of the individual author(s) and contributor(s) and not of MDPI and/or the editor(s). MDPI and/or the editor(s) disclaim responsibility for any injury to people or property resulting from any ideas, methods, instructions or products referred to in the content.



Academic Open
Access Publishing

mdpi.com

ISBN 978-3-7258-2082-5